Aerosol Formation and Growth in Aromatic Hydrocarbon/NO_x Systems

Thesis by
Jennifer E. Stern

In Partial Fulfillment of the Requirements

for the Degree of

Doctor of Philosophy

Department of Chemical Engineering

California Institute of Technology

Pasadena, California

1988

(Submitted November 25, 1987)

ACKNOWLEDGEMENTS

I would never have made it this far without the help of many people, both at Caltech and miles away. For guidance and moral support, I owe many thanks to my advisor, John Seinfeld. I have benefited not only from his ideas and insights when I have been thinking about a problem, but also from his understanding when things seemed disastrously wrong to me. I have become a much better scientist under his constant insistence that I back up all of my statements with real calculations. I also owe a great deal to my co-advisor, Rick Flagan, who helped me develop the experimental technique and ability to conduct such a complicated and large-scale experimental investigation. I thank Rick especially for always treating me as an equal in philosophical discussions about aerosol experimentation. Without the advice and ideas I got from both advisors, my thesis would have taken infinitely longer to complete.

In addition, I give special thanks to two co-workers whose input was invaluable for this work. Dale Warren helped me get started both in the lab and on the computer. His computer expertise certainly made my life easier. Without Toby Petti, I would not have completed a year's worth of experiments. No one could have been better company for all the many hours spent on the roof, watching the sun rise, second-guessing the weather people and crawling around on hands and knees. Who else would have sanctioned lunch at 10:00 a.m.?

One of the great things about working in the air pollution group was the camaraderie among the students in the group. I have shared some wonderful times with my co-workers, and will continue to enjoy many friendships when I leave

Caltech. For this, I especially thank Carol Jones Adkins, Gidi Sageev Grader, Jin Jwang Wu, Hung Nguyen, Sonia Kreidenweis-Dandy, Brian Wong, Ranajit Sahu, and Suzanne Paulson.

Those who deserve the most credit for making my years here enjoyable are the friends I have made and kept in the years from high school until the present. Naming them all here would not be unlike trying to draw up an invitation list for a very small wedding – inevitably some would be forgotten and others would feel left out. I would therefore like to thank all of them (in one encompassing statement) for the bridge games, dinner parties, afternoon walks, backrubs, tea breaks at the Red Door, phone calls, letters and cards. In addition, I would like to extend extra-special appreciation to (in alphabetical order) Liz, Jeff, Walter, Sue, Joe, Jeff, Donna, and the Tylers for helping me keep straight the important things in life.

I gratefully acknowledge the financial support of the National Science Foundation Fellowship program, and of the Coordinating Research Council, project AP-6.

From 3000 miles away, my mother has provided me with inspiration and love for all of my years here. I finally have the chance to thank her for everything she has done for me.

Most importantly, I want to thank my husband, Jeffrey, who has shared the good times and helped me through the difficult times, and has always been an unfailing source of support, friendship, and love.

ABSTRACT

The formation of secondary organic aerosol in the atmosphere remains one of the most poorly understood aspects of the air pollution problem in urban areas. Photooxidation of gas-phase emissions produces low vapor pressure species that are converted to the aerosol phase either by homogeneous nucleation of new particles or by condensation onto existing particles. One of the goals in studying aerosol dynamics in atmospheric systems is to determine the factors that govern which of these two pathways dominates in the conversion of gas-phase species to the aerosol phase.

We have conducted an extensive series of experiments aimed at elucidating the physics of atmospheric organic aerosol formation. An outdoor smog chamber was used to study the formation and growth of secondary aerosol resulting from the photooxidation of aromatic hydrocarbons (toluene, m-xylene, ethyl benzene, and 1,3,5-trimethyl benzene) in the presence of NO_x. In the experiments, particular emphasis was given to the effect of primary aerosol on the subsequent aerosol evolution in the system. We observed that with a sufficient number concentration of initial seed particles in the system, homogeneous nucleation could be suppressed and all gas-to-particle conversion occurred via condensation onto the seed particles.

Aerosol yields by mass from the gas phase were calculated for each experiment. These yields were somewhat dependent on the initial hydrocarbon/NO_x ratio in each experiment, which is an indication of the system reactivity. Average yields for each aromatic species were: toluene – 4.8%, m-xylene – 3.5%, ethyl benzene – 1.9%, and 1,3,5-trimethyl benzene – 2.4%. These results are in good agreement

with previous determinations of aerosol yield for the toluene and m-xylene systems.

Several models were used to describe the observed aerosol dynamics. An integral model assuming a monodisperse aerosol, developed by Warren and Seinfeld (1984, 1985b), was used to determine apparent saturation vapor pressures of condensible species from the observations of nucleation events. Overall predictions of final number concentrations with the integral model, based on these saturation vapor pressures, were fairly close to the experimentally observed number concentrations.

An analysis of the rate of aerosol growth was carried out for those experiments exhibiting uniform condensational growth. This analysis provided estimates for the gas-phase partial pressures of the condensible species, which could be compared with the integral model vapor pressures to give approximate saturation ratios during these periods of growth.

Full aerosol size distribution simulations were performed using the sectional model ESMAP (Warren and Seinfeld, 1985a), based on the work of Gelbard et al. (1980). Number concentrations resulting from these predictions were higher than those of the integral model, since the condensation rate on a polydisperse aerosol is smaller than that on a monodisperse distribution, leading to a higher nucleation rate. Comparisons of predicted and observed size distributions during the course of each experiment were limited in accuracy by the numerical diffusion associated with current versions of the sectional model.

TABLE OF CONTENTS

LIST OF TABLES

LIST OF FIGURES

CHAPTER 1

INTRODUCTION

Atmospheric aerosols can be categorized as either primary or secondary. Primary aerosol particles are emitted directly into the atmosphere; some examples are dust and ash. Secondary aerosol is formed by gas-to-particle conversion of gaseous emissions, either by condensation onto pre-existing particles or by the homogeneous nucleation of new particles. These two processes are in competition for the available condensible vapors. Atmospheric aerosols are typically multicomponent, often with a significant organic content. Figure 1.1 shows some of the species that constitute atmospheric aerosol, along with the mechanisms leading to their formation. The most poorly understood pathway shown in this schematic diagram is the formation of secondary organic aerosol. Secondary organics constitute an important component of the aerosol in urban areas where photooxidation of gas-phase emissions produces large amounts of condensible vapors. In order to develop effective control strategies for particulate air pollutants, we need to understand the mechanisms leading to the formation of secondary aerosol, which includes knowing which are the important gas-phase precursors, as well as the mechanisms that lead to their conversion to the aerosol phase.

It is relatively straightforward to determine the amount of elemental versus organic carbon in an atmospheric aerosol sample, giving an indication of whether the aerosol is primary or secondary. However, it is much more difficult to obtain detailed chemical analysis of individual organic species. This speciation information is important not only because it assists in identifying the precursor species, but also because it allows the determination of physical property data necessary to

model aerosol formation, since precise modeling of the processes of nucleation and condensation requires knowledge of the molecular weights, surface tensions, and vapor pressures of the condensible species. If the compositions of the condensible species are not known, their physical properties must be estimated. Aerosol modeling will help us to discover which mechanisms of gas-to-particle conversion are important for the formation of atmospheric organic aerosol; that is, we would like to determine whether homogeneous nucleation is a significant mechanism for organic aerosol formation, or whether most of the organic aerosol in the atmosphere is produced by condensation onto pre-existing particles. We are also interested in discovering to what extent we can simulate organic aerosol formation and growth processes using the governing equation for aerosol dynamics, the General Dynamic Equation.

The present work is a study of aerosol formation and growth resulting from aromatic organic atmospheric reactions. Using an outdoor smog chamber, we conducted an experimental study of the formation and growth of the aerosol produced from the photooxidation of aromatic hydrocarbons in the presence of NO and NO_2. Aromatic hydrocarbons were chosen for this study because of their importance as aerosol precursors in the atmosphere (Kopczynski, 1964; Wilson et al., 1973; Schwartz, 1974; O'Brien et al., 1975; Grosjean, 1977). Aromatics are important components of anthropogenic emissions, produced from a variety of sources including vehicular exhaust, industrial processes, and solvent usage (Nelson et al., 1983). Aerosol data were obtained continuously from each experiment over a period of several hours. These data serve as the basis for gaining insight into the mechanisms of nucleation and condensation in such atmospheric systems. Particularly close attention was given to the influence of primary aerosol on secondary aerosol formation to assess our understanding of homogeneous nucleation theory in such systems.

Aerosols undergo a complex array of processes, including homogeneous nucleation, condensational growth, deposition on surfaces, and coagulation. The effect of each process on an aerosol size distribution is described by the General Dynamic Equation (GDE). In its continuous form, where the size distribution of particles can be represented by $n(v,t)$, the GDE is (Seinfeld, 1986):

$$\frac{\partial n(v,t)}{\partial t} + \frac{\partial [I(v,t)n(v,t)]}{\partial v} = \frac{1}{2}\int_0^v K(v-\tilde{v},\tilde{v})n(v-\tilde{v},t)n(\tilde{v},t)d\tilde{v}$$

$$-n(v,t)\int_0^\infty K(v,\tilde{v})n(\tilde{v},t)d\tilde{v} + S(v,t) - \mathcal{R}(v,t)n(v,t) \qquad (1.1)$$

subject to the boundary conditions

$$n(v,0) = n_0(v)$$

$$n(0,t) = 0.$$

In this equation, $I(v,t)$ is the net rate of change of the volume of a particle of volume v due to condensation and evaporation processes, the right-hand side integrals represent changes in the distribution due to coagulation, $S(v,t)$ is a particle source term (e.g., homogeneous nucleation), and $\mathcal{R}(v,t)$ is a first-order rate constant for removal (e.g., deposition). A discrete analogue of (1.1) can also be written in which the volume v is replaced by an index indicating the number of monomer units in a particle. No analytical solution of the GDE in its complete form exists, and, moreover, it is difficult to solve numerically, as it is nonlinear with a possible range of many orders of magnitude in size and number concentration.

Simplifying assumptions based on the physics of the system under consideration lead to special cases of the GDE. For example, in a system of very high number concentration, coagulation is frequently the dominant mechanism for particle dynamics. In the absence of particle sources and sinks, the GDE reduces to the so-called Coagulation Equation:

$$\frac{\partial n(v,t)}{\partial t} = \frac{1}{2}\int_0^v K(v-\tilde{v},\tilde{v})n(v-\tilde{v},t)n(\tilde{v},t)d\tilde{v}$$

$$-n(v,t)\int_0^\infty K(v,\tilde{v})n(\tilde{v},t)d\tilde{v}. \qquad (1.2)$$

Solutions of the Coagulation Equation in either discrete or continuous form have been widely reported (e.g., Drake, 1972; Tambour and Seinfeld, 1980; Williams, 1984.).

Alternatively, when coagulation can be neglected and growth or evaporation processes predominate, the GDE reduces to the Condensation Equation:

$$\frac{\partial n(v,t)}{\partial t} + \frac{\partial}{\partial v}\left[I(v,t)n(v,t)\right] = S(v,t) - \mathcal{R}(v,t)n(v,t). \qquad (1.3)$$

Analytical solutions of the Condensation Equation have been reported by several researchers (e.g., Brock, 1972; Gelbard and Seinfeld, 1979; Williams, 1983). A summary of reported solutions to the GDE for different physical systems can be found in Gelbard (1979).

The most general available numerical solution of the aerosol GDE is the code ESMAP (Warren and Seinfeld, 1985a), an extension of the widely-used code MAEROS (Gelbard, 1982). Both programs are based on the work of Gelbard et al. (1980), in which the particle size range is broken into a discrete number of sections, hence allowing the efficient evaluation of the coagulation integrals. ESMAP also allows, in addition to coagulation, a particle source term, homogeneous nucleation, condensational growth, and deposition by a variety of mechanisms. The numerical solution of the GDE by the sectional approach can lead to inaccuracies in representing the first-order condensation growth term (Warren and Seinfeld, 1985a).

Three levels of analysis are employed in evaluating the experimental data. The first is an integral model (the SNM model described originally by Warren and Seinfeld (1984, 1985b)), which includes a vapor source, condensational growth,

homogeneous nucleation, and particle deposition, and is based on the assumption that the aerosol distribution can be represented by two monodisperse modes. The system can then be described by ordinary differential equations representing a mass balance on the vapor phase (the saturation ratio, S), and number and mass balances (N and M) on the two aerosol modes. From this analysis we can derive apparent saturation vapor pressures from the experimental data. These are necessary in the absence of molecular composition data for the condensible species. Secondly, we utilize an analytical solution of the Condensation Equation to obtain growth-law parameters that characterize the growth mechanism in our experiments. The growth-law parameters can be used to determine the concentration of condensible species in the gas phase; these values can then be compared with the vapor pressures obtained from the integral model to give estimates for the supersaturation in the systems undergoing steady condensational growth. Finally, we use the sectional model (ESMAP) to simulate the complete size distribution evolution and to compare the results with the integral model calculations. The full sectional model allows us to obtain the best estimate of the competition between nucleation and condensation in these systems, and to evaluate the effectiveness of the more simplistic integral model in simulating these processes.

The remainder of this thesis is organized as follows. Chapter 2 contains a description of the experimental facility and a summary of the experiments conducted. Chapter 3 addresses the inversion of the aerosol data, namely the procedures needed to generate aerosol size distributions from the raw data. The integral model simulations are detailed in Chapter 4. Chapter 5 outlines the analytical solution of the Condensation Equation and the comparison of the growth-law parameters with the integral model vapor pressures. The comparison of the sectional representation with the monodisperse integral representation is discussed in Chapter 6. Finally, we present conclusions and recommendations for further

study.

The Appendices contain the bulk of the experimental data collected in this study, the data inversion program employed in their analysis, a summary of the aerosol yields from the gas phase for each experiment, and a paper analyzing the effects of spatial inhomogeneities in a system undergoing simultaneous nucleation and condensation.

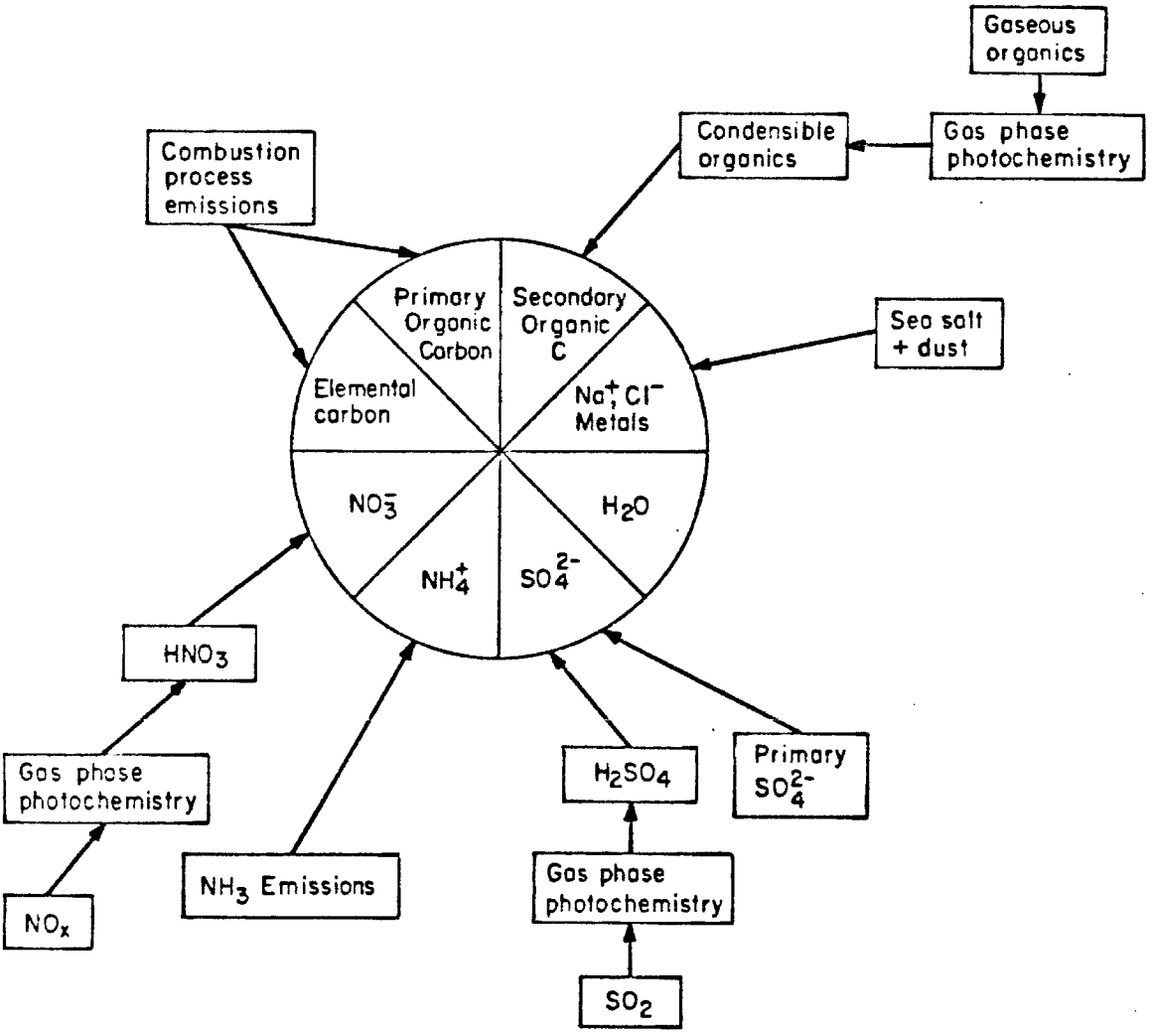

FIGURE 1.1. Schematic diagram of the sources and composition of atmospheric aerosols

CHAPTER 2

DESCRIPTION OF EXPERIMENTS

2.1 The Outdoor Smog Chamber Facility

Experiments were performed in a flexible outdoor smog chamber on the roof of the three-story Keck Laboratory on the Caltech campus. Two chambers were used for this study; one measured 6.1 m (20') by 9.1 m (30'), and one measured 6.1 m (20') by 10.4 m (34'). Each was constructed by heat-sealing 10 1.2 m-(4'-) wide panels of 2-mil thick Teflon to form a pillow-shaped chamber. The seals were reinforced with Mylar tape. Four Teflon ports were installed for filling the chamber and sampling from it. The bottom of the chamber was supported approximately 65 cm (26") above the rooftop to allow for the circulation of air beneath the chamber. A dark tarpaulin was placed on the rooftop underneath the chamber to minimize reflective heating of the chamber contents. During an experiment, the contents of the chamber were well-mixed by the wind acting on the flexible chamber walls.

The chamber could be operated in either single-chamber or dual-chamber mode. When operated as a single reactor, the chamber volume was approximately 60 m^3, as measured by the injection of known amounts of NO or NO_2. In dual-chamber mode, a PVC pipe was placed across the center of the chamber to create two identical reactors. Air leaks across the divider were undetectable, as determined by sampling from both sides of the chamber with different gas phase concentrations or species on either side. Each side of the divided chamber was approximately 25 m^3 in volume.

The major instrumentation for the experiments was housed in a laboratory adjacent to the chamber. All of the gas-phase instruments and some of the aerosol-phase instruments operated inside the laboratory. The laboratory also contained the computer used for some of the data acquisition, the gas cylinders used in setting up the experiments, the air purification system for filling the chamber, and the seed aerosol generator. Gas-phase sampling was done through Teflon lines that extended 20 cm (8") into the chamber through the Teflon ports. Aerosol samples were drawn through separate copper tubing that extended about 15 cm (6") into the chamber. Copper lines were chosen for aerosol sampling since Teflon tends to carry a charge, which would enhance the depositional loss of the charged aerosol particles. In dual-chamber mode, an actuator valve was used to automatically switch sampling from one side of the divided chamber to the other. The side of the divided chamber closest to the laboratory was designated "side A" and the farther side, "side B."

2.2 Experimental Protocol

For each experiment, the chamber was filled with purified air, beginning the evening before the experiment. Laboratory compressed air at a flow rate of approximately 80 ℓ min^{-1} was purified by passing through three consecutive packed beds containing, in order, Purafil (Purafil, Inc.), drierite with 13X molecular sieves (Union Carbide), and activated charcoal. The Purafil removed any NO_x from the air stream, and the molecular sieves and the activated charcoal removed any hydrocarbons present. Each bed was 7.5 cm (3") in diameter and 45 cm (18") long. The resulting air routinely contained less than 20 ppb of total NO_x. The dry purified air was passed through a total particle filter to remove any aerosol that carried through the beds, and was then weakly humidified by passing through a jug of distilled water before entering the chamber. The relative humidity could be

controlled to a small extent by heating the distilled water jug, although generally the water was maintained at room temperature. The resulting relative humidity depended strongly on the ambient temperature on the day of the experiment, but was usually between 40% and 65%, as measured by a Hygrometrix, Inc. relative humidity meter. Approximately 8 – 10 hours were allowed for the filling of the chamber.

Injection of the gas-phase reactants began approximately two hours before each experiment started. The aromatic hydrocarbon was injected by syringe into a glass bulb and evaporated into the chamber with the assistance of a heat gun. NO and NO_2 were each added using certified cylinders containing about 600 ppm of the gas in ultrapure nitrogen (Scott-Marrin, Inc.). During the entire filling and injecting process, a dark tarpaulin covered the chamber in order to shield the contents from solar radiation. The initial concentrations of the gas-phase species were measured just before the experiment began.

Initial aerosol was optionally added to the entire chamber or to one side of the divided chamber. The seed particles were ammonium sulfate, generated with a stainless-steel constant rate atomizer (Liu and Lee, 1975) from a solution of 2 g ℓ^{-1} $(NH_4)_2SO_4$ in distilled water. The aerosol was passed through a Kr-85 decharger before injection into the chamber. In order to minimize variations in the aerosol size distribution from day to day, the atomizer and syringe pump delivering the solution to the atomizer were operated at the same pressures and flowrates for each experiment; the initial aerosol loading was varied by adjusting the length of time the atomizer fed particles into the system. The aerosol generator was always operated for at least 15 minutes before beginning addition of aerosol to the chamber, to avoid transient fluctuations. The aerosol was usually the last addition to the chamber before beginning the experiment in order to minimize

depositional losses.

The time at which the dark tarpaulin was removed from the chamber was considered to be the starting time for each experiment. Gas-phase measurements obtained were O_3, NO, NO_x, the aromatic species (toluene, m-xylene, ethyl benzene, or 1,3,5-trimethyl benzene), chamber temperature, sample-line temperature, relative humidity, and total solar radiation. The aromatic hydrocarbons were measured using a Hewlett-Packard Model 5830 gas chromatograph (GC) equipped with an HNU photoionization detector. The column used was a 6' by 1/8" stainless-steel column packed with SP1240DA on 100/120 mesh Supelcoport at 353 K. The GC was calibrated before each experiment using certified cylinders containing about 5 ppm of the aromatic in ultrapure nitrogen (Scott-Marrin, Inc.). The GC was programmed to sample air automatically from the smog chamber using two solenoid valves, a 6-port Valco sampling valve, and a Valco valve actuator. The aromatic concentration was measured every 5 or 10 minutes and output as a series of peaks on a chart recorder. Data from the other gas-phase instruments were taken by hand, usually every 15 minutes in single-chamber mode, and every 10 minutes in dual-chamber mode, just before the actuator switched sides. Table 2.1 summarizes the gas-phase instruments used, their corresponding calibration methods, and the estimated uncertainty in each measurement.

The aerosol measurements were obtained by three different instruments. In single-chamber mode, two TSI Model 3030 Electrical Aerosol Analyzers (EAA's) sampled continuously from the chamber contents. The EAA's give size distribution information in the size range from 0.0056 μm – 1.0 μm, nominally, but they are considered most trustworthy in the size range from 0.02 μm – 0.3 μm (see Table 2.2). The two EAA's were placed side by side on a covered cart that was moved outside, next to the supporting rack by the center of the chamber. This

configuration allowed for the shortest sampling lines; copper tubing (0.5" o.d.) extended approximately 2 m (6') from under the chamber to the instruments. A PDP 11-03 series minicomputer housed inside of the laboratory both controlled the two instruments and collected data from them in cycles of about three minutes each.

A Royco Model 226 Laser Optical Particle Counter (OPC), housed inside the laboratory, was used to monitor aerosol growth in the larger size range, above 0.12 μm (see Table 2.2). Since the OPC can operate properly only with number concentrations below 1500 cm^{-3}, a dilution system was built to deliver approximately 100 times dilution of the sample before it entered the OPC. The diluter was located outside of the laboratory, with 0.5" o.d. copper tubing between it and the chamber, and 0.25" o.d. copper tubing carrying the diluted sample into the laboratory to the OPC. The initial aerosol in the chamber was too small to be detected by the OPC, so the diluter, although remaining in line, was not turned on for the first part of each experiment. When the number concentration detected by the OPC approached the 1500 cm^{-3} limit, the diluter was turned on. The dilution ratio was determined by matching the number concentration of particles before dilution with the number concentration of particles after dilution multiplied by the dilution ratio. The OPC printed out counts per channel on a paper tape every two minutes.

Two Environment|One Model Rich 100 Condensation Nuclei Counters (CNC's) were available for a rough determination of overall number concentration in the chamber. These were useful for monitoring a burst of nucleation, since their cycle time was considerably shorter than the other size-resolving instruments. A summary of all of the aerosol instruments is included in Table 2.2.

All of the aerosol instruments were checked before each experiment to deter-

mine their response to particle-free air. A total filter was placed on the inlet to each instrument to ensure that the output showed no particles. After this check, the instruments were connected to the chamber before any injections to verify that the system contained no aerosol. All of the instruments regularly zeroed very well.

In dual-chamber mode, the EAA's were used to obtain a continuous record of the size distribution in each side of the chamber. The instruments were computer-controlled, with one instrument connected to each side of the divided chamber. To determine any effects of instrument bias, the sample lines were manually switched for several cycles at intervals during each experiment. Very little bias was observed while the particles were fairly small ($<0.1\ \mu m$). The two EAA's diverged somewhat in the larger channels ($>0.2\ \mu m$), but when the aerosol was in that size range the OPC was used more reliably than the EAA's for size distribution information. In dual-chamber mode, the OPC and one CNC were connected to the central switching valve, thus sampling for 10 minutes alternately on each side of the chamber. The OPC diluter was run constantly during the dual-chamber experiments, as the residence time in the diluter when there was no dilution air was too large to allow the OPC to receive unmixed samples from each side of the chamber. For the m-xylene, ethyl benzene and 1,3,5-trimethyl benzene experiments, the dilution ratio was measured after each experiment by diluting the aerosol concentration in the chamber to below 1500 cm^{-3} and comparing the number concentrations reaching the OPC with and without the dilution. A full schematic of the experimental set-up is shown in Figure 2.1.

After each experiment, the chamber was emptied and re-filled for a "bake-out" in the sunlight the following day. Between some experiments, this procedure was performed more than once. This flushing of the chamber and exposure to the sun removed any residual reactants and products from the walls of the chamber. It was

found that continual flushing of the chamber contents with clean air during the "bake-out" helped to minimize ozone levels in the chamber. Using this procedure, we found the experimental results to be very reproducible.

2.3 Summary of Experiments Conducted

A total of 40 smog chamber experiments were carried out between June, 1985 and May, 1986 for collecting continuous gas-phase and aerosol-phase data. In addition, single-chamber experiments were run for each aromatic solely to produce aerosol to be collected for molecular composition studies. Molecular composition information for these samples has not yet been obtained. There were a total of 17 toluene photooxidations, 7 m-xylene photooxidations, 6 1,3,5-trimethyl benzene photooxidations, 5 ethyl benzene photooxidations and 5 experiments in which different aromatics were injected into each side of the divided chamber. The 17 toluene experiments were performed in the first of the two chambers used in the study; the remaining experiments were carried out in the second chamber.

The first 10 experiments conducted were single-chamber experiments with toluene as the aromatic starting species; the remaining experiments were run in dual-chamber mode. Most dual-chamber experiments were designed to have the same gas-phase concentrations on each side of the chamber and initial particles on one side. This arrangement allowed us to determine directly the effect of initial aerosol on the nucleation and condensation behavior of the system. Several experiments were conducted to compare directly different aromatic starting species under the same reaction conditions, and some experiments were designed to test the effect of varying hydrocarbon/NO_x ratio for the same aromatic; these were generally performed with no initial aerosol. A summary of the experiments conducted can be found in Tables 2.3 – 2.5. As noted in the Tables, several experiments provided data for only the gas phase or only the aerosol phase.

The experiments varied between two and six hours in length; most experiments ran for four hours. This length of time was generally sufficient to obtain the important gas-phase and aerosol-phase data. By the end of an experiment, the aromatic decay had usually slowed, and the ozone level had reached its maximum, giving an indication of the oxidative potential of the system. In this length of time, the partial pressure of the aerosol precursor species had generally built up to supersaturated levels and been relieved by nucleation of new particles or condensational growth of the existing aerosol. No rapid changes in the gas-phase kinetics or the aerosol size distributions were occurring when the experiments ended.

Initial hydrocarbon/NO_x ratios varied between 6.4 and 44.2 ppmC/ppm. We attempted to hold this ratio approximately constant through a series of experiments for each aromatic in order to reproduce the gas-phase reactivity while varying the aerosol loading. Variations occurred in the actual hydrocarbon/NO_x ratio obtained because of differences in the initial fullness of the chamber. All of the m-xylene, ethyl benzene and 1,3,5-trimethyl benzene experiments that included aerosol information were planned for two different hydrocarbon/NO_x levels to give a relatively fast-reacting system and a relatively slow-reacting system in which to study aerosol behavior.

The average temperature in the experiments varied between 291 K and 322 K. Initial aerosol number concentrations were generally below 7500 cm^{-3}, although one experiment had a higher initial aerosol level (17,000 cm^{-3}). Maximum aerosol number concentrations after nucleation ranged from 1500 cm^{-3} to 33,000 cm^{-3}, depending greatly on the aromatic starting species and the hydrocarbon/NO_x ratio.

TABLE 2.1. Summary of measured gas-phase parameters and analytical methods

Parameter/ Species	Instrument/Method	Calibration	Estimated Uncertainty (%)
NO,NO_x	Thermo Electron Model 14D/E	Gas Cylinder (Scott-Marrin, Inc.)	±10
O_3	Dasibi Model 1008-PC	Dasibi Environmental Corp.	±5
Aromatics	Hewlett-Packard Model 5830A with HNU PID detector	Gas Cylinders (Scott-Marrin, Inc.)	±15
Chamber Temperature	YSI Model 741A Thermistor	Precision thermometer	≤5
Sample Temperature	YSI Model 43 Thermistor	Precision thermometer	≤5
Relative Humidity	*Hygrometrix* Model 8501	*Factory Calibration*	≤5
Total Solar Radiation	Eppley Laboratory Model 8-48 Pyranometer	Factory Calibration	≤7

TABLE 2.2. Summary of aerosol instruments

Instrument	Size range of particles (diameter)	Estimated uncertainty (%)
TSI Model 3030 Electrical Aerosol Analyzer (EAA)	0.0056 μm – 1.0 μm Most reliable for 0.02 μm – 0.3 μm	±20 (Serial #132) ±10 (Serial #250)
Royco Model 226 Optical Particle Counter (OPC)	0.12 μm – 5.0 μm Most reliable for $\geq$ 0.2 μm	±10
Environment/One Model Rich 100 Condensation Nuclei Counter (CNC)	$\geq$ 0.005 μm	±40 (Serial #219) ±20 (Serial #230)

TABLE 2.3. Record of experiments

Experiment	Date	Aromatic[a]	t_{start} (hr.)	Duration (min.)	T (K)	Comments
MTMA16	6-20-85	Tol	12:30	270	307	
MTLA18	6-27-85	Tol	11:30	285	315	
MTMA20	6-29-85	Tol	11:30	300	311	
MTMA22	7-3-85	Tol	11:00	300	318	
MTNA26	7-12-85	Tol	11:00	330	313	
MTHA31	7-22-85	Tol	11:45	225	309	
MTNA35	7-26-85	Tol	11:00	330	313	
HTNA37	7-29-85	Tol	11:15	315	309	
HTMA39	7-31-85	Tol	11:15	315	309	
HTLA41	8-5-85	Tol	11:15	315	312	
DHNA43,A[b]	8-28-85	Tol	12:30	240	319	
B		Tol				
DMMA45,A	8-30-85	Tol	11:45	265	322	
B		Tol				
DMXA48,A	9-13-85	Tol	11:30	240	315	
B		Tol				
DQXA53,A	9-20-85	Tol	12:15	240	312	
B		Tol				
DQXA55,A	9-23-85	Tol	12:00	240	315	
B		Tol				
DQXA57,A	9-25-85	Tol	12:00	220	312	
B		Tol				
DXLA60,A	10-2-85	Tol	11:30	240	315	
B		Tol				
XA08,A	11-2-85	Xyl	10:15	245	310	
B		Xyl				
XB10,A	11-4-85	Xyl	10:50	180	305	Gas-phase data not modeled
B		Xyl				
XB12,A	11-6-85	Xyl	9:30	240	308	
B		Xyl				
XG15,A	11-13-85	Xyl	9:40	240	291	
B		Xyl				
XK17,A	11-18-85	Xyl	9:30	240	294	
B		Xyl				
XJ19,A	11-20-85	Xyl	9:30	240	296	
B		Xyl				

TABLE 2.3, CONTINUED

Experiment	Date	Aromatic[a]	t_{start} (hr.)	Duration (min.)	T (K)	Comments
XTQ27,A	12-13-85	Xyl	9:40	240	297	No aerosol data planned
B		Tmb				
XEP30,A	12-17-85	Xyl	9:30	240	306	No aerosol data planned
B		Eb				
TER32,A	1-7-86	Tmb	9:20	250	299	No aerosol data planned
B		Eb				
XJ34,A	1-10-86	Xyl	9:30	240	305	
B		Xyl				
TE36,A	1-19-86	Tmb	9:30	240	304	
B		Tmb				
TE39,A	1-28-86	Tmb	9:30	240	302	
B		Tmb				
TI43,A	3-4-86	Tmb	10:00	240	307	
B		Tmb				
TO46,A	3-20-86	Tmb	10:00	240	309	No NO_x data
B		Tmb				
TN49,A	3-24-86	Tmb	10:15	210	310	No NO_x data
B		Tmb				
TN52,A	3-27-86	Tmb	10:20	180	311	No NO_x data
B		Tmb				
ED62,A	4-19-86	Eb	9:30	300	309	No aerosol data, too slow
B		Eb				
EC64,A	4-21-86	Eb	9:50	300	309	
B		Eb				
EH66,A	4-23-86	Eb	10:30	240	304	
B		Eb				
EM70,A	4-28-86	Eb	10:10	240	311	
B		Eb				
EL73,A	5-2-86	Eb	10:30	240	310	
B		Eb				
TXU75,A	5-5-86	Tmb	10:40	120	307	Gas-phase data not modeled
B		Xyl				
LEV77,A	5-8-86	Tol	10:20	210	308	
B		Eb				

[a] Tol=toluene, Xyl=m-xylene, Tmb=1,3,5-trimethylbenzene, Eb=ethylbenzene

[b] A and B indicate the two sides of the divided chamber

TABLE 2.4. Gas-phase data

Experiment	Aromatic	$[HC]_0$ (ppm)	$[NO]_0$ (ppm)	$[NO_2]_0$ (ppm)	$[HC/NO_x]_0$ (ppmC/ppm)	O_3 peak (ppm)	t_{peak} (min.)	% HC reacted
MTMA16	Tol	0.96	0.38	0.14	12.9			32
MTLA18	Tol	1.30	0.46	0.18	14.2			43
MTMA20	Tol	1.45	0.43	0.16	17.2			29
MTMA22	Tol	1.25	0.49	0.14	13.9			32
MTNA26	Tol	0.79	0.44	0.11	10.1			46
MTHA31	Tol	1.25	0.29	0.12	21.3			37
MTNA35	Tol	1.08	0.40	0.13	14.3			59
HTNA37	Tol	3.80	1.26	0.37	16.3			47
HTMA39	Tol	4.30	1.30	0.40	17.7			40
HTLA41	Tol	3.10	1.37	0.41	12.2			42
DHNA43,A	Tol	4.90	1.30	0.30	21.4			27
B	Tol	3.90	1.30	0.30	17.1			21
DMMA45,A	Tol	1.18	0.42	0.11	15.6			43
B	Tol	1.18	0.42	0.11	15.6			43
DMXA48,A	Tol	1.45	0.61	0.11	14.1			32
B	Tol	1.45	0.61	0.11	14.1			37
DQXA53,A	Tol	2.71	0.44	0.13	33.3			30
B	Tol	2.71	0.44	0.13	33.3			28
DQXA55,A	Tol	2.65	0.51	0.14	28.5			36
B	Tol	2.74	0.51	0.14	29.5			32
DQXA57,A	Tol	2.95	0.57	0.12	29.9			30
B	Tol	2.83	0.57	0.12	28.7			30
DXLA60,A	Tol	3.00	0.59	0.10	30.4			34
B	Tol	1.42	0.59	0.10	14.4			36
XA08,A	Xyl	1.41	0.98	0.250	9.2	0.865	105	83
B	Xyl	1.44	1.10	0.250	8.5	0.932	115	81
XB10,A	Xyl	1.86	1.92	0.40	6.4	—	—	—
B	Xyl	1.86	1.95	0.35	6.5	—	—	—
XB12,A	Xyl	2.18	1.88	0.320	7.9	1.161	160	78
B	Xyl	2.18	1.85	0.310	8.1	1.139	170	80
XG15,A	Xyl	2.32	1.91	0.360	8.2	0.768	200	65
B	Xyl	1.17	0.434	0.078	18.3	0.385	110	55
XK17,A	Xyl	1.18	0.465	0.063	17.9	0.422	90	53
B	Xyl	1.17	0.469	0.058	17.8	0.415	100	57
XJ19,A	Xyl	1.31	0.420	0.069	21.4	0.386	90	53
B	Xyl	1.34	0.420	0.071	21.8	0.386	80	55

TABLE 2.4, CONTINUED

Experiment	Aromatic	$[HC]_0$ (ppm)	$[NO]_0$ (ppm)	$[NO_2]_0$ (ppm)	$[HC/NO_x]_0$ (ppmC/ppm)	O_3 peak (ppm)	t_{peak} (min.)	% HC reacted
XTQ27,A	Xyl	1.97	0.403	0.071	33.2	0.384	90	38
B	Tmb	1.69	0.384	0.074	33.2	0.421	80	45
XEP30,A	Xyl	1.88	0.403	0.076	31.4	0.490	60	48
B	Eb	1.98	0.405	0.074	33.1	0.537	150	24
TER32,A	Tmb	1.44	0.392	0.071	28.0	0.520	80	66
B	Eb	2.56	0.392	0.071	44.2	max not reached		26
XJ34,A	Xyl	1.25	0.485	0.076	17.8	0.539	90	63
B	Xyl	1.24	0.485	0.071	17.8	0.535	100	64
TE36,A	Tmb	2.47	1.66	0.41	10.7	1.372	110	91
B	Tmb	2.47	1.66	0.41	10.7	1.361	105	93
TE39,A	Tmb	1.92	1.60	0.39	8.7	1.198	130	94
B	Tmb	1.91	1.57	0.44	8.6	1.197	120	93
TI43,A	Tmb	3.03	2.02	0.33	11.6	1.378	100	96
B	Tmb	1.26	0.46	0.10	20.3	0.697	70	91
TO46,A	Tmb	1.9	~0.83	~0.19	~16.8	0.957	50	94
B	Tmb	1.9	~0.81	~0.19	~17.1	0.961	60	94
TN49,A	Tmb	2.32	~0.80	~0.23	~20.3	1.251	60	94
B	Tmb	2.32	~0.79	~0.22	~21.1	1.240	62	95
TN52,A	Tmb	2.30	~1.1	~0.29	~14.9	1.262	55	96
B	Tmb	2.30	~1.1	~0.27	~15.1	1.261	63	96
ED62,A	Eb	3.15	2.02	0.41	10.4	max not reached		15
B	Eb	3.15	1.98	0.42	10.5	max not reached		18
EC64,A	Eb	2.33	1.05	0.20	14.9	max not reached		22
B	Eb	2.33	1.03	0.16	15.7	max not reached		22
EH66,A	Eb	3.22	1.24	0.30	16.7	max not reached		18
B	Eb	3.27	0.550	0.125	38.8	0.616	180	31
EM70,A	Eb	2.19	0.430	0.080	34.4	0.543	190	37
B	Eb	2.19	0.420	0.075	35.4	0.544	180	40
EL73,A	Eb	2.39	0.485	0.100	32.7	0.567	200	32
B	Eb	2.39	0.485	0.105	32.4	0.522	190	31
TXU75,A	Tmb	3.59	0.97	0.18	28.1	—	—	—
B	Xyl	2.37	0.97	0.22	15.9	—	—	—
LEV77,A	Tol	4.28	1.36	0.09	20.7	0.814	180	32
B	Eb	3.03	1.12	0.06	20.5	max not reached		24

TABLE 2.5. Aerosol data

Experiment	Aromatic	$[HC/NO_x]_0$ (ppmC/ppm)	N_i^a 10^3 cm^{-3}	N_{max}^b 10^3 cm^{-3}	t_{nucl} (min.)
MTMA16	Tol	12.9	7.0	—	—
MTLA18	Tol	14.2	1.0	12.0	90
MTMA20	Tol	17.2	7.4	—	—
MTMA22	Tol	13.9	4.7	6.1	60
MTNA26	Tol	10.1	0.0	6.3	140
MTHA31	Tol	21.3	8.0	—	—
MTNA35	Tol	14.3	0.0	13.2	100
HTNA37	Tol	16.3	0.0	11.7	120
HTMA39	Tol	17.7	6.8	—	—
HTLA41	Tol	12.2	3.0	4.0	90
DHNA43,A	Tol	21.4	0.0	16.5	105
B	Tol	17.1	0.0	10.8	150
DMMA45,A	Tol	15.6	3.6	6.4	110
B	Tol	15.6	3.4	5.2	110
DMXA48,A	Tol	14.1	6.7	—	—
B	Tol	14.1	0.0	9.5	170
DQXA53,A	Tol	33.3	2.0	20.0	75
B	Tol	33.3	0.0	29.0	70
DQXA55,A	Tol	28.5	16.9	—	—
B	Tol	29.5	0.0	22.3	110
DQXA57,A	Tol	29.9	5.9	—	—
B	Tol	28.7	0.0	23.7	95
DXLA60,A	Tol	30.4	2.0	15.1	80
B	Tol	14.4	2.1	—	—
XA08,A	Xyl	9.2	6.3	—	—
B	Xyl	8.5	0.0	11.5	50
XB10,A	Xyl	6.4	1.6	—	—
B	Xyl	6.5	0.0	3.4	75
XB12,A	Xyl	7.9	2.1	—	—
B	Xyl	8.1	0.25	4.6	60
XG15,A	Xyl	8.2	0.5	2.0	125
B	Xyl	18.3	0.5	4.7	65
XK17,A	Xyl	17.9	3.0	—	—
B	Xyl	17.8	0.0	5.7	40
XJ19,A	Xyl	21.4	7.4	—	—
B	Xyl	21.8	0.25	14.7	40

TABLE 2.5, CONTINUED

Experiment	Aromatic	$[HC/NO_x]_0$ (ppmC/ppm)	N_i^a 10^3 cm^{-3}	N_{max}^b 10^3 cm^{-3}	t_{nucl} (min.)
XJ34,A	Xyl	17.8	5.2	—	—
B	Xyl	17.8	0.4	11.5	45
TE36,A	Tmb	10.7	2.0	2.7	—
B	Tmb	10.7	0.4	4.0	60
TE39,A	Tmb	8.7	2.2	—	—
B	Tmb	8.6	0.1	3.2	60
TI43,A	Tmb	11.6	0.7	2.3	60
B	Tmb	20.3	0.2	5.9	45
TO46,A	Tmb	16.8	3.4	—	—
B	Tmb	17.1	0.8	5.5	35
TN49,A	Tmb	20.3	5.0	—	—
B	Tmb	21.1	0.4	2.1	30
TN52,A	Tmb	14.9	6.6	—	—
B	Tmb	15.1	0.2	6.8	35
EC64,A	Eb	14.9	5.8	—	—
B	Eb	15.7	1.1	—	—
EH66,A	Eb	16.7	0.7	—	—
B	Eb	38.8	0.7	7.6	135
EM70,A	Eb	34.4	3.0	10.2	140
B	Eb	35.4	0.2	17.0	110
EL73,A	Eb	32.7	5.4	—	—
B	Eb	32.4	0.0	5.4	105
TXU75,A	Tmb	28.1	1.3	2.8	30
B	Xyl	15.9	0.8	18.0	40
LEV77,A	Tol	20.7	0.4	5.6	130
B	Eb	20.5	1.0	—	—

[a] Initial number concentration

[b] Maximum number observed. — indicates no observed nucleation

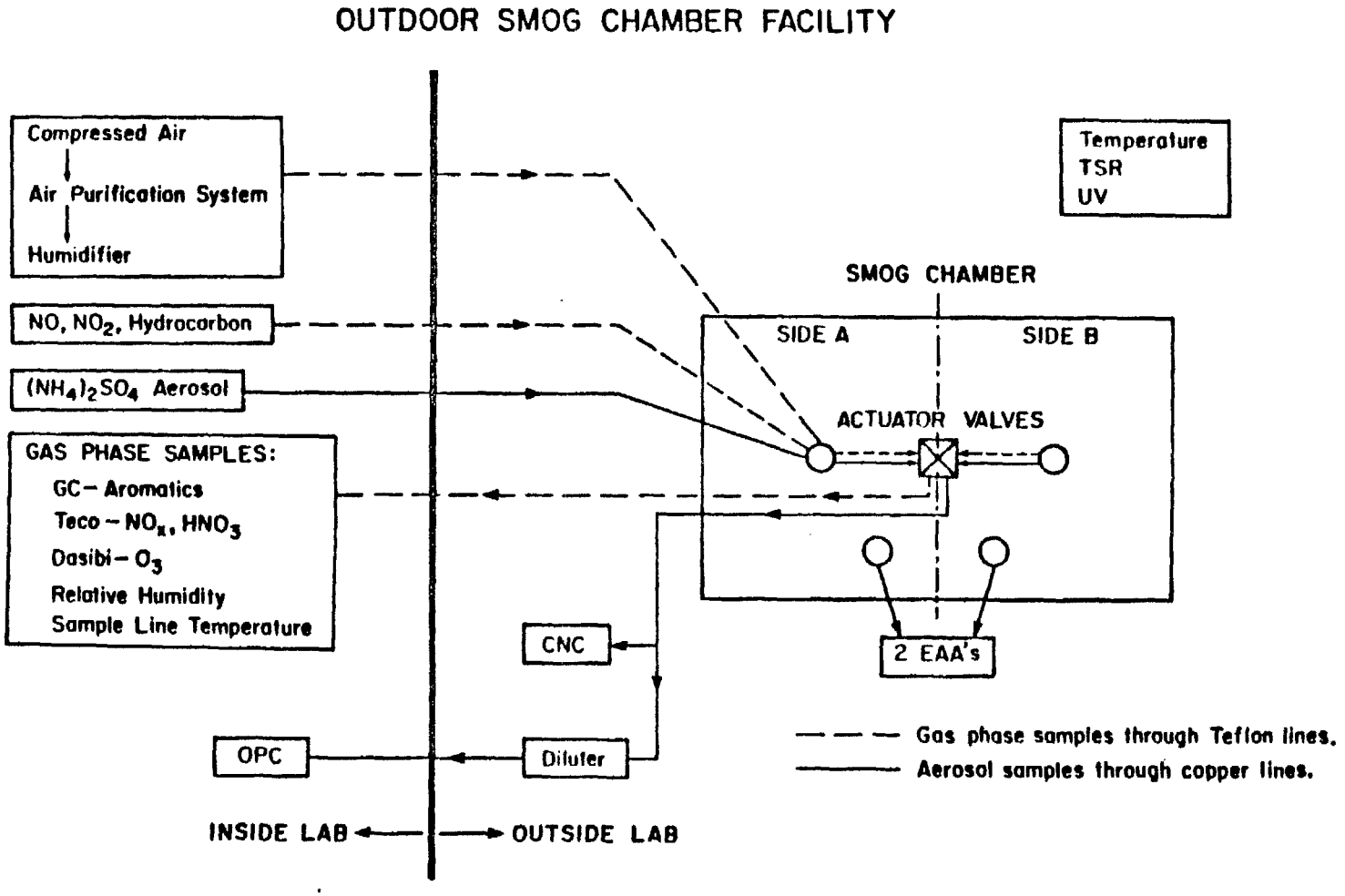

FIGURE 2.1. Schematic diagram of the outdoor smog chamber facility used for the experiments.

CHAPTER 3

AEROSOL DATA INVERSION

3.1 Introduction

The EAA and the OPC are the main sources of information about the aerosol size distribution in the experiments. Both of these instruments classify the aerosol particles in discrete intervals with ideal cut-points in diameter between the intervals. However, non-idealities in the instrument behavior lead to some particles appearing in the wrong sections; this is known as instrument cross-sensitivity. In addition, the particular instrument may exhibit a size bias, so that the diameter cut-points are shifted slightly from the ideal sizes specified by the manufacturer. Because of these factors, the size distribution can not be inferred directly from the signal in each discrete interval, and an inversion problem must be solved.

The inversion problem for a single instrument is not a new problem. Many researchers have derived algorithms to determine what true signal is giving an observed instrument response (e.g., Twomey, 1963, 1965, 1975; Strand and Westwater, 1968; Hanson, 1971; McWhirter and Pike, 1978; Crump and Seinfeld, 1982a,b; Kaijser, 1983; Maher and Laird, 1985). For our experimental system, we would like to know the size distribution of aerosol that gives rise to the observed EAA and OPC readings. This need is further complicated by the differing size ranges of the two instruments. The EAA is optimal for sensing small particles; the OPC can detect only larger particles (see Table 2.2). The size range of overlap for the reliable signals from the instruments is only approximately 0.2 μm – 0.3 μm in diameter, so there are few sets of experimental data where the performance of both instruments can be compared.

A general mathematical formulation of the aerosol inversion problem is:

$$y_i = \int K_i(D_p) f(D_p) dD_p, \tag{3.1}$$

where y_i are the experimental observations in channel i, and $K_i(D_p)$ is the kernel function that describes the instrument response in channel i, including the instrument cross-sensitivity as determined by calibration. Here, $f(D_p)$ is usually the size distribution of aerosol, but it can be a different distribution function, depending on the instrument used for the measurements. For example, the electrical aerosol analyzer signal consists of current differences in each channel of the instrument; for an inversion of EAA data, therefore, $f(D_p)$ can be the current distribution function that produces the current differences, y_i.

A discrete analogue of Equation (3.1) can be written at an array of preset diameters, D_{p_j}, in the size range of interest:

$$y_i = \sum_{D_{p_j}} K_i(D_{p_j}) f(D_{p_j}) \Delta D_{p_j}, \tag{3.2}$$

where D_{p_j} are the aerosol diameters at which the kernel functions are defined, and ΔD_{p_j} is the width of the discrete interval. Since we do not have a continuous representation for $K_i(D_p)$ but rather discrete values at calibration diameters, we shall use Equation (3.2) to obtain aerosol size distributions from the observed EAA and OPC signals, y_i. There is an additional constraint for the aerosol problem that the computed size distribution must be positive.

3.2 The Smoothed-Twomey Inversion

One of the widely used algorithms for the inversion problem is that of Twomey (1965, 1975). Twomey proposed a nonlinear iterative technique to obtain the function $f(D_p)$ in Equation (3.1). An initial guess, $f_1(D_p)$, is made and the y_i values are calculated from Equation (3.1) (or its discrete analogue). The ratio of

the observed y_i to the calculated y_i is denoted $r_1^{(i)}$. In general, the p^{th} estimate for $f(D_p)$ is obtained from performing the iteration:

$$f_p^{(i)}(D_p) = \left[1 + (r_p^{(i-1)} - 1)K_i(D_p)\right] f_p^{(i-1)}(D_p) \tag{3.3}$$

over each of the i observations. The kernel functions, $K_i(D_p)$, must be less than one for convergence of Equation (3.3). Twomey's iteration essentially corrects the predicted $f(D_p)$ in proportion to the deviation of $y_{i,calc}$ from $y_{i,obs}$, weighted by the magnitude of the kernel functions. If the changes resulting from each iteration are small, the new estimate for $f(D_p)$ reduces to a series expansion in $K_i(D_p)$ (Twomey, 1975).

The Twomey algorithm, however, can give rise to oscillatory results that still satisfy Equation (3.1). Addition of a sine or cosine term to the function $f(D_p)$ will not appear in the predicted y_i values as long as the oscillation is at a sufficiently high frequency. To eliminate the choice of highly oscillatory results as satisfactory solutions to the inversion problem, a smoothing step can be added (Markowski, 1987). In between each iteration, the resulting function $f_p(D_p)$ is smoothed according to a simple smoothing algorithm. A full iteration, then, consists of a Twomey step plus a smoothing step, and the inversion is therefore referred to as a smoothed-Twomey inversion.

3.3 Inversion of the Aerosol Data

For a single aerosol instrument, we have developed a routine based on the smoothed-Twomey inversion that allows the input of experimental tolerances for each channel of the instrument, and a set of kernel functions at specified diameters. The inversion routine attempts to find the smoothest number distribution $n(D_{p_j})$ satisfying

$$y_i = \sum_{D_{p_j}} K_i(D_{p_j}) n(D_{p_j}) \Delta D_{p_j}, \tag{3.4}$$

within the experimental tolerances given. With approximately 100 data sets for each experiment, a quickly converging, robust scheme was needed. Twomey's routine was well-suited for our inversion, as it satisfies these criteria and always provides a reasonably smooth distribution function.

For the EAA inversion, the kernel functions for a standard instrument were obtained from Richards (1979). Richards provides discrete values for the response function $F_i(D_{p_j})$, which is the fraction of the electrometer current appearing in channel i due to particles of size D_{p_j}. In addition, a sensitivity function, $S_i(D_{p_j})$, is provided that uniquely relates the electrometer current to the number distribution. The kernel functions $K_i(D_{p_j})$ that produce signals in units of current from a number distribution, therefore, are given by $K_i(D_{p_j}) = S_i(D_{p_j})F_i(D_{p_j})$. These kernel functions are shown in Figure 3.1, and have units of $\mathrm{pA}/(\#\ \mathrm{cm}^{-3})$. For the OPC, the kernel functions are simply the fraction of particles of size D_{p_j} appearing in each channel i; these were given by Crump (1983) from a calibration on our own instrument, and are shown in Figure 3.2.

The resulting inversion routines gave satisfactory results for the EAA and the OPC individually. However, we must obtain the aerosol size distribution that gave rise to both the observed EAA and OPC readings. This can be done only by combining the data from both instruments and inverting all of the experimental observations simultaneously. Such a multi-instrument inversion technique has not been reported previously.

The kernel functions for the OPC were interpolated to give values at the same reference diameters as given for the EAA. Since the OPC data and EAA data were not collected with the same cycle times, the OPC readings were time-interpolated to the same times available for the EAA. This provided data sets at just under 3-minute intervals over the course of an experiment. The inversion routine MISTI (Multi-Instrument Smoothed-Twomey Inversion) uses channels 3 – 11 of the EAA

(nominally 0.01 μm – 1.0 μm) and channels 1 – 6 of the OPC (nominally 0.12 μm – 1.17 μm) for a total of 15 experimental signals to fit. The inverted size distribution has 49 diameters from 0.01 μm – 1.0 μm, 24 per decade in particle size.

It is essential to test the performance of an inversion routine by inputting a known distribution, generating y_i values, and determining how well the inversion reproduces the input distribution. For this test, a lognormal distribution or a sum of lognormal distributions is often used. We tested MISTI with both single-mode and bimodal lognormal distributions. As long as the tolerances were kept fairly strict (relative error $\leq 0.1\%$), the inversion reproduced the unimodal distributions. Figure 3.3 shows an input lognormal number distribution with $\overline{D}_{p_g} = 0.1$ μm and $\sigma_g = 1.3$, and the inverted distribution generated by MISTI. We see little difference between the input distribution and the inverted result. The response of MISTI to bimodal distributions was also determined. For bimodal distributions where the modes were non-overlapping or highly overlapped, we again achieved an excellent inversion result. Figure 3.4 shows a sum of lognormal distributions with $\overline{D}_{p_{g1}} = 0.04$ μm, $\overline{D}_{p_{g2}} = 0.2$ μm, $\sigma_{g1} = \sigma_{g2} = 1.3$, and 5% of the total volume in the first mode. Figure 3.5 shows a sum of lognormal distributions where there is a great deal of overlap: $\overline{D}_{p_{g1}} = 0.08$ μm, $\overline{D}_{p_{g2}} = 0.15$ μm, $\sigma_{g1} = \sigma_{g2} = 1.3$, and 10% of the volume in the smaller mode. With two distinct modes of aerosol, or with very close modes, the inversion is very close to the original distribution. However, when there is some overlap between the two modes, as in Figure 3.6, the inversion does not perform as well. In Figure 3.6, we have $\overline{D}_{p_{g1}} = 0.08$ μm, $\overline{D}_{p_{g2}} = 0.2$ μm, $\sigma_{g1} = \sigma_{g2} = 1.3$, and 10% of the volume in the smaller mode. For all of the test inversions shown, the relative error allowed by MISTI was set at 0.1%.

For inversion of experimental data, the initial guess for the first dataset was taken from the simple EAA histogram inversion procedure, in which the current

differences in each channel are multiplied by an average kernel function to obtain the number of particles in each channel (Liu and Pui, 1975). This number distribution was interpolated linearly to give the starting number distribution at each of the inversion diameters, D_{p_j}. Since the first dataset was generally at the beginning of an experiment, when the particles were too small for the OPC to detect, this was a reasonably good approximation for beginning the iterations. After the first dataset in a series, the initial guess for the subsequent data was taken as the previous inverted dataset in order to speed convergence. Experimental tolerances were set at 10% relative error for EAA channels 3 - 8 and OPC channels 2 - 6, 15% for EAA channels 9 and 10, and 20% for EAA channel 11 and OPC channel 1, where the instruments are at their detection limits.

The routine encountered convergence difficulties when the Twomey iteration was performed over all 15 channels prior to smoothing. Since the EAA currents and the OPC counts per channel were independent measurements, the iteration was broken down into two steps. The Twomey iteration was performed over all of the channels in one instrument, the result was smoothed, the iterations continued for the other instrument, and the final result was smoothed again. At this point, the curvature of the inverted distribution was calculated, to determine whether to continue the procedure. The resulting inverted distribution depended on the order in which the instrument signals were considered, fitting the observed signals of the second instrument more closely. Therefore, early in an experiment the routine iterated over the OPC channels first, followed by the EAA channels; late in an experiment, when the particles were larger, the routine iterated over the EAA channels first, followed by the OPC channels. The order of the instruments was determined by calculating the average particle size in the inverted distribution – when the particles were smaller than 0.2 μm, the following dataset used the OPC then the EAA channels, and when they were larger, the order of the instruments

was reversed. This procedure sometimes led to discontinuities in the time sequence of the moments of the inverted size distributions (total number concentration and total volume concentration) when the instruments were not in good agreement. A complete listing of MISTI can be found in Appendix III.

Figures 3.7 and 3.8 show the inverted number and volume distributions at half-hour intervals for the single-chamber toluene experiment MTHA31. These distributions were obtained by averaging all of the distributions within a $\pm$7.5-minute interval of the given time. There was no nucleation in this experiment, and the distributions are typical of a growing aerosol. We see a fairly broad initial number distribution that narrows and grows between one hour and three hours. The volume distribution is very small until the particles grow larger. Between 3.5 and 4.0 hours the distributions show particle loss by deposition.

We present in Appendix IV the inverted data from all of the smog chamber experiments. The total number, total volume, and mean particle size are shown as a function of time, along with the raw data from all of the aerosol instruments. In addition, we present the averaged number and volume distributions at half-hour intervals throughout each experiment.

3.4 Conclusions

We have developed a multi-instrument inversion routine for the analysis of the experimental EAA and OPC data. The routine is based on Twomey's iteration (Twomey, 1975) with an additional smoothing step added to minimize the likelihood of resulting oscillatory size distributions (Markowski, 1987). Our routine, MISTI, was used to invert the data obtained from all of the smog chamber experiments.

Discontinuities in the inverted results sometimes occurred when the experimental signals from the EAA and the OPC were not consistent. This highlights

the need for an inversion routine that is equally robust but mathematically more rigorous. Although MISTI was tested on lognormal distributions, there exists no independent way to verify the inverted experimental data. Inverting these data by another inversion routine would allow us to assess better the accuracy of the smoothed-Twomey inversion.

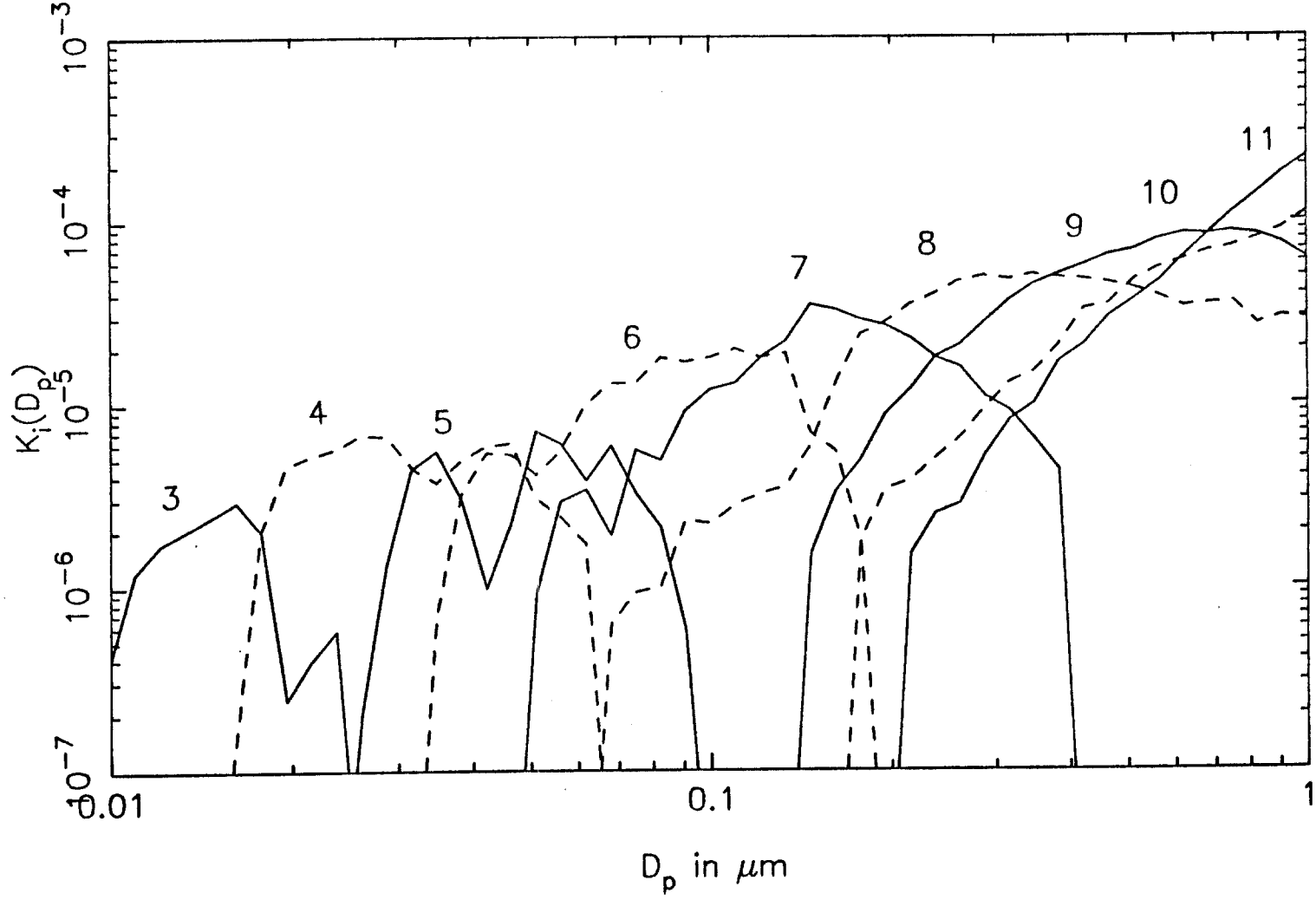

FIGURE 3.1. Kernel functions for the EAA, channels 3 – 11.

Units for $K_i(D_{p_j})$ are pA/#cm^{-3}.

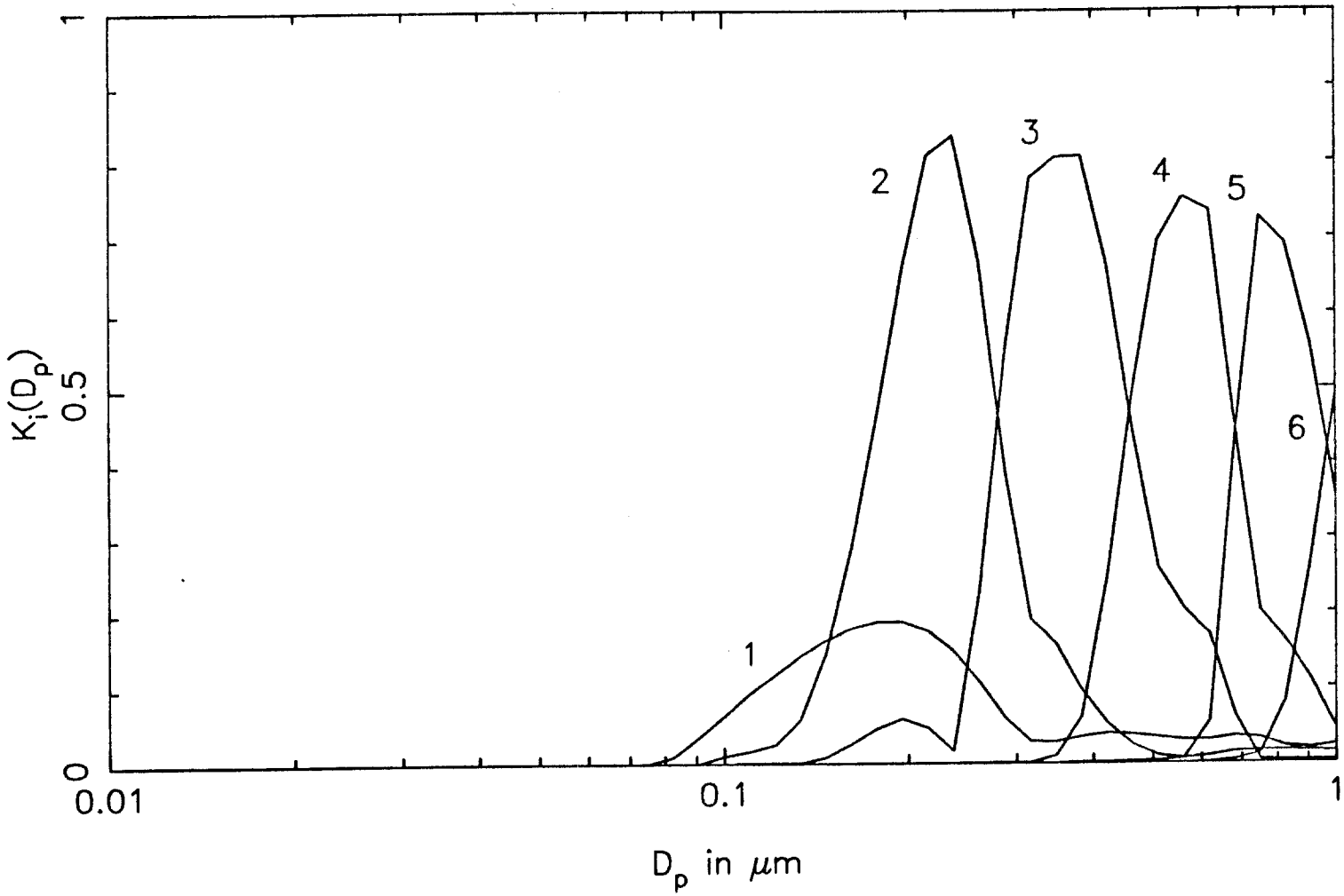

FIGURE 3.2. Kernel functions for the OPC, channels 1 – 6.

Units for $K_i(D_{p,})$ are $1/\#\text{cm}^{-3}$.

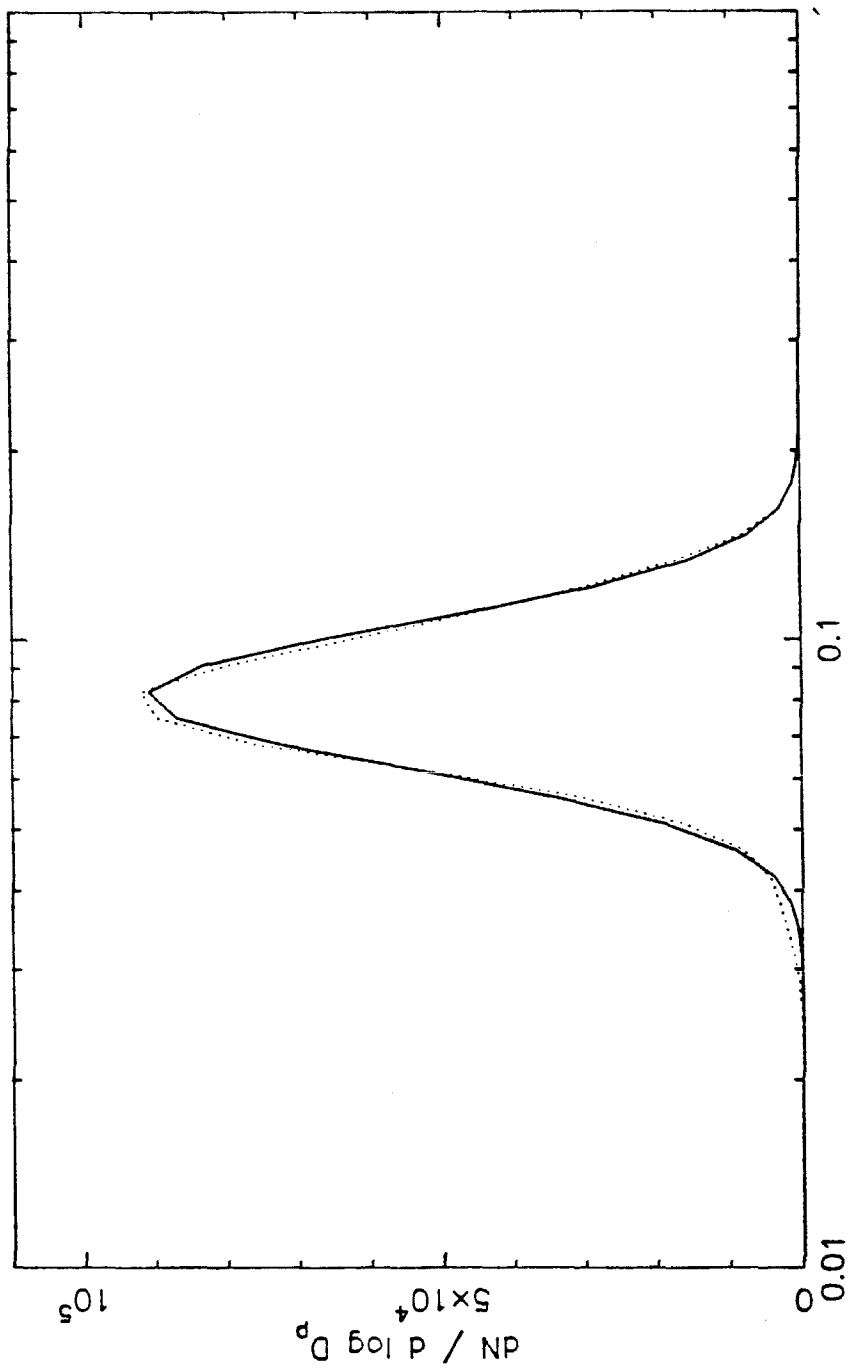

FIGURE 3.3. Test single-mode lognormal distribution with $\overline{D}_{p_n} = 0.1$ μm and $\sigma_{ll} =$

— input distribution, ··· inverted distribution

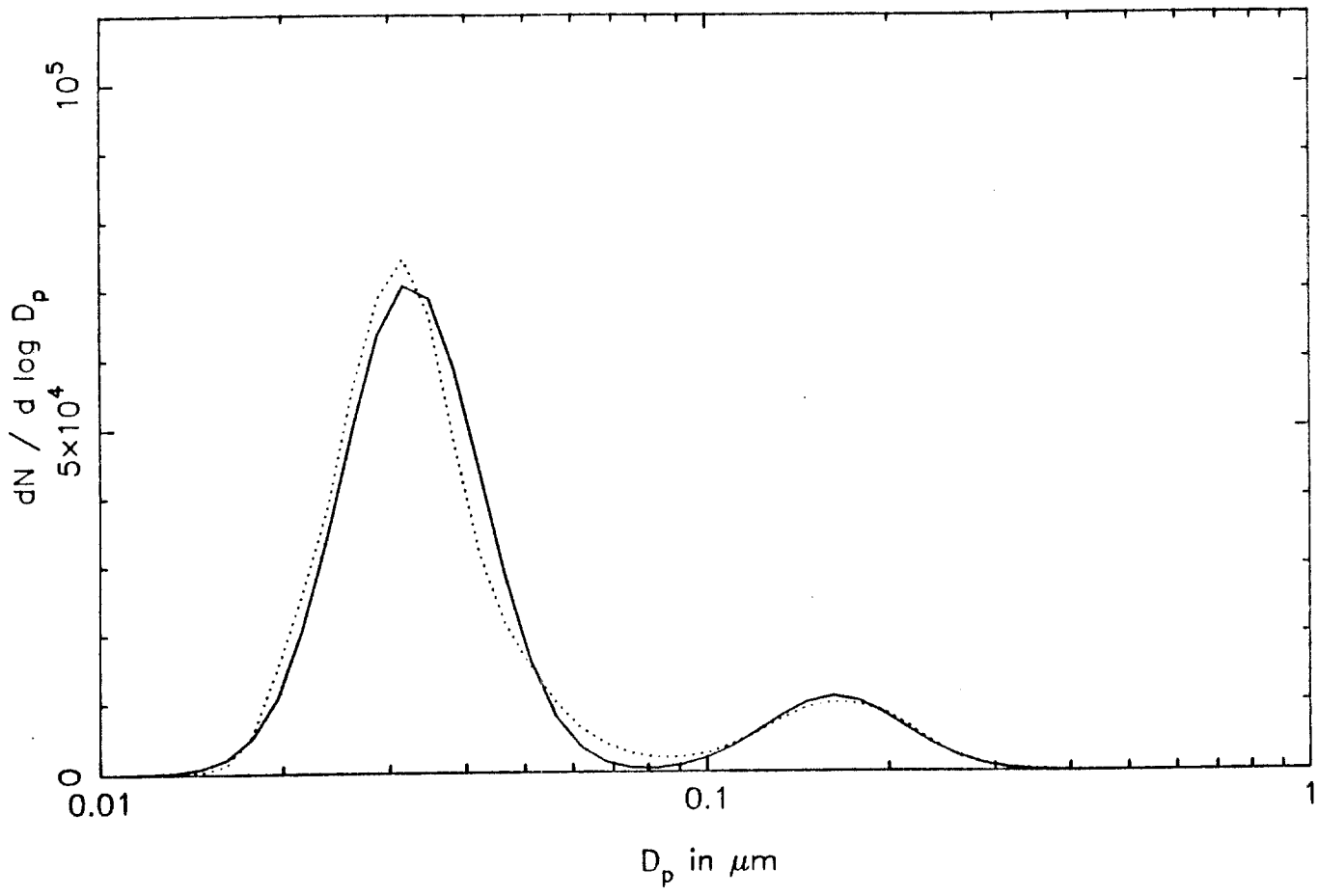

FIGURE 3.4. Test bimodal lognormal distribution with $\overline{D}_{p_{g1}} = 0.04\ \mu$m, $\overline{D}_{p_{g2}} = 0.2\ \mu$m, $\sigma_{g1} = \sigma_{g2} = 1.3$, and 5% of the total volume in the first mode.

— input distribution, ··· inverted distribution

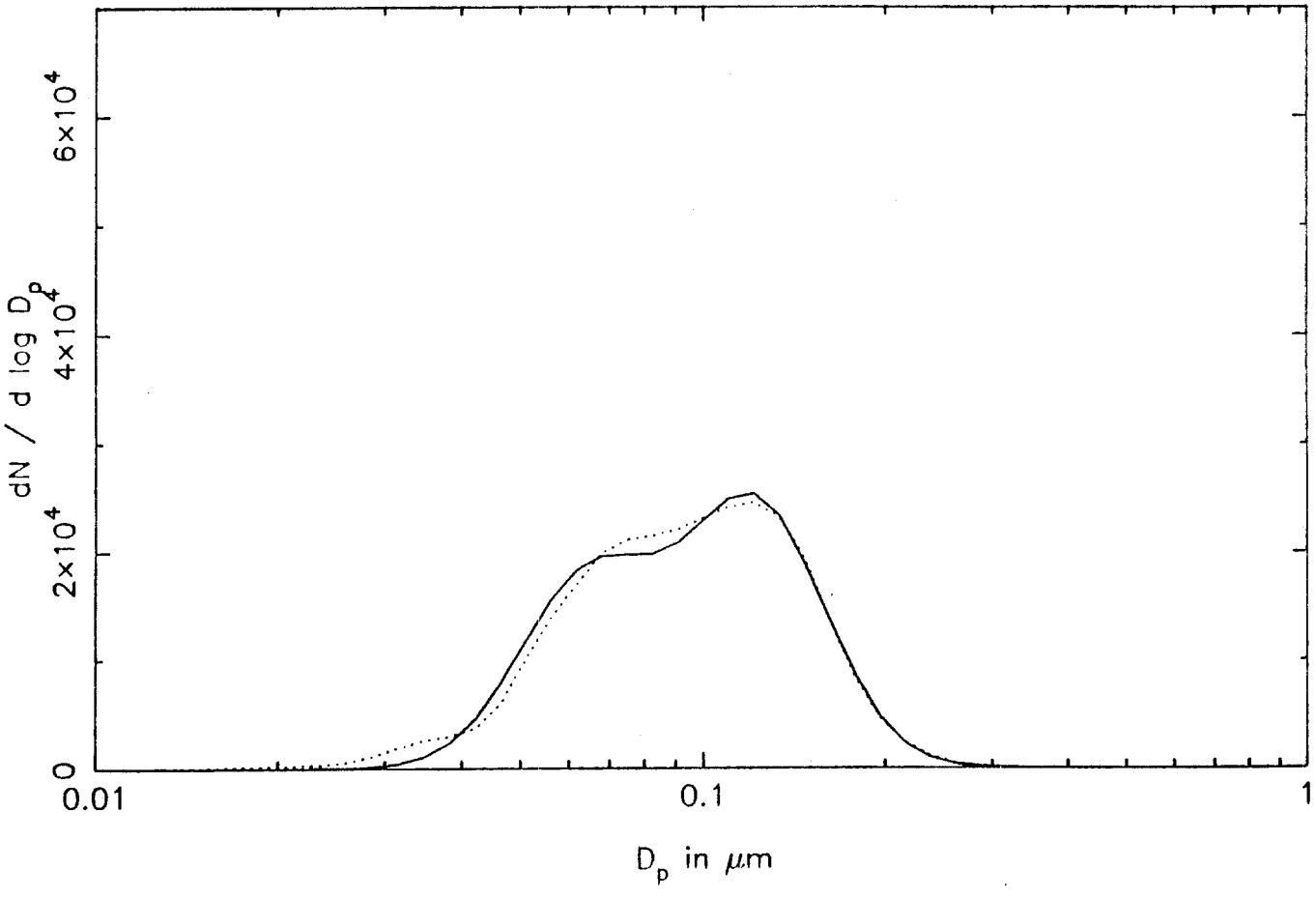

FIGURE 3.5. Test bimodal lognormal distribution with $\overline{D}_{p_{g1}} = 0.08\ \mu$m; $\overline{D}_{p_{g2}} = 0.15\ \mu$m, $\sigma_{g1} = \sigma_{g2} = 1.3$, and 10% of the total volume in the first mode.

— input distribution, ··· inverted distribution

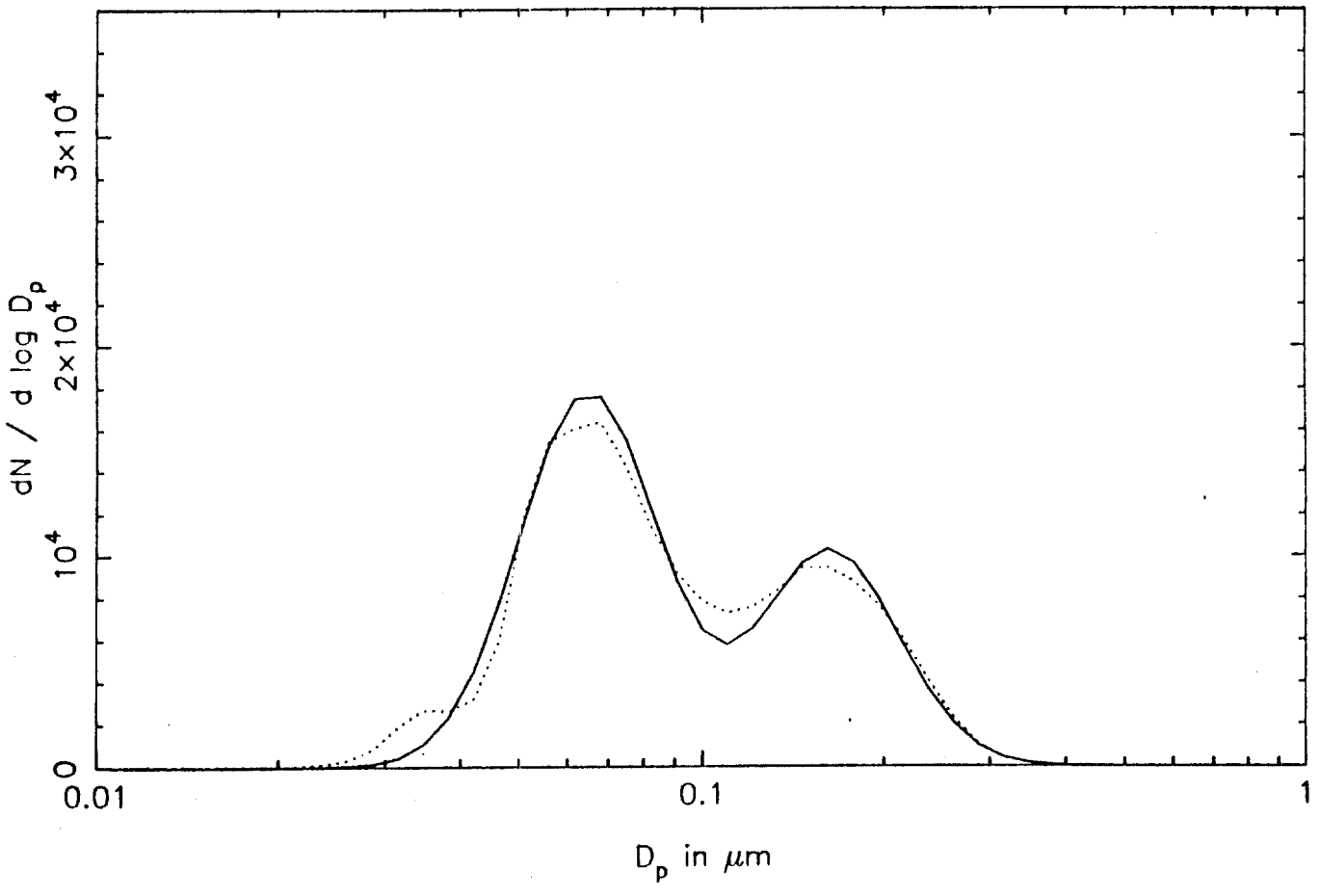

FIGURE 3.6. Test bimodal lognormal distribution with $\overline{D}_{p_{g1}} = 0.08\ \mu$m, $\overline{D}_{p_{g2}} = 0.2\ \mu$m, $\sigma_{g1} = \sigma_{g2} = 1.3$, and 10% of the total volume in the first mode.

— input distribution, ··· inverted distribution

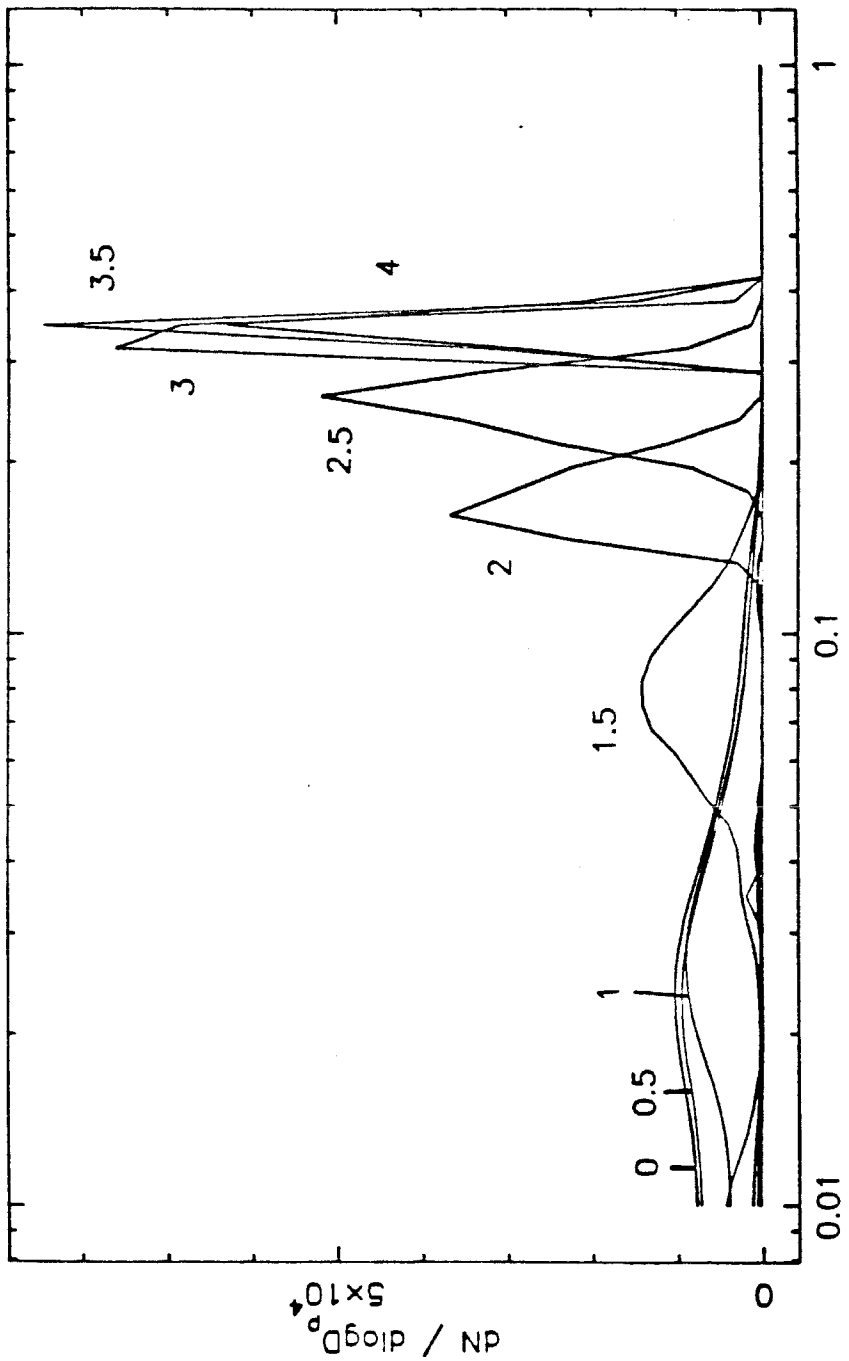

FIGURE 3.7. Inverted number distributions at half-hour intervals for MTHA31.

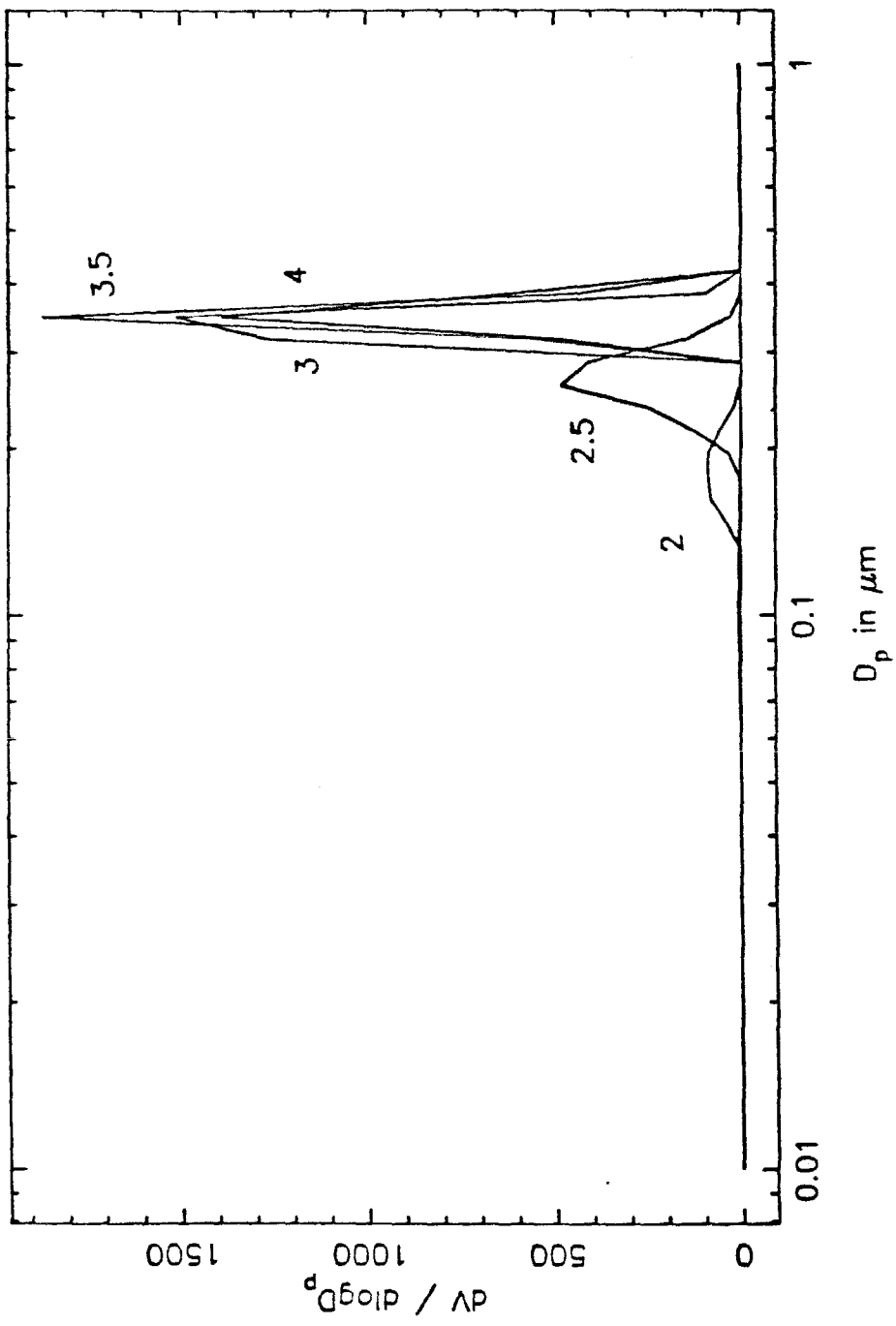

FIGURE 3.8. Inverted volume distributions at half-hour intervals for MTHA31.

CHAPTER 4

USE OF AN INTEGRAL MODEL FOR NUCLEATION/CONDENSATION MODELING

4.1 Introduction

The smog chamber experiments generated a large data base with information on particle formation and growth in aromatic photooxidations. By applying aerosol models to these data, we can learn about the microphysics of aerosol dynamics in such systems. In particular, the experiments demonstrated the effect of primary aerosol on the nucleation behavior of these systems. In a system with a source of condensible vapor and no initial particles, the partial pressure in the vapor phase can build up to highly supersaturated levels, at which point homogeneous nucleation can occur and aerosol particles are formed. Subsequent condensation onto these particles will help relieve the vapor phase supersaturation, causing nucleation eventually to cease. After this point, subsequent gas-to-particle conversion will occur by condensation. However, in the presence of initial particles, condensational growth can begin as soon as the saturation point of the low vapor pressure species is passed. With a sufficiently large number of initial particles it is possible that the vapor will never achieve the supersaturation needed for nucleation, as condensational growth will always be the dominant mechanism for gas-to-particle conversion.

The analysis of the experimental data tests our ability to simulate simultaneous nucleation and condensation in such photooxidation systems. The principal unknown quantity in the description of aerosol formation and growth is the rate of homogeneous nucleation of the aerosol precursors. Indeed, predicting the rate of homogeneous nucleation of a substance is one of the long-standing challenges

in condensed matter physics. The two most popular nucleation theories, the so-called classical theory and the Lothe-Pound theory differ in their predicted rates by something approaching 20 orders of magnitude (Lothe and Pound, 1961). Thus, the data obtained from the smog chamber experiments on the rates of particle formation and growth will aid in assessing our ability to describe nucleation of organic aerosol constituents. Moreover, studying how those rates are modified in the presence of foreign particles provides additional measures of the nucleation rate as the condensing species concentration is altered by condensation onto the pre-existing particles.

In this chapter, we present an analysis of the competition between nucleation and condensation in our experimental system using an integral model of aerosol dynamics. The integral model is an excellent tool for beginning a comprehensive study such as this one; because of its simplicity, it is flexible enough to accommodate variations in assumptions about the physics occurring in the system with only minor changes in the equations.

4.2 Theoretical Analysis of Aerosol Formation and Growth

The integral aerosol model used for this study is called the "SNM model" because it describes the saturation ratio in the vapor phase, number concentration and mass concentration of aerosol (Warren and Seinfeld, 1984, 1985b). It treats the aerosol distribution as two monodisperse modes: a primary mode that contains the seed aerosol, and a secondary mode created by homogeneous nucleation from the vapor phase. The processes included in the analysis are a source of condensible vapor, homogeneous nucleation, condensational growth, and particle loss by deposition. The number concentrations in our experiments were low enough so that the amount of coagulation is insignificant; for example, for a system with 10,000 cm^{-3} particles of 0.1 μm diameter, the characteristic time for coagulation

is approximately 30 hours. The model consists of balances on mass and number in the two aerosol modes, and a mass balance on the vapor phase:

Vapor concentration:

$$\frac{d}{dt}N_v = R_G - g_s R_J - R_{c1} - R_{c2} \tag{4.1}$$

Primary aerosol:

$$\frac{d}{dt}N_{p1} = -\beta_1 N_{p1} \tag{4.2}$$

$$\frac{d}{dt}M_{p1} = m_1 R_{c1} - m_1 \beta_1 N_{p1} \tag{4.3}$$

Secondary aerosol:

$$\frac{d}{dt}N_{p2} = R_J - \beta_2 N_{p2} \tag{4.4}$$

$$\frac{d}{dt}M_{p2} = m_1 g_s R_J + m_1 R_{c2} - m_1 \beta_2 N_{p2}, \tag{4.5}$$

where R_G represents the source rate of condensible vapor, R_J represents the nucleation rate, and R_{c1} and R_{c2} are the rates of condensation onto the two modes of aerosol, all in number cm^{-3} s^{-1}. β_1 and β_2 are the deposition coefficients of the two modes in s^{-1}, and m_1 is the monomer mass in grams. It is assumed that the secondary aerosol forms at the thermodynamically determined critical cluster size, g_c, and grows rapidly to an assumed cluster size, g_s. The characteristic time for condensational growth of freshly nucleating particles in our system is approximately one millisecond. Since this free-molecular regime growth is fast, the assumption that particles form at size g_s instead of g_c is reasonable.

The following parameters are needed for use in this model: physical property data, the source rate of condensible vapor, deposition parameters (electric field, particle charge, and coefficient of eddy diffusivity) and nucleation parameters (nucleation rate expression and g_s). For nucleation and condensation modeling, we need to know the vapor pressure, surface tension, density and molecular weight

of the condensible species. Moreover, we need to account for the temperature dependence of these properties since the average temperature of the outdoor smog chamber varied from experiment to experiment. However, the molecular composition of the condensing species in our system is unknown, and therefore we cannot easily predict the physical property data needed.

In addition to the aerosol physical property data, the gas-phase source rate of condensible vapor is the other major unknown in our system. Ideally one would predict this rate from knowledge of the detailed gas-phase kinetics. Such knowledge is not yet available for these systems. In the absence of this information the source rate can be estimated from the overall aerosol growth. To determine the rate of generation of condensible species, the measured aerosol volume profile was interpolated over half-hour intervals. The growth rate was determined in discrete intervals from each data point to the next. Thus the source rate used in the model was variable, increasing or decreasing in steps. For intervals where the aerosol volume decreased because of depositional loss, the source rate was taken to be zero.

The rate of deposition on the wall of the chamber is the result of diffusional and gravitational deposition as described in the theory of Crump and Seinfeld (1981). In addition, if the particles are charged, electrostatic deposition is important, since Teflon film chambers tend to develop an electric field. McMurry and Rader (1985) have shown that electrostatic deposition is especially significant for particles between 0.1 μm and 1.0 μm, the size range of interest in our experiments. We assumed the turbulent mixing coefficient in the Crump-Seinfeld theory to be k_e = 0.1 s^{-1}, and the electric field on the Teflon to be 40 V cm^{-1}, approximately the values found by McMurry and Rader in their Teflon chambers. If the aerosol particles are singly charged, the theory predicts a deposition coefficient, β, on the order of 10^{-4} s^{-1}, which is dependent on particle size.

The predicted number concentrations are not particularly sensitive to the choice of deposition parameters, since nucleation occurs over an extremely short time period, during which depositional losses are insignificant. We chose the deposition parameters to match the removal observed during the period of steady condensational growth that follows nucleation. The parameters reported here predict depositional losses close to those observed experimentally.

We have assumed initially that each aromatic starting species will produce one condensible species. It is believed that the aerosol precursors come from the ring-preserving reaction pathway of the aromatic photooxidation mechanism (e.g., Grosjean, 1977). Therefore, we have assumed that the condensible species for all of the aromatics have a molecular weight of 150, representative of a nitrogenated or oxygenated ring compound. We assumed a surface tension of 30 dynes cm^{-1}, independent of temperature, a value typical of organic liquids, and a density of 1 g cm^{-3}. The temperature effects were included by variation of the vapor pressure of the condensing species.

The Clausius-Clapeyron equation states that for an ideal gas, vapor pressure and temperature are related by

$$\ln p_{sat} = \frac{A}{T} + B, \tag{4.6}$$

where A and B are species-dependent constants. Since our experiments were carried out over a range of temperatures, we assume that this functional form describes the variation in vapor pressure of the condensible species between experiments. Because the molecular composition of the aerosol species was not known, it was necessary to estimate the vapor pressure for the condensed species from the experimental data. From our observations of nucleation in systems with few or no initial particles, it is possible to determine the vapor pressure required to predict the observed number of particles resulting from the nucleation event.

Doing so for each relevant experiment gave a collection of (p_{sat}, T) points for each aromatic; from these we could determine a best fit of the vapor pressure for each system using Equation (4.6). The vapor pressure estimates are given in Figures 4.1 – 4.3 for toluene, m-xylene, and 1,3,5-trimethyl benzene, respectively. The ethyl benzene system did not generate sufficient aerosol, and the temperature range of those experiments was narrow enough, that there were not sufficient data to determine a p_{sat}/T relationship. Since the aromatic decay in the ethyl benzene system most closely resembled that of toluene, the toluene vapor pressures have been used provisionally for ethyl benzene. The 1,3,5-trimethyl benzene data were taken over a limited temperature range, so a constant average vapor pressure was used for data analysis of this species.

Although for experimental purposes it was necessary to employ initial aromatic concentrations about 1 ppm, ambient aromatic levels are on the order of 50 ppb (Grosjean and Fung, 1984). If the aerosol yield for toluene, for example, is about 3%, as we have found (see discussion on aerosol yield in the Appendix), there should be approximately 1.5 ppb of gas-phase toluene aerosol precursors produced in the atmosphere. The vapor pressure of the toluene aerosol constituents that is consistent with the observed rate of nucleation is approximately 10^{-5} dynes cm^{-2}, which is about 0.01 ppb. This level yields a saturation ratio of about 150, which is sufficiently high for gas-to-particle conversion, either by nucleation or by condensation, to occur under atmospheric conditions.

Finally, we need to consider the nucleation rate expression and the size of the nucleating particles. The nucleating cluster size in the SNM model, g_s, was assumed to be 200; with our other assumptions, g_c was on the order of 100 at the onset of nucleation and decreased as the saturation ratio rose. The effect of the assumption of $g_s = 200$ was tested by changing g_s to 500. No change was noted in our predicted aerosol behavior, so the system is insensitive to the choice of g_s.

We thus used $g_s = 200$ in our simulations. The nucleation rate expression used is the classical rate expression of Becker, Doring and Zeldovich (Friedlander, 1977). An enhancement in the nucleation rate of about 10^7 over that predicted by the classical theory has been observed in some experimental systems (Okuyama et al., 1987; Warren et al., 1987). Including such an enhancement in our analysis shifted the vapor pressure/temperature curve somewhat, and gave a slightly greater temperature dependence, but did not significantly alter our predictions. Therefore, classical nucleation theory was used for the results that follow.

4.3 Predicted and Observed Aerosol Dynamics

Using the vapor pressure/temperature relations of Figures 4.1 – 4.3, the SNM model was used to predict the variation of number concentration with time for each experiment in which aerosol data were recorded. Required information for each simulation included the temperature, the number of initial particles if seed particles were added, and the condensible species generation rate. Each simulation started at the time the experiment commenced and continued through the final time for which data were available.

A comparison of the final or maximum number predicted by the model and that observed experimentally is given in Figure 4.4 for all of the aromatic species. In cases where no nucleation was observed, the initial number is the maximum number observed and is therefore the number we have plotted. "Perfect" results would fall on the dashed line shown in each figure. Although there is some scatter in the data, the overall agreement is fairly good. The points that fall exactly on the dashed line are those experiments in which both observation and simulation show total suppression of nucleation and therefore in which the number shown is equal to the initial number of particles in the system. We note that more points fall below the dashed line than above it; this indicates that our model generally

underpredicts nucleation for this system.

We present in Figures 4.5 – 4.7 a comparison of a typical simulation with experimental data for a case with no nucleation. The experimental data presented are the inverted data, obtained as described in Chapter 3. The system simulated is one side of a dual-chamber toluene experiment in which nucleation was suppressed by the presence of initial aerosol (DMXA48, side A). The seed aerosol concentration was 6700 cm^{-3}, and the initial particle diameter was approximately 0.06 μm. Figure 4.5 shows the predicted and observed total number concentrations; both the experiment and the simulation show the total number decaying with time as particles are lost to the walls of the chamber. Here we evaluate our ability to model deposition and the validity of our assumptions about deposition parameters. The total volume concentrations predicted and observed are shown in Figure 4.6. Since we are using the experimental observations directly to give the rate of condensible species generation, the simulation is predictably close to the data. The prediction of aerosol volume lies just below the experimental observation. This is because of our use of the aerosol volume profile to give the vapor source rate; since the condensation and nucleation rates are driven by a gas-phase supersaturation, not all of the mass in the vapor phase can be converted back to the aerosol phase while gas-to-particle conversion is occurring. The two experimental diameters shown in Figure 4.7 are the measured volume-averaged and number-averaged diameters. Since the SNM model represents the aerosol in terms of two monodisperse modes, there is only one average diameter. As in Figure 4.6, we see condensational growth starting about two hours into the experiment.

Figure 4.8 shows another example of the predicted and observed average particle size as a function of time. These data are from a m-xylene run in which there were 250 cm^{-3} initial particles (XJ19, side B). We see condensational growth starting very early. Approximately 35 minutes into the experiment there is a nu-

cleation burst and the average particle size falls sharply as the secondary aerosol mode of smaller particles begins to dominate. This behavior is apparent in both the experimental profiles and the simulation. For this experiment, approximately $10,500\ cm^{-3}$ particles were formed in the nucleation event.

The simulation of a nucleation event is shown in Figure 4.9. This is one side of a dual-chamber toluene experiment in which $400\ cm^{-3}$ initial particles allowed approximately $5000\ cm^{-3}$ nucleating particles (LEV77, side A). Although the onset of nucleation in the simulation occurs at the same time as the experimental observation, the model predicts that nucleation will occur much faster than we observe experimentally. Some of this time lag could be due to the imperfect response of our aerosol instruments to a rapidly changing aerosol size distribution at their lower size detection limit.

One of the main objectives of this work was to determine the effect of initial particles on nucleation in aromatic photooxidation systems. Theoretical predictions and experimental observations of nucleation suppression in systems with initial aerosol have been reported in systems driven by a high initial supersaturation (Warren et al., 1987), and theoretical predictions have been reported for systems driven by a constant source rate (Warren and Seinfeld, 1985b; Stern et al., 1986). However, no data have been reported on experimentally observed nucleation suppression in source rate-driven systems such as the present one.

Figure 4.10 shows the theoretically-predicted nucleation suppression by initial aerosol in a system with a constant vapor source. N_{J_0} is the number of particles expected to form by nucleation in the absence of initial aerosol, N_i is the initial aerosol concentration, and N_f is the final number predicted. If initial particles had no effect on nucleation, this curve would be a line at $\frac{N_f}{N_i+N_{J_0}}$ equal to one. Physically, at both low and high initial number concentrations this ratio is one, as predicted by the theory. At low initial number, there will be almost no effect

on nucleation and

$$\frac{N_f}{N_i + N_{J_0}} \approx \frac{N_{J_0}}{N_i + N_{J_0}} \approx 1 \qquad N_i \ll N_{J_0}. \tag{4.7}$$

At high initial number concentrations, all nucleation will be suppressed and

$$\frac{N_f}{N_i + N_{J_0}} \approx \frac{N_i}{N_i + N_{J_0}} \approx 1 \qquad N_i \gg N_{J_0}. \tag{4.8}$$

In our experimental system, N_{J_0} can be measured experimentally in dual-chamber experiments with no initial particles on one side of the chamber and some initial particles on the other, with identical gas-phase chemistry on each side. For these cases we can construct an experimental analogue of Figure 4.10. The results for all four aromatic species are shown in Figure 4.11, along with the calculated points based on the final number predicted from the simulation and the measured N_i and N_{J_0}. Although the agreement of all but two sets of points looks excellent, we must note that all of the points for which there is perfect agreement represent systems where no nucleation was observed on the side with initial particles, hence both observation and prediction fall on the $N_i = N_f$ curve.

There are, however, some toluene experiments not shown in Figure 4.11 for which N_{J_0} could not be determined (single-chamber runs or experiments with initial particles on both sides), as well as some points in Figure 4.11, where we observed nucleation when the simulations predict no significant amounts of nucleation. For these experiments, the aerosol vapor pressure needed to simulate the observed nucleation is up to an order of magnitude lower than that determined for nucleating systems with no initial particles. In other words, the apparent vapor pressure of these systems is not consistent with the observations used to generate Figures 4.1 – 4.3, the vapor pressure/temperature relations for each aromatic species. These few experiments in which nucleation was observed but not predicted based on the vapor pressure determined from seed-free experiments pose an interesting question concerning our representation of nucleation.

A possible explanation for the underpredicted rate of nucleation is the existence of two nucleating species. To account for this possibility, the SNM model can be expanded to include a hypothetical second gas-phase aerosol-producing species. Call the original species A, and postulate the existence of a second lower vapor pressure species B. Assume that the vapor pressure of species B is a constant fraction of the vapor pressure of A, but that all other physical properties of B and A are identical. Therefore, $\gamma = p_{sat,B}/p_{sat,A}$ is one new adjustable parameter in the model. Furthermore, let us assume that a constant fraction of the aerosol source rate can be assigned to A and the remainder to B. Therefore, for some source rate, R_G, and fraction to B, ς, $R_{G_A} = (1-\varsigma)R_G$ and $R_{G_B} = \varsigma R_G$, where R_{G_A} and R_{G_B} are the vapor source rates of A and B, respectively. With these assumptions, the system can be represented by:

Vapor concentrations:

$$\frac{d}{dt}N_{vA} = (1-\varsigma)R_G - g_s R_{JA} - R_{c1A} - R_{c2A} \tag{4.9}$$

$$\frac{d}{dt}N_{vB} = \varsigma R_G - g_s R_{JB} - R_{c1B} - R_{c2B} \tag{4.10}$$

Primary aerosol:

$$\frac{d}{dt}N_{p1} = -\beta_1 N_{p1} \tag{4.11}$$

$$\frac{d}{dt}M_{p1} = m_1 R_{c1A} + m_1 R_{c1B} - m_1\beta_1 N_{p1} \tag{4.12}$$

Secondary aerosol:

$$\frac{d}{dt}N_{p2} = R_{JA} + R_{JB} - \beta_2 N_{p2} \tag{4.13}$$

$$\frac{d}{dt}M_{p2} = m_1 g_s R_{JA} + m_1 g_s R_{JB} + m_1 R_{c2A} + m_1 R_{c2B} - m_1\beta_2 N_{p2}. \tag{4.14}$$

To test this two-species hypothesis, we considered four toluene experiments at approximately the same temperatures. Two of these systems had no initial particles (DHNA43, sides A and B), one had 1000 cm^{-3} initial particles (MTLA18),

and the fourth had 4700 cm^{-3} initial particles (MTMA22). In all four systems nucleation was observed (see Table 2.5). We shall refer to these four cases as Cases I – IV, respectively. In simulating each experiment, γ was held fixed and ς varied between 0 and 1. These limits represent the systems with all aerosol precursor being species A and B, respectively. We varied the vapor pressure of A (hence indirectly varying the vapor pressure of B) until the model predicted the amount of observed nucleation.

If two nucleating species were to explain our experimental observations, there should be some combination of ς and γ that would allow the nucleation observed in all four systems to be predicted by the same vapor pressure. Therefore, we can present our results as $p_{sat,A}$ needed to achieve observed nucleation versus ς, the fraction of the source rate designated as species B. Figure 4.12 shows these results for $\gamma = 0.1$ and $\gamma = 0.01$, systems with a secondary species of one and of two orders of magnitude lower vapor pressure. The four lines represent the systems we have chosen to study. At $\varsigma = 0$ we have the single-species case, where all of the aerosol is A. The vapor pressures at this point are exactly the vapor pressures we determined previously that predicted the observed amount of nucleation.

As we increase the amount of source designated as B, we must adjust $p_{sat,A}$, since the B vapor will affect the overall condensation and nucleation behavior in the system. For the $\gamma = 0.1$ case we see an initial dip in the curves as ς is increased. This is because not enough of the vapor source is going to species B to allow it to undergo significant gas-to-particle conversion. The net result is to deplete the concentration of A, so that we need a lower vapor pressure to achieve the same amount of nucleation that we observe. As we increase ς, we get more and more B being produced. Since B has a lower vapor pressure, its saturation ratio rises much faster and we get nucleation and condensation more easily. Therefore, we must compensate by raising the input $p_{sat,A}$, and so we see the rise in $p_{sat,A}$

with increasing ς. With high levels of species B, we see B nucleating before the saturation level of A increases high enough to allow significant nucleation rates. The supersaturation of A is then relieved by condensation onto the newly nucleated B particles. Thus, we have essentially a condensing species and a nucleating species.

We seek some change in the behavior of Cases I - IV as we increase the amount of source designated as B. For instance, at $\varsigma = 0$, $p_{sat,A}$ is an order of magnitude smaller for Case IV than it is for Case I. This is because our simulation predicts that the 4700 cm^{-3} initial particles in Case IV provide so much surface area for condensation that nucleation is effectively suppressed using the $p_{sat,A}$ for Case I. We need to assume a much lower vapor pressure to simulate the nucleation that was observed. Increasing ς, if the vapor pressures for the four experiments begin to converge, this would indicate that the higher levels of initial aerosol would not lead to as much nucleation suppression in the presence of a secondary lower vapor pressure nucleation species as they do with only one gas-phase species. Unfortunately, we do not observe this behavior either at $\gamma = 0.1$ or at $\gamma = 0.01$. Adding a second species affects Cases I - IV equally, and the curves move predictably upwards towards the $\varsigma = 1$ limit, where all of the vapor source goes to B and $p_{sat,B}$ equals $p_{sat,A}$ at $\varsigma = 0$ (recalling that $p_{sat,B} = \gamma p_{sat,A}$).

The previous calculations used classical nucleation theory and assumed that species A and B were non-interacting. In some systems, such as sulfuric acid and water, enhanced nucleation rates occur because of the interaction of the two species. Binary nucleation theory has been developed to account for these thermodynamic interactions (Mirabel and Katz, 1974; Stauffer, 1976). The two-species nucleation calculations were repeated using binary nucleation theory. For these calculations we assumed that the organic species behaved as ideal solutions, along with the assumptions previously stated for the non-interacting case.

The results of these simulations are presented in Figure 4.13. Again there is no indication that binary nucleation theory can account for the experimentally observed nucleation with high levels of initial aerosol. This question still remains to be resolved.

4.4 Conclusions

We have considered the effects of pre-existing particles on the competition between nucleation and condensation in aromatic hydrocarbon/NO_x systems. In the absence of pre-existing particles, aerosol formation must occur by homogeneous nucleation, whereas with a large quantity of pre-existing particles, condensation of the "condensible" products of photooxidation onto existing particles will maintain the saturation ratios low enough that nucleation will not occur. As one repeats an experiment with ever more increasing primary aerosol levels, a point is reached at which homogeneous nucleation is fully suppressed. Our experiments clearly illustrate this effect. Data on nucleation suppression are valuable in assessing the theoretical rate of homogeneous nucleation.

Simulations of the aerosol behavior in the aromatic systems were carried out using a simple integral aerosol model. Vapor pressure data were estimated from observations of nucleation in systems with few or no initial particles. Using the vapor pressure/temperature correlation we obtained from these observations, we attempted to simulate the total number concentration time profile, the volume concentration time profile, and the average particle size during each experiment. We found reasonably good agreement with the experiments, as we have shown in Figures 4.5 – 4.9 for several experimental systems.

In addition, we compared the predictions of nucleation suppression by initial particles with the observed suppression. Although the simulations of such systems generally agree with the experimental observations, several experiments with ini-

tial particles in the toluene system exhibited nucleation when the model predicted that nucleation should not occur. Assuming the existence of a second lower vapor pressure species that could nucleate independently or participate in binary nucleation with the original species could not account for the observed nucleation. This question still remains to be resolved.

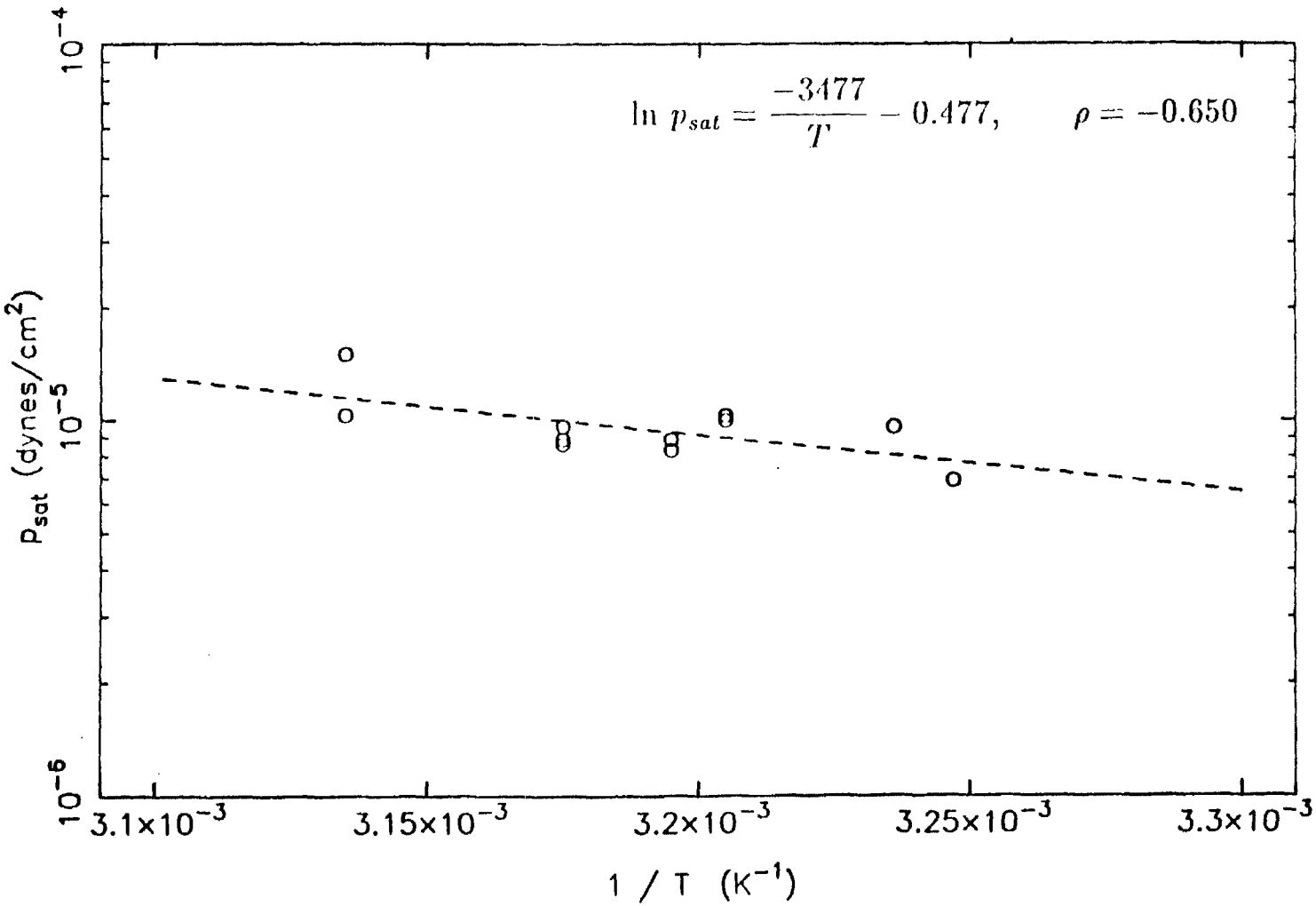

FIGURE 4.1. Vapor pressure as a function of inverse temperature for toluene aerosol constituents, including best-fit line.

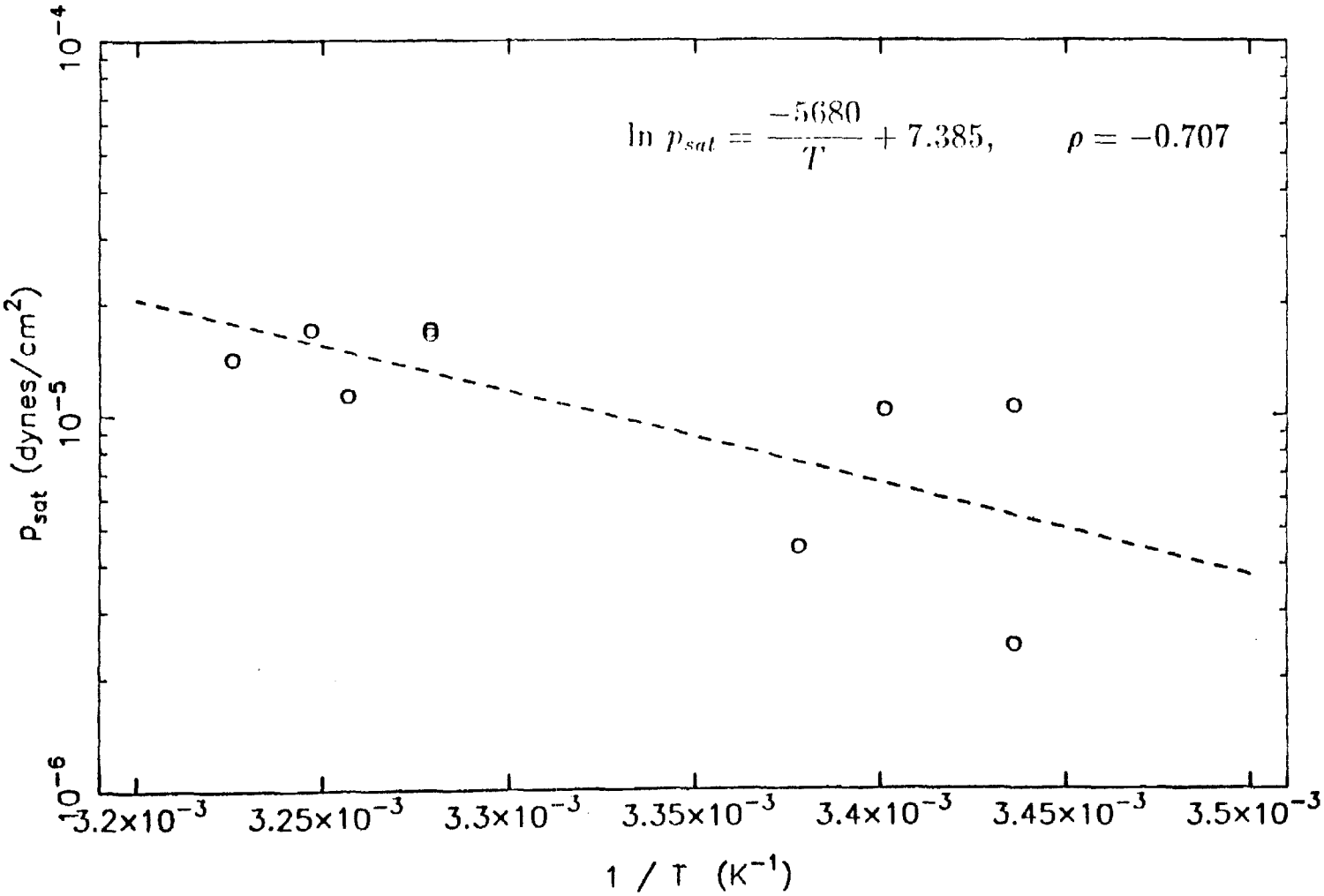

FIGURE 4.2. Vapor pressure as a function of inverse temperature for m-xylene aerosol constituents, including best-fit line.

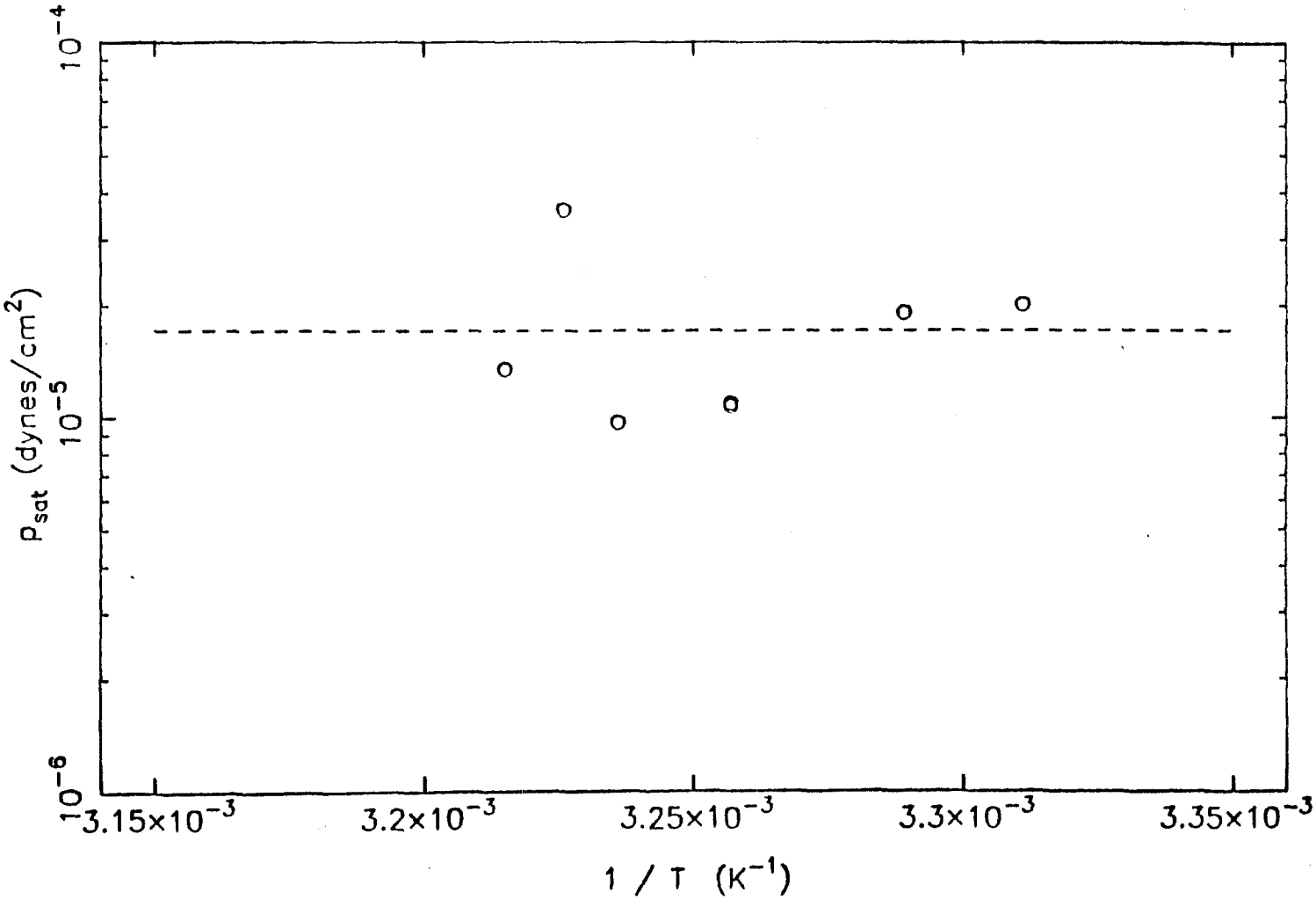

FIGURE 4.3. Vapor pressure as a function of inverse temperature for 1,3,5-trimethyl benzene aerosol constituents, including average vapor pressure line.

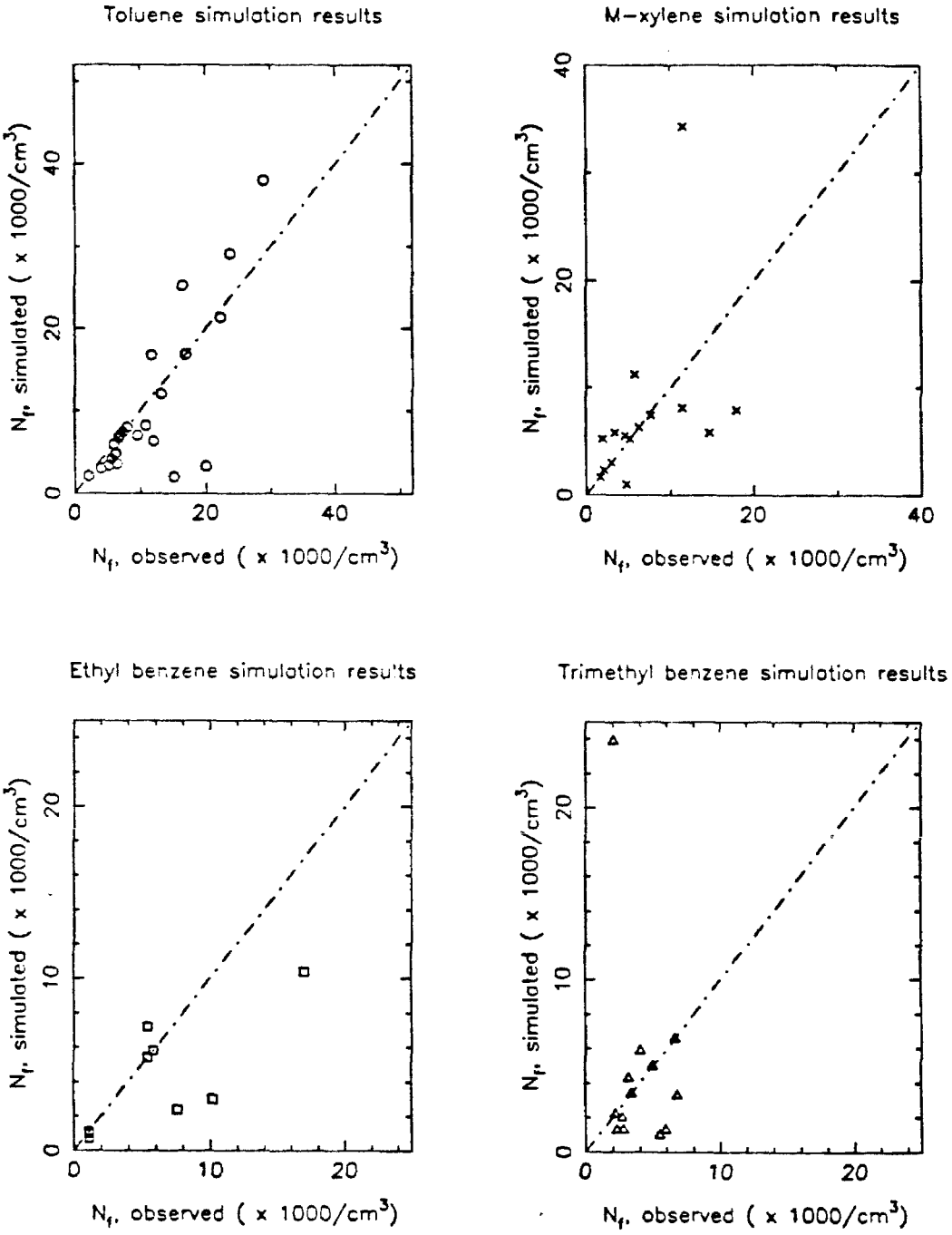

FIGURE 4.4. Predicted and observed final or maximum aerosol number concentrations for all experiments.

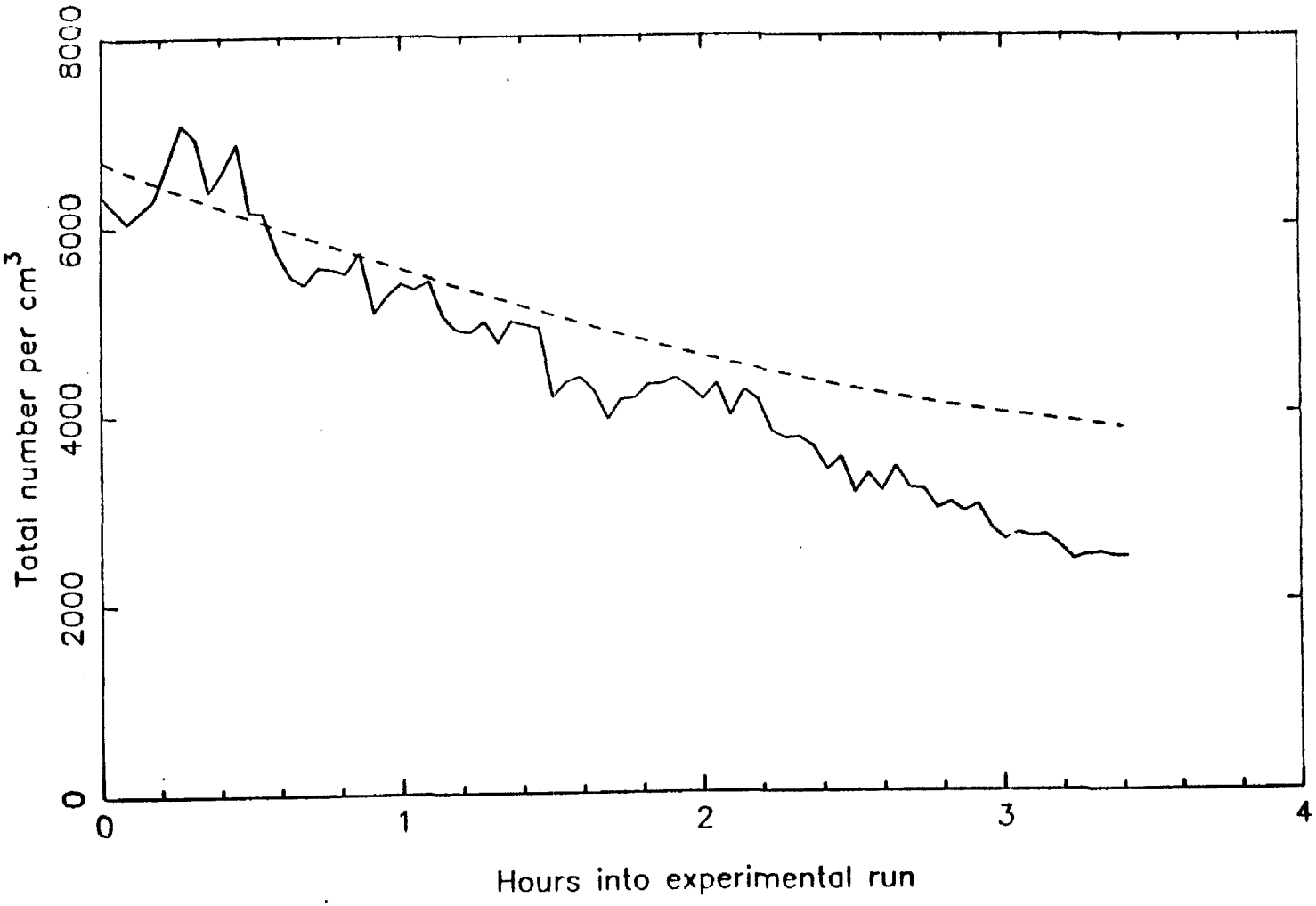

FIGURE 4.5. Predicted and observed total aerosol number concentration for experiment DMXA48, A.

— observed, - - - predicted

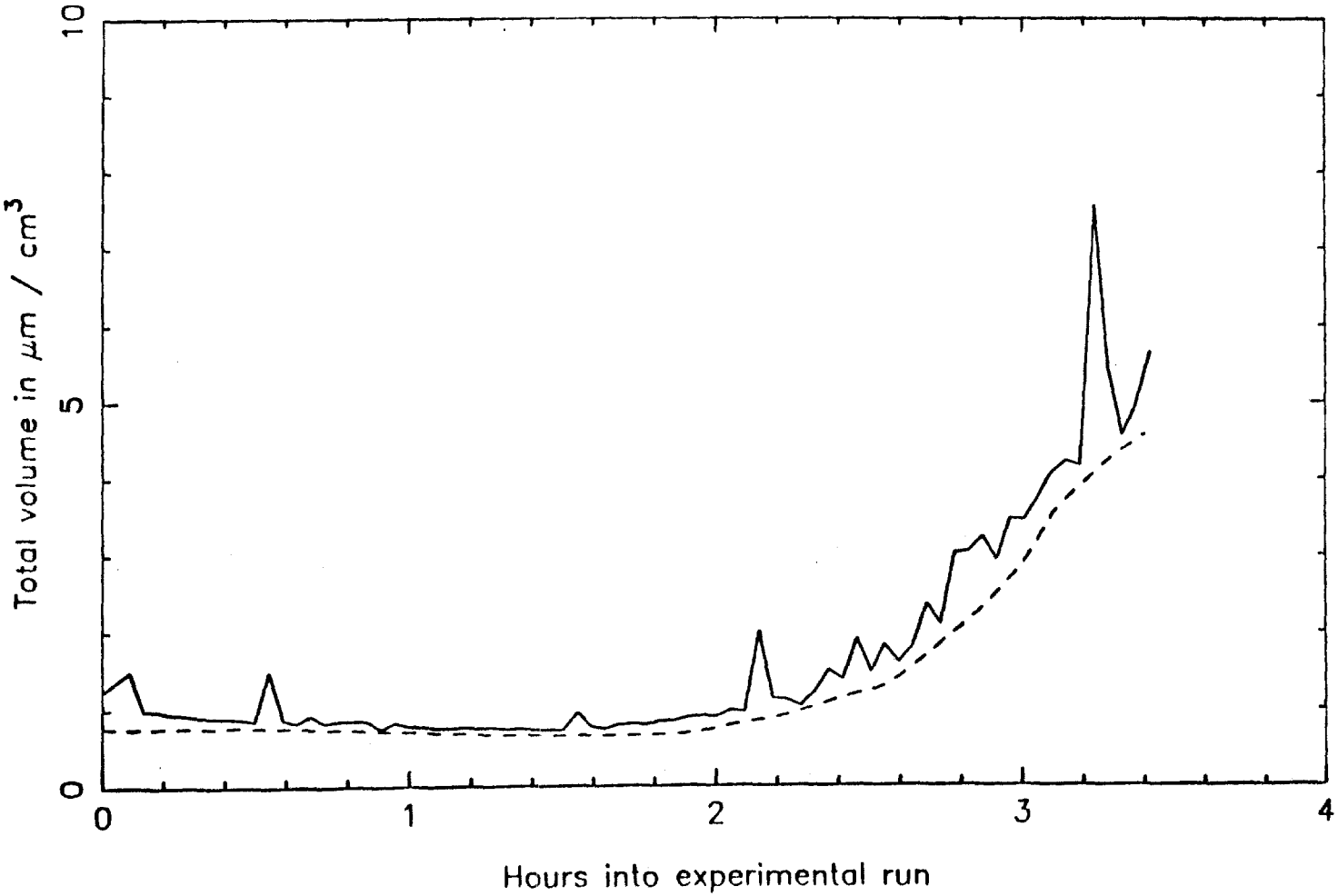

FIGURE 4.6. Predicted and observed total aerosol volume concentration for experiment DMXA48, A.

— observed, - - - predicted

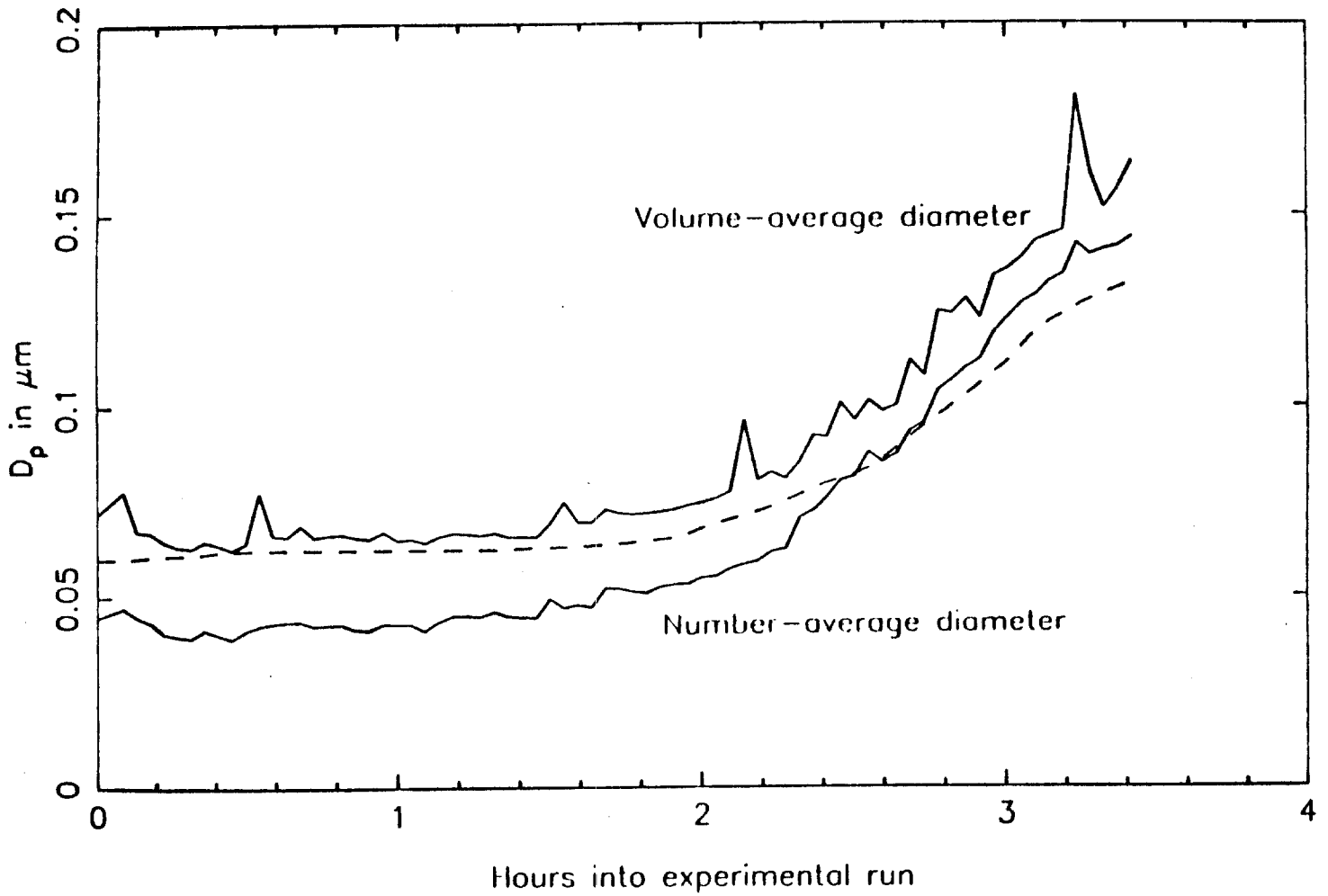

FIGURE 4.7. Predicted and observed average aerosol particle diameter for experiment DMXA48, A.

— observed, - - - predicted

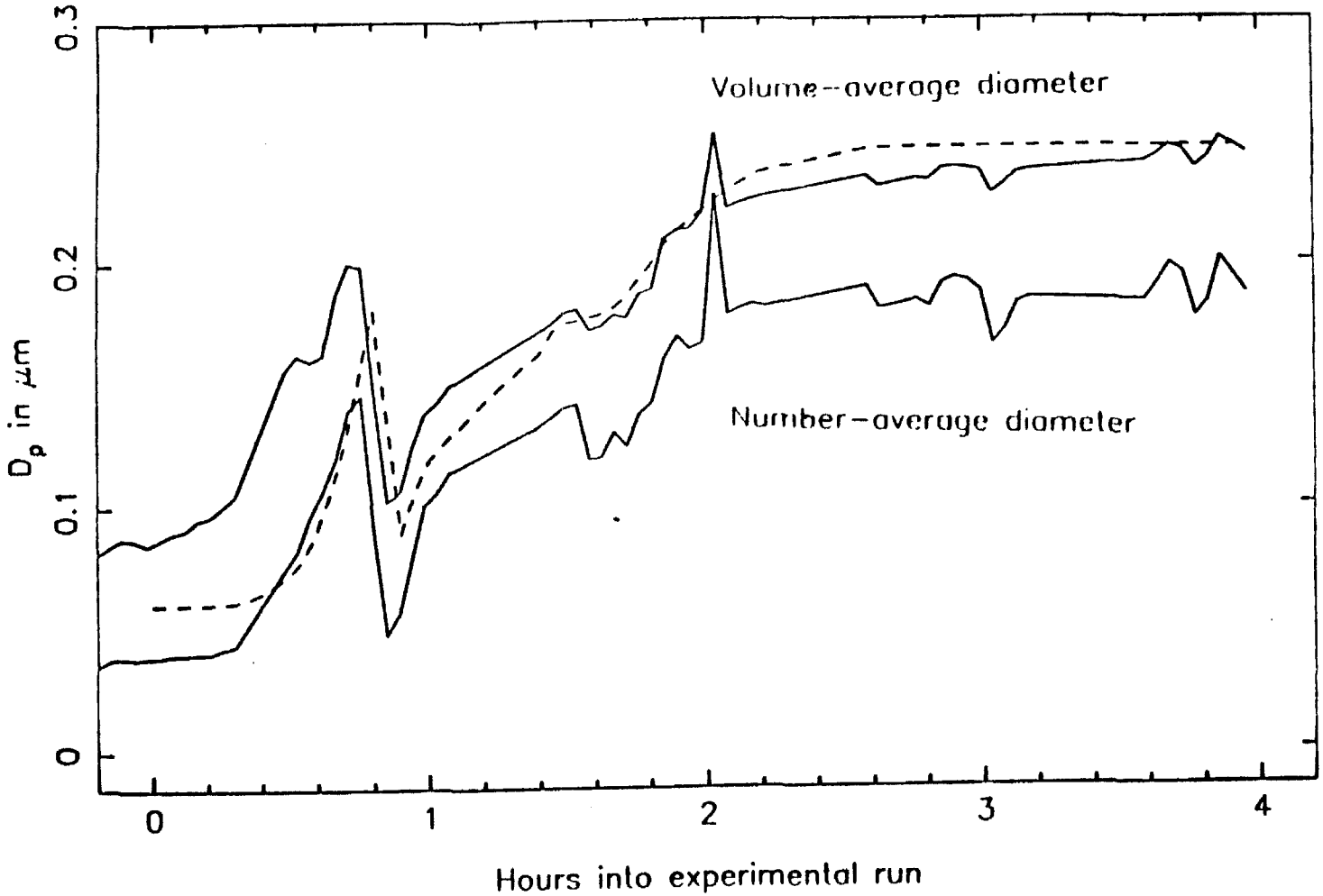

FIGURE 4.8. Predicted and observed average aerosol particle diameter for experiment XJ19, B.

— observed, - - - predicted

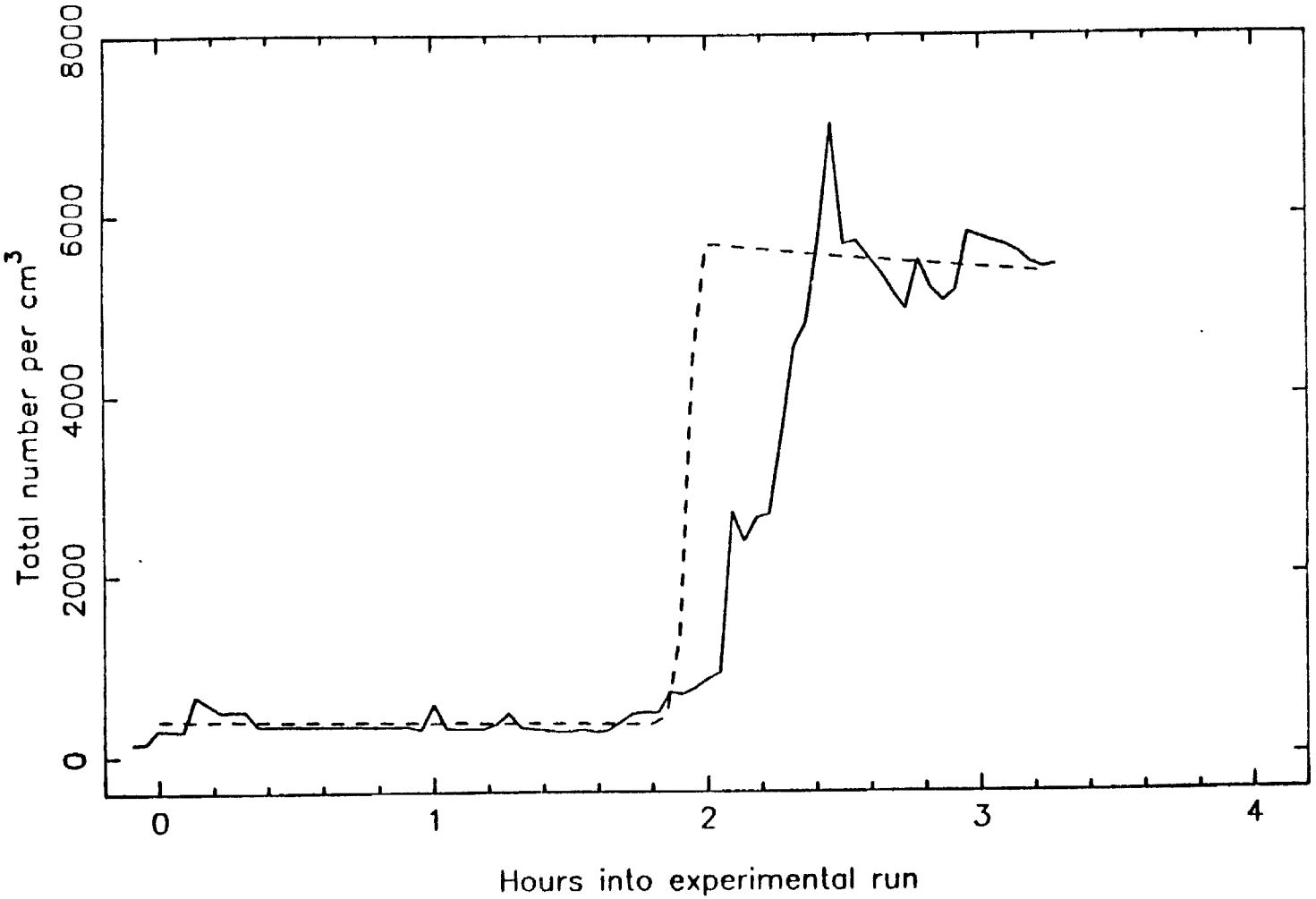

FIGURE 4.9. Predicted and observed total aerosol number concentration for experiment LEV77, A.

— observed, - - - predicted

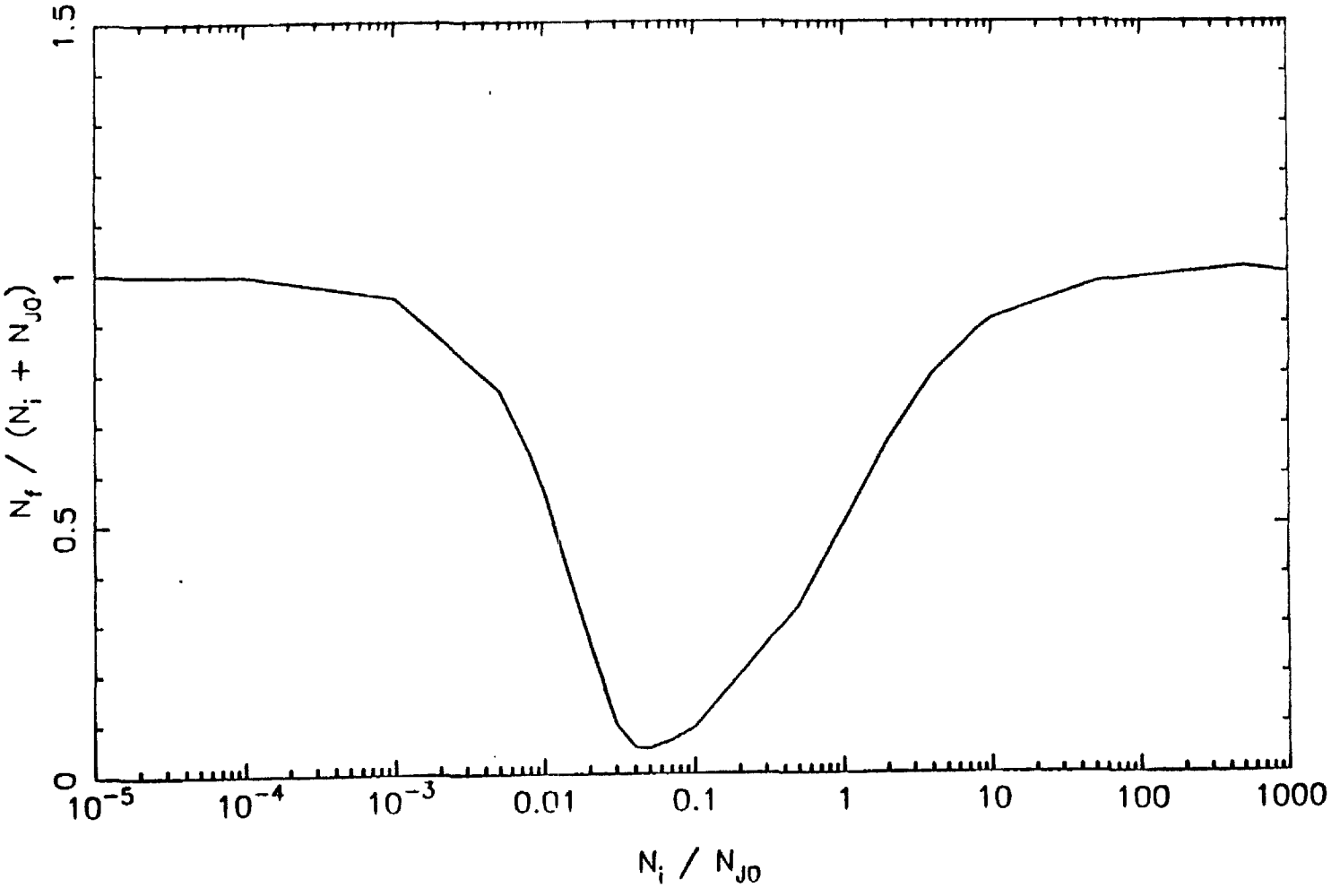

FIGURE 4.10. Predicted suppression of nucleation as a function of initial particle loading for a constant source rate system.

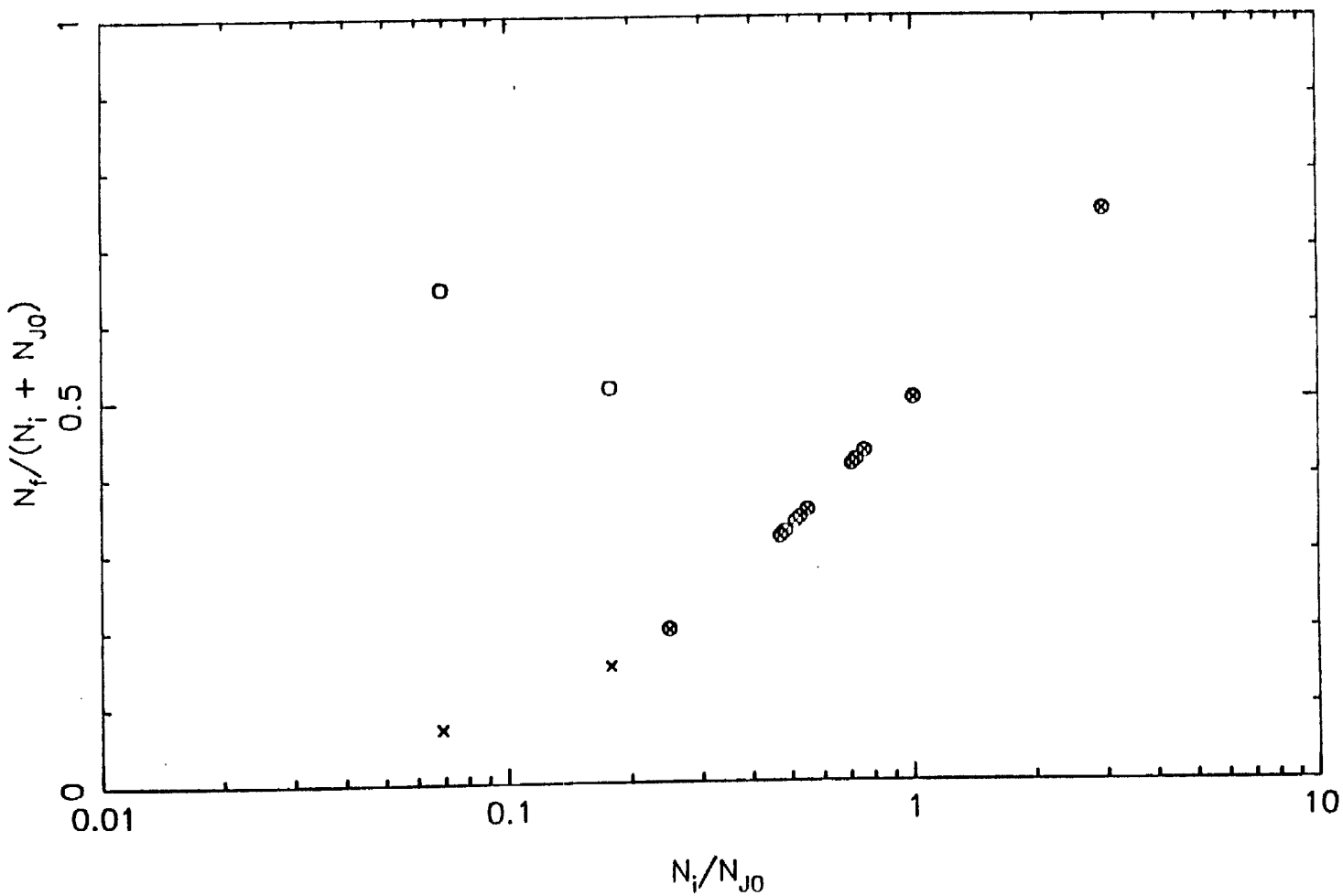

FIGURE 4.11. Observed and predicted suppression of nucleation as a function of initial particle loading in the experimental system.

o observed, × predicted

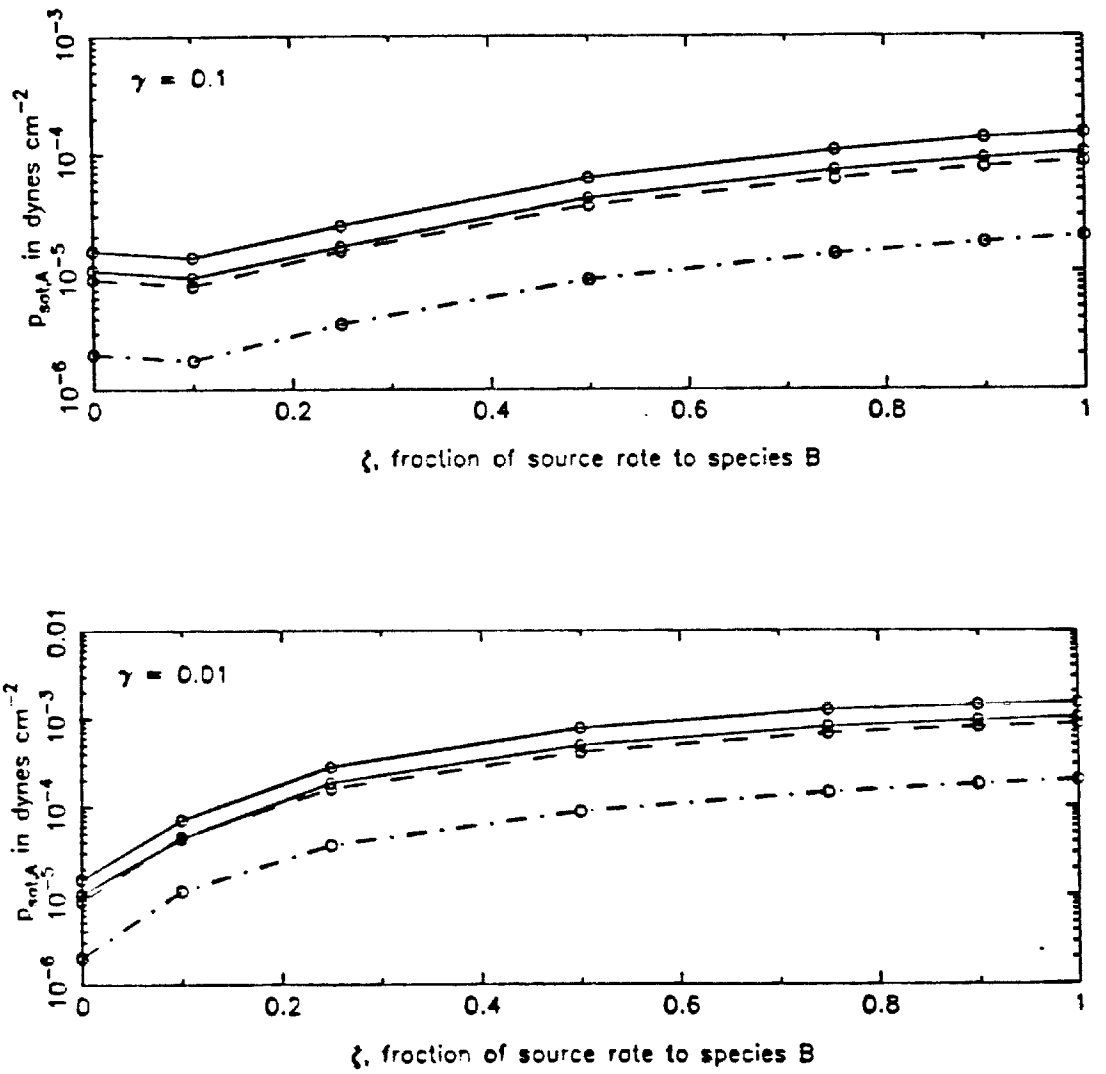

FIGURE 4.12. Vapor pressure of species A needed to achieve observed nucleation as a function of ζ; classical nucleation theory. For four toluene experiments with different initial aerosol loadings. $\gamma = 0.1$ and $\gamma = 0.01$. — 0 cm^{-3}; - - - 1000 cm^{-3}; - · - 4700 cm^{-3}.

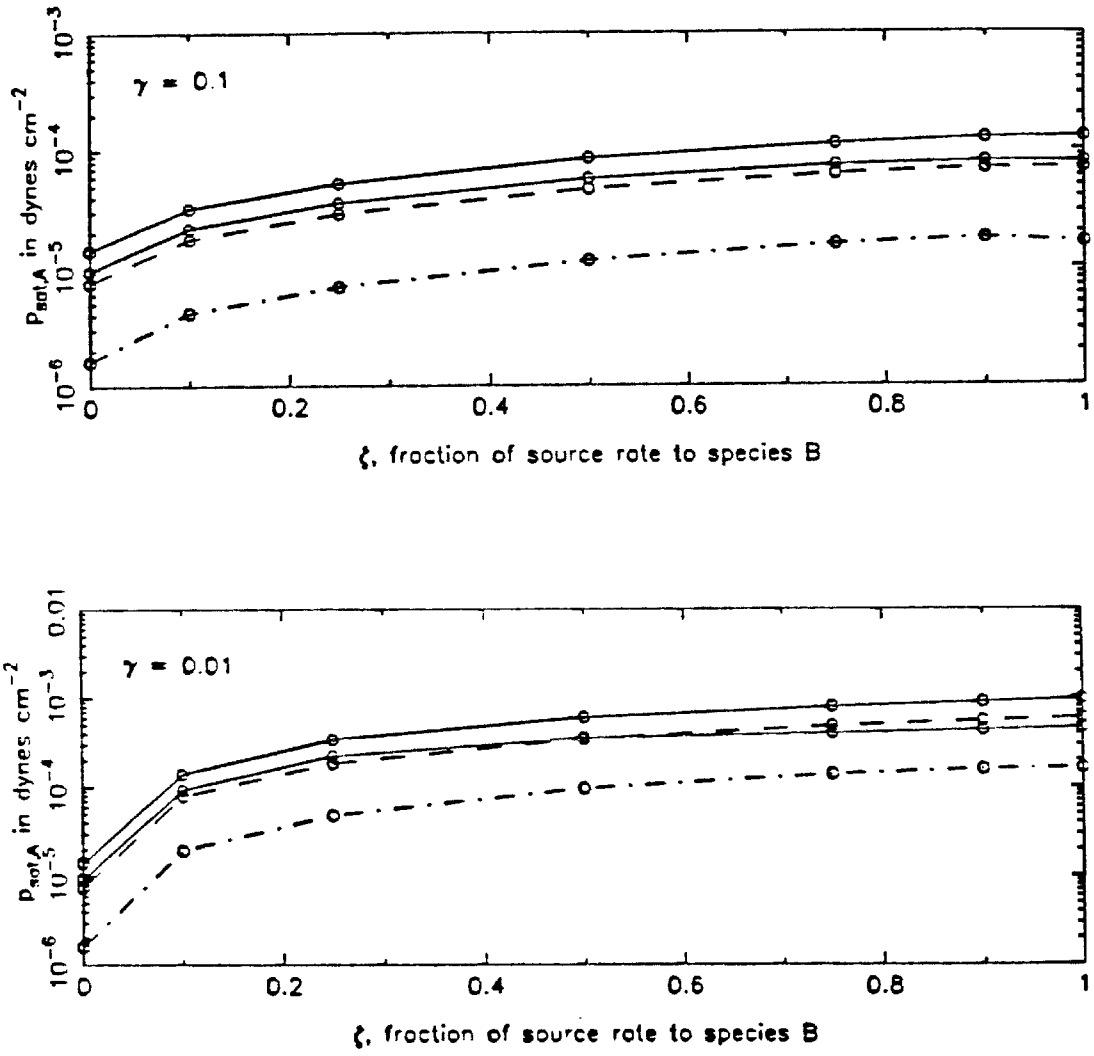

FIGURE 4.13. Vapor pressure of species A needed to achieve observed nucleation as a function of ζ; binary nucleation theory. For four toluene experiments with different initial aerosol loadings. $\gamma = 0.1$ and $\gamma = 0.01$. — 0 cm^{-3}; - - - 1000 cm^{-3}; - · - 4700 cm^{-3}.

CHAPTER 5

DETERMINATION OF GROWTH-LAW PARAMETERS FOR AROMATIC AEROSOLS

5.1 Introduction

The integral model of aerosol dynamics described in the previous chapter characterizes the evolution of the moments of the size distribution. To simulate the evolution of the size distribution itself, we need to consider the full aerosol General Dynamic Equation (GDE), Equation (1.1). Since we have shown that coagulation can be ignored in our experimental system, we can focus instead on solution of the Condensation Equation, Equation (1.3). At some point in each experiment the dominant aerosol process occurring is condensational growth. At this point it is, in fact, unimportant whether the growing particles are the $(NH_4)_2SO_4$ seed particles or the secondary aerosol formed by homogeneous nucleation. These particles grow according to a growth law, $dv/dt = I(v,t)$, that can be written as a function of aerosol Knudsen number, Kn.

The Condensation Equation can be solved numerically or analytically using the full growth law, but an analytical solution using an approximate growth law can be useful in evaluating the nature of the growth process. Therefore, in this chapter, we explore the behavior of the growing aerosol as observed in our experiments by using a simplified power-law growth expression. We can compare the growth law parameters that fit the observed aerosol size distribution evolution with a full growth expression to estimate the gas-phase partial pressures of the condensing vapors. These pressures can then be compared with the vapor pressures obtained in the previous chapter using the integral model to obtain gas-phase supersaturations. The integral model vapor pressures were derived from the observations

of nucleation in these systems; the calculations described here are based on observations of condensation. These two approaches are complementary in nature, and therefore it is of interest to draw a comparison between their predictions of gas-phase pressures for the condensible species. This kind of analysis has not been reported previously.

After performing these calculations with the power-law representation of the growth law, we use the full growth law in the analytical solution to obtain directly gas-phase partial pressures for the condensing species. These can be compared with the partial pressures estimated with the approximate growth law to evaluate the usefulness of employing a simplified expression in analyses of growing aerosols. Since power-law forms of the growth law are often used in the analysis of aerosol data, this is a useful comparison.

5.2 General Solution of the Condensation Equation

The analytical solution that follows is based on the solution by Williams (1983). Using the variable transformation $M(v,t) = I(v,t)n(v,t)$, (1.3) can be converted to:

$$\frac{1}{I(v,t)}\frac{\partial M(v,t)}{\partial v} = S(v,t) - \left(\frac{\mathcal{R}(v,t)}{I(v,t)} - \frac{\partial I(v,t)/\partial t}{[I(v,t)]^2}\right) M(v,t). \qquad (5.1)$$

Exact solution of (5.1) is possible only if we assume that the particle growth law $I(v,t)$ is separable in v and t. In such a case we have

$$\frac{dv}{dt} = I(v,t) = f(v)H(t). \qquad (5.2)$$

Integrating this, we have

$$\int \frac{dv'}{f(v')} = \int H(t')dt' + C_1, \qquad (5.3)$$

or, equivalently,

$$F(v) = G(t) + C_1,$$

where C_1 is for the moment an unspecified constant. This gives the equations of the characteristics:

$$v(t) = F^{-1}(G(t) + C_1). \tag{5.4}$$

Along the characteristics (5.1) becomes

$$\frac{dM(v(t),t)}{dt} + \left(\mathcal{R}(v(t),t) - \frac{dH(t)/dt}{H(t)}\right) M(v(t),t) = S(v(t),t)f(v(t))H(t). \tag{5.5}$$

This equation can be solved with an integrating factor. Thus, let

$$\Delta(t) = \exp\left\{\int \left[\mathcal{R}(v(t'),t') - \frac{dH(t')/dt'}{H(t')}\right] dt'\right\}, \tag{5.6}$$

and we have the solution of (5.5):

$$M(v(t),t)\Delta(t) = \int S(v(t'),t')f(v(t'))H(t')\Delta(t')dt' + C_2. \tag{5.7}$$

Applying the boundary condition at $t = 0$, we get

$$M(v,0) = M_0(v) = I(v,0)n_0(v) = f(v)H(0)n_0(v). \tag{5.8}$$

Letting $C_2 = \Lambda(F(v)-G(t)) = \Lambda(C_1)$, and replacing v at time 0 with $v = F^{-1}(C_1 + G(0)) = F^{-1}(F(v) - G(t) + G(0))$, Equation (5.7) at time 0 becomes

$$M_0\left(F^{-1}(F(v) - G(t) + G(0))\right)\Delta(0) =$$

$$\int^0 S(v(t'),t')f(v(t'),t')H(t')\Delta(t')dt' + \Lambda(C_1), \tag{5.9}$$

from which we derive the expression for $\Lambda(F(v) - G(t))$. Substituting back into (5.7), we get

$$M(v(t),t) = M_0\left(F^{-1}(F(v) - G(t) + G(0))\right)\frac{\Delta(0)}{\Delta(t)}$$

$$+\frac{1}{\Delta(t)}\int_0^t S(v(t'),t')f(v(t'))H(t')\Delta(t')dt'. \qquad (5.10)$$

Finally, we can replace $\Delta(t)$ by noting that (5.6) simplifies to become

$$\Delta(t) = \frac{1}{H(t)}\exp\left\{\int \mathcal{R}(v(t'),t')dt'\right\}. \qquad (5.11)$$

Substitution into (5.10) yields the general solution:

$$M(v(t),t) = M_0\left(F^{-1}(F(v) - G(t) + G(0))\right)\frac{H(t)}{H(0)}\exp\left\{\int_0^t \mathcal{R}(v(t'),t')dt'\right\}$$
$$+H(t)\int_0^t S(v(t'),t')f(v(t'))\exp\left\{\int_{t'}^t \mathcal{R}(v(t''),t'')dt''\right\}dt', \qquad (5.12)$$

where $M(v,t) = f(v)H(t)n(v,t)$.

5.3 Power-Law Simplification

We have derived a general analytical solution of the Condensation Equation that assumes only that the growth law, $I(v,t)$, is separable with respect to v and t. To implement this solution one needs to specify the functional forms of $f(v)$, $H(t)$, $\mathcal{R}(v,t)$ and $S(v,t)$. These functions are not generally available for the aromatic hydrocarbon/NO_x photooxidation system in the outdoor smog chamber. As an initial simplification, therefore, we confine our attention to a growing aerosol distribution in the absence of nucleation and deposition. The general solution for $S(v,t) = \mathcal{R}(v,t) = 0$ becomes

$$M(v,t) = M_0\left(F^{-1}(F(v) - G(t) + G(0))\right)\frac{H(t)}{H(0)}. \qquad (5.13)$$

Furthermore, we assume a power-law form for the growth law:

$$I(v,t) = H_\alpha v^\alpha \qquad (5.14)$$

or

$$f(v) = v^\alpha, \qquad H(t) = H_\alpha.$$

The power-law approximation is reasonable when we consider the possible mechanisms of growth for an atmospheric aerosol, including diffusion-limited, surface

reaction-limited and volume reaction-limited growth, as described below. The characteristic curves of the system corresponding to (5.14) are:

$$v^{1-\alpha} = v_0^{1-\alpha} + (1-\alpha)H_\alpha t, \tag{5.15}$$

where v_0 is the initial volume of the particle that has grown to volume v at time t. Substituting $M(v,t) = H_\alpha v^\alpha n(v,t)$ and $M_0(v_0) = H_\alpha v_0^\alpha n_0(v_0)$ into (5.13) and solving for $n(v,t)$, we get

$$n(v,t) = n_0(v_0)\left(\frac{v_0}{v}\right)^\alpha, \tag{5.16}$$

with v and v_0 related along a characteristic by (5.15). Equation (5.16) is the analytical expression for the size distribution during pure condensational growth with a power-law growth rate and no particle source or removal mechanisms.

At this point, let us examine the significance of the parameters H_α and α. The values of α determine how each particle size grows relative to the other particle sizes and is indicative of the method of growth. If the dominant mechanism for aerosol growth is diffusion-limited transport in the continuum regime, the growth law $I(v,t) = k_c v^{\frac{1}{3}}$, where k_c includes the pressure driving force for condensation as well as some numerical and physical constants. Diffusional growth in the free-molecular regime can be represented by $I(v,t) = k_{fm} v^{\frac{2}{3}}$, where k_{fm} is, like k_c, a group of constants. Growth by surface reaction can be represented by $I(v,t) = k_s v^{\frac{2}{3}}$, and for growth by volume reaction, $I(v,t) = k_v v$, where k_s and k_v include rate constants and other parameters of the system. Therefore, we can see that most important mechanisms for growth can be represented by $I(v,t) = H_\alpha v^\alpha$.

While α specifies the shape of an evolving size distribution, and suggests the mechanism by which it grows, H_α determines how rapid the growth is. The value of H_α gives us information on the physical parameters governing the growth in the system. If the growth mechanism is reaction-controlled, H_α depends on the rate

constants of the reactions. If the aerosol is undergoing diffusion-limited growth, H_α depends on the driving force for the transport of vapor molecules to the particle surface. For instance, for diffusion-controlled growth in the free-molecular regime, kinetic theory gives:

$$\frac{dv}{dt} = \left(\frac{9\pi}{16}\right)^{\frac{1}{3}} \frac{\bar{c}v_1}{kT}(p_A - p_s)\, v^{\frac{2}{3}}, \tag{5.17}$$

where $\bar{c}$ is the mean molecular speed of the vapor molecules, v_1 is the molecular volume, and $(p_A - p_s)$ is the difference between the partial pressure of the condensing species in the gas phase, p_A, and its partial pressure over the surface of the particle, p_s. From a measurement of H_α for a value of $\alpha = \frac{2}{3}$, we can determine $p_A - p_s$.

We assumed that the growth law is separable in v and t. We can see in Equation (5.17) above that the volume term can be separated from the rest of the expression as long as all of the physical constants as well as p_A and p_s are volume-independent. This is true as long as p_s is not dependent on the curvature of the particle surface, that is, that the Kelvin effect can be neglected. For 0.1 μm particles at 300 K, molecular weight of 150 g mole-1, density of 1 g cm^{-3}, and surface tension of 30 dynes cm^{-1}, the Kelvin effect predicts $p_s/p_{sat} = 1.07$. Therefore, for particles in the size range of our experimental system, this is a reasonably good assumption.

5.4 Determination of Experimental Growth-Law Parameters

As we have shown, analyses of the evolution of a size distribution can offer insight into the mechanisms of growth (Heisler and Friedlander, 1977; McMurry and Wilson, 1982; Seinfeld and Bassett, 1982; McMurry and Grosjean, 1985). We are interested in applying this method of analysis to our measured aerosol size distributions to determine if the data are consistent with a particular type of growth law, and to estimate gas-phase partial pressures of the condensing species.

To apply the analytical solution to our measured size distributions, we chose time intervals of steady growth in each experiment considered, as judged by the total volume versus time profile. Since aerosol growth does not commence immediately, the "initial time" for this analysis was considered to be the time at which observable growth began. The aerosol number distribution at this time was determined by averaging the distributions over a ± 7.5 minute interval. The evolving number distribution was considered at half-hour intervals (again averaged over ± 7.5 minutes) throughout the period of steady growth. The final time was taken to be that at which the total aerosol volume ceased increasing. This period ranged from 1.0 to 1.5 hours in most experiments considered. The experiments chosen represent those in which the number distributions were reasonably smooth and the volume versus time profile showed a steady increase over some time period.

The initial number distribution, $n_0(v_0)$, is specified at the diameters used for the inversion of the data. Using (5.15) to determine the volumes, v, at each half-hour interval for these initial volumes, we can then calculate $n(v,t)$ from (5.16). By adjusting the parameters H_α and α, we can attempt to fit the evolution of the size distribution at half-hour intervals from the designated starting distribution.

Figure 5.1 shows a typical number distribution time evolution for a single-chamber toluene experiment, MTHA31. All of the distributions that we show are expressed as $dN/d \log D_p$. The initial and final times for observed growth in this experiment were 1.5 and 3.0 hours, respectively. The simulated and observed volume distributions ($dV/d \log D_p$) for this experiment are shown in Figure 5.2, and the total aerosol volume evolution is given in Figure 5.3. We see from Figure 5.3 that the aerosol volume increases in this 1.5 hour period by a factor of about 100. H_α and α were estimated to be 0.41 μm hour^{-1} and $\frac{2}{3}$, respectively. As we can see, the simulated distributions are very close to the observed distributions.

Since no aerosol-phase chemical reactions are expected to be occurring, we

anticipate the aerosol in the systems studied here to grow by a diffusion-limited mechanism, consistent with a value of α between $\frac{1}{3}$ and $\frac{2}{3}$. A value of $\alpha = \frac{2}{3}$ was found to fit most of the experiments extremely well. This value of α corresponds to free-molecular regime growth. The particles are typically at the large end of this regime; the potential inaccuracy in using the growth law for smaller particles will be explored later. Therefore, α was fixed at $\frac{2}{3}$, and H_α varied to obtain a best-fit of the experimental distributions. Table 5.1 lists all of the experiments considered, the initial and final times for aerosol growth in each system, and the best-fit value for H_α. The experiments simulated include all four aromatic starting species, both single- and dual-chamber experiments, the full range of experimental temperatures, and growing primary and secondary aerosol particles.

For the 1,3,5-trimethyl benzene experiments, it appears that the value of α producing the best fit of observed and predicted size distributions is closer to 1 than to $\frac{2}{3}$. Figure 5.4 shows a growing number distribution for side A of a dual-chamber trimethyl benzene experiment (TE36) with 2000 cm^{-3} initial ammonium sulfate particles, and $\alpha = 0.98$. Although a value of $\alpha = 1$ corresponds to volume-reaction limited growth, there are no differences in the photooxidation mechanism for trimethyl benzene that would suggest an aerosol-phase chemical reaction-controlled growth mechanism. In addition, a value of $\alpha = 1$ implies that the aerosol size distribution does not narrow as the aerosol grows. The apparently different behavior of the trimethyl benzene aerosol can be explained if we consider the nature of the aerosol generated in these systems. The aerosol produced from the trimethyl benzene photooxidation tends to grow very quickly such that the few initial particles will be fairly large by the time the aerosol volume loading in the system is significant. The time we have defined as $t = 0$ for the growth-law analysis of this experiment is 1.0 hours into the experiment, by which time the aerosol distribution is already quite narrow. However, the distributions that are

obtained from the raw data are constrained not to be smaller than a minimum width by the smoothing function in our data inversion. Therefore, these inverted distributions do not narrow with time, and we obtain a best-fit α close to 1, an artifact of the inversion we have used.

Since α close to 1 has no physical basis in our system, we fixed $\alpha = \frac{2}{3}$ for the trimethyl benzene experiments as well. Figure 5.5 shows the predicted number distributions for TE36, A, after one hour of growth, for $\alpha = 0.98$ ($H_\alpha = 3.01$) and $\alpha = \frac{2}{3}$ ($H_\alpha = 1.07$). Although the $\alpha = 0.98$ prediction clearly provides a better fit, the assumption of $\alpha = \frac{2}{3}$ does predict accurately the mean particle diameter after one hour of growth.

To complete this analysis, using assumed physical properties of the condensing species we can estimate their gas-phase partial pressures, which can be compared with the vapor pressures determined using the integral model to give estimates of saturation ratios during these periods of condensational growth. The vapor pressures obtained using the integral model were based on observations of nucleation rates. The gas-phase partial pressures obtained by this approach are based on observations of condensation rates. Thus, these two approaches are complementary in nature, and if the gas-phase partial pressures agree well with one another, they lend credence to both rate expressions. Such a comparison in an experimental system has not been previously reported. We note here that the integral model vapor pressures generally were obtained by considering nucleation events in experiments different from those we have used in the growth-law analysis, and that the nucleation events occur in all systems before substantial amounts of growth are observed. However, since we are considering a representative sampling of the experiments, we anticipate that the effect of these differences will be minimal.

Assuming $\alpha = \frac{2}{3}$, we use (5.17) to obtain gas-phase partial pressures for each growing aerosol. Without detailed knowledge of the composition of the aerosol, we

need to make estimates for any required physical properties. For Equation (5.17), we need only an assumption about molecular weight; for these calculations, we assume as in Chapter 4 that the condensible vapor has a molecular weight of 150.

We can now estimate $(p_A - p_s)$ for each of the experiments listed in Table 5.1; these partial pressures are given in Table 5.2. If we assume that the Kelvin effect is negligible, then $p_s = p_{sat}$, and the tabulated values are $p_{sat}\ (S - 1)$, where S is the saturation ratio. Using the vapor pressures obtained for each aromatic from the simulation with the integral model, we obtain a value for S for each experiment. These saturation ratios are also included in Table 5.2. Most of the values lie between 3.5 and 13, with two higher values for experiments that were at the lowest temperatures observed, leading to low saturation vapor pressures. These values represent a reasonable range for the supersaturation in a system undergoing condensational growth. Much lower supersaturations would not cause detectable growth to occur; much higher values would tend to make nucleation more significant than observed. Using the additional physical property assumptions of Chapter 4 that $\sigma = 30$ dynes cm^{-1}, and $\rho_p = 1$ g cm^{-3}, and assuming $p_{sat} = 1 \times 10^{-5}$ dynes cm^{-2}, we estimate the nucleation rate even at the highest saturation ratio, $S \approx 30$, to be only approximately 10^{-6} cm^{-3} sec^{-1}, which does not produce appreciable nucleation. We note that if the Kelvin effect is not negligible, the saturation ratios will be slightly higher, as $p_A - p_s$ will be equal to $p_{sat}\,[S - \exp(\frac{D_K}{D_p})]$, instead of $p_{sat}(S - 1)$, where D_K is the Kelvin diameter.

We finally address the assumption that deposition is negligible in these systems. Over the course of one hour in most of these experiments, depositional losses account for a decrease in the total number of particles of approximately 10 %. Therefore, this is not a significant effect, and our neglecting deposition does not introduce substantial error into these calculations.

5.5 Full Transition Regime Representation

Although from the approximate growth-law analysis of these systems it appears that the aromatic aerosols are undergoing free-molecular regime growth, the particles are too large to be considered strictly in this regime. We desire, therefore, to use Equation (5.13) with a full transition-regime growth law to simulate the growing aerosol. Again, to use the analytical solution we must assume that the growth law $I(v,t)$ is separable in v and t.

For the transition regime, the growth law $I(v,t)$ can be given by (Seinfeld, 1986):

$$I(v,t) = (48\pi^2)^{\frac{1}{3}} \frac{D_A M_A}{\rho_p RT} v^{\frac{1}{3}} (p_A - p_s) f_{Kn}(\mathrm{Kn}), \tag{5.18}$$

where $f_{Kn}(\mathrm{Kn})$ is an interpolation formula for the transition regime that makes the growth-law approach the correct continuum and free-molecular expressions. The mean free path of a condensing vapor can be related to its diffusivity by (Seinfeld, 1986):

$$\frac{D_A}{\lambda_A \bar{c}} = \frac{3\pi}{32}(1+z), \tag{5.19}$$

where z is the ratio of the molecular weight of the condensing species to the molecular weight of air. The most common assumption relating λ_A to D_A is that of Fuchs and Sutugin (1971),

$$\frac{D_A}{\lambda_A \bar{c}} = \frac{1}{3} \tag{5.20}$$

which by comparison to (5.19) corresponds to an aerosol of very low molecular weight. For an aerosol of molecular weight 150, this ratio should be set equal to 1.818, reducing the mean free path from Equation (5.20) by a factor of 5.5. Using a diffusivity expression given from kinetic theory by (Davis, 1983):

$$D_A = \frac{3}{8\pi} \sqrt{\frac{1}{2}\pi RT \left(\frac{1}{M_A} + \frac{1}{M_{air}} \right)} \Big/ n_{air} d_{A,air}^2, \tag{5.21}$$

we estimate λ_A from Equation (5.19) to be 0.165 μm at 300 K. A typical 0.1 μm particle in our system will have Kn = 0.33, clearly a transition-regime aerosol. We will use Equation (5.19) for all of our calculations involving the mean free path.

The most commonly used $f_{Kn}(\mathrm{Kn})$ is also that of Fuchs and Sutugin (1971) which is based on Equation (5.20) for the mean free path. Since this is not the assumption we will make, we will instead employ the transition regime interpolation formula from Fuchs' earlier work involving flux-matching (Fuchs, 1964):

$$f_{Kn}(\mathrm{Kn}) = \frac{1 + \frac{2\Delta}{D_p}}{1 + \frac{8D_A}{\bar{c}D_p}\left[1 + \frac{2\Delta}{D_p}\right]}, \tag{5.22}$$

where Δ is the distance at which the continuum and free-molecular fluxes are equated. Assuming that $\Delta = \lambda_A$, and using Equation (5.19), we obtain

$$f_{Kn}(\mathrm{Kn}) = \frac{1 + \mathrm{Kn}}{1 + 7.272\mathrm{Kn} + 7.272\mathrm{Kn}^2} \tag{5.23}$$

for an aerosol of molecular weight 150.

We now return to the solution of Equation (5.13) using the growth law, (5.18). We assume that there is no time-dependence in any of the terms in Equation (5.18) and obtain the expression for $n(v,t)$:

$$n(v,t) = n_0(v_0)\left(\frac{v_0}{v}\right)^{\frac{1}{3}} \frac{f_{Kn}(\mathrm{Kn}_0)}{f_{Kn}(\mathrm{Kn})}. \tag{5.24}$$

The form of the growth law now used makes it impossible to obtain an explicit equation for the particle size along the characteristics, as we previously obtained (Equation (5.15)); the characteristics are found from Equation (5.4) to be:

$$0.5(D_p^2 - D_{p_0}^2) + 12.544\lambda(D_p - D_{p_0}) + 4\lambda_A^2 \ln\left(\frac{D_p + 2\lambda_A}{D_{p_0} + 2\lambda_A}\right)$$

$$-\frac{4D_A M_A}{\rho_p RT}(p_A - p_s)t = 0, \tag{5.25}$$

where a particle with initial diameter of D_{p_0} grows to size D_p at time t.

Using similar techniques as with the power-law growth analysis, we use Equations (5.24) and (5.25) to predict the evolution of experimental distributions through periods of steady growth. The only parameter varied in this assumed growth law is the gas-phase pressure differential, $p_A - p_s$. The new particle diameters at each half-hour interval are found from Equation (5.25) by a Newton iteration, and the new number distribution is calculated. This procedure is repeated over each half-hour interval, and the sum of squares difference between the observed and predicted number distributions is calculated. The best-fit $p_A - p_s$ is obtained by minimizing the total sum of squares over all of the time intervals considered.

We present in Figures 5.6 and 5.7 the observed and predicted number and volume distributions for the single-chamber toluene experiment discussed previously (MTHA31, Figures 5.1 - 5.3). The agreement of the simulated distributions with the experimental distributions is clearly not as good as with the power-law expression using $\alpha = \frac{2}{3}$. The simulated distribution narrows more than the observed distribution, but the peak diameter is accurately predicted. Using the full growth law, we obtained $p_A - p_s = 1.27 \times 10^{-4}$ dynes cm^{-2} for this experiment. Comparing this with the $p_A - p_s$ derived from the best-fit H_α found in the power-law analysis, $p_A - p_s = 7.22 \times 10^{-5}$ dynes cm^{-2}, we see that the values are close, but that the full growth law predicts a larger pressure difference.

The $p_A - p_s$ values obtained for all of the experiments previously considered are presented in Table 5.3. If we again consider $p_A - p_s = p_{sat}(S - 1)$, we can use the integral model vapor pressures to obtain approximate saturation ratios; these are also given in Table 5.3. We see that the saturation ratios are slightly higher than those predicted by the approximate growth law (Table 5.2), but they are reasonably close. If we directly compare the values for $p_A - p_s$ for the two different growth laws, we find that the power-law approximation generally gives pressure

differentials that are approximately 60% of those given by the full transition-regime growth law. The ratios of these pressure differentials are also included in Table 5.3.

5.6 Conclusions

We have used an analytical solution to the Condensation Equation, assuming $S = \mathcal{R} = 0$, to simulate the size distribution evolution in those smog chamber experiments that exhibit periods of steady aerosol growth. The analysis was performed using two different growth laws, $I(v,t)$. We initially approximated the growth law with a power-law expression, $I(v,t) = H_\alpha v^\alpha$, and fit the observed size distribution evolution by varying α and H_α. We then used a complete growth-law expression, given by Equation (5.18) and fit the observed distributions by directly varying the gas-phase pressure driving force, $p_A - p_s$.

We found with the power-law analysis that the observed distributions could be simulated very well using a value of $\alpha = \frac{2}{3}$ and varying H_α only. A value of $\alpha = \frac{2}{3}$ corresponds to diffusional growth in the free-molecular regime. From the full growth law governing diffusion in this regime, we could obtain $p_A - p_s$ values from the best-fit values for H_α. When these were compared with the integral model predictions of vapor pressure, approximate saturation ratios during these periods of growth were found to be generally 3 - 13. This is a reasonable range of values for a system undergoing condensational growth.

Since the aerosol particles in these experiments were not strictly of free-molecule size, the analysis was repeated using a full transition-regime growth law. The gas-phase partial pressures could be directly compared with those obtained from the power-law simulations to evaluate the accuracy of the simplified growth law. We found that the power-law expression predicted consistently lower $p_A - p_s$ values, but that the predictions were not qualitatively different. We can conclude

from this that the use of a power-law simplification for growth-law analyses can be used for qualitative but not quantitative results when the full growth law makes the analysis difficult or impossible.

TABLE 5.1. Estimated growth-law parameters for smog chamber experiments

Experiment	Aromatic	t_i (*hours*)	t_f (*hours*)	H_a*
MTMA16	Tol	2.0	3.5	0.19
MTMA22	Tol	1.5	3.0	0.38
MTHA31	Tol	1.5	3.0	0.41
MTNA35	Tol	2.5	3.5	0.15
DMMA45,A	Tol	1.5	2.5	0.36
DMMA45,B	Tol	1.5	2.5	0.35
XA08,A	Xyl	0.5	2.0	0.78
XB10,A	Xyl	1.0	2.5	0.77
XG15,B	Xyl	1.0	2.0	0.83
XK17,B	Xyl	1.0	2.0	0.66
XJ19,A	Xyl	1.0	2.5	0.34
XJ19,B	Xyl	1.0	2.0	0.19
XJ34,A	Xyl	0.5	1.5	0.70
TE36,A	Tmb	1.0	2.0	1.07
TE39,A	Tmb	1.0	2.0	0.87
TI43,B	Tmb	1.0	2.5	0.25
TO46,A	Tmb	1.0	2.0	0.24
TN52,A	Tmb	0.5	1.5	0.86
EH66,A	Eb	2.5	3.5	0.31
EM70,B	Eb	2.5	3.5	0.13
EL73,A	Eb	1.5	3.0	0.44
TXU75,A	Tmb	1.0	1.5	0.36

* H_a was determined by a least-squares fit over all of the half-hour intervals.

TABLE 5.2. Estimated gas-phase partial pressures and saturation ratios for smog chamber experiments, power-law growth expression

Experiment	Temperature	$p_A - p_s$	p_{sat}	S
	K	dynes cm^{-2}	dynes cm^{-2}	
MTMA16	307	3.567×10^{-5}	7.484×10^{-6}	5.77
MTMA22	318	7.260×10^{-5}	1.107×10^{-5}	7.56
MTHA31	309	7.722×10^{-5}	8.053×10^{-6}	10.59
MTNA35	313	2.843×10^{-5}	9.299×10^{-6}	4.06
DMMA45,A	322	6.921×10^{-5}	1.268×10^{-5}	6.46
DMMA45,B	322	6.729×10^{-5}	1.268×10^{-5}	6.31
XA08,A	310	1.471×10^{-4}	1.778×10^{-5}	9.27
XB10,A	305	1.441×10^{-4}	1.316×10^{-5}	11.95
XG15,B	291	1.517×10^{-4}	5.374×10^{-6}	29.23
XK17,B	294	1.212×10^{-4}	6.559×10^{-6}	19.48
XJ19,A	296	6.267×10^{-5}	7.473×10^{-6}	9.39
XJ19,B	296	3.502×10^{-5}	7.473×10^{-6}	5.69
XJ34,A	305	1.310×10^{-4}	1.316×10^{-5}	10.95
TE36,A	304	1.999×10^{-4}	1.713×10^{-5}	12.67
TE39,A	302	1.620×10^{-4}	1.713×10^{-5}	10.46
TI43,B	307	4.693×10^{-5}	1.713×10^{-5}	3.74
TO46,A	309	4.520×10^{-5}	1.713×10^{-5}	3.64
TN52,A	311	1.625×10^{-4}	1.713×10^{-5}	10.49
EH66,A	304	5.791×10^{-5}	6.693×10^{-6}	9.65
EM70,B	311	2.456×10^{-5}	8.658×10^{-6}	3.84
EL73,A	310	8.300×10^{-5}	8.351×10^{-6}	10.94
TXU75,A	307	6.758×10^{-5}	1.713×10^{-5}	4.95

TABLE 5.3. Gas-phase partial pressures and saturation ratios for smog chamber experiments, full growth expression

Experiment	Temperature	$p_A - p_s$	S	Ratio of $p_A - p_s$
	K	dynes cm^{-2}		power-law/full growth
MTMA16	307	4.88×10^{-5}	7.52	0.731
MTMA22	318	9.18×10^{-5}	9.29	0.791
MTHA31	309	1.27×10^{-4}	16.77	0.608
MTNA35	313	5.26×10^{-5}	6.66	0.540
DMMA45,A	322	1.01×10^{-4}	8.97	0.685
DMMA45,B	322	9.56×10^{-5}	8.54	0.704
XA08,A	310	2.32×10^{-4}	14.05	0.634
XB10,A	305	3.47×10^{-4}	27.37	0.415
XG15,B	291	2.00×10^{-4}	38.22	0.759
XK17,B	294	1.11×10^{-4}	17.92	1.092
XJ19,A	296	1.20×10^{-4}	17.06	0.522
XJ19,B	296	5.31×10^{-5}	8.11	0.660
XJ34,A	305	2.03×10^{-4}	16.43	0.645
TE36,A	304	5.33×10^{-4}	32.12	0.375
TE39,A	302	3.54×10^{-4}	21.67	0.458
TI43,B	307	6.70×10^{-5}	4.91	0.700
TO46,A	309	1.03×10^{-4}	7.01	0.439
TN52,A	311	3.10×10^{-4}	19.10	0.524
EH66,A	304	9.79×10^{-5}	15.63	0.592
EM70,B	311	3.86×10^{-5}	5.46	0.636
EL73,A	310	1.40×10^{-4}	17.76	0.593
TXU75,A	307	1.64×10^{-4}	10.57	0.412

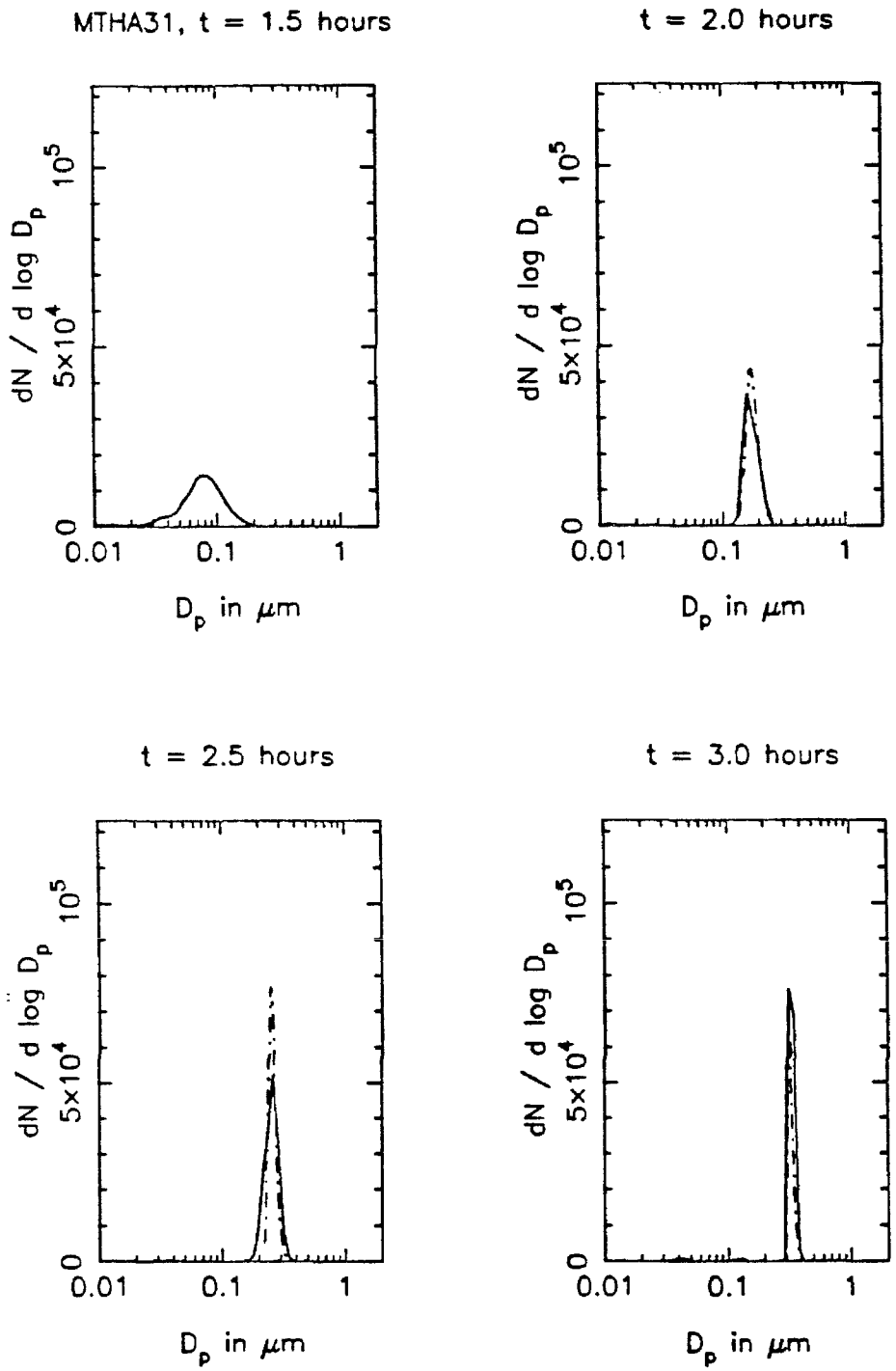

FIGURE 5.1. Predicted and observed aerosol number distributions at half-hour intervals for MTHA31, from $t = 1.5$ hours to $t = 3.0$ hours.

$\alpha = \frac{2}{3}$, $H_a = 0.41$

— observed, – · – predicted

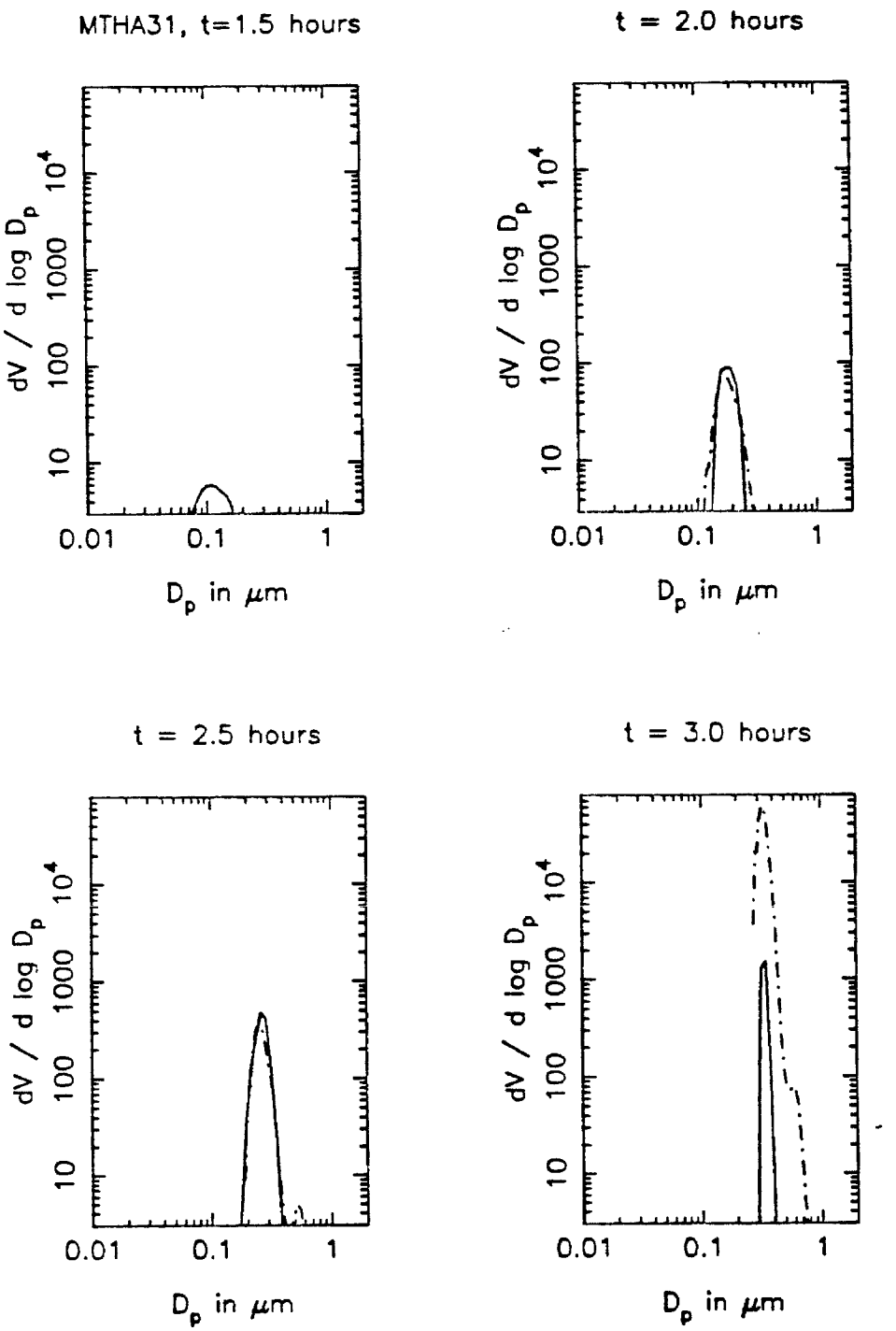

FIGURE 5.2. Predicted and observed aerosol volume distributions at half-hour intervals for MTHA31, from $t = 1.5$ hours to $t = 3.0$ hours.

$\alpha = \frac{2}{3}$, $H_\alpha = 0.41$

— observed, – · – predicted

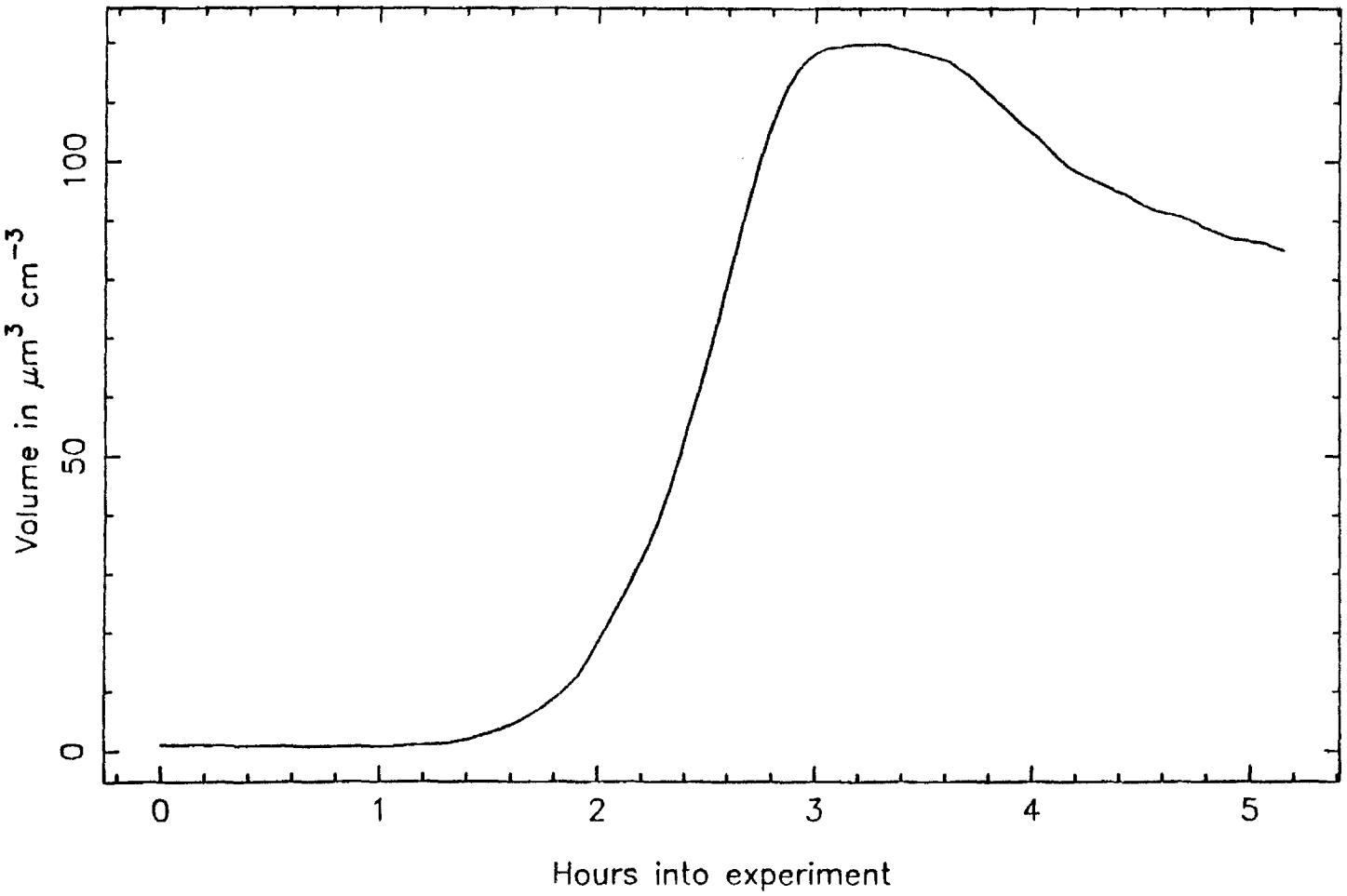

FIGURE 5.3. Observed total aerosol volume concentration as a function of time for MTHA31.

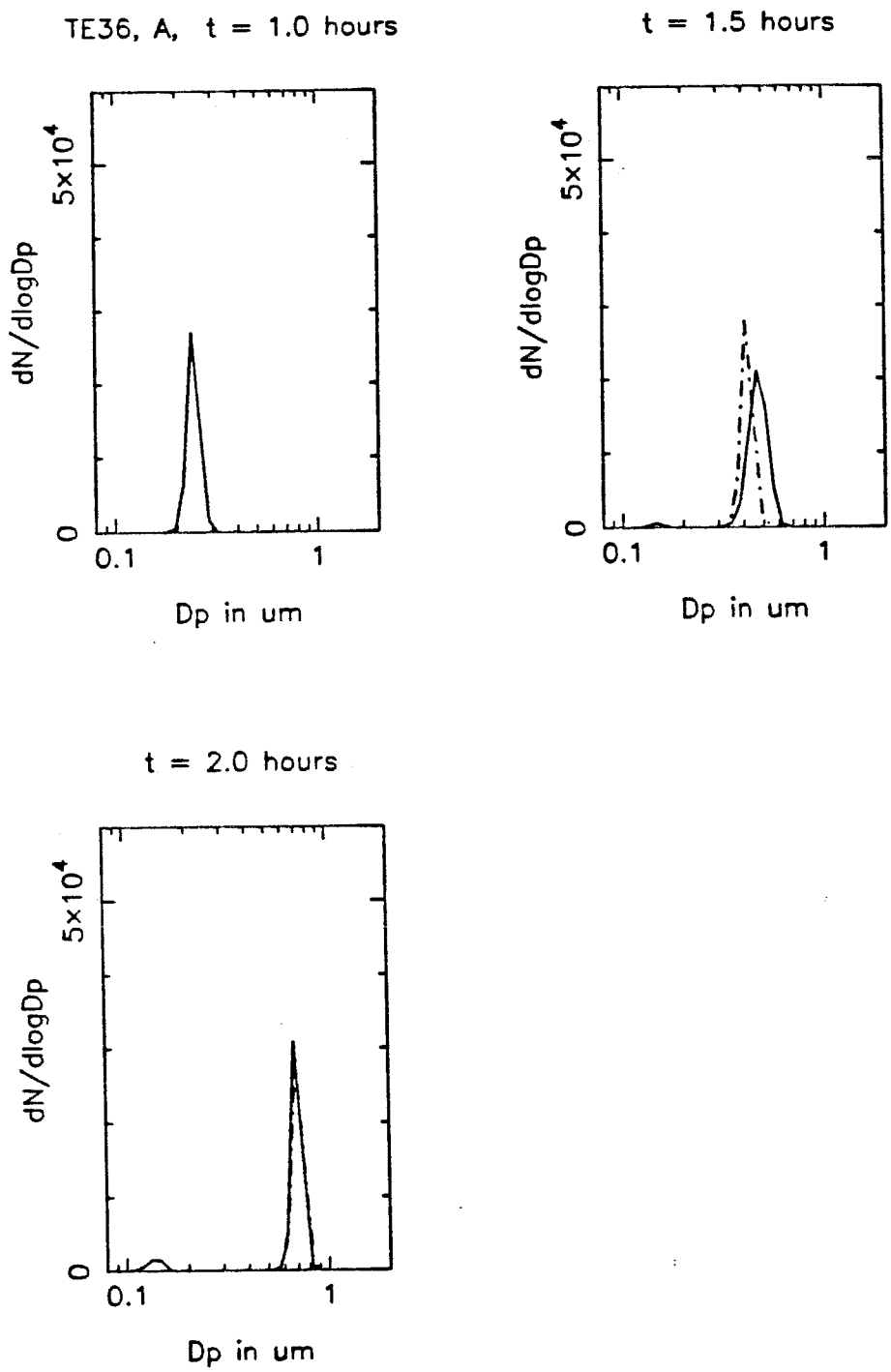

FIGURE 5.4. Predicted and observed aerosol number distributions at half-hour intervals for TE36,A, from $t = 1.0$ hours to $t = 2.0$ hours.

$\alpha = 0.98$, $H_\alpha = 3.01$

— observed, – · – predicted

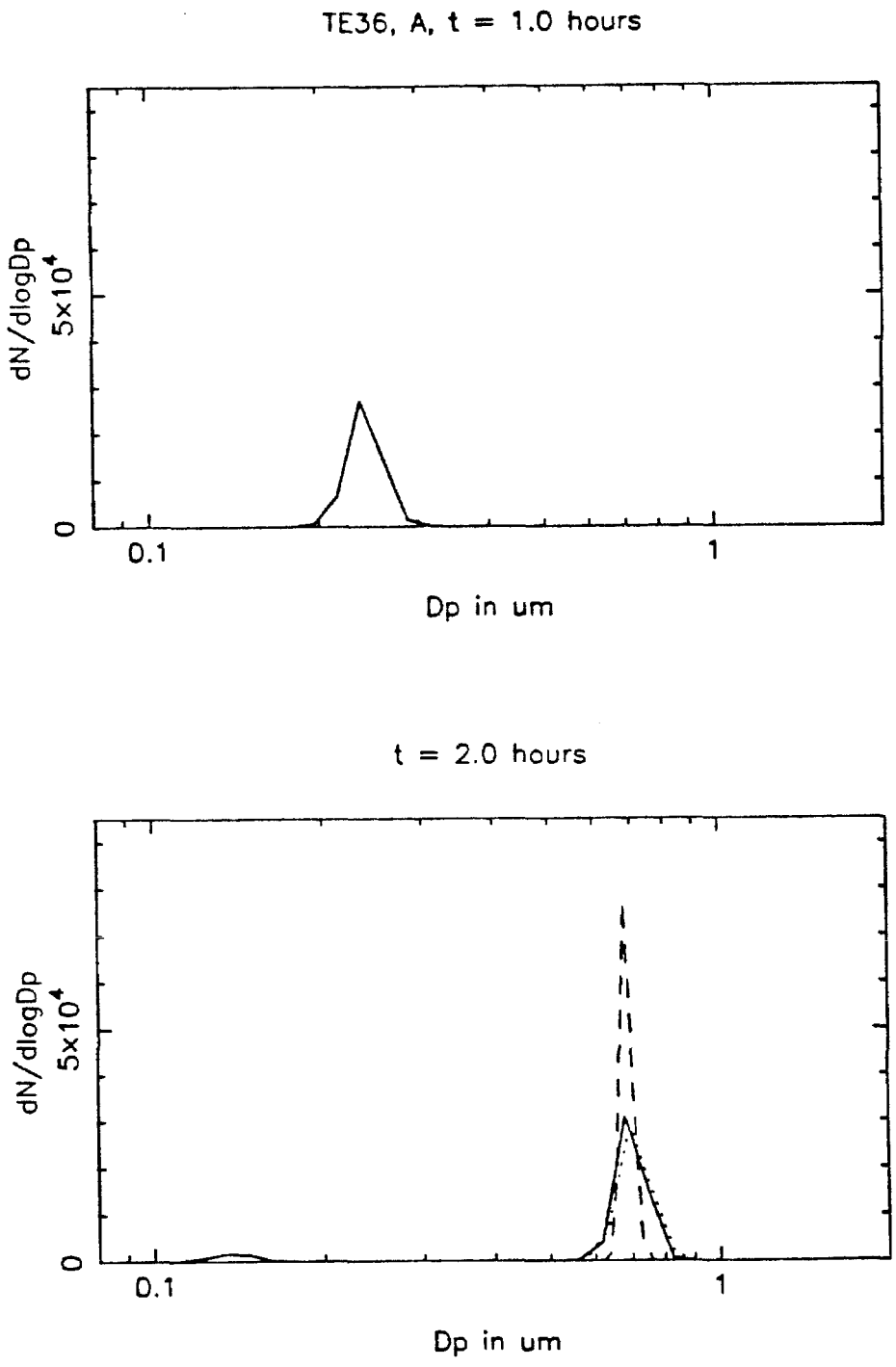

FIGURE 5.5. *Predicted and observed aerosol number* distributions at $t = 1.0$ hours and $t = 2.0$ hours.

$\alpha = \frac{2}{3}$, $H_\alpha = 1.07$ and $\alpha = 0.98$, $H_\alpha = 3.01$

— observed, $\cdots$ $\alpha = 0.98$, $- - -$ $\alpha = \frac{2}{3}$

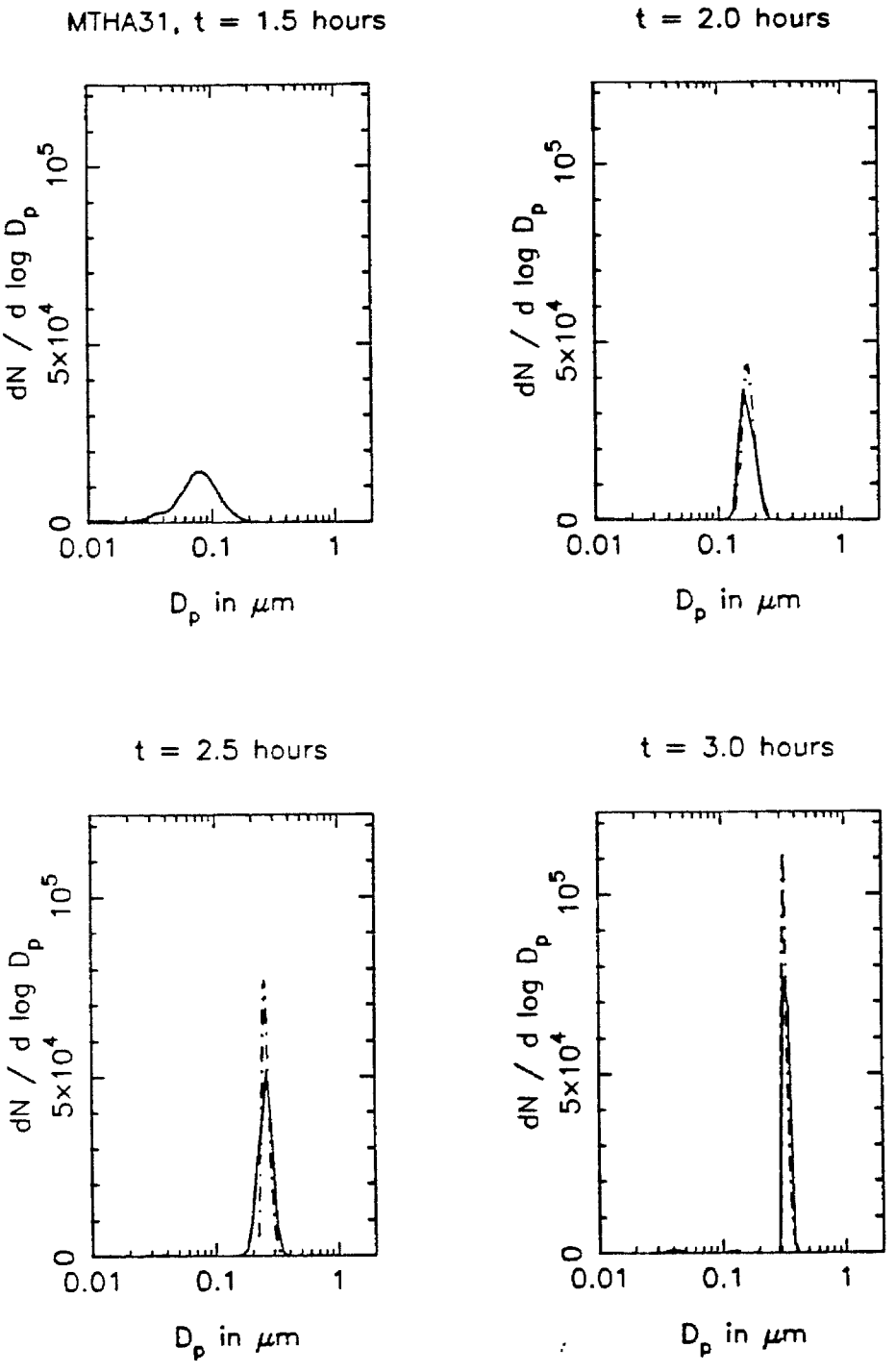

FIGURE 5.6. Predicted and observed aerosol number distributions at half-hour intervals for MTHA31, using full transition-regime growth law.

$t = 1.5$ hours to $t = 3.0$ hours, $p_A - p_s = 1.27 \times 10^{-4}$

— observed, – · – predicted

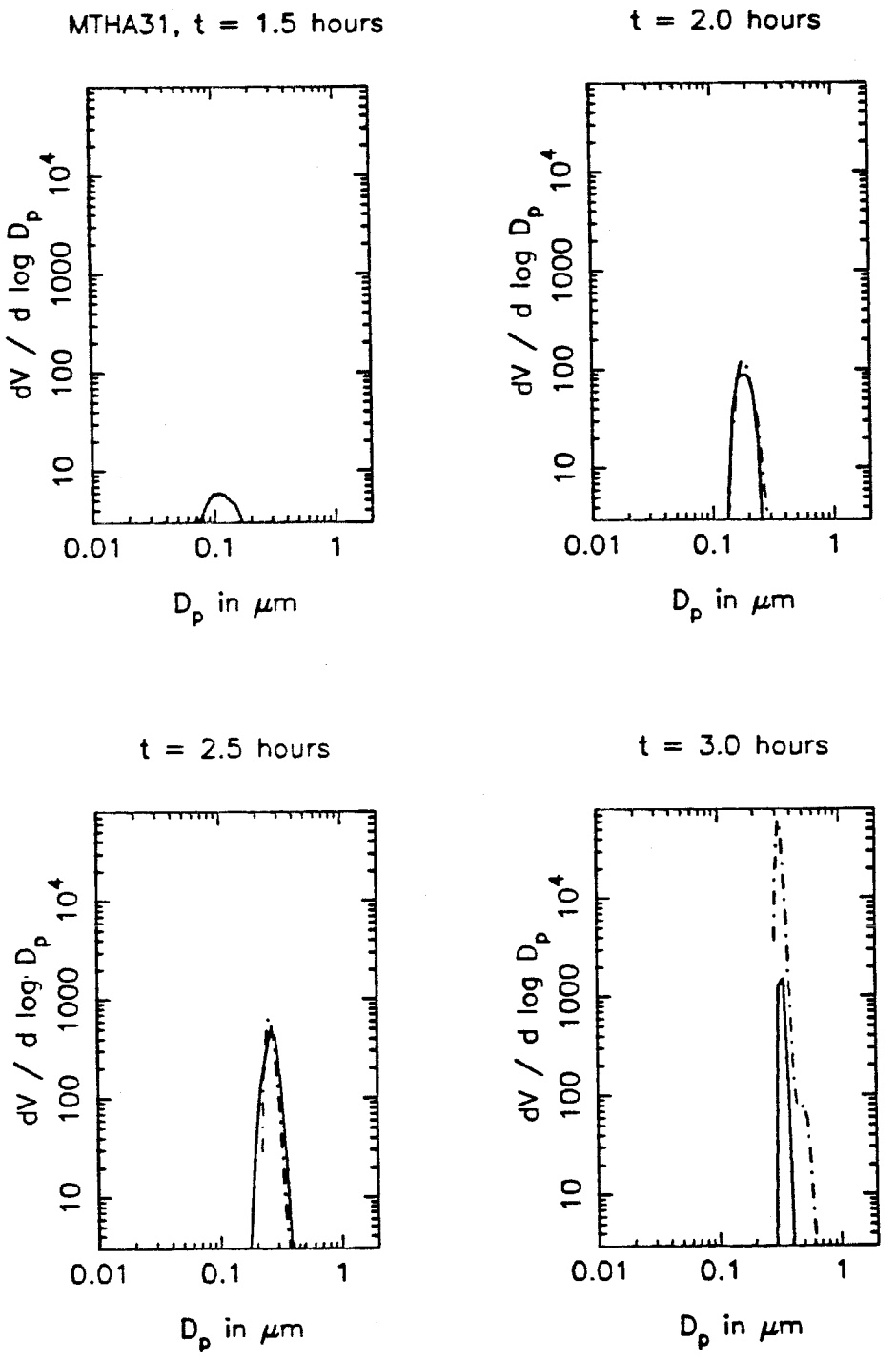

FIGURE 5.7. Predicted and observed aerosol volume distributions at half-hour intervals for MTHA31, using full transition-regime growth law.

$t = 1.5$ hours to $t = 3.0$ hours, $p_A - p_s = 1.27 \times 10^{-4}$

— observed, – · – predicted

CHAPTER 6

SIMULATIONS OF SIZE DISTRIBUTION EVOLUTION USING A SECTIONAL MODEL

6.1 Introduction

In the previous chapter, we considered the full size distribution evolution of the photochemical aerosol only for those experiments that exhibited uniform condensational growth. We now simulate the complete size distribution evolution over the course of an experiment, including with condensation the processes of nucleation and deposition. A powerful and convenient way of numerically simulating aerosol processes is the sectional solution of the GDE developed by Gelbard et al. (1980). The original sectional code, MAEROS (Gelbard, 1982) was extended in the code ESMAP (Warren and Seinfeld, 1985a) to include new particle formation by homogeneous nucleation and to treat intersectional condensation more accurately.

We describe here further alterations to the existing computer code to make it suitable for simulation of the smog chamber experiments. These simulations will be used to compare the number concentrations both predicted by the integral model and observed, in order to evaluate the performance of the simpler integral model for simulating organic aerosol formation as an alternative to the full size distribution model. In addition, we will compare the predicted and observed aerosol size distributions over the course of the experiments. This comparison will allow us to evaluate to what extent we can model the processes occurring in the smog chamber experiments.

6.2 Input Parameters for Modeling of Smog Chamber Experiments

For a sectional method simulation, the following information is needed: physical property data for the condensible species, including vapor pressure and surface tension, a vapor source rate, and an initial aerosol mass distribution. Minor modifications were made to ESMAP so that it was suitable for smog chamber simulations. Temperature was included as a direct input, so that a vapor pressure/temperature relation of the type obtained in the integral model calculations could be specified to fix the vapor pressure used in each simulation. An equation to couple the mass change in the vapor phase to the aerosol phase had been included in ESMAP for a constant vapor source; however, for our simulations we needed to use a varying source rate, as the generation of condensible vapor varied with time in the experiments. As in the integral model calculations, this vapor source was taken from the aerosol volume profile obtained experimentally. The source rate was determined by smoothing the aerosol volume versus time profile and interpolating between the times for which data were available.

The initial aerosol mass distribution is a critical input for the sectional model simulations. ESMAP requires the specification of the aerosol mass concentration in each section at $t = 0$. However, it is not possible to specify both mass and number concentrations for each section, since these are fixed relative to one another by the choice of section boundaries. The assumptions that the mass concentration profile is flat across each section gives, for section l:

$$N_l = Q_l \left(\frac{e^{-x_l} - e^{-x_{l+1}}}{x_{l+1} - x_l} \right), \tag{6.1}$$

where x is the logarithm of the mass of the particle, and N_l and Q_l are the number and mass concentrations in section l, respectively. Specification of the initial number and volume (or mass) distributions for each experiment, therefore,

can not be made independently.

Let us consider the nature of the feed aerosol distribution in a typical experiment. Figure 6.1 shows the number and volume distributions for the initial aerosol in side A of the dual-chamber m-xylene experiment, XJ19. Although both distributions are unimodal, the median diameters are very different. If we attempted to represent this distribution with one lognormal distribution centered at 0.03 μm, the median diameter for the number distribution, the volume distribution would not exhibit the large peak at 0.14 μm. Conversely, if we assumed a single mode of particles centered around 0.14 μm, the large number concentration of small particles would not be represented. The solution to this mismatch was to assume that the initial distribution consisted of two lognormal distributions, the sum of which produced the number and volume distributions in Figure 6.1.

A lognormal distribution is characterized by three parameters – ordinarily N, $\overline{D}_{p_g}$, and σ_g for a number distribution, and V, $\overline{D}_{p_g}$, and σ_g for a volume distribution, where $\overline{D}_{p_g}$ is a median diameter for the distribution and σ_g is the geometric standard deviation. Two lognormal distributions require 6 parameters, and for the modeling we choose N, V, $\overline{D}_{p_g 1N}$, $\overline{D}_{p_g 2V}$, σ_{g1} and σ_{g2}, where the subscripts 1 and 2 refer to the smaller and larger modes, respectively. Here, $\overline{D}_{p_g 1N}$ is the number-average diameter of the first mode, determined by the shape of the number distribution curve, $\overline{D}_{p_g 2V}$ is the volume-average diameter of the second mode, determined by the volume distribution curve, and σ_{g1} and σ_{g2} are the geometric standard deviations of each mode. For any lognormal distribution, the number-average and volume-average diameters are uniquely related by σ_g. Specification of N and V allows the determination of the number of particles and volume in each mode by conserving total number and total volume subject to the given diameters and standard deviations. The resulting distribution is shown in Figure 6.2, superimposed upon the experimental distribution.

Here we set $\sigma_{g1} = 1.7$, $\sigma_{g2} = 1.4$, $\overline{D}_{p_g1N} = 0.03\ \mu$m, $\overline{D}_{p_g2V} = 0.14\ \mu$m, $N = 8000\ \text{cm}^{-3}$, and $V = 1.06\ \mu\text{m}^3\ \text{cm}^{-3}$. The σ_g values were obtained by fitting a single lognormal distribution to each mode individually.

Generally, for all the experiments, the diameters and standard deviations of the initial aerosol did not vary significantly, indicating that the generation of the seed aerosol was fairly reproducible. Usually, $0.025\ \mu\text{m} \leq \overline{D}_{p_g1N} \leq 0.033\ \mu\text{m}$, $0.12\ \mu\text{m} \leq \overline{D}_{p_g2V} \leq 0.16\ \mu\text{m}$, $1.6 \leq \sigma_{g1} \leq 1.8$, and $1.3 \leq \sigma_{g2} \leq 1.6$. Therefore, we assumed $\overline{D}_{p_g1N} = 0.03\ \mu\text{m}$, $\overline{D}_{p_g2V} = 0.14\ \mu\text{m}$, $\sigma_{g1} = 1.7$, and $\sigma_{g2} = 1.4$, and input N and V for each experiment to obtain a representation of the initial aerosol distribution for that experiment.

The bimodal lognormal mass distribution obtained in this manner was converted to mass per section for use in ESMAP, and then normalized so that the total initial number concentration was conserved. As we showed previously, the number per section and mass per section can not be specified independently; without normalization the number concentrations obtained from the sectionalized mass distributions were approximately twice the experimental initial number concentrations. When the simulated and observed initial number concentrations were set equal, the resulting initial mass loading was lower than experimentally observed; however, since it represents such a small fraction of the eventual total mass in the system, the inaccuracy associated with this is unimportant. This point will be demonstrated later.

6.3 Predictions of Number Concentrations

Our first goal was to assess how the full size distribution simulation of number concentration compared with the number concentrations predicted by the integral model. We used the vapor pressure/temperature predictions from the SNM model calculations and the physical property assumptions about molecular weight,

surface tension, and particle density that we had used previously to carry out the initial sectional method simulations. The source rate was inferred from the aerosol growth information, and the initial distributions were obtained as outlined above. Coagulation was not included since, as previously shown, it is expected to be insignificant in these systems.

Figure 6.3 shows the predicted and observed final number concentrations for each of the original aromatic species. As in the discussion of the integral model results, the points that fall exactly on the dashed line represent those experiments where the inital aerosol loading suppressed nucleation entirely and the final number (both observed and predicted) equaled the initial number. We see from Figure 6.3 that the agreement between the predicted and observed number concentrations is generally within a factor of two. If we compare these results with Figure 4.4, the analogous predictions for the integral model simulations, we note that the amount of scatter is quite similar. This comparison shows that the two models are in substantial agreement; that is, the vapor pressures from the integral model, obtained by fitting the observed and simulated nucleation events, lead to similar amounts of nucleation when used in the sectional model.

Warren and Seinfeld (1985a) compared the integral and sectional models and found that the final number concentration predicted by the sectional model for a system with no initial particles and a constant vapor source was found to be higher than that predicted by the integral model by a factor of two to three. For systems both with and without initial particles, with a varying vapor source. we note, as earlier, that the sectional model generally predicts more nucleation in the system, with most points falling above the dashed line. This behavior is to be expected, since in the integral model, the assumption that the aerosol is monodisperse maximizes the predicted condensation rate, hence minimizing the nucleation rate. If we compare, for instance, the condensation rate for a lognormal

aerosol of the same total mass, M, and total number, N, as that of an equivalent monodisperse distribution, it can be shown that

$$R_{C,lognormal} = R_{C,monodisperse} \exp(-\ln^2 \sigma_g).$$

For a lognormal distribution with $\sigma_g = 1.6$, the condensation rate is 0.8 times that for a monodisperse distribution. Therefore, when we use the integral model vapor pressures in a full size distribution simulation, the predicted condensation rate will be lower because of the polydispersity, and therefore the predicted nucleation rate will be higher.

We can artificially depress the condensation rate in the integral model by a so-called "polydispersity factor," α_p. In order to determine whether the increased nucleation observed with the sectional model simulations results from using a full aerosol size distribution, the integral model calculations described in the previous chapter were repeated with the condensation rate given by:

$$R_{C,polydisperse} = \alpha_p \, R_{C,monodisperse}. \tag{6.2}$$

We set $\alpha_p = 0.8$, approximating the condensation rate for a lognormal distribution with $\sigma_g = 1.6$. Figure 6.4 shows the final number concentration predicted for each toluene experiment using the SNM model with $\alpha_p = 1.0$ (monodisperse), and with $\alpha_p = 0.8$, as well as the final number concentration predicted from the ESMAP simulations. We show only the toluene results as an example. Since we are interested in comparing the "polydisperse" SNM and the ESMAP predictions of number concentration, these are both plotted against the monodisperse SNM results. The final number concentrations predicted by both simulations with polydisperse aerosols are higher than those predicted by the monodisperse integral model, and are, in fact, quite close to one another. These findings demonstrate that the greater nucleation predicted when using the integral model vapor pres-

sures with the sectional model can be attributed to the polydisperse representation of the aerosol in the system.

We calculated the best-fit vapor pressure/temperature relationship for the set of toluene experiments using the sectional model, to compare with those obtained from the integral model. These predictions of vapor pressure based on the sectional model are shown in Figure 6.5, along with the best-fit vapor pressures from the integral model. We expect that the vapor pressures predicted using the sectional model will be somewhat higher than those predicted with the integral model, since species with higher vapor pressures produce fewer particles when condensation and nucleation are competing for the same source of condensible vapor. A higher vapor pressure will decrease the saturation ratio for the same gas-phase partial pressures of condensible vapors, hence decreasing the nucleation rate. The best-fit vapor pressure/temperature lines for both models are also given in Figure 6.5. We note there is a slightly stronger temperature dependence in the sectional model predictions.

As an additional note with regard to these simulations, we find, as in the integral model discussion, that nucleation is underpredicted in systems with initial particles, as was found with the integral model. This question remains unresolved.

6.4 Simulations of Size Distribution Evolution

We shall now consider the predictions of the full size distribution evolution of several representative experiments. First, we will consider an experiment in which there was no observed nucleation, to evaluate the simulated behavior of a growing aerosol. This experiment will be used to evaluate the effects of different assumptions for the initial aerosol mass loading. The simulation of an experiment with no initial particles allows us to evaluate the representation of the nucleation event and the resulting single mode of secondary aerosol. Finally, we will con-

sider an experiment with seed aerosol and a burst of nucleation, which allows the simulation of both primary and secondary modes of aerosol.

Figure 6.6 shows the total aerosol number and volume concentrations as a function of time for the m-xylene experiment, XJ19, side A. There were 7400 cm^{-3} initial particles in the system, with a total volume of 0.82 μm^3 cm^{-3}. In this experiment, there was no observed nucleation. The total number decays with time as particles are lost by deposition, while the total volume increases early in the experiment and then eventually decreases because of depositional loss. The evolution of the aerosol volume distribution is shown in Figure 6.7. These simulations were performed with 18 sections per decade in particle diameter over two decades, evenly spaced on a logarithmic diameter axis. The experimental distributions shown are the inverted data averaged over a $\pm$7.5-minute interval. After one hour, the primary aerosol has increased in size and in total volume, and the simulated distribution is quite close to that observed. After 2.0 hours of growth, and after 3.5 hours, the observed distribution has narrowed considerably more than the simulated distribution because of numerical diffusion inherent in the sectional representation of condensation in ESMAP.

In order to evaluate the effect of the starting volume distribution used in the simulations on the predicted distributions, we considered a variety of initial distributions in one simulation. We carried out the m-xylene simulation described above with three different initial distributions: the normalized sum of lognormals, as outlined in Section 6.2, the unnormalized initial mass distribution, which conserves total volume but not total number, and an exact duplication of the observed initial volume distribution, which neglects the large mode of smaller particles. Each of these starting distributions is shown in Figure 6.8. The initial number concentrations for these three cases are 7.4×10^3 cm^{-3} (the correct initial number concentration), 1.40×10^4 cm^{-3}, and 7.53×10^3 cm^{-3}.

The simulated mass distributions after 3.5 hours of growth are shown in Figure 6.8 along with the observed distribution. The main differences in the simulated distributions at this point arise from the different initial number concentrations. The two distributions that start with approximately 7500 cm^{-3} initial particles look almost identical after growth has occurred, yet their initial volume distributions are not similarly shaped, nor is the total volume initially the same. The initial number concentration is close to the observed initial number only coincidentally. The unnormalized initial distribution produces a distribution after growth has occurred that is similar in shape to the other two but has a much smaller median diameter. Because of the increased number of initial particles, each can not grow as large. From these simulations it appears that matching the shape of the initial volume distribution is not as important as matching the initial number concentrations. The normalized sum of lognormals is therefore an excellent choice for a starting distribution, since it reproduces approximately both the number and volume distributions while conserving initial number.

The total number and total volume profiles for one side of a dual-chamber toluene experiment (DQXA57, side B) are shown in Figure 6.9. There were no initial particles in this system, and nucleation was observed after approximately 1.5 hours. We present in Figure 6.10 the simulated volume distributions for this experiment. At $t = 1.5$ hours, no secondary aerosol is evident, but at $t = 2.0$ hours new particles have formed and grown to over 0.1 μm in size. The simulated volume distributions at 2.0 hours and at 3.5 hours show approximately the same average diameters as the observed distributions, but are much broader.

Figure 6.11 shows the evolution of the volume distribution for the single-chamber toluene experiment, HTLA41. In this experiment there were approximately 3000 cm^{-3} initial particles, and nucleation was observed late in the experiment, beginning at $t \approx 3.5$ hours. After 2.5 hours of growth, the primary aerosol

has increased in size and in volume, and the simulated distribution is somewhat broader than the observed distribution. After 4.0 hours, the burst of new particles appears, in both the observed and the predicted distributions. We see, however, that after 5.0 hours the resolution of the two modes is lost in the simulated distribution, while the experimental distribution still retains separate primary and secondary aerosol modes. This is another illustration of the numerical diffusion associated with the sectional method.

6.5 Conclusions

We have shown that the sectional model calculations of number concentration agree reasonably well with the integral model calculations, but predict a slightly higher number of nucleating particles for the same input vapor pressures. This behavior can be attributed to the decrease in condensation rate that attends a polydisperse rather than a monodisperse aerosol. Such a decrease leads to an increase in nucleation rate, since the two processes are in competition for the available vapor. Re-predicting the vapor pressures as a function of temperature using the sectional model yields results that are qualitatively similar to those of the integral model. In predicting the time evolution of the volume distribution, we found that the sectional solution method produced significant amounts of numerical diffusion, which is a limiting feature of current versions of the method.

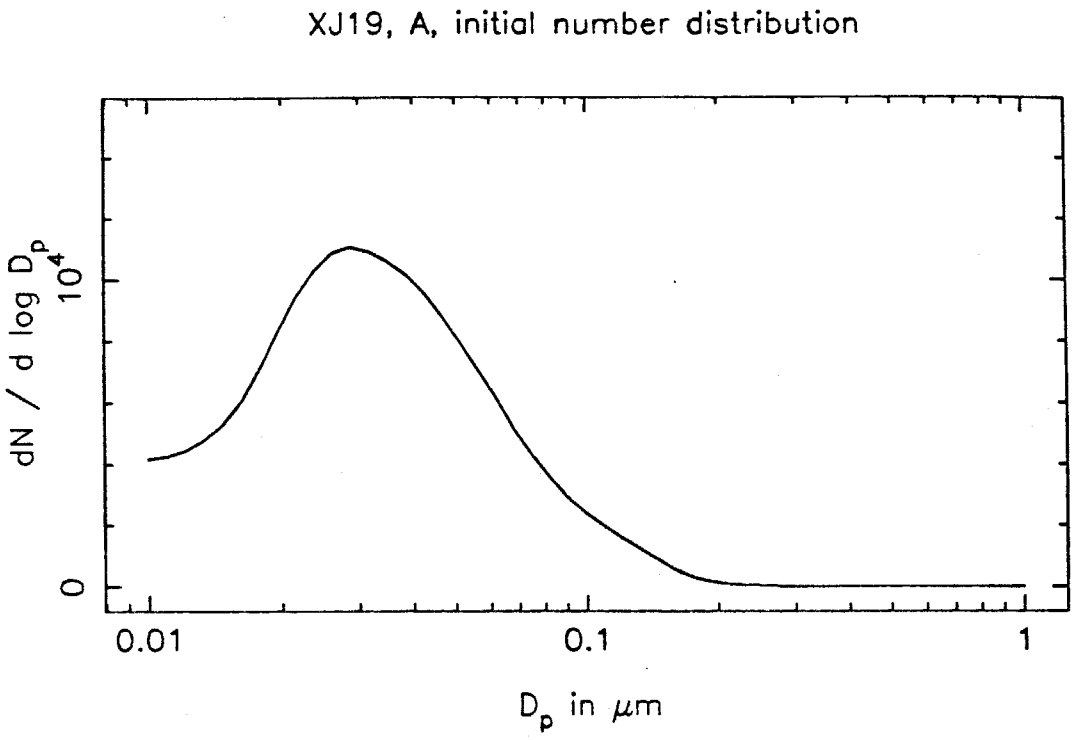

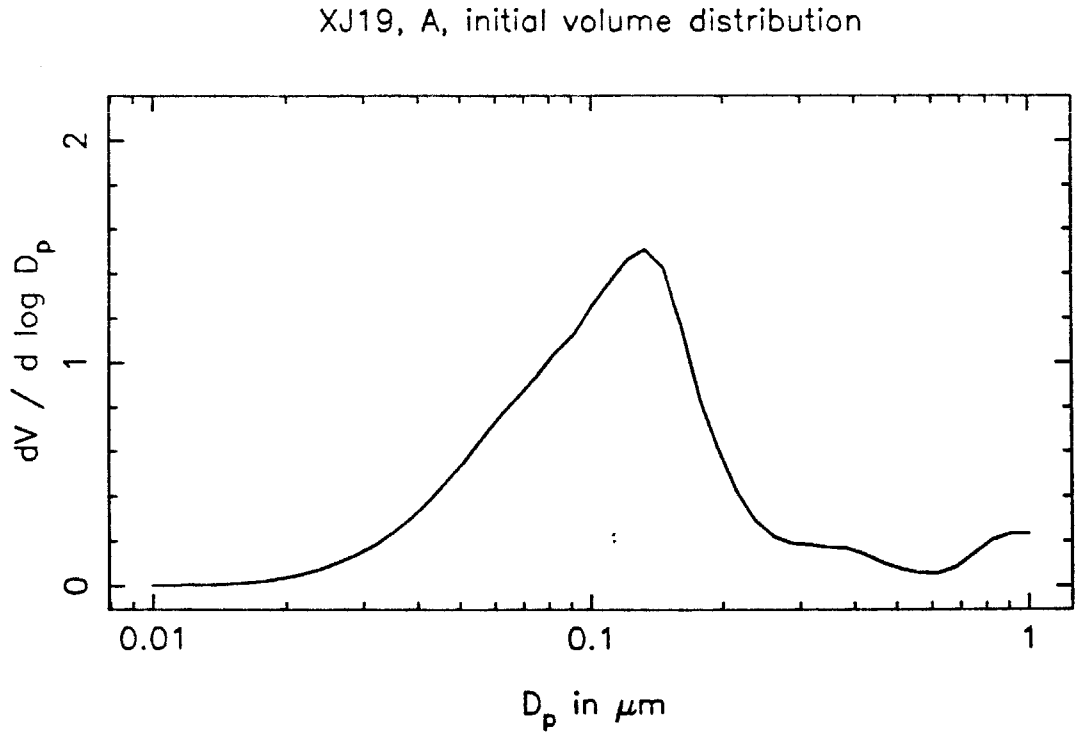

FIGURE 6.1. Initial aerosol number and volume distributions for the experiment XJ19, A.

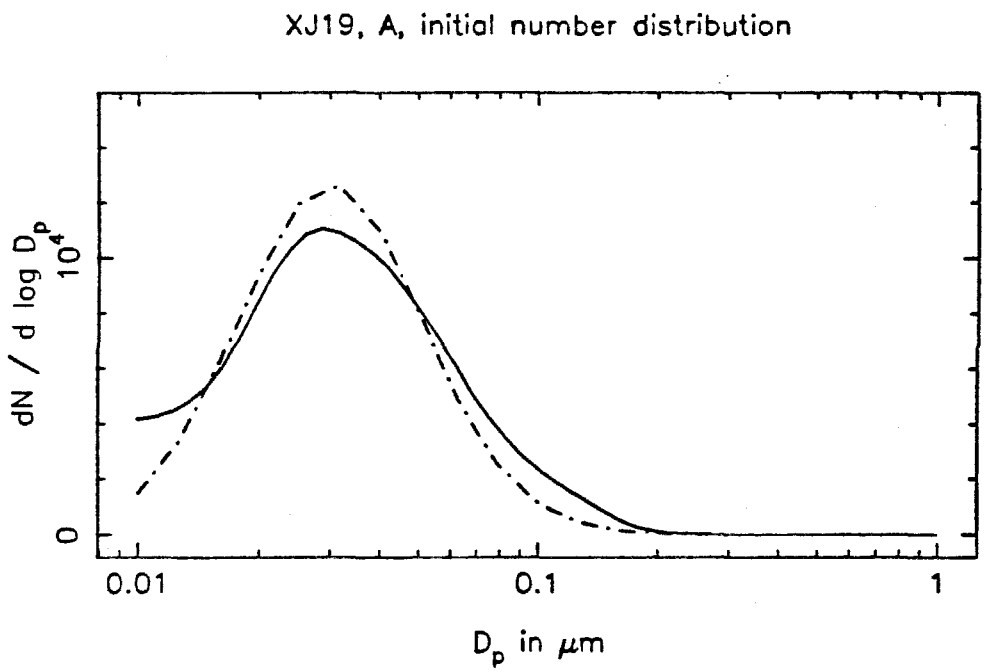

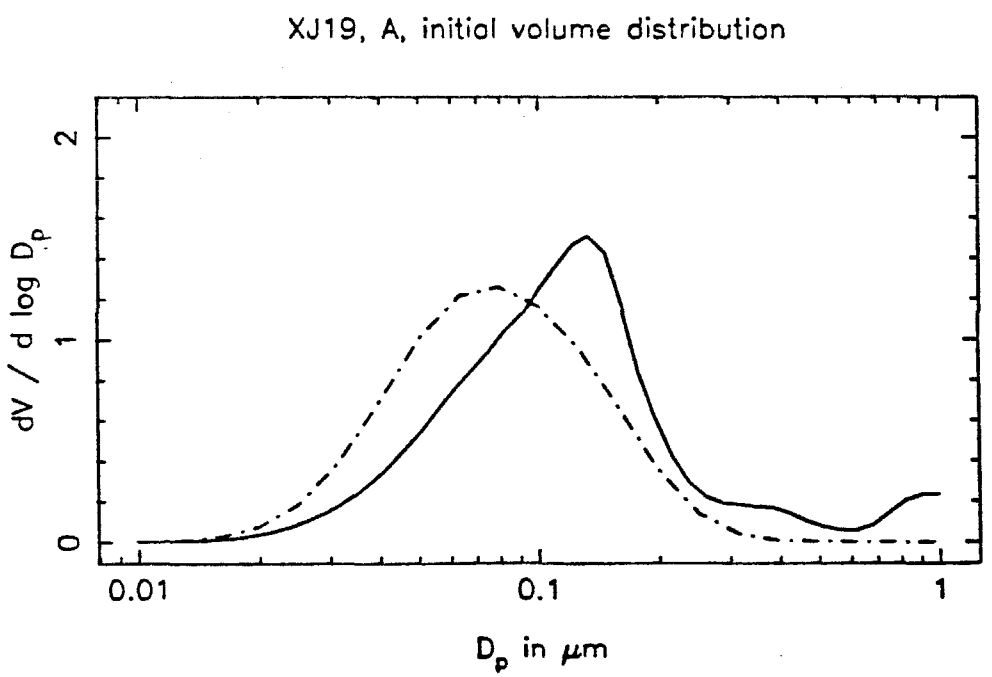

FIGURE 6.2. Sum of two lognormal distributions representation of the initial number and volume distributions for XJ19, A.

— observed distributions; - · - simulated bimodal distributions

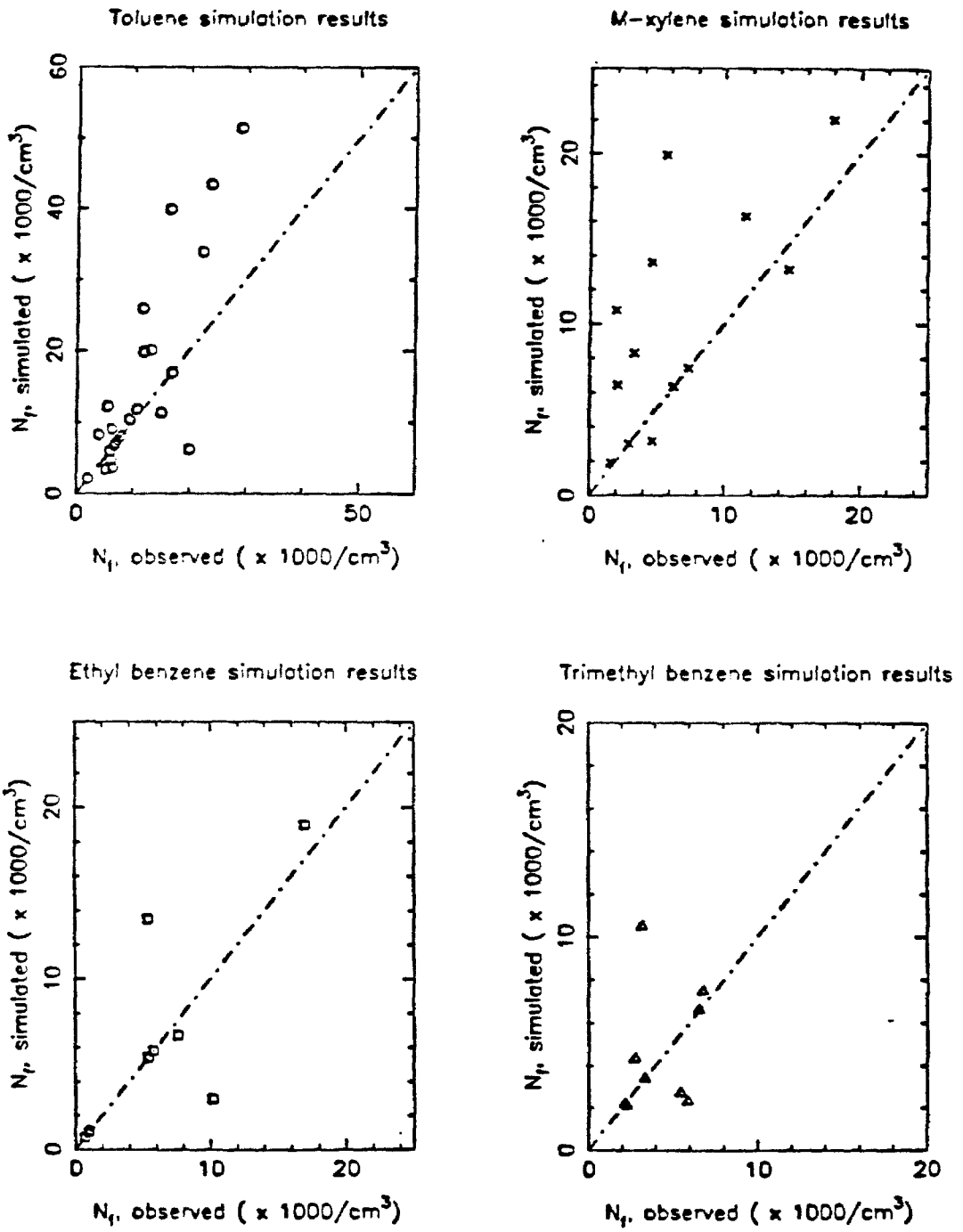

FIGURE 6.3. Predicted and observed final or maximum aerosol number concentrations for all experiments.

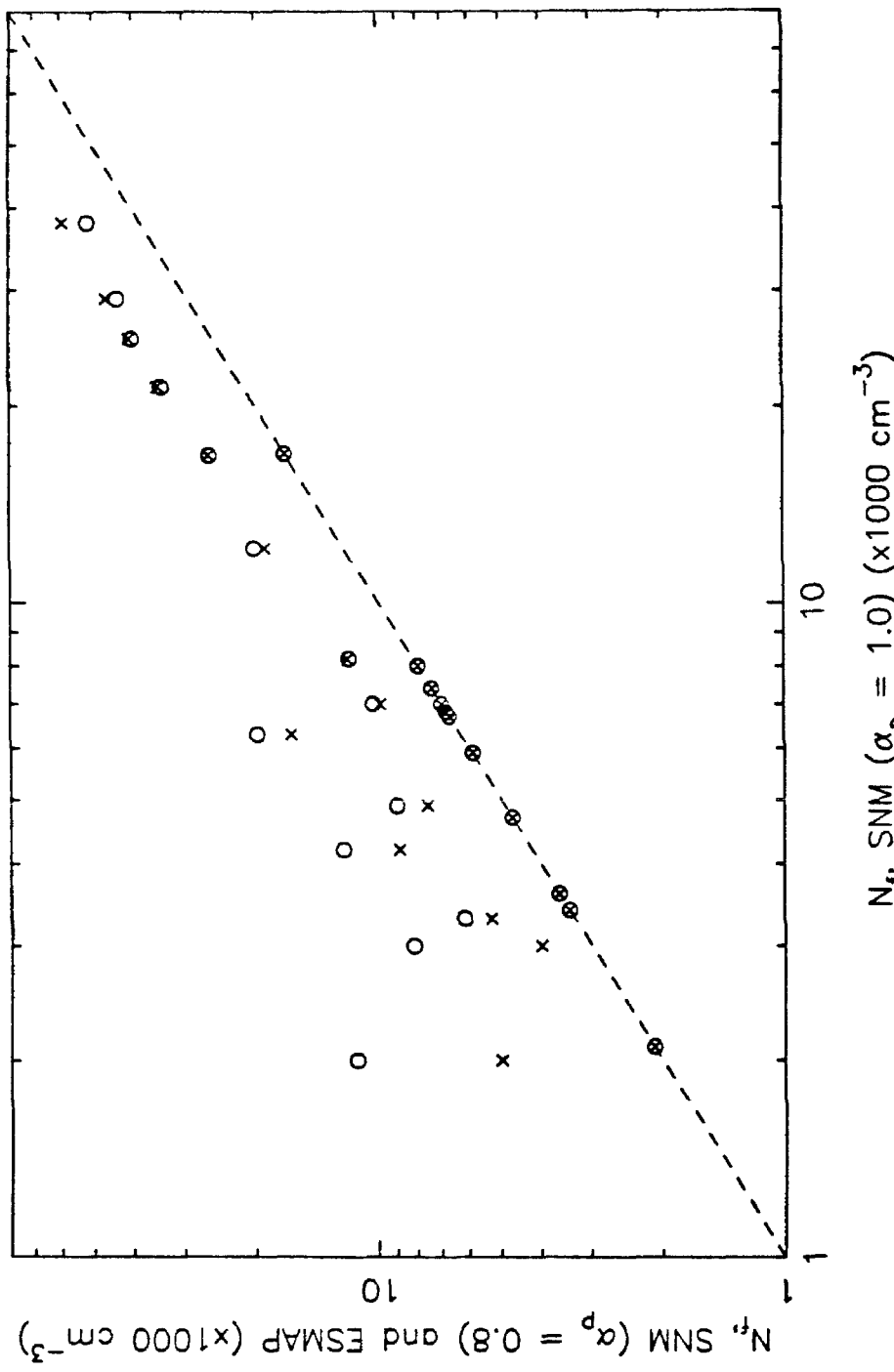

FIGURE 6.4. Predictions of final number concentrations for integral and sectional models for all toluene experiments.

×: integral model, $\alpha_p = 0.8$; o: sectional model

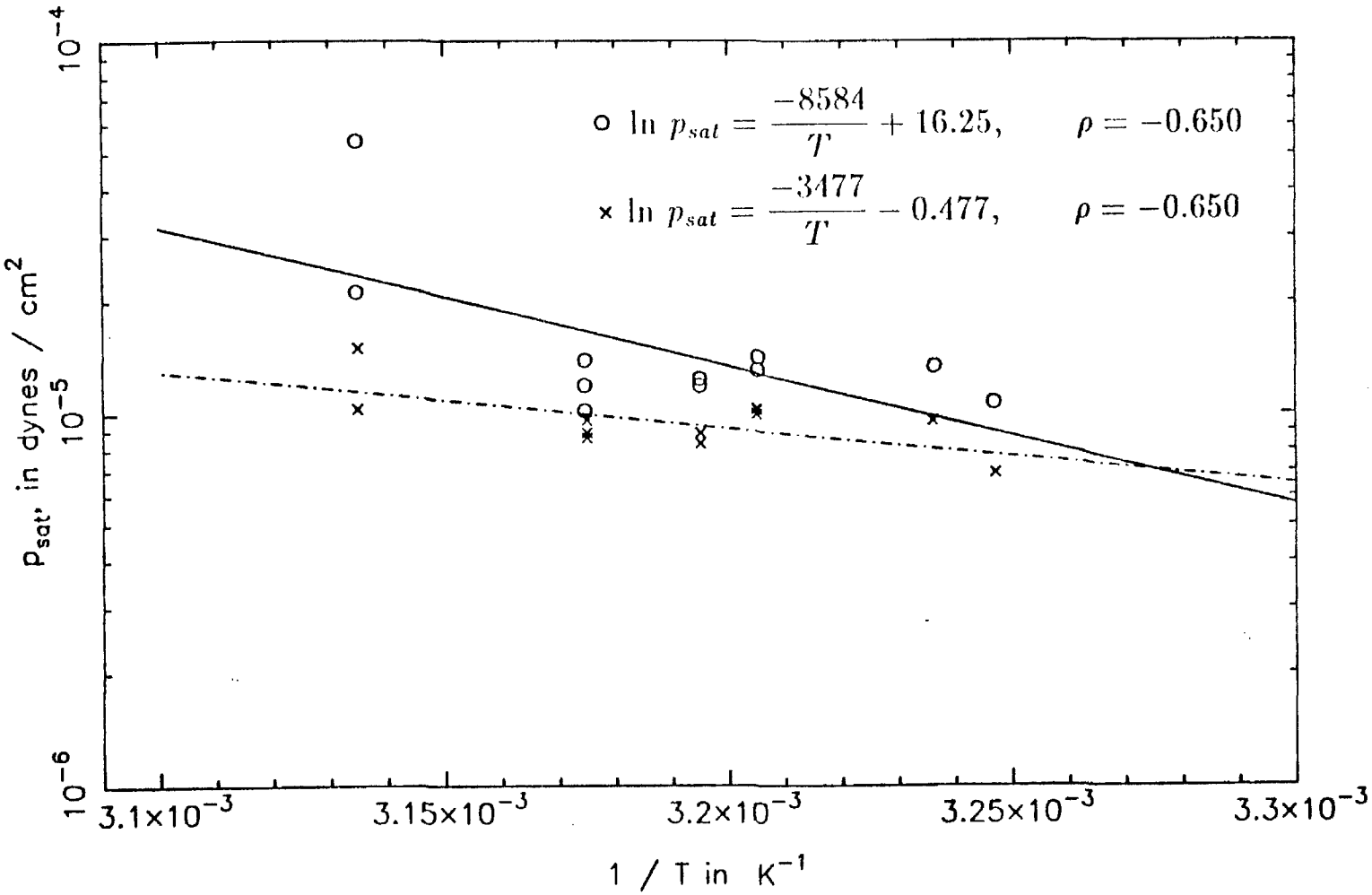

FIGURE 6.5. Vapor pressures as a function of inverse temperature for toluene aerosol constituents for integral and sectional models, including best-fit lines.

×: integral model; o: sectional model

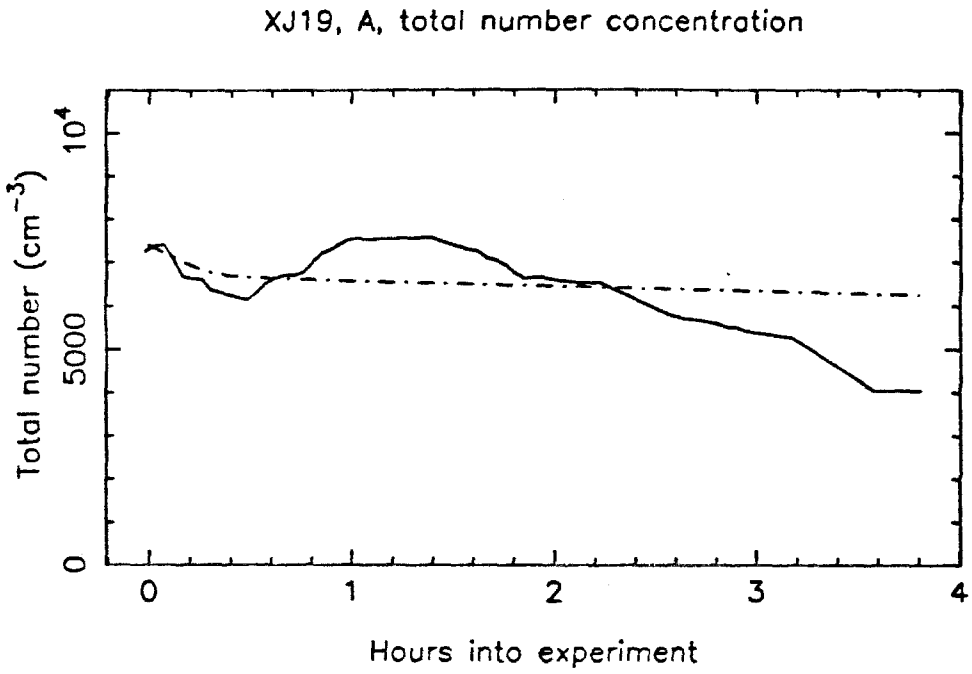

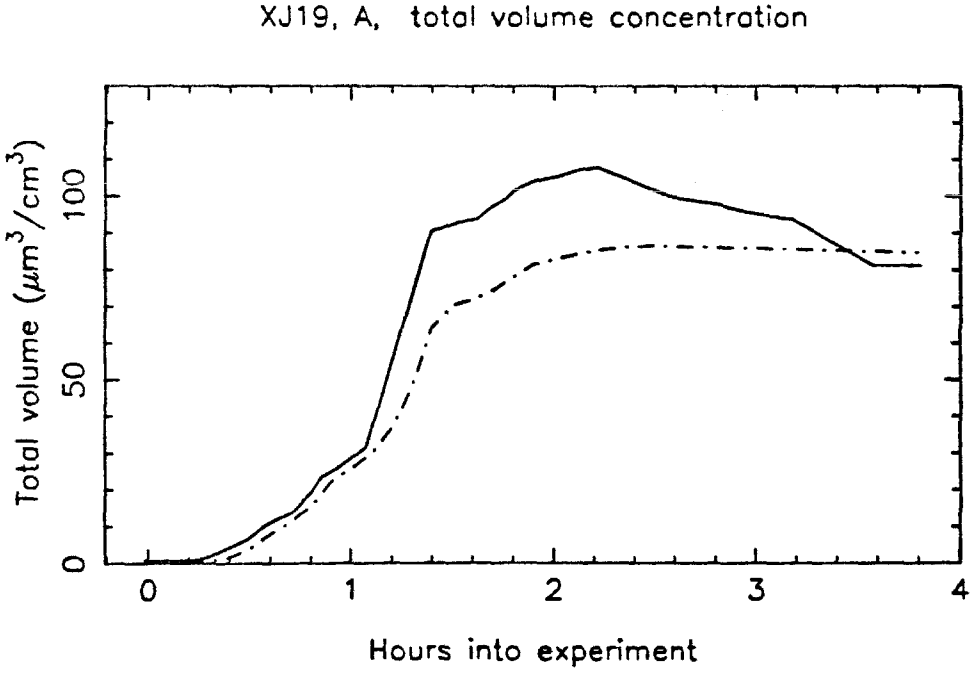

FIGURE 6.6. Predicted and observed total aerosol number and volume concentrations as a function of time for experiment XJ19, A.

— observed, - - - predicted

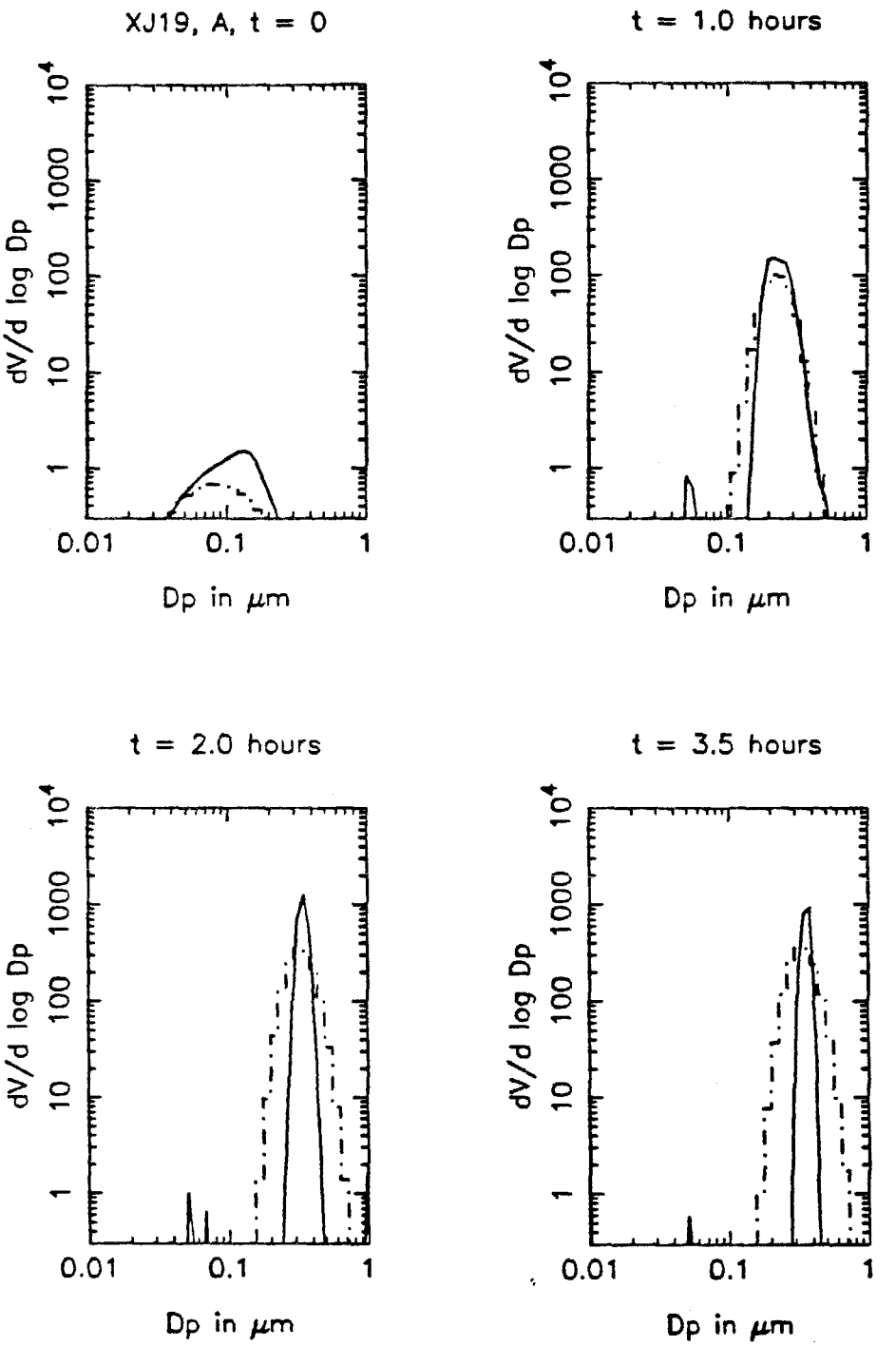

FIGURE 6.7. Predicted and observed aerosol volume distributions for XJ19, A, at $t = 0$, $t = 1.0$ hours, $t = 2.0$ hours, and $t = 3.5$ hours.

— observed, - - - predicted

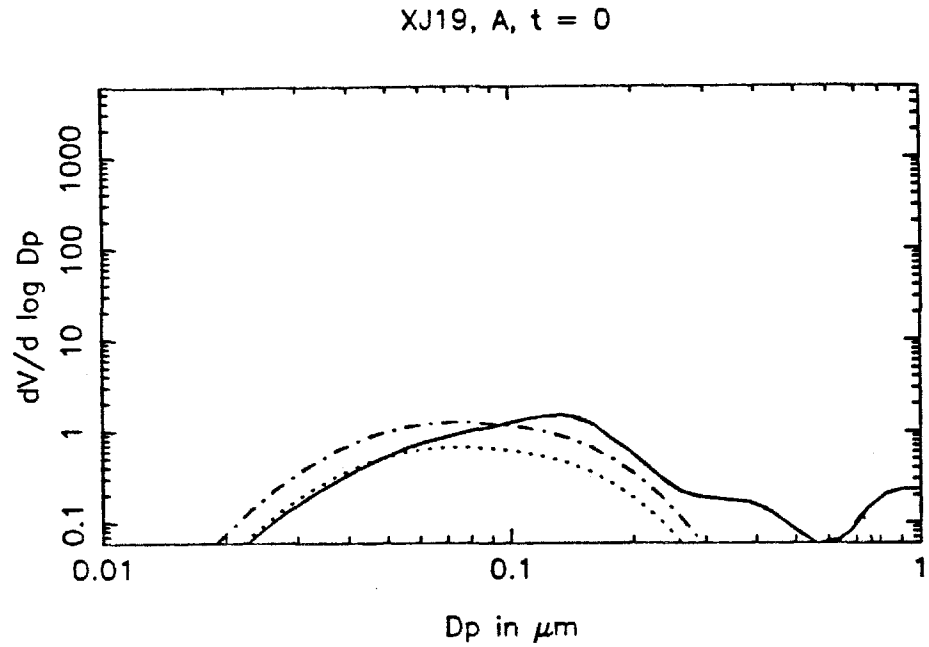

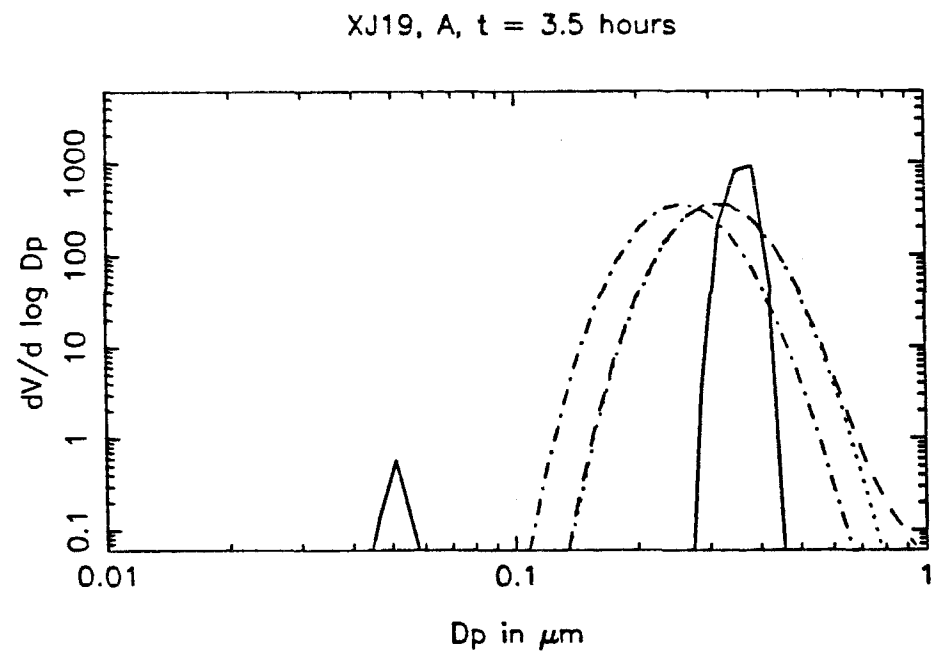

FIGURE 6.8. Predicted and observed volume distributions for XJ19, A, at $t = 0$ and $t = 3.5$ hours, showing the effect of initial distribution assumptions. — observed, ··· normalized sum of lognormals, – · – unnormalized sum of lognormals, – – – exact initial volume distribution

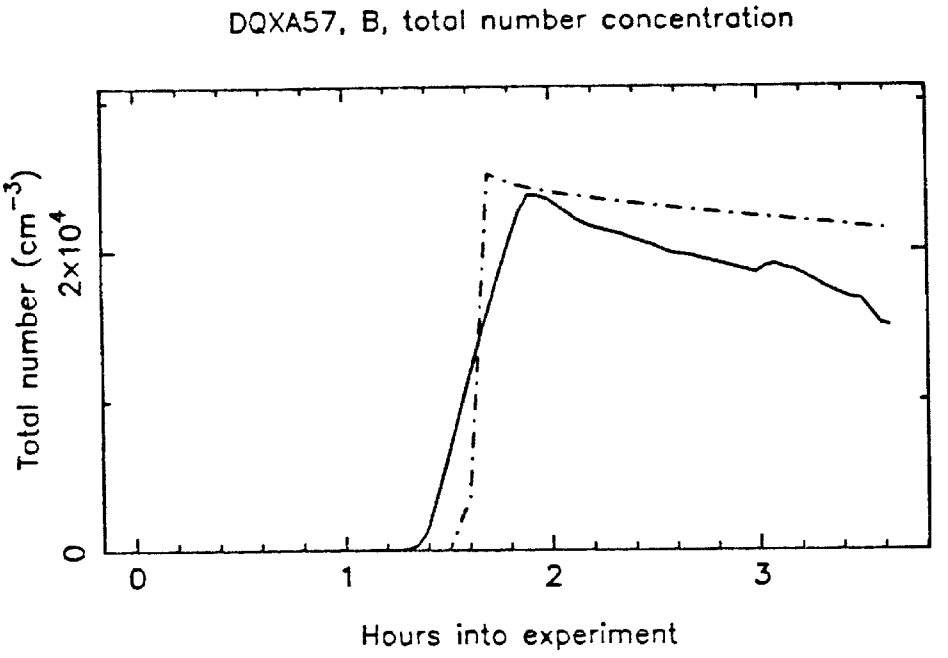

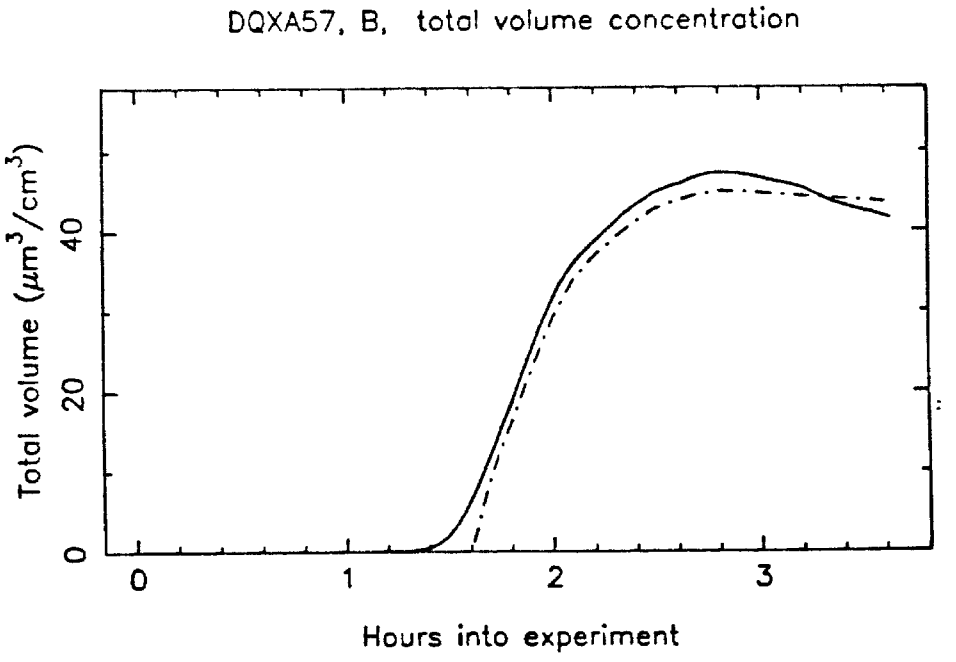

FIGURE 6.9. Predicted and observed total aerosol number and volume concentrations as a function of time for experiment DQXA57, B.

— observed, - - - predicted

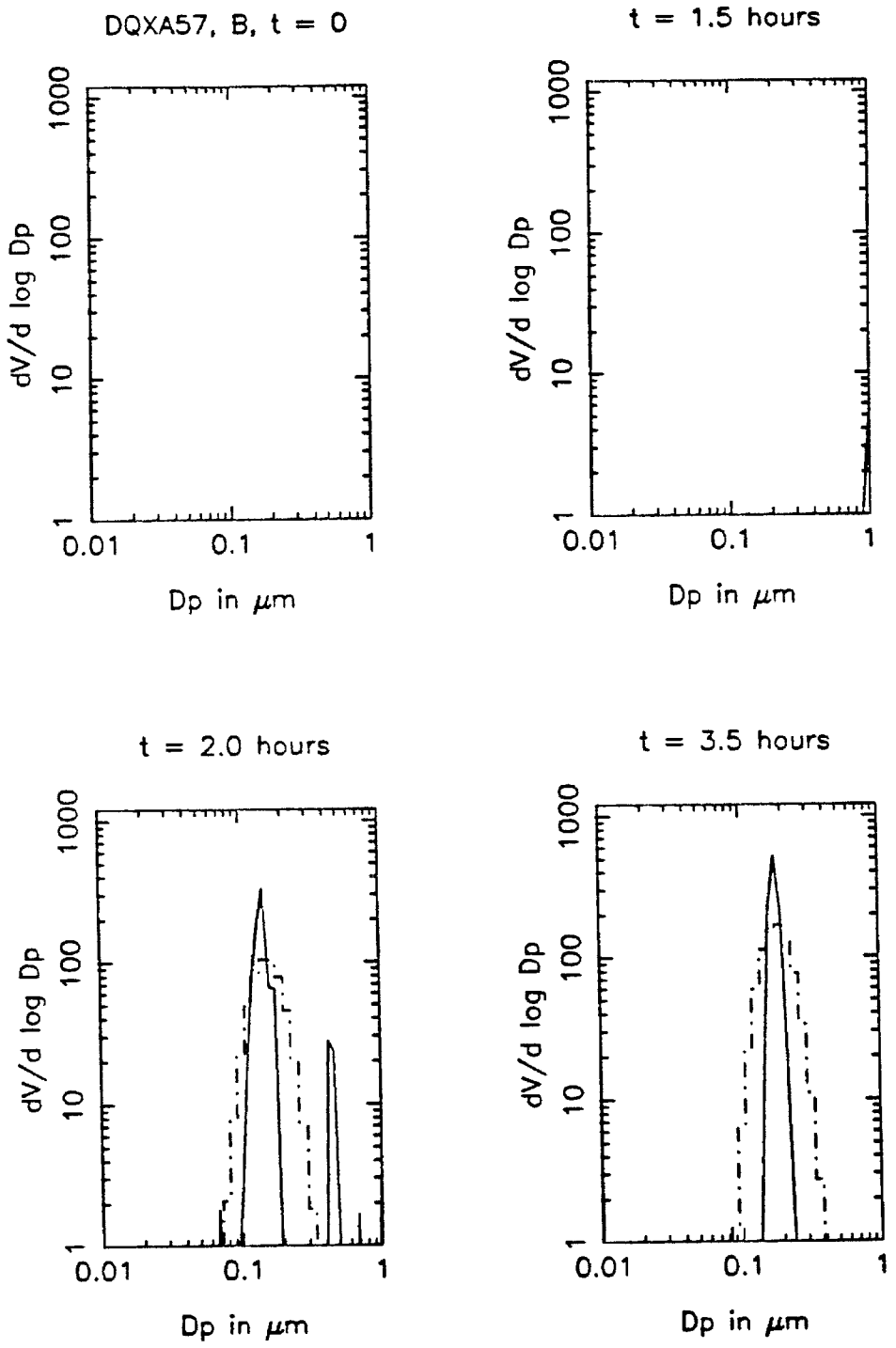

FIGURE 6.10. Predicted and observed aerosol volume distributions for DQXA57, B, at $t = 0$, $t = 1.5$ hours, $t = 2.0$ hours, and $t = 3.5$ hours.

— observed, - - - predicted

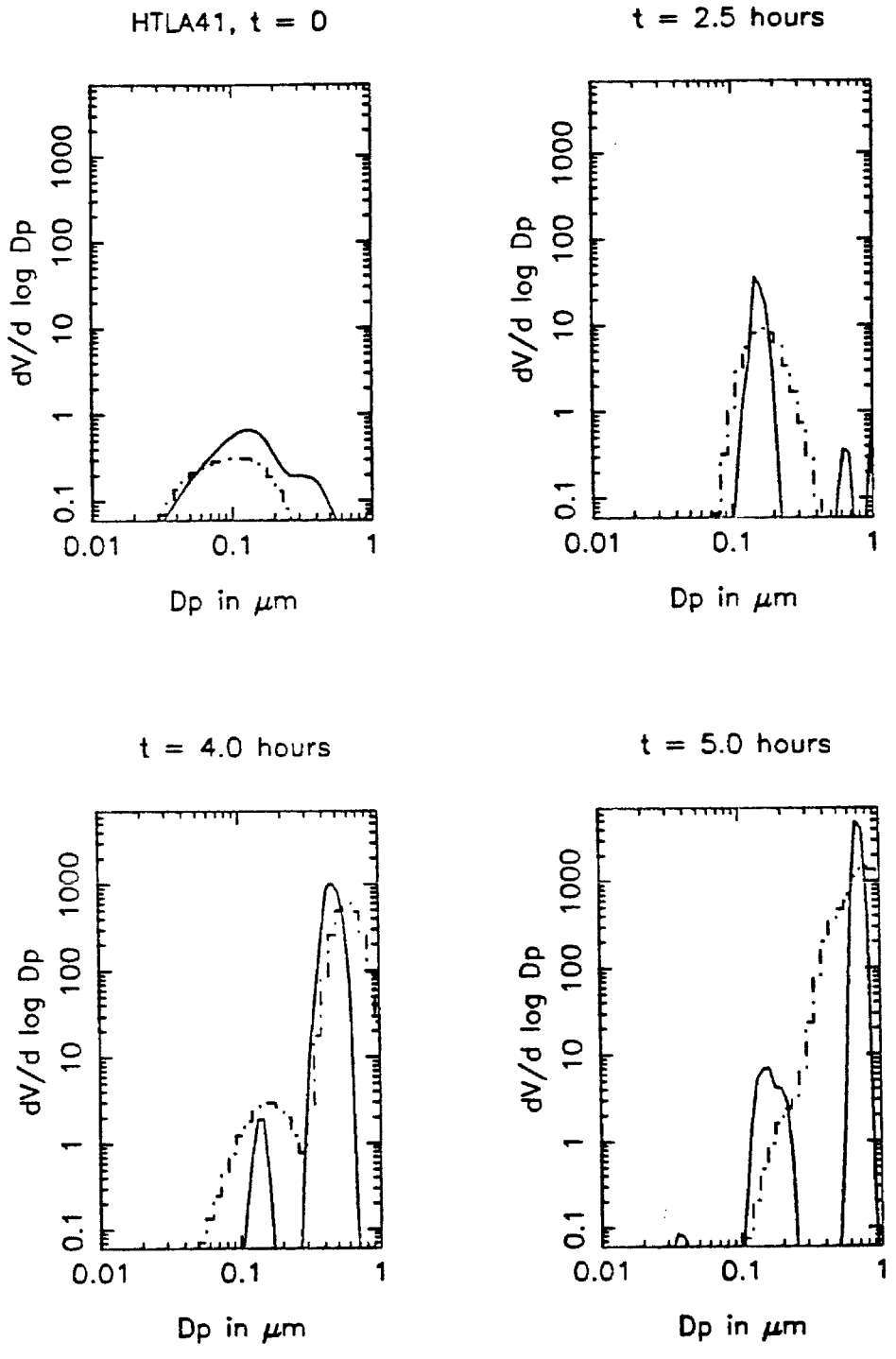

FIGURE 6.11. Predicted and observed aerosol volume distributions for HTLA41, at $t = 0$, $t = 2.5$ hours, $t = 4.0$ hours, and $t = 5.0$ hours.

— observed, - - - predicted

CHAPTER 7

CONCLUSIONS AND RECOMMENDATIONS FOR FURTHER STUDY

7.1 Summary

We have carried out an extensive experimental study of secondary organic aerosol formation and growth in aromatic hydrocarbon/NO_x systems. Outdoor smog chamber experiments were designed to study the gas-phase reaction kinetics, the aerosol physics, and the aerosol-forming potential of the photooxidations of toluene, m-xylene, ethyl benzene, and 1,3,5-trimethyl benzene. Aerosol data were collected at approximately 3-minute intervals during each several-hour experiment, generating a significant data base for modeling studies.

A multi-instrument inversion routine was developed to determine the aerosol size distributions from the raw data throughout each experiment. This routine performs a series of smoothed-Twomey iterations (Twomey, 1975; Markowski, 1987) on the combined electrical aerosol analyzer and optical particle counter observations to produce an estimate of the aerosol size distribution in the system at each sample time. Such a multi-instrument inversion has not been reported previously.

Several aerosol models were used to describe the observed aerosol dynamics. The integral (SNM) model developed by Warren and Seinfeld (1984, 1985b) was used to determine saturation vapor pressures for the condensible species in the system by fitting the observed nucleation events as a function of temperature. Physical property data for these systems must be estimated from the observed aerosol dynamics in the absence of molecular composition information for the condensible vapors. Predictions of final number concentrations for each experiment obtained

using these vapor pressures were very close to the observed number concentrations, except in some systems with initial aerosol where nucleation was observed. For these experiments, the integral model generally underpredicted the observed amount of nucleation. Expansion of the model to include two condensible species with different vapor pressures could not account for the observed nucleation.

Preliminary size distribution simulations were performed using a growth-law analysis of the experiments that included periods of steady condensational growth. An analytical solution of the Condensation Equation (Williams, 1983) was used with two different growth laws to explore the mechanism of growth in these systems. From a power-law approximation of the growth law, it was found that the experiments exhibited behavior consistent with diffusion-limited growth in the free-molecular regime. Since the aerosol particles were generally too large to be considered free-molecular, the analysis was repeated using the full transition-regime growth expression. Vapor-phase partial pressures were obtained by fitting the predicted and observed evolution of the size distribution; these, when compared with the integral model vapor pressures, gave apparent saturation ratios in the system. These saturation ratios were found to be in the range of 4 to 20, a reasonable range for condensational growth to be occurring.

A full size distribution simulation of the experiments was carried out using the sectional model ESMAP (Warren and Seinfeld, 1985a), which is an extension of the code MAEROS (Gelbard, 1982). Predictions of final number concentration using the integral model vapor pressures were higher with the sectional model than with the monodisperse integral model; this is because the predicted overall condensation rate is lower for a polydisperse aerosol, leading to higher nucleation rates. Comparisons of the predicted and observed size distribution evolutions were difficult because of numerical diffusion limitations of current versions of ESMAP.

7.2 Nucleation in the Atmosphere

One of the goals of this work was to determine whether homogeneous nucleation of organic aerosol occurs in the atmosphere. From the experiments and the simulations, we can estimate the physical parameters needed to carry out a simulation of atmospheric aerosol dynamics, for the formation of secondary organic aerosol from aromatic hydrocarbons. We will use a typical atmospheric aerosol and the sectional code ESMAP to estimate whether nucleation does, in fact, occur in the atmosphere or whether most secondary organic aerosol is formed by condensation onto existing particles.

An aerosol volume distribution on a typical Los Angeles day was obtained from Larson (1988) to use as the starting distribution for ESMAP. As in the previous calculations in this study, the aerosol density was assumed to be 1.0 g cm^{-3}, the molecular weight of the condensible organic, 150 g $mole^{-1}$, and the surface tension, 30 dynes cm^{-1}. Aerosol deposition in the system was taken to be the same as observed in the smog chamber. The vapor pressure was assumed to be 1×10^{-5} dynes cm^{-2}, approximately the value found for the smog chamber experiments, and the temperature was set at 300 K. The source rate of condensible vapor was assumed constant, and set to 0.02 μg m^{-3} sec^{-1}. This was an average source rate for the aromatic concentrations in the smog chamber experiments, and should be significantly higher than that for the atmosphere, where the quantity of initial aromatic hydrocarbon is much lower than in the experiments. Atmospheric concentrations of aromatic hydrocarbons are on the order of 50 ppb (Grosjean and Fung, 1984), and the smog chamber concentrations of aromatics were approximately 2 ppm; the source rate of condensible organics in the smog chamber is therefore approximately 40 times that expected in the atmosphere. Using the smog chamber source rate in the simulation should give us an upper bound for

the source rate of condensible vapors in the atmosphere. The calculation was carried out for four hours of simulation time. No explicit particle sources were included; the only new particles introduced into the system were those generated by homogeneous nucleation.

Figure 7.1 shows the aerosol volume and number concentration profiles for the four-hour simulation. No nucleation is observed, and the aerosol volume decreases initially, then increases steadily over the four hours. The predicted initial decrease in volume is caused by the depositional loss of the larger particles in the starting atmospheric distribution. We present in Figure 7.2 the aerosol volume distributions at $t = 0$, 0.5 hours, 1.0 hours and 4.0 hours. The initial volume distribution has a coarse mode of particles (> 2 μm) and a fine mode; after one hour most of the coarse particles have deposited out. The volume distribution at $t = 4$ hours shows virtually no coarse particle mode, but substantial condensational growth of the fine mode.

We can conclude from this simulation that it is unlikely that homogeneous nucleation of organic aerosols occurs in the atmosphere. It is possible that inhomogeneities in the atmosphere could still provide a means for some small amount of nucleation to occur, but we assume that condensational growth is the dominant mechanism for gas-to-particle conversion of condensible organic species from the aromatic hydrocarbon photooxidation.

7.3 Recommendations for Future Work

There are several areas in which we could improve our understanding of organic aerosol formation. Characterization of the source rate of condensible vapor in the smog chamber experiments remains one of the major uncertainties in this work. A better understanding of the gas-phase chemistry, along with molecular composition data on the aerosol-phase species, would allow the prediction of the vapor source

rate directly from the gas-phase observations. Molecular composition analysis of the organic aerosol would help provide physical property data that is essential for the condensation and nucleation modeling. Other methods for estimating physical property data for the aerosol species in this system would be valuable as well, for example, vapor pressure measurements using the differential mobility analyzer (Rader et al., 1987).

It is difficult to estimate the aerosol size distributions in the experiments from the signals of the aerosol instruments used in this study. More accurate data inversion methods are needed to assess the performance of the multi-instrument smoothed-Twomey inversion of the raw aerosol data from these instruments. This analysis would allow us to verify the accuracy of our inverted size distribution data, and is crucial in order to trust the comparisons between simulations and observations. Alternatively, aerosol instruments that provide better size resolution over the range of particle sizes encountered in these experiments (such as the differential mobility analyzer/condensation nuclei counter combination) would give data that are more easily inverted.

The growth-law analyses can be extended to model a system with nucleation and deposition. This extension may require a large effort in determining how to treat nucleation, since solutions that follow trajectories in particle size, such as the method of characteristics technique used here, are not readily extended to include the initiation of new trajectories as nucleation occurs.

Finally, the sectional code, MAEROS, has recently been modified to use a moving-grid technique to eliminate numerical diffusion inaccuracies in the treatment of condensation (Gelbard, 1987). This code, however, does not include homogeneous nucleation, which would be necessary before the code could be used to model the smog chamber experiments.

Further experiments to study aerosol formation and growth should be carried

out in a better-characterized system. In a system with known aerosol-phase precursor species, many of the modeling uncertainties would be reduced. The outdoor smog chamber will always have limitations because of the inability to control temperature and concentrations precisely, but it remains a valuable tool for studying gas-phase kinetics and aerosol dynamics in atmospheric systems.

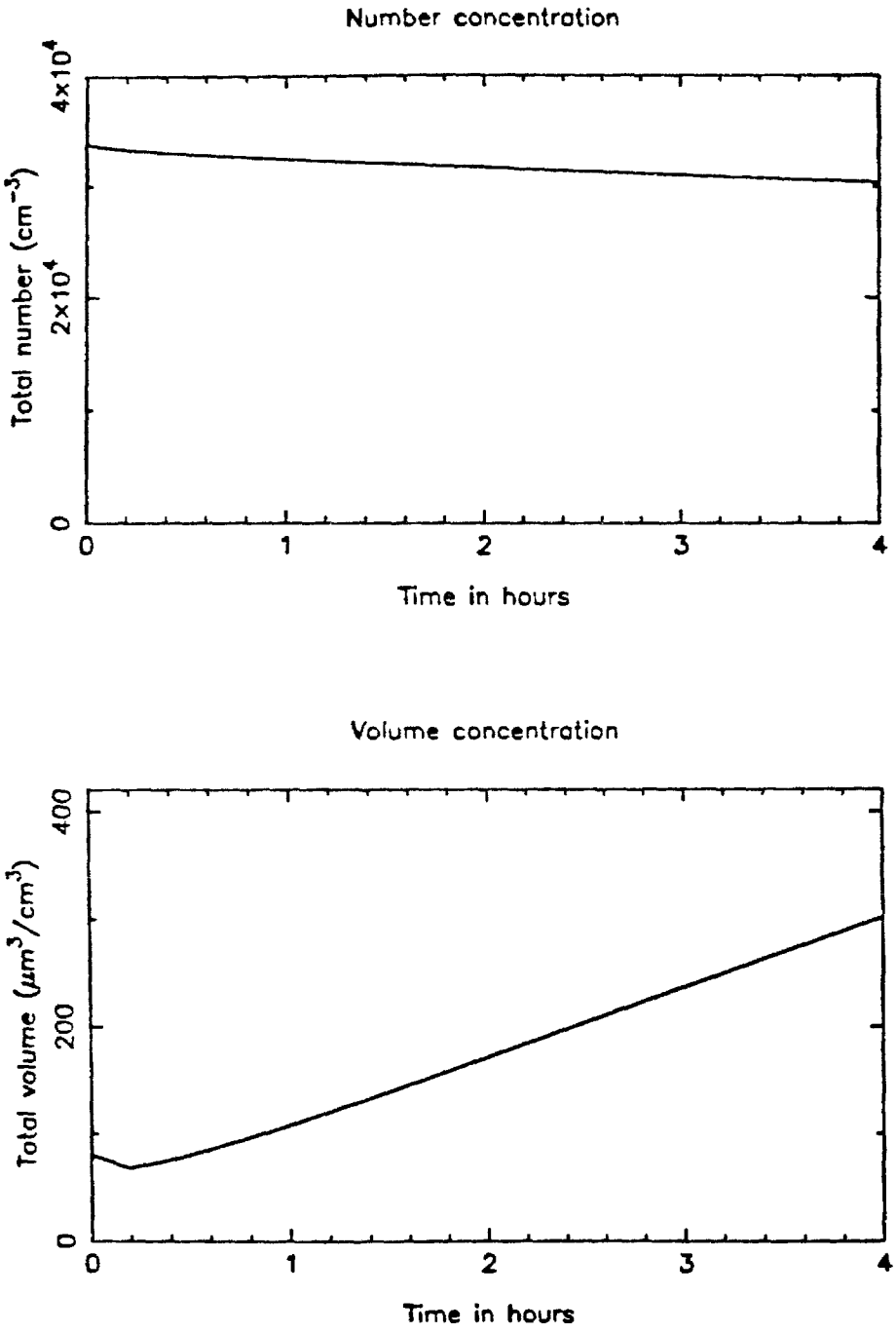

FIGURE 7.1. Predicted total aerosol volume and number concentrations as a function of time for simulation of atmospheric organic aerosol formation. Initial aerosol distribution from measurements of Larson (1988) for September 21, 1984 in Pasadena, CA.

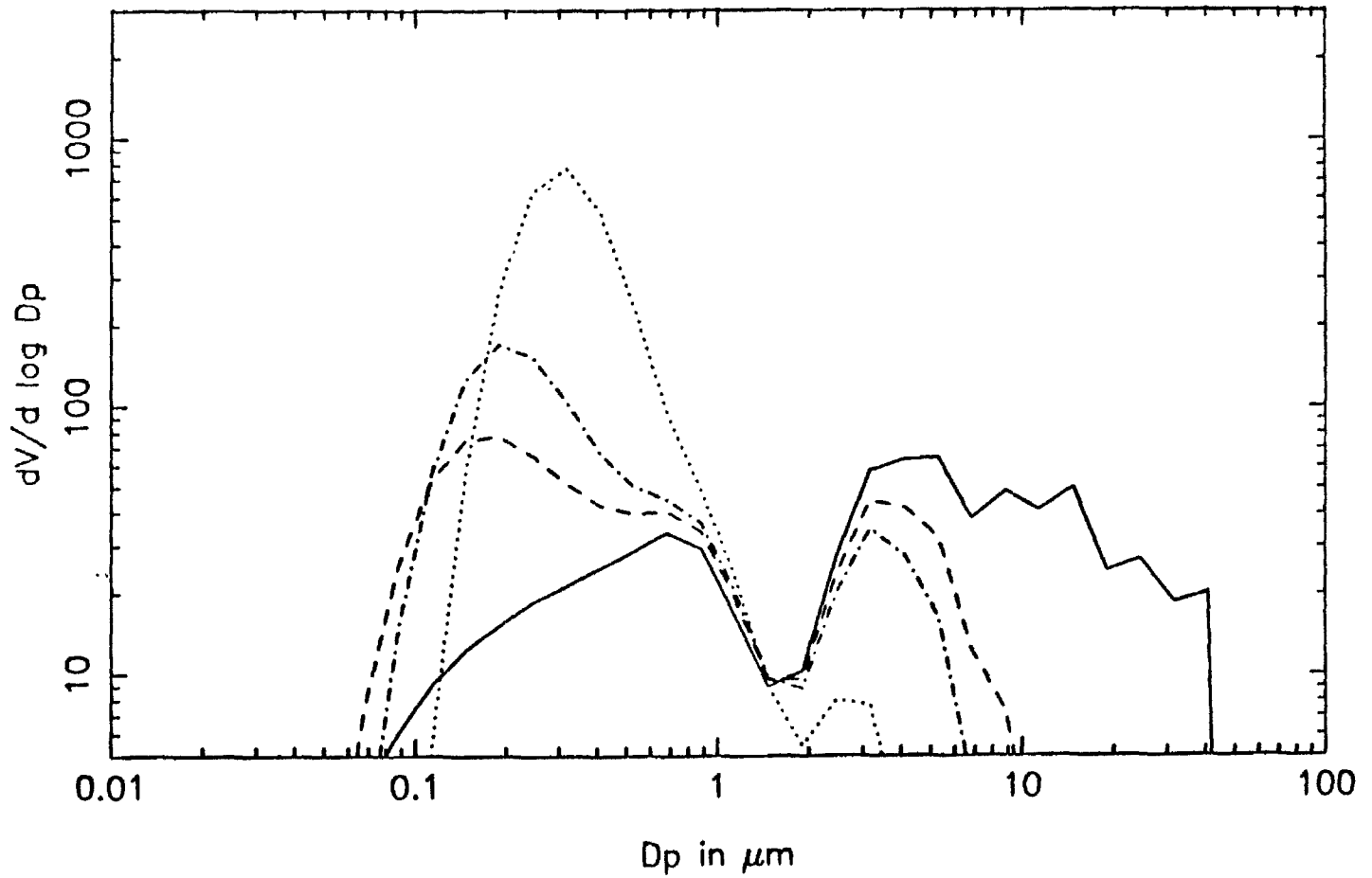

FIGURE 7.2. Predicted aerosol volume distributions at $t = 0$, $t = 0.5$ hours, $t = 1.0$ hours, and $t = 4.0$ hours for simulation of atmospheric organic aerosol formation.

— $t = 0$, – – – $t = 0.5$ hours, – · – $t = 1.0$ hours, ··· $t = 4.0$ hours

REFERENCES

Brock J.R. (1972),
Condensational Growth of Atmospheric Aerosols, J. Colloid Interface Sci., **39**, 32 – 36.

Crump J.G. (1983),
Aerosol Deposition, Growth, and Dynamics in the Continuous Stirred Tank Reactor, Ph.D. Thesis, California Institute of Technology.

Crump J.G. and Seinfeld J.H. (1981),
Turbulent Deposition and Gravitational Sedimentation of an Aerosol in a Vessel of Arbitrary Shape, J. Aerosol Sci., **12**, 405 – 415.

Crump J.G. and Seinfeld J.H. (1982a),
A New Algorithm for the Inversion of Aerosol Size Distribution Data , Aerosol Sci. Technol., **1**, 15 – 34.

Crump J.G. and Seinfeld J.H. (1982b),
Further Results on Inversion of Aerosol Size Distribution Data: Higher-Order Sobolev Spaces and Constraints , Aerosol Sci. Technol., **1**, 363 – 369.

Davis E.J. (1983),
Transport Phenomena with Single Aerosol Particles, Aerosol Sci. Technol., **2**, 121 – 144.

Drake R.L. (1972),
A General Mathematical Survey of the Coagulation Equation, in "Topics in Current Aerosol Research, part 2," G.M. Hidy and J.R. Brock (Eds.), Pergamon, New York, 201 – 376.

Friedlander S.K. (1977),
Smoke, Dust and Haze, John Wiley and Sons, New York.

Fuchs N.A. (1964),
The Mechanics of Aerosols, Pergamon, New York.

Fuchs N.A. and Sutugin A.G. (1971),
High-Dispersed Aerosols, in "Topics in Current Aerosol Research," G.M. Hidy and J.R. Brock (Eds.), Pergamon, New York, 1 – 200.

Gelbard F. (1979),
The General Dynamic Equation for Aerosols, Ph.D. Thesis, California Institute

of Technology.

Gelbard F. (1982),
MAEROS User Manual, Sandia National Laboratories, SAND80-0822, Albuquerque, New Mexico.

Gelbard F. (1987),
Multicomponent Aerosol Condensation and Coagulation, presented at AAAR Annual Meeting, September, 1987, Seattle, WA.

Gelbard F. and Seinfeld J.H. (1979),
Exact Solution of the General Dynamic Equation for Aerosol Growth by Condensation, J. Colloid Interface Sci., **68**, 173 - 183.

Gelbard F., Tambour Y., and Seinfeld J.H. (1980),
Sectional Representations for Simulating Aerosol Dynamics, J. Colloid Interface Sci., **76**, 541 - 556.

Grosjean D. (1977),
Aerosols, in "Ozone and Other Photochemical Oxidants," National Academy of Sciences, Washington D.C., 45 - 125.

Grosjean D. and Fung K. (1984),
Hydrocarbons and Carbonyls in Los Angeles Air, J. Air Pollut. Control Assoc., **34**, 537 - 543.

Hanson R.J. (1971),
A Numerical Method for Solving Fredholm Integral Equations of the First Kind Using Singular Values, SIAM J. Numer. Anal., **8**, 616 - 622.

Heisler, S.L. and Friedlander S.K. (1977),
Gas-to-Particle Conversion in Photochemical Smog: Aerosol Growth Laws and Mechanisms for Organics, Atmos. Environ., **11**, 157 - 168.

Kaijser T. (1983),
A Simple Inversion Method for Determining Aerosol Size Distributions, J. Comput. Phys., **52**, 80 - 104.

Kopczynski S.L. (1964),
Photo-oxidation of Alkylbenzene-Nitrogen Dioxide Mixtures in Air, Int. J. Air Water Pollut., **8**, 107 - 120.

Larson S.M. (1988),
A Study of Summer Midday Low-Visibility Events in the Los Angeles Area, Ph.D. Thesis, California Institute of Technology.

Liu B.Y.H. and Lee K.W. (1975),
An Aerosol Generator of High Stability, Amer. Ind. Hyg. Assoc. J., **36**, 861 - 865.

Liu B.Y.H. and Pui D.Y.H. (1975),
On the Performance of the Electrical Aerosol Analyzer, J. Aerosol Sci., **6**, 249 - 264.

Lothe J. and Pound G.M. (1961),
Reconsiderations of Nucleation Theory, J. Chem. Phys., **36**, 2080 - 2085.

Maher E.F. and Laird N.M. (1985),
EM Algorithm Reconstruction of Particle Size Distributions from Diffusion Battery Data, J. Aerosol Sci., **16**, 557 - 570.

Markowski G.R. (1987),
Improving Twomey's Algorithm for Inversion of Aerosol Measurement Data, Aerosol Sci. Technol., **7**, 127 - 141.

McMurry P.H. and Grosjean D. (1985),
Photochemical Formation of Organic Aerosols: Growth Laws and Mechanisms, Atmos. Environ., **19**, 1445 - 1451.

McMurry P.H. and Rader D.J. (1985),
Aerosol Wall Losses in Electrically Charged Chambers, Aerosol Sci. Technol., **4**, 249 - 268.

McMurry P.H. and Wilson J.C. (1982),
Growth Laws for the Formation of Secondary Ambient Aerosols: Implications for Chemical Conversion Mechanisms, Atmos. Environ., **16**, 121 - 134.

McWhirter J.G. and Pike, E.R. (1978),
On the Numerical Inversion of the Laplace Transform and Similar Fredholm Integrals of the First Kind, J. Phys. A: Math-Gen., **11**, 1729 - 1745.

Mirabel P. and Katz J.L. (1974),
Binary Homogeneous Nucleation as a Mechanism for the Formation of Aerosols, J. Chem. Phys., **60**, 1138 - 1144.

Nelson P.F., Quigley S.M., and Smith M.Y. (1983),
Sources of Atmospheric Hydrocarbons in Sydney: A Quantitative Determination Using a Source Reconciliation Technique, Atmos. Environ., **17**, 439 - 449.

O'Brien R.J., Holmes J.R., and Bockian A.H. (1975),
Formation of Photochemical Aerosol from Hydrocarbons: Chemical Reactivity and Products, Environ. Sci. Technol., **9**, 568 - 576.

Okuyama K., Kousaka Y., Warren D.R., Flagan R.C., and Seinfeld J.H. (1987),
Homogeneous Nucleation by Continuous Mixing of High Temperature Vapor with Room Temperature Gas, Aerosol Sci. Technol., **6**, 15 - 27.

Rader D.J., McMurry P.H., and Smith S. (1987),
Evaporation Rates of Monodisperse Organic Aerosols in the 0.02 - 0.2 μm-

Diameter Range, Aerosol Sci. Technol., **6**, 247 - 260.

Richards L.W. (1979),
The Reduction of Data from the Electrical Aerosol Analyzer, in "Aerosol Measurement," D.A. Lundgren, et al. (Eds.), University Presses of Florida, Gainesville, 438 - 450.

Schwartz W.D. (1974),
Chemical Characterization of Model Aerosols, EPA Report # EPA-650|3-74-011, Washington, D.C.

Seinfeld J.H. (1986),
Atmospheric Chemistry and Physics of Air Pollution, John Wiley and Sons, New York.

Seinfeld J.H. and Bassett M. (1982),
Effect of the Mechanism of Gas-to-Particle Conversion on the Evolution of Aerosol Size Distributions, in "Heterogeneous Atmospheric Chemistry," D.R. Schryer (Ed.), American Geophysical Union, Washington, D.C., 6 - 12.

Stauffer D. (1976),
Kinetic Theory of Two-Component ("Heteromolecular") Nucleation and Condensation, J. Aerosol Sci., **7**, 319 - 333.

Stern J.E., Wu J.J., Flagan R.C., and Seinfeld J.H. (1986),
Effect of Spatial Inhomogeneities on the Rate of Homogeneous Nucleation in Systems with Aerosol Particles, J. Colloid Interface Sci., **110**, 533 - 543.

Strand O.N. and Westwater E.R. (1968),
Minimum-RMS Estimation of the Numerical Solution of a Fredholm Integral of the First Kind, SIAM J. Numer. Anal., **5**, 287 - 295.

Tambour Y. and Seinfeld J.H. (1980),
Solution of the Discrete Coagulation Equation, J. Colloid Interface Sci., **74**, 260 - 272.

Twomey S. (1963),
On the Numerical Solution of Fredholm Integral Equations of the First Kind by the Inversion of the Linear System Produced by Quadrature, J. Assoc. Comput. Mach., **10**, 97 - 101.

Twomey S. (1965),
The Application of Numerical Filtering to the Solution of Integral Equations Encountered in Indirect Sensing Measurements, J. Franklin Inst., **279**, 95 - 109.

Twomey S. (1975),
Comparison of Constrained Linear Inversion and an Iterative Nonlinear Al-

gorithm Applied to the Indirect Estimation of Particle Size Distributions, J. Comput. Phys., **18**, 188 - 200.

Warren D.R., Okuyama K., Kousaka Y., Seinfeld J.H., and Flagan R.C. (1987), *Homogeneous Nucleation in Supersaturated Vapor Containing Foreign Seed Aerosol*, J. Colloid Interface Sci., **116**, 563 - 581.

Warren D.R. and Seinfeld J.H. (1984), *Nucleation and Growth of Aerosol from a Continuously Reinforced Vapor*, Aerosol Sci. Technol., **3**, 135 - 153.

Warren D.R. and Seinfeld J.H. (1985a), *Simulation of Aerosol Size Distribution Evolution in Systems with Simultaneous Nucleation, Condensation, and Coagulation*, Aerosol Sci. Technol., **4**, 31 - 43.

Warren D.R. and Seinfeld J.H. (1985b), *Prediction of Aerosol Concentrations Resulting from a Burst of Nucleation*, J. Colloid Interface Sci., **105**, 136 - 142.

Williams, M.M.R. (1983), *The Time-Dependent Behavior of Aerosols with Growth and Deposition. I. Without Coagulation*, J. Colloid Interface Sci., **93**, 252 - 263.

Williams, M.M.R. (1984), *On Some Exact Solutions to the Space- and Time-Dependent Coagulation Equation for Aerosols*, J. Colloid Interface Sci., **101**, 19 - 26.

Wilson W.E. Jr., Miller D.F., Levy A., and Stone R.K. (1973), *The Effect of Fuel Composition on Atmospheric Aerosol Due to Auto Exhaust*, J. Air Pollut. Control Assoc., **23**, 949 - 956.

APPENDICES

APPENDIX I

EFFECT OF SPATIAL INHOMOGENEITIES ON THE RATE OF HOMOGENEOUS NUCLEATION IN SYSTEMS WITH AEROSOL PARTICLES

Jennifer E. Stern, Jin-Jwang Wu,* Richard C. Flagan,* and John H. Seinfeld

Department of Chemical Engineering

California Institute of Technology

Pasadena, California 91125

Appeared in *J. Colloid Interface Sci.*, **110**, 533–543 (1986).

i.1 Abstract

The presence of growing particles in a system leads to spatial inhomogeneities in the vapor concentration. The effect of these spatial variations on the rate of formation of new particles by homogeneous nucleation is examined theoretically using a cell model. Results indicate that the presence of these inhomogeneities in systems both with and without initial aerosol generally has little effect on the final number concentration of particles following a nucleation "event."

* Department of Environmental Engineering Science

i.2 Introduction

Classical nucleation theory predicts the rate of formation of aerosol particles in a system containing a highly supersaturated vapor. In the presence of growing particles there exist local vapor concentration and temperature profiles around each particle. These spatial inhomogeneities will cause the overall nucleation rate in the system to differ from that based on the average vapor concentration and temperature. In this paper we examine the magnitude of the effect of these local spatial inhomogeneities on the rate of formation of new particles by homogeneous nucleation.

The rate of formation of new particles by homogeneous nucleation is most commonly represented by the classical theory of Volmer, Becker, Doring and Zeldovich (Springer, 1978):

$$J = S^2 N_s^2 \, 2v_1 \sqrt{\frac{\sigma}{2\pi m_1}} \exp\left(\frac{-16\pi\sigma^3 v_1^2}{3k^3 T^3 \ln^2 S}\right) . \qquad (i.1)$$

Equation $(i.1)$ expresses the rate of formation of new particles as a function of the local saturation ratio of vapor, S, and the local temperature, T. The particles formed have a surface tension σ, molecular volume v_1, and molecular mass m_1. After some particles form, vapor depletion by condensation, as well as nucleation, will diminish the vapor supersaturation and quench the nucleation process (Warren and Seinfeld, 1984, 1985). Condensational growth of the particles then dominates to relieve the excess vapor supersaturation.

Since depletion of the vapor by condensation will quickly dominate once a sufficient number of particles are present, nucleation will effectively cease. Warren and Seinfeld (1984, 1985) have shown how one therefore can predict a final number concentration of particles that will be formed for a given set of conditions. Considering a spatially homogeneous system containing a condensible vapor and aerosol

particles in which homogeneous nucleation, condensation, and vapor generation are occurring, mass and number balances on the system give:

$$\frac{d}{dt}N_v = R_G - g_s J - R_c \qquad (i.2)$$

$$\frac{d}{dt}N_p = J \qquad (i.3)$$

$$\frac{d}{dt}M_p = m_1 g_s J + m_1 R_c \ , \qquad (i.4)$$

where N_v is the vapor phase concentration, N_p is the aerosol number concentration, and M_p is the total mass loading in the aerosol phase. R_G, J, and R_c are the rates of vapor generation, nucleation and condensation, respectively. g_s is the assumed number of vapor molecules in the nucleating particles. The vapor concentration, N_v, determined from a mass balance, corresponds to the average saturation ratio in the system.

From the form of the nucleation rate expression, Equation $(i.1)$, we can see that there is a very strong dependence on saturation ratio. Therefore, local spatial inhomogeneities in a system containing particles could significantly influence the overall nucleation rate and the resulting number concentration.

Many researchers have considered the effects of interparticle competition for vapor in the context of the diffusional growth problem (Reiss and LaMer, 1950; Reiss, 1951; Frisch and Collins, 1952, 1953; Reiss et al., 1977). These efforts have been concentrated largely on solving the diffusion equation around a single particle, then extending that solution to an ensemble of particles. There are some mathematical difficulties that arise in the boundary conditions, as the growing particle imparts to the problem a moving boundary. This moving boundary problem has been solved by a number of different mathematical techniques, including perturbation methods (Frisch, 1952; Frisch and Collins, 1953; Goodrich, 1966), other approximate numerical solutions (Reiss and LaMer, 1950) and approximate

analytical solutions (Reiss et al., 1977). There have been several treatments of the competition between simultaneous nucleation and growth (Zaiser and LaMer, 1948; Reiss and LaMer, 1950), but none that attempts to account for the local profiles around an aerosol particle. Here we will concentrate on nucleation in a macroscopically homogeneous system, and the effect of the local spatial inhomogeneities around each growing particle on the overall rate of new particle formation. [Note that this is in contrast to the macroscopically inhomogeneous system considered by Becker and Reiss (1976) and McGraw and McMurry (1983).]

The effect of local spatial inhomogeneities on the rate of homogeneous nucleation during the early stages of nucleation has been considered by Pesthy et al. (1981) and Alam (1984). In these studies the conservation equations for heat and mass transfer were solved for the steady-state vapor concentration around a single growing aerosol particle. Boundary conditions were taken at the particle surface and at infinity, and the resulting vapor saturation ratio profile was written as a function of S_∞, T_∞ and r, assuming some known concentration at the particle surface. The nucleation rate was determined therefore as a function of radial distance from the particle. If the system considered is sufficiently dilute, the temperature effects can be neglected, as any substantial heat transfer will be dissipated by collisions with air molecules. This means that the heat released by gas-to-particle conversion will not have a significant effect on the temperature of the system, and the nucleation rate expression will be dependent only on S_∞ and r.

A radius, ρa, was then defined around the particle of radius a, such that the nucleation rate averaged over all of space equals the nucleation rate based on S_∞ from ρa to infinity,

$$\int_a^\infty J(S(r))\ 4\pi r^2 dr = \int_{\rho a}^\infty J(S_\infty)\ 4\pi r^2 dr\ . \qquad (i.5)$$

Thus, the volume between a and ρa is treated as a dead zone for nucleation. The

nucleation rate was approximated by a step function at radius ρa, the edge of this so-called *clearance volume.*

In a system of particles, the same idea can be applied, but a total fractional clearance volume is defined:

$$\Omega = \int_0^\infty \frac{4}{3}\pi(\rho a)^3 n(a)da \qquad (i.6)$$

for a particle number distribution $n(a)$. If $\Omega = 1$, the nucleation rate is zero in all of the available space. The clearance volume approach is valid, however, only in the limit of very small effects. In this situation, each particle can be considered to be in isolation, and the total fractional clearance volume, $\Omega \ll 1$. If we attempt to extend it past these limits, many additional uncertainties are introduced, as clearance volumes can overlap, and the saturation ratio cannot reach a value at infinity. Thus, it is not valid to extend the theory for Ω approaching one. The object of the present work is to develop a general theory for the effect of growing particles on the rate of homogeneous nucleation of a vapor that is valid over the entire range of times from very early to very late in the evolution of the system.

i.3 The Cell Model

A new approach is needed to predict nucleation behavior in systems that are beyond the scope of the clearance volume theory. We can extend the idea of a fully developed steady-state vapor concentration profile around a particle by considering each particle as existing within its own cell. Thus, we associate a certain volume of space with each particle. The vapor concentration at the edge of the cell is the same for all particles, and the cell sizes are chosen so that the entire volume of the system is accounted for. Note that this kind of treatment has been applied as a method for dealing with interparticle competition in the diffusional growth problem (Reiss and LaMer, 1950; Reiss, 1951; Reiss et al., 1977).

We start by writing the steady-state conservation equations for the vapor with boundary conditions at the particle edge and at the cell edge. As noted previously, the system is assumed to be dilute, so that the temperature effects caused by condensation of vapor on the particle are negligible. Thus we have:

$$\frac{1}{r^2}\frac{d}{dr}(cr^2V_r^*) = 0 \qquad (i.7)$$

$$V_r^*\frac{dx_A}{dr} = \frac{D}{r^2}\frac{d}{dr}(r^2\frac{dx_A}{dr}) \ , \qquad (i.8)$$

$$x_A = x'_A \qquad r = a$$

$$x_A = x_{AL} \qquad r = L$$

$$N_A = cV_r^* \qquad r = a \ ,$$

where c is the total concentration in the vapor phase, x_A is the mole fraction of vapor A, L is the cell radius, and V_r^* is the molar average velocity resulting from the flux of vapor molecules to the particle surface. To obtain an expression for x'_A, the mole fraction of vapor just above the particle surface, that is valid from the continuum to the free molecule regimes, we employ the idea of flux-matching (Fuchs and Sutugin, 1971). Flux-matching describes the vapor flux in the vicinity of a particle by the kinetic theory results for the free molecular regime; far from the particle, the flux is modeled in the continuum regime. At some boundary sphere, the fluxes are matched. When this boundary sphere is at the particle edge, we obtain the boundary condition (Alam, 1984):

$$x'_A = x_{A0} + (x_{AL} - x_{A0})\frac{\beta\,\mathrm{Kn}}{1+\beta\,\mathrm{Kn}} \ , \qquad (i.9)$$

where x_{A0} is the mole fraction above the particle surface based on the size and composition of the particle, and β is a dimensionless diffusivity given by:

$$\beta = \frac{4D}{\lambda_1\bar{c}_1} \ . \qquad (i.10)$$

Here, λ_1 is the mean free path of the condensing species and $\bar{c}_1$ is its kinetic velocity. The Kelvin equation gives x_{A0} in terms of the saturation mole fraction above a flat surface as:

$$x_{A0} = x_{A_{\text{sat}}} \exp\left(\frac{2\sigma v_1}{akT}\right) . \qquad (i.11)$$

Finally, we note that the vapor mole fraction at the cell edge, x_{AL}, is at the moment an unknown quantity.

Solution of Equations $(i.7)$ and $(i.8)$ gives the vapor mole fraction distribution as a function of radial position around the particle,

$$\left(\frac{1-x_A}{1-x'_A}\right) = \left(\frac{1-x_{AL}}{1-x'_A}\right)^{\frac{\frac{1}{a}-\frac{1}{r}}{\frac{1}{a}-\frac{1}{L}}} . \qquad (i.12)$$

We expect $\frac{1-x_{AL}}{1-x'_A}$ to be close to one, since the vapor phase mole fractions are very small, so we rewrite the right-hand side of this equation as a first-order binomial expansion

$$\left(\frac{1-x_{AL}}{1-x'_A}\right)^{\frac{\frac{1}{a}-\frac{1}{r}}{\frac{1}{a}-\frac{1}{L}}} = \left(1-\left(1-\frac{1-x_{AL}}{1-x'_A}\right)\right)^{\frac{\frac{1}{a}-\frac{1}{r}}{\frac{1}{a}-\frac{1}{L}}}$$

$$\cong 1 - \left(\frac{\frac{1}{a}-\frac{1}{r}}{\frac{1}{a}-\frac{1}{L}}\right)\left(1-\frac{1-x_{AL}}{1-x'_A}\right) . \qquad (i.13)$$

This corresponds to the exact solution of the steady-state conservation equations assuming $V_r^* = 0$. Physically, this assumes that the vapor phase is extremely dilute, so that $\ln\left(\frac{1-x'_A}{1-x_{AL}}\right) \cong 0$. To test the validity of neglecting the Stefan flow contribution we can take, for example, a "worst case" of an extremely small cell relative to particle size, and a high vapor concentration mole fraction. Taking L/a equal to 200, and x'_A equal to 0.01, the maximum difference between the concentration profiles with and without Stefan flow included is less than 0.01%. Thus, we can neglect this effect in all subsequent calculations.

We have also assumed a steady-state vapor concentration profile. This is a good assumption for most cases of interest, as the characteristic time for diffusion is

much less than the characteristic time for nucleation or for condensation. However, it is important to note what effect this would have on our results if it were in fact a poor assumption for certain systems. A growing particle has its first effects in the region immediately surrounding it, depleting the vapor phase in that region. If the steady-state assumption is not a good one, the resulting predicted nucleation rate will be lower than it actually is. This is because the effects far from the particle will be minimal, but near the particle we will have assumed a maximally depleted vapor phase. If the profile has not reached steady-state, a large portion of this predicted depletion will not have occurred.

Combining Equations $(i.9)$, $(i.11)$, and $(i.13)$, and dividing the mole fraction by the saturation mole fraction, we have an expression for the saturation ratio as a function of radial position:

$$S(r) = \left(\frac{\frac{1}{a} - \frac{1}{r}}{\frac{1}{a} - \frac{1}{L}} \right) (S_L - \alpha) \frac{1}{1 + \beta \, \mathrm{Kn}} + (S_L - \alpha) \frac{\beta \, \mathrm{Kn}}{1 + \beta \, \mathrm{Kn}} + \alpha, \qquad (i.14)$$

where

$$\alpha = \exp\left[\frac{2\sigma v_1}{akT} \right] . \qquad (i.15)$$

We can now define the average saturation ratio in a cell, and from that obtain the average saturation ratio in the system. Furthermore, knowing the nucleation rate explicitly as a function of radial position in each cell, by integrating this rate over the volume of each cell, we obtain the average nucleation rate in the system. Thus,

$$\bar{S}_{\mathrm{cell}} = \frac{\int_a^{L(a)} S(r) \; 4\pi r^2 dr}{\int_a^{L(a)} 4\pi r^2 dr} , \qquad (i.16)$$

$$\bar{S}_{\mathrm{system}} = \int_0^{\infty} \frac{4}{3} \pi L^3(a) \, n(a) \bar{S}_{\mathrm{cell}}(a) \, da , \qquad (i.17)$$

and similarly

$$\bar{J}_{\mathrm{cell}} = \frac{\int_a^{L(a)} J(S(r)) \; 4\pi r^2 dr}{\int_a^{L(a)} 4\pi r^2 dr} , \qquad (i.18)$$

$$\bar{J}_{\text{system}} = \int_0^\infty \frac{4}{3}\pi L^3(a)\, n(a) \bar{J}_{\text{cell}}(a)\, da \ . \qquad (i.19)$$

i.4 Dynamics of a Spatially Inhomogeneous System with Homogeneous Nucleation, Vapor Source, and Condensation

We now consider a system with a vapor source, homogeneous nucleation, and condensational growth. Equations $(i.2)$, $(i.3)$, and $(i.4)$ can be used identically, except that the expressions for R_c and J must be modified to account for spatial inhomogeneities. The nucleation rate is based on the system average rate, and the condensation rate expression must be based on the vapor supersaturation at the cell edge as the driving force, instead of the average supersaturation in the system. Therefore, we define correction factors f_J and f_C as:

$$f_J = \frac{\bar{J}_{\text{system}}}{J(\bar{S})} \qquad (i.20)$$

$$f_C = \frac{R_c(S_L)}{R_c(\bar{S})} \ , \qquad (i.21)$$

with $\bar{S}$ the average saturation ratio in the system, determined from a mass balance on the vapor phase.

As Warren and Seinfeld have shown (Warren and Seinfeld, 1984, 1985), the time scales for homogeneous nucleation and condensational growth are very different in a system where both are occurring. Gas-to-particle conversion via nucleation occurs fast enough relative to conversion by condensation that we may assume that all secondary aerosol forms at once and grows simultaneously. Then the secondary aerosol mode will be monodisperse. If the system has a pre-existing monodisperse aerosol present, the particle size distribution will be bimodal, and the governing equations must be modified. In this case, the dynamic model for the system is:

$$\frac{d}{dt} N_v = R_G - g_s J\, f_J - (R_{c1} + R_{c2})\, f_C \qquad (i.22)$$

$$\frac{d}{dt}N_{p1} = 0 \tag{i.23}$$

$$\frac{d}{dt}N_{p2} = J\, f_J \tag{i.24}$$

$$\frac{d}{dt}M_{p1} = m_1 R_{c1}\, f_C \tag{i.25}$$

$$\frac{d}{dt}M_{p2} = m_1 g_s J\, f_J + m_1 R_{c2}\, f_C \ , \tag{i.26}$$

with the subscript 1 for primary aerosol and 2 for secondary aerosol. The nucleation rate expression, J, is given by Equation $(i.1)$ with $S = \bar{S}$, the average saturation ratio determined from a mass balance on the vapor phase. The condensation rate expression for a particle of radius a is (Warren and Seinfeld, 1985):

$$R_c = N_s \bar{c}_1 \pi a^2 (S - \exp(\frac{a_K}{a}))f(\mathrm{Kn}) \ , \tag{i.27}$$

for a vapor whose saturated number concentration is N_s. Here, the exponential term is from the Kelvin effect, with a_K the characteristic Kelvin radius, given for a monomer of radius a_1 by $a_K = 4\pi a_1^2 \sigma / (3kT)$. $f(\mathrm{Kn})$ is an interpolation function to account for the regime of the particle, e.g., the Fuchs-Sutugin formula:

$$f(\mathrm{Kn}) = \frac{(4/3)\mathrm{Kn}^* (1 + \mathrm{Kn}^*)}{1 + 1.71\mathrm{Kn}^* + (4/3)(\mathrm{Kn}^*)^2}, \tag{i.28}$$

where Kn^* is defined by:

$$\mathrm{Kn}^* = \frac{\lambda_1}{a}\frac{3D}{\lambda_1 \bar{c}_1} = \frac{3}{4}\beta\, \mathrm{Kn} \ . \tag{i.29}$$

Each mode of particles is assumed to be monodisperse, so the integrals for average saturation ratio and average nucleation rate in the system become summations:

$$\bar{S}_{\mathrm{system}} = \sum_{i=1}^{2} \frac{4}{3}\pi L_i^3 N_{pi} \bar{S}_i \tag{i.30}$$

$$\bar{J}_{\text{system}} = \sum_{i=1}^{2} \frac{4}{3}\pi L_i^3 N_{pi} \bar{J}_i \ . \qquad (i.31)$$

We now need to consider the question of defining the cell size when particles of different sizes are present. In the case of only one mode of particles, the cells can be defined to be space-filling, or:

$$\frac{4}{3}\pi L^3 N_p = 1 \ . \qquad (i.32)$$

Since we define S_L to be a given value at the edge of every cell, some care must be taken in how to define the cell size with an inhomogeneous number concentration of particles. We will consider two limiting cases. In the first, the size of the aerosol has no effect on the volume it influences. In this case, Equation (i.32) still holds, with N_p given by $N_{p1} + N_{p2}$. At the other extreme, the cell radius will vary directly with the particle radius. Thus, the ratio $\kappa = L/a$ will be constant, and

$$\sum_{i=1}^{2} \frac{4}{3}\pi (\kappa a_i)^3 N_{pi} = 1 \ . \qquad (i.33)$$

Physically, the dependence on particle size is expected to be somewhere within these two limits.

The solution procedure will be to determine S_L from $\bar{S}$ at each time step. Knowing S_L, the correction factors f_J and f_C can be calculated, and the improved J and R_c returned to the system of ODE's to take the next time step.

i.5 Simulations and Discussion

In the numerical simulations that follow, we attempt to determine the relative importance of the inhomogeneities in the vapor phase in predicting the final number concentration of particles after a nucleation event. We will first consider systems with no initial aerosol, varying the source rate of condensible vapor and

comparing the resulting number concentration with that which results when the spatial inhomogeneities are ignored. We will then consider systems with a pre-existing monodisperse aerosol and look for the same effect.

We will present the results in terms of certain dimensionless parameters. The number concentration is non-dimensionalized with respect to the number concentration of monomer vapor at saturation, $N^* = N_p/N_s$. Similarly, the vapor source rate is non-dimensionalized with respect to the characteristic rate of monomer-monomer collisions in the saturated vapor, $R^* = R_G/R_\beta$. This collision rate, $R_\beta = N_s^2 \bar{c}_1 s_1/4$, where s_1 is the monomer surface area. The time is rescaled with respect to the time needed to regenerate the saturated vapor state, $\tau = t/\tau_G$ with $\tau_G = N_s/R_G$.

Figure I.1 shows the average saturation ratio and dimensionless number concentration from the numerical simulation of a system with no initial particles, with a dimensionless source rate, $R^* = 10^{-8}$. Other parameters used in the simulation are:

T = 298 K

p = 1 atm

$m_1 = 1.66 \times 10^{-22}$ g

$v_1 = 1.66 \times 10^{-22}$ cm^3

$\rho = 1.0$ g cm^{-3}

D = 0.0411 cm^2 sec^{-1}

$p_{sat} = 10^{-5}$ dynes cm^{-2}

$\tau_\beta = 44.8$ sec

$\Theta = 8.$

These correspond to a typical low vapor pressure organic of molecular weight 100. Here, τ_β is the characteristic time for collisions between monomers in a saturated vapor, and equals N_s/R_β. Θ is the dimensionless surface tension, given by $\Theta = \frac{\sigma s_1}{kT}$. Note that this definition is consistent with Warren and Seinfeld (1984), but differs from Warren and Seinfeld (1985) by a factor of 2/3.

The difference between the predictions that account for spatial variations and those that do not is imperceptible. It appears that with such a low dimensionless source rate, employing the average system supersaturation to predict the nucleation rate is entirely adequate. There is not sufficient nucleation to make the effects of the nucleated particles noticeable.

This calculation was repeated with the higher dimensionless source rate, $R^* = 10^{-2}$ (Figure 1.2). As expected, at higher source rates, more nucleation occurs, and we therefore expect the effect of particles to be more significant. Although the total predicted resulting number concentration is lower with the inhomogeneities accounted for, nucleation continues over a slightly longer period of time. This observation indicates that the rate of new particle formation is reduced for the duration of the nucleation event. This can be explained by considering the competing events of nucleation and condensation. Determining the saturation ratio far from the particle allows us to predict the condensation rate more accurately than when the average saturation ratio is used. From Equation (i.27) we know that the driving force for condensation is directly proportional to the saturation ratio unaffected by the particle. Thus, we need the asymptotic value of this profile, not the average value, to accurately determine condensation rate. With a slightly higher predicted condensation rate, as this allows, the predicted average system supersaturation will be lower than when local spatial inhomogeneities are neglected. Thus, the predicted nucleation rate will also be depleted, and the

overall amount of nucleation observed will be decreased.

In Figure I.3 we present final predicted dimensionless number concentrations versus dimensionless source rate for systems with no initial aerosol. Two surface tensions are considered. The lower one, $\Theta = 8$, corresponds to a hypothetical low vapor pressure organic species. The higher one, $\Theta = 15$, is typical for many other organic species. Most organics will fall somewhere between these two values. The simulation was carried out for dimensionless source rates less than one, where the condensible vapor is being generated at the same rate as the saturation monomer-monomer collision rate. Beyond a dimensionless source rate of one, the assumptions of classical steady-state nucleation theory probably break down, and the classical nucleation rate expression may no longer be valid.

We observe again that the particles' influence on the vapor concentration makes no appreciable difference in the resulting final number concentration of particles. At the higher surface tension, where less nucleation is predicted, the effect is naturally less important. At $\Theta = 8$, we can begin to see some effect at high source rates, but even this is insignificant. At $R^* = 1$, where the maximum effect is observed, the difference in the resulting number concentrations is less than 20%. Thus, it appears that in systems with no primary aerosol, homogeneous nucleation rates can be predicted with no significant error introduced by neglecting the effect of the spatial inhomogeneities due to the particles. All of the remaining simulations are based on $\Theta = 8$, where more deviation was observed.

In systems with pre-existing aerosol, we expect to see a greater effect than when no aerosol is present initially. Figures I.4 and I.5 show the change in number concentration that results when nucleation occurs in systems with initial aerosol. In these systems two dimensionless source rates are considered, $R^* = 10^{-3}$ and $R^* = 1$. The system shown in Figure I.4 has seed particles in the free-molecular

regime, with radii of 0.005 μm, whereas Figure 1.5 shows the results in a system with continuum-sized seed particles, 0.5 μm in radius. The cell model predicts less nucleation, again with only a small effect on final number concentrations. The cell size, even with pre-existing aerosol, is very large compared with the particle size. Still, the increased condensation rate will yield lower supersaturations and hence predict less overall nucleation.

We see that in all cases considered, a sufficiently small number of initial particles has no effect on the final number concentration; the curves are linear with a slope of -1. With higher number concentrations, nucleation is effectively quenched; the curves approach $N_f/N_i = 1$. At this limit, the effects of variations in the vapor concentration are negligible, and the curves with and without the cell model approach one another.

With initial aerosol in the system, we must address the question posed earlier about how to define the cell size. Results indicate that there is no observable difference between making the cells uniformly sized for both modes of aerosols and linking the cell size to the particle size. Therefore, in all calculations presented here the cells are uniformly sized for all particles in the system, as given in Equation $(i.32)$.

In Figure 1.6 we present these results in a somewhat different format. For $R^* = 1$ we have plotted final dimensionless number concentration as a function of initial seed particle size for initial number concentrations of 1×10^{-7}, 5×10^{-7}, and 1×10^{-6}. If the seed particles are very small, they have no effect on the final number concentration; the curves show no dependence on primary aerosol size. The transition to the region where the initial particles affect the final number concentration is quite sharp, and occurs at a smaller particle size for higher initial number concentrations. Again we note that the effect of accounting for the spatial

inhomogeneities in the vapor phase is a slight decrease in the resulting number concentration of particles.

Figure I.7 is a comparison of the contributions of nucleation and condensation to the total mass of vapor converted to aerosol for a range of initial number concentrations of particles. A high source rate, $R^* = 1$, and large seed particles, $a = 0.5\ \mu$m, were considered in order to enhance any observed effects of the vapor phase spatial variations. On the ordinate, we have plotted the ratio of mass that is converted via homogeneous nucleation to the total mass converted to the aerosol phase at the end of the nucleation event. Subsequent to the nucleation event, virtually all mass will go to condensational growth of the particles. Here we note that the effect of spatial inhomogeneities in the vapor phase concentration profiles is more pronounced. We have previously seen that the cell model predicts less nucleation than when the average saturation ratio is used. In addition, it will predict a greater rate of condensation because the driving force is slightly greater when the saturation ratio at the edge of the cell is used instead of the average value over the entire system. The combined effects will give us the greater difference we observe.

i.6 Conclusions

In a nucleating vapor system the presence of particles leads to inhomogeneities in the vapor phase concentration. The condensation rate is slightly enhanced by using (properly) the asymptotic limit of the saturation ratio profile far from the particle as the driving force for condensation, instead of the average value. This enhanced condensation rate also serves to reduce nucleation, as does any effect that favors gas-to-particle conversion by heterogeneous condensation. These combined effects yield lower resulting number concentrations following a nucleation event. This is observed in systems both with and without pre-existing aerosol. Numerical

calculations show, however, that in reasonably dilute systems with low source rates we may accurately ignore the effects of the local vapor phase spatial variations in making nucleation predictions.

Acknowledgement

This work was supported by National Science Foundation grant ATM-8208625.

i.7 References

Alam, M. K. (1984),
Nucleation and Condensational Growth of Aerosols: Application to Silicon Production, Ph.D. Thesis, California Institute of Technology.

Becker C. and Reiss H. (1976),
Nucleation in a Nonuniform Vapor, J. Chem. Phys., **65**, 2066 - 2070.

Frisch H.L. (1952),
Durch Diffusion Kontrolliertes Phasenwachstum, Z. Elektrochem., **56**, 324 - 326.

Frisch H.L. and Collins F.C. (1952),
Diffusional Processes in the Growth of Aerosol Particles, J. Chem. Phys. **20**, 1797 - 1801, and **21**, 1116.

Frisch H.L. and Collins F.C. (1953),
Diffusional Processes in the Growth of Aerosol Particles. II., J. Chem. Phys., **21**, 2158 - 2165.

Fuchs N.A. and Sutugin A.G. (1971),
High-Dispersed Aerosols, in "Topics in Current Aerosol Research," G.M. Hidy and J.R. Brock (Eds.), Pergamon, New York, 1 - 200.

Goodrich F.C. (1966),
On Diffusion-Controlled Particle Growth: the Moving Boundary Problem, J. Phys. Chem., **70**, 3660 - 3665.

McGraw R. and McMurry P.H. (1983),
The Coupling of Nucleation and Diffusion Near an Aerosol Particle, J. Colloid Interface Sci., **92**, 584 - 587.

Pesthy A.J., Flagan R.C. and Seinfeld J.H. (1981),
The Effect of a Growing Aerosol on the Rate of Homogeneous Nucleation of a Vapor, J. Colloid Interface Sci., **82**, 465 - 479.

Reiss H. (1951),
The Growth of Uniform Colloidal Dispersions, J. Chem. Phys., **19**, 482 - 487.

Reiss H. and LaMer V.K. (1950),
Diffusional Boundary Value Problems Involving Moving Boundaries, Connected with the Growth of Colloidal Particles, J. Chem. Phys., **18**, 1 - 12.

Reiss H., Patel J.R. and Jackson K.A. (1977),
Approximate Analytical Solutions of Diffusional Boundary-Value by the Method of Finite Zone Continuity, J. Appl. Phys., **48**, 5274 - 5278.

Springer G.S. (1978),
in "Advances in Heat Transfer" (T. F. Irvine and J. P. Hartnett, Eds.), Vol. 14, Academic Press, New York.

Warren D.R. and Seinfeld J.H. (1984),
Nucleation and Growth of Aerosol from a Continuously Reinforced Vapor, Aerosol Sci. Technol., **3**, 135 - 153.

Warren D.R. and Seinfeld J.H. (1985),
Prediction of Aerosol Concentrations Resulting from a Burst of Nucleation, J. Colloid Interface Sci., **105**, 136 - 142.

Zaiser E.M. and LaMer V.K. (1948),
The Kinetics of the Formation and Growth of Monodispersed Sulfur Hydrosols, J. Colloid Sci., **3**, 571 - 598.

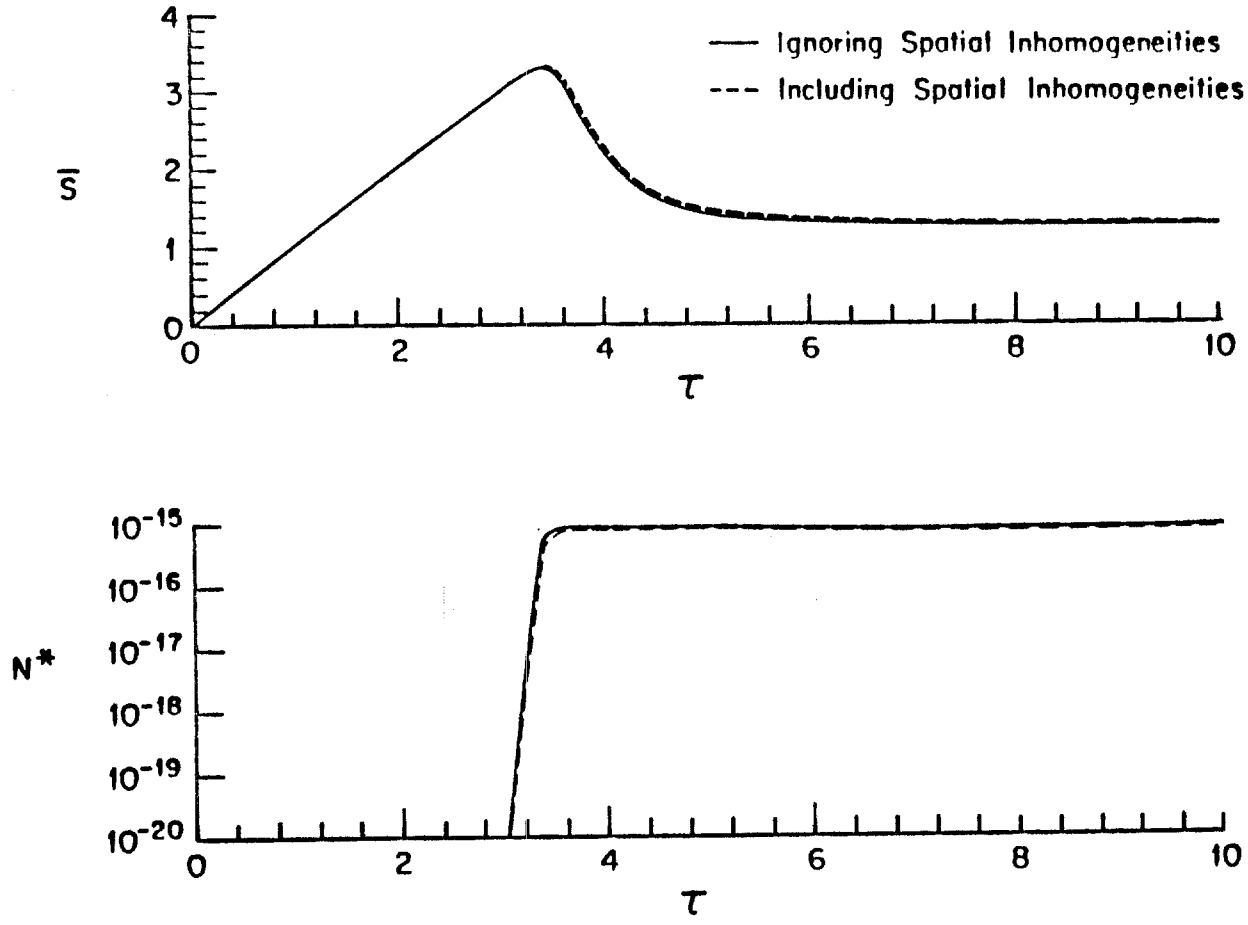

FIGURE 1.1. $\bar{S}$ and N^* as a function of τ for $R^* = 10^{-8}, \Theta = 8$, and no initial aerosol.

$\bar{S}$: Average system saturation ratio, N^*: Dimensionless number concentration

τ: Dimensionless time

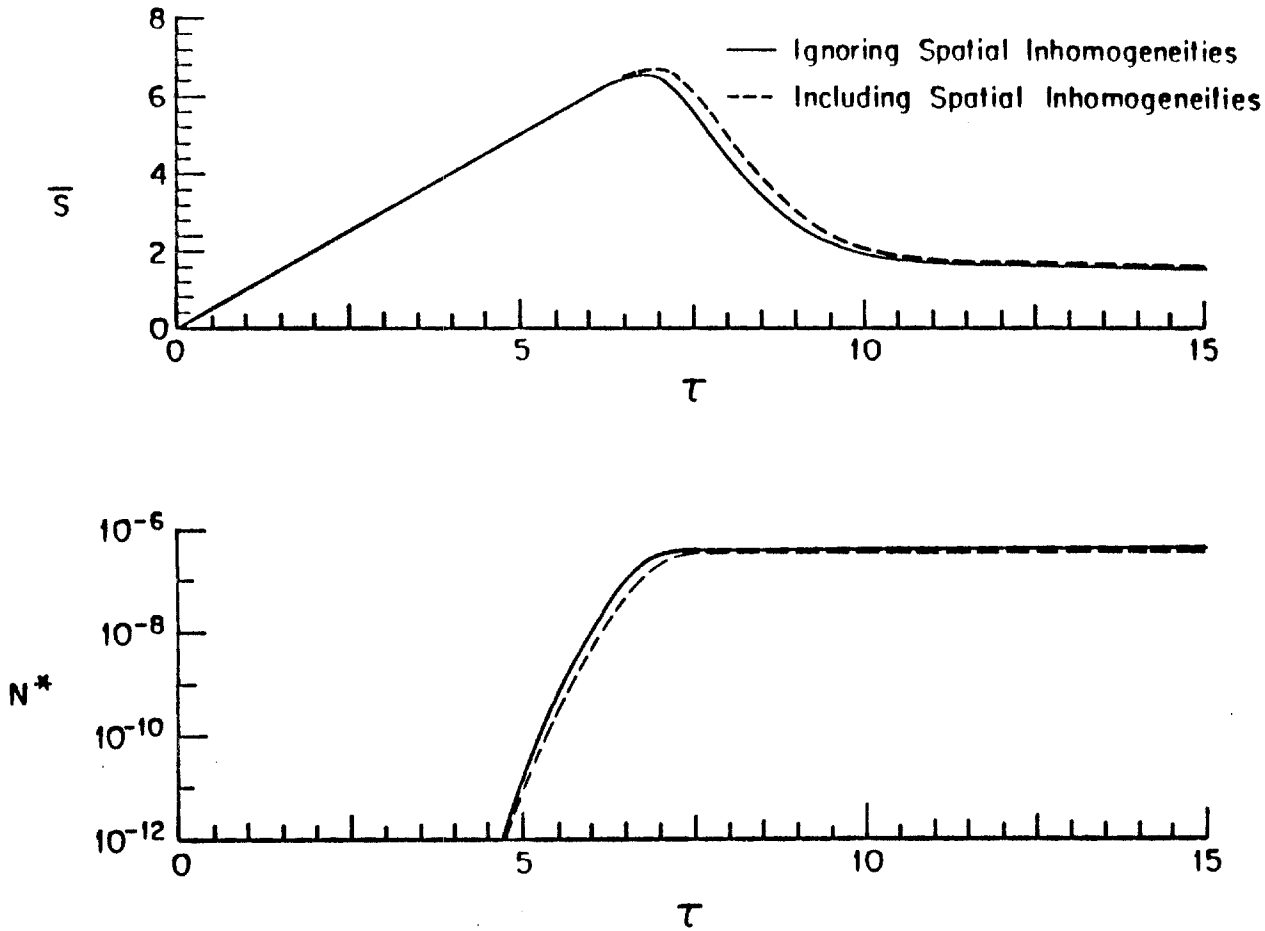

FIGURE 1.2. S and N^* as a function of τ for $R^* = 10^{-8}, \Theta = 8$, and no initial aerosol.

S: Average system saturation ratio, N^*: Dimensionless number concentration

τ: Dimensionless time

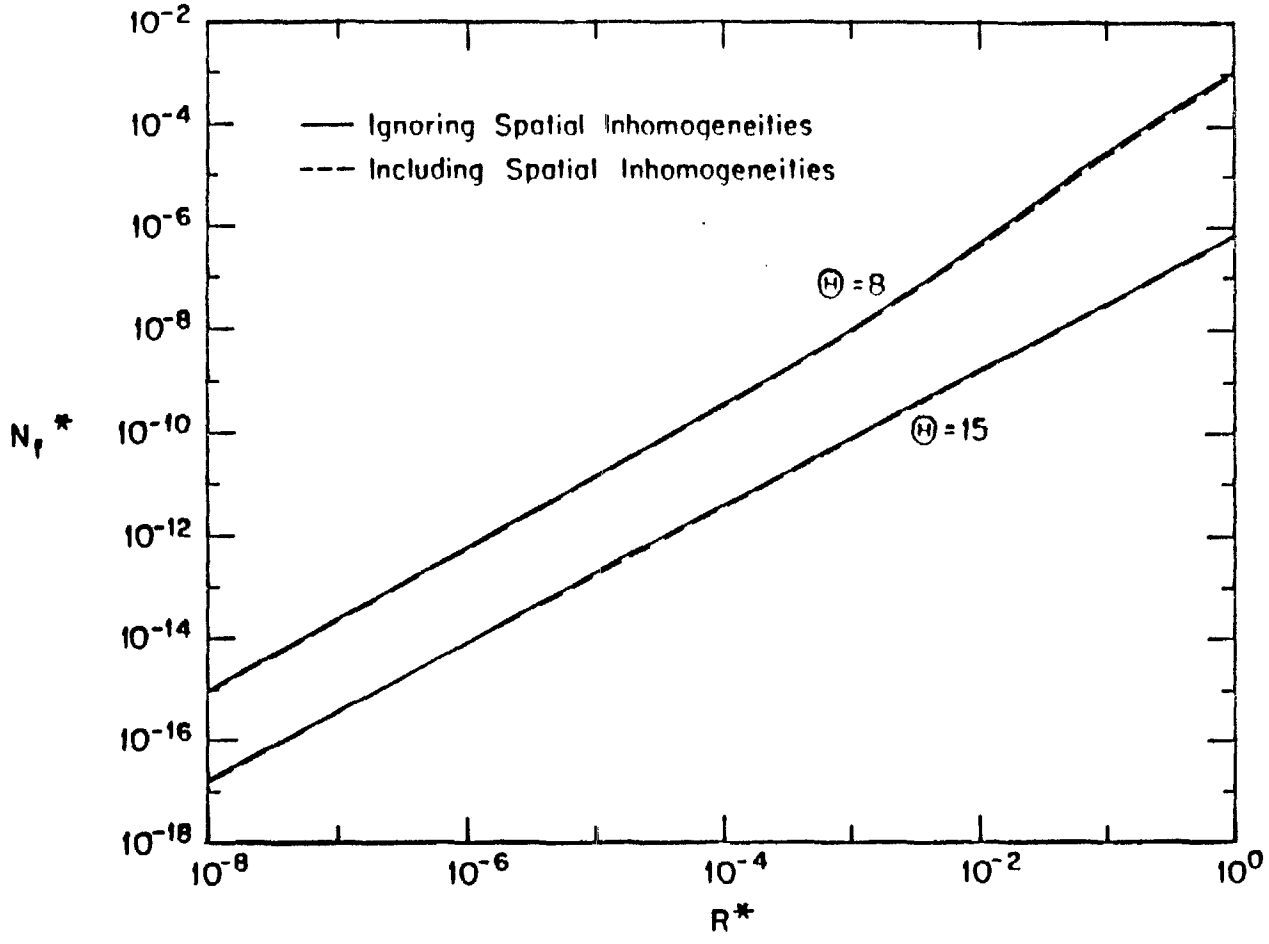

FIGURE I.3. Dimensionless final number concentration, N_f^*, as a function of dimensionless source rate, R^*, for a system with no initial aerosol.

The two curves represent $\Theta = 8$ and $\Theta = 15$.

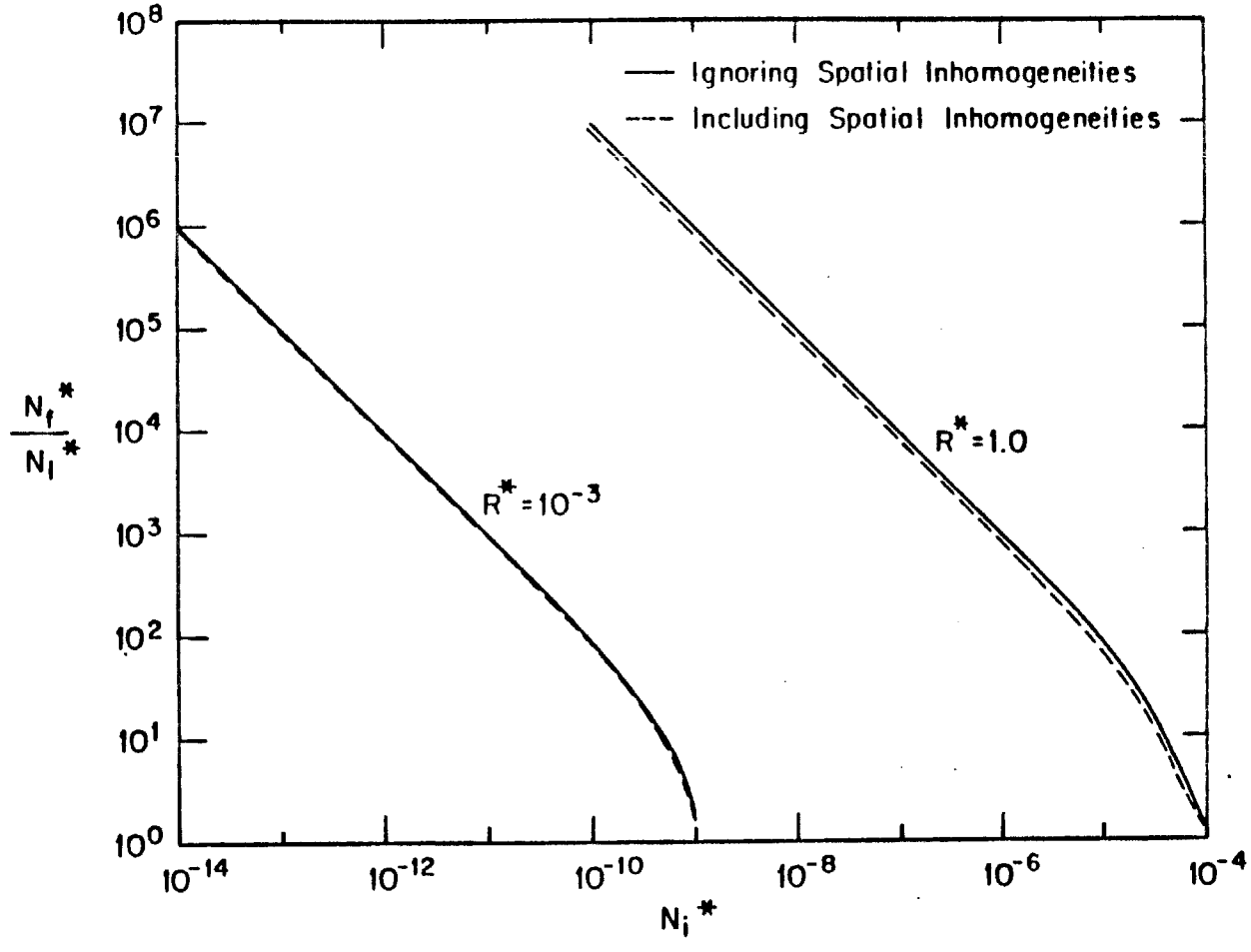

FIGURE 1.4. The change in dimensionless number concentration as a function of dimensionless initial number concentration. $a = 0.005\ \mu m$.

Initial particles of radius $a = 0.005\ \mu m$, $R^* = 10^{-3}$ and $R^* = 1.0$, $\Theta = 8$.

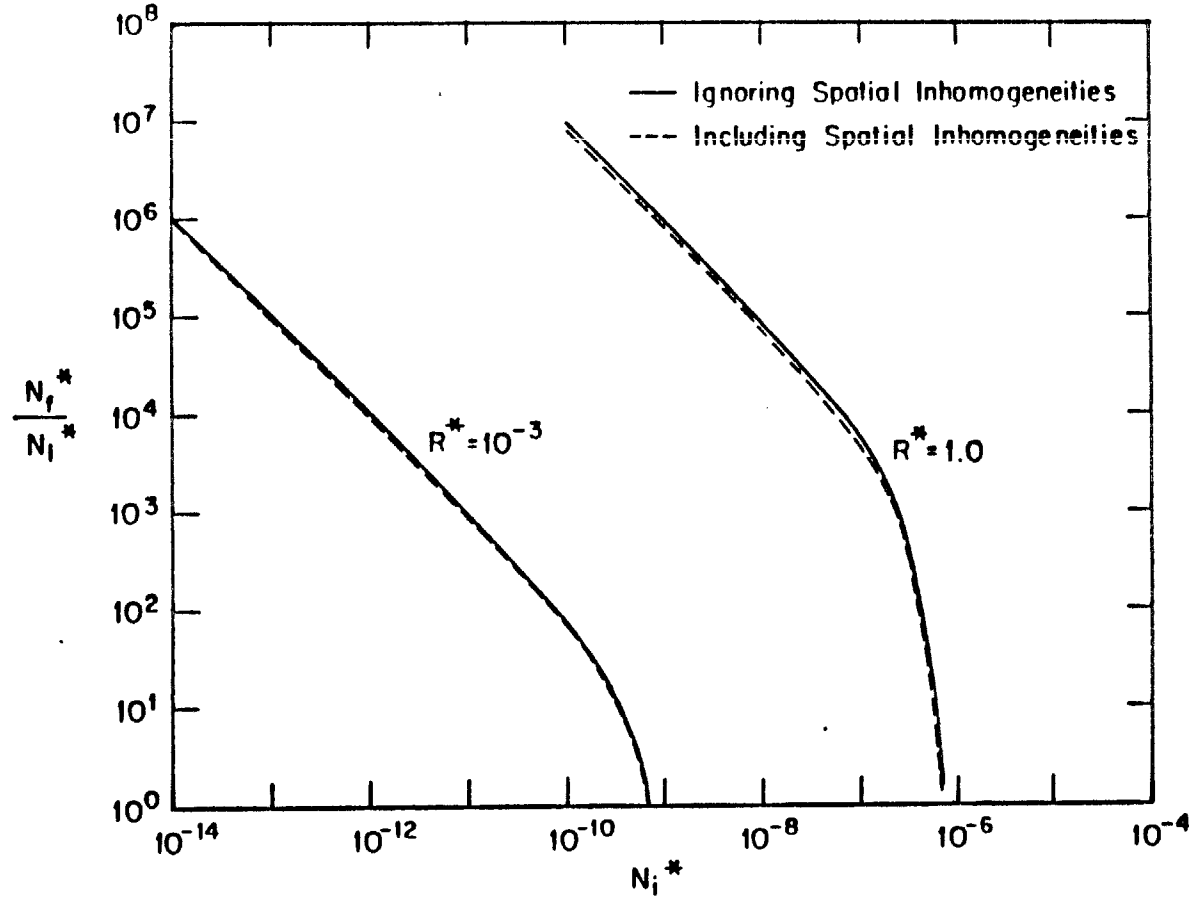

FIGURE 1.5. The change in dimensionless number concentration as a function of dimensionless initial number concentration. $a = 0.5\ \mu m$.

Initial particles of radius $a = 0.5\ \mu m$, $R^* = 10^{-3}$ and $R^* = 1.0$, $\Theta = 8$.

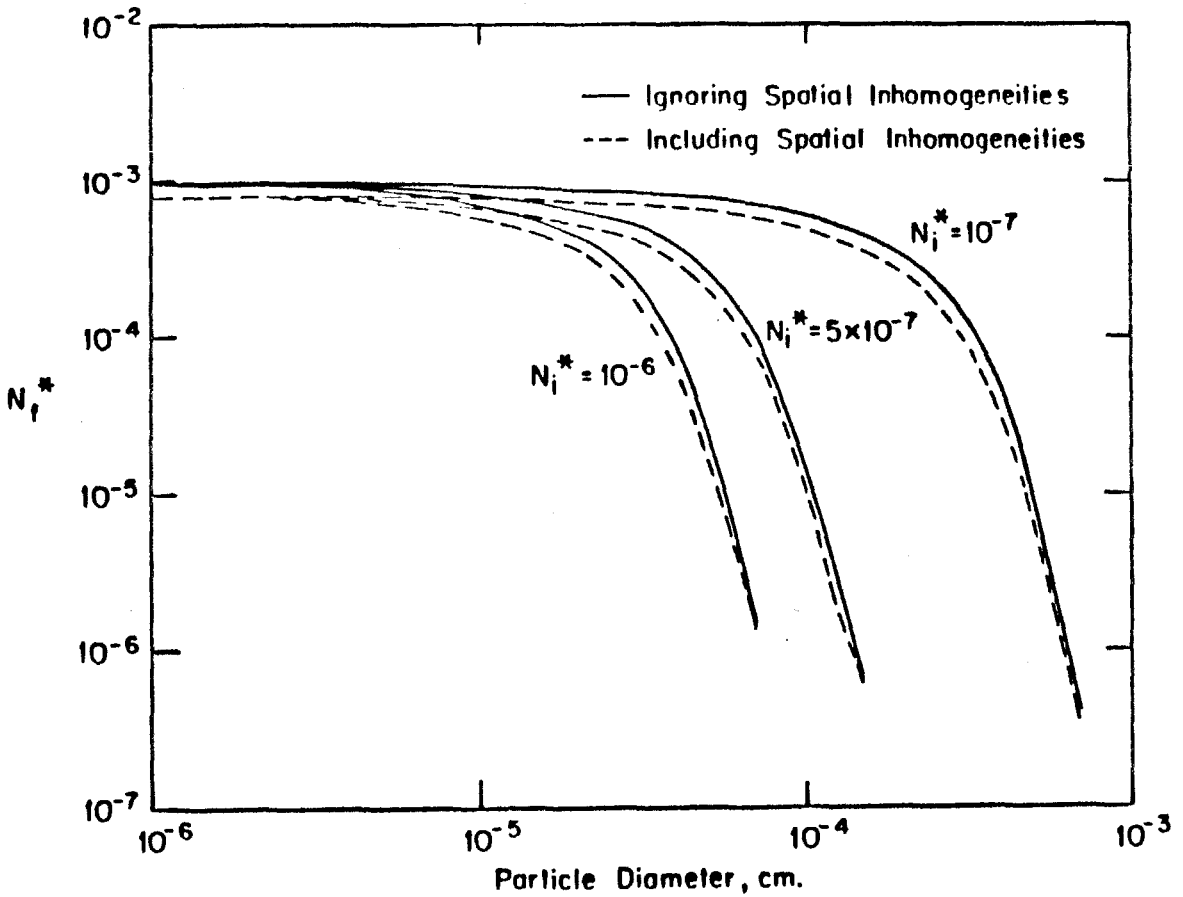

FIGURE 1.6. Dimensionless final number concentration, N_f^*, as a function of seed particle diameter for varying dimensionless initial number concentrations.

$R^* = 1.0$ and $\Theta = 8$

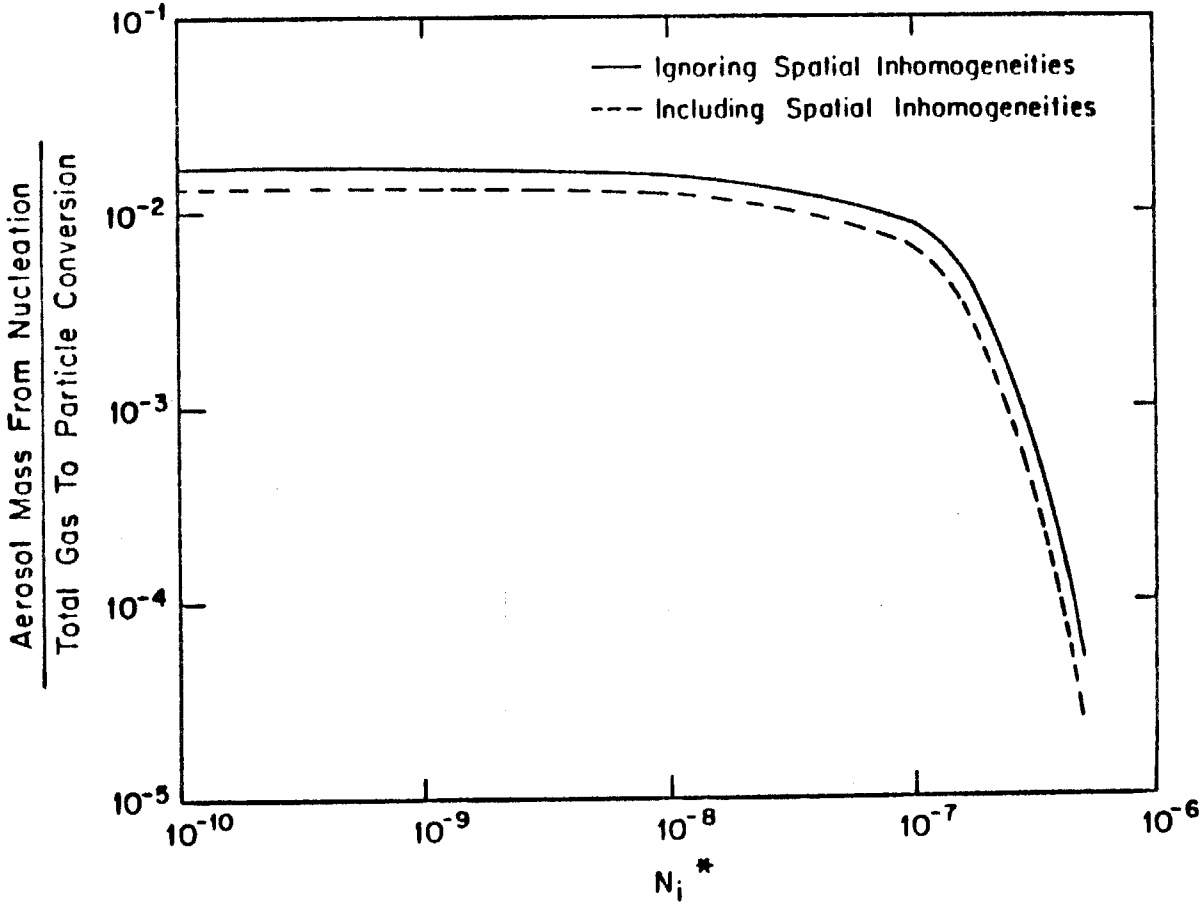

FIGURE 1.7. The ratio of mass converted by homogeneous nucleation to total mass converted to the aerosol phase as a function of N_i^*.

$R^* = 1.0$, $a = 0.5\ \mu m$, and $\Theta = 8$.

APPENDIX II

CALCULATION OF AEROSOL YIELD

An important goal of this work was to determine the quantity of the initial hydrocarbon that was converted to aerosol-phase precursor. This is an important calculation, for it provides information not only to help determine gas-phase reaction pathways, but also to assess in an overall way the aerosol-forming potential of the organic species.

We must first define the concept of aerosol "yield" in the photooxidation experiments. There is no unique way to define the percent yield of aerosol from the photooxidation of an organic species. For instance, the yield can be expressed on a mass or a molar basis. The molar definition of yield will reveal how many aromatic molecules undergo the transition to aerosol-phase products, or what percentage of the initial carbon atoms become aerosol-phase products. However, aerosol data are collected on a basis of aerosol volume per unit volume of air, and without detailed knowledge of the aerosol molecular composition it is difficult to convert these data to molar terms. If we consider as an example a toluene photooxidation in which (for simplicity) the aerosol is assumed to be entirely dinitro-cresol, we have:

Toluene has a molecular weight of 92 and a density of 0.87 g cm^{-3}; dinitro-cresol has a molecular weight of 198 and a density of approximately 1.3 g cm^{-3}. If for each mole m^{-3} of toluene reacting, 0.01 moles m^{-3} of dinitro-cresol form as aerosol, we have a molar yield of 1%. However, if we express this yield on a mass basis,

we have 92 g m^{-3} of toluene forming 1.98 g m^{-3} of dinitro-cresol, or a mass yield of 2.15% . In addition, this would be measured as 1.52 μm^3 of aerosol per cm^3 of air.

Conversion from the gas phase occurs primarily by two routes: homogeneous nucleation of secondary aerosol particles, and heterogeneous condensation onto primary (pre-existing) and secondary aerosol modes. The rate of gas-to-particle conversion will vary over the course of an experiment. Initially, no secondary aerosol is formed while the partial pressures of the condensible species build up to saturation levels. After the saturation point of $S = 1$ is passed, the supersaturation can be relieved either by condensation onto pre-existing aerosol or by nucleation and subsequent condensation. During a nucleation event, conversion to the aerosol phase is rapid. Late in the experiment, after significant gas-to-particle conversion has occurred, the partial pressures of the condensing species may fall below saturation levels and conversion to the aerosol phase will stop. Thus, we must define an overall yield that best represents an entire photooxidation event.

The calculation of aerosol yield is further complicated by aerosol volume loss by deposition, which can reach significant levels late in an experiment. To avoid having to account for aerosol wall losses in the calculation of yield, we have determined the yield at the point in time where the aerosol volume profile reaches its maximum. At this point, aerosol loss has been estimated to be less than about 10%. Since the starting aromatic species have densities below 1 g cm^{-3} and some previously identified aerosol products have densities just above 1 g cm^{-3}, and since we lack other information, we have assumed for these calculations that the aerosol has a density of 1.0 g cm^{-3}.

Finally, we note that in experiments where there is initial aerosol, the mass of this seed aerosol generally represents less than 1% of the aerosol volume at its maximum level, so no attempt has been made to correct for the presence

of seed aerosol when calculating aerosol yield. The measured aerosol yields by mass for each experiment are given in Tables II.1 – II.4. We have also included the HC/NO_x ratio for each experiment in the Tables, since there is a correlation between the system reactivity, which is dependent on the HC/NO_x ratio, and the percent conversion to the aerosol phase.

The average aerosol yield by mass was about 1 – 5% for each aromatic, although some toluene experiments had yields around 10%. Average yields for each aromatic species were: toluene – 4.8%, m-xylene – 3.5%, ethyl benzene – 1.9%, 1,3,5-trimethyl benzene – 2.4%. Previous studies of the gas-phase mechanisms of aromatic hydrocarbons have included aerosol yields based on percent of reacted carbon in order to complete a mass balance on the carbon loading in the system (Schwartz, 1974; Schwartz et al., 1976; Spicer and Jones, 1977; Grosjean et al., 1978; Gery et al., 1985; Leone et al., 1985; Gery et al., 1987). These researchers have found aerosol yields in the range of 1 – 6% for the toluene and m-xylene systems. Although our yield determination was calculated on a mass basis instead of an elemental carbon basis, we can note that our numbers are generally in good agreement with the values found in previous studies.

References:

Gery M.W., Fox D.L., Jeffries H.E., Stockburger L., and Weathers L.S. (1985), *A Continuous Stirred Tank Reactor Investigation of the Gas-Phase Reaction of Hydroxyl Radicals and Toluene*, Int. J. Chem. Kinet., **17**, 931 - 955.

Gery M.W., Fox D.L., Kamens R.M., and Stockburger L. (1987), *Investigation of Hydroxyl Radical Reactions with o-Xylene and m-Xylene in a Continuously Stirred Tank Reactor*, Environ. Sci. Technol., **21**, 339 - 348.

Grosjean D., Van Cauwenberghe K., Fitz D.R., and Pitts J.N. Jr. (1978), *Photooxidation Products of Toluene-NO_x Mixtures Under Simulated Atmospheric Conditions*, ACS Division Environ. Chem. Preprints, **18**, 354 - 356.

Leone J.A., Flagan R.C., Grosjean D., and Seinfeld J.H. (1985), *An Outdoor Smog Chamber and Modeling Study of Toluene-NO_x Photooxidation*, Int. J. Chem. Kinet., **17**, 177 - 216.

Schwartz W.D. (1974), *Chemical Characterization of Model Aerosols*, EPA Report # EPA-650/3-74-011, Washington, D.C.

Schwartz W.D., Mendenhall G.D., Jones P.W., Riggle C.J., Graffeo A.P., and Miller D.F. (1976), *Chemical Characterization of Model Aerosols*, EPA Report # EPA-600/3-76-085, Washington, D.C.

Spicer C.W. and Jones P.W. (1977), *The Fate of Aromatic Hydrocarbons in Photochemical Smog Systems:Toluene*, J. Air Pollut. Control Assoc., **27**, 1122 - 1125.

TABLE II.1. Aerosol yields for toluene experiments

Experiment	Temp. (K)	$[HC/NO_x]_0$ (ppmC/ppm)	HC mass conc. ($\mu g\ m^{-3}$)	Aerosol mass conc. ($\mu g\ m^{-3}$)	Yield (%)
MTMA16	307	12.9	1132	28.6	2.53
MTLA18	315	14.2	1851	88.0	4.76
MTMA20	311	17.2	1334	48.2	3.61
MTMA22	318	13.9	1305	53.7	4.11
MTNA26	313	10.1	1218	49.8	4.09
MTHA31	309	21.3	1597	119.9	7.51
MTNA35	313	14.3	2078	111.0	5.34
HTNA37	309	16.3	6495	558.3	8.60
HTMA39	309	17.7	6023	747.4	12.41
HTLA41	312	12.2	4671	416.3	8.91
DHNA43,A	319	21.4	4850	648.7	13.38
B		17.1	4218	286.8	6.80
DMMA45,A	322	15.6	1776	52.0	2.93
B		15.6	1776	50.8	2.86
DMXA48,A	315	14.1	1637	5.4	0.33
B		14.1	1922	21.1	1.10
DQXA53,A	312	33.3	2480	119.6	4.82
B		33.3	2516	188.0	7.47
DQXA55,A	316	28.5	2171	107.6	4.95
B		29.5	2848	30.7	1.08
DQXA57,A	312	29.9	2803	97.2	3.47
B		28.7	2336	47.3	2.02
DXLA60,A	315	30.4	2919	87.6	3.00
B		14.4	1815	10.2	0.56
LEV77,A	308	20.7	4696	113.4	2.41

TABLE II.2. Aerosol yields for m-xylene experiments

Experiment	Temp. (K)	$[HC/NO_x]_0$ (ppmC/ppm)	HC mass conc. ($\mu g\ m^{-3}$)	Aerosol mass conc. ($\mu g\ m^{-3}$)	Yield (%)
XA08, A	310	9.2	4751	184.8	3.89
B		8.5	4417	198.3	4.49
XB10, A	305	6.4	4532	165.1	3.64
B		6.5	4532	80.4	1.77
XB12, A	308	7.9	7130	287.9	4.04
B		8.1	6543	404.2	6.18
XG15, A	291	8.2	3773	93.4	2.48
B		18.3	2752	58.0	1.54
XK17, A	294	17.9	2592	88.4	3.41
B		17.8	2373	88.7	3.74
XJ19, A	296	21.4	2619	107.8	4.12
B		21.8	2750	77.6	2.82
XJ34, A	305	17.8	2711	92.9	3.43
B		17.8	2838	70.5	2.48
TXU75,B	307	15.9	5302	233.1	4.40

TABLE II.3. Aerosol yields for ethyl benzene experiments

Experiment	Temp. (K)	$[HC/NO_x]_0$ (ppmC/ppm)	HC mass conc. ($\mu g\ m^{-3}$)	Aerosol mass conc. ($\mu g\ m^{-3}$)	Yield (%)
EC64, A	309	14.9	2634	15.9	0.60
B		15.7	2634	12.0	0.45
EH66, A	304	16.7	2465	15.4	0.63
B		38.8	4037	188.6	4.67
EM70, A	311	34.4	3531	63.4	1.80
B		35.4	3531	94.7	2.68
EL73, A	310	32.7	2750	82.1	2.99
B		32.4	3084	80.5	2.61
LEV77,B	308	20.5	3188	28.7	0.90

TABLE II.4. Aerosol yields for 1,3,5-trimethyl benzene experiments

Experiment	Temp. (K)	$[HC/NO_x]_0$ (ppmC/ppm)	HC mass conc. ($\mu g\ m^{-3}$)	Aerosol mass conc. ($\mu g\ m^{-3}$)	Yield (%)
TE36, A	304	10.7	8996	356.4	3.96
B		10.7	10006	433.7	4.33
TE39, A	302	8.7	7942	304.8	3.84
B		8.6	8039	290.3	3.61
TI43, A	307	11.6	13243	311.6	2.35
B		20.3	5050	69.8	1.38
TO46, A	309	16.8	7478	121.1	1.62
B		17.1	6626	115.7	1.75
TN49, A	310	20.3	8869	120.0	1.35
B		21.1	9294	142.1	1.53
TN52, A	311	14.9	8982	145.8	1.62
B		15.1	9264	124.7	1.35
TXU75,A	307	28.1	8861	180.5	2.04

APPENDIX III

MISTI (MULTI-INSTRUMENT SMOOTHED-TWOMEY INVERSION) DOCUMENTATION AND PROGRAM LISTING

MISTI – Multi-Instrument Smoothed-Twomey Inversion – is a modified Twomey routine for the inversion of datasets from the EAA and the OPC. It is based on the routine THREATS, written by Dale Warren, based on a code by Greg Markowski. EAA data must be entered as current differences, not as raw currents. This can easily be modified in future revisions to the code. This program incorporates the following features:

- *time searching to start the inversion only when both instruments* have recorded data.
- time interpolation to bring OPC data to the same time as each EAA dataset. Both datasets are then inverted simultaneously at the EAA time.
- an initial size distribution estimate using the simple EAA raw data histogram for the first dataset. Thereafter, the previous distribution is used as a starting guess for the inversion.
- a smoothing routine to take out unrealistic waviness in the number distribution that may result from the Twomey algorithm.
- a Twomey inversion routine assuming a 49-element response matrix based on L. W. Richards' EAA kernel functions and tabulated instrument sensitivity functions, and OPC kernel functions based on spline-fits from Jim Crump's OPC calibration data. These 49 sizes range from 0.01 μm to 1.0 μm.
- iteration of the smoothing-Twomey cycles until the curvature of the distribution approaches a minimum, constrained by agreement with the measured data to within user-selected tolerances.

- for additional information, see references listed in source code, source code comments, and THREATS (analogous EAA code) documentation in Dale Warren's Ph.D. thesis (1986) (Reference in Appendix IV).

By default, MISTI goes through 20 loops, each consisting of up to 30 Twomey iterations (stopping on each channel as soon as the error tolerance is met) and one sub-channel distribution smoothing (1/2 prior value + 1/2 neighbors' average value). The Twomey iterations are done sequentially by instrument, with the OPC channels first followed by the EAA channels for particles smaller than 0.2 μm, and by the EAA first followed by the OPC for large particles. Alternately (using Markowski's suggestions), the routine can be made to stop when the prior two iterations have decreased the curvature by less than a set percentage. The final exit occurs after a set of Twomey iterations (not smoothings, as then error tolerance might not be met). The user may override these conditions if desired by setting values in MISTI.TOL, the tolerance input file. The appropriate tolerances will depend upon the stability of the measured aerosol and the precision with which the data were taken.

It is quite possible that MISTI will not meet the error tolerances on experimental data. This is probably due to errors in the calibration matrix. Nonetheless, we believe that this is the best multi-instrument inversion we have available to use on data such as these.

MISTI also allows the user to generate composite log-normal distributions for testing of the code with perfect aerosol data.

The following files are relevant to MISTI, and contain further information about the program:

MISTI.FOR	FORTRAN source file, with comments.
MISTI.EXE	Executable program
EAA.EI	Default input EAA data file.
OPC.OP	Default input OPC data file.
MISTI.TOL	Default experimental tolerances file
MTEST.TOL	Default test distribution tolerances file.
MISTI.OUT	Default text output file, suitable for printing.
STATS.OUT	Default output run statistics file.
MISTI.NUM	Output unformatted number distributions at each time.
DIST.#	Optionally created number and volume dists by inversion.
HISE.#	Optionally created number and volume dists by EAA histogram.
HISO.#	Optionally created number and volume dists by OPC histogram.

The following files are generated by MANAGE, the program that will read and interpret the unformatted .NUM file generated by MISTI.

NANDV.PRO	Total number and volume by histogram and by inversion.
MISTI.SUM	Total number, volume, and mean particle size by inversion.
DIST.#	Optionally created number and volume dists by inversion.
HISE.#	Optionally created number and volume dists by EAA histogram.
HISO.#	Optionally created number and volume dists by OPC histogram.

MISTI.NUM contains the following information in columns i:

1	Time
2–16	Number in channel $k, k = 1,15$ (raw data by both instruments)
17–65	Number distribution in channel $j, j = 1,49$ (inverted)

MISTI.SUM contains the following information in column i:

1	Time
2	Total number by inversion, $D_p > 0.01$ μm
3	Total number by inversion, $D_p > 0.02$ μm
4	Total volume by inversion
5	Number-average mean diameter
6	Volume-average mean diameter

NANDV.PRO contains the following information in column i:

1	Time
2	Total number by inversion, $D_p > 0.01$ μm
3	Total number by EAA histogram, channels 3-11
4	Total number by OPC histogram, channels 1-6
5	Total volume by inversion
6	Total volume by EAA histogram
7	Total volume by OPC histogram

DIST and HISE, HISO files contain the calculated size distributions, in the following order of variables:

DIST col.1:	$D_p(i)$, diameter of ith size range [microns]
DIST col.2:	dV/d log $D_p(i)$, volume distribution by MISTI
DIST col.3:	dN/d log $D_p(i)$, number distribution by MISTI
HISE col.1:	$D_p(k)$, EAA channel cut sizes
HISE col.2:	dV_h/d log $D_p(k)$, volume distribution by histogram
HISE col.3:	dN_h/d log $D_p(k)$, number distribution by histogram
HISO col.1:	$D_p(k)$, OPC channel cut sizes
HISO col.2:	dV_h/d log $D_p(k)$, volume distribution by histogram
HISO col.3:	dN_h/d log $D_p(k)$, number distribution by histogram

Program listings follow for MISTI, MANAGE (the data manipulation program to handle the unformatted output files of MISTI), and SMOOTH (the smoothing program that generates smoothed size distribution moment profiles). In addition, sample tolerance files for MISTI are given for inversion of experimental data (MISTI.TOL) and test distributions (MTEST.TOL).

```
      PROGRAM MISTI
C                    (Multi-Instrument Smoothed-Twomey Inversion)
C
C MARKOWSKI-TWOMEY INVERSION ALGORITHM
C
C   This code is currently set up to produce a number distribution
C     with 49 diameters between .01 um and 1.0 um.  As input, it
C     takes 2 datasets -- one from an EAA, and one from an OPC
C     Thus there are 16 input data for each inversion dataset:
C     10 EAA channels and 6 OPC channels.
C   This particular version of the code neglects channel 2 of the EAA,
C     hence using only 15 input data.
C   The inversion routine used is a Twomey inversion with repeated
C     smoothings between inversions to try to suppress some of the
C     wiggles which often result from a Twomey inversion. (See the
C     references below for more information.)  This program was
C     developed from a combination of the THREATS EAA inversion
C     routine and the STOPC OPC inversion routine, both of which use
C     this smoothed-Twomey inversion.
C   Note that PARAMS.INC must be in the same directory when compiling
C     so that it can be included in the code.
C   Note also that all EAA data must be entered at present as current
C     differences, not raw currents.  This can be changed in the future.
C
C   Generalization comments:
C       To generalize this code, several things must be done.  Flags
C       must be set up so that all of the indices can increment
C       automatically (k=1,9 e.g. for EAA), and output can still
C       be nicely formatted.  In addition, certain parameters that
C       have been designated instrument-specific by adding an E
C       or an O to the variable name should be made into vectors
C       (e.g. HOURE, and HOURO should become an array of HOUR(2,200)).
C       A QUERY input routine will allow the instruments desired to be
C       selected with the code automatically scaling itself properly.
C     Input procedure and formatting must be greatly improved.
C
C
C  REFERENCES:
C 1.  S. TWOMEY, COMPARISON OF CONSTRAINED LINEAR INVERSION
C     AND AN ITERATIVE NONLINEAR ALGORITHM APPLIED TO THE
C     INDIRECT ESTIMATION OF PARTICLE SIZE DISTRIBUTIONS,
C       J. COMP. PHYS., 18:188-200 (1979).
C 2.  GREGORY R. MARKOWSKI, IMPROVING TWOMEY'S ALGORITHM
C     FOR INVERSION OF AEROSOL MEASUREMENT DATA,
C       AEROSOL SCI & TECHNOL., 7:127-141 (1987).
C       3.  L. W. RICHARDS, THE REDUCTION OF DATA FROM THE ELECTRICAL
C         AEROSOL ANALYZER, PROCEEDINGS FROM AEROSOL MEASUREMENT
C             WORKSHOP, U. FLORIDA, MARCH 24-26, 1976.  PUBLISHED IN
C             AEROSOL MEASUREMENT, ED. D.A. LUNDGREN, (1979).
```

```
C
$INCLUDE: 'PARAMS.INC'
C
C   PARAMS.INC includes the values for NMIN,KMIN,NMAX and KMAX.
C    If the number of input channels changes, change KMAX.
C    If the number of output diameters in the distribution changes,
C     change NMAX.  All arrays will automatically be dimensioned
C     properly.
C
      COMMON /FLAG/ IPRNT,INFO,TESTD
      COMMON /TEST/ DG(3),SG(3),VM(3)
      COMMON /INFO/ HEAD,IMAXE,IMAXO
      COMMON /SIZE/ DIA(NMAX),DEAA(9),DOPC(7),DAVG(6)
      COMMON /DATA/ HOURE(200),HOURO(200),EAA(10,200),OPC(6,200)
      COMMON /RESMAT/ RM(KMAX,NMAX),RI(NMAX,KMAX),H(NMAX)
      COMMON /SET/ TARGET(KMAX),CTOL(KMAX),RFIT(KMAX),AFIT(KMAX)
      COMMON /DROP/ NDZERO,CMINE,CMINO
      COMMON /INVRT/ MAXTWO,MAXSMO,ISMAX,MINSMO,SMTOL
      COMMON /STATS/ JSET,JLOOP,JTWO,JCON,SUMSIG,BEGSIG,SUMCUR,BEGCUR
      CHARACTER*20 DFILE,SFILE,PFILE,TFILE,QFILE
      CHARACTER*70 HEAD
      CHARACTER*4 DNAME,ENAME,ONAME
      LOGICAL INFO,SAVDIS,SAVPRO,TESTD
      CHARACTER*1 ASK
      DIMENSION CURRNT(9),SENS(9),S(9)
      DIMENSION COUT(KMAX),HISTV(KMAX), HISTN(KMAX)
      DIMENSION TRIAL(NMAX), ATRIAL(NMAX)
      REAL SDIST(NMAX), VDIST(NMAX), RAT(NMAX), NDIST(NMAX)
      DIMENSION TOTNUM(2),STNUM(2),HISNUM(4),HISVOL(2)
C
      DATA S / 4.17E5, 1.67E5, 8.70E4, 4.44E4,
     #         2.41E4, 1.23E4, 6.67E3, 3.51E3, 1.80E3 /
C
      DO 3 I=1,9
 3      SENS(I) = S(I)
C
C  S and SENS are the instrument sensitivities (del N / del I) given in
C   the EAA manual.
C
      NOWSET = 0
C
C    First:  Set up response matrix for inversion and all relevant
C      diameters.
C
       CALL RESPONSE
C
C
C    Determine what info should be saved from the inversion:
C
```

```
C Current defaults will save the Output number dist. (.NUM)
C on which the MANAGE program may operate (dn/dlogdp).
C        MANAGE can create distributions (DIST.#) and histograms
C        (HIST.#) and a summary file (.SUM).
C        See MANAGE documentation for further info.
C
      WRITE(*,600)
 600  FORMAT(/' Save number distribution [Y] ? '\)
      READ(*,666) ASK
      SAVPRO=.TRUE.
      IF (ASK.EQ.'n' .OR. ASK.EQ.'N') THEN
          SAVPRO=.FALSE.
      ELSE
          WRITE(*,601)
 601      FORMAT(' Name of output file [MISTI.NUM] ? '\)
          READ(*,667) PFILE
 667      FORMAT(A)
          IF (PFILE.EQ.' ') PFILE='MISTI.NUM'
          WRITE(*,637)
 637      FORMAT(' Name of stats file [STATS.OUT] ? '\)
          READ(*,667) TFILE
          IF (TFILE.EQ.' ') TFILE='STATS.OUT'
      END IF
      WRITE(*,602)
 602  FORMAT(' Save each distribution and histograph [N] ? '\)
      READ(*,666) ASK
      SAVDIS=.FALSE.
      IF (ASK.EQ.'Y' .OR. ASK.EQ.'y') SAVDIS=.TRUE.
      WRITE(*,606)
 606  FORMAT(' Print detailed info [N] ? '\)
      READ(*,666) ASK
      INFO=.FALSE.
      IF (ASK.EQ.'Y' .OR. ASK.EQ.'y') INFO=.TRUE.
      WRITE(*,608)
 608  FORMAT(' Print intermediate dists (Y/N/S/T) [N] ? '\)
      READ(*,666) ASK
      IPRNT=0
      IF (ASK.EQ.'Y'.OR. ASK.EQ.'y') IPRNT=10
      IF (ASK.EQ.'S'.OR. ASK.EQ.'s') IPRNT=2
      IF (ASK.EQ.'T'.OR. ASK.EQ.'t') IPRNT=1
 666  FORMAT(A1)
      WRITE(*,609)
 609  FORMAT(' Use test distribution [N] ? '\)
      READ(*,666) ASK
      TESTD=.FALSE.
      IF (ASK.EQ.'Y' .OR. ASK.EQ.'y') TESTD=.TRUE.
      WRITE(*,*) ' '
C
      DNAME='DIST'
```

```
      ENAME='HISE'
      ONAME='HISO'
      IF (SAVPRO) THEN
        OPEN (11,FILE=PFILE,STATUS='NEW',FORM='UNFORMATTED')
        OPEN (12,FILE=TFILE,STATUS='NEW',FORM='FORMATTED')
      ENDIF
C
C         Get input parameters by INPUT subroutine
C
 200  CALL INPUT (NOWSET)
C
C   For experimental data, all of the data have been entered into
C   arrays/vectors.  We must first determine where to start joining
C   the datasets by seeing at what time both instruments have
C   recorded data.
C
       IF (.NOT.TESTD) THEN
         FIRST = HOURE(1)
         IF (HOURO(1).GE.FIRST) FIRST = HOURO(1)
C
C   The following are indices to indicate the first useful time.
C    Once they are set, they will not increment again.  Once both
C    are set, exit the loop and continue.
C
         IEAA = 0
         IOPC = 0
C
        DO 87 I=1,200
         IF (IEAA.EQ.0.AND.HOURE(I).GE.FIRST) IEAA = I
         IF (IOPC.EQ.0.AND.HOURO(I).GT.FIRST) IOPC = I
 87      IF (IEAA.NE.0.AND.IOPC.NE.0) GOTO 88
 88     CONTINUE
C
       END IF
C
C         USE FOLLOWING IF TARGET WAS NOT ENTERED AS AS A DATA SET;
C   ON TESTD = .TRUE. GENERATE SIZE DISTRIBUTION AND CALCULATE
C   TARGET FROM DISTRIBUTION PARAMETERS AND RESPONSE MATRIX.
C INIT sets SDIST array to zero.
C LOGNRM adds lognormal modes to SDIST (volume).
C RESP finds response TARGET from pseudocurrent TRIAL.
C
 700  IF ( TESTD ) THEN
        WRITE(*,121)
 121    FORMAT(' Enter information for up to 3 lognormal distributions')
        WRITE(*,122)
 122    FORMAT(' ENTER DG(I) I = 1 - 3 :  '\)
        READ (*,127) (DG(I),I=1,3)
        WRITE(*,123)
```

```
 123    FORMAT(' ENTER SG(I) I = 1 - 3 :  '\)
        READ (*,127) (SG(I),I=1,3)
        WRITE(*,126)
 126    FORMAT(' ENTER VOLUME(I) I = 1 - 3 :   '\)
        READ (*,127) (VM(I),I=1,3)
 127    FORMAT(3E10.3)
C
        WRITE(6,133) ( I,DG(I),SG(I),VM(I), I=1,3 )
 133    FORMAT(' MODE ',I2, ':   DG =',F6.3,'   SG =', F5.2,
     #         '   Vm =',F11.6)
        CALL INIT ( SDIST, NMAX, 0. )
        CALL LOGNRM ( 1, SDIST  )
        CALL LOGNRM ( 2, SDIST  )
        CALL LOGNRM ( 3, SDIST  )
C
C  We must convert the volume distribution returned by LOGNRM to
C   number distribution ATRIAL, from which TARGET will be created.
C
        CALL GETNUM ( ATRIAL, SDIST )
        CALL RESP ( ATRIAL, TARGET )
        DO 623 I=1,9
 623      CURRNT(I) = TARGET(I)
        IF (INFO) THEN
          WRITE(6,*) ' CALCULATED SUM OF LOGNORMAL DISTRIBUTIONS'
          WRITE(6,624)
          WRITE(6,625) (I, DIA(I), SDIST(I), ATRIAL(I), I=NMIN,NMAX)
        END IF
 624    FORMAT ( 2('   I     Dp    dV/dlDp    ATRIAL ',1X))
 625    FORMAT ( 2(I4,0PF8.4,F10.4,1PE10.3,2X) )
C
      ELSE
C
C  Set up TARGET for experimental data:
C   Exit if we have reached the last EAA data set with corresponding
C   OPC datasets on either side.
C
        HOUR = HOURE( IEAA + NOWSET - 1 )
 496    IF (HOURO(IOPC).LT.HOUR) THEN
            IOPC = IOPC + 1
            GOTO 496
        END IF
         IF (IOPC.GT.IMAXO) GOTO 990
C
        TIMEO = ( HOUR - HOURO(IOPC - 1) ) /
     +              ( HOURO(IOPC) - HOURO(IOPC-1) )
C
       DO 500 I = 1,9
         TARGET(I) = EAA ( I+1 , IEAA + NOWSET - 1 )
 500     CURRNT(I) = TARGET(I)
```

```
C
      DO 510 I = 1,6
 510    TARGET(I+9) = (1.-TIMEO)*OPC(I,IOPC-1) + TIMEO*OPC(I,IOPC)
C
C  This sets up TARGET as:
C     channels 1-9         EAA current differences from .EI files
C     channels 10-15       OPC counts from .OP files
C
      END IF
C
C Write out value for each target channel in table.
C Calculate total tolerances from RFIT(K) and AFIT(K)
C
C  Only print this out on the first pass:
C
      IF (NOWSET.LE.1) THEN
C
       DPAVG = 0.02
C
C   Just to initialize for first inversion
C
         WRITE(*,112) (K+2, K=1,9)
         WRITE(6,112) (K+2, K=1,9)
         WRITE(6,117) (RFIT(K),K=1,9)
         WRITE(*,117) (RFIT(K),K=1,9)
         WRITE(6,118) (AFIT(K),K=1,9)
         WRITE(*,118) (AFIT(K),K=1,9)
         WRITE(*,111) (K-9, K=10,15)
         WRITE(6,111) (K-9, K=10,15)
         WRITE(6,113) (RFIT(K),K=10,15)
         WRITE(*,113) (RFIT(K),K=10,15)
         WRITE(6,114) (AFIT(K),K=10,15)
         WRITE(*,114) (AFIT(K),K=10,15)
      END IF
C
 112  FORMAT (/' EAA CHANNEL',1X,I2,9I7 )
 117  FORMAT (' RFIT TOL', 9F7.4 )
 118  FORMAT (' AFIT TOL', 9F7.4 )
 111  FORMAT (/' OPC CHANNEL',I6,5I10)
 113  FORMAT (' RFIT TOL', 6F10.3 )
 114  FORMAT (' AFIT TOL', 6F10.3 )
C
      WRITE(*,124) NOWSET,HOUR
      WRITE(6,124) NOWSET,HOUR
 124  FORMAT(/'  EAA Dataset # ',I3,' at time ',F8.4 )
C
      WRITE(*,112) (K+2, K=1,9)
      WRITE(6,112) (K+2, K=1,9)
C
```

```
      WRITE(*,210) (TARGET(K), K=1,9)
      WRITE(6,210) (TARGET(K), K=1,9)
C
      WRITE(*,111) (K-9, K=10,15)
      WRITE(6,111) (K-9, K=10,15)
C
      WRITE(*,212) (TARGET(K), K=10,15)
      WRITE(6,212) (TARGET(K), K=10,15)
C
 210  FORMAT (' CURRENT ',9F7.3)
 212  FORMAT (' COUNTS  ',6F10.2)
C
C   Set minimum value.
C
      CALL NONEG(CURRNT)
C        This removes negative current differences from EAA target
C
      DO 140 K = 1,9
         TARGET(K) = CURRNT(K)
         IF (TARGET(K).LE.CMINE) TARGET(K)=CMINE
 140     CTOL(K) = RFIT(K) * TARGET(K) + AFIT(K)
      DO 141 K = 10,15
         IF (TARGET(K).LE.CMINO) TARGET(K)=CMINO
 141     CTOL(K) = RFIT(K) * TARGET(K) + AFIT(K)
C
      WRITE(6,211) (TARGET(K),K=1,9)
      WRITE(*,211) (TARGET(K),K=1,9)
      WRITE(*,104) (CTOL(K),K=1,9)
      WRITE(6,104) (CTOL(K),K=1,9)
      WRITE(6,213) (TARGET(K),K=10,KMAX)
      WRITE(*,213) (TARGET(K),K=10,KMAX)
      WRITE(*,105) (CTOL(K),K=10,KMAX)
      WRITE(6,105) (CTOL(K),K=10,KMAX)
 104  FORMAT(' EAA CTOL',9F7.3)
 105  FORMAT(' OPC CTOL ',6x,6F8.2)
 211  FORMAT (/' Corrected',F6.3,8F7.3)
 213  FORMAT (/' Corrected',6x,6F8.2)
      WRITE(6,*) ' '
      WRITE(*,*) ' '
C
C        Calculate beginning guess
C
C   For NOWSET <= 1, this is the first dataset.  The EAA current
C   distribution will give the initial guess.  After that, TRIAL
C   (the solution vector) will be used as the starting guess for
C   the next dataset.  Subroutine GUESS is left in for the user
C   to optionally change the starting guess routine.
C
      IF (NOWSET.LE.1) THEN
```

```
         CALL GUESS(TRIAL,TARGET,SENS)
      ELSE
        DO 23 I=1,NMAX
 23       ATRIAL(I)=TRIAL(I)
      END IF
C
C        Smoooth initial guess
C
      CALL SMOOTH ( TRIAL, NDZERO )
      IF (INFO) WRITE (6,*) ' BEGINNING TRIAL DISTRIBUTION'
      IF (INFO) WRITE (6,640) (I, TRIAL(I), I = NMIN,NMAX)
 640  FORMAT ( 4(I4,1pe10.3) )
C
C        Write ideal response matrix
C
      IF (INFO.AND.NOWSET.EQ.1) THEN
           WRITE (6, 610 )
 610       FORMAT ( // 20X, ' EAA RESPONSE MATRIX ')
           WRITE (6,611) (I, I = 3,11 )
 611       FORMAT (8X, 9I8)
           WRITE(6,613) (I,DIA(I),(RI(I,K), K=1,9),I=NMIN,NMAX)
 613       FORMAT (I3,F7.4,1X,9E8.2)
           WRITE (6, 612 )
 612       FORMAT ( // 16X, ' OPC RESPONSE MATRIX ')
           WRITE (6,614) (I, I = 1,6 )
 614       FORMAT (11X, 6I8,)
           WRITE(6,615) (I,DIA(I),(RI(I,K), K=10,15),I=NMIN,NMAX)
 615       FORMAT (I3,F7.4,2X,6F8.3)
           WRITE(6,*) ' '
      END IF
C
C        Save first trial values
C Optionally print size distribution
C Note: SDIST is starting true volume distribution if
C               TESTD.EQ.TRUE
C
      IF (.NOT.TESTD) THEN
        DO 190 I = NMIN,NMAX
 190       ATRIAL(I) = TRIAL(I)
      END IF
        CALL GETVOL ( ATRIAL, SDIST, STVOL, STNUM )
C
      CALL HISTO ( TARGET, SENS, HISTV, HISTN, HISVOL, HISNUM )
      IF (INFO) THEN
        WRITE (6,*) ' TRIAL (STARTING NUMBER DISTRIBUTION) :'
        WRITE (6,617) (TRIAL(I), I=NMIN,NMAX)
        WRITE (6,*) ' SDIST (STARTING VOLUME DISTRIBUTION) :'
        WRITE( 6,617) (SDIST(I), I=NMIN,NMAX)
        WRITE(6,*) ' TARGET (TRUE VALUES) :'
```

```
       WRITE (6,616) (TARGET(K), K=1,9)
       WRITE (6,617) (TARGET(K), K=10,15)
 616  FORMAT (9F7.3)
 617  FORMAT (1PE10.3,5E10.3)
      END IF
C
C PRELIMINARIES DONE . . . Invert the data.
C
C INVERT repeatedly applies the TWOMEY algorithm and smooths.
C     DPAVG is passed because the order of the TWOMEY corrections will
C      be based on the average particle size in the inverted dist.
C
      CALL INVERT (TRIAL, COUT, DPAVG )
C
C Get calculated volume distrib in VDIST (DV/DLOGDP)
C
      CALL GETVOL (TRIAL, VDIST, TOTVOL, TOTNUM)
C
      DPAVG = (TOTVOL/TOTNUM(1) *6./3.14159 ) ** (1./3.)
c
C Save or display the final results
C
      WRITE(*,629) 'INITL',STVOL,STNUM
      WRITE(*,629) 'HISTE',HISVOL(1),(HISNUM(I),I=1,2)
      WRITE(*,629) 'HISTO',HISVOL(2),(HISNUM(I),I=3,4)
      WRITE(*,629) 'INVRT',TOTVOL,TOTNUM
      WRITE(6,629) 'INITL',STVOL,STNUM
      WRITE(6,629) 'HISTE',HISVOL(1),(HISNUM(I),I=1,2)
      WRITE(6,629) 'HISTO',HISVOL(2),(HISNUM(I),I=3,4)
      WRITE(6,629) 'INVRT',TOTVOL,TOTNUM
 629  FORMAT(/' Method ',A5,' gives  TV = ',1pe10.2,'   TN = ',2E10.2)
      WRITE(6,*) ' '
      IF (INFO) WRITE(6,620) HEAD
 620  FORMAT(/A)
      WRITE(6,*) ' '
      WRITE(6,644)
 644  FORMAT(5X,'DIAMETER    START    FINAL     VOLUME       RATIO'
     #/    '   I    DP       NDIST    NDIST      DIST        Fi/St')
C
      DO 300 I = NMIN,NMAX
C  Add the following check and fake RAT to avoid divide-by-zero errors
        IF (SDIST(I).LT.1.E-12) THEN
         RAT(I) = 111111.11
        ELSE
         RAT(I) = VDIST(I)/SDIST(I)
        END IF
 300  CONTINUE
C
      WRITE(6,125)  (I,DIA(I),ATRIAL(I),TRIAL(I),VDIST(I),
```

```
     #                RAT(I), I=NMIN,NMAX)
 125  FORMAT ( I4, F8.4, F10.1, F10.1, F10.3, F10.2 )
C
C  Unformatted Output   MISTI.NUM
C 1 HOUR
C               2-16 TARGET(K)
C               17-65   NDIST(I)
C
      IF (SAVPRO) WRITE(11) HOUR,(TARGET(K),K=1,KMAX),
     #    (TRIAL(I),I=1,NMAX)
C
C     Display true and calculated TARGET values
C
      WRITE(*,621)
      WRITE(6,621)
 621  FORMAT(/'  EAA  MIDPOINT  MEASURED  CALC     RATIO     DIFF' /
     #        ' CHAN    DIA      CURR     CURR     Ic/Im     Ic-Im')
      DO 220 K=1,9
         CRAT=COUT(K)/TARGET(K)
         CDIF=COUT(K)-TARGET(K)
         WRITE(*,622) K+2, DEAA(K), TARGET(K), COUT(K), CRAT, CDIF
         WRITE(6,622) K+2, DEAA(K), TARGET(K), COUT(K), CRAT, CDIF
 220  CONTINUE
 622  FORMAT(I4, F8.4 ,F9.4, F9.4, F10.3, F9.3)
      WRITE(*,723)
      WRITE(6,723)
 723  FORMAT(/'  OPC  MIDPOINT MEASURED   CALC     RATIO      DIFF' /
     #        ' CHAN    DIA     COUNTS    COUNTS   Nc/Nm      Nc-Nm')
      DSUM = 0.
      CSUM = 0.
      DO 222 K=10,15
         CRAT=COUT(K)/TARGET(K)
         CDIF=COUT(K)-TARGET(K)
         CSUM = CSUM + TARGET(K)
         DSUM = DSUM + CDIF
         WRITE(*,627) K, DAVG(K-9), TARGET(K), COUT(K), CRAT, CDIF
         WRITE(6,627) K, DAVG(K-9), TARGET(K), COUT(K), CRAT, CDIF
 222  CONTINUE
 627  FORMAT(I4, F8.4 ,2x,1PE10.3, 1PE10.3, 0PF9.3, F11.3)
      DPERC = ABS(DSUM/CSUM) * 100.
      WRITE(6,630) DSUM
      WRITE(*,630) DSUM
      WRITE(6,631) CSUM,DPERC
      WRITE(*,631) CSUM,DPERC
 630  FORMAT ('  Total OPC number difference: final-initial ',f10.3)
 631  FORMAT ('                    with initial number: ',1pe10.3,
     #          ' or ',0pf7.2,' percent',/)
      WRITE(*,*) ' '
      WRITE(6,*) ' '
```

```
      WRITE(*,*) '-----------------------------------------'
C
C Option to save each distribution as DIST.# and HIST.#
c
      IF (SAVDIS) THEN
        IF (NOWSET.LT.10) THEN
           WRITE(DFILE,201) DNAME,NOWSET
           WRITE(SFILE,201) ENAME,NOWSET
           WRITE(QFILE,201) ONAME,NOWSET
        ELSEIF (NOWSET.LT.100) THEN
           WRITE(DFILE,202) DNAME,NOWSET
           WRITE(SFILE,202) ENAME,NOWSET
           WRITE(QFILE,202) ONAME,NOWSET
        ELSE
           WRITE(DFILE,203) DNAME,NOWSET
           WRITE(SFILE,203) ENAME,NOWSET
           WRITE(QFILE,203) ONAME,NOWSET
        ENDIF
 201    FORMAT(A,'.',I1)
 202    FORMAT(A,'.',I2)
 203    FORMAT(A,'.',I3)
C
C DIST.n will contain the following table of results:
C         Dp  Vol(SmTw)  N(SmTw)
C
        OPEN (9,FILE=DFILE,STATUS='NEW',FORM='FORMATTED')
        DO 800 I=NMIN,NMAX
 800       WRITE(9,810) DIA(I),VDIST(I),TRIAL(I)
 810     FORMAT(1X,F7.4,2X,2F11.4)
         CALL CLOSE(9)
C
C HISTE.n will contain the following table of results.
C   Dp{min/max}  Vol(Sim)  N(Sim)     for EAA
C
        EAAHLF = 10.**0.125
        OPEN (8,FILE=SFILE,STATUS='NEW',FORM='FORMATTED')
           WRITE(8,860) DEAA(1)/EAAHLF,0.,0.
        DO 850 K=1,9
           WRITE(8,860) DEAA(K)/EAAHLF,HISTV(K),HISTN(K)
 850       WRITE(8,860) DEAA(K)*EAAHLF,HISTV(K),HISTN(K)
 860    FORMAT(1X,F7.4,2X,F10.4,2X,F11.2)
        CALL CLOSE(8)
C
C HISTO.n will contain the following table of results.
C   Dp{min/max}  Vol(Sim)  N(Sim)     for OPC
C
        OPEN (7,FILE=QFILE,STATUS='NEW',FORM='FORMATTED')
           WRITE(7,860) DOPC(1),0.,0.
        DO 870 K=10,15
```

```
          WRITE(7,860) DOPC(K-9),HISTV(K),HISTN(K)
 870      WRITE(7,860) DOPC(K-8),HISTV(K),HISTN(K)
        CALL CLOSE(7)
      ENDIF
C
C     Process next EAA dataset (and associated OPC dataset)
C        Optionally, allow another test distribution to be input.
C
      IF (.NOT.TESTD) THEN
        NOWSET = NOWSET + 1
        IF ((IEAA+NOWSET).LE.IMAXE) GOTO 700
      ELSE
        WRITE (*,872)
 872    FORMAT(1X,' Do you want to do another test distribution? '\)
        READ(*,666) ASK
        IF (ASK.EQ.'Y' .OR. ASK.EQ.'y') THEN
           NOWSET = 0
           GOTO 200
        END IF
      END IF
C
C         Inversion procedure done
C
 990  CALL CLOSE (6)
      IF (SAVPRO) CALL CLOSE(11)
      IF (JSET.GT.0) THEN
        SETS=FLOAT(JSET)
        AVLOOP=FLOAT(JLOOP)/SETS
        AVTWO=FLOAT(JTWO)/SETS
        AVTWOL=AVTWO/AVLOOP
        AVCON=100.*FLOAT(JCON)/SETS
        AVCUR=SUMCUR/SETS
        AVCURO=BEGCUR/SETS
        AVSIG=SUMSIG/SETS
        AVSIGO=BEGSIG/SETS
        WRITE(*,995) JSET,AVLOOP,AVTWO,AVTWOL,AVCON
        WRITE(6,995) JSET,AVLOOP,AVTWO,AVTWOL,AVCON
        WRITE(12,995) JSET,AVLOOP,AVTWO,AVTWOL,AVCON
 995    FORMAT(/10X,'Statistics for',I4,' Datasets:'/
     #  ' Average Smoothing Loops = ',F7.2 /
     #  ' Average Twomey Iterations = ',F7.2 /
     #  ' Average Twomey Iterations per Loop = ',F7.2 /
     #  ' Percentage of Datasets meeting TOLERANCE = ',F6.1,' %' )
        WRITE(*,996) AVSIGO,AVSIG,AVCURO,AVCUR
        WRITE(6,996) AVSIGO,AVSIG,AVCURO,AVCUR
        WRITE(12,996) AVSIGO,AVSIG,AVCURO,AVCUR
 996    FORMAT(' Average Initial Sigma (del/tol) = ',F12.3 /
     #  ' Average Final Sigma = ',F12.3 /
     #  ' Average Initial Curvature = ',1PE11.3 /
```

```
     #   ' Average Final Curvature = ',1PE11.3 /)
         ELSE
           WRITE(*,997)
           WRITE(6,997)
           WRITE(12,997)
 997     FORMAT(/' No Statistics Available !?'/)
         END IF
         STOP 'Multi-instrument Inversion Program MISTI Done.'
         END
C
C=======================================================================
C
         SUBROUTINE RESPONSE
C
C  Sets up response matrix and diameters for inversion.
C
$INCLUDE: 'PARAMS.INC'
         COMMON /SIZE/ DIA(NMAX),DEAA(9),DOPC(7),DAVG(6)
         COMMON /RESMAT/ RM(KMAX,NMAX),RI(NMAX,KMAX),H(NMAX)
         DIMENSION RME(9,NMAX),RMO(6,NMAX),Q(NMAX)
         DIMENSION RMX(252), RMY(189)
         EQUIVALENCE (RMX(1),RME(1,1)) , (RMY(1),RME(1,29))
         DIMENSION RMW(264),RMZ(30)
         EQUIVALENCE (RMW(1),RMO(1,1)) , (RMZ(1),RMO(1,45))
C
C
C        Below are the EAA kernel functions as directly out of THREATS.
C RME was split into RMX and RMY so DATA had <10 Continuations
C        These are rows 1-49 of the response matrix.
C
         DATA RMX /  0.5,8*0., .95,8*0., 1.,8*0., 1.,8*0., 1.,8*0.,
        1   .95,.05,7*0., .5,.5,7*0., .05,.95,7*0., .07,.93,7*0.,
        2   .09,.91,7*0., 0.,.97,.03,6*0., 0.,.84,.16,6*0.,
        3   0.,.51,.49,6*0., 0.,.37,.56,.07,5*0., 0.,.44,.27,.29,5*0.,
        4   0.,.48,.08,.44,5*0., 0.,.45,.16,.39,5*0., 0.,.20,.47,.27,
        5   .06,4*0., 0.,.14,.36,.33,.17,4*0., 0.,.09,.20,.53,.18,4*0.,
        6   2*0.,.28,.60,.09,.03,3*0., 2*0.,.14,.58,.24,.04,3*0.,
        7   2*0.,.08,.69,.19,.04,3*0., 2*0.,.02,.58,.32,.08,3*0.,
        8   3*0.,.57,.36,.07,3*0., 3*0.,.55,.37,.08,3*0.,
        9   3*0.,.46,.46,.08,3*0., 3*0.,.42,.50,.08,3*0. /
C
         DATA RMY / 3*0.,.14,.71,.12,.03,2*0., 3*0.,.10,.60,.24,.06,2*0.,
        1   3*0.,.03,.47,.39,.08,.03,0., 4*0.,.40,.42,.13,.05,0.,
        2   4*0.,.31,.46,.16,.05,.02, 4*0.,.22,.48,.21,.06,.03,
        3   4*0.,.17,.50,.23,.07,.03, 4*0.,.11,.48,.27,.09,.05,
        4   4*0.,.08,.42,.32,.11,.07, 4*0.,.05,.40,.35,.12,.08,
        5   4*0.,.03,.34,.36,.15,.12, 5*0.,.30,.36,.21,.13,
        6   5*0.,.26,.37,.20,.17, 5*0.,.22,.35,.24,.19, 5*0.,.18,.36,
        7   .25,.21, 5*0.,.14,.35,.25,.26, 5*0.,.13,.31,.25,.31,
```

```
     8   5*0.,.12,.29,.24,.35, 5*0.,.08,.25,.24,.43,
     9   5*0.,.08,.20,.24,.48, 5*0.,.07,.15,.26,.52 /
C
C  Below is the so-called H-function, or delta I / delta N.
C   [This is entered as Q, and transferred to H so that it can
C    be passed in COMMON]
C   This, multiplied by the previous kernel functions, will give
C   a new kernel function which will produce current values from
C   number distribution.
C    These values come from the paper by Richards referenced at
C    the start of the program.
C
       DATA Q /
     1    8.11E-7, 1.3E-6, 1.7E-6, 2.0E-6, 2.4E-6, 3.0E-6, 3.9E-6,
     2    4.8E-6, 5.6E-6, 6.3E-6, 7.0E-6, 8.0E-6, 8.88E-6, 9.88E-6,
     3    1.12E-5, 1.22E-5, 1.36E-5, 1.51E-5, 1.69E-5, 1.88E-5,
     4    2.09E-5, 2.32E-5, 2.58E-5, 2.87E-5, 3.20E-5, 3.56E-5,
     5    3.96E-5, 4.41E-5, 4.90E-5, 5.46E-5, 6.07E-5, 6.75E-5,
     6    7.51E-5, 8.36E-5, 9.31E-5, 1.04E-4, 1.15E-4, 1.28E-4,
     7    1.43E-4, 1.59E-4, 1.77E-4, 1.97E-4, 2.19E-4, 2.43E-4,
     8    2.71E-4, 3.01E-4, 3.35E-4, 3.73E-4, 4.15E-4 /
C
C  Now enter the OPC kernel functions into RMW and RMZ.  These will
C    be combined into RMO (avoiding too many continuations, again)
C      -- RME and RMO will be combined to give RM
C
       DATA RMW /  132*0.,.009,5*0., .035,5*0., .063,.010,4*0.,
     1   .092,.016,.001,3*0., .117,.025,.001,3*0., .142,.059,.001,3*0.,
     2   .163,.145,.008,3*0., .179,.286,.026,3*0., .188,.465,.046,3*0.,
     3   .188,.656,.059,3*0., .175,.808,.047,3*0., .148,.833,.016,3*0.,
     4   .107,.670,.223,3*0., .060,.390,.548,.001,2*0., .029,.191,
     5   .778,.001,2*0., .028,.157,.805,.010,2*0., .035,.096,.807,
     6   .061,.001,0., .039,.052,.663,.246,.001,0.,
     7   .038,.024,.442,.495,.002,0., .034,.010,.259,.694,.003,0.,
     8   .030,.006,.205,.752,.006,0., .030,.009,.169,.735,.055,.001 /
       DATA RMZ /
     1   .035,.014,.063,.451,.431,.004, .032,.016,.004,.202,.725,.012,
     2   .021,.016,.003,.161,.692,.081, .019,.015,.003,.110,.557,.267,
     3   .023,.014,.003,.044,.354,.491 /
C
       DO 60 I=1,NMAX
 60     H(I) = Q(I)
C
C   Set diameters for inverted distribution from 0.01 um to 1.0 um
C
      DIA(1) = 0.01
      DO 100 I = 2,NMAX
 100     DIA(I) = DIA(I-1) *  1.100694
C          Note that 1.100694 is 10**(1./24) for 24 sizes per decade.
```

```
C
C  Now set diameters for EAA channels 2-10.  These are average diameters.
C
      DEAA(1) = 0.01333521
      DO 110 K = 2,9
 110     DEAA(K) = DEAA(K-1) * 1.778279
C
C  Now set diameters for OPC.
C  DOPC are the cut sizes at the bottoms of each channel.  To get
C    the average particle size (DAVG) multiply i by i+1 and take sqrt.
C
      DOPC(1) = 0.12
      DOPC(2) = 0.17
      DOPC(3) = 0.27
      DOPC(4) = 0.42
      DOPC(5) = 0.62
      DOPC(6) = 0.87
      DOPC(7) = 1.17
C
      DO 111 K = 1,6
 111     DAVG(K) = SQRT(DOPC(K)*DOPC(K+1))
C
C  Now set up the response matrix RM by combining RME (the EAA response
C   matrix) and RMO (the OPC response matrix)
C
      DO 50 I=1,NMAX
       DO 30 J=1,9
 30      RM(J,I) = RME(J,I) * H(I)
       DO 40 J=10,15
 40      RM(J,I) = RMO(J-9,I)
 50   CONTINUE
C
C        Transfer RM to RI in proper order
C
      DO 120 I = 1,NMAX
         DO 115 K = 1, KMAX
              RI(I,K) = RM(K,I)
 115     CONTINUE
 120  CONTINUE
C
      RETURN
      END
C
C-----------------------------------------------------------------------
C
      SUBROUTINE INPUT ( NOWSET )
C
C  This subroutine reads the input from 3 files.
C  Unit 2 is the raw EAA data, Unit 3 is the raw OPC data,
```

```
C   and Unit 5 is the tolerance file.
C  The user will be queried for file names.
C
C  Next the times and data will be read and stored for each instrument.
C   This will be passed back to the main program, which will do time-
C   interpolation to bring the datasets to the same time to create
C   the TARGET vector.
C
C---Unit 2-------------  *.INP  ------------------------------------
C1>  A70 Text to Identify Dataset
C2>  * KDIF{1=delta currents}
C3+> 11F7.0 HOUR, EAA(K),K=1,10
C
C----Unit 3-------------  *.OP  -------------------------------------
C1+> F7.0,7E10.3 HOUR, TOTNUM, OPC(K),K=1,6
C
C---Unit 5-------------  *.TOL  ------------------------------------
C1> A70 Text to Identify Tolerances
C2> 9F7.0 RFIT(K),K=1,9 {relative tolerance, -1. repeats}
C3> 6F7.0 RFIT(K),K=10,15
C4> 9F7.0 AFIT(K),K=1,9 {absolute tolerance, -1. repeats}
C5> 6F7.0 AFIT(K),K=10,15
C6> 4I7,F7.0            MAXTWO,MAXSMO,ISMAX,MINSMO,SMTOL
C7> I7,2F7.0 NDZERO,CMINE,CMINO
C
C-------------------------------------------------------------------------
C
$INCLUDE: 'PARAMS.INC'
      COMMON /FLAG/ IPRNT,INFO,TESTD
      COMMON /TEST/ DG(3),SG(3),VM(3)
      COMMON /INFO/ HEAD,IMAXE,IMAXO
      COMMON /SET/ TARGET(KMAX),CTOL(KMAX),RFIT(KMAX),AFIT(KMAX)
      COMMON /INVRT/ MAXTWO,MAXSMO,ISMAX,MINSMO,SMTOL
      COMMON /DROP/ NDZERO,CMINE,CMINO
      COMMON /STATS/ JSET,JLOOP,JTWO,JCON,SUMSIG,BEGSIG,SUMCUR,BEGCUR
      COMMON /DATA/ HOURE(200),HOURO(200),EAA(10,200),OPC(6,200)
      CHARACTER*20 OFILE,EFILE,PFILE,TFILE
      CHARACTER*70 HEAD
      LOGICAL INFO,TESTD
      DIMENSION OPCNUM(200)
C
      IF (NOWSET.EQ.0) THEN
C
C   Initialize variables
C
        MAXTWO=0
MAXSMO=0
ISMAX=0
        MINSMO=0
```

```
SMTOL=0.
NDZERO=0
        CMINE=0.
        CMINO=0.
        JSET=0
        JLOOP=0
        JTWO=0
        JCON=0
        SUMSIG=0.
        BEGSIG=0.
        SUMCUR=0.
        BEGCUR=0.
        WRITE(*,50) 'Enter Tolerances Filename [MISTI.TOL]: '
        READ (*,55) TFILE
        WRITE(*,50) 'Enter Output Filename [MISTI.OUT]: '
        READ (*,55) OFILE
  50    FORMAT(1X,A\)
  55    FORMAT(A)
        IF (TFILE.EQ.' ') TFILE='MISTI.TOL'
        IF (OFILE.EQ.' ') OFILE='MISTI.OUT'
        OPEN(5,FILE=TFILE,STATUS='OLD')
        OPEN(6,FILE=OFILE,STATUS='NEW')
        WRITE (6,101) TFILE,OFILE
 101    FORMAT (2X, 2(A20,2X) )
        READ (5,104) HEAD
 104    FORMAT (A70)
        WRITE (6,104) HEAD
        WRITE (*,104) HEAD
C
C       Read in *.TOL
C
        READ (5,300) (RFIT(K),K=1,9)
        READ (5,320) (RFIT(K),K=10,15)
        READ (5,300) (AFIT(K),K=1,9)
        READ (5,320) (AFIT(K),K=10,15)
 300    FORMAT(9F7.0)
 320    FORMAT(6F7.0)
        READ (5,180) MAXTWO,MAXSMO,ISMAX,MINSMO,SMTOL
 180    FORMAT (4I7,F7.0)
        READ (5,185) NDZERO,CMINE,CMINO
 185    FORMAT(I7,2F7.0)
        CALL CLOSE(5)
C
C        Fit tolerance for each stage
C
C Use -1. in RFIT or AFIT to use last value for remainder
C If no last value, default to RFIT(K)=.05, AFIT(K)=.002
C
        IF (RFIT(KMIN).LT.0.) THEN
```

```
  RFIT(KMIN)=0.05
  RFIT(KMIN+1)=-1.
ENDIF
IF (AFIT(KMIN).LT.0.) THEN
  AFIT(KMIN)=0.1
  AFIT(KMIN+1)=-1.
ENDIF
        DO 196 K=KMIN+1,KMAX
           IF (RFIT(K).LT.0.) THEN
             DO 192 I=K,KMAX
 192 RFIT(I)=RFIT(K-1)
   END IF
           IF (AFIT(K).LT.0.) THEN
             DO 194 I=K,KMAX
 194            AFIT(I)=AFIT(K-1)
           END IF
 196    CONTINUE
C
C Set defaults
C
      IF (MAXTWO.EQ.0) MAXTWO = 30
      IF (MAXSMO.EQ.0) MAXSMO = 20
      IF (ISMAX.EQ.0) ISMAX = 5
      IF (MINSMO.EQ.0) MINSMO = 5
      IF (SMTOL.EQ.0.) SMTOL = 1.2
      IF (CMINE.LE.0.) CMINE = 1.E-5
      IF (CMINO.LE.0.) CMINO = 1.E-3
C            Note that CMIN is needed since Twomey will not change
C              an initial guess of zero.
C
        IF (TESTD) THEN
          NOWSET = NOWSET + 1
          RETURN
        END IF
C
C             Otherwise, open data file and start reading in data
C
        WRITE(*,50) 'Enter EAA Input Data Filename [EAA.EI]: '
        READ (*,55) EFILE
        IF (EFILE.EQ.' ') EFILE='EAA.EI'
        OPEN(2,FILE=EFILE,STATUS='OLD')
C
        WRITE(*,50) 'Enter OPC Input Data Filename [OPC.OP]: '
        READ (*,55) PFILE
        IF (PFILE.EQ.' ') PFILE='OPC.OP'
        OPEN(3,FILE=PFILE,STATUS='OLD')
C
        START = 0.
        WRITE(*,50) 'Enter Run Starting Time in hours [0.]: '
```

```
        READ (*,60) START
 60     FORMAT (F6.4)
C
       END IF
C
C  Now read in the time vectors and data for both instruments.
C   These will be needed to bring datasets together at the proper times.
C   Note that EAA data are in real time, not run time.
C   START time will convert everything to run time.
C
C  First delete header on EAA file.
C
       DO 230 I=1,2
         READ(2,220) HEAD
 220     FORMAT (A70)
 230   CONTINUE
C
       DO 400 I=1,200
         READ(2,250,END=410) HOURE(I),(EAA(K,I), K=1,10)
 250     FORMAT( F7.4, 10(F7.4) )
         HOURE(I) = HOURE(I) - START
 400     IMAXE = I
 410   CONTINUE
C
       DO 460 I=1,200
         READ(3,270,END=470) HOURO(I),OPCNUM(I),
     #      (OPC(K,I), K=1,6)
 270     FORMAT(1X,F7.3,E10.3,1X,6E10.3)
 460     IMAXO = I
 470   CONTINUE
C
 880  NOWSET = NOWSET + 1
 900  CALL CLOSE(2)
      CALL CLOSE(3)
      CALL CLOSE(4)
C
      RETURN
      END
C
C-----------------------------------------------------------------------
C
      SUBROUTINE GUESS(TRIAL,TARGET,SENS)
C
C  Subroutine GUESS will calculate an initial distribution for the
C   first TARGET value.  Since this is usually the beginning of an
C   experimental run, the initial EAA target will be used to create an
C   initial distribution.  This will be done by converting the raw
C   data to a number distribution at the 9 average channel diameters,
C   then doing a linear interpolation in between these points.
```

```
C   After the first dataset, the previous distribution will be used
C   as the starting guess for the next dataset.   This should be a
C   relatively good guess and should speed up the inversion a bit,
C   as well as increasing the chances of convergence.
C
$INCLUDE: 'PARAMS.INC'
      COMMON /SIZE/ DIA(NMAX),DEAA(9),DOPC(7),DAVG(6)
      COMMON /RESMAT/ RM(KMAX,NMAX),RI(NMAX,KMAX),H(NMAX)
      DIMENSION SENS(9),DNUM(9)
      DIMENSION TRIAL(NMAX),TARGET(KMAX)
C
      DO 100 K=1,9
C
C   The 4 is 1 / DLOGDP for the EAA channels
C
        DNUM(K) = SENS(K) * TARGET(K) * 4.
 100  CONTINUE
C
      TRIAL(1) = DNUM(1) * 0.5
      TRIAL(2) = DNUM(1) * 0.667
      TRIAL(3) = DNUM(1) * 0.833
C
      DO 150 I=1,8
         TRIAL(6*I - 2) = DNUM(I)
         TRIAL(6*I - 1) = 0.833*DNUM(I) + 0.167*DNUM(I+1)
         TRIAL(6*I) = 0.667*DNUM(I) + 0.333*DNUM(I+1)
         TRIAL(6*I + 1) = 0.5*DNUM(I) + 0.5*DNUM(I+1)
        IF (I.NE.8) THEN
         TRIAL( 6*I + 2 ) = 0.333*DNUM(I) + 0.667*DNUM(I+1)
         TRIAL( 6*I + 3 ) = 0.167*DNUM(I) + 0.833*DNUM(I+1)
        END IF
 150  CONTINUE
C
      RETURN
      END
C
C-------------------------------------------------------------------------
C
      SUBROUTINE INIT ( A, N, CONST )
C
C         INIT merely initializes array A to CONST.
C
      DIMENSION A(N)
      DO 10 J = 1,N
  10    A(J) = CONST
      RETURN
      END
C
C-----------------------------------------------------------------
```

```
C
      SUBROUTINE LOGNRM ( NDIS, SIZD )
C
C     LOGNRM calculates a lognormal volume distribution, SIZD, using
C     diameter DG and deviation SG and volume VM indicated by NDIS
C
C>    SUBROUTINES USED -- NONE
C
$INCLUDE: 'PARAMS.INC'
      COMMON /TEST/ DG(3),SG(3),VM(3)
      COMMON /SIZE/ DIA(NMAX),DEAA(9),DOPC(7),DAVG(6)
      DIMENSION SIZD(NMAX)
      SDLOG = ALOG ( SG(NDIS) )
C
C Normal distribution prefactor is 1./SQRT(2.*PI)
C Note ln(10) pops up because we use dV/dlog10(dp)
C
      ANORM = ALOG(10.)/(SQRT(2.*3.14159)) * VM(NDIS) / SDLOG
      DPMEAN = DG(NDIS)
      WRITE(*,25) NDIS,DPMEAN,SG(NDIS),VM(NDIS)
  25  FORMAT(' LOGNORMAL DISTRIBUTION #',I2,':  Dp=',F9.4,
     #          '  Sg=',F9.4,'  Vm=',F9.4)
C
      DO 50 I = NMIN,NMAX
         Z = ALOG ( DIA(I)/DPMEAN ) / SDLOG
         A = ANORM * EXP ( - Z * Z / 2. )
         SIZD(I) = SIZD(I) + A
 50   CONTINUE
      RETURN
      END
C
C-------------------------------------------------------------------------------
C
      SUBROUTINE GETVOL ( TRIAL, VDIST, TOTVOL, TOTNUM )
C
C Calculate volume distribution from number distribution
C
$INCLUDE: 'PARAMS.INC'
      COMMON /SIZE/ DIA(NMAX),DEAA(9),DOPC(7),DAVG(6)
       DIMENSION VDIST(NMAX),TRIAL(NMAX),TOTNUM(2)
C
C TOTNUM(1) includes all, TOTNUM(2)>.02 um
C
       TOTVOL = 0.
       TOTNUM(1) = 0.
       TOTNUM(2) = 0.
       DLOGDP = ALOG10(DIA(2)/DIA(1))
C
      DO 200 I= 1,NMAX
```

```
          D= DIA(I)
          ANUM = TRIAL(I) * DLOGDP
          VOLUM = ANUM * 3.141593 * D*D*D / 6.
          VDIST(I) = VOLUM / DLOGDP
          TOTVOL = TOTVOL + VOLUM
          TOTNUM(1) = TOTNUM(1) + ANUM
          IF (D.GT.0.02) TOTNUM(2) = TOTNUM(2) + ANUM
 200  CONTINUE
       RETURN
       END
C
C-----------------------------------------------------------------------
C
      SUBROUTINE GETNUM ( NDIST, VDIST )
C
C Calculate number distribution from volume distribution
C
$INCLUDE: 'PARAMS.INC'
      COMMON /SIZE/ DIA(NMAX),DEAA(9),DOPC(7),DAVG(6)
      REAL VDIST(NMAX),NDIST(NMAX)
C
      DO 200 I= NMIN,NMAX
         D= DIA(I)
 200     NDIST(I) = VDIST(I) * 6. / (3.141593 * D*D*D )
C
      RETURN
      END
C
C-----------------------------------------------------------------------
C
      SUBROUTINE HISTO ( COUT, SENS, HISTV, HISTN, TVOL, TNUM )
C
C This is the simple data inversion method, which assumes
C no cross-sensitivity.  Both the EAA simple inversion and the
C       OPC simple inversion will be performed.
C
C       TNUM(1) contains total number by EAA, channel 3+
C       TNUM(2) contains total number by EAA, channel 4+
C       TNUM(3) contains total number by OPC, including all channels
C       TNUM(4) contains total number by OPC, channel 2+
C
C       TVOL(1) contains total volume by EAA
C       TVOL(2) contains total volume by OPC
C
$INCLUDE: 'PARAMS.INC'
      COMMON /SIZE/ DIA(NMAX),DEAA(9),DOPC(7),DAVG(6)
      DIMENSION COUT(KMAX), HISTV(KMAX), HISTN(KMAX)
      DIMENSION TNUM(4),TVOL(2),SENS(9)
      TVOL(1) = 0.
```

```
      TVOL(2) = 0.
      DO 20 I=1,4
 20      TNUM(I) = 0.
C
C   Invert the EAA channels first
C    DLOGDP for the EAA is 0.25, since there are 4 channels per decade
C      (hence the multiplication by 4 for HISTN and HISTV)
C
      DO 100 K=1,9
         ANUM = SENS(K) * COUT(K)
         HISTN(K) = 4. * ANUM
         TNUM(1) = TNUM(1) + ANUM
         IF (K.GE.2) TNUM(2) = TNUM(2) + ANUM
         AVOL = 3.141593 * ANUM * DEAA(K)**3 / 6.
         HISTV(K) = 4. * AVOL
         TVOL(1) = TVOL(1) + AVOL
 100  CONTINUE
C
C   Next invert the OPC channels
C
      DO 120 K=10,15
         DLOGDP = ALOG10(DOPC(K-8)/DOPC(K-9))
         ANUM = COUT(K)
         HISTN(K) = ANUM / DLOGDP
         TNUM(3) = TNUM(3) + ANUM
         IF (K.GE.11) TNUM(4) = TNUM(4) + ANUM
         AVOL = 3.141593 * ANUM * DAVG(K-9)**3 / 6.
         HISTV(K) = AVOL / DLOGDP
         TVOL(2) = TVOL(2) + AVOL
 120  CONTINUE
C
      RETURN
      END
C
C-----------------------------------------------------------------------
C
      SUBROUTINE SMOOTH ( Y, NDZERO)
C
C     SMOOTH smooths an array Y as follows:
C
C new Y(I) = 0.25*Y(I-1) + 0.50*Y(I) + 0.25*Y(I+1)
C
C     For the end points, assume:
C          IF NDZERO=0    Y(out-of-bounds)=Y(endpoint)
C   IF NDZERO=1    Y(out-of-bounds)=0.
C Note that NDZERO=1 still only weakly zeros the tails.
C
$INCLUDE: 'PARAMS.INC'
      DIMENSION Y(NMAX)
```

```
      LM1= NMAX - 1
      PAST = 0.
      IF (NDZERO.EQ.0) PAST = Y(NMIN)
      DO 10 J = NMIN,LM1
         CURR = Y(J)
         Y(J) = .25*PAST + .5*CURR + .25*Y(J+1)
         PAST = CURR
 10   CONTINUE
      IF (NDZERO.EQ.0) THEN
          Y(NMAX) = .25*PAST + .75*Y(NMAX)
       ELSE
          Y(NMAX) = .25*PAST + .50*Y(NMAX)
      END IF
      RETURN
      END
C
C-----------------------------------------------------------------------
C
      SUBROUTINE NONEG(CURR)
C
$INCLUDE: 'PARAMS.INC'
      REAL CURR(9)
C
C Negativity compensation algorithm.
C Insists that all differences be positive, or at least zero.
C If CURR(K)<0. then will attempt to split the negativity with
C  the neighboring points, spreading out as far as necessary
C  to eliminate the impossible negative signal.  An endpoint
C  is a perfect sink.  At each distance from the negative
C  signal, the algorithm attempts to split the negative
C  burden evenly, and if still not satisfied will take whatever
C  is needed from the remaining positive signal (never driving
C  any signal negative), and spread out further, bilaterally,
C  from the negative source if necessary.
C
C J = distance from source K (1,2,3 . . .)
C COVER = amount of negative current still needing to be covered
C UP = maximum signal that up channel K+J could cover
C DOWN = maximum signal that down channel K-J could cover
C
      DO 500 K=1,9
         IF (CURR(K).LT.0.) THEN
    COVER=-CURR(K)
            J=1
 200        KD=K-J
            KU=K+J
            DOWN=COVER
    UP=COVER
            IF (KD.GE.KMIN) DOWN=CURR(KD)
```

```
            IF (KU.LE.KMAX) UP=CURR(KU)
            IF (DOWN.LT.0.) DOWN=0.
            IF (UP.LT.0.) UP=0.
            PLAY=DOWN+UP
            IF (PLAY.GE.COVER) GOTO 400
            COVER=COVER-PLAY
            IF (KU.LE.KMAX .AND. CURR(KU).GT.0.) CURR(KU)=0.
            IF (KD.GE.KMIN .AND. CURR(KD).GT.0.)  CURR(KD)=0.
            J=J+1
            IF (J.LE.4) GOTO 200
            WRITE(*,*) 'NONEG WARNING:  Cannot Cover Difference!'
            GOTO 450
 400        IF (UP.GE.0.5*COVER .AND. DOWN.GE.0.5*COVER) THEN
               IF (KD.GE.KMIN) CURR(KD)=CURR(KD)-0.5*COVER
               IF (KU.LE.KMAX) CURR(KU)=CURR(KU)-0.5*COVER
            ELSE IF (UP.LT.0.5*COVER) THEN
               IF (KU.LE.KMAX .AND. CURR(KU).GT.0.) CURR(KU)=0.
               IF (KD.GE.KMIN) CURR(KD)=CURR(KD)-COVER+UP
            ELSE IF (DOWN.LT.0.5*COVER) THEN
               IF (KD.GE.KMIN .AND. CURR(KD).GT.0.) CURR(KD)=0.
               IF (KU.LE.KMAX) CURR(KU)=CURR(KU)-COVER+DOWN
            ELSE
               STOP 'LOGIC ERROR IN NONEG!'
            ENDIF
 450        CURR(K)=0.
         END IF
C     WRITE(*,222) (CURR(J),J=KMIN,KMAX)
C222  FORMAT(' Curr ',9F7.4)
 500  CONTINUE
      RETURN
      END
C
C-------------------------------------------------------------------------
C
      SUBROUTINE RESP ( TRIAL, COUT )
C
C RESP computes the measured output COUT given the size
C distribution in TRIAL and the response matrix in RM.
C
C Find response COUT(K) from assumed distribution TRIAL
C
$INCLUDE: 'PARAMS.INC'
      COMMON /SIZE/ DIA(NMAX),DEAA(9),DOPC(7),DAVG(6)
      COMMON /RESMAT/ RM(KMAX,NMAX),RI(NMAX,KMAX),H(NMAX)
      DIMENSION TRIAL(NMAX),COUT(KMAX)
      DLOGDP = ALOG10(DIA(2)/DIA(1))
      DO 50 K=KMIN,KMAX
         A = 0.
         DO 20 I=NMIN,NMAX
```

```
C
C  The following IF block is to prevent underflow errors caused
C    by small values of TRIAL
C
             IF (TRIAL(I).LE.1.E-35) THEN
               TEMP=0.
             ELSE
               TEMP=TRIAL(I)
             END IF
C
             A = A + RI(I,K) * TEMP * DLOGDP
C
  20      CONTINUE
          COUT(K)=A
  50  CONTINUE
      RETURN
      END
C
C-----------------------------------------------------------------------
C
      SUBROUTINE INVERT ( TRIAL, COUT, DPAVG )
C
C This is the inversion routine driver.
C     INVERT calls the TWOMEY routine and controls the smoothing
C     and intermediate output.  The solution is returned.
C
C>    SUBROUTINES USED -- RESP,CHKOUT,FITCHK,TWOMEY,SMOOTH
C
$INCLUDE: 'PARAMS.INC'
      COMMON /SET/ TARGET(KMAX),CTOL(KMAX),RFIT(KMAX),AFIT(KMAX)
      COMMON /FLAG/ IPRNT,INFO,TESTD
      COMMON /RESMAT/ RM(KMAX,NMAX),RI(NMAX,KMAX),H(NMAX)
      COMMON /INVRT/ MAXTWO,MAXSMO,ISMAX,MINSMO,SMTOL
      COMMON /DROP/ NDZERO,CMINE,CMINO
      COMMON /STATS/ JSET,JLOOP,JTWO,JCON,SUMSIG,BEGSIG,SUMCUR,BEGCUR
      LOGICAL INFO,TESTD
      DIMENSION TRIAL(NMAX),COUT(KMAX)
      DIMENSION CURVE(20), TLAST(NMAX), CLAST(KMAX)
C
C        Initialize variables
C
      NIT = 0
      LOOPS = 0
      WRITE(6,106) MAXTWO,MAXSMO,ISMAX,NDZERO,SMTOL
 106  FORMAT(' MAXTWO=',I3,'  MAXSMO=',I3,'  ISMAX=',I3,
     #       '  NDZERO=',I2,'  SMTOL=',F7.3 )
C
C        DO loop to do Twomey-Smoothing up to 15 (MAXSMO) times
C
```

```
      DO 60 NS = 1, MAXSMO
        ISM = 0
        IF (NS.EQ.1) GOTO 40
C
C        Smooth until differences are large enough, ISMAX (5) TIMES
C        Note:  Setting  SMTOL sets a trade-off between smoothness and
C          accuracy of solution.  Clearly sigma < 1 is too much
C          accuracy, as sigma=1 is the designated instrument tolerance.
C          Smooth the data as much as possible given this trade-off.
C        The default here is SMTOL = sigma = 1.2.
C
  20    CALL SMOOTH (TRIAL, NDZERO)
        ISM = ISM + 1
  40    CALL RESP ( TRIAL, COUT )
        CALL FITCHK ( COUT, SIGMA )
        IF ( SIGMA.LT.SMTOL .AND. ISM.LT.ISMAX .AND. NS.GT.1) GOTO 20
C
C        End of inner smoothing loop
C
        LOOPS = LOOPS + 1
        ID = 2
C                ID = 2 causes printing after the smoothing loop.
C
        CALL CHKOUT(ID,LOOPS,0,NIT,ISM,TRIAL,SIGMA,CURVAT)
C
C   Now initialize the sigma and the curvature for post-run statistics.
C
        IF (LOOPS.EQ.1) THEN
            BEGSIG=BEGSIG+SIGMA
            BEGCUR=BEGCUR+CURVAT
        END IF
C
C        Run TWOMEY to correct for smoothing.  IT iterations done.
C
        CALL TWOMEY ( TRIAL, COUT, IT, SIGMA, DPAVG )
C
        NIT = NIT + IT
        ID = 1
C                ID = 1 causes printing after the Twomey loop.
        CALL CHKOUT(ID,LOOPS,IT,NIT,0,TRIAL,SIGMA,CURVAT)
        CURVE(NS) = CURVAT
C
C Option to do MINSMO smoothing loops, override automatic exit
C
        IF (LOOPS.LT.MINSMO) GOTO 50
C
C        Stop smoothing loop if curvature increases
C
        IF (NS.GT.2 .AND. CURVAT .GT. CURVE(NS-1)) GOTO 70
```

```
C
C         Quit if less than 2.5% decrease in last 2 iterations
C
        IF (NS.GT.3 .AND. CURVAT .GE. .975*CURVE(NS-2)) GOTO 90
C
C         Save this TRIAL and COUT in TLAST and CLAST
C
  50    DO 59 I = NMIN,NMAX
  59       TLAST(I) = TRIAL(I)
        DO 56 K = KMIN,KMAX
  56       CLAST(K) = COUT(K)
  60  CONTINUE
C
      WRITE(6,65) MAXSMO
      WRITE(*,65) MAXSMO
  65  FORMAT(' *** MAXIMUM ',I2,' TWOMEY-SMOOTHING LOOPS DONE.')
      GOTO 100
C
C         Use prior trial and output instead of new ones
C
  70  DO 72 MM = NMIN,NMAX
  72     TRIAL(MM) = TLAST(MM)
      DO 74 MM = KMIN,KMAX
  74     COUT(MM) = CLAST(MM)
      WRITE(*,*) ' Curvature Increased so PRIOR TRIAL USED'
      WRITE(6,*) ' PRIOR TRIAL USED'
C
  90  WRITE(6,95) LOOPS
  95  FORMAT(/' *** INVERSION USED ',I2,' TWOMEY-SMOOTHING LOOPS.'/)
 100  WRITE(6,105) (CURVE(J), J=1,LOOPS)
 105  FORMAT(' CURVAT ',8e9.2)
      JSET=JSET+1
      IF (SIGMA.LE.1.0) JCON=JCON+1
      JLOOP=JLOOP+LOOPS
      JTWO=JTWO+NIT
      SUMSIG=SUMSIG+SIGMA
      SUMCUR=SUMCUR+CURVAT
      RETURN
      END
C
C-----------------------------------------------------------------------
C
      SUBROUTINE TWOMEY ( TRIAL,COUT,IT,SIGMA,DPAVG )
C
C         TWOMEY does the Twomey iteration until SIGMA is < 1
C     of until SIGMA is no longer changing significantly (< .1%).
C     TWOMEY corrections are performed across each instrument
C     separately, then a new TRIAL distribution is calculated and
C     TWOMEY corrections applied for the channels corresponding to
```

```
C     the next instrument, etc.  This seems to make the fit better
C     by a significant margin.
C
C     Iteration for a stage is skipped if the trial and true
C     values are within the specified fit tolerance.
C
$INCLUDE: 'PARAMS.INC'
      COMMON /SET/ TARGET(KMAX),CTOL(KMAX),RFIT(KMAX),AFIT(KMAX)
      COMMON /RESMAT/ RM(KMAX,NMAX),RI(NMAX,KMAX),H(NMAX)
      COMMON /INVRT/ MAXTWO,MAXSMO,ISMAX,MINSMO,SMTOL
      DIMENSION TRIAL(NMAX), RATIO(KMAX)
      DIMENSION COUT(KMAX)
C
C       Do up to 30 (MAXTWO) Twomey iterations
C   Iterate on channel index K first
C     Skip channel if it is within tolerance
C     Check agreement with actual TARGET values
C   Display progress on screen
C Continue Twomey iterations if agreement is inadequate, SIGMA>1
C         or until SIGMA stops changing.
C
      DO 50 J = 1, MAXTWO
         IT = J
C
      IF (DPAVG.LE.0.2) THEN
C
C  Do TWOMEY correction on the EAA after the OPC.
C
         CALL OPCT(TRIAL,COUT)
         CALL EAAT(TRIAL,COUT)
      ELSE
C
C  Do TWOMEY correction on the OPC after the EAA.
C
         CALL EAAT(TRIAL,COUT)
         CALL OPCT(TRIAL,COUT)
      ENDIF
C
C  Check fit:
C
         CALL FITCHK ( COUT, SIGMA )
C
         IF (ABS((SIGMA-SIGOLD)/SIGMA).LE.1.E-3) RETURN
         IF (SIGMA .LT. 1.) RETURN
         SIGOLD = SIGMA
  50  CONTINUE
C
      WRITE(6,*) ' *** FIT NOT MET AFTER MAXIMUM TWOMEY ITERATIONS'
      RETURN
```

```
      END
C
C-----------------------------------------------------------------
C
        SUBROUTINE EAAT(TRIAL,COUT)
C
$INCLUDE: 'PARAMS.INC'
      COMMON /SET/ TARGET(KMAX),CTOL(KMAX),RFIT(KMAX),AFIT(KMAX)
      COMMON /RESMAT/ RM(KMAX,NMAX),RI(NMAX,KMAX),H(NMAX)
      DIMENSION COUT(KMAX),RATIO(KMAX),TRIAL(NMAX)
C
         DO 40 K = KMIN,9
          IF (COUT(K).LE.1.E-35) THEN
            TEMP = 1.E-35
          ELSE
            TEMP = COUT(K)
          END IF
          RATIO(K) = TARGET(K)/TEMP - 1
C
            CERR = TARGET(K) - COUT(K)
C
C Could try to make sufficiently good fit better by
C unconditionally doing the next IF block, but this would
C decrease the smoothness.
C
            IF ( ABS(CERR) .GE. CTOL(K) ) THEN
               A  = RATIO(K)
               DO 30 I = NMIN, NMAX
                  B = RI(I,K)
C
C  Now, to re-normalize the kernel function so that the Twomey
C    correction will make a significant step towards convergence,
C    the response matrix element B is divided by the instrument
C    sensitivity, H (for the EAA only, k=1,9).
C
                  B=B/H(I)
                  TRIAL(I) = TRIAL(I)*(1.+A*B)
 30            CONTINUE
            END IF
 40       CONTINUE
C
         CALL RESP ( TRIAL, COUT )
C
       RETURN
       END
C
C-----------------------------------------------------------------
C
        SUBROUTINE OPCT(TRIAL,COUT)
```

```
C
$INCLUDE: 'PARAMS.INC'
      COMMON /SET/ TARGET(KMAX),CTOL(KMAX),RFIT(KMAX),AFIT(KMAX)
      COMMON /RESMAT/ RM(KMAX,NMAX),RI(NMAX,KMAX),H(NMAX)
      DIMENSION COUT(KMAX),RATIO(KMAX),TRIAL(NMAX)
C
         DO 41 K = 10,15
          IF (COUT(K).LE.1.E-35) THEN
            TEMP = 1.E-35
          ELSE
            TEMP = COUT(K)
          END IF
          RATIO(K) = TARGET(K)/TEMP - 1
C
            CERR = TARGET(K) - COUT(K)
C
            IF ( ABS(CERR) .GE. CTOL(K) ) THEN
               A  = RATIO(K)
               DO 31 I = NMIN, NMAX
                  B = RI(I,K)
                  TRIAL(I) = TRIAL(I)*(1.+A*B)
 31            CONTINUE
            END IF
 41      CONTINUE
C
         CALL RESP ( TRIAL, COUT )
C
         RETURN
         END
C
C-------------------------------------------------------------------------
C
      SUBROUTINE FITCHK ( COUT, SIGMA )
C
C        FITCHK computes a fractional discrepancy in the
C desired signal TARGET from the calculated signal COUT,
C and finds a normalized error parameter SIGMA.
C
$INCLUDE: 'PARAMS.INC'
      COMMON /SET/ TARGET(KMAX),CTOL(KMAX),RFIT(KMAX),AFIT(KMAX)
      DIMENSION COUT(KMAX)
      NCHAN = KMAX-KMIN+1
      SIGMA = 0.
      DO 10 K = KMIN,KMAX
         A = (COUT(K)-TARGET(K)) / CTOL(K)
         SIGMA = SIGMA + A*A
  10  CONTINUE
      SIGMA = SQRT( SIGMA/NCHAN )
      RETURN
```

```
      END
C
C-----------------------------------------------------------------
C
      SUBROUTINE CHKOUT(ID,LOOPS,IT,NIT,ISM,TRIAL,SIGMA,CURVAT)
C
C     CHKOUT prints intermediate inversion results and gets
C     curvature parameter. IPRNT=1 causes TRIAL to be printed after
C     TWOM, 2=after SMOOTH only.
C
C     CHKOUT essentially calculates a derivative to indicate smoothness
C
$INCLUDE: 'PARAMS.INC'
      COMMON /FLAG/ IPRNT,INFO,TESTD
      LOGICAL INFO,TESTD
      DIMENSION TRIAL(NMAX)
      REAL A(3)
C
C        Calculate CURVATURE parameter (must skip endpoints)
C
      CURVAT = 0.
      DO 10 I = NMIN+1, NMAX-1
         A(1) = TRIAL(I-1)
         A(2) = TRIAL(I)
         A(3) = TRIAL(I+1)
        DO 12 J=1,3
C
C   Again to prevent underflow errors, values < 1.e-35 are zeroed.
C
 12       IF (A(J).LT.1.E-35) A(J) = 0.
         CURVAT = CURVAT + ABS( (A(2) - A(1)) + (A(2) - A(3)))
 10   CONTINUE
      NCOUNT = NMAX-NMIN-1
      CURVAT = CURVAT / NCOUNT
C
C Print out status of TWOMEY-SMOOTHING scheme
C
      WRITE(6,90) LOOPS,IT,NIT,ISM,SIGMA,CURVAT
      WRITE(*,90) LOOPS,IT,NIT,ISM,SIGMA,CURVAT
  90  FORMAT(' Loop',I3,'   Tw=',I3,' =>',I4,'   Sm=',I3,
     # '   SIGMA=',F8.2,'   CURV=',F10.4)
C
      IF (ID.EQ.IPRNT.OR.IPRNT.GE.10) THEN
C        Print TRIAL in 4 columns
        NCOL = 4
        NLIN = (NMAX-NMIN)/NCOL + 1
        DO 200 I = 1,NLIN
           JJ=NCOL-1
           IF (I+JJ*NLIN.GT.NMAX) JJ=JJ-1
```

```
          WRITE(6,110) (I+J*NLIN,TRIAL(I+J*NLIN),J=0,JJ)
 110      FORMAT(5(I3,1PE10.3,3X))
 200    CONTINUE
      END IF
 900  RETURN
      END
C
C=======================================================================
*
```

```
MISTI.TOL:
 Trial Tolerances for experimental data
 0.10      .10    .10    .10    .10    .10    .15    .15    .20
 0.20      .10    .10    .10    .10    .10
 0.001    .001   .001   .001   .001   .001   .001   .001   .001
    1.      1.    0.5    0.1    0.1    0.1
    50      15      4      4   1.3
     0  1.e-5 1.e-03
^*****^^*****^^*****^^*****^ MISTI.TOL ****^^*****^^*****^^*****^^*****^
 MAXTWO MAXSMO  ISMAX MINSMO  SMTOL
 NDZERO CMINE   CMINO
 LINE 1 is a line of identifying text.  A70
 LINE 2 contains the relative EAA error tolerances, RFIT.   9F7.0
Note that a -1. will give all remaining channels
  the last RFIT listed (e.g., use 0.05      -1.)
 LINE 3 contains the relative OPC error tolerances, RFIT.
        -1. repeats as with line 2                          6F7.0
 LINES 4 and 5 contain the absolute error tolerances, AFIT. 9F7.0 and
                                                            6F7.0
Likewise, a -1. repeats the last value given.
 LINE 6 contains MAXTWO, MAXSMO, ISMAX, MINSMO, SMTOL 5I7,F7.0
MAXTWO is the maximum Twomey iterations per loop, default 30.
MAXSMO is the maximum number of smoothing loops, default 20.
ISMAX is the maximum number of smooths in a loop, default 3.
        MINSMO positive forces at least MINSMO smoothing loops, def 5.
SMTOL is the smoothing tolerance, the value of SIGMA
  above which no more smooths occur in a loop, default 1.2
Note LINE 6 may be omitted entirely and defaults used.
 LINE 7 contains NDZERO, CMINE, CMINO                    I7,2F7.0
        NDZERO nonzero will smooth the endpoints towards zero, def 0.
CMINE is the smallest EAA voltage allowed (NOT 0.), def 1.E-5
CMINO is the smallest OPC counts allowed (NOT 0.),  def 1.E-3
Note this line may be omitted and defaults used.

MTEST.TOL:
 Trial Tolerances for test data
 0.001     -1.
 0.001     -1.
 0.0001 .0001  .0001  .0001  .0001  .0001  .0001  .0001  .0001
   .001   .001  .0005  .0001  .0001  .0001
   500     20      4      5   1.4
     0  1.e-5 1.e-05
^*****^^*****^^*****^^*****^ MISTI.TOL ****^^*****^^*****^^*****^^*****^
 MAXTWO MAXSMO  ISMAX MINSMO  SMTOL
 NDZERO CMINE   CMINO
 LINE 1 is a line of identifying text.  A70
 LINE 2 contains the relative EAA error tolerances, RFIT.   9F7.0
Note that a -1. will give all remaining channels
  the last RFIT listed (e.g., use 0.05      -1.)
```

```
 LINE 3 contains the relative OPC  error tolerances, RFIT.
        -1. repeats as with line 2                              6F7.0
 LINES 4 and 5 contain the absolute error tolerances, AFIT.  9F7.0 and
                                                               6F7.0
Likewise, a -1. repeats the last value given.
 LINE 6 contains MAXTWO, MAXSMO, ISMAX, MINSMO, SMTOL 5I7,F7.0
MAXTWO is the maximum Twomey iterations per loop, default 30.
MAXSMO is the maximum number of smoothing loops, default 20.
ISMAX is the maximum number of smooths in a loop, default 3.
        MINSMO positive forces at least MINSMO smoothing loops, def 5.
SMTOL is the smoothing tolerance, the value of SIGMA
  above which no more smooths occur in a loop, default 1.2
Note LINE 6 may be omitted entirely and defaults used.
 LINE 7 contains NDZERO, CMINE, CMINO                       I7,2F7.0
        NDZERO nonzero will smooth the endpoints towards zero, def 0.
CMINE is the smallest EAA voltage allowed (NOT 0.), def 1.E-5
CMINO is the smallest OPC counts allowed (NOT 0.),  def 1.E-3
Note this line may be omitted and defaults used.
```

```
      PROGRAM MANAGE
C
C   MANIPULATES INVERTED NUMBER DISTIBUTIONS AT USER-SELECTED TIMES
C
C   THE INPUT FILE IS THE INVERTED MISTI (.NUM) UNFORMATTED DATAFILE
C
C MANAGE will find the user-selected time, optionally smoothing
C its data, and output data to DIST.# files, HISE.# files, and
C       HISO.# files, representing the inverted distribution, the
C       input EAA histogram, and the input OPC histogram.  Also, it
C will optionally creating number/volume/size summary (.SUM)
C
C          This program closely follows SELECT, the EAA management
C           program, and CHOOSE, the OPC management program.
C
C      DATA FILES:
C
C 20 CFILE MISTI.NUM Inverted N Density (INPUT)
C 11 NFILE NANDV.PRO Inverted Number and Volume
C        7      EFILE   HISE.#          EAA Histogram Distribution
C        8 HFILE HISO.# OPC Histogram Distribution
C        9 DFILE DIST.# Inverted Distribution
C 25 SFILE MISTI.SUM Totals and average Dps.
C
C
$INCLUDE: 'PARAMS.INC'
      COMMON /SIZE/ DIA(NMAX),DEAA(9),DOPC(7),DAVG(6)
      COMMON /STORE/ TIME(200),RAWS(KMAX,200),DEN(NMAX,200)
      COMMON /WHERE/ NOW,NEXT
      REAL RAW(KMAX)
      REAL PRAW(KMAX),POUT(NMAX),PVIST(NMAX)
      REAL VDIST(NMAX),NDIST(NMAX),TVOL(2),TOTNUM(3)
      REAL HISTV(KMAX),HISTN(KMAX),HISNUM(4),HISVOL(2)
      REAL S(9),SENS(9)
      CHARACTER*20 DFILE,HFILE,NFILE,VFILE,CFILE,SFILE,EFILE
      CHARACTER*4 DNAME,HNAME,ENAME
      CHARACTER*1 ASK
      LOGICAL SAVPRO,SAVDIS,SAVSUM
C
      DATA S / 4.17E5, 1.67E5, 8.70E4, 4.44E4,
     #         2.41E4, 1.23E4, 6.67E3, 3.51E3, 1.80E3 /
C
      DO 3 I=1,9
 3      SENS(I) = S(I)
C
C
C   Set diameters for inverted distribution from 0.01 um to 1.0 um
C
      DIA(1) = 0.01
```

```
      DO 100 I = 2,NMAX
 100      DIA(I) = DIA(I-1) * 1.100694
C
C  Now set diameters for EAA channels 2-10.  These are average diameters.
C
      DEAA(1) = 0.01333521
      DO 110 K = 2,9
 110     DEAA(K) = DEAA(K-1) * 1.778279
C
C  Now set diameters for OPC.
C  DOPC are the cut sizes at the bottoms of each channel.  To get
C    the average particle size (DAVG) multiply i by i+1 and take sqrt.
C
      DOPC(1) = 0.12
      DOPC(2) = 0.17
      DOPC(3) = 0.27
      DOPC(4) = 0.42
      DOPC(5) = 0.62
      DOPC(6) = 0.87
      DOPC(7) = 1.17
C
      DO 111 K = 1,6
 111     DAVG(K) = SQRT(DOPC(K)*DOPC(K+1))
C
C         WHAT INFO SHOULD BE SAVED FROM THE INVERSION?
C
      WRITE(*,190)
 190  FORMAT(/20X,'*** MANAGE - MISTI PROFILE HANDLER ***'/)
      WRITE(*,200) 'Name of MISTI output file [MISTI.NUM] : '
 200  FORMAT(/1X,A\)
      READ(*,202) CFILE
 202  FORMAT(A)
      IF (CFILE.EQ.' ') CFILE='MISTI.NUM'
C
      DNAME='DIST'
      HNAME='HIS0'
      ENAME='HISE'
      OPEN (20,FILE=CFILE,STATUS='OLD',FORM='UNFORMATTED')
C
      WRITE(*,200) 'Shall N & V profiles be created? [Y] '
      READ(*,666) ASK
 666  FORMAT(A1)
      SAVPRO=.TRUE.
      IF (ASK.EQ.'N' .OR. ASK.EQ.'n') SAVPRO=.FALSE.
      IF (SAVPRO) THEN
        WRITE(*,200) 'Name of profile file [NANDV.PRO] : '
        READ(*,202) NFILE
        IF (NFILE.EQ.' ') NFILE='NANDV.PRO'
        OPEN (11,FILE=NFILE,STATUS='NEW',FORM='FORMATTED')
```

```
      ENDIF
      WRITE(*,200) 'Shall summary file (.SUM) be created? [Y] '
      READ(*,666) ASK
      SAVSUM=.TRUE.
      IF (ASK.EQ.'N' .OR. ASK.EQ.'n') SAVSUM=.FALSE.
      IF (SAVSUM) THEN
        WRITE(*,200) 'Name of output file [MISTI.SUM] : '
        READ(*,202) SFILE
        IF (SFILE.EQ.' ') SFILE='MISTI.SUM'
        OPEN (25,FILE=SFILE,STATUS='NEW',FORM='FORMATTED')
      ENDIF
C
C*********************************************************************
C
C Unformatted Files of the Number Distribution with Time
C
C  MISTI.NUM
C 1 HOUR
C 2-16    RAW(K)
C 17-65   NDIST(K)
C
C     Formatted Summary (.SUM) File format: (unit 25)
C
C      1       2       3         4      5      6
C    TIME    NT>0.01 NT>0.02    TV     DPnav  DPvav
C
C            Formatted NANDV.PRO file format: (unit 11)
C
C      1      2       3       4        5        6       7
C    TIME   NT,dist NT,EAA  NT,OPC    V,dist  V,EAA   V,OPC
C
C*********************************************************************
C
      NOW = 0
C
C         READ IN MISTI DATASET
C
 300  READ(20,END=400,ERR=400) HOUR,(RAW(K),K=1,KMAX),
     #        (NDIST(I),I=1,NMAX)
C
      NOW = NOW + 1
      IF (SAVPRO.OR.SAVSUM) THEN
         CALL HISTO ( RAW, SENS, HISTV, HISTN, HISVOL, HISNUM )
         CALL GETVOL ( NDIST, VDIST, TOTVOL, TOTNUM )
      ENDIF
      IF (SAVPRO) THEN
         WRITE(11,307) HOUR,TOTNUM(1),HISNUM(1),HISNUM(3),TOTVOL,
     #                 HISVOL(1),HISVOL(2)
 307     FORMAT(1X,F7.3,3F9.1,3F9.3)
```

```
      ENDIF
      IF (SAVSUM) THEN
         CALL FINDAV(VDIST,NDIST,DPVAV,DPNAV)
         WRITE(25,290) HOUR,TOTNUM(1),TOTNUM(2),TOTVOL,DPNAV,DPVAV
 290     FORMAT(1X,F7.3,2F9.1,F9.3,2F7.4)
      ENDIF
      TIME(NOW)=HOUR
      DO 310 K=1,KMAX
 310     RAWS(K,NOW)=RAW(K)
      DO 320 I=1,NMAX
 320     DEN(I,NOW)=NDIST(I)
      IF (NOW.LT.200) GOTO 300
C
 400  CONTINUE
C
      ENDTIM=HOUR
      WRITE(*,*) NOW,' Datasets Read up to Time ',ENDTIM
      CALL CLOSE (20)
      CALL CLOSE (11)
C
C All inverted data have been read in.
C Now average the datasets over a user-specified interval.
C
      WRITE(*,200) 'AVERAGING Interval (Hours; 0. nearest pt.): '
      READ(*,*) TINT
      WRITE(*,200) 'Time Into Run for FIRST Plot (Hours): '
      READ(*,*) BEGIN
      WRITE(*,200) 'Time STEP Between Plots (Hours): '
      READ(*,*) TSTEP
C
C Initialize Plotting Loop
C
      NEXT=1
      PTIME=BEGIN
 500  CALL AVERAG(PTIME,TINT,PRAW,POUT)
C
C Note if there are no data near PTIME, AVERAG will use the
C  first time after PTIME to provide data, rather than exit.
C
      CALL HISTO ( PRAW, SENS, HISTV, HISTN, HISVOL, HISNUM )
      CALL GETVOL ( POUT, PVIST, TOTVOL, TOTNUM )
C
C OPTION TO SAVE EACH DISTRIBUTION AS DIST.# AND HIST.#
C
      IF (NEXT.LT.10) THEN
         WRITE(DFILE,401) DNAME,NEXT
         WRITE(HFILE,401) HNAME,NEXT
         WRITE(EFILE,401) ENAME,NEXT
      ELSEIF (NEXT.LT.100) THEN
```

```
         WRITE(DFILE,402) DNAME,NEXT
         WRITE(HFILE,402) HNAME,NEXT
         WRITE(EFILE,402) ENAME,NEXT
      ELSE
         WRITE(DFILE,403) DNAME,NEXT
         WRITE(HFILE,403) HNAME,NEXT
         WRITE(EFILE,403) ENAME,NEXT
      ENDIF
 401  FORMAT(A,'.',I1)
 402  FORMAT(A,'.',I2)
 403  FORMAT(A,'.',I3)
C
C DIST.n will contain the following results:
C           Dp  Vol(Cin)  N(Cin)
C
      OPEN (9,FILE=DFILE,STATUS='NEW',FORM='FORMATTED')
      DO 800 I=NMIN,NMAX
 800     WRITE(9,810) DIA(I),PVIST(I),POUT(I)
 810  FORMAT(1X,F7.4,2X,F10.4,2X,F12.3)
      CALL CLOSE(9)
C
C HISE.n will contain the following table of results.
C Dp{min/max}  Vol(Sim)  N(Sim)
C
      EAAHLF = 10.**0.125
      OPEN (7,FILE=EFILE,STATUS='NEW',FORM='FORMATTED')
         WRITE(7,860) DEAA(1)/EAAHLF,0.,0.
      DO 840 K=1,9
         WRITE(7,860) DEAA(K)/EAAHLF,HISTV(K),HISTN(K)
 840     WRITE(7,860) DEAA(K)*EAAHLF,HISTV(K),HISTN(K)
      CALL CLOSE(7)
C
C HISO.n will contain the following table of results.
C Dp{min/max}  Vol(Sim)  N(Sim)
C
      OPEN (8,FILE=HFILE,STATUS='NEW',FORM='FORMATTED')
         WRITE(8,860) DOPC(1),0.,0.
      DO 850 K=10,15
         WRITE(8,860) DOPC(K-9),HISTV(K),HISTN(K)
 850     WRITE(8,860) DOPC(K-8),HISTV(K),HISTN(K)
 860  FORMAT(1X,F7.4,2X,F10.4,F10.1)
      CALL CLOSE(8)
C
C Go on to the next data set.
C
      NEXT=NEXT+1
      PTIME=PTIME+TSTEP
      IF (PTIME.LT.ENDTIM) GOTO 500
C
```

```
C   Inversion procedure done.
C
 990  CONTINUE
      WRITE (*,*) ' '
      STOP 'Data Management Program MANAGE Done.
      END
C
C-----------------------------------------------------------------
C
      SUBROUTINE GETVOL ( NDIST, VDIST, TOTVOL, TOTNUM )
C
C Calculate volume distribution from number distribution
C
$INCLUDE: 'PARAMS.INC'
       COMMON /SIZE/ DIA(NMAX),DEAA(9),DOPC(7),DAVG(6)
       REAL VDIST(NMAX),NDIST(NMAX),TOTNUM(2)
C
C TOTNUM(1) includes all, TOTNUM(2)>.02 um
C
       TOTVOL = 0.
       TOTNUM(1) = 0.
       TOTNUM(2) = 0.
       DLOGDP = ALOG10(DIA(2)/DIA(1))
C
      DO 200 I= 1,NMAX
          D= DIA(I)
          ANUM = NDIST(I) * DLOGDP
          VOLUM = ANUM * 3.141593 * D*D*D / 6.
          VDIST(I) = VOLUM / DLOGDP
          TOTVOL = TOTVOL + VOLUM
          TOTNUM(1) = TOTNUM(1) + ANUM
          IF (D.GT.0.02) TOTNUM(2) = TOTNUM(2) + ANUM
 200  CONTINUE
       RETURN
       END
C
C-----------------------------------------------------------------
C
      SUBROUTINE HISTO ( RAW, SENS, HISTV, HISTN, TVOL, TNUM )
C
C This is the simple data inversion method, which assumes
C no cross-sensitivity.  Both the EAA simple inversion and the
C       OPC simple inversion will be performed.
C
C       TNUM(1) contains total number by EAA, channel 3+
C       TNUM(2) contains total number by EAA, channel 4+
C       TNUM(3) contains total number by OPC, including all channels
C       TNUM(4) contains total number by OPC, channel 2+
C
```

```
C       TVOL(1) contains total volume by EAA
C       TVOL(2) contains total volume by OPC
C
$INCLUDE: 'PARAMS.INC'
      COMMON /SIZE/ DIA(NMAX),DEAA(9),DOPC(7),DAVG(6)
      DIMENSION RAW(KMAX), HISTV(KMAX), HISTN(KMAX)
      DIMENSION TNUM(4),TVOL(2),SENS(9)
      TVOL(1) = 0.
      TVOL(2) = 0.
      DO 20 I=1,4
 20      TNUM(I) = 0.
C
C   Invert the EAA channels first
C    DLOGDP for the EAA is 0.25, since there are 4 channels per decade
C      (hence the multiplication by 4 for HISTN and HISTV)
C
      DO 100 K=1,9
         ANUM = SENS(K) * RAW(K)
         HISTN(K) = 4. * ANUM
         TNUM(1) = TNUM(1) + ANUM
         IF (K.GE.2) TNUM(2) = TNUM(2) + ANUM
         AVOL = 3.141593 * ANUM * DEAA(K)**3 / 6.
         HISTV(K) = 4. * AVOL
         TVOL(1) = TVOL(1) + AVOL
 100  CONTINUE
C
C   Next invert the OPC channels
C
      DO 120 K=10,15
      .  DLOGDP = ALOG10(DOPC(K-8)/DOPC(K-9))
         ANUM = RAW(K)
         HISTN(K) = ANUM / DLOGDP
         TNUM(3) = TNUM(3) + ANUM
         IF (K.GE.11) TNUM(4) = TNUM(4) + ANUM
         AVOL = 3.141593 * ANUM * DAVG(K-9)**3 / 6.
         HISTV(K) = AVOL / DLOGDP
         TVOL(2) = TVOL(2) + AVOL
 120  CONTINUE
C
      RETURN
      END
C
C-----------------------------------------------------------------------
C
      SUBROUTINE AVERAG ( PTIME, TINT, PRAW, POUT )
C
C Finds AVERAGE OPC values at PTIME within Interval TINT
C     (from PTIME-TINT/2 to PTIME+TINT/2 in hours)
C
```

```
$INCLUDE: 'PARAMS.INC'
      REAL PRAW(KMAX), POUT(NMAX)
      COMMON /STORE/ TIME(200),RAWS(KMAX,200),DEN(NMAX,200)
      COMMON /WHERE/ NOW,NEXT
C
c  Starting and stopping times:
c
      PSTAR=PTIME-TINT/2.
      PSTOP=PTIME+TINT/2.
c
c  Look for the first time greater than PSTAR
c
      J=1
   25 IF (TIME(J).GT.PSTAR) GOTO 100
      J=J+1
      IF (J.GT.NOW) STOP 'PTIME too large'
      GOTO 25
c
c  Having found this time, initialize PRAW and POUT
c    which will hold the averaged values.
c
  100 DO 110 K=1,KMAX
  110    PRAW(K)=RAWS(K,J)
      DO 120 I=1,NMAX
  120    POUT(I)=DEN(I,J)
      KOUNT=1
  200 J=J+1
      IF (J.GT.NOW .OR. TIME(J).GT.PSTOP) GOTO 500
c
c  Add the raw values to PRAW and the distribution values to POUT
c   for as many times as can fit before PSTOP.
c
      DO 210 K=1,KMAX
  210    PRAW(K)=PRAW(K)+RAWS(K,J)
      DO 220 I=1,NMAX
  220    POUT(I)=POUT(I)+DEN(I,J)
      KOUNT=KOUNT+1
      GOTO 200
c
c  Now divide by the number of values that were added in.
c
  500 COUNT=FLOAT(KOUNT)
      DO 510 K=1,KMAX
  510    PRAW(K)=PRAW(K)/COUNT
      DO 520 I=1,NMAX
  520    POUT(I)=POUT(I)/COUNT
c
      WRITE(*,900) NEXT,PTIME,KOUNT
  900 FORMAT(' DISTribution #',I3,' at TIME ',F7.3,' from',I3,
```

```
     # ' DATASETS.')
      RETURN
      END
C
C-----------------------------------------------------------------
C
      SUBROUTINE FINDAV ( VDIST, NDIST, DPVAV, DPNAV )
C
$INCLUDE: 'PARAMS.INC'
      COMMON /SIZE/ DIA(NMAX),DEAA(9),DOPC(7),DAVG(6)
      REAL VDIST(NMAX),NDIST(NMAX)
C
C    FINDAV finds moments of the size distribution.
C
      SUMN=0.
      SUMV=0.
      SUM1=0.
      DO 100 I=NMIN,NMAX
         SUMN=SUMN+NDIST(I)
         SUMV=SUMV+VDIST(I)
         SUM1=SUM1+NDIST(I)*DIA(I)
 100  CONTINUE
      DPVAV= (6*SUMV/SUMN/3.141593)**(1./3.)
      DPNAV= SUM1/SUMN
      RETURN
      END
C
C-----------------------------------------------------------------------
C
      SUBROUTINE GETNUM ( NDIST, VDIST )
C
C Calculate number distribution from volume distribution
C
$INCLUDE: 'PARAMS.INC'
      COMMON /SIZE/ DIA(NMAX),DEAA(9),DOPC(7),DAVG(6)
      REAL VDIST(NMAX),NDIST(NMAX)
C
      DO 200 I= NMIN,NMAX
         D= DIA(I)
 200     NDIST(I) = VDIST(I) * 6. / (3.141593 * D*D*D )
C
      RETURN
      END
C
C=======================================================================
Z
```

```
      PROGRAM SMOOTH
C
C SMOOTHS TOTAL VOLUME AND TOTAL NUMBER PROFILES OVER SELECTED INTERVAL
C
C  SMOOTH takes as input the profile files created by MANAGE from the
C   output files of MISTI.  It reads the data in from the .P1,.P2,.PA
C   or .PB file, asks for the averaging interval (suggested: 1/2 hour)
C   and smooths the total number and total volume by inversion.  The
C   output is written to a user-specified file (Unit 11).
C
      COMMON /WHERE/ NOW,NEXT
      REAL TOTNUM,EAANUM,OPCNUM,TOTVOL,EAAVOL,OPCVOL
      REAL TIME(200),NUM(200),VOL(200)
      REAL TINT,FIRSTTIME,ENDTIME
      CHARACTER*20 NFILE,CFILE
      CHARACTER*1 ASK
C
      WRITE(*,200) 'Name of .PA or .PB file to be smoothed : '
 200  FORMAT(/1X,A\)
      READ(*,202) CFILE
 202  FORMAT(A)
C
      OPEN (20,FILE=CFILE,STATUS='OLD',FORM='FORMATTED')
C
        WRITE(*,200) 'Name of smoothed output file [SMOOTH.OUT] : '
        READ(*,202) NFILE
        IF (NFILE.EQ.' ') NFILE='SMOOTH.OUT'
        OPEN (11,FILE=NFILE,STATUS='NEW',FORM='FORMATTED')
C
      NOW = 0
      NOWMIN = 0
C
C         READ IN DATASET
C
 300  READ(20,*,END=400,ERR=400) HOUR,TOTNUM,EAANUM,OPCNUM,TOTVOL,
     #        EAAVOL,OPCVOL
C
      IF (NOW.EQ.0) FIRSTTIME=HOUR
      NOW = NOW + 1
      TIME(NOW)=HOUR
      IF (HOUR.LT.0) NOWMIN = NOW
      NUM(NOW)=TOTNUM
      VOL(NOW)=TOTVOL
      IF (NOW.LT.200) GOTO 300
C
 400  CONTINUE
C
      ENDTIM=HOUR
      WRITE(*,*) NOW,' Datasets Read up to Time ',ENDTIM
```

```
      CALL CLOSE (20)
C
C All unsmoothed data have been read in.
C Now average the datasets over a user-specified interval.
C
      WRITE(*,200) 'AVERAGING Interval (Hours; 0. nearest pt.): '
      READ(*,*) TINT
C
      NEXT=NOWMIN
      PTIME = TIME(NOWMIN)
      IF (FIRSTTIME.GT.0) THEN
         PTIME=FIRSTTIME
         NEXT = 1
      END IF
C
 500  CALL AVERAG(PTIME,TINT,TIME,NUM,VOL)
C
C Note if there are no data near PTIME, AVERAG will use the
C  first time after PTIME to provide data, rather than exit.
C
C Go on to the next point.
C
      NEXT=NEXT+1
      PTIME=TIME(NEXT)
      IF (NEXT.LE.NOW) GOTO 500
C
 990  CONTINUE
      WRITE (*,*) ' '
      STOP 'Smoothing program SMOOTH Done.'
      END
C
C-----------------------------------------------------------------------
C
      SUBROUTINE AVERAG ( PTIME, TINT, TIME, NUM, VOL)
C
C Finds AVERAGE values at PTIME within Interval TINT
C     (from PTIME-TINT/2 to PTIME+TINT/2 in hours)
C
      REAL TIME(200),NUM(200),VOL(200)
      COMMON /WHERE/ NOW,NEXT
C
c  Starting and stopping times:
c
      PSTAR=PTIME-TINT/2.
      PSTOP=PTIME+TINT/2.
c
c  Look for the first time greater than PSTAR
c
      J=1
```

```
  25  IF (TIME(J).GT.PSTAR) GOTO 100
      J=J+1
      IF (J.GT.NOW) STOP 'PTIME too large'
      GOTO 25
C
C  Having found this time, initialize ANUM and AVOL which will hold
C     the averaged number and volume values.
C
 100  ANUM = NUM(J)
      AVOL = VOL(J)
      KOUNT=1
 200  J=J+1
      IF (J.GT.NOW .OR. TIME(J).GT.PSTOP) GOTO 500
c
c  Add the number to ANUM and the volume to AVOL for as many times as
c    can fit before PSTOP.
c
      ANUM = ANUM + NUM(J)
      AVOL = AVOL + VOL(J)
      KOUNT=KOUNT+1
      GOTO 200
c
c  Now divide by the number of values that were added in.
c
 500  COUNT=FLOAT(KOUNT)
        ANUM = ANUM/COUNT
        AVOL = AVOL/COUNT
c
      WRITE(11,800) PTIME,AVOL,ANUM
 800  FORMAT(2X,F8.4,4X,F9.3,4X,F9.2)
C
      RETURN
      END
C
C=======================================================================
*
```

APPENDIX IV

DATA FROM SMOG CHAMBER EXPERIMENTS

iv.1 Summary of smog chamber data files

Data from these experiments are recorded in many different files, from raw data through inverted results. In the following section, we summarize the path these data follow between acquisition and final inverted distributions. Most of the programs used for these manipulations can be found in Warren (1986). A complete summary of the suffix coding for the files is given in Table IV.1 following.

Raw EAA data are recorded by the PDP-11 computer in the laboratory on 8" floppy disks. These data are labeled with the experiment name followed by the suffix .E2R, to indicate 2 EAA's, raw data. The PDP-11 program VTEAA creates the more compact files .EA1, .EA2, .EA3, or .EA4. The .EA1 and .EA2 files represent EAA132 and EAA250 readings, respectively. For dual-chamber experiments, .EA1 indicates EAA132 recording data from side A of the chamber, .EA2 represents EAA250 on side B, .EA3 represents EAA132 on side B, and .EA4 represents EAA250 on side A.

The PDP-11 program EAAINT creates .EI# files from the .EA# files, where the numbering remains the same. This program simply time-interpolates each channel of the EAA to correct for the length of the sampling cycle, and stores the data as EAA voltage differences per channel instead of the voltages per channel recorded in the .EA# files.

Data from the OPC are output on paper tape from the instrument and entered by hand into the PDP-11 computer. The suffixes .OPC and .DOP apply to single-

chamber experiments, before and after the diluter is turned on. These files are combined into an .OP file, which gives the time and number concentration in each channel for channels 1 - 6. For the dual-chamber experiments, .OPA and .OPB files are created from the paper tapes, for sides A and B. These are multiplied by the dilution ratio and put in the same format as the .OP files, and labeled .POA and .POB.

CNC data are recorded by hand, then entered into the computer as .CN1 and .CN2 files when both instruments are running for a single-chamber experiment, or as a .CNC file for only one instrument. The designations "1" and "2" referred to CNC219 and CNC230, respectively. In dual-chamber experiments, .CNA and .CNB files contain the time versus number concentration data.

The .EA# files and .OP files for single-chamber experiments are inverted simultaneously by MISTI, producing .N1 and .N2 files. These are unformatted files that contain the number distributions with time for the combined EAA132/OPC data and the combined EAA250/OPC data, respectively. Using the program MANAGE, also given in Appendix III, .P1 and .P2 profile files are created from the .N1 and .N2 files; these contain time, total number concentration of particles by inversion, EAA and OPC, and total volume concentrations by inversion, EAA and OPC. MANAGE also creates .S1 and .S2 summary files that contain time, total number concentration of particles $\geq$0.01 μm by inversion, total number concentration $\geq$0.02 μm, total volume concentration and number-average and volume-average diameters. The .P1 and .P2 files are smoothed over a half-hour interval to create .SM1 and .SM2 files. Aerosol number and volume distributions averaged over $\pm$7.5-minute intervals are created by MANAGE, and stored as DISTxxx.#, where the xxx designates the number of the experiment and the # ranges from 1 - 12, for each half-hour interval, with 1 being the experimental initial distribution.

For dual-chamber experiments, the designations are the same, with A and B being used instead of 1 and 2 to designate the side of the chamber.

TABLE IV.1. File suffixes for smog chamber data

EAA files:	
.E2R	Raw EAA data taken from both EAA's
.EA1	EAA132, single-chamber experiments, raw data in voltages
.EA2	EAA250, single-chamber experiments, raw data in voltages
.EA1	EAA132, dual-chamber experiments, side A, raw data in voltages
.EA2	EAA250, dual-chamber experiments, side B, raw data in voltages
.EA3	EAA132, dual-chamber experiments, side B, raw data in voltages
.EA4	EAA250, dual-chamber experiments, side A, raw data in voltages
.EA#	Time-interpolated voltages, stored as voltage differences. Same numbering as above
OPC files:	
.OPC	Raw OPC data as entered into the PDP-11. Undiluted, single-chamber experiments, number of counts per OPC printout
.DOP	Raw OPC, single-chamber experiment, diluter on
.OP	Combination of .OPC and .DOP, containing hours into experiment, total number concentrations, and number in each channel for channels 1 – 6
.OPA,.OPB	Raw OPC data for sides A and B of dual-chamber experiments. Diluter on
.POA,.POB	Same as .OP description above, for dual-chamber experiments
CNC files:	
.CN1	Time and number concentration from CNC219
.CN2	Time and number concentration from CNC230
.CNC	Time and number concentration for single-chamber experiment with only one CNC operating
.CNA,.CNB	Time and number concentration for sides A and B of dual-chamber experiments
MISTI files:	
.N1	Unformatted number distributions with time for single-chamber experiments, using EAA132 and OPC data
.N2	Unformatted number distributions with time for single-chamber experiments, using EAA250 and OPC data
.P1,.P2	Profile files created by MANAGE from .N1 and .N2 files. Contain time, total number concentrations by inversion, EAA, and OPC, and total volume concentrations by inversion, EAA, and OPC
.S1,.S2	Summary files created by MANAGE from .N1 and .N2 files. Contain time, total number $\geq 0.01\ \mu$m, total number $\geq 0.02\ \mu$m, total volume, number-average and volume-average diameters
.SM1,.SM2	Smoothed summary files containing time, volume concentration and number concentration interpolated over half-hour intervals
.NA,.NB	Unformatted number distributions for dual-chamber experiments
.PA,.PB	Profile files for dual-chamber experiments
.SA,.SB	Summary files for dual-chamber experiments
.SMA,.SMB	Smoothed summary files for dual-chamber experiments
DISTxxx.#	Inverted distributions at half-hour intervals, averaged over ± 7.5 minutes. Contains diameter, $dV/d \log D_p$, $dN/d \log D_p$. xxx identifies experiment, # indicates which half-hour interval

iv.2 Plots of smog chamber aerosol data

We present here the plots of the aerosol data from each smog chamber experiment for which aerosol data were recorded. For each experiment, we include plots of the total aerosol number concentration, the total aerosol volume concentration, and the average particle size for each aerosol instrument and for the inverted result. In addition, we show number and volume distributions at half-hour intervals over the course of each experiment. A key to the symbols on the total number, total volume and average particle size plots follows:

+	EAA132
×	EAA250
○	OPC
⋆	CNC219
*	CNC230
—	Inverted result

The dashed line in the inverted result curve indicates the area of overlap of the EAA and OPC. When these two instruments are in poor agreement, the accuracy of the inversion procedure is in question; the dashed line indicates the uncertainty in this region.

For the mean diameter plots, the inverted volume-average diameter is presented.

In the total number plots, the OPC data always start at zero particles cm^{-3}, as the particle size is below the detection limit of the instrument. In addition, in the average particle size plots, random scatter early in an experiment may be

the result of noise signals from the instruments (e.g., no initial particles in the system).

As CNC219 is generally unreliable, CNC230 was used exclusively for the dual-bag system.

Reference

Warren D.R. (1986),
Nucleation and Growth of Aerosols, Ph.D. Thesis, California Institute of Technology.

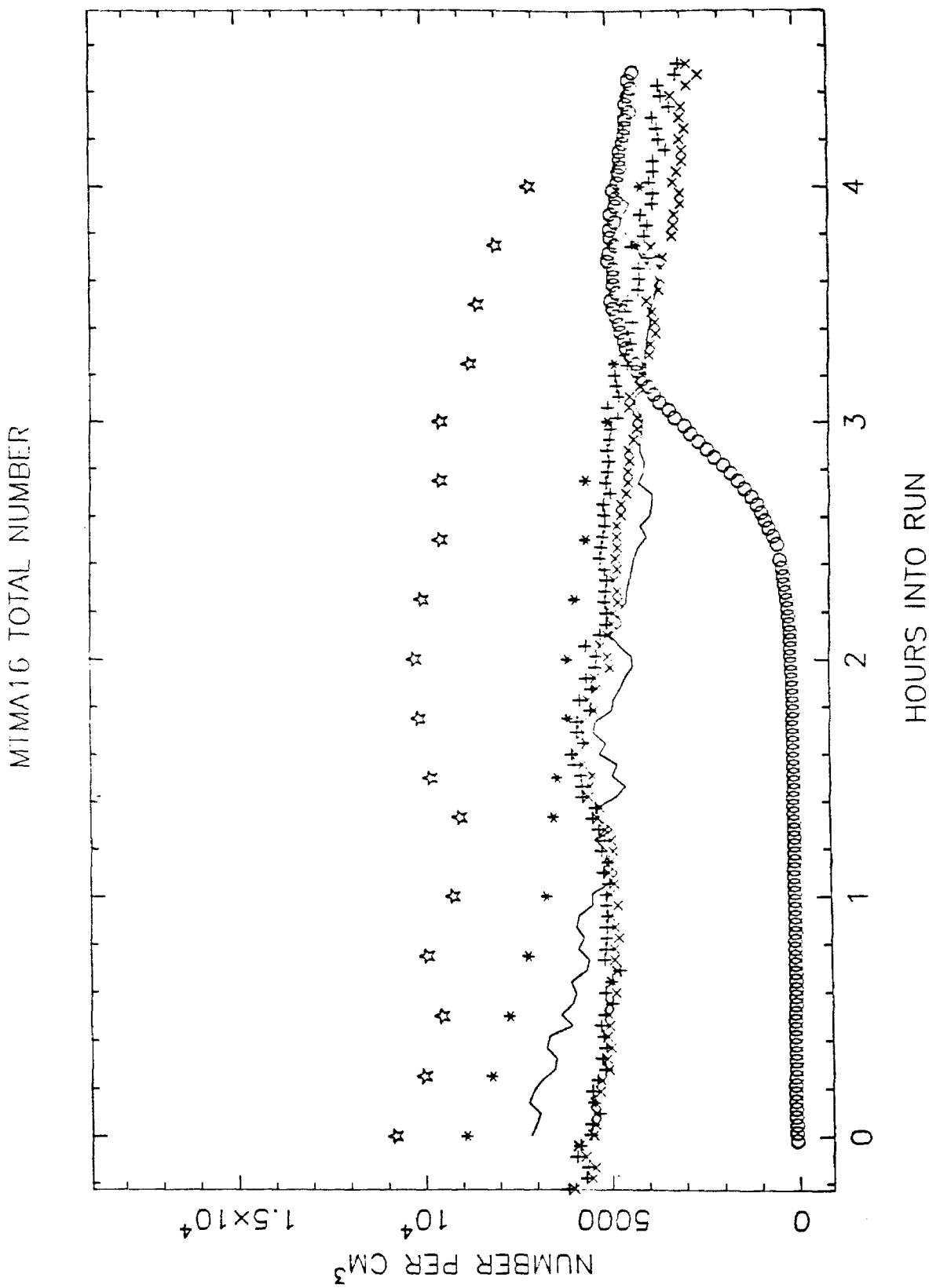
MIMA16 TOTAL NUMBER
NUMBER PER CM3
0
5000
10^4
1.5x10^4
0
1
2
3
4
HOURS INTO RUN

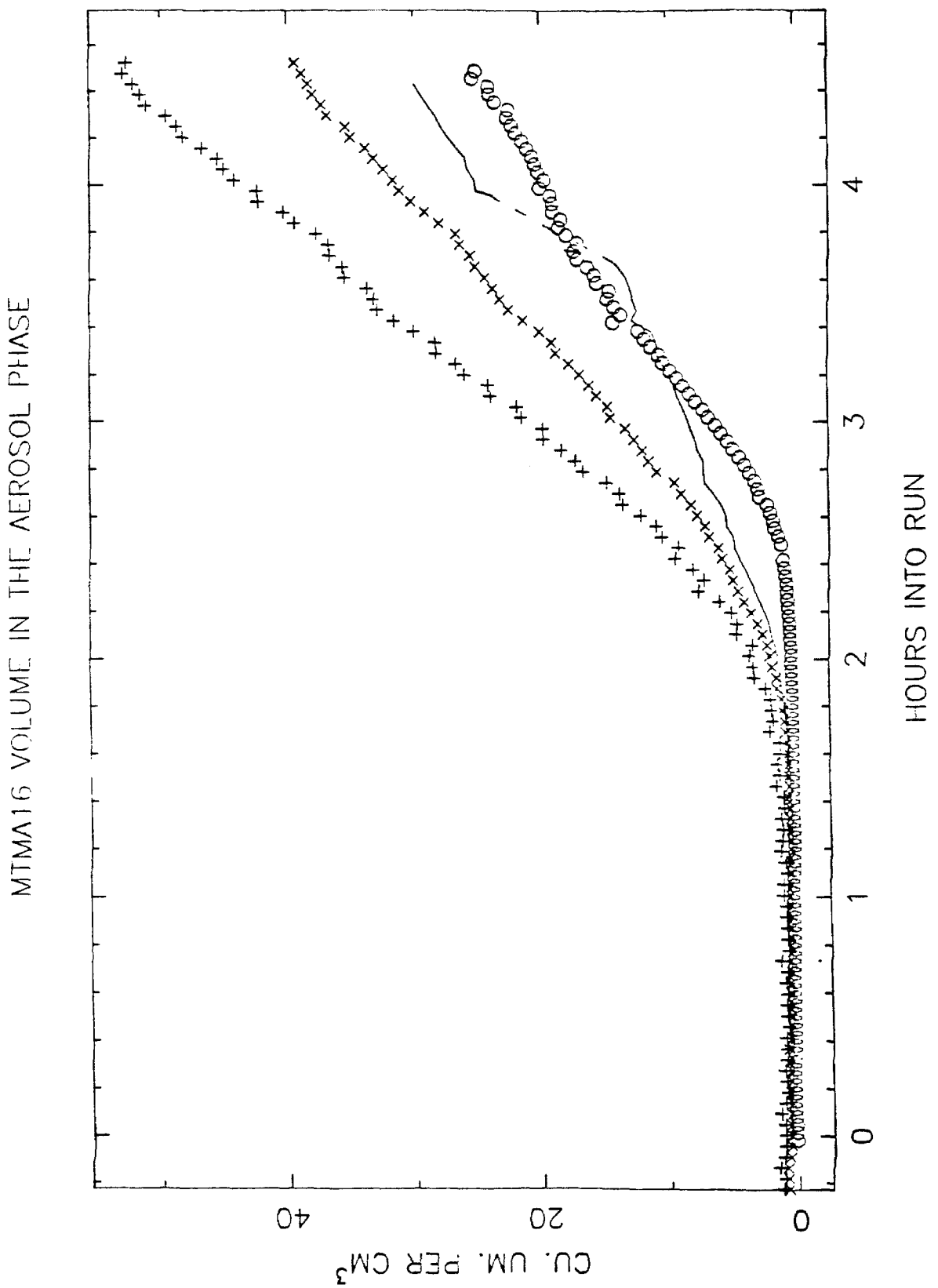
MTMA16 VOLUME IN THE AEROSOL PHASE
CU. UM. PER CM3
0
20
40
0
1
2
3
4
HOURS INTO RUN

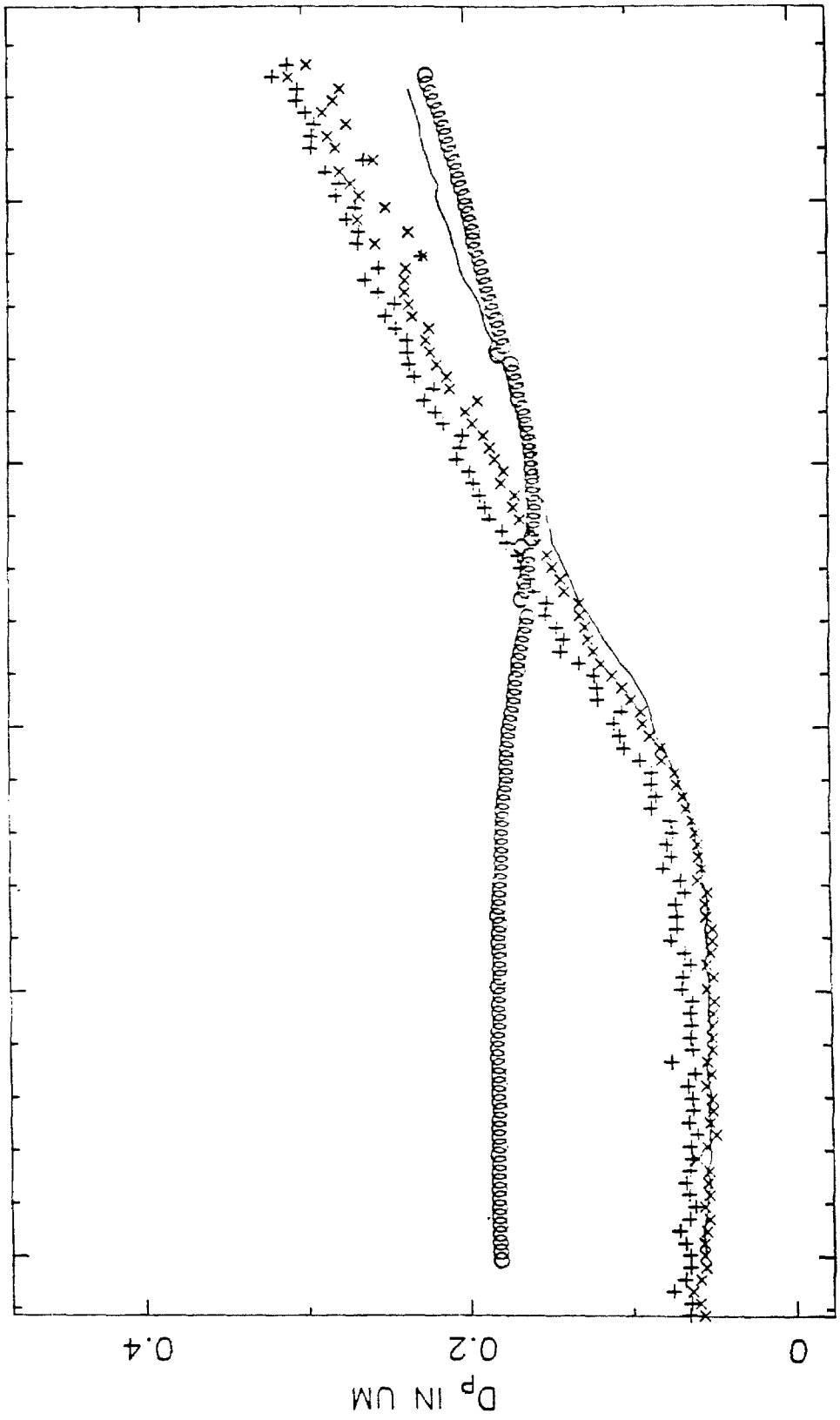
MTMA16 MEAN PARTICLE SIZE
D_p IN UM
0
0.2
0.4
0
1
2
3
4
HOURS INTO RUN

MTMA16 NUMBER DISTRIBUTION, T=0

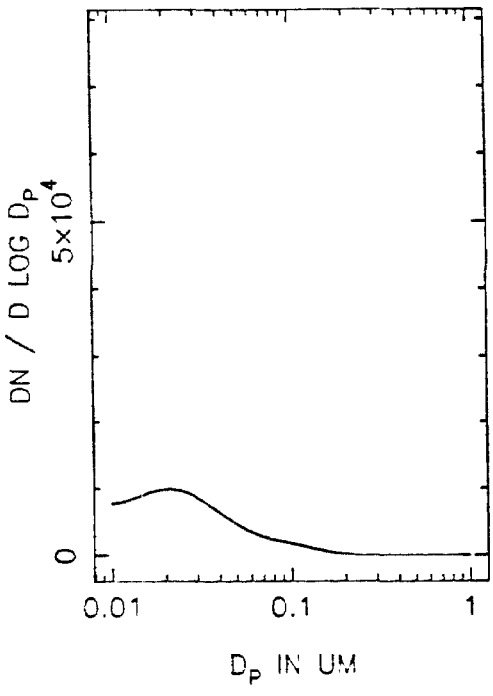

T=0.5 HOURS

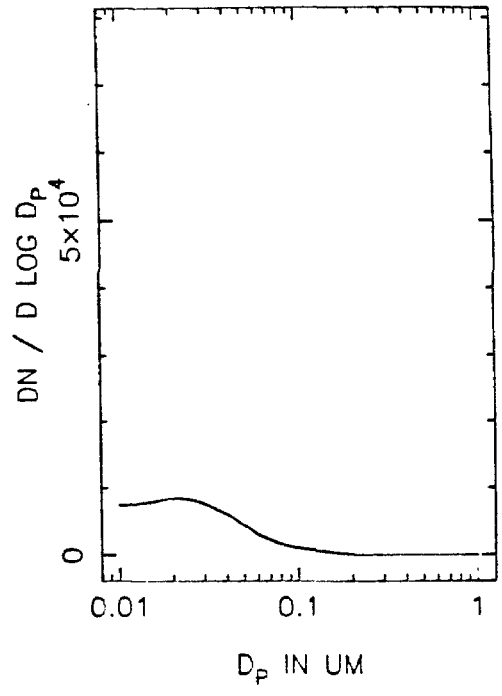

T=1.0 HOURS

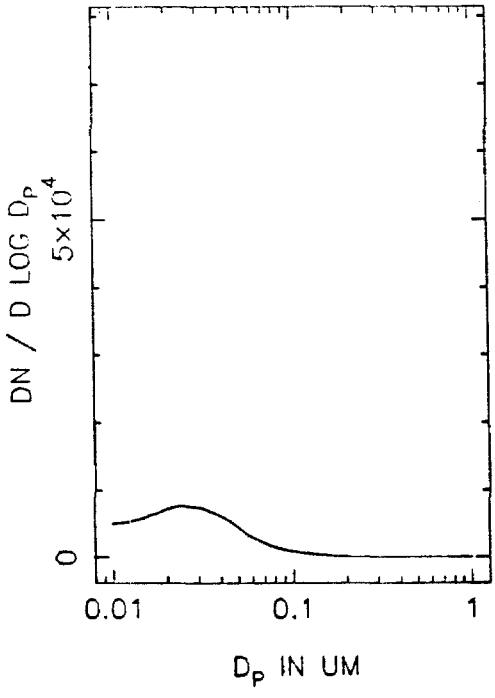

T=1.5 HOURS

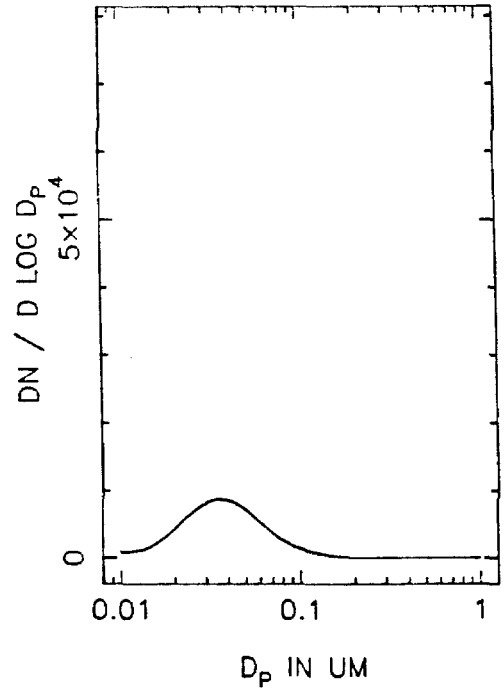

MTMA16 NUMBER DISTRIBUTION, T=2.0

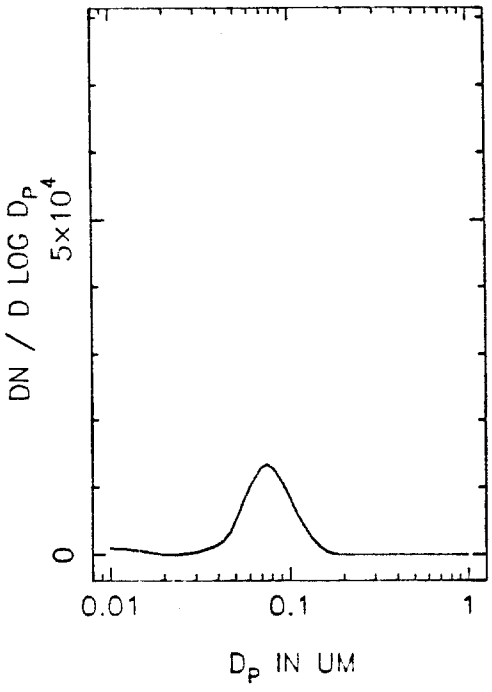

T=2.5 HOURS

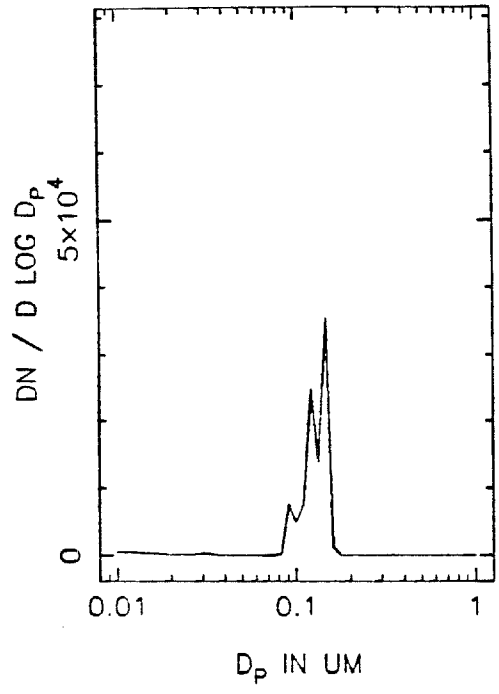

T=3.0 HOURS

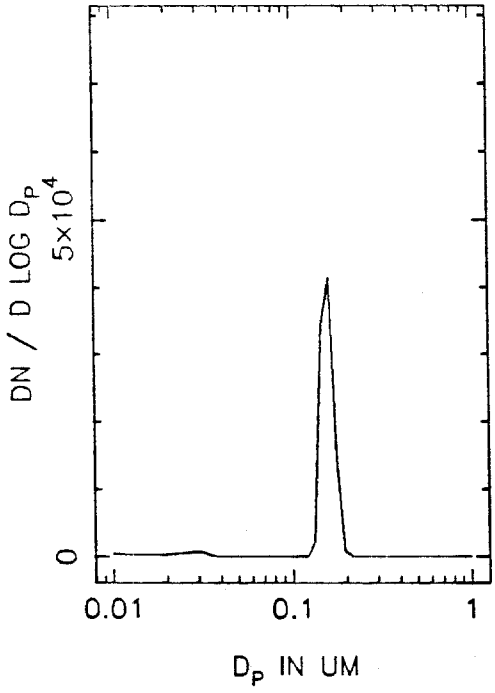

T=3.5 HOURS

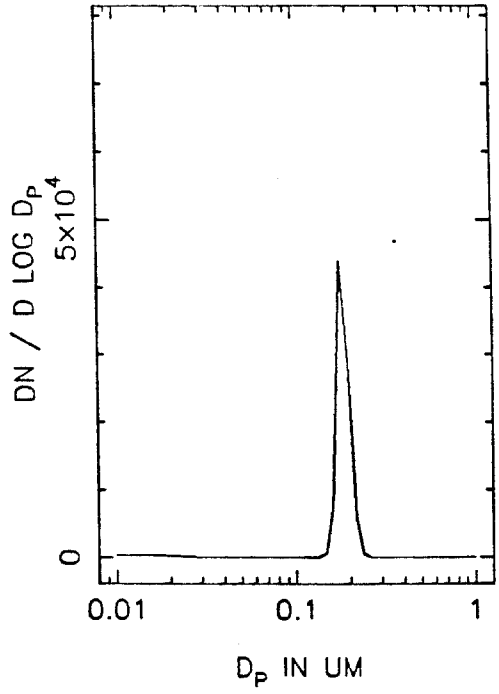

MTMA16 NUMBER DISTRIBUTION, T=4.0

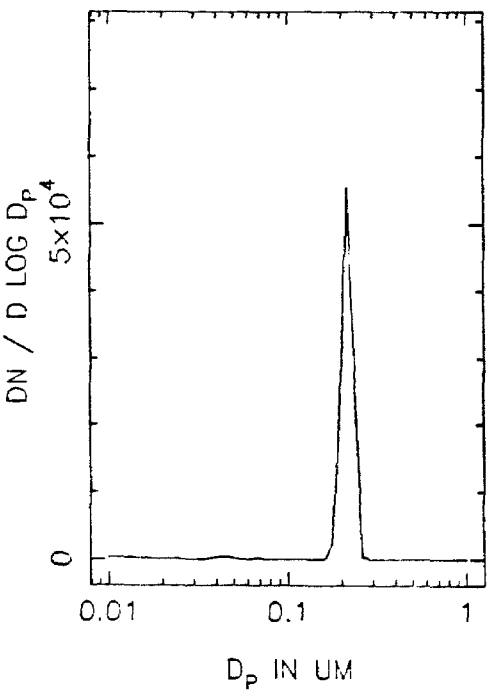

MTMA16 VOLUME DISTRIBUTION, T=0

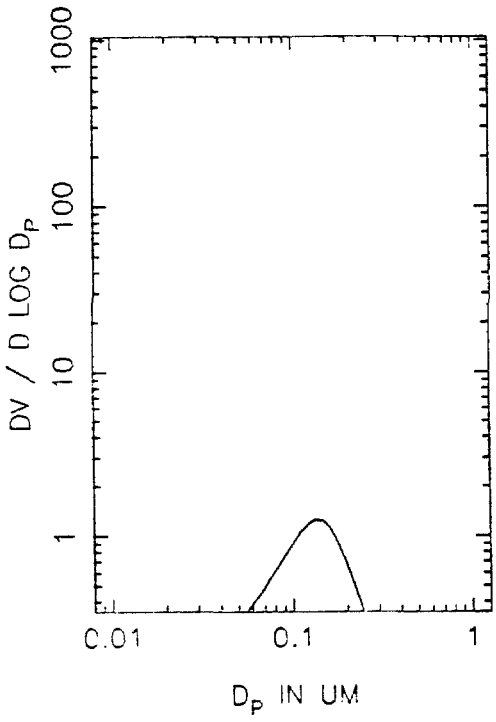

T=0.5 HOURS

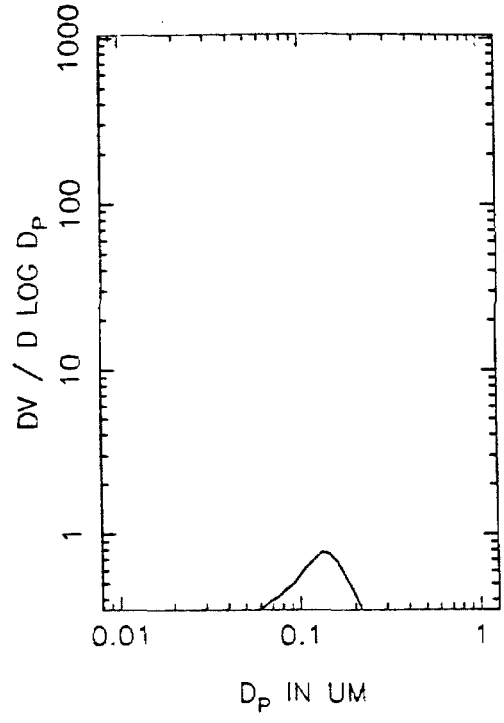

T=1.0 HOURS

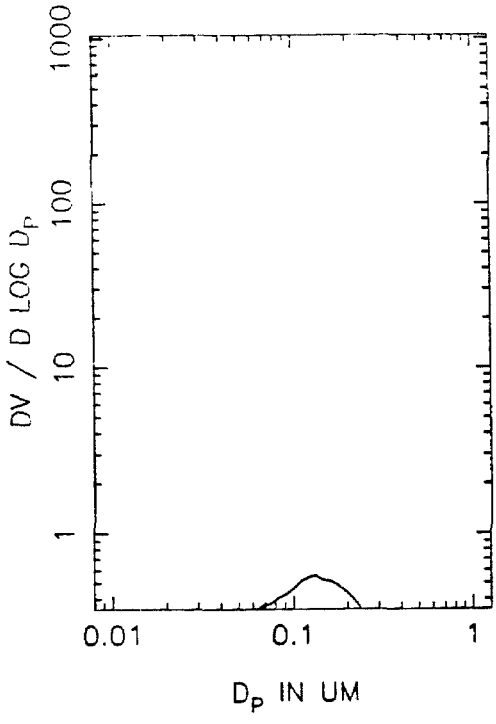

T=1.5 HOURS

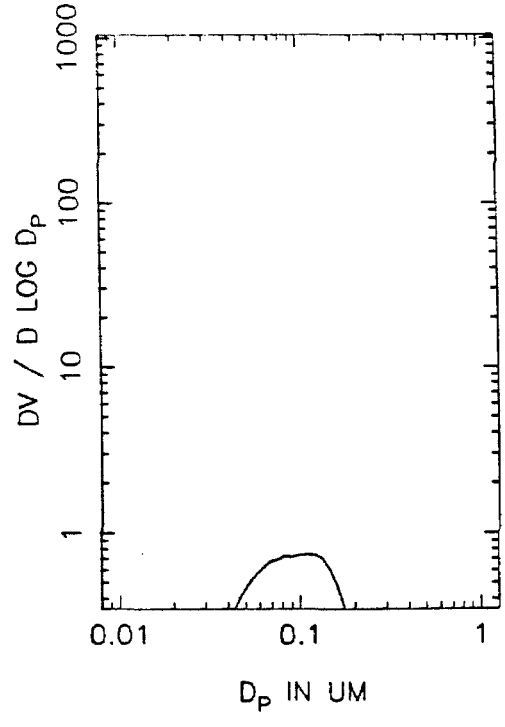

MTMA16 VOLUME DISTRIBUTION, T=2.0

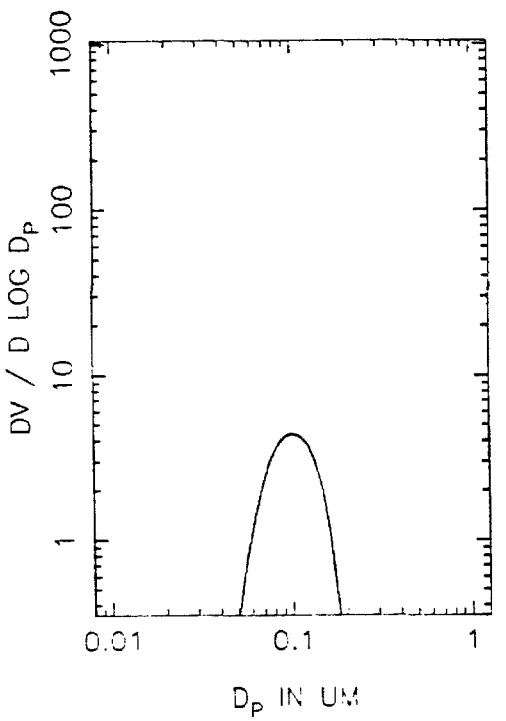

T=2.5 HOURS

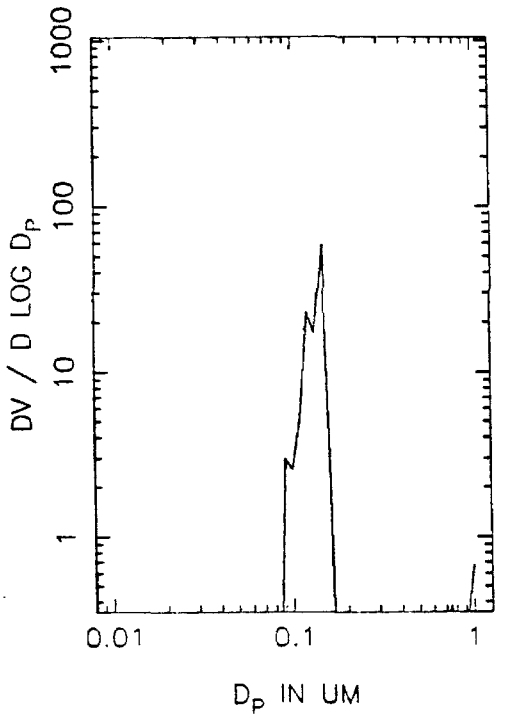

T=3.0 HOURS

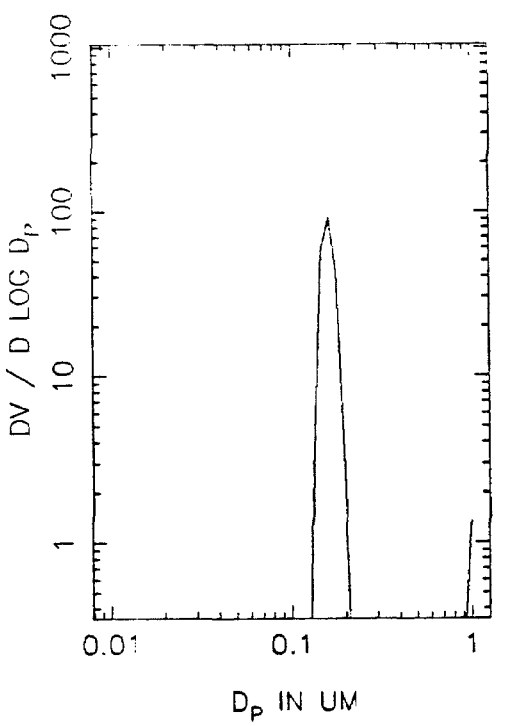

T=3.5 HOURS

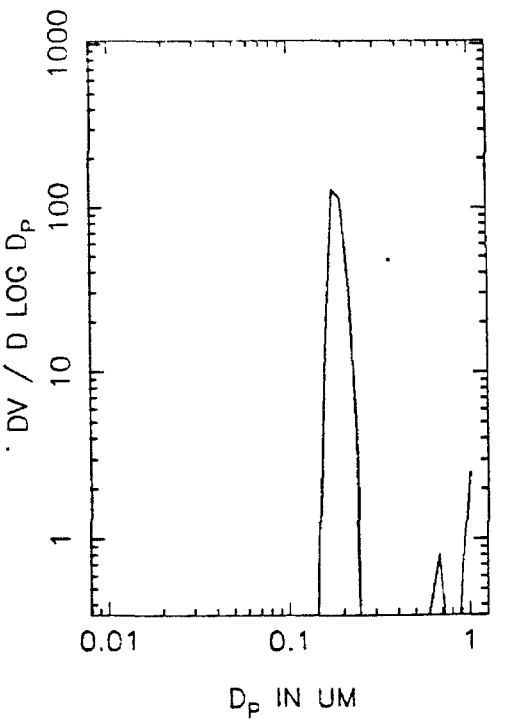

MTMA16 VOLUME DISTRIBUTION, T=4.0

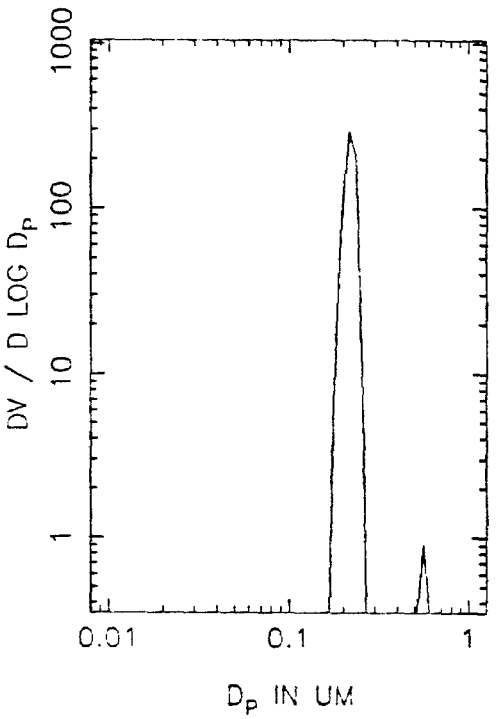

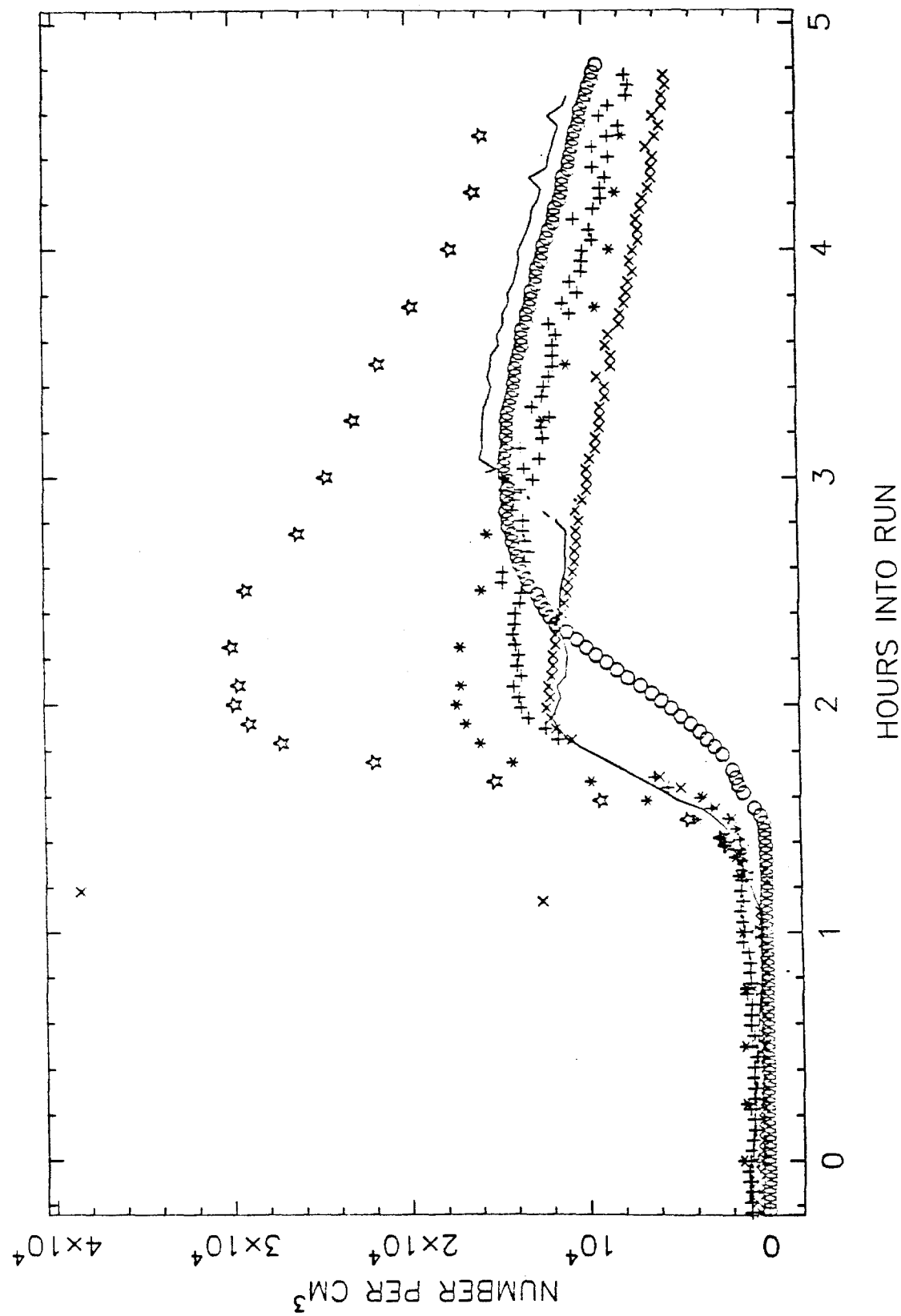
MTLA18 TOTAL NUMBER
NUMBER PER CM3
0
10^4
2×10^4
3×10^4
4×10^4
0
1
2
3
4
5
HOURS INTO RUN

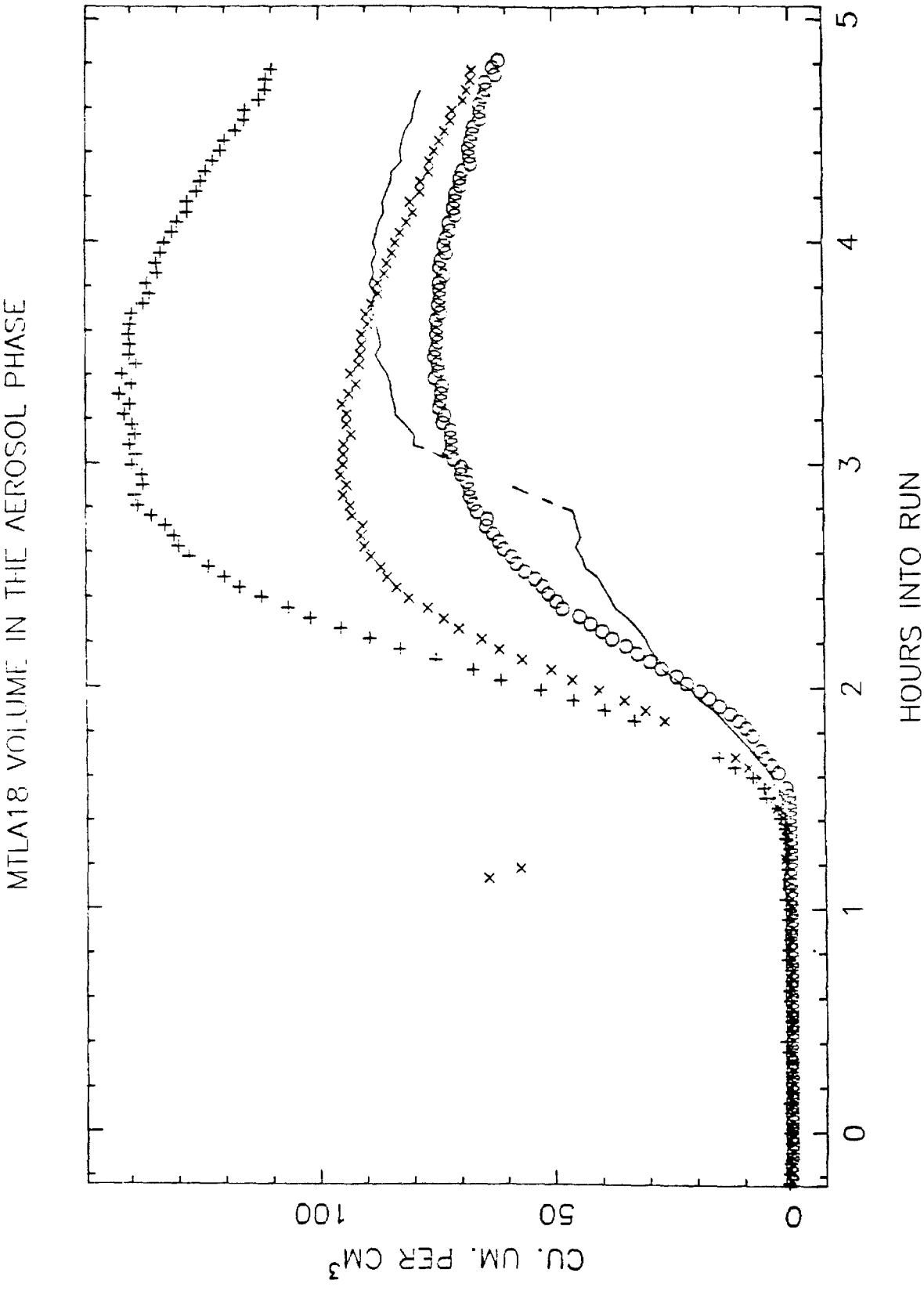
MTLA18 VOLUME IN THE AEROSOL PHASE
CU. UM. PER CM3
0
50
100
0
1
2
3
4
5
HOURS INTO RUN

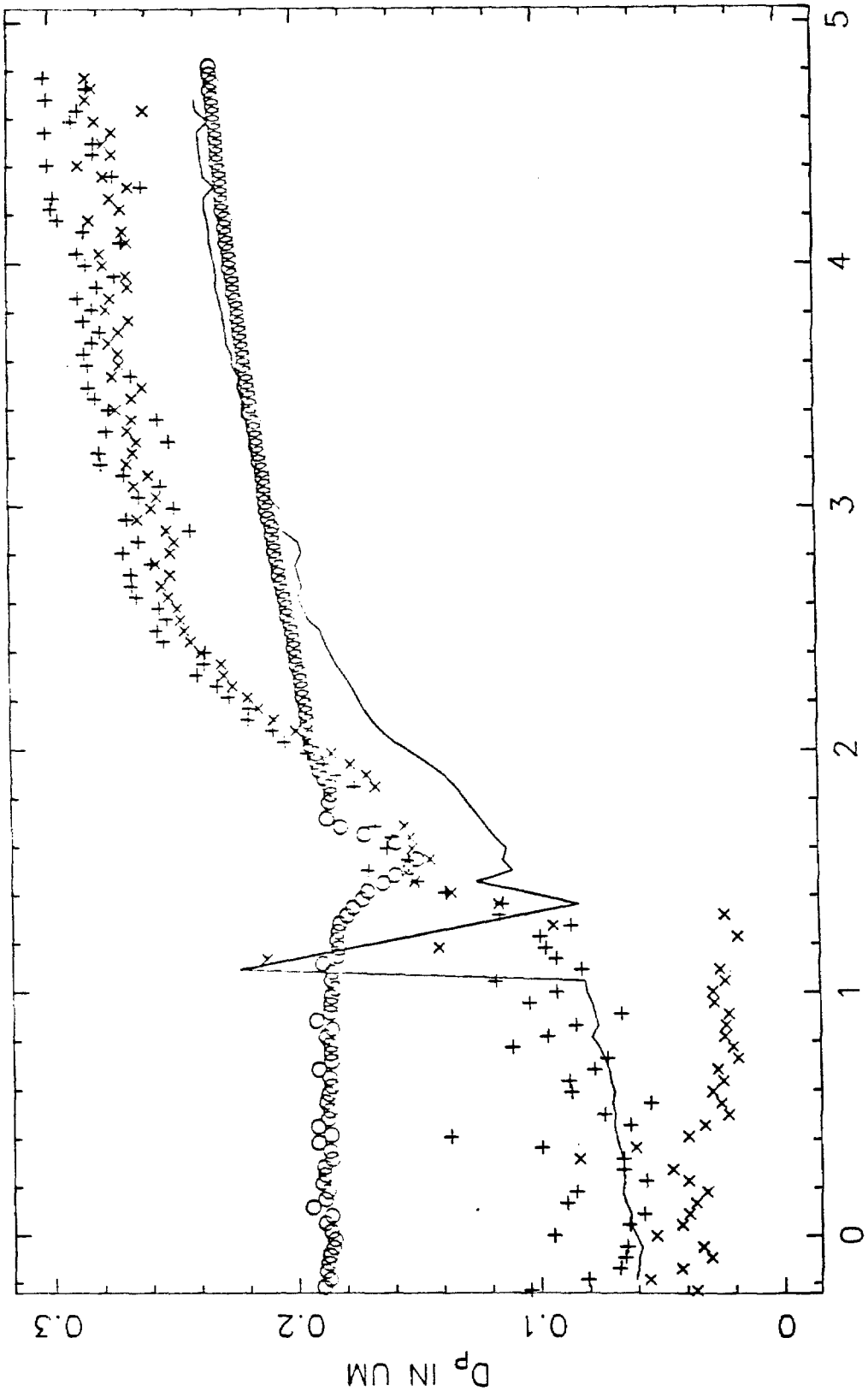
MTLA18 MEAN PARTICLE SIZE
D_p IN UM
0
0.1
0.2
0.3
0
1
2
3
4
5
HOURS INTO RUN

MTLA18 NUMBER DISTRIBUTION, T=0

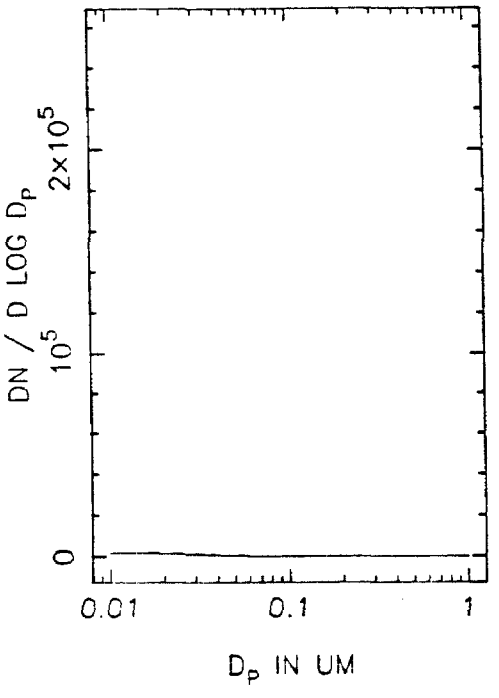

T=0.5 HOURS

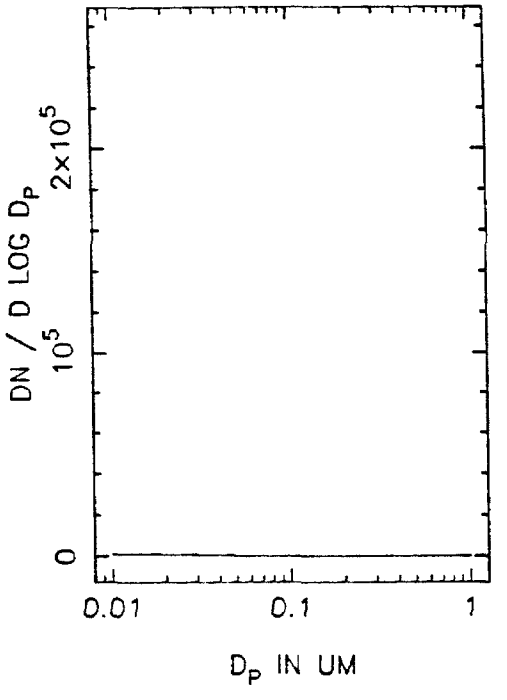

T=1.0 HOURS

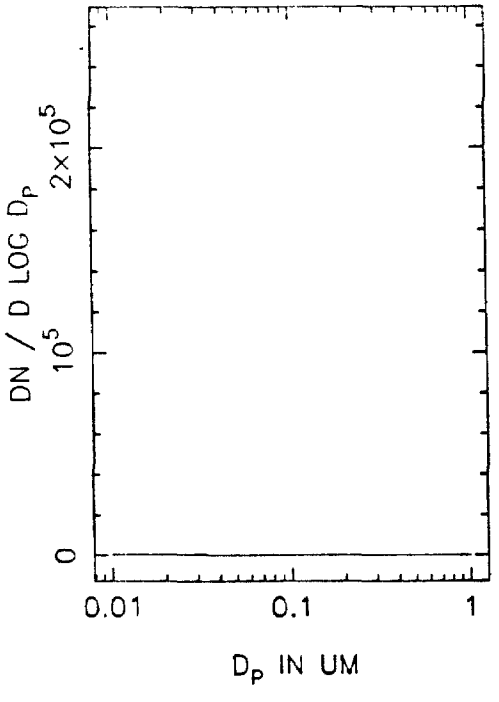

T=1.5 HOURS

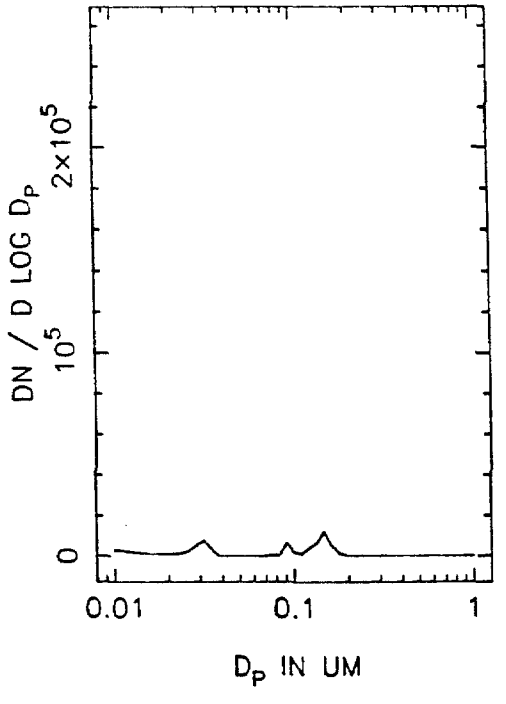

MTLA18 NUMBER DISTRIBUTION, T=2.0

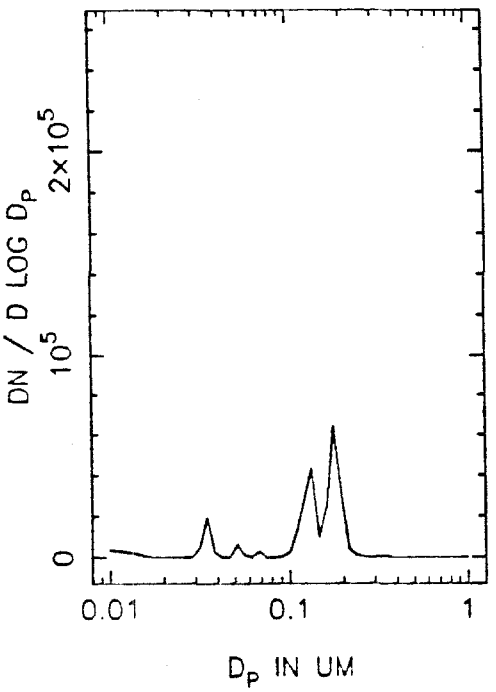

T=2.5 HOURS

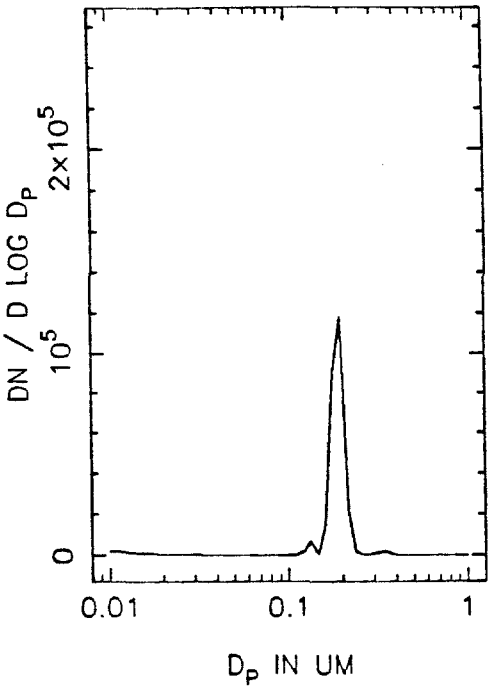

T=3.0 HOURS

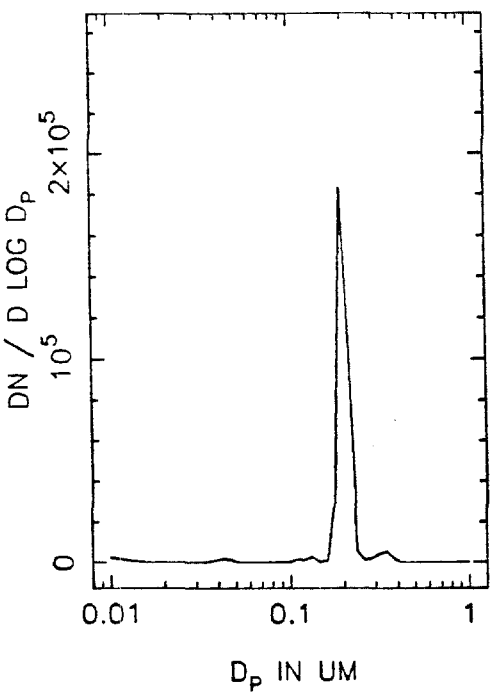

T=3.5 HOURS

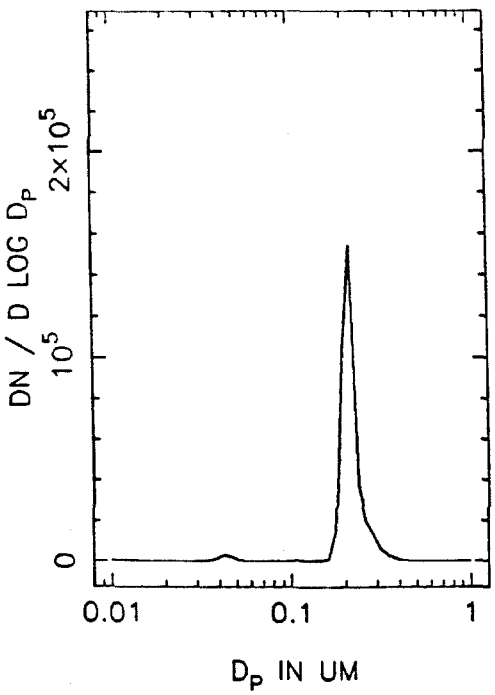

MTLA18 NUMBER DISTRIBUTION, T=4.0

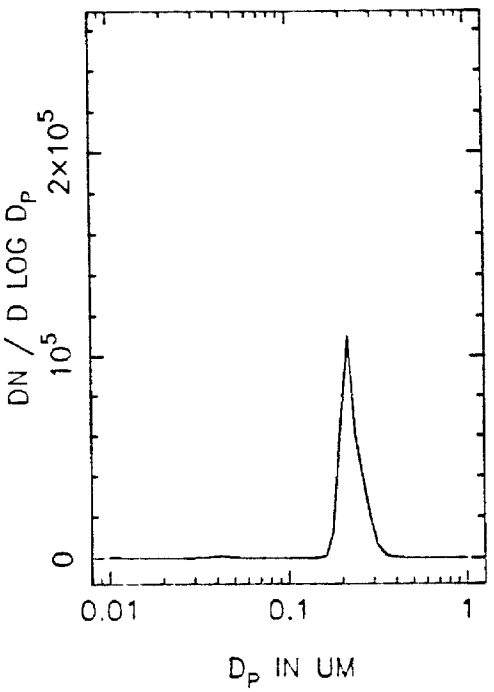

T=4.5 HOURS

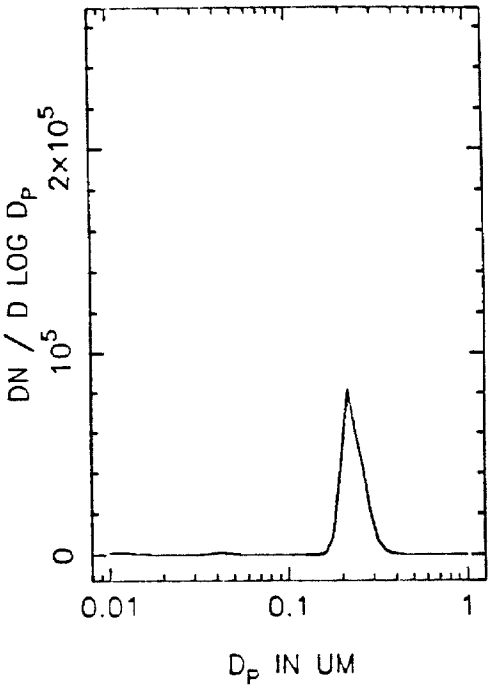

MTLA18 VOLUME DISTRIBUTION, T=0

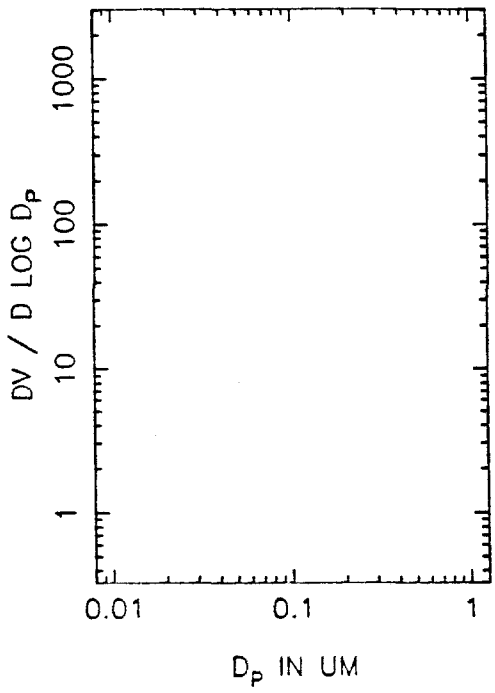

T=0.5 HOURS

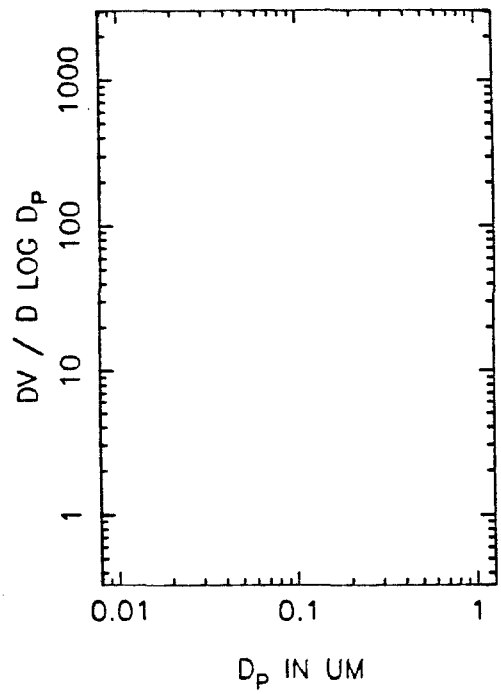

T=1.0 HOURS

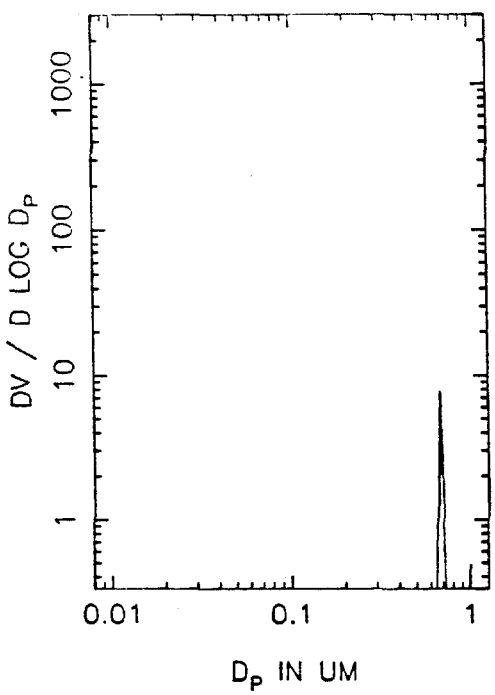

T=1.5 HOURS

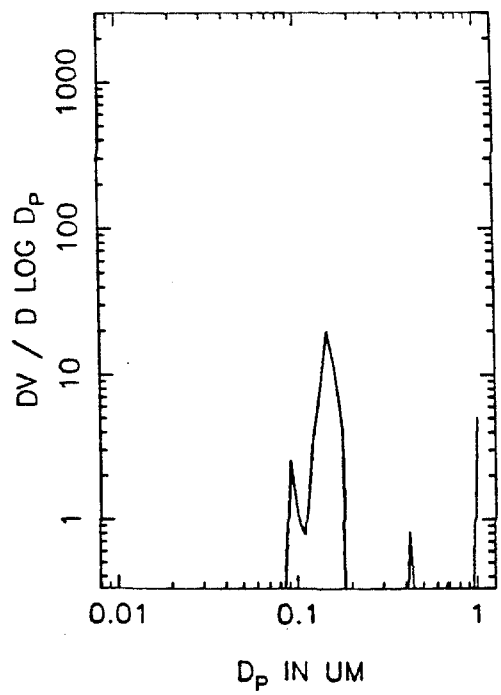

MTLA18 VOLUME DISTRIBUTION, T=2.0

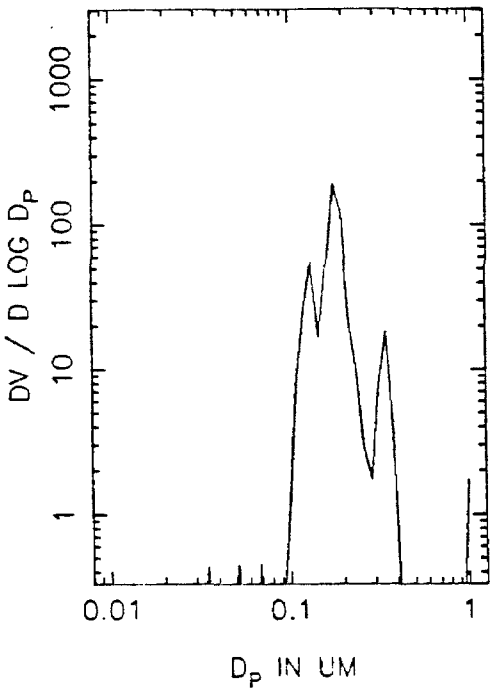

T=2.5 HOURS

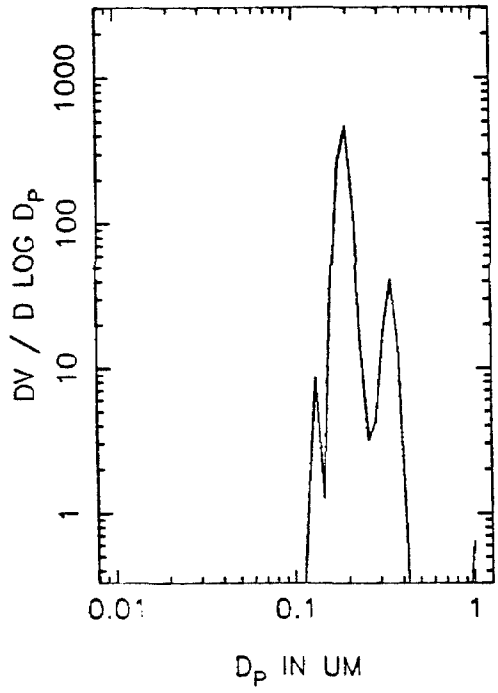

T=3.0 HOURS

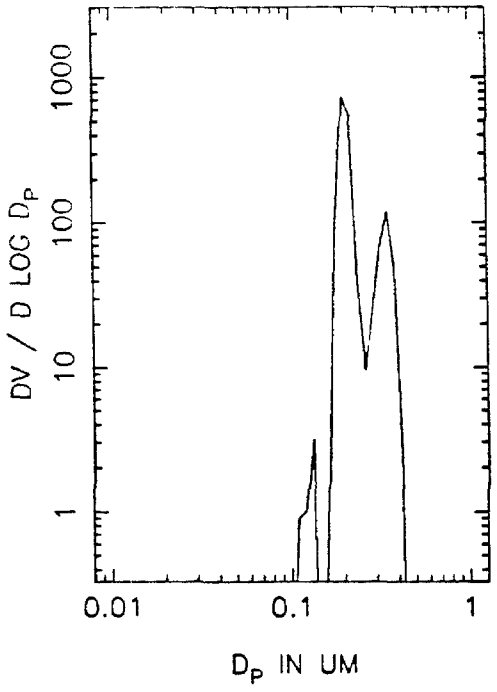

T=3.5 HOURS

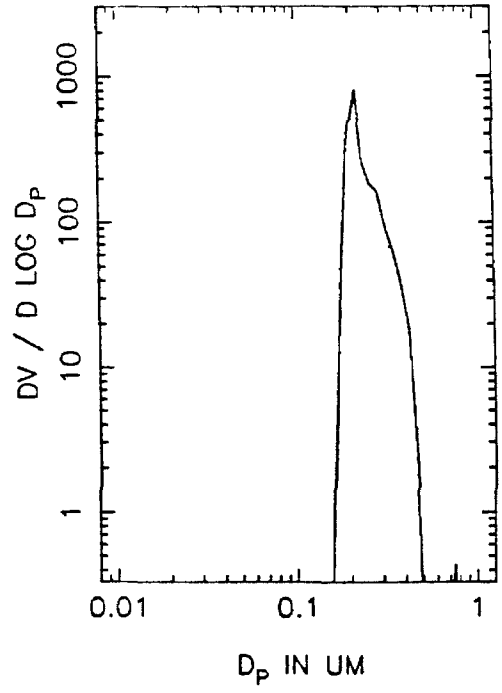

MTLA18 VOLUME DISTRIBUTION, T=4.0

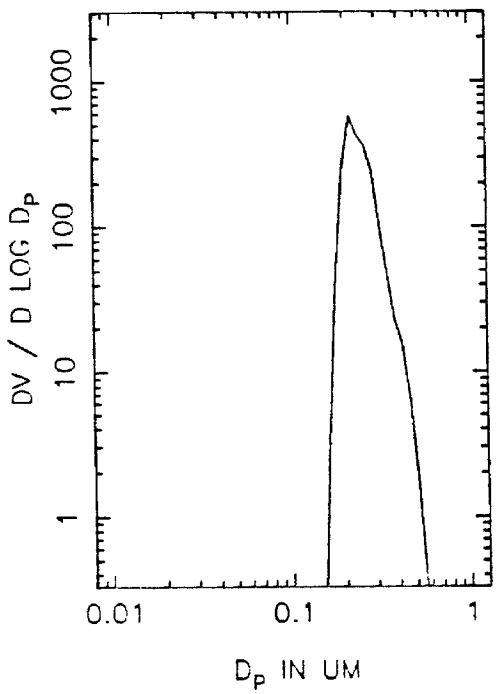

T=4.5 HOURS

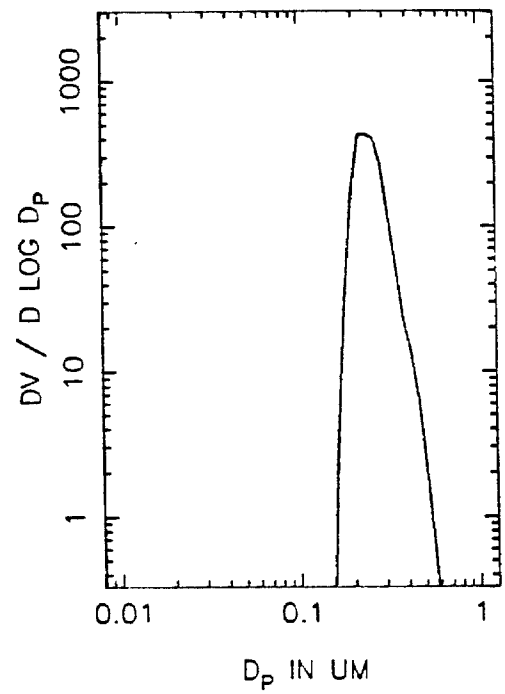

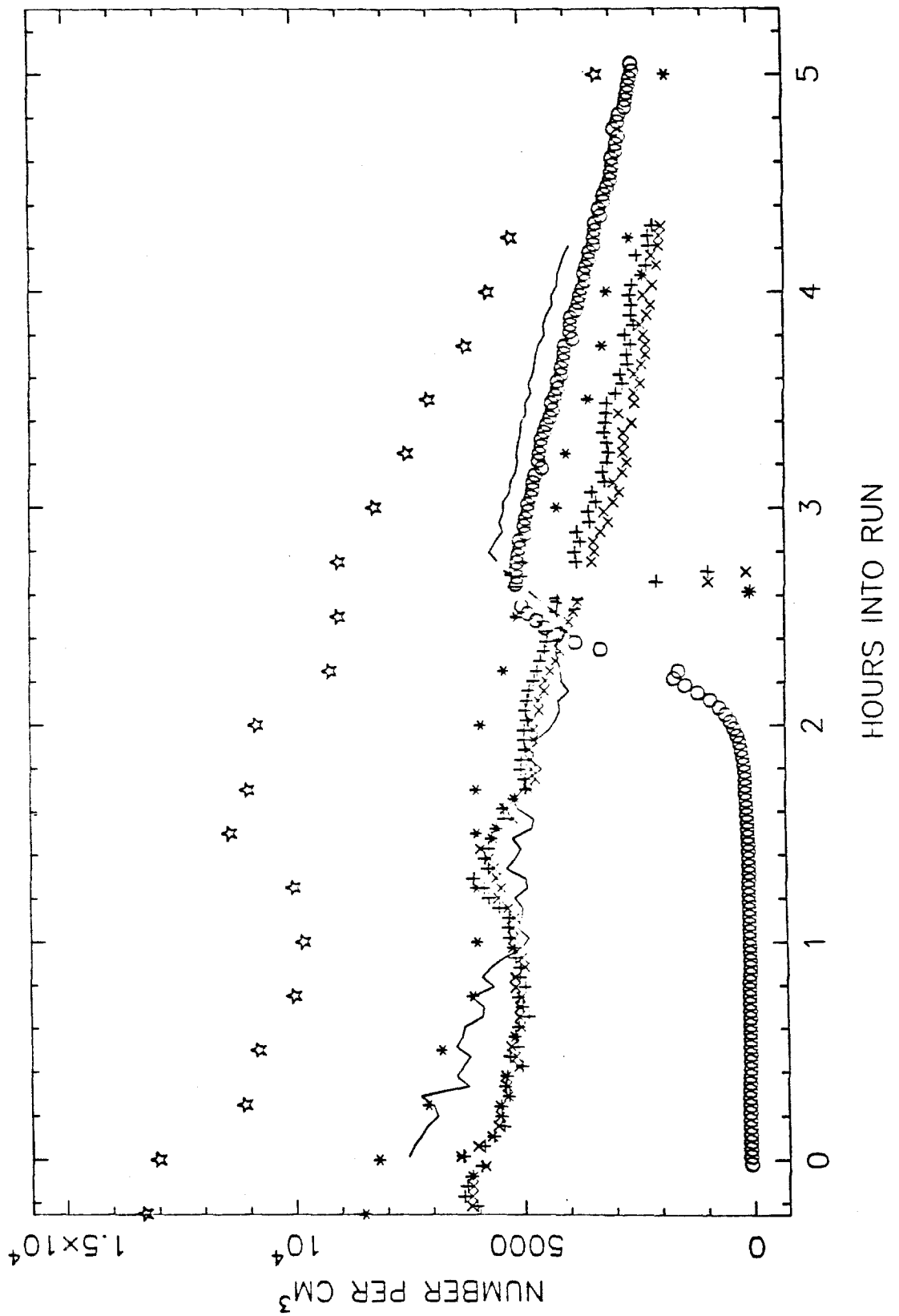
MTMA20 TOTAL NUMBER
NUMBER PER CM3
0
5000
10^4
1.5×10^4
0
1
2
3
4
5
HOURS INTO RUN

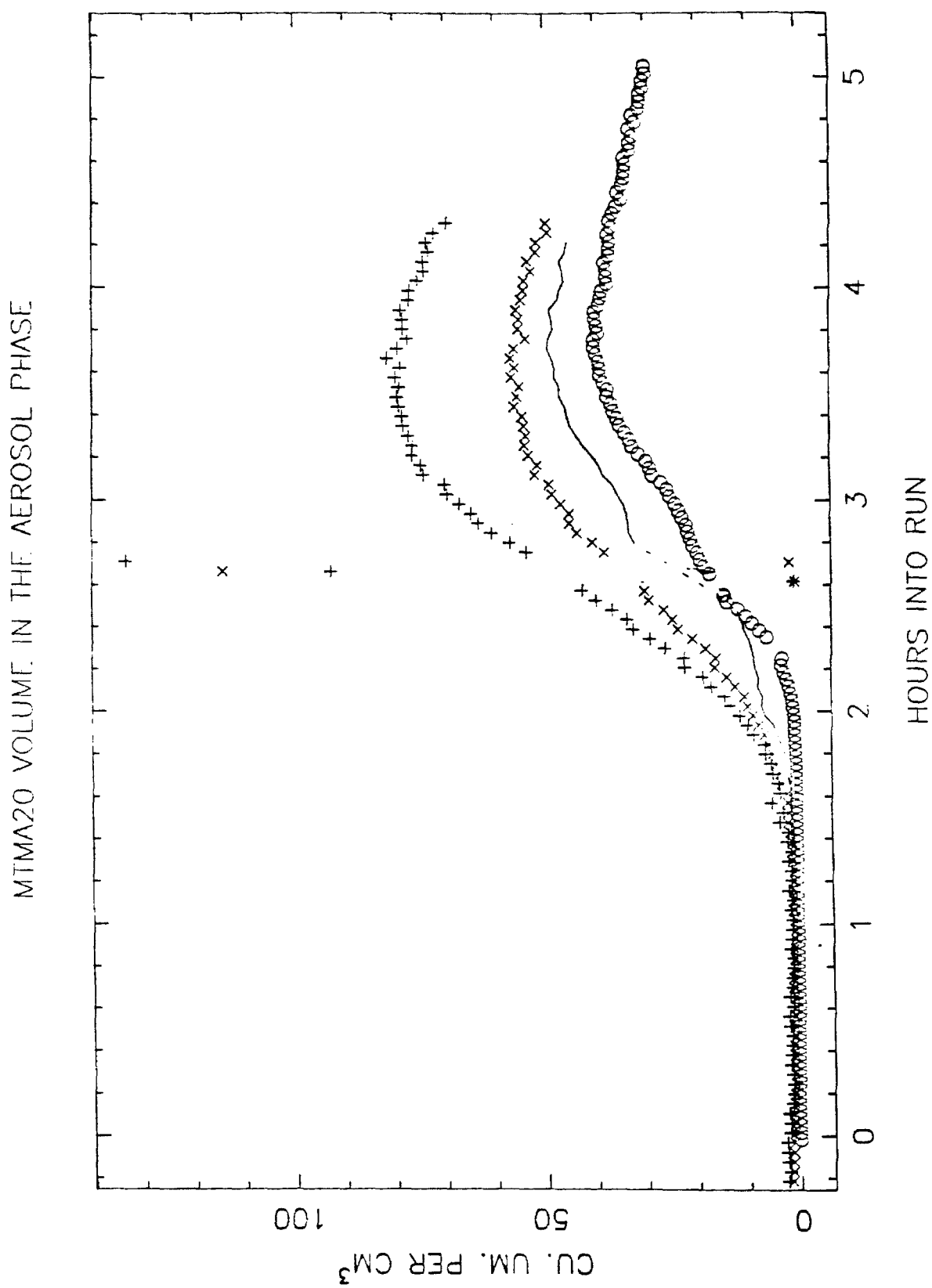
MTMA20 VOLUME IN THE AEROSOL PHASE
CU. UM. PER CM3
0
50
100
0
1
2
3
4
5
HOURS INTO RUN

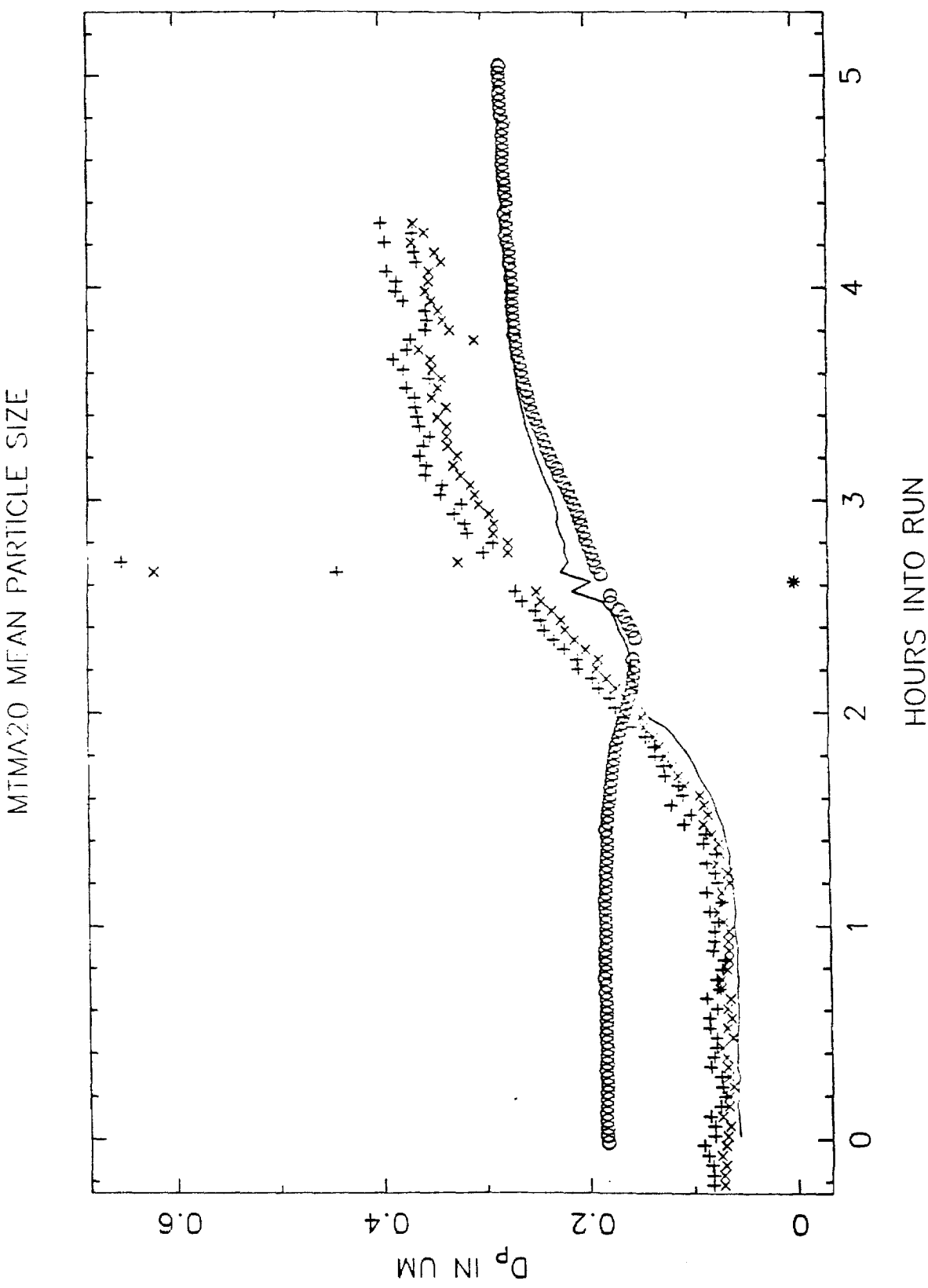
MTMA20 MEAN PARTICLE SIZE
D_p IN UM
0
0.2
0.4
0.6
0
1
2
3
4
5
HOURS INTO RUN

MTMA20 NUMBER DISTRIBUTION, T=0

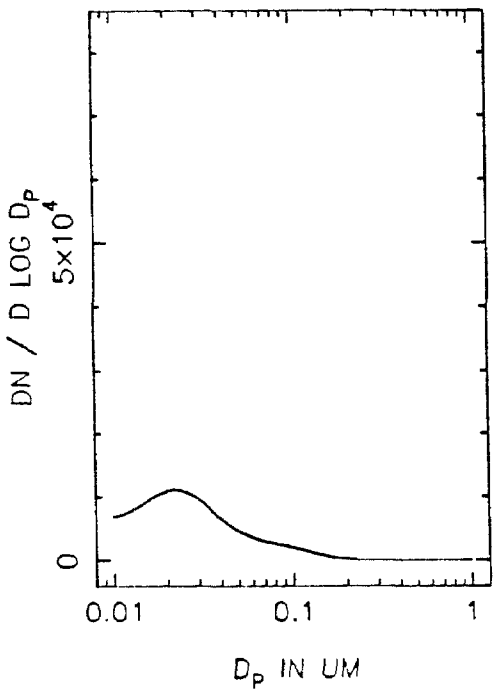

T=0.5 HOURS

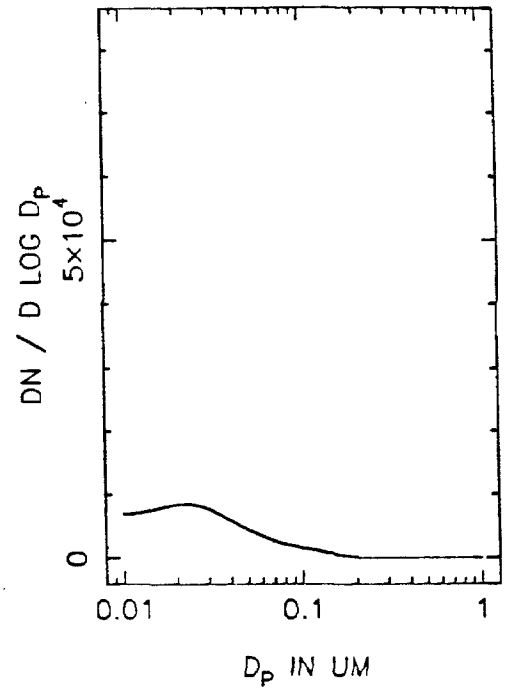

T=1.0 HOURS

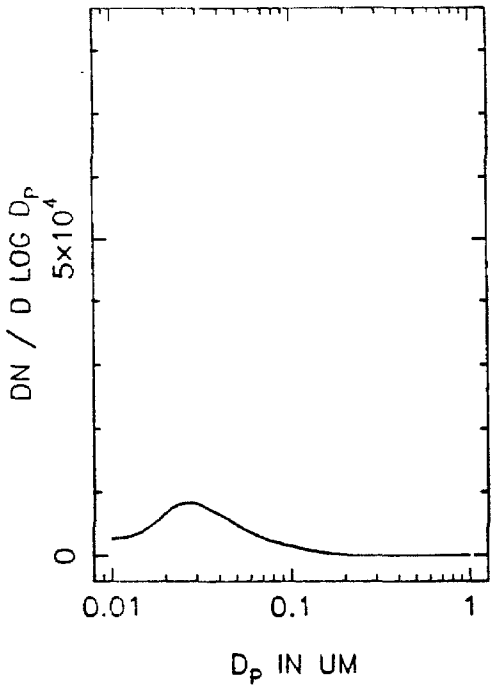

T=1.5 HOURS

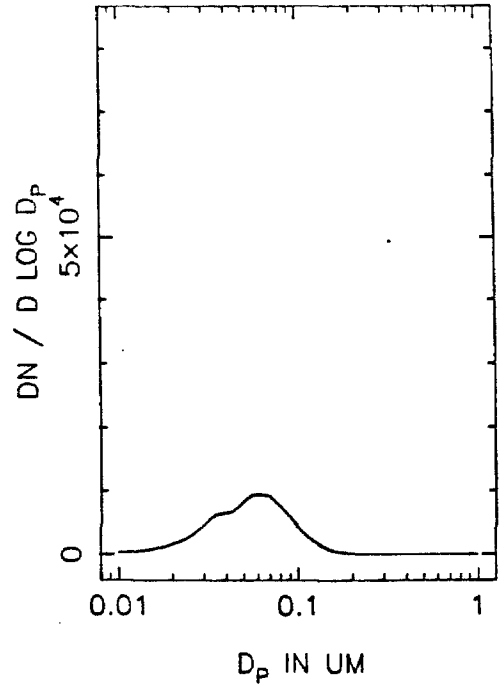

MTMA20 NUMBER DISTRIBUTION, T=2.0

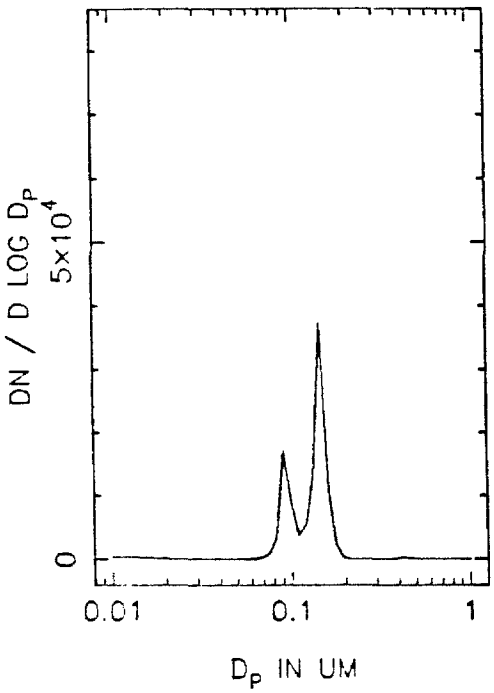

T=2.5 HOURS

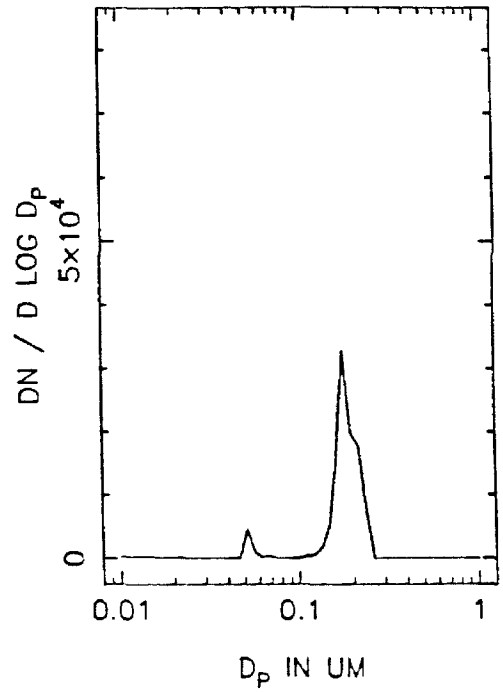

T=3.0 HOURS

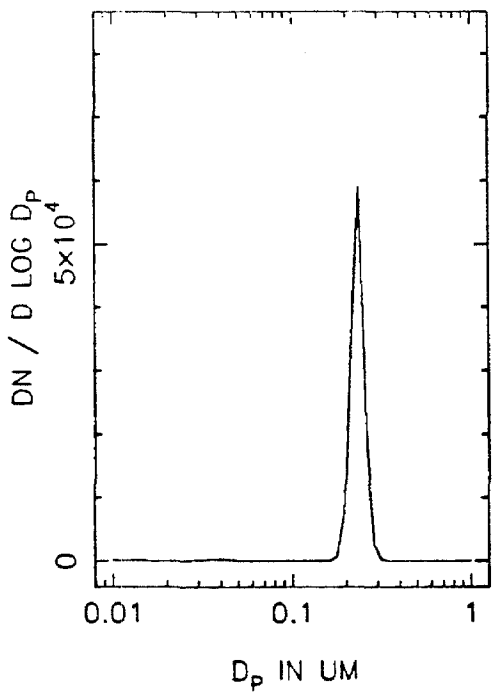

T=3.5 HOURS

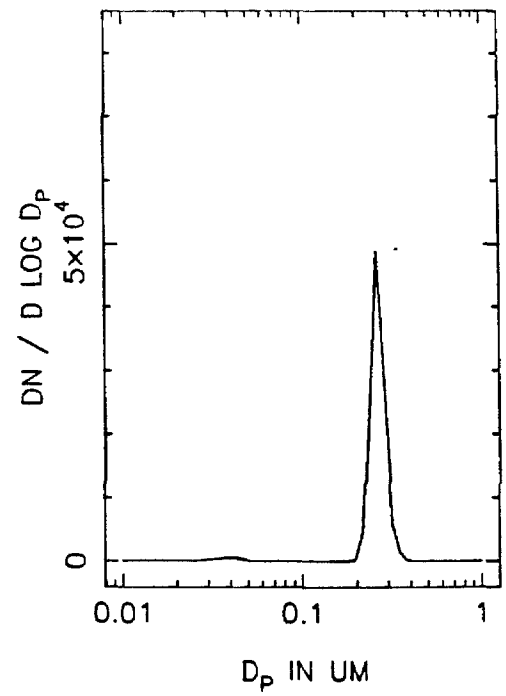

MTMA20 NUMBER DISTRIBUTION, T=4.0

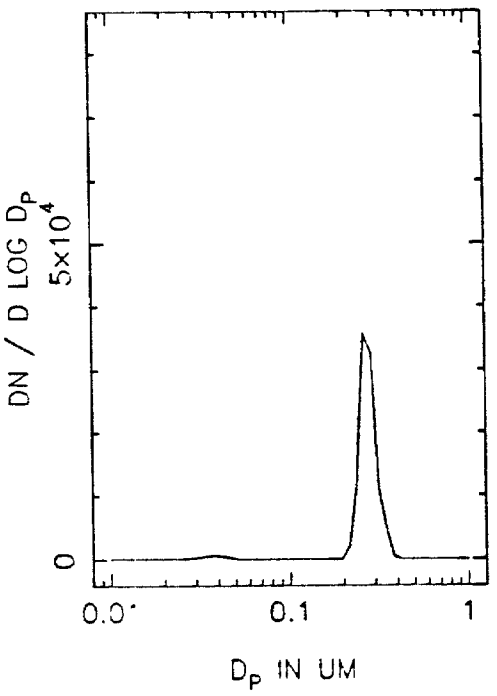

MTMA20 VOLUME DISTRIBUTION, T=0

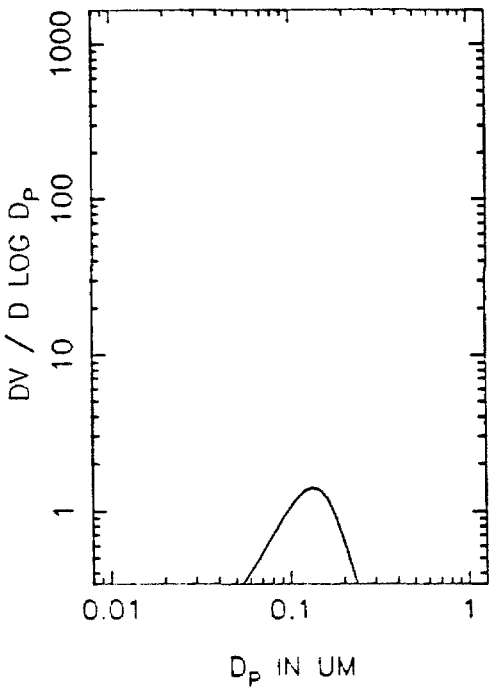

T=0.5 HOURS

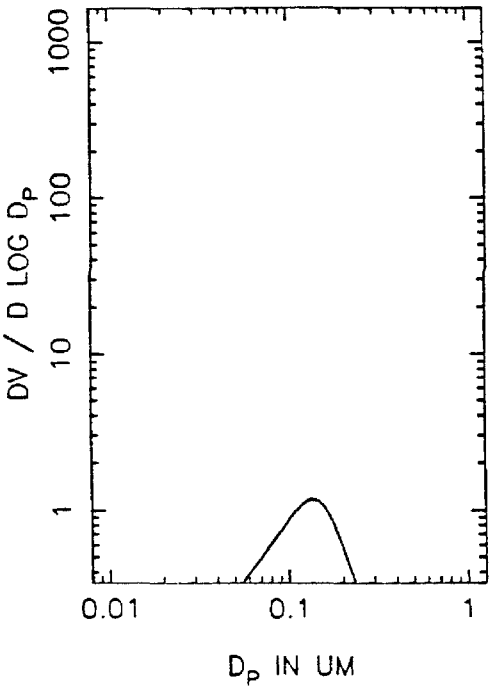

T=1.0 HOURS

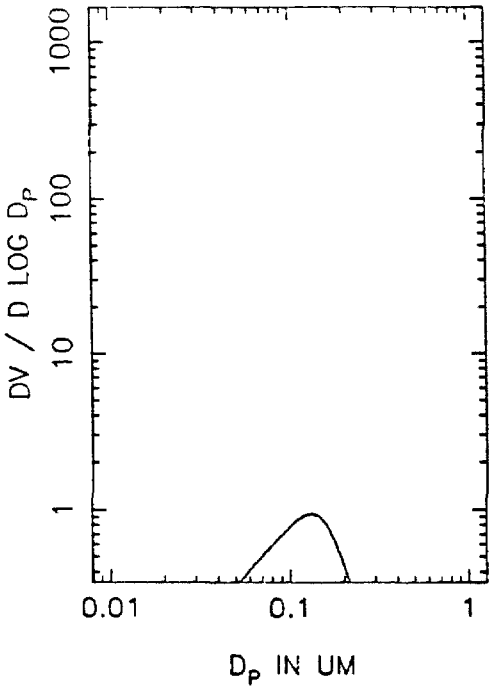

T=1.5 HOURS

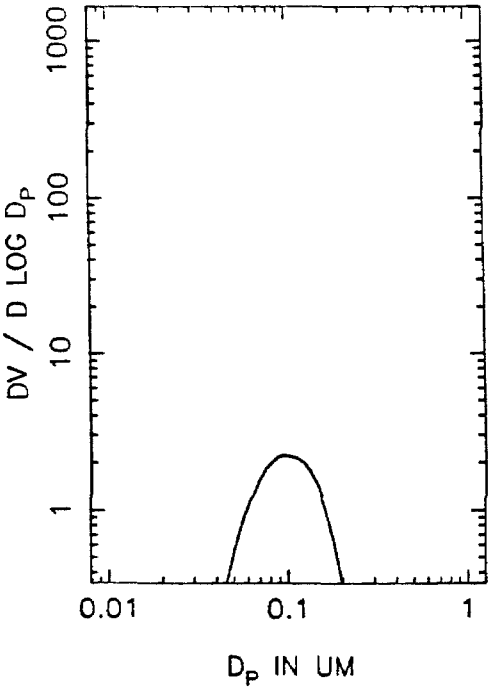

MTMA20 VOLUME DISTRIBUTION, T=2.0

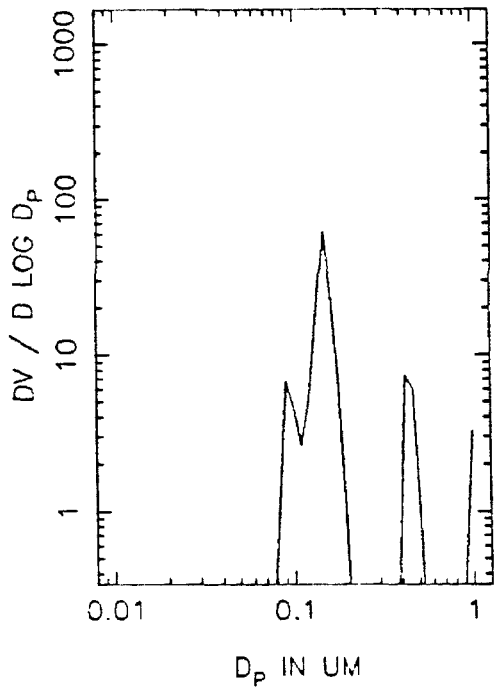

T=2.5 HOURS

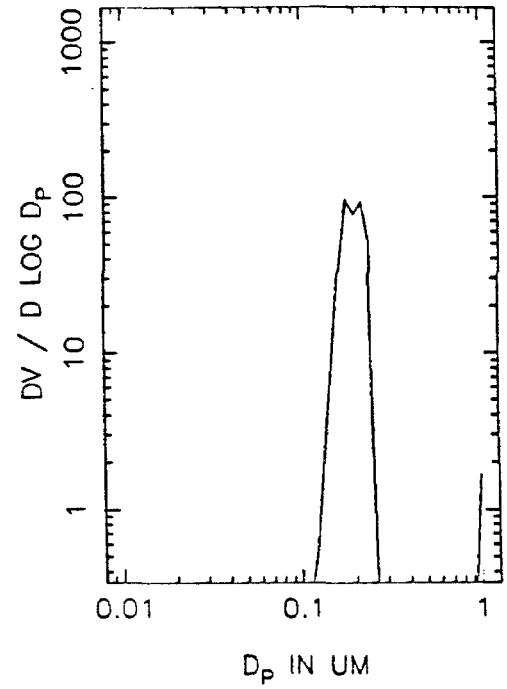

T=3.0 HOURS

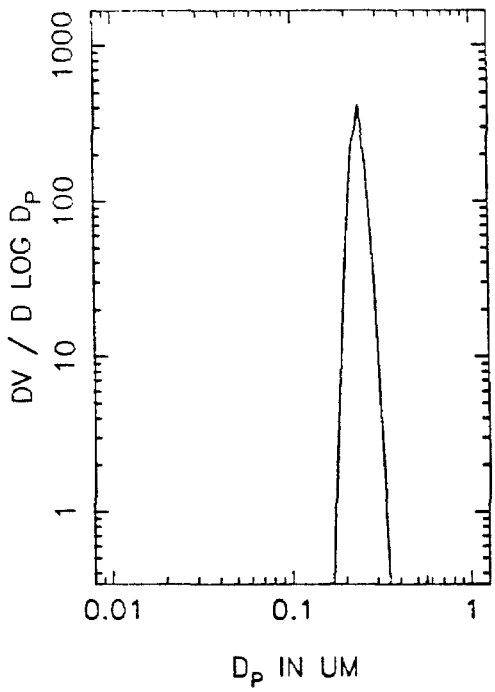

T=3.5 HOURS

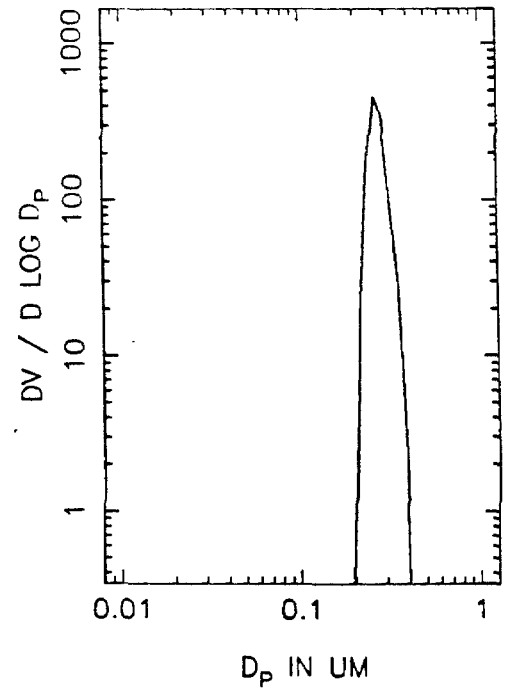

MTMA20 VOLUME DISTRIBUTION, T=4.0

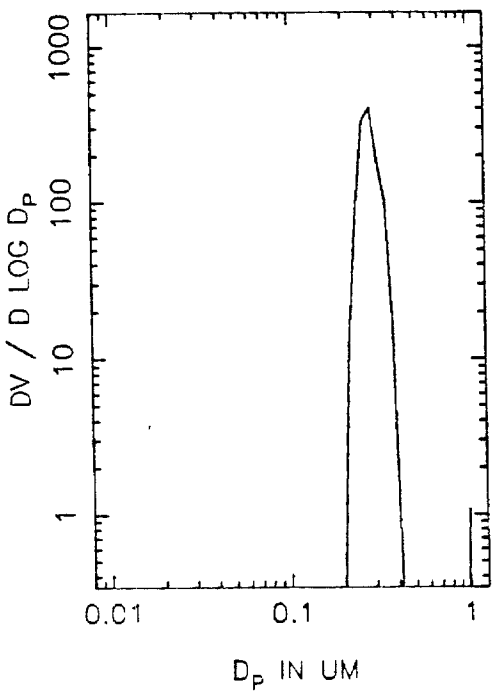

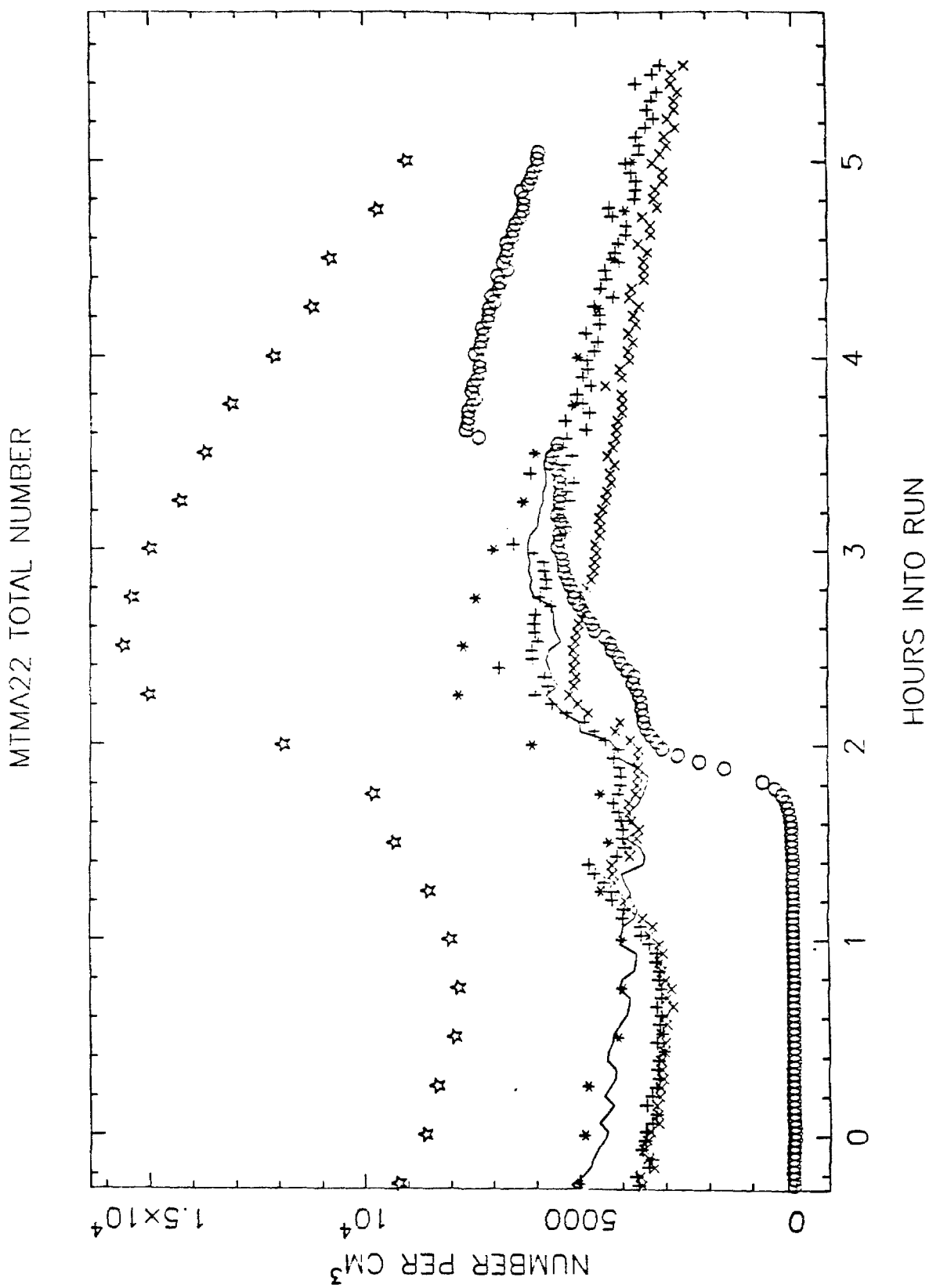
MTMA22 TOTAL NUMBER
NUMBER PER CM^3
1.5×10^4
10^4
5000
0
0
1
2
3
4
5
HOURS INTO RUN

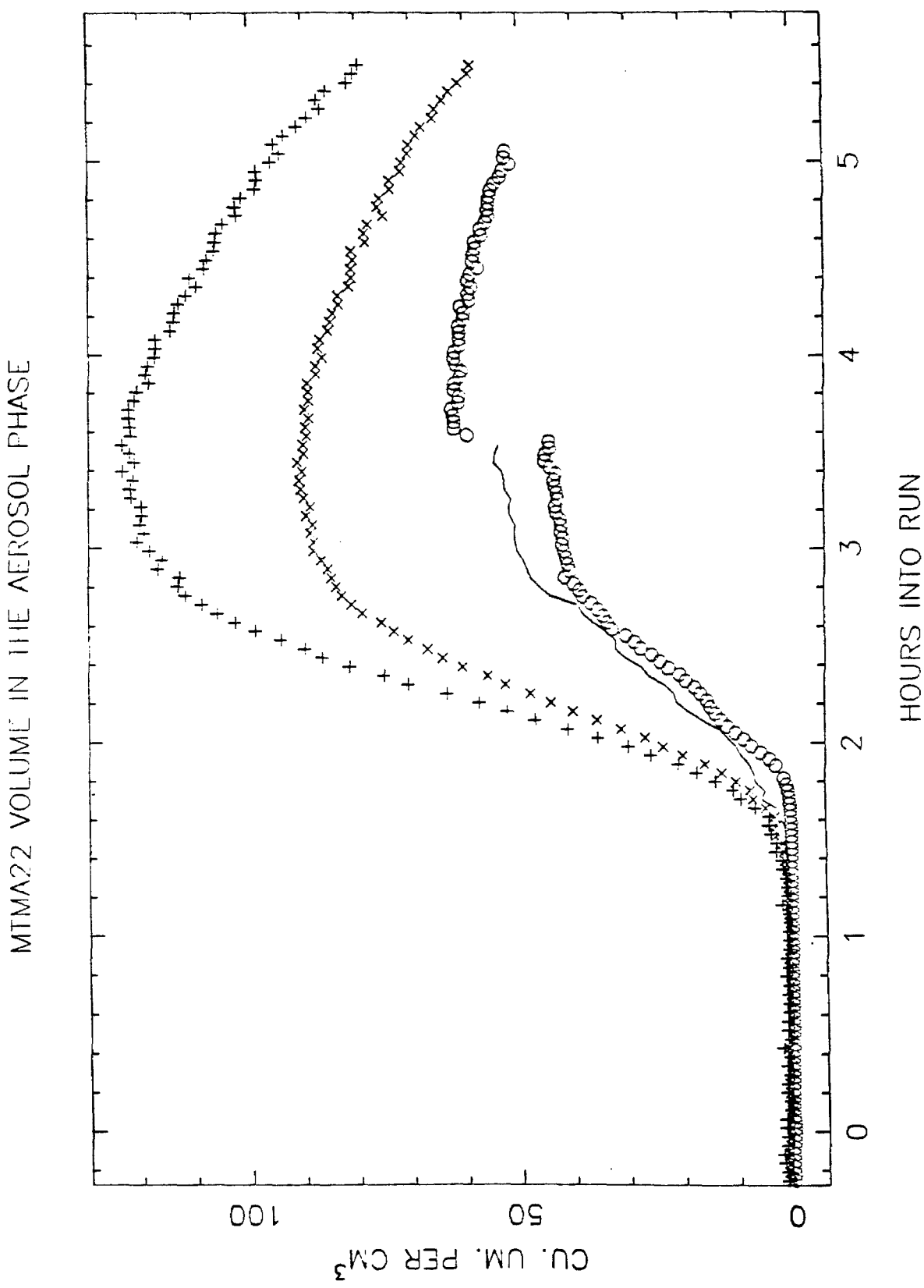
MTMA22 VOLUME IN THE AEROSOL PHASE
CU. UM. PER CM3
0
50
100
0
1
2
3
4
5
HOURS INTO RUN

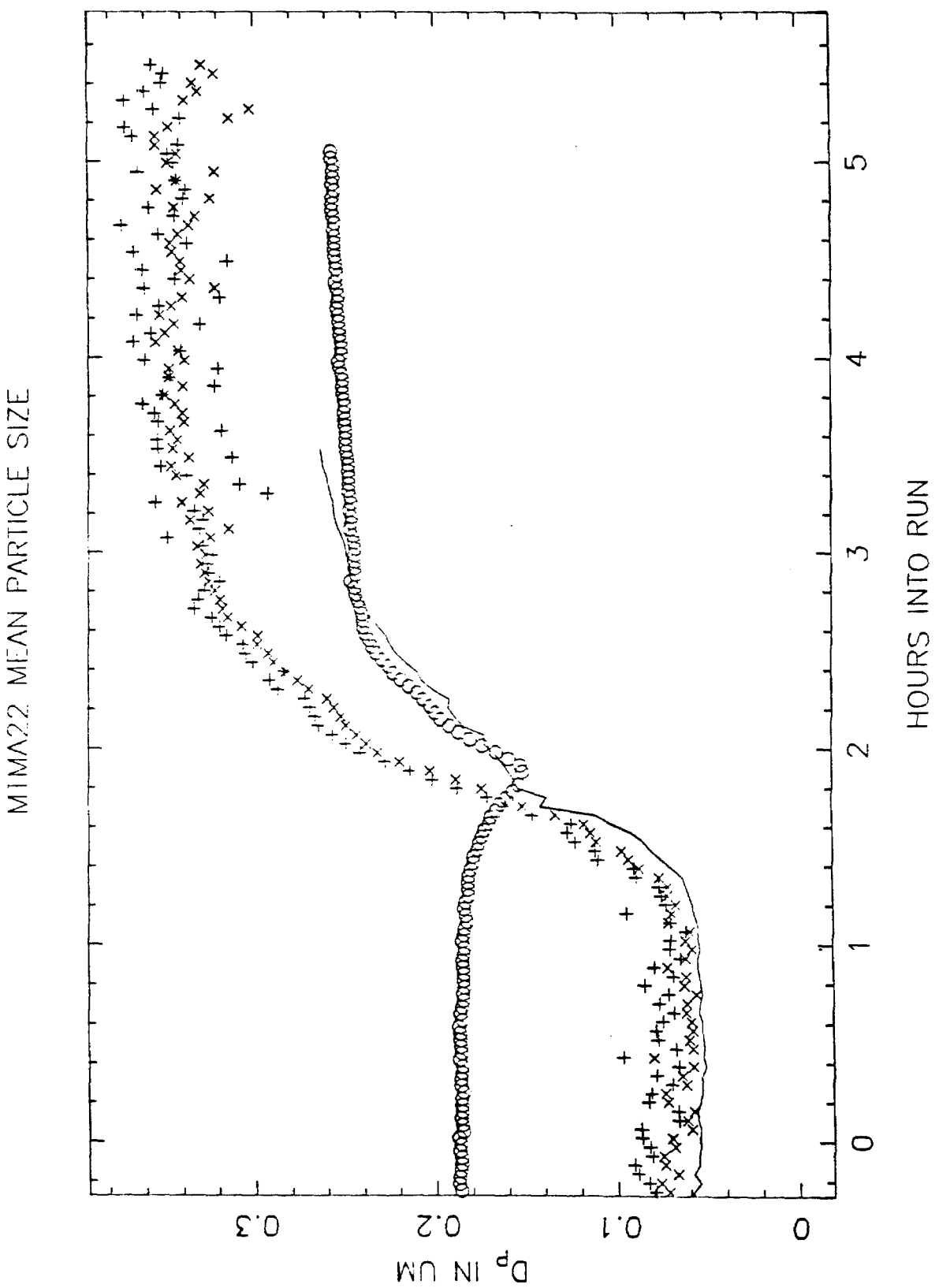
MIMA22 MEAN PARTICLE SIZE
D_p IN UM
0
0.1
0.2
0.3
0
1
2
3
4
5
HOURS INTO RUN

MTMA22 NUMBER DISTRIBUTION, T=0

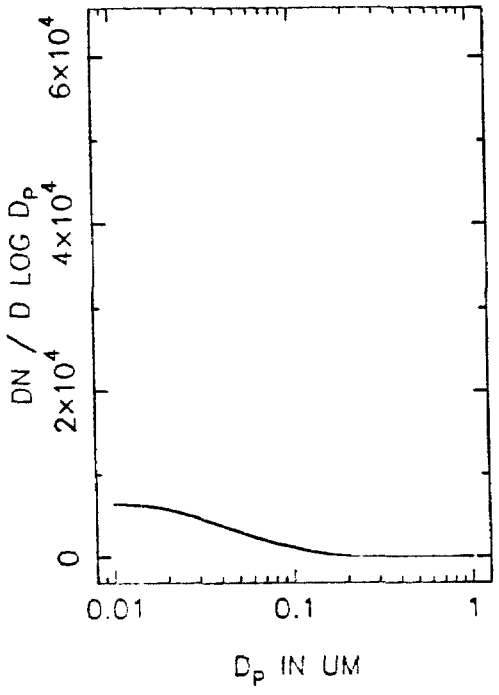

T=0.5 HOURS

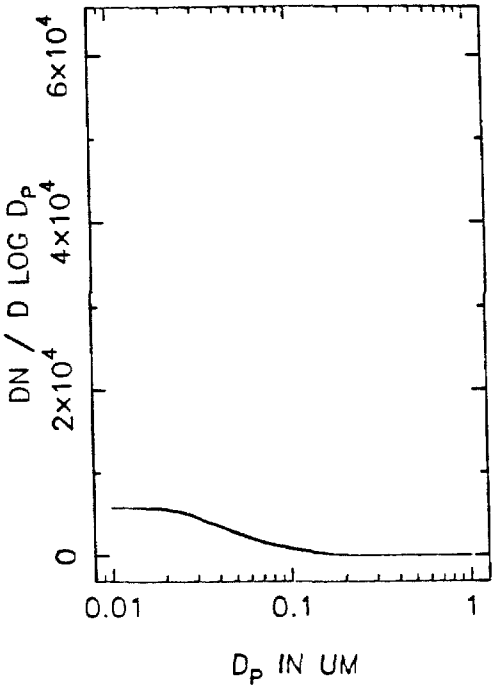

T=1.0 HOURS

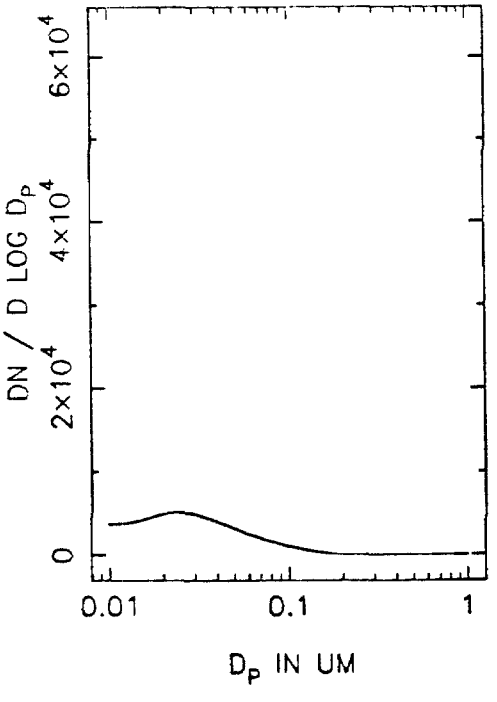

T=1.5 HOURS

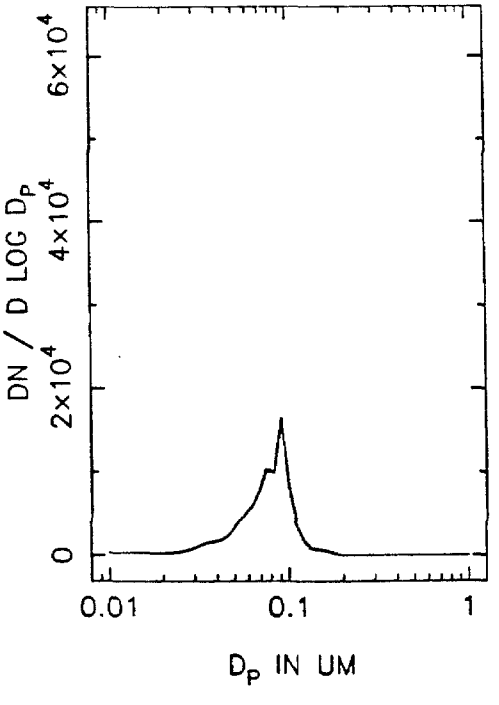

MTMA22 NUMBER DISTRIBUTION, T=2.0

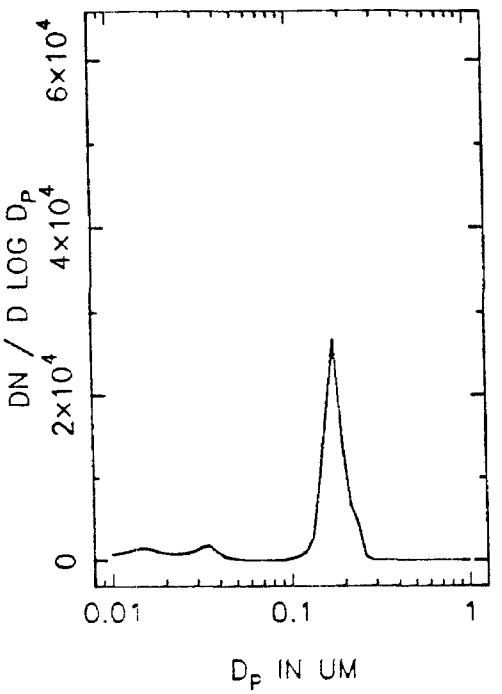

T=2.5 HOURS

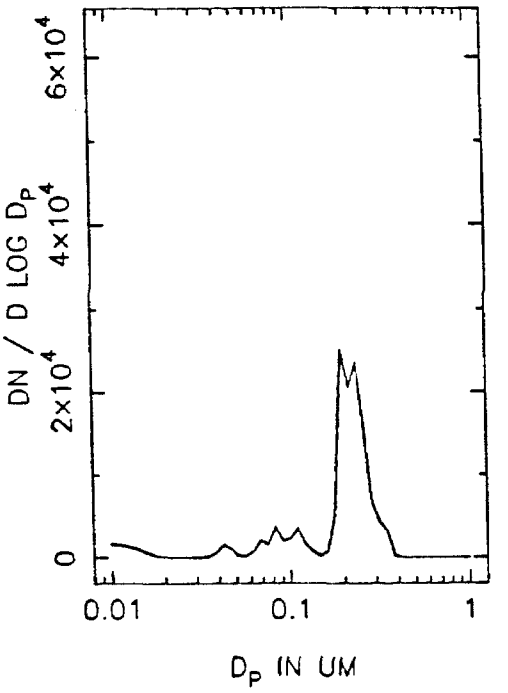

T=3.0 HOURS

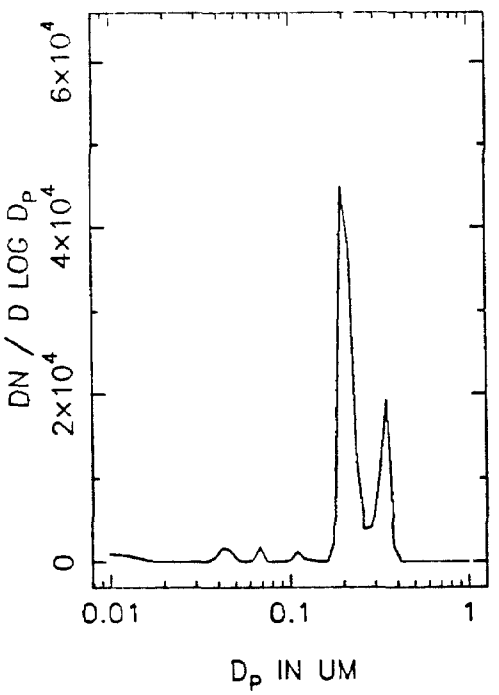

T=3.5 HOURS

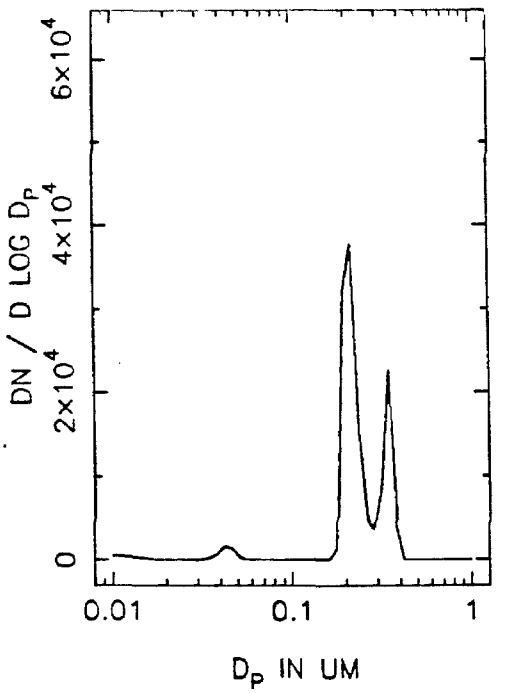

MTMA22 VOLUME DISTRIBUTION, T=0

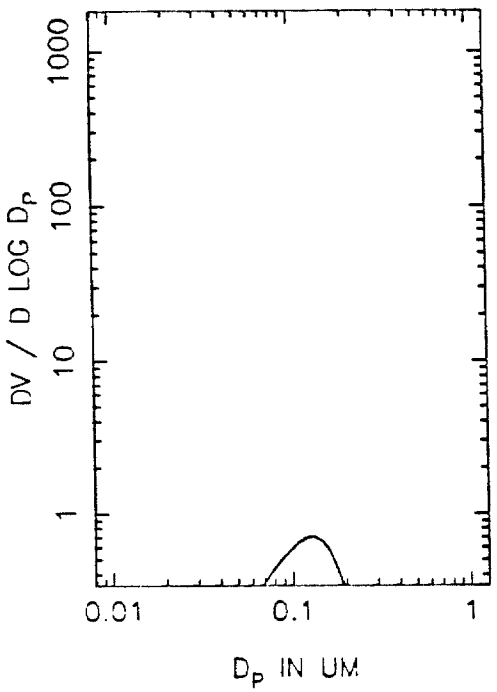

T=0.5 HOURS

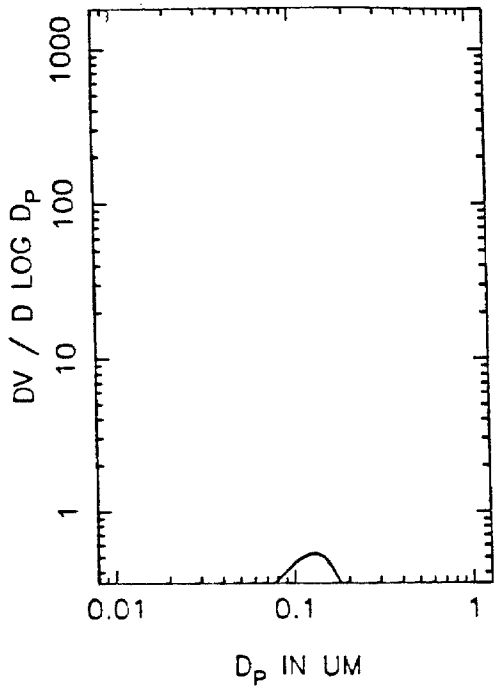

T=1.0 HOURS

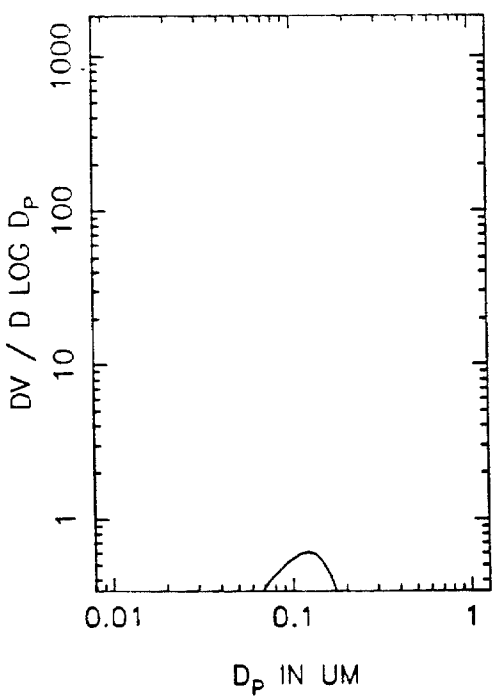

T=1.5 HOURS

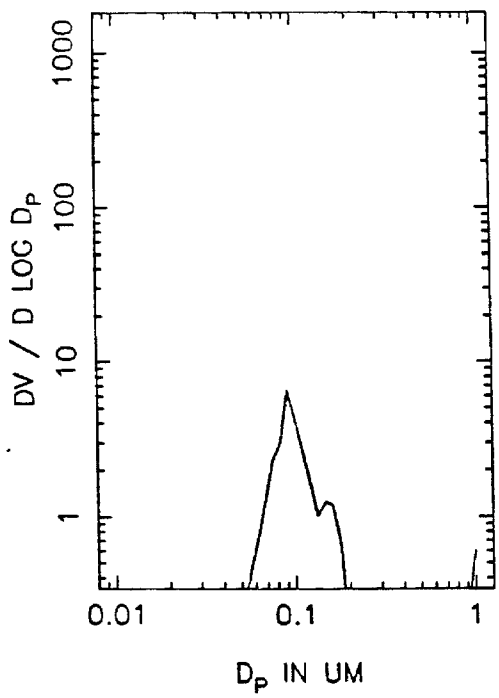

MTMA22 VOLUME DISTRIBUTION, T=2.0

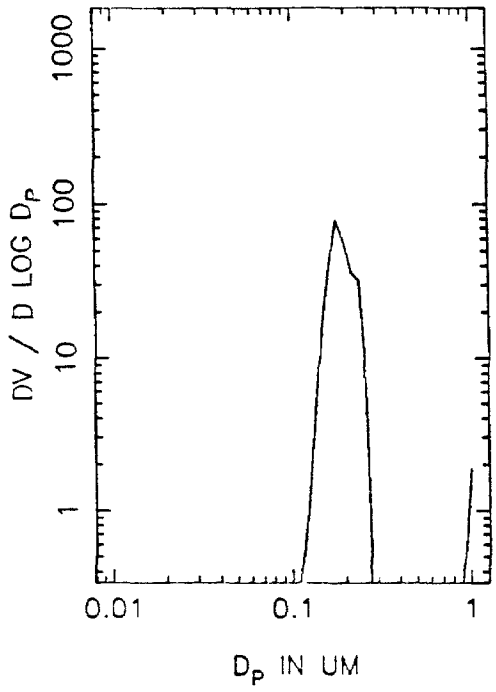

T=2.5 HOURS

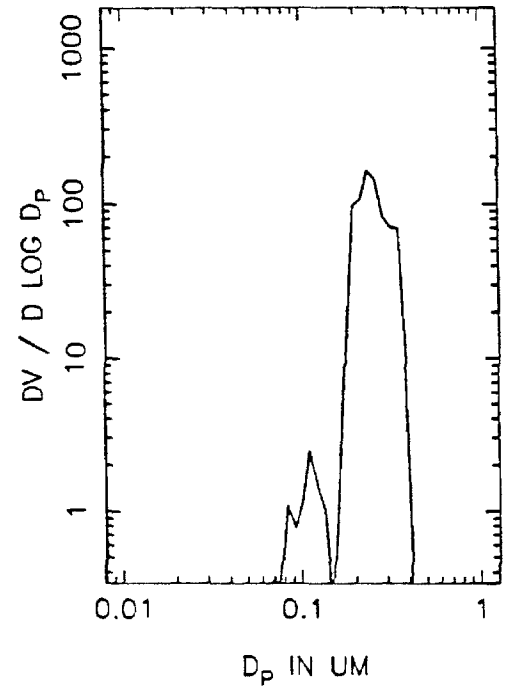

T=3.0 HOURS

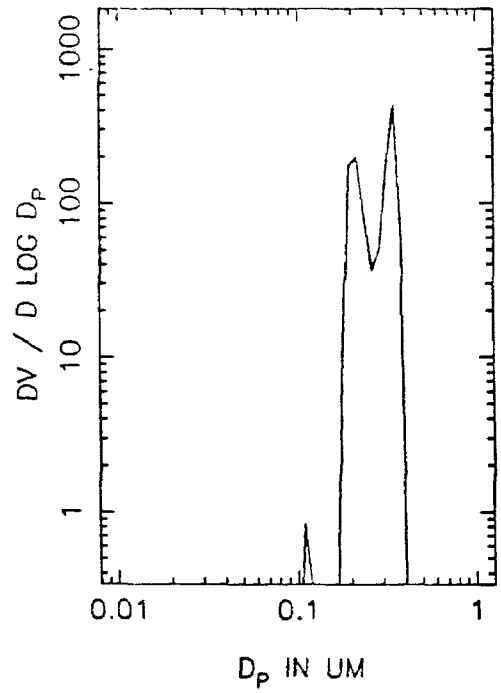

T=3.5 HOURS

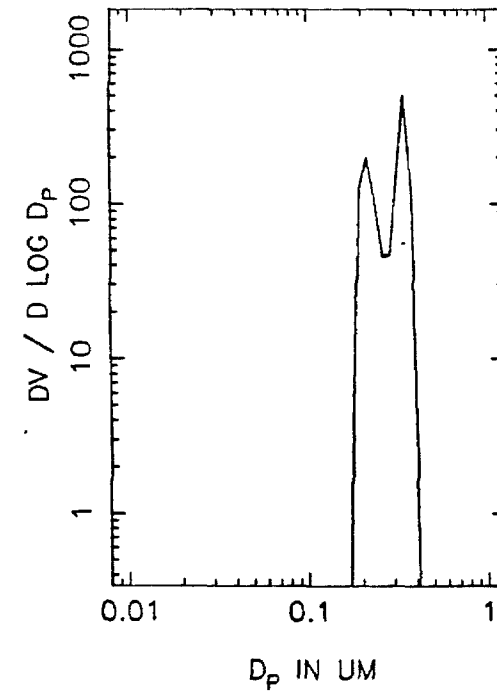

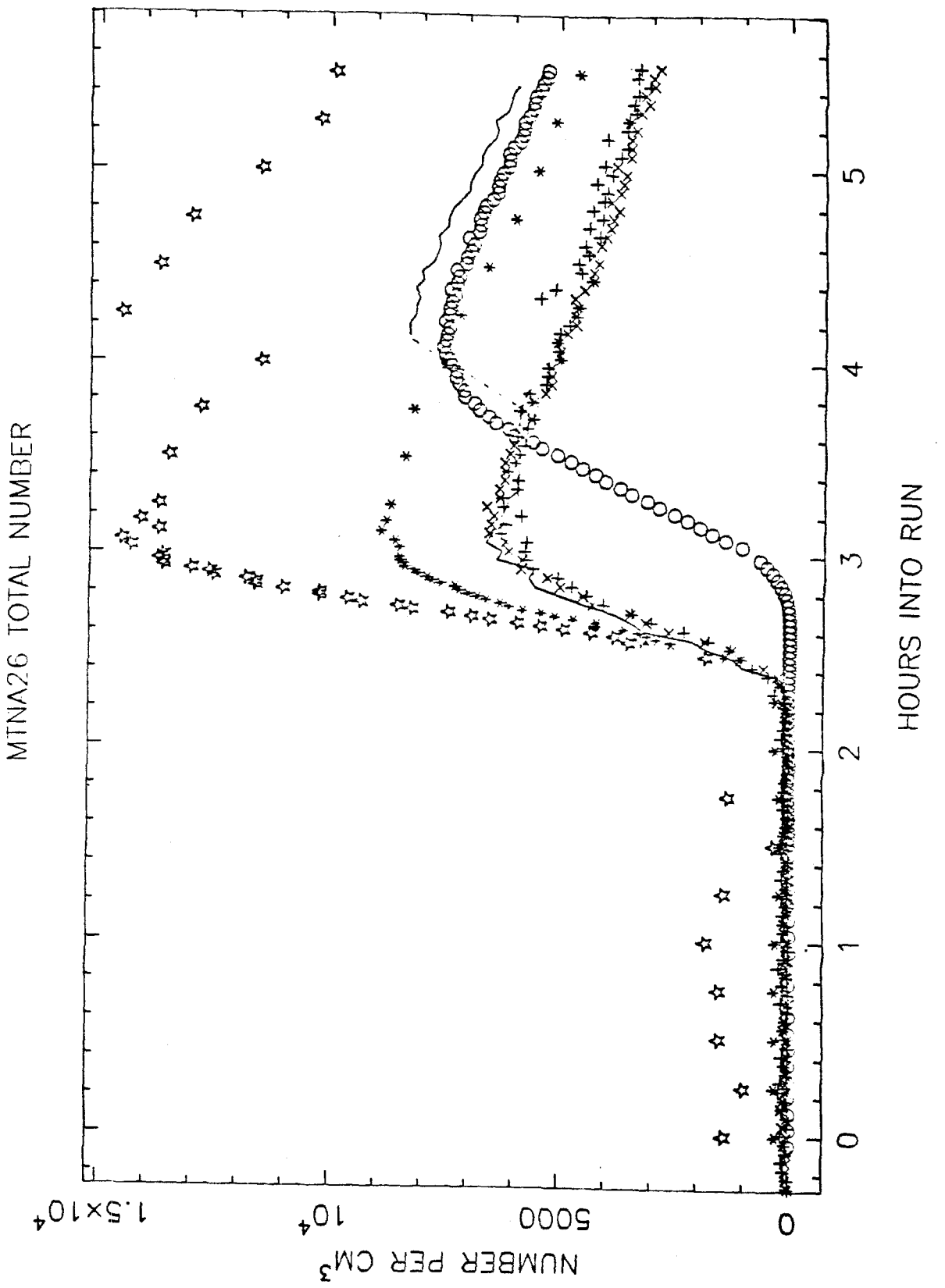
MTNA26 TOTAL NUMBER
NUMBER PER CM^3
0
5000
10^4
1.5×10^4
0
1
2
3
4
5
HOURS INTO RUN

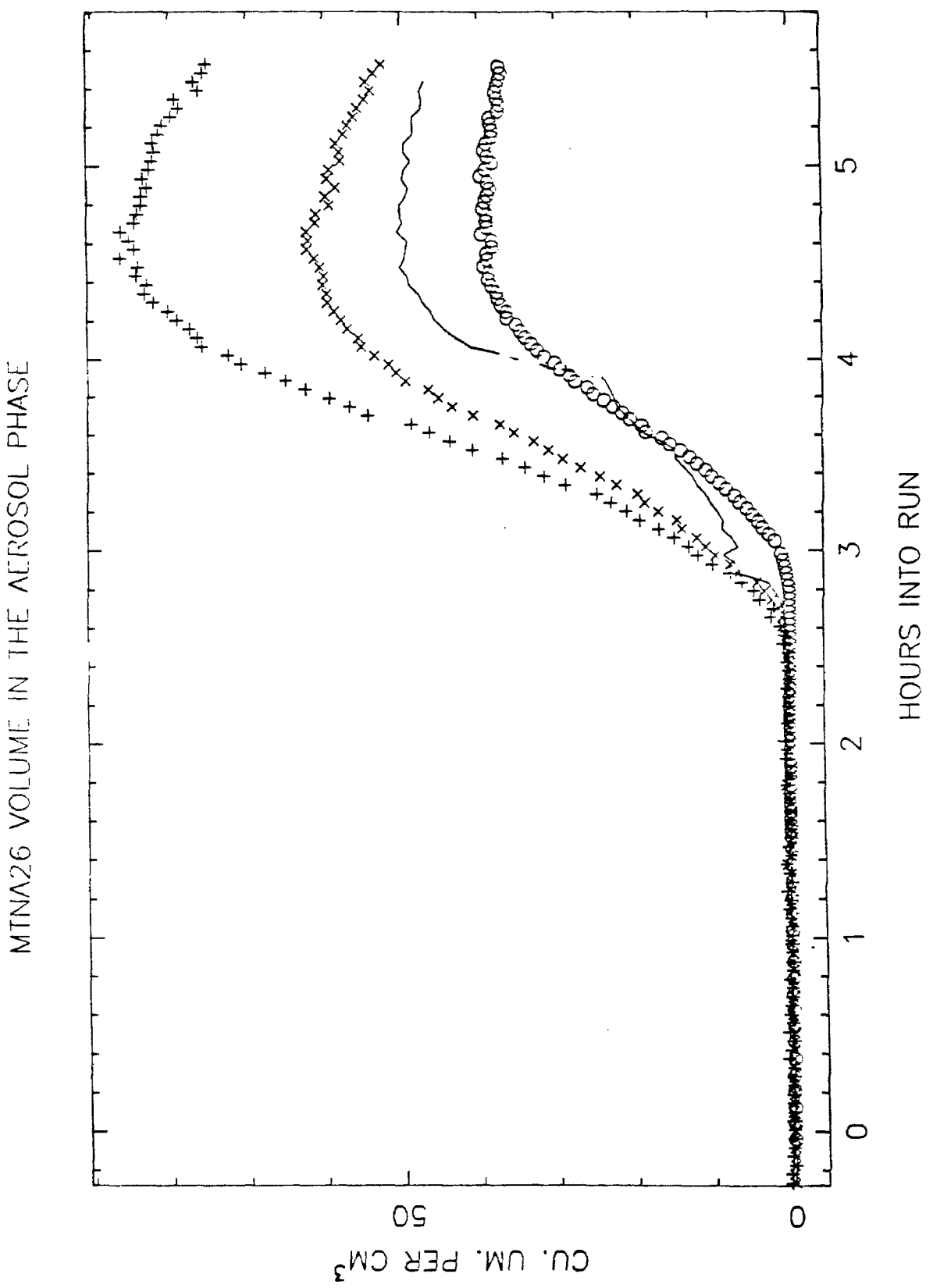
MTNA26 VOLUME IN THE AEROSOL PHASE
CU. UM. PER CM3
0
50
0
1
2
3
4
5
HOURS INTO RUN

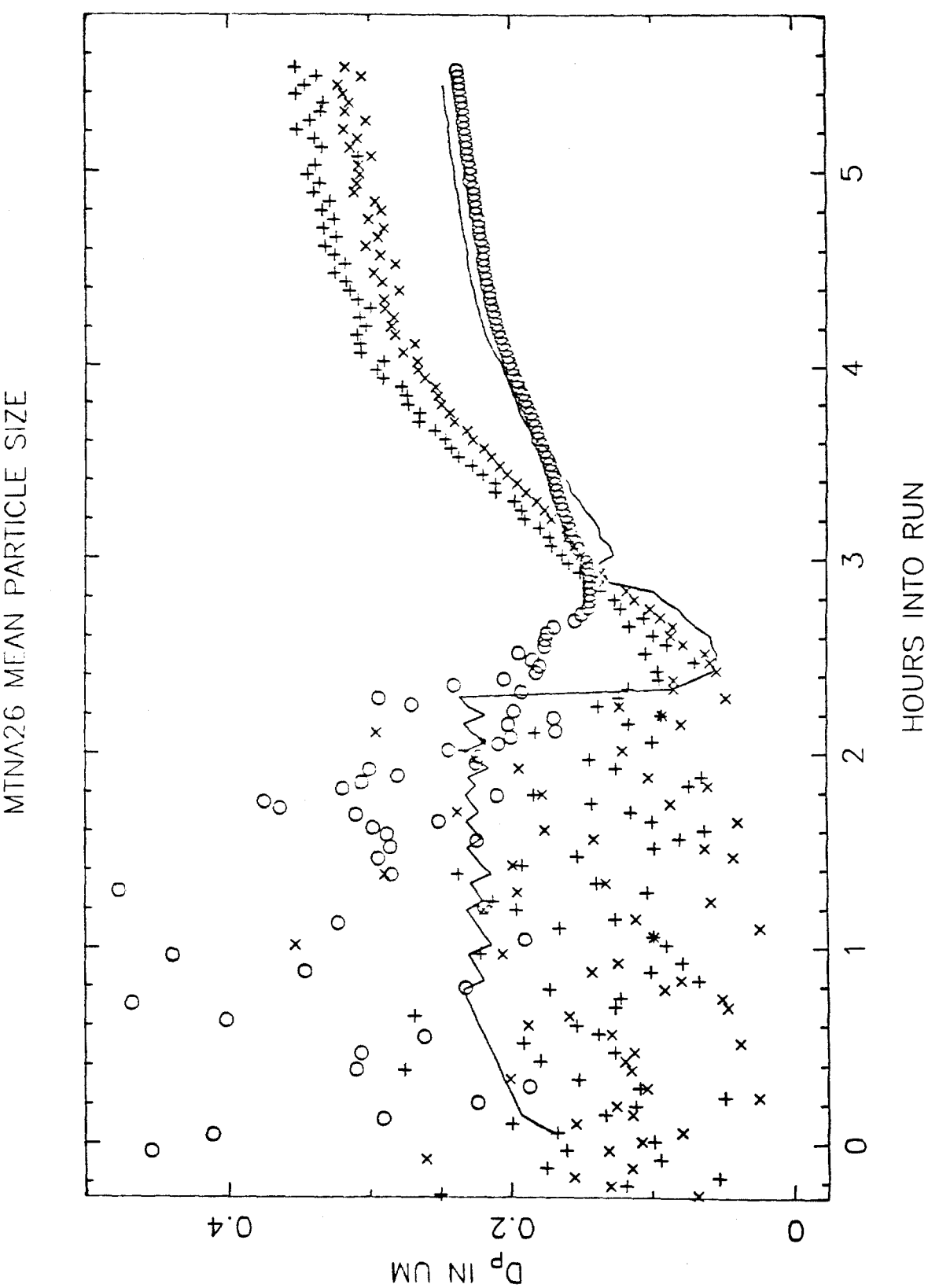
MTNA26 MEAN PARTICLE SIZE
D_p IN UM
0
0.2
0.4
0
1
2
3
4
5
HOURS INTO RUN

MTNA26 NUMBER DISTRIBUTION, T=0

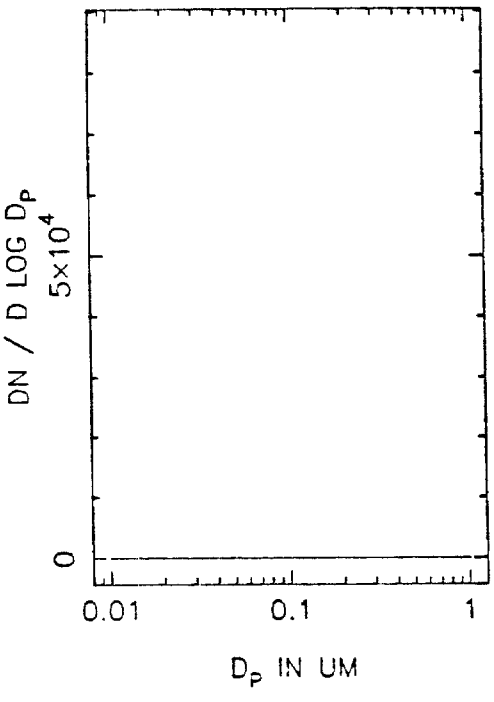

T=0.5 HOURS

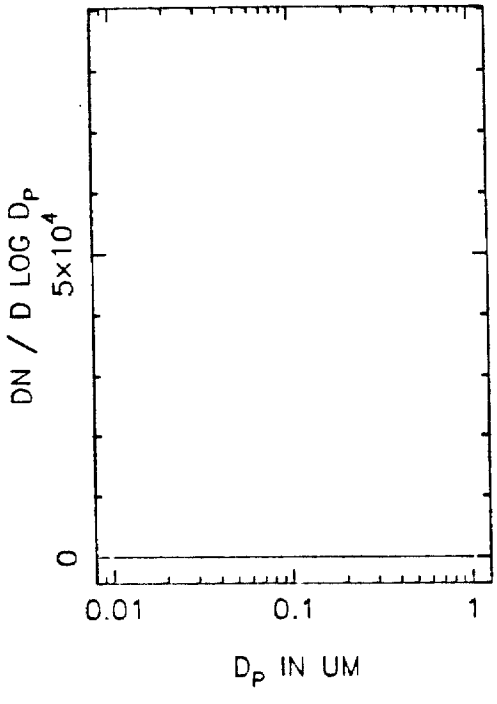

T=1.0 HOURS

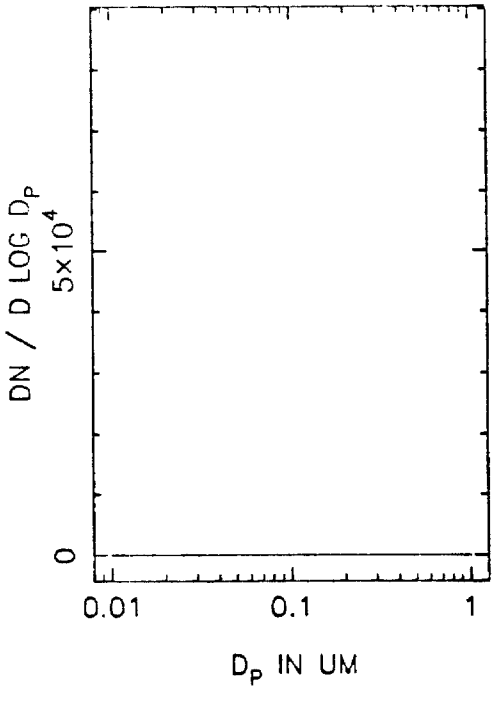

T=1.5 HOURS

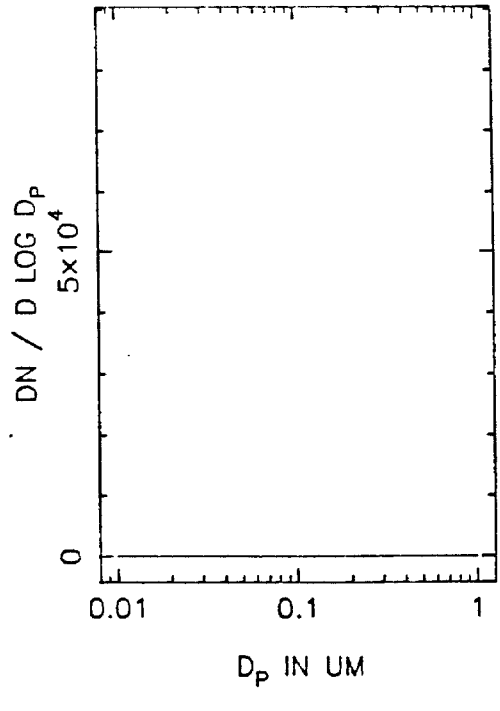

MTNA26 NUMBER DISTRIBUTION, T=2.0

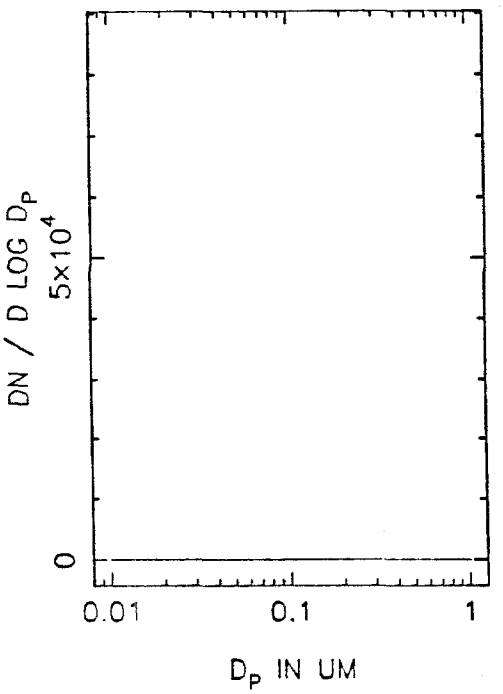

T=2.5 HOURS

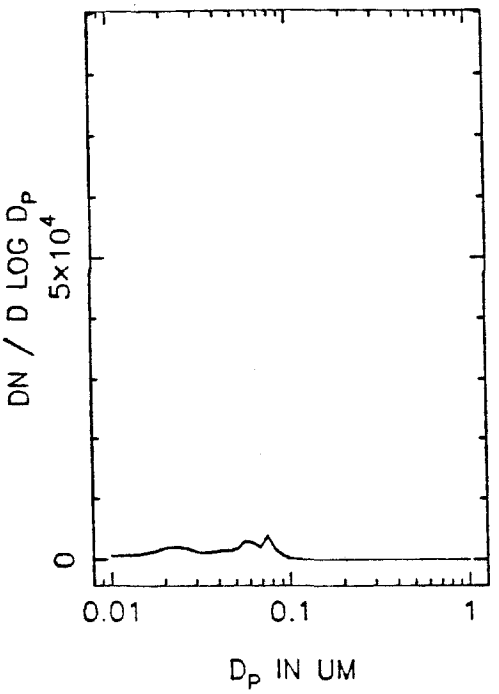

T=3.0 HOURS

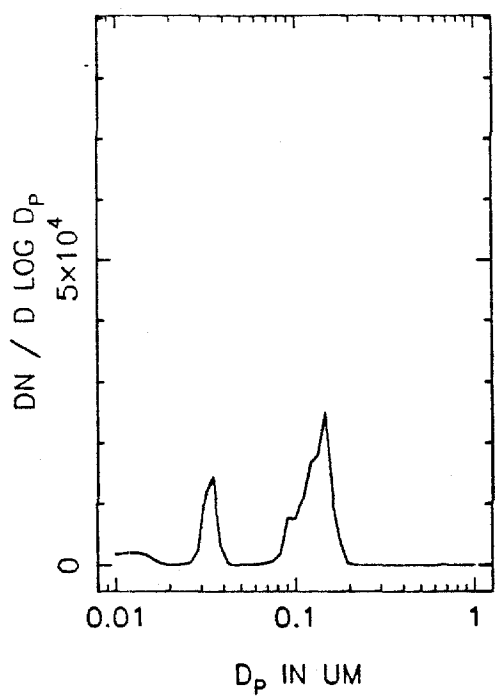

T=3.5 HOURS

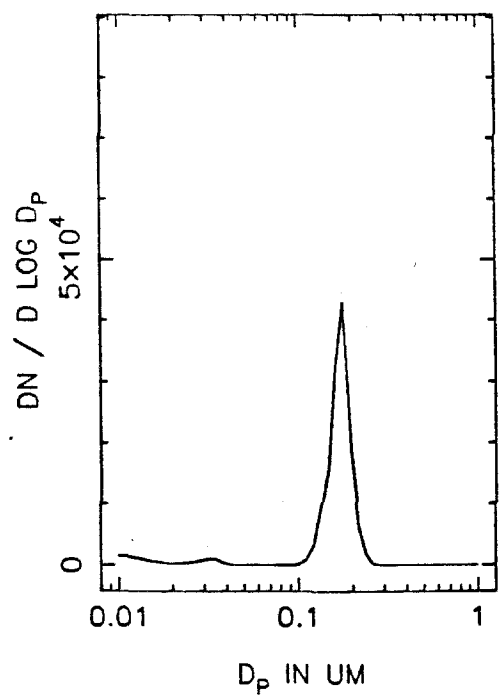

MTNA26 NUMBER DISTRIBUTION, T=4.0

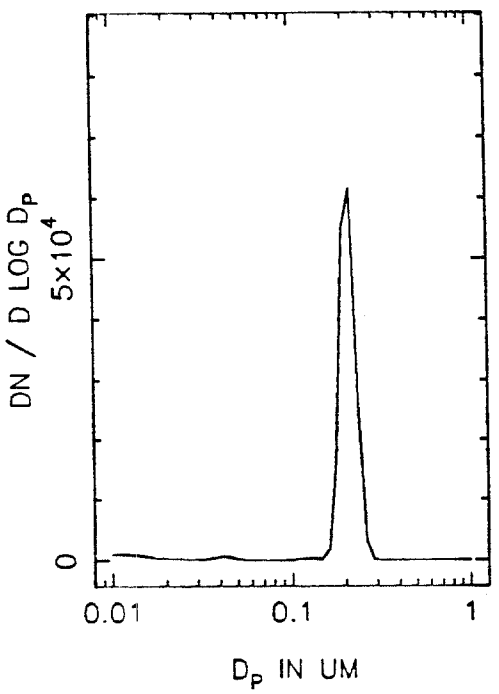

MTNA26 VOLUME DISTRIBUTION, T=0

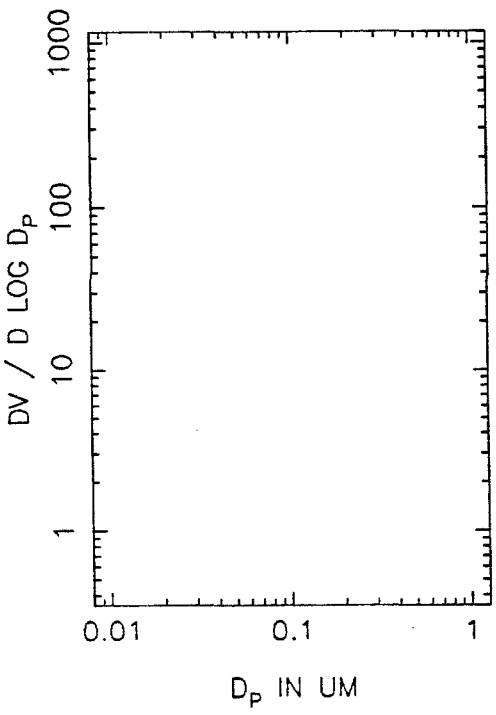

T=0.5 HOURS

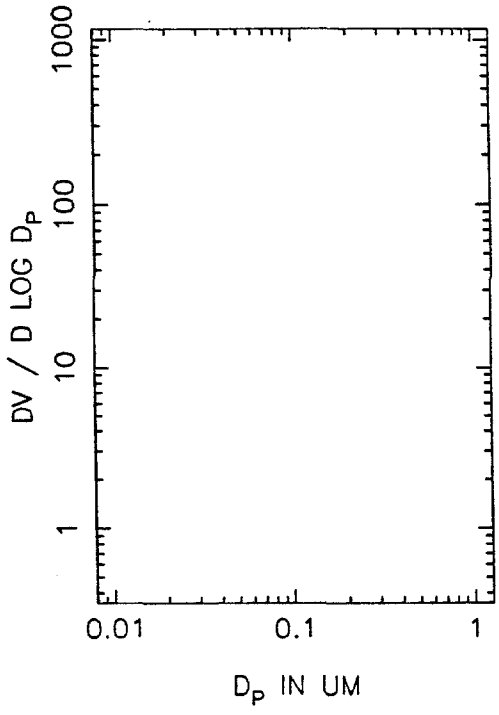

T=1.0 HOURS

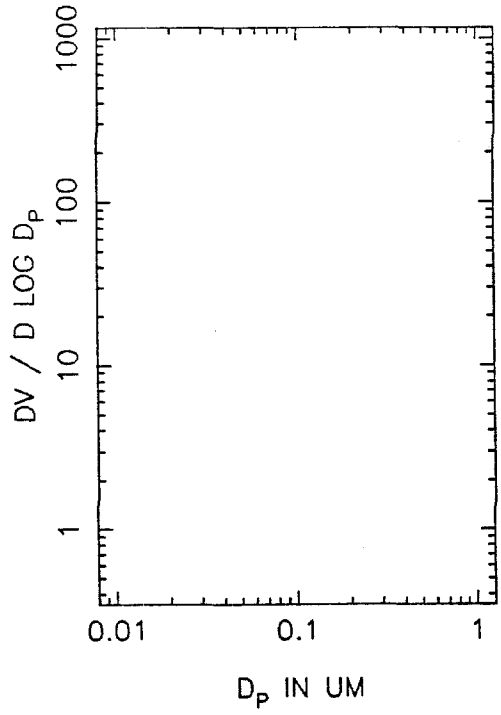

T=1.5 HOURS

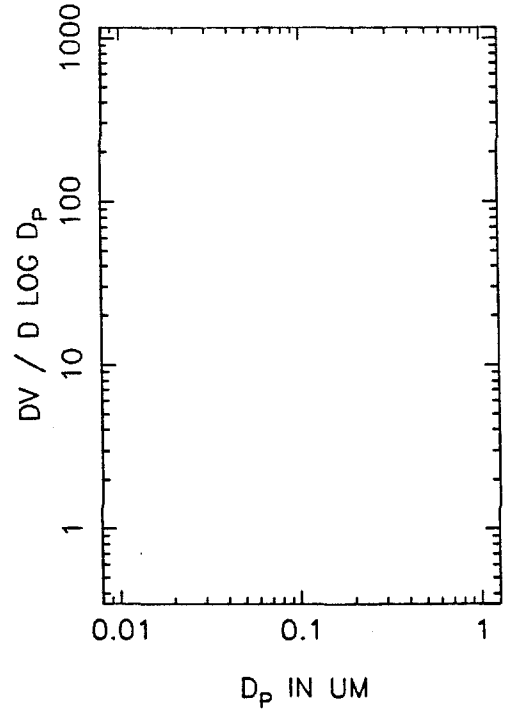

MTNA26 VOLUME DISTRIBUTION, T=2.0

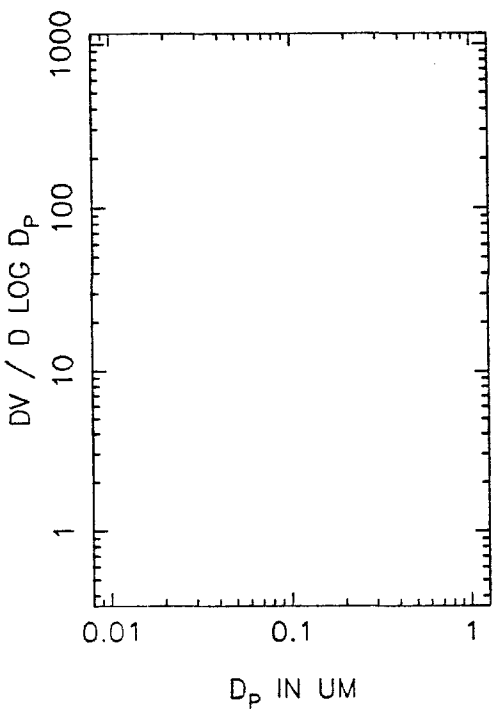

T=2.5 HOURS

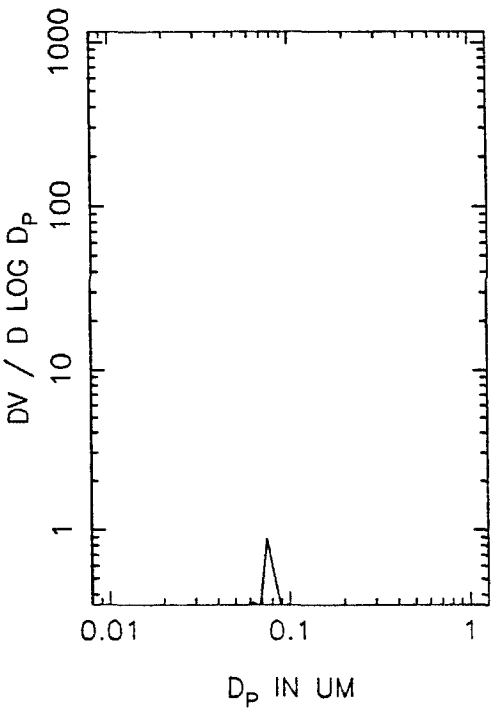

T=3.0 HOURS

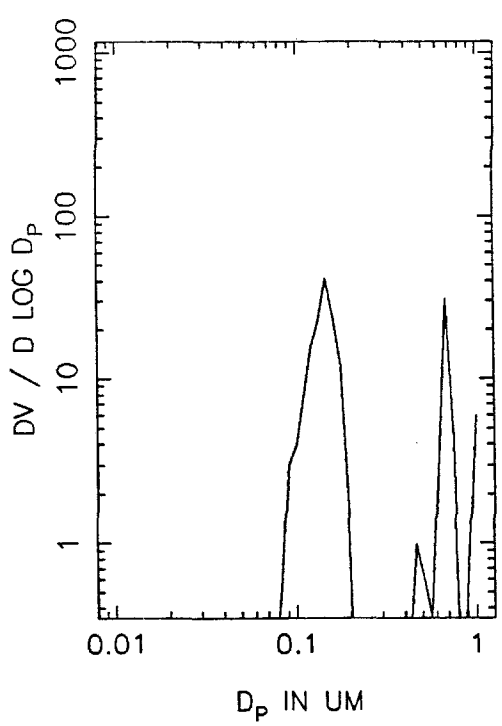

T=3.5 HOURS

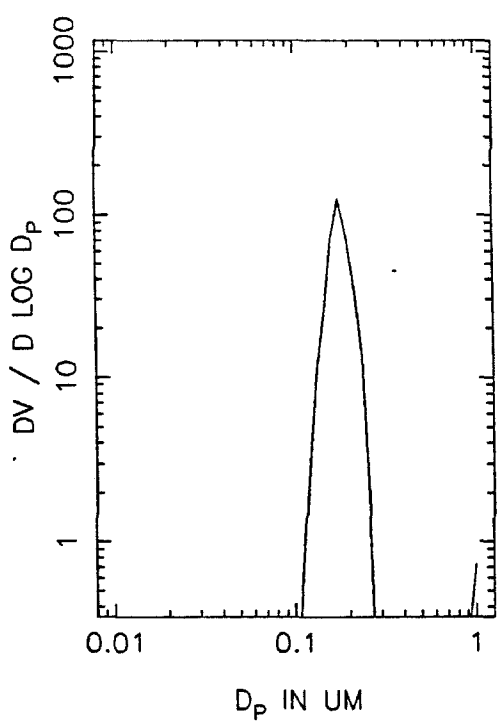

MTNA26 VOLUME DISTRIBUTION, T=4.0

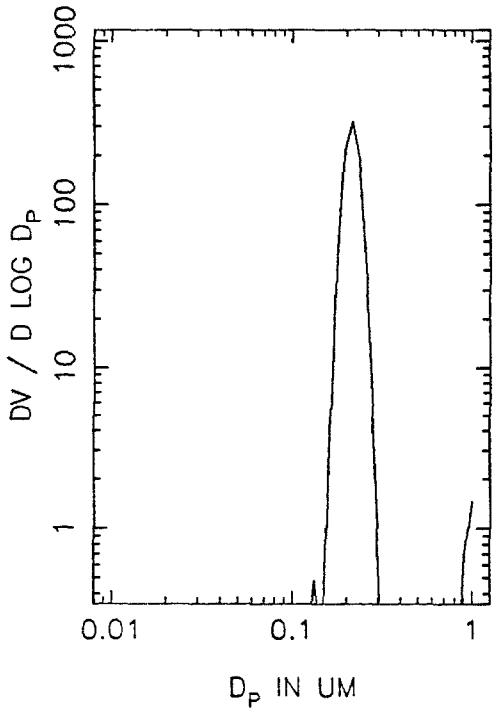

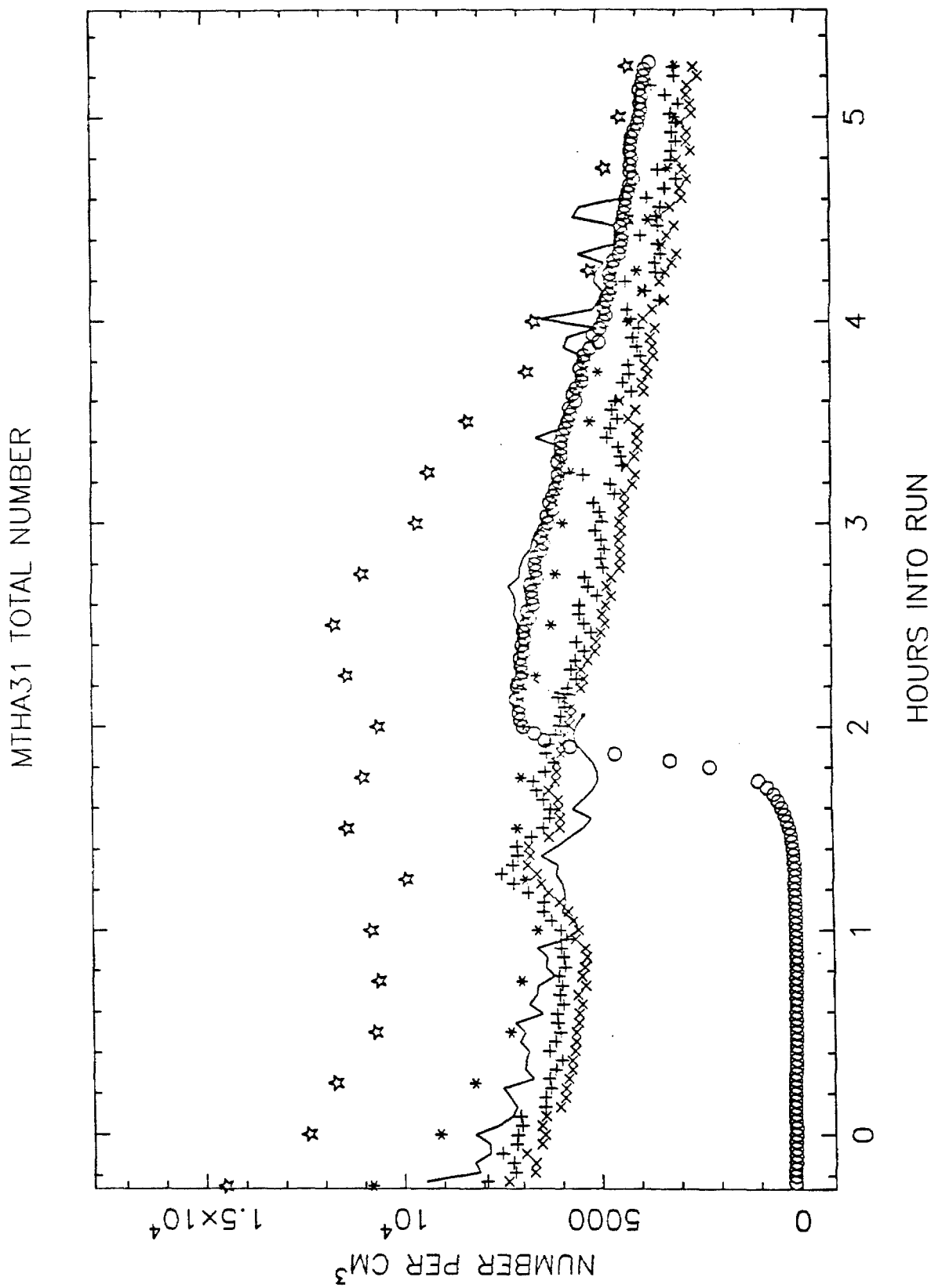
MTHA31 TOTAL NUMBER
NUMBER PER CM^3
0
5000
10^4
1.5×10^4
0
1
2
3
4
5
HOURS INTO RUN

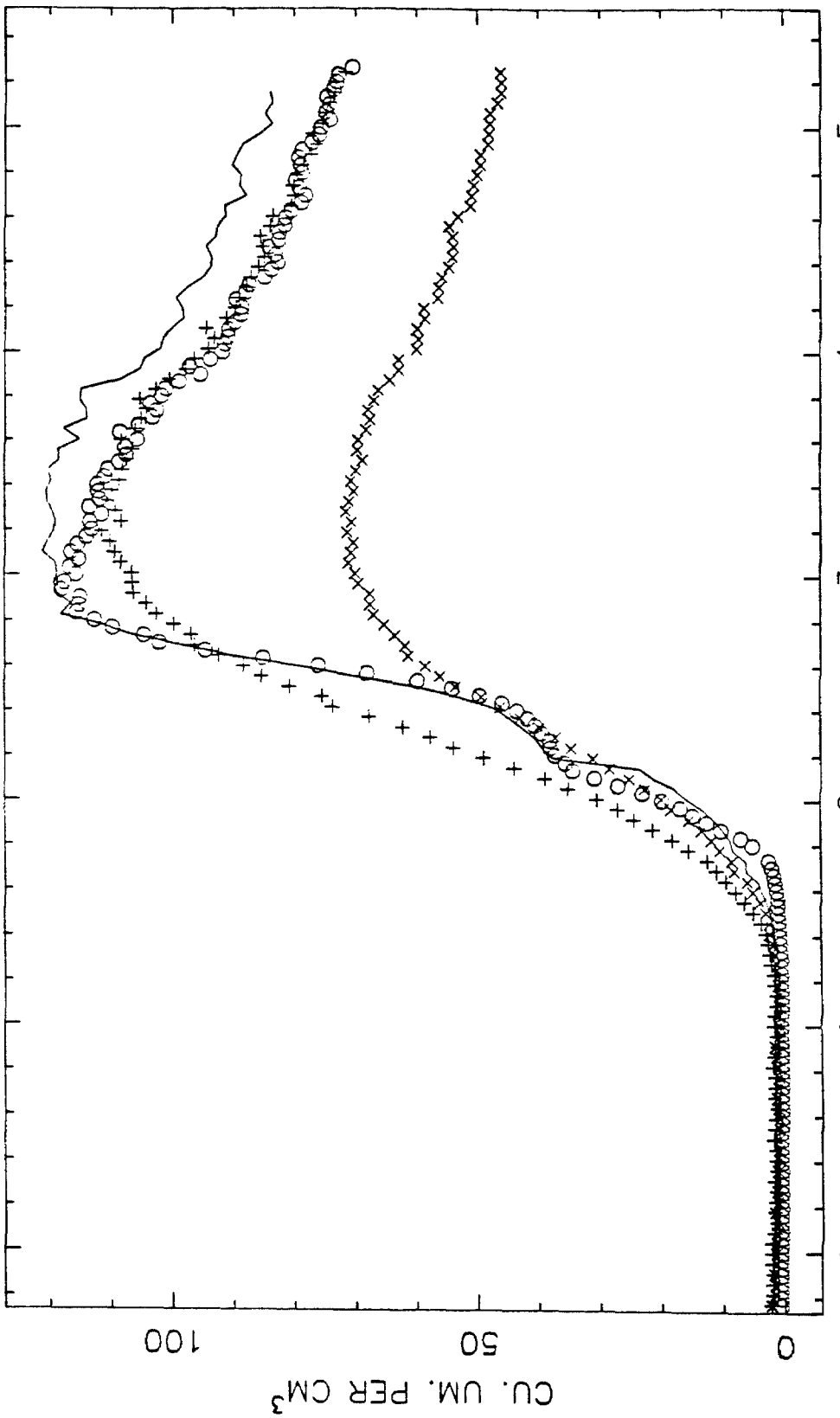
MTHA31 VOLUME IN THE AEROSOL PHASE
CU. UM. PER CM3
0
50
100
0
1
2
3
4
5
HOURS INTO RUN

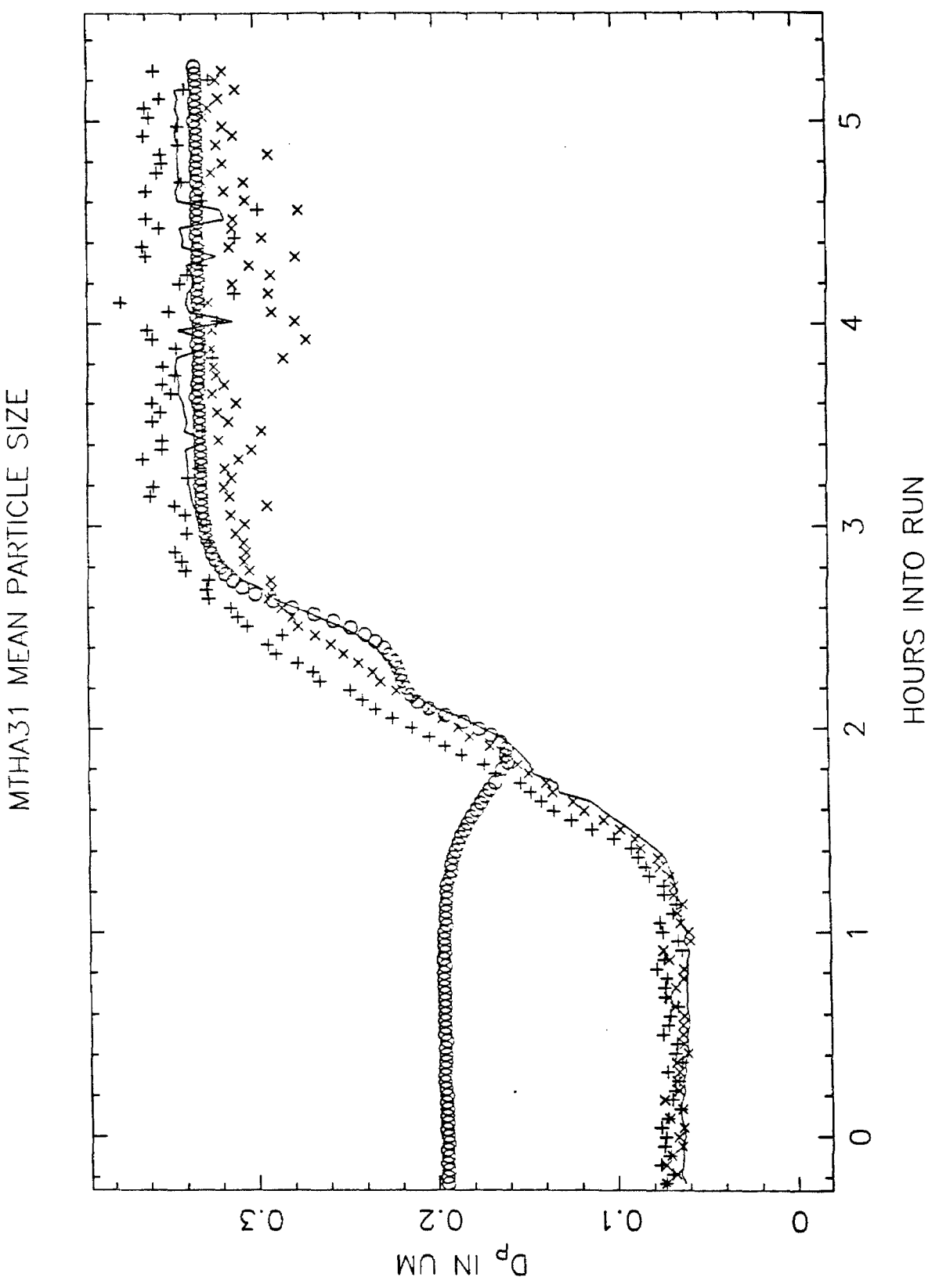
MTHA31 MEAN PARTICLE SIZE
D_p IN UM
0
0.1
0.2
0.3
0
1
2
3
4
5
HOURS INTO RUN

MTHA31 NUMBER DISTRIBUTION, T=0

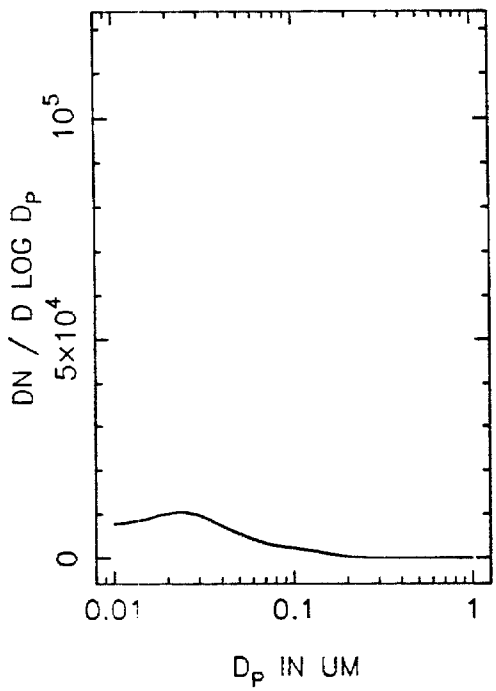

T=0.5 HOURS

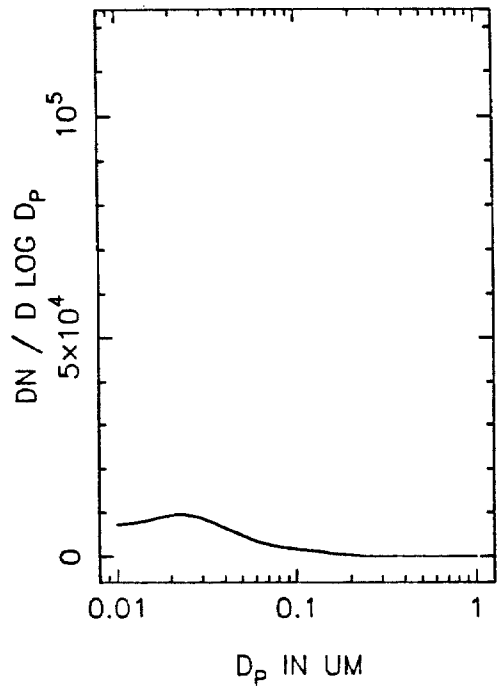

T=1.0 HOURS

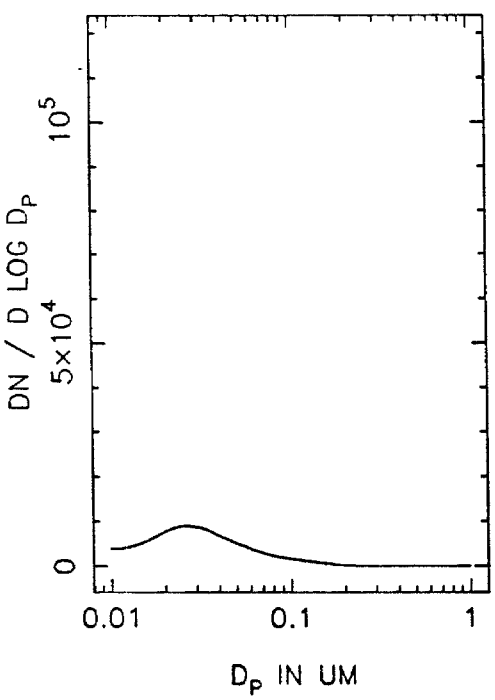

T=1.5 HOURS

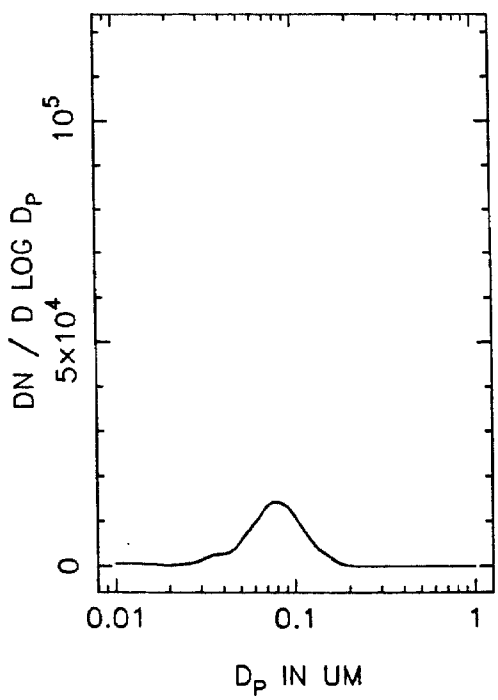

MTHA31 NUMBER DISTRIBUTION, T=2.0

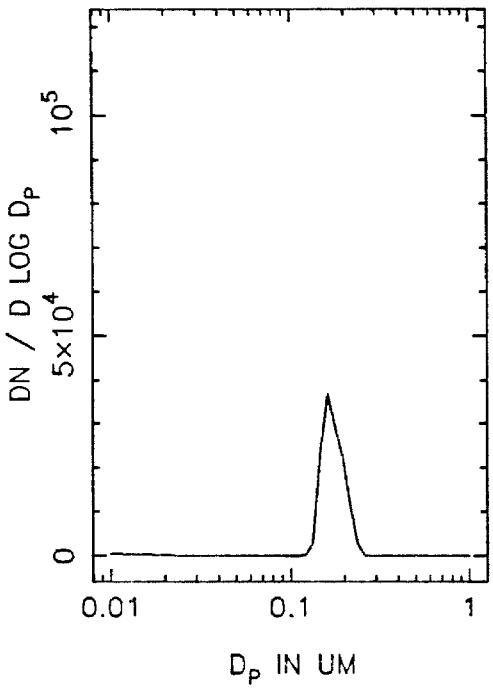

T=2.5 HOURS

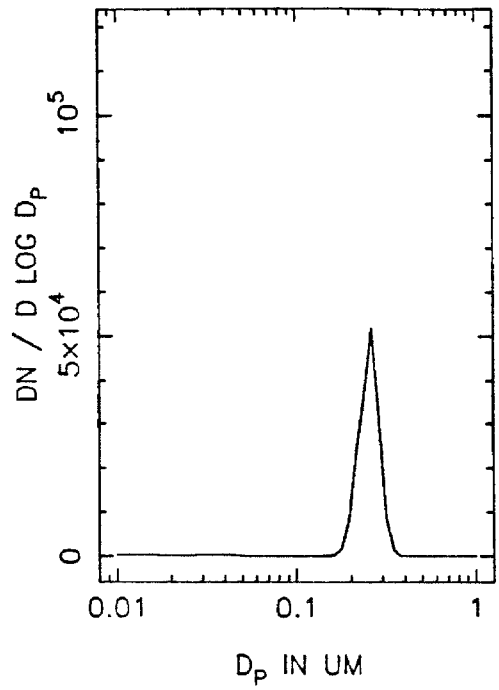

T=3.0 HOURS

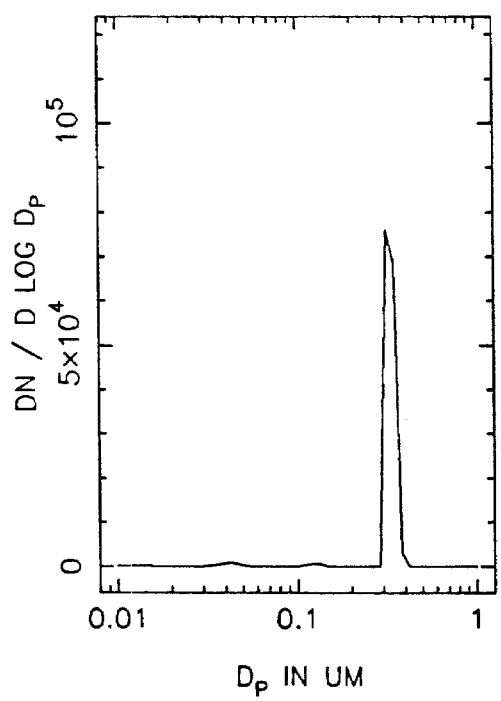

T=3.5 HOURS

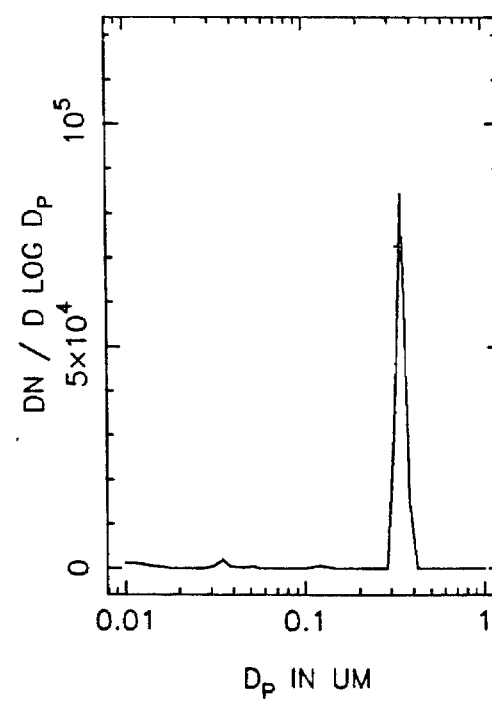

MTHA31 NUMBER DISTRIBUTION, T=4.0

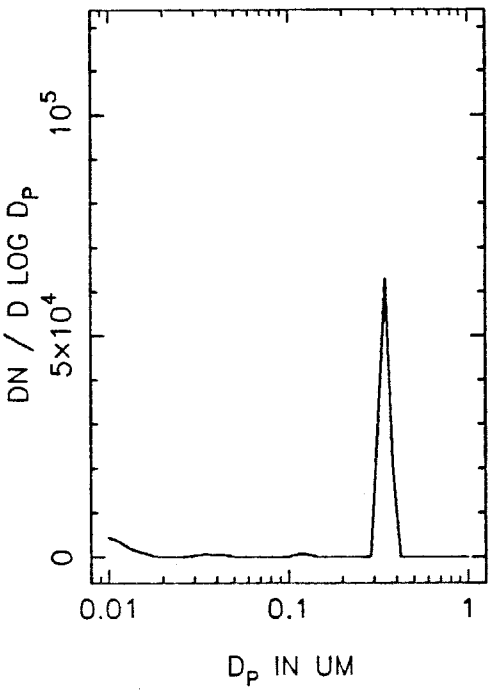

T=4.5 HOURS

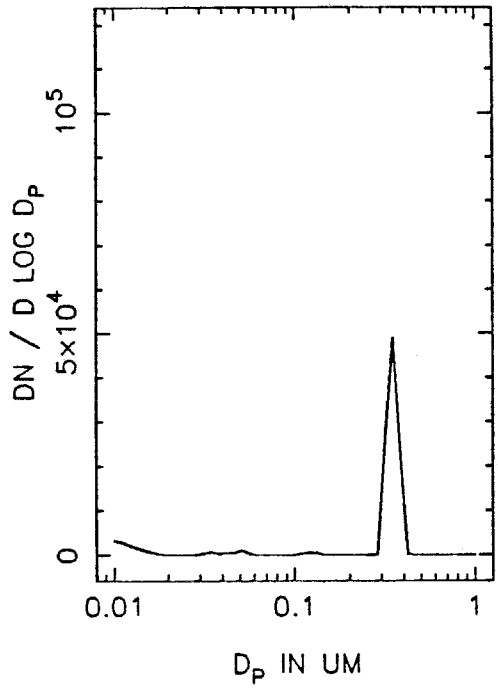

T=5.0 HOURS

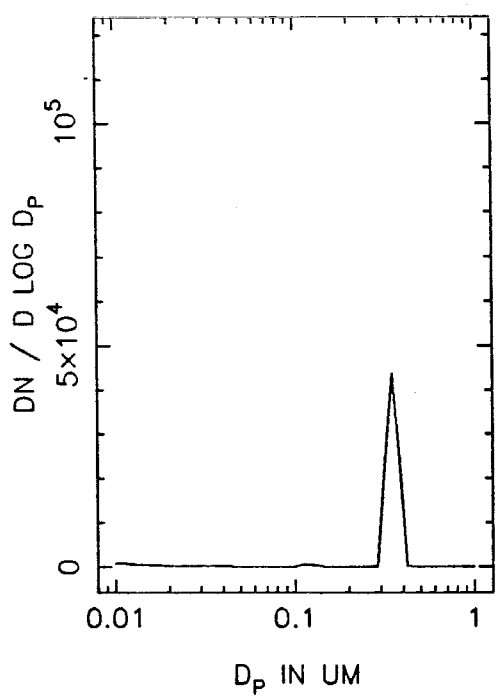

MTHA31 VOLUME DISTRIBUTION, T=0

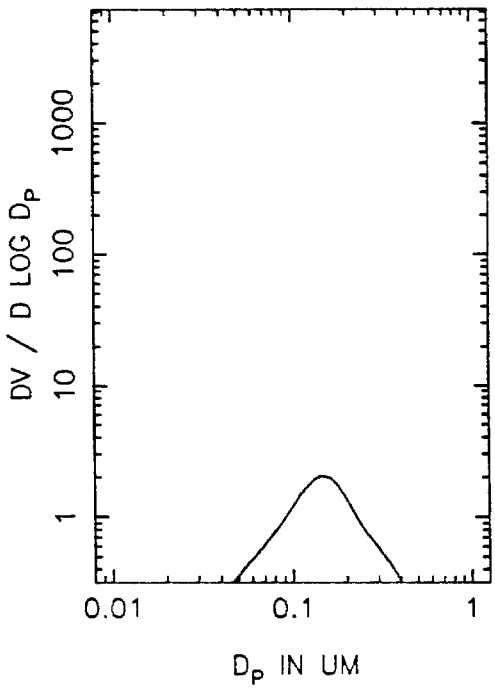

T=0.5 HOURS

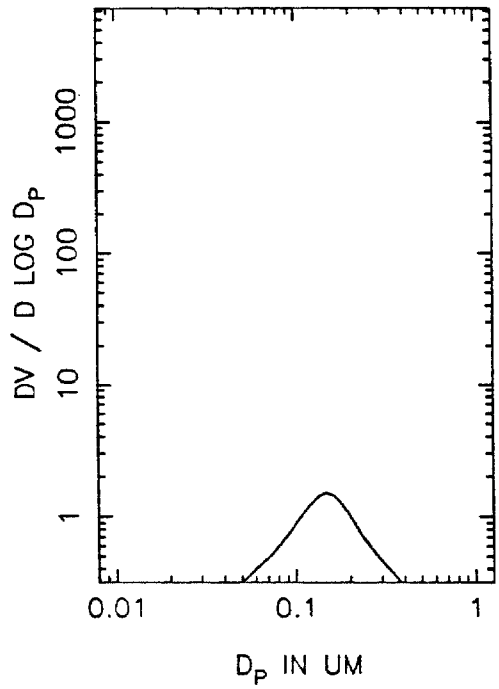

T=1.0 HOURS

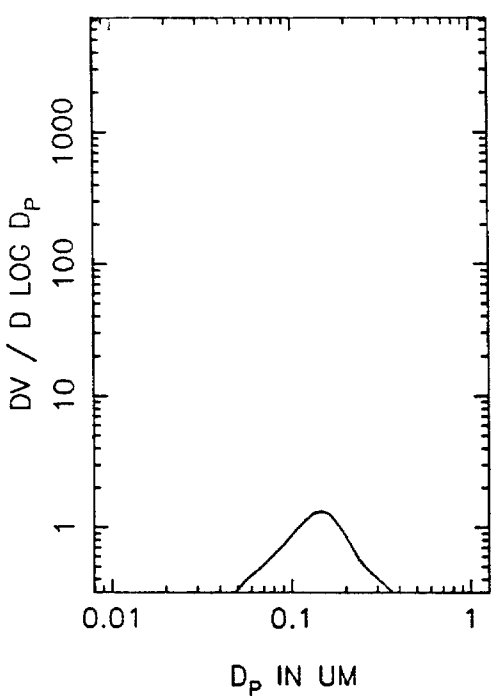

T=1.5 HOURS

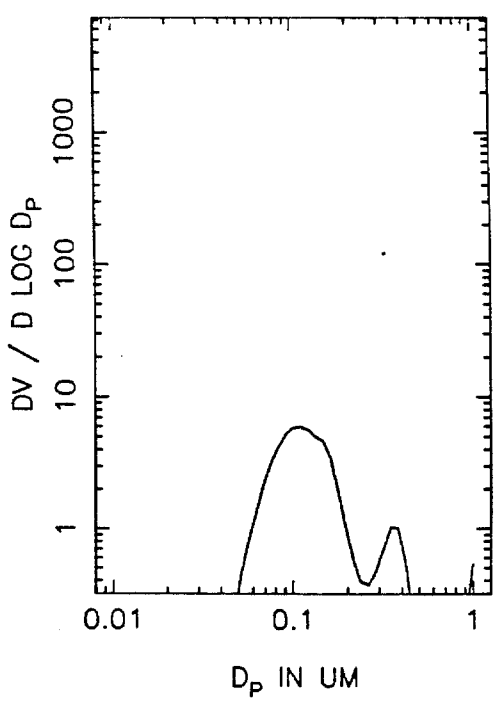

MTHA31 VOLUME DISTRIBUTION, T=2.0

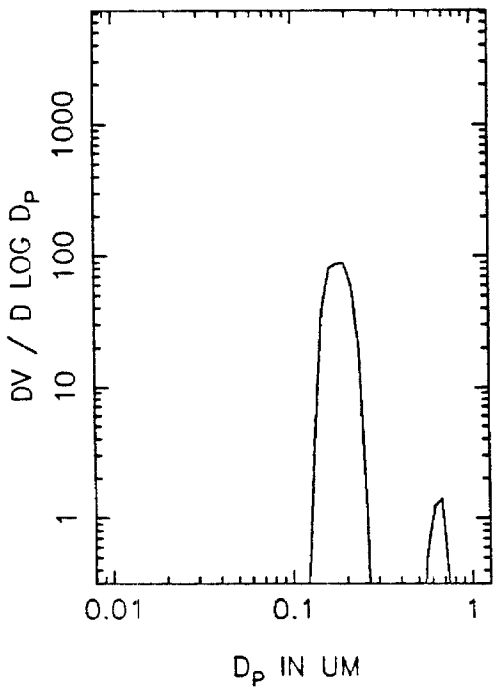

T=2.5 HOURS

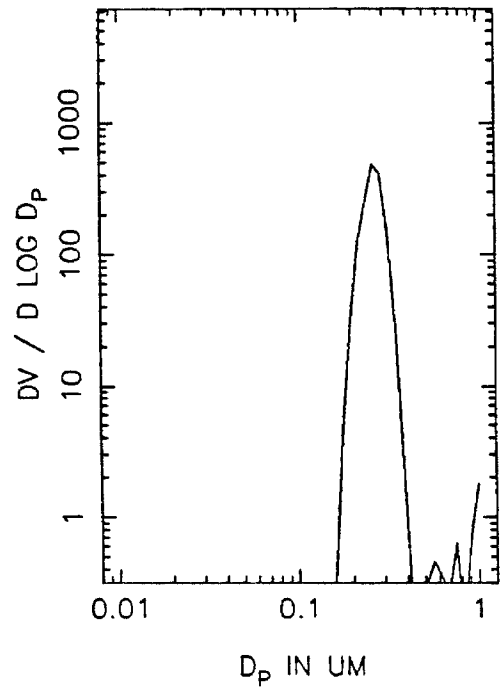

T=3.0 HOURS

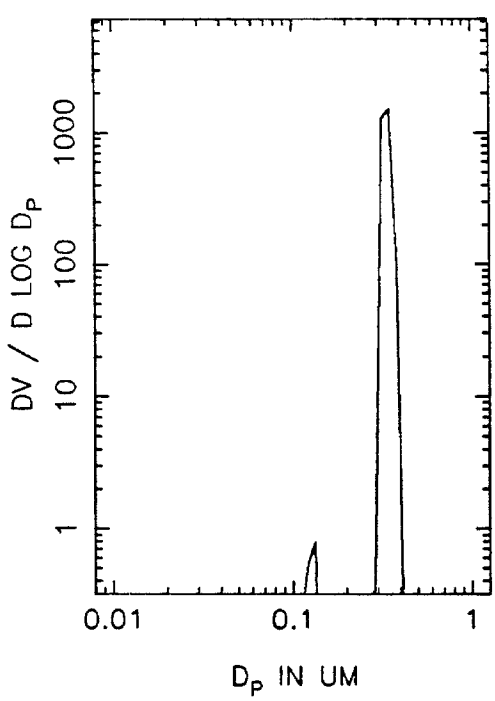

T=3.5 HOURS

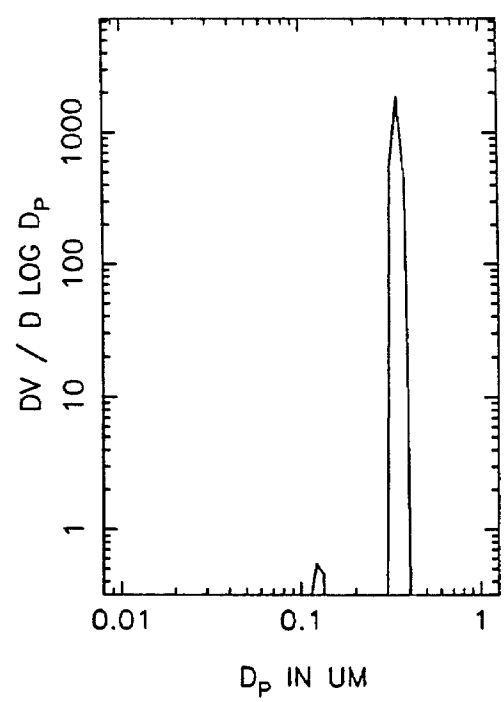

MTHA31 VOLUME DISTRIBUTION, T=4.0

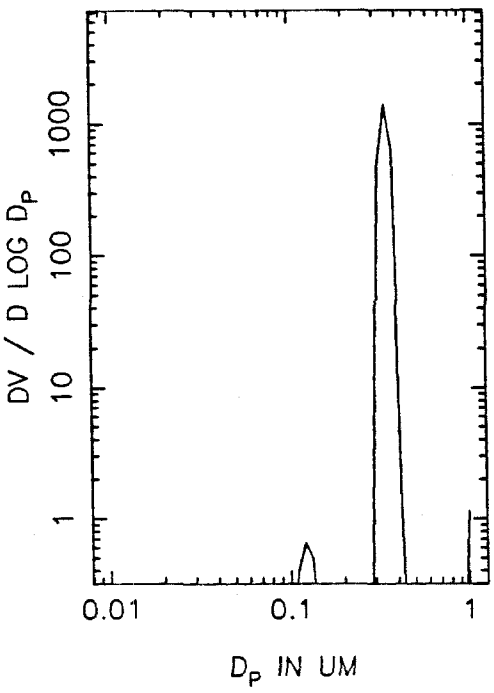

T=4.5 HOURS

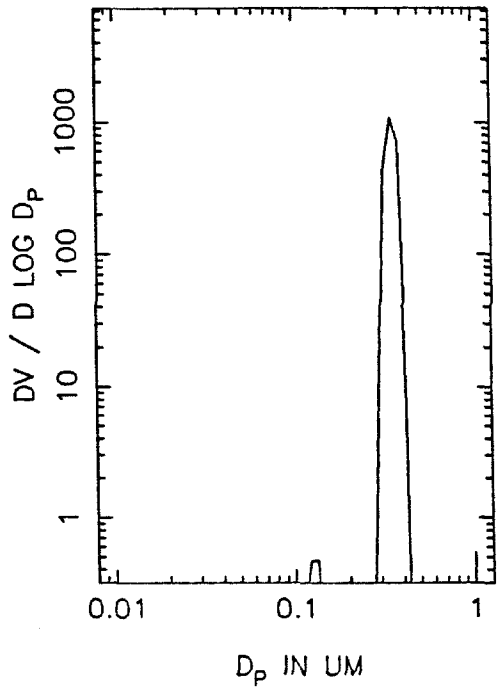

T=5.0 HOURS

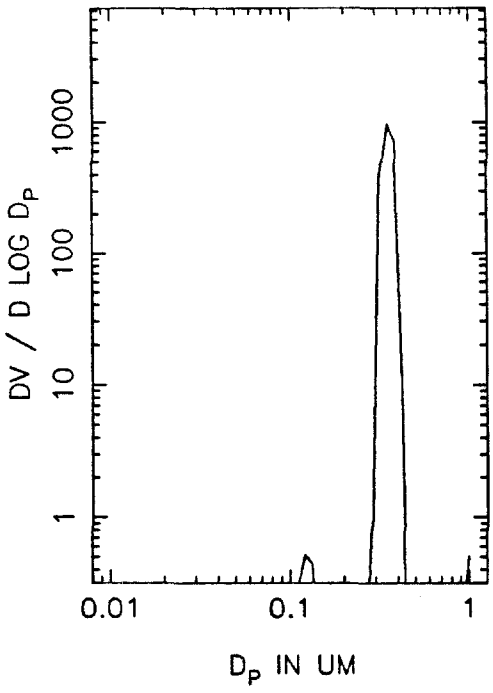

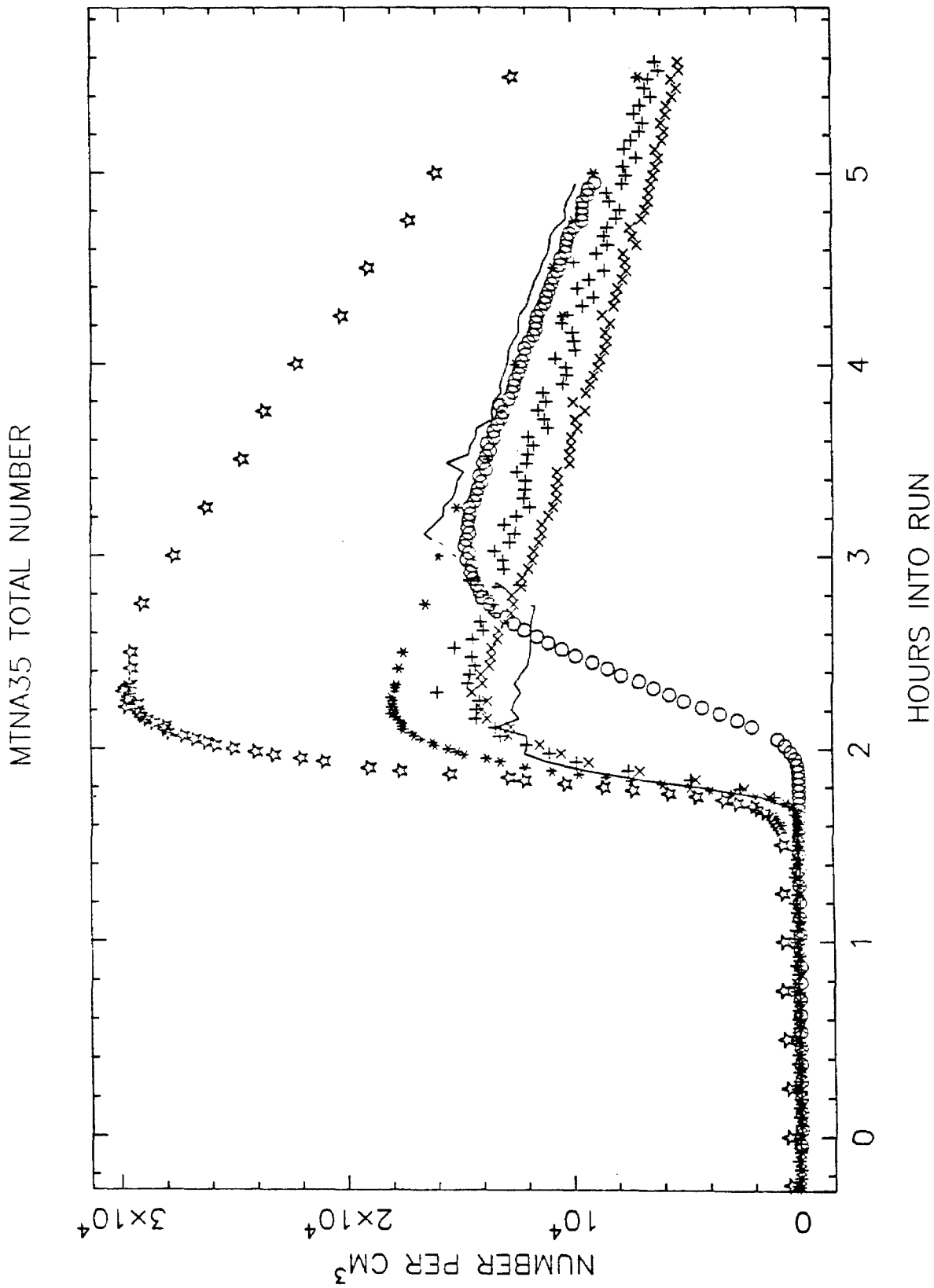
MTNA35 TOTAL NUMBER
NUMBER PER CM3
0
10^4
2×10^4
3×10^4
0
1
2
3
4
5
HOURS INTO RUN

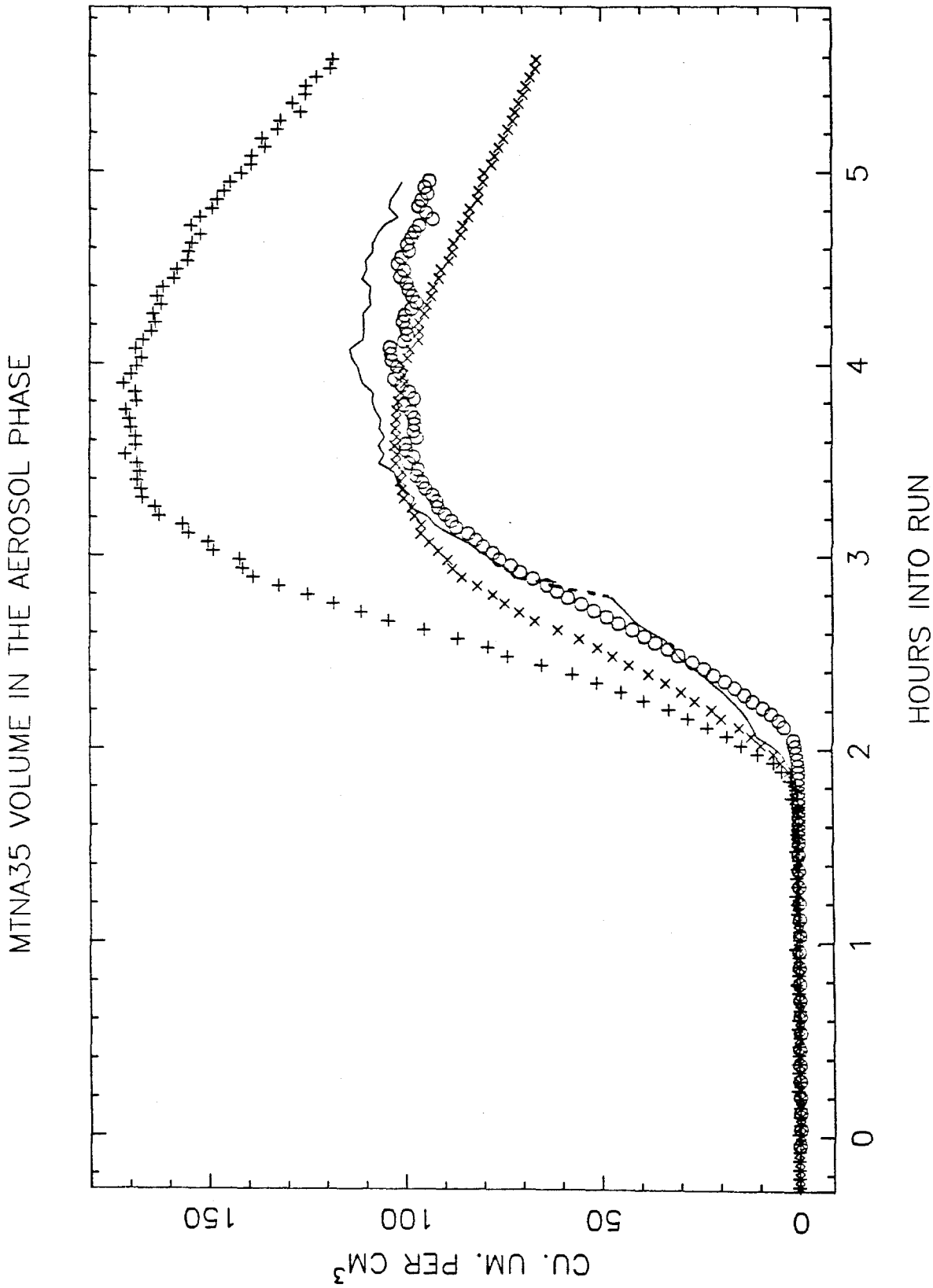
MTNA35 VOLUME IN THE AEROSOL PHASE
CU. UM. PER CM^3
0
50
100
150
0
1
2
3
4
5
HOURS INTO RUN

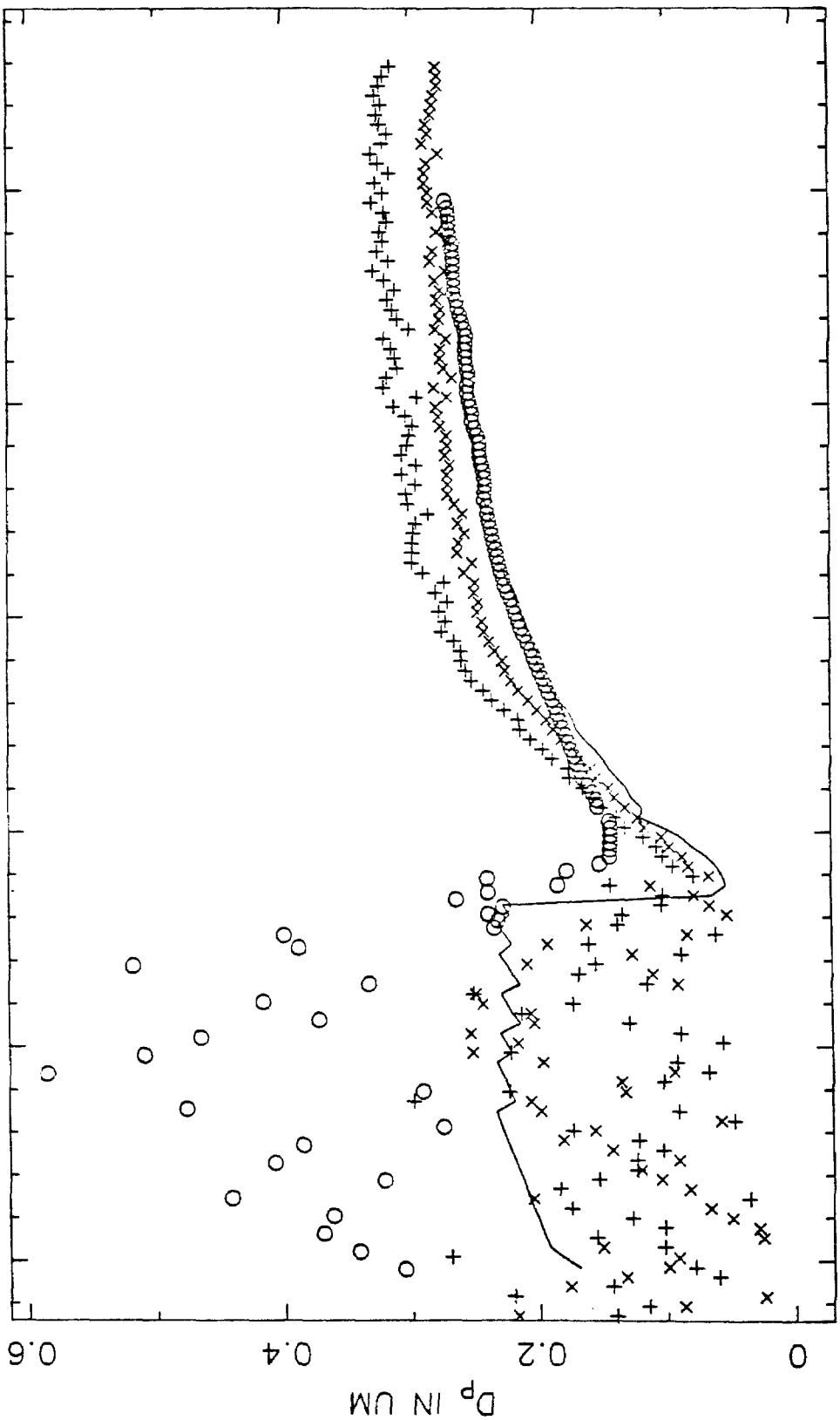
MTNA35 MEAN PARTICLE SIZE
D_p IN UM
0
0.2
0.4
0.6
0
1
2
3
4
5
HOURS INTO RUN

MTNA35 NUMBER DISTRIBUTION, T=0

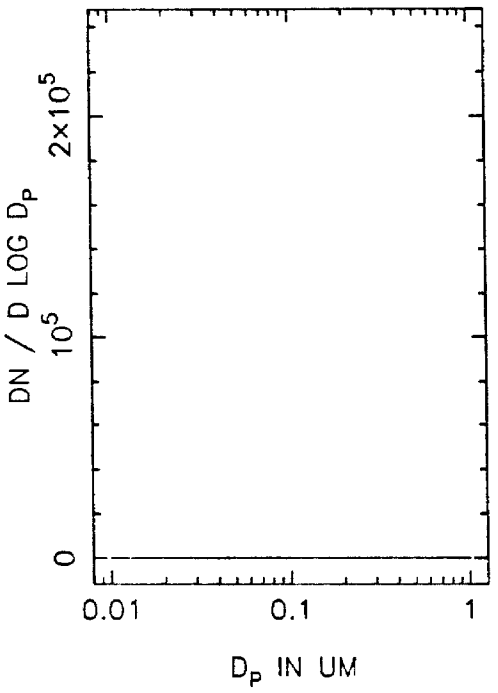

T=0.5 HOURS

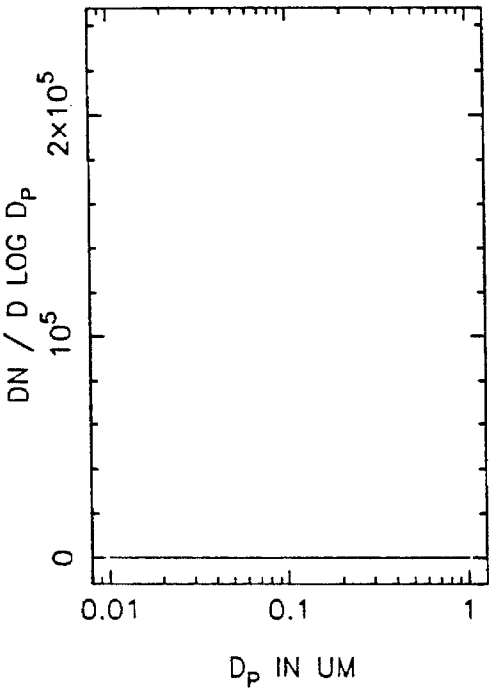

T=1.0 HOURS

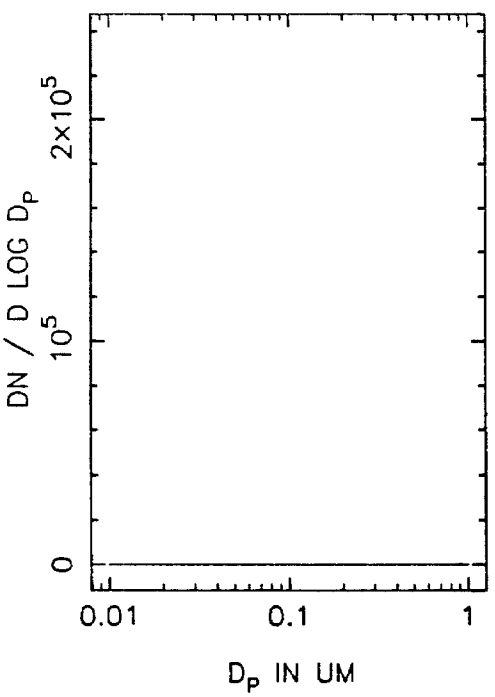

T=1.5 HOURS

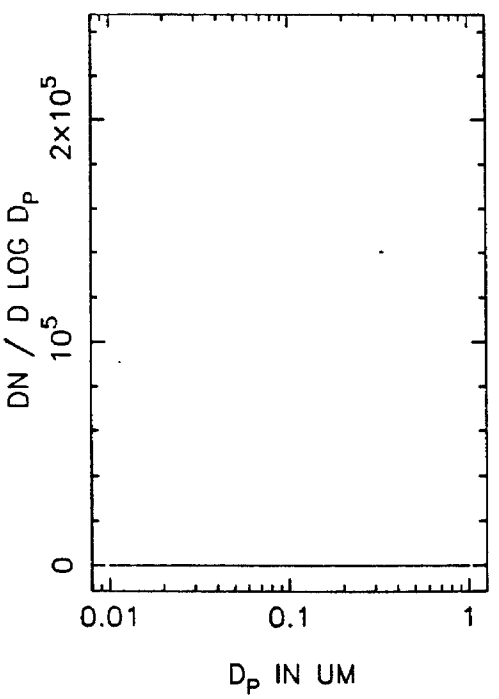

MTNA35 NUMBER DISTRIBUTION, T=2.0

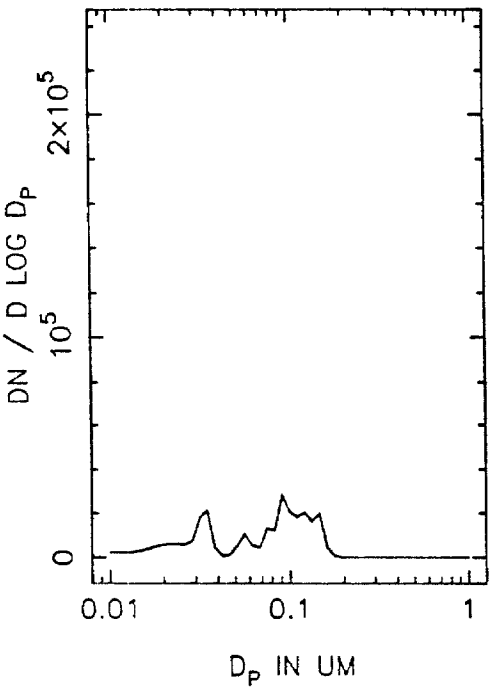

T=2.5 HOURS

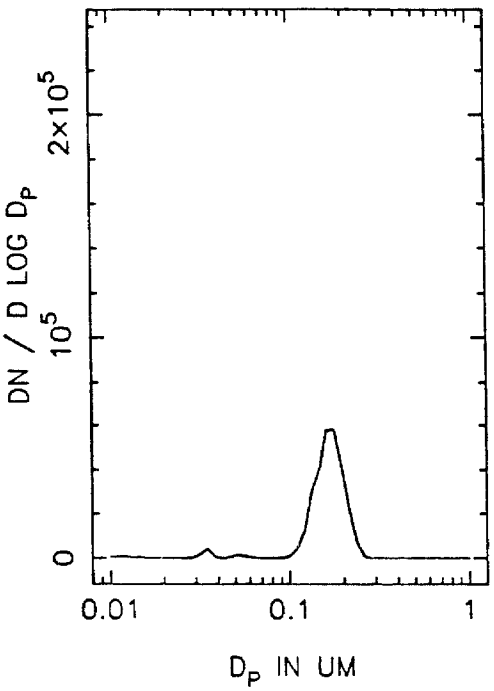

T=3.0 HOURS

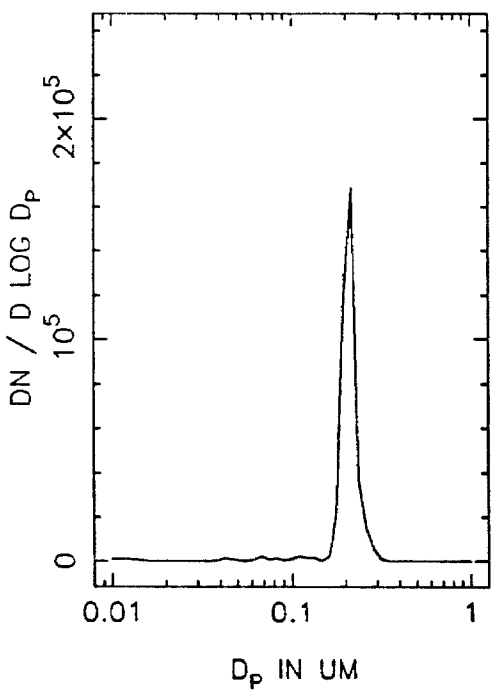

T=3.5 HOURS

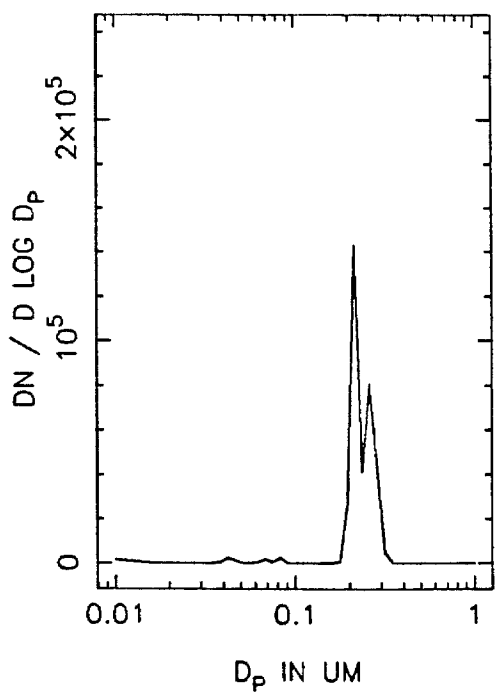

MTNA35 NUMBER DISTRIBUTION, T=4.0

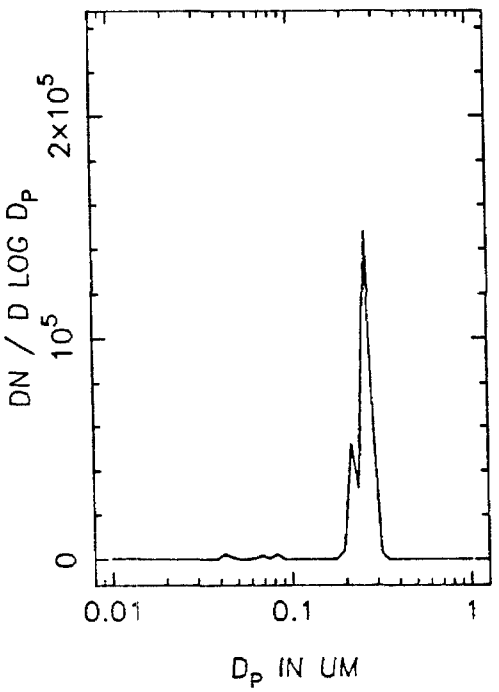

T=4.5 HOURS

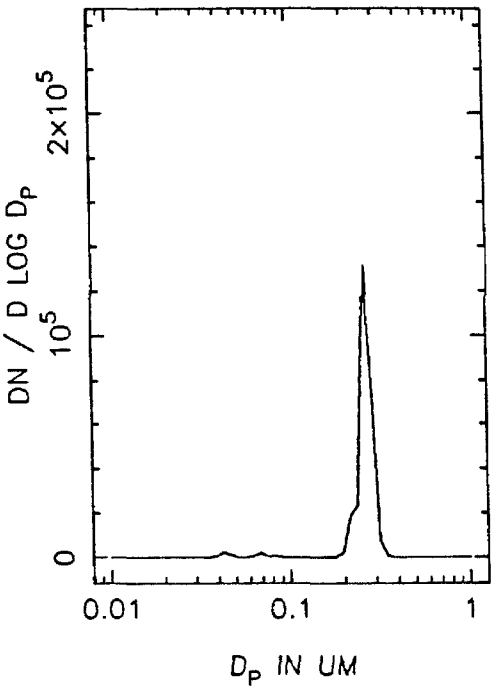

MTNA35 VOLUME DISTRIBUTION, T=0

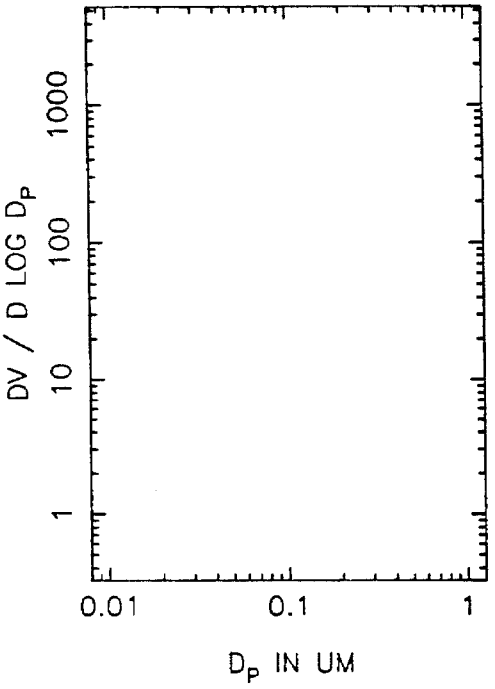

T=0.5 HOURS

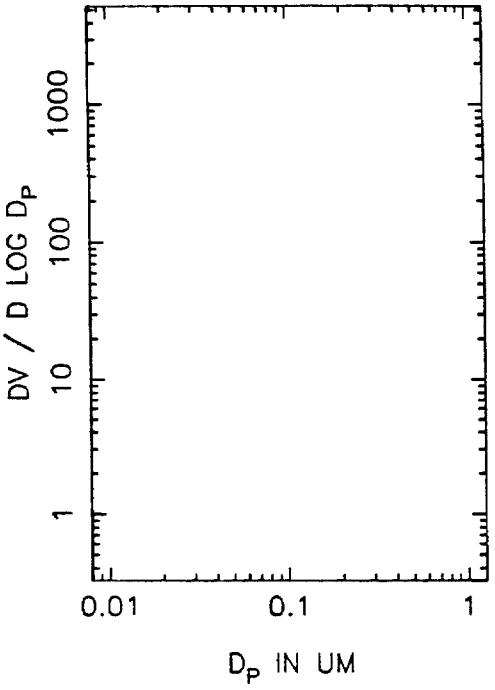

T=1.0 HOURS

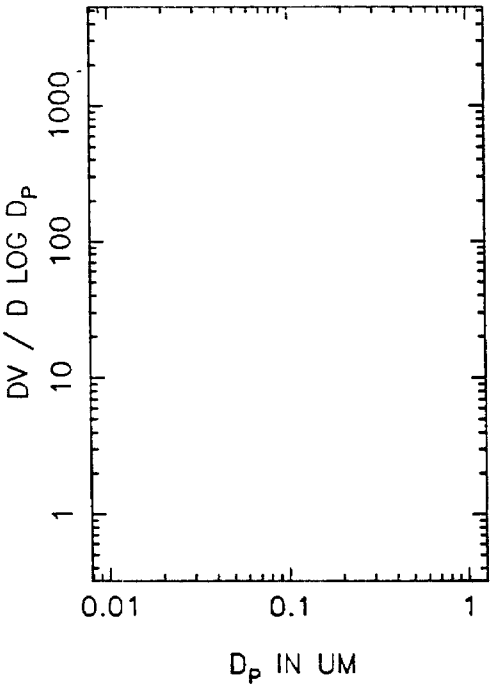

T=1.5 HOURS

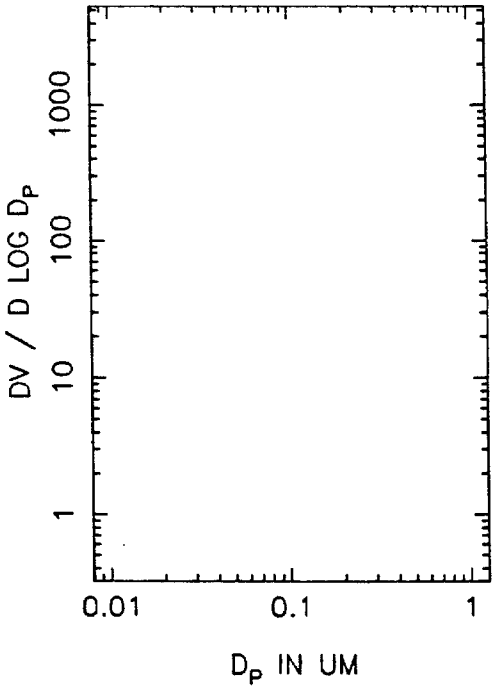

MTNA35 VOLUME DISTRIBUTION, T=2.0

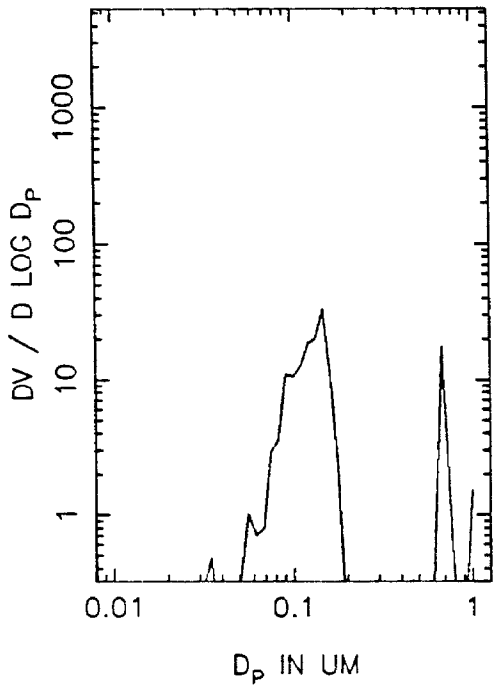

T=2.5 HOURS

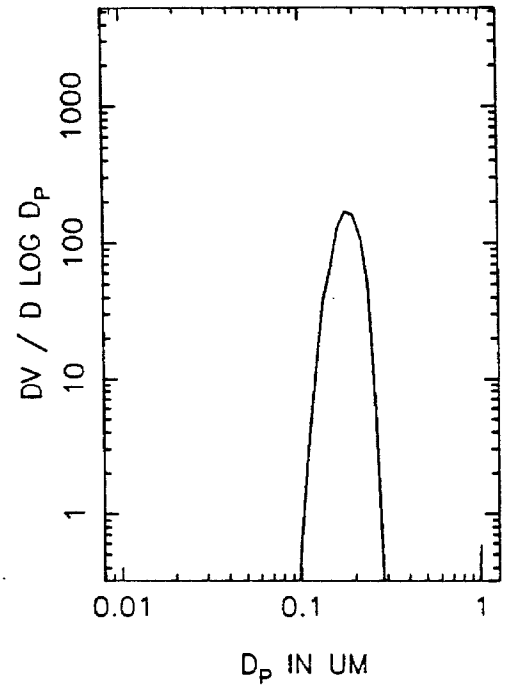

T=3.0 HOURS

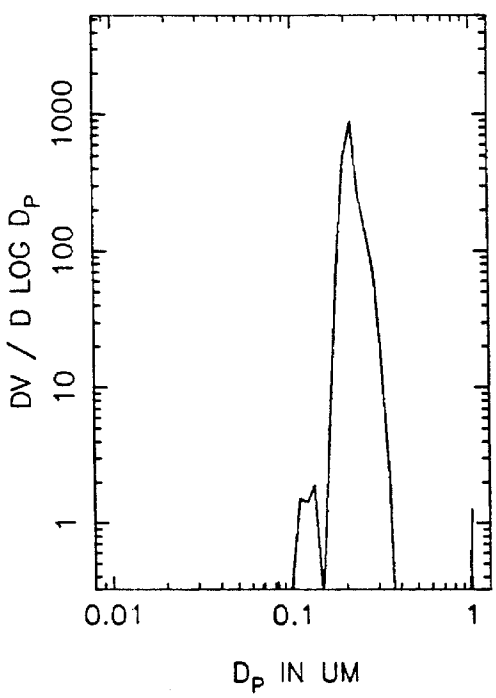

T=3.5 HOURS

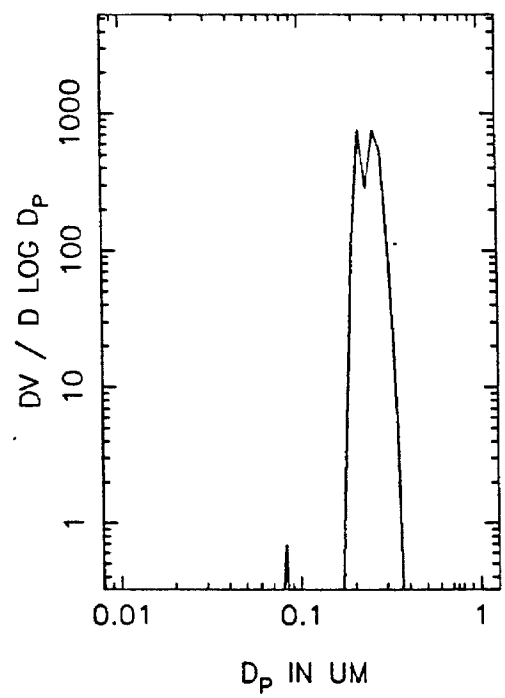

MTNA35 VOLUME DISTRIBUTION, T=4.0

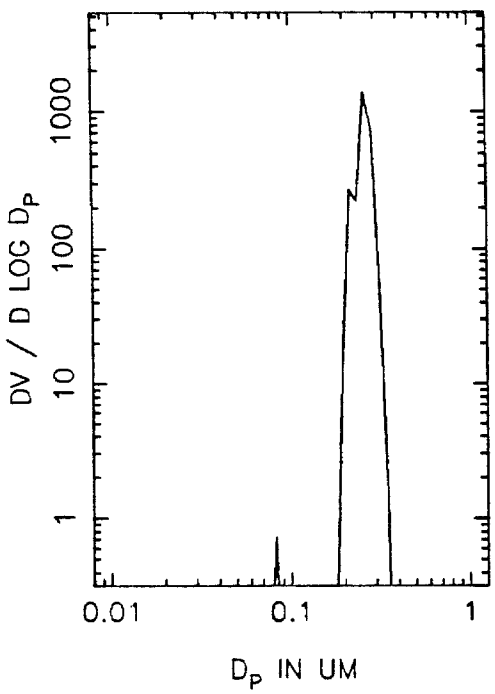

T=4.5 HOURS

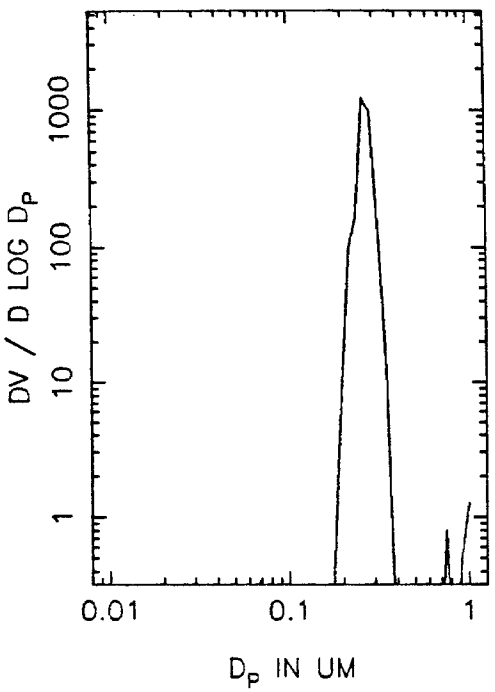

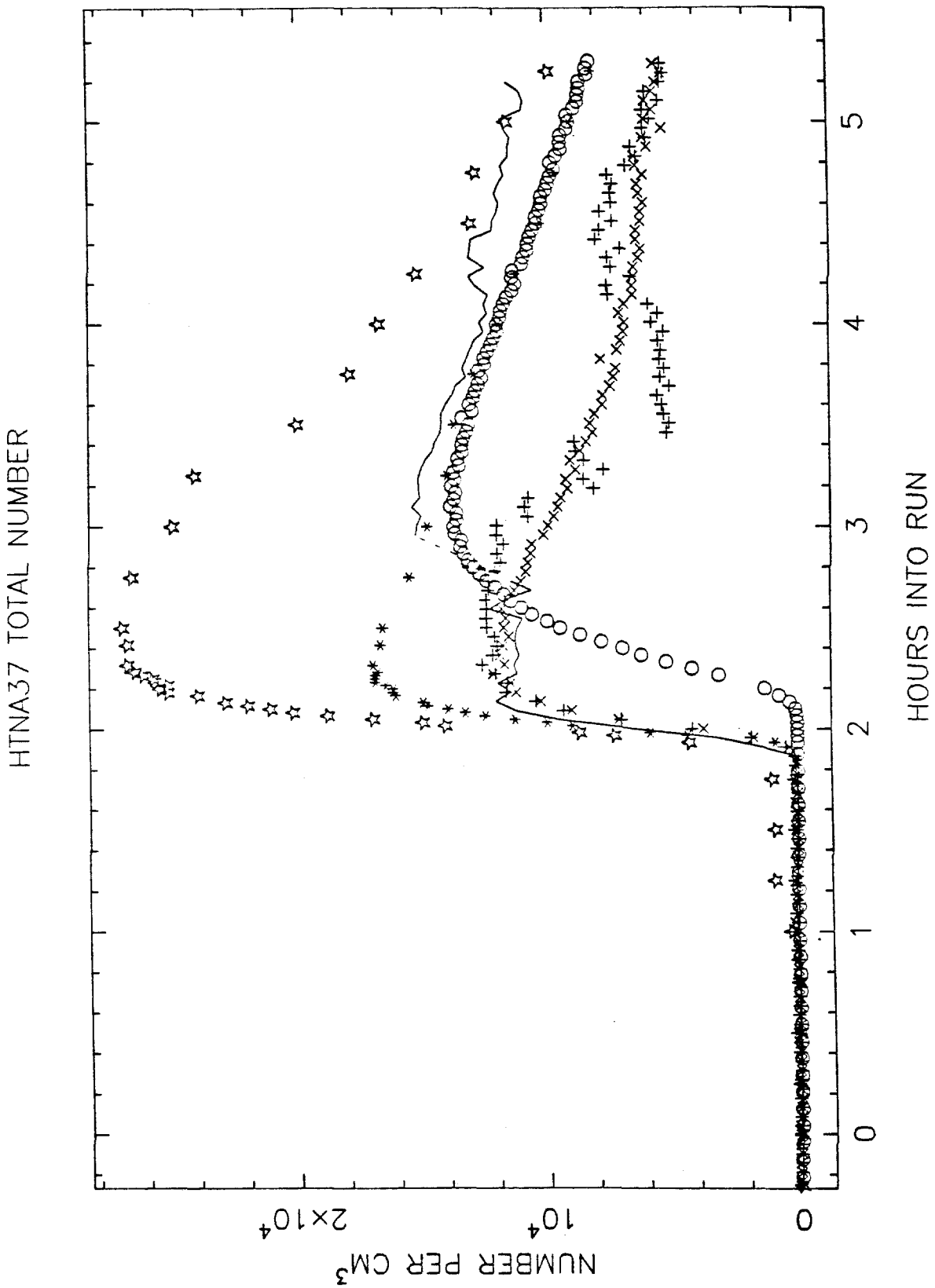
HTNA37 TOTAL NUMBER
NUMBER PER CM3
0
10^4
2×10^4
0
1
2
3
4
5
HOURS INTO RUN

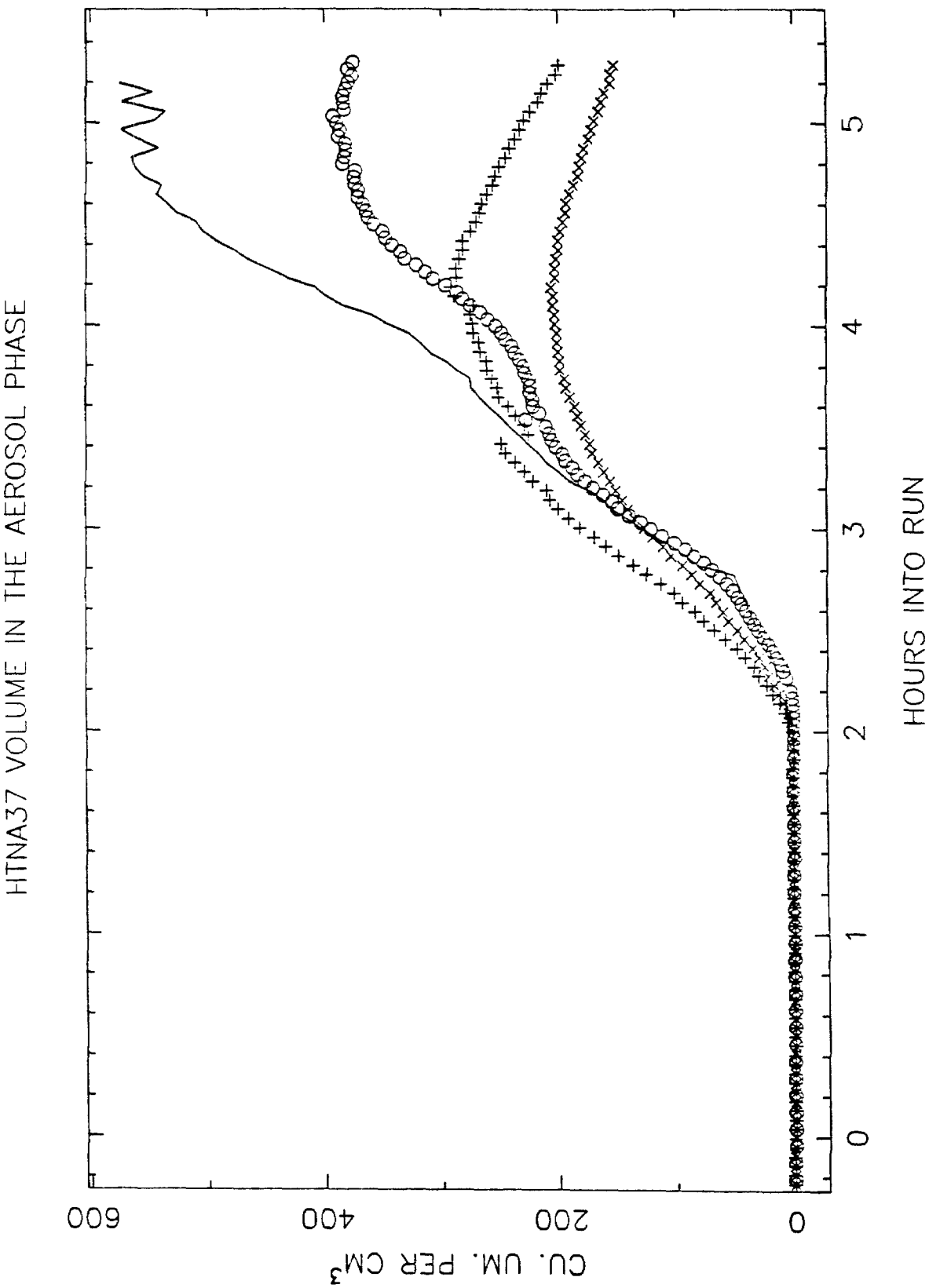
HTNA37 VOLUME IN THE AEROSOL PHASE
CU. UM. PER CM3
0
200
400
600
0
1
2
3
4
5
HOURS INTO RUN

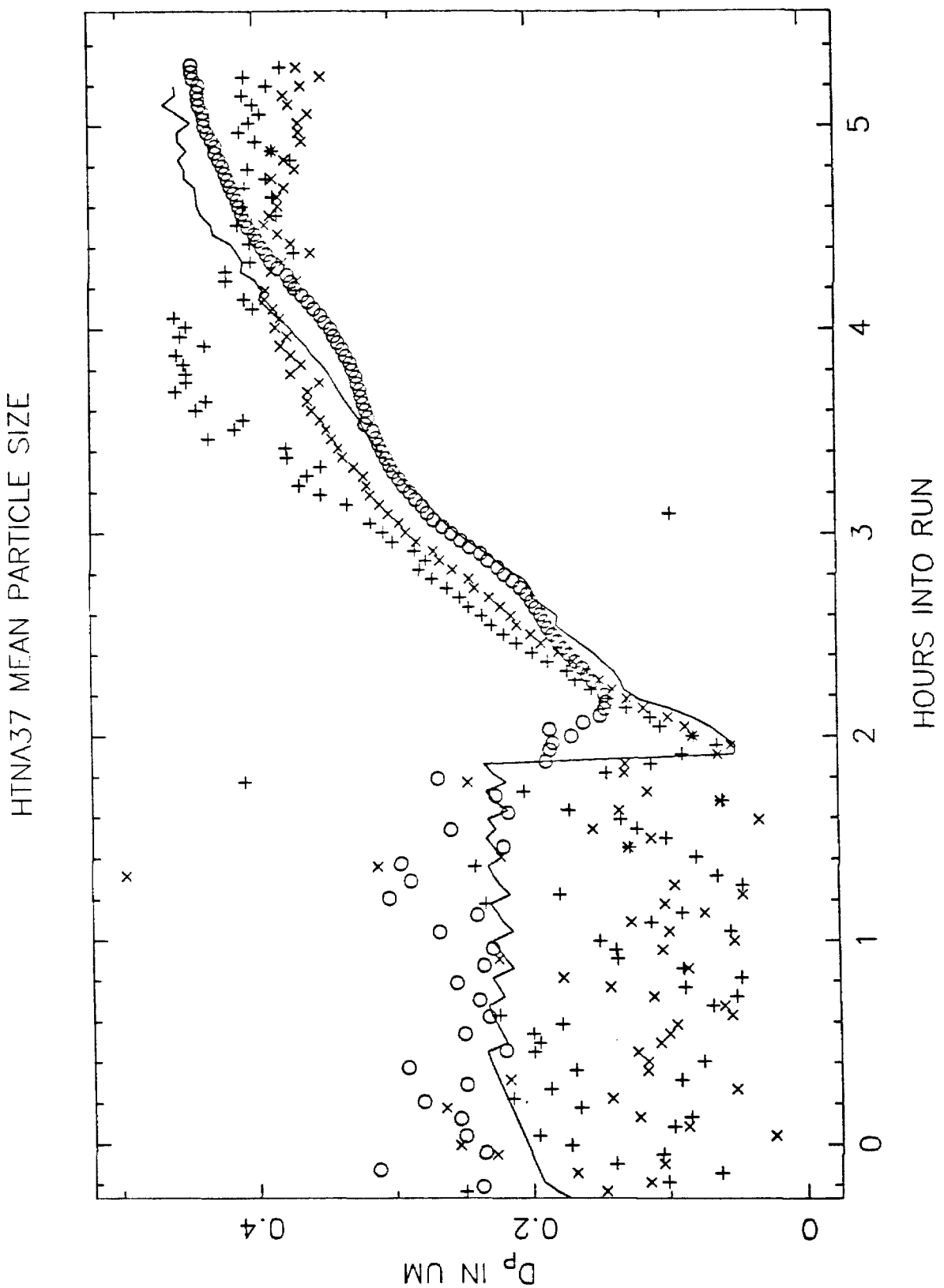
HTNA37 MEAN PARTICLE SIZE
D_p IN UM
0
0.2
0.4
0
1
2
3
4
5
HOURS INTO RUN

HTNA37 NUMBER DISTRIBUTION, T=0

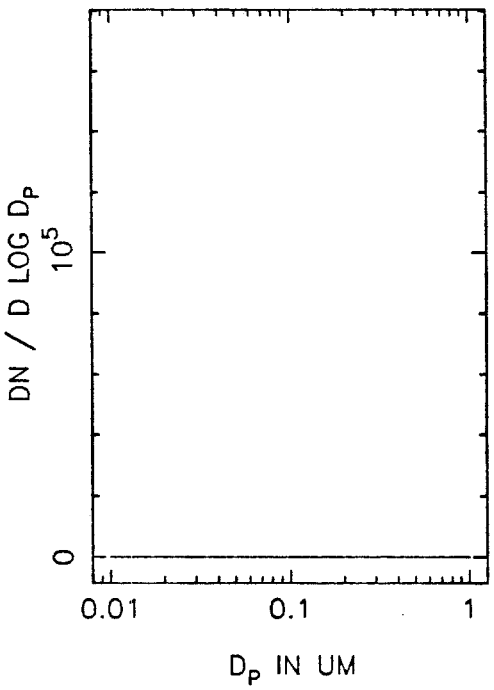

T=0.5 HOURS

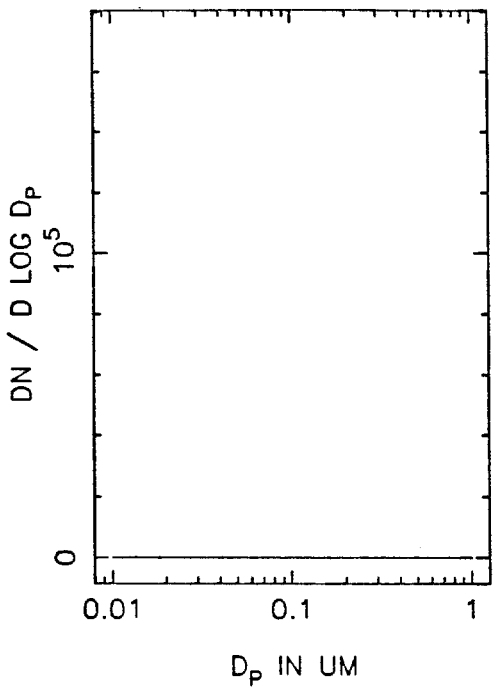

T=1.0 HOURS

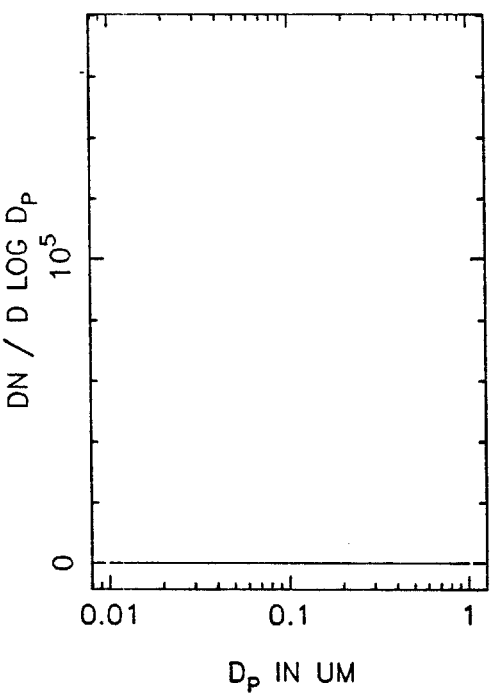

T=1.5 HOURS

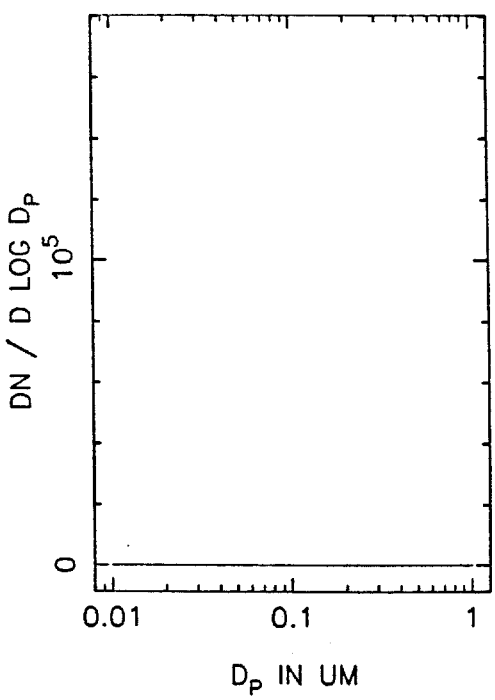

HTNA37 NUMBER DISTRIBUTION, T=2.0

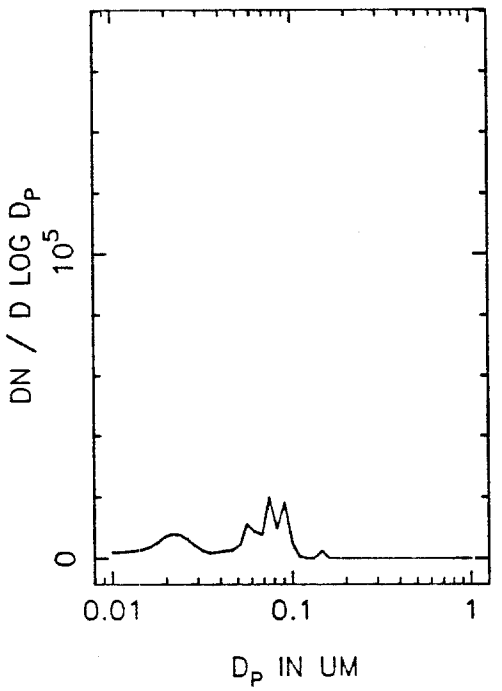

T=2.5 HOURS

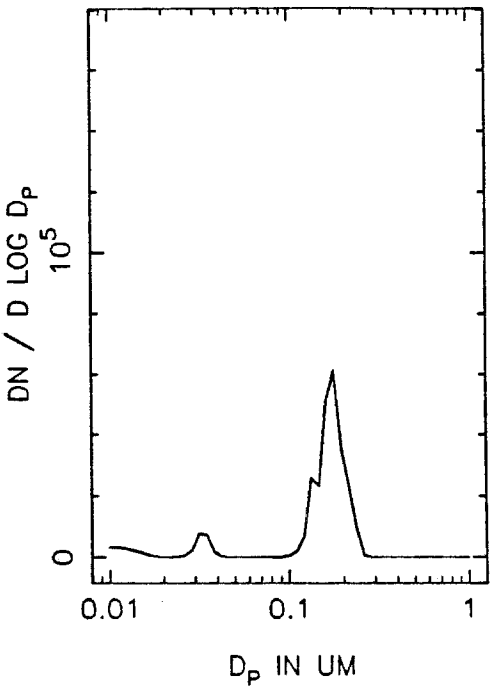

T=3.0 HOURS

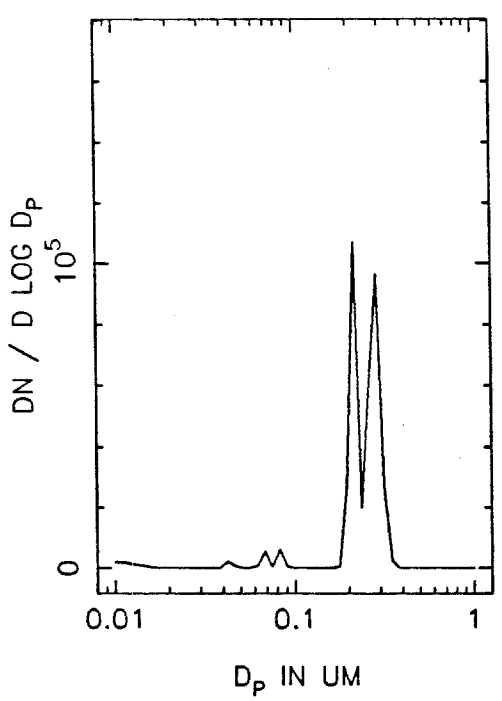

T=3.5 HOURS

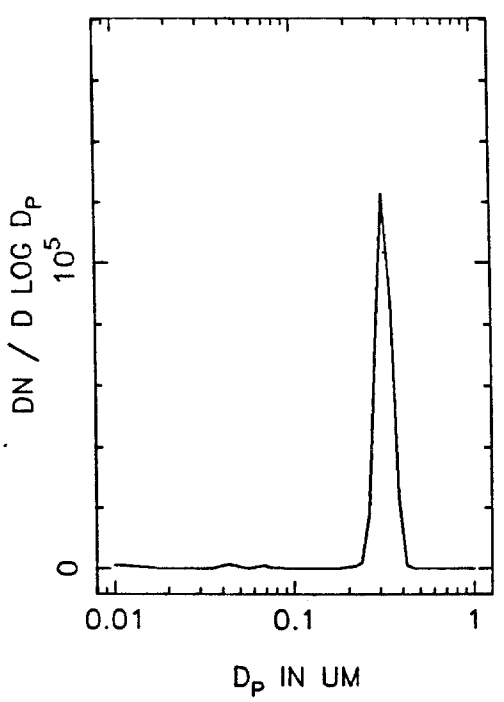

HTNA37 NUMBER DISTRIBUTION, T=4.0

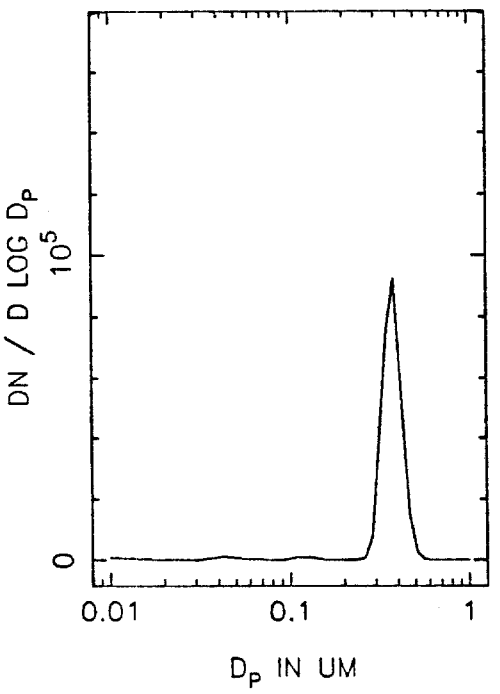

T=4.5 HOURS

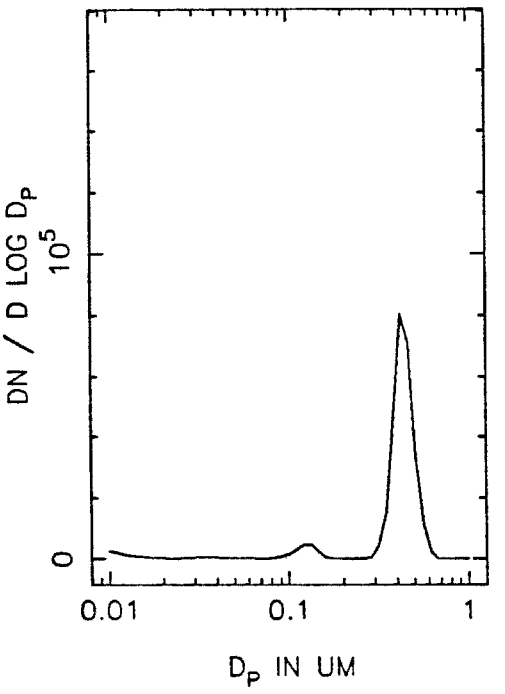

T=5.0 HOURS

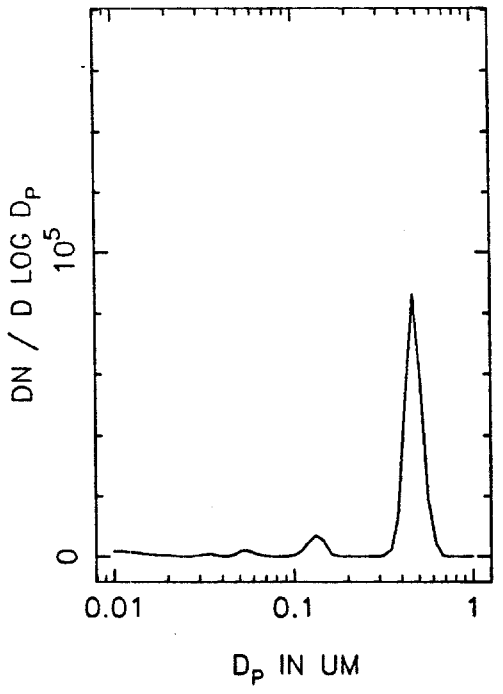

HTNA37 VOLUME DISTRIBUTION, T=0

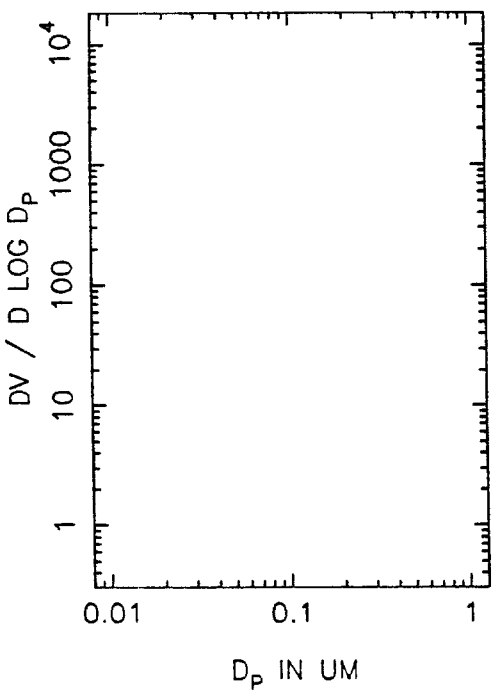

T=0.5 HOURS

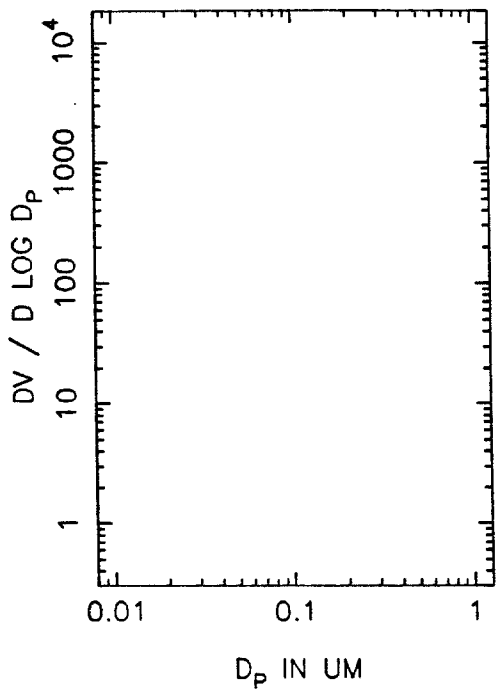

T=1.0 HOURS

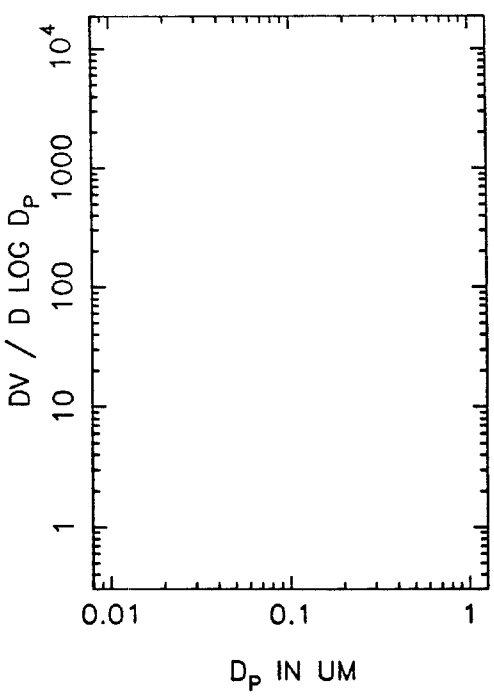

T=1.5 HOURS

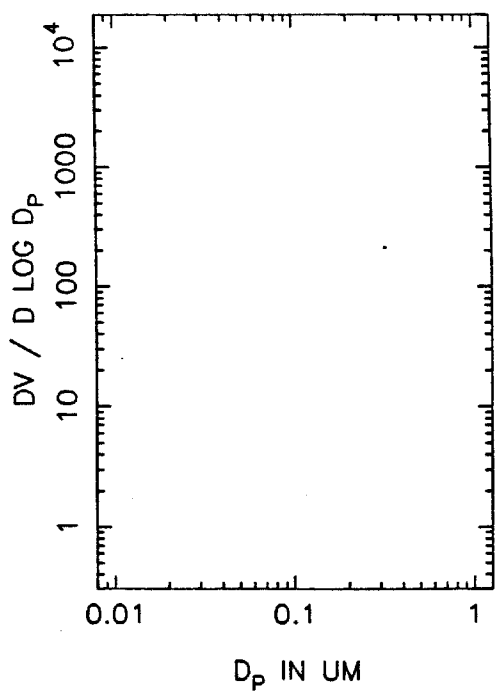

HTNA37 VOLUME DISTRIBUTION, T=2.0

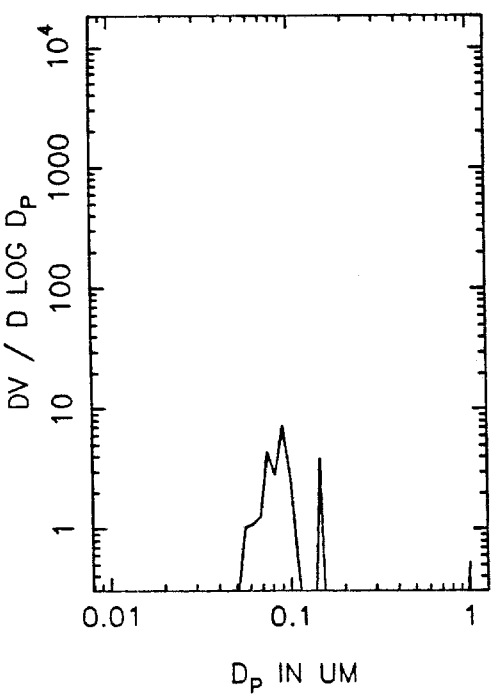

T=2.5 HOURS

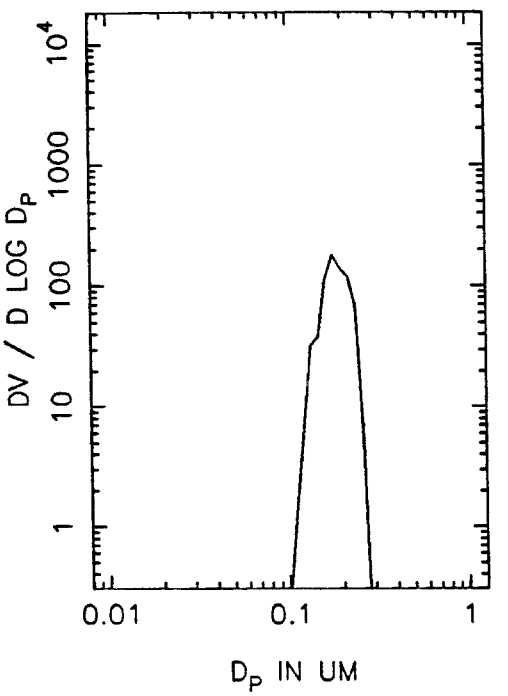

T=3.0 HOURS

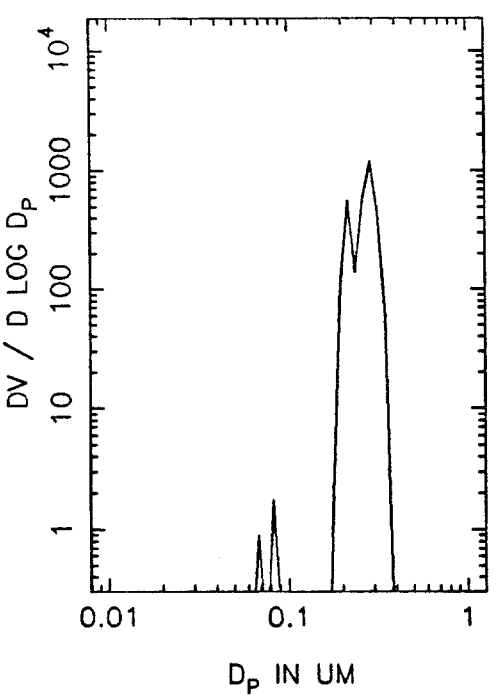

T=3.5 HOURS

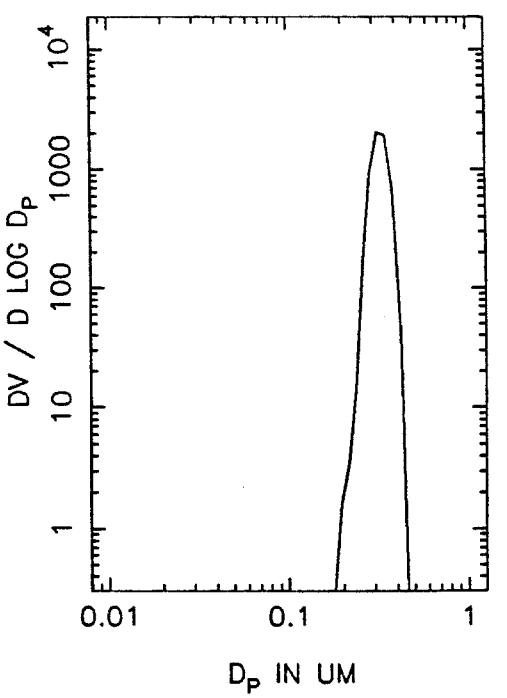

HTNA37 VOLUME DISTRIBUTION, T=4.0

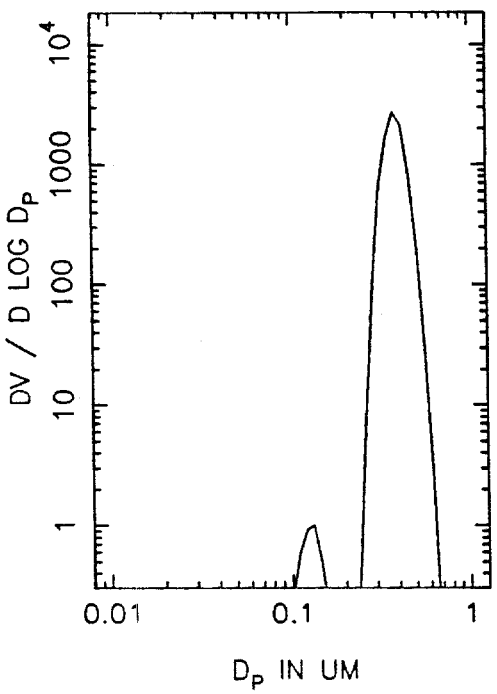

T=4.5 HOURS

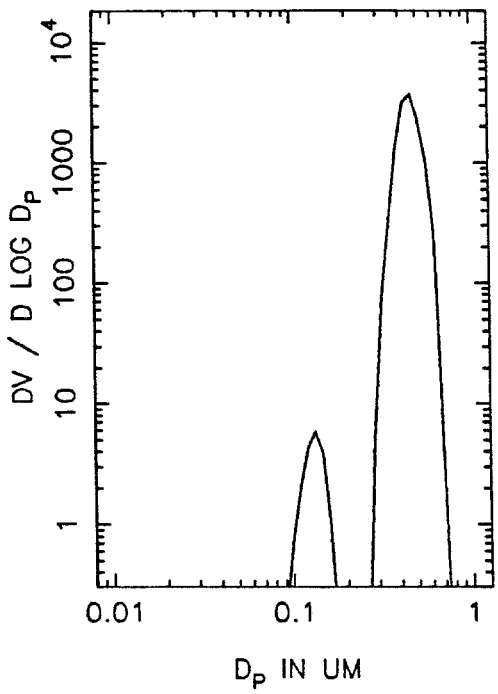

T=5.0 HOURS

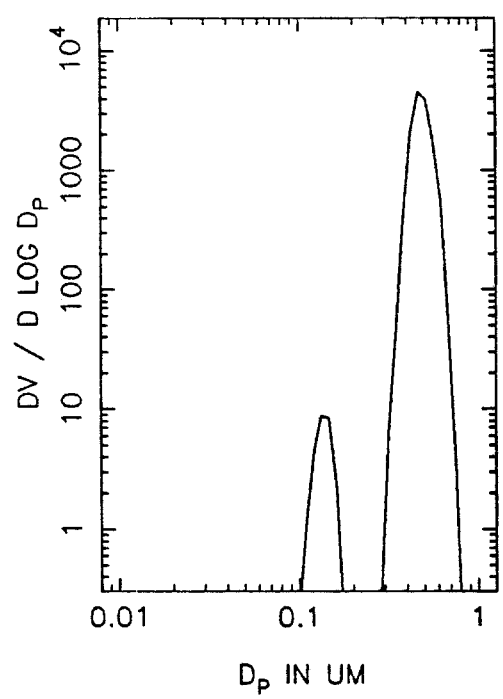

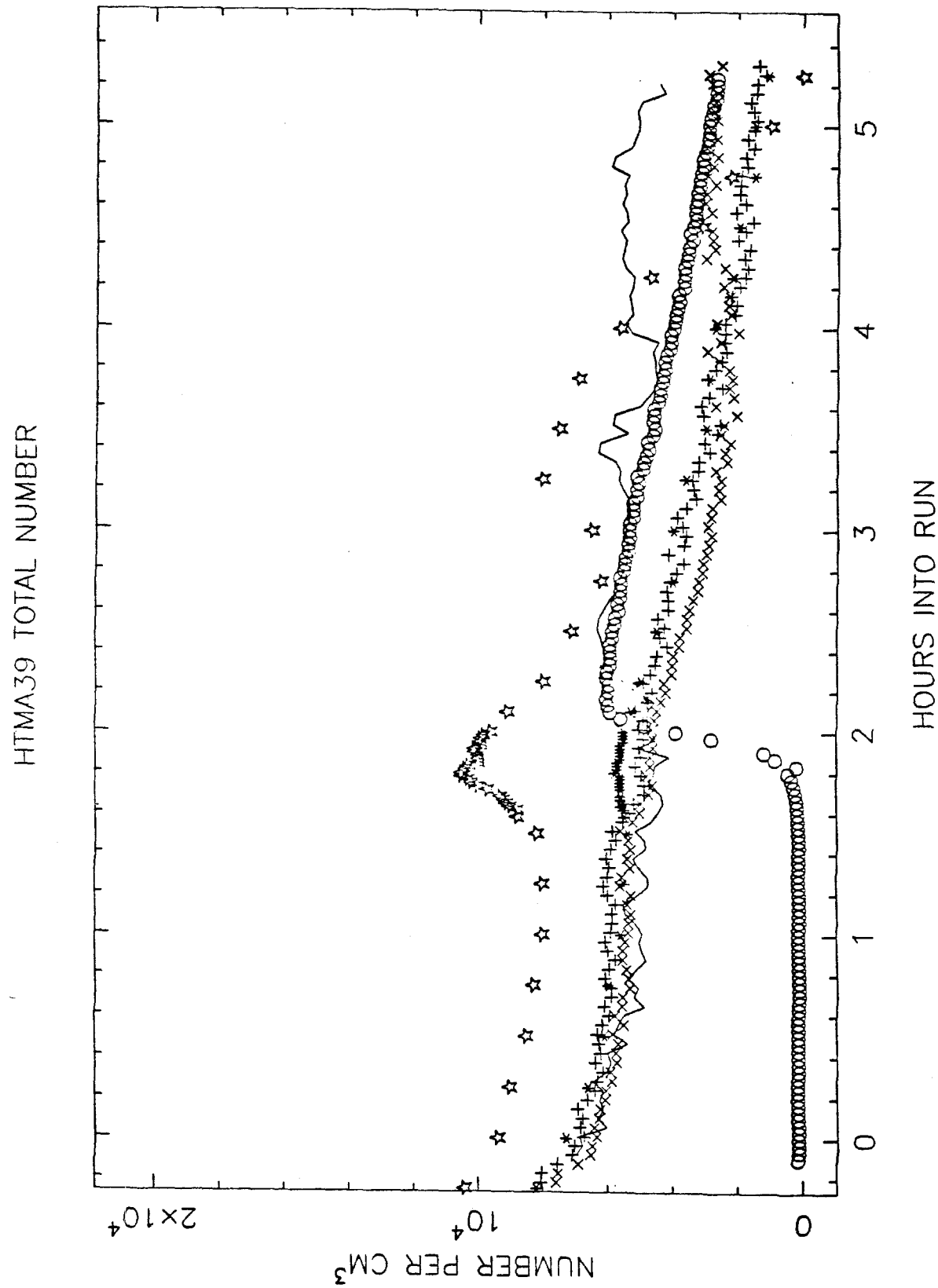
HTMA39 TOTAL NUMBER
NUMBER PER CM3
2×10⁴
10⁴
0
0
1
2
3
4
5
HOURS INTO RUN

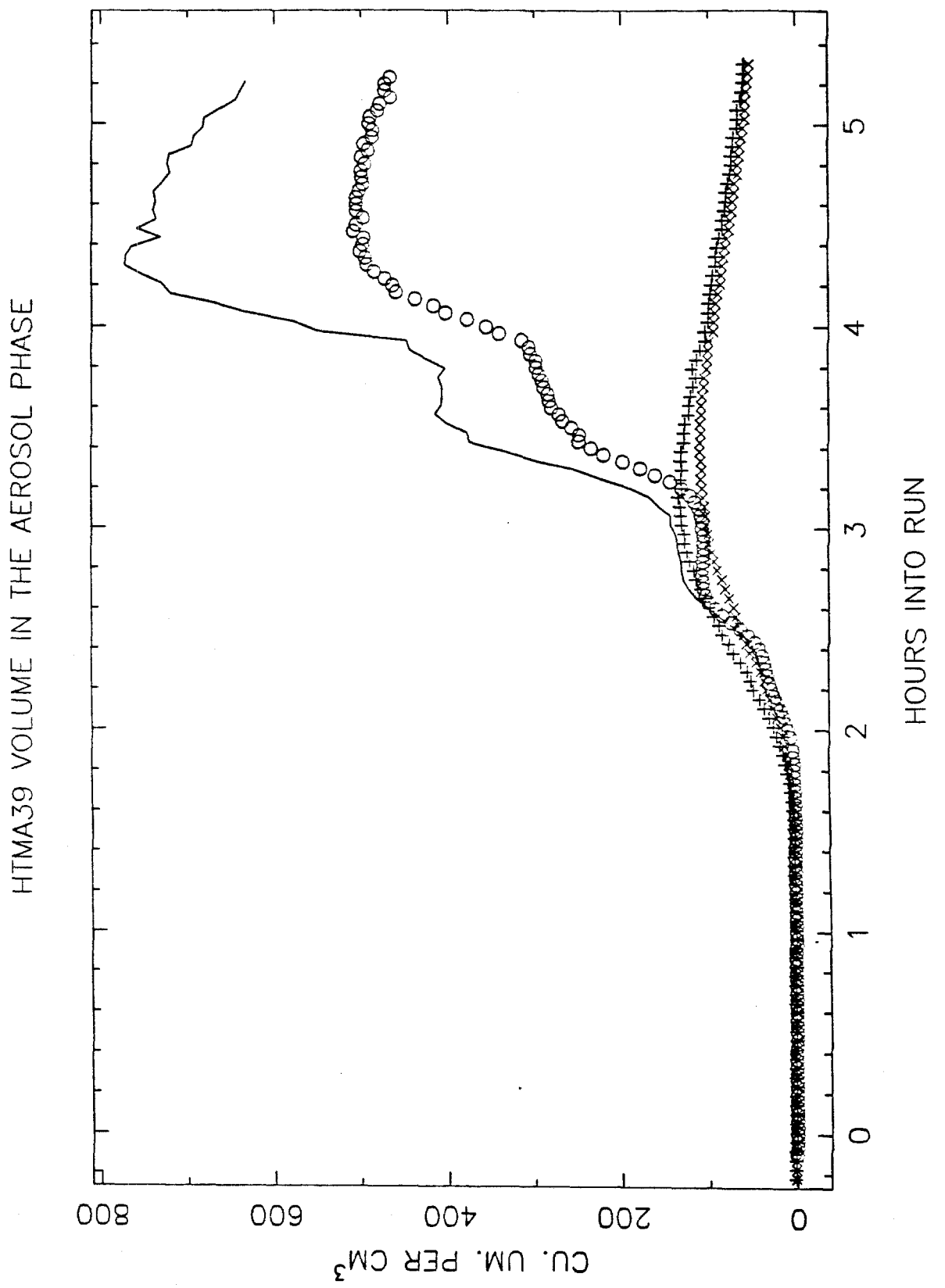
HTMA39 VOLUME IN THE AEROSOL PHASE
CU. UM. PER CM3
0
200
400
600
800
0
1
2
3
4
5
HOURS INTO RUN

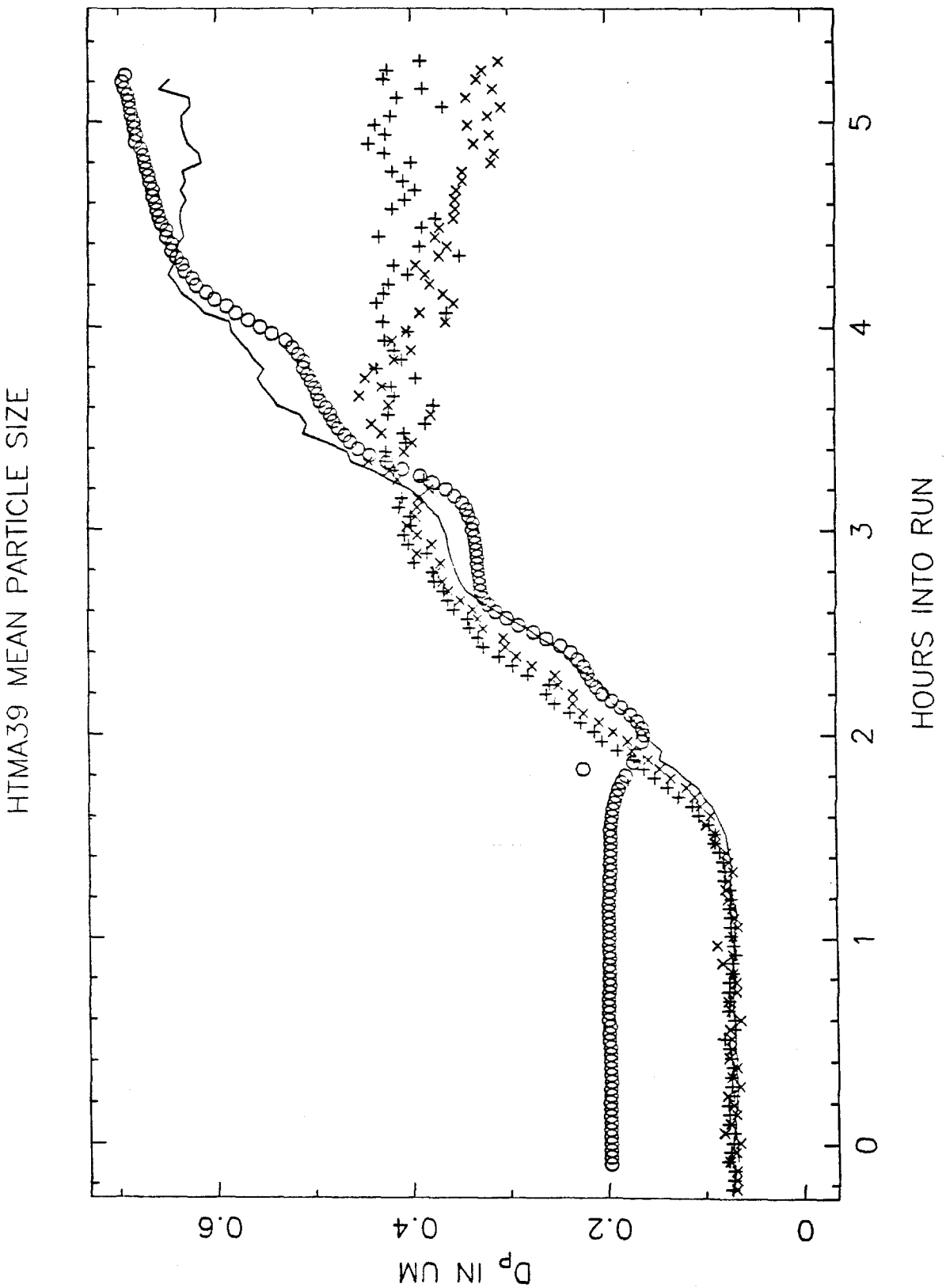
HTMA39 MEAN PARTICLE SIZE
D_p IN UM
0
0.2
0.4
0.6
0
1
2
3
4
5
HOURS INTO RUN

HTMA39 NUMBER DISTRIBUTION, T=0

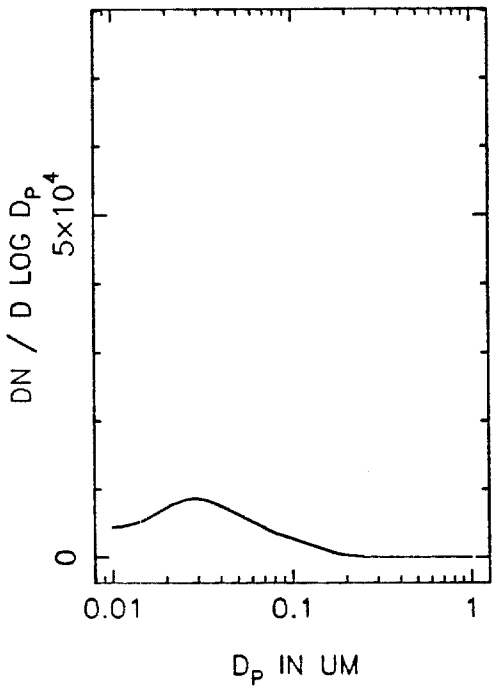

T=0.5 HOURS

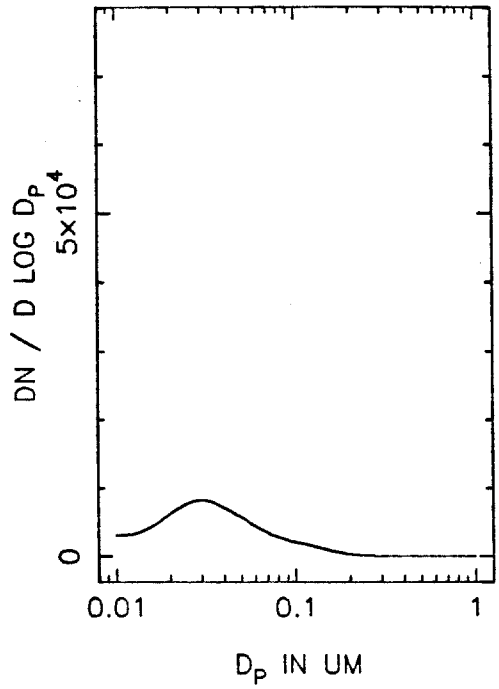

T=1.0 HOURS

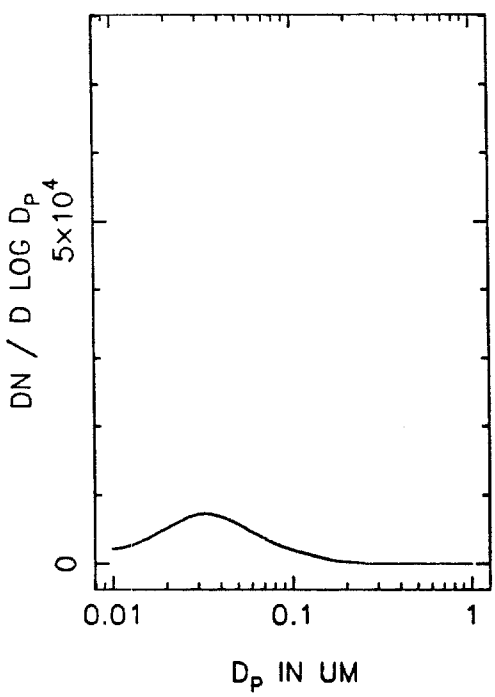

T=1.5 HOURS

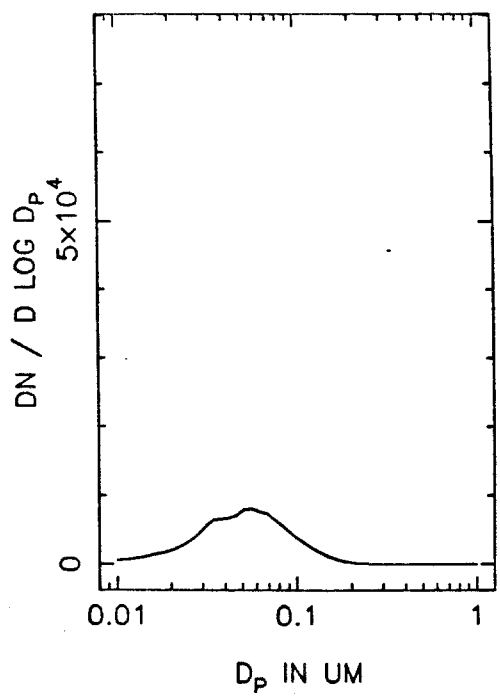

HTMA39 NUMBER DISTRIBUTION, T=2.0

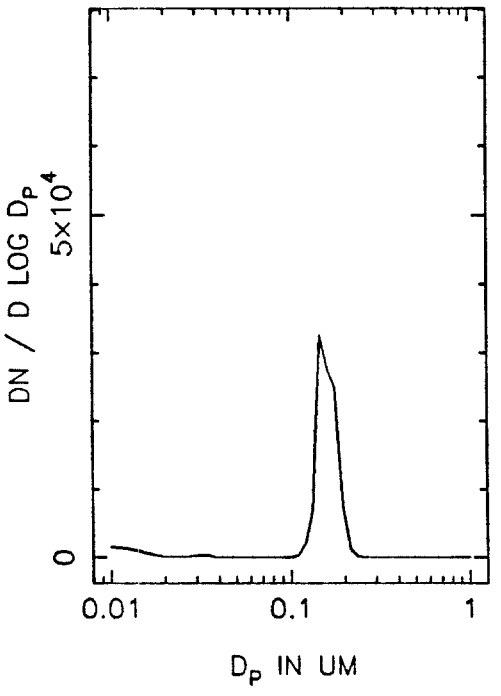

T=2.5 HOURS

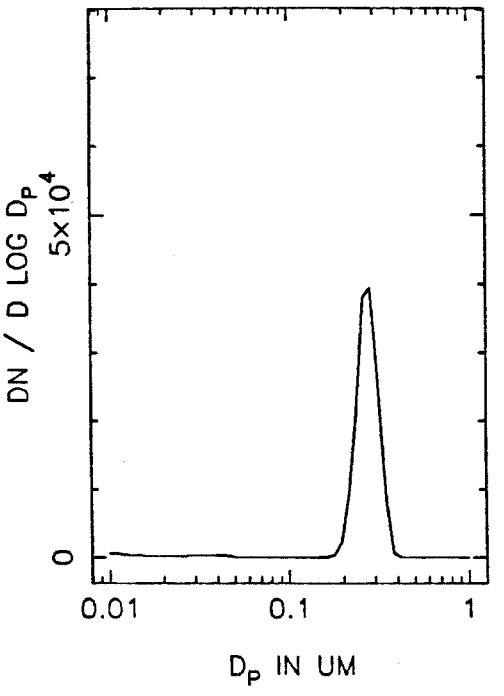

T=3.0 HOURS

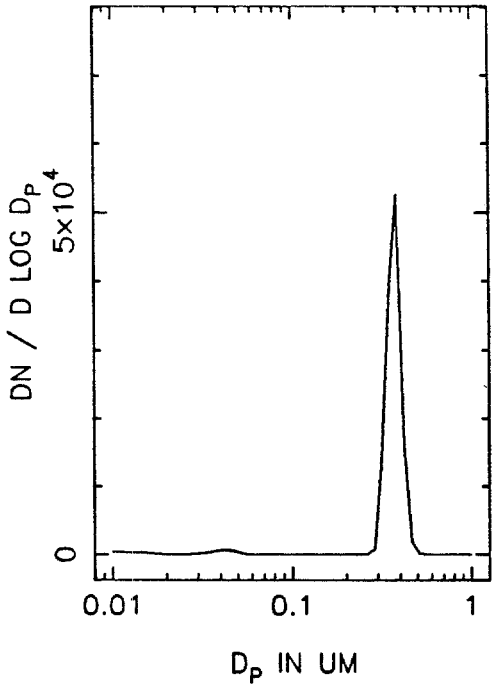

T=3.5 HOURS

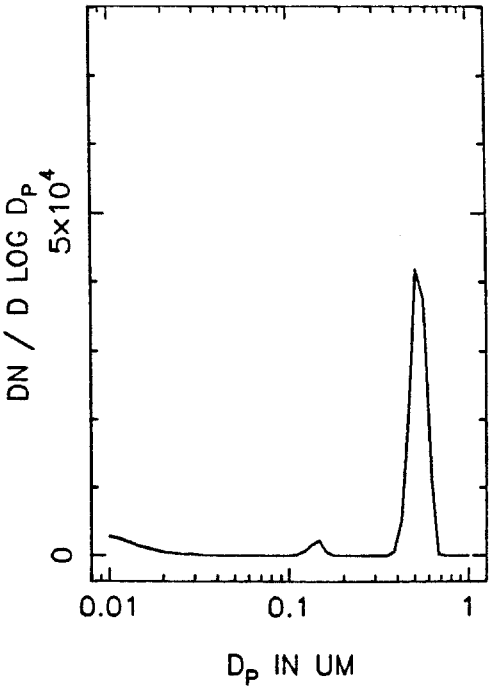

HTMA39 NUMBER DISTRIBUTION, T=4.0

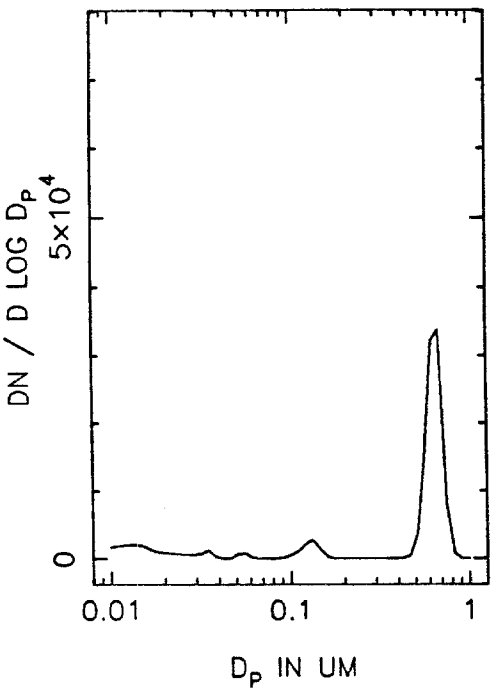

T=4.5 HOURS

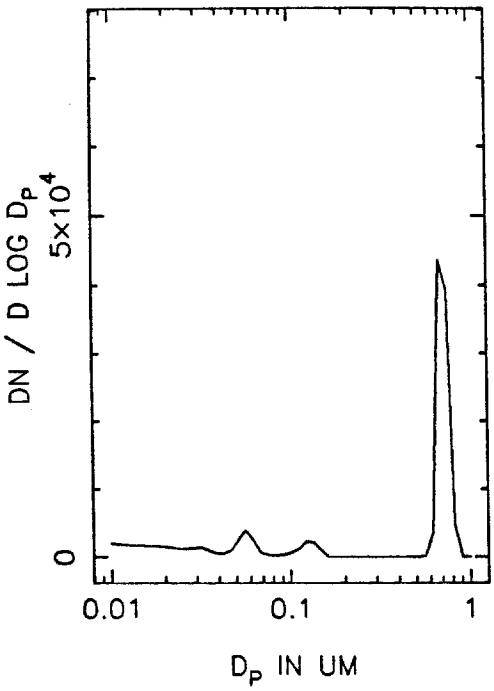

T=5.0 HOURS

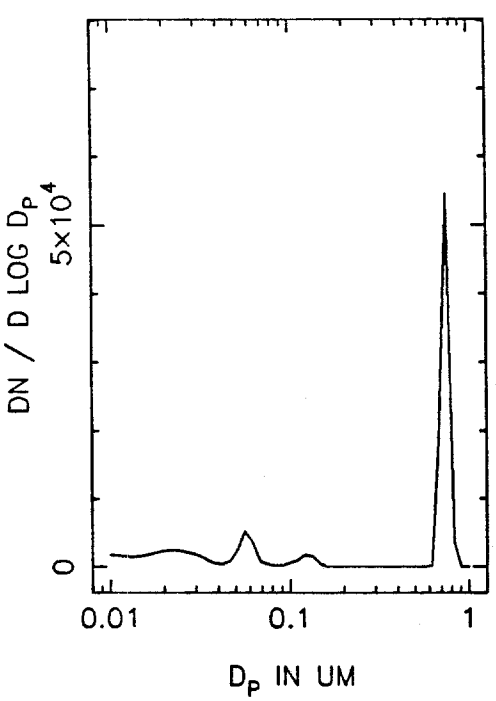

HTMA39 VOLUME DISTRIBUTION, T=0

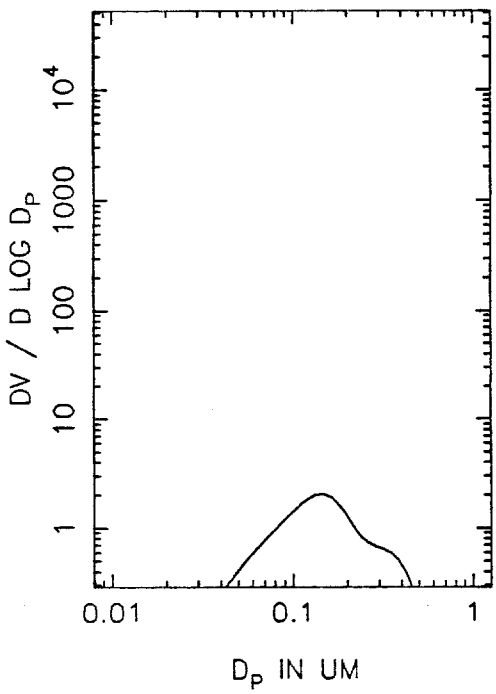

T=0.5 HOURS

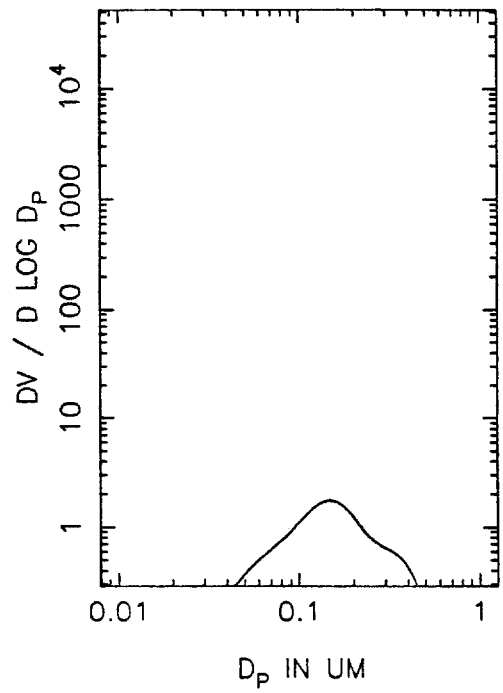

T=1.0 HOURS

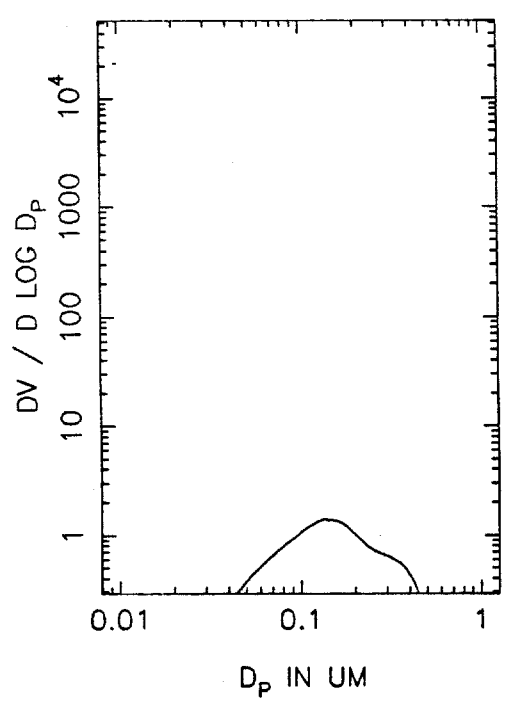

T=1.5 HOURS

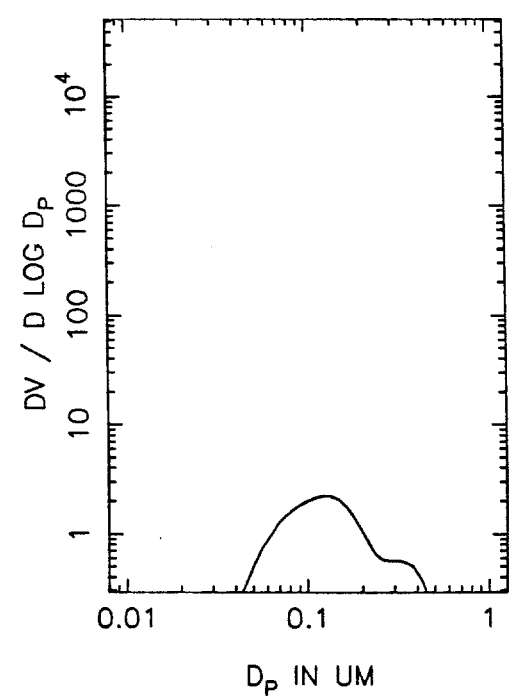

HTMA39 VOLUME DISTRIBUTION, T=2.0

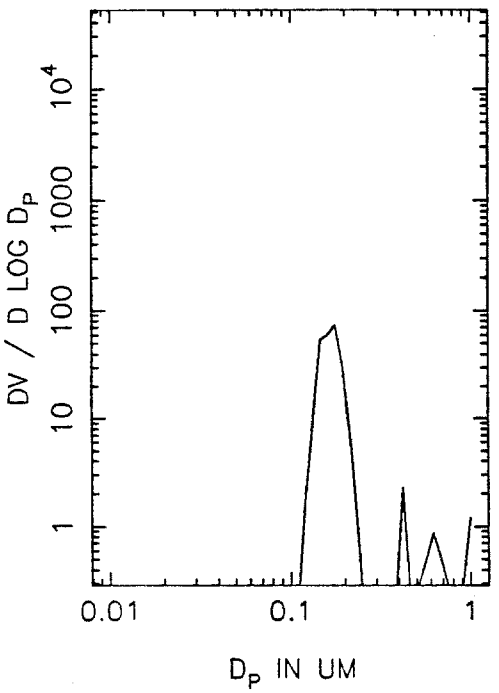

T=2.5 HOURS

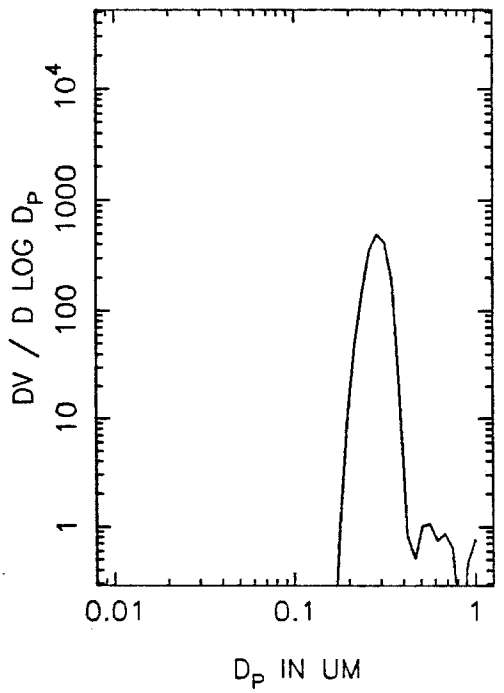

T=3.0 HOURS

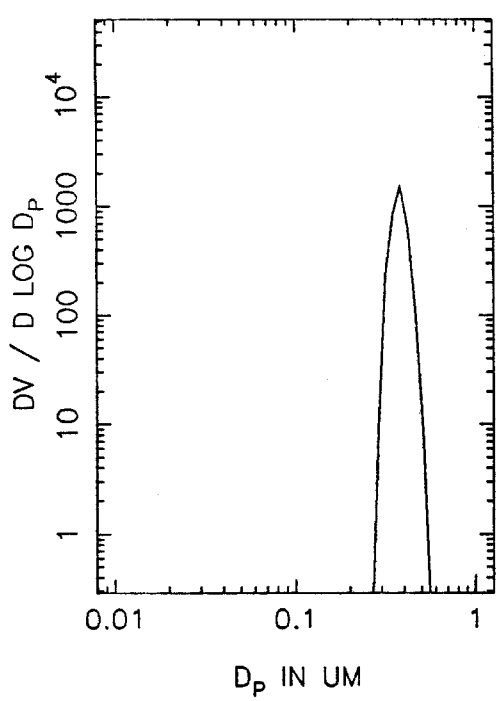

T=3.5 HOURS

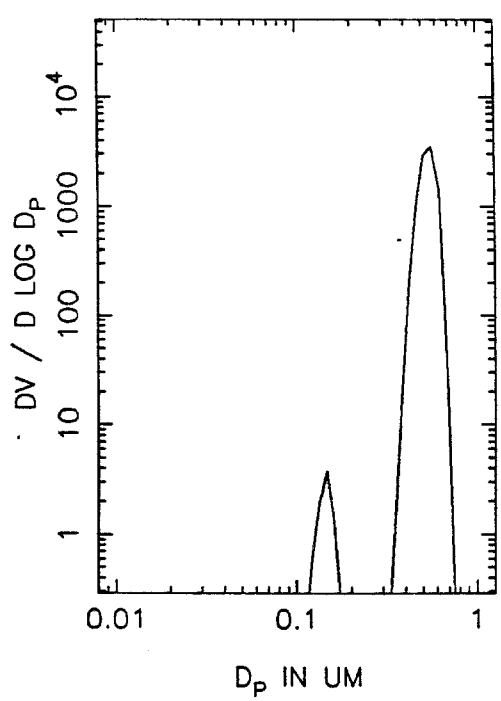

HTMA39 VOLUME DISTRIBUTION, T=4.0

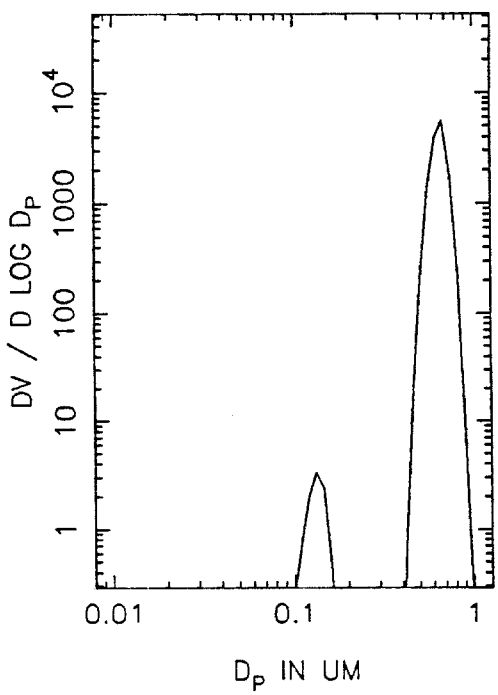

T=4.5 HOURS

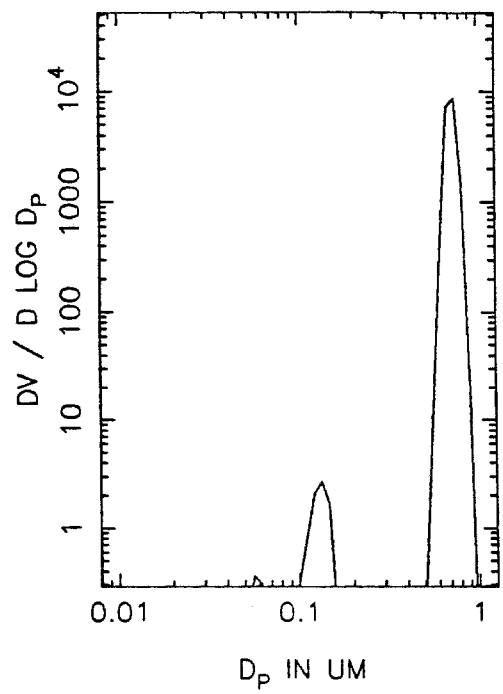

T=5.0 HOURS

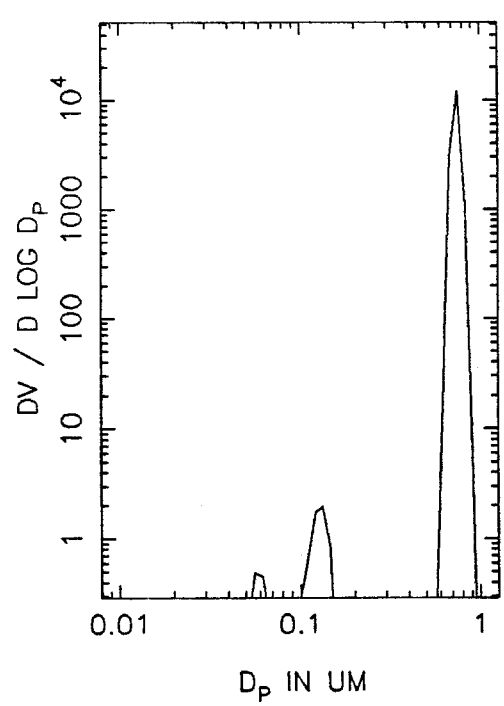

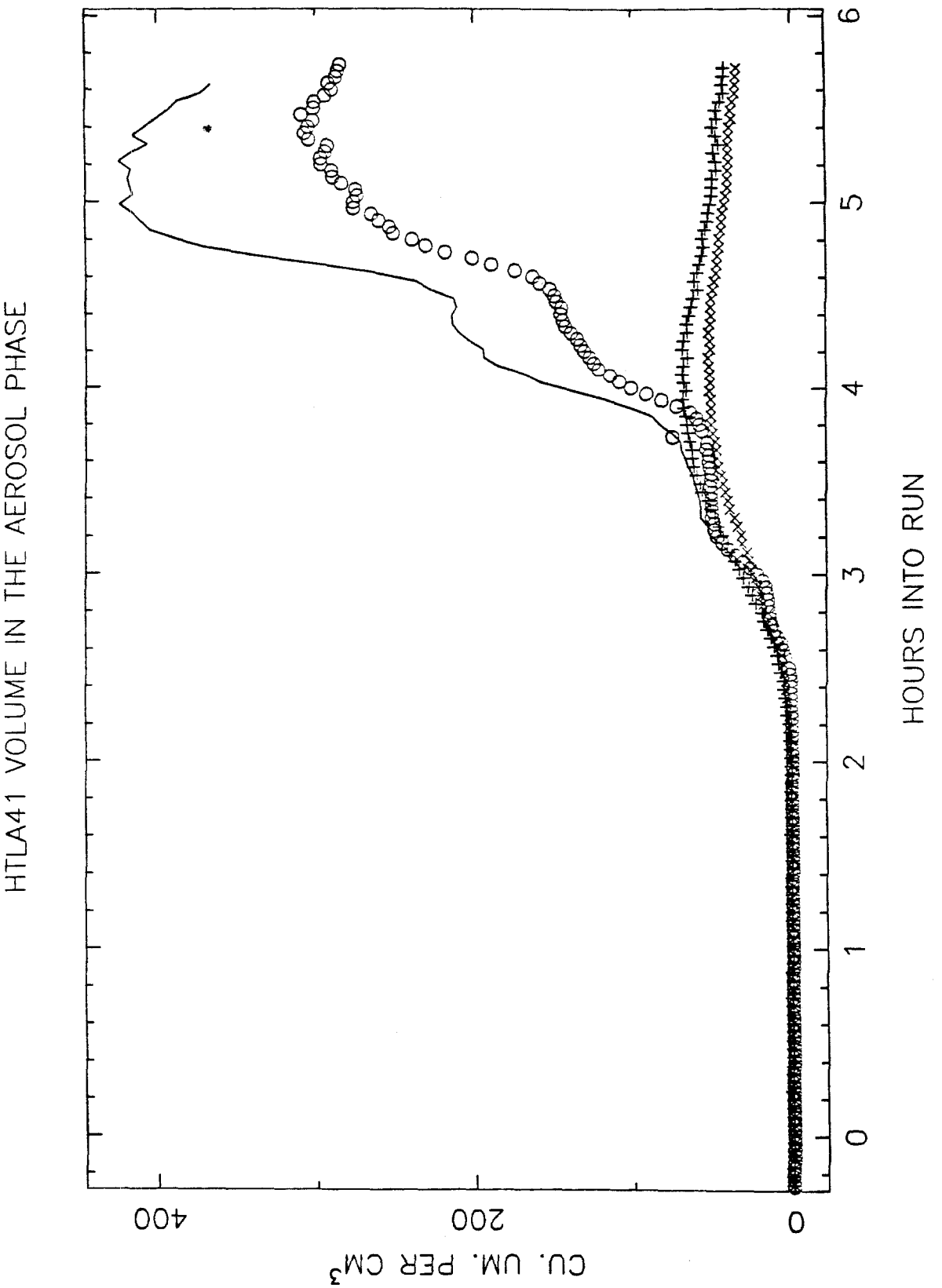
HTLA41 VOLUME IN THE AEROSOL PHASE
CU. UM. PER CM^3
0
200
400
0
1
2
3
4
5
6
HOURS INTO RUN

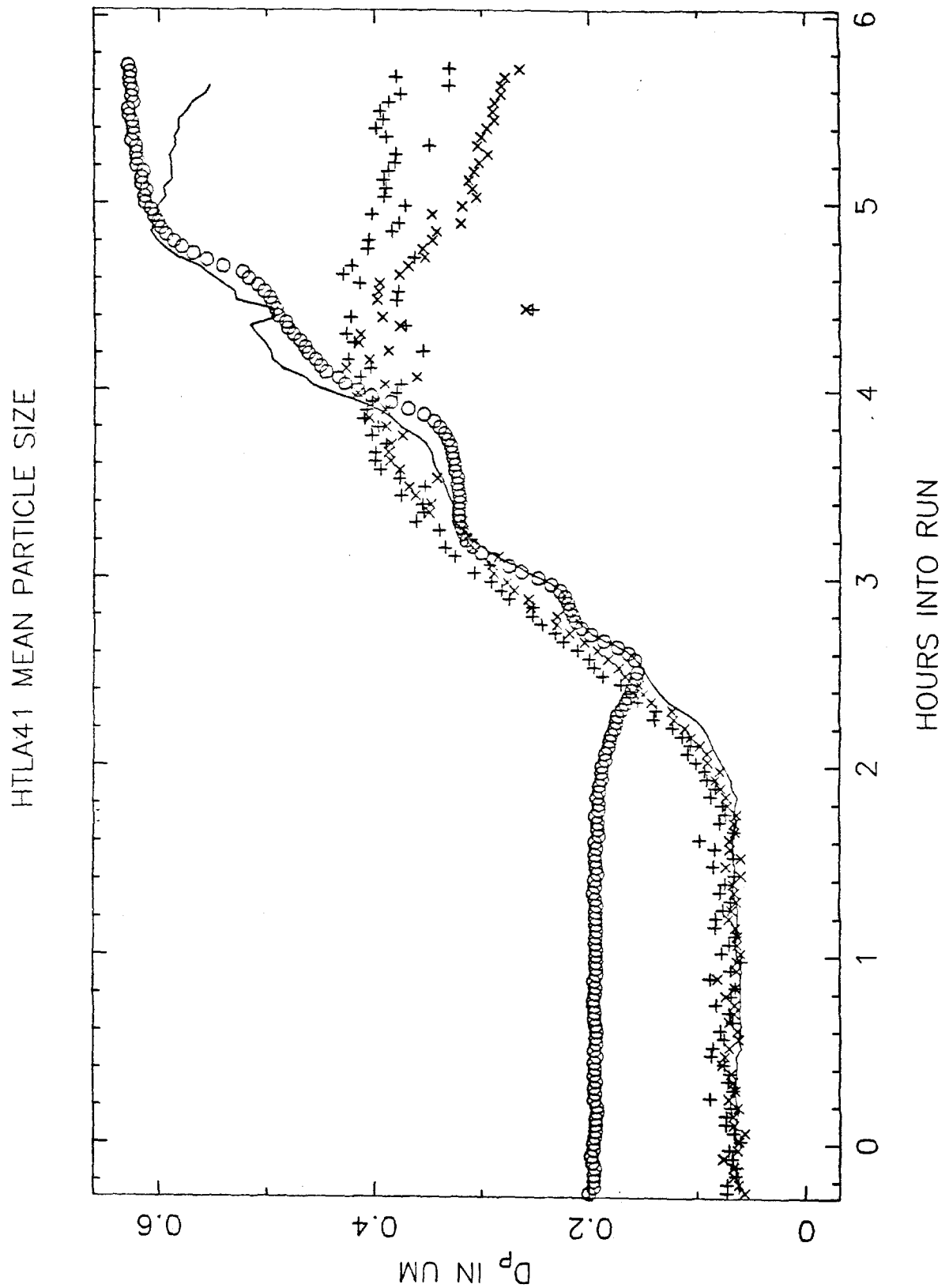
HTLA41 MEAN PARTICLE SIZE
D_p IN UM
0
0.2
0.4
0.6
HOURS INTO RUN
0
1
2
3
4
5
6

HTLA41 NUMBER DISTRIBUTION, T=0

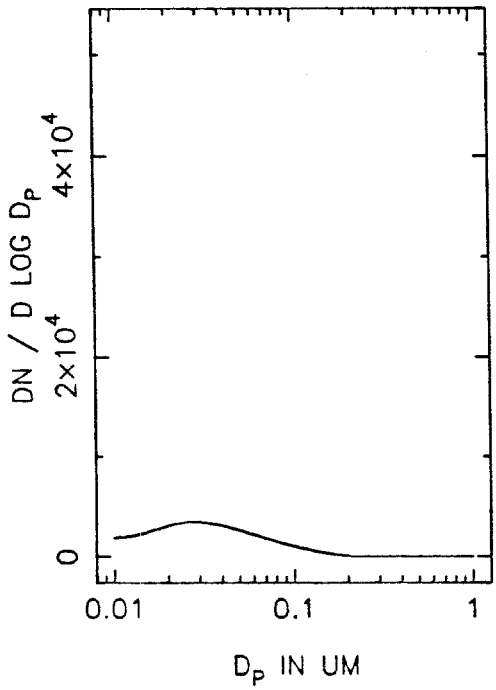

T=0.5 HOURS

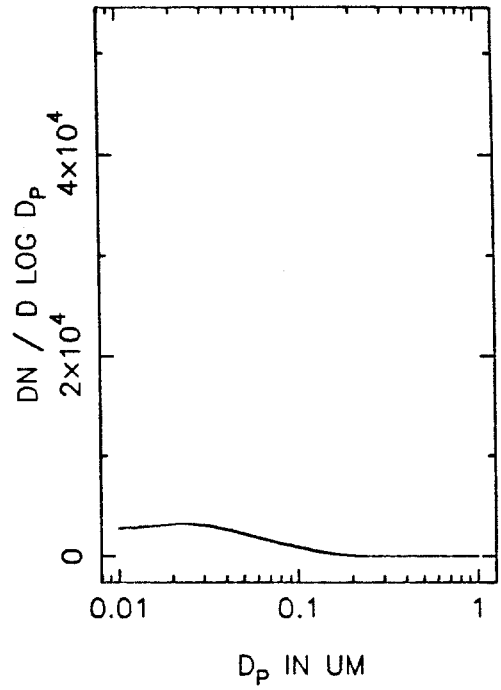

T=1.0 HOURS

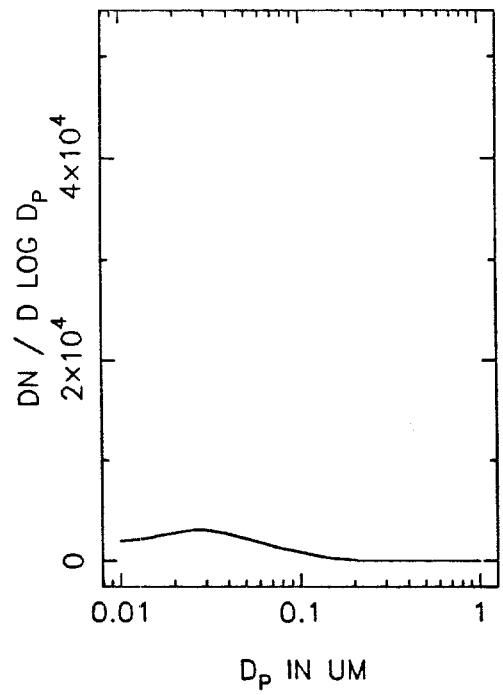

T=1.5 HOURS

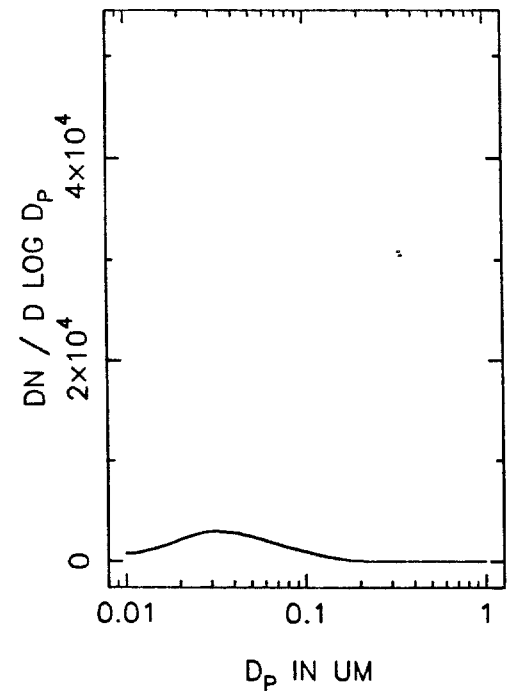

HTLA41 NUMBER DISTRIBUTION, T=2.0

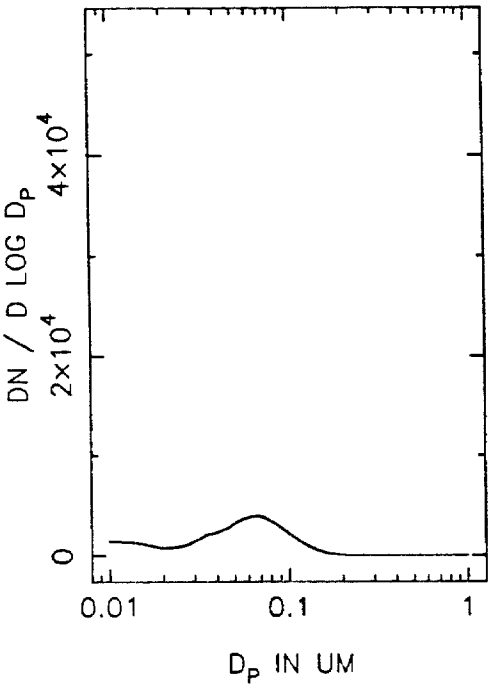

T=2.5 HOURS

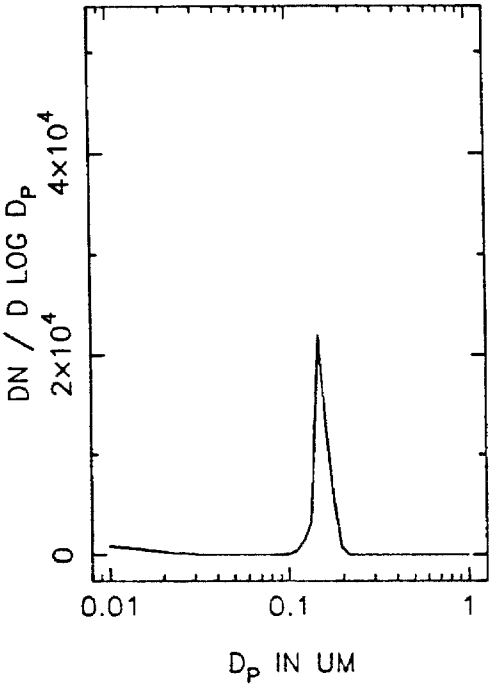

T=3.0 HOURS

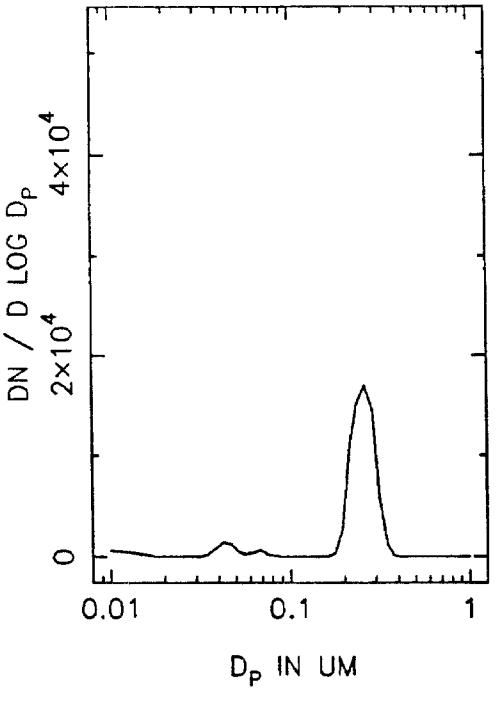

T=3.5 HOURS

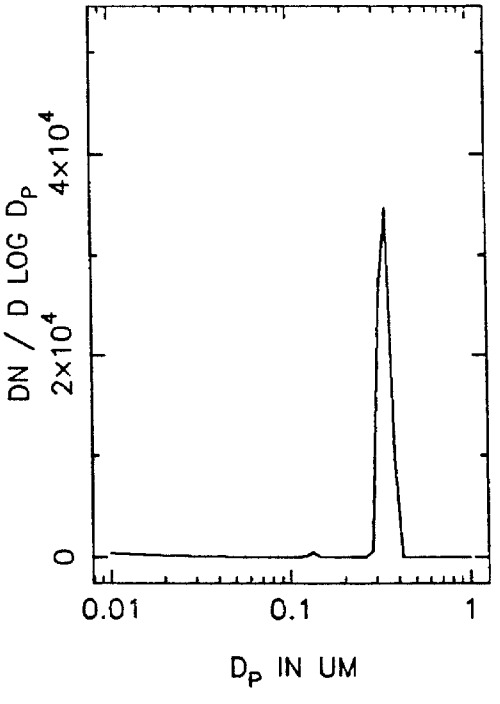

HTLA41 NUMBER DISTRIBUTION, T=4.0

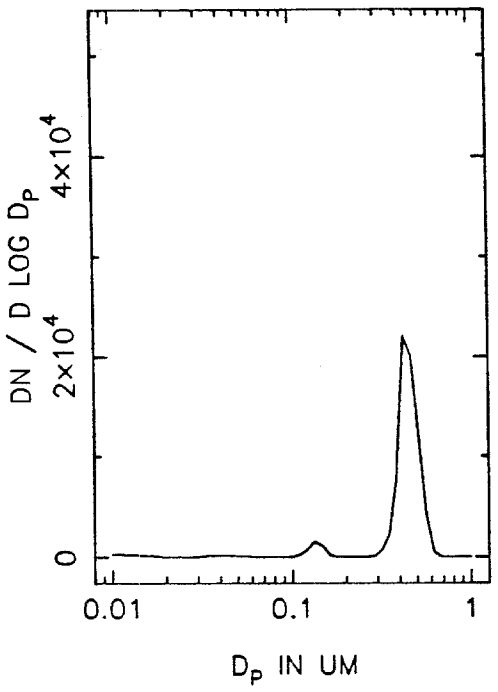

T=4.5 HOURS

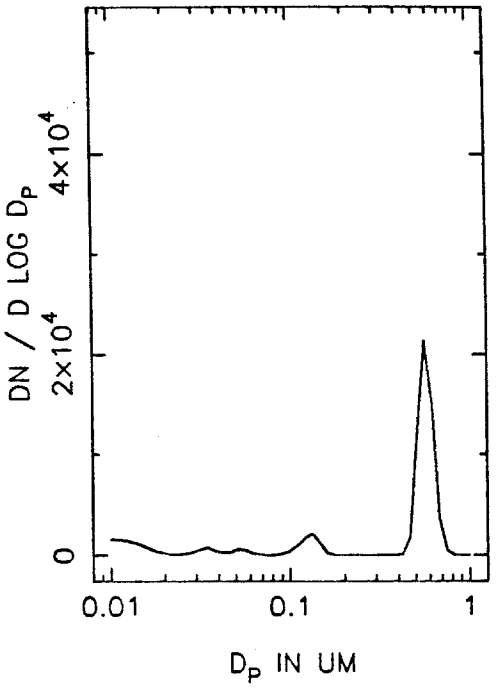

T=5.0 HOURS

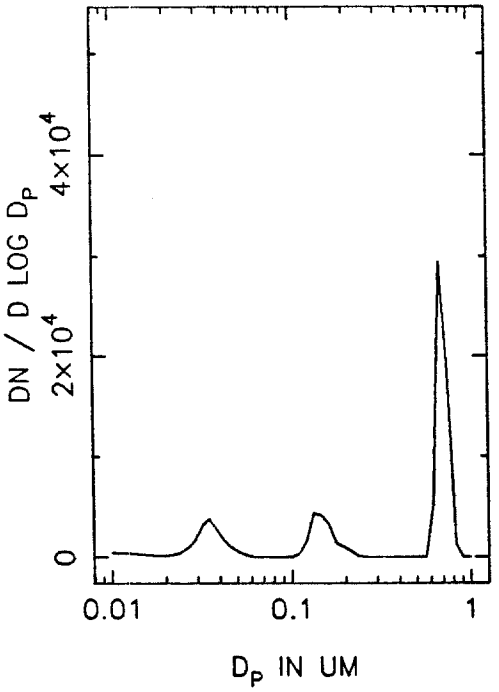

T=5.5 HOURS

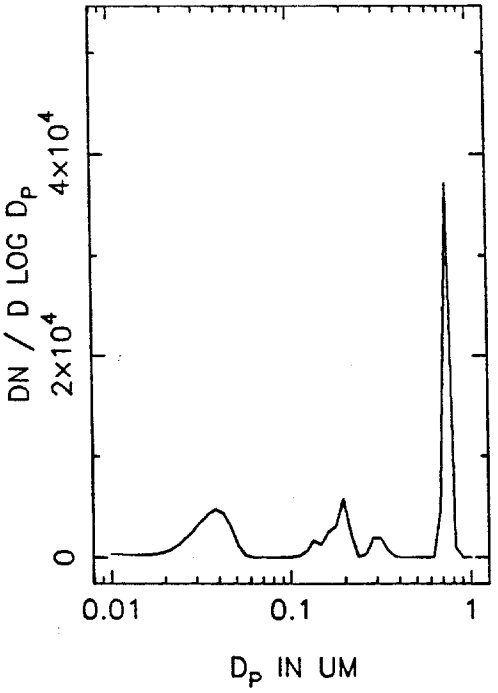

HTLA41 VOLUME DISTRIBUTION, T=0

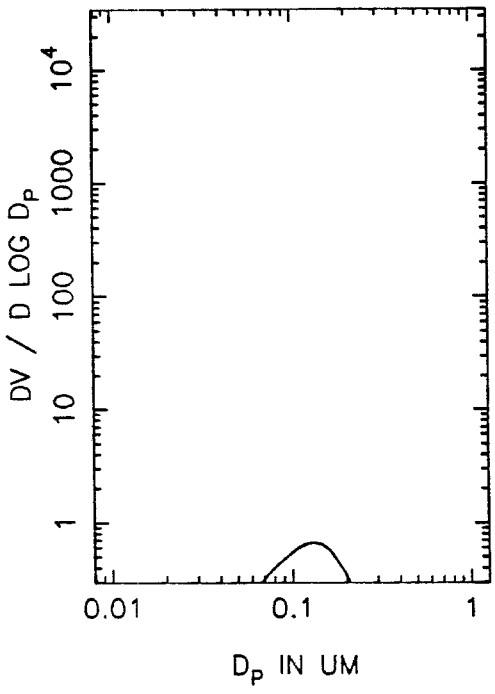

T=0.5 HOURS

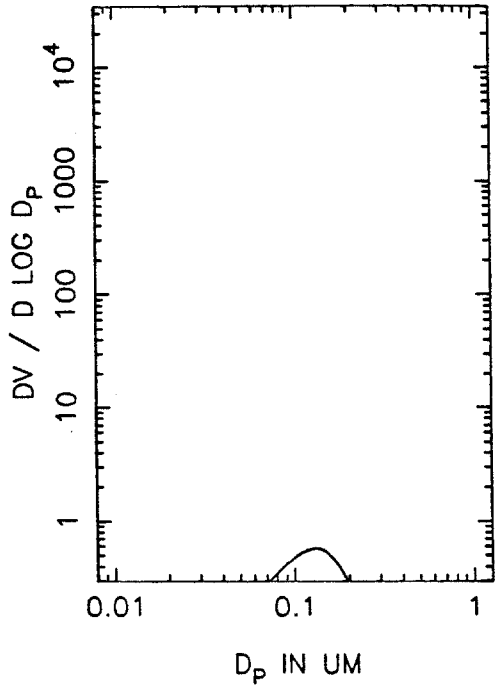

T=1.0 HOURS

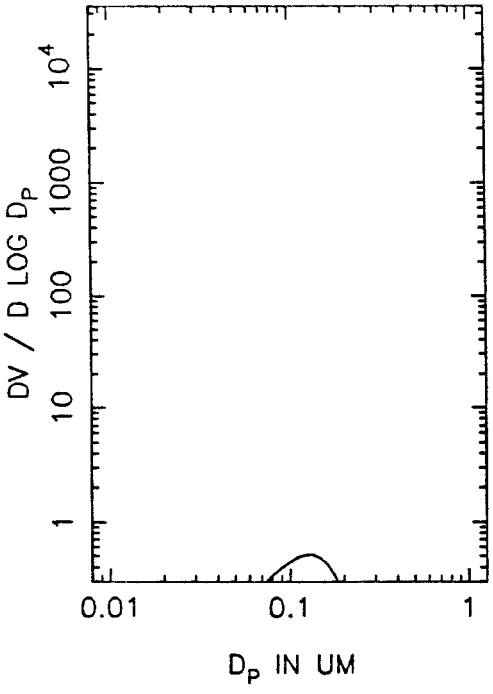

T=1.5 HOURS

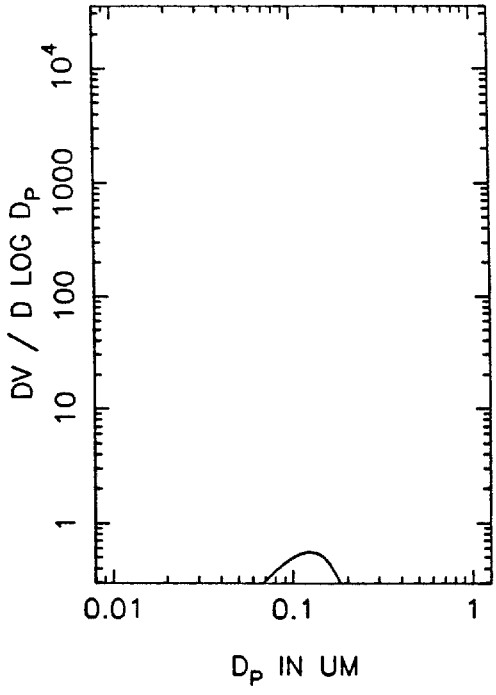

HTLA41 VOLUME DISTRIBUTION, T=2.0

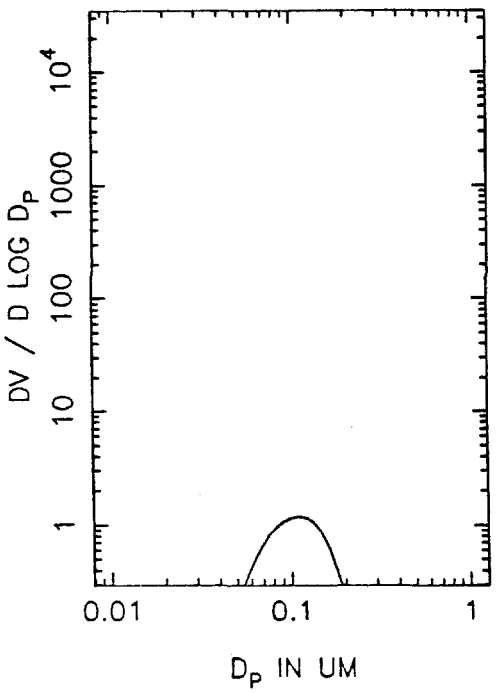

T=2.5 HOURS

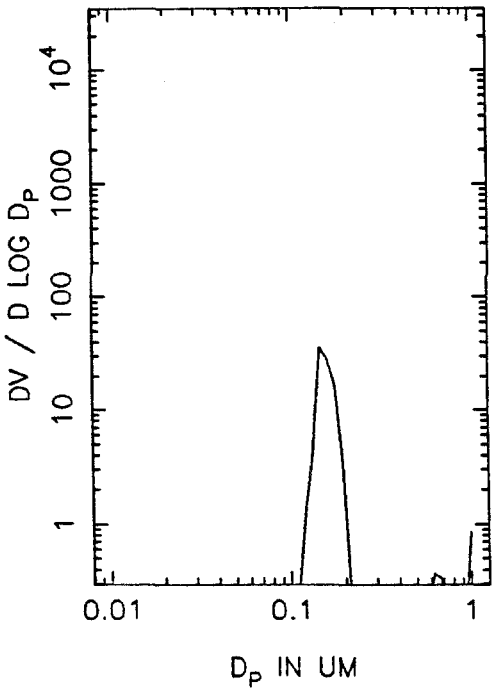

T=3.0 HOURS

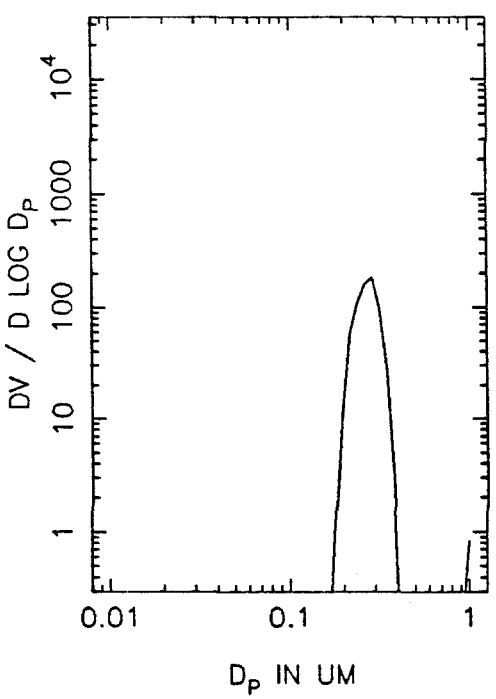

T=3.5 HOURS

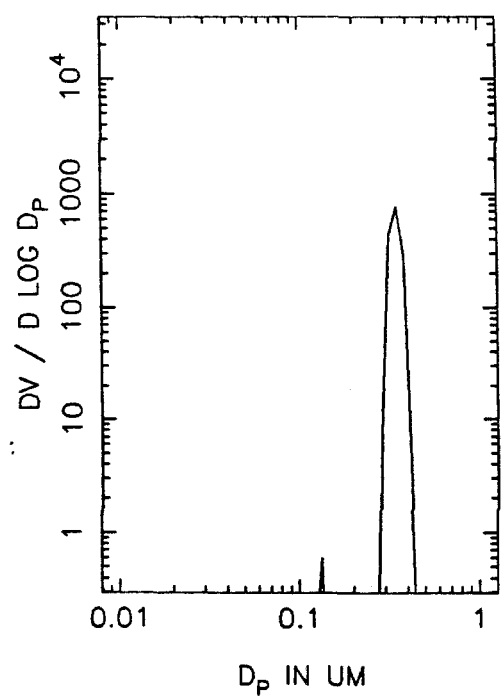

HTLA41 VOLUME DISTRIBUTION, T=4.0

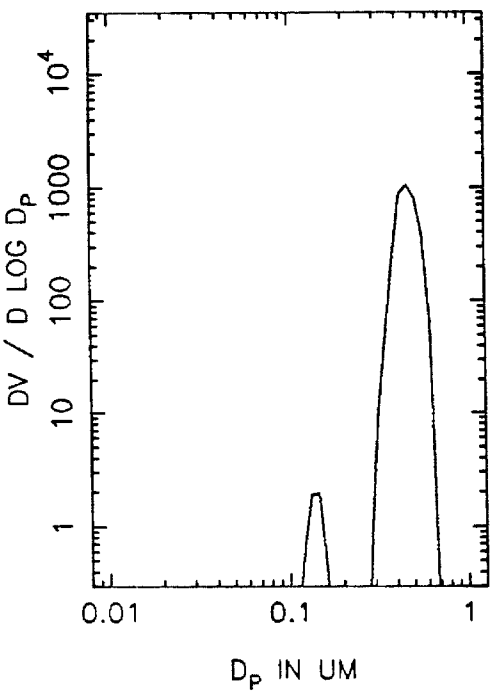

T=4.5 HOURS

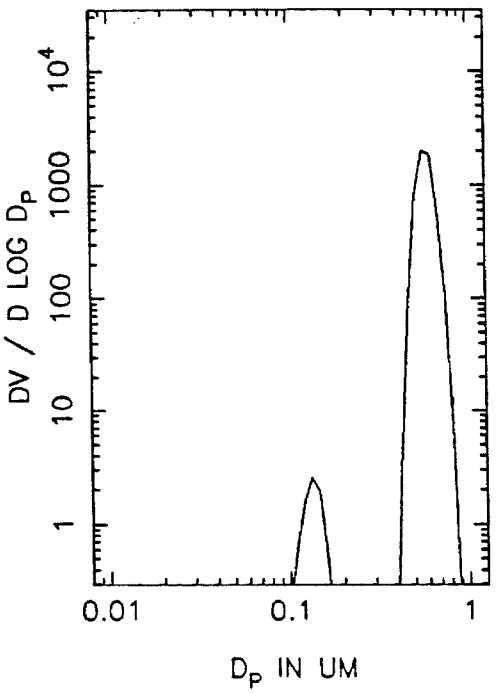

T=5.0 HOURS

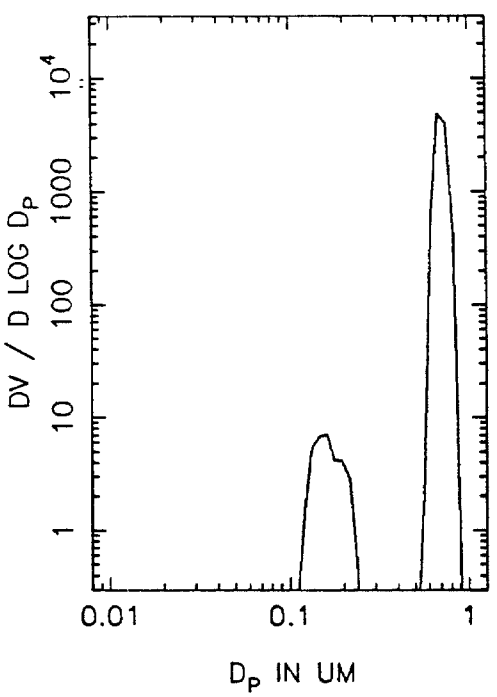

T=5.5 HOURS

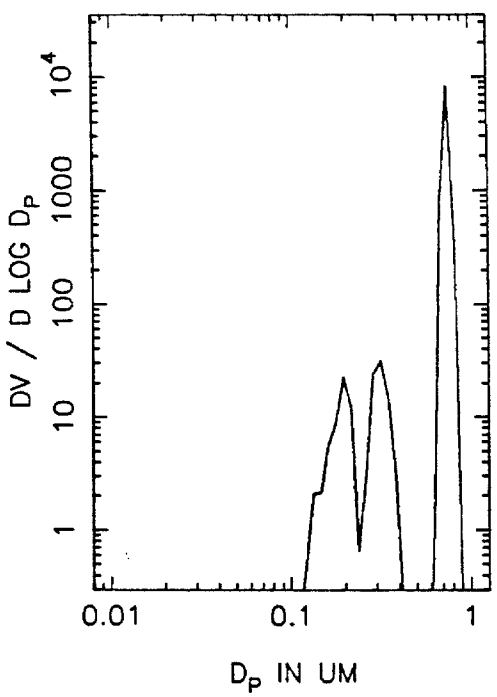

DHNA43 TOTAL NUMBER, SIDE A

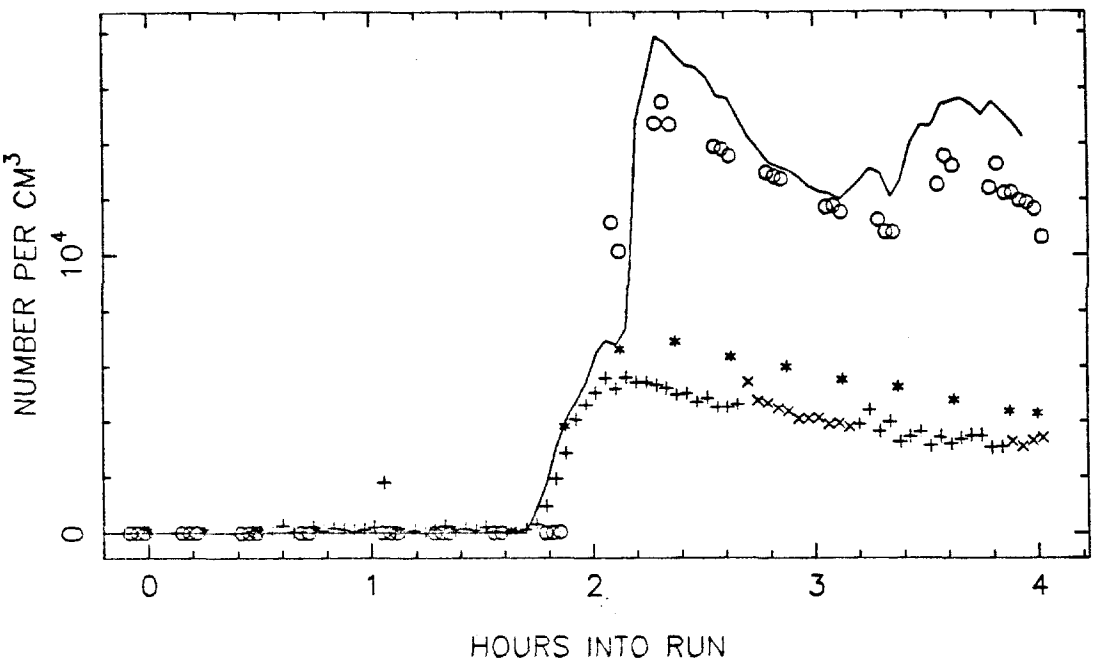

SIDE B

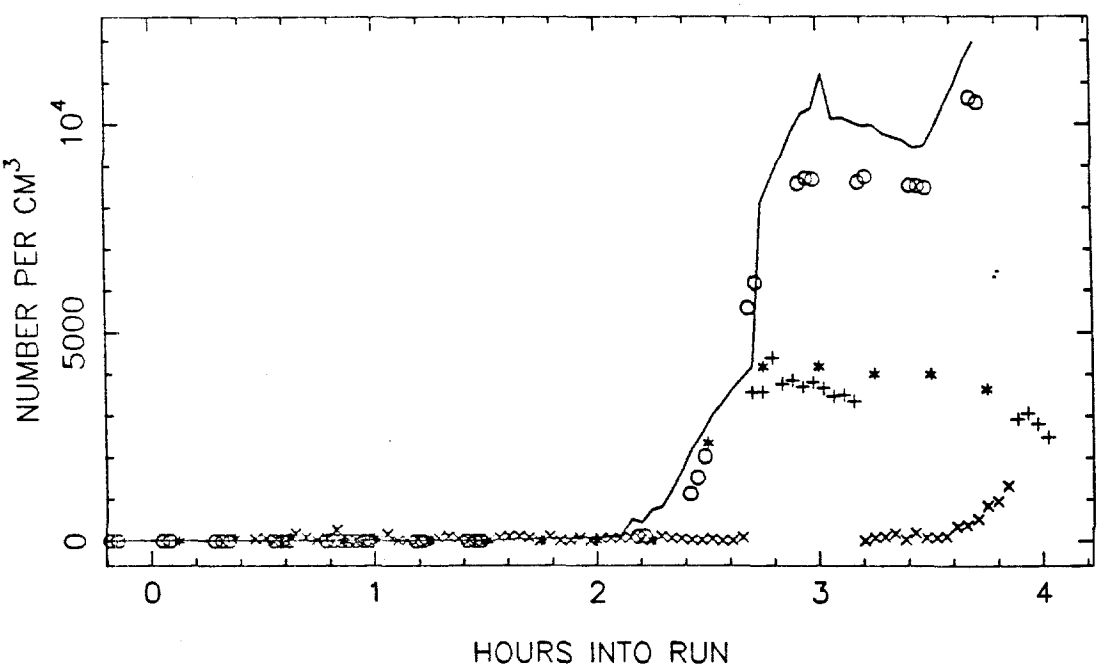

DHNA43 VOLUME IN THE AEROSOL PHASE, SIDE A

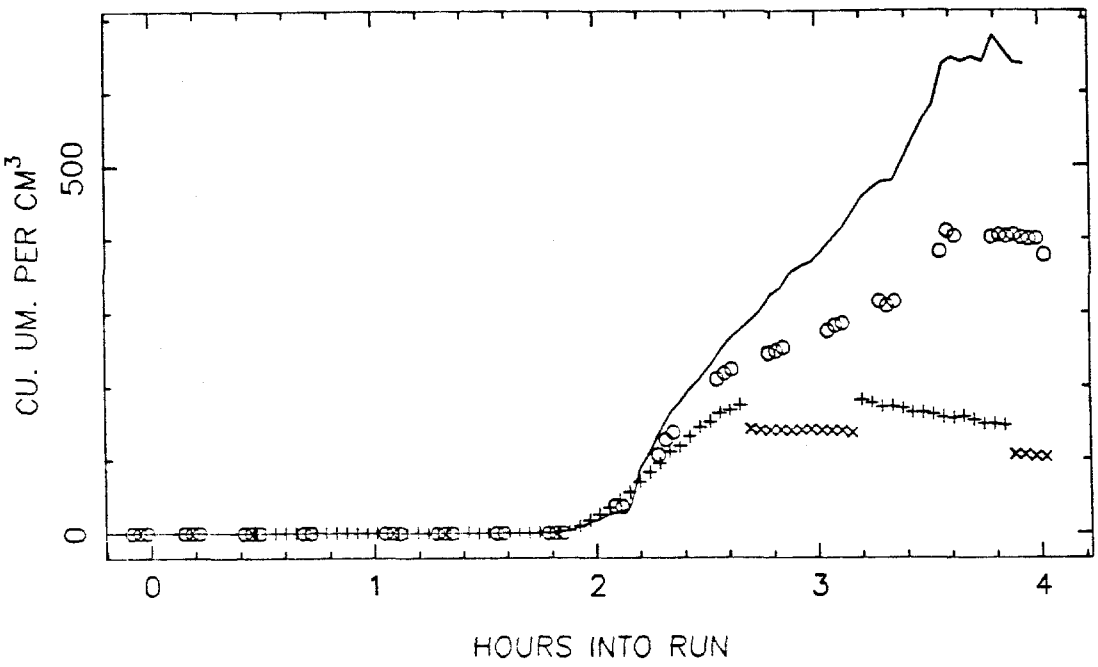

SIDE B

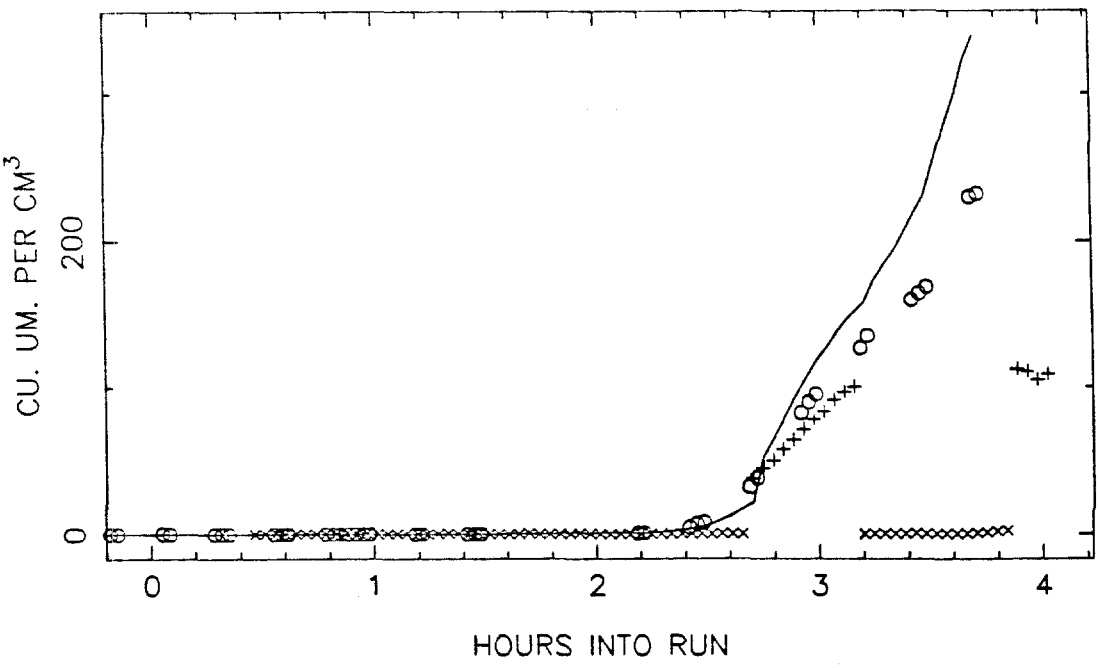

DHNA43 MEAN PARTICLE SIZE, SIDE A

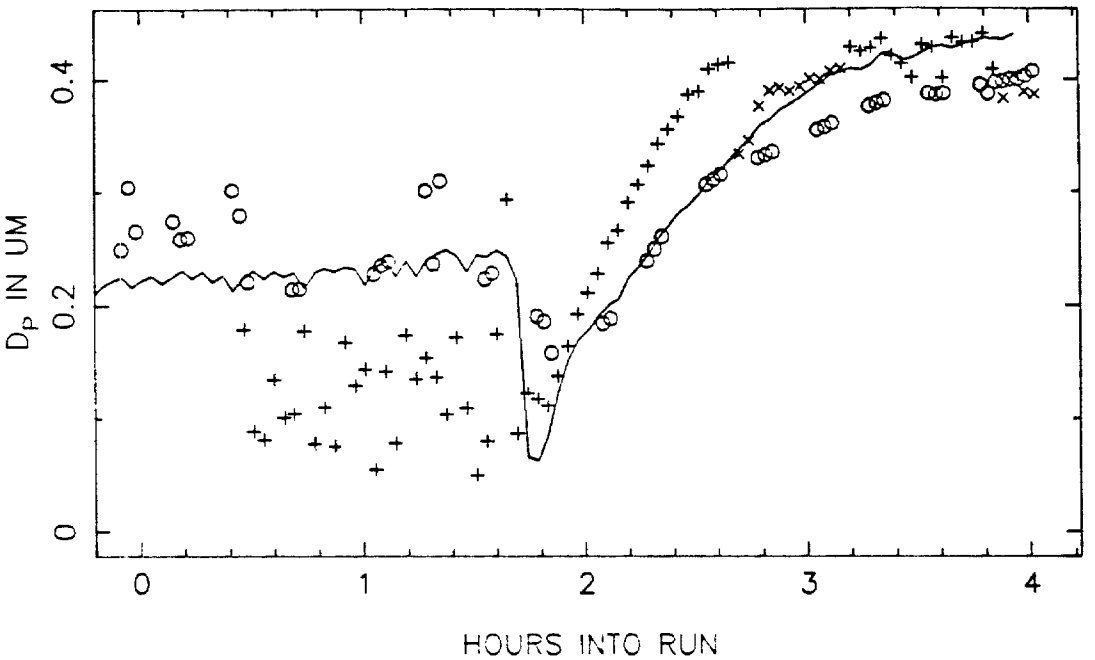

SIDE B

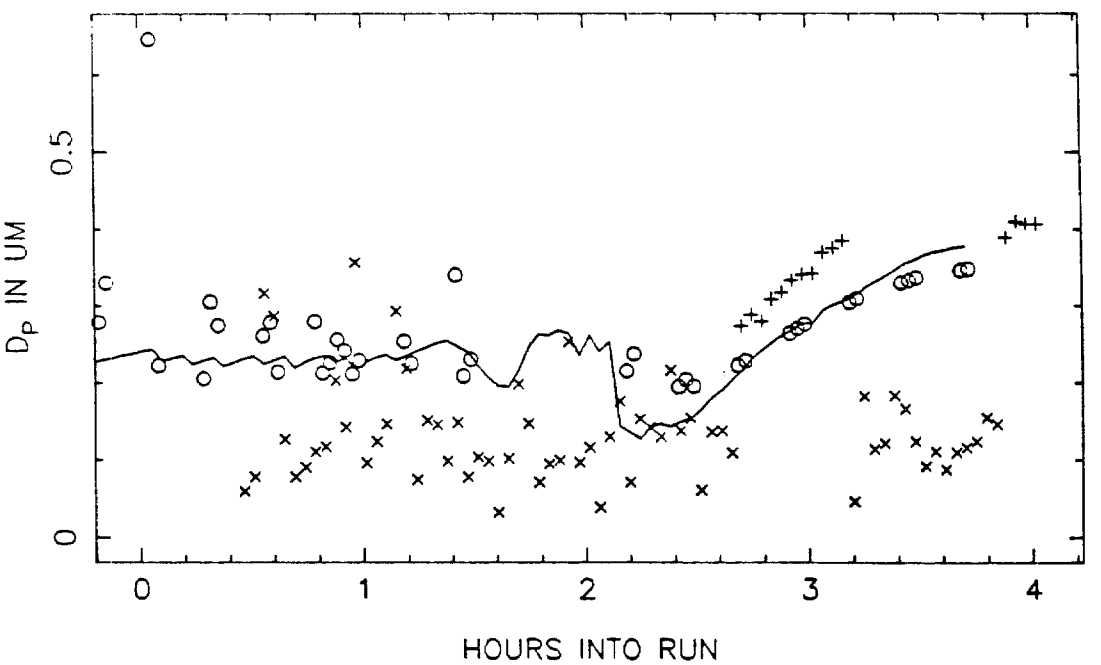

DHNA43A NUMBER DISTRIBUTION, T=0

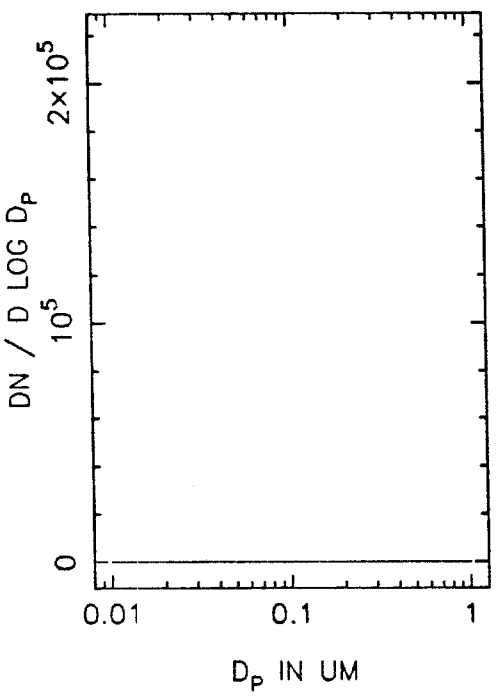

T=0.5 HOURS

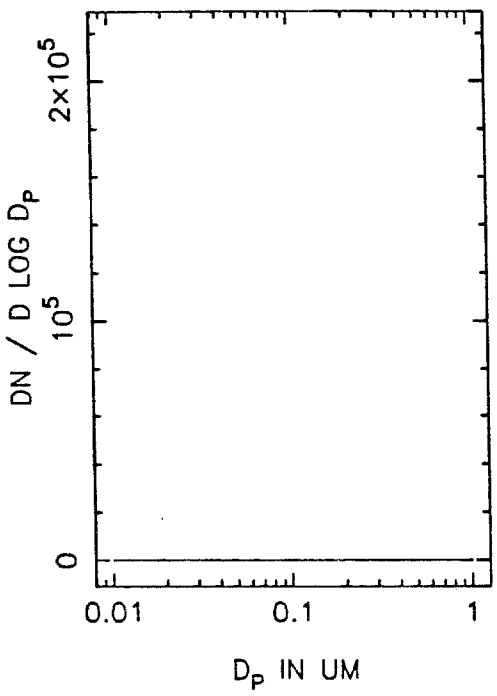

T=1.0 HOURS

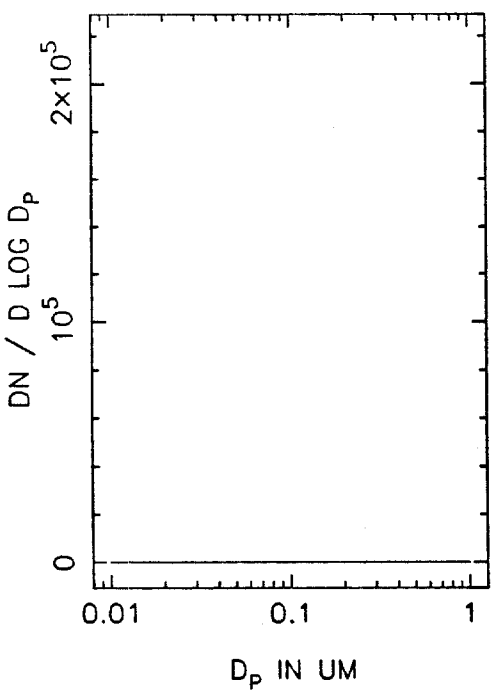

T=1.5 HOURS

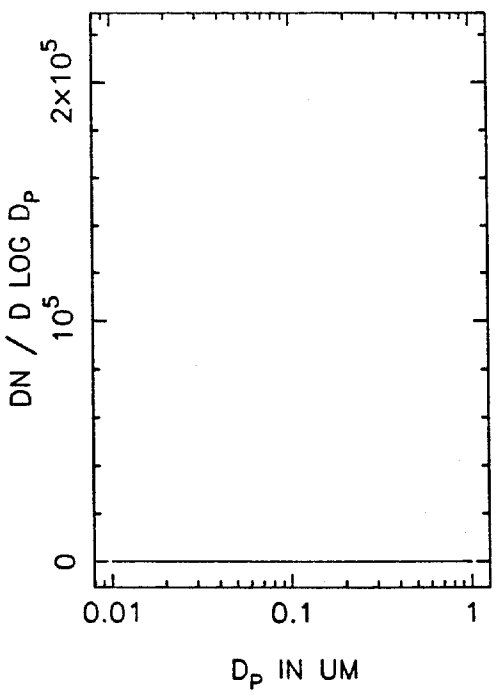

DHNA43A NUMBER DISTRIBUTION, T=2.0

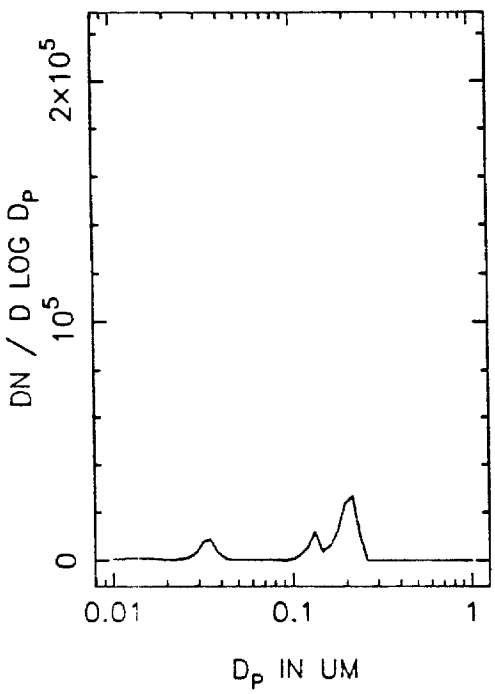

T=2.5 HOURS

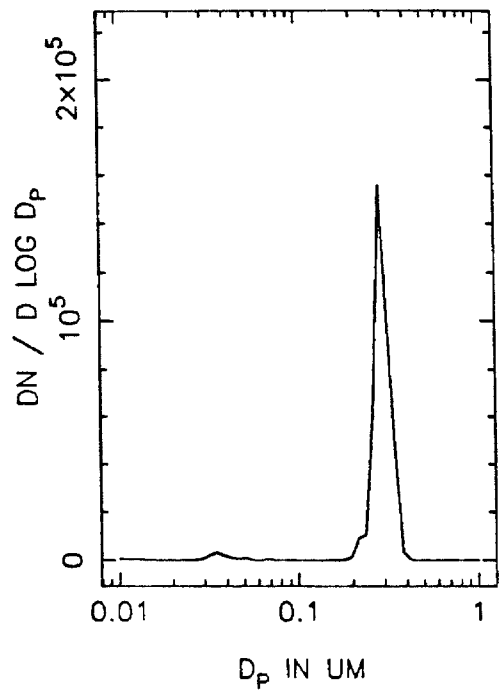

T=3.0 HOURS

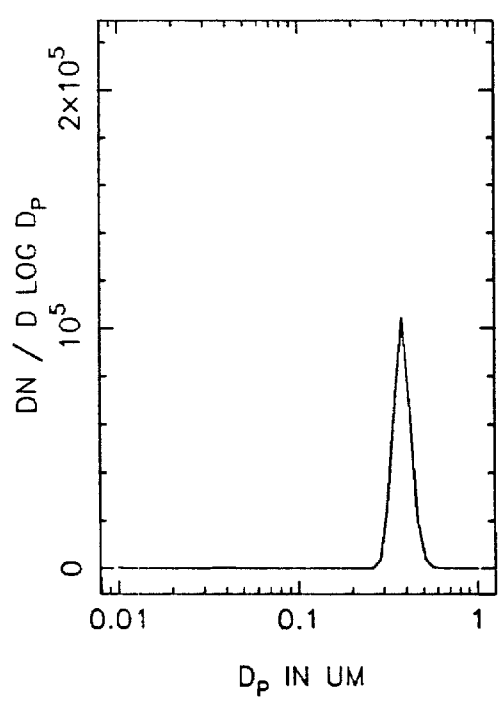

T=3.5 HOURS

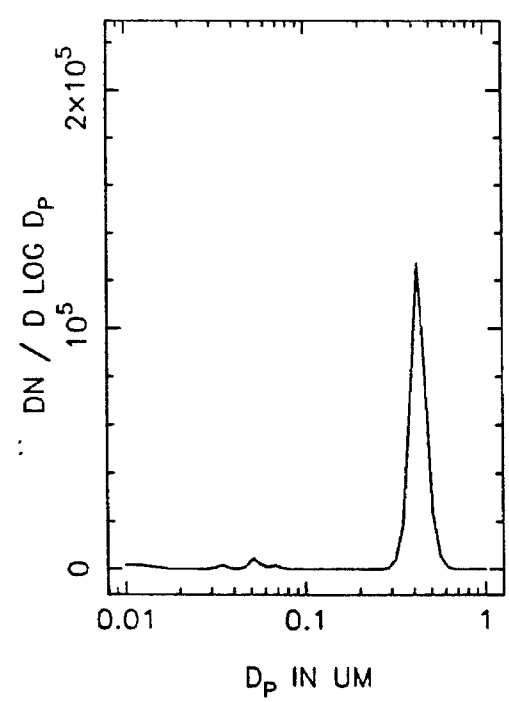

DHNA43A VOLUME DISTRIBUTION, T=0

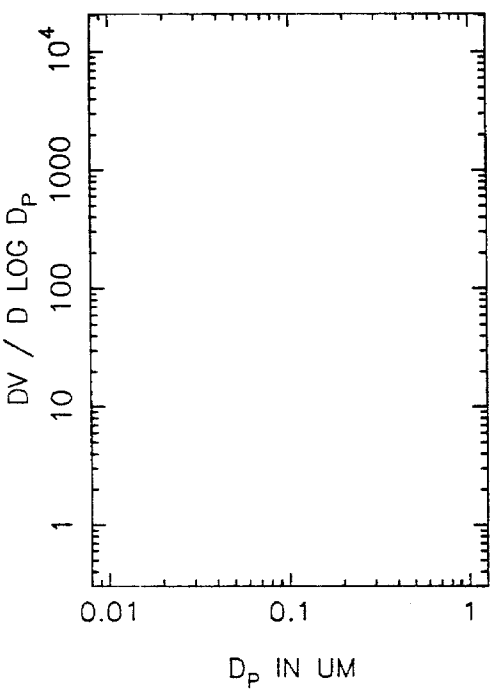

T=0.5 HOURS

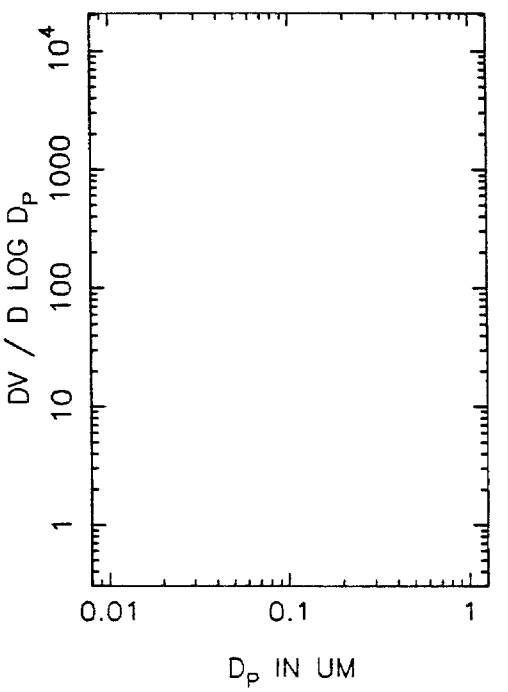

T=1.0 HOURS

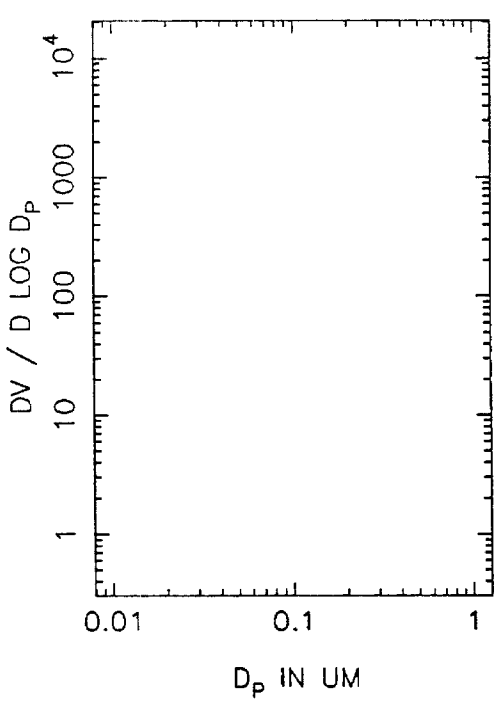

T=1.5 HOURS

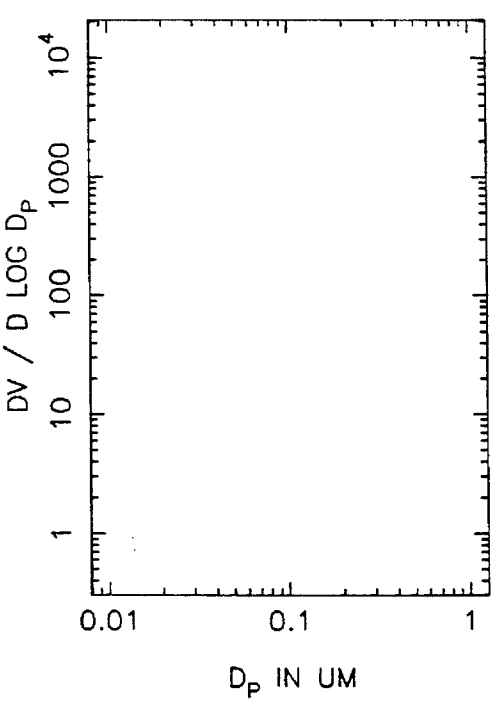

DHNA43A VOLUME DISTRIBUTION, T=2.0

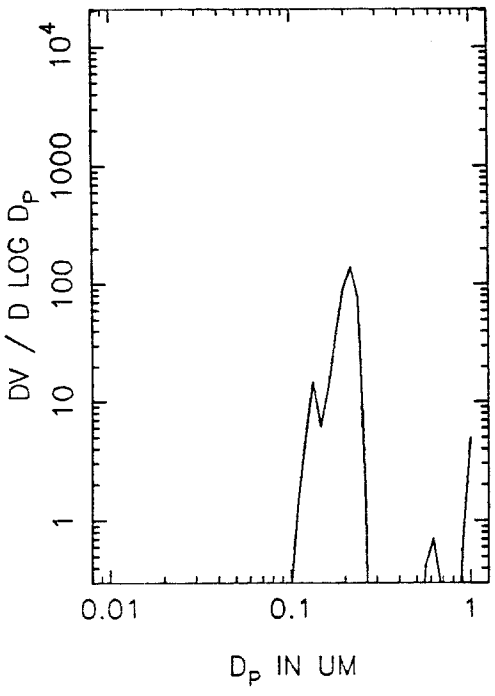

T=2.5 HOURS

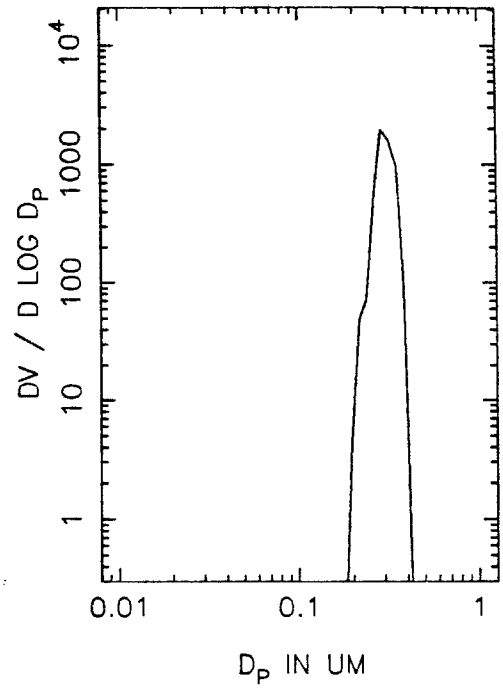

T=3.0 HOURS

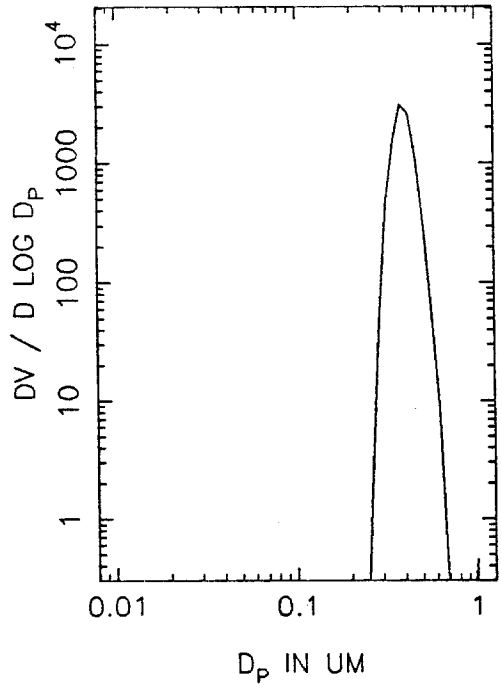

T=3.5 HOURS

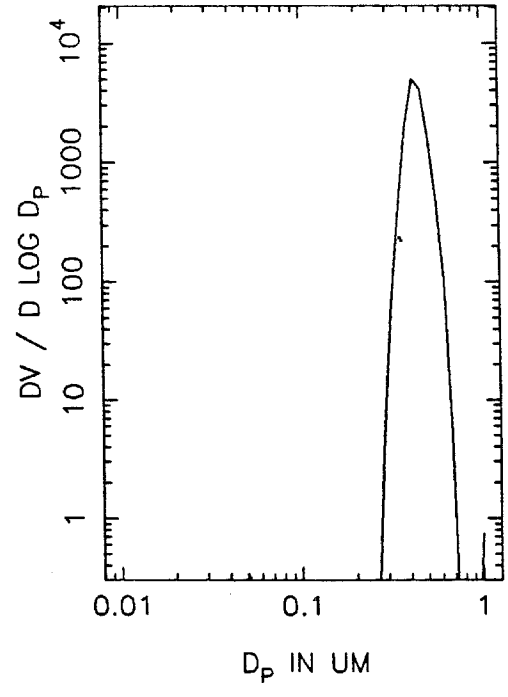

DHNA43B NUMBER DISTRIBUTION, T=0

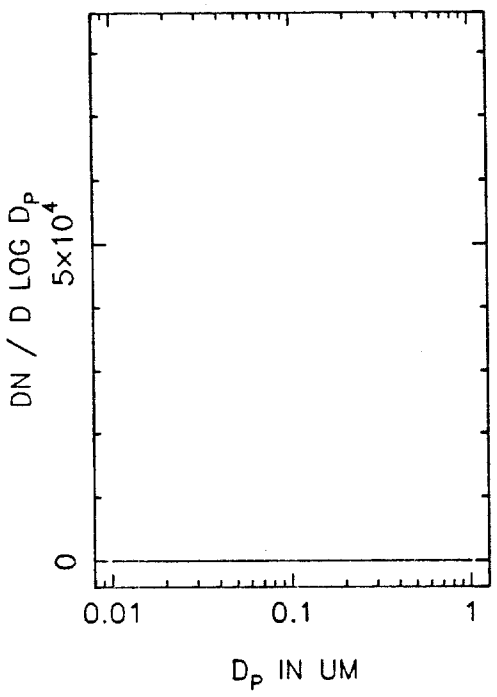

T=0.5 HOURS

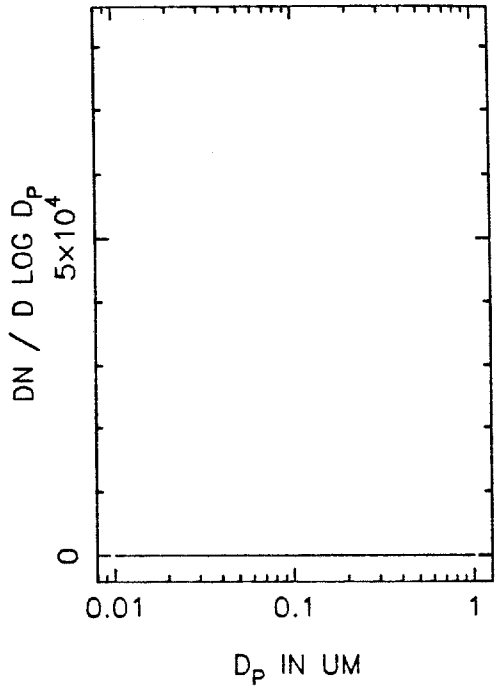

T=1.0 HOURS

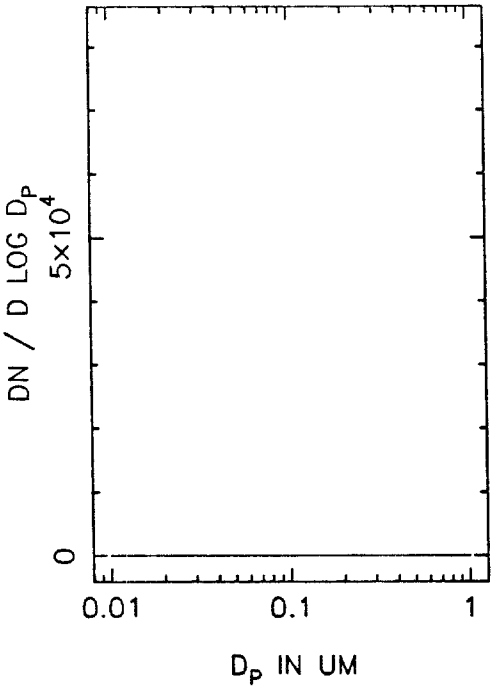

T=1.5 HOURS

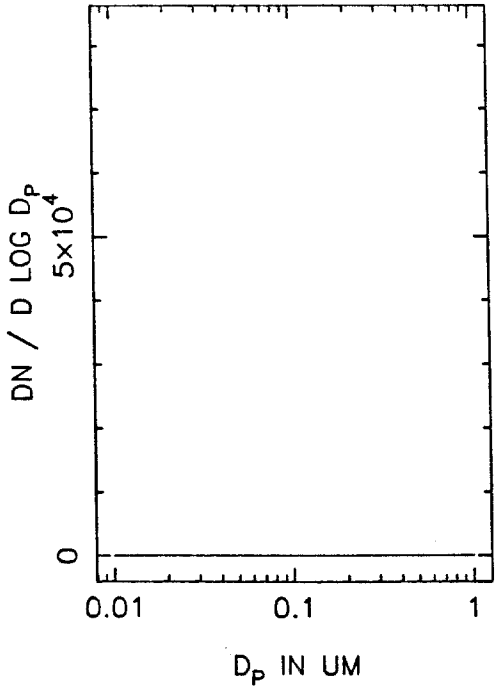

DHNA43B NUMBER DISTRIBUTION, T=2.0

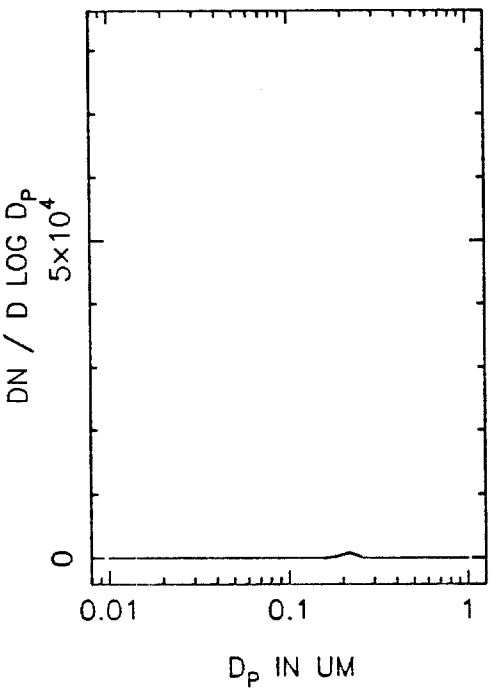

T=2.5 HOURS

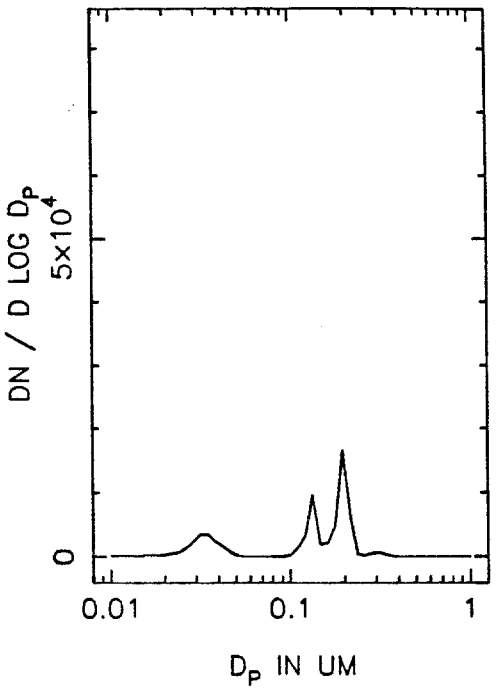

T=3.0 HOURS

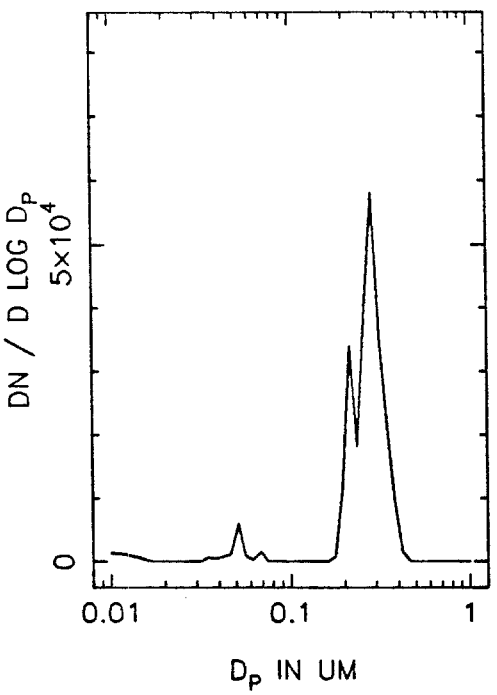

T=3.5 HOURS

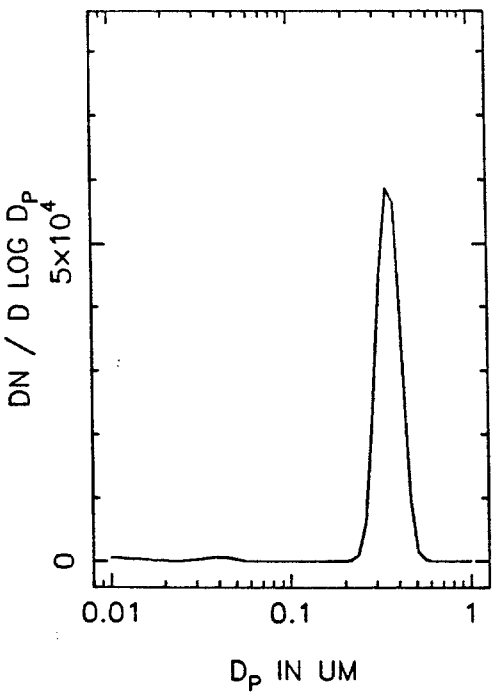

DHNA43B VOLUME DISTRIBUTION, T=0

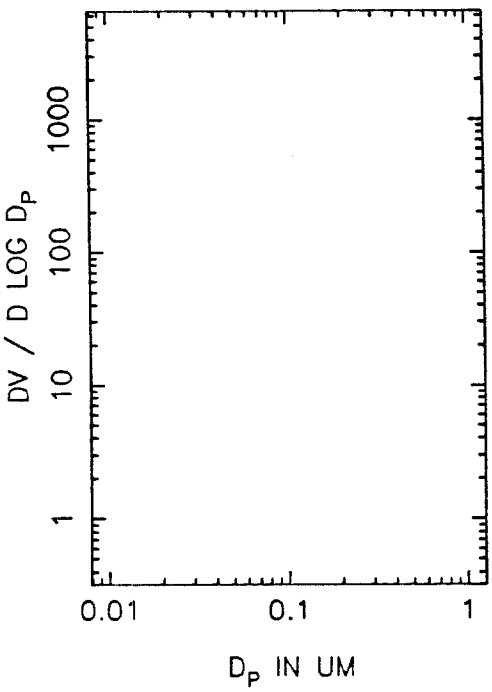

T=0.5 HOURS

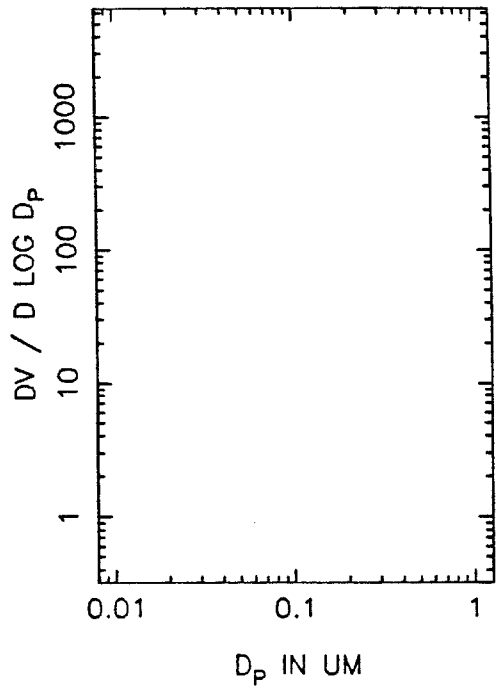

T=1.0 HOURS

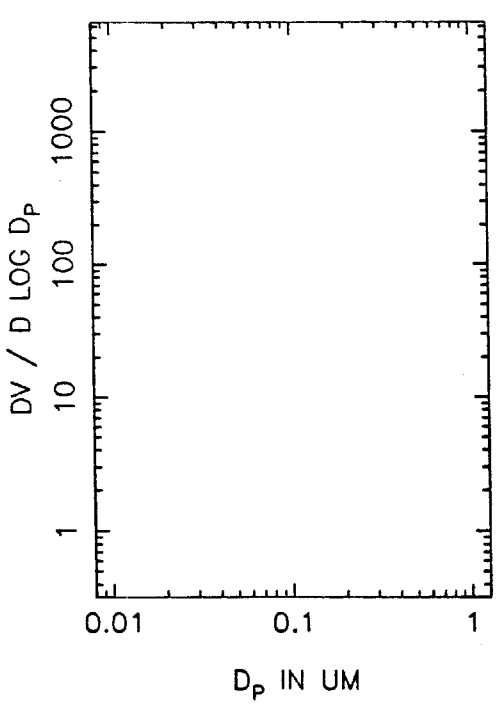

T=1.5 HOURS

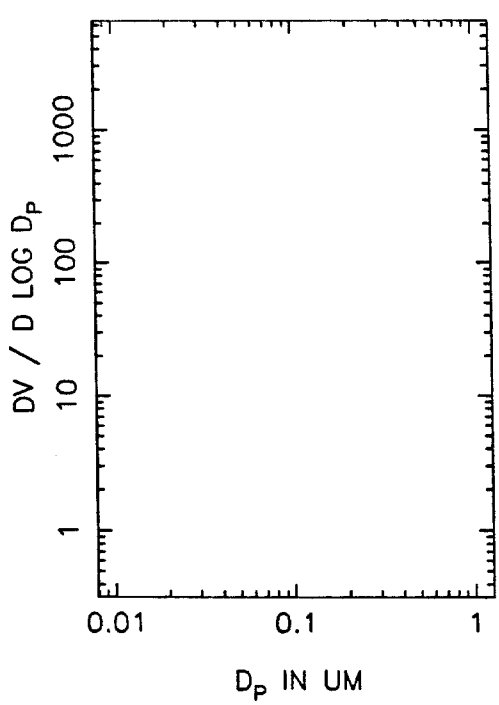

DHNA43B VOLUME DISTRIBUTION, T=2.0

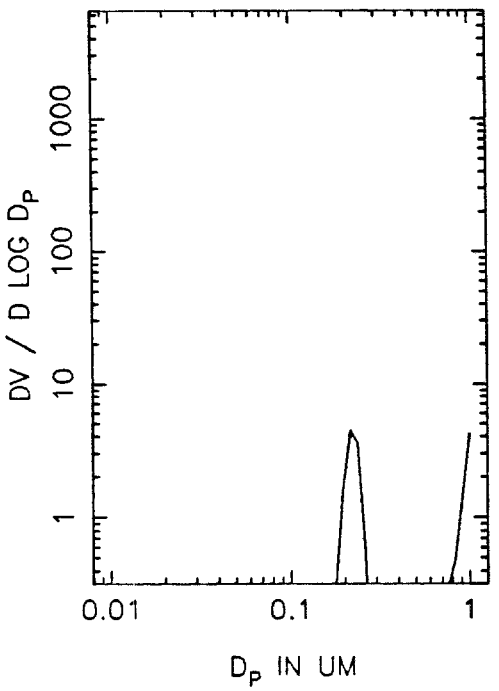

T=2.5 HOURS

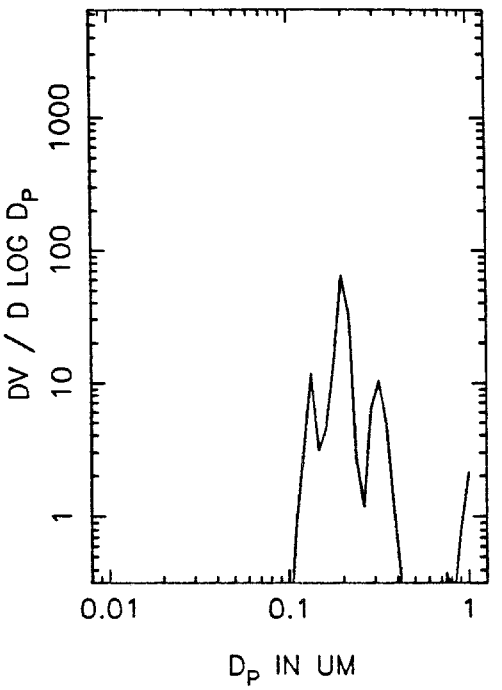

T=3.0 HOURS

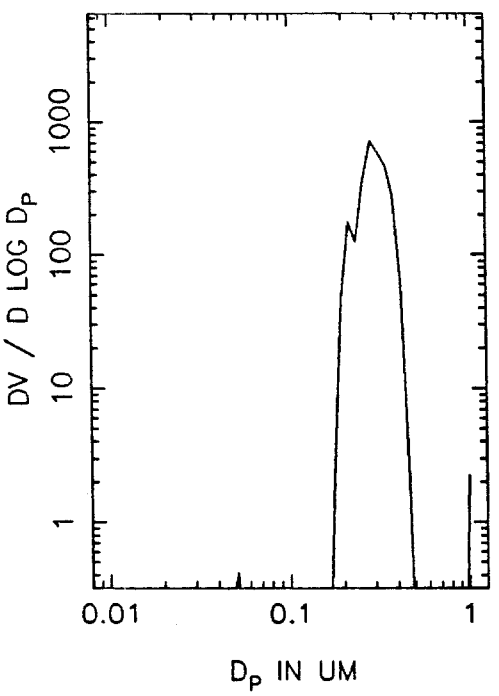

T=3.5 HOURS

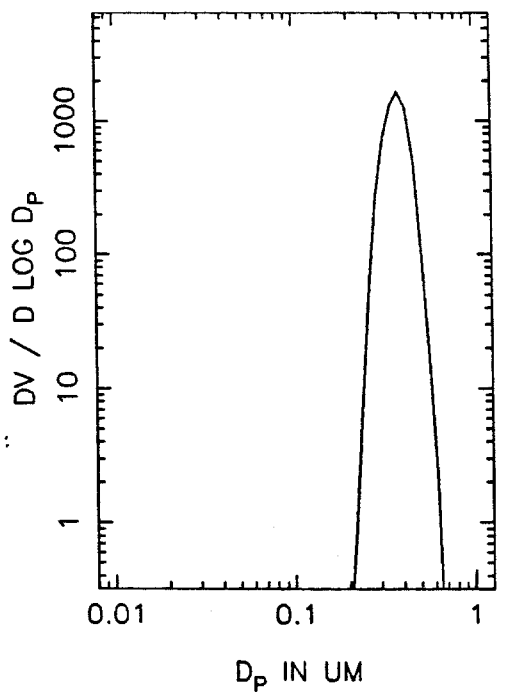

DMMA45 TOTAL NUMBER, SIDE A

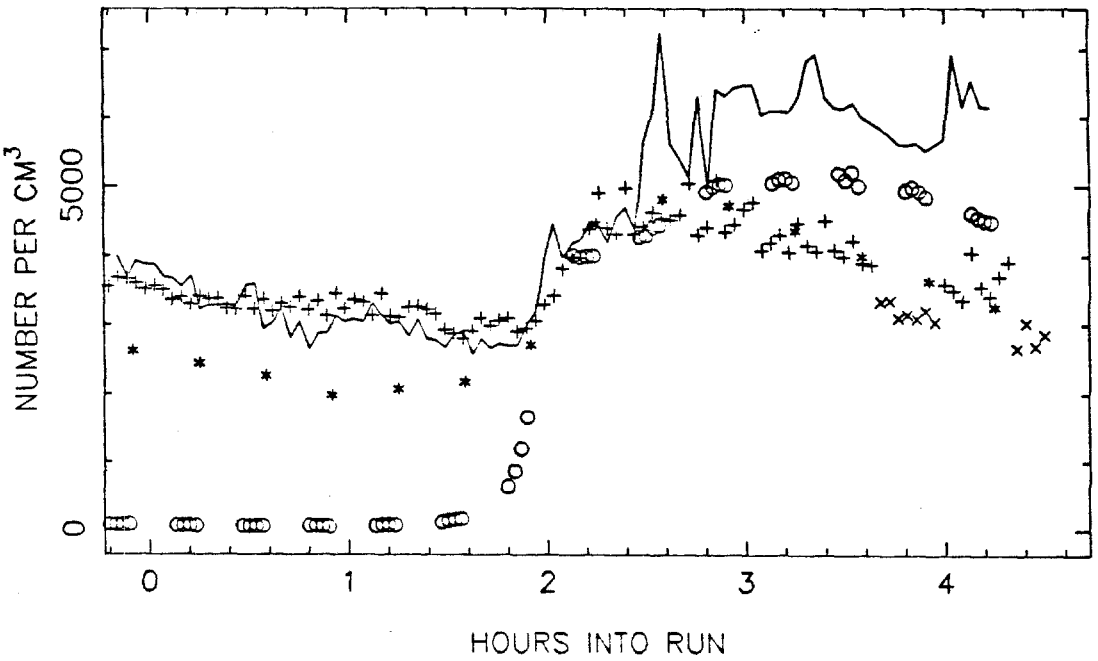

SIDE B

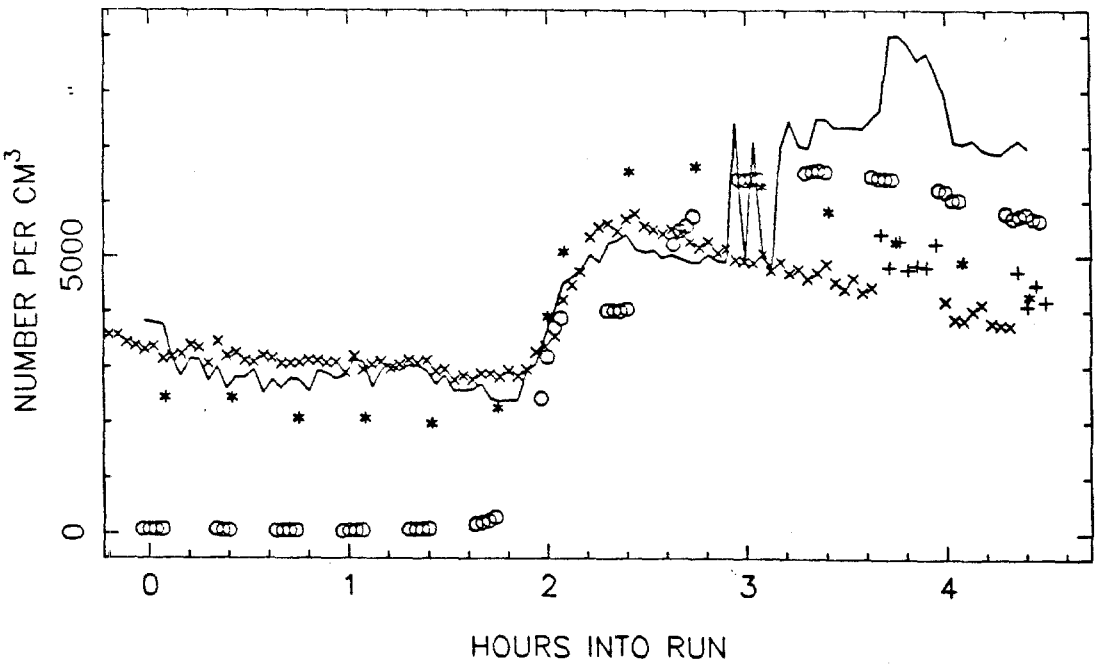

DMMA45 VOLUME IN THE AEROSOL PHASE, SIDE A

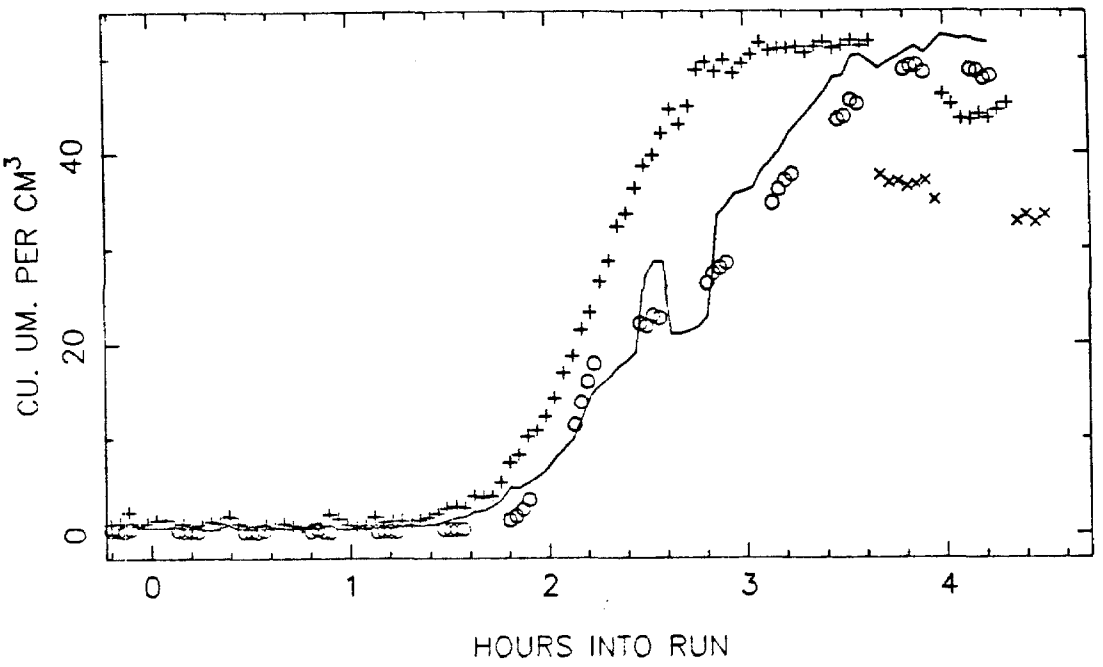

SIDE B

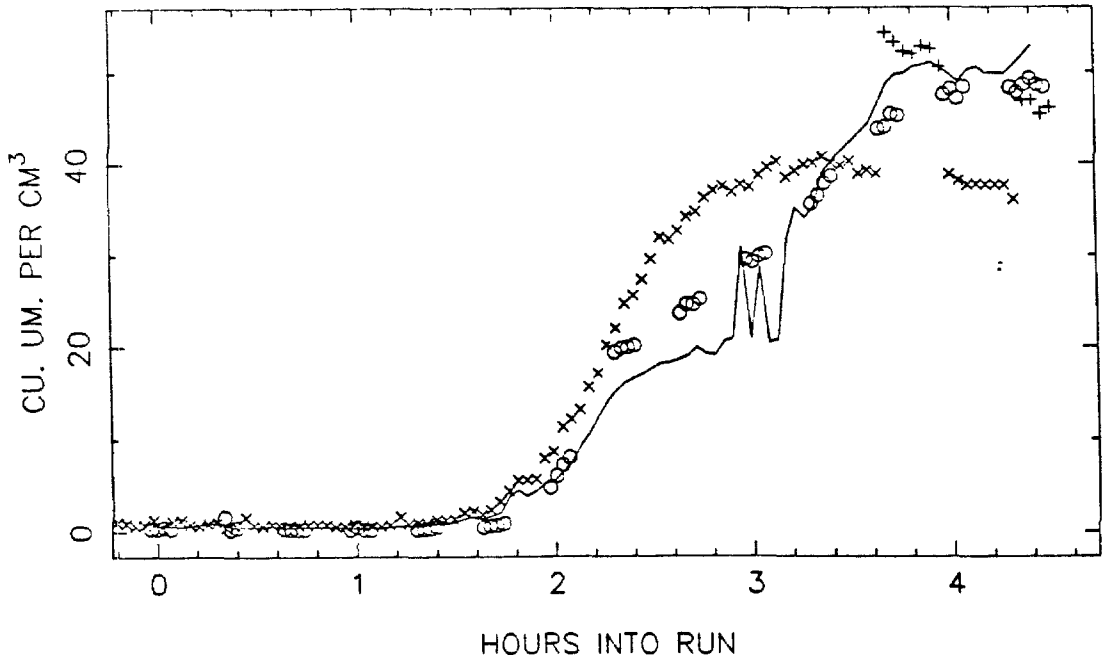

DMMA45 MEAN PARTICLE SIZE, SIDE A

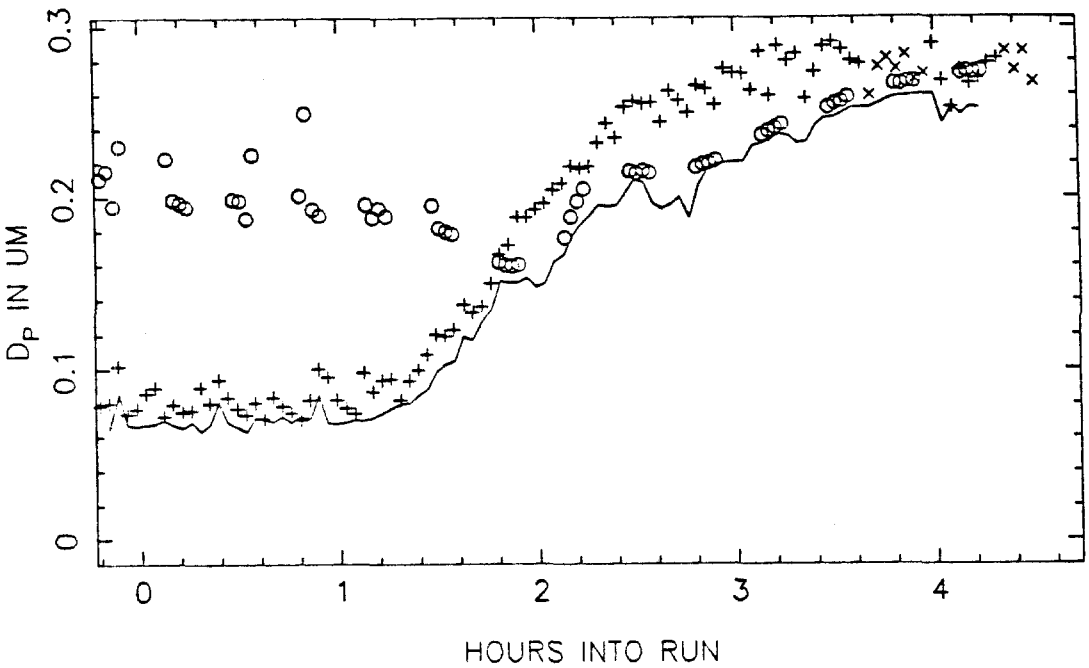

SIDE B

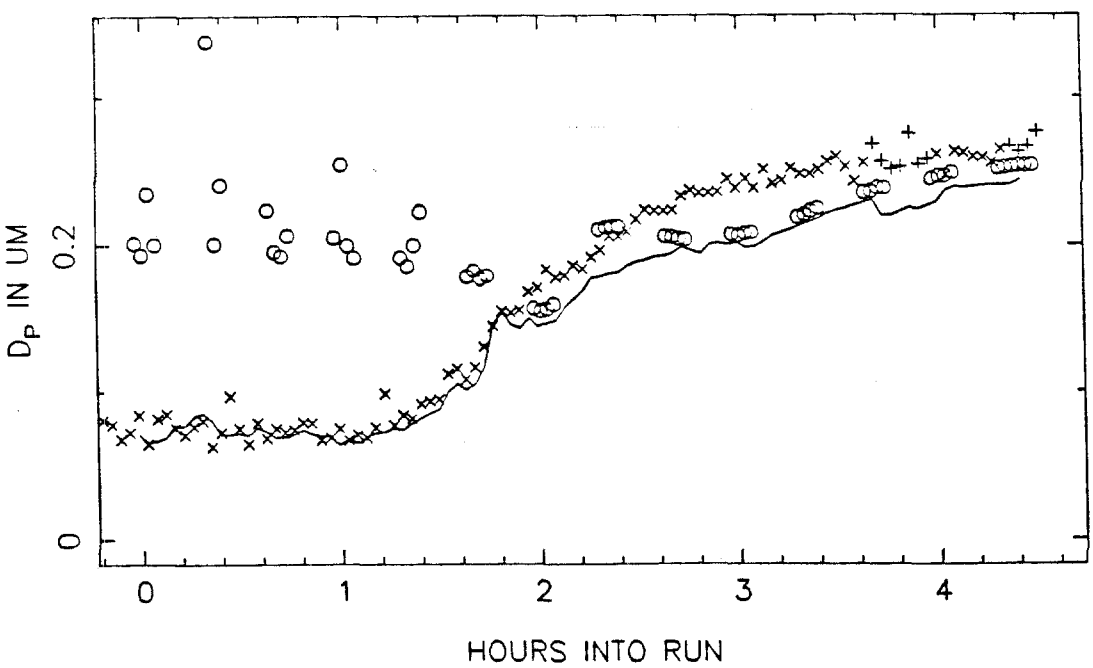

DMMA45A NUMBER DISTRIBUTION, T=0

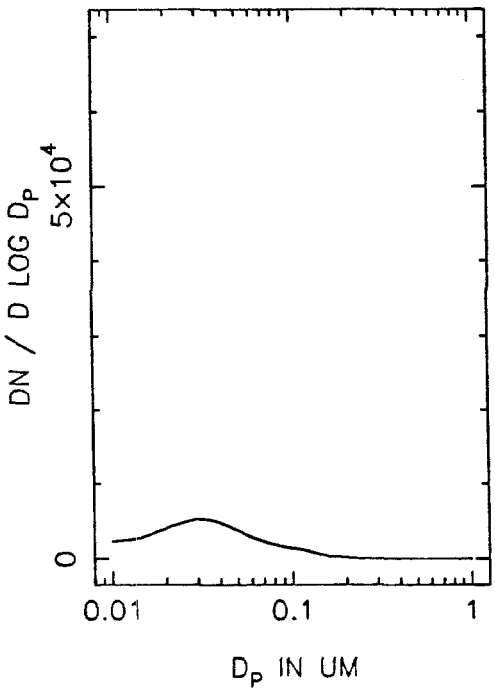

T=0.5 HOURS

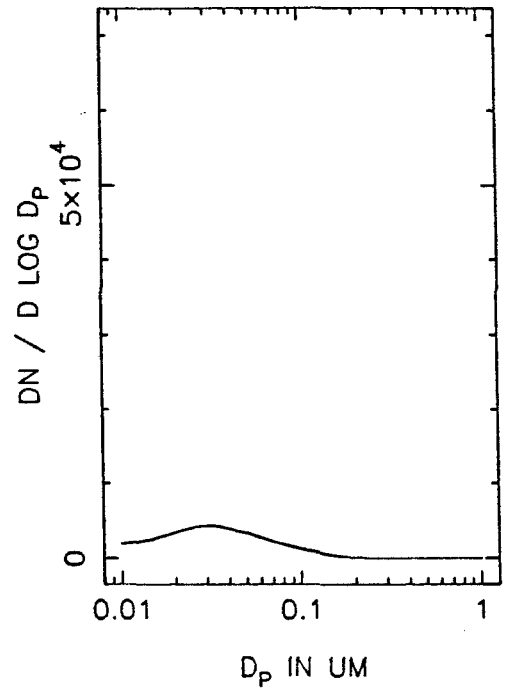

T=1.0 HOURS

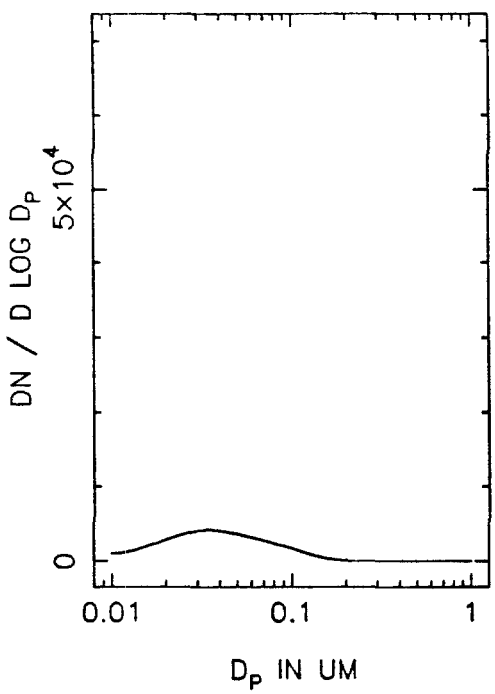

T=1.5 HOURS

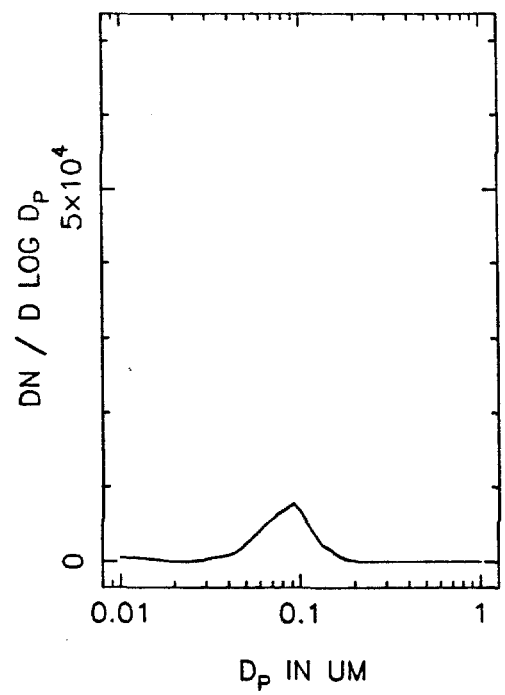

DMMA45A NUMBER DISTRIBUTION, T=2.0

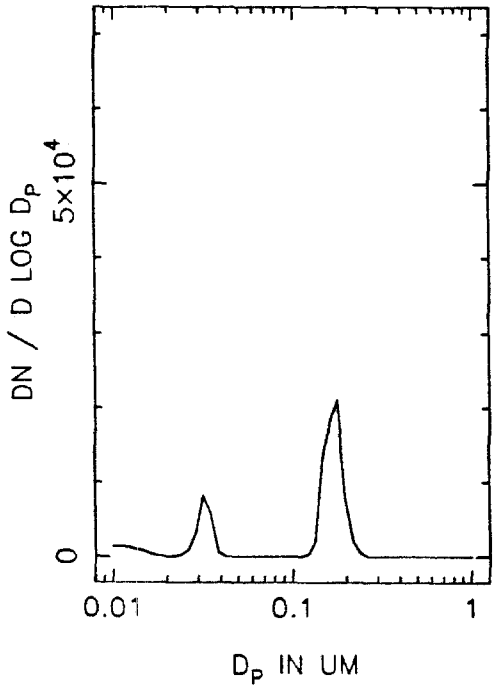

T=2.5 HOURS

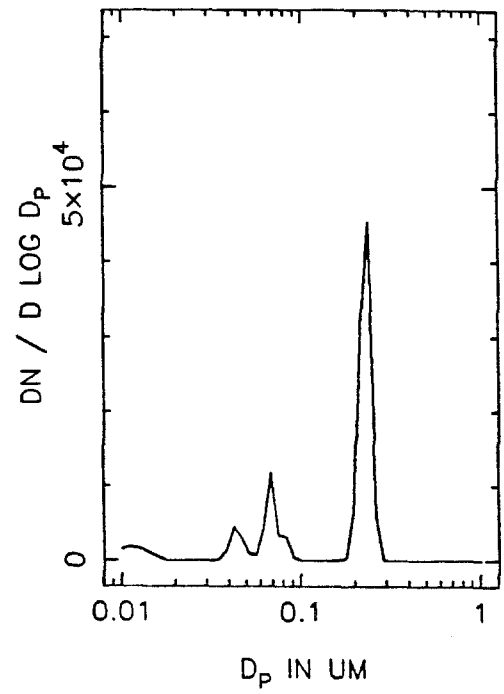

T=3.0 HOURS

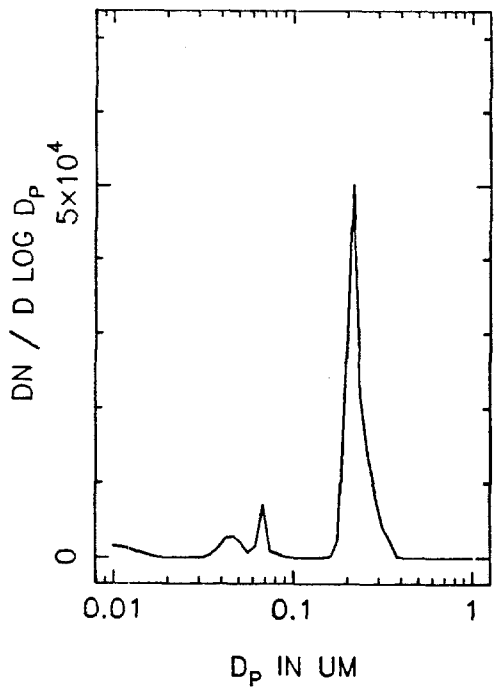

T=3.5 HOURS

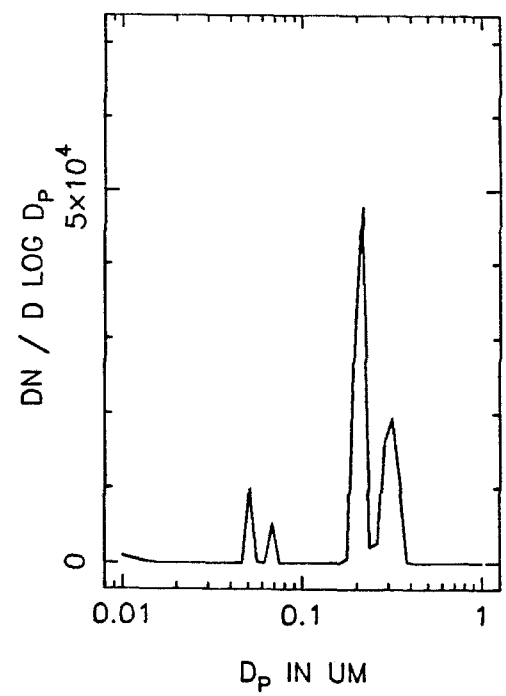

DMMA45A NUMBER DISTRIBUTION, T=4.0

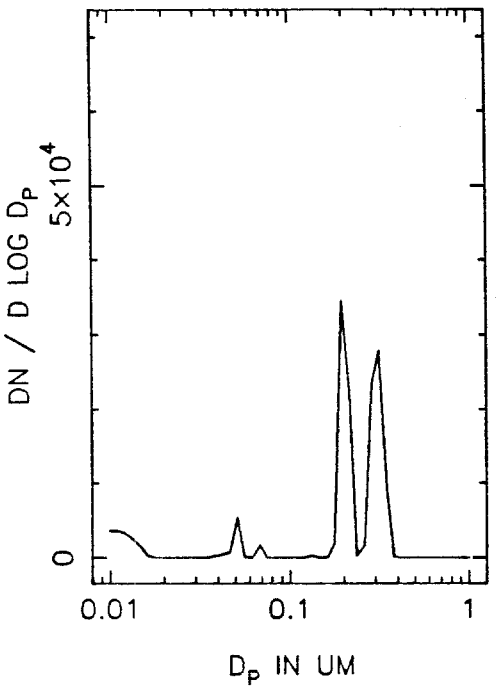

DMMA45A VOLUME DISTRIBUTION, T=0

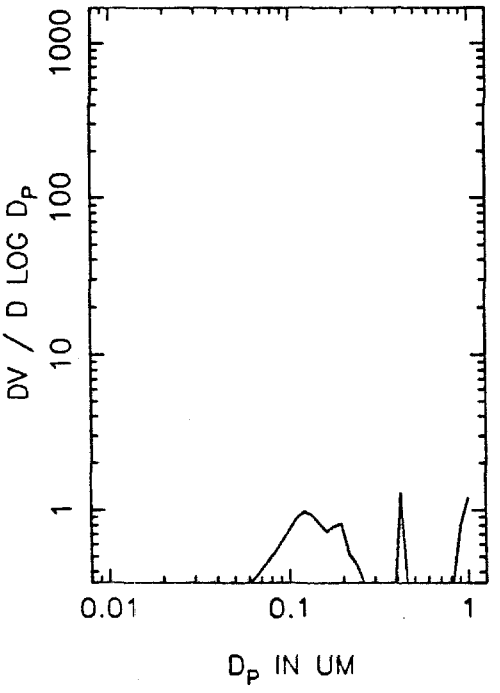

T=0.5 HOURS

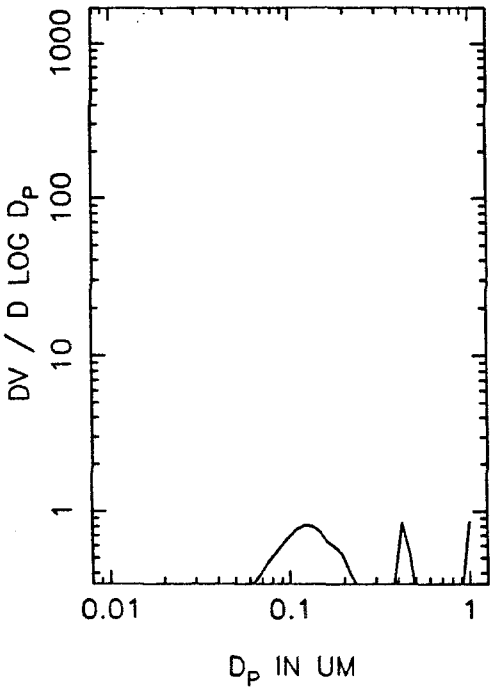

T=1.0 HOURS

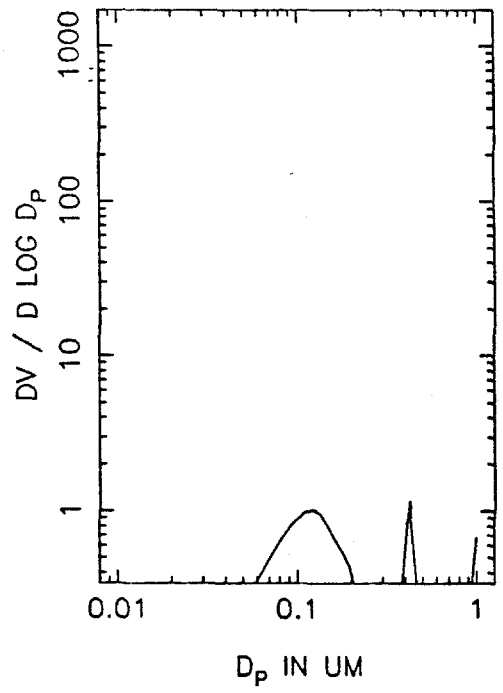

T=1.5 HOURS

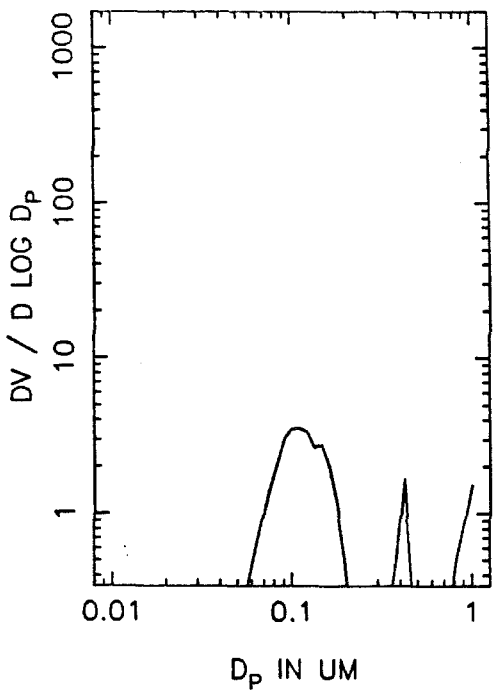

DMMA45A VOLUME DISTRIBUTION, T=2.0

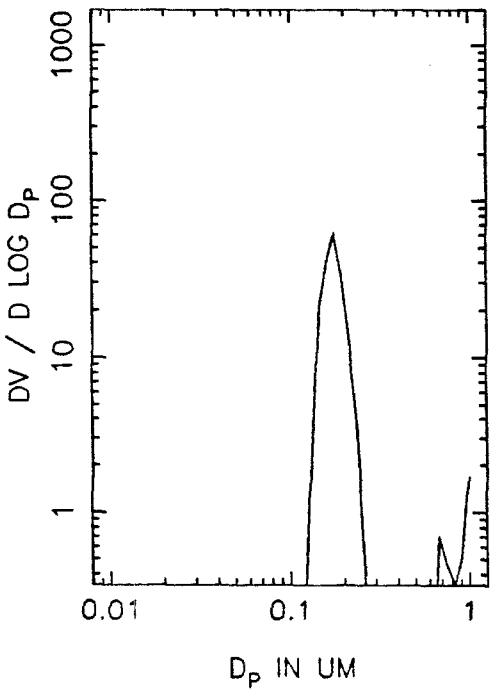

T=2.5 HOURS

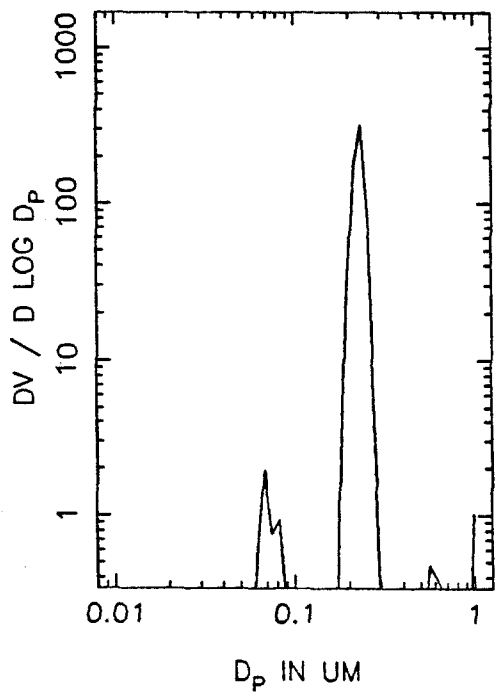

T=3.0 HOURS

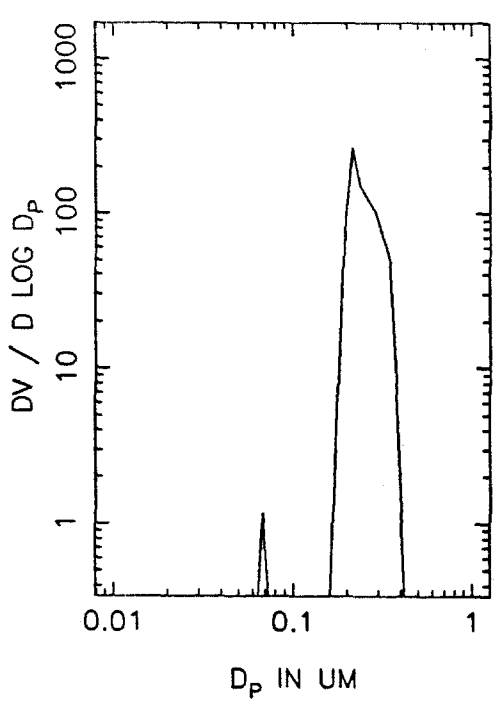

T=3.5 HOURS

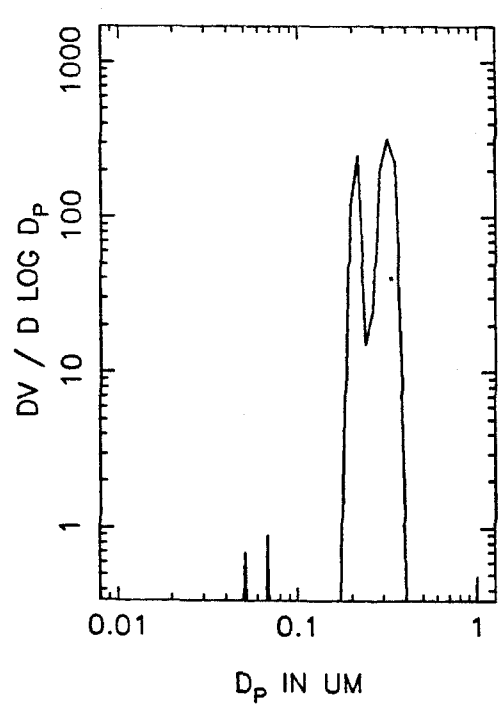

DMMA45A VOLUME DISTRIBUTION, T=4.0

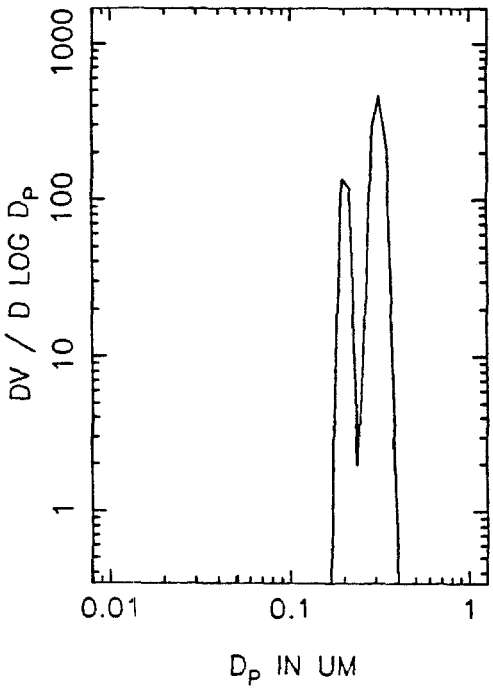

DMMA45B NUMBER DISTRIBUTION, T=0

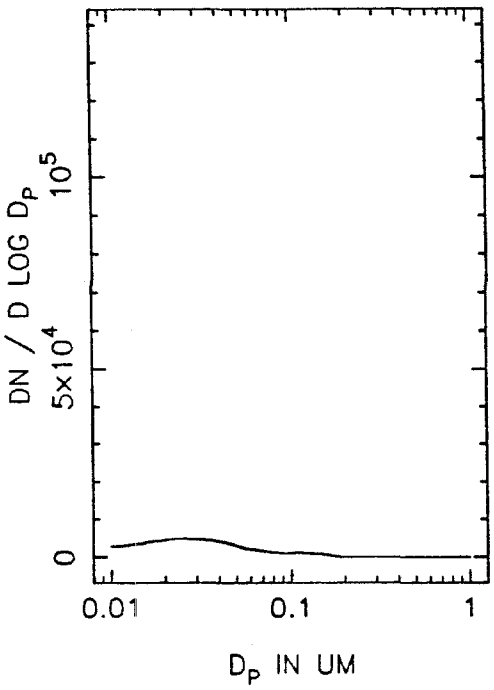

T=0.5 HOURS

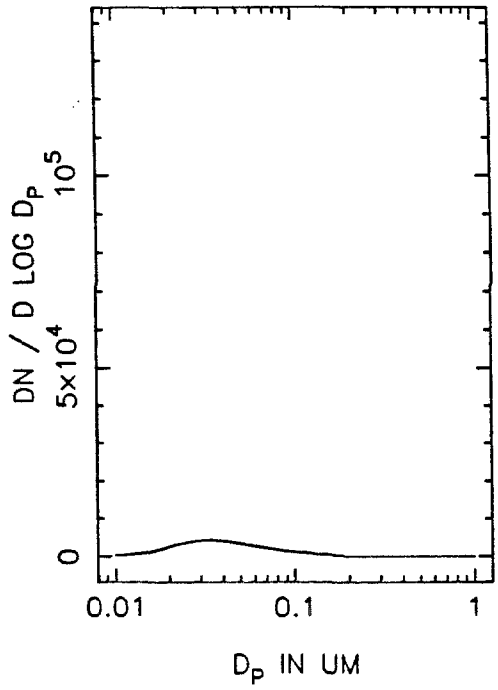

T=1.0 HOURS

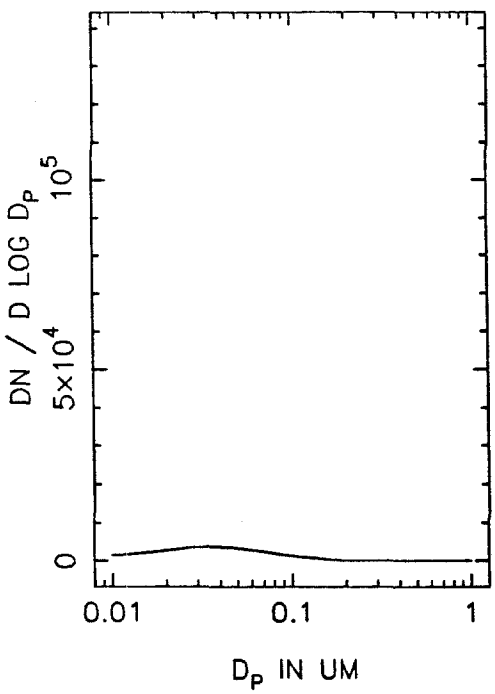

T=1.5 HOURS

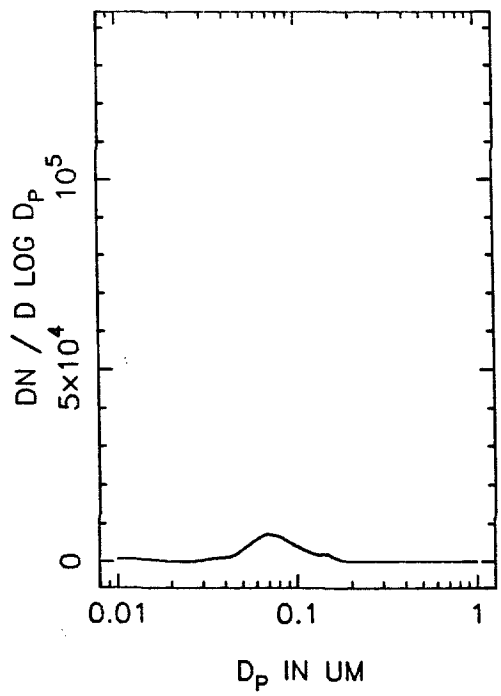

DMMA45B NUMBER DISTRIBUTION, T=2.0

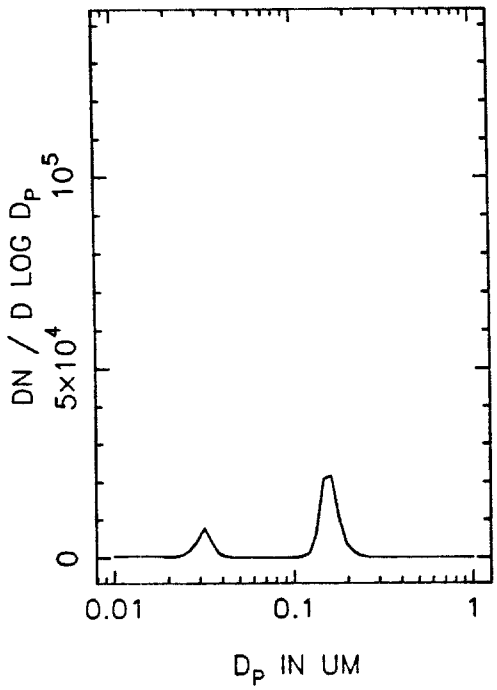

T=2.5 HOURS

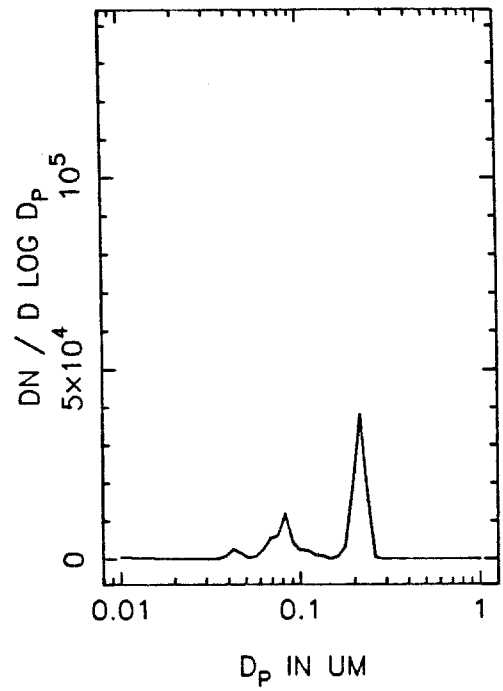

T=3.0 HOURS

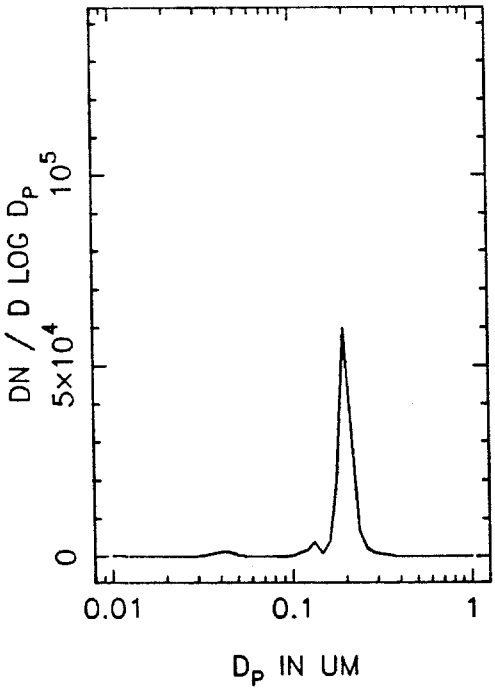

T=3.5 HOURS

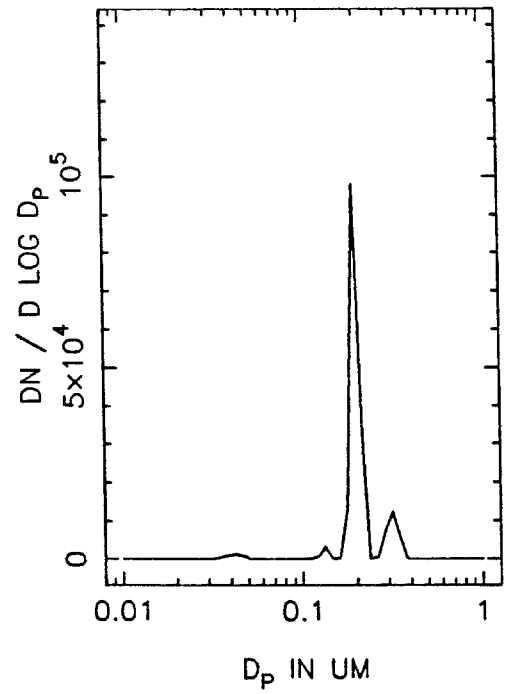

DMMA45B NUMBER DISTRIBUTION, T=4.0

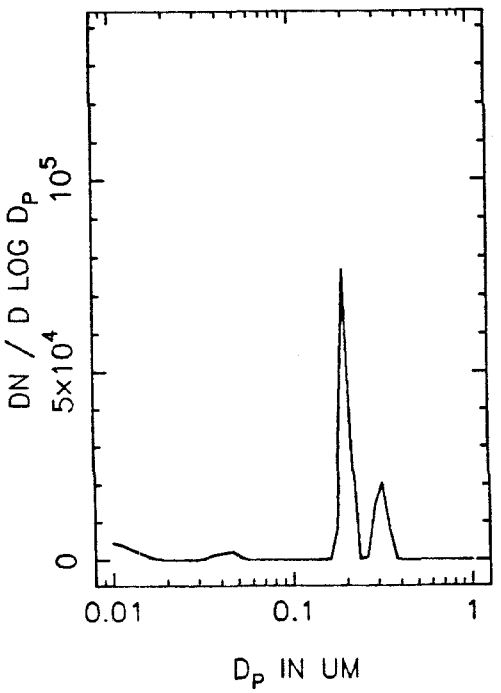

DMMA45B VOLUME DISTRIBUTION, T=0

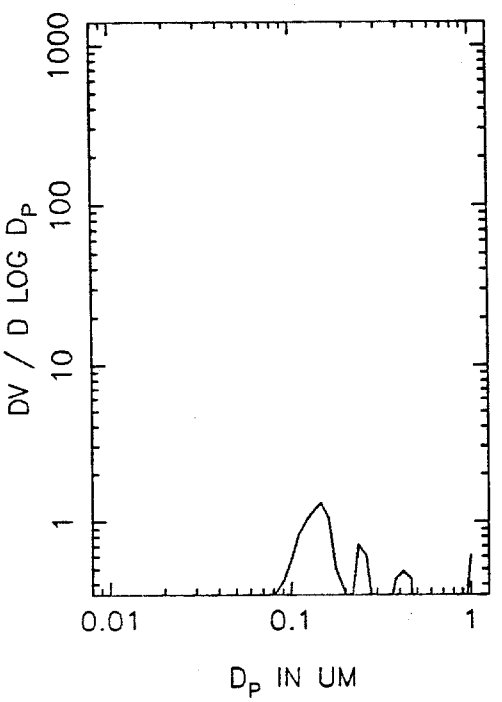

T=0.5 HOURS

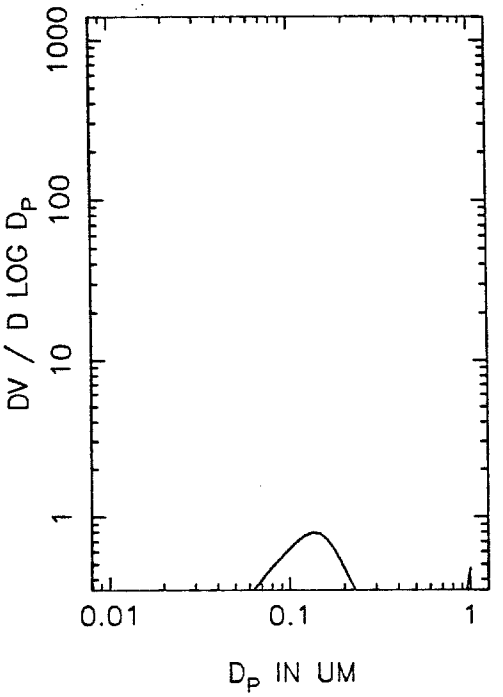

T=1.0 HOURS

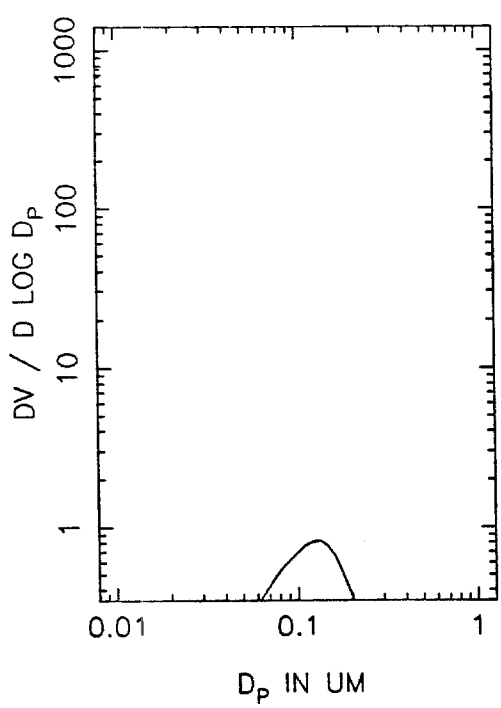

T=1.5 HOURS

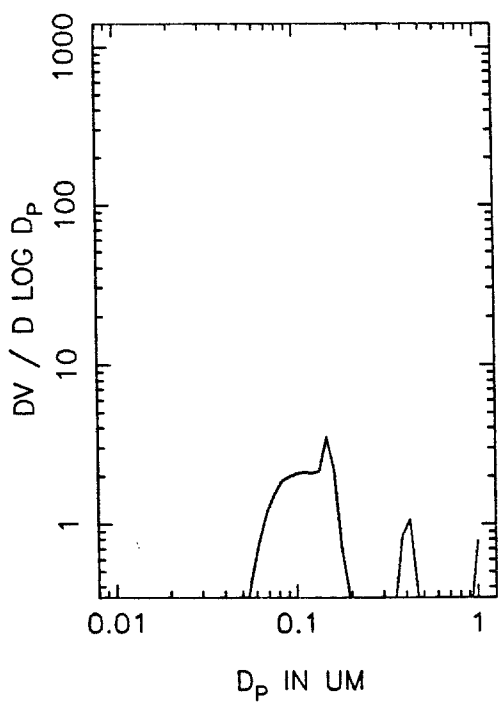

DMMA45B VOLUME DISTRIBUTION, T=2.0

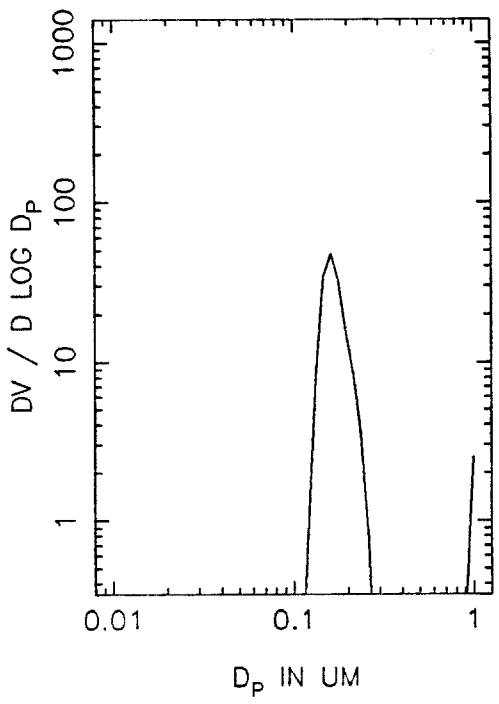

T=2.5 HOURS

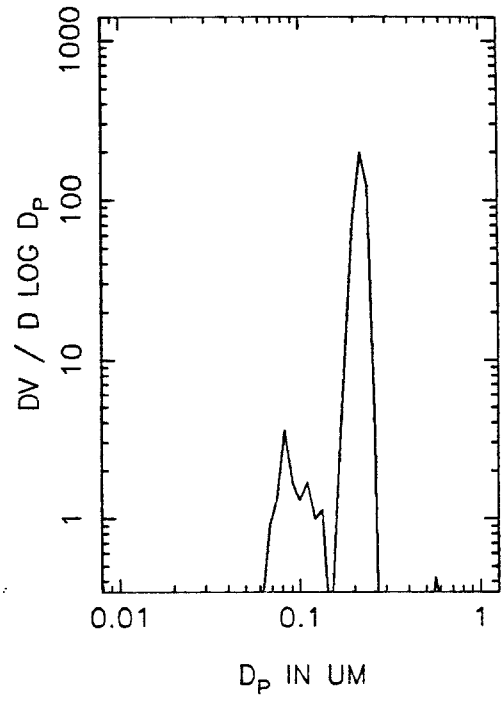

T=3.0 HOURS

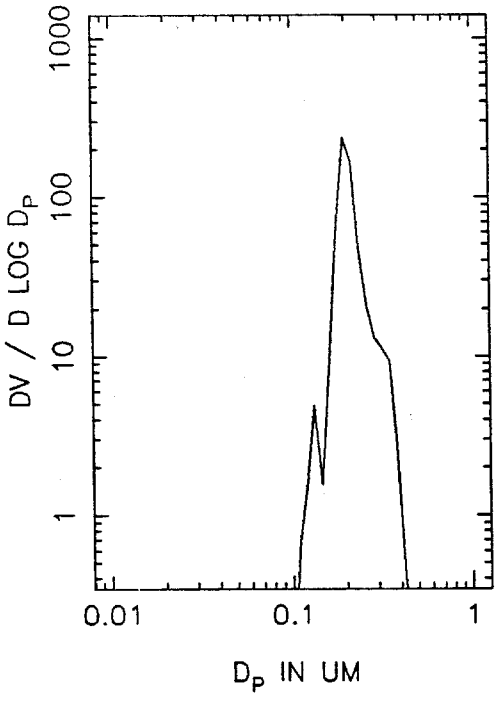

T=3.5 HOURS

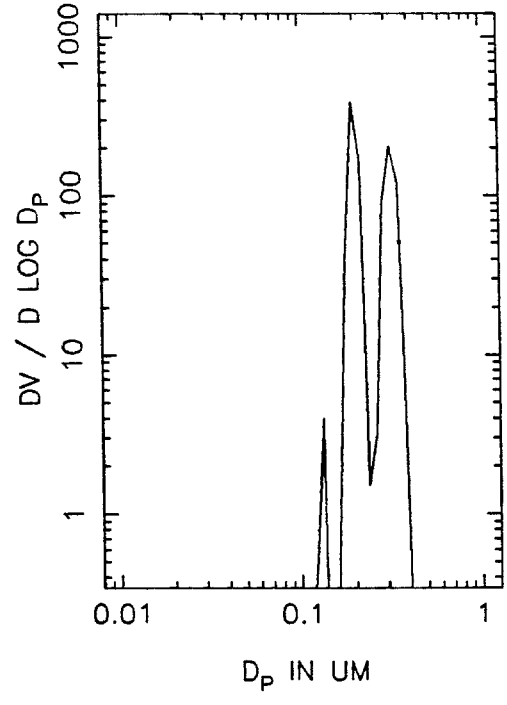

DMMA45B VOLUME DISTRIBUTION, T=4.0

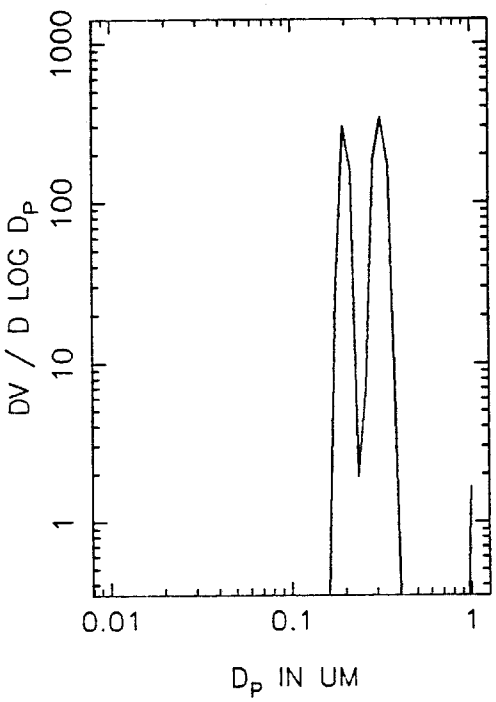

DMXA48 TOTAL NUMBER, SIDE A

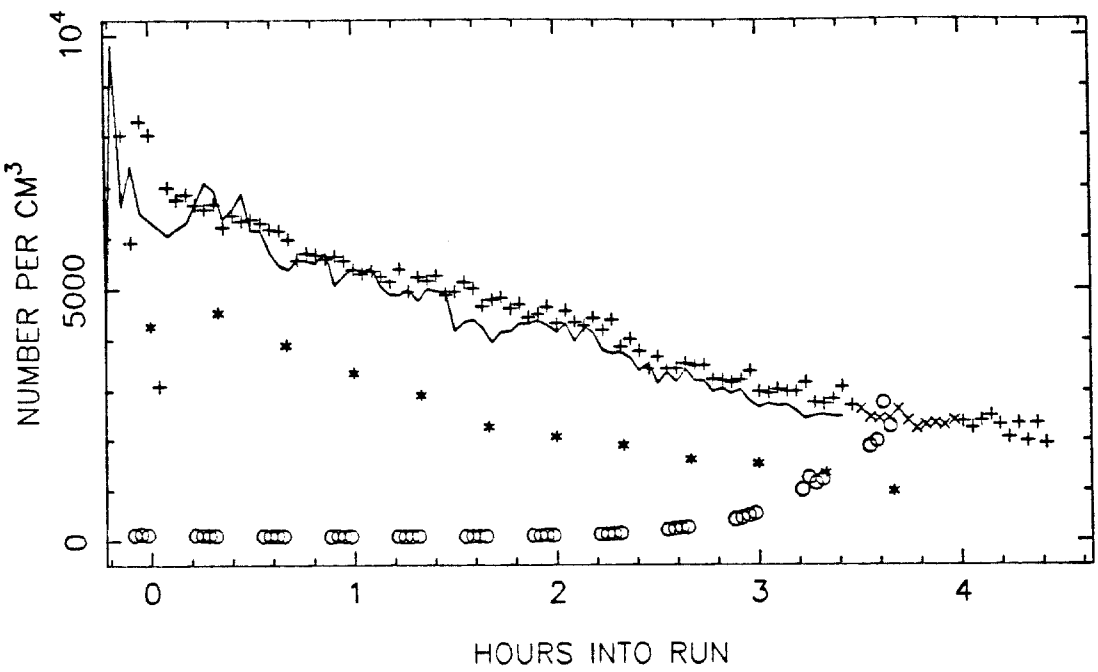

SIDE B

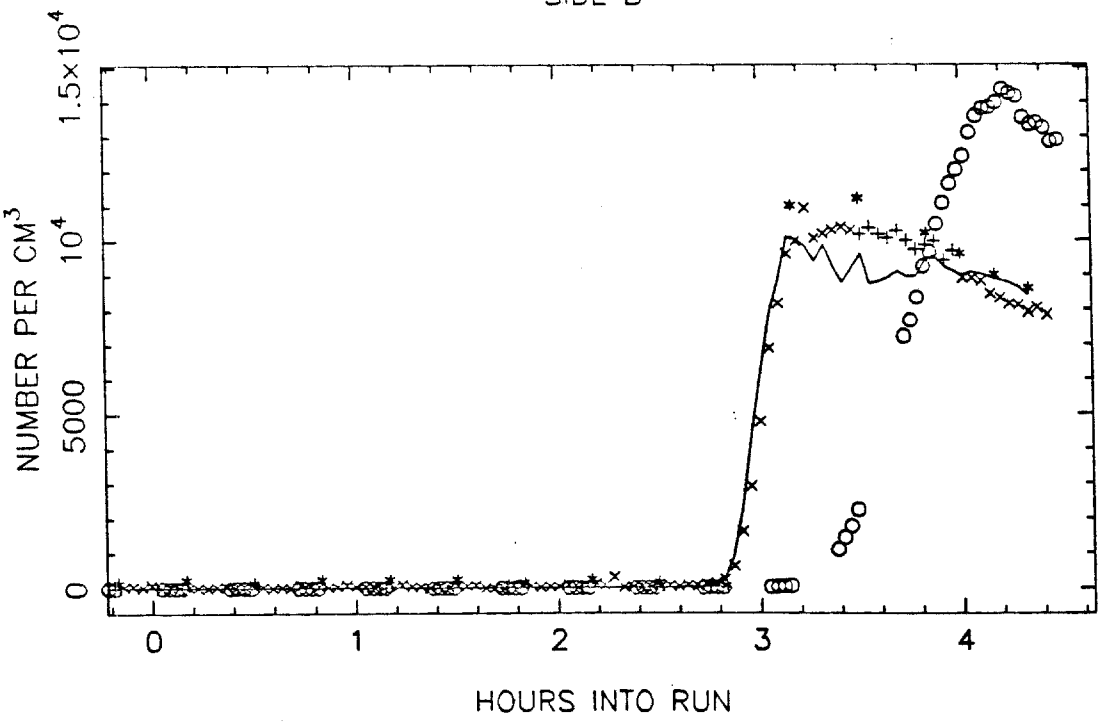

DMXA48 VOLUME IN THE AEROSOL PHASE, SIDE A

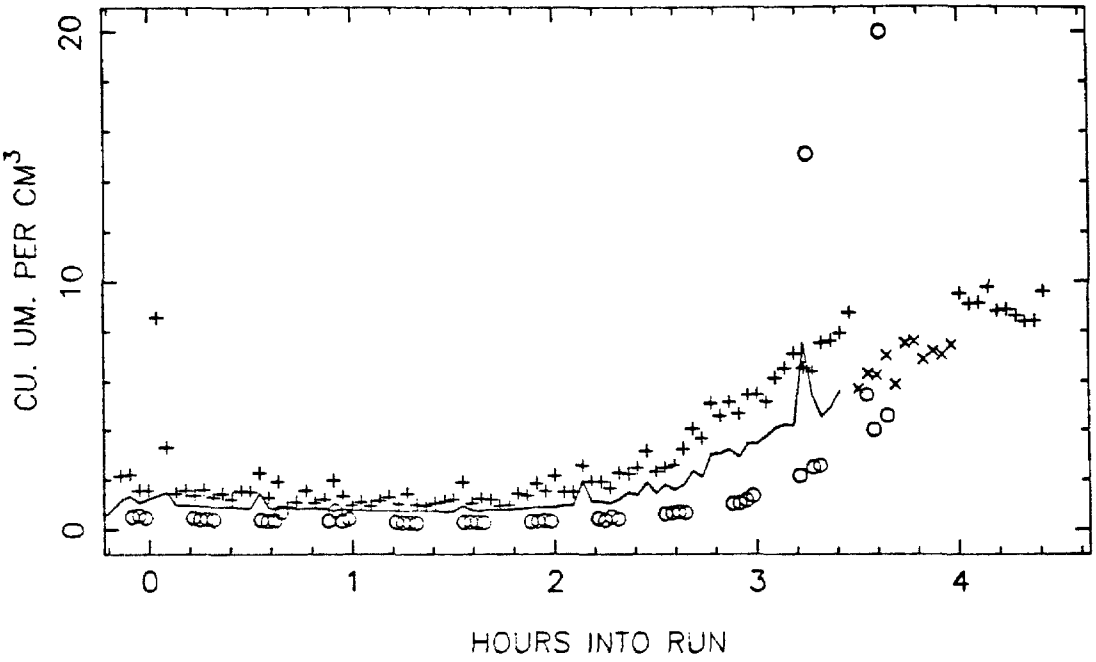

SIDE B

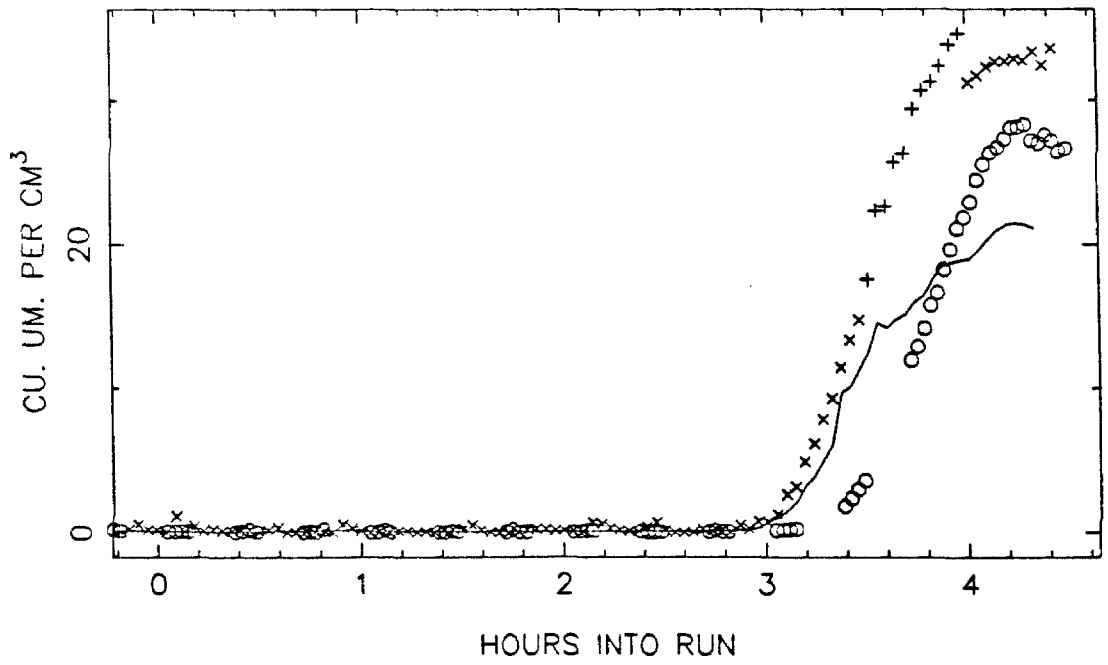

DMXA48 MEAN PARTICLE SIZE, SIDE A

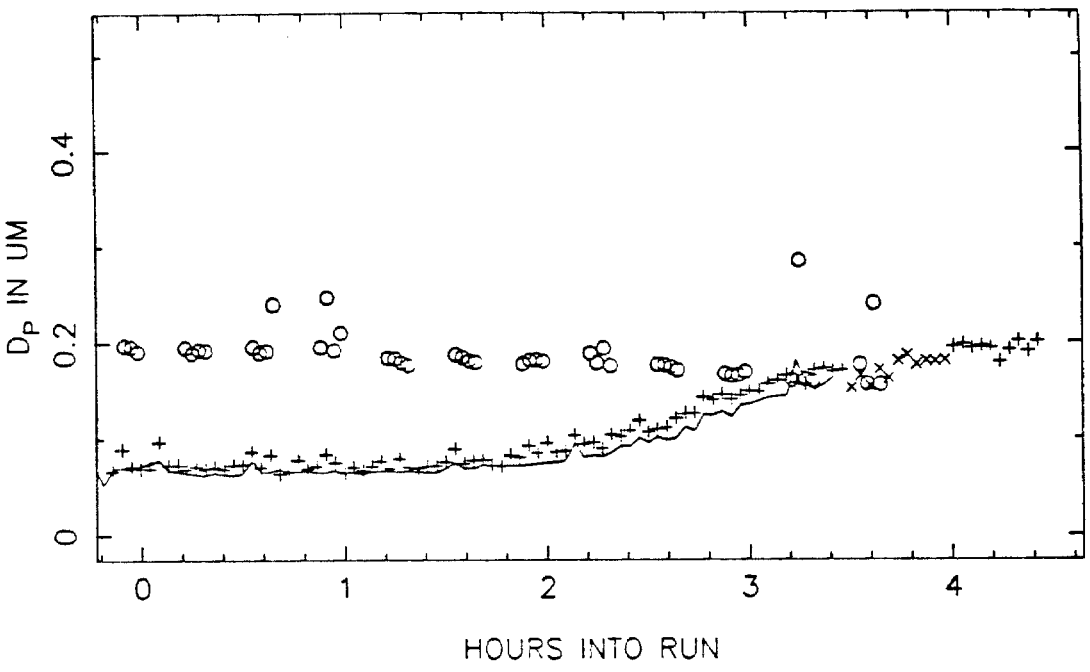

SIDE B

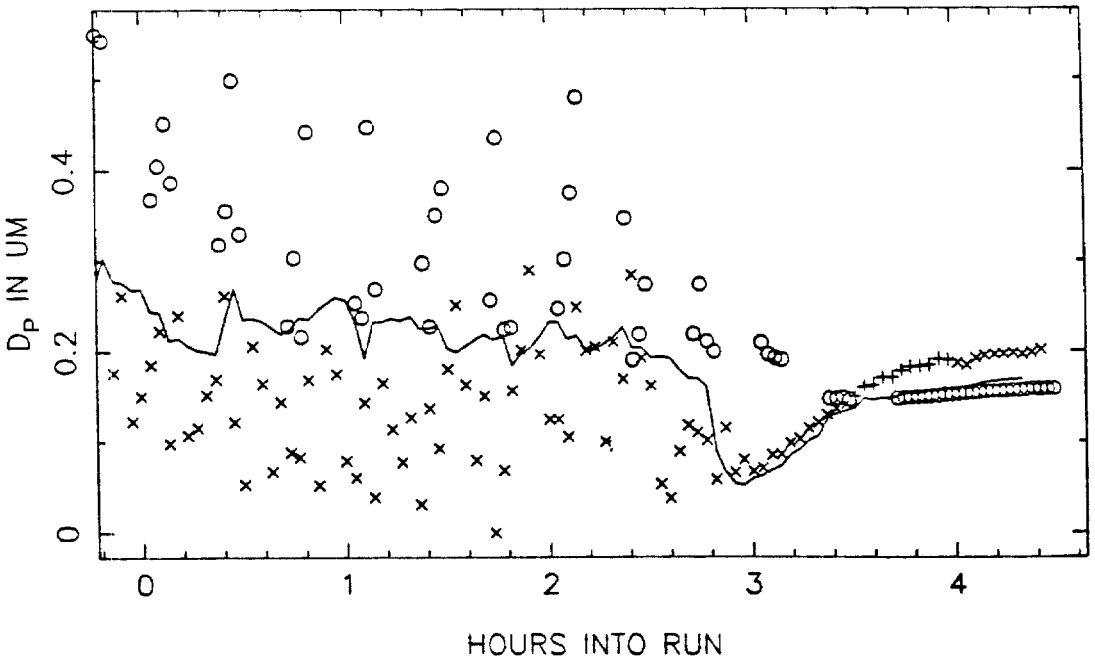

DMXA48A NUMBER DISTRIBUTION, T=0

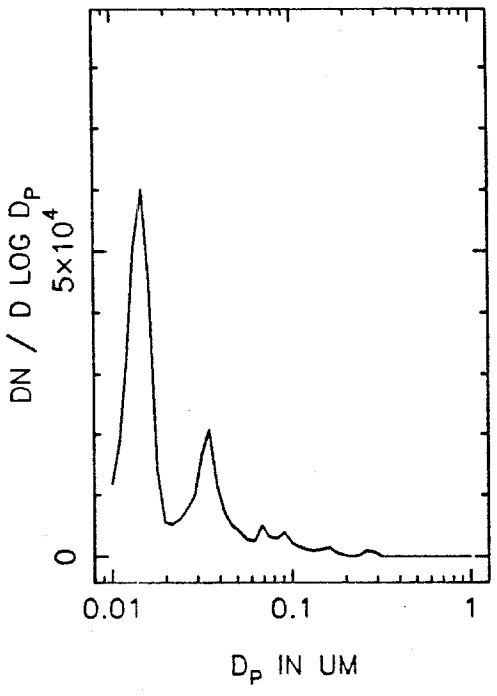

T=0.5 HOURS

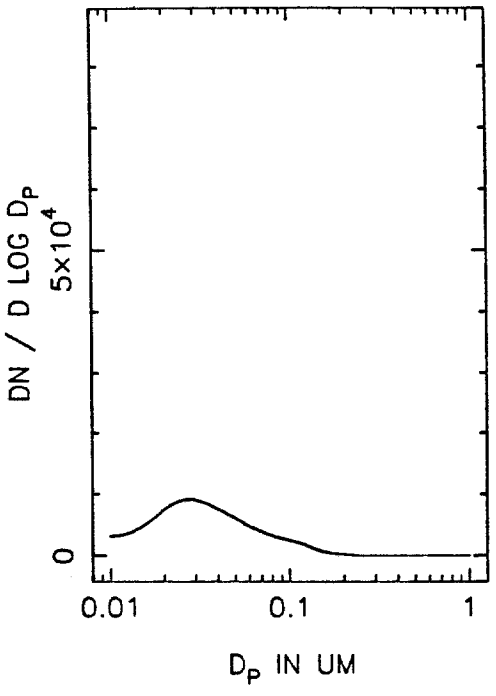

T=1.0 HOURS

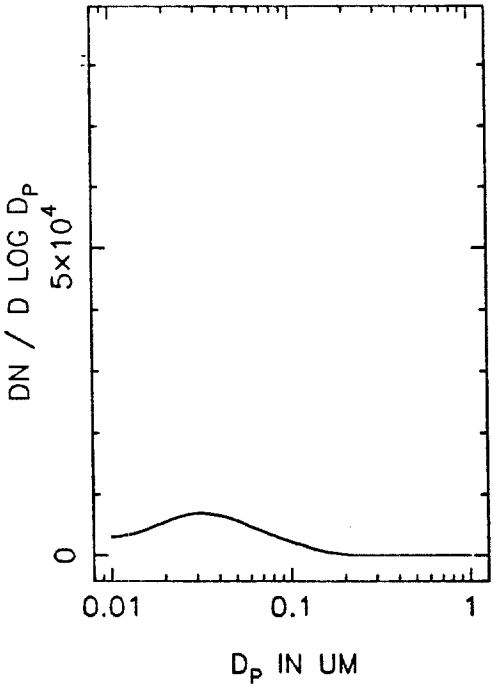

T=1.5 HOURS

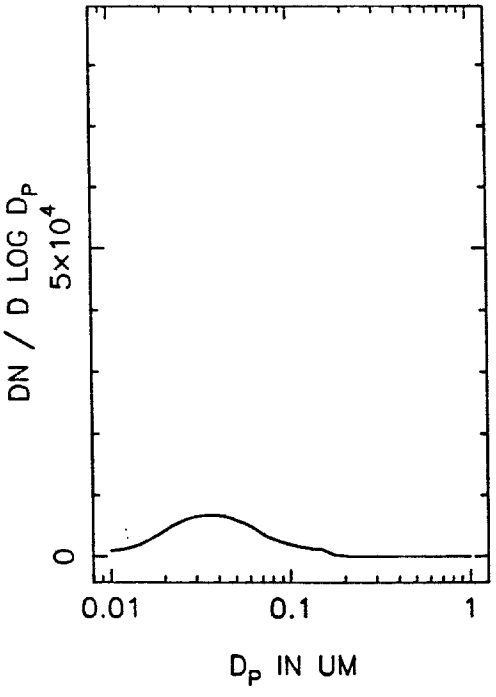

DMXA48A NUMBER DISTRIBUTION, T=2.0

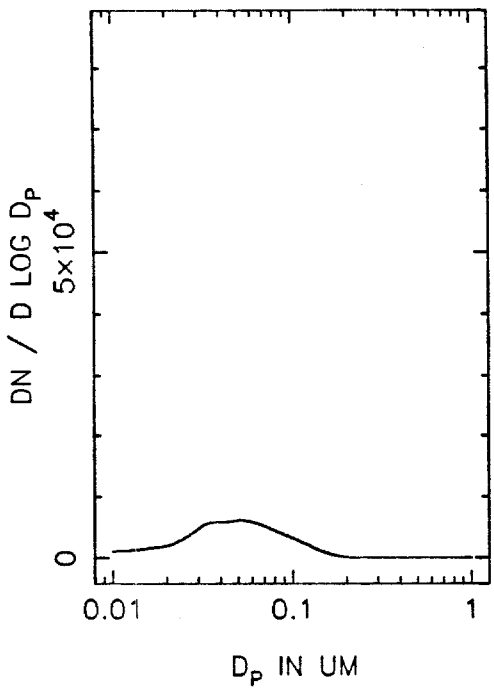

T=2.5 HOURS

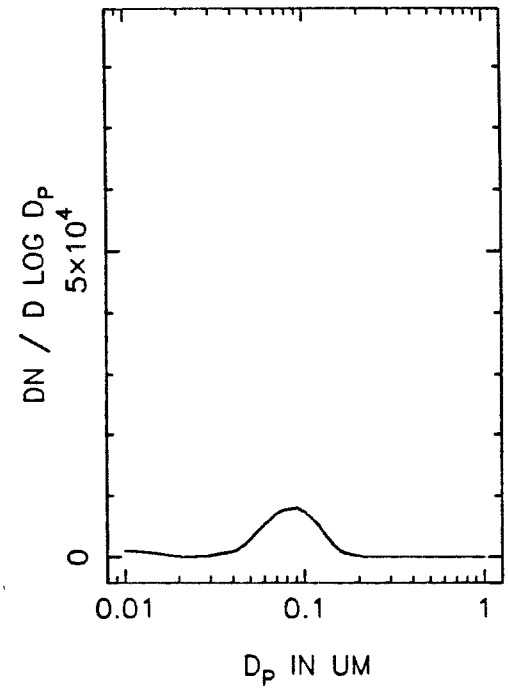

T=3.0 HOURS

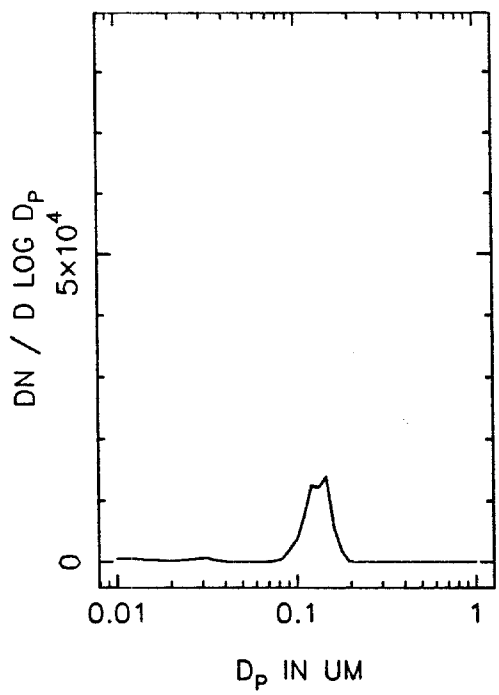

T=3.5 HOURS

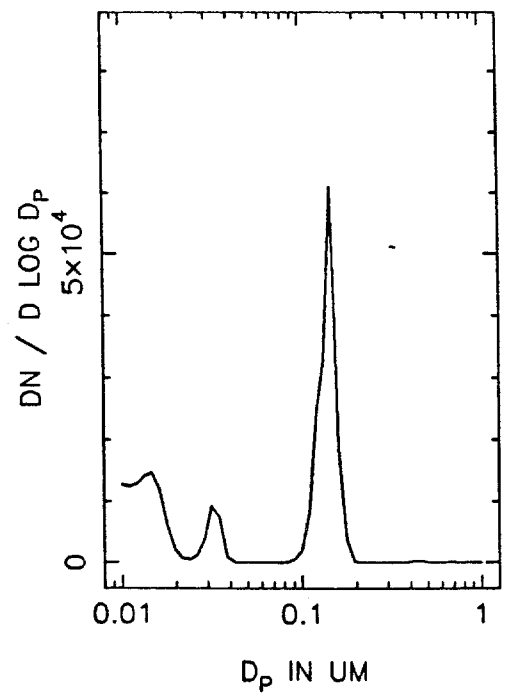

DMXA48A VOLUME DISTRIBUTION, T=0

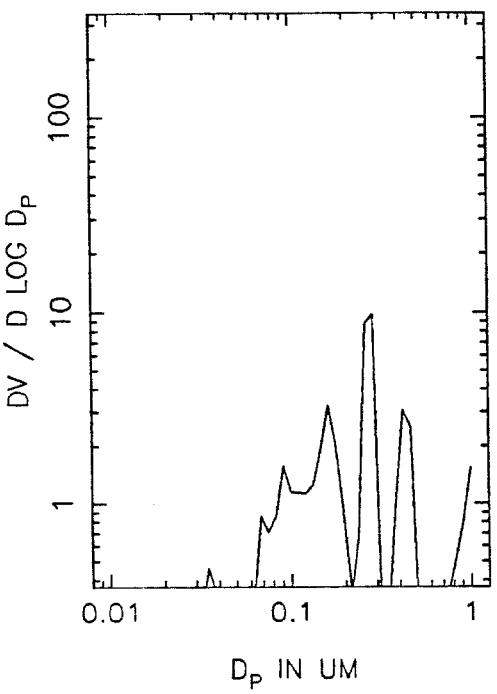

T=0.5 HOURS

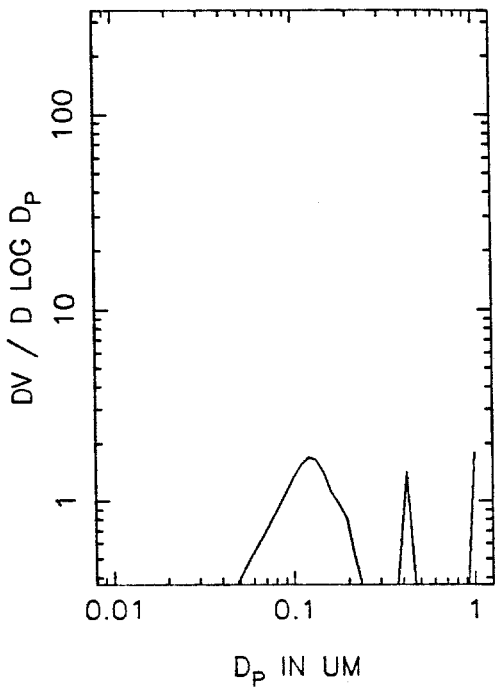

T=1.0 HOURS

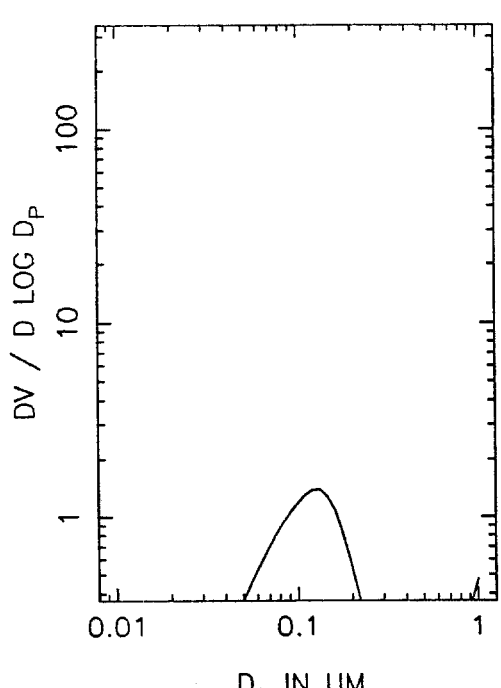

T=1.5 HOURS

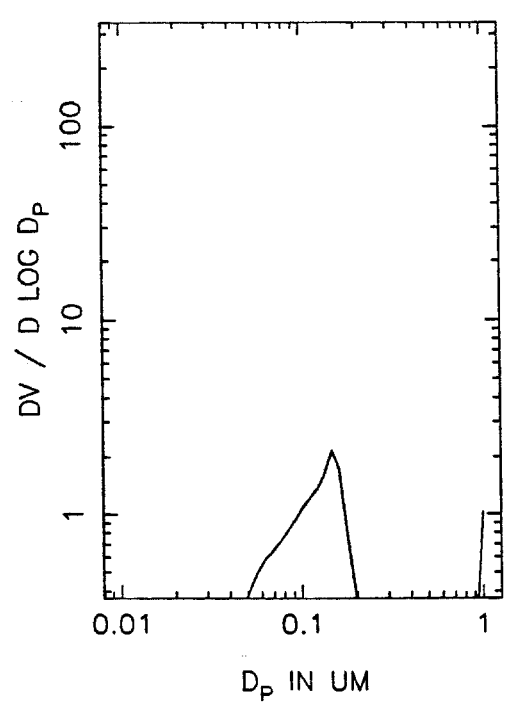

DMXA48A VOLUME DISTRIBUTION, T=2.0

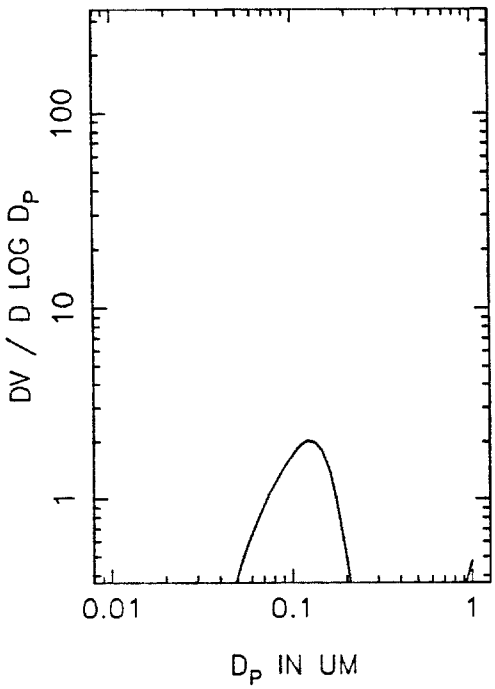

T=2.5 HOURS

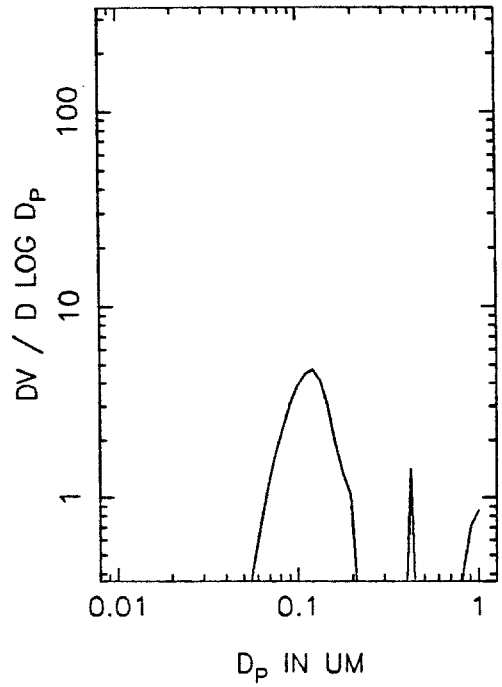

T=3.0 HOURS

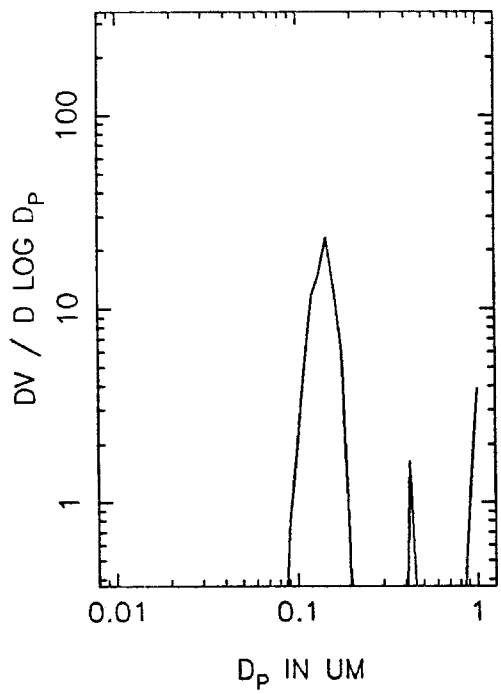

T=3.5 HOURS

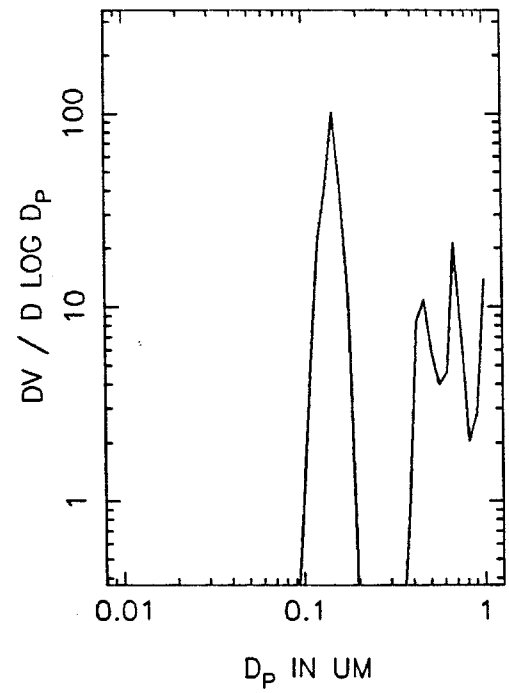

DMXA48B NUMBER DISTRIBUTION, T=0

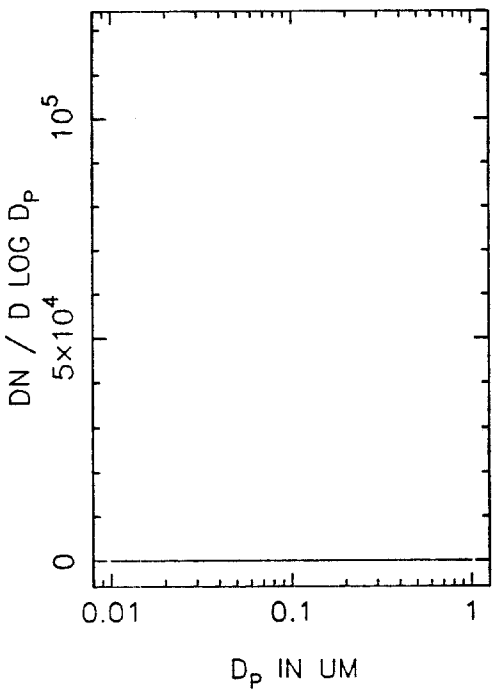

T=0.5 HOURS

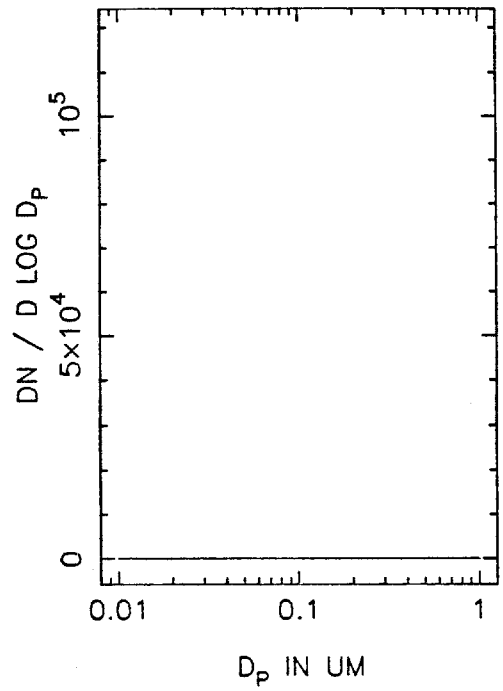

T=1.0 HOURS

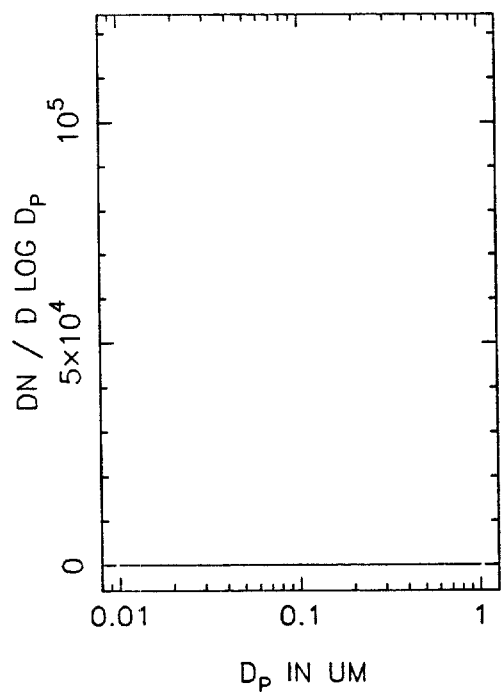

T=1.5 HOURS

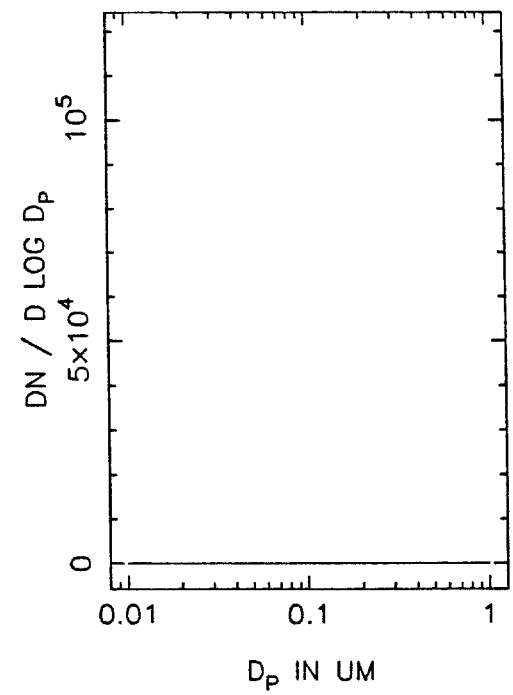

DMXA48B NUMBER DISTRIBUTION, T=2.0

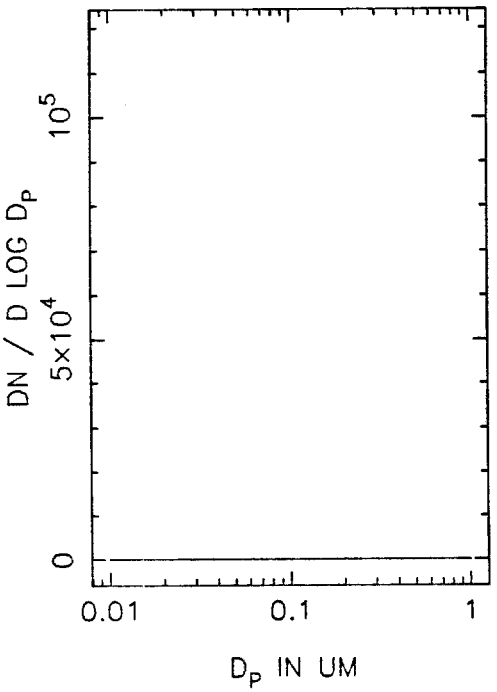

T=2.5 HOURS

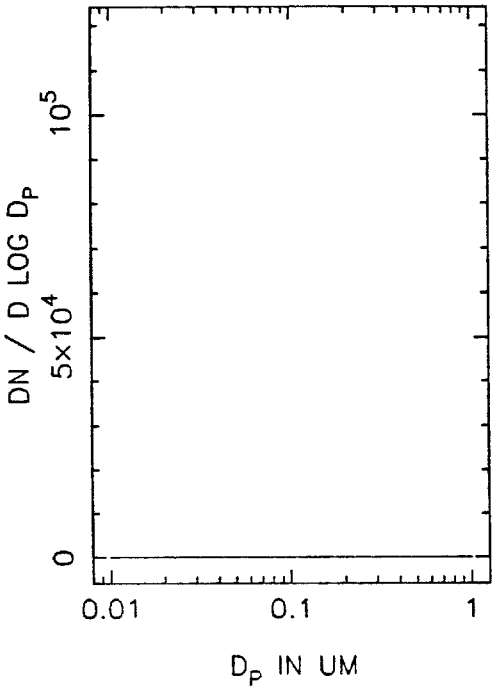

T=3.0 HOURS

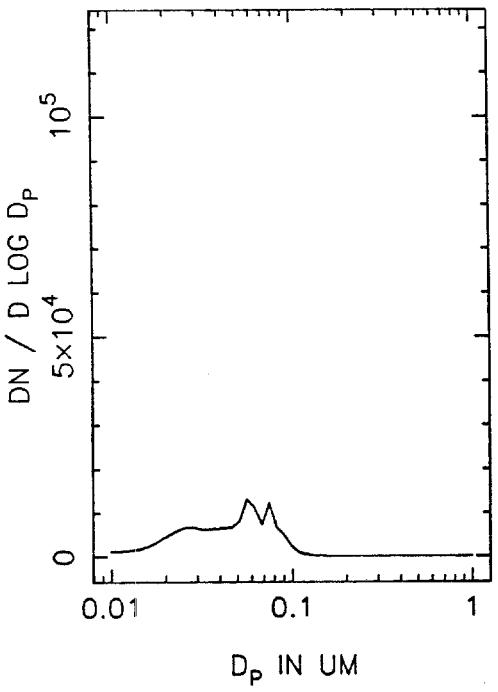

T=3.5 HOURS

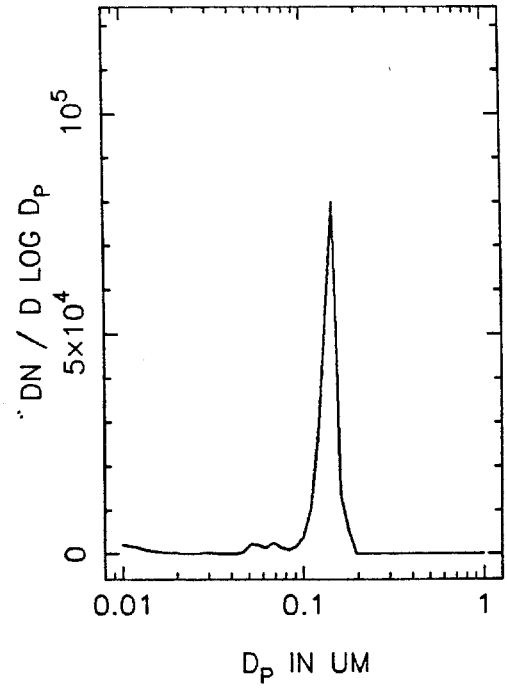

DMXA48B NUMBER DISTRIBUTION, T=4.0

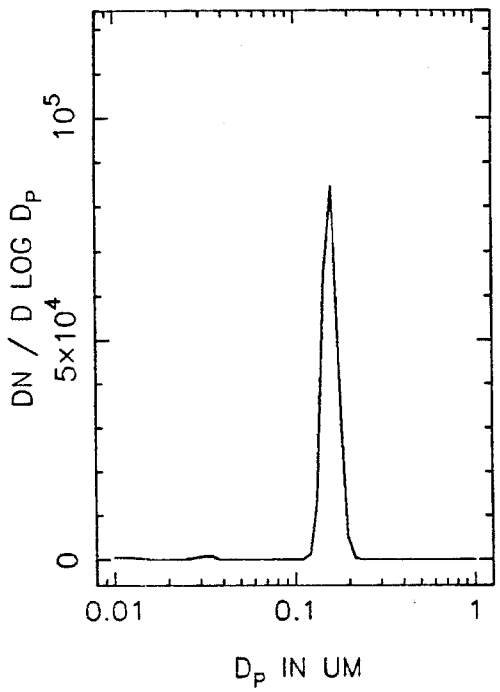

DMXA48B VOLUME DISTRIBUTION, T=0

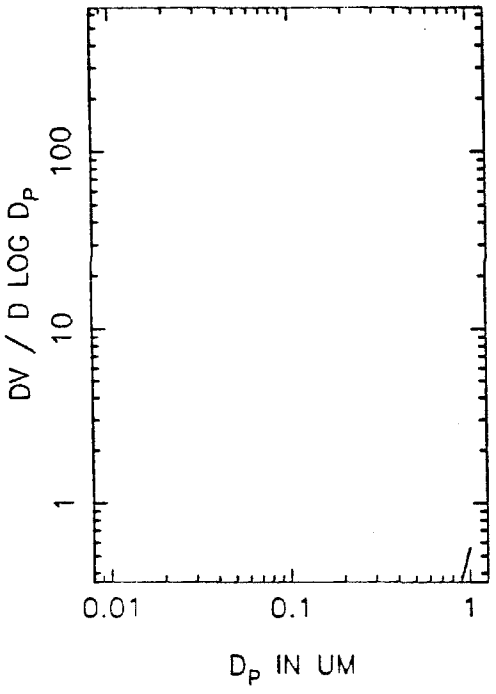

T=0.5 HOURS

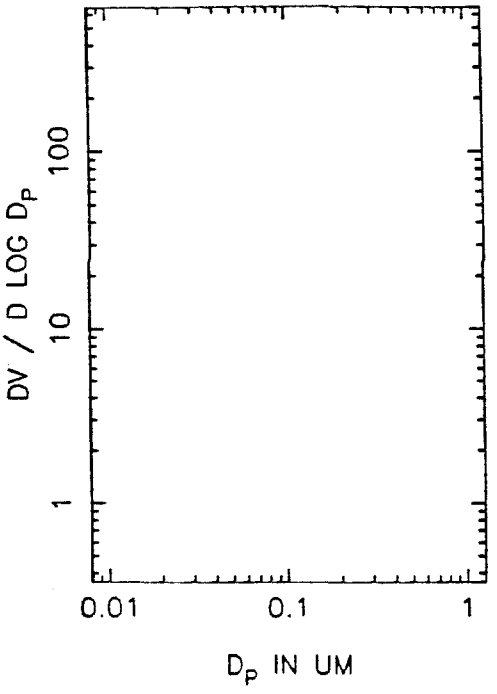

T=1.0 HOURS

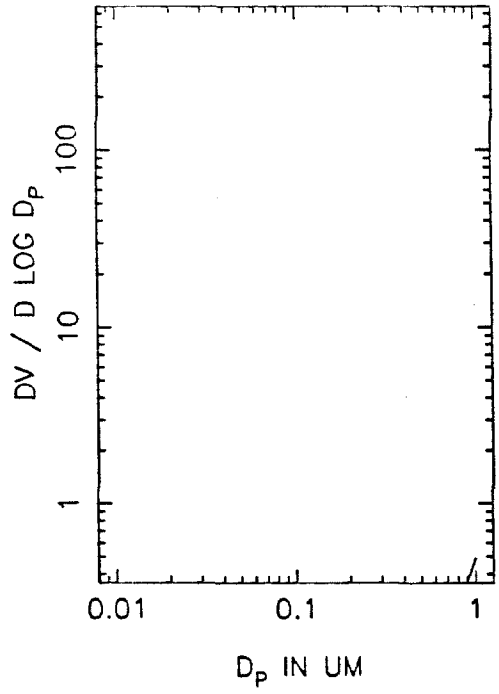

T=1.5 HOURS

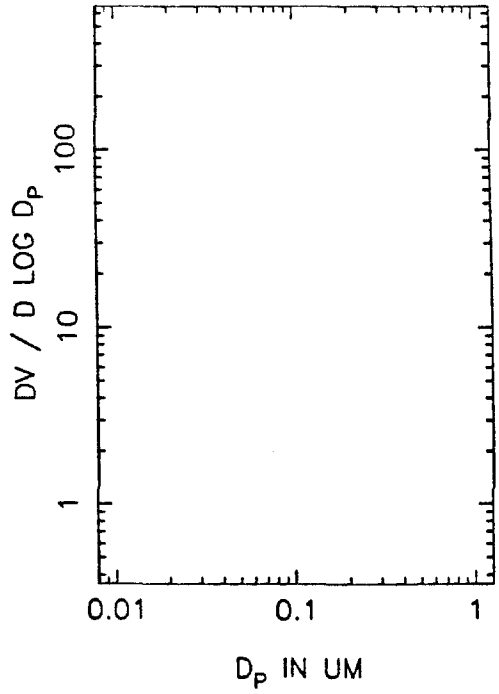

DMXA48B VOLUME DISTRIBUTION, T=2.0

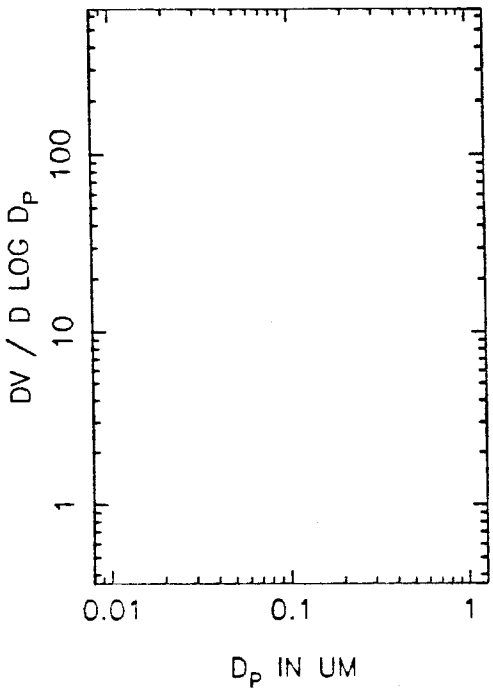

T=2.5 HOURS

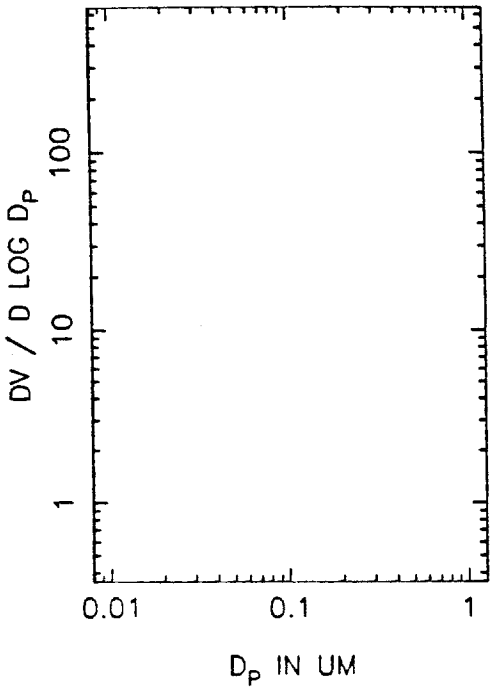

T=3.0 HOURS

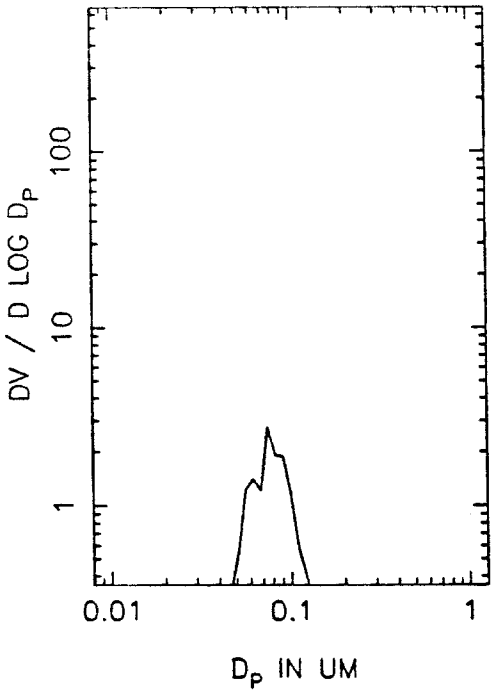

T=3.5 HOURS

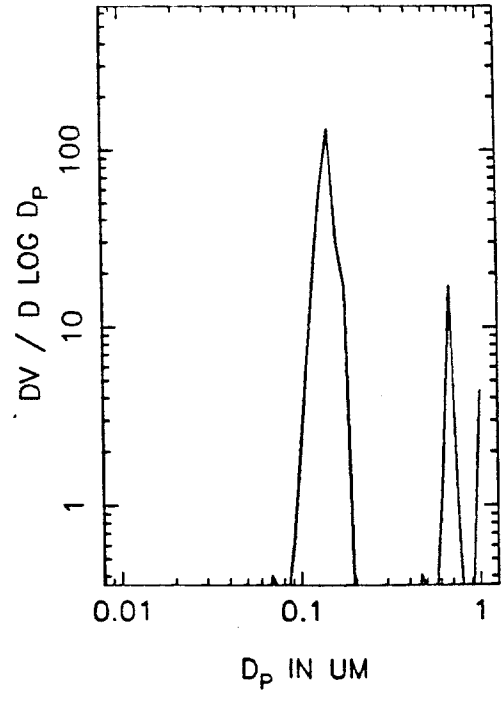

DMXA48B VOLUME DISTRIBUTION, T=4.0

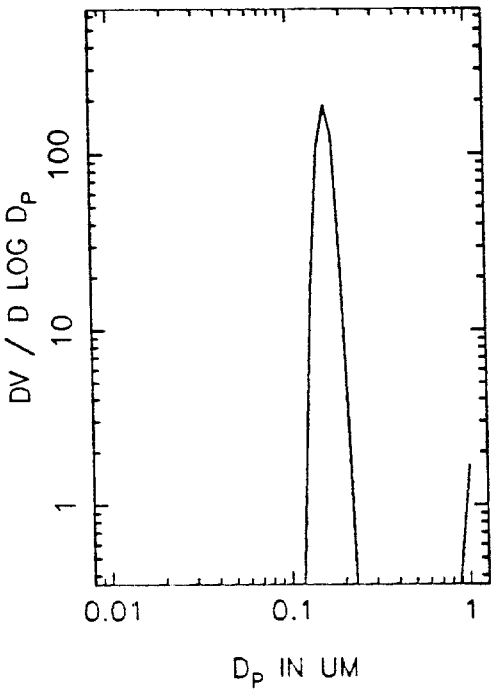

DQXA53 TOTAL NUMBER, SIDE A

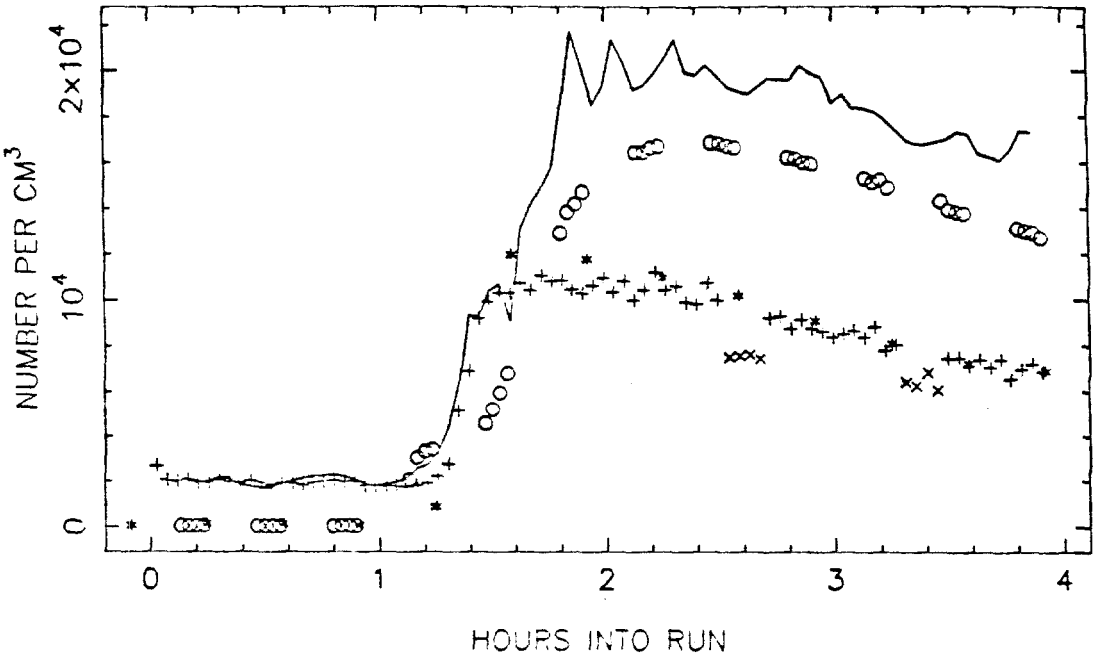

SIDE B

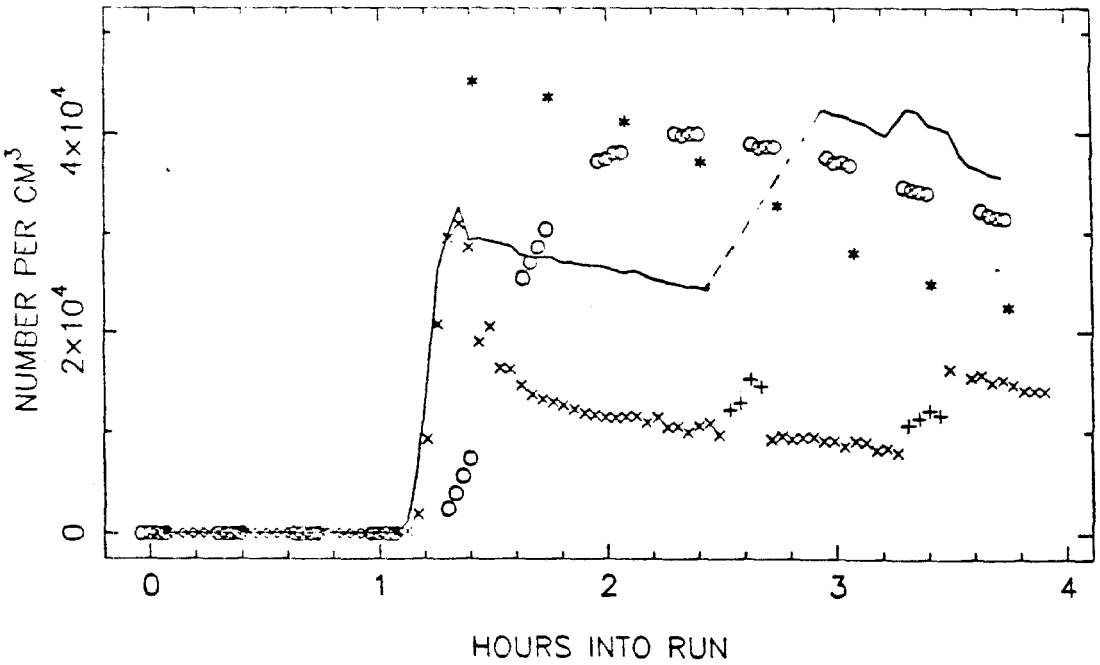

DQXA53 VOLUME IN THE AEROSOL PHASE, SIDE A

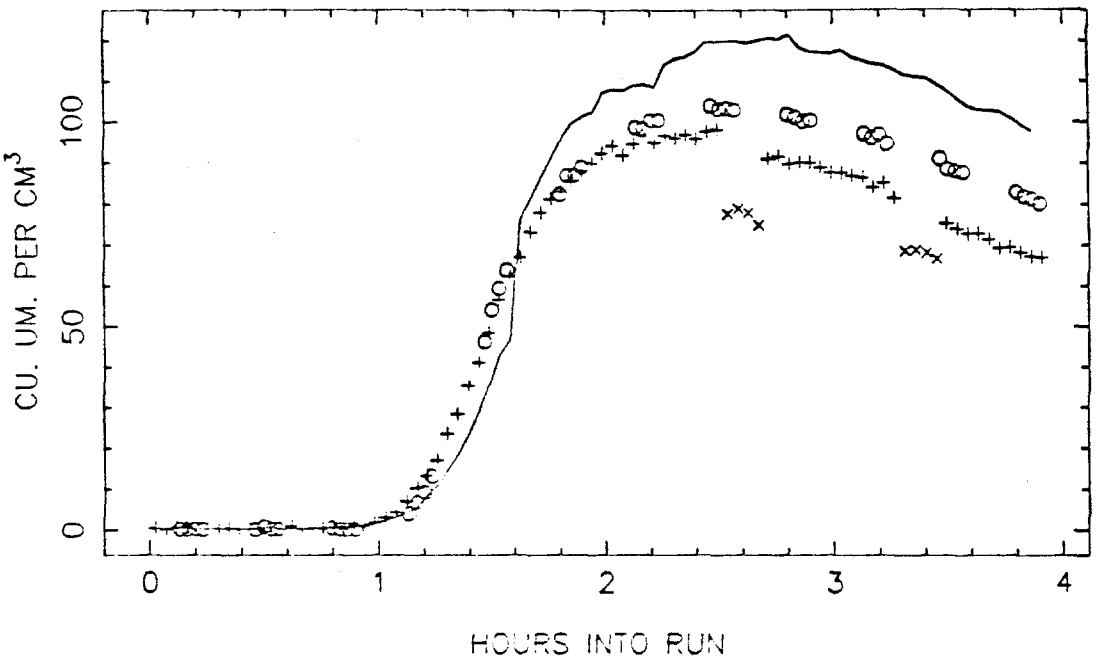

SIDE B

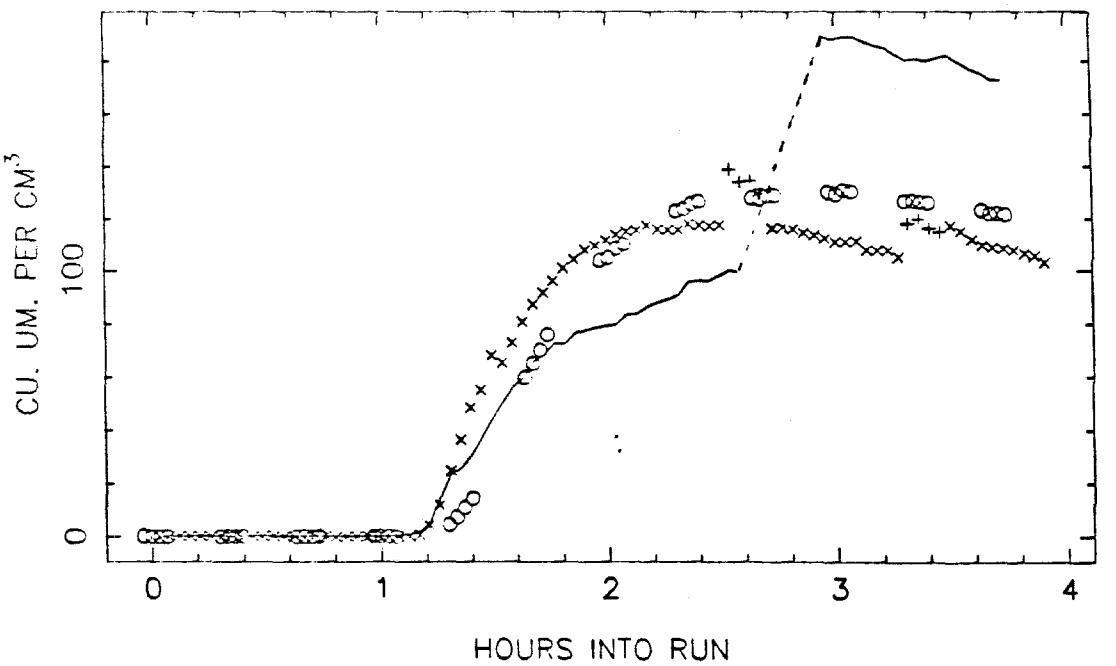

DQXA53 MEAN PARTICLE SIZE, SIDE A

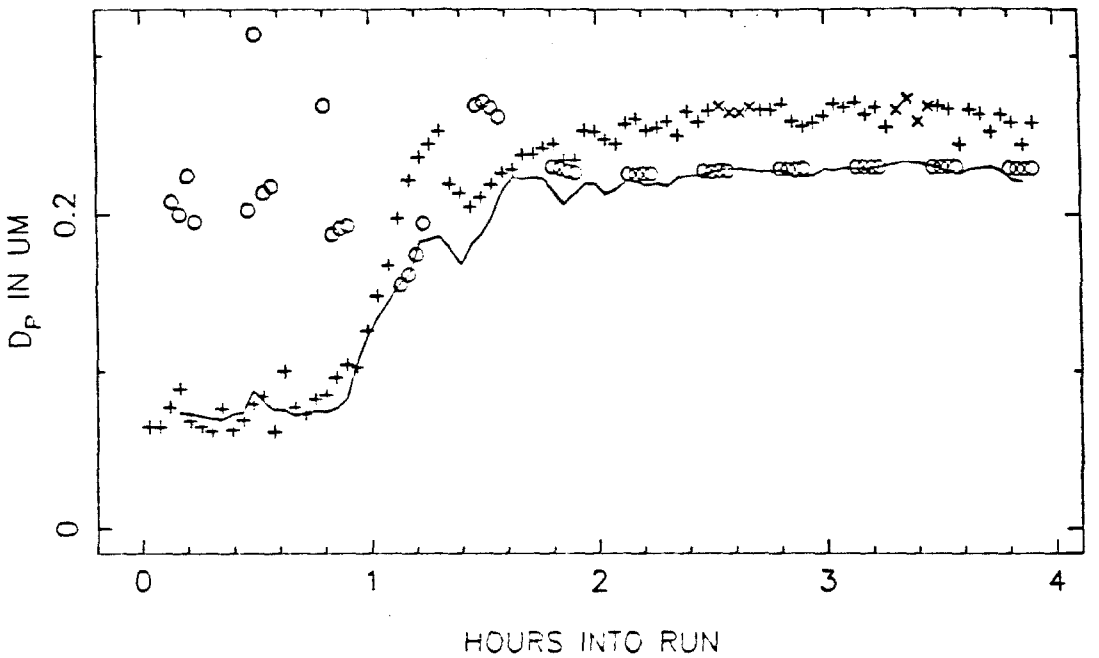

SIDE B

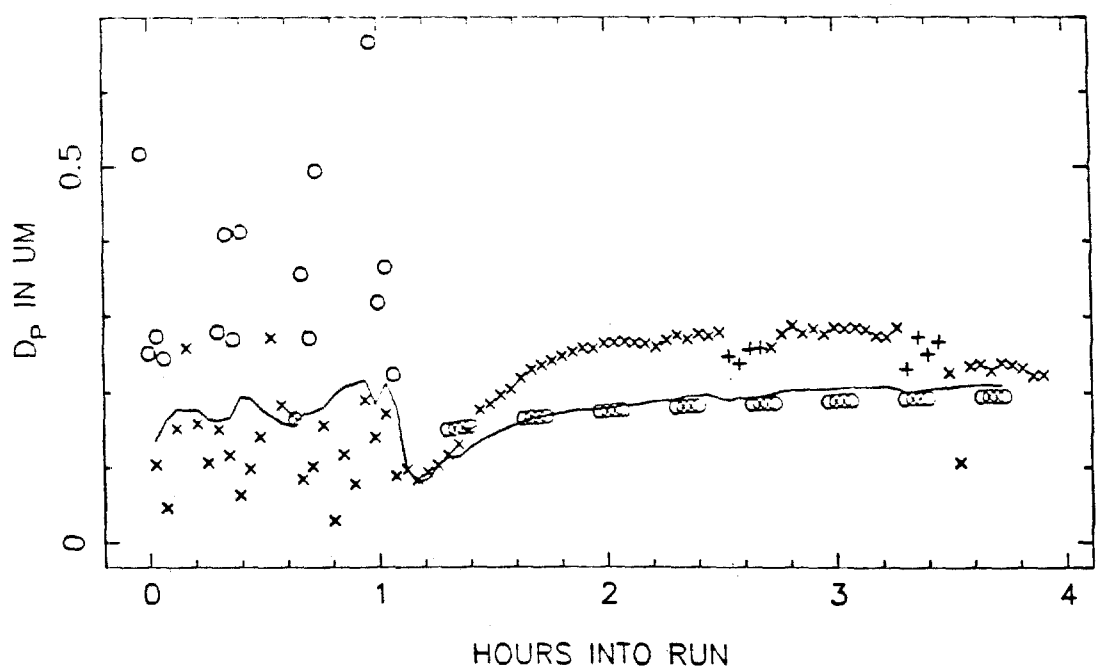

DQXA53A NUMBER DISTRIBUTION, T=0

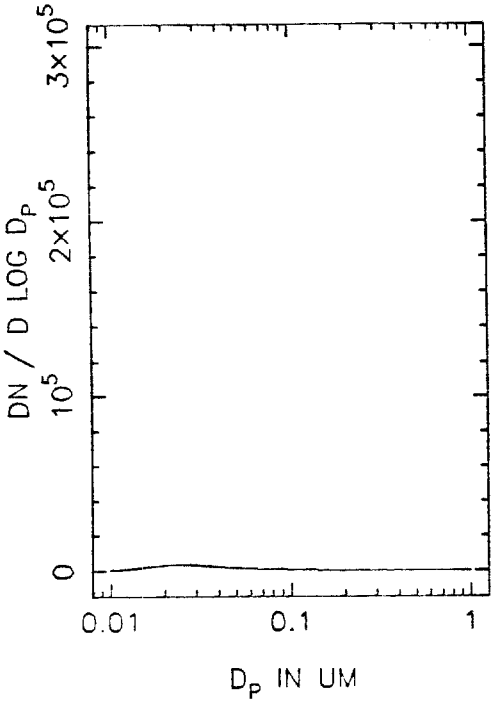

T=0.5 HOURS

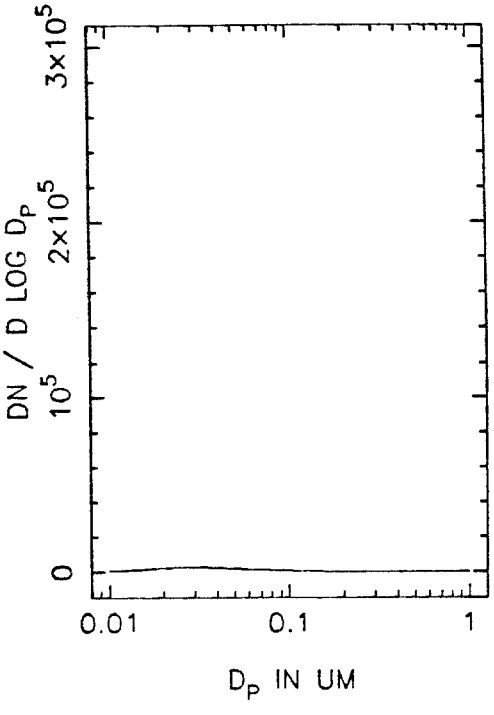

T=1.0 HOURS

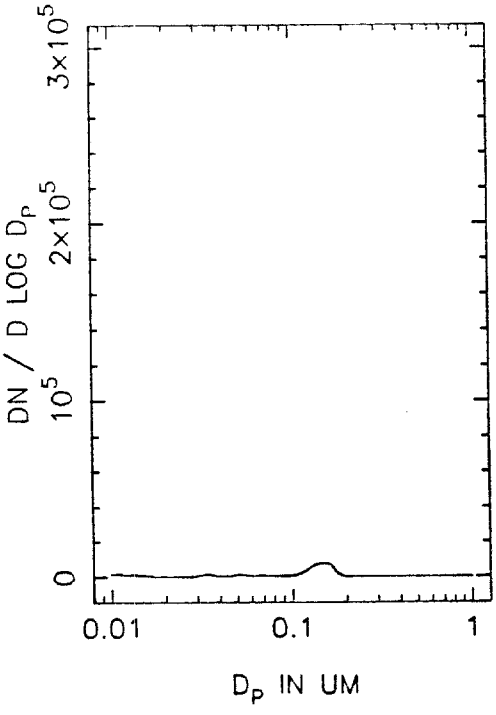

T=1.5 HOURS

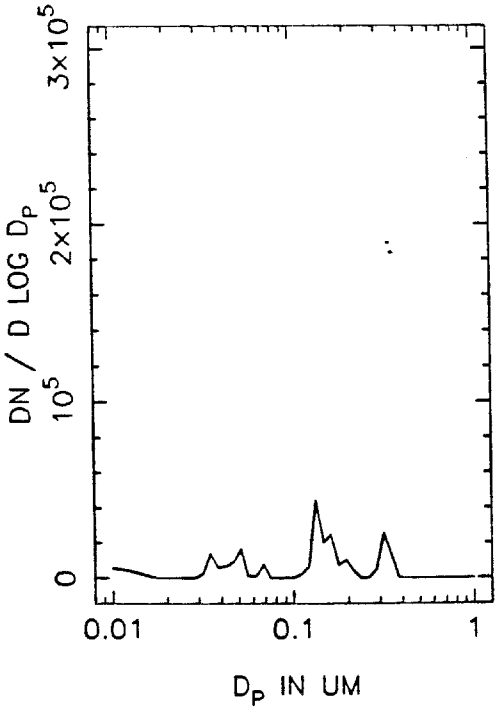

DQXA53A NUMBER DISTRIBUTION, T=2.0

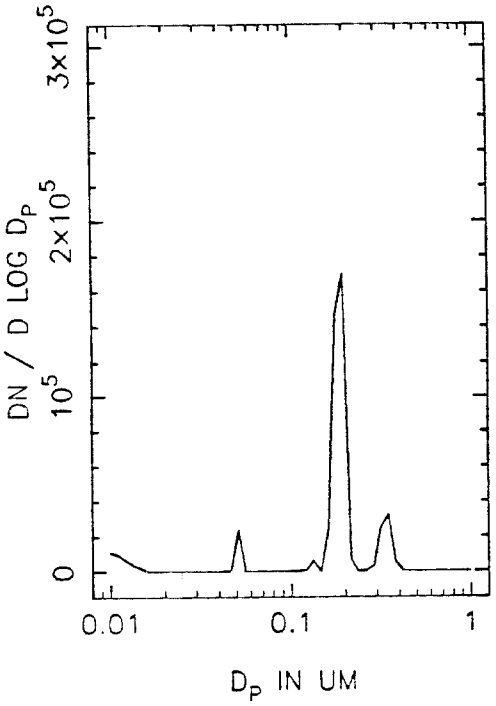

T=2.5 HOURS

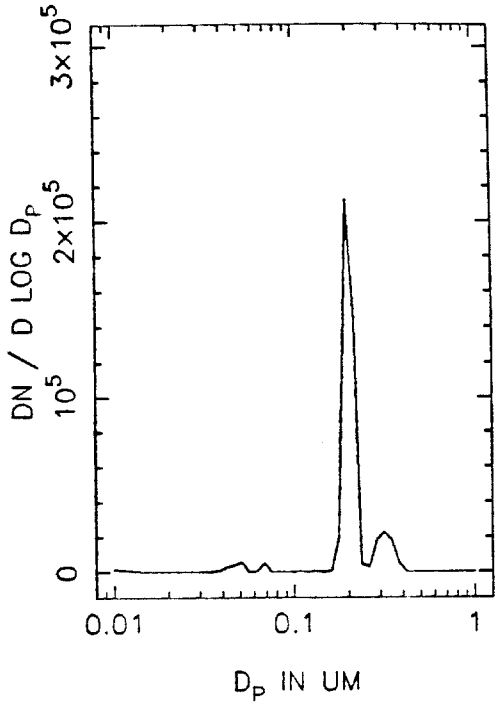

T=3.0 HOURS

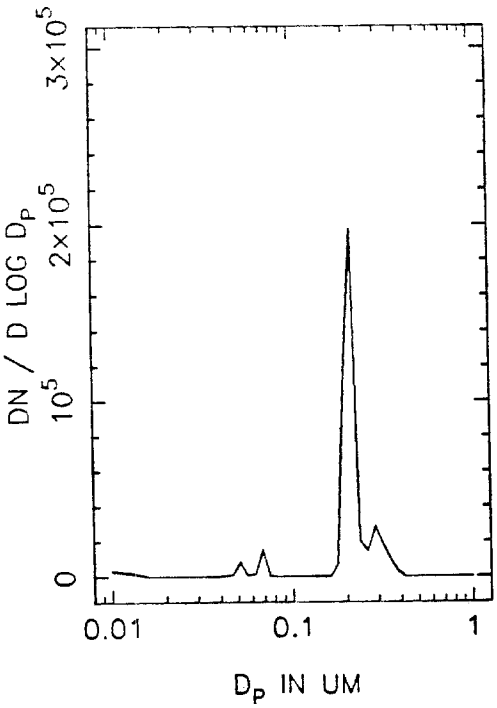

T=3.5 HOURS

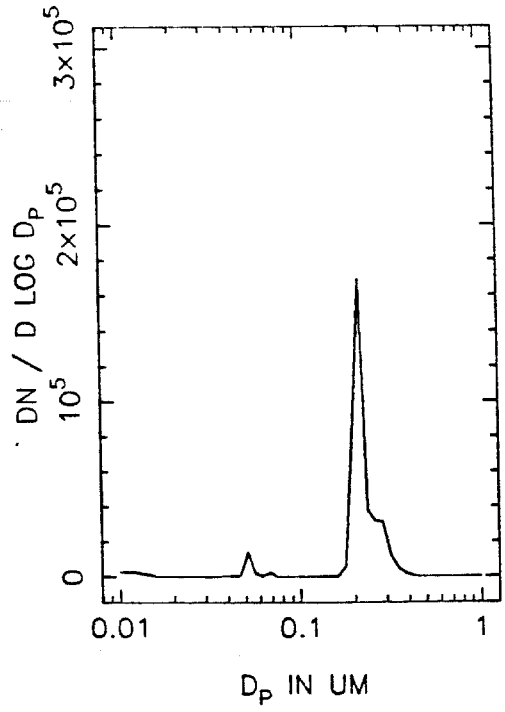

DQXA53A VOLUME DISTRIBUTION, T=0

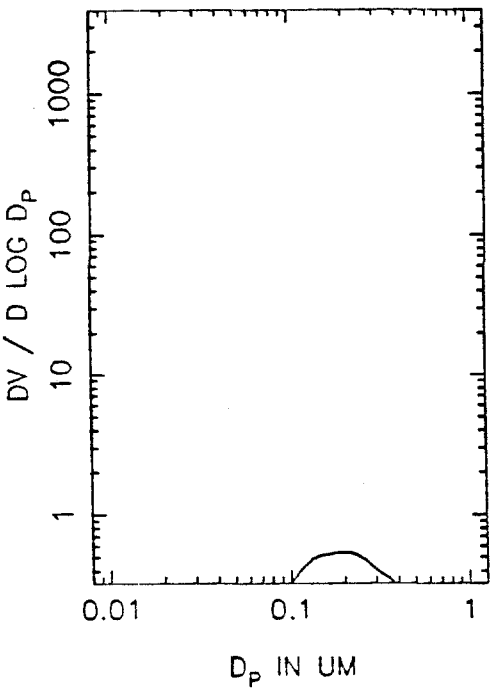

T=0.5 HOURS

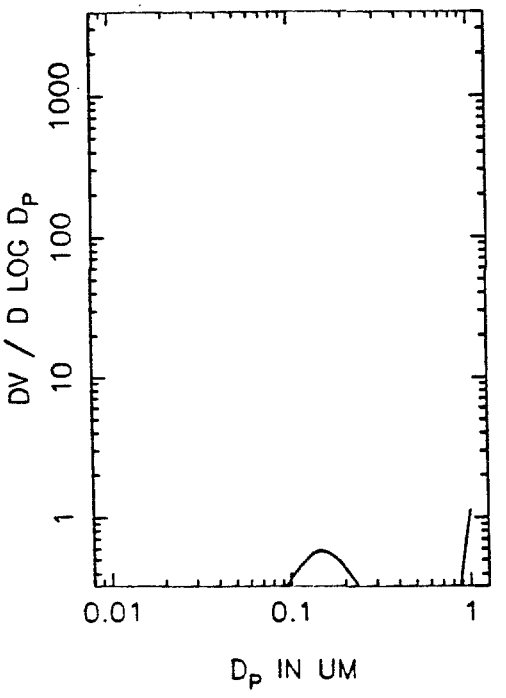

T=1.0 HOURS

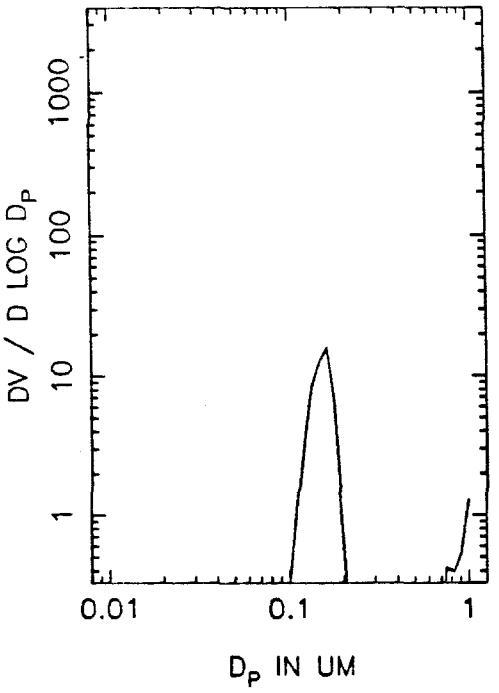

T=1.5 HOURS

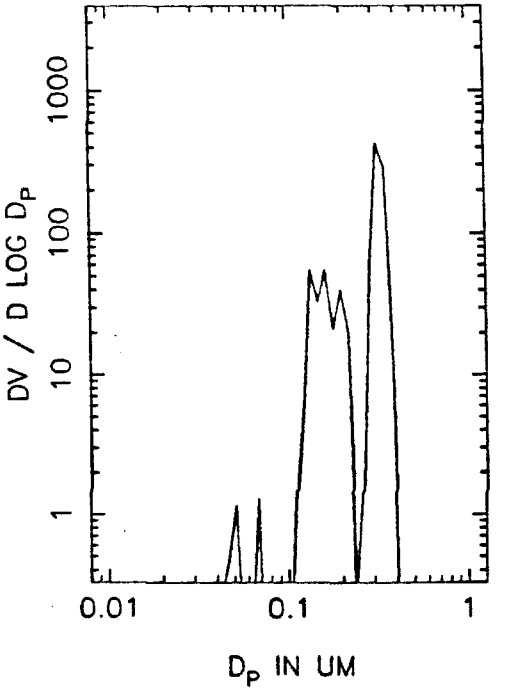

DQXA53A VOLUME DISTRIBUTION, T=2.0

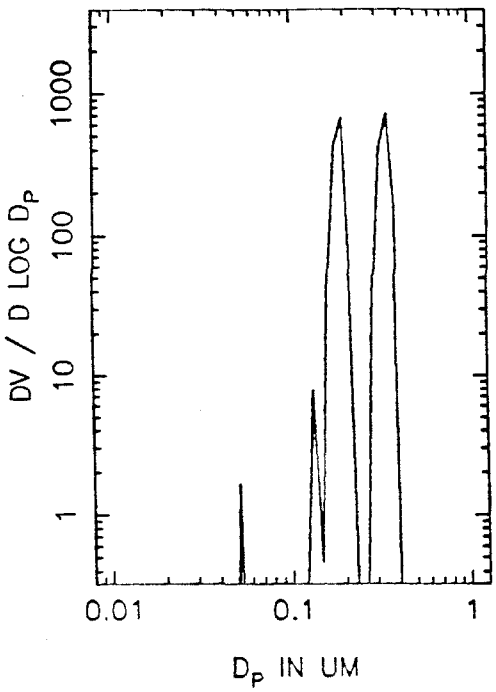

T=2.5 HOURS

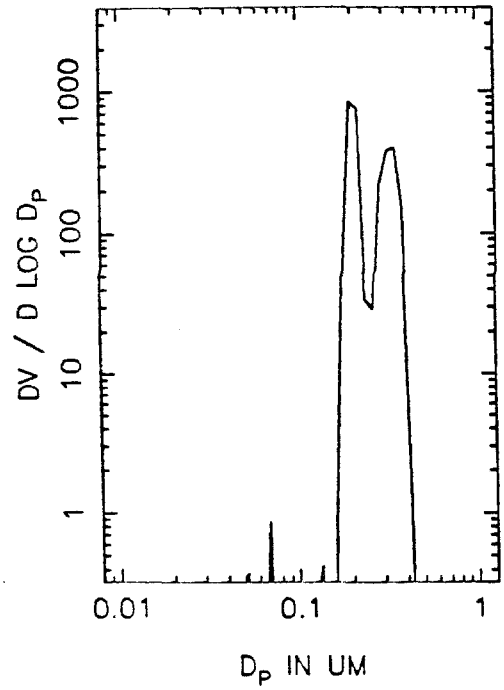

T=3.0 HOURS

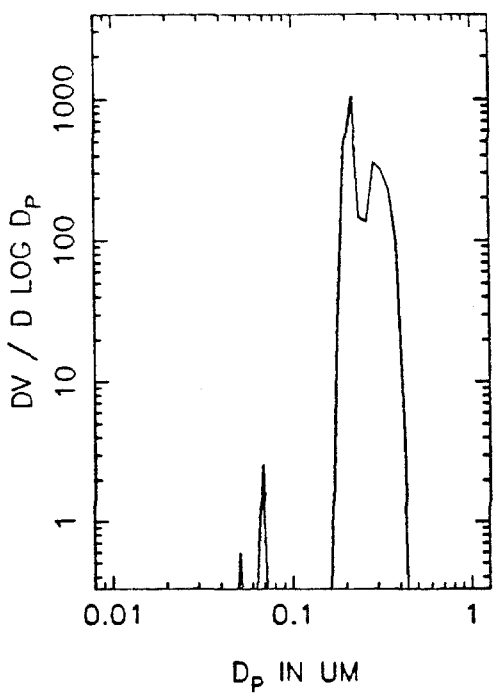

T=3.5 HOURS

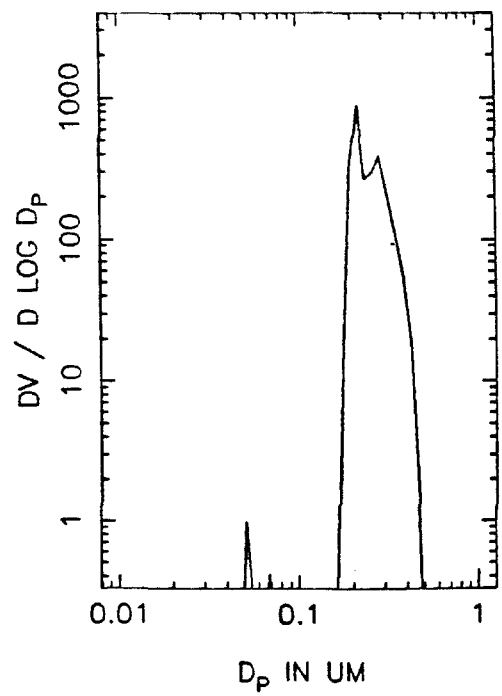

DQXA53B NUMBER DISTRIBUTION, T=0

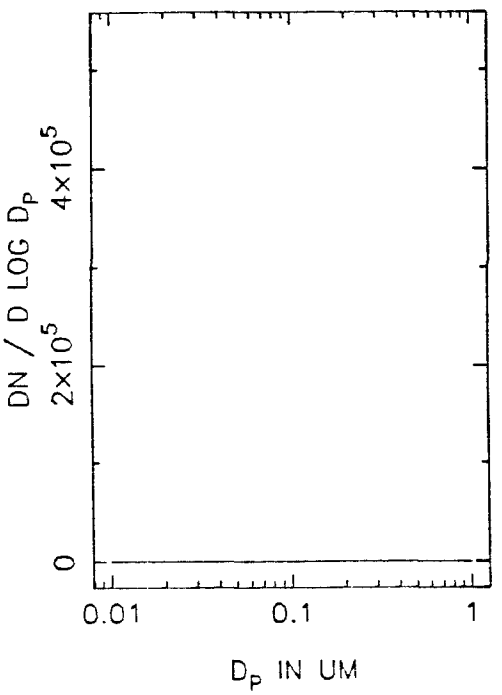

T=0.5 HOURS

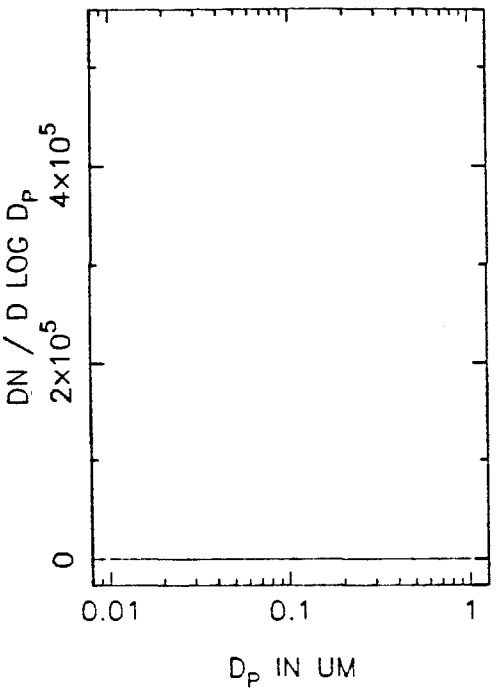

T=1.0 HOURS

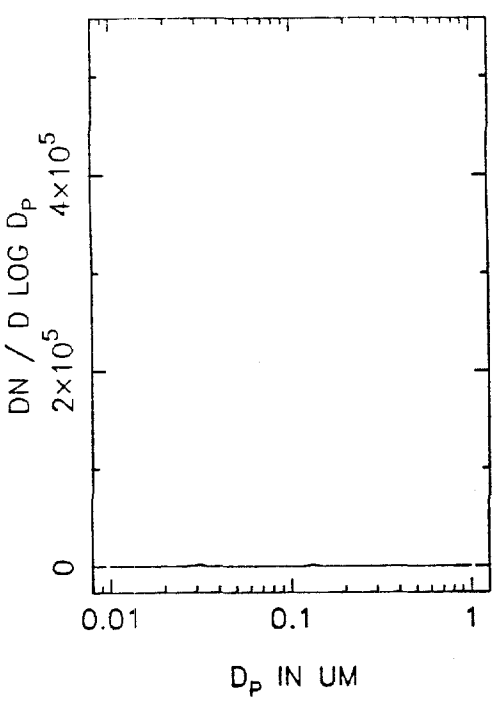

T=1.5 HOURS

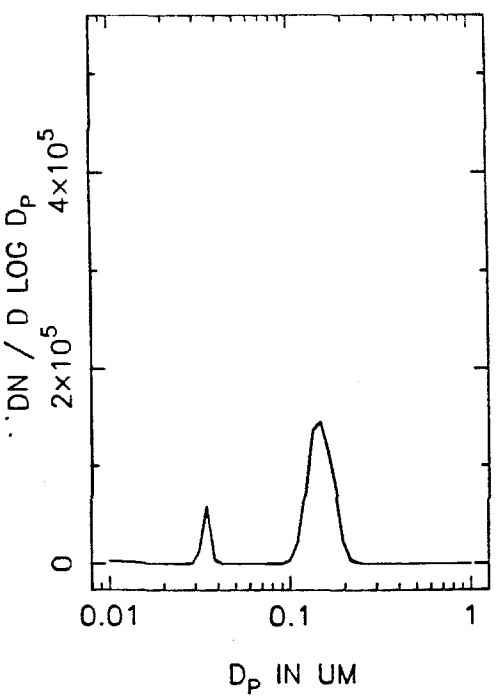

DQXA53B NUMBER DISTRIBUTION, T=2.0

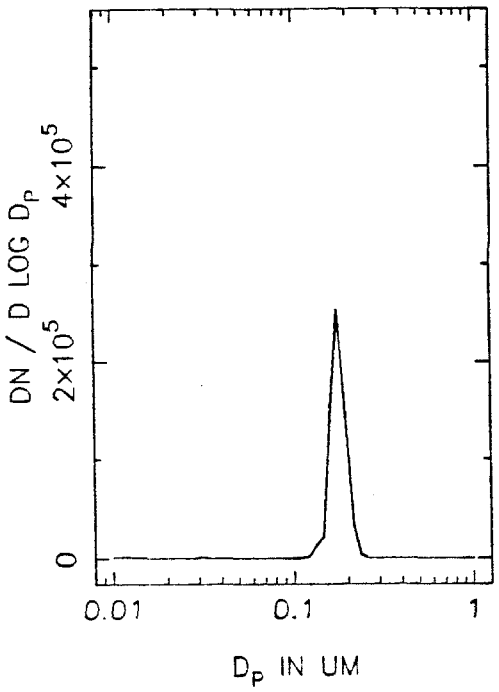

T=2.5 HOURS

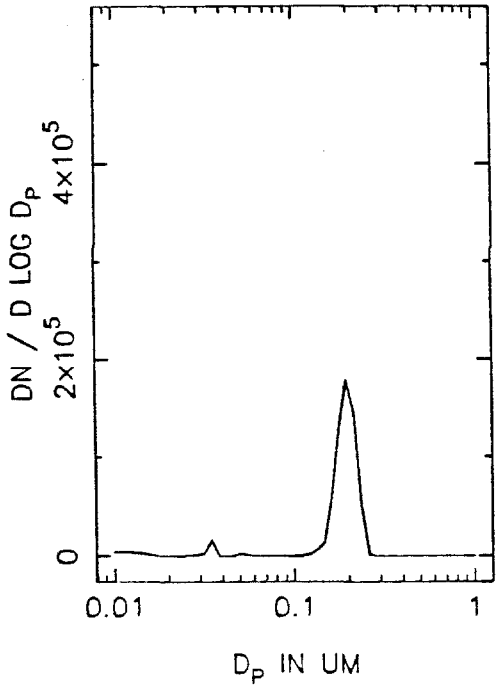

T=3.0 HOURS

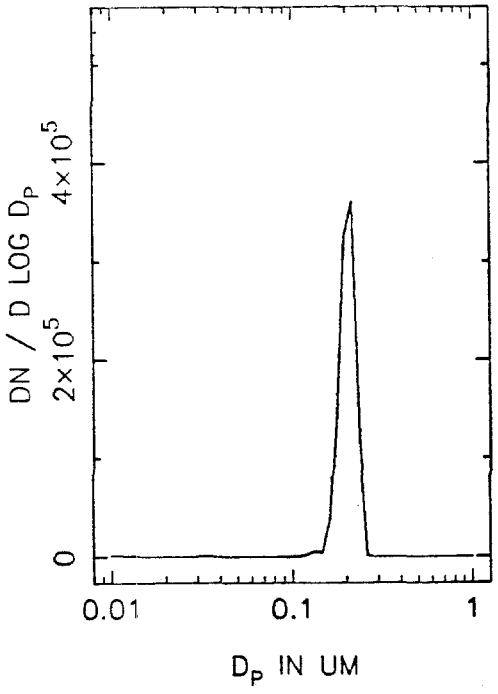

T=3.5 HOURS

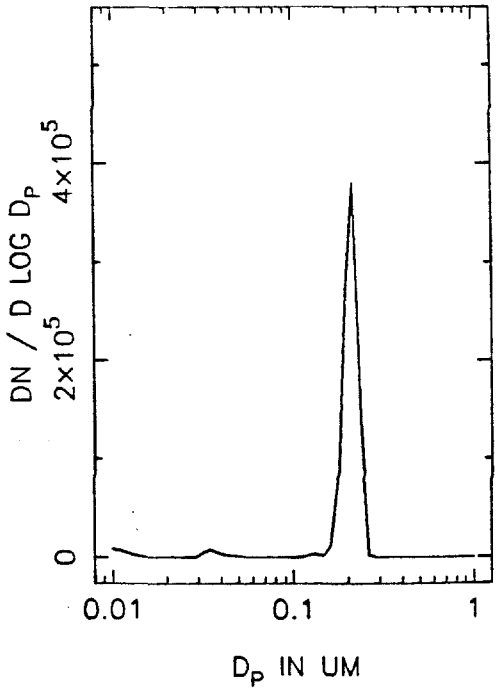

DQXA53B VOLUME DISTRIBUTION, T=0

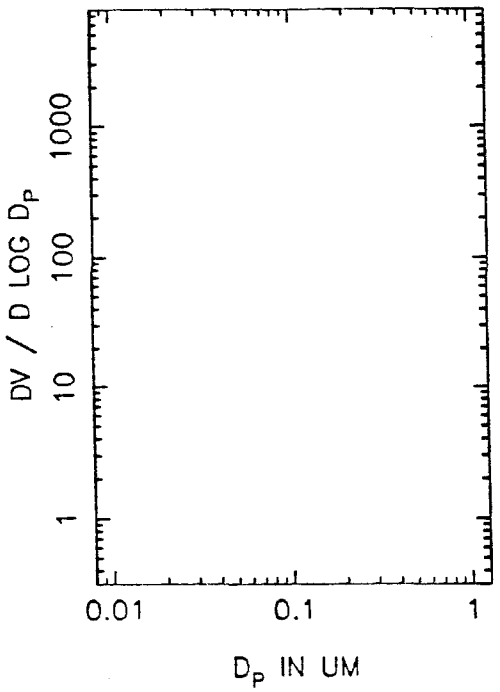

T=0.5 HOURS

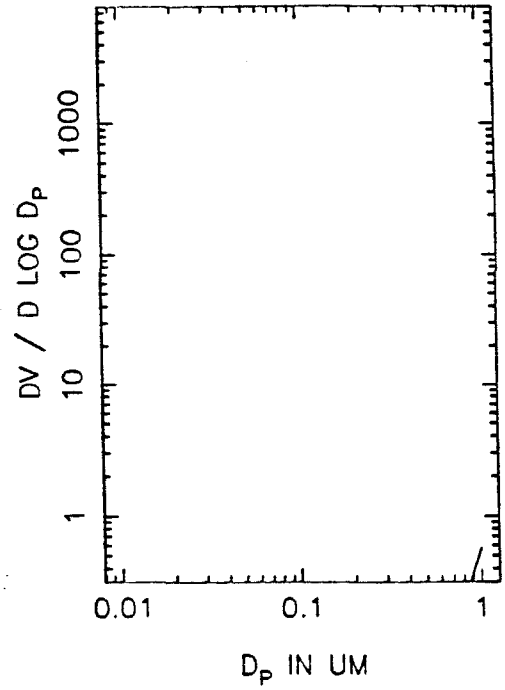

T=1.0 HOURS

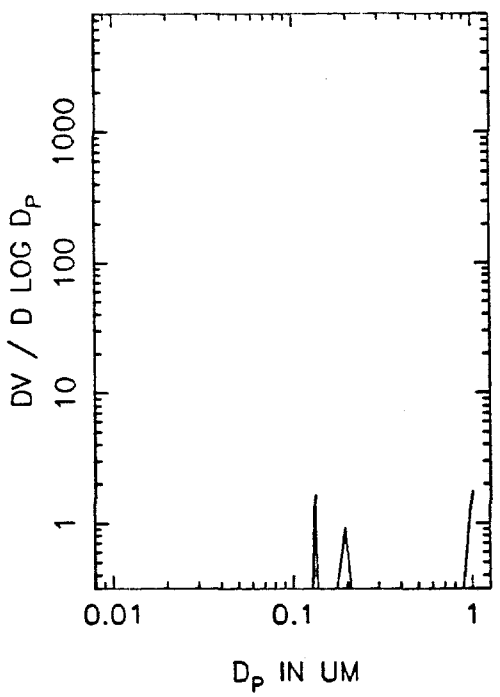

T=1.5 HOURS

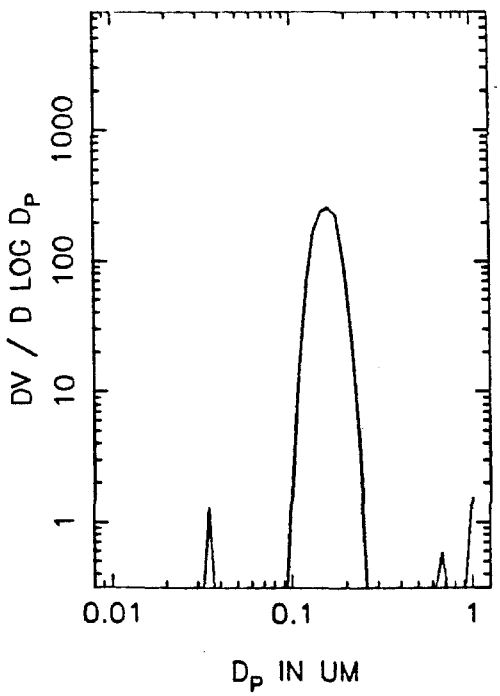

DQXA53B VOLUME DISTRIBUTION, T=2.0

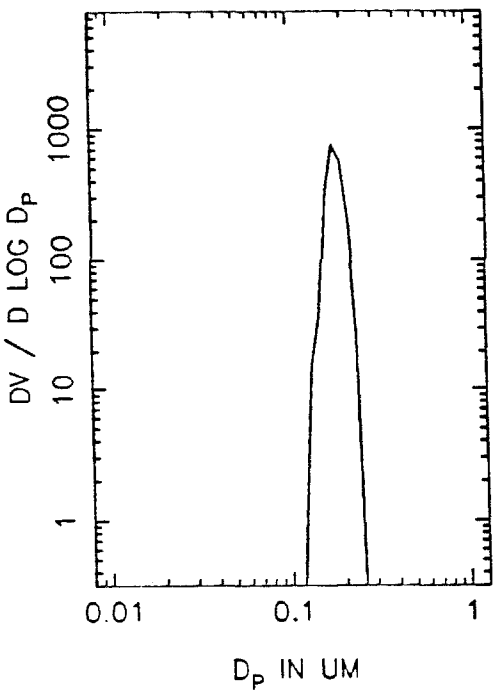

T=2.5 HOURS

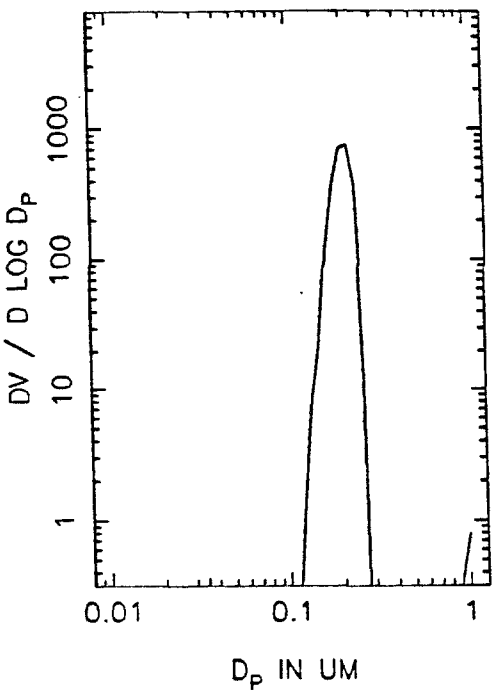

T=3.0 HOURS

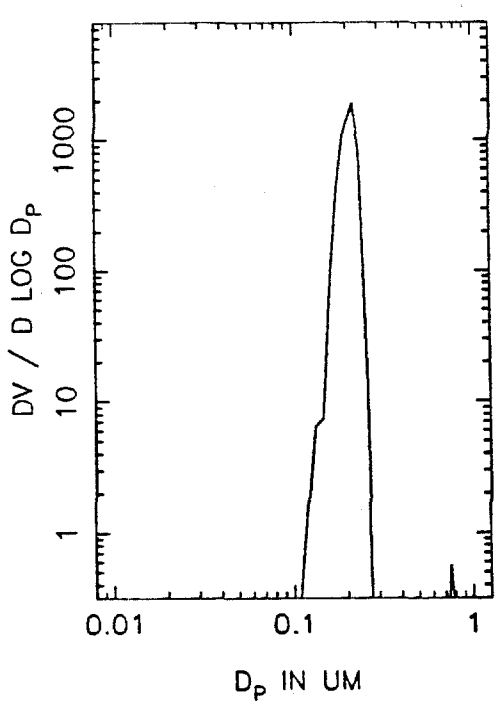

T=3.5 HOURS

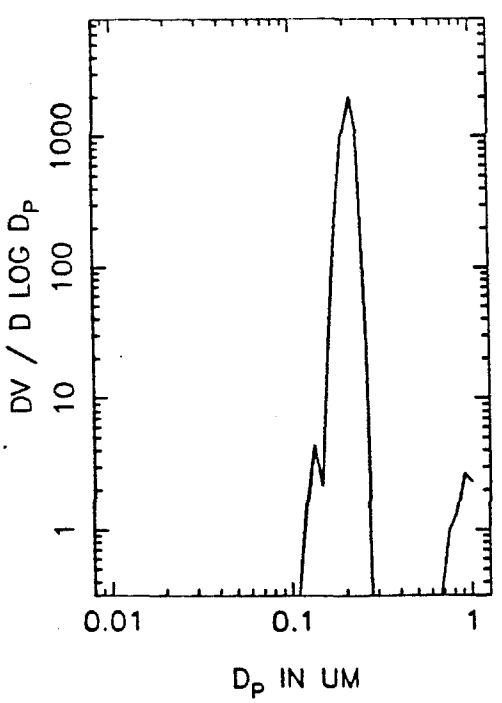

DQXA55 TOTAL NUMBER, SIDE A

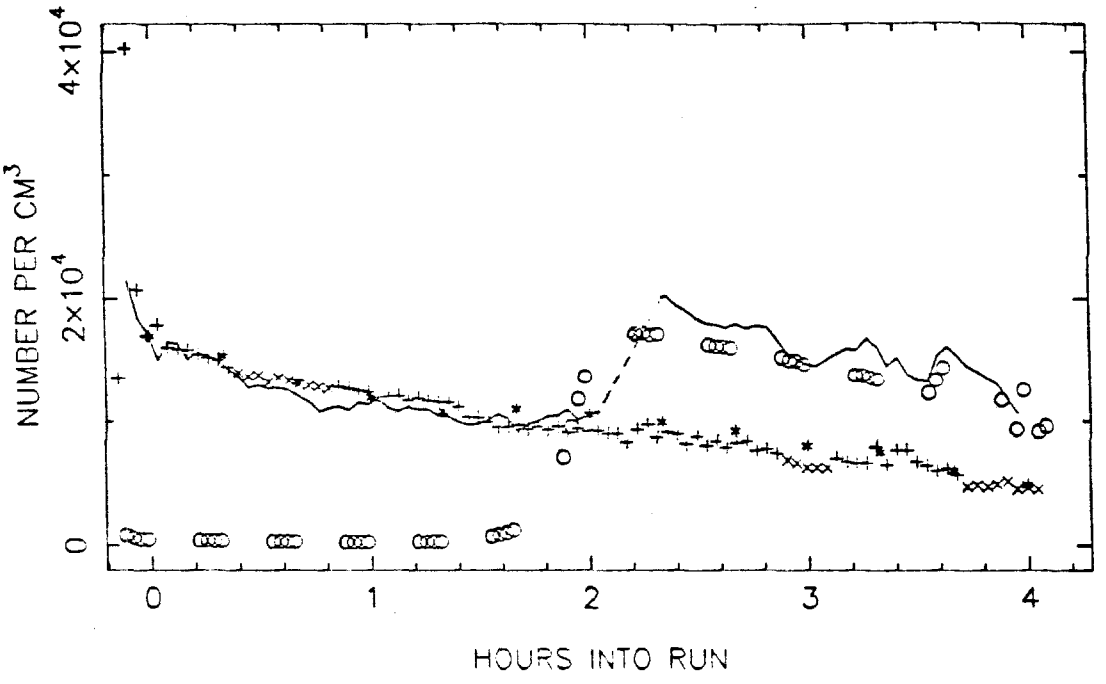

SIDE B

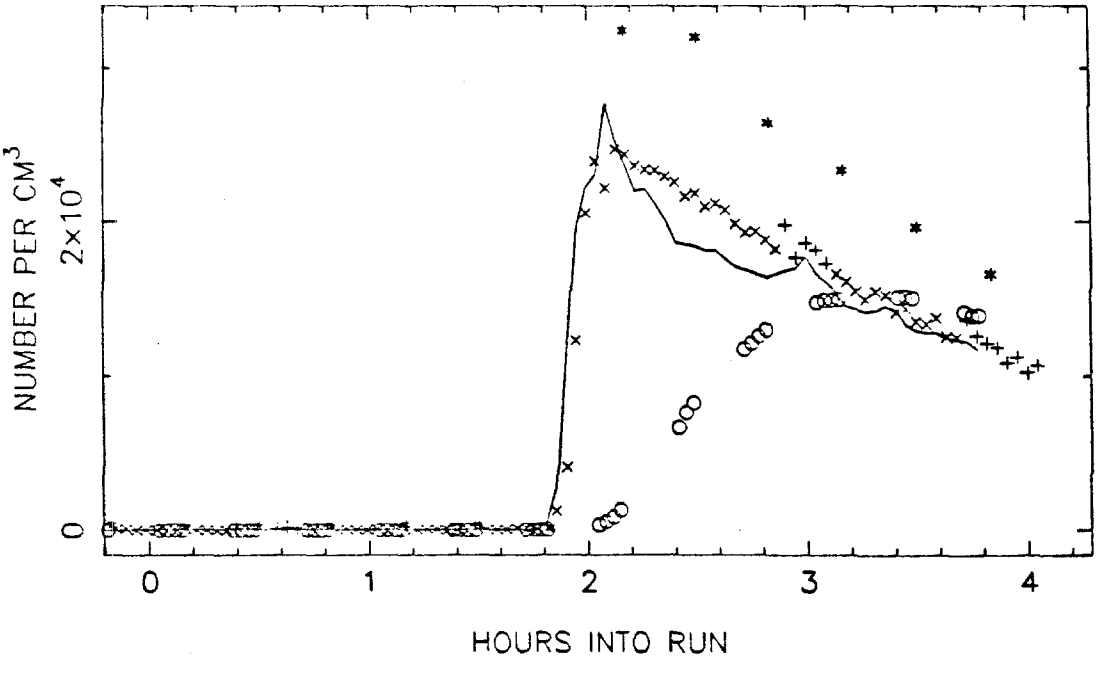

DQXA55 VOLUME IN THE AEROSOL PHASE, SIDE A

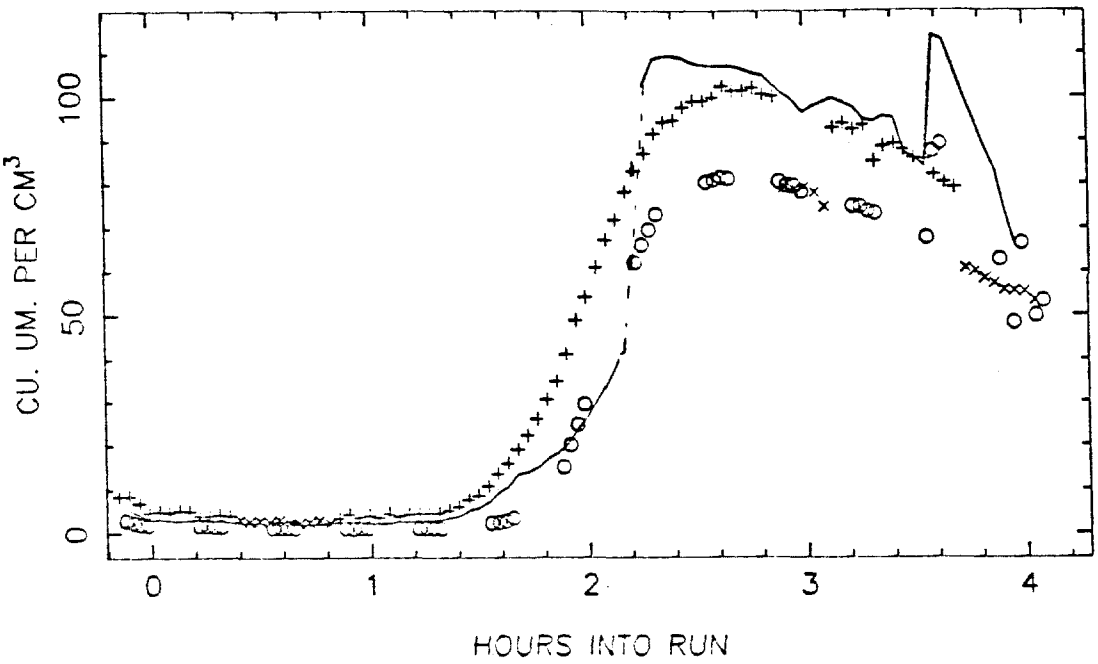

SIDE B

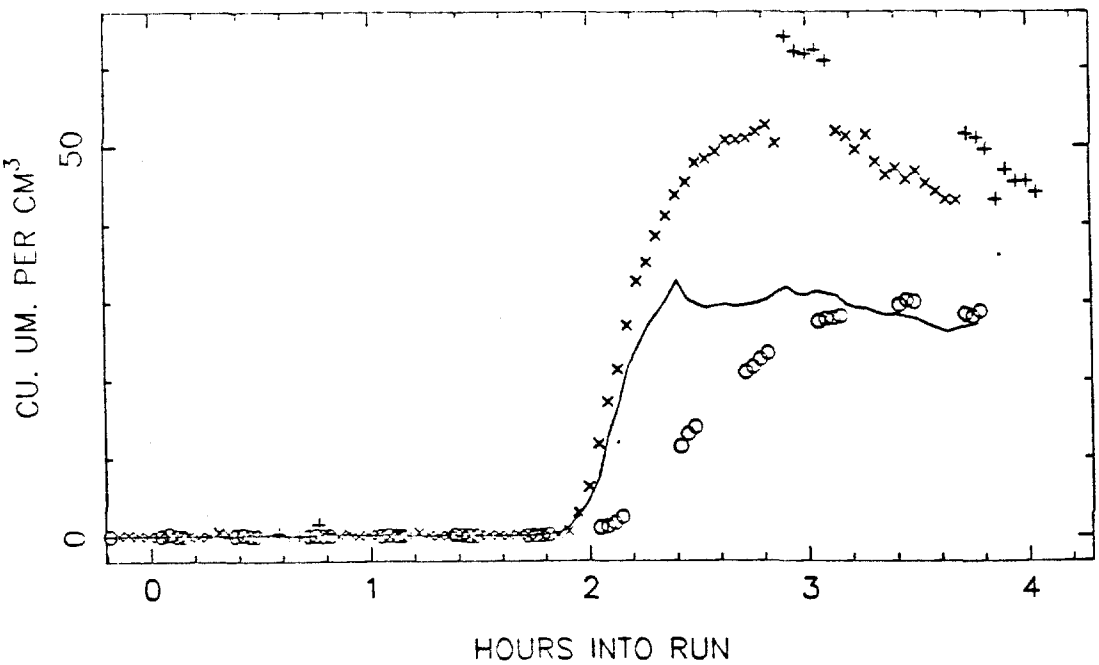

DQXA55 MEAN PARTICLE SIZE, SIDE A

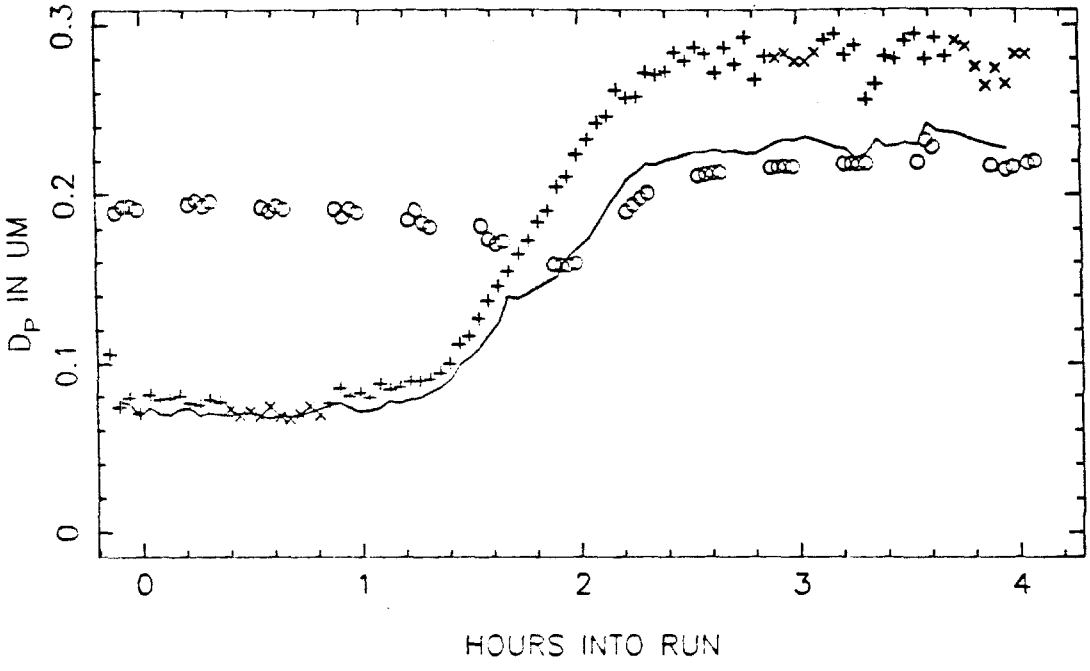

SIDE B

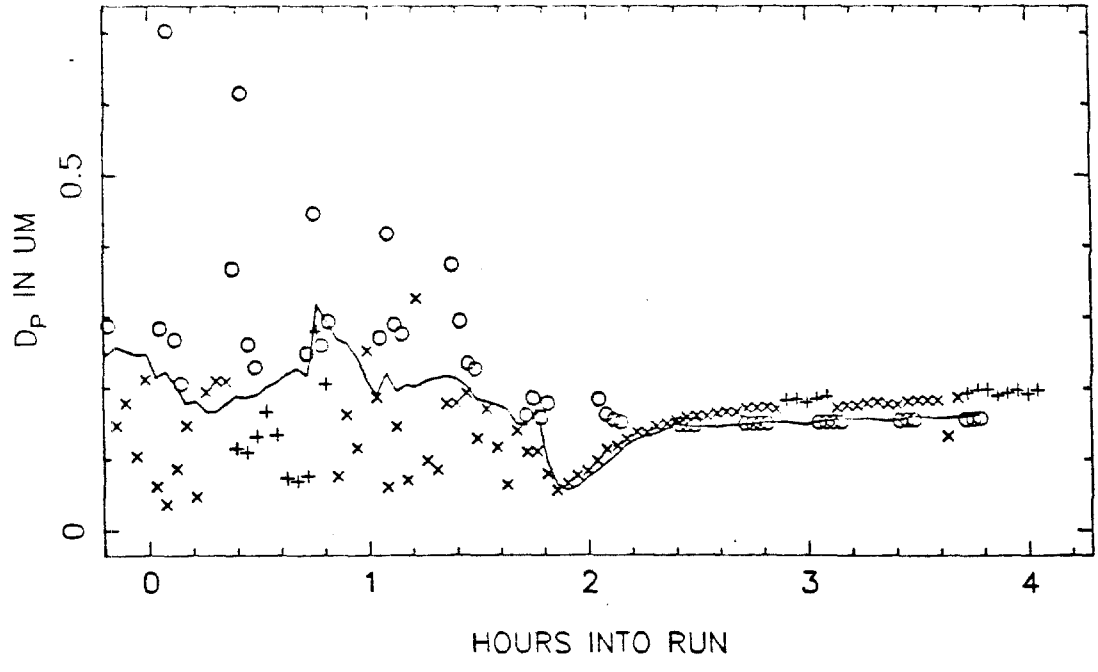

DQXA55A NUMBER DISTRIBUTION, T=0

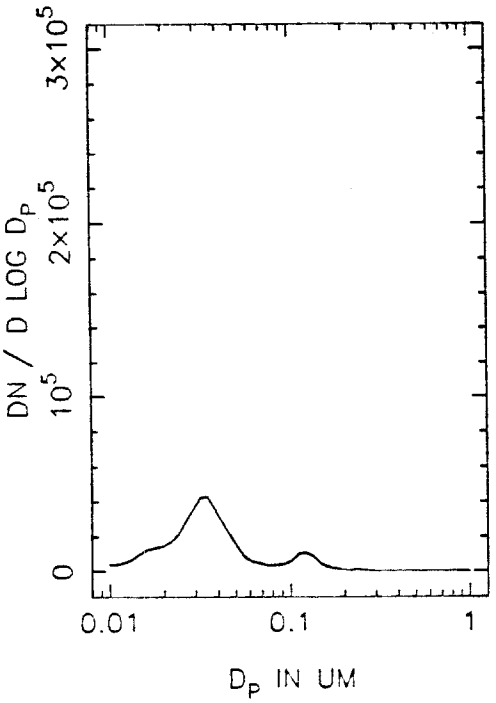

T=0.5 HOURS

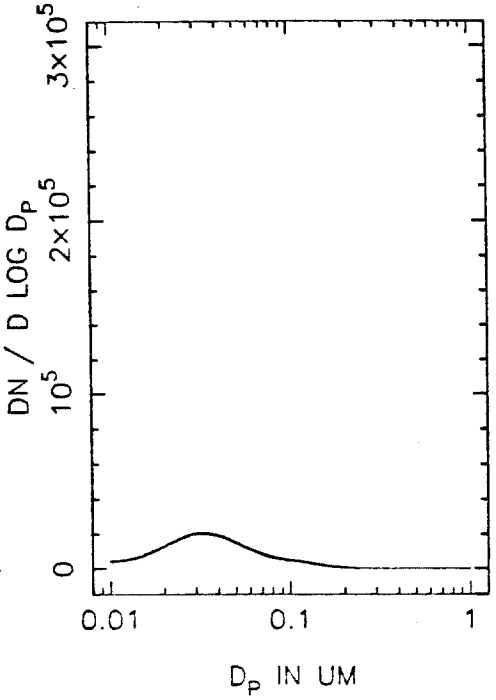

T=1.0 HOURS

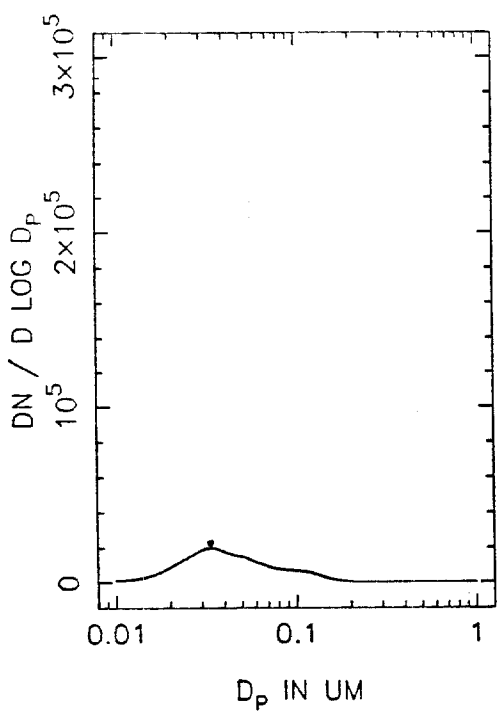

T=1.5 HOURS

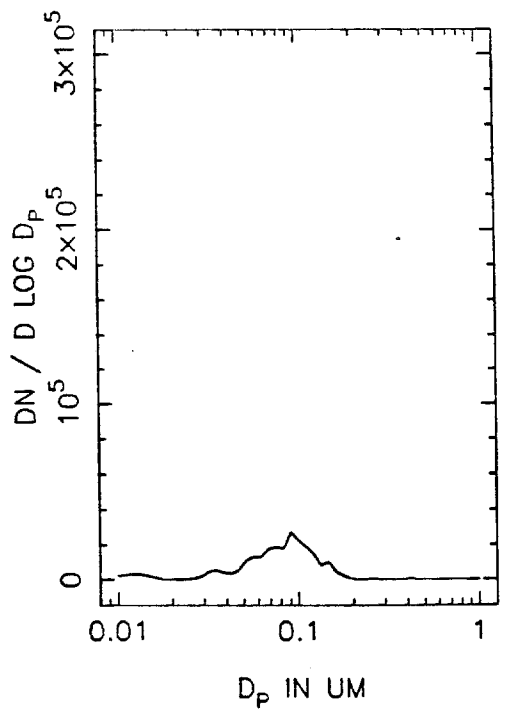

DQXA55A NUMBER DISTRIBUTION, T=2.0

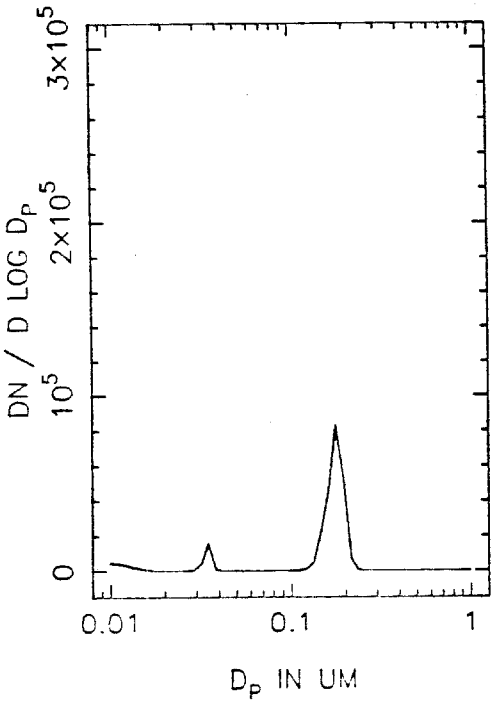

T=2.5 HOURS

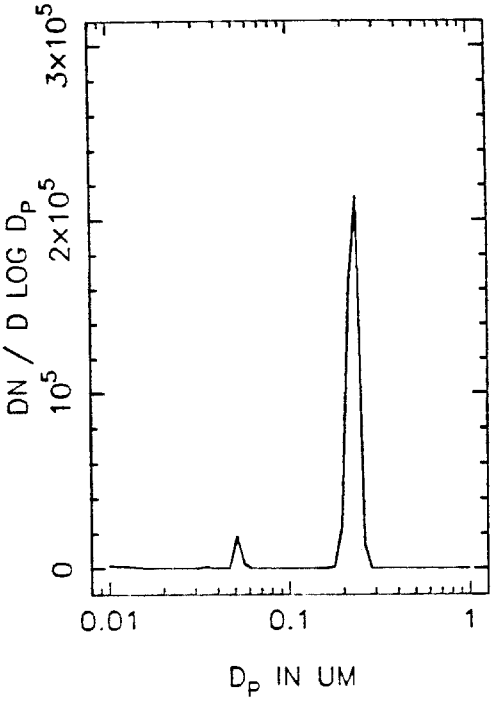

T=3.0 HOURS

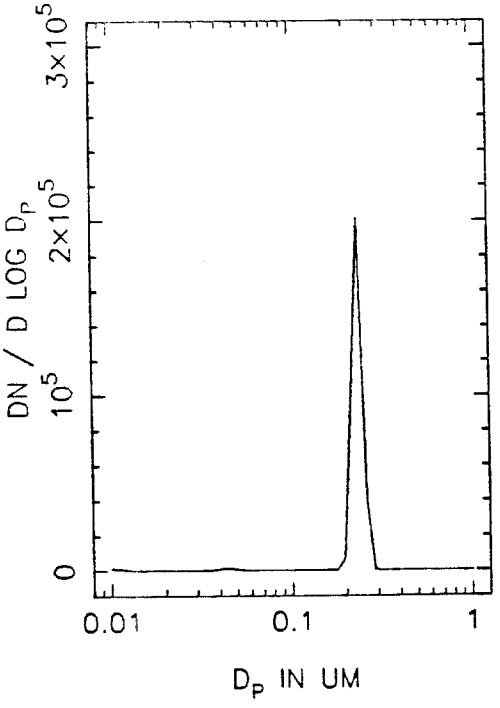

T=3.5 HOURS

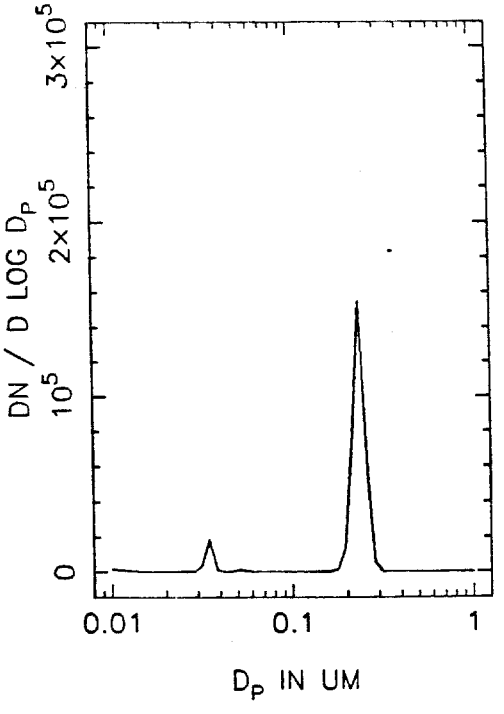

DQXA55A VOLUME DISTRIBUTION, T=0

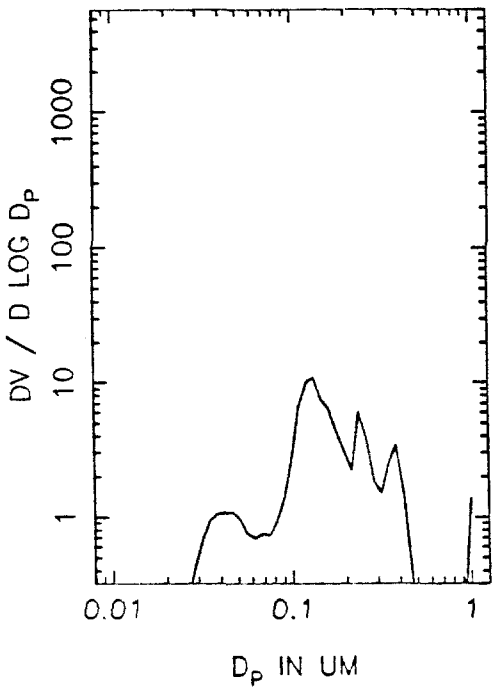

T=0.5 HOURS

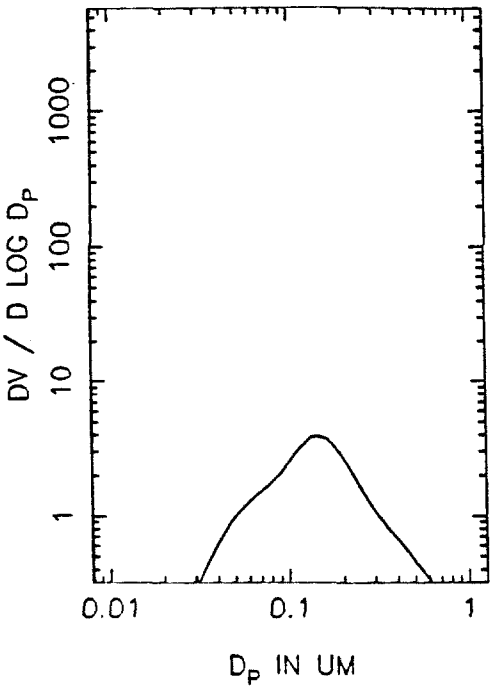

T=1.0 HOURS

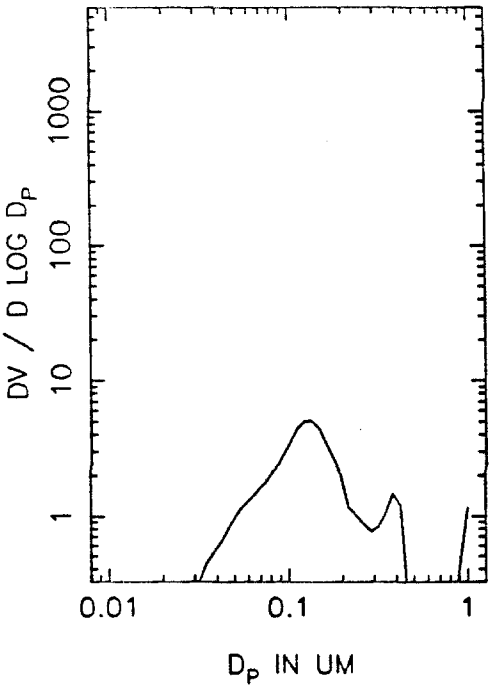

T=1.5 HOURS

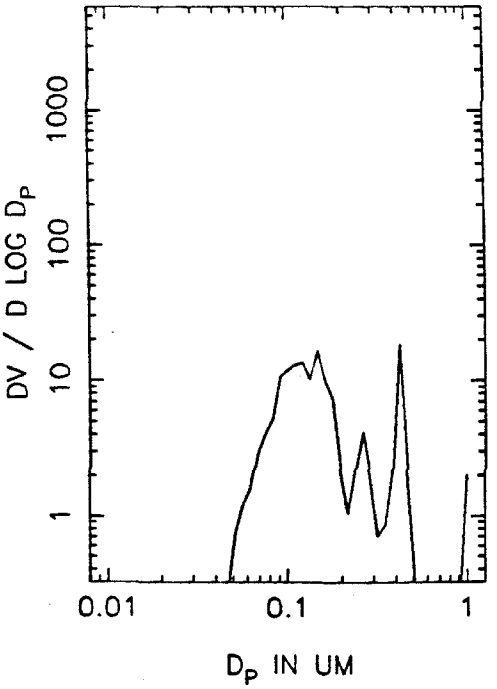

DQXA55A VOLUME DISTRIBUTION, T=2.0

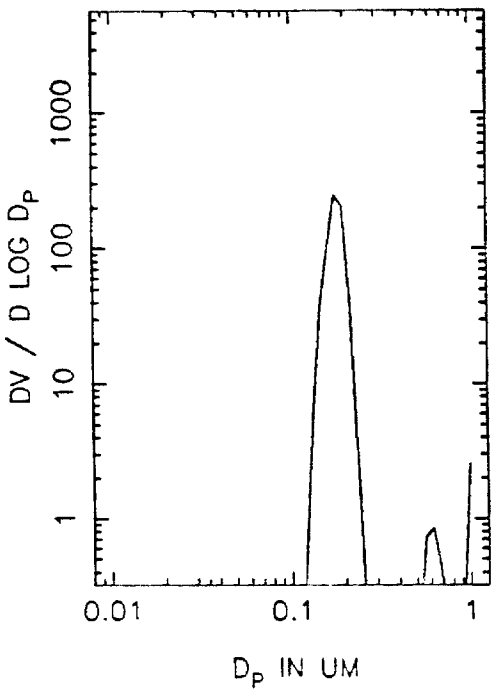

T=2.5 HOURS

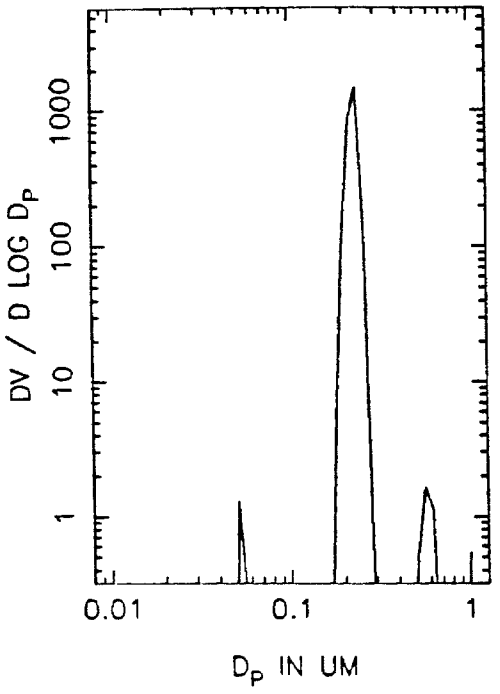

T=3.0 HOURS

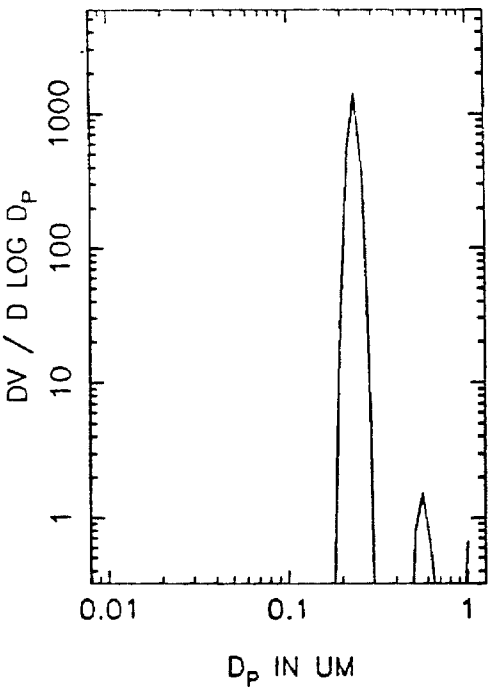

T=3.5 HOURS

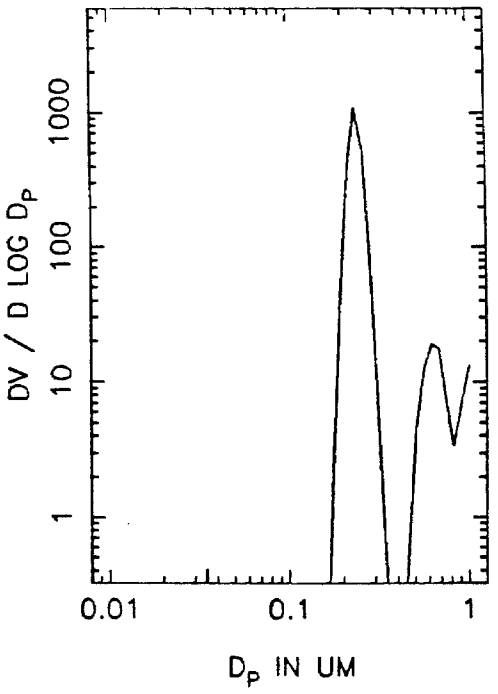

DQXA55B NUMBER DISTRIBUTION, T=0

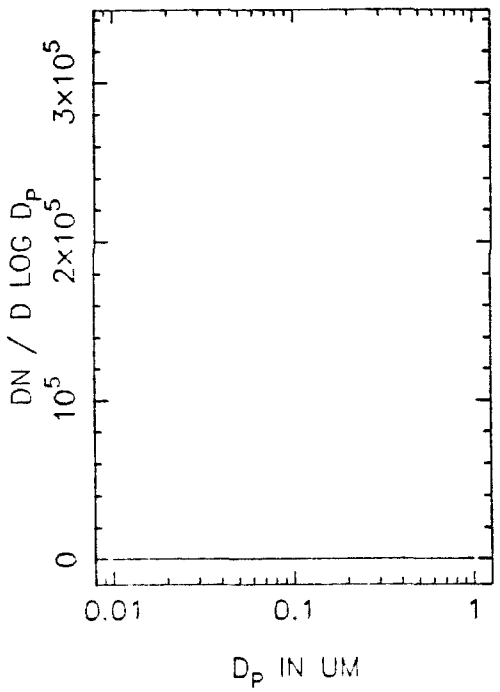

T=0.5 HOURS

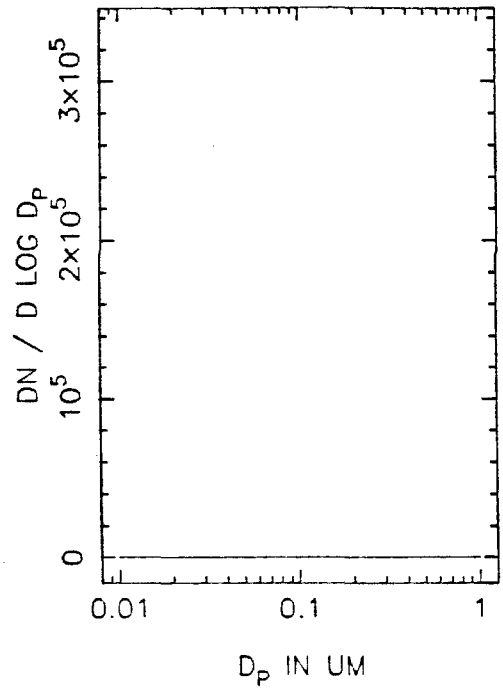

T=1.0 HOURS

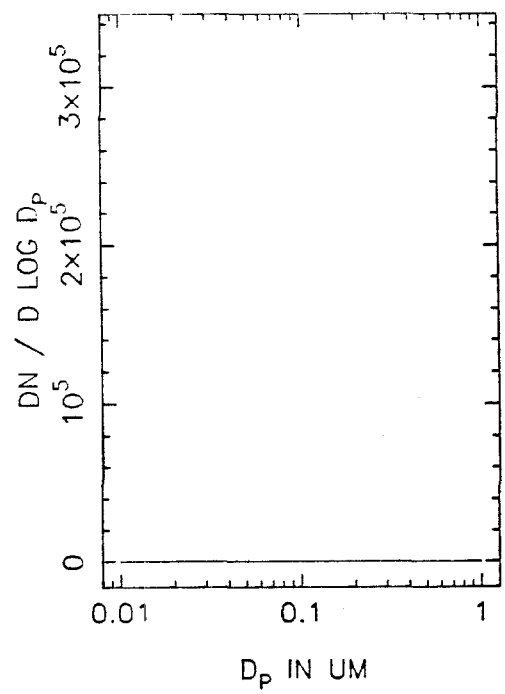

T=1.5 HOURS

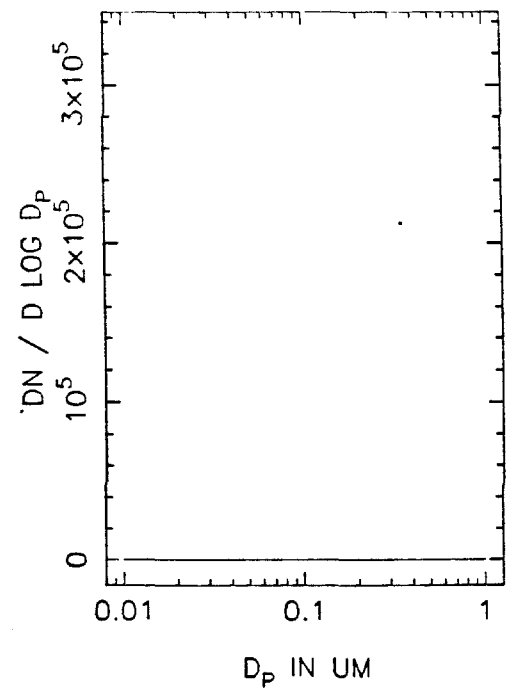

DQXA55B NUMBER DISTRIBUTION, T=2.0

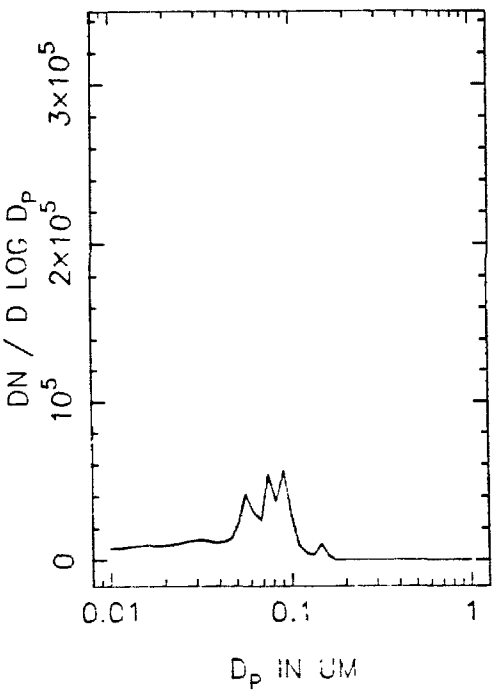

T=2.5 HOURS

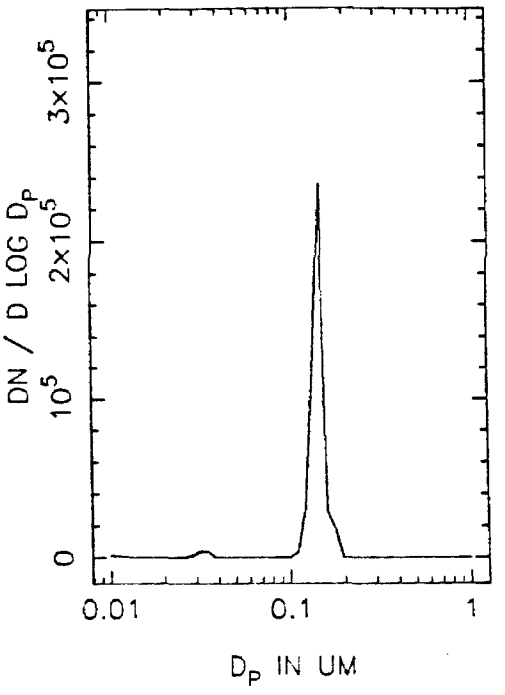

T=3.0 HOURS

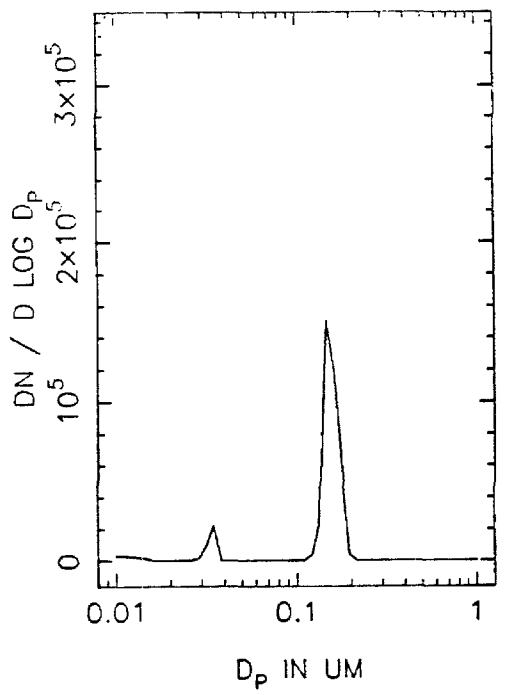

T=3.5 HOURS

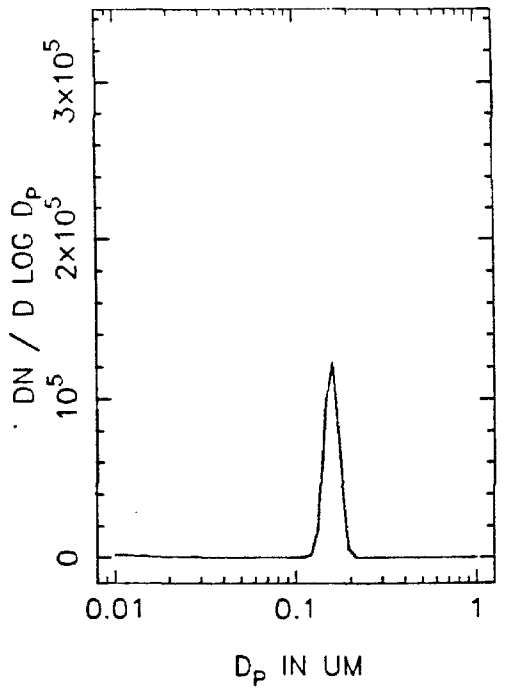

DQXA55B VOLUME DISTRIBUTION, T=0

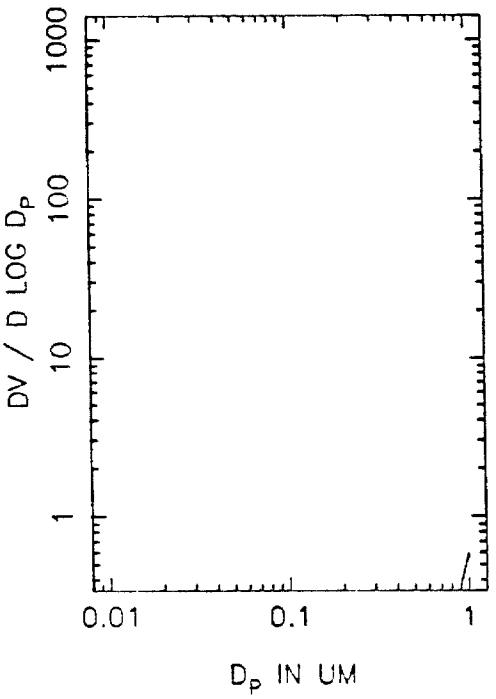

T=0.5 HOURS

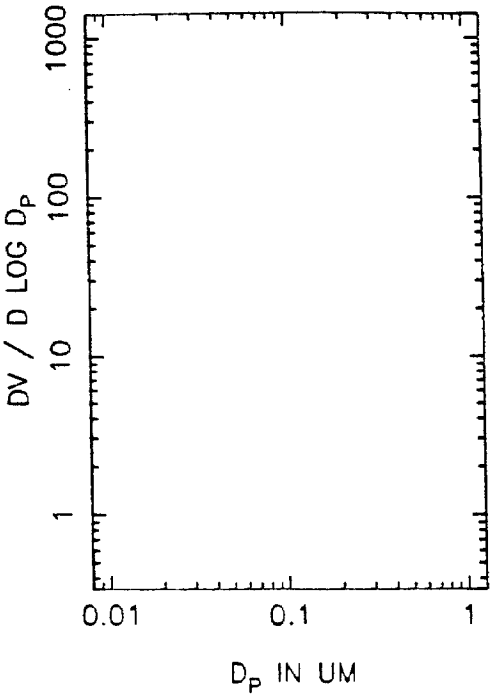

T=1.0 HOURS

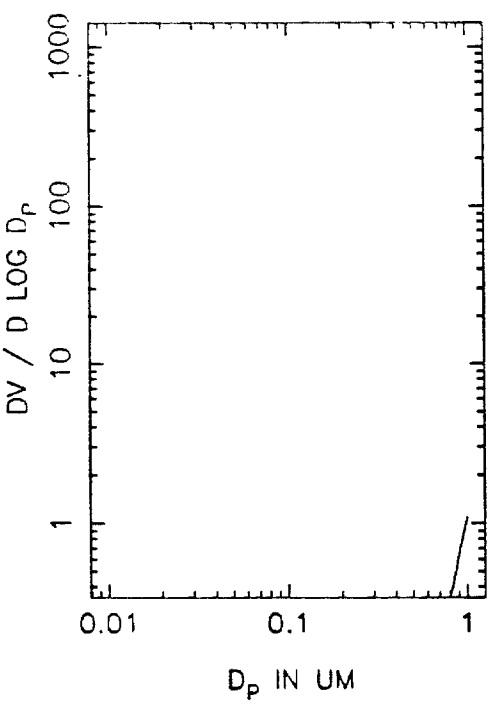

T=1.5 HOURS

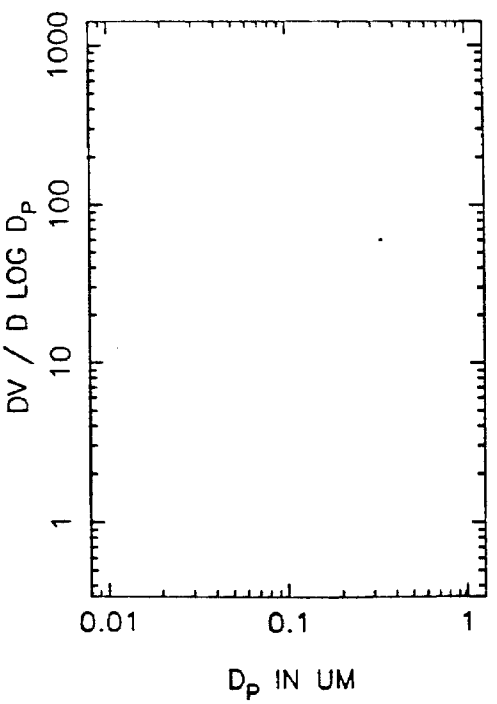

DQXA55B VOLUME DISTRIBUTION, T=2.0

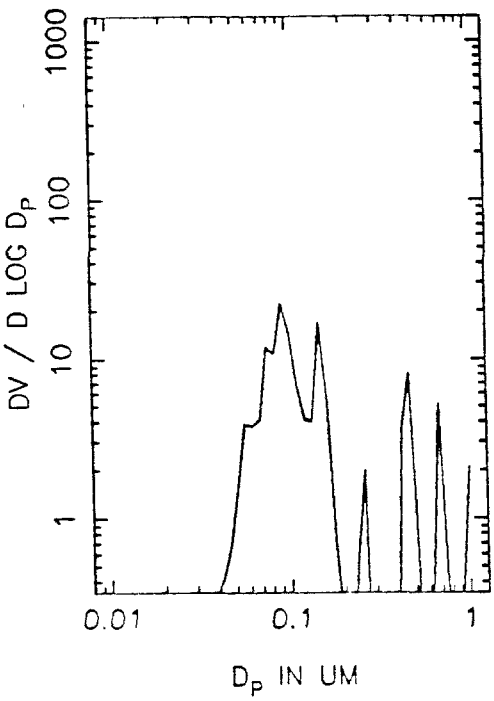

T=2.5 HOURS

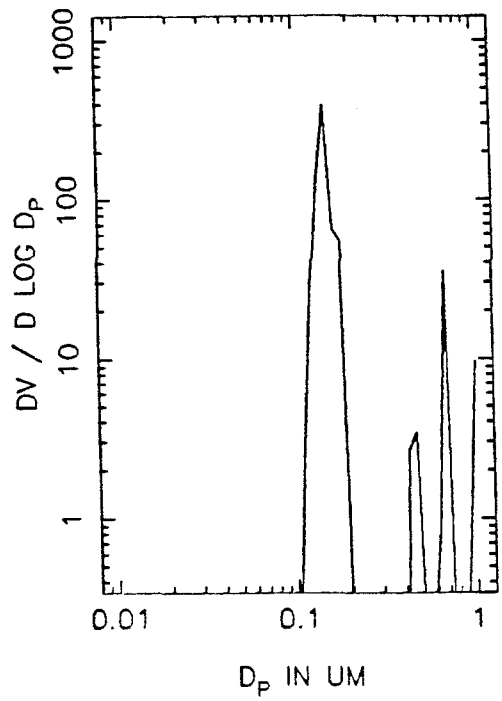

T=3.0 HOURS

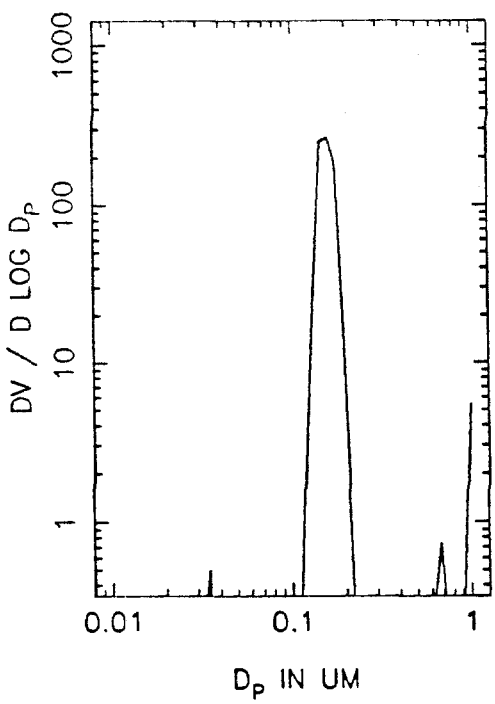

T=3.5 HOURS

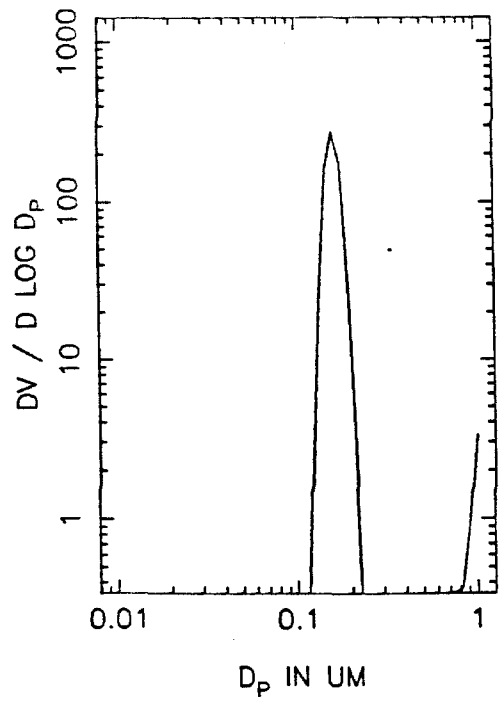

DQXA57 TOTAL NUMBER, SIDE A

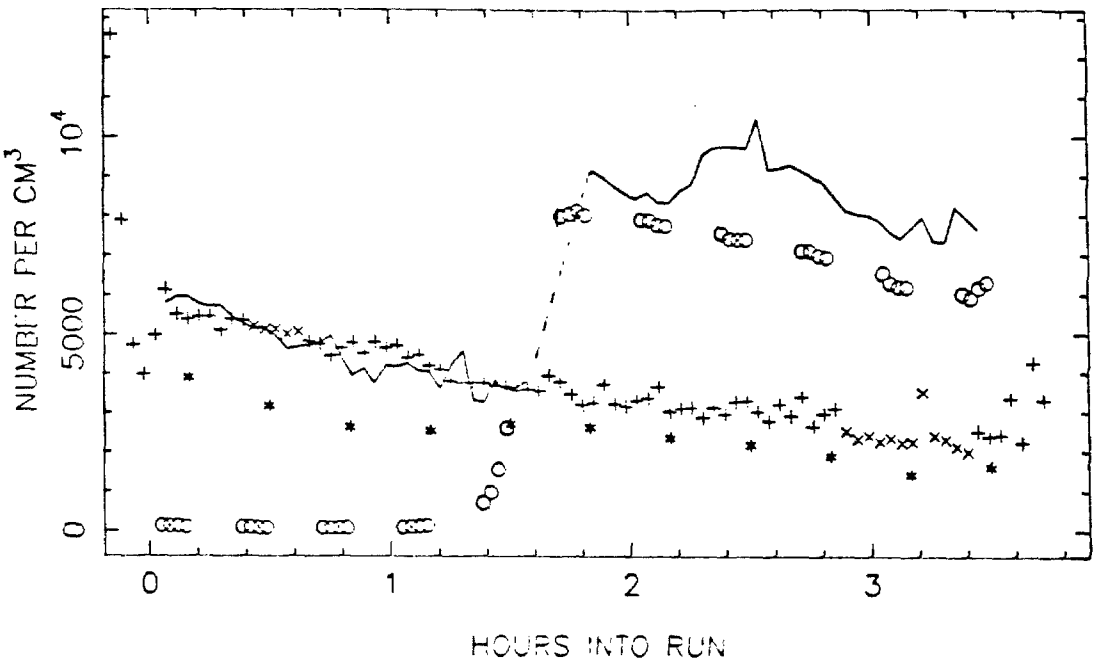

SIDE B

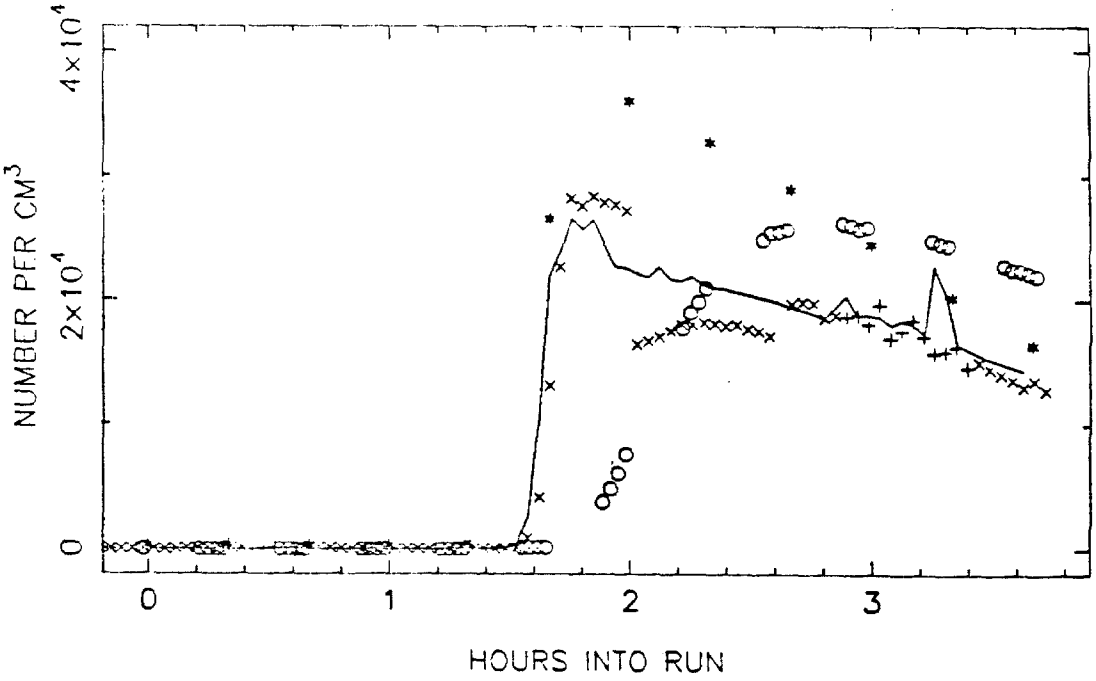

DQXA57 VOLUME IN THE AEROSOL PHASE, SIDE A

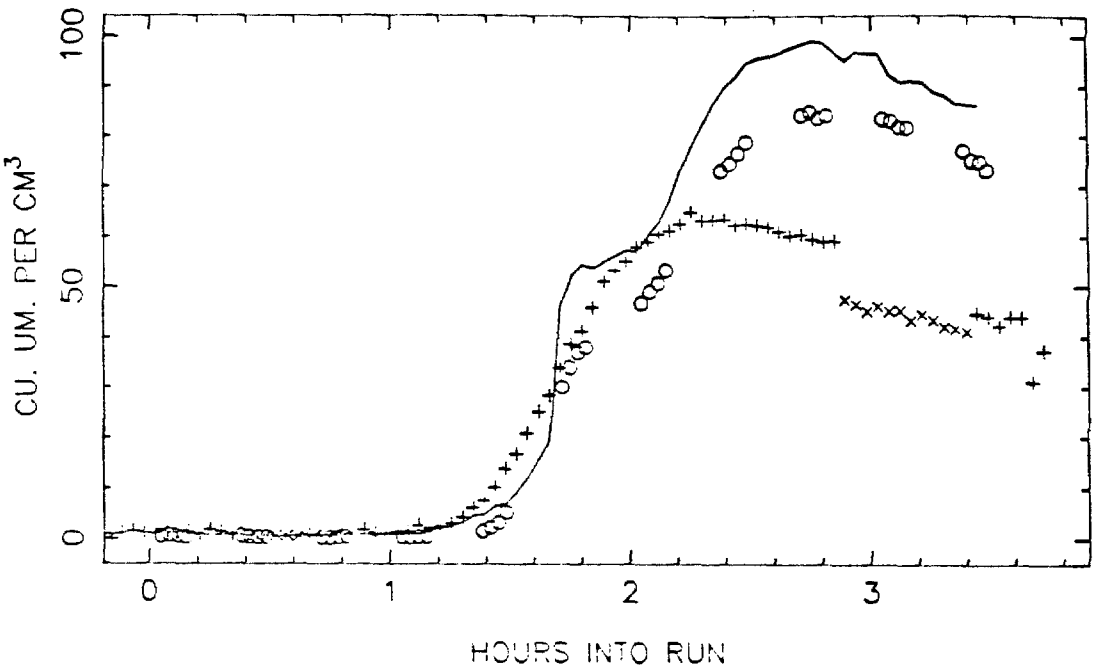

SIDE B

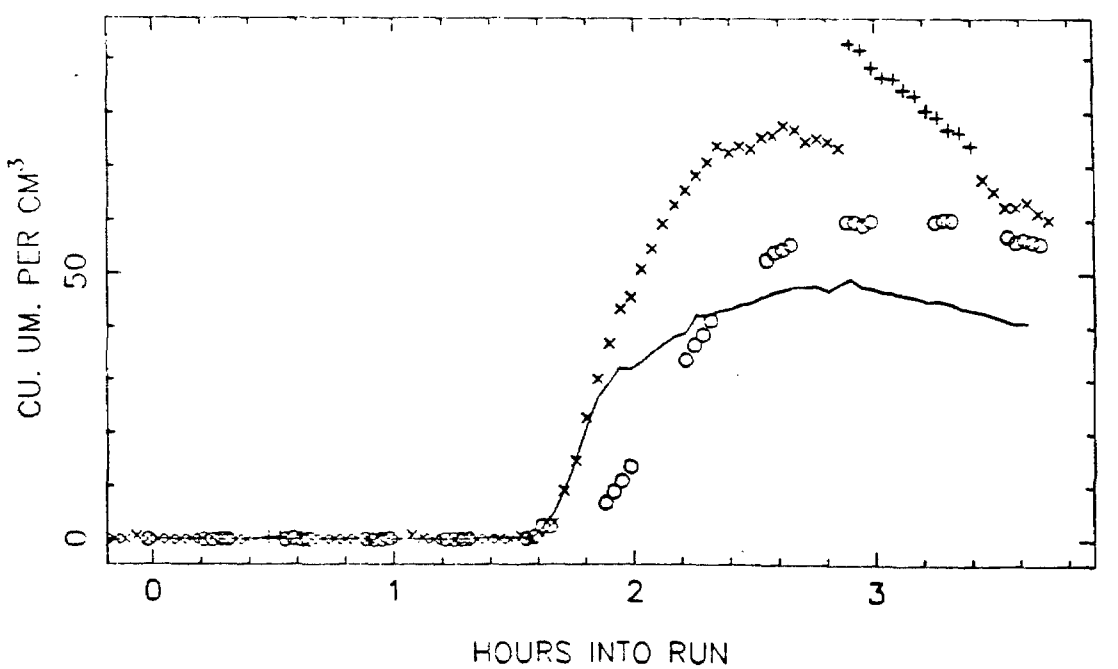

DQXA57 MEAN PARTICLE SIZE, SIDE A

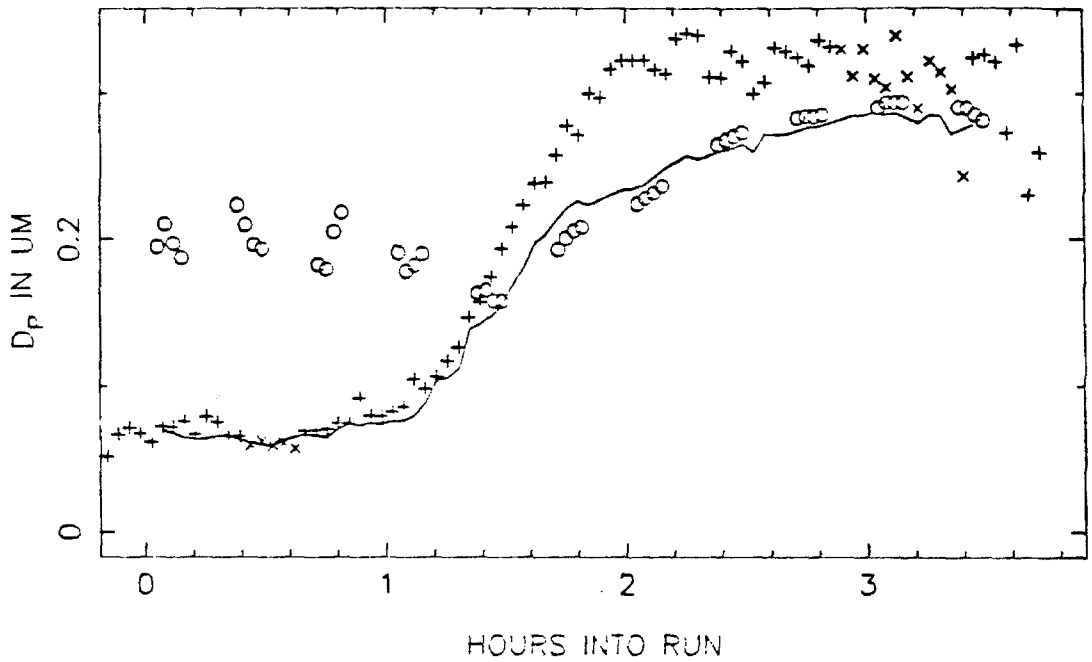

SIDE B

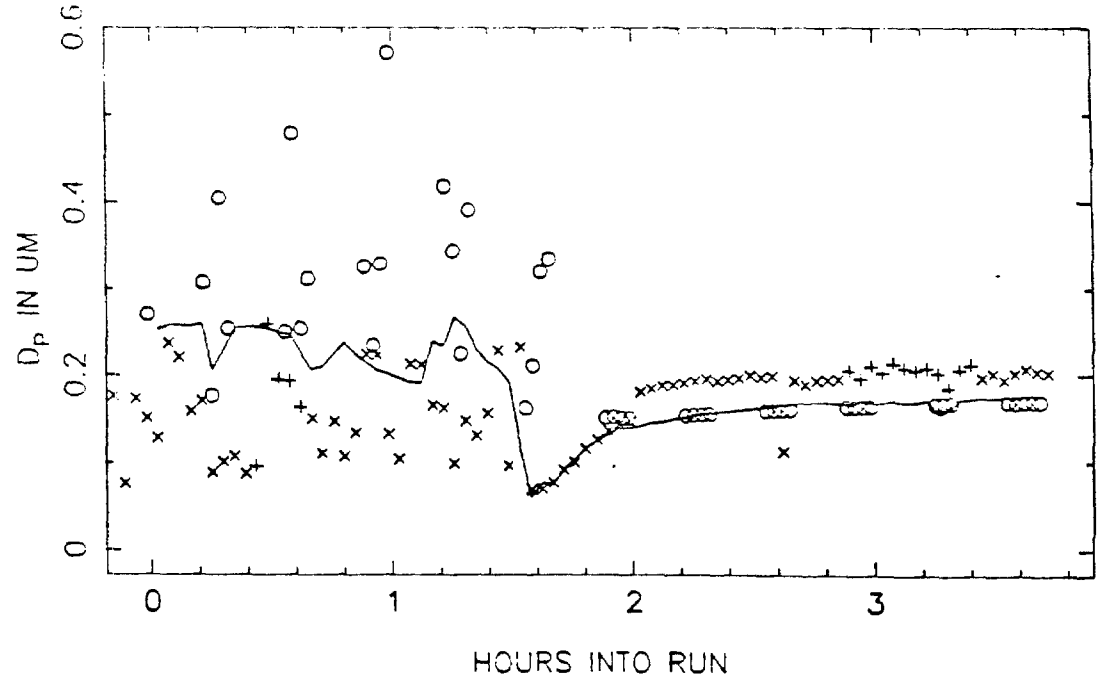

DQXA57A NUMBER DISTRIBUTION, T=0

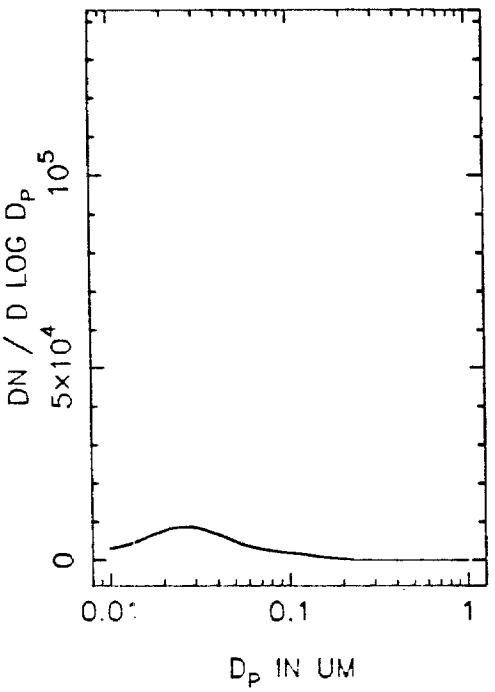

T=0.5 HOURS

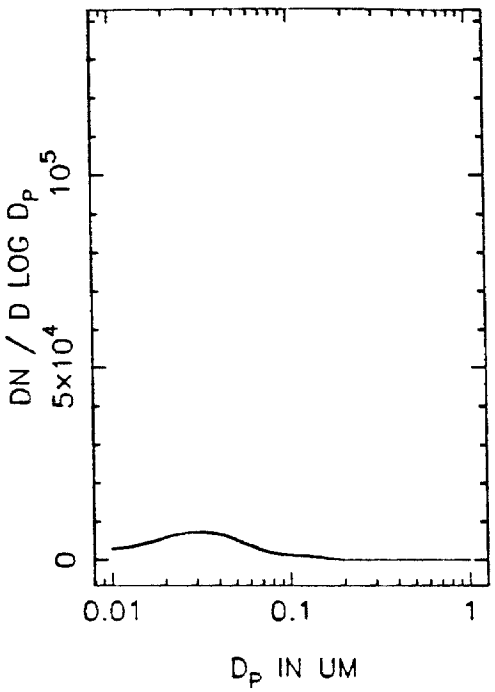

T=1.0 HOURS

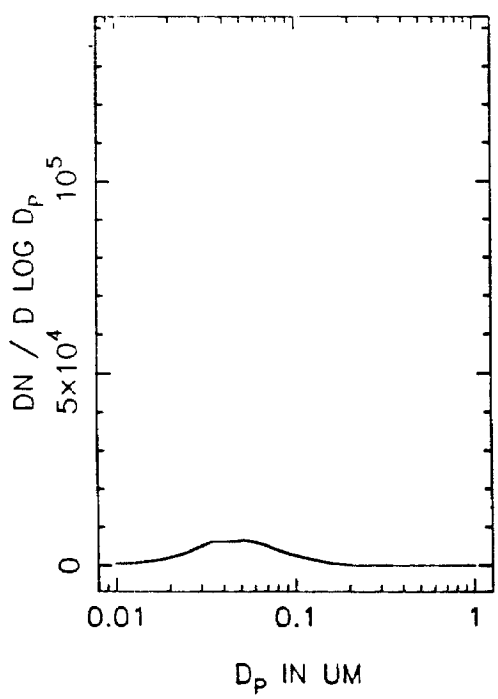

T=1.5 HOURS

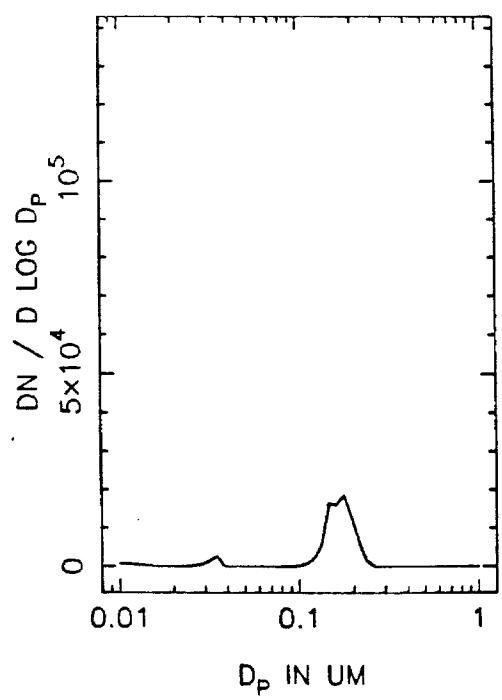

DQXA57A NUMBER DISTRIBUTION, T=2.0

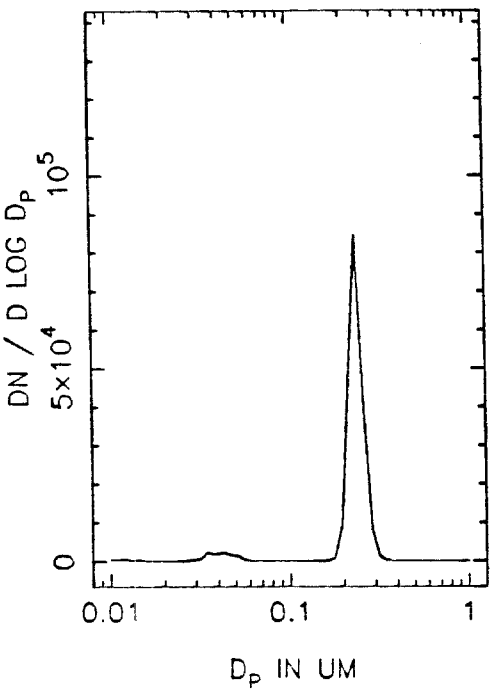

T=2.5 HOURS

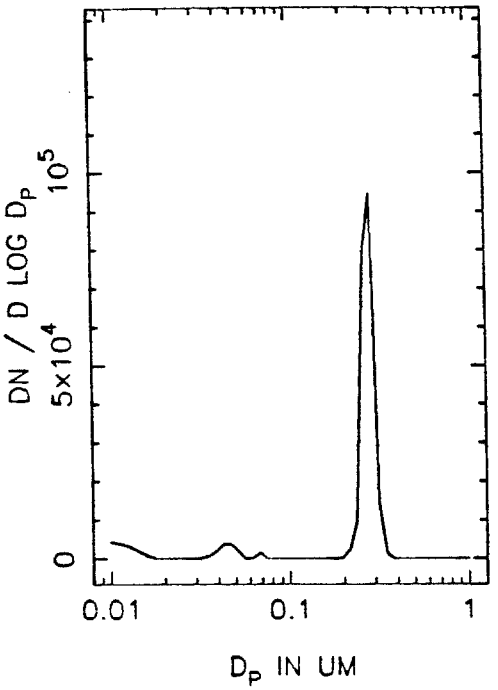

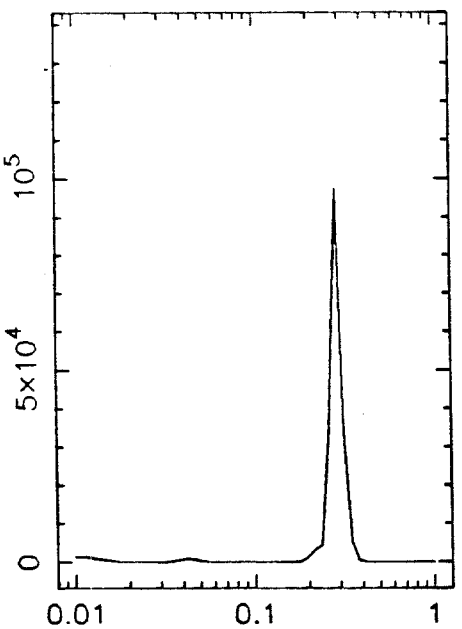

DQXA57A VOLUME DISTRIBUTION, T=0

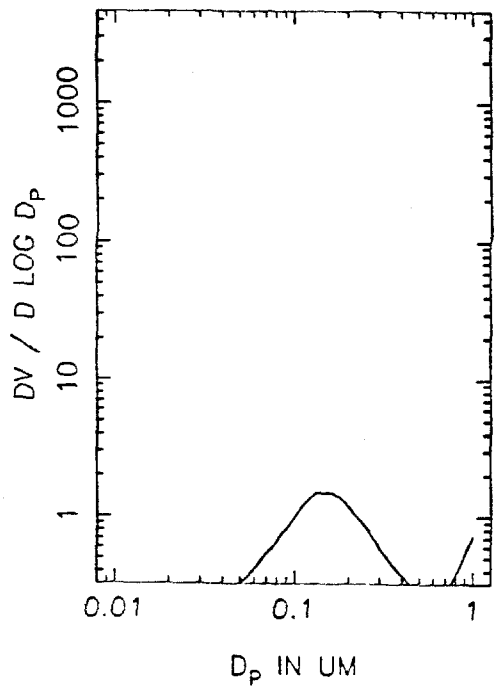

T=0.5 HOURS

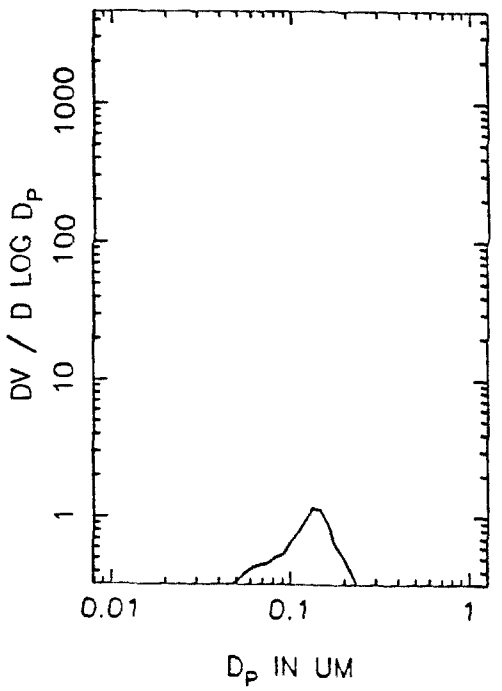

T=1.0 HOURS

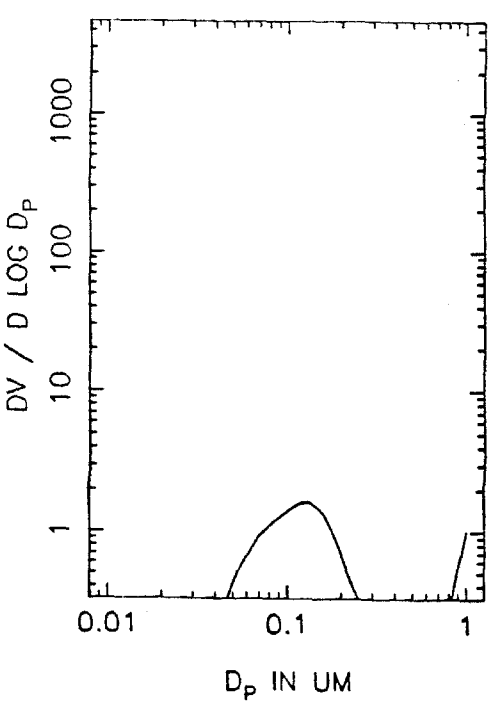

T=1.5 HOURS

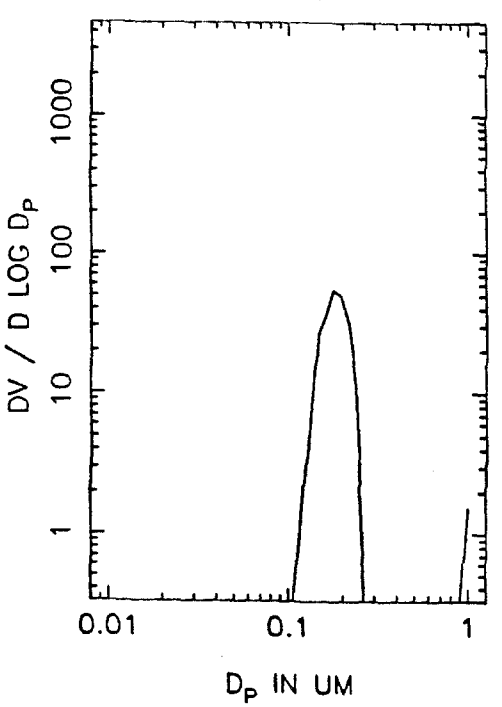

DQXA57A VOLUME DISTRIBUTION, T=2.0

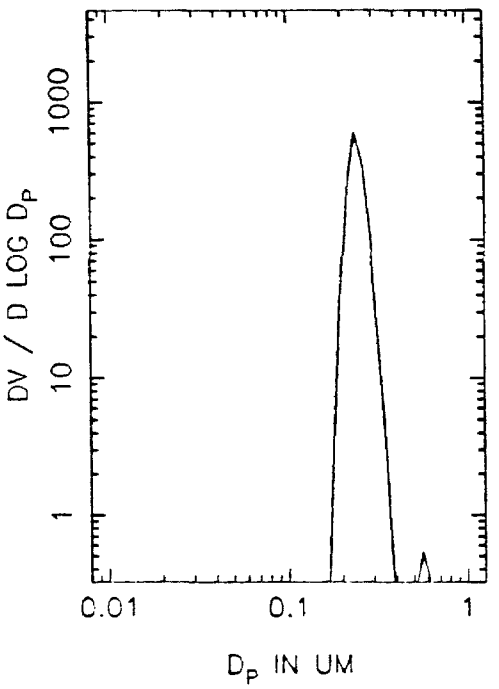

T=2.5 HOURS

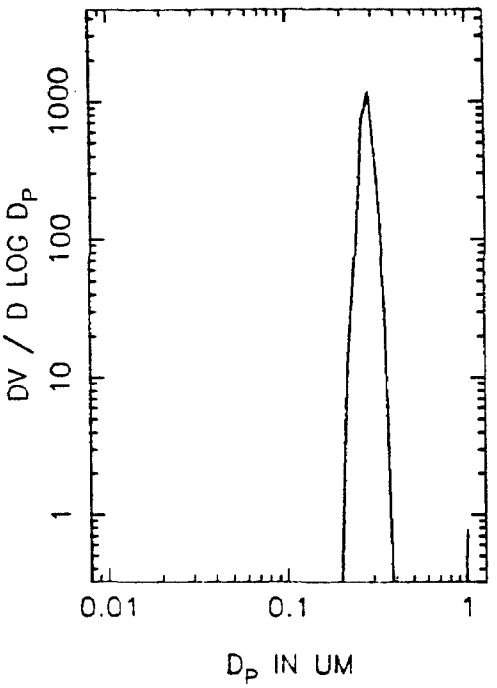

T=3.0 HOURS

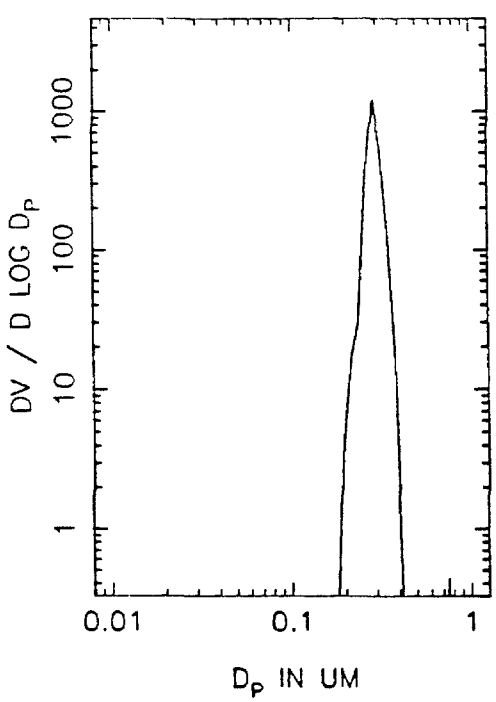

DQXA57B NUMBER DISTRIBUTION, T=0

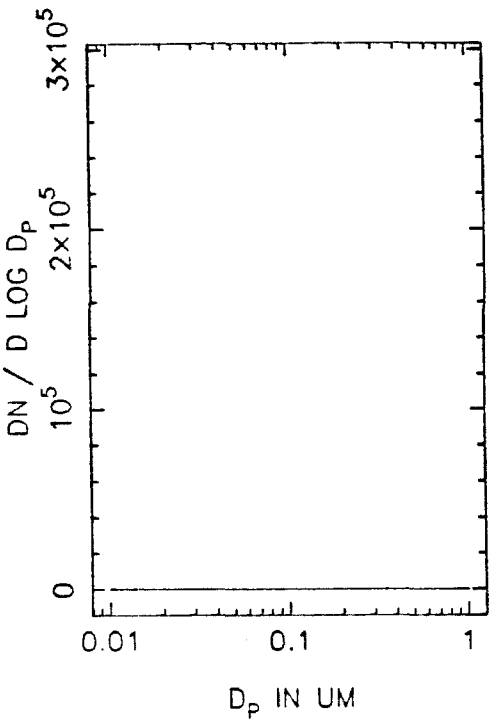

T=0.5 HOURS

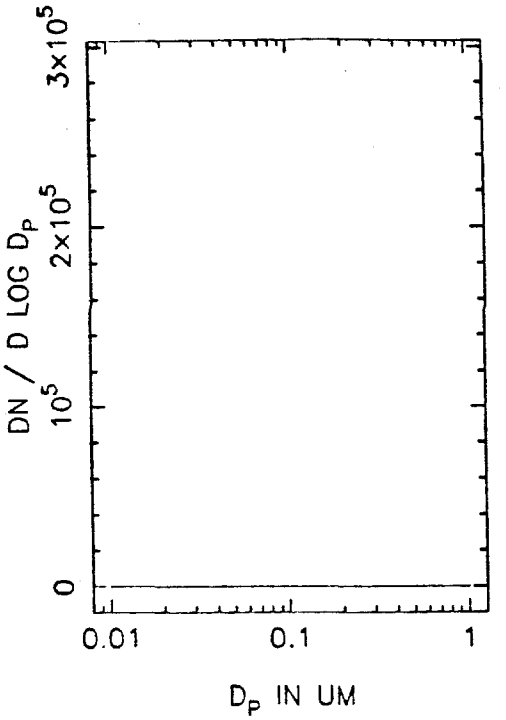

T=1.0 HOURS

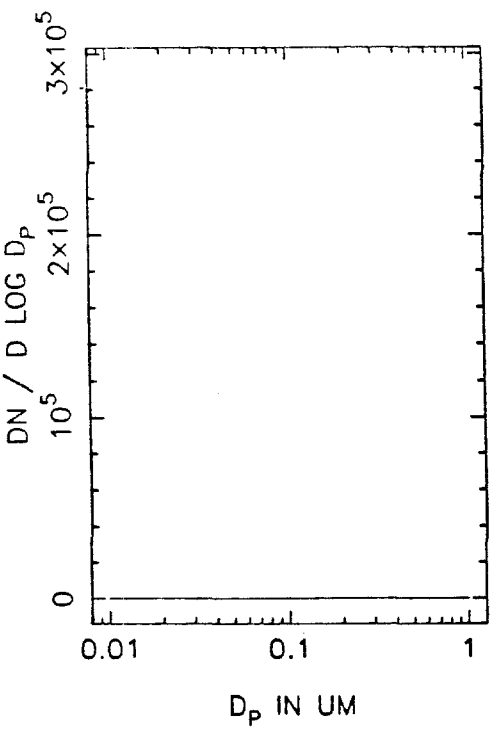

T=1.5 HOURS

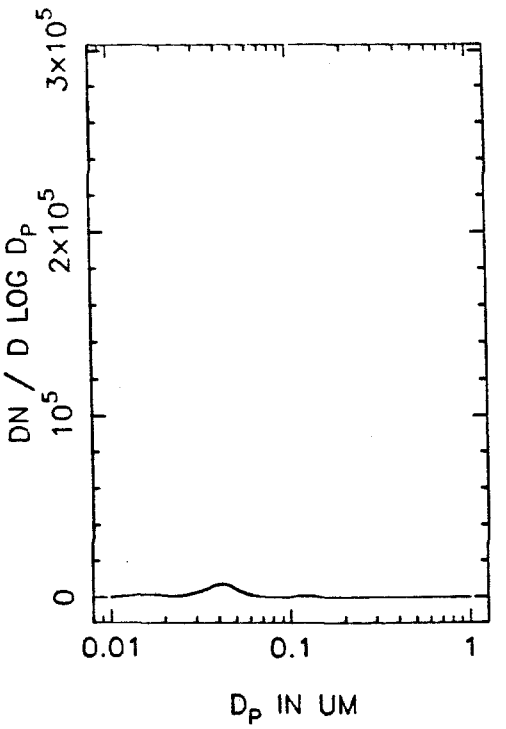

DQXA57B NUMBER DISTRIBUTION, T=2.0

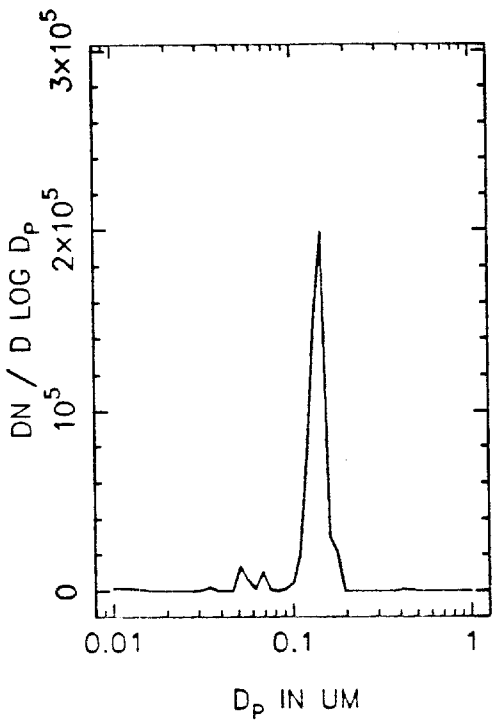

T=2.5 HOURS

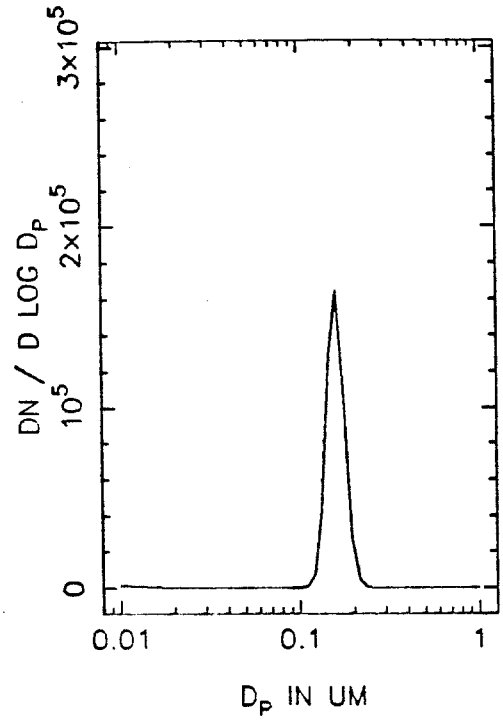

T=3.0 HOURS

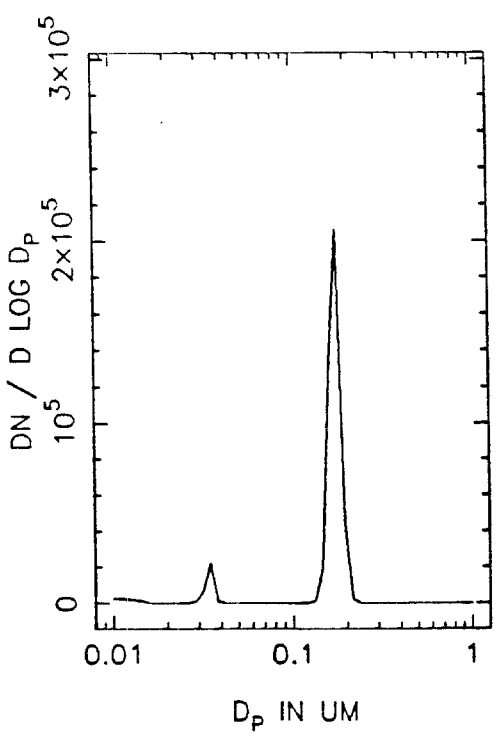

T=3.5 HOURS

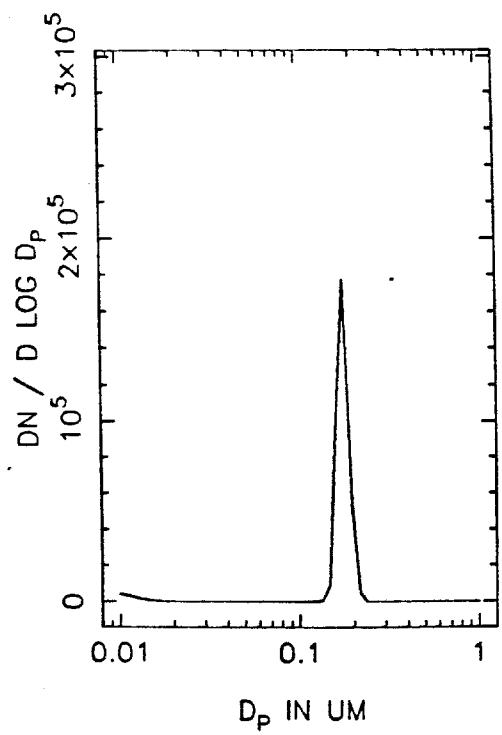

DQXA57B VOLUME DISTRIBUTION, T=0

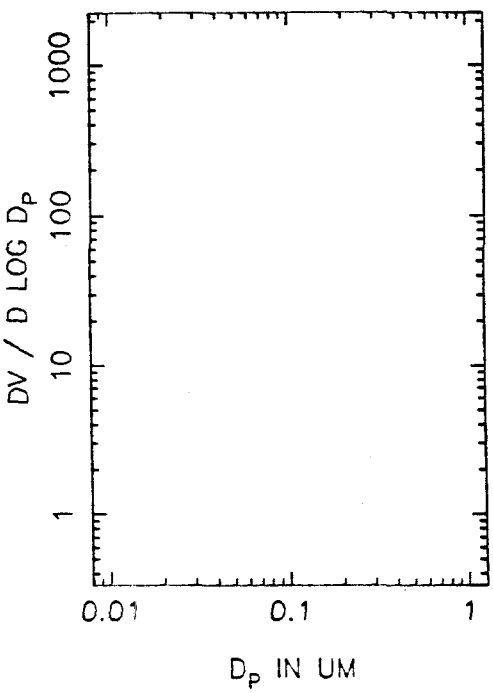

T=0.5 HOURS

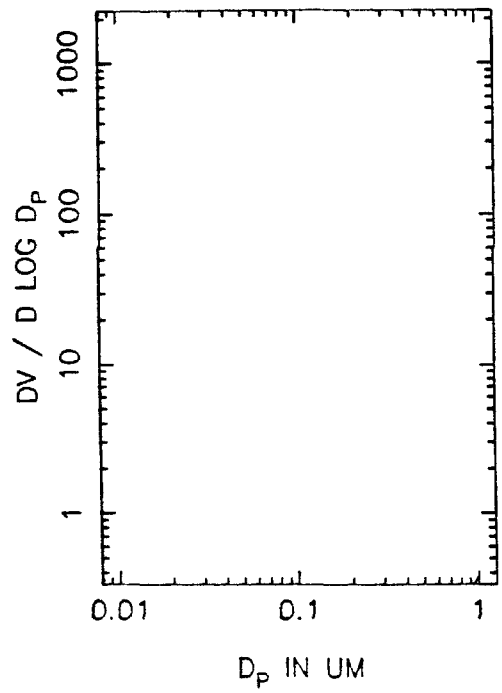

T=1.0 HOURS

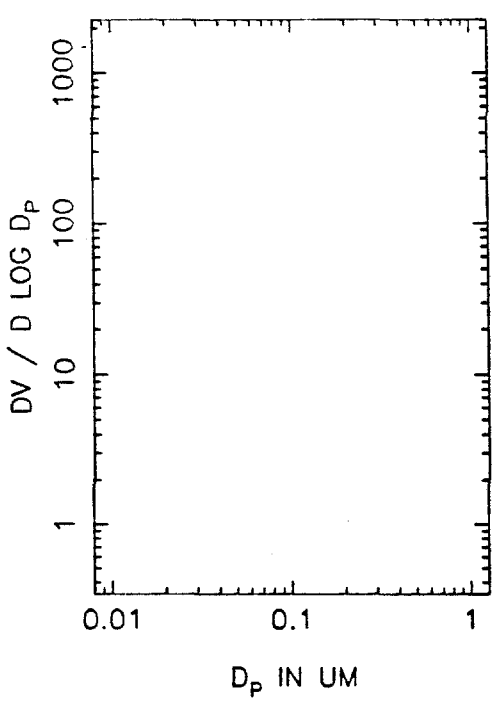

T=1.5 HOURS

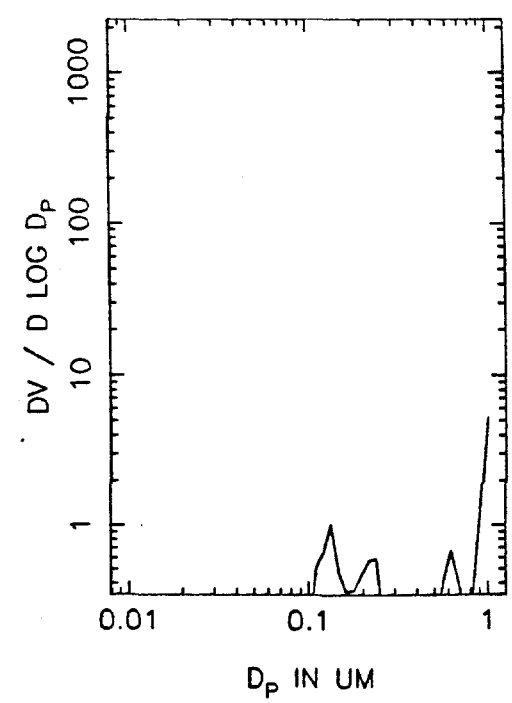

DQXA57B VOLUME DISTRIBUTION, T=2.0

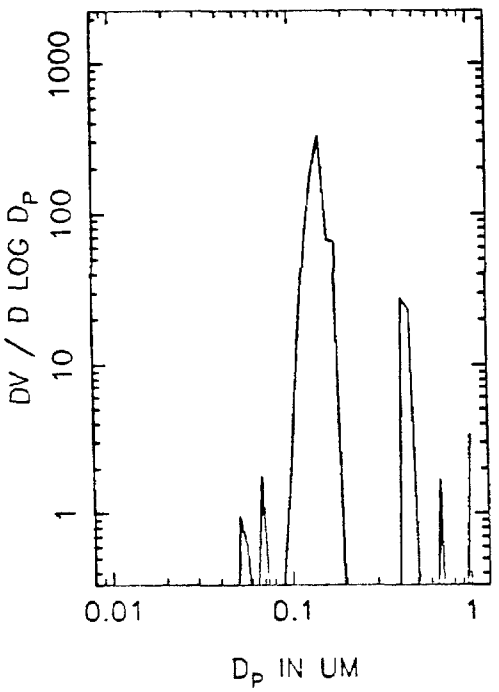

T=2.5 HOURS

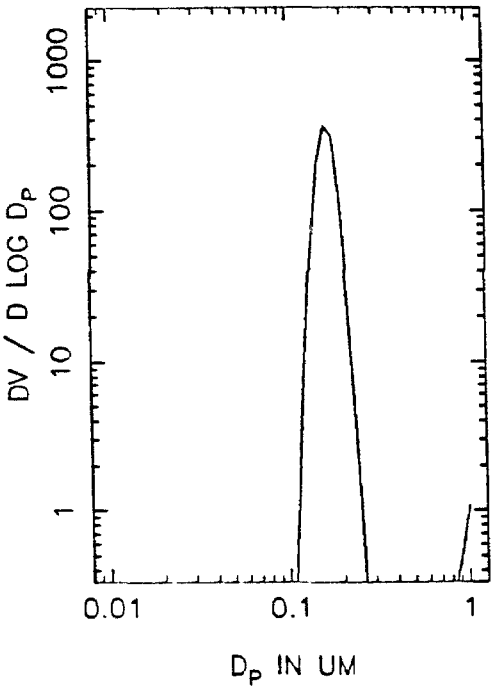

T=3.0 HOURS

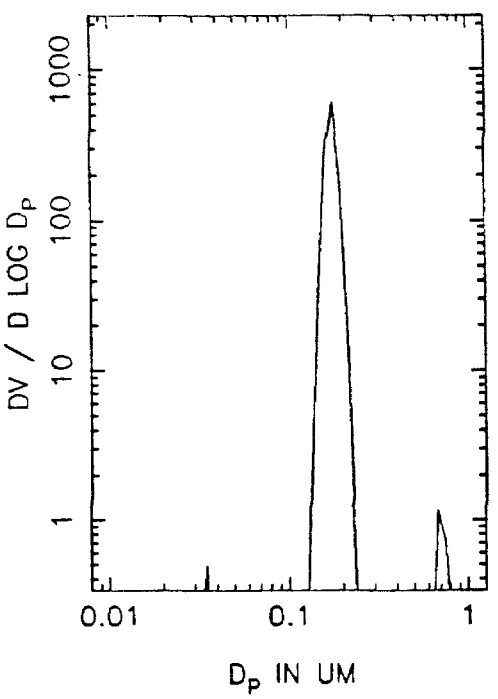

T=3.5 HOURS

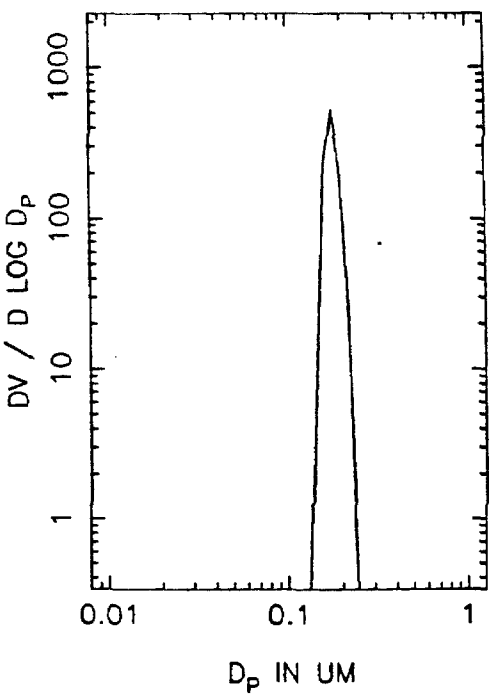

DXLA60 TOTAL NUMBER, SIDE A

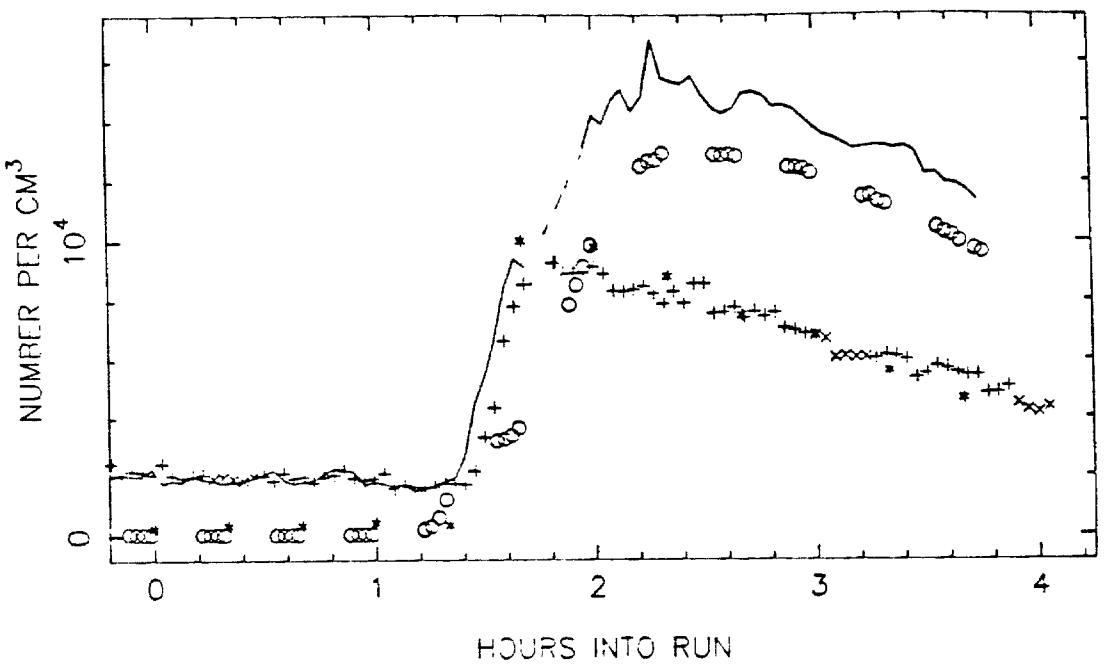

SIDE B

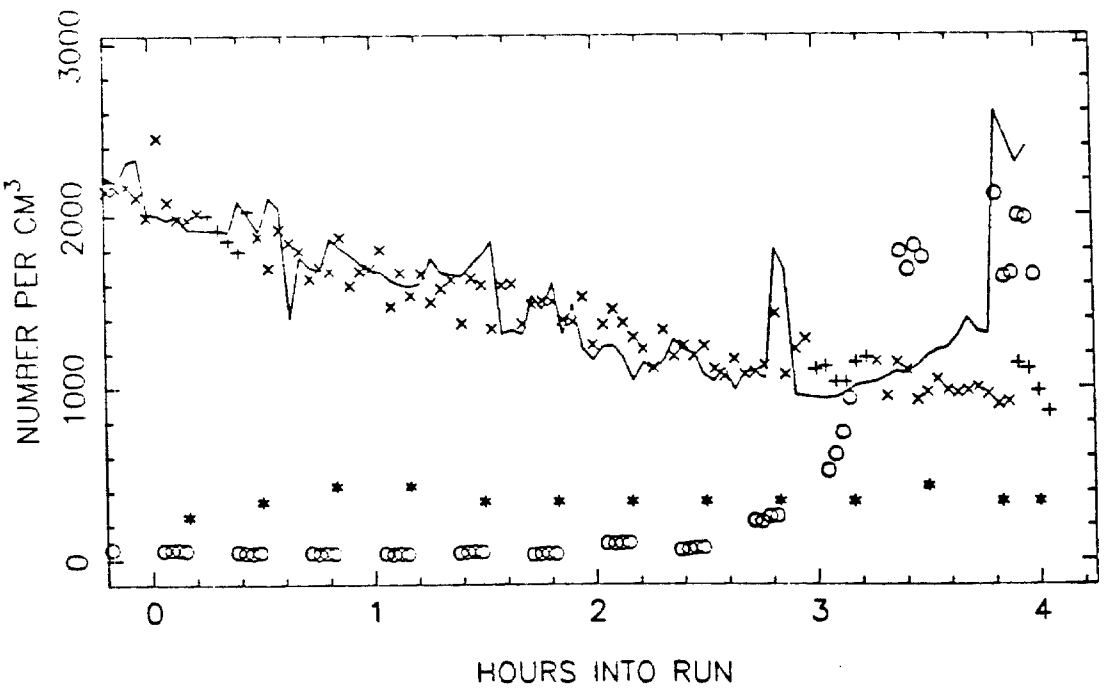

DXLA60 VOLUME IN THE AEROSOL PHASE, SIDE A

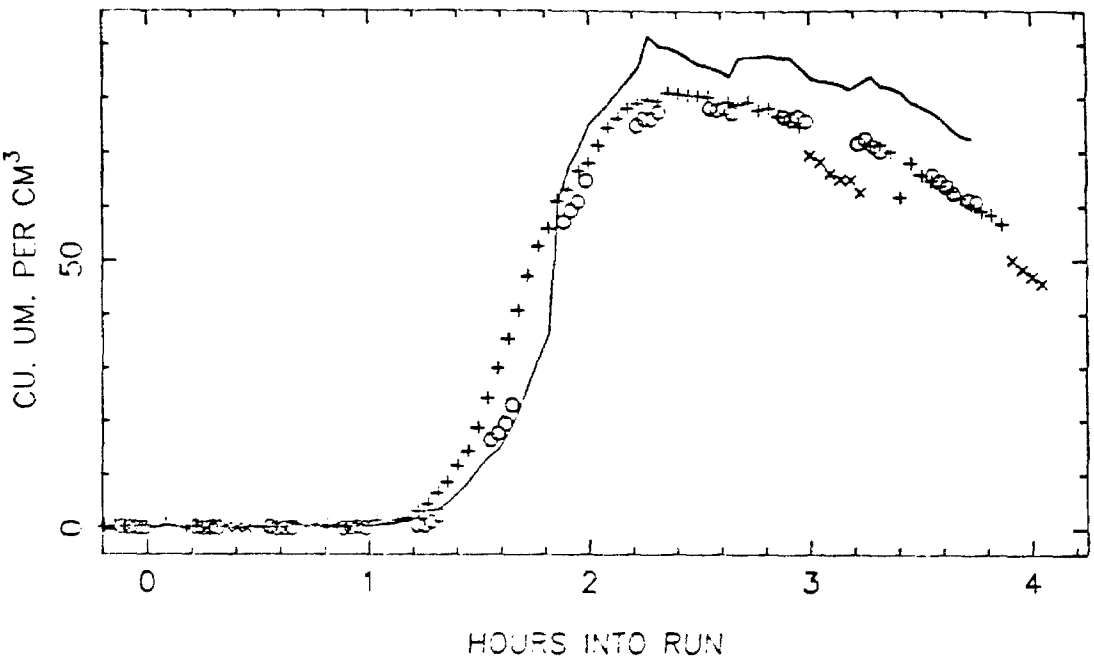

SIDE B

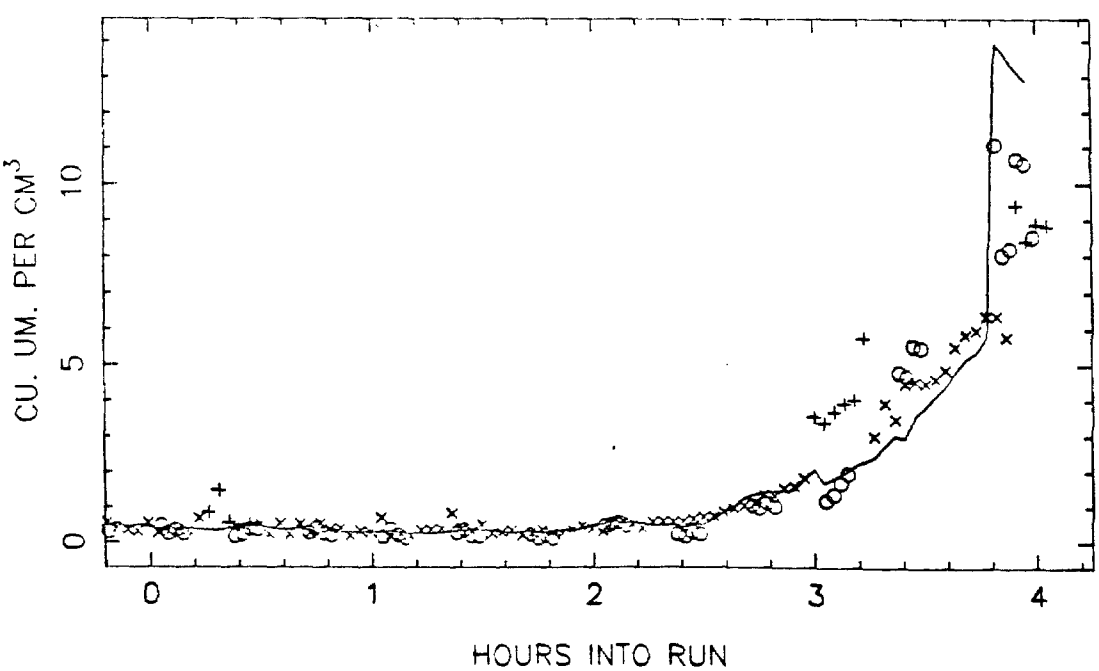

DXLA60 MEAN PARTICLE SIZE, SIDE A

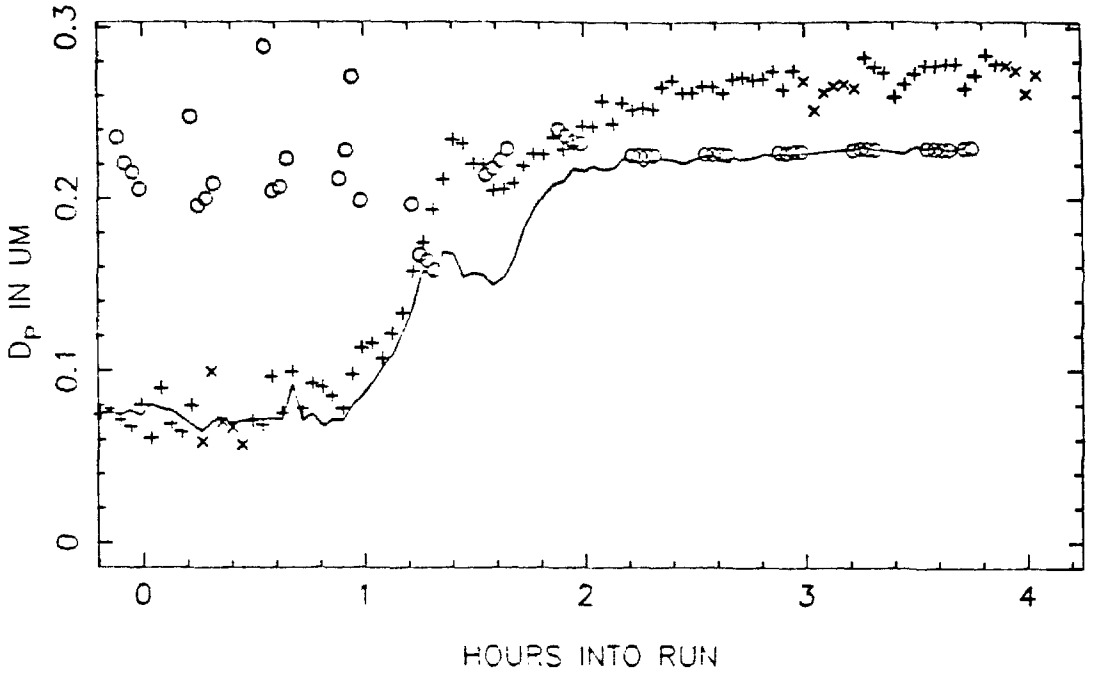

SIDE B

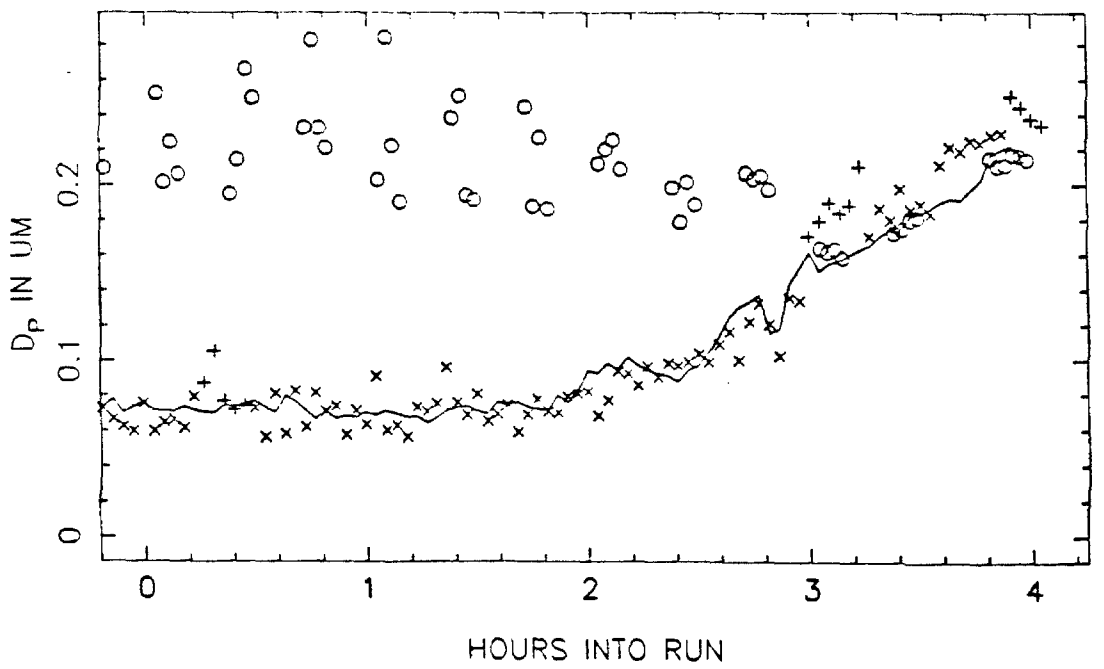

DXLA60A NUMBER DISTRIBUTION, T=0

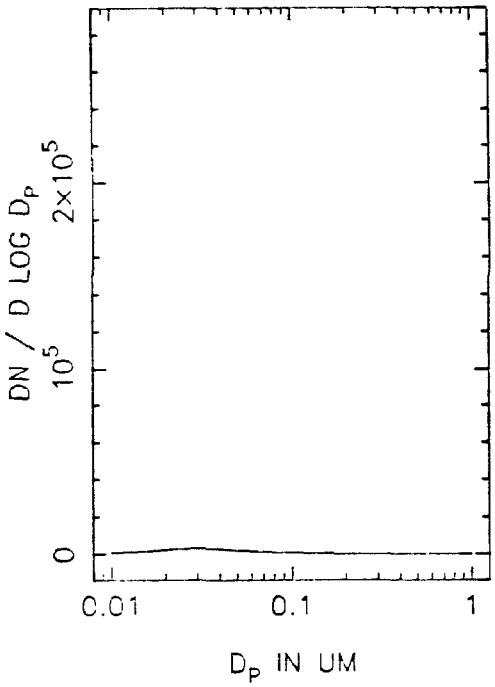

T=0.5 HOURS

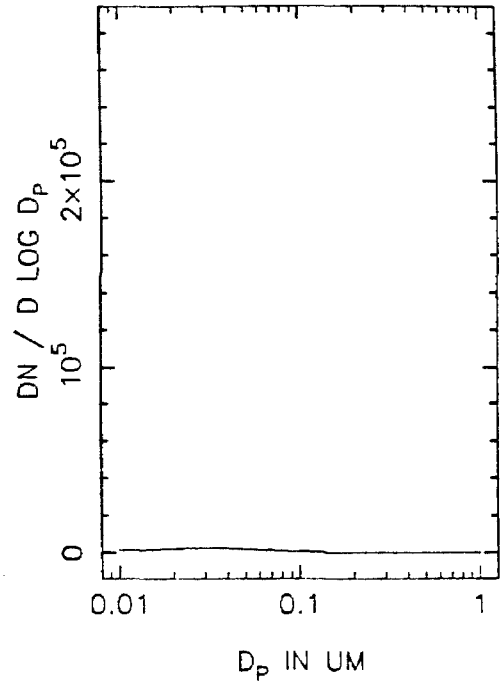

T=1.0 HOURS

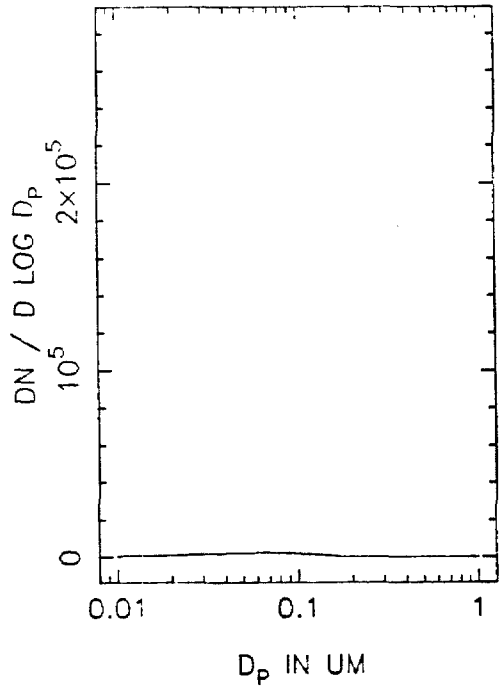

T=1.5 HOURS

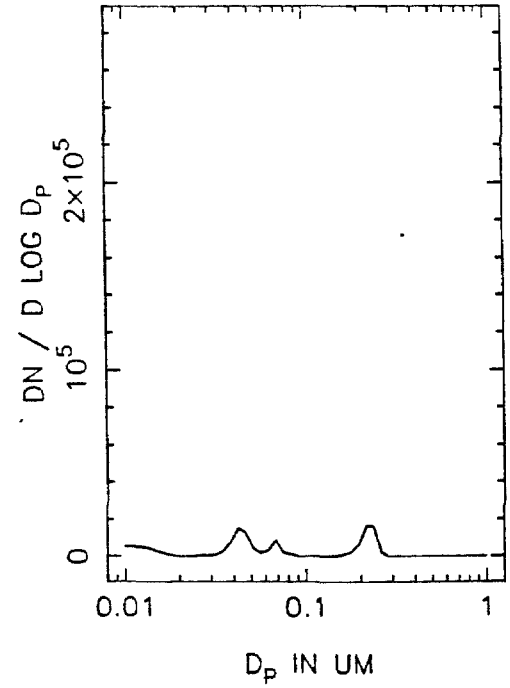

DXLA60A NUMBER DISTRIBUTION, T=2.0

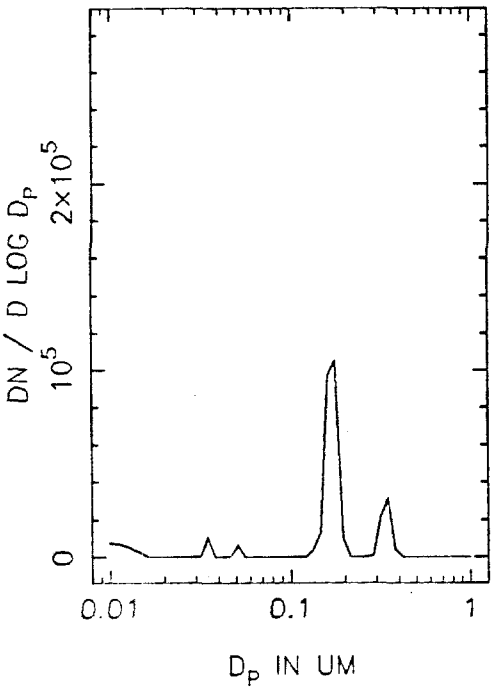

T=2.5 HOURS

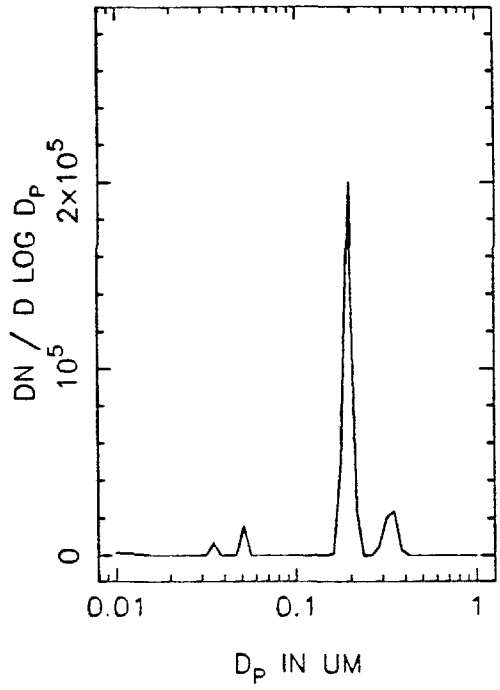

T=3.0 HOURS

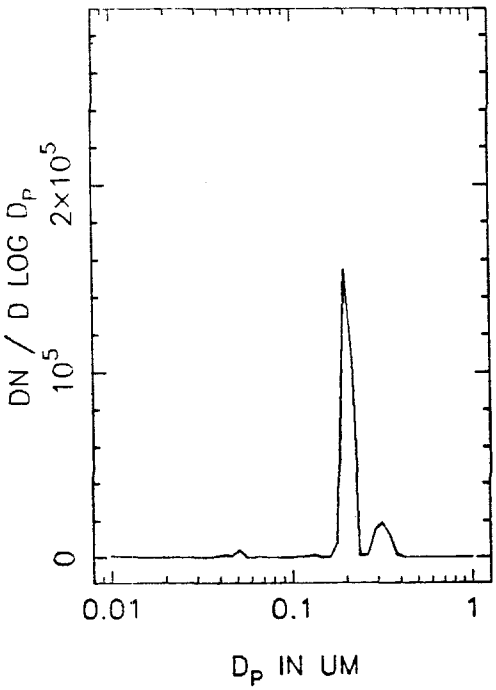

T=3.5 HOURS

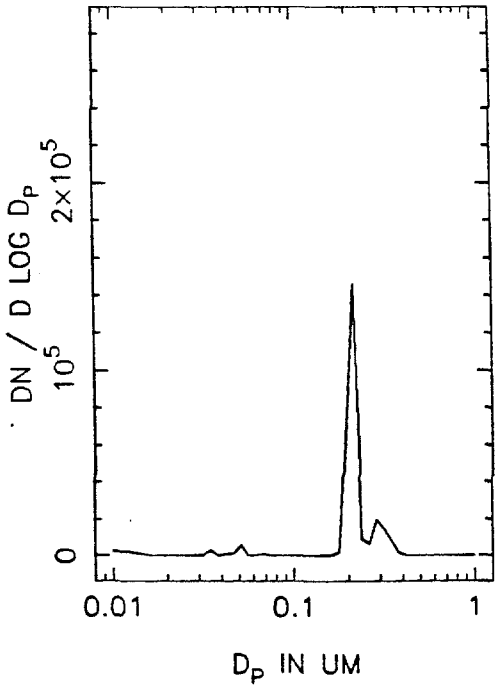

DXLA60A VOLUME DISTRIBUTION, T=0

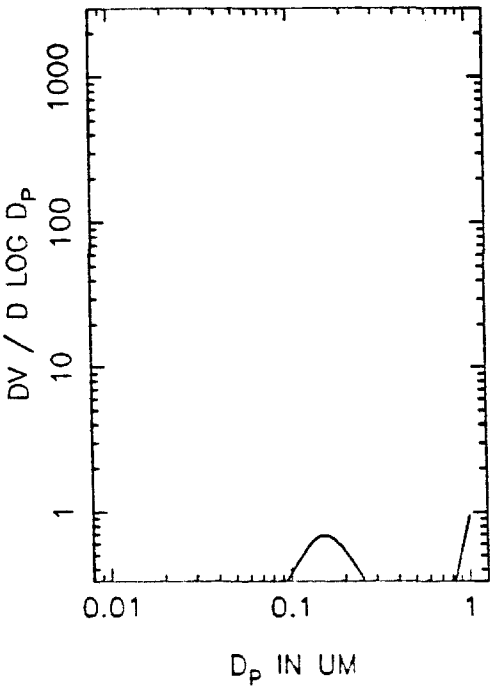

T=0.5 HOURS

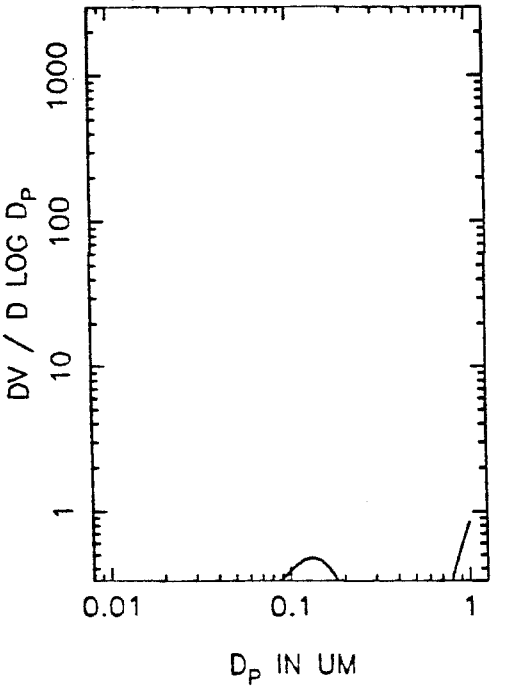

T=1.0 HOURS

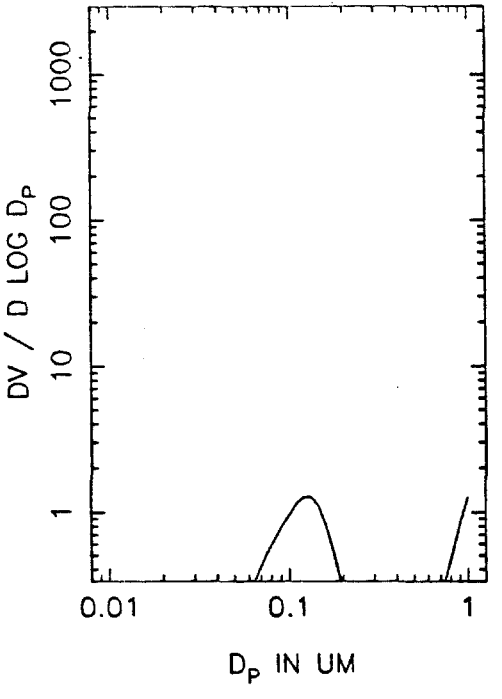

T=1.5 HOURS

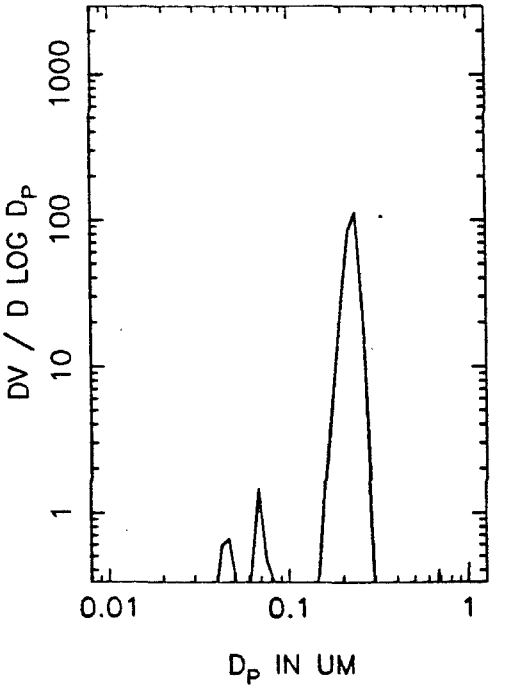

DXLA60A VOLUME DISTRIBUTION, T=2.0

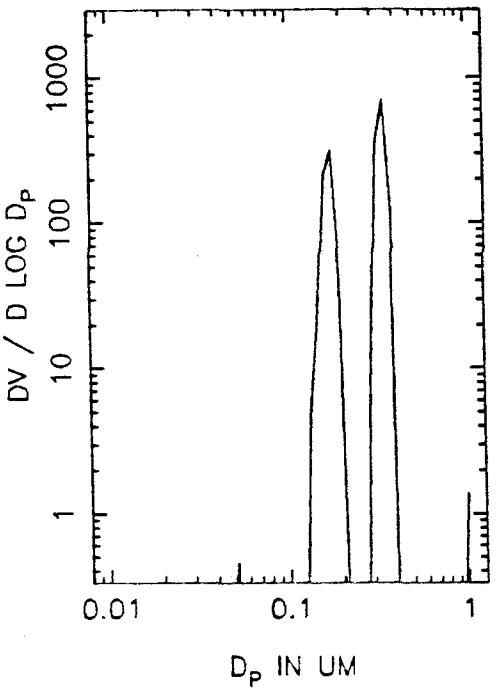

T=2.5 HOURS

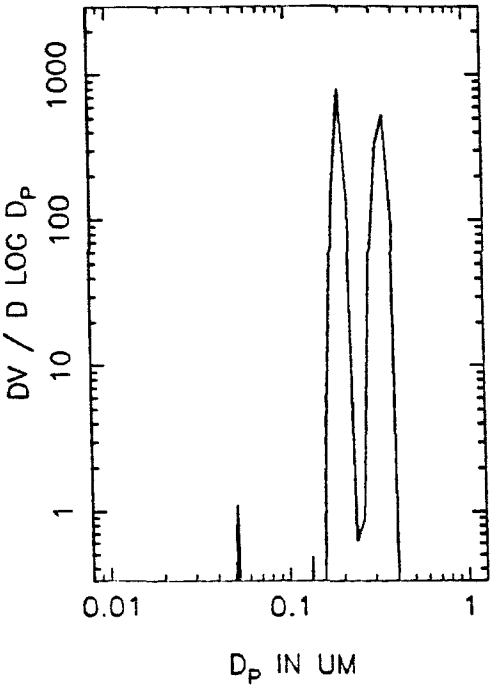

T=3.0 HOURS

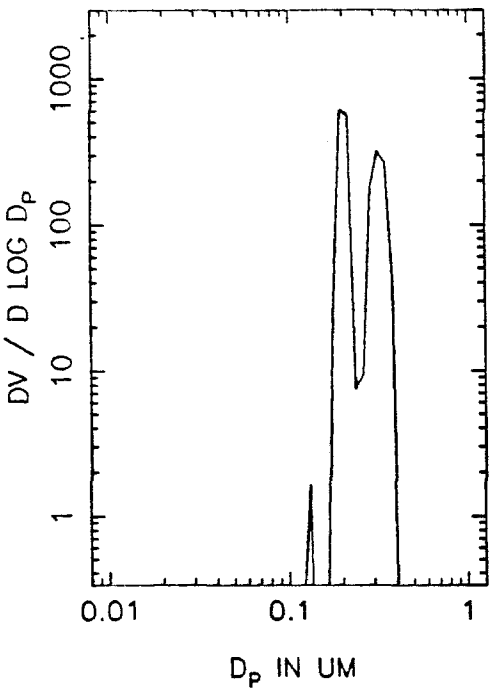

T=3.5 HOURS

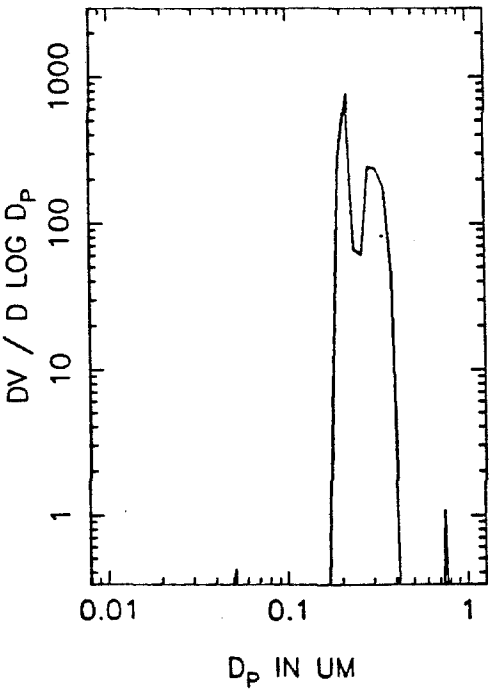

DXLA60B NUMBER DISTRIBUTION, T=0

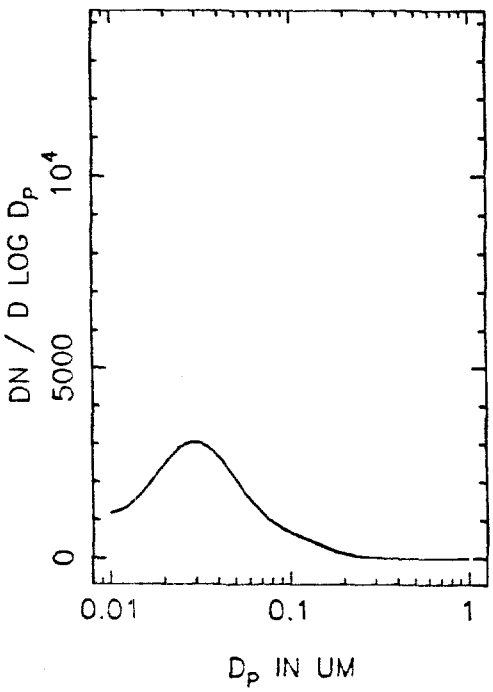

T=0.5 HOURS

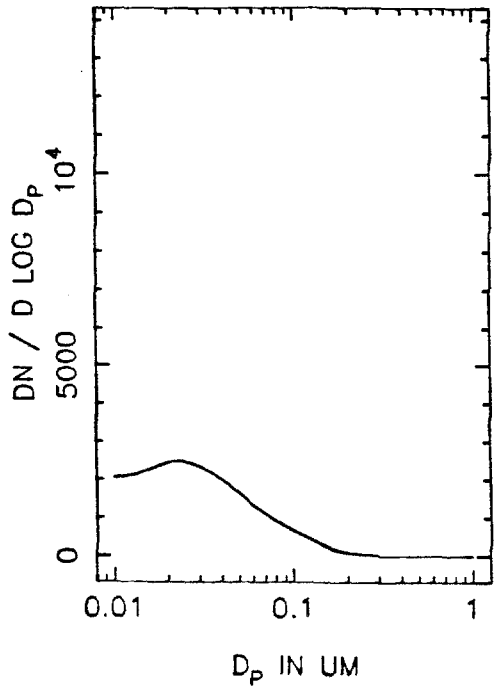

T=1.0 HOURS

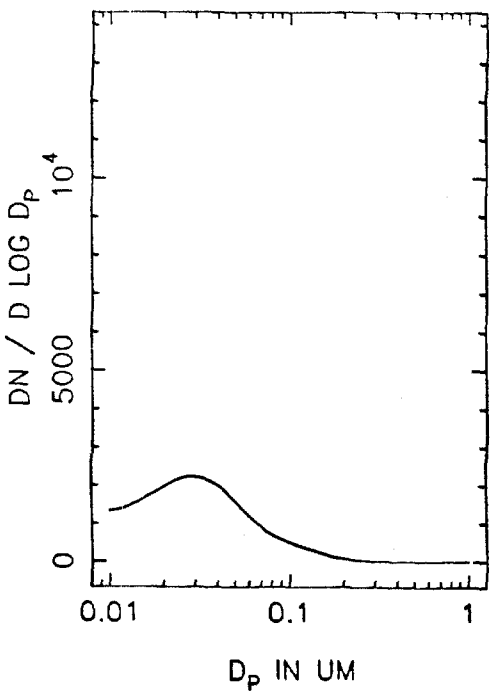

T=1.5 HOURS

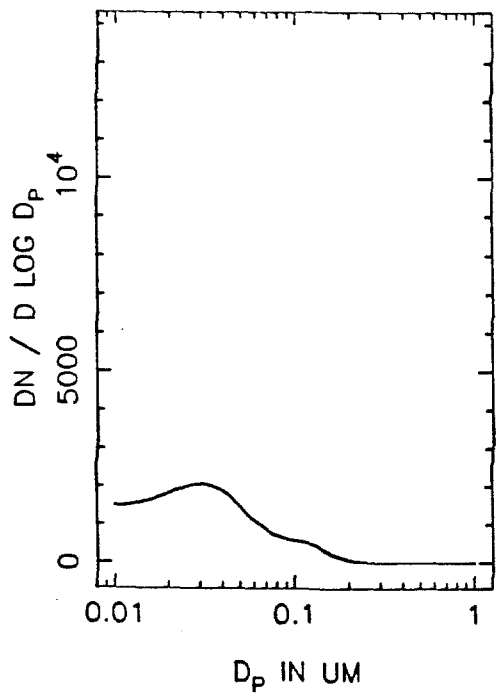

DXLA60B NUMBER DISTRIBUTION, T=2.0

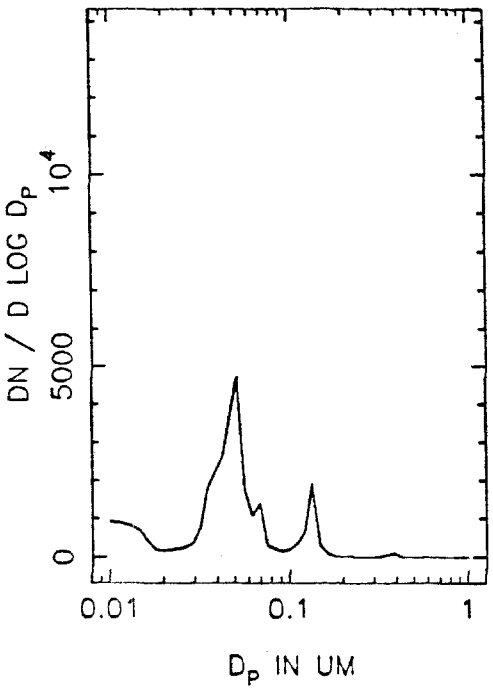

T=2.5 HOURS

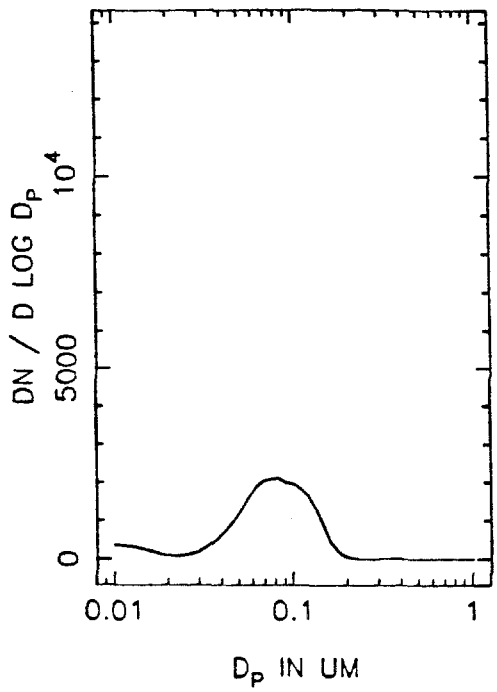

T=3.0 HOURS

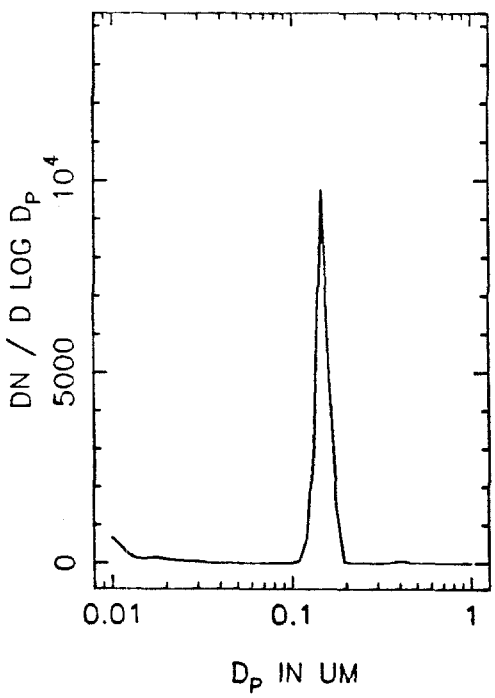

T=3.5 HOURS

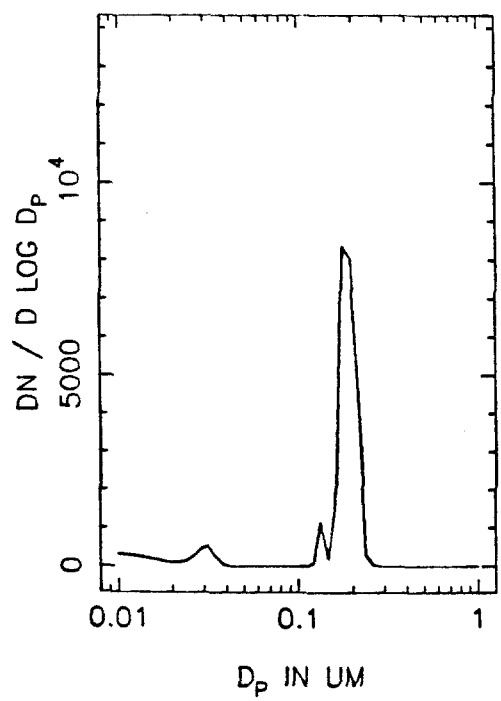

DXLA60B VOLUME DISTRIBUTION, T=0

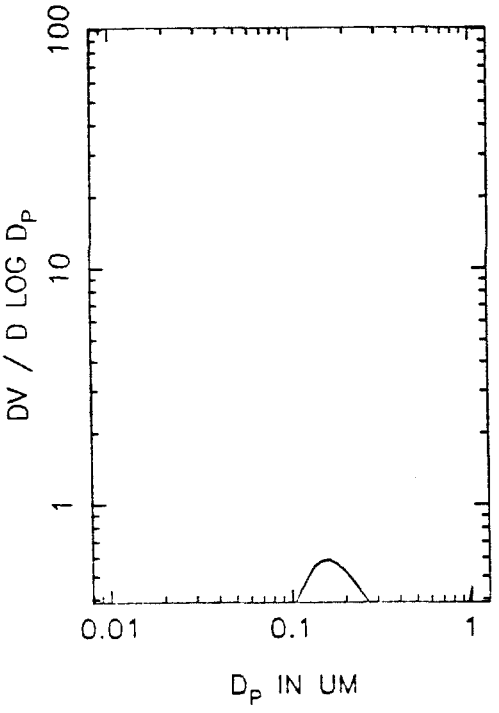

T=0.5 HOURS

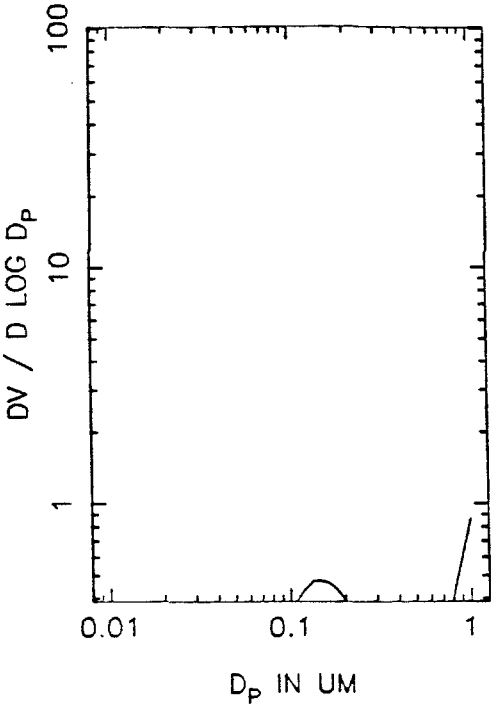

T=1.0 HOURS

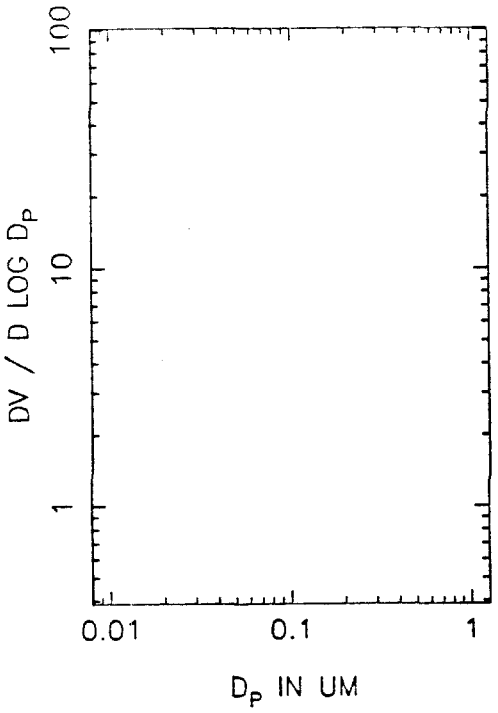

T=1.5 HOURS

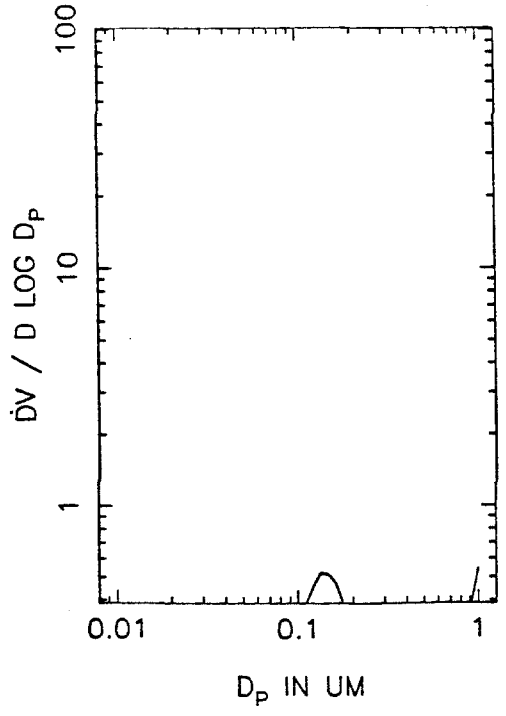

DXLA60B VOLUME DISTRIBUTION, T=2.0

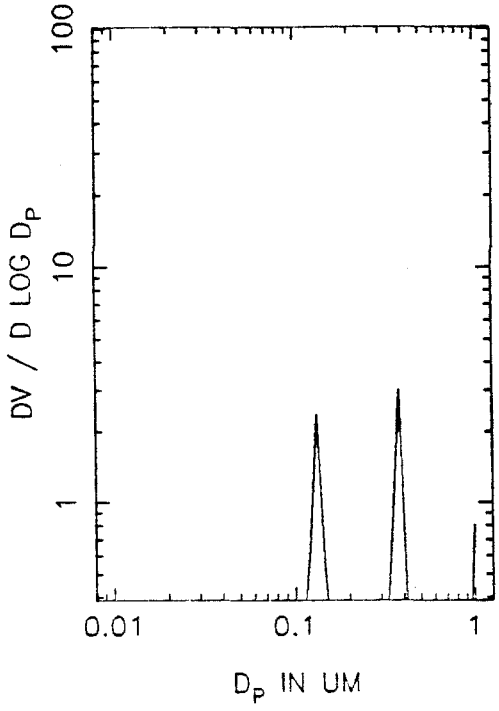

T=2.5 HOURS

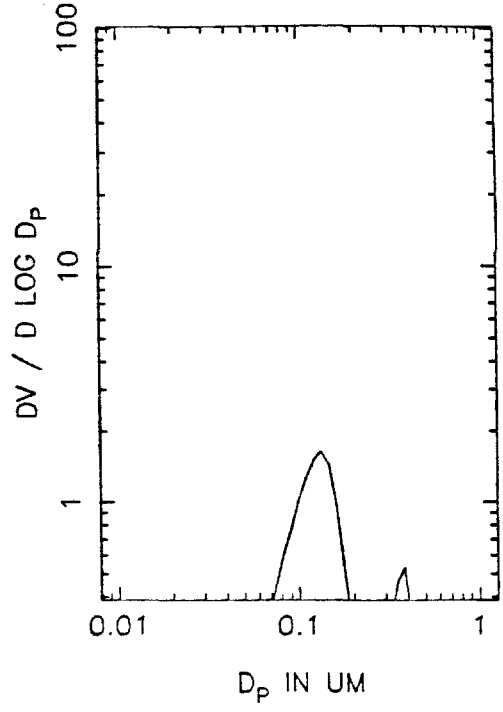

T=3.0 HOURS

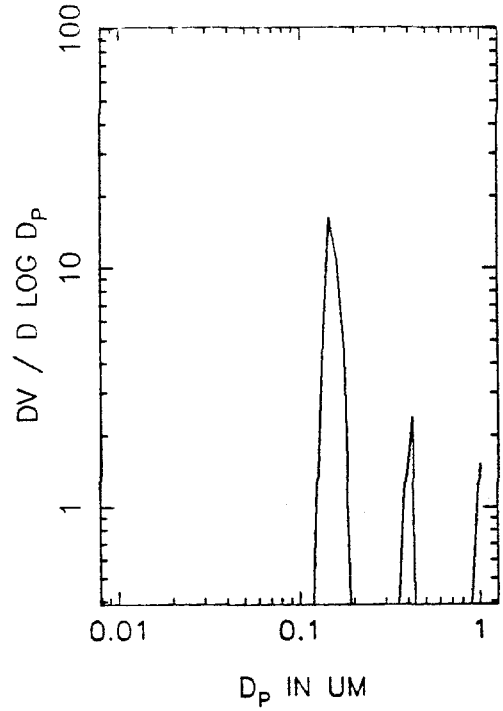

T=3.5 HOURS

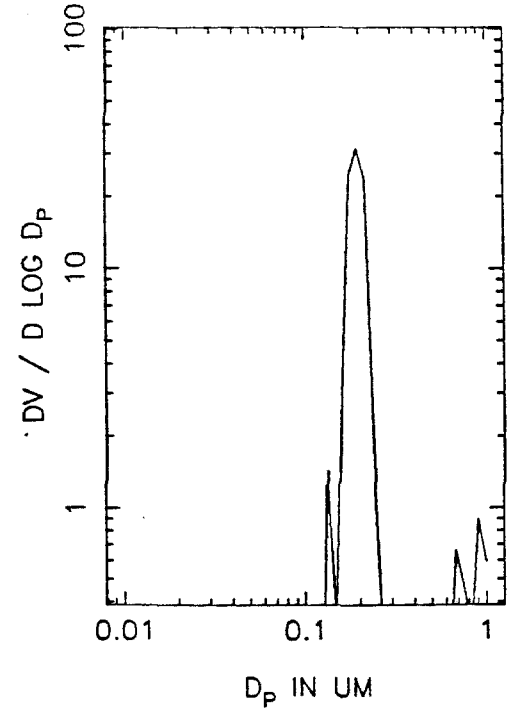

XA08 TOTAL NUMBER, SIDE A

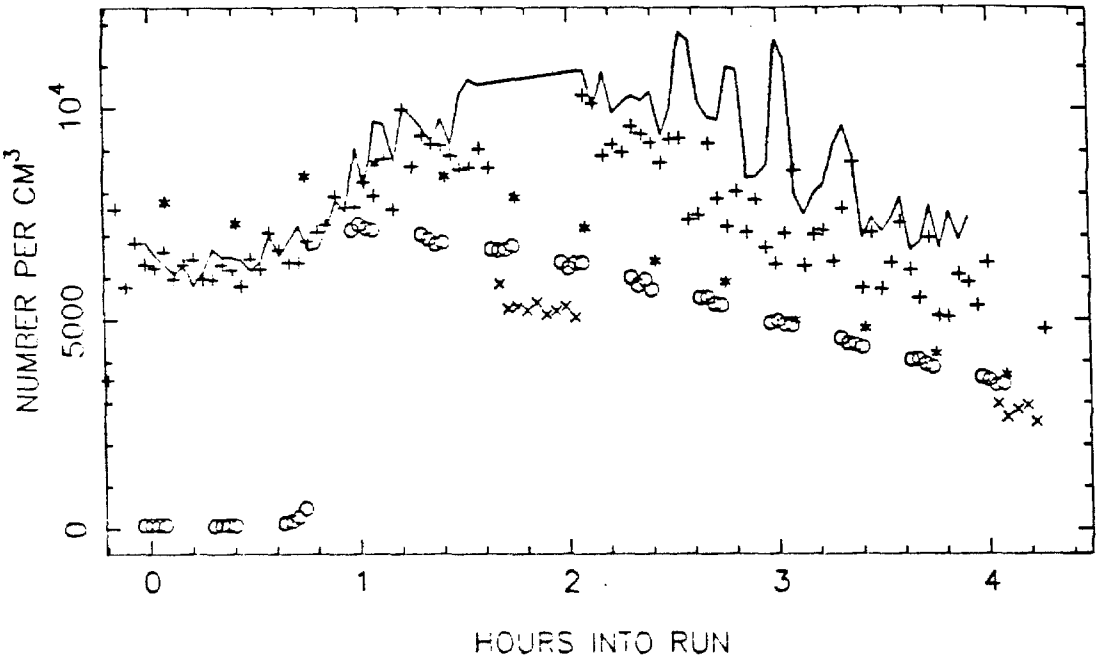

SIDE B

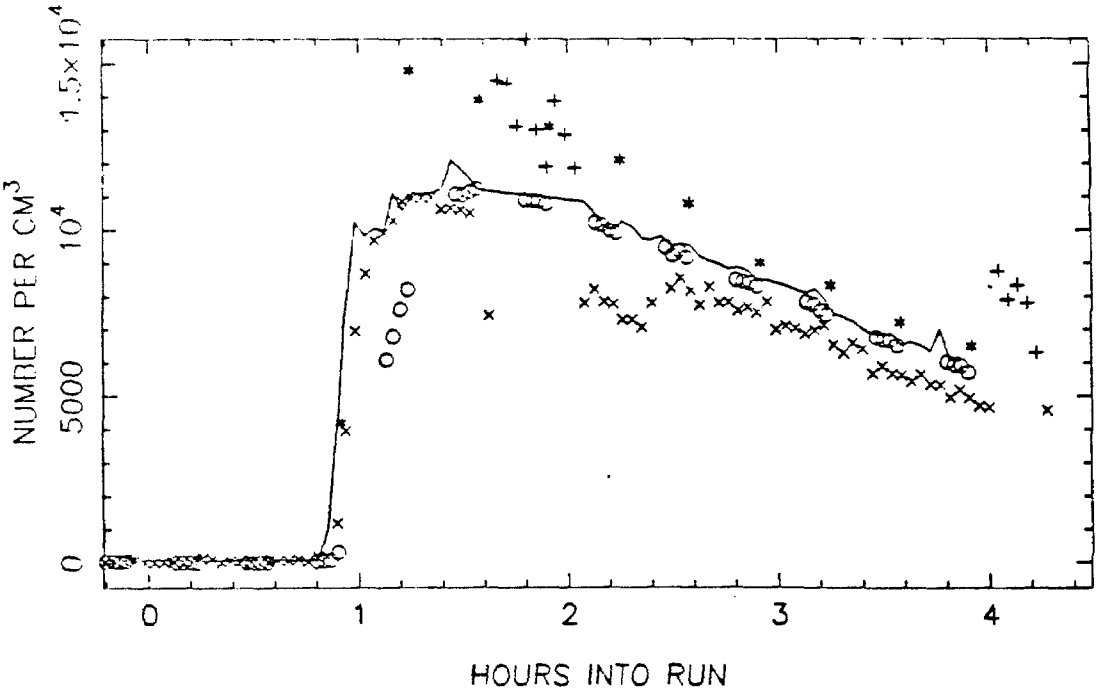

XA08 VOLUME IN THE AEROSOL PHASE, SIDE A

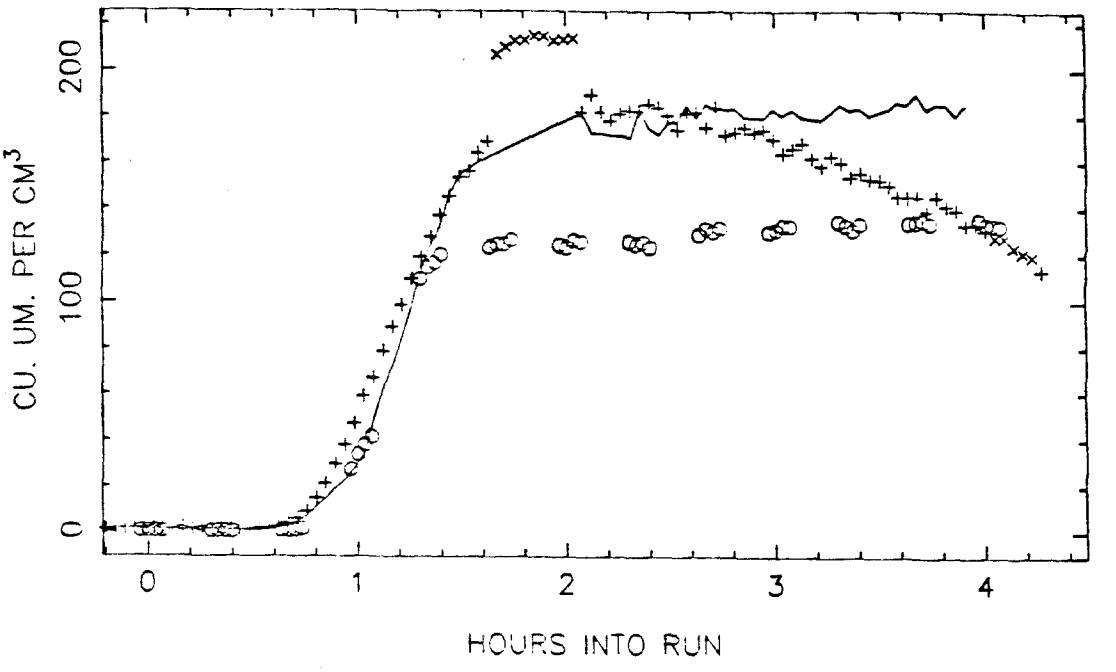

SIDE B

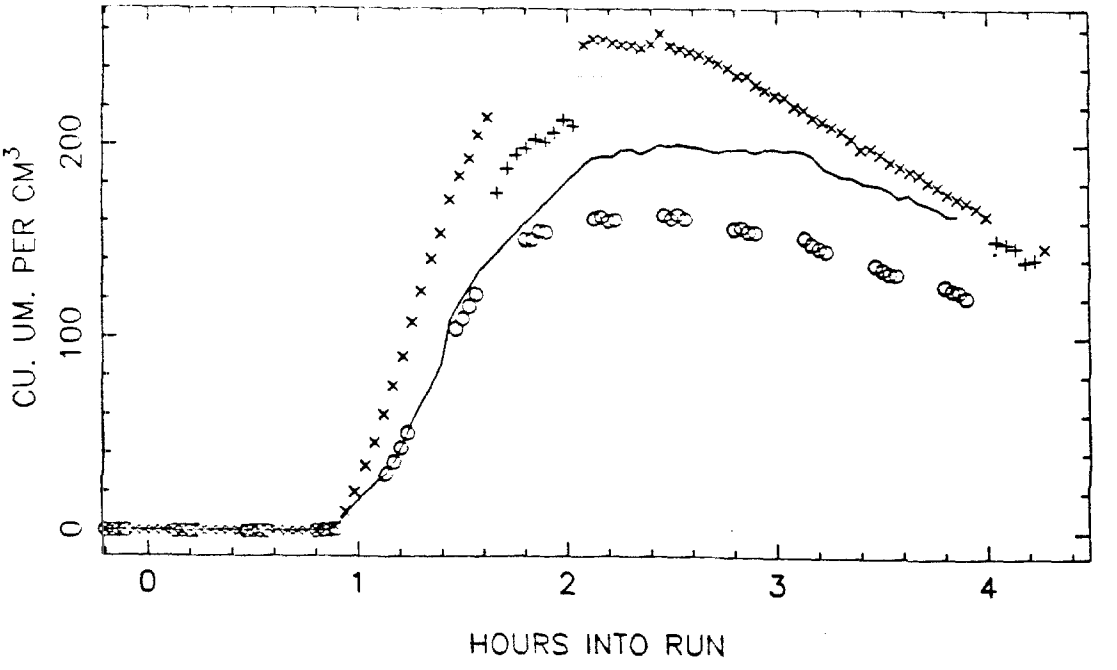

XA08 MEAN PARTICLE SIZE, SIDE A

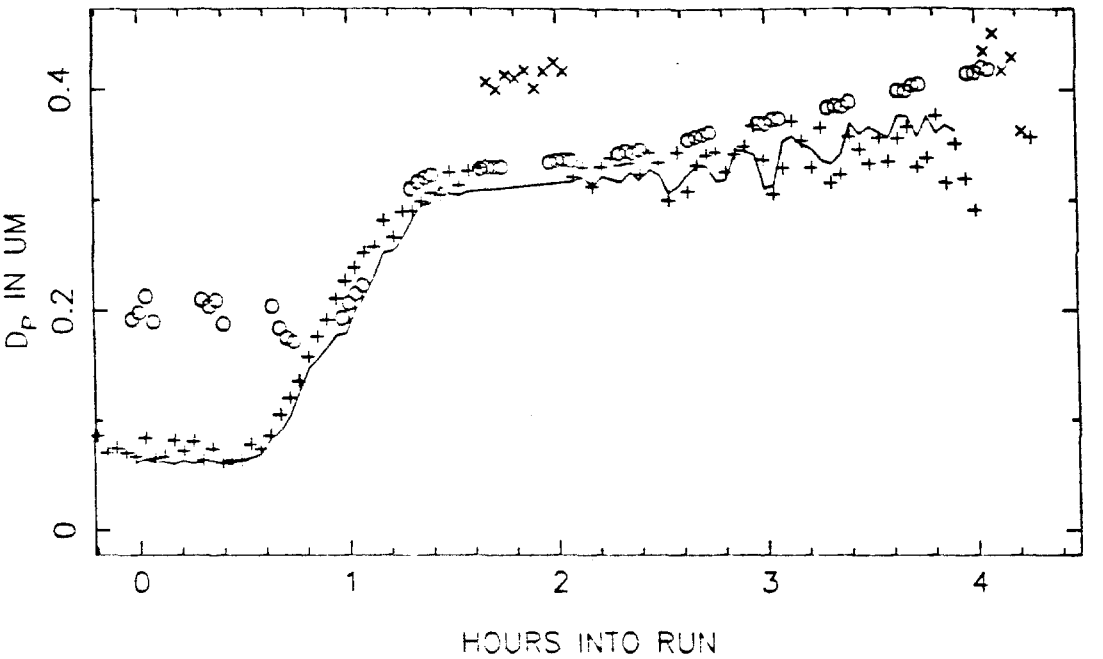

SIDE B

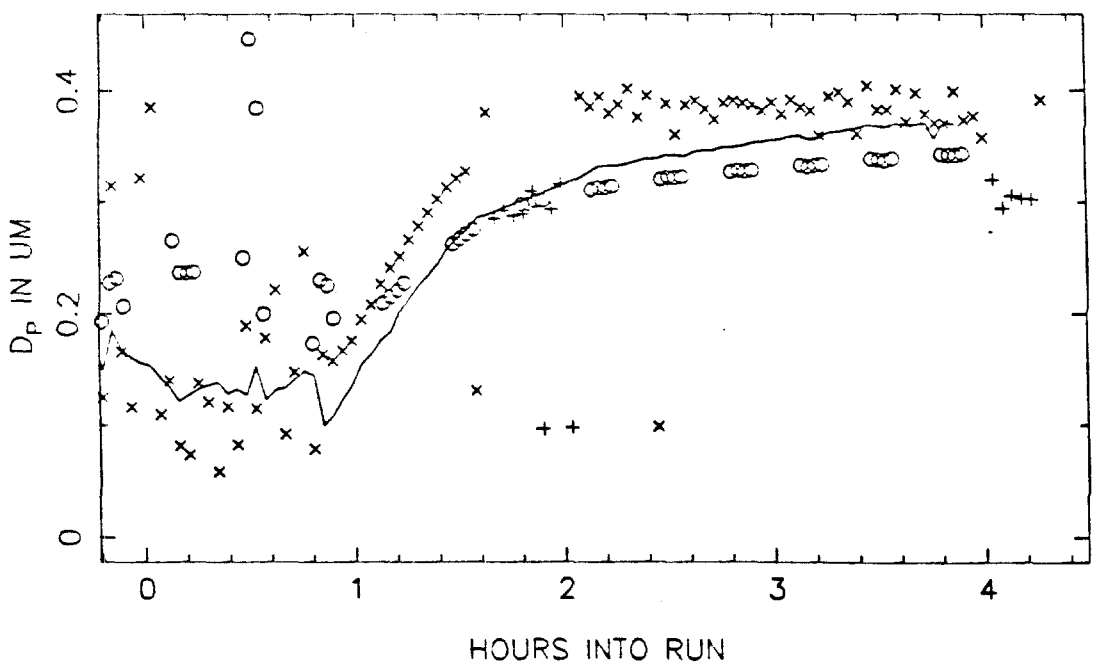

XA08A NUMBER DISTRIBUTION, T=0

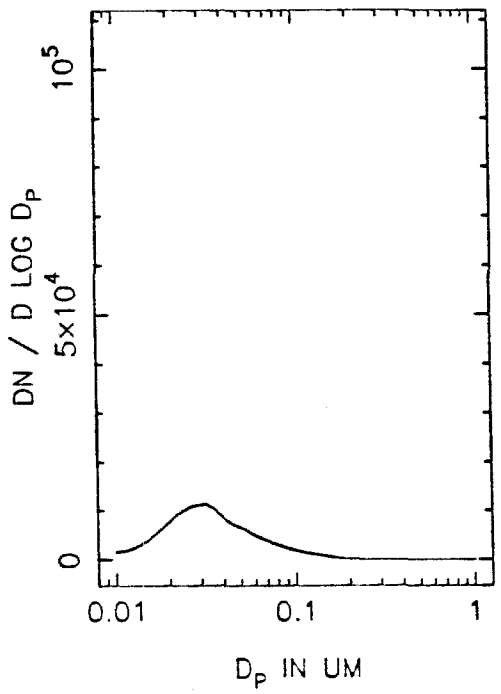

T=0.5 HOURS

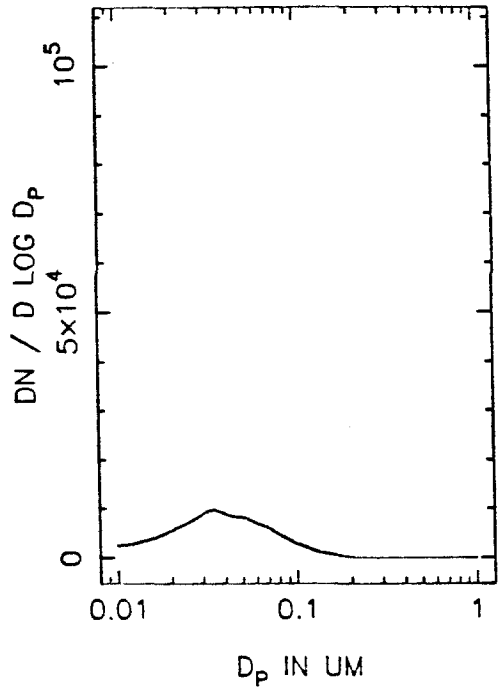

T=1.0 HOURS

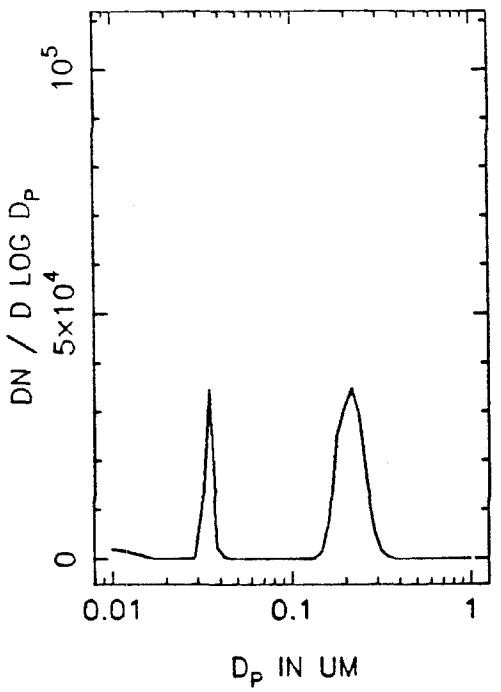

T=1.5 HOURS

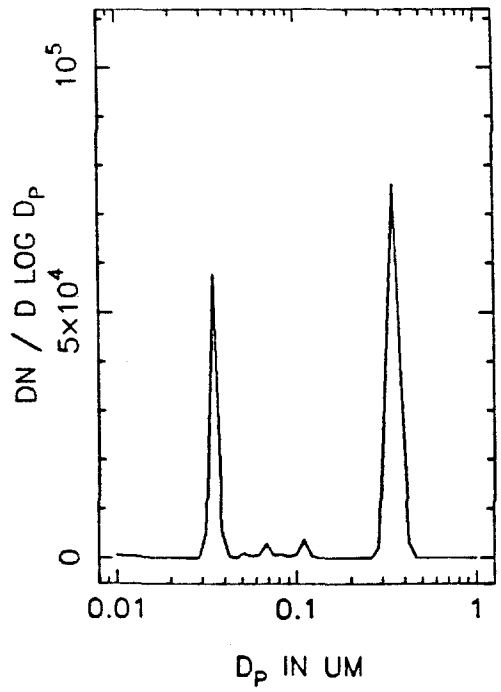

XA08A NUMBER DISTRIBUTION, T=2.0

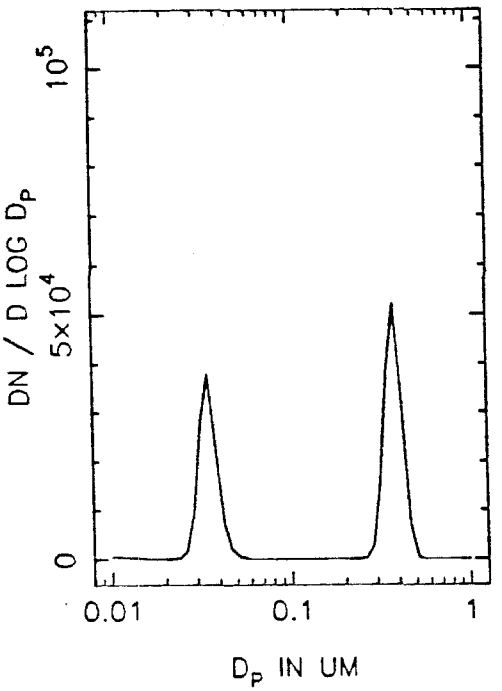

T=2.5 HOURS

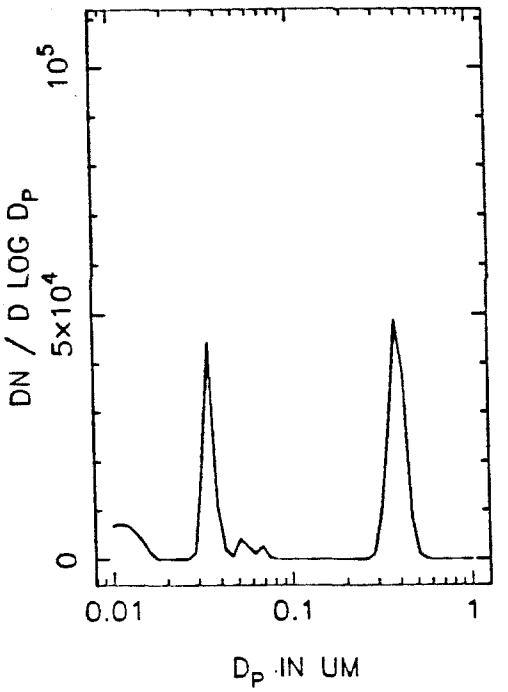

T=3.0 HOURS

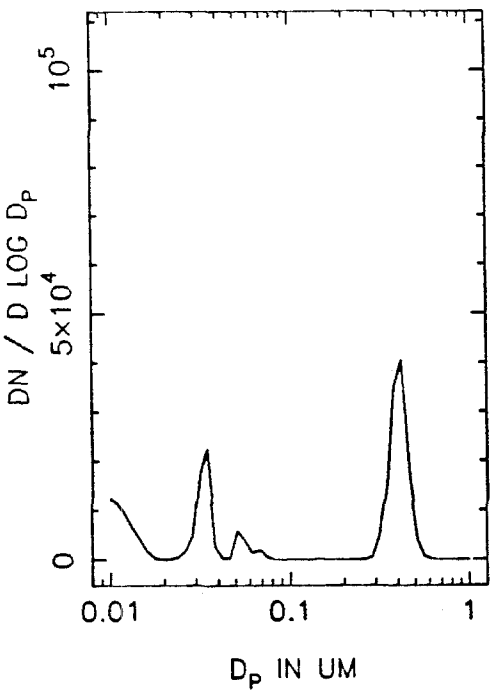

T=3.5 HOURS

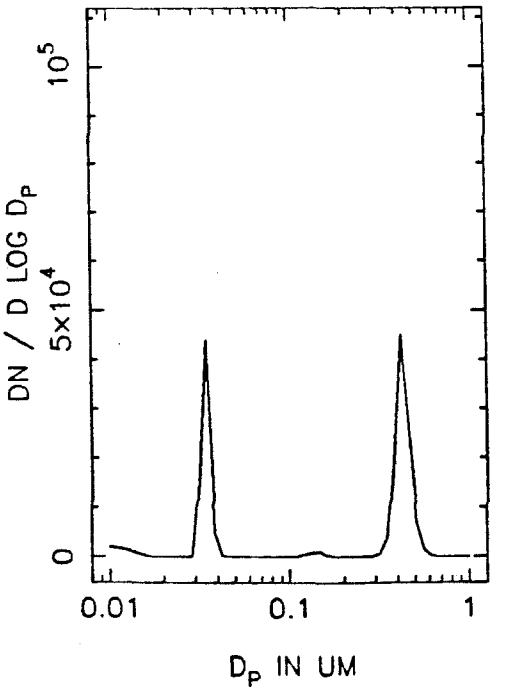

XA08A VOLUME DISTRIBUTION, T=0

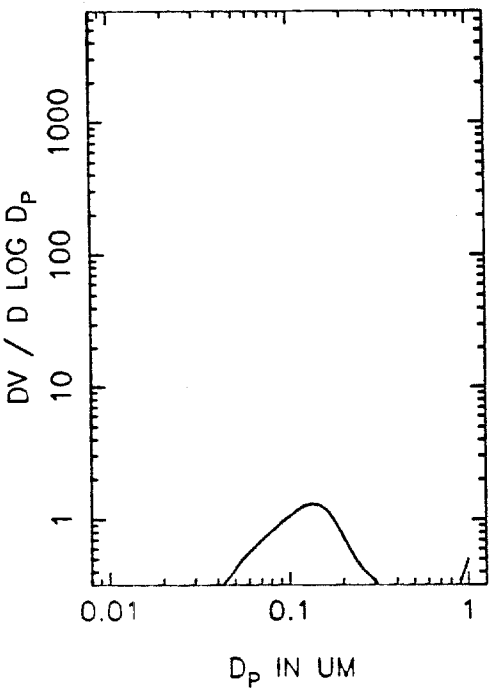

T=0.5 HOURS

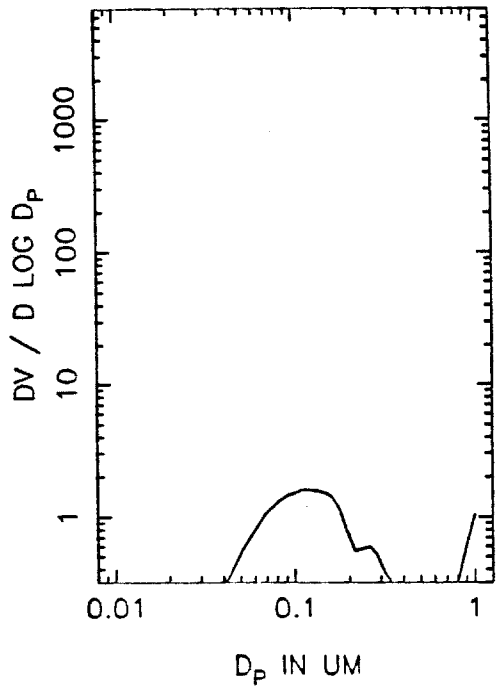

T=1.0 HOURS

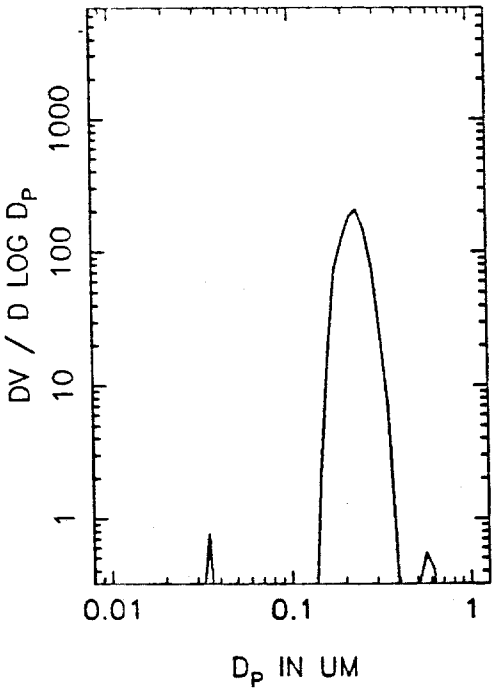

T=1.5 HOURS

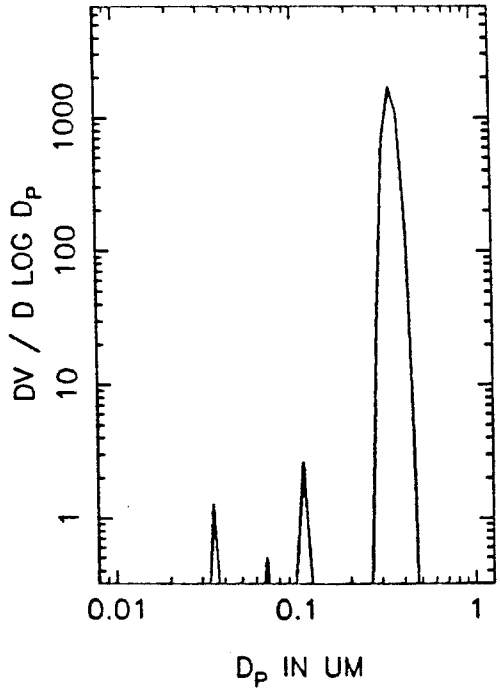

XA08A VOLUME DISTRIBUTION, T=2.0

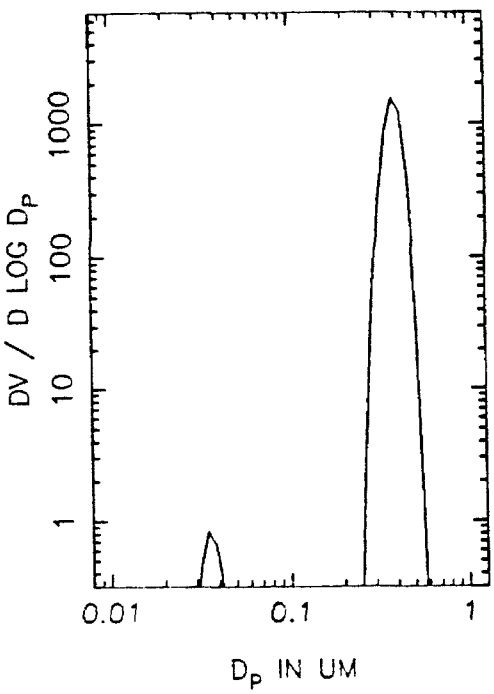

T=2.5 HOURS

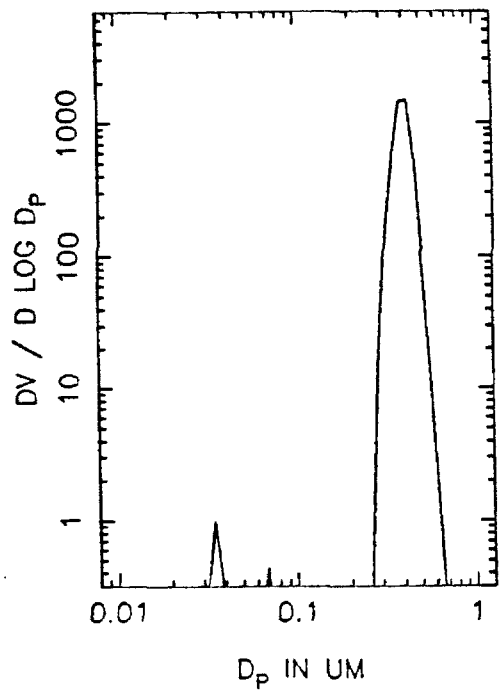

T=3.0 HOURS

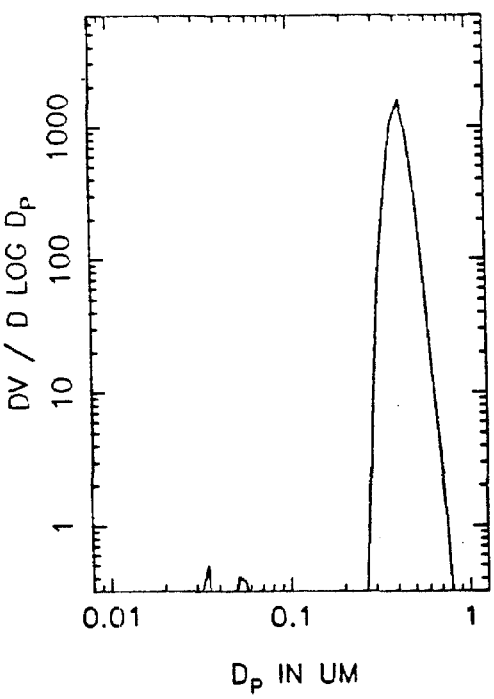

T=3.5 HOURS

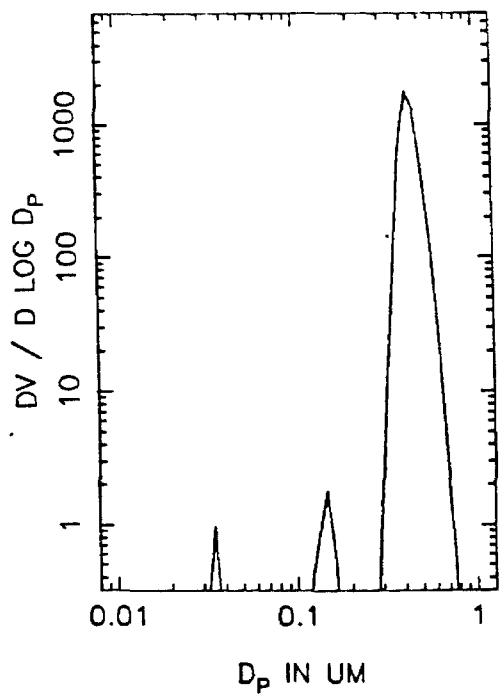

XA08B NUMBER DISTRIBUTION, T=0

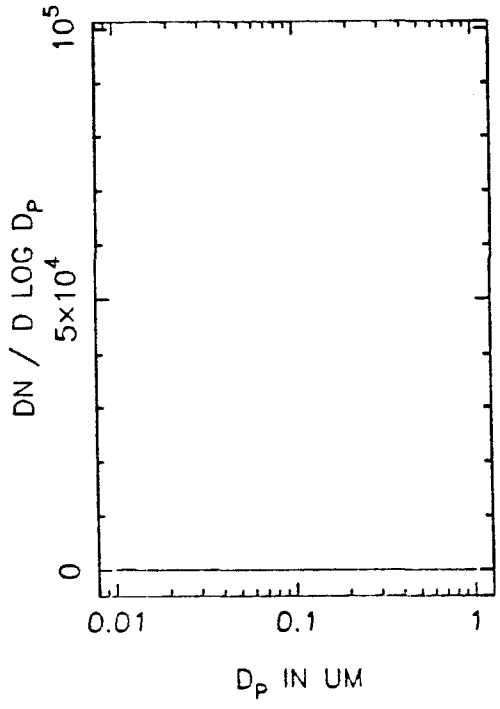

T=0.5 HOURS

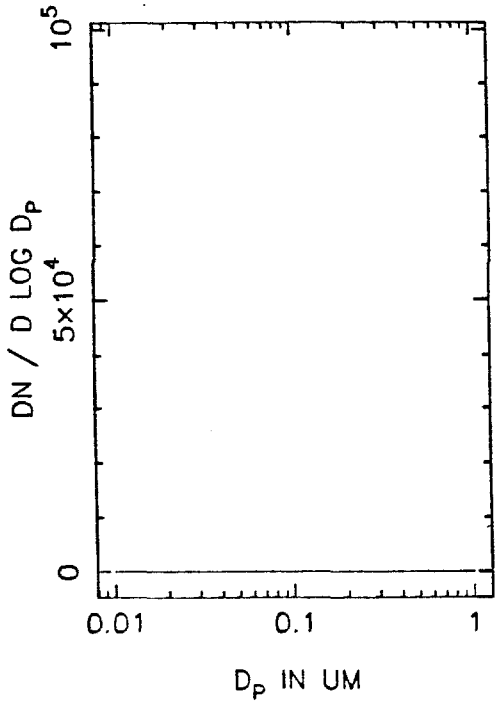

T=1.0 HOURS

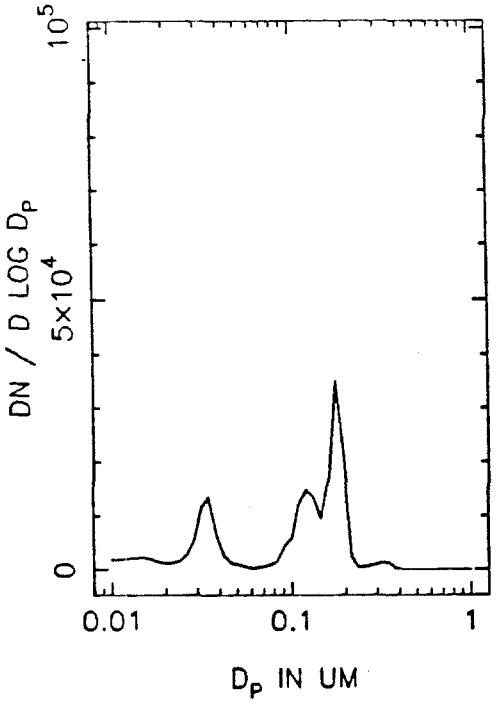

T=1.5 HOURS

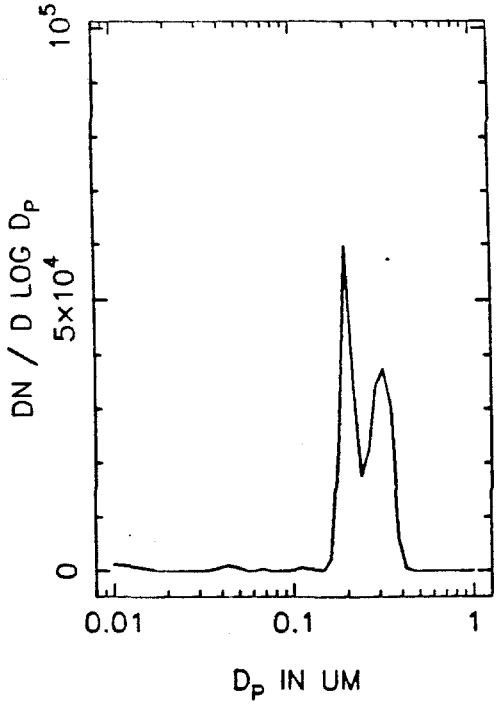

XA08B NUMBER DISTRIBUTION, T=2.0

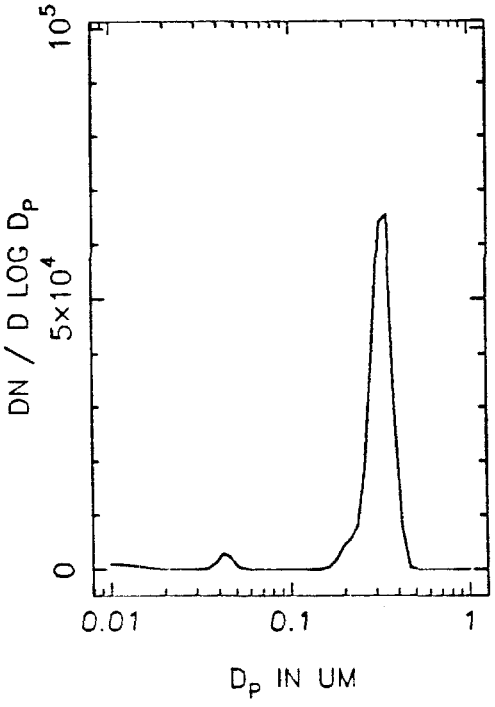

T=2.5 HOURS

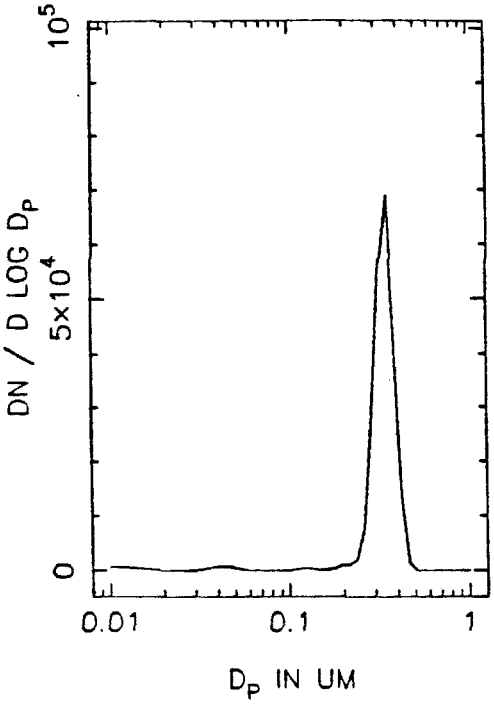

T=3.0 HOURS

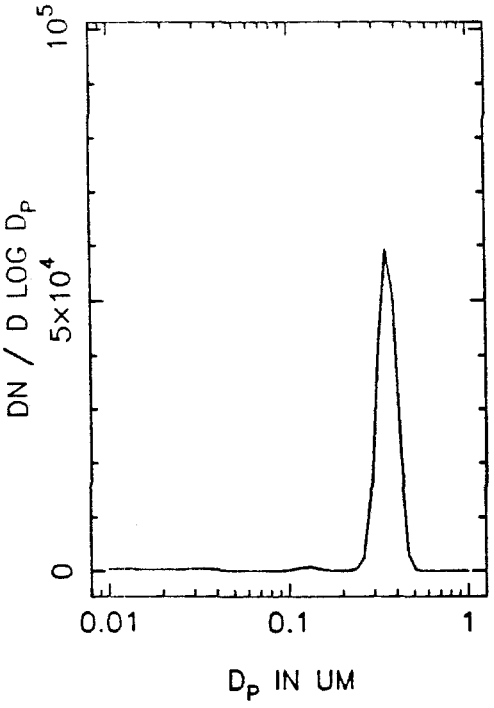

T=3.5 HOURS

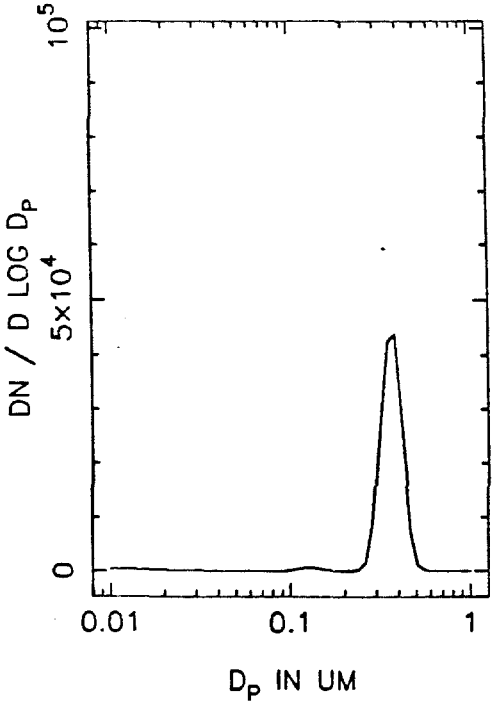

XA08B VOLUME DISTRIBUTION, T=0

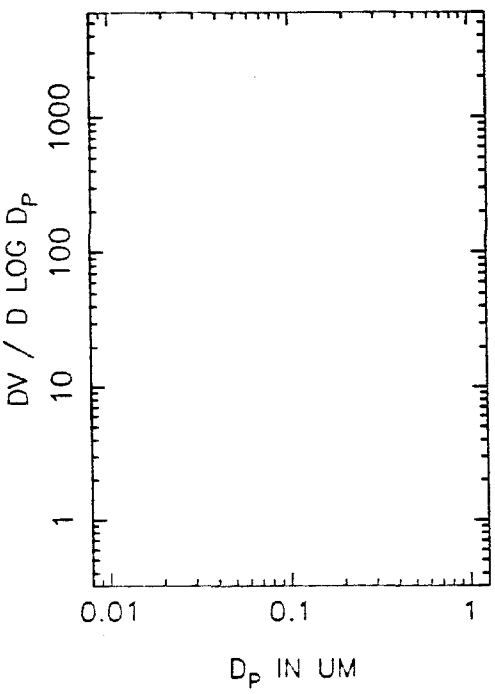

T=0.5 HOURS

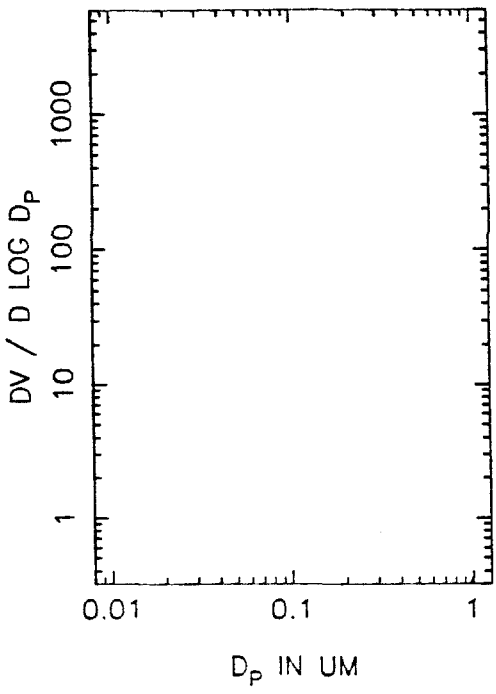

T=1.0 HOURS

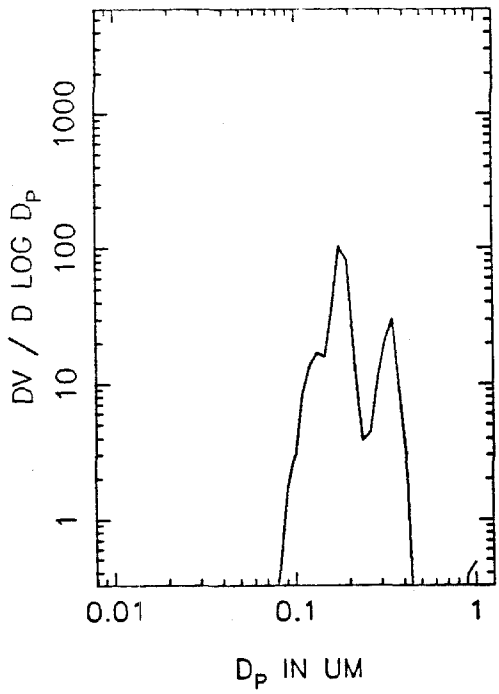

T=1.5 HOURS

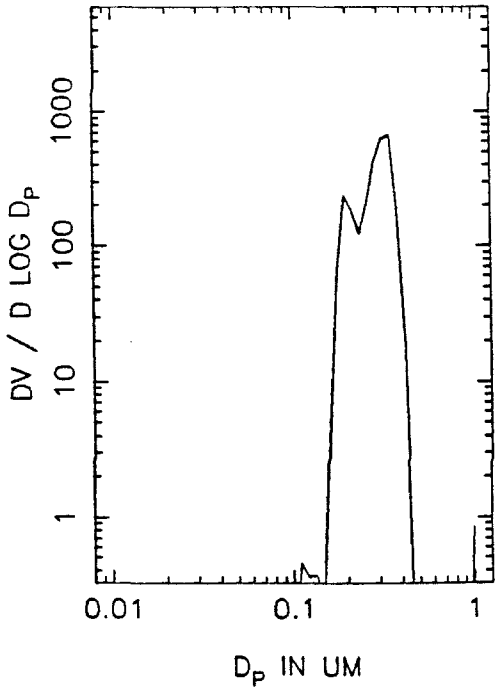

XA08B VOLUME DISTRIBUTION, T=2.0

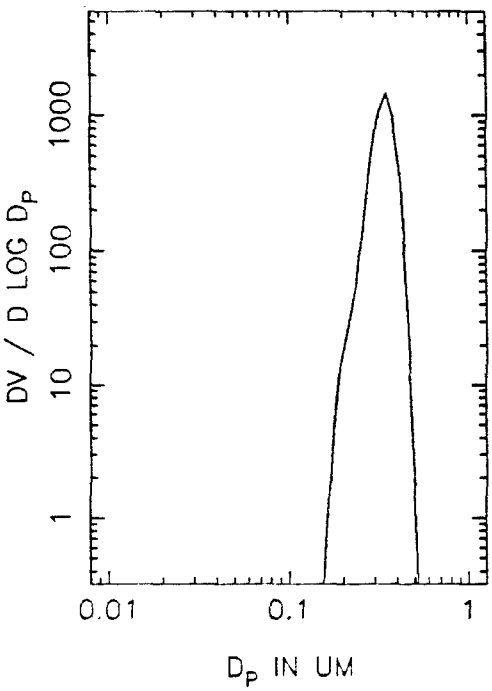

T=2.5 HOURS

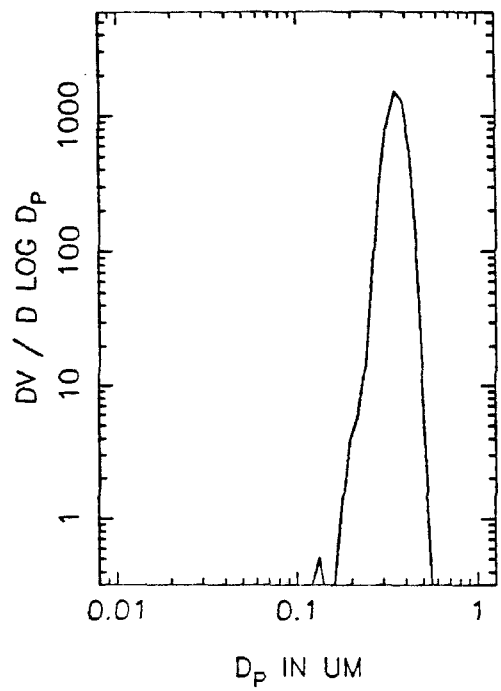

T=3.0 HOURS

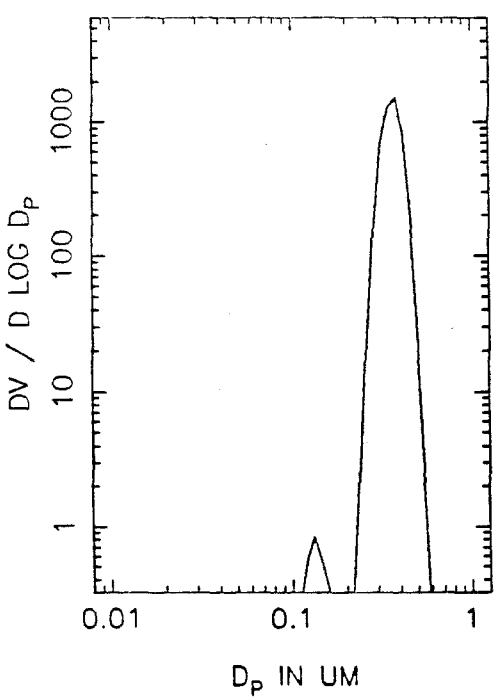

T=3.5 HOURS

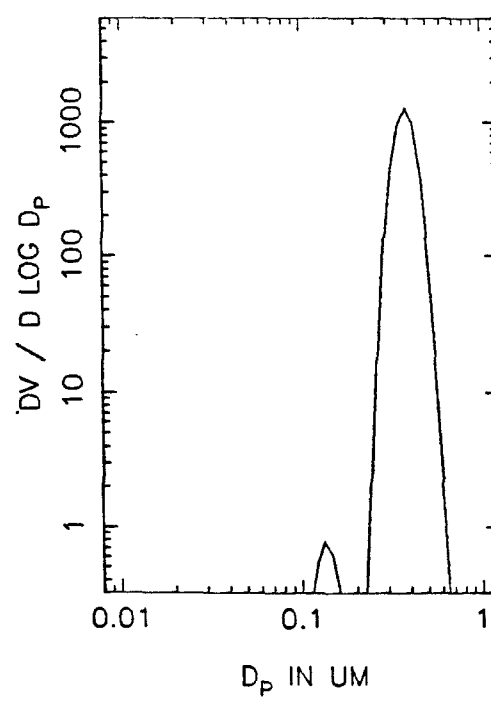

XB10 TOTAL NUMBER, SIDE A

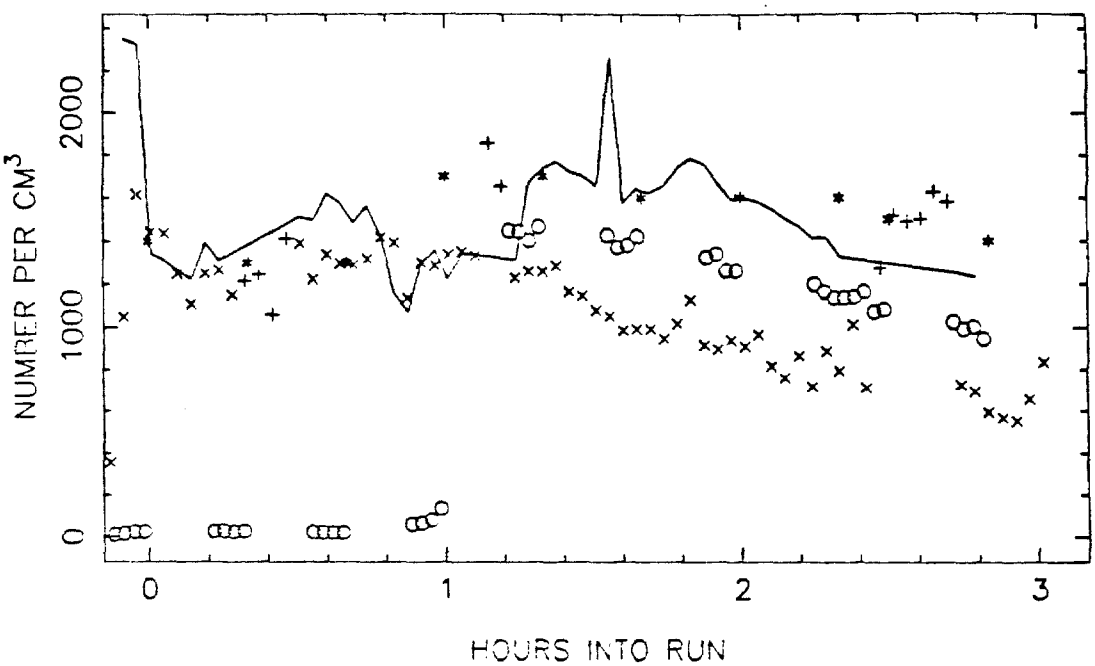

SIDE B

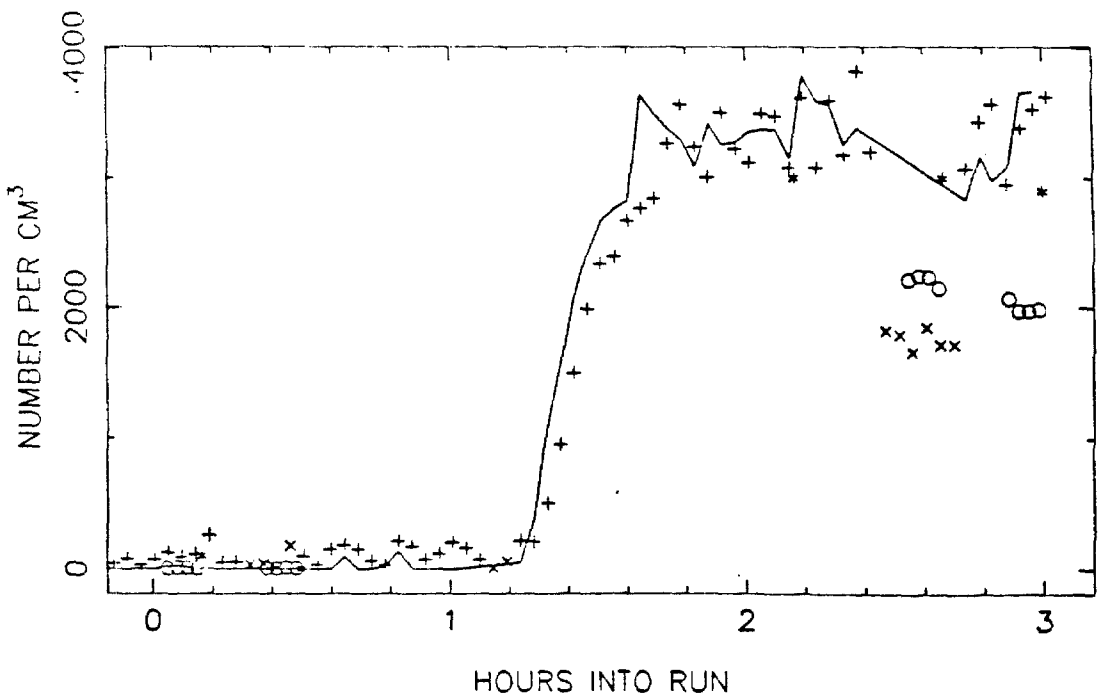

XB10 VOLUME IN THE AEROSOL PHASE, SIDE A

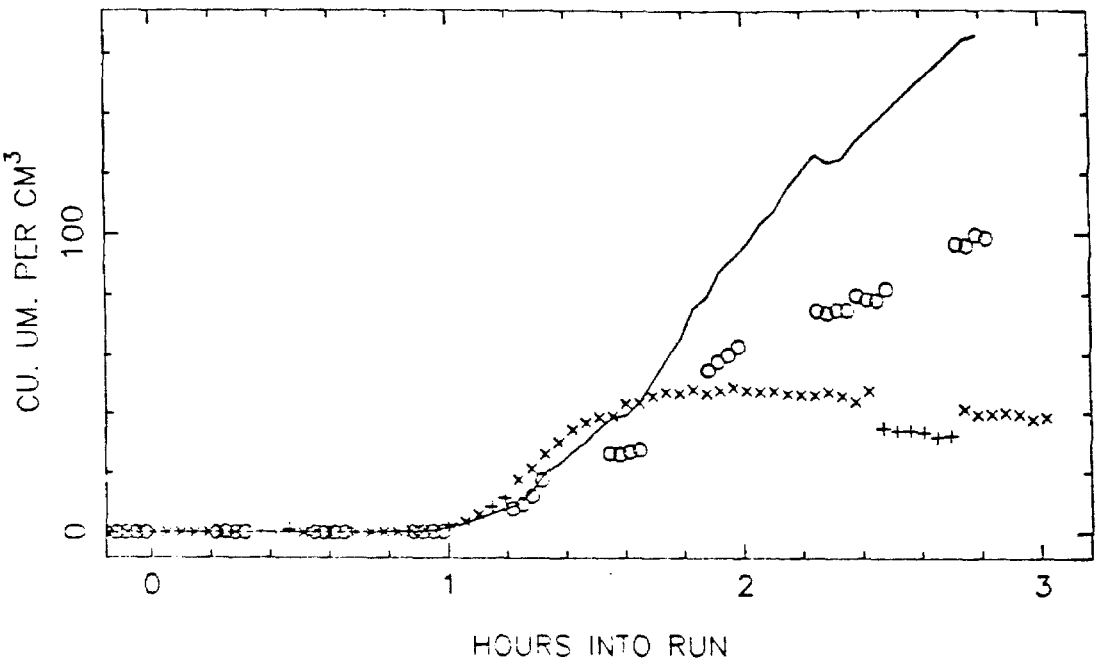

SIDE B

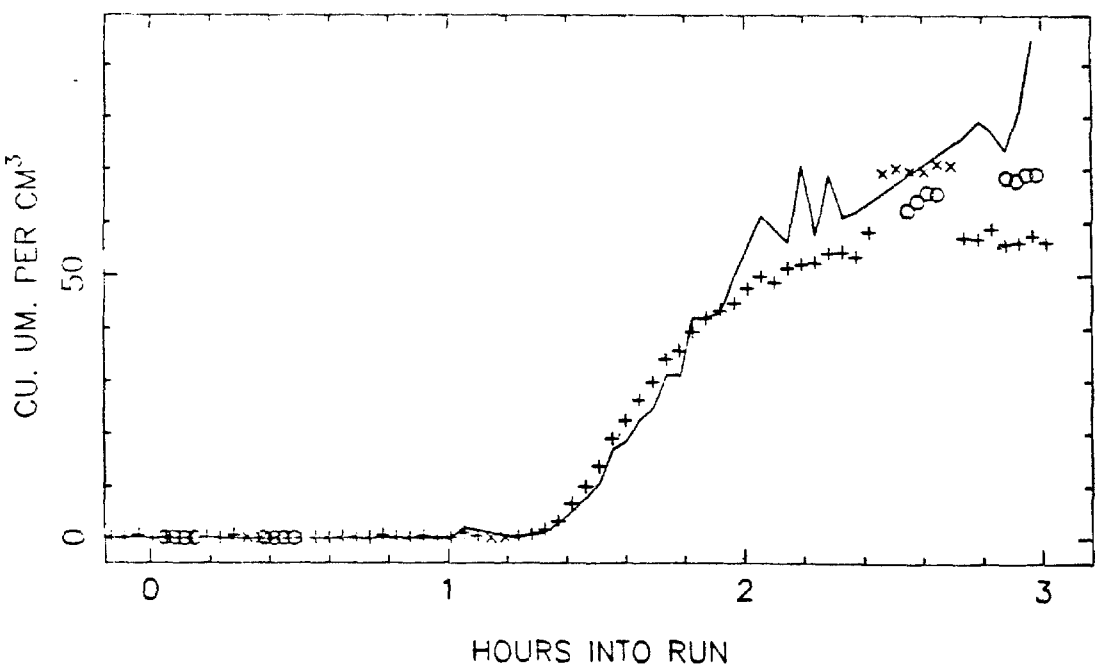

XB10 MEAN PARTICLE SIZE, SIDE A

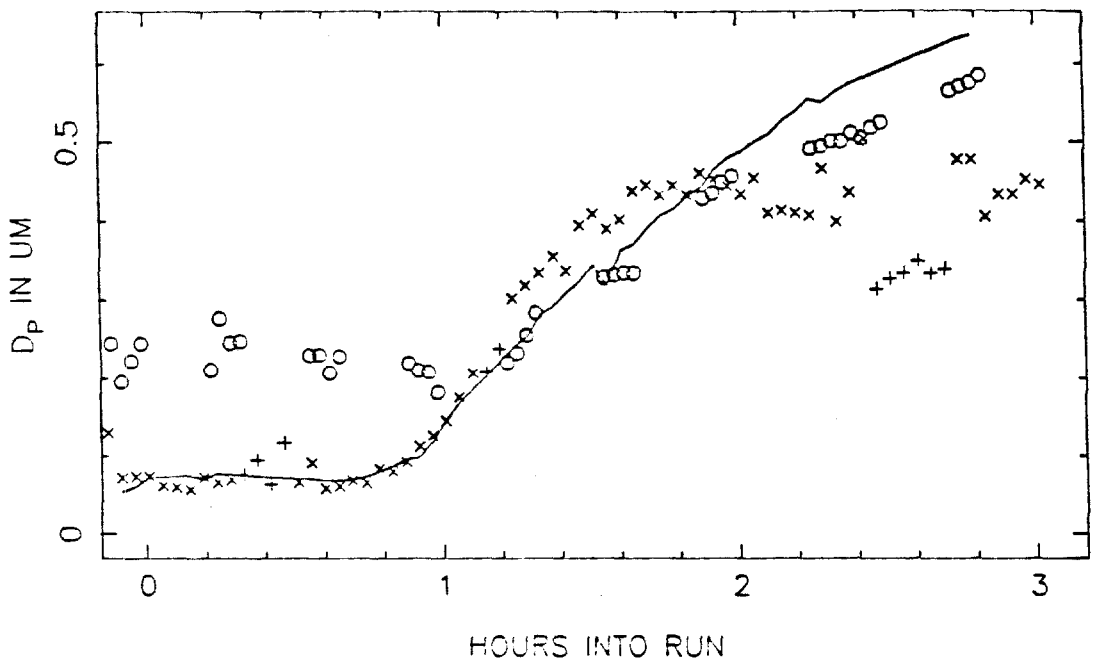

SIDE B

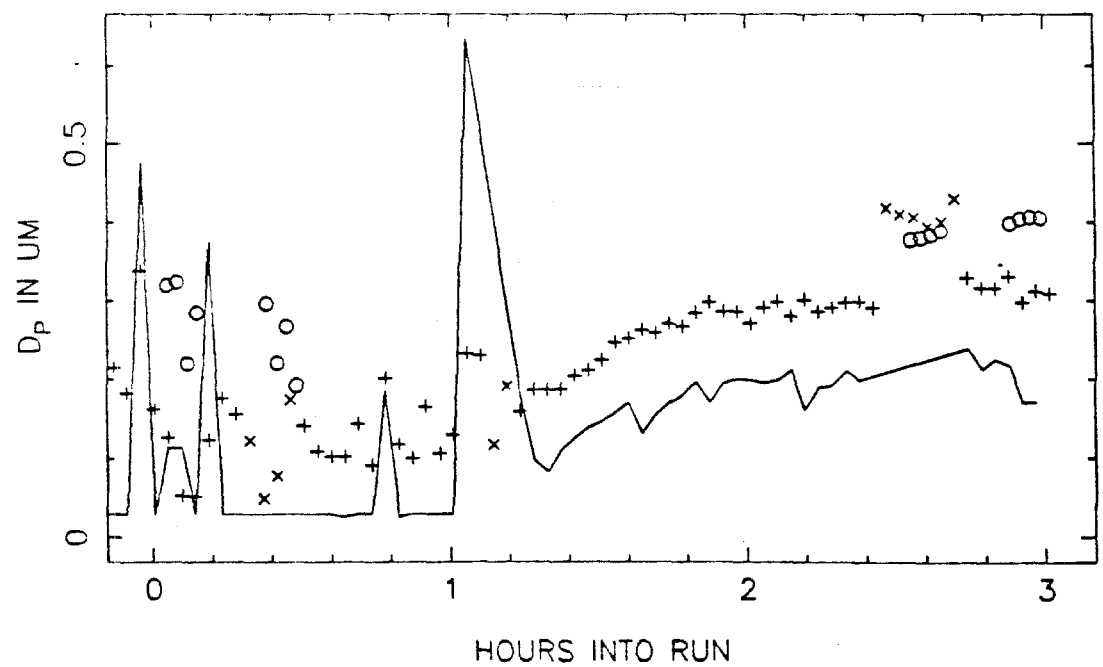

XB10A NUMBER DISTRIBUTION, T=0

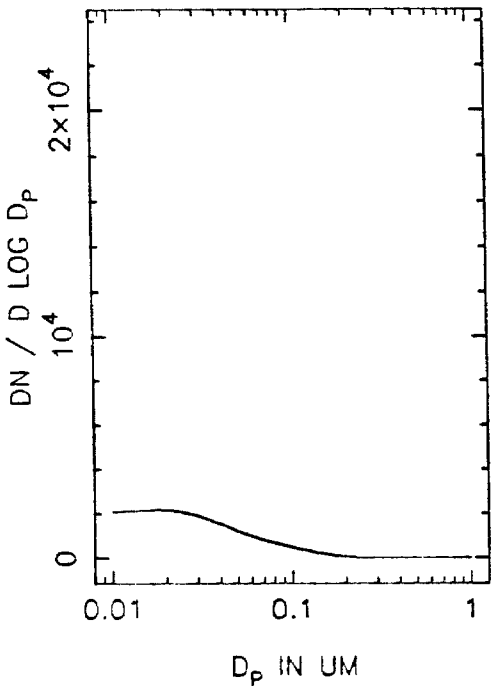

T=0.5 HOURS

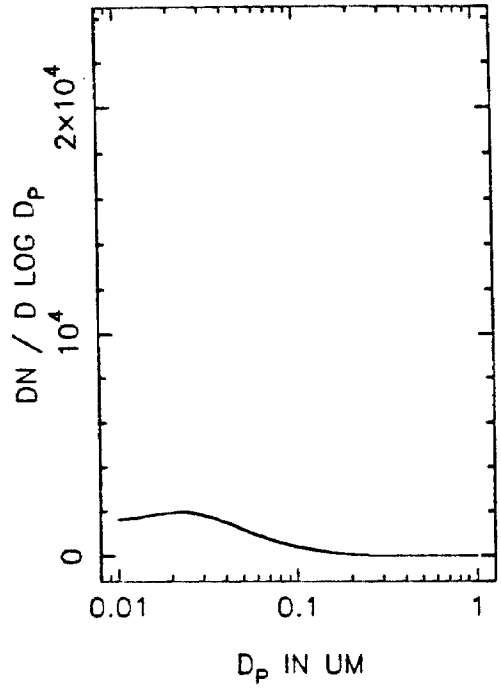

T=1.0 HOURS

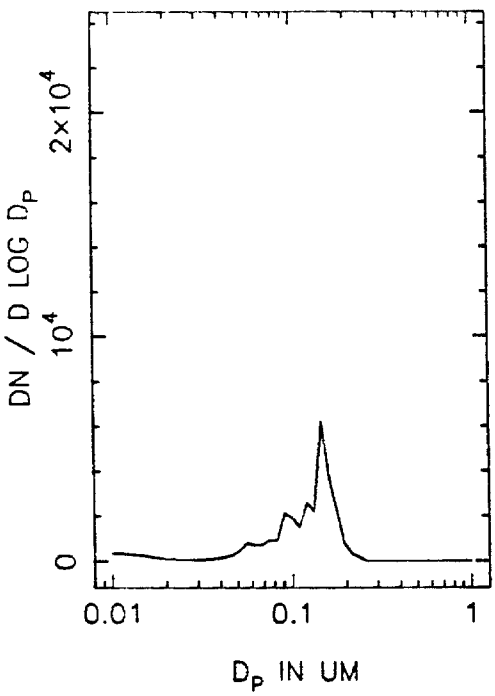

T=1.5 HOURS

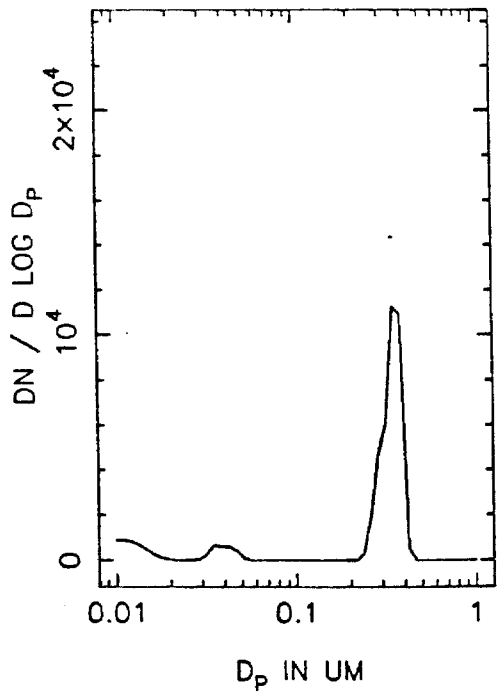

XB10A NUMBER DISTRIBUTION, T=2.0

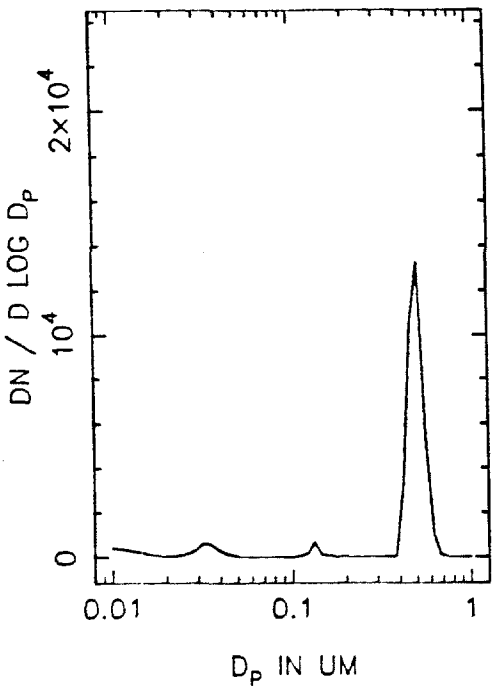

T=2.5 HOURS

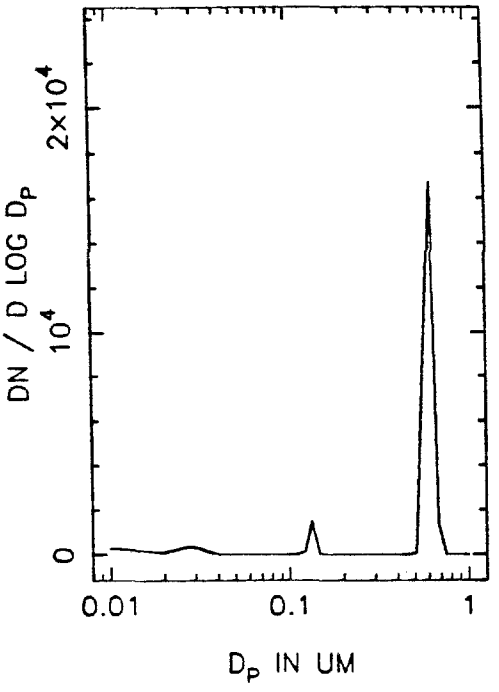

XB10A VOLUME DISTRIBUTION, T=0

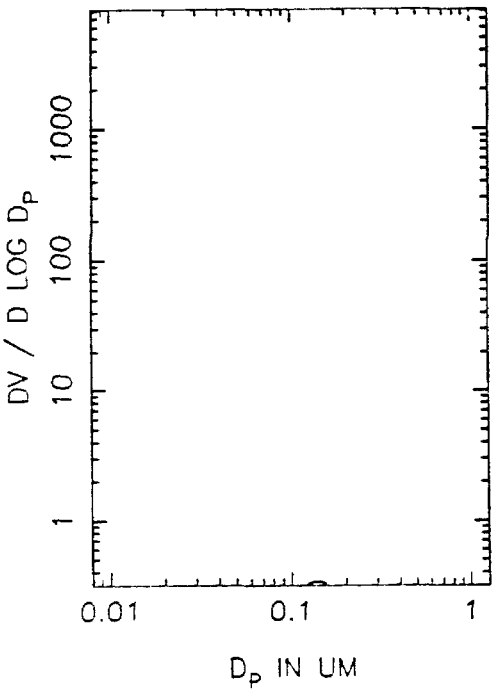

T=0.5 HOURS

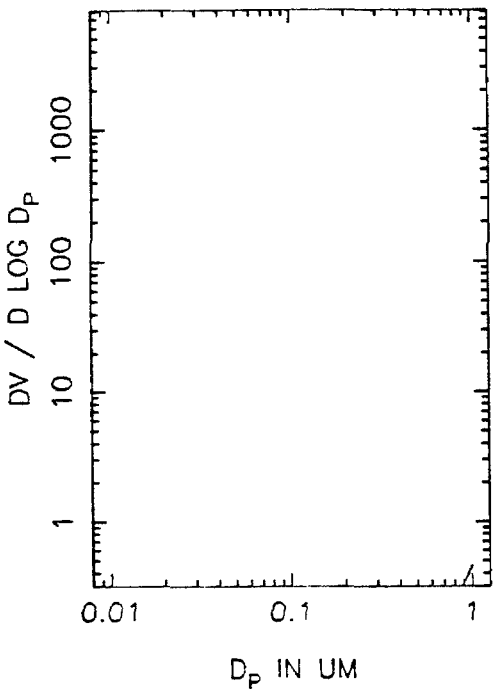

T=1.0 HOURS

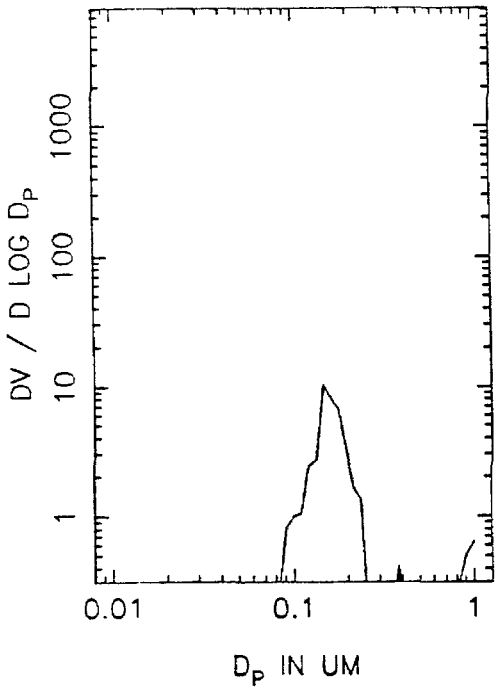

T=1.5 HOURS

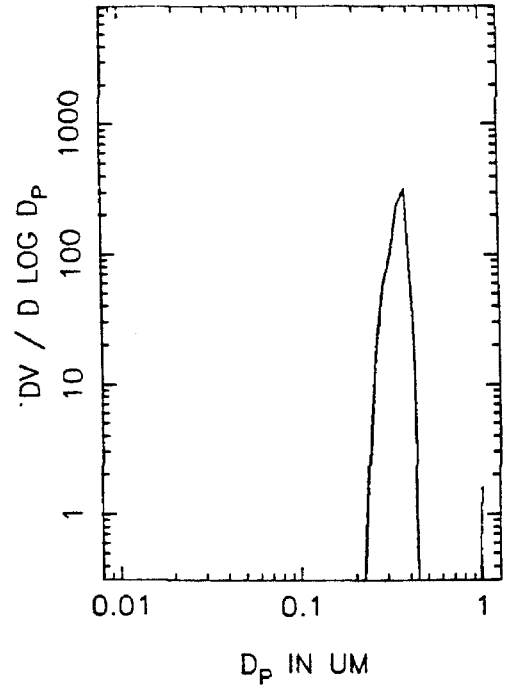

XB10A VOLUME DISTRIBUTION, T=2.0

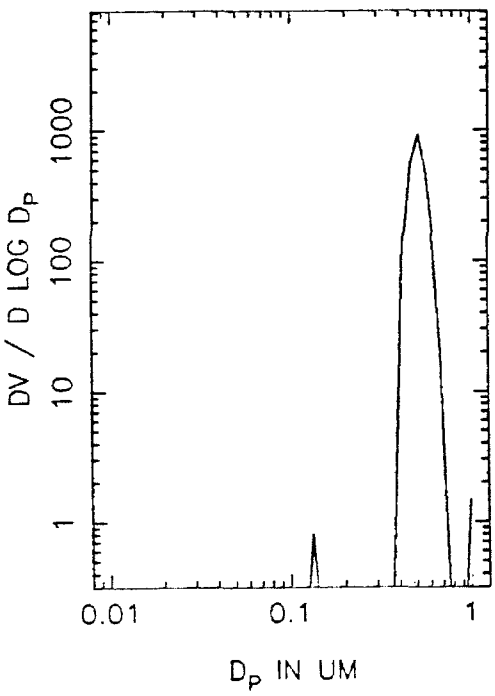

T=2.5 HOURS

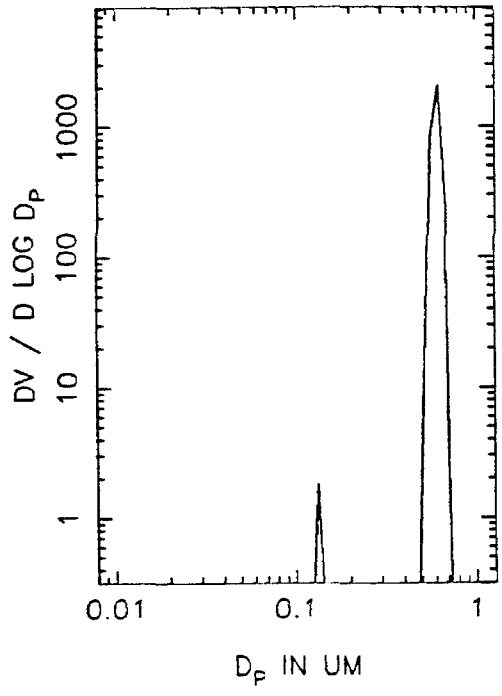

XB10B NUMBER DISTRIBUTION, T=0

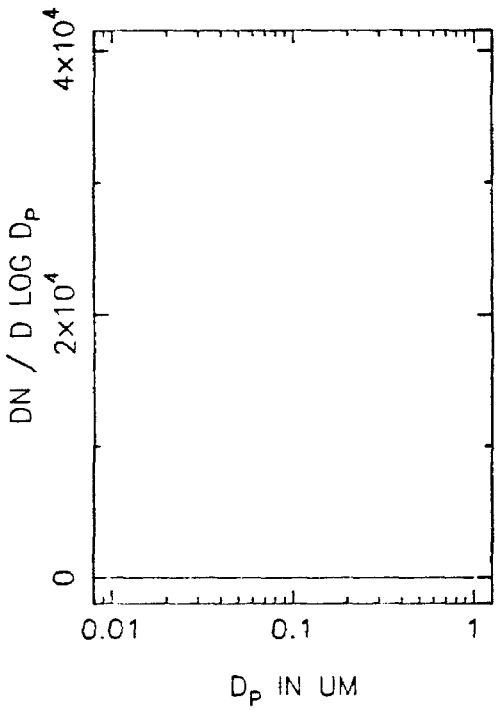

T=0.5 HOURS

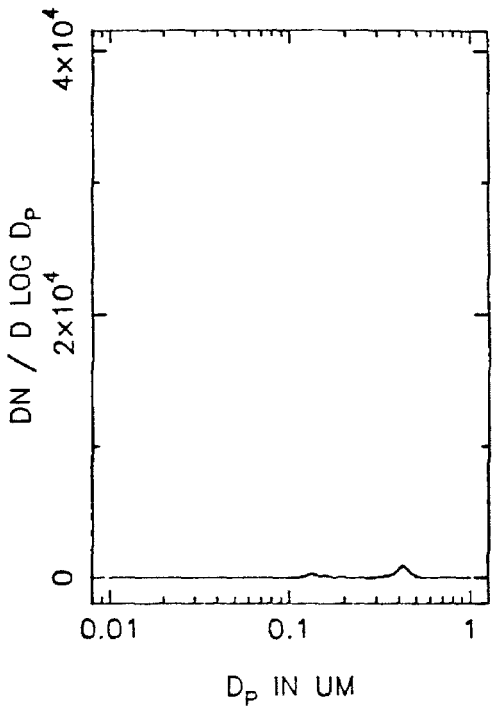

T=1.0 HOURS

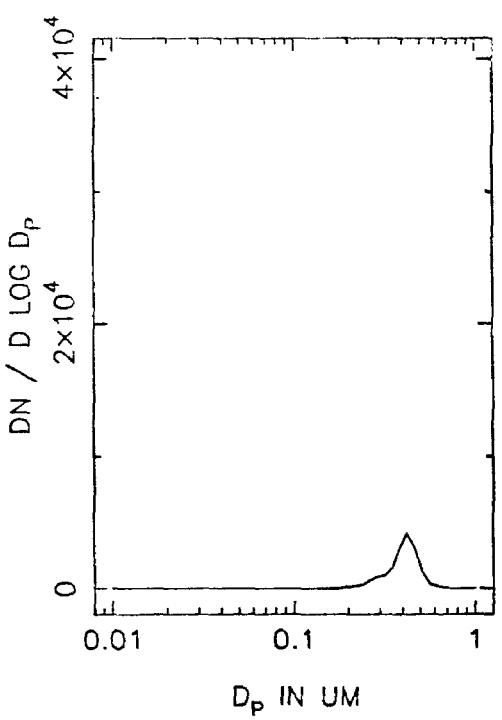

T=1.5 HOURS

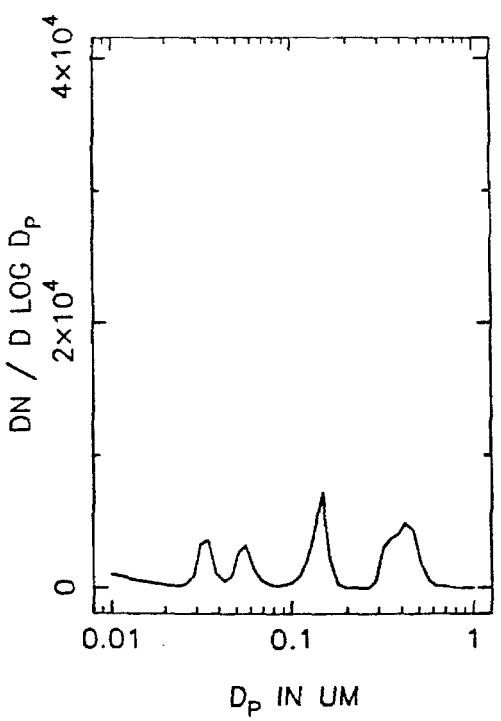

XB10B NUMBER DISTRIBUTION, T=2.0

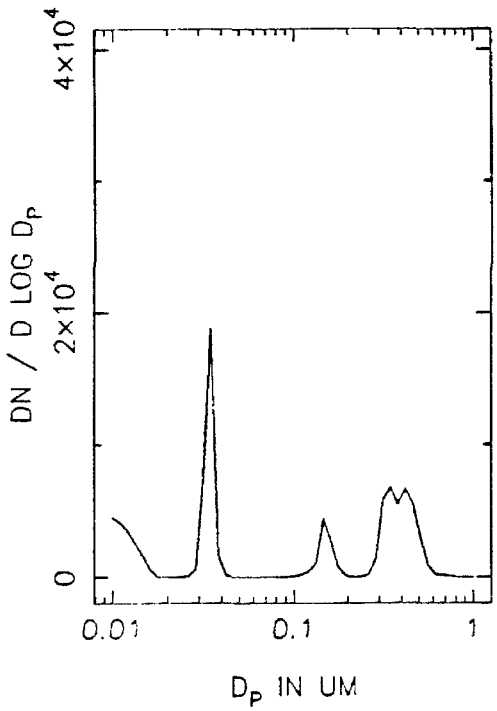

T=2.5 HOURS

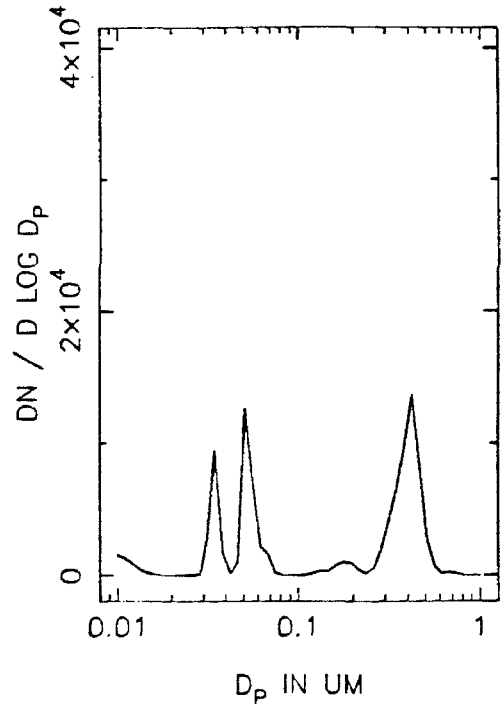

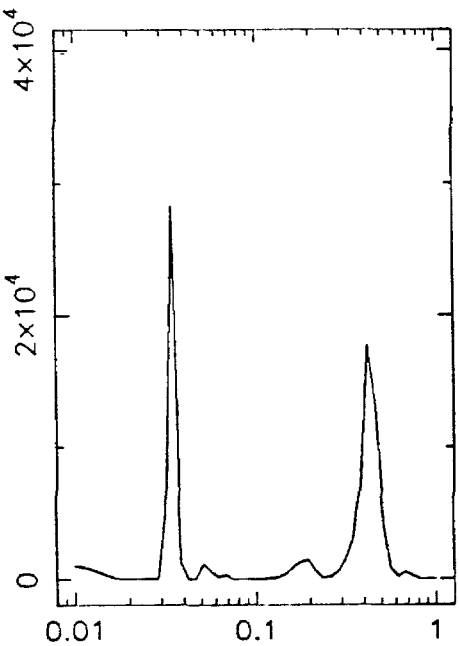

XB10B VOLUME DISTRIBUTION, T=0

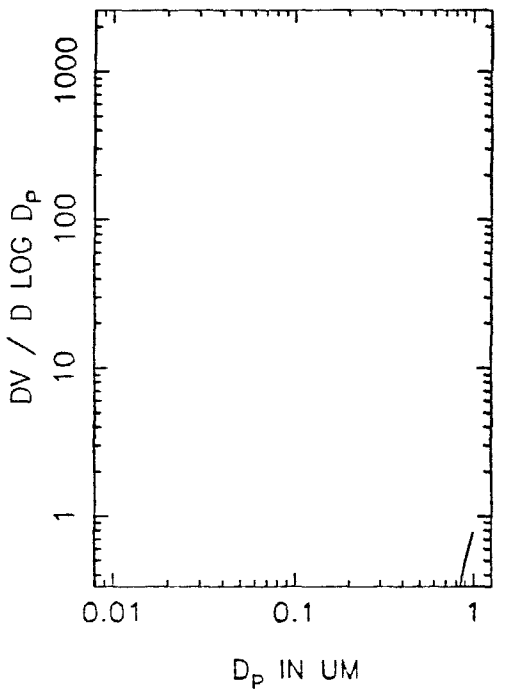

T=0.5 HOURS

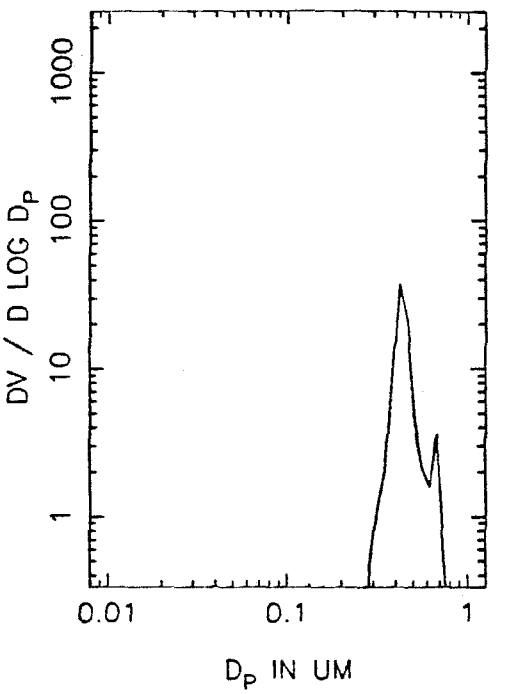

T=1.0 HOURS

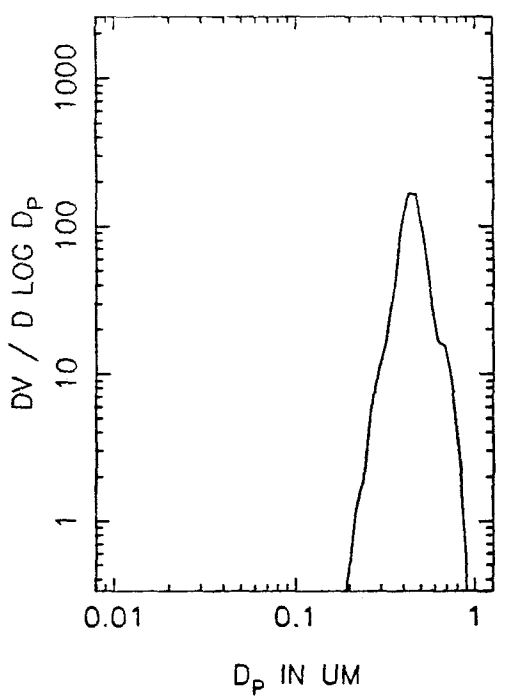

T=1.5 HOURS

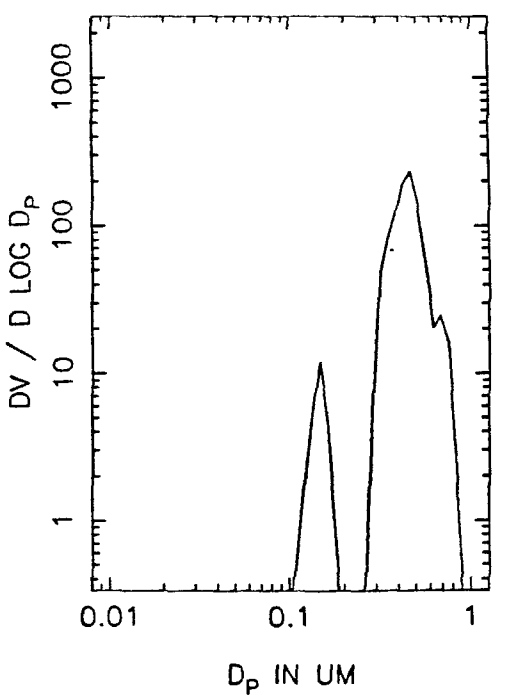

XB10B VOLUME DISTRIBUTION, T=2.0

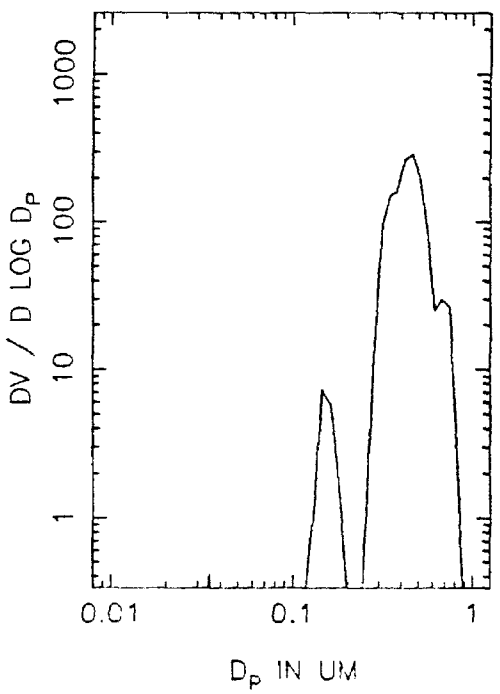

T=2.5 HOURS

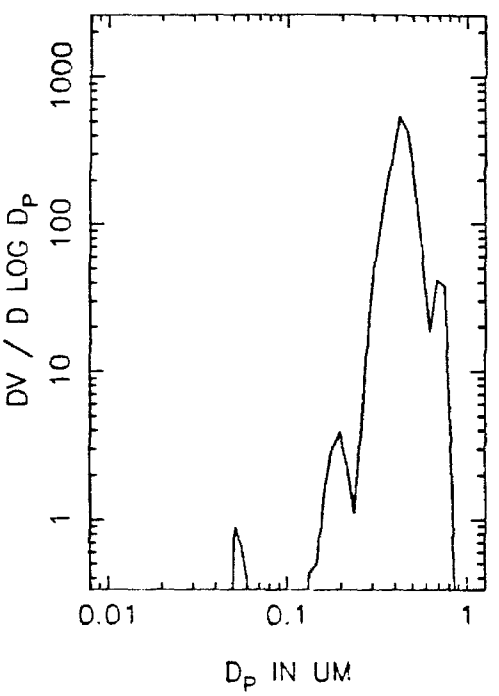

T=3.0 HOURS

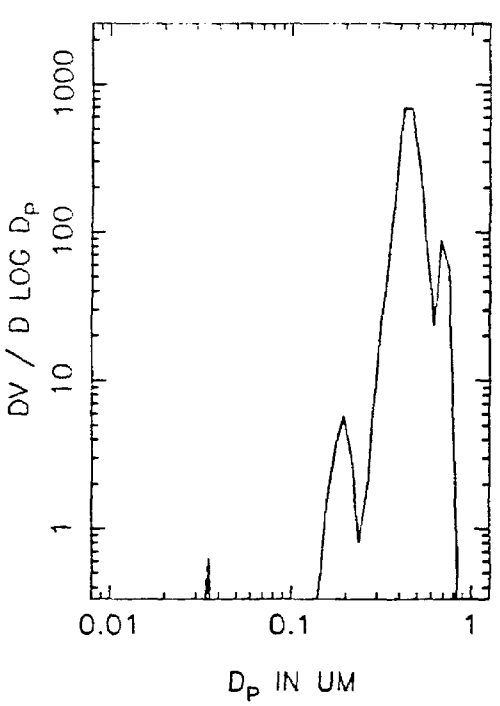

XB12 TOTAL NUMBER, SIDE A

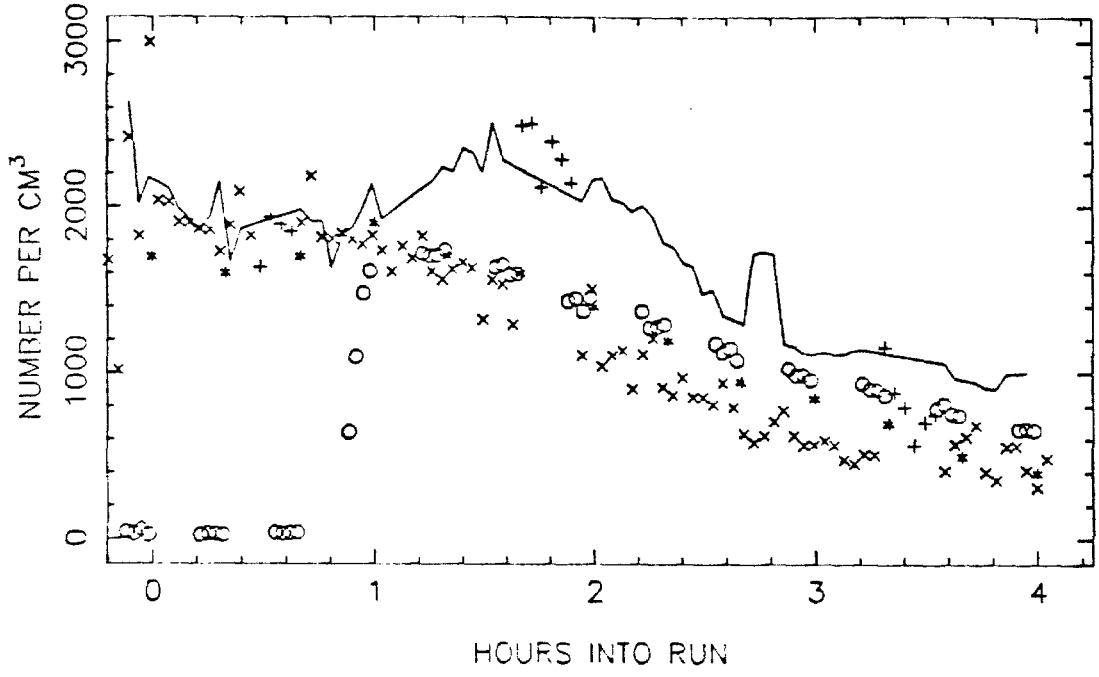

SIDE B

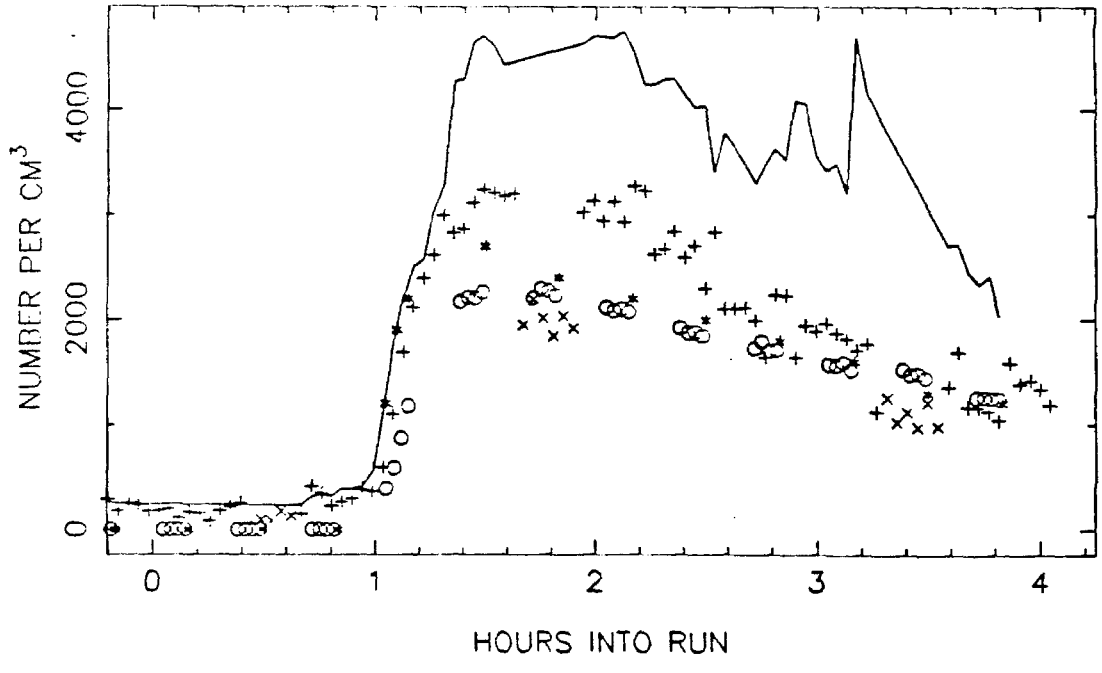

XB12 VOLUME IN THE AEROSOL PHASE, SIDE A

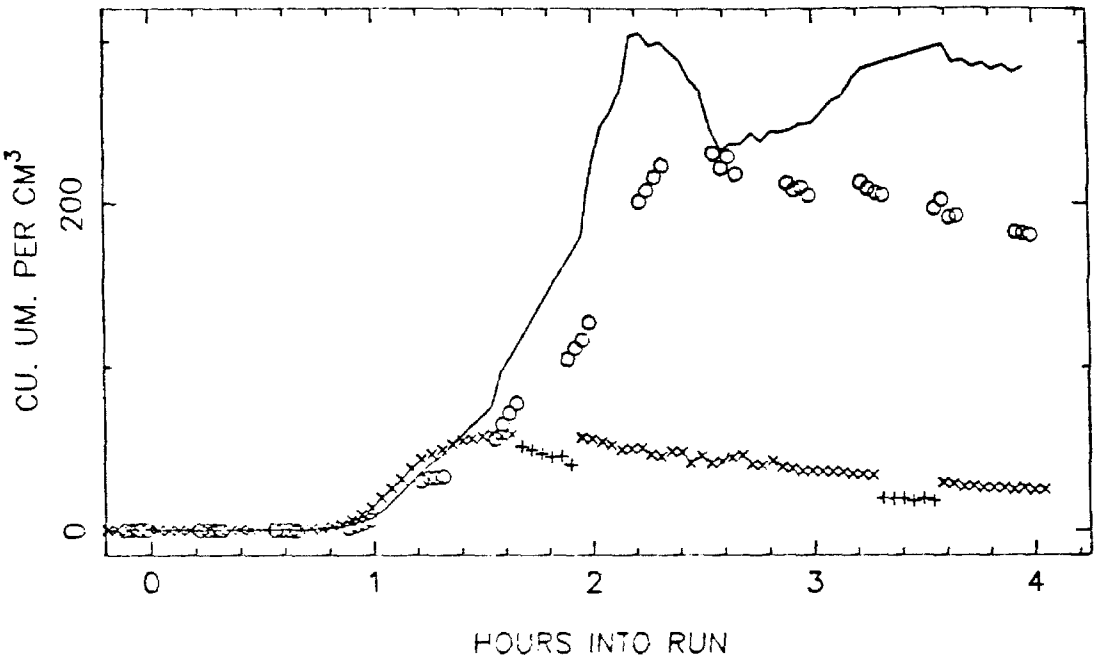

SIDE B

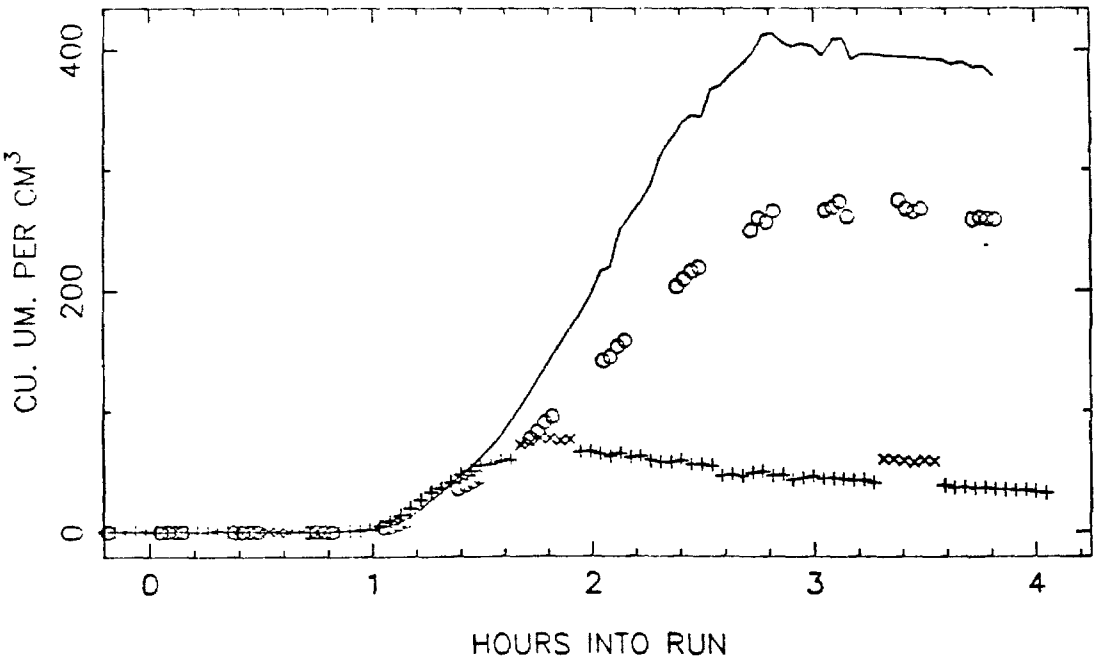

XB12 MEAN PARTICLE SIZE, SIDE A

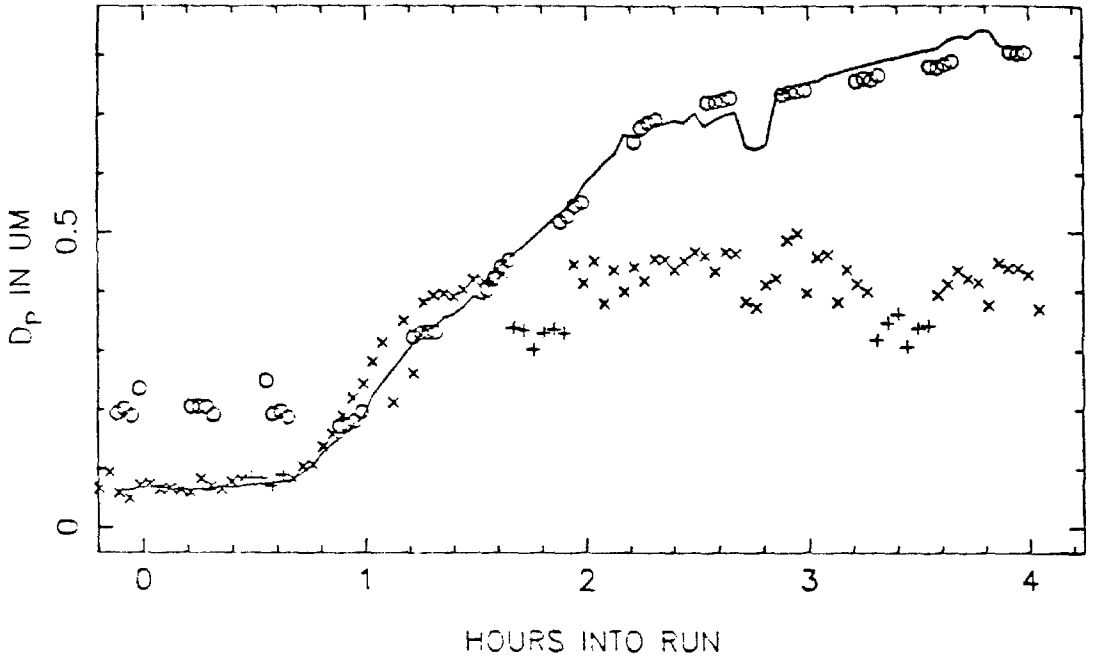

SIDE B

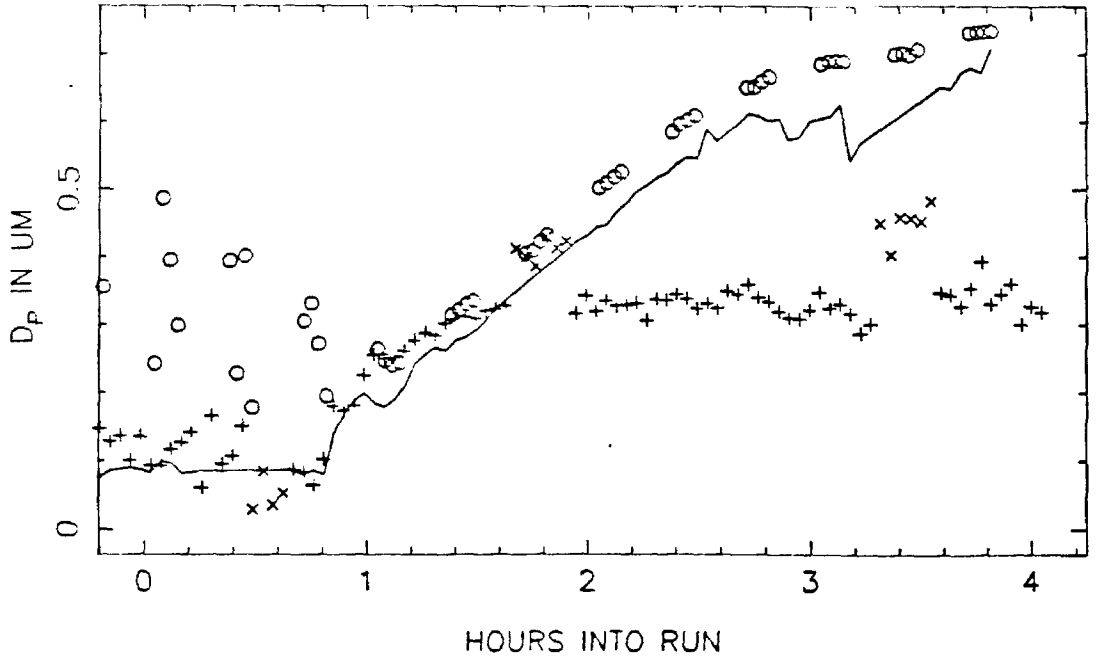

XB12A NUMBER DISTRIBUTION, T=0

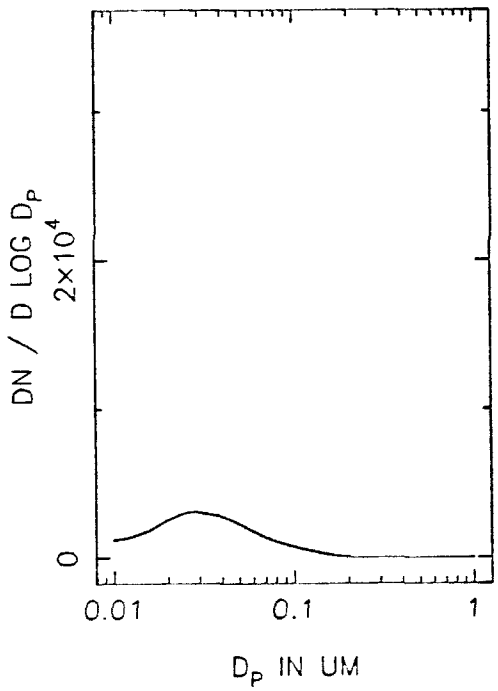

T=0.5 HOURS

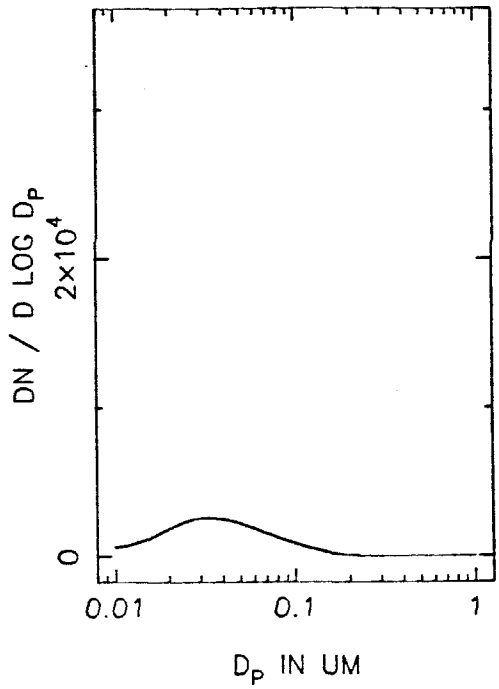

T=1.0 HOURS

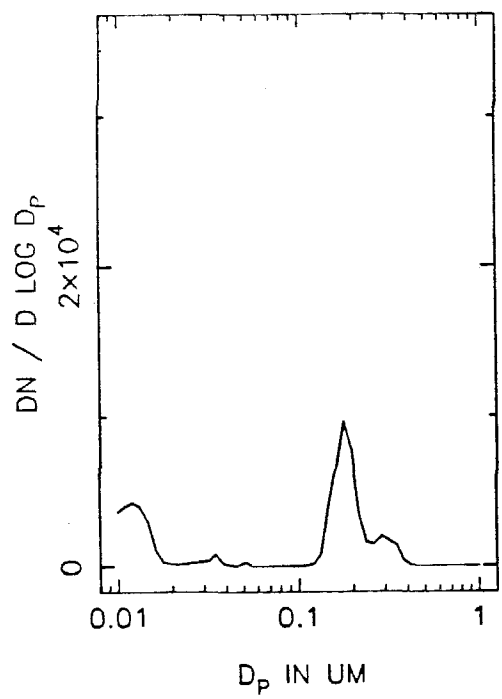

T=1.5 HOURS

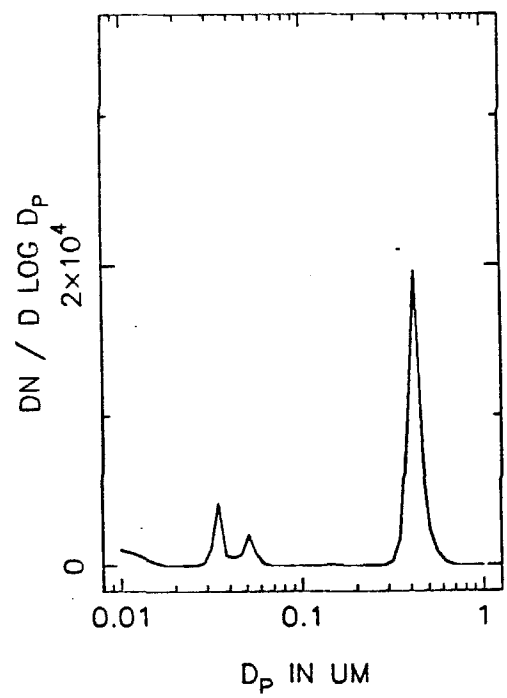

XB12A NUMBER DISTRIBUTION, T=2.0

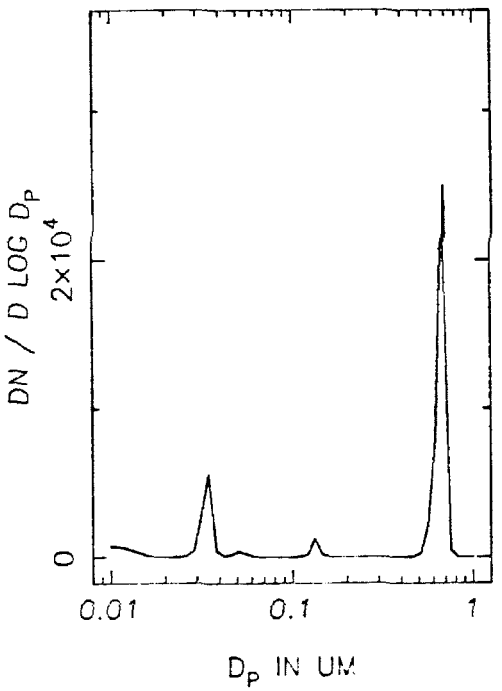

T=2.5 HOURS

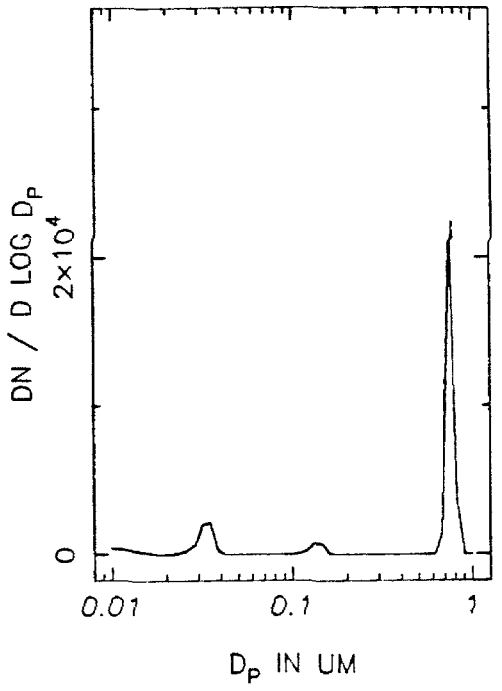

T=3.0 HOURS

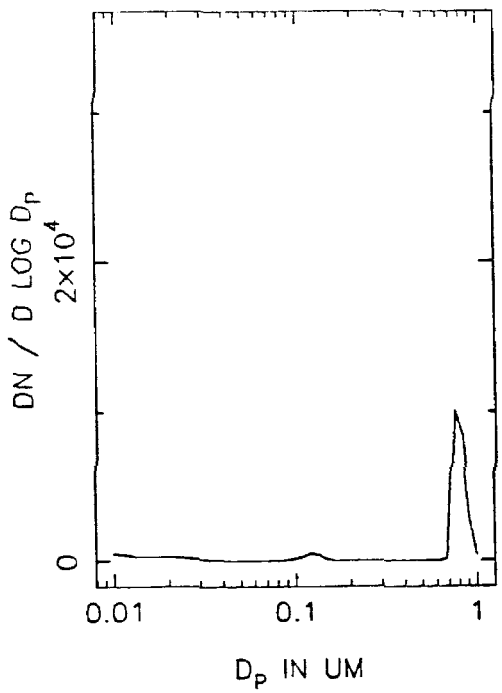

T=3.5 HOURS

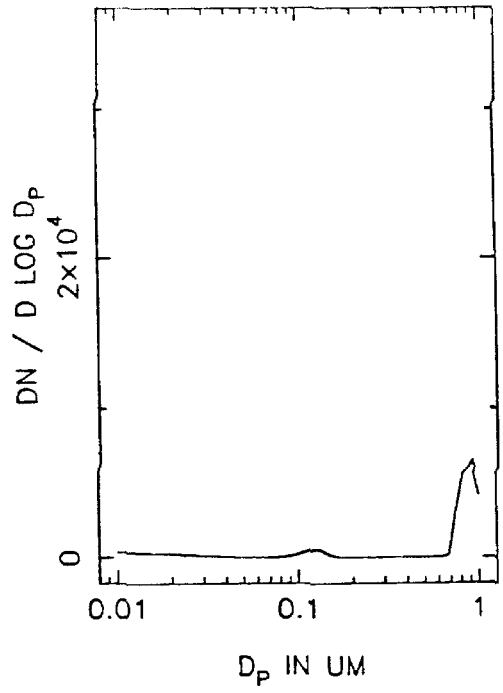

XB12A NUMBER DISTRIBUTION, T=4.0

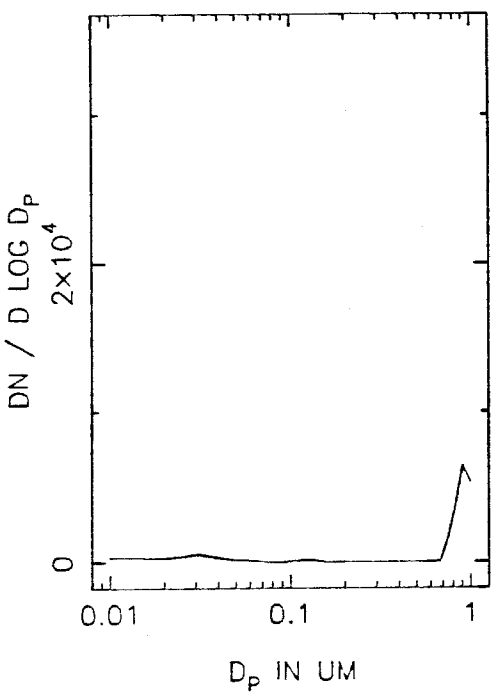

XB12A VOLUME DISTRIBUTION, T=0

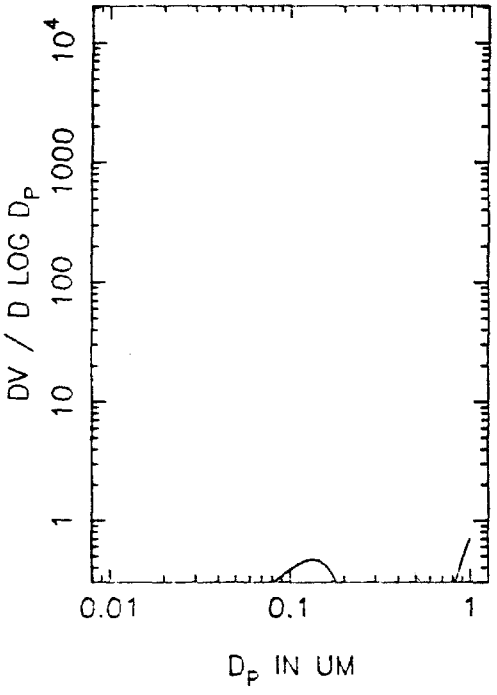

T=0.5 HOURS

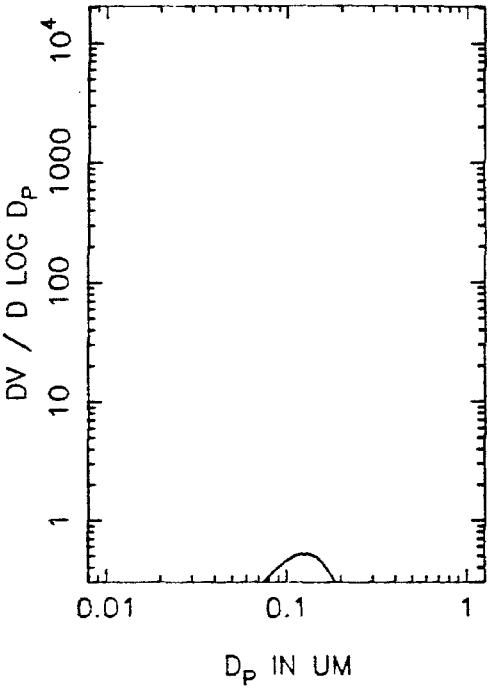

T=1.0 HOURS

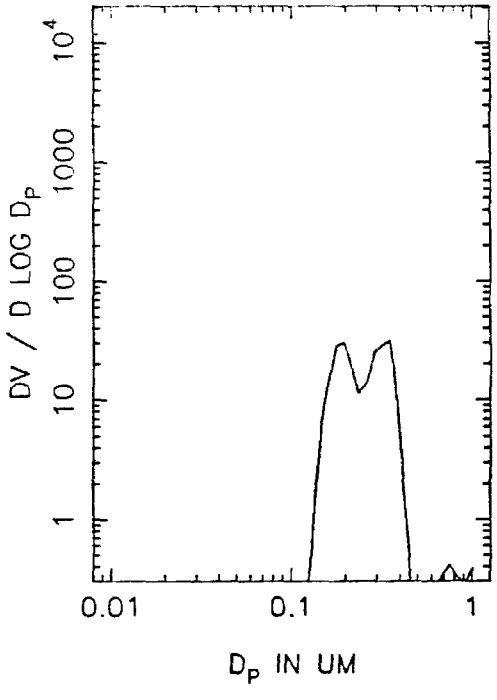

T=1.5 HOURS

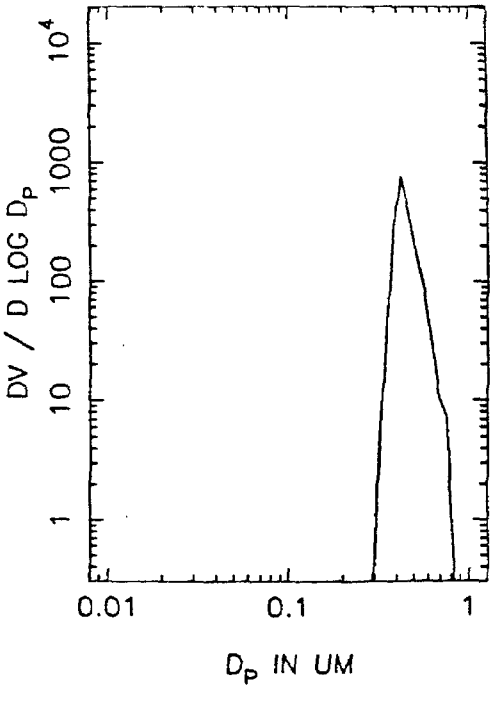

XB12A VOLUME DISTRIBUTION, T=2.0

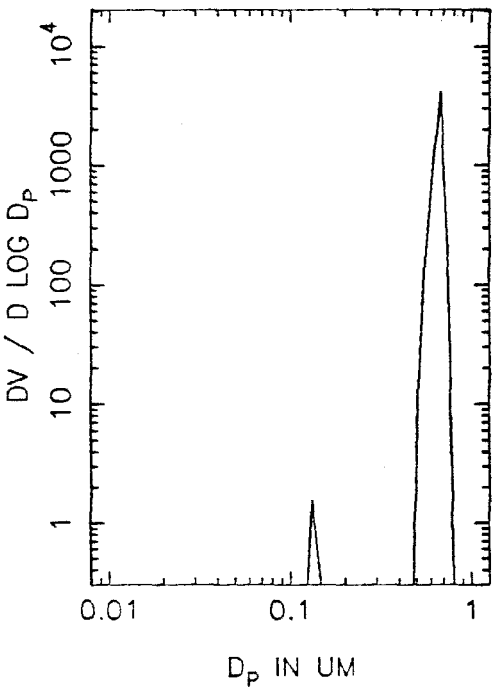

T=2.5 HOURS

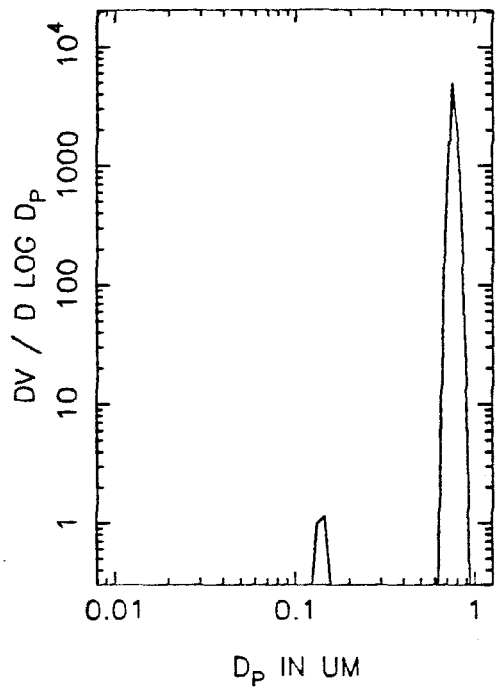

T=3.0 HOURS

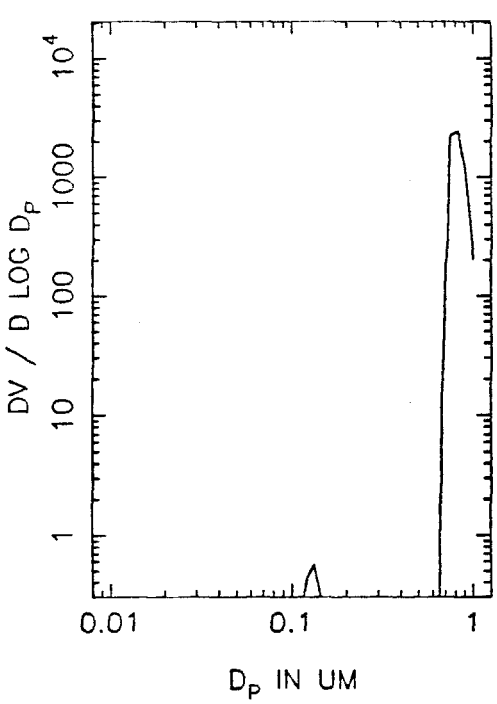

T=3.5 HOURS

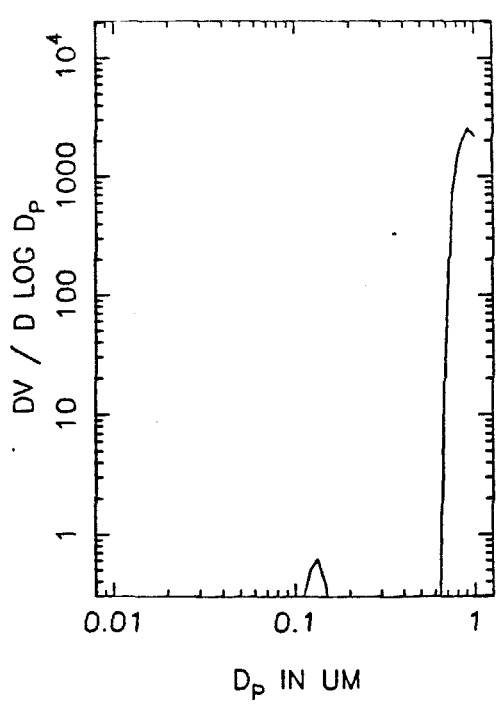

XB12A VOLUME DISTRIBUTION, T=4.0

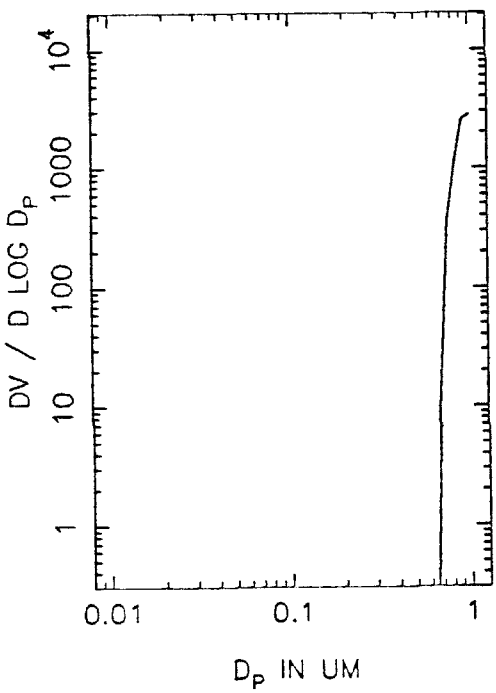

XB12B NUMBER DISTRIBUTION, T=0

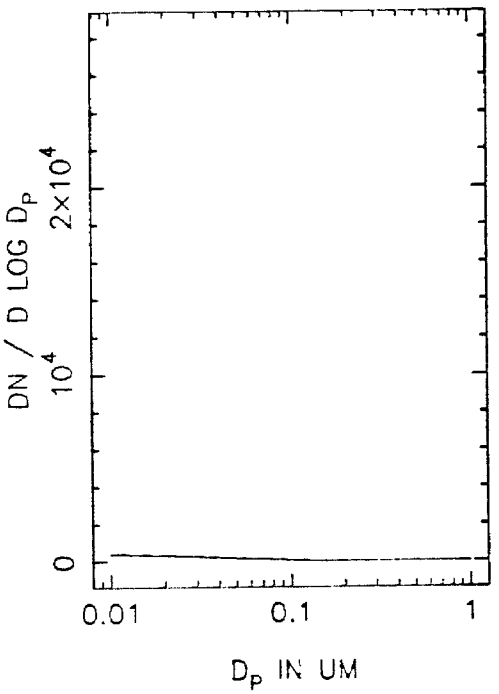

T=0.5 HOURS

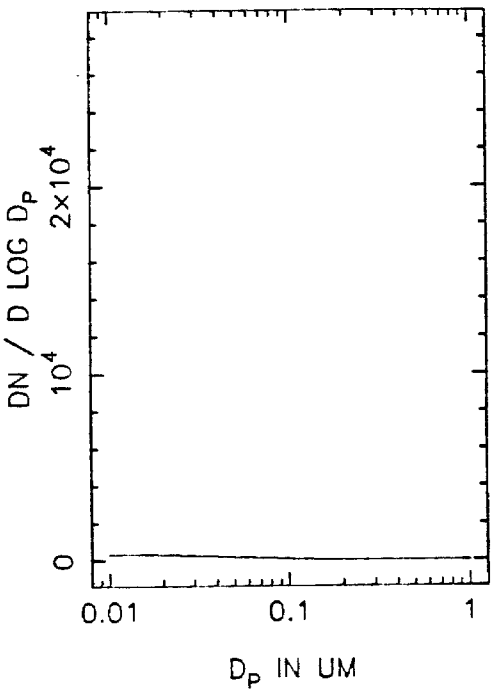

T=1.0 HOURS

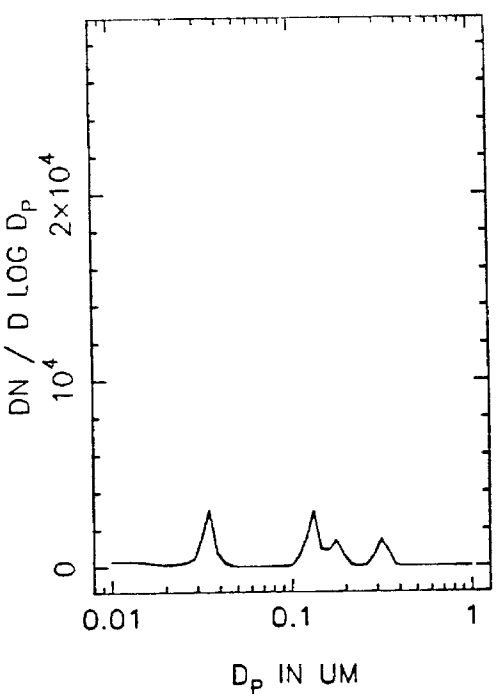

T=1.5 HOURS

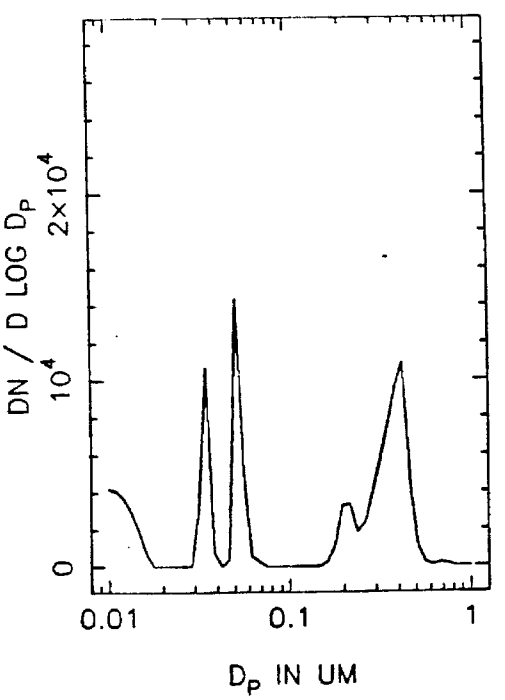

XB12B NUMBER DISTRIBUTION, T=2.0

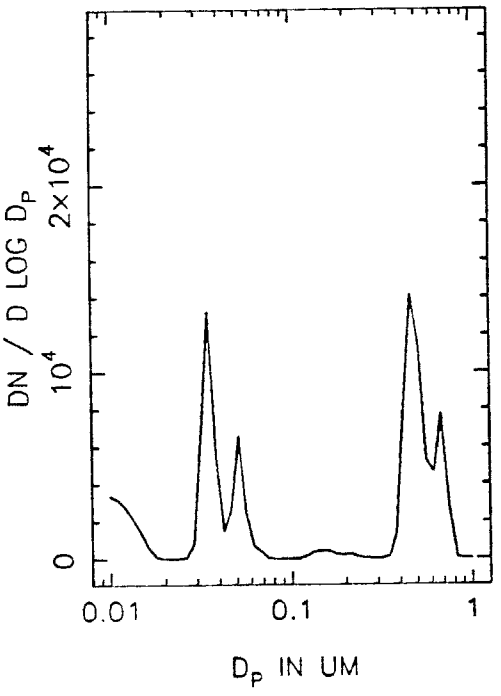

T=2.5 HOURS

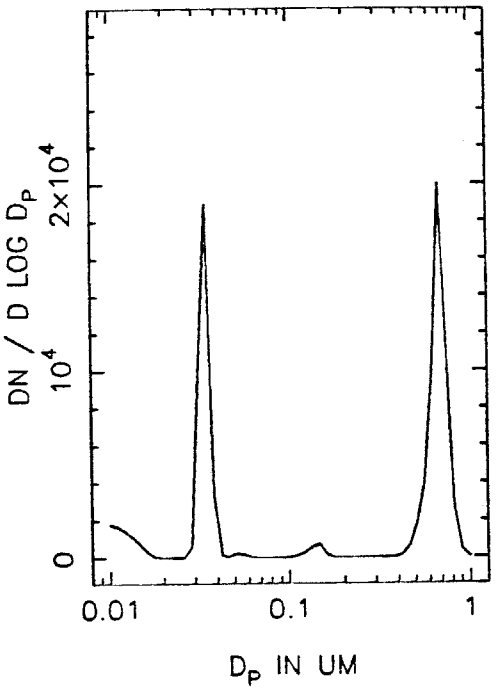

T=3.0 HOURS

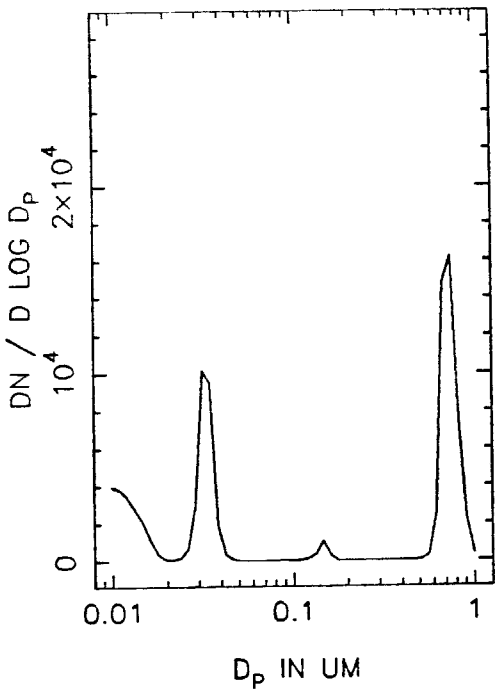

T=3.5 HOURS

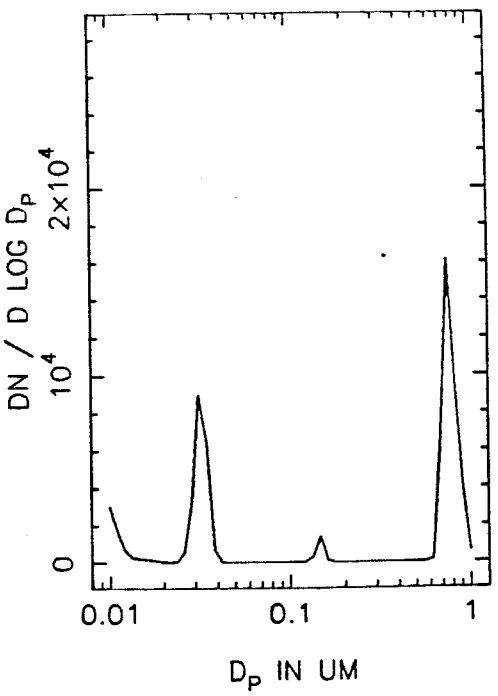

XB12B VOLUME DISTRIBUTION, T=0

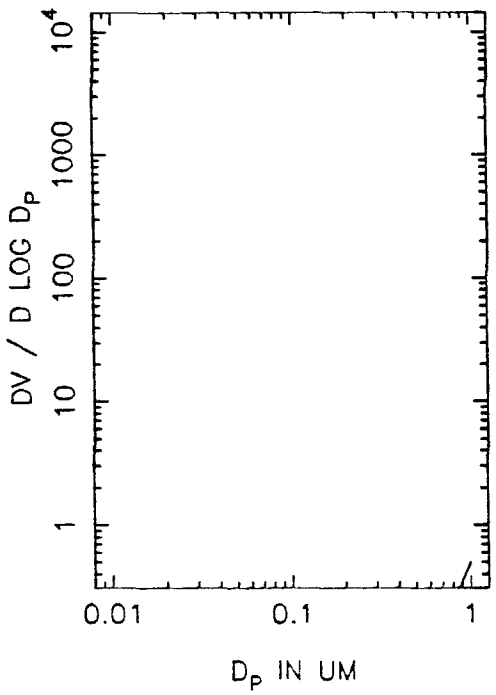

T=0.5 HOURS

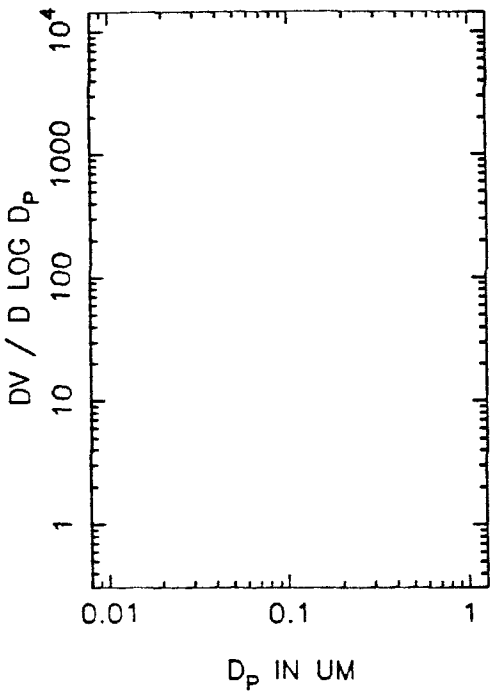

T=1.0 HOURS

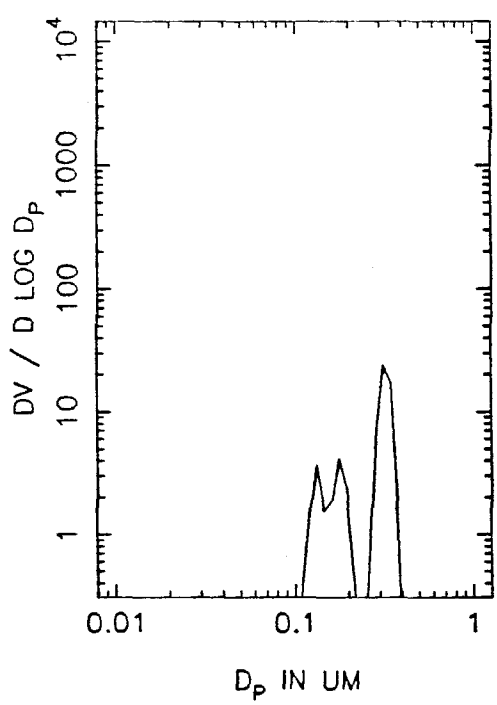

T=1.5 HOURS

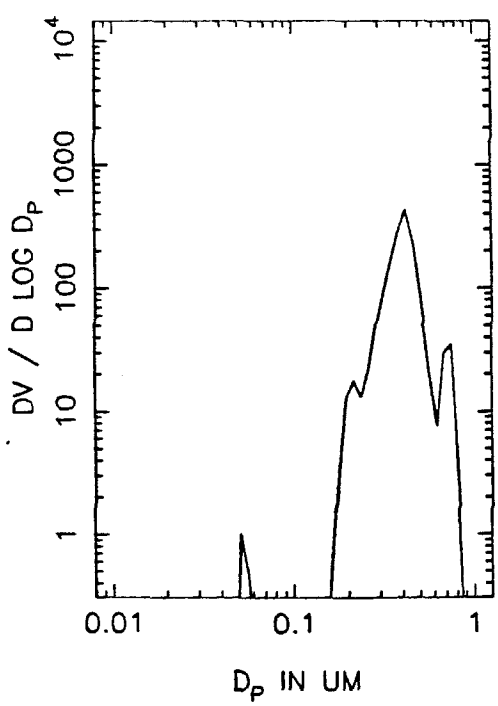

XB12B VOLUME DISTRIBUTION, T=2.0

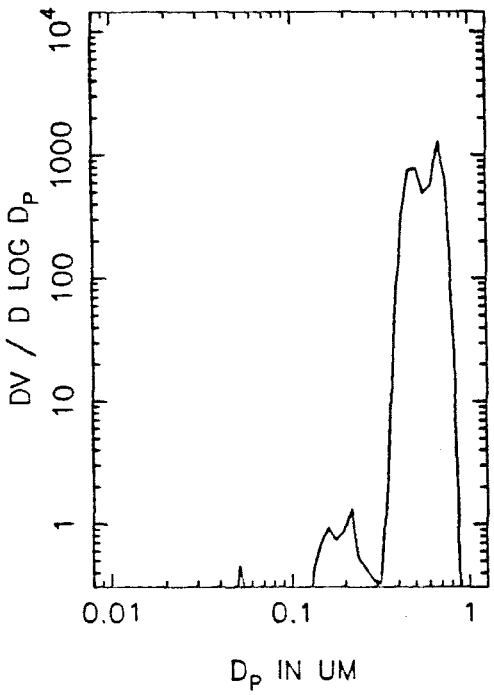

T=2.5 HOURS

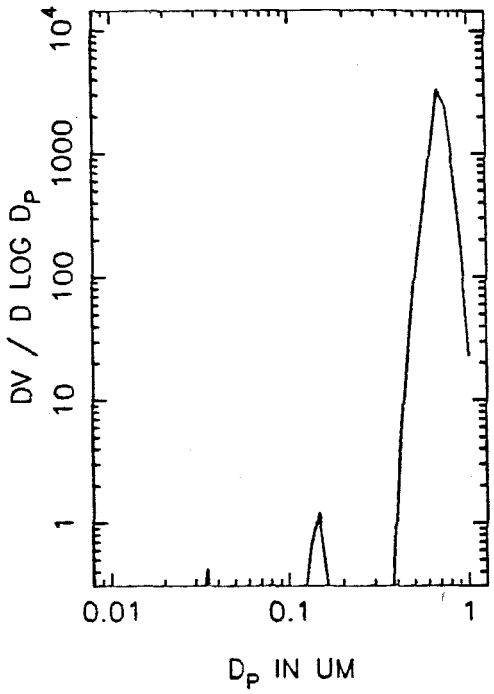

T=3.0 HOURS

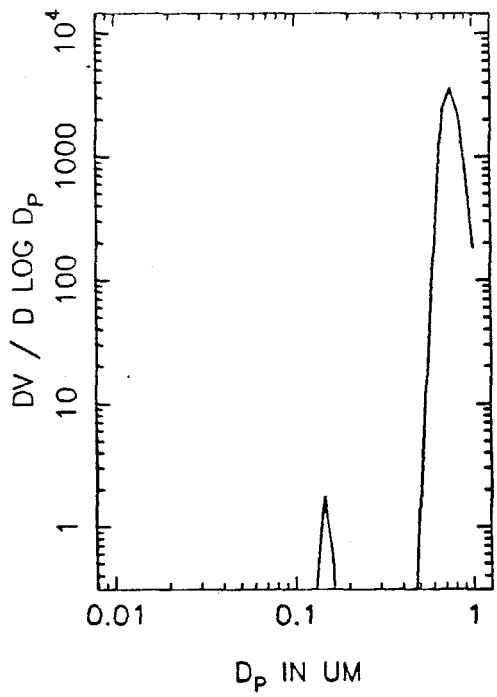

T=3.5 HOURS

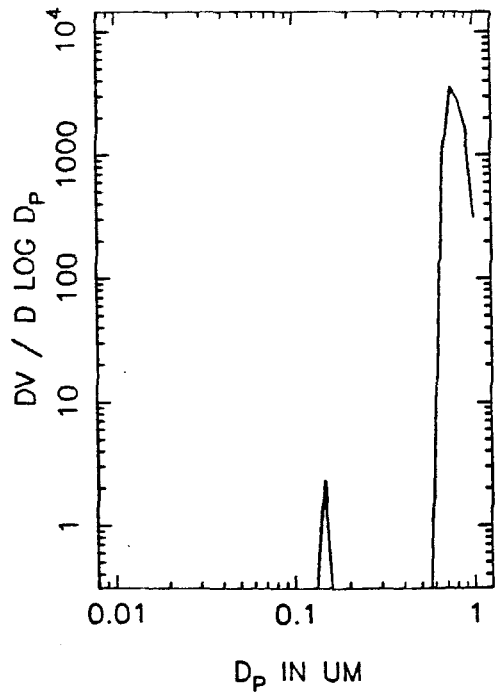

XG15 TOTAL NUMBER, SIDE A

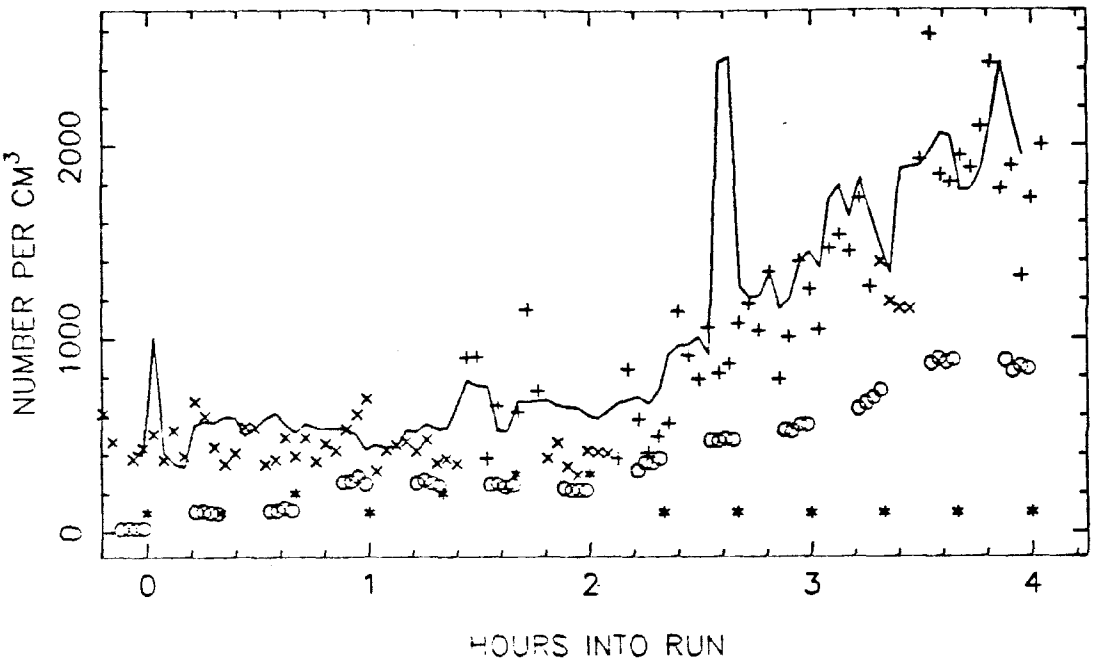

SIDE B

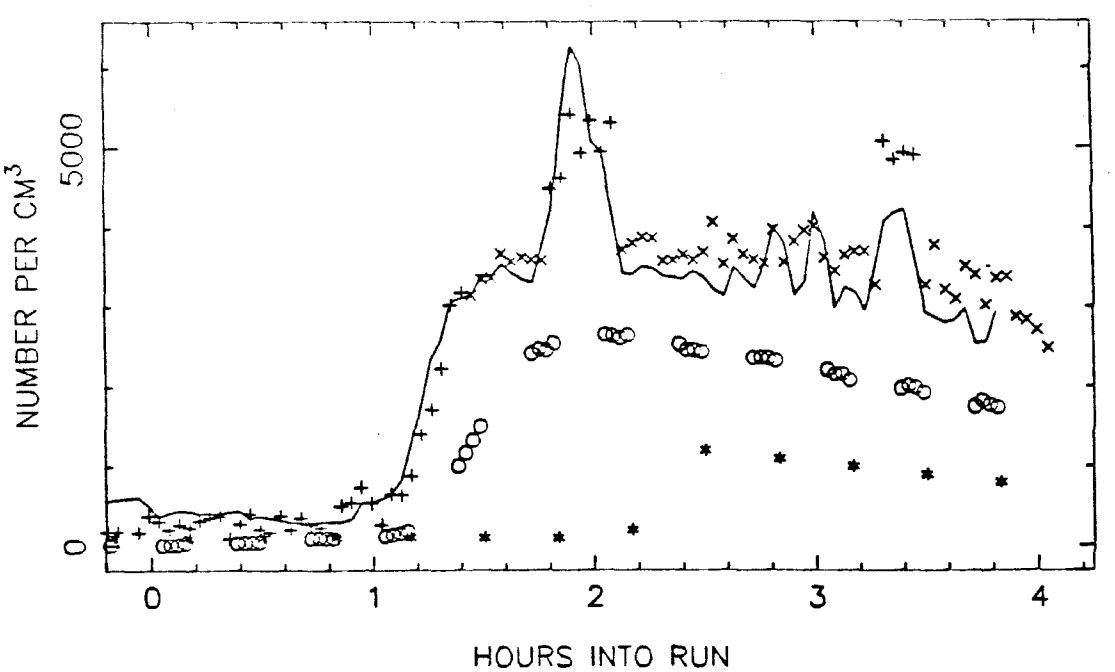

XG15 VOLUME IN THE AEROSOL PHASE, SIDE A

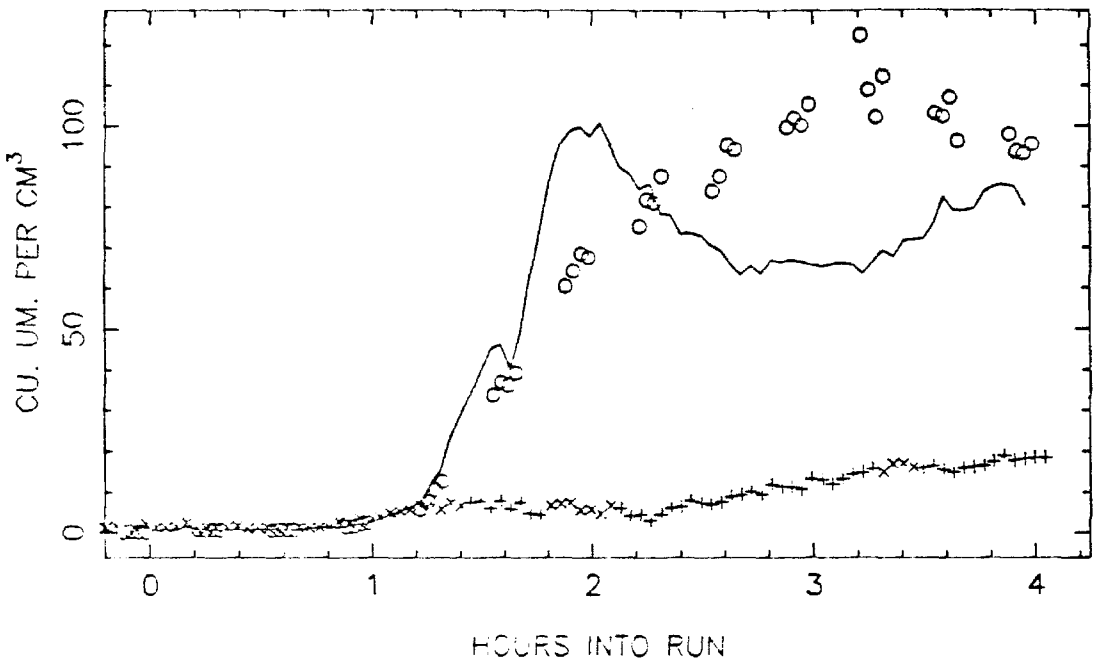

SIDE B

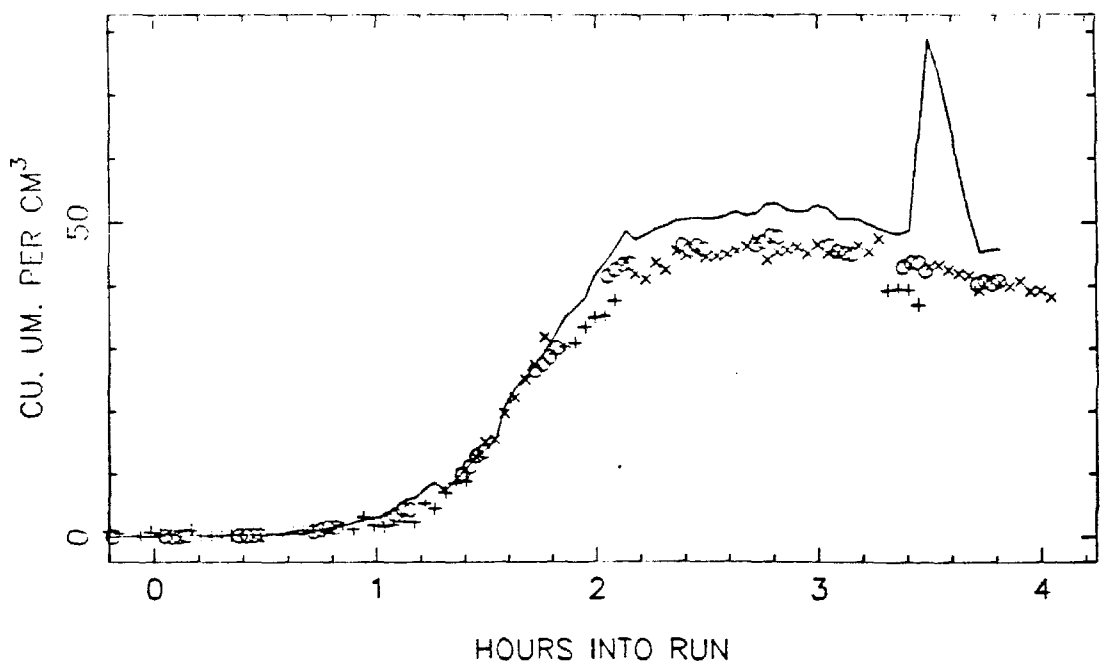

XG15 MEAN PARTICLE SIZE, SIDE A

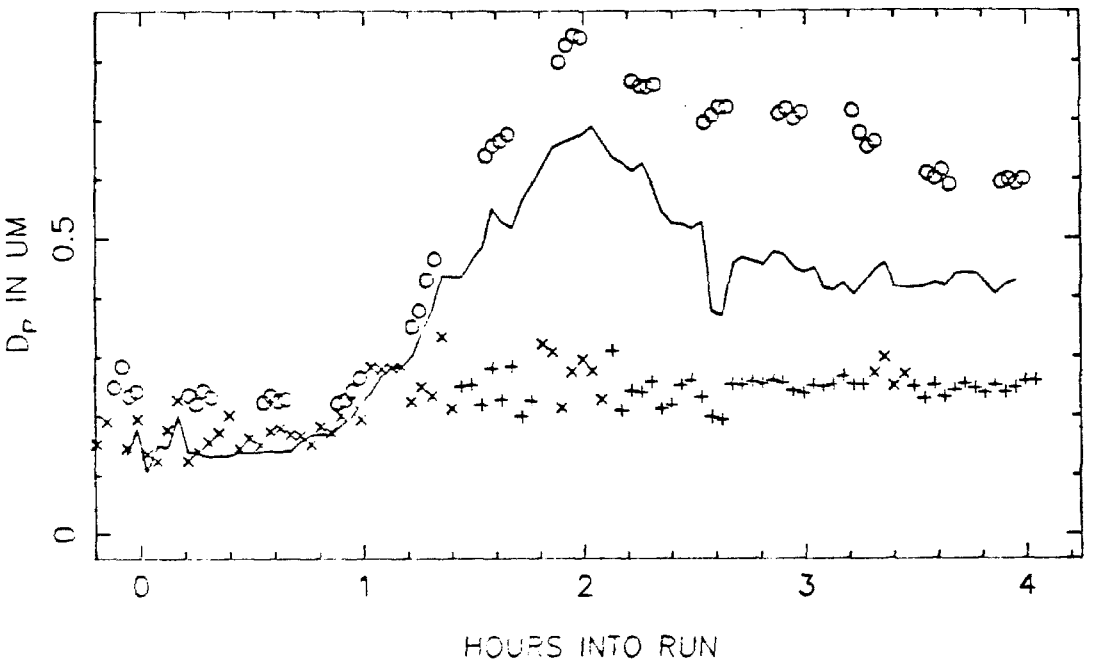

SIDE B

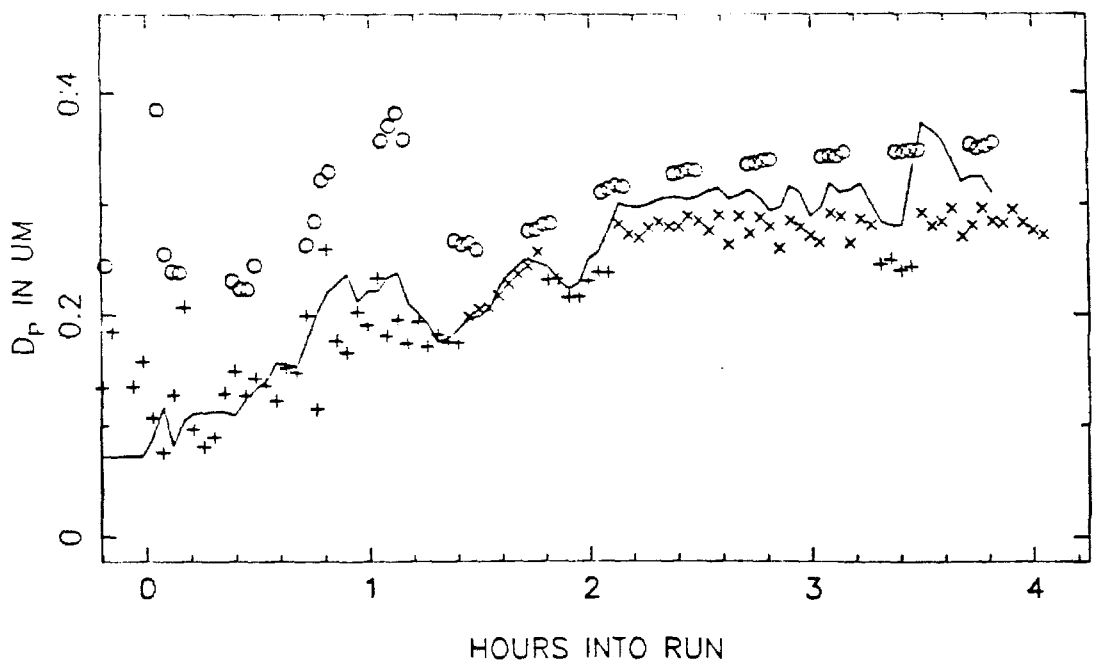

XG15A NUMBER DISTRIBUTION, T=0

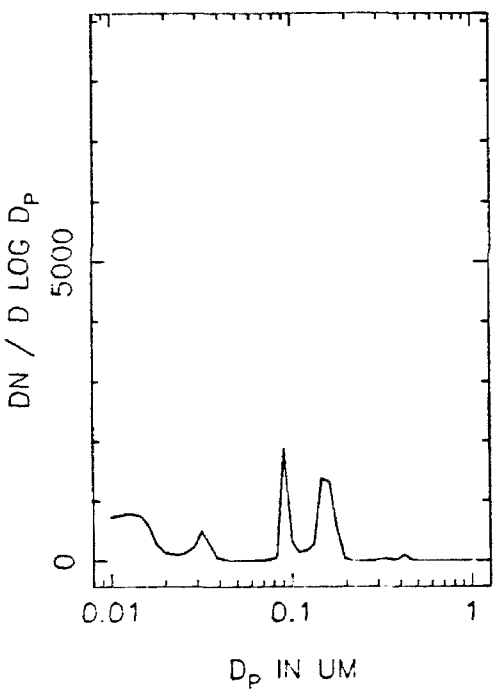

T=0.5 HOURS

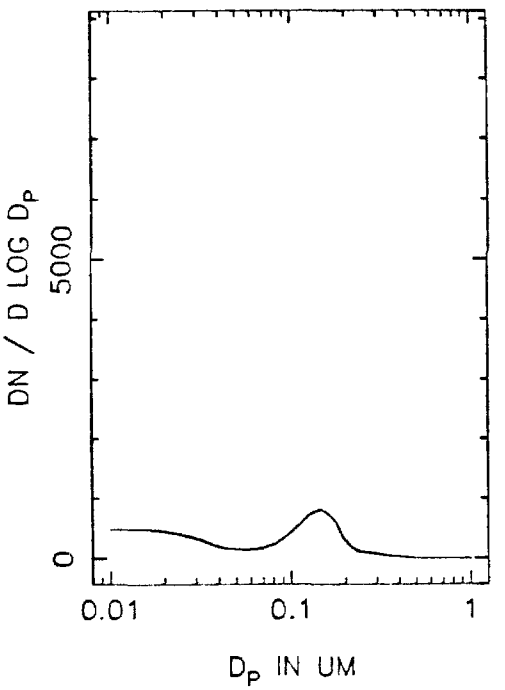

T=1.0 HOURS

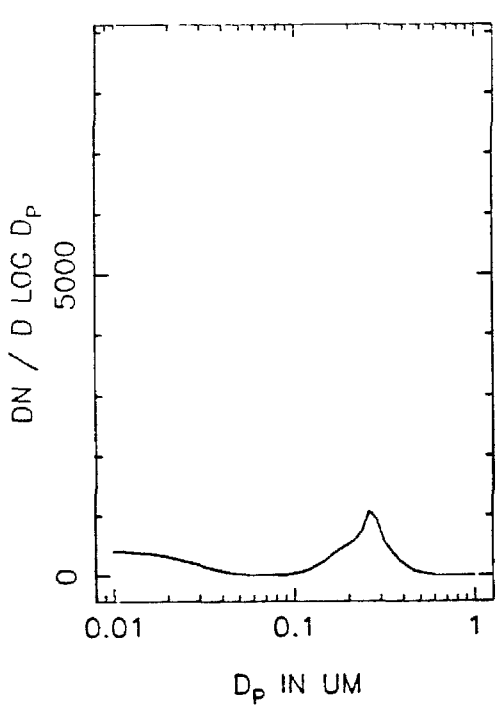

T=1.5 HOURS

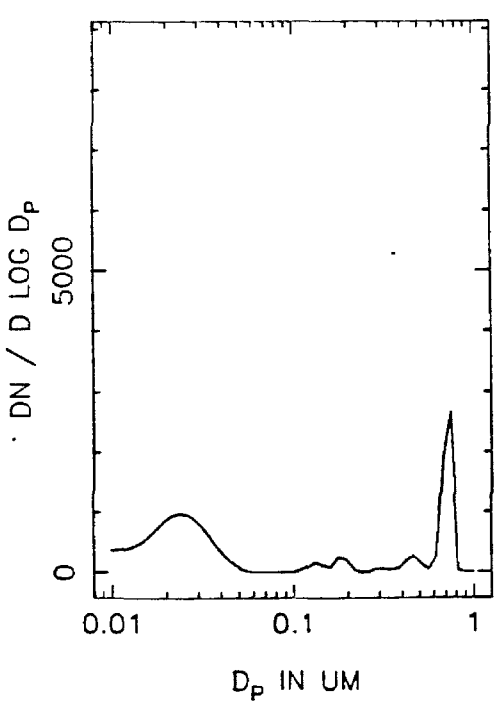

XG15A NUMBER DISTRIBUTION, T=2.0

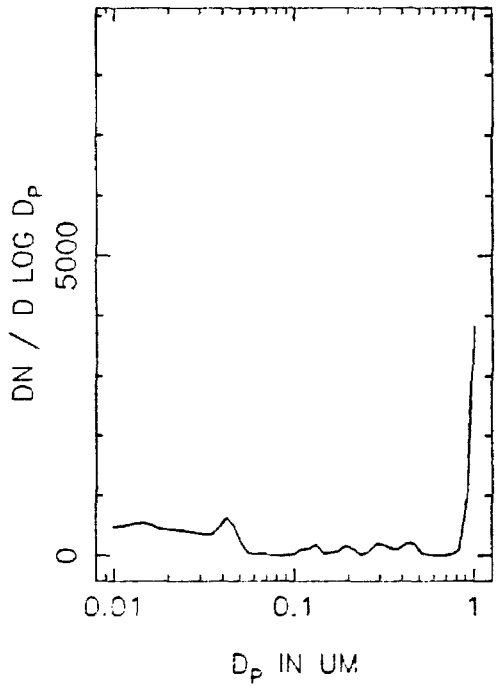

T=2.5 HOURS

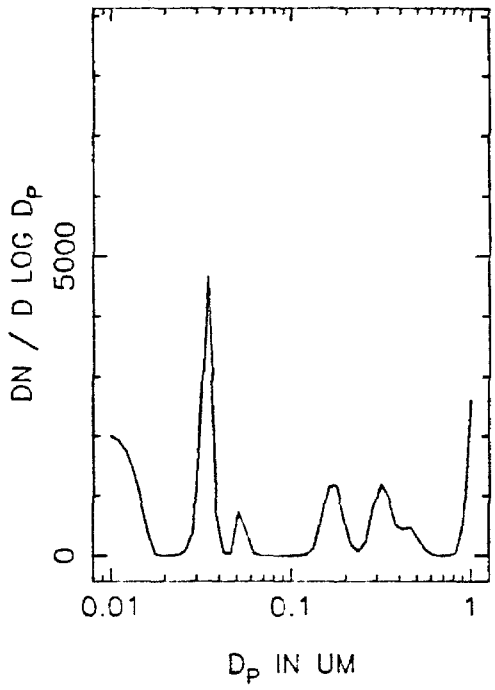

T=3.0 HOURS

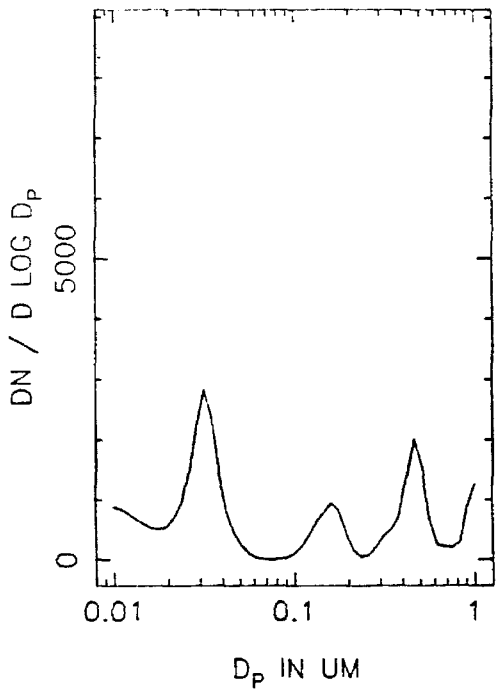

T=3.5 HOURS

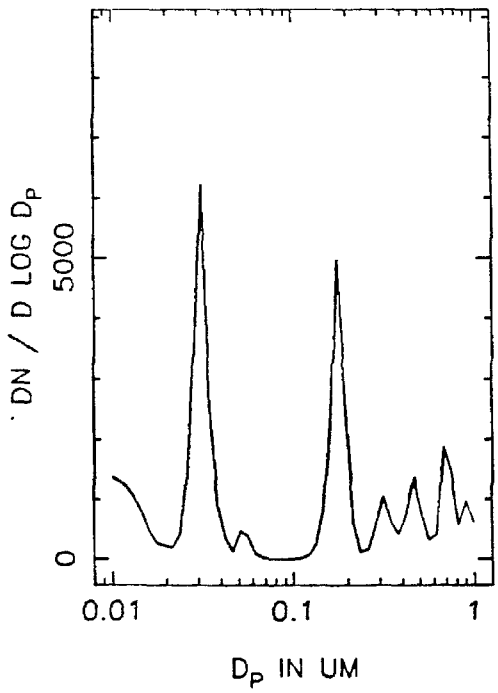

XG15A NUMBER DISTRIBUTION, T=4.0

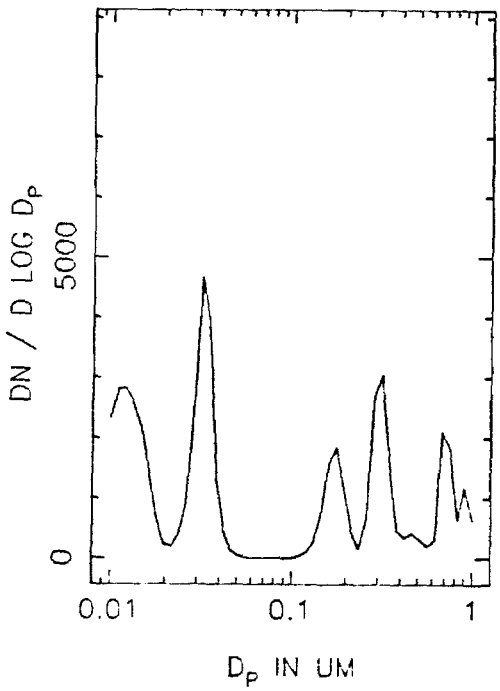

XG15A VOLUME DISTRIBUTION, T=0

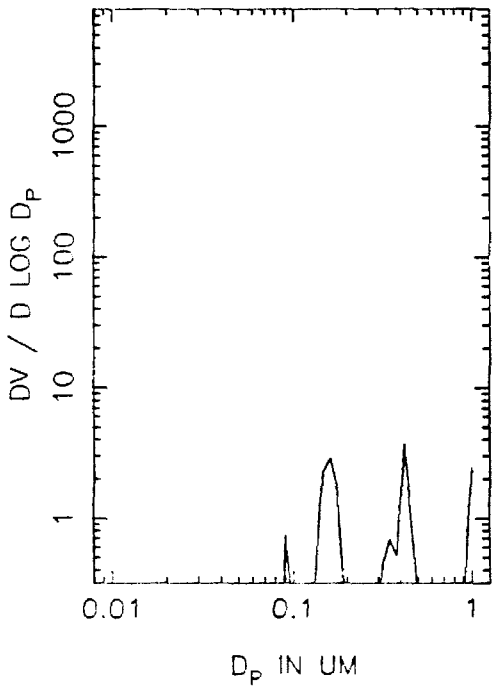

T=0.5 HOURS

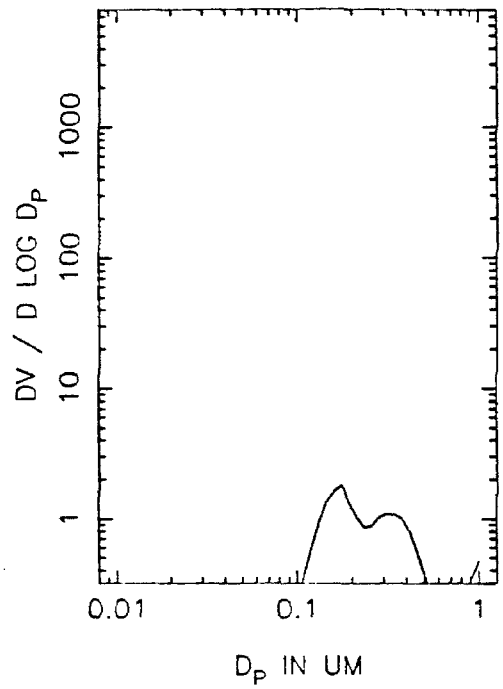

T=1.0 HOURS

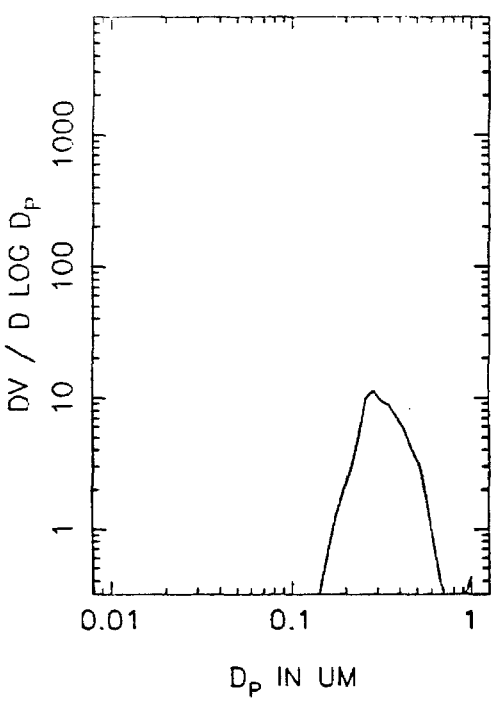

T=1.5 HOURS

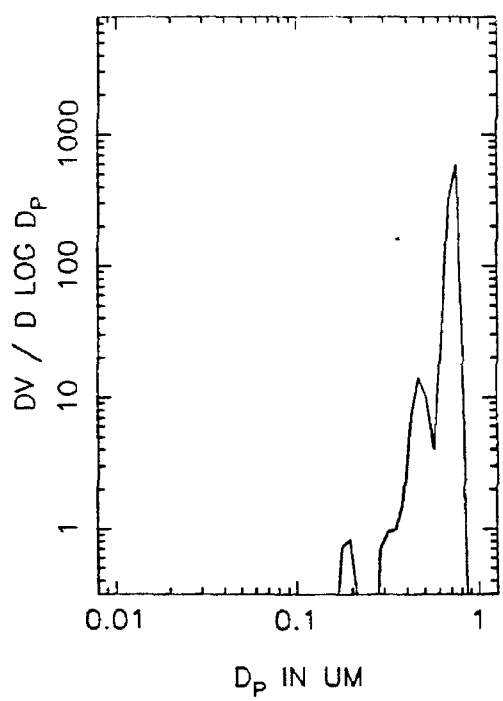

XG15A VOLUME DISTRIBUTION, T=2.0

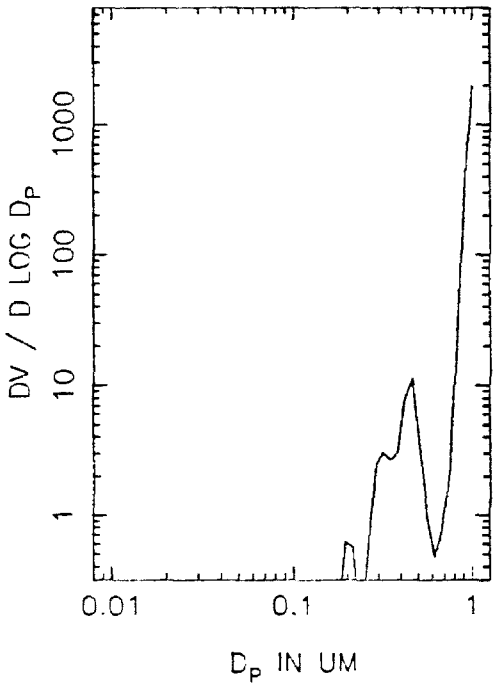

T=2.5 HOURS

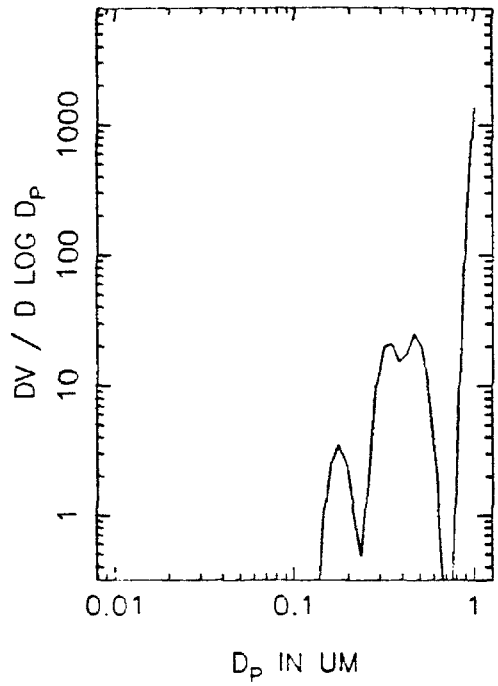

T=3.0 HOURS

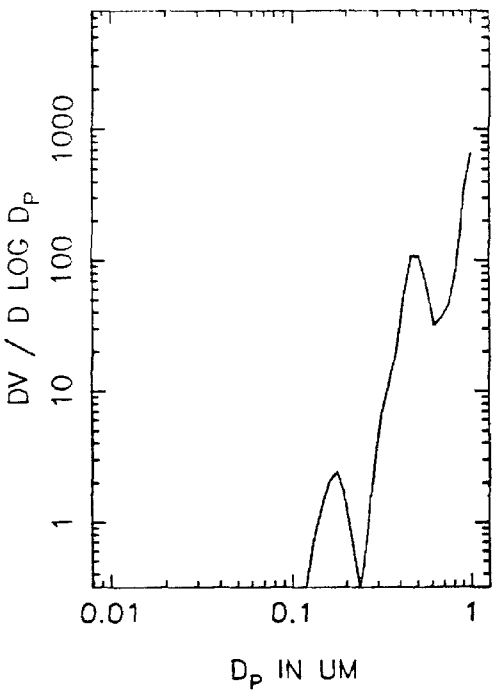

T=3.5 HOURS

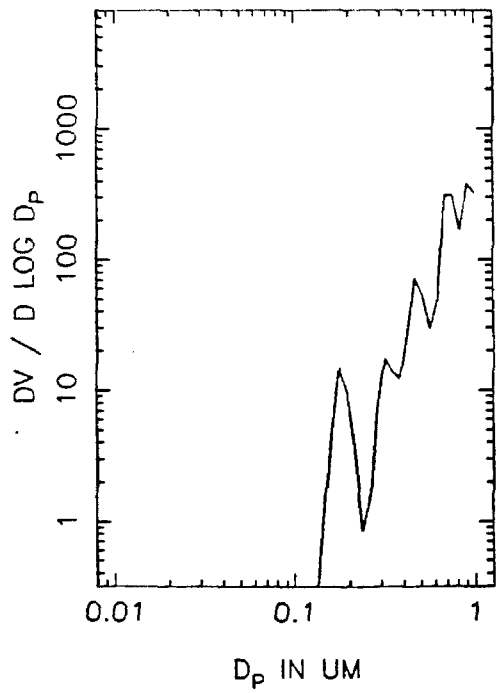

XG15A VOLUME DISTRIBUTION, T=4.0

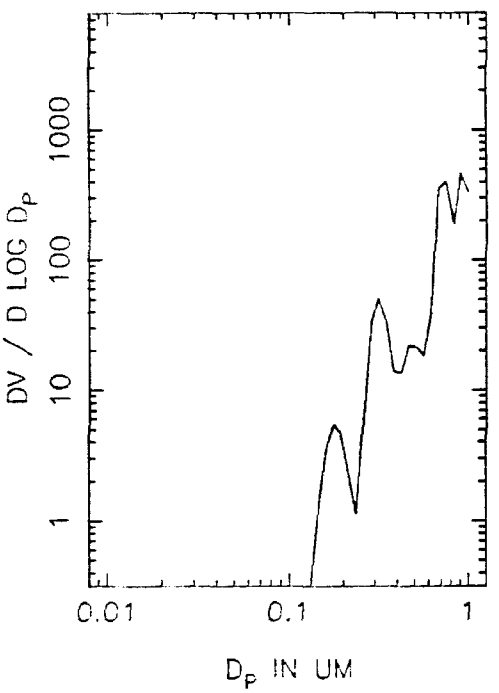

XG15B NUMBER DISTRIBUTION, T=0

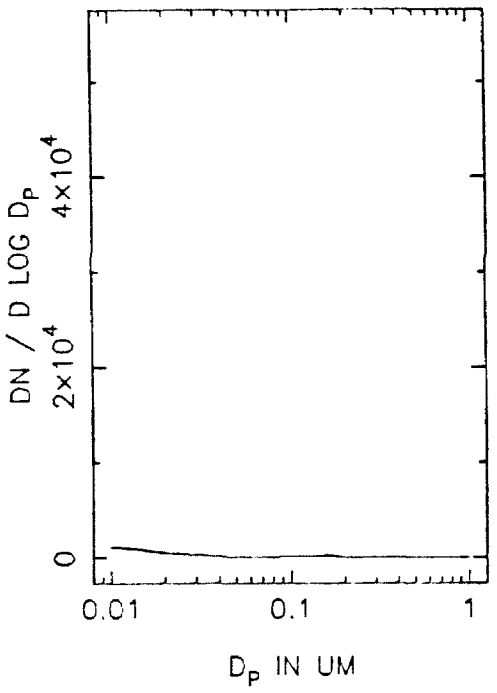

T=0.5 HOURS

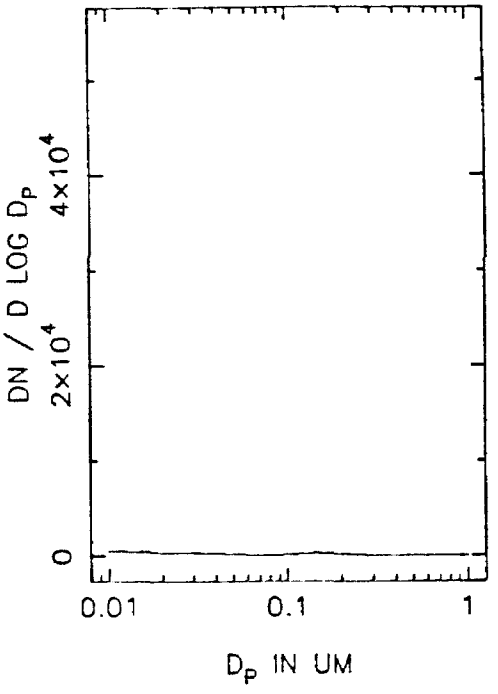

T=1.0 HOURS

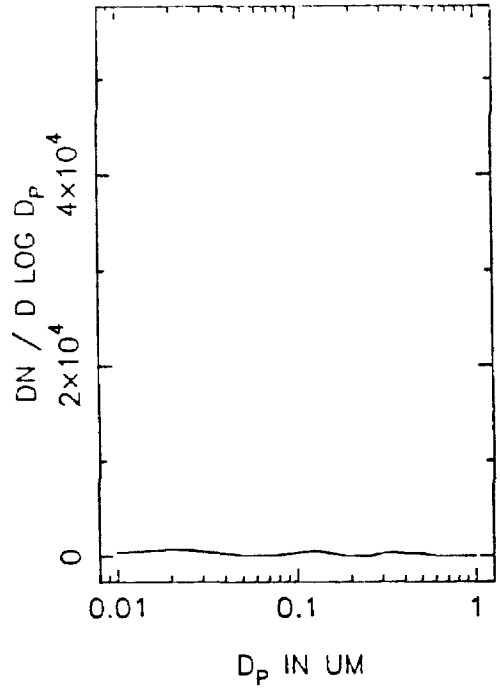

T=1.5 HOURS

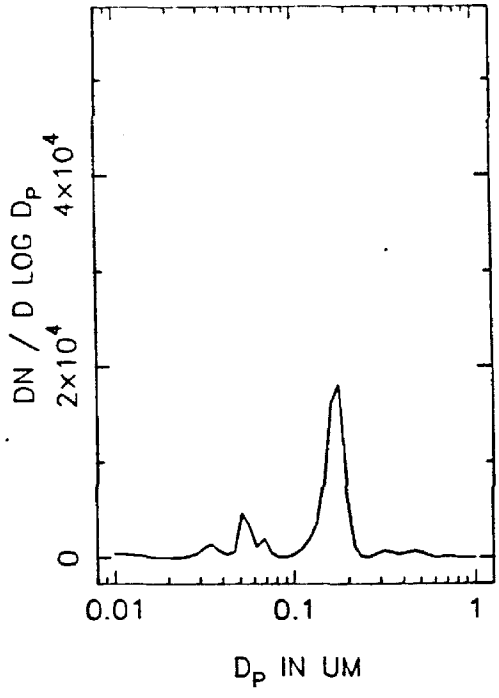

XG15B NUMBER DISTRIBUTION, T=2.0

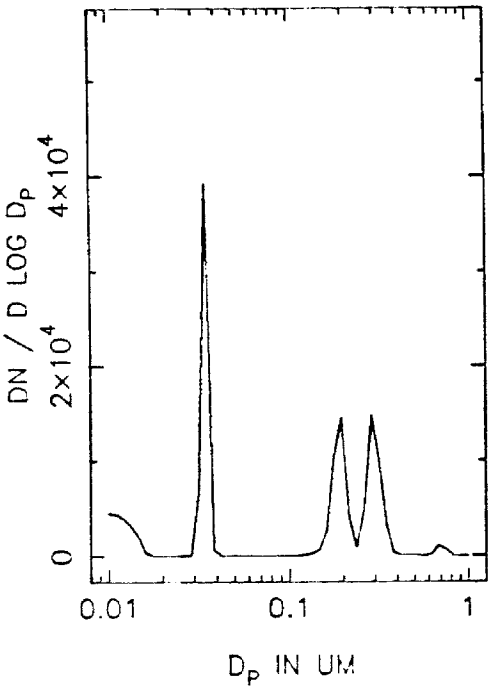

T=2.5 HOURS

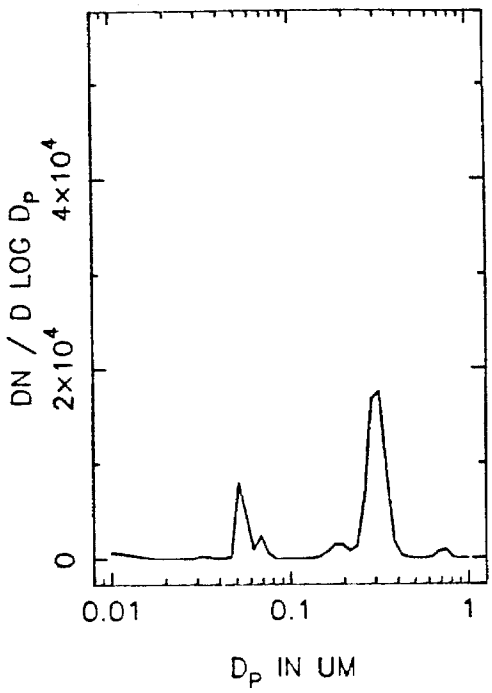

T=3.0 HOURS

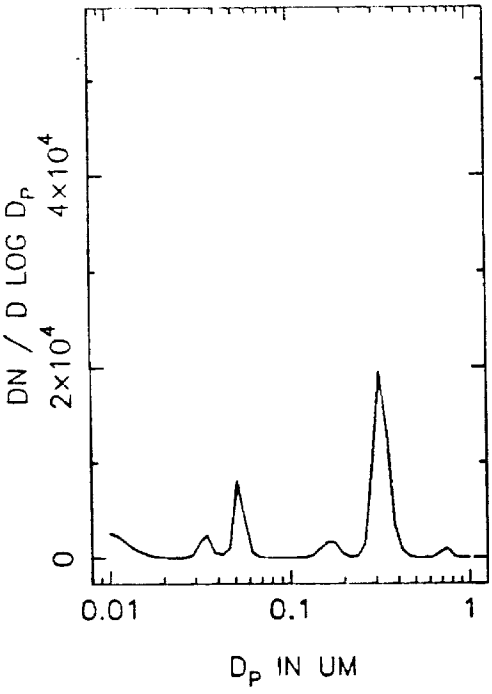

T=3.5 HOURS

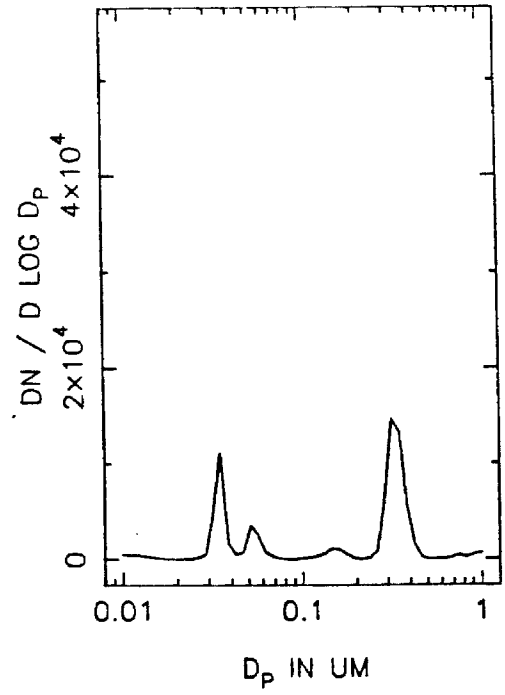

XG15B VOLUME DISTRIBUTION, T=0

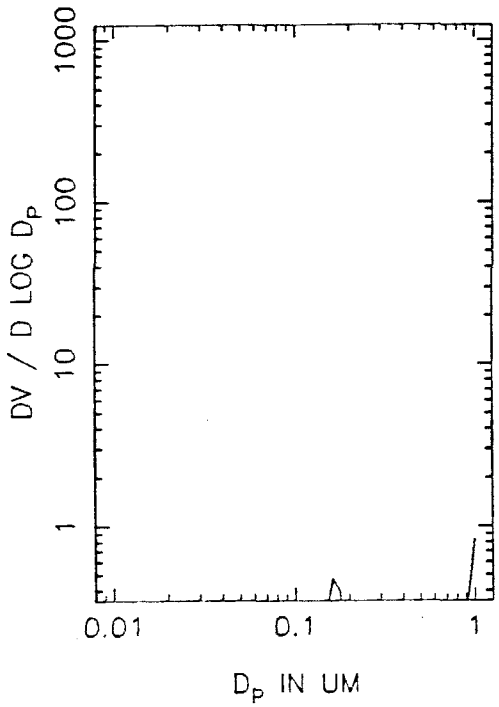

T=0.5 HOURS

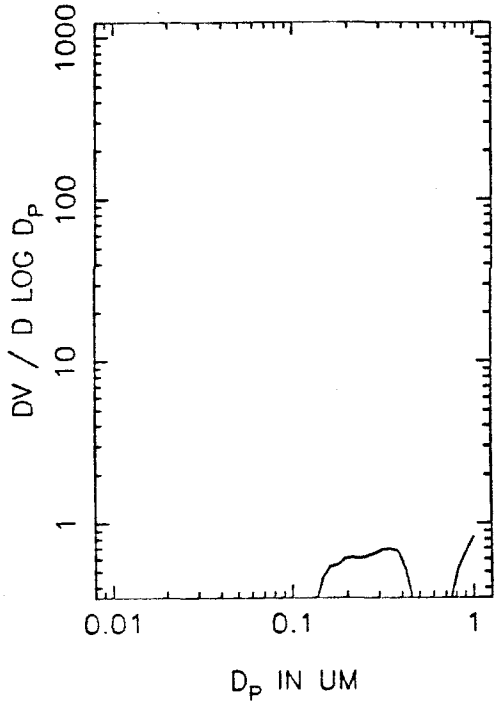

T=1.0 HOURS

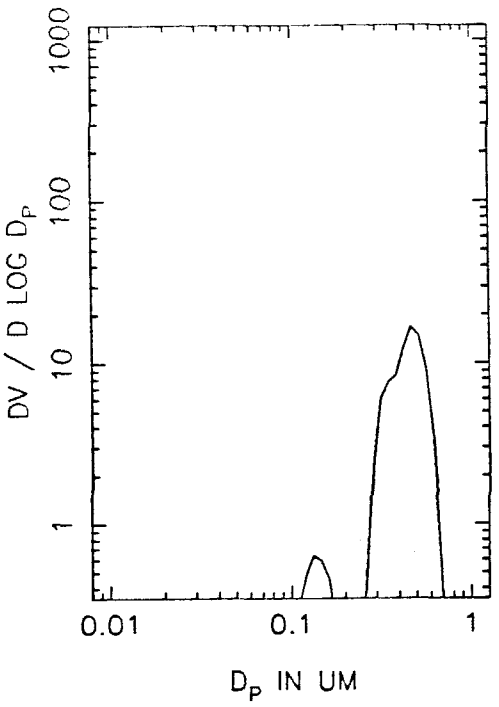

T=1.5 HOURS

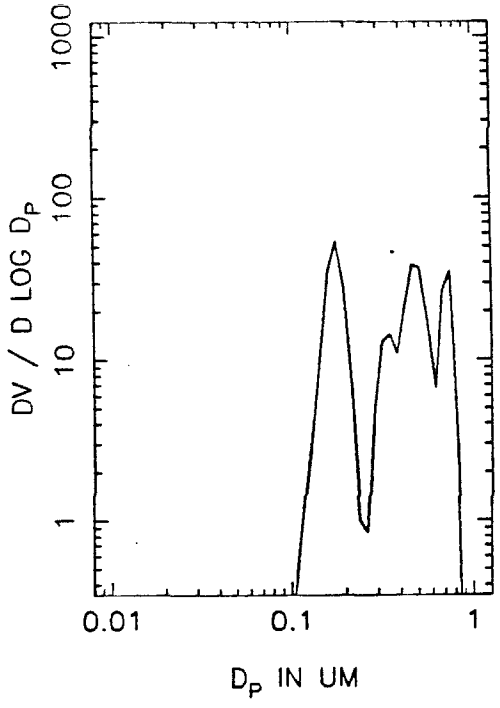

XG15B VOLUME DISTRIBUTION, T=2.0

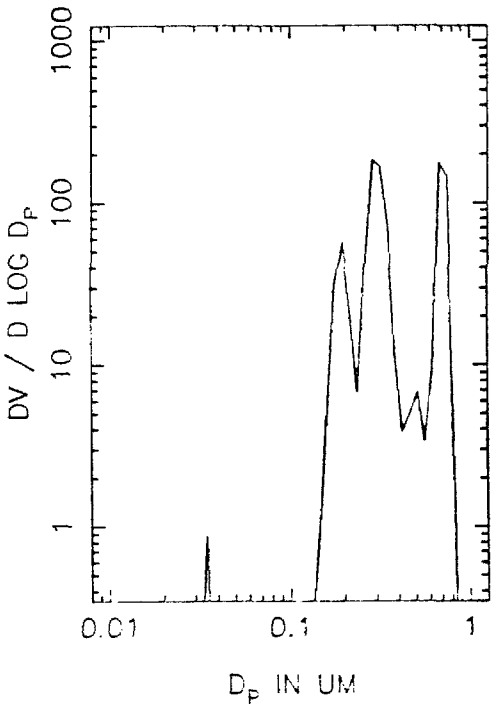

T=2.5 HOURS

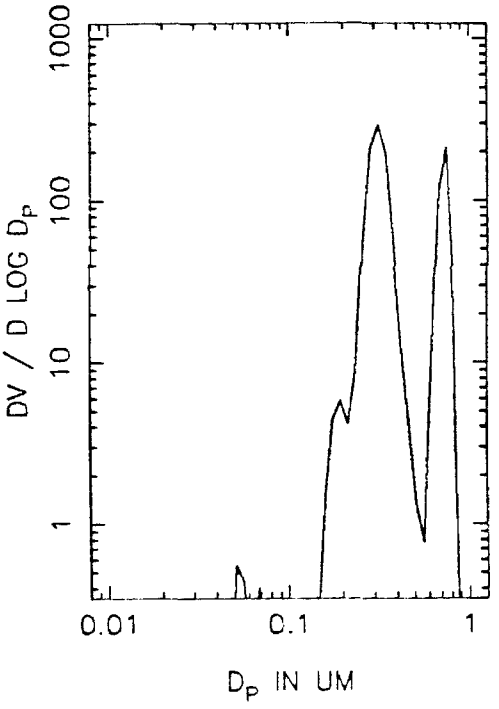

T=3.0 HOURS

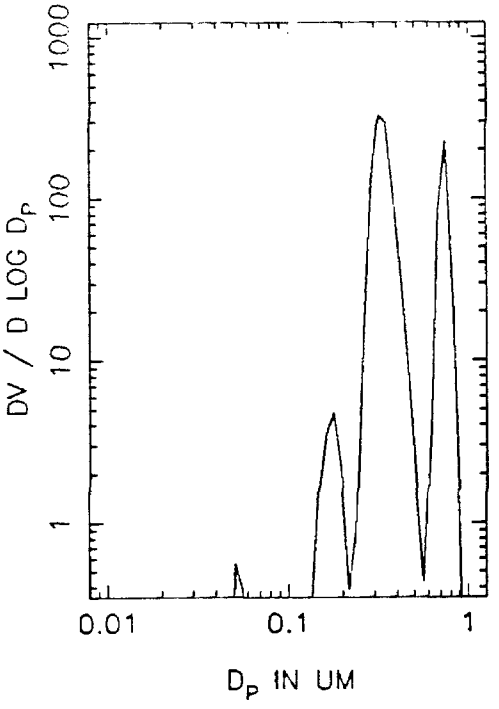

T=3.5 HOURS

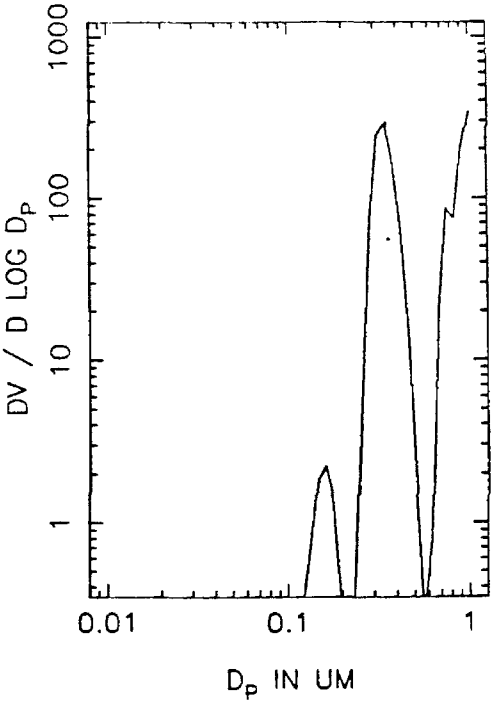

XK17 TOTAL NUMBER, SIDE A

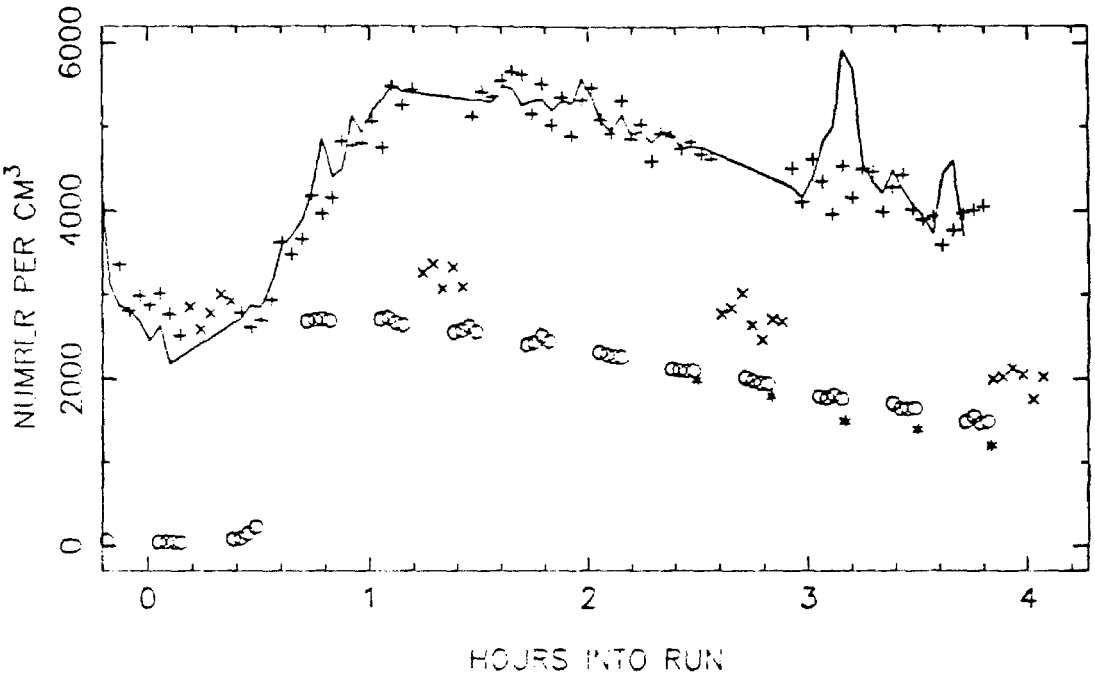

SIDE B

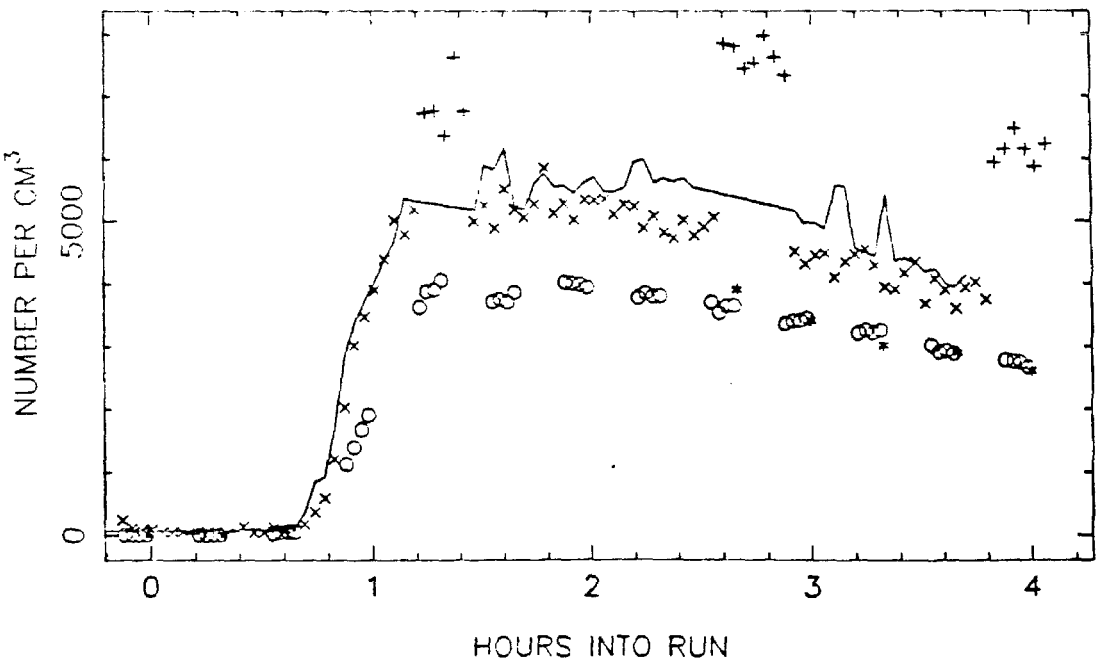

XK17 VOLUME IN THE AEROSOL PHASE, SIDE A

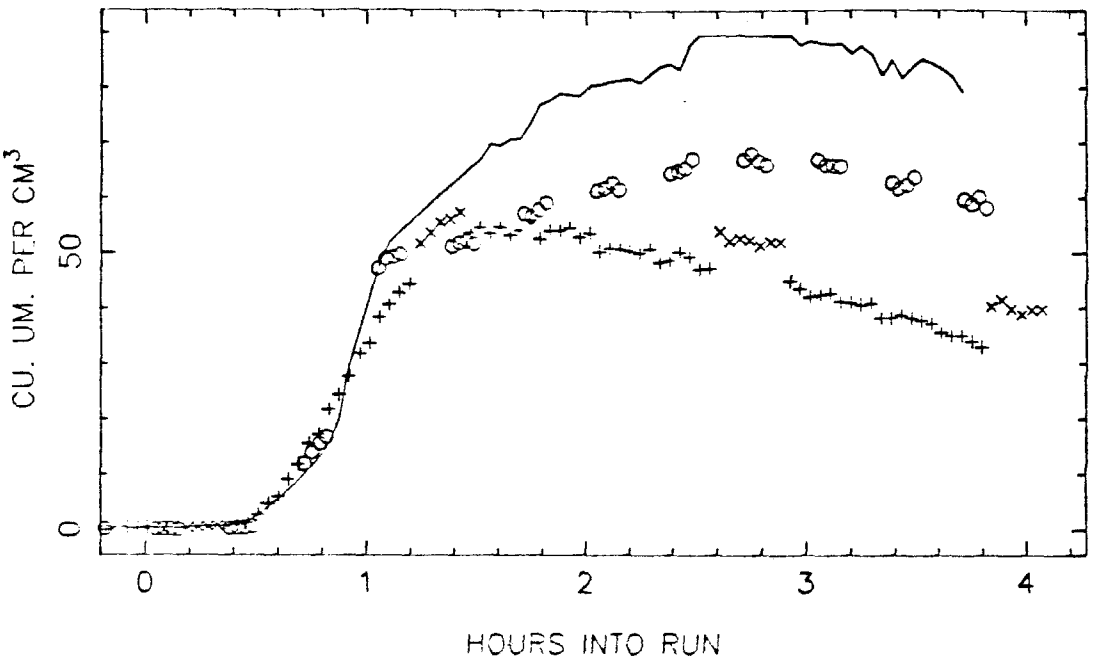

SIDE B

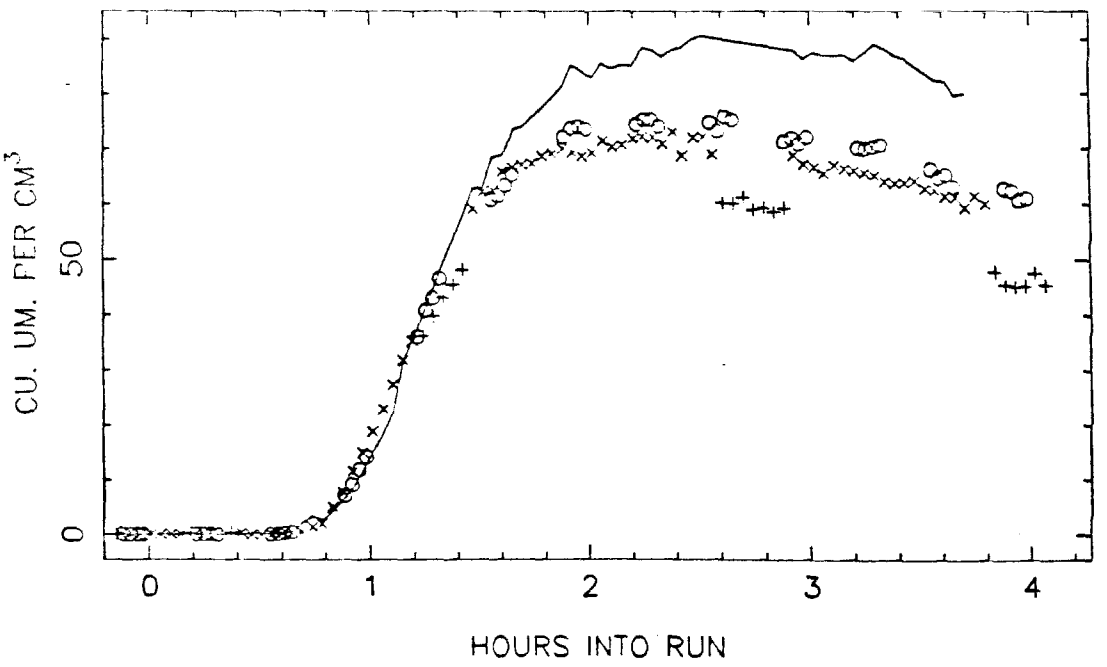

XK17 MEAN PARTICLE SIZE, SIDE A

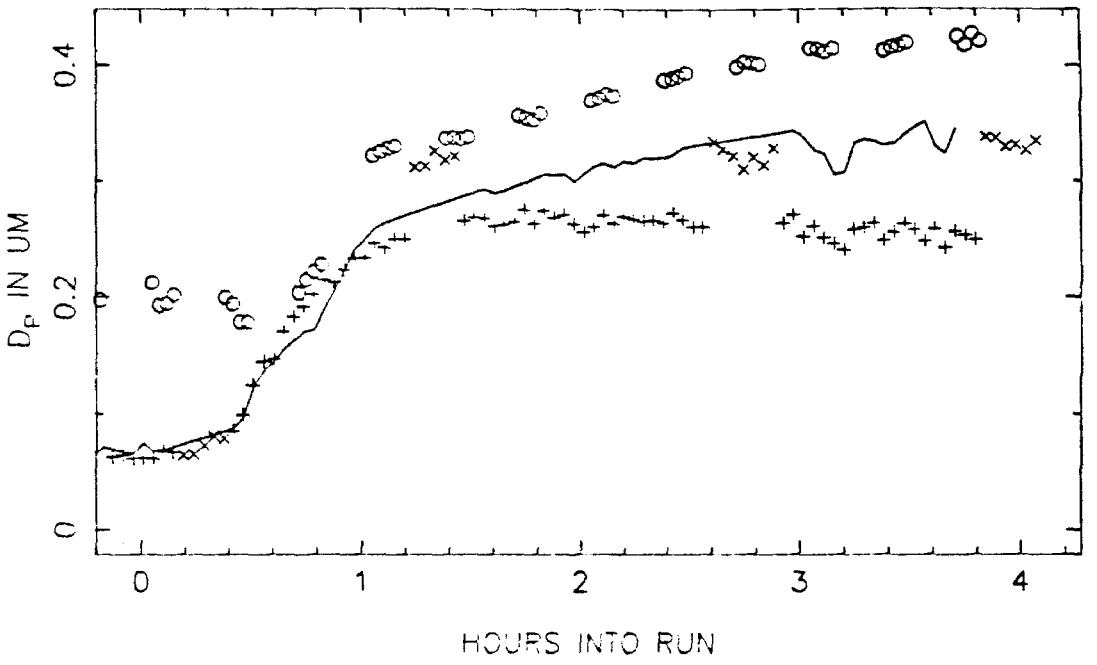

SIDE B

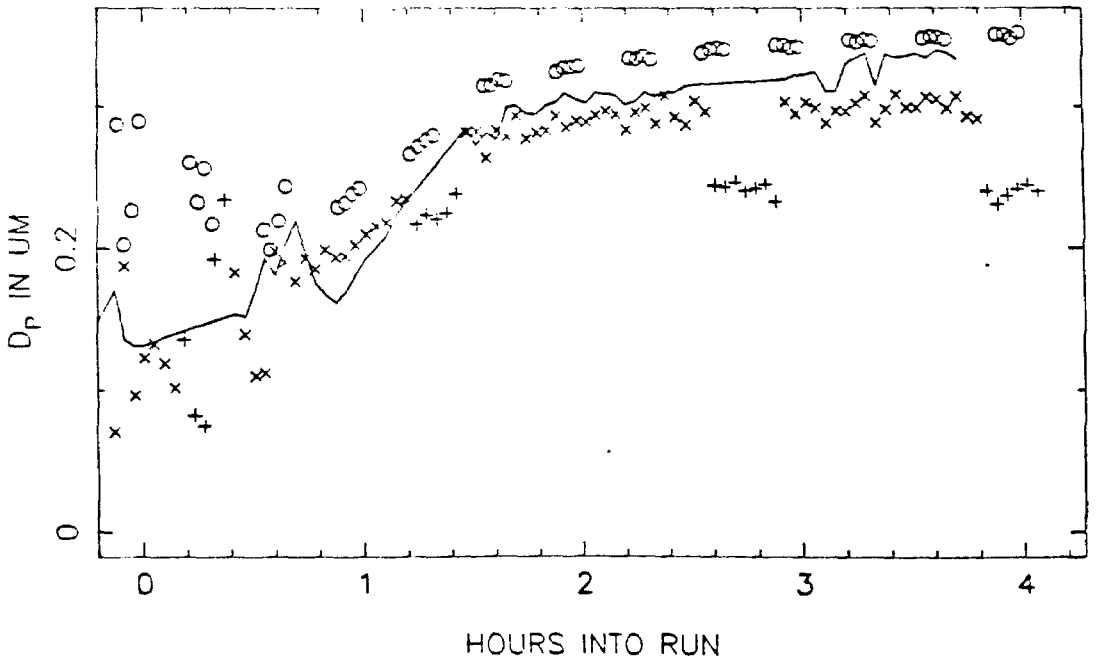

XK17A NUMBER DISTRIBUTION, T=0

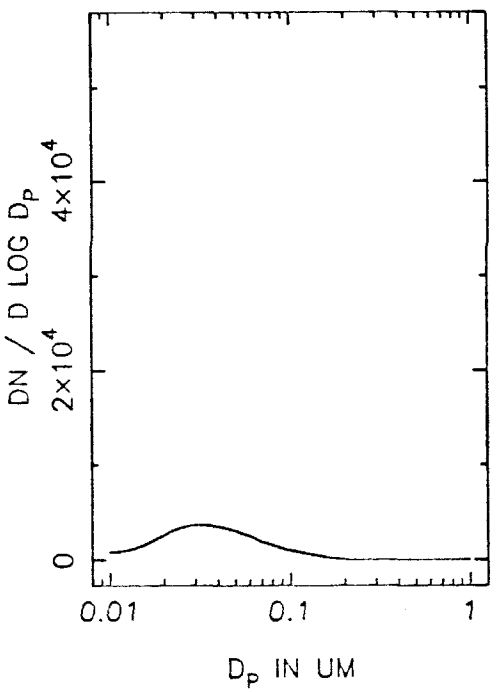

T=0.5 HOURS

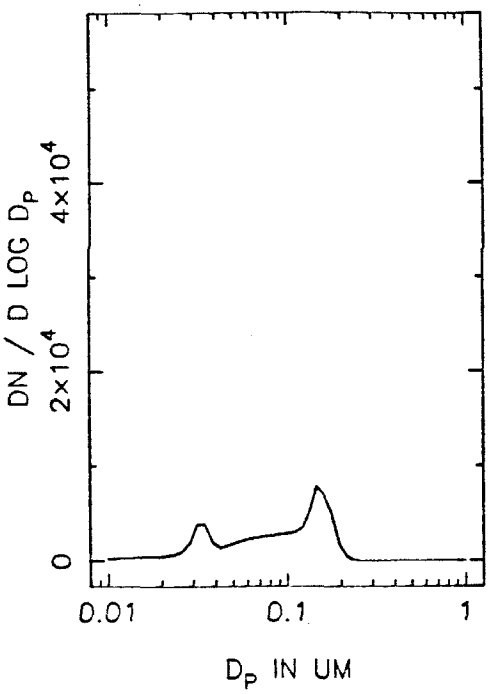

T=1.0 HOURS

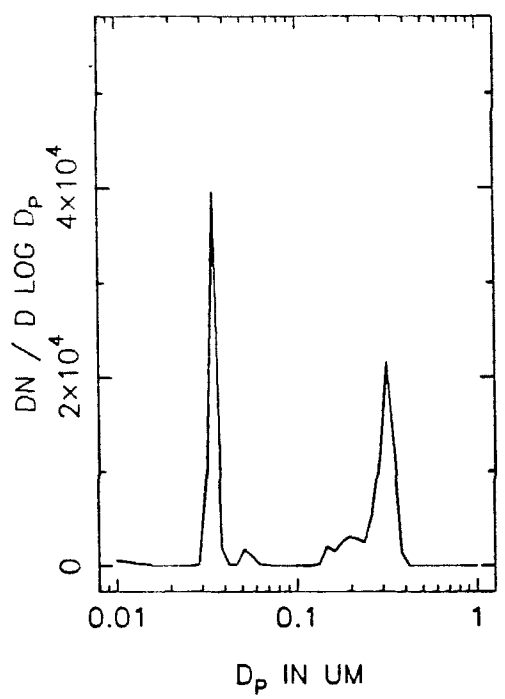

T=1.5 HOURS

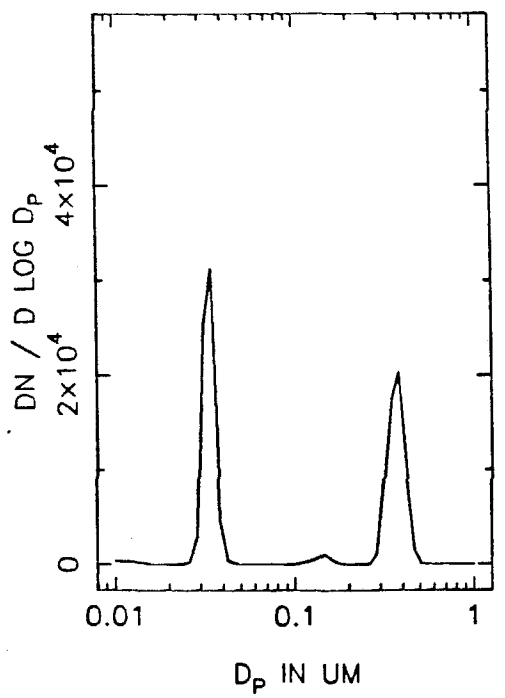

XK17A NUMBER DISTRIBUTION, T=2.0

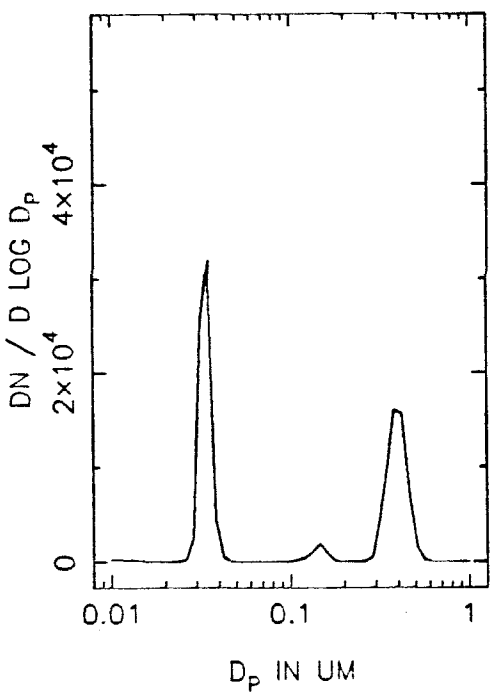

T=2.5 HOURS

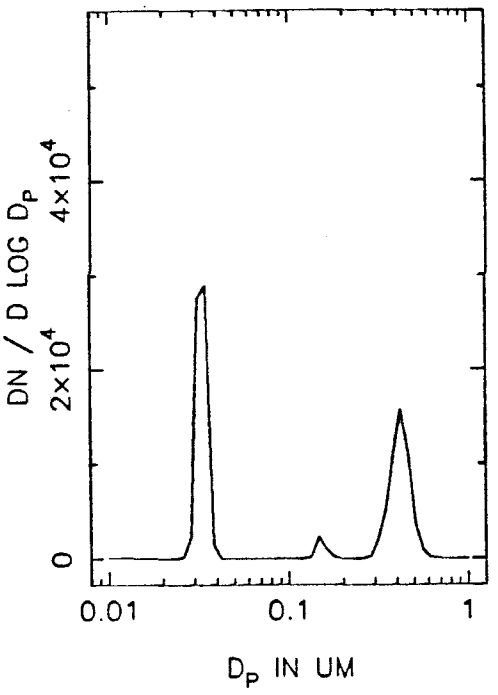

T=3.0 HOURS

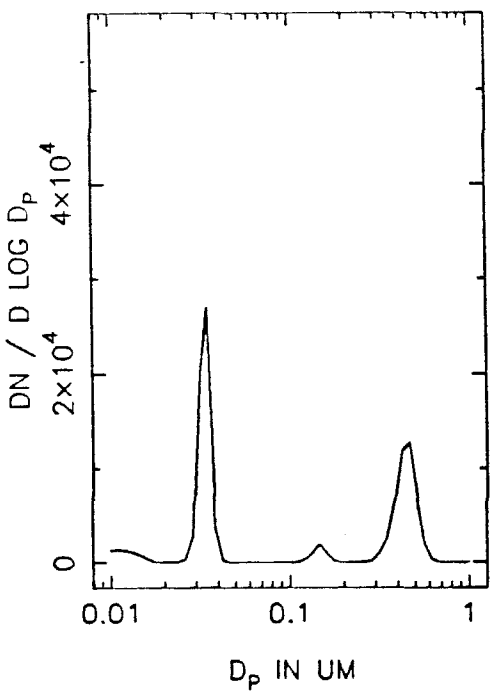

T=3.5 HOURS

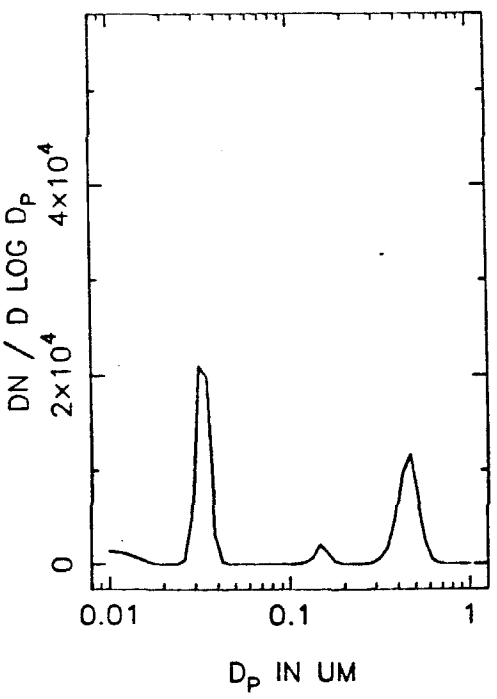

XK17A VOLUME DISTRIBUTION, T=0

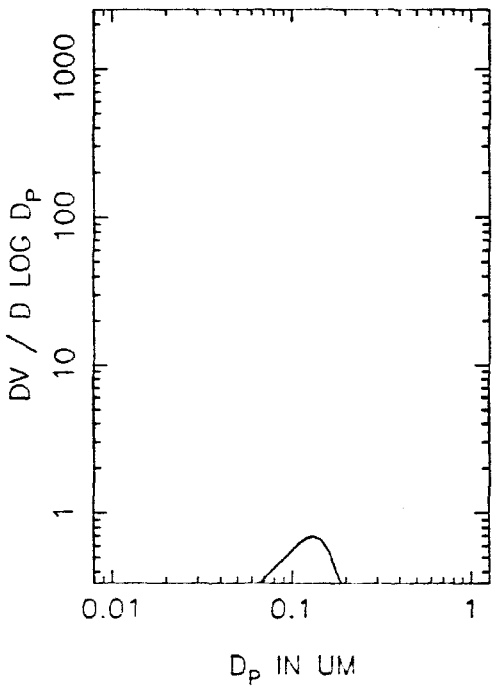

T=0.5 HOURS

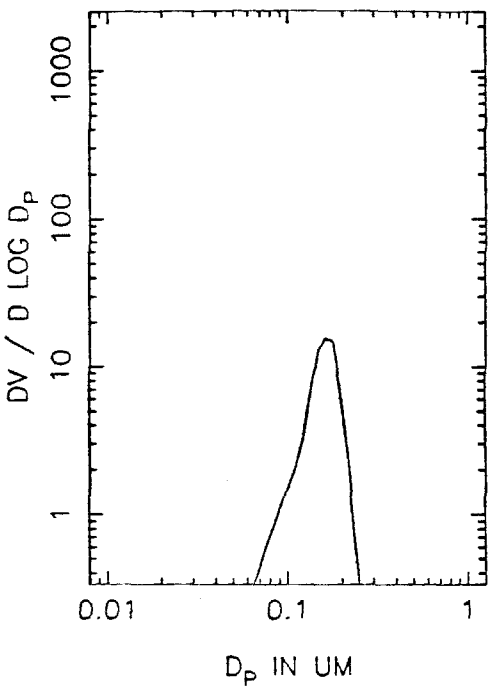

T=1.0 HOURS

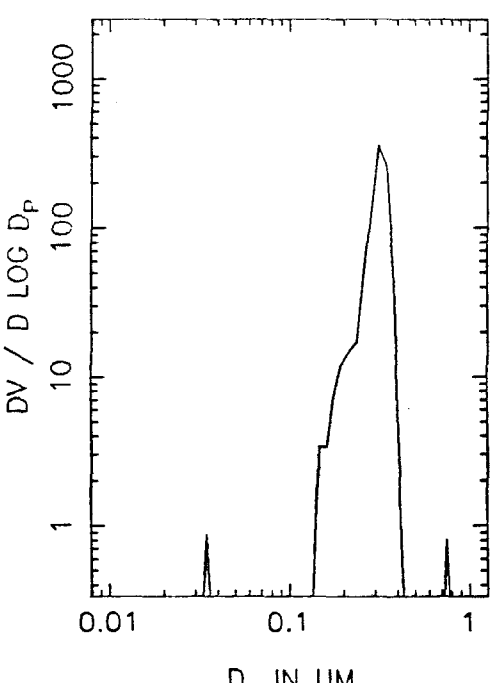

T=1.5 HOURS

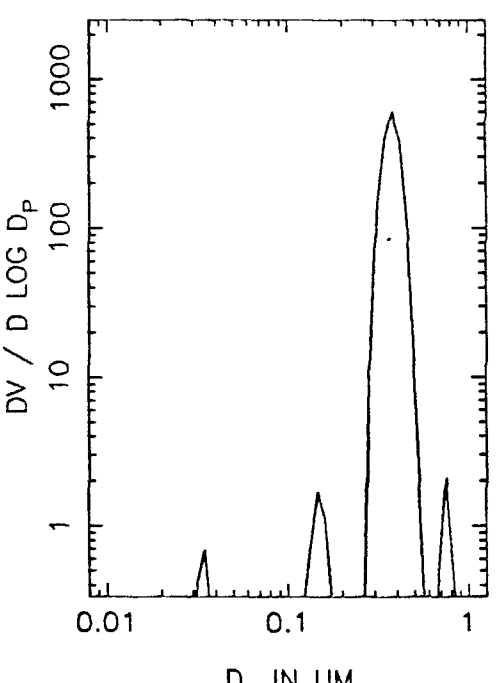

XK17A VOLUME DISTRIBUTION, T=2.0

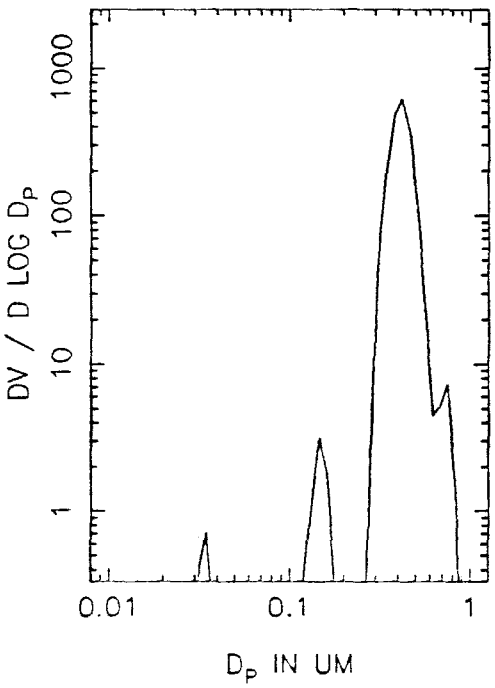

T=2.5 HOURS

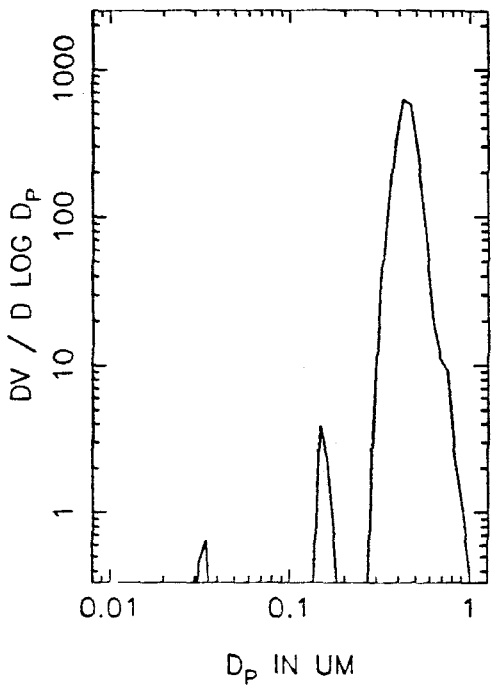

T=3.0 HOURS

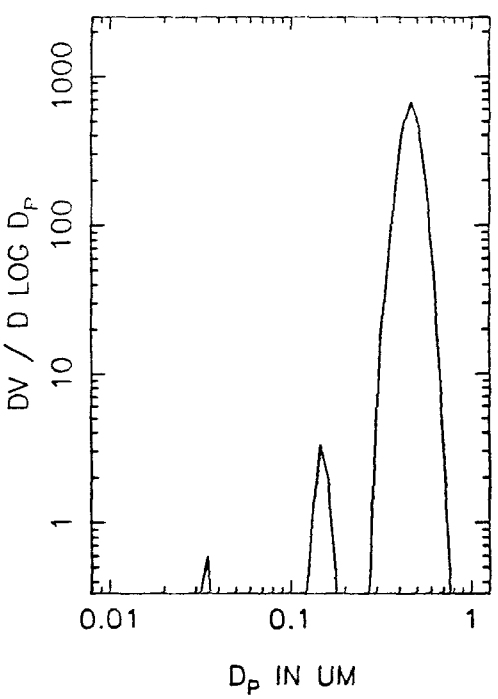

T=3.5 HOURS

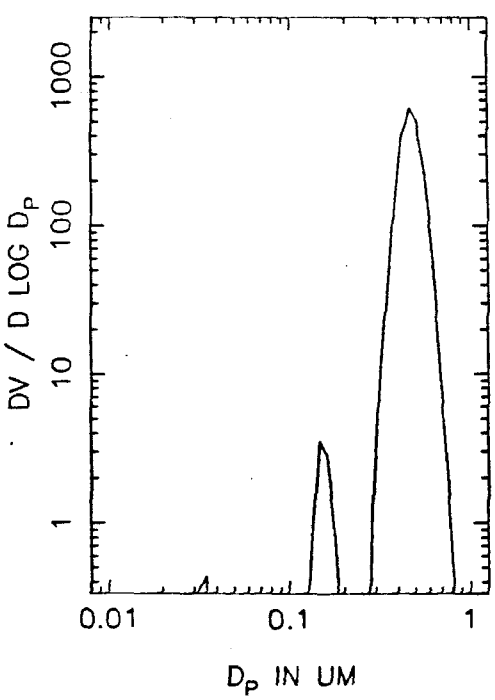

XK17B NUMBER DISTRIBUTION, T=0

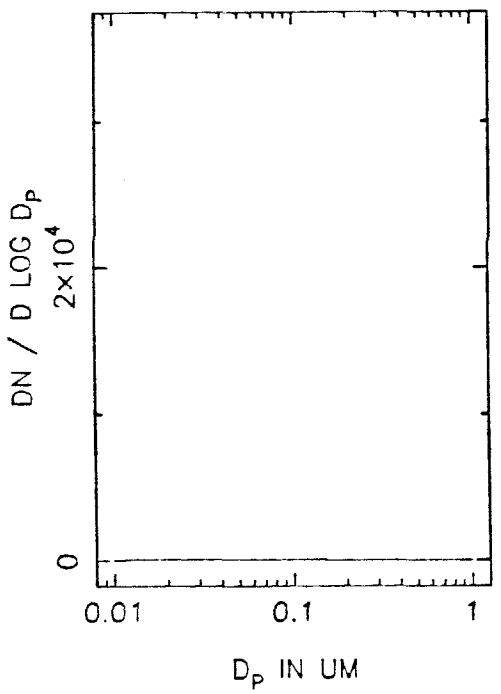

T=0.5 HOURS

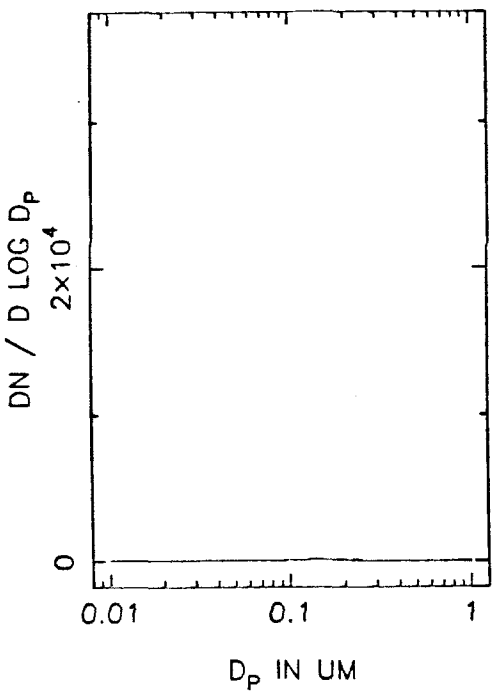

T=1.0 HOURS

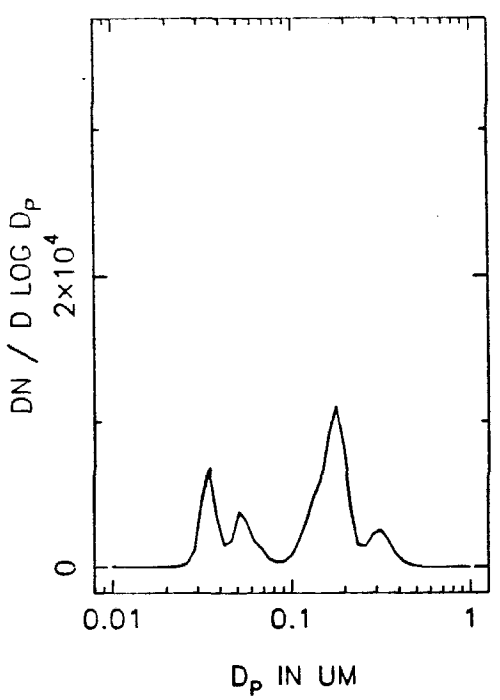

T=1.5 HOURS

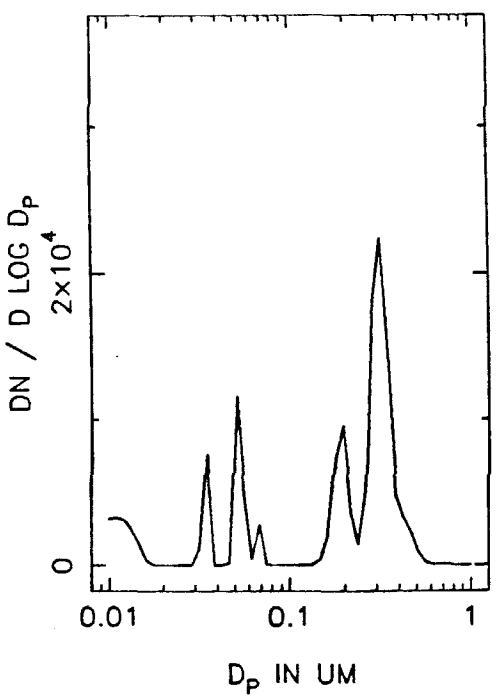

XK17B NUMBER DISTRIBUTION, T=2.0

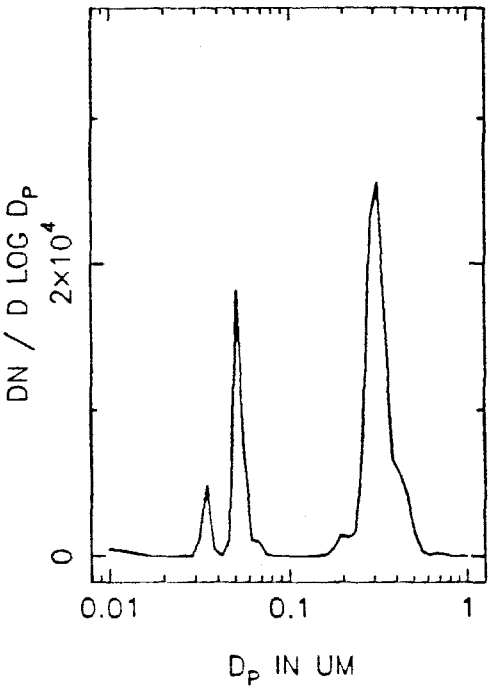

T=2.5 HOURS

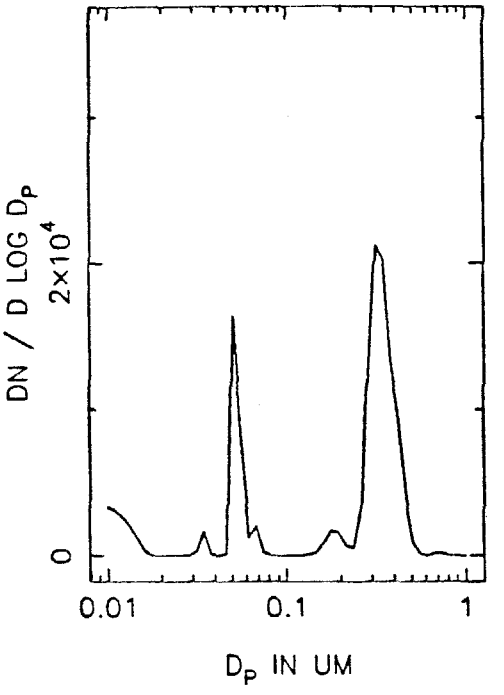

T=3.0 HOURS

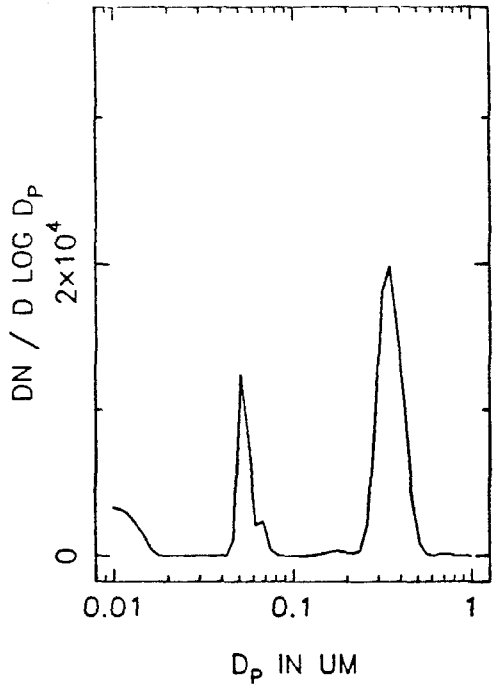

T=3.5 HOURS

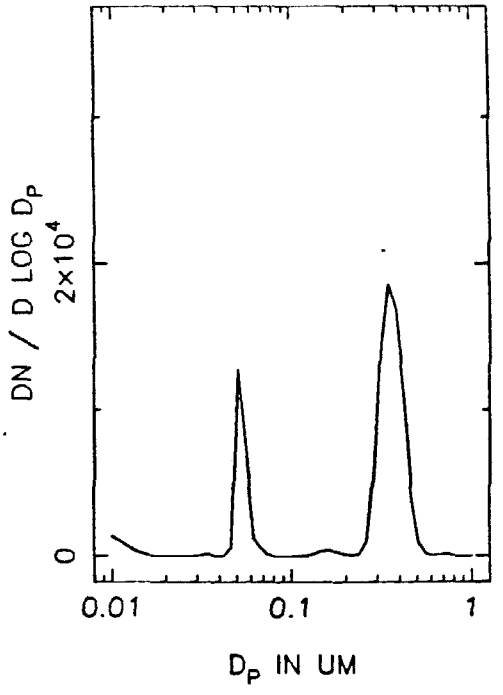

XK17B VOLUME DISTRIBUTION, T=0

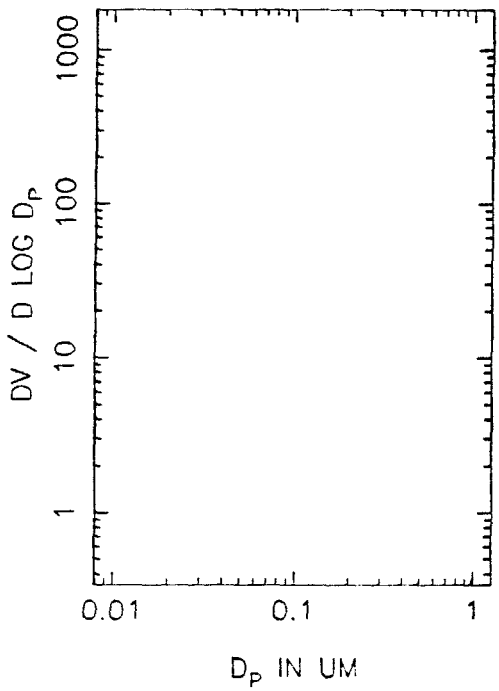

T=0.5 HOURS

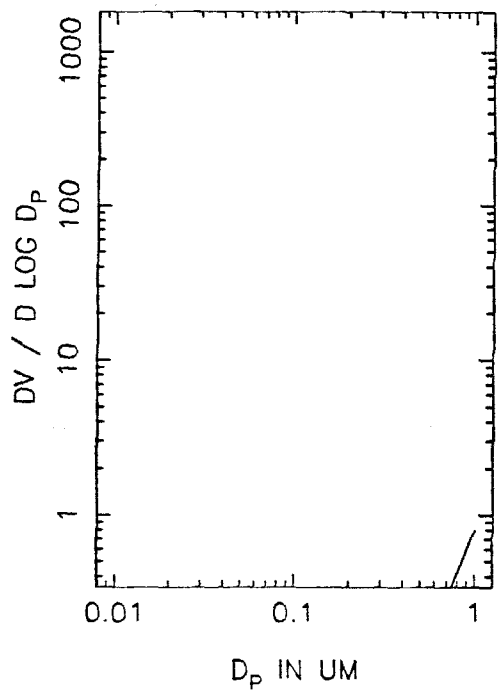

T=1.0 HOURS

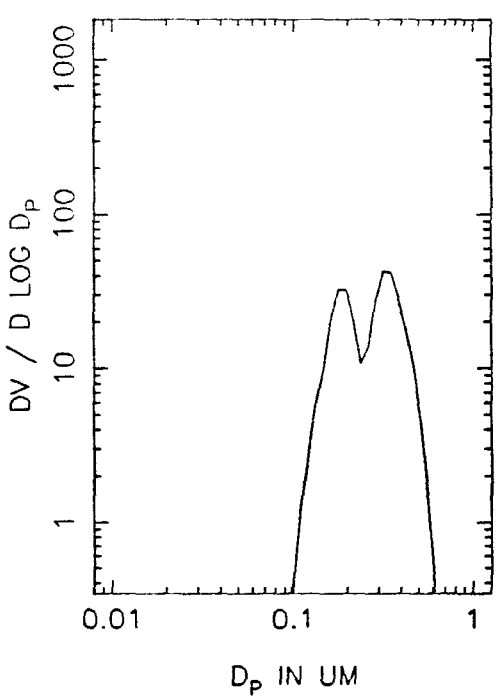

T=1.5 HOURS

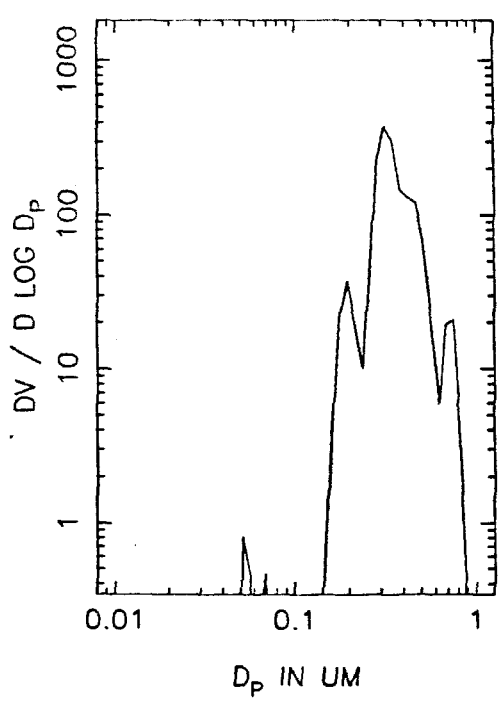

XK17B VOLUME DISTRIBUTION, T=2.0

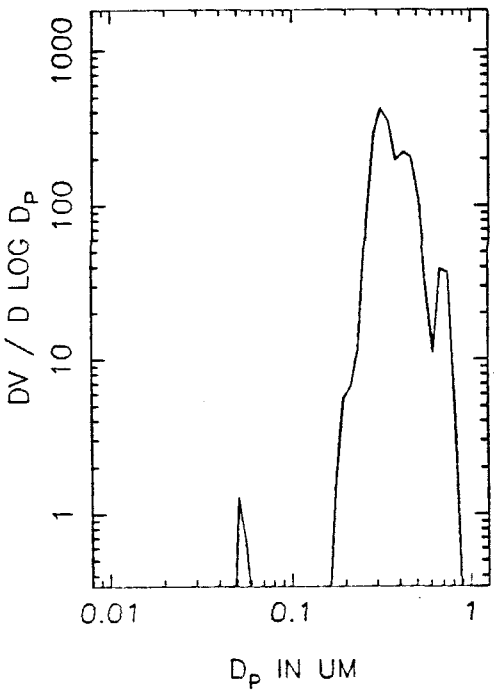

T=2.5 HOURS

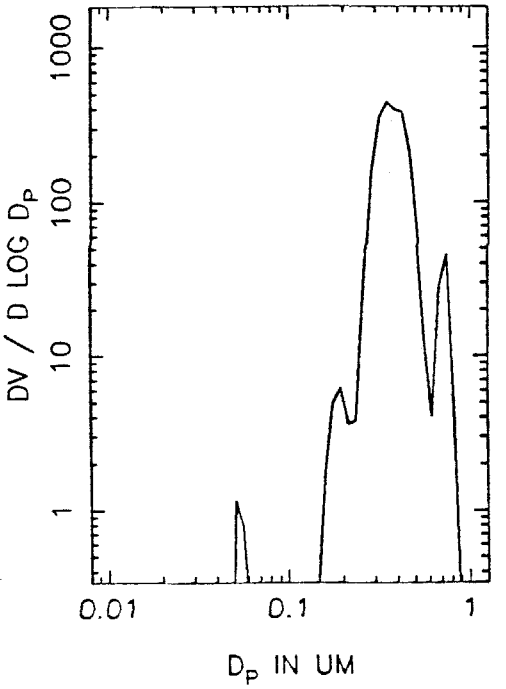

T=3.0 HOURS

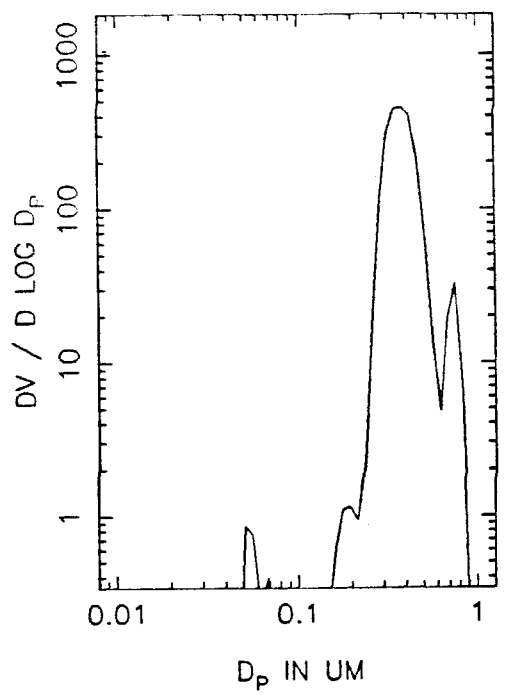

T=3.5 HOURS

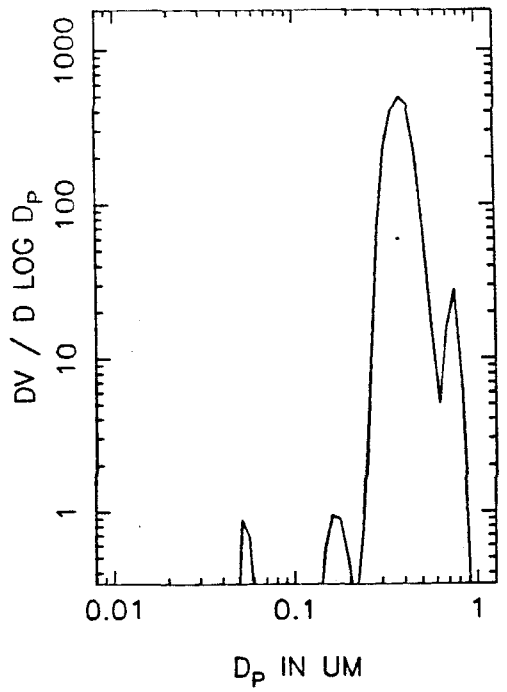

XJ19 TOTAL NUMBER, SIDE A

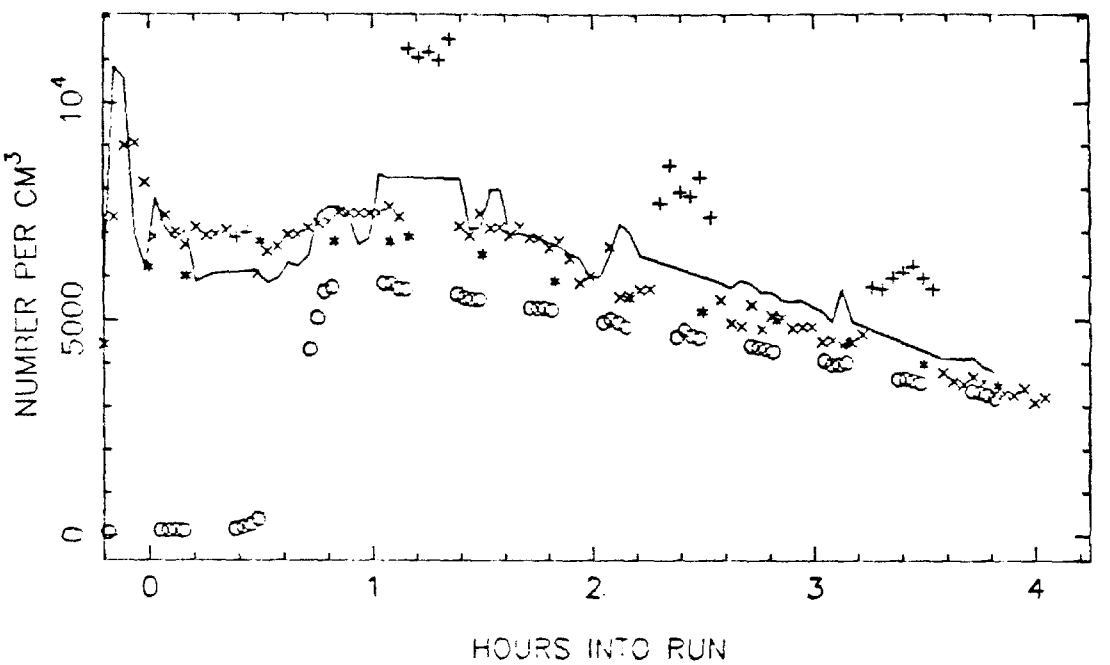

SIDE B

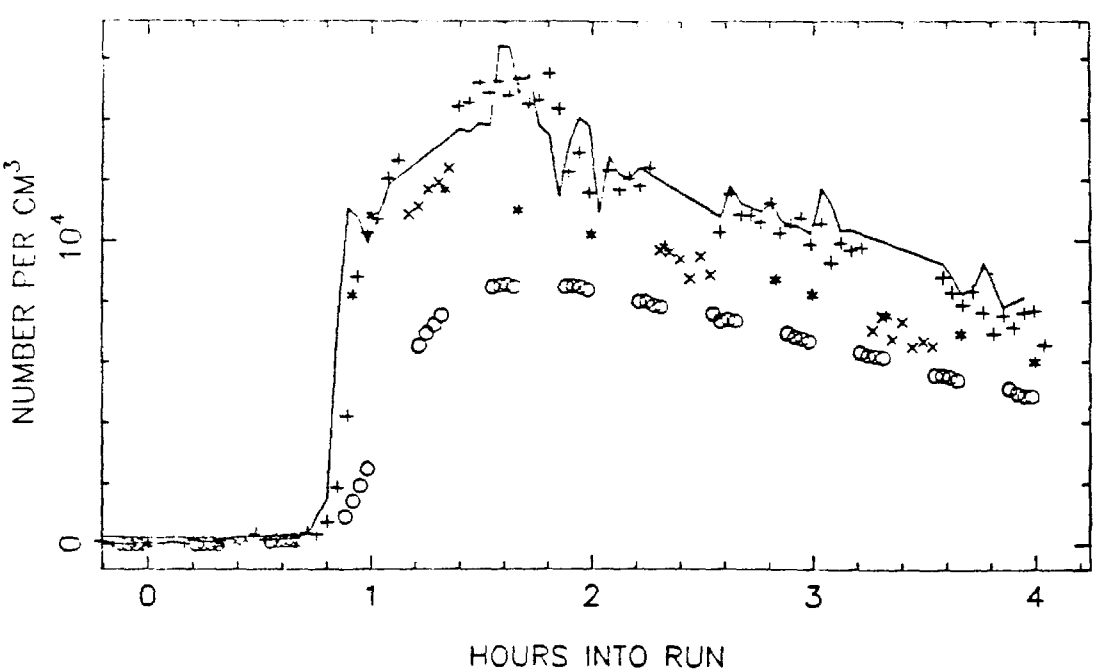

XJ19 VOLUME IN THE AEROSOL PHASE, SIDE A

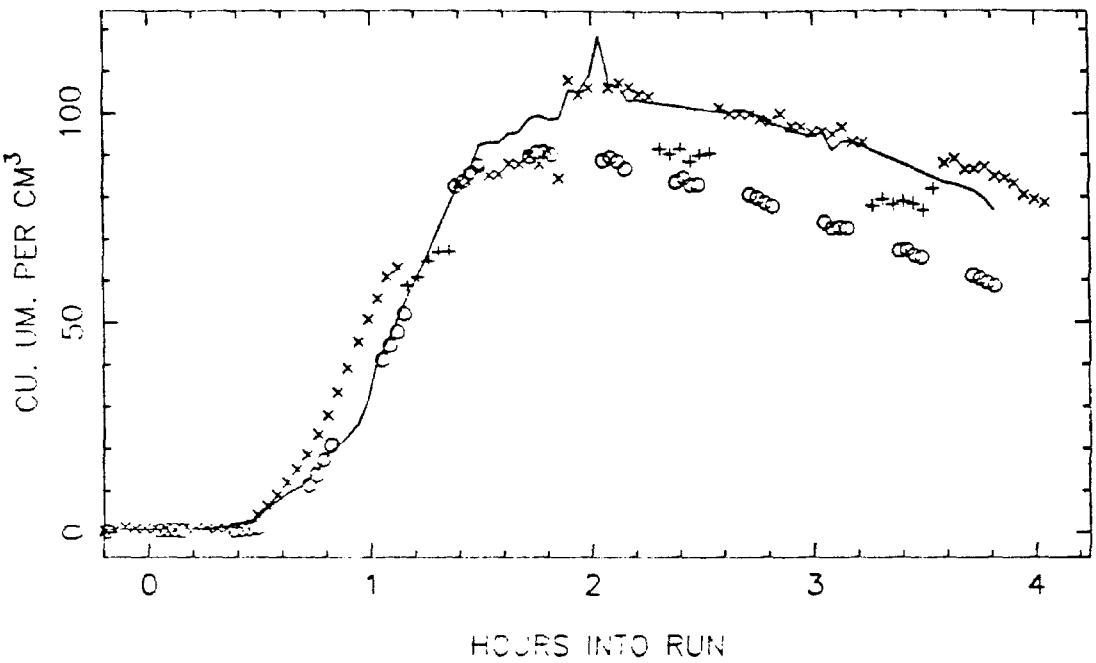

SIDE B

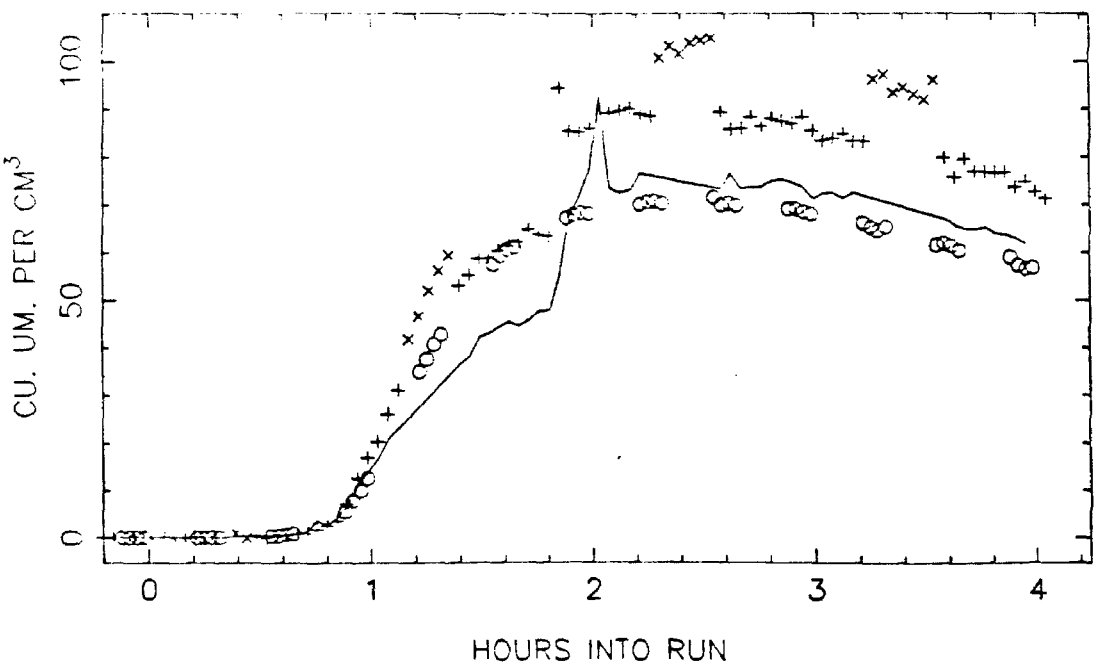

XJ19 MEAN PARTICLE SIZE, SIDE A

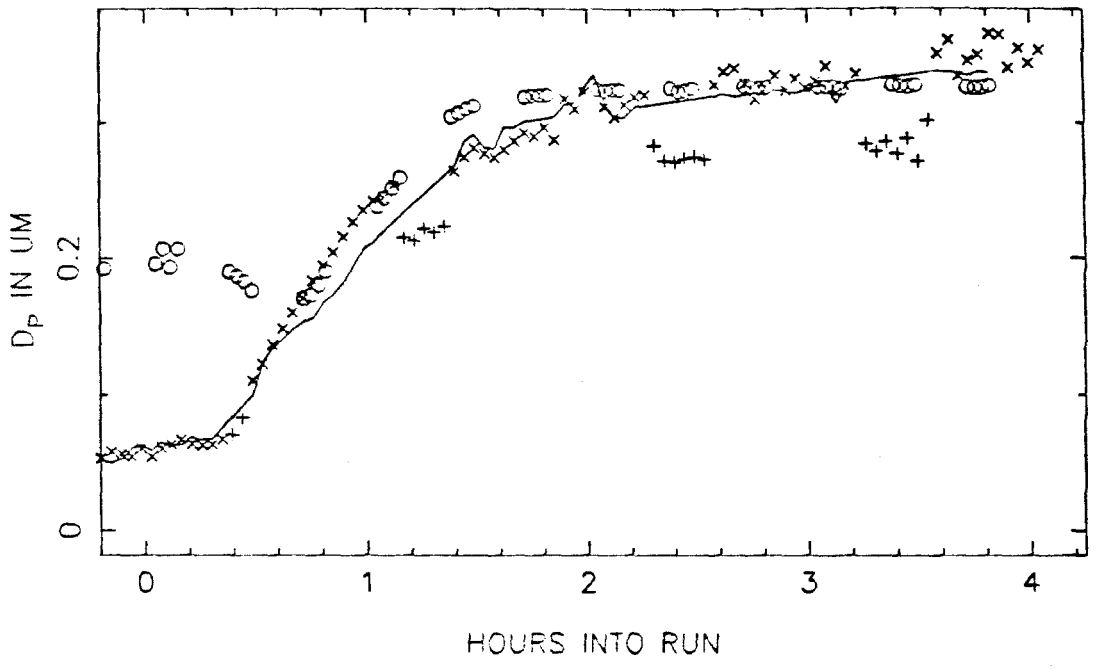

SIDE B

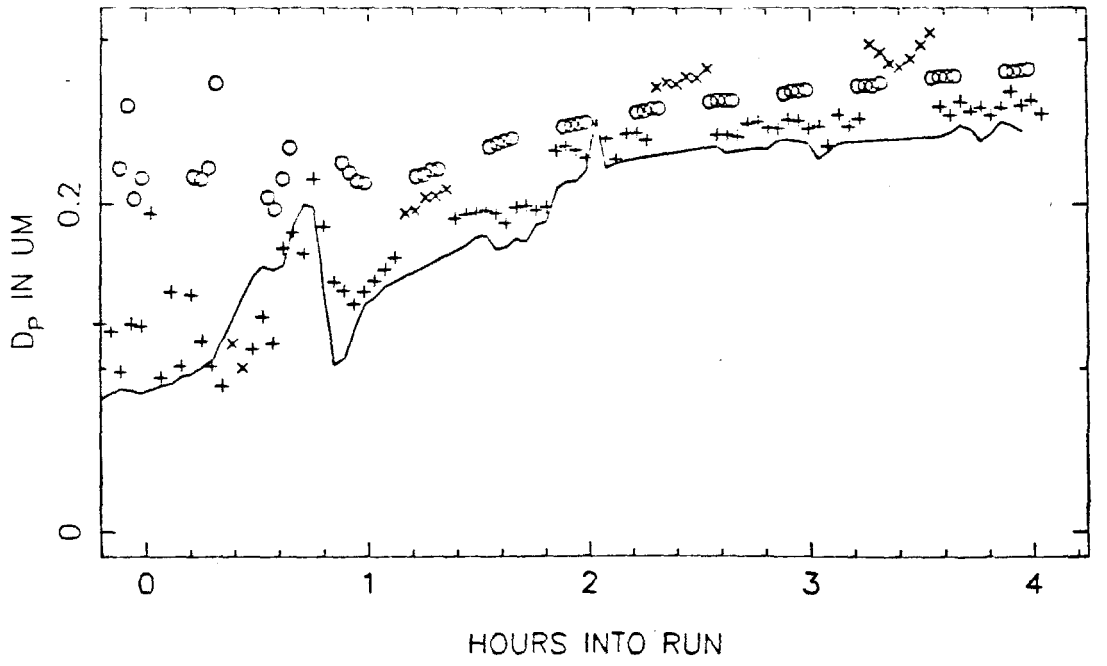

XJ19A NUMBER DISTRIBUTION, T=0

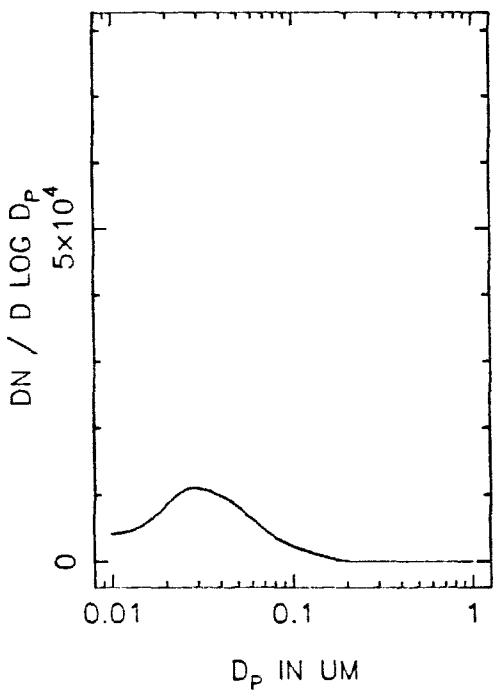

T=0.5 HOURS

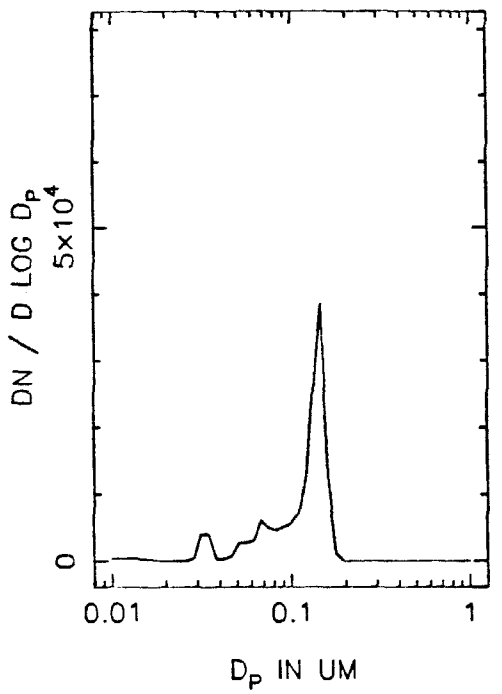

T=1.0 HOURS

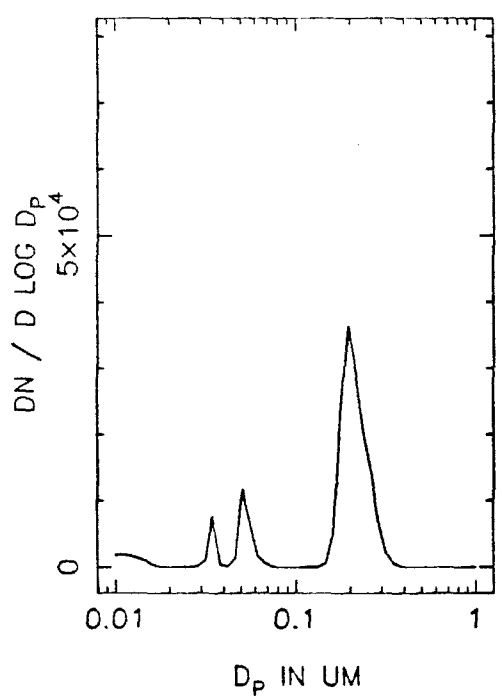

T=1.5 HOURS

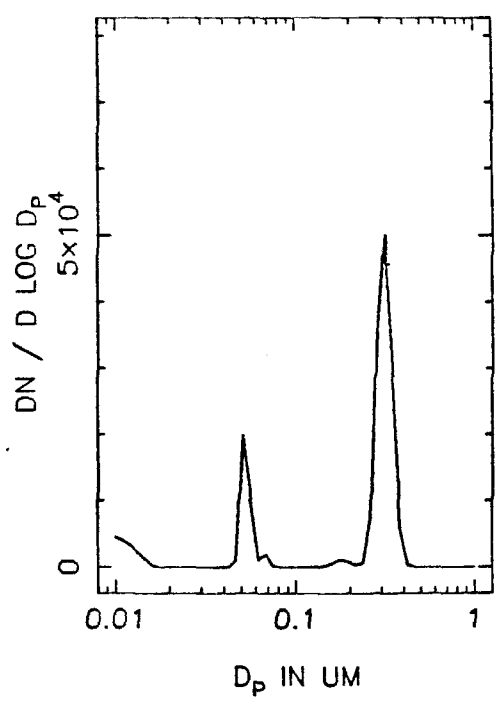

XJ19A NUMBER DISTRIBUTION, T=2.0

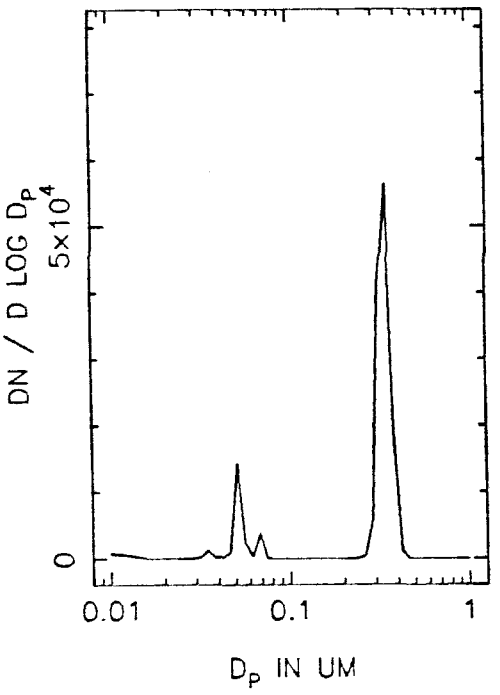

T=2.5 HOURS

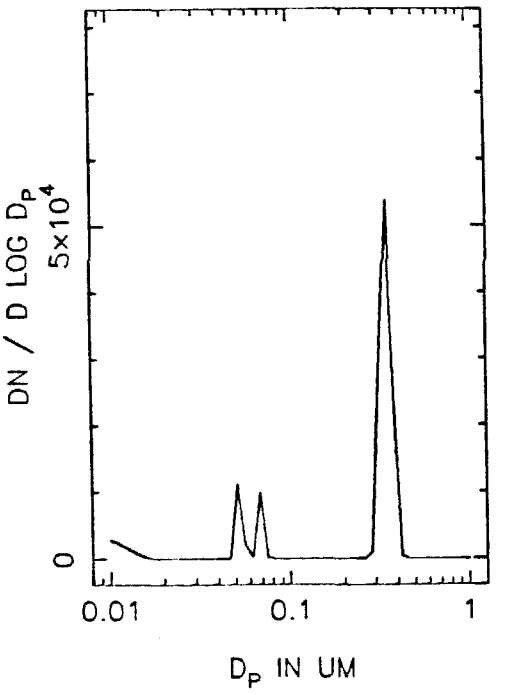

T=3.0 HOURS

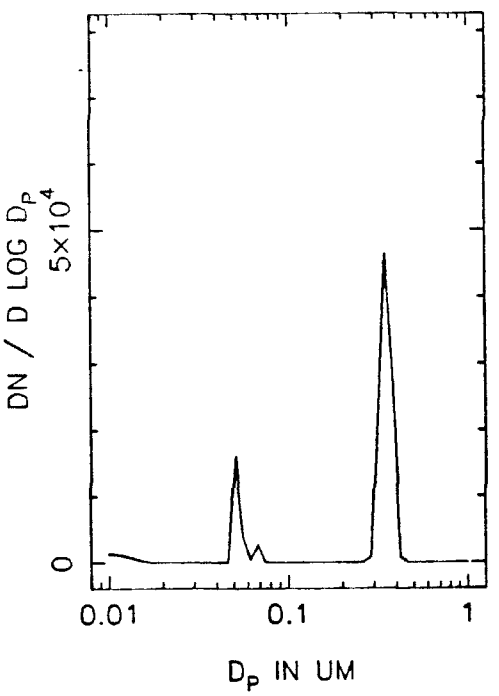

T=3.5 HOURS

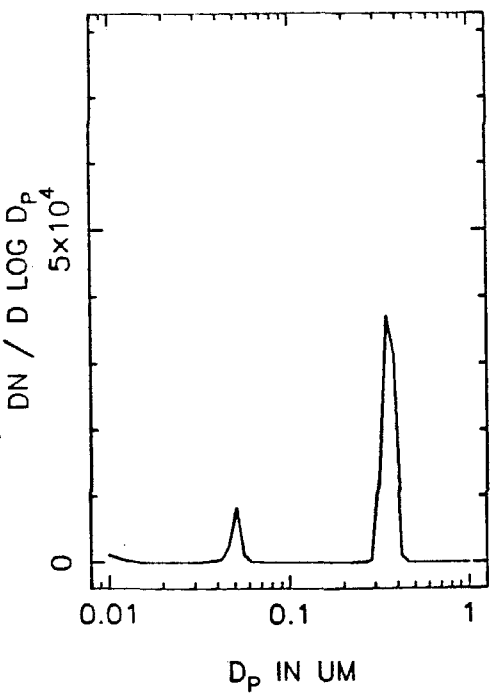

XJ19A VOLUME DISTRIBUTION, T=0

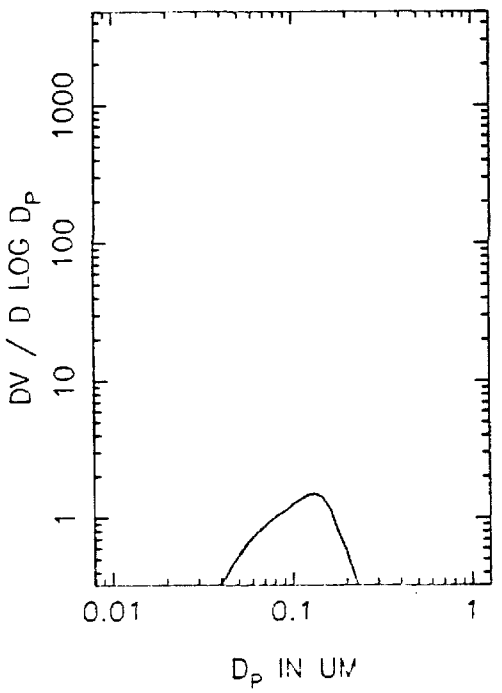

T=0.5 HOURS

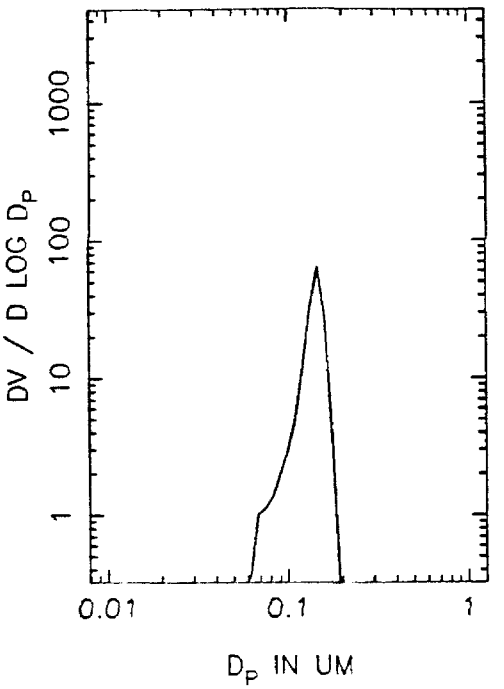

T=1.0 HOURS

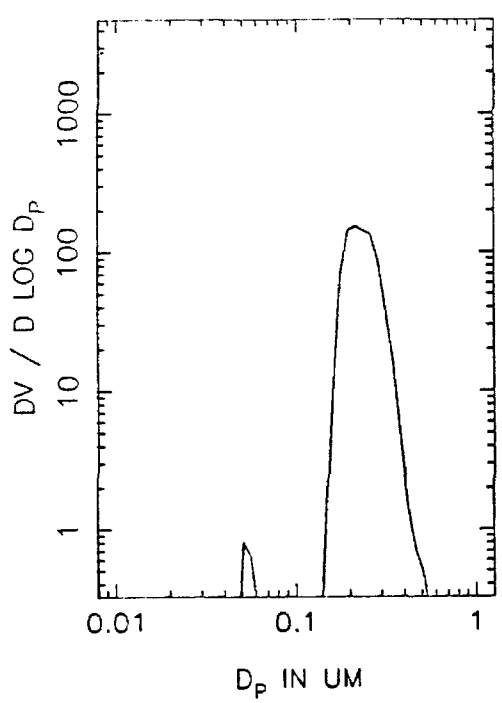

T=1.5 HOURS

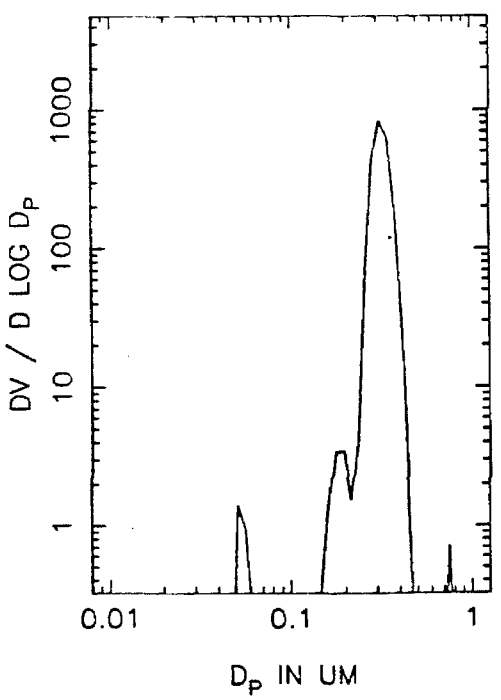

XJ19A VOLUME DISTRIBUTION, T=2.0

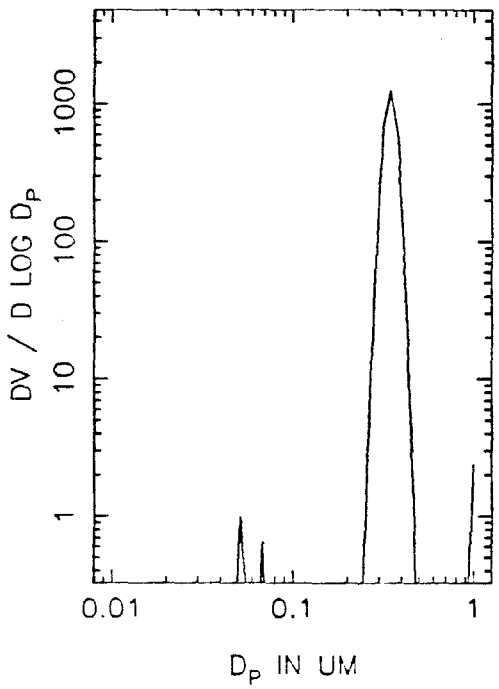

T=2.5 HOURS

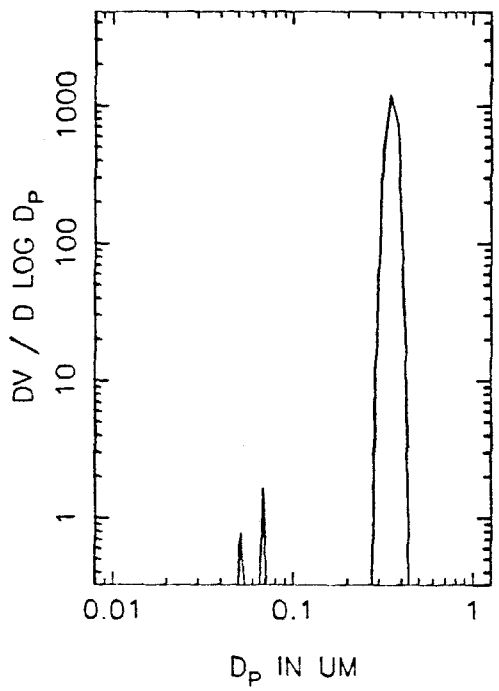

T=3.0 HOURS

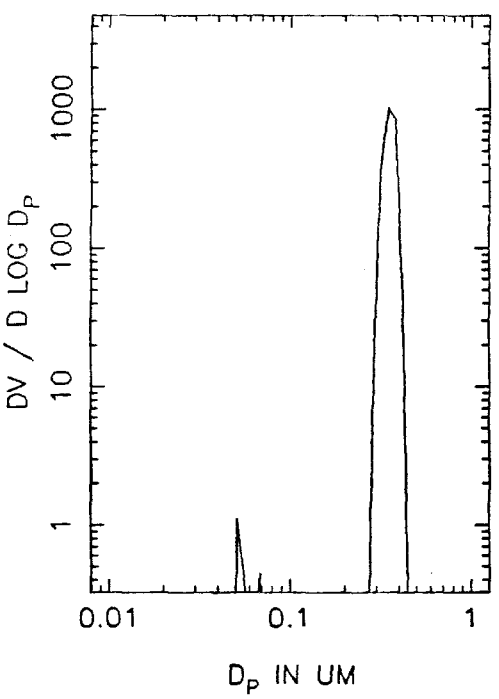

T=3.5 HOURS

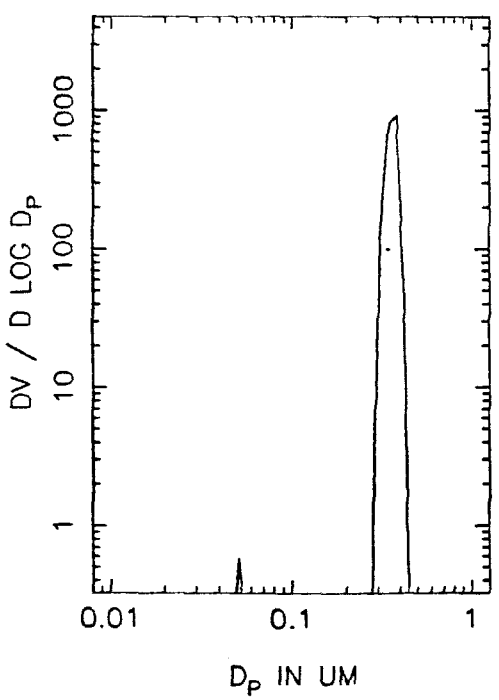

XJ19B NUMBER DISTRIBUTION, T=0

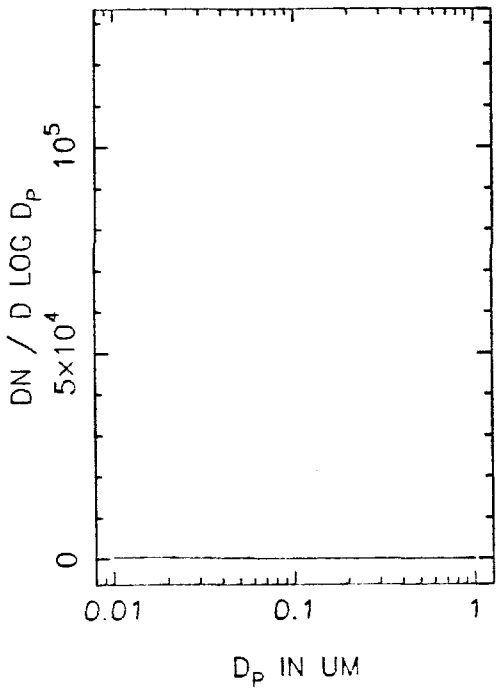

T=0.5 HOURS

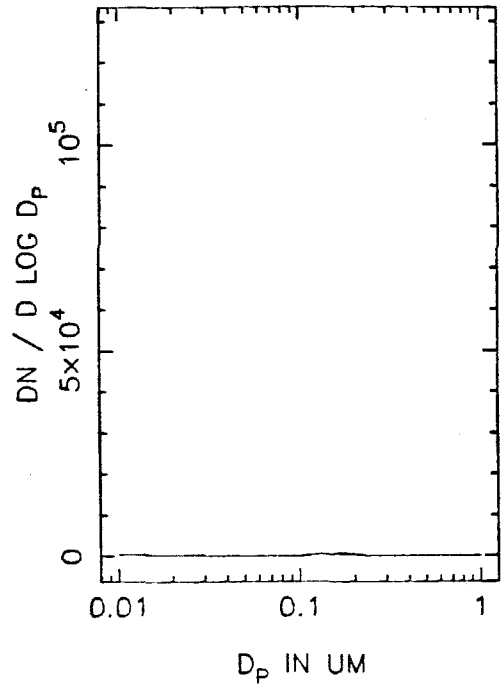

T=1.0 HOURS

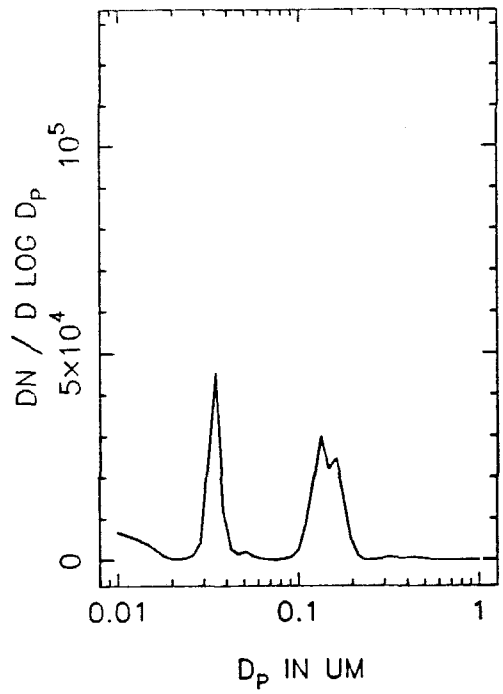

T=1.5 HOURS

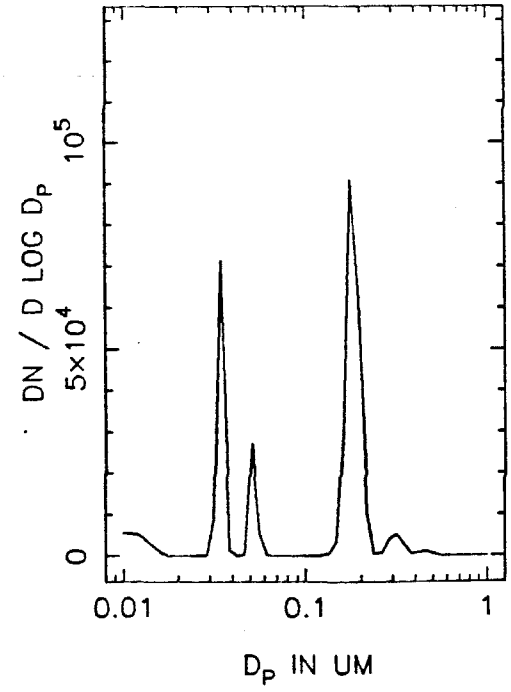

XJ19B NUMBER DISTRIBUTION, T=2.0

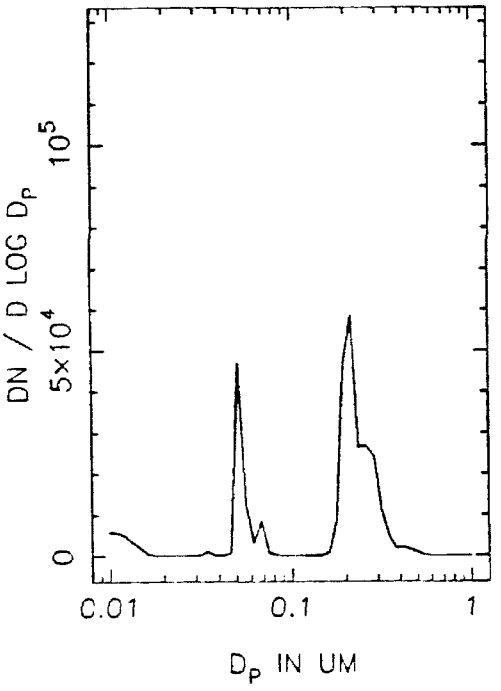

T=2.5 HOURS

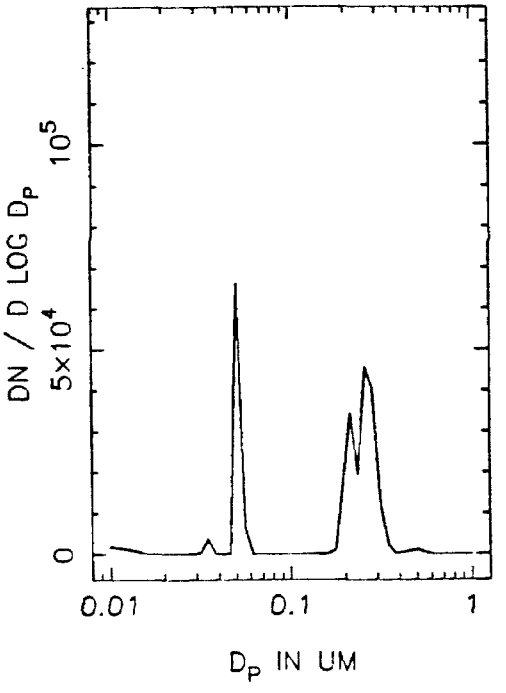

T=3.0 HOURS

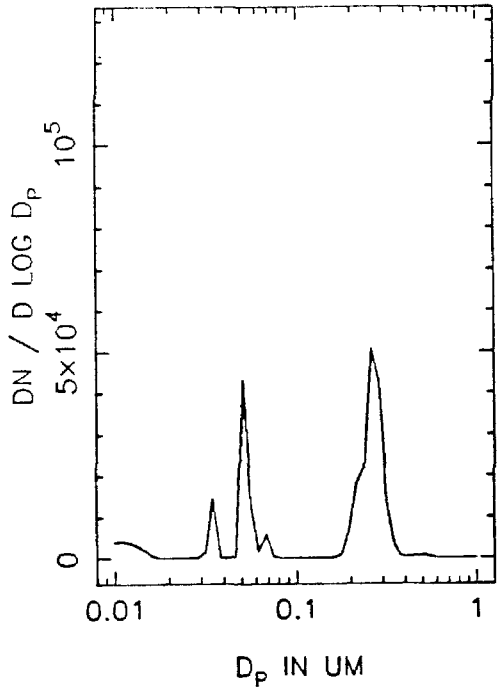

T=3.5 HOURS

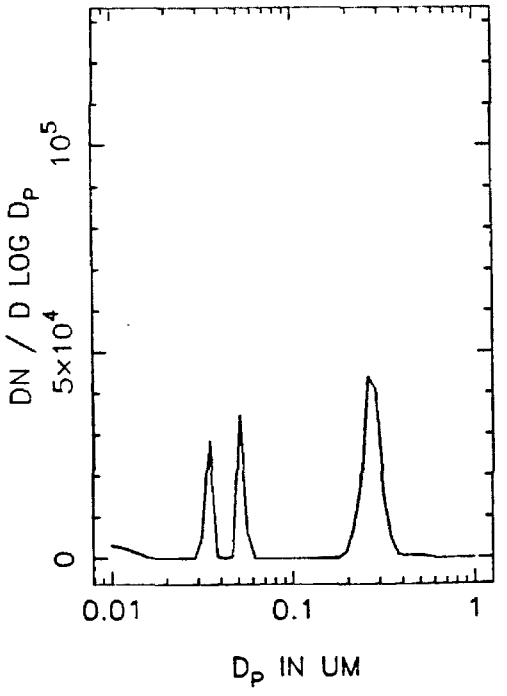

XJ19B NUMBER DISTRIBUTION, T=4.0

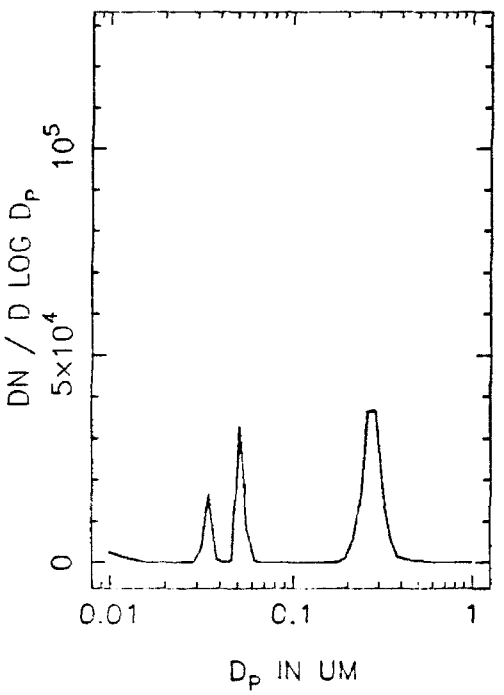

XJ19B VOLUME DISTRIBUTION, T=0

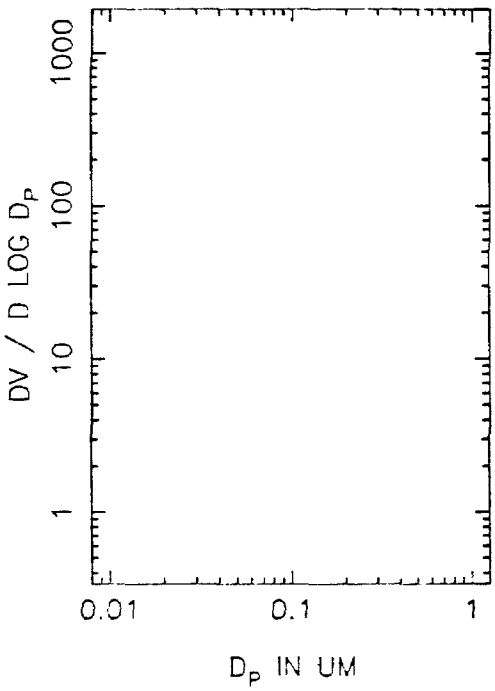

T=0.5 HOURS

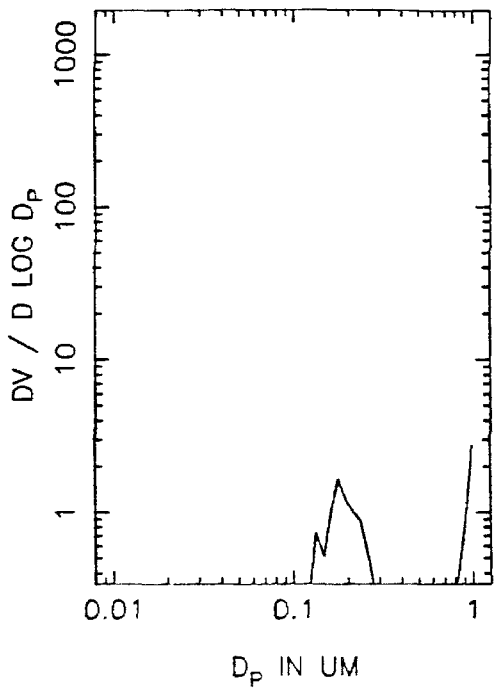

T=1.0 HOURS

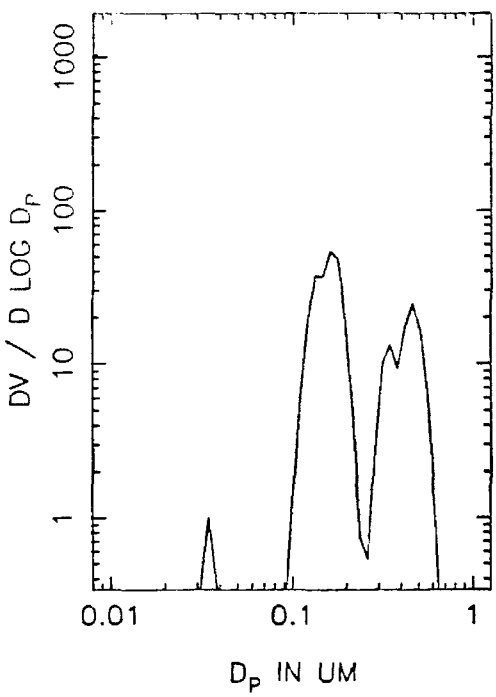

T=1.5 HOURS

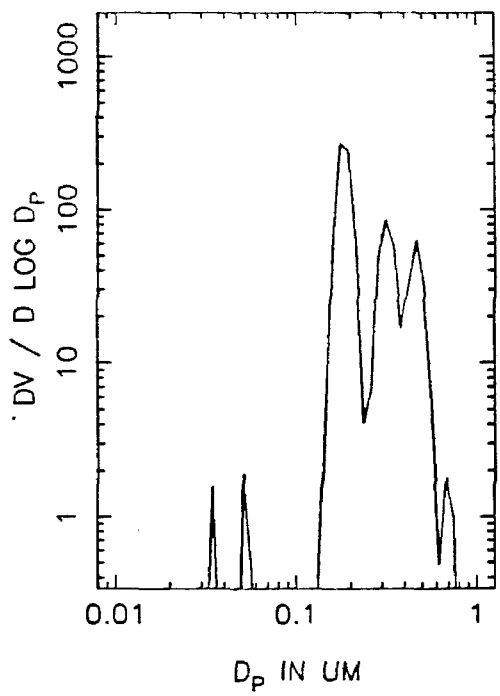

XJ19B VOLUME DISTRIBUTION, T=2.0

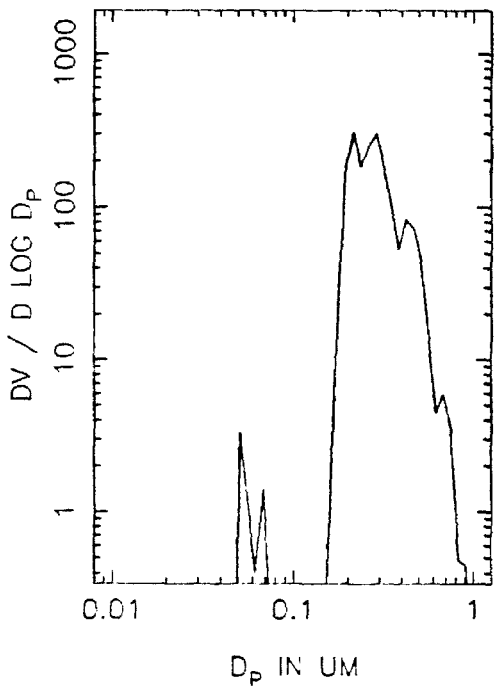

T=2.5 HOURS

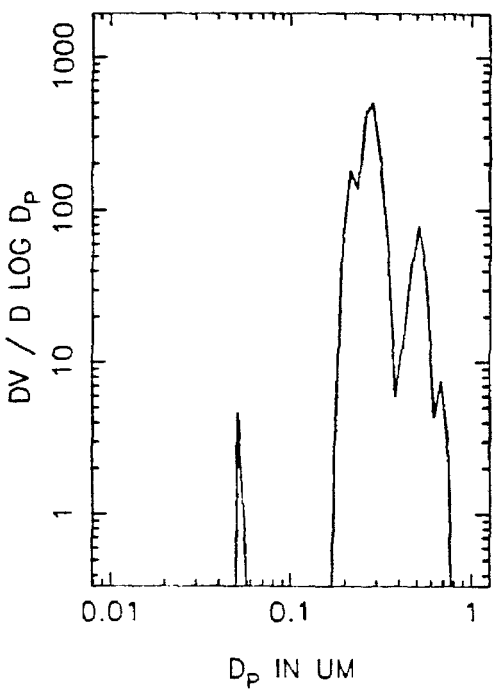

T=3.0 HOURS

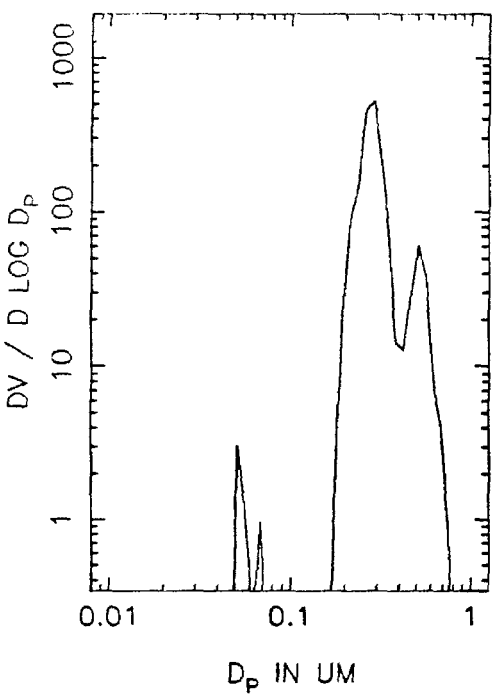

T=3.5 HOURS

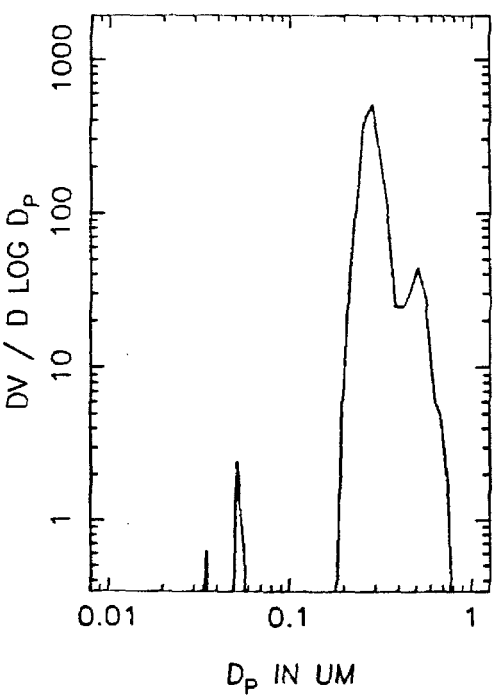

XJ19B VOLUME DISTRIBUTION, T=4.0

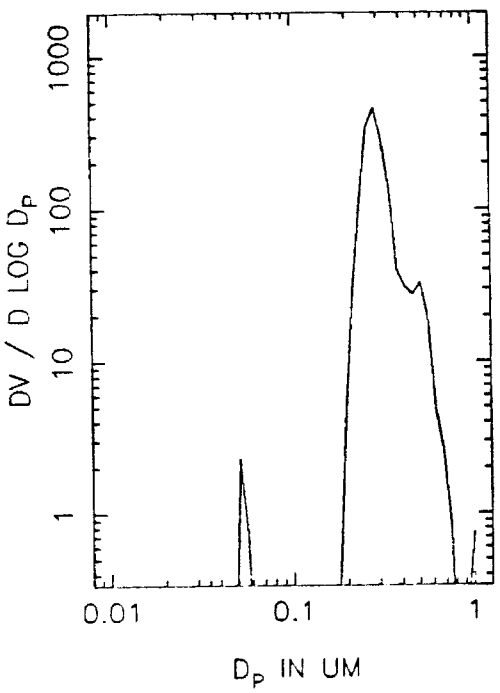

XJ34 TOTAL NUMBER, SIDE A

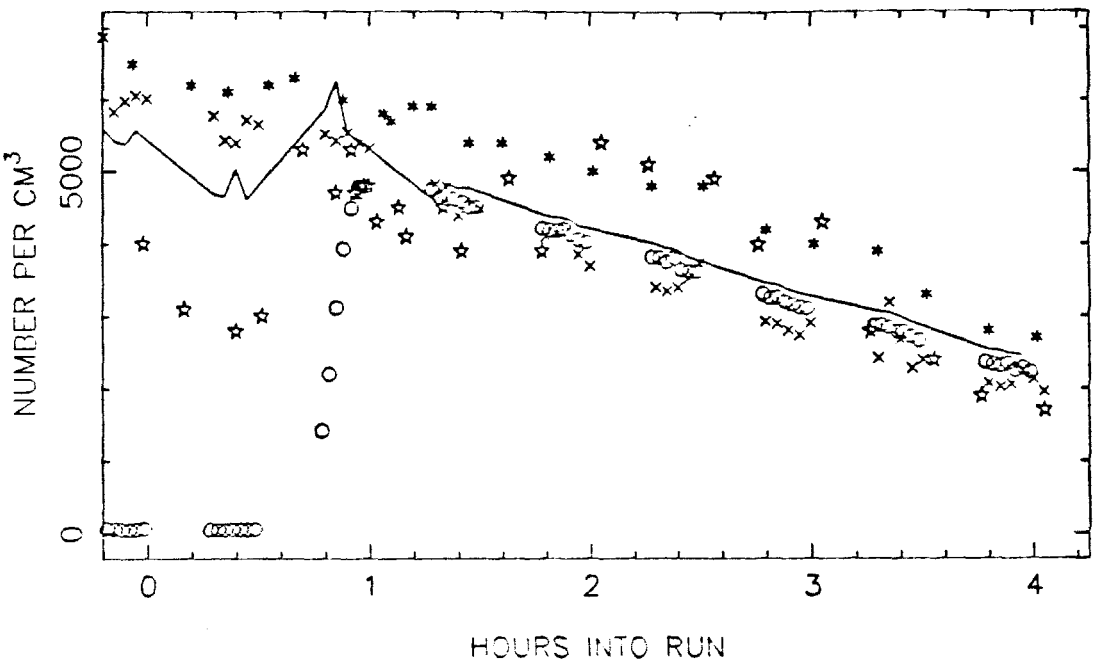

SIDE B

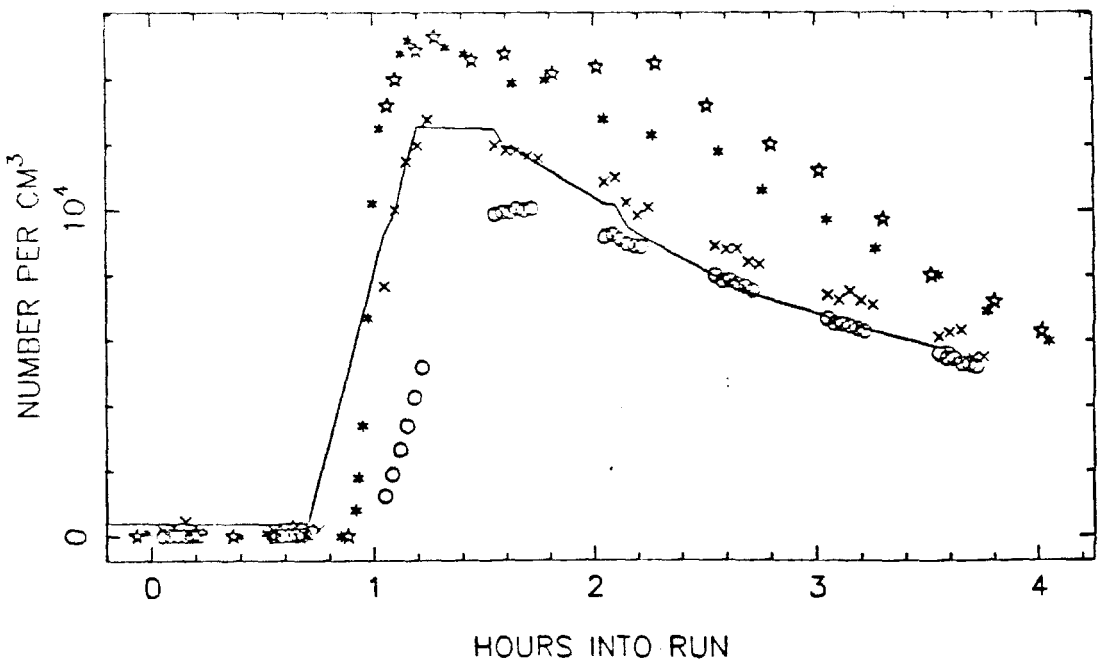

XJ34 VOLUME IN THE AEROSOL PHASE, SIDE A

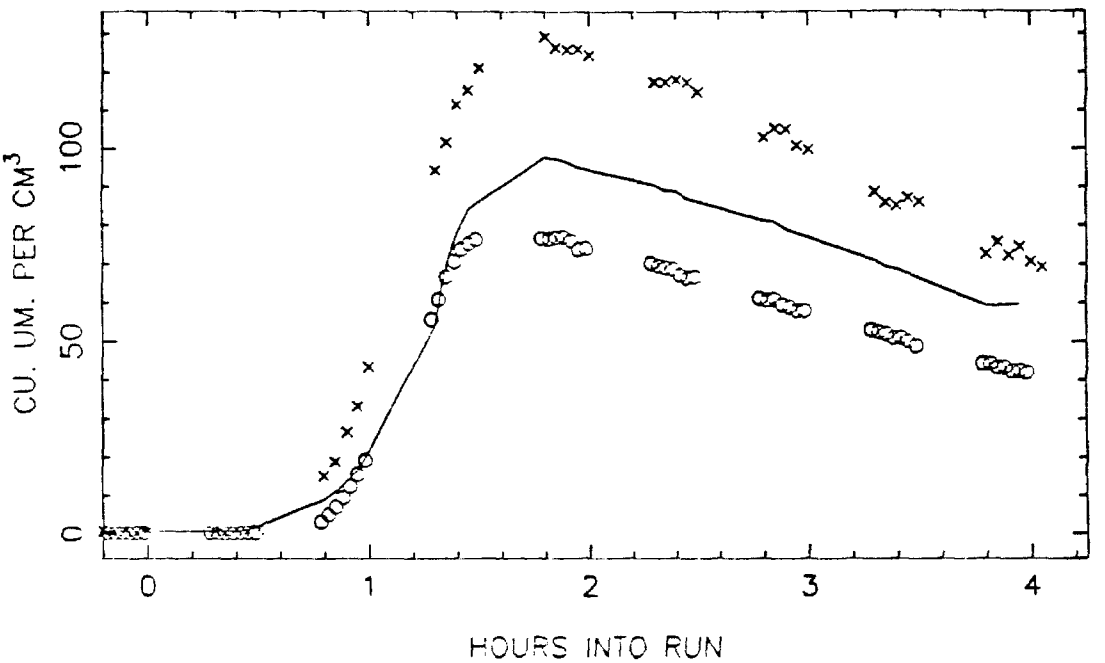

SIDE B

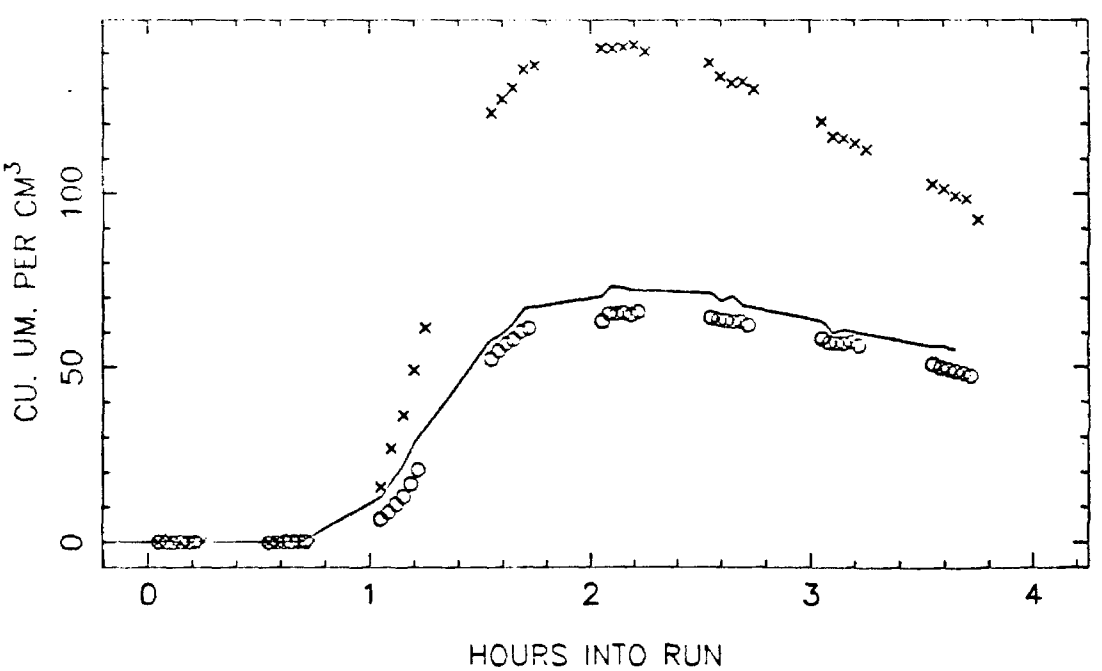

XJ34 MEAN PARTICLE SIZE, SIDE A

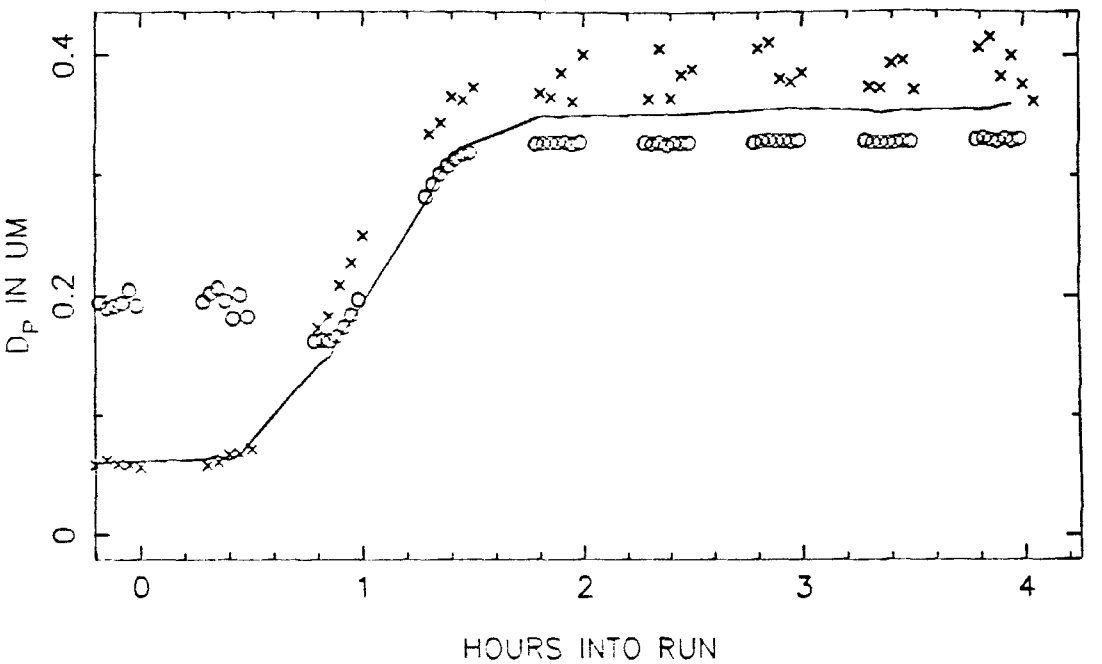

SIDE B

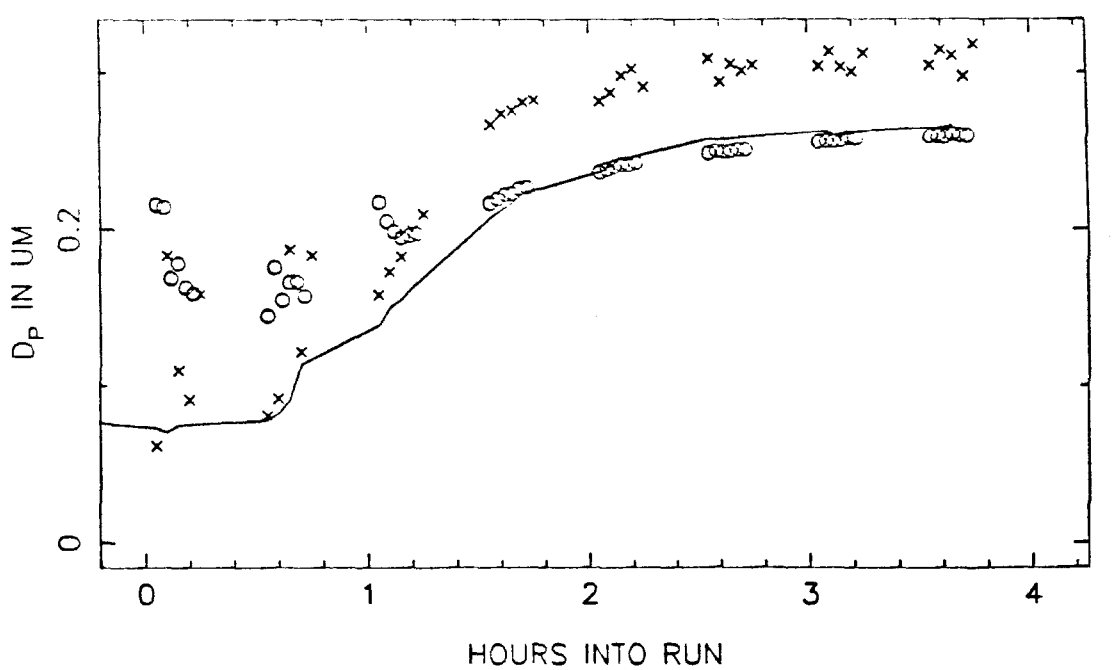

XJ34A NUMBER DISTRIBUTION, T=0

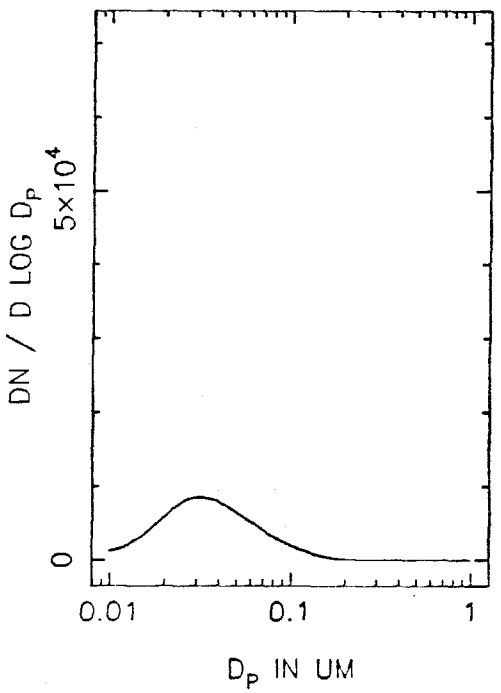

T=0.5 HOURS

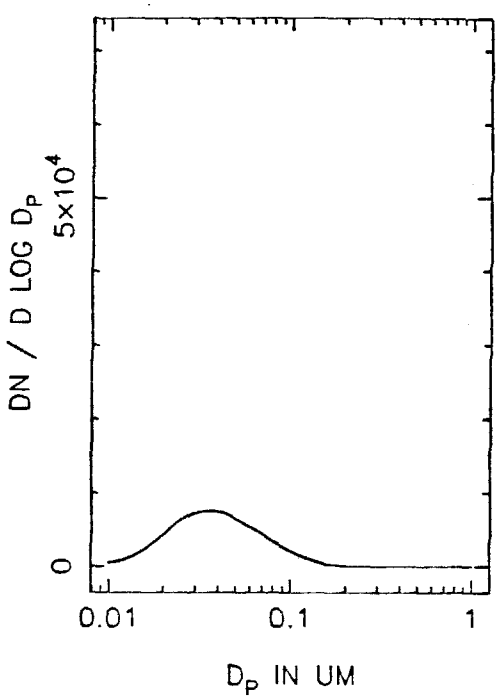

T=1.0 HOURS

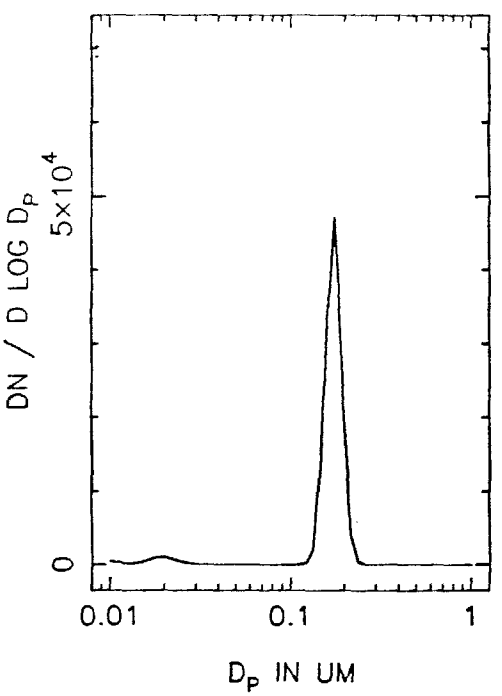

T=1.5 HOURS

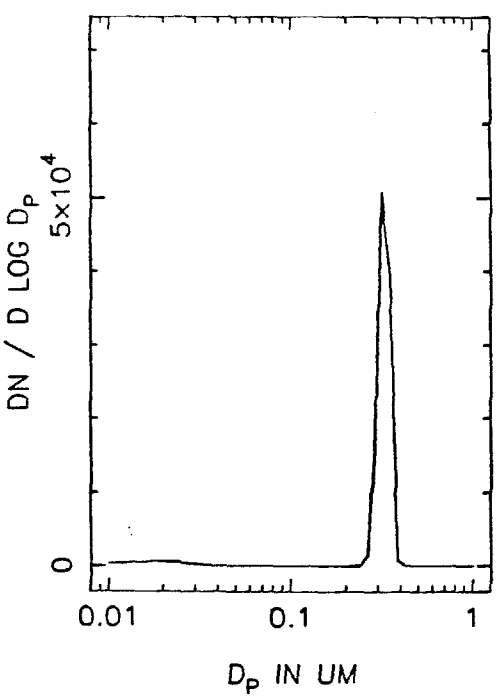

XJ34A NUMBER DISTRIBUTION, T=2.0

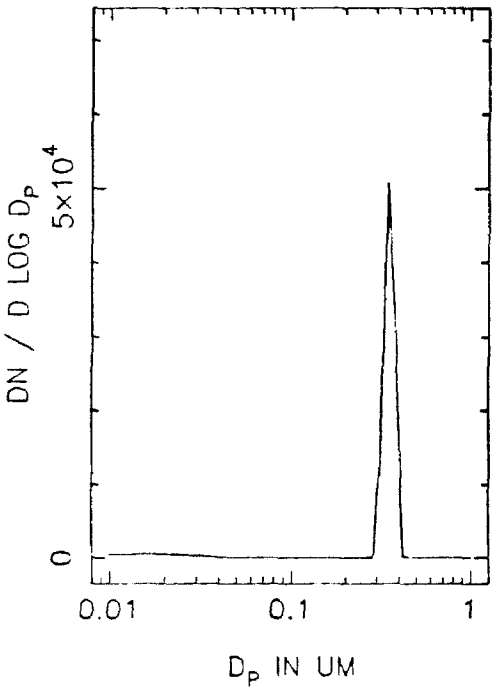

T=2.5 HOURS

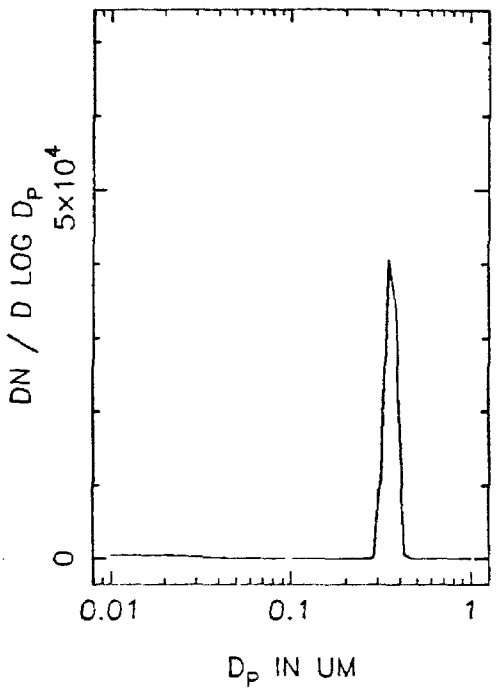

T=3.0 HOURS

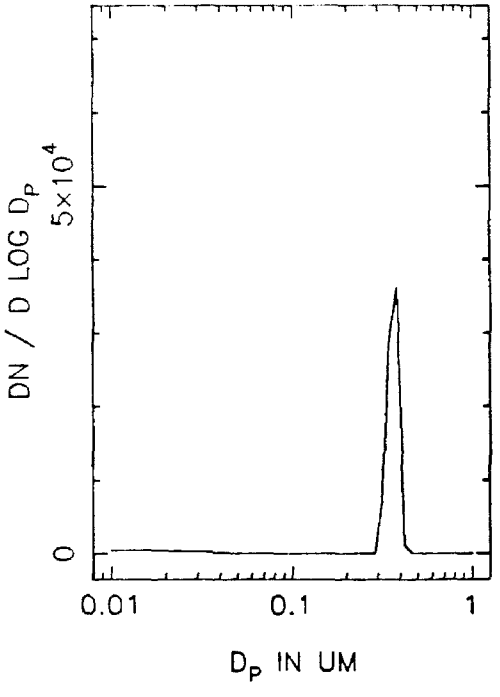

T=3.5 HOURS

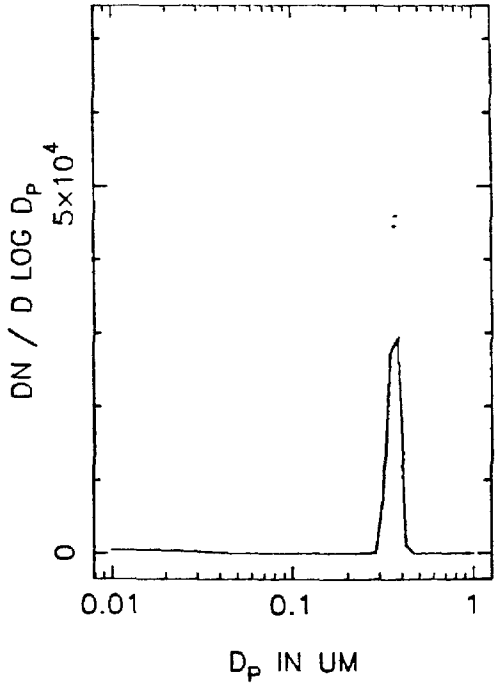

XJ34A NUMBER DISTRIBUTION, T=4.0

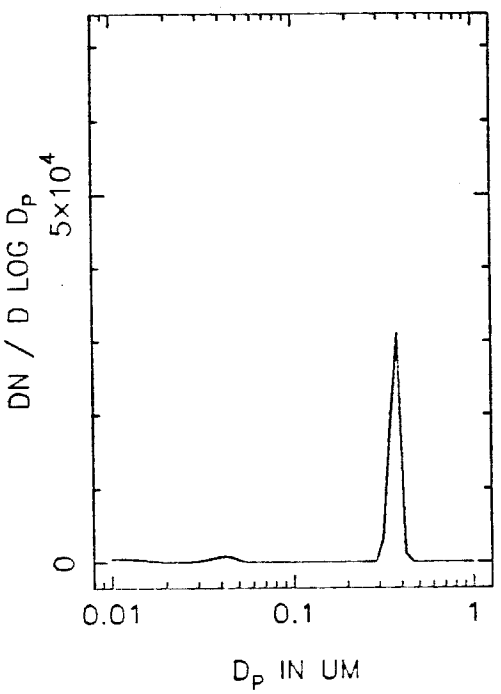

XJ34A VOLUME DISTRIBUTION, T=0

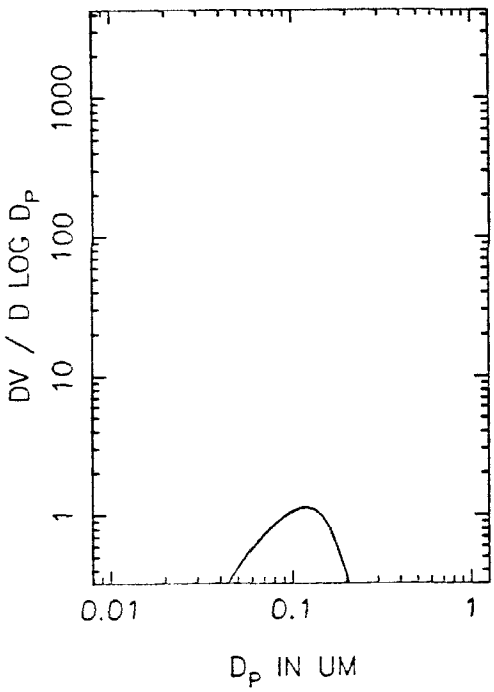

T=0.5 HOURS

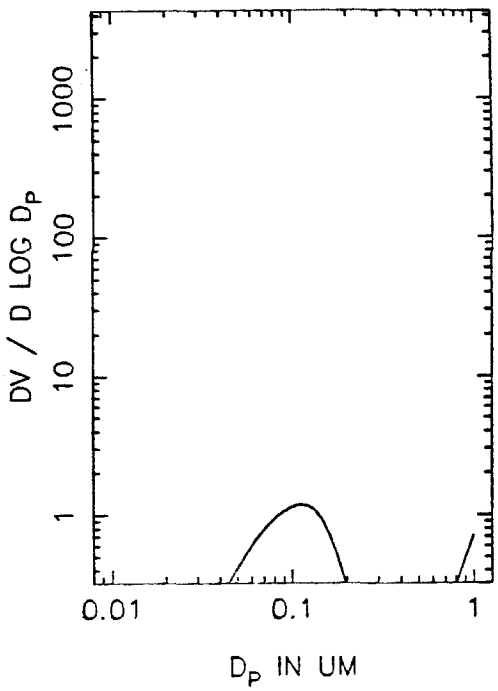

T=1.0 HOURS

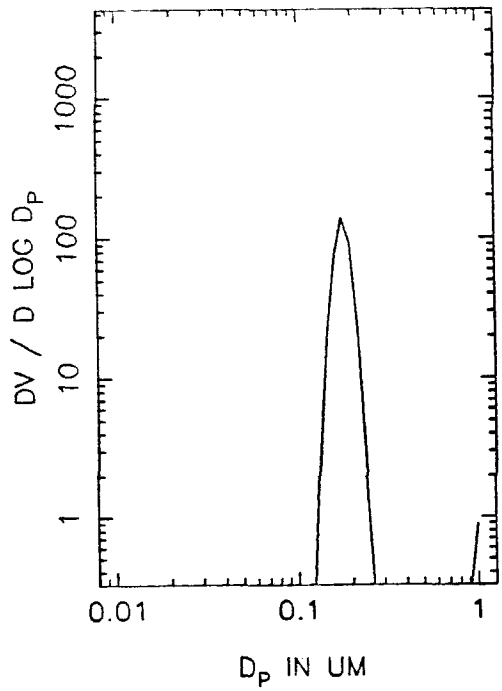

T=1.5 HOURS

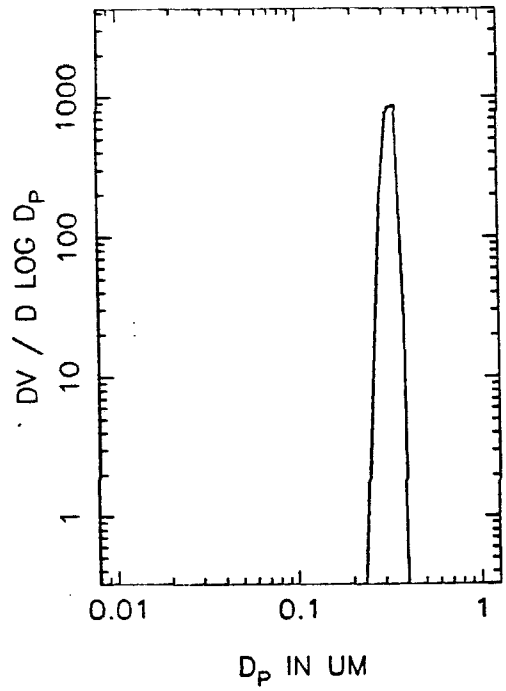

XJ34A VOLUME DISTRIBUTION, T=2.0

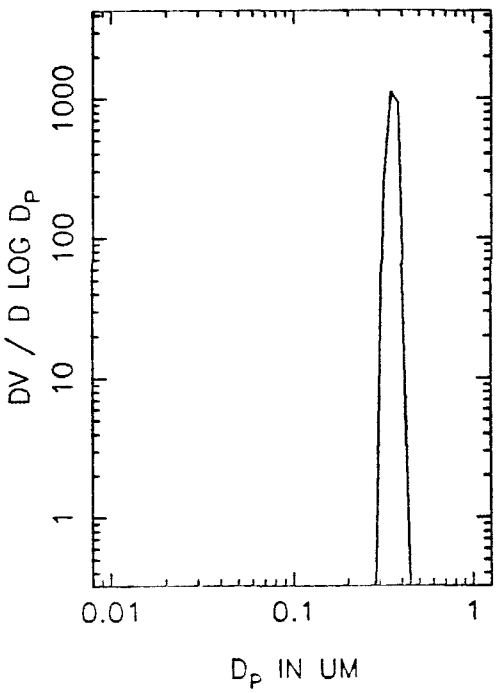

T=2.5 HOURS

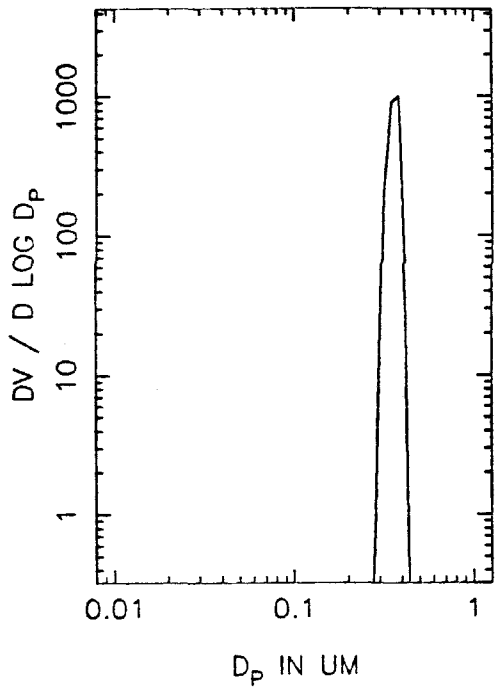

T=3.0 HOURS

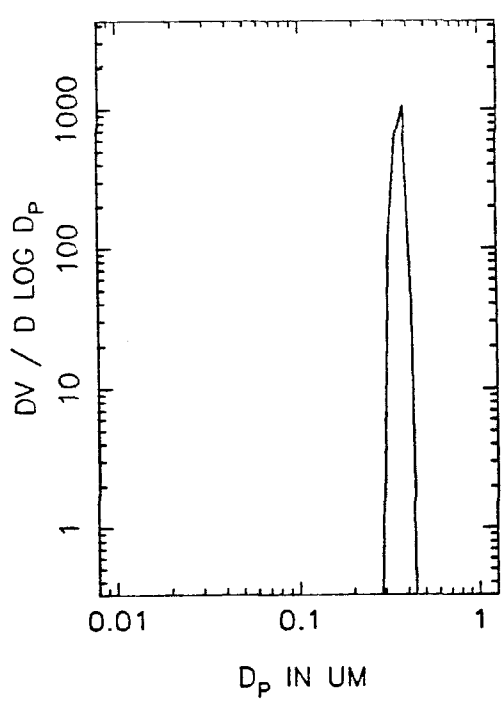

T=3.5 HOURS

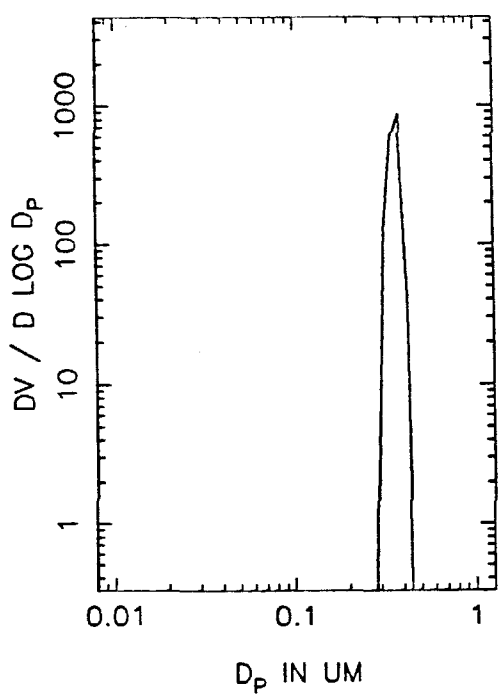

XJ34A VOLUME DISTRIBUTION, T=4.0

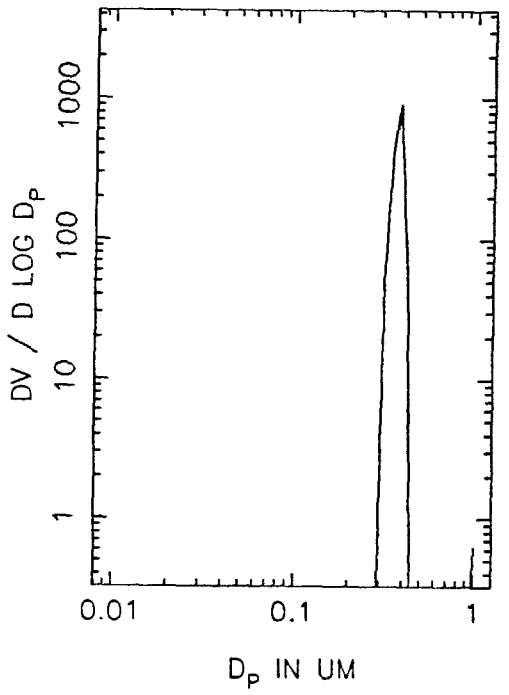

XJ34B NUMBER DISTRIBUTION, T=0

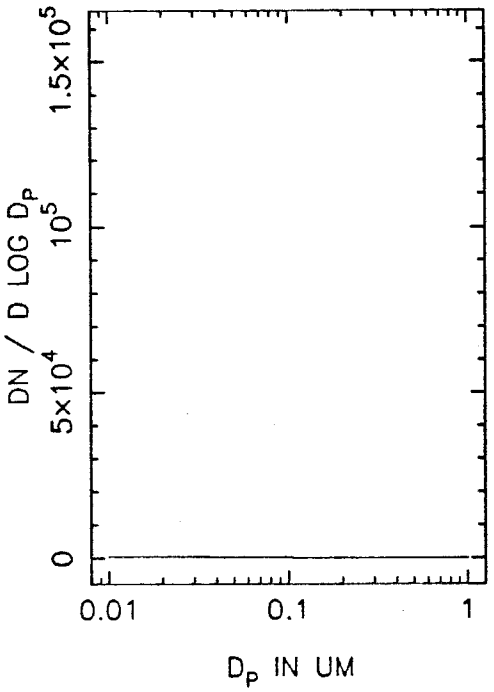

T=0.5 HOURS

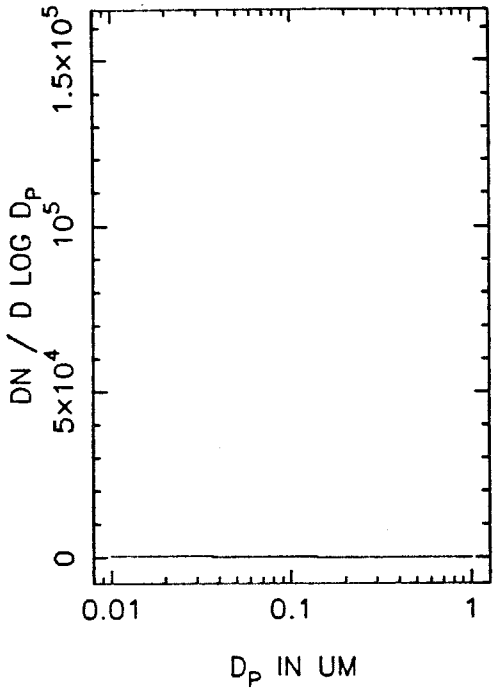

T=1.0 HOURS

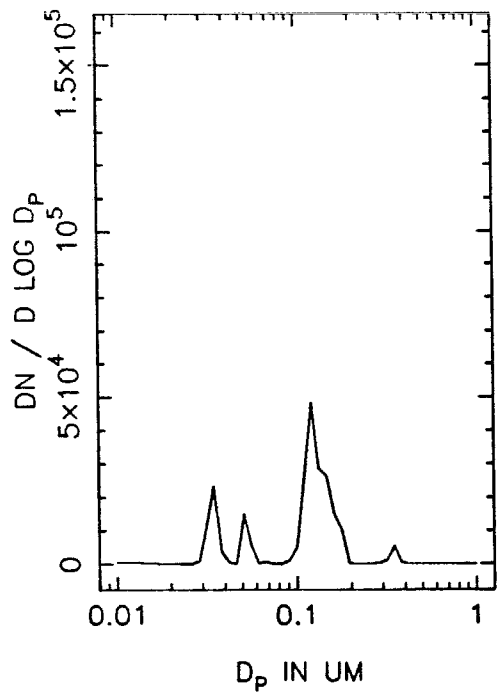

T=1.5 HOURS

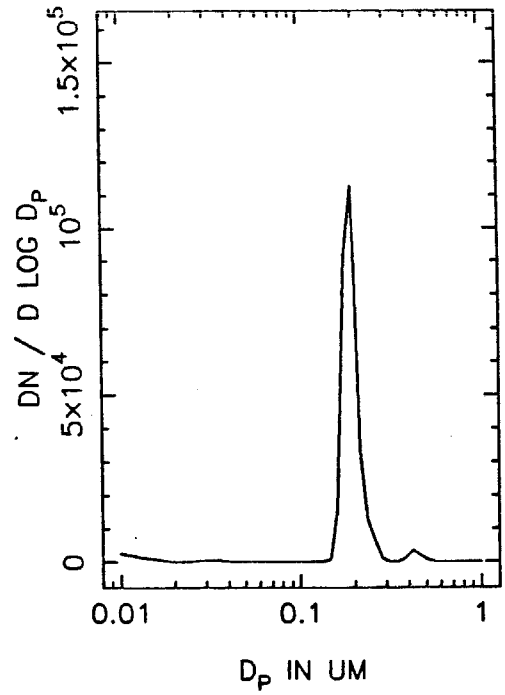

XJ34B NUMBER DISTRIBUTION, T=2.0

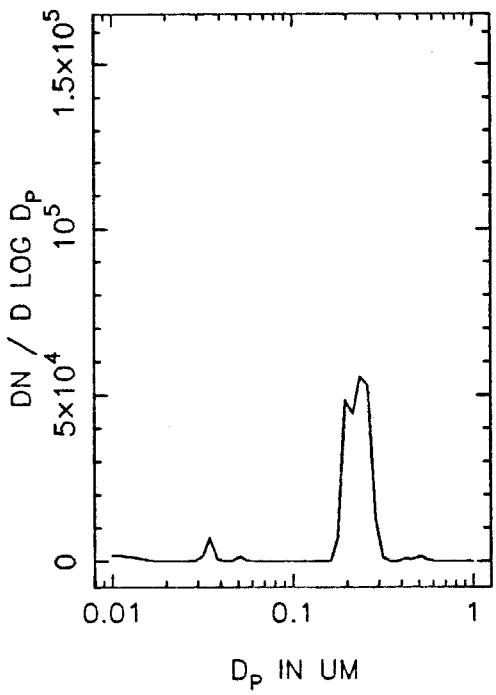

T=2.5 HOURS

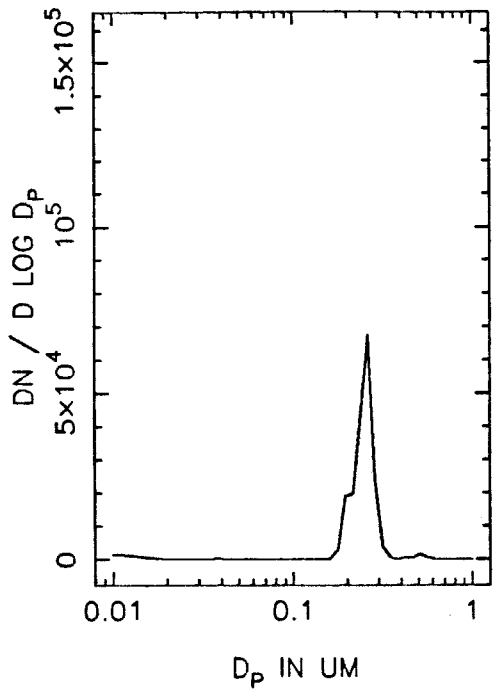

T=3.0 HOURS

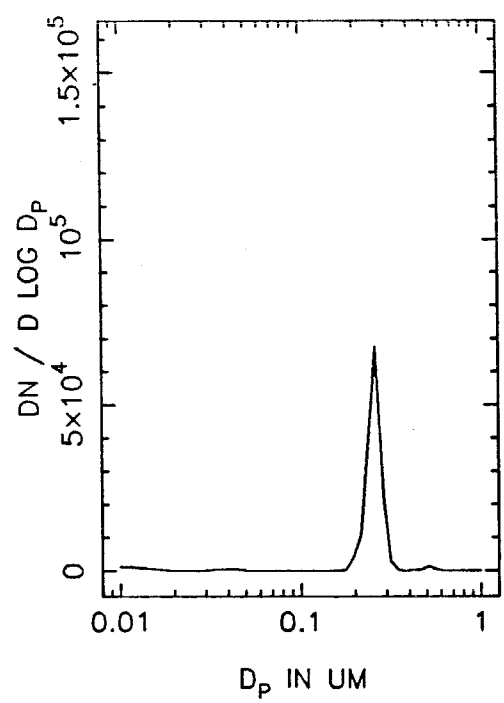

T=3.5 HOURS

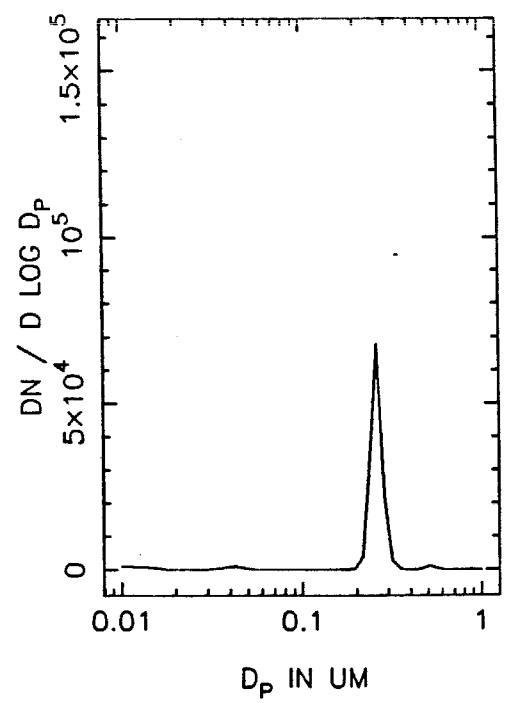

XJ34B VOLUME DISTRIBUTION, T=0

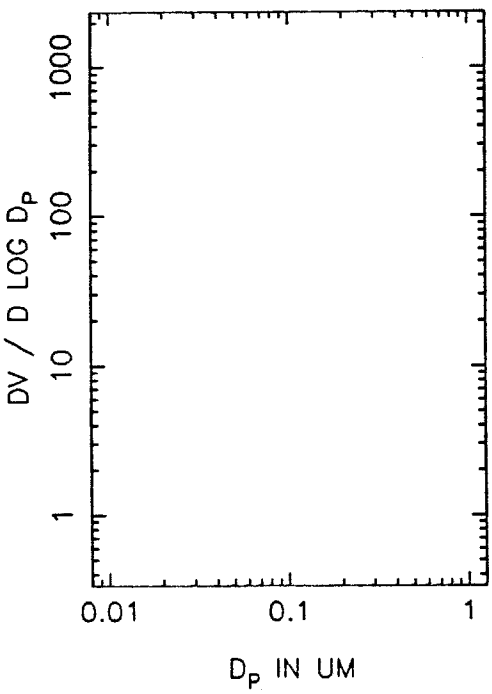

T=0.5 HOURS

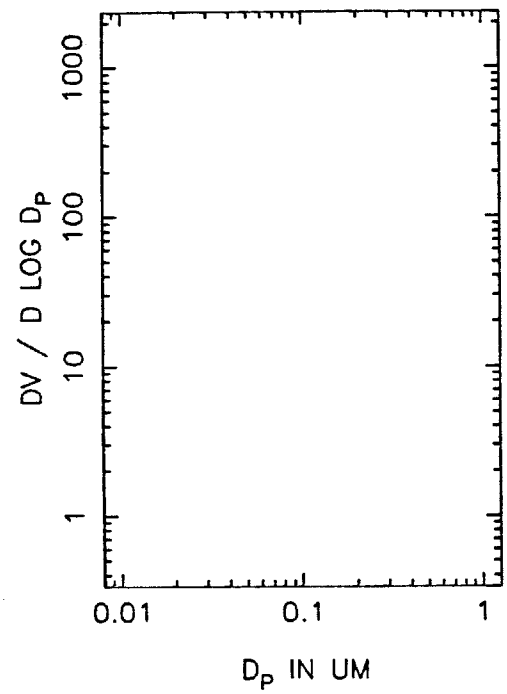

T=1.0 HOURS

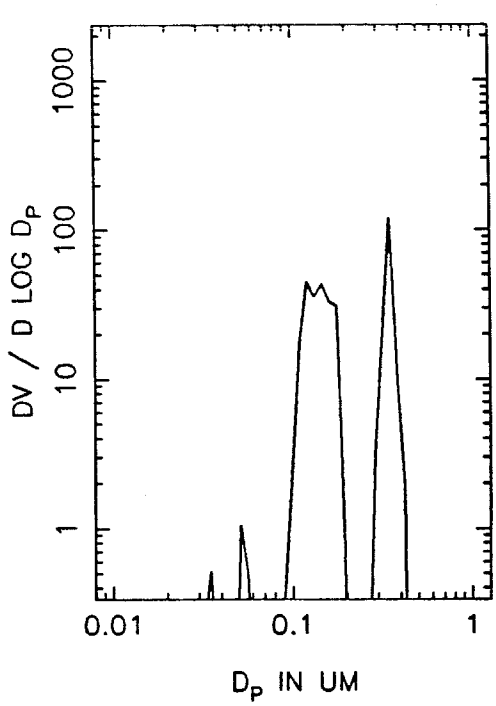

T=1.5 HOURS

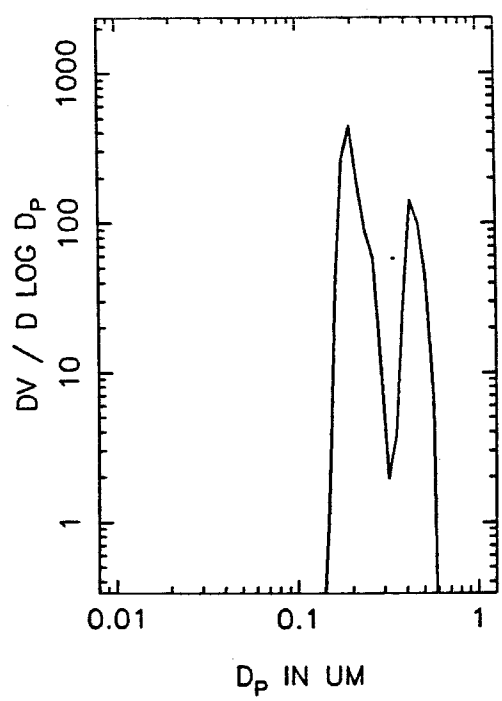

XJ34B VOLUME DISTRIBUTION, T=2.0

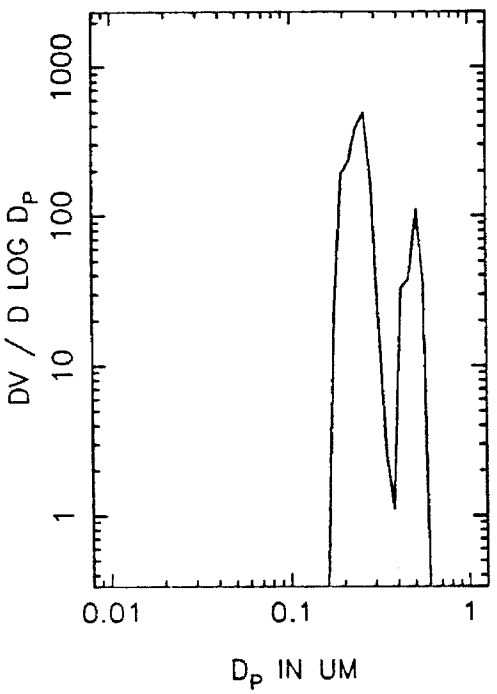

T=2.5 HOURS

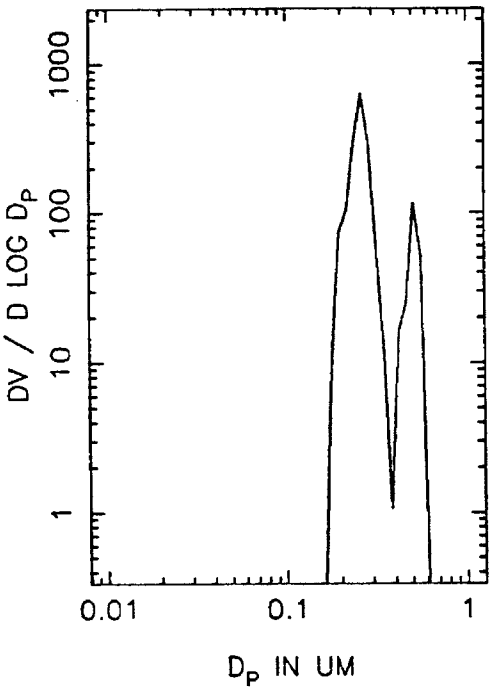

T=3.0 HOURS

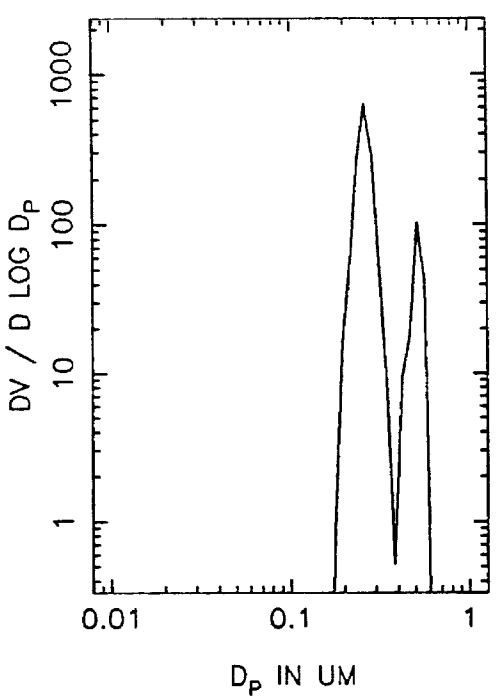

T=3.5 HOURS

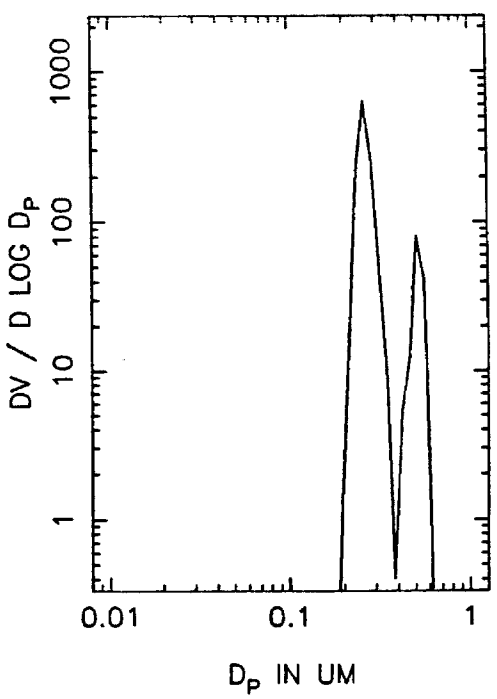

TE36 TOTAL NUMBER, SIDE A

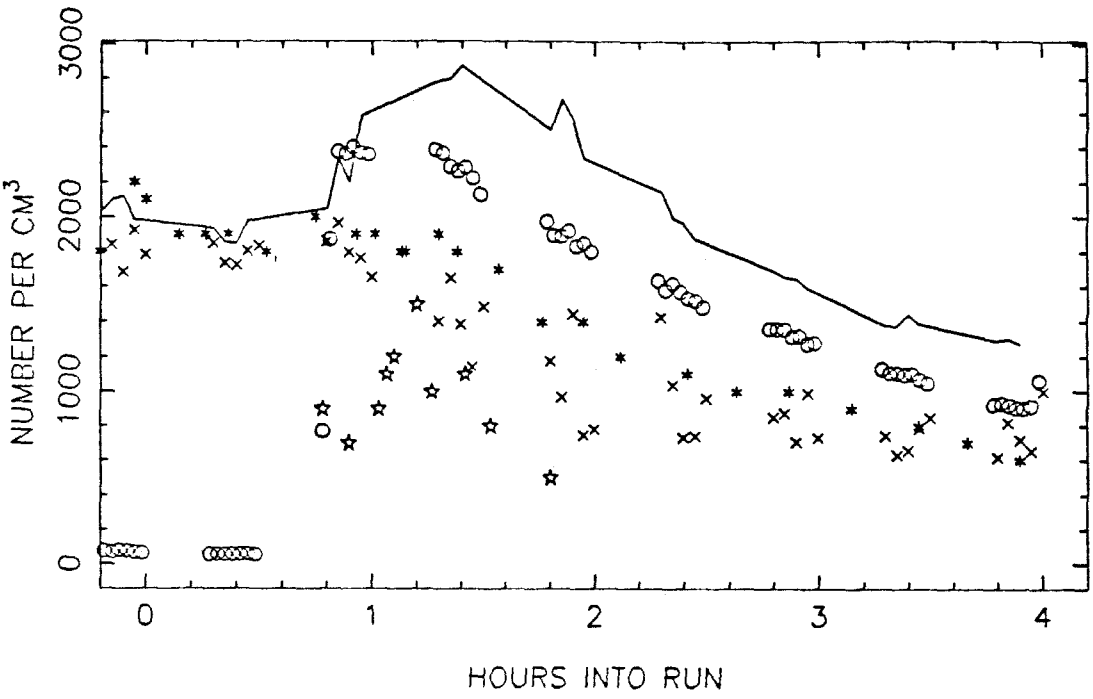

SIDE B

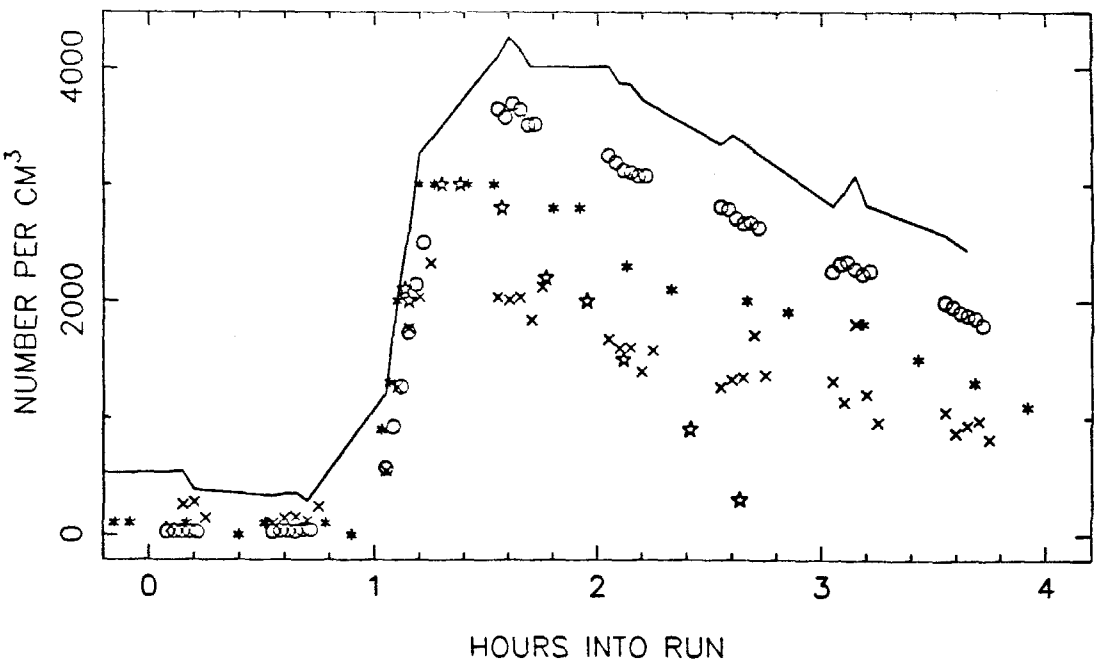

TE36 VOLUME IN THE AEROSOL PHASE, SIDE A

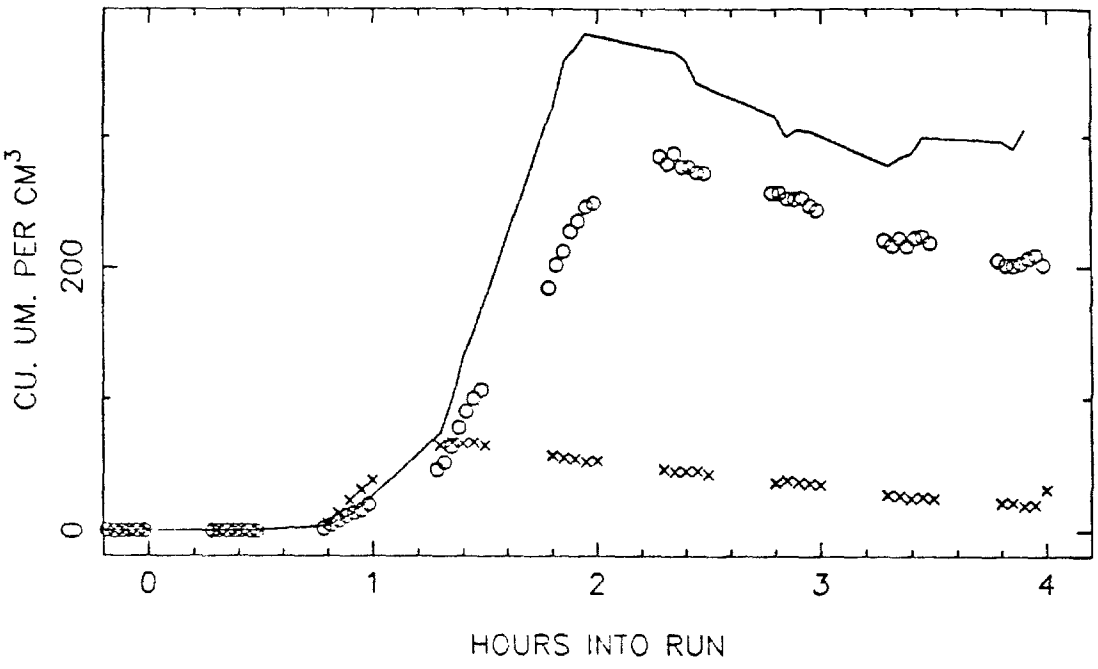

SIDE B

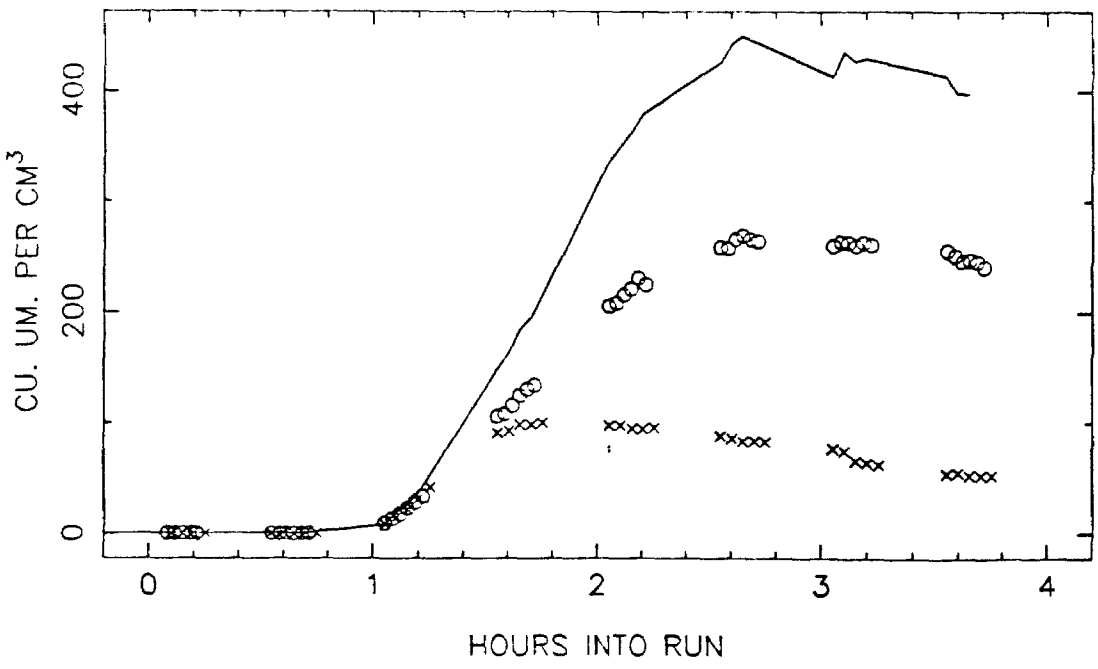

TE36 MEAN PARTICLE SIZE, SIDE A

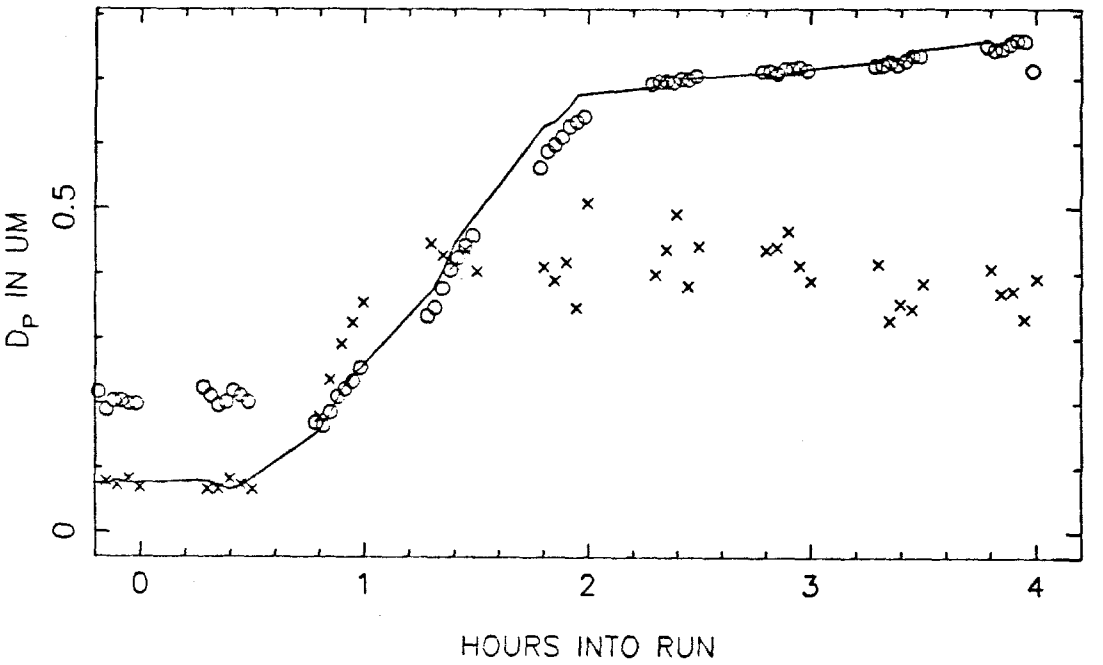

SIDE B

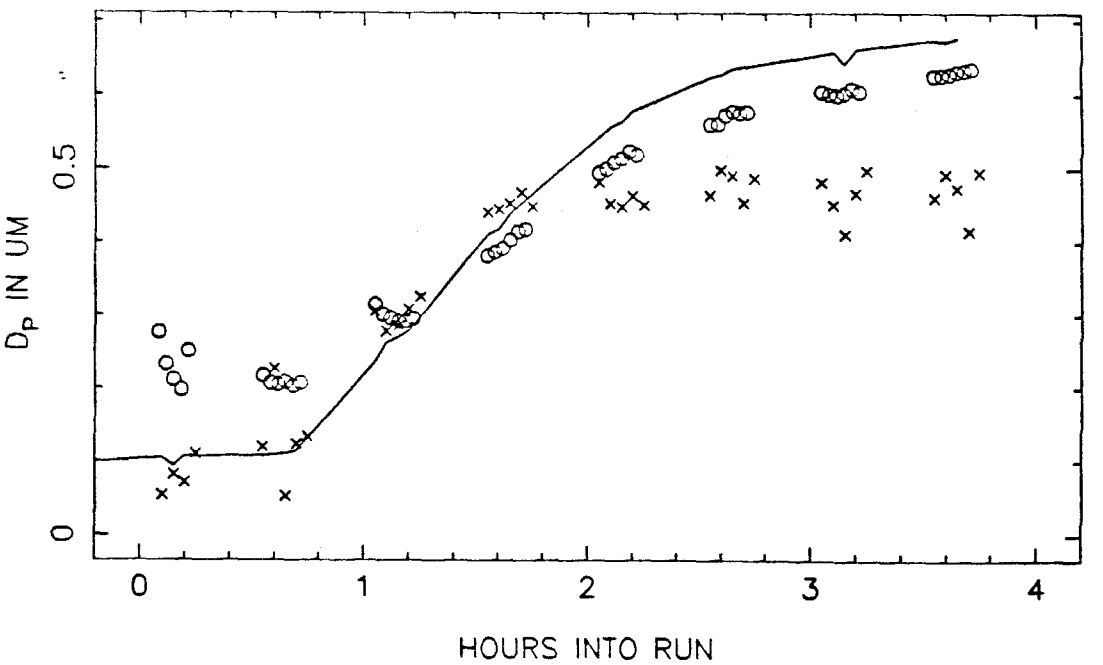

TE36A NUMBER DISTRIBUTION, T=0

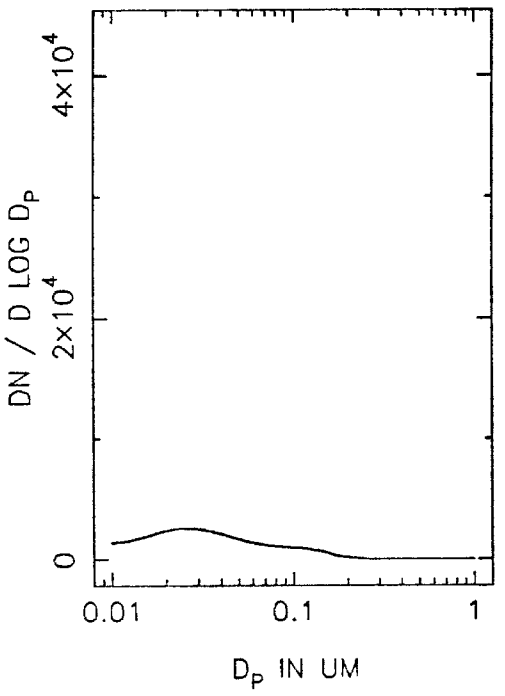

T=0.5 HOURS

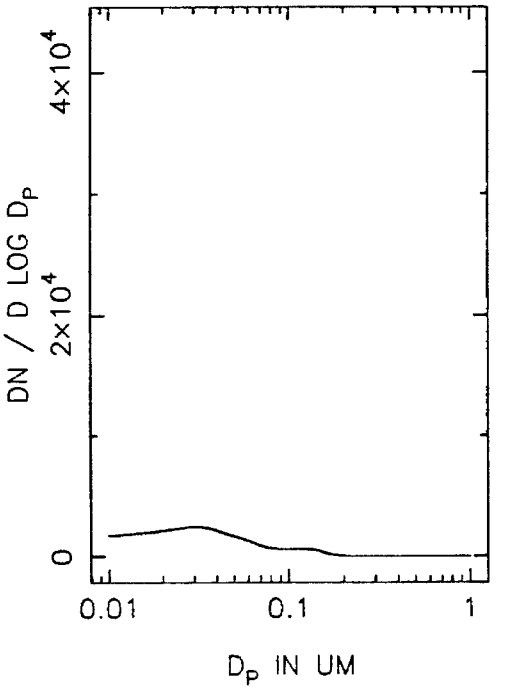

T=1.0 HOURS

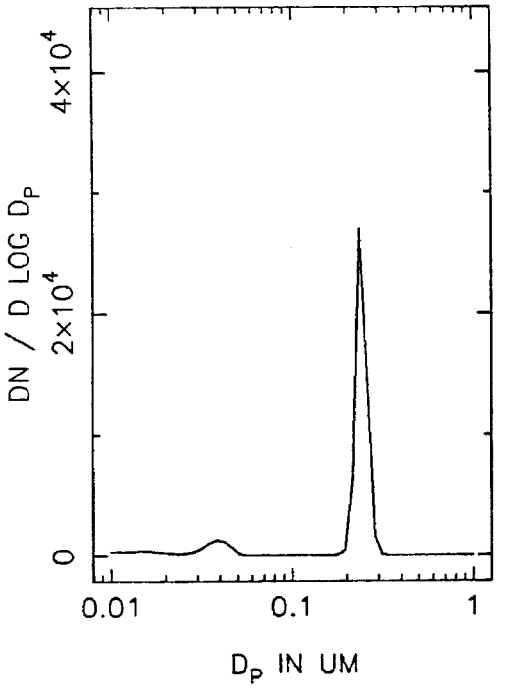

T=1.5 HOURS

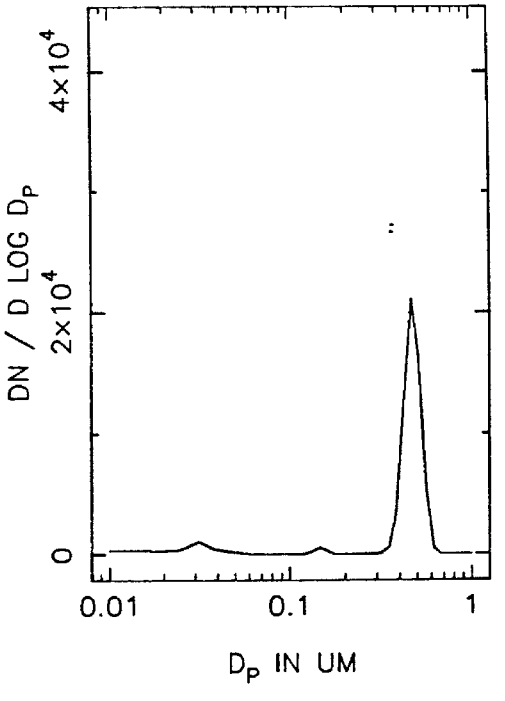

TE36A NUMBER DISTRIBUTION, T=2.0

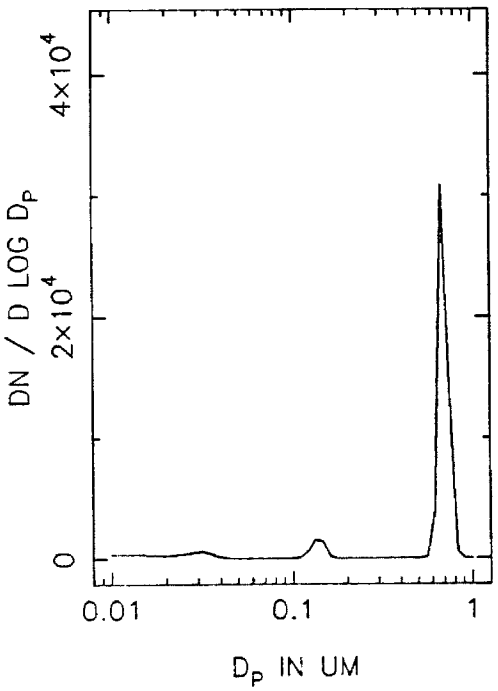

T=2.5 HOURS

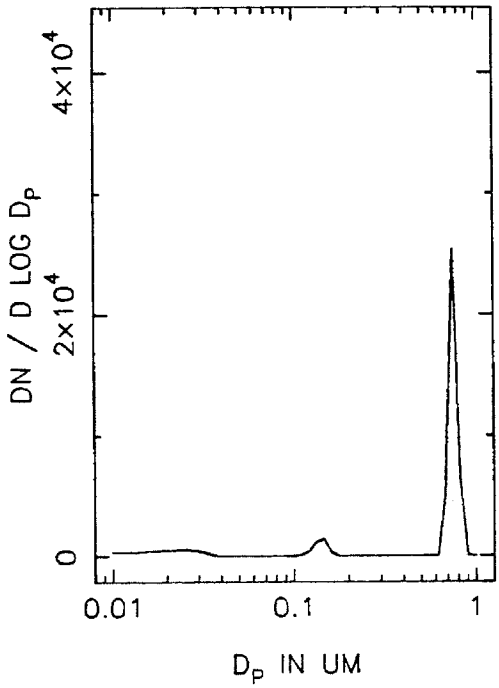

T=3.0 HOURS

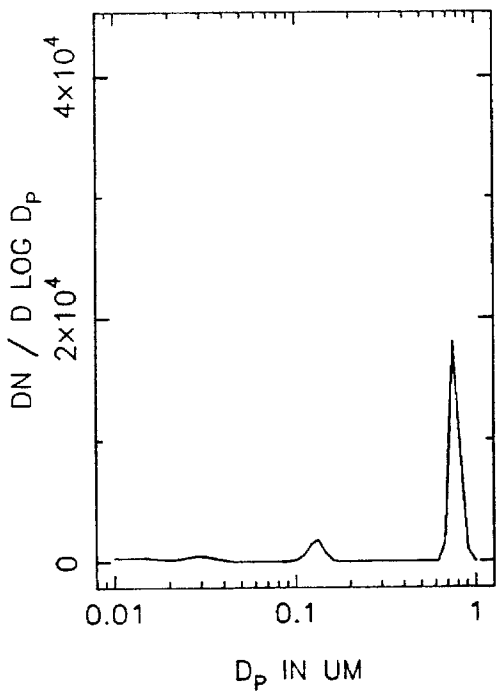

T=3.5 HOURS

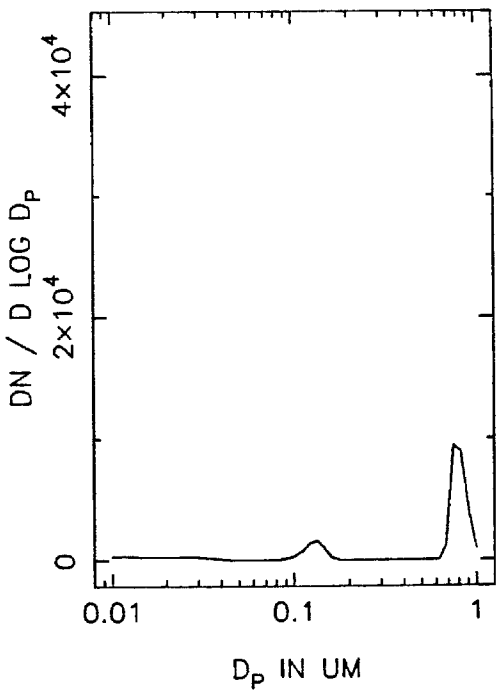

TE36A VOLUME DISTRIBUTION, T=0

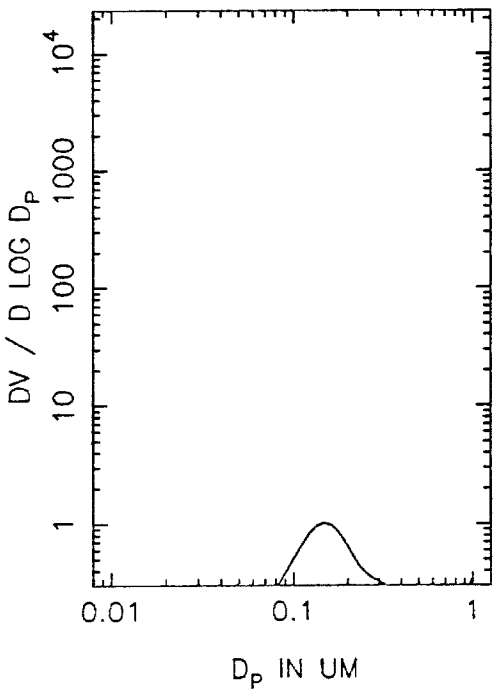

T=0.5 HOURS

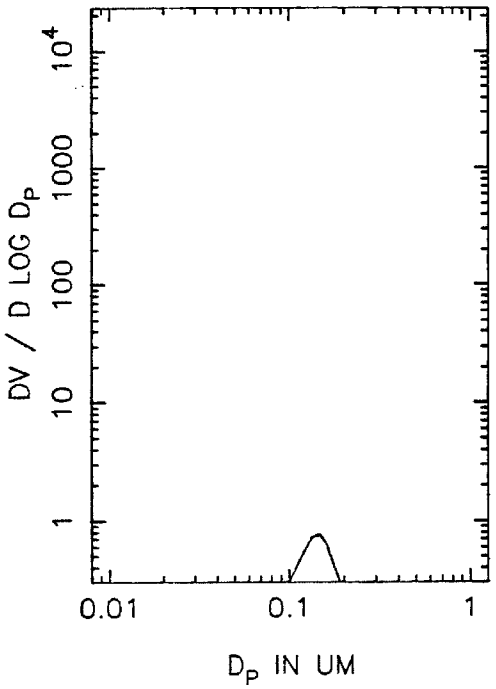

T=1.0 HOURS

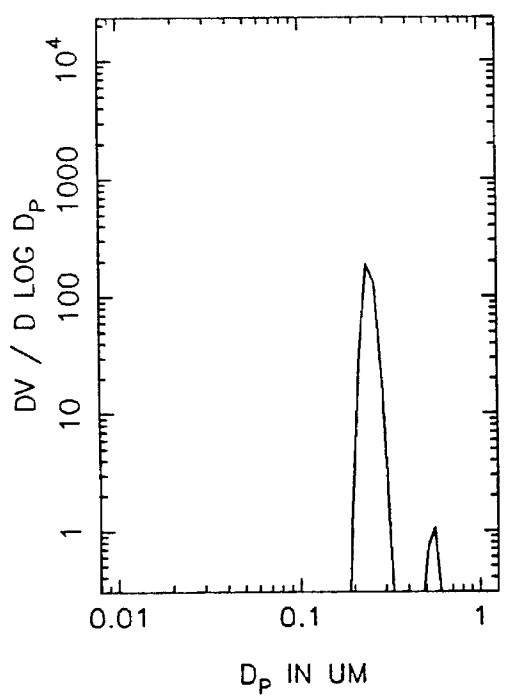

T=1.5 HOURS

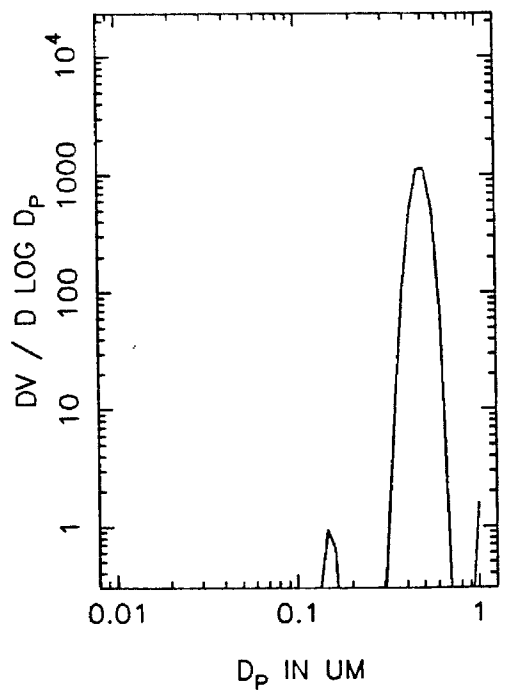

TE36A VOLUME DISTRIBUTION, T=2.0

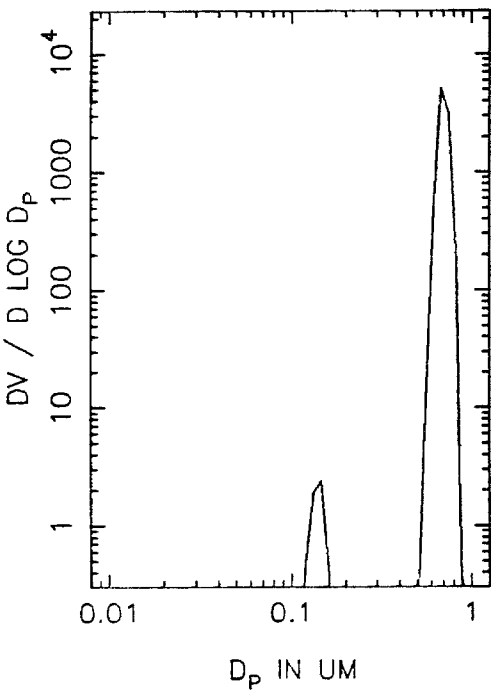

T=2.5 HOURS

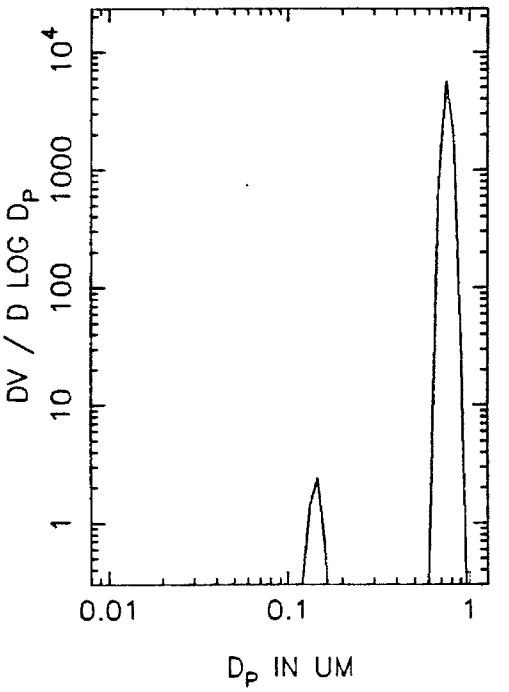

T=3.0 HOURS

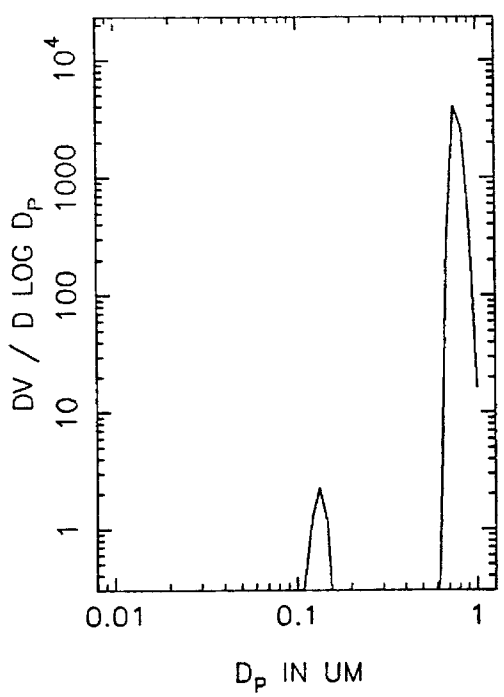

T=3.5 HOURS

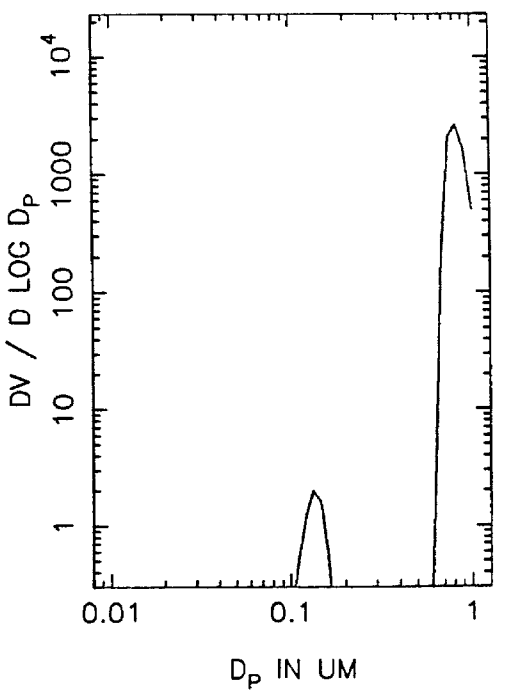

TE36B NUMBER DISTRIBUTION, T=0

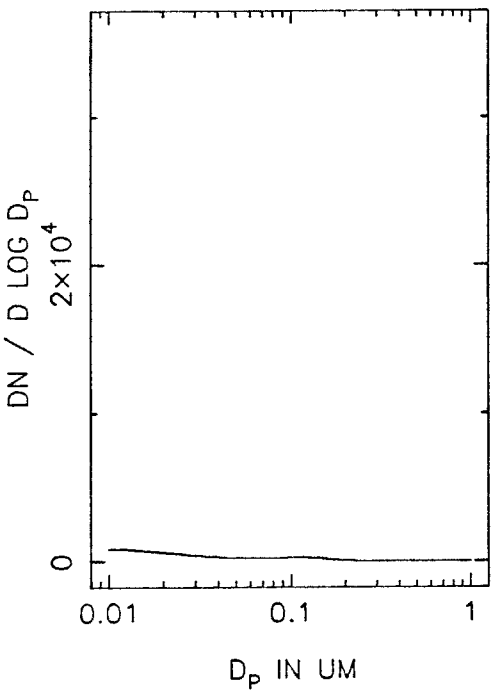

T=0.5 HOURS

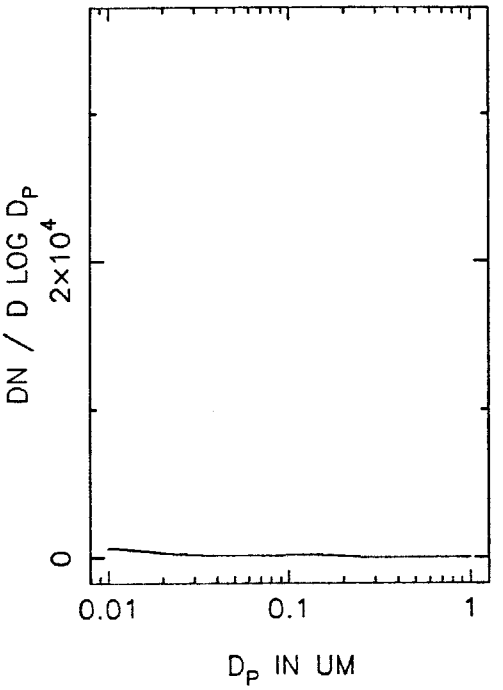

T=1.0 HOURS

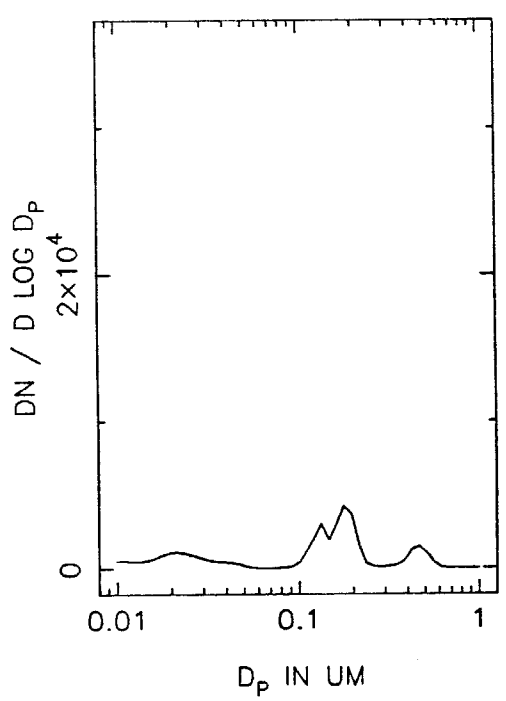

T=1.5 HOURS

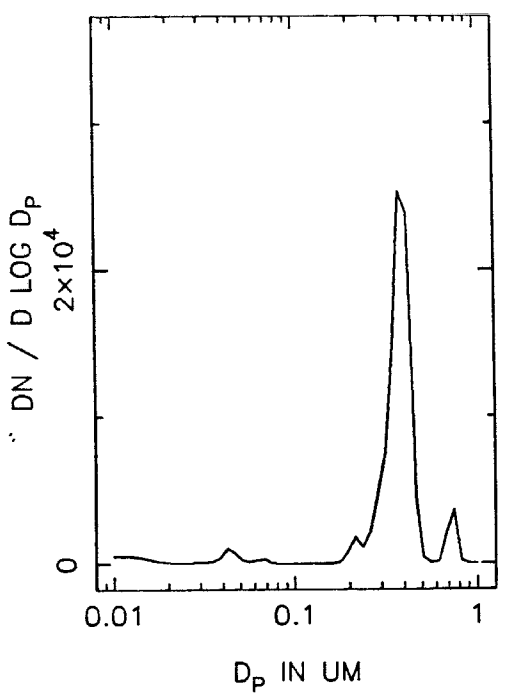

TE36B NUMBER DISTRIBUTION, T=2.0

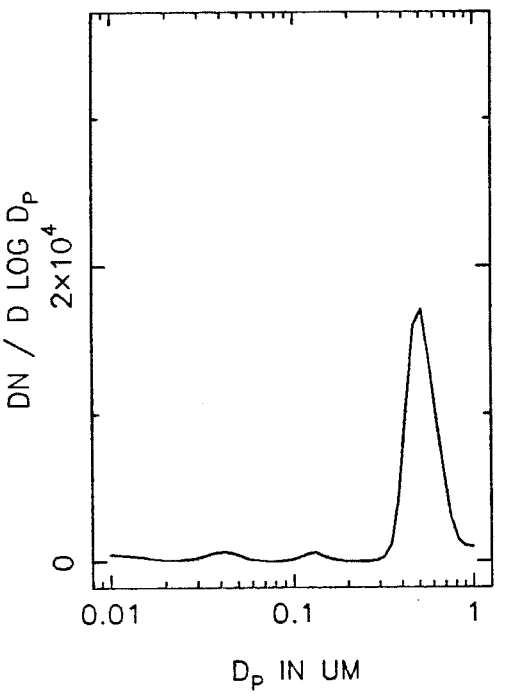

T=2.5 HOURS

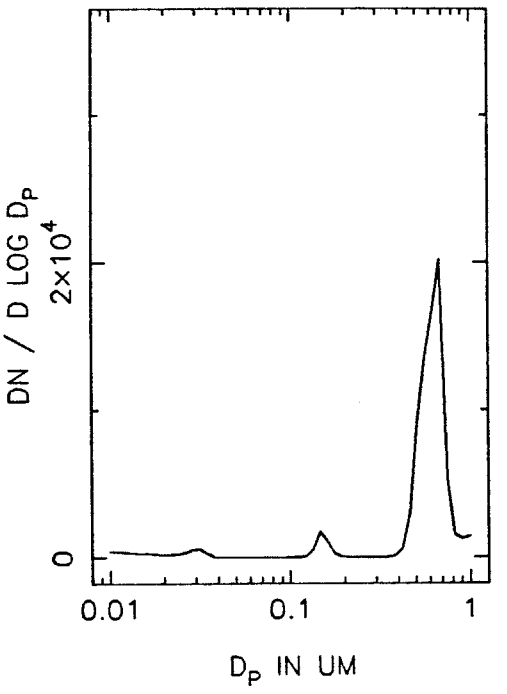

T=3.0 HOURS

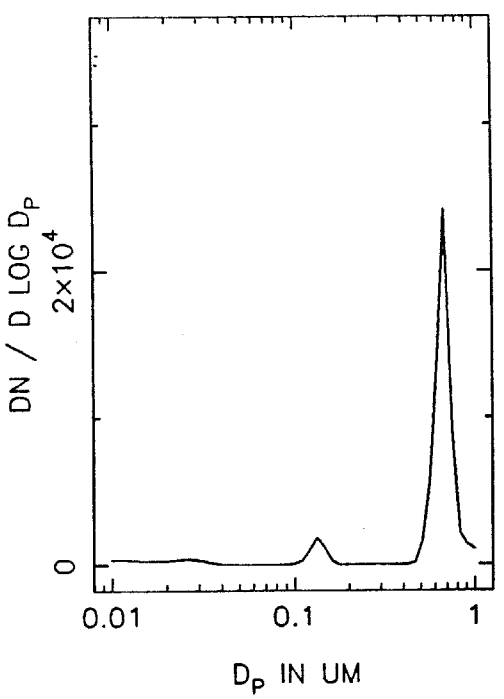

T=3.5 HOURS

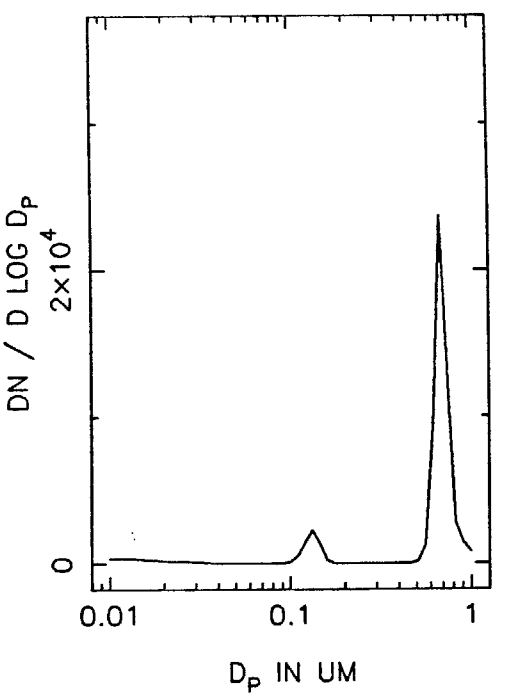

TE36B VOLUME DISTRIBUTION, T=0

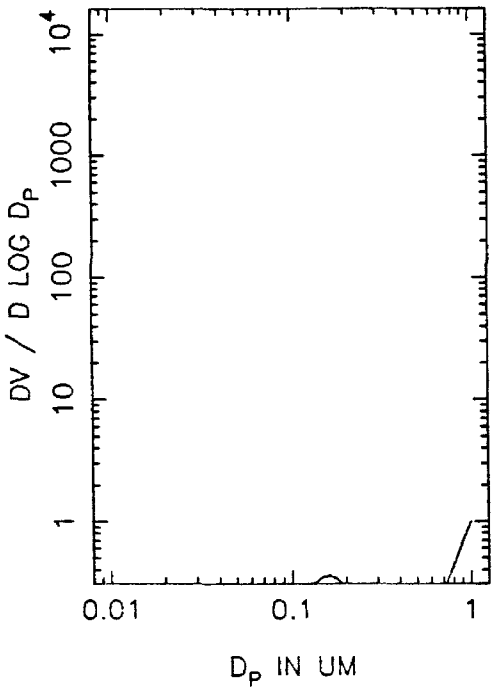

T=0.5 HOURS

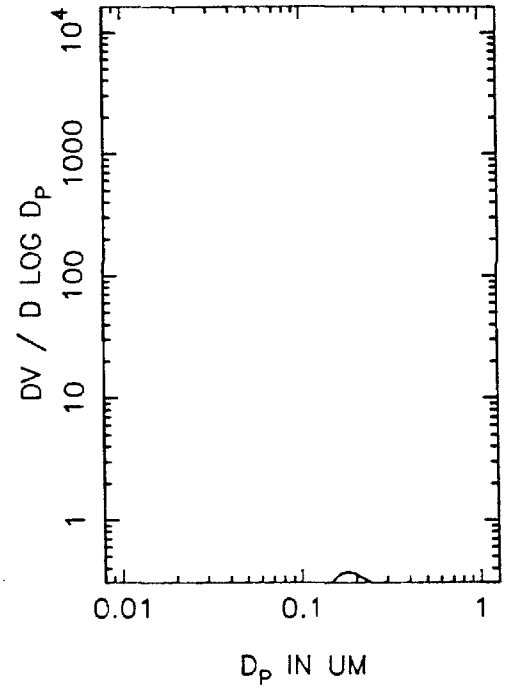

T=1.0 HOURS

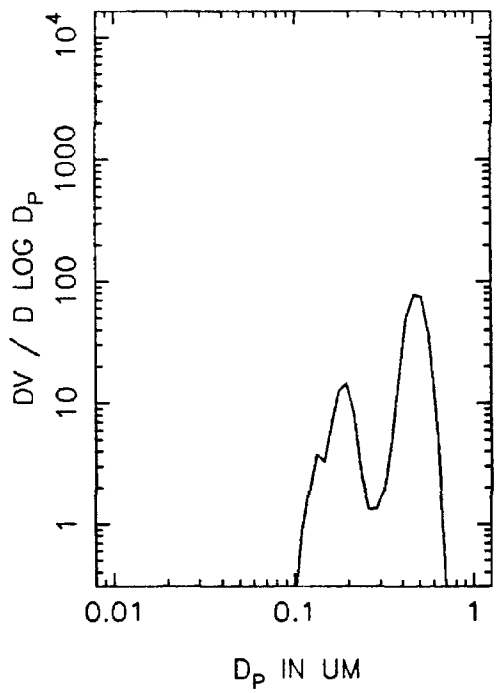

T=1.5 HOURS

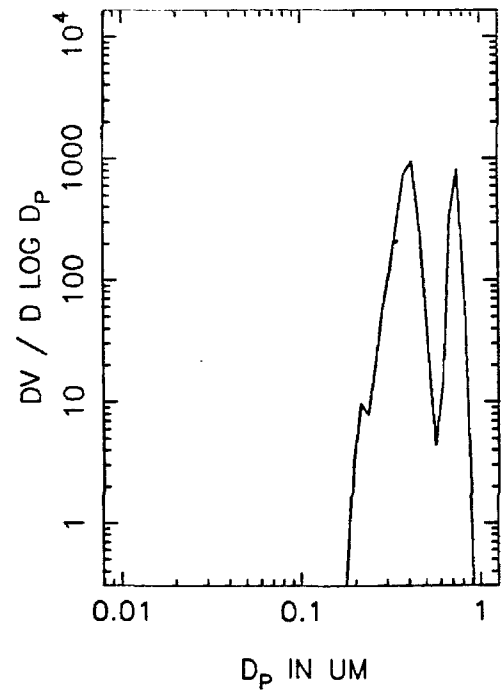

TE36B VOLUME DISTRIBUTION, T=2.0

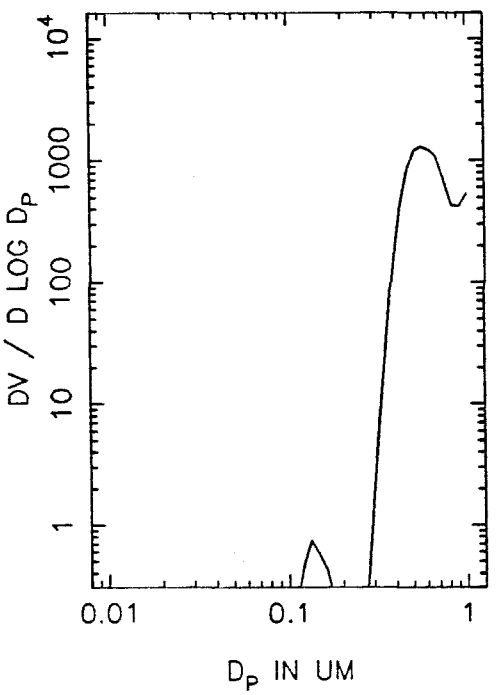

T=2.5 HOURS

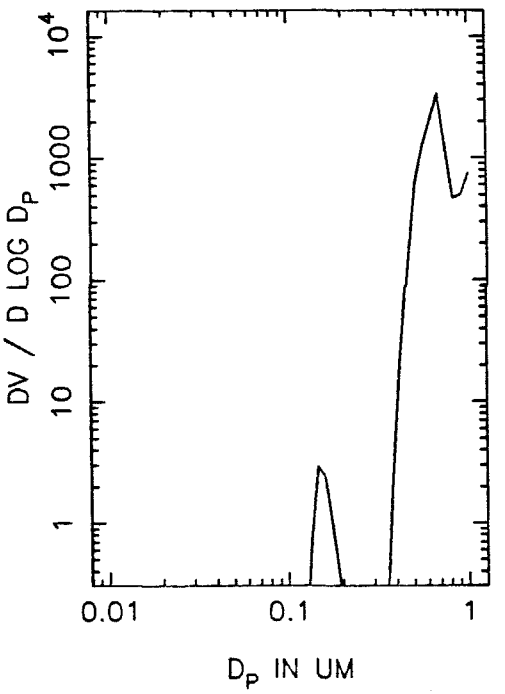

T=3.0 HOURS

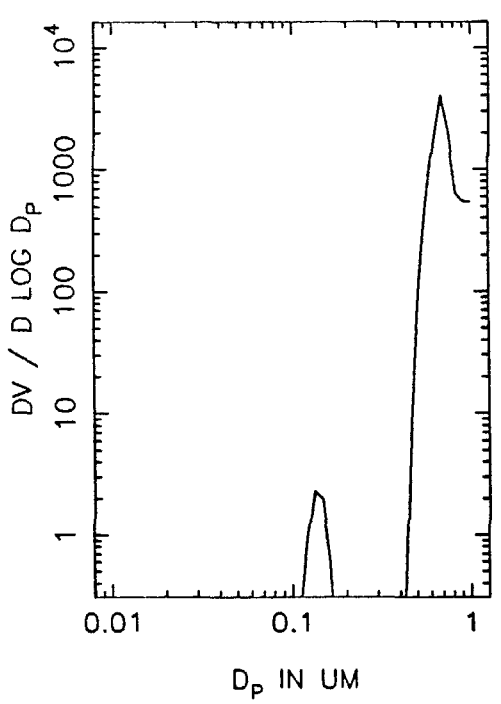

T=3.5 HOURS

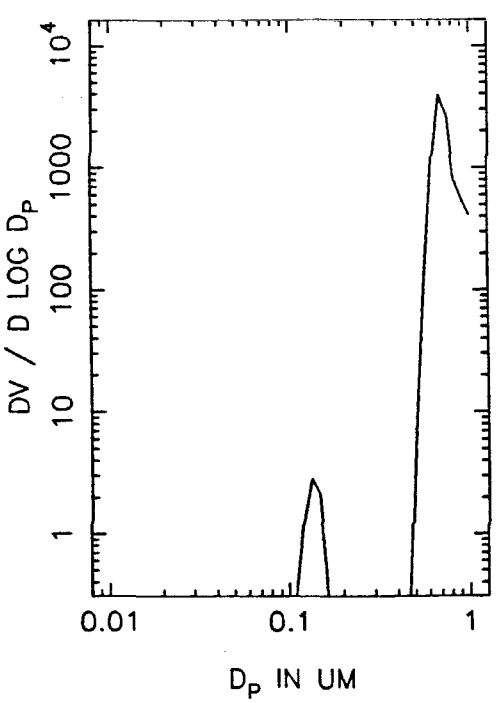

TE39 TOTAL NUMBER, SIDE A

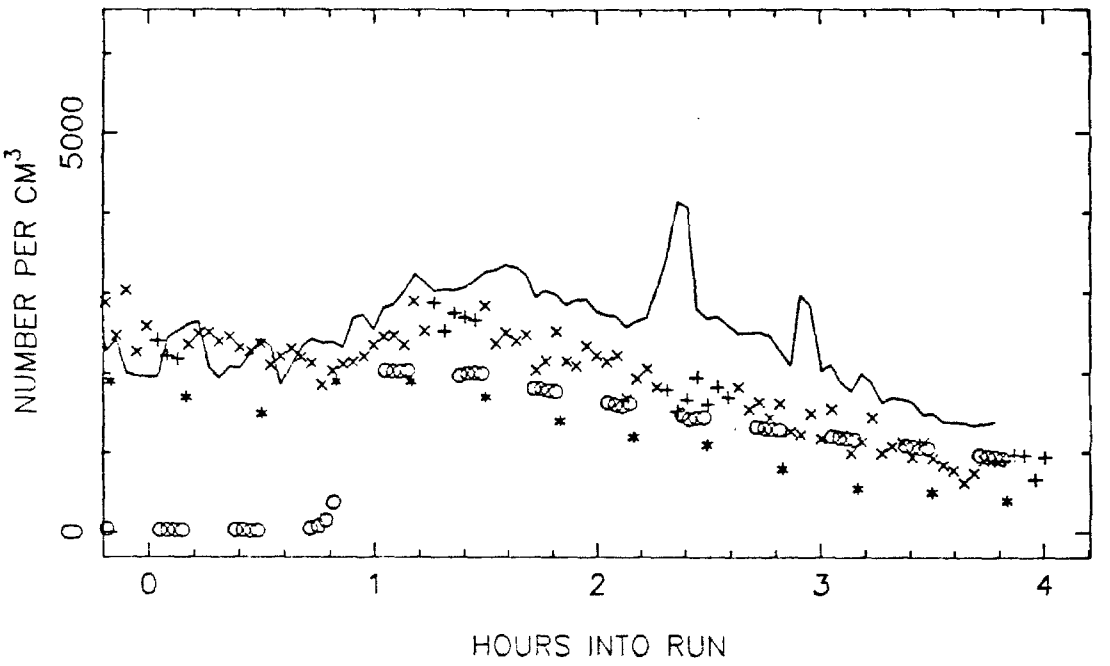

SIDE B

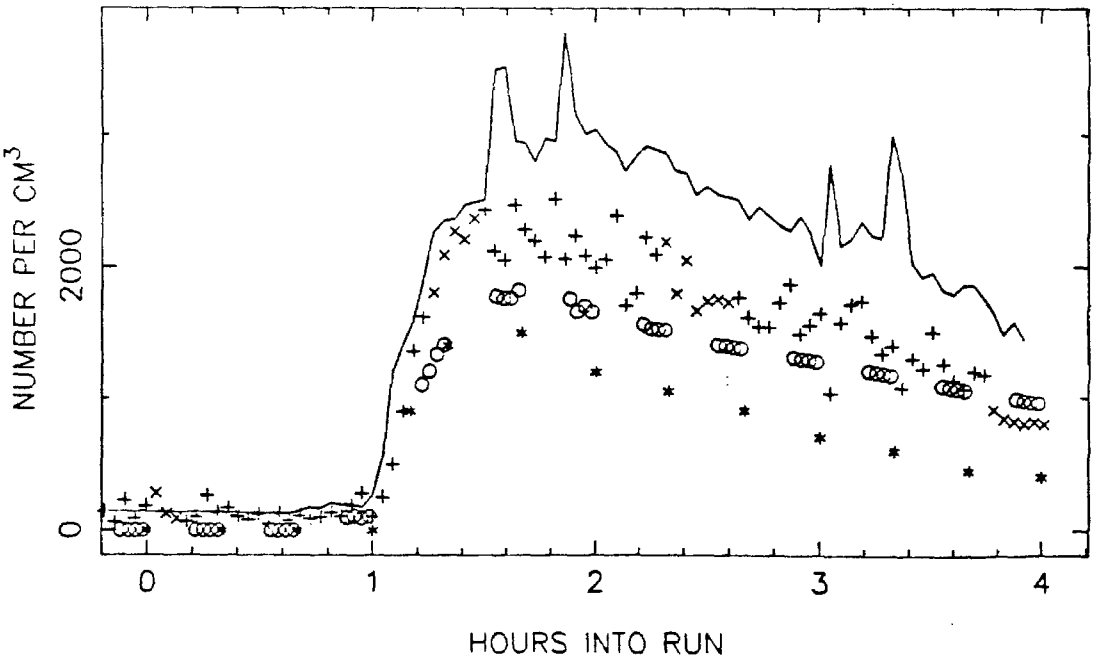

TE39 VOLUME IN THE AEROSOL PHASE, SIDE A

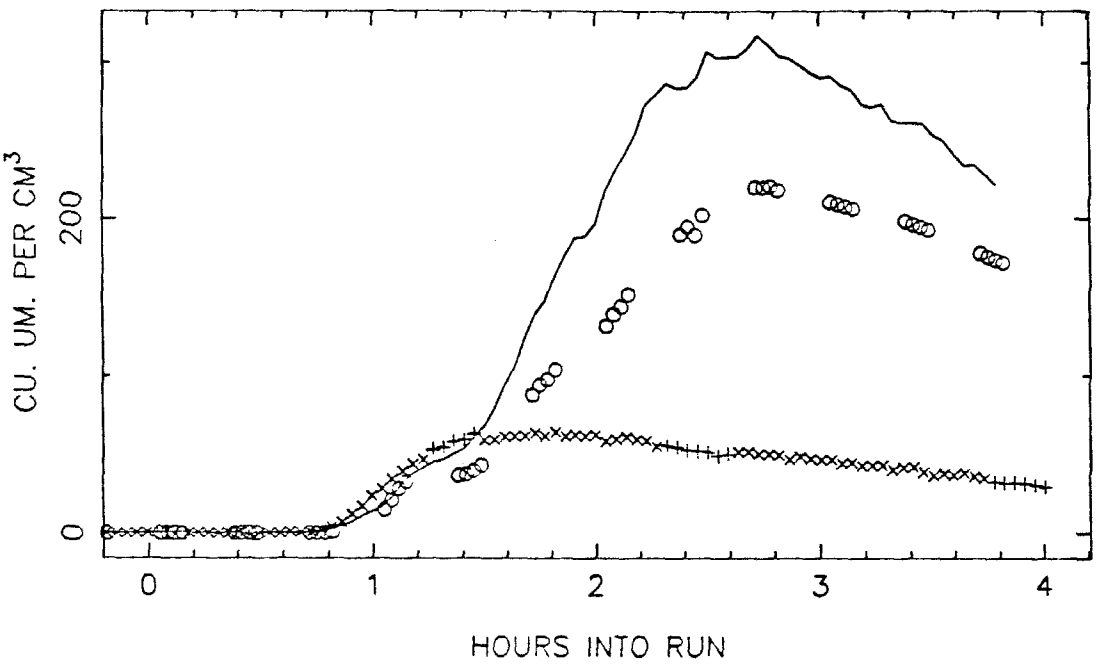

SIDE B

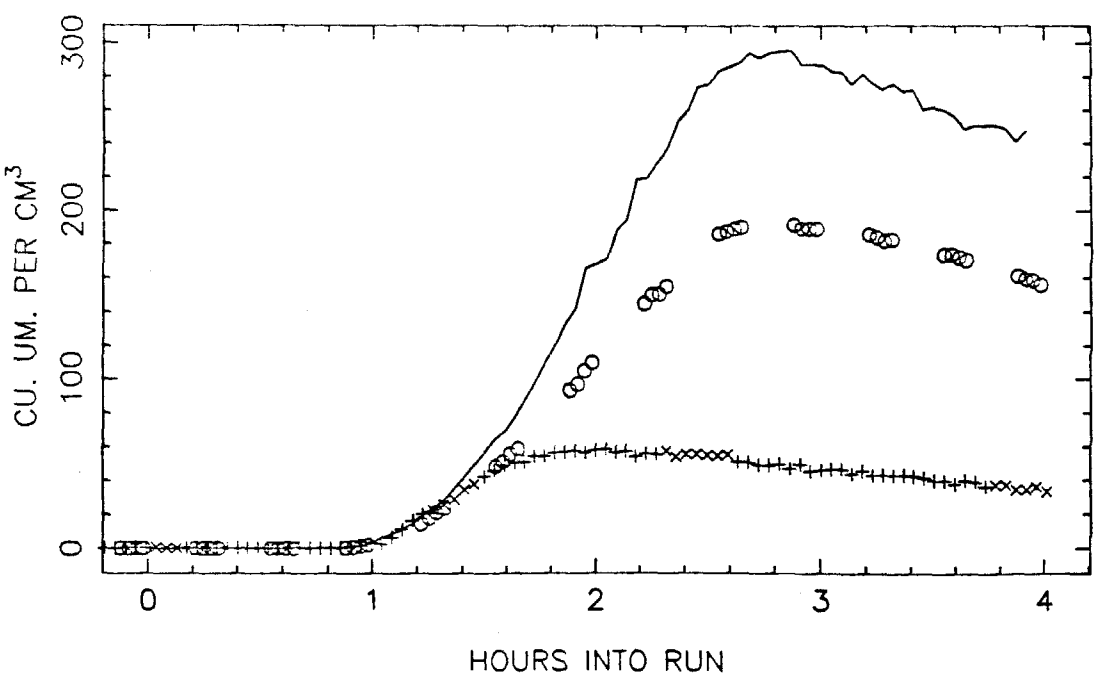

TE39 MEAN PARTICLE SIZE, SIDE A

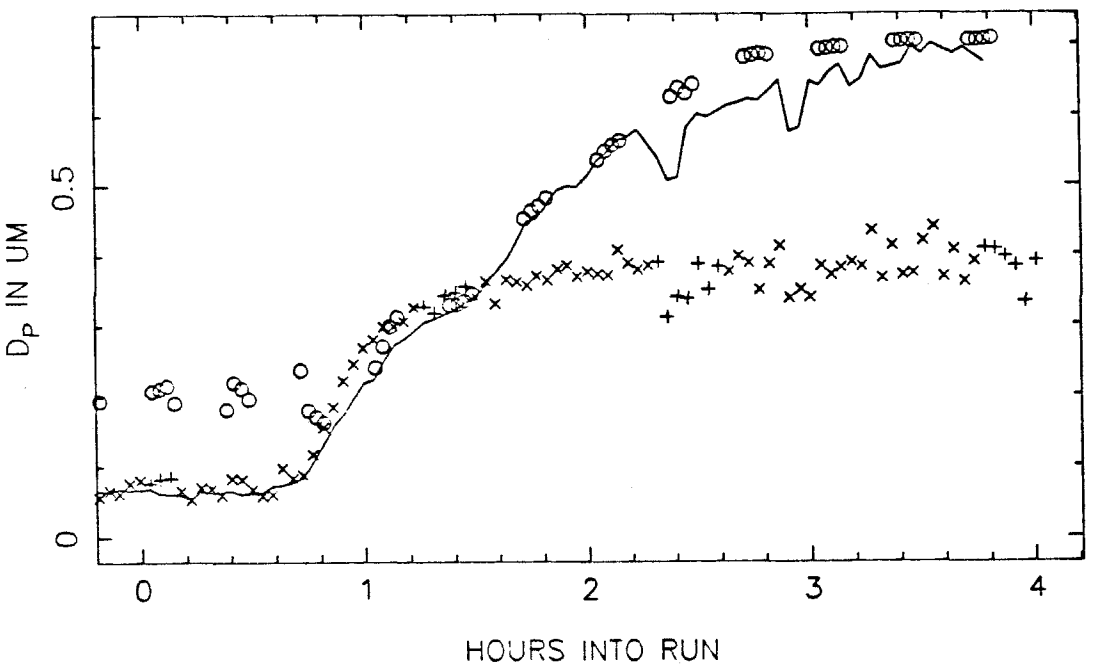

SIDE B

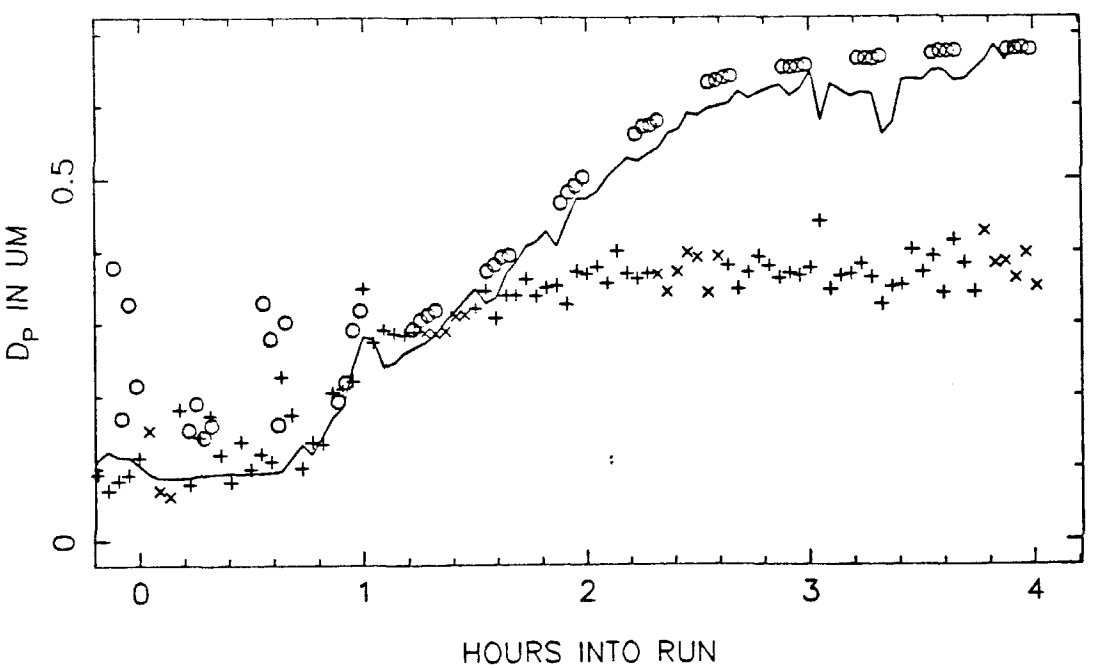

TE39A NUMBER DISTRIBUTION, T=0

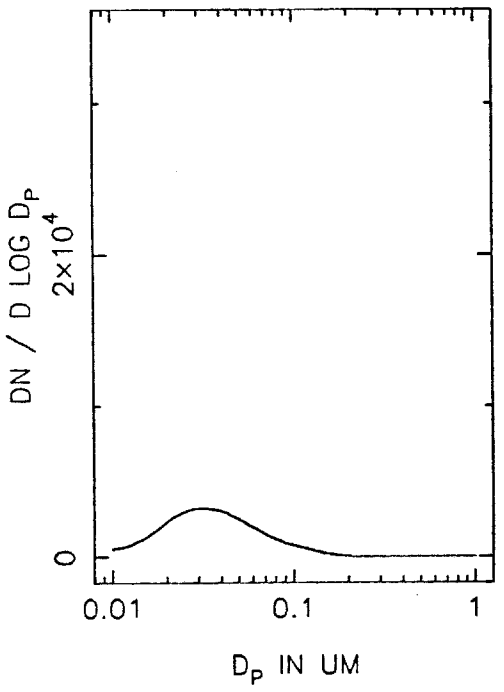

T=0.5 HOURS

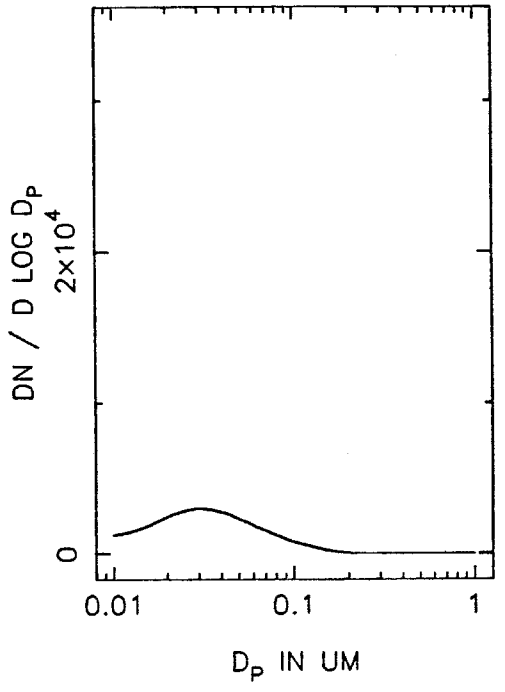

T=1.0 HOURS

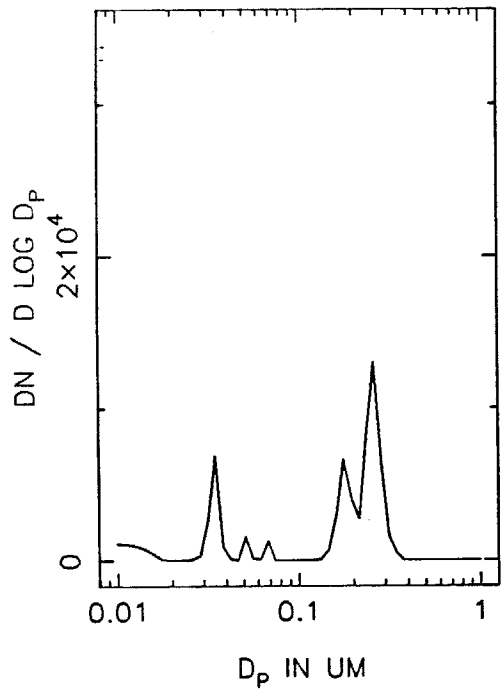

T=1.5 HOURS

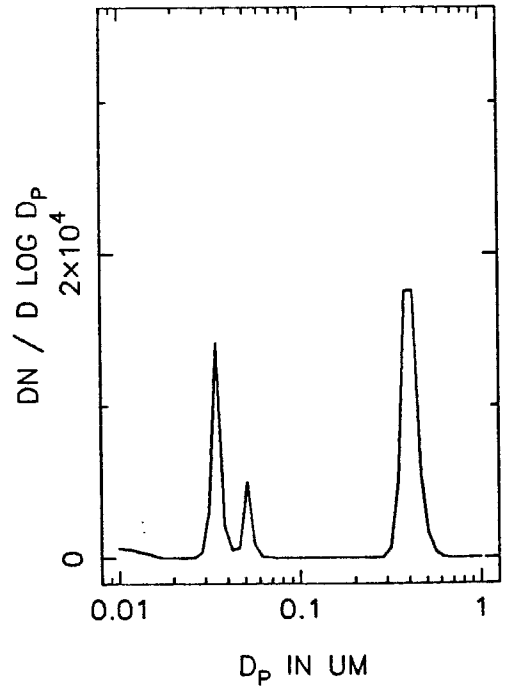

TE39A NUMBER DISTRIBUTION, T=2.0

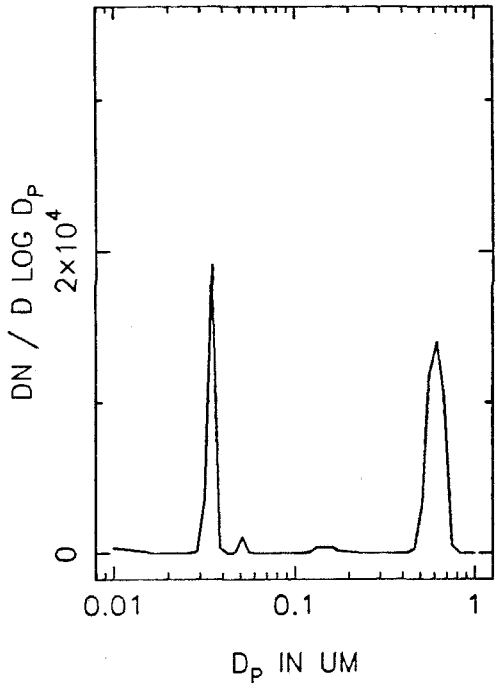

T=2.5 HOURS

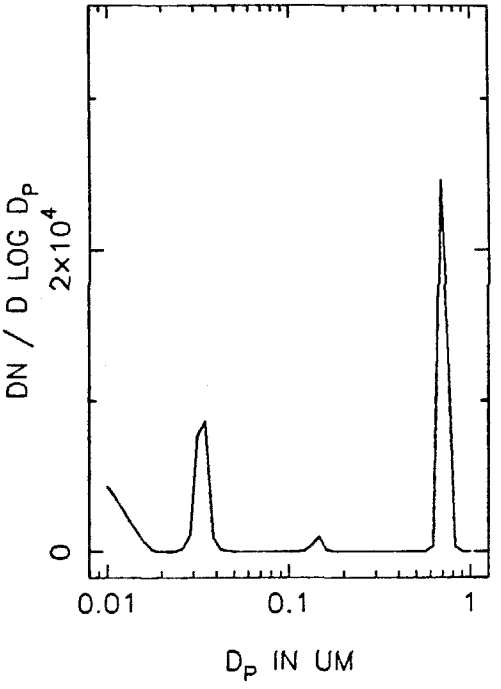

T=3.0 HOURS

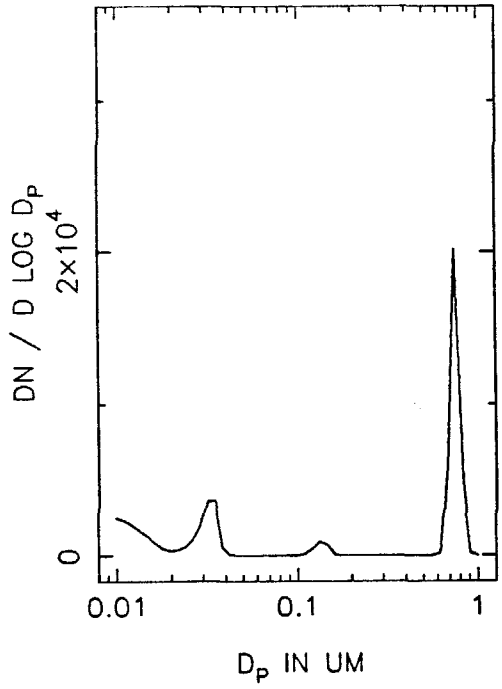

T=3.5 HOURS

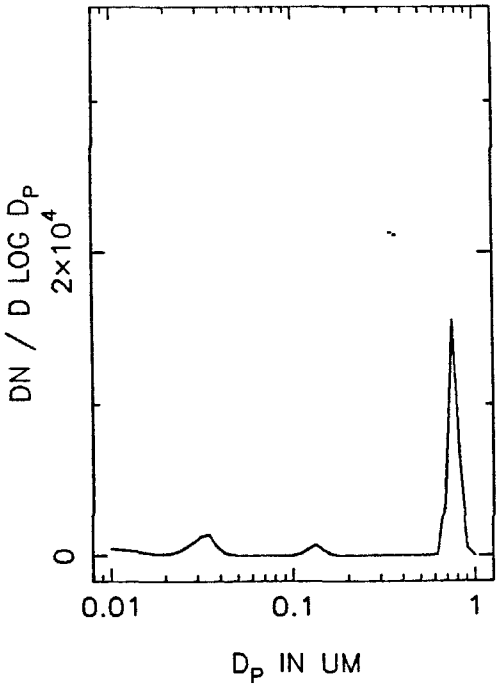

TE39A VOLUME DISTRIBUTION, T=0

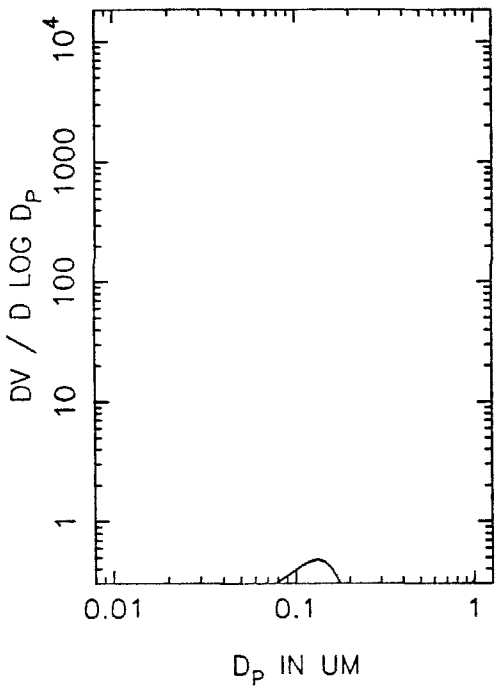

T=0.5 HOURS

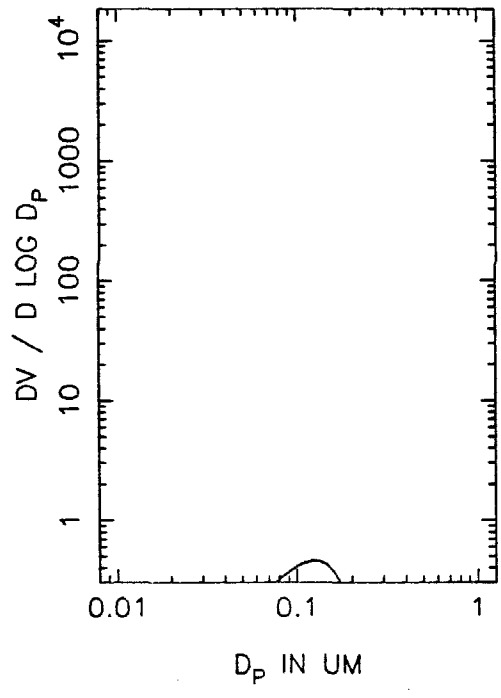

T=1.0 HOURS

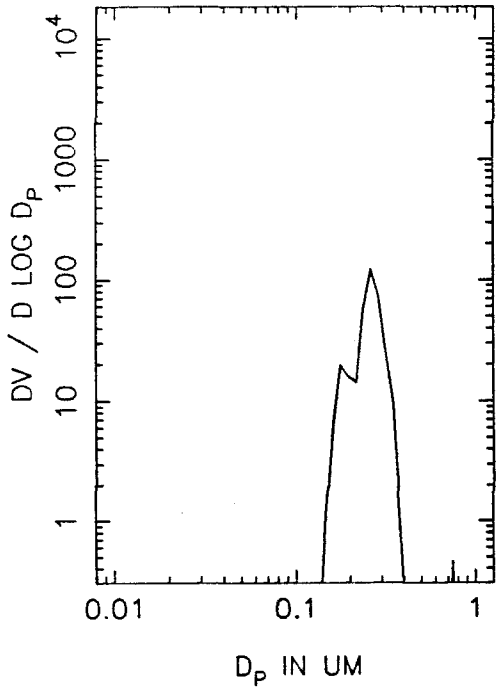

T=1.5 HOURS

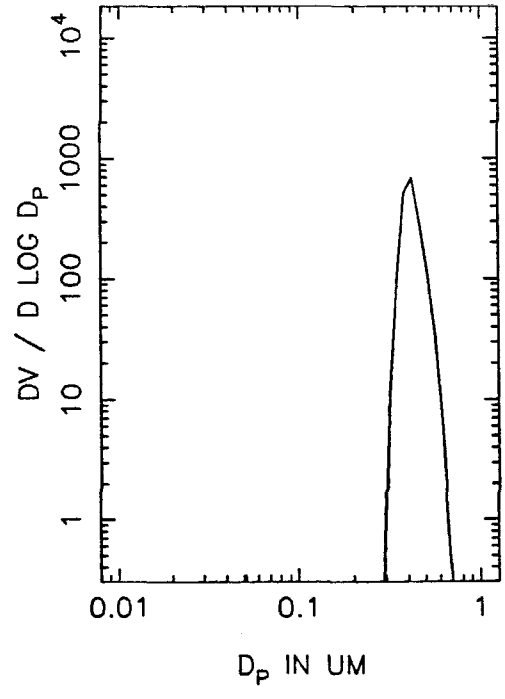

TE39A VOLUME DISTRIBUTION, T=2.0

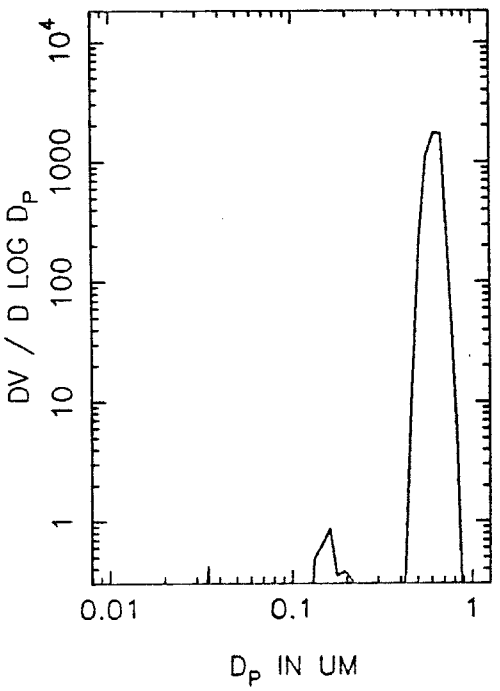

T=2.5 HOURS

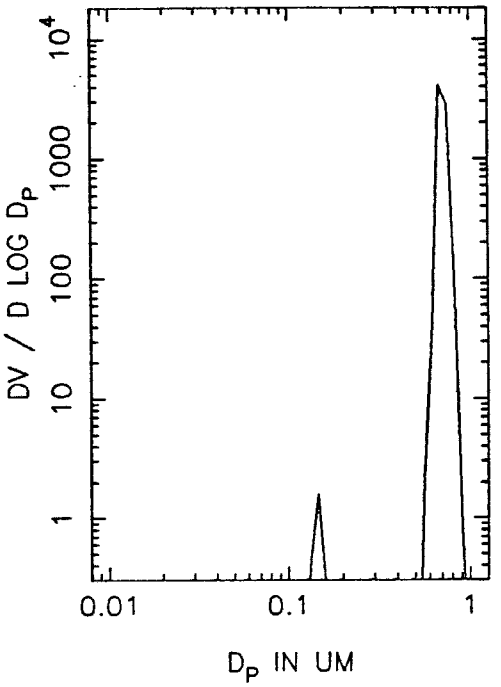

T=3.0 HOURS

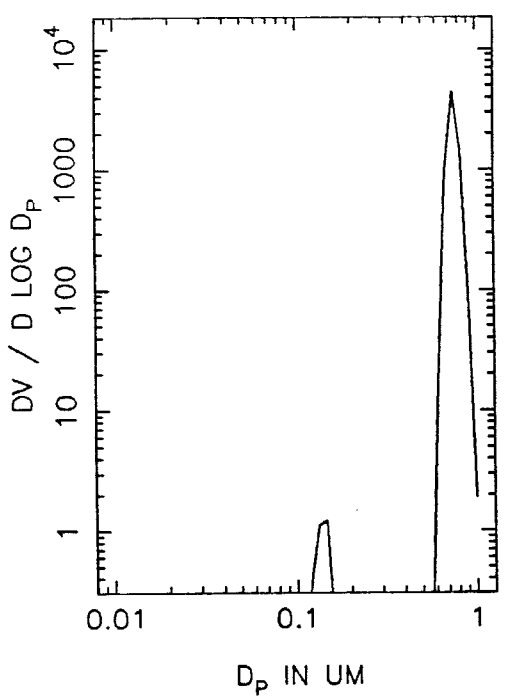

T=3.5 HOURS

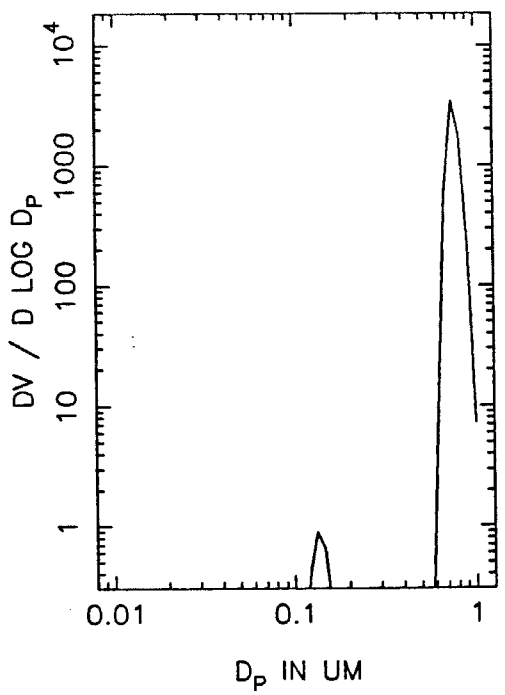

TE39B NUMBER DISTRIBUTION, T=0

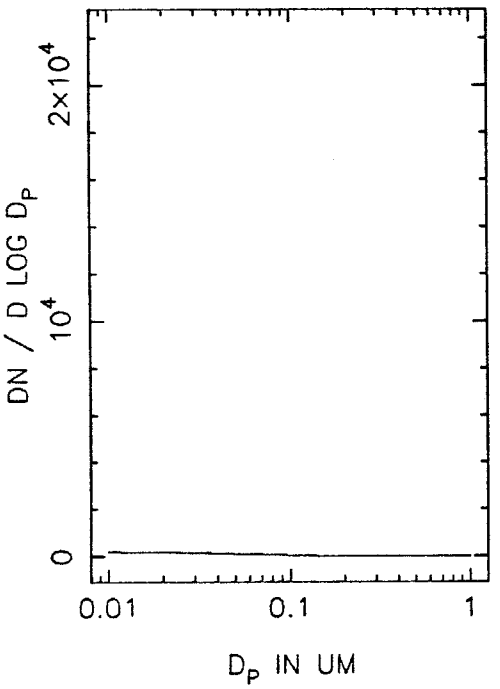

T=0.5 HOURS

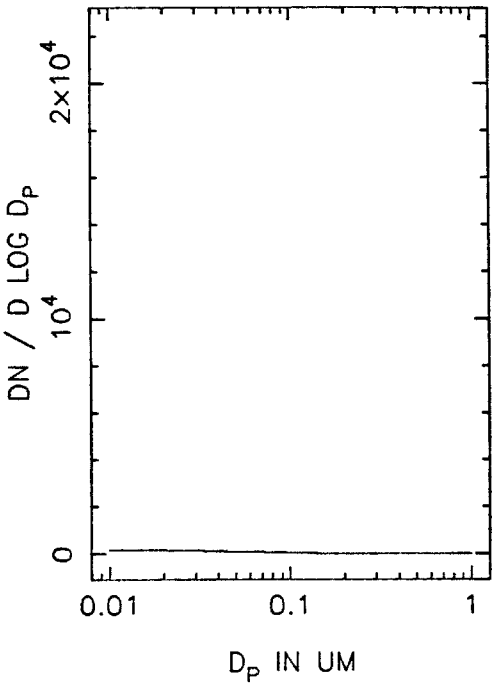

T=1.0 HOURS

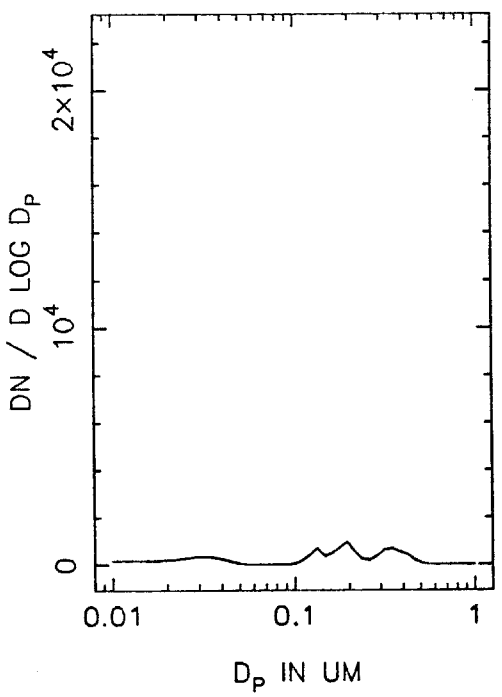

T=1.5 HOURS

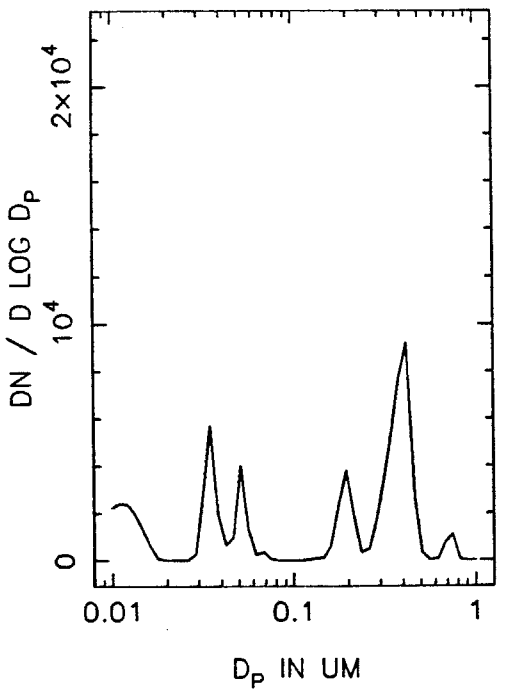

TE39B NUMBER DISTRIBUTION, T=2.0

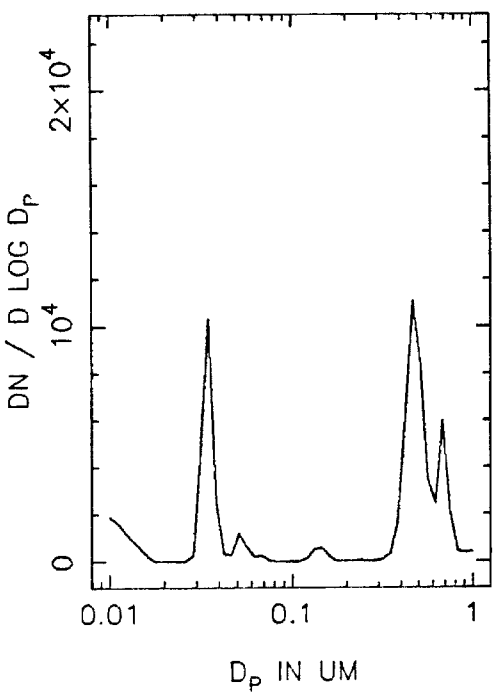

T=2.5 HOURS

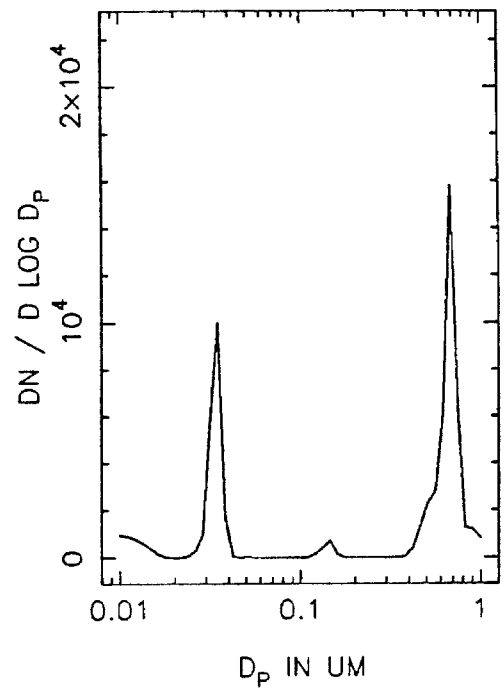

T=3.0 HOURS

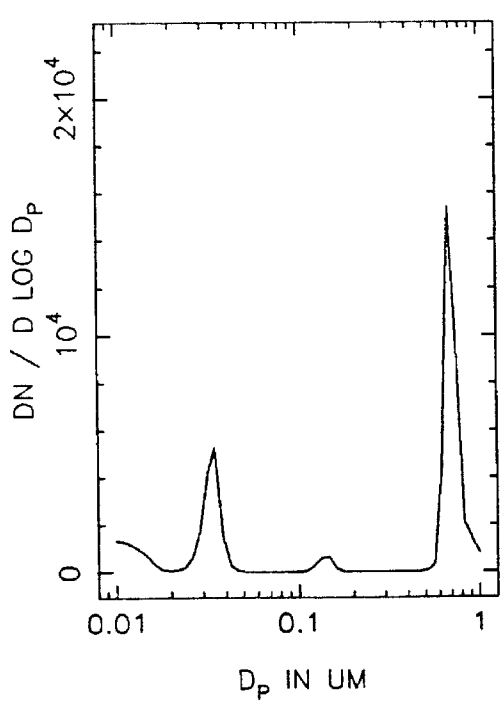

T=3.5 HOURS

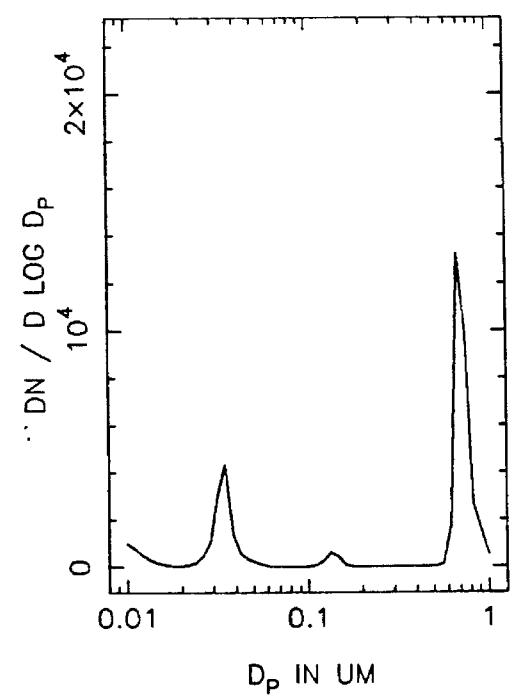

TE39B VOLUME DISTRIBUTION, T=0

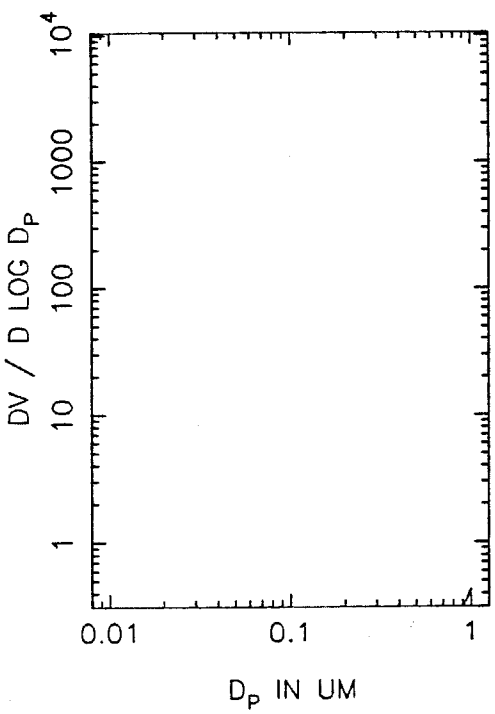

T=0.5 HOURS

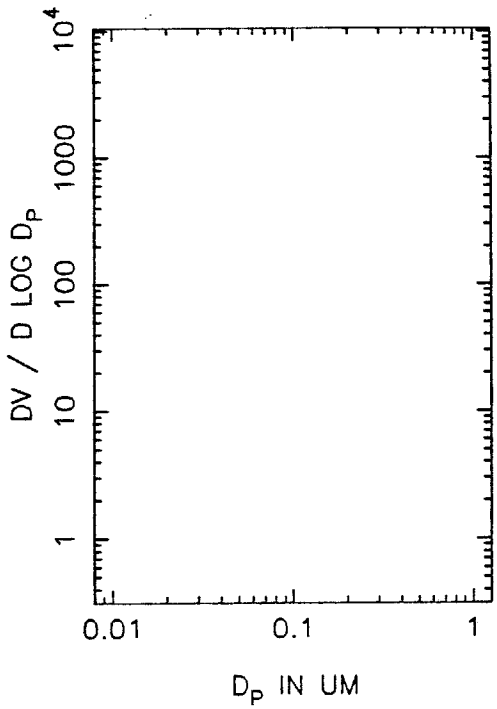

T=1.0 HOURS

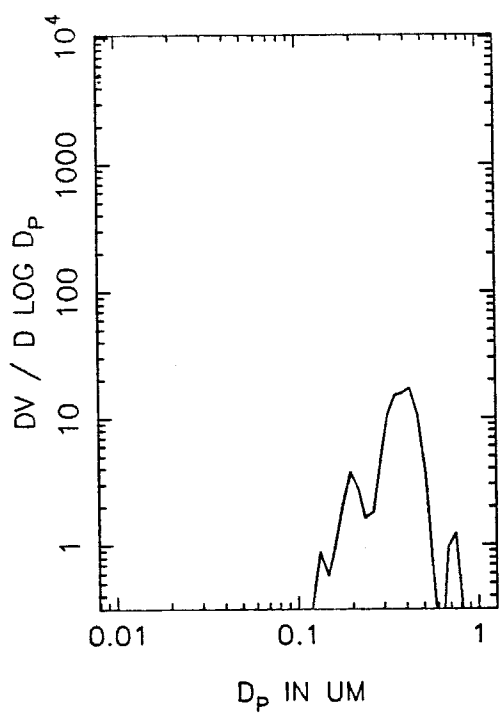

T=1.5 HOURS

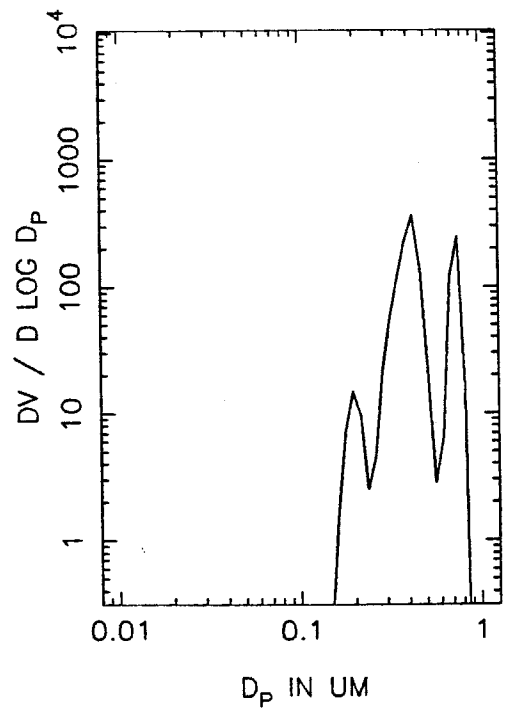

TE39B VOLUME DISTRIBUTION, T=2.0

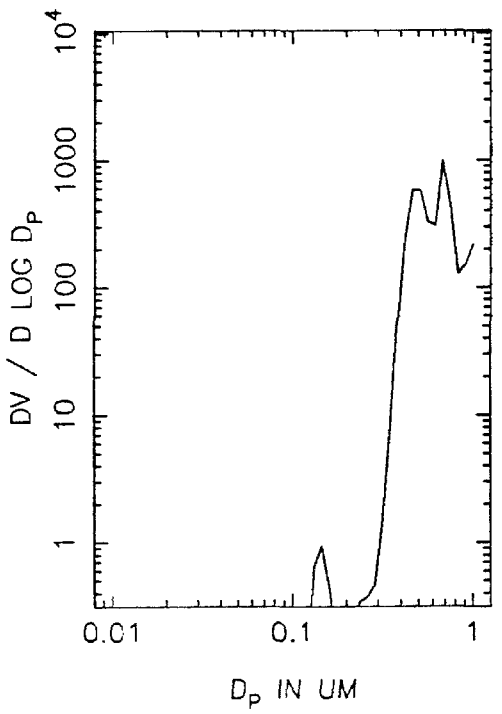

T=2.5 HOURS

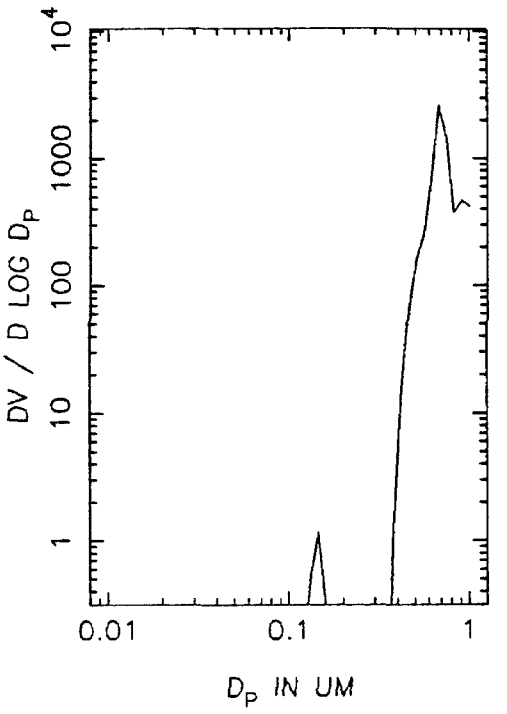

T=3.0 HOURS

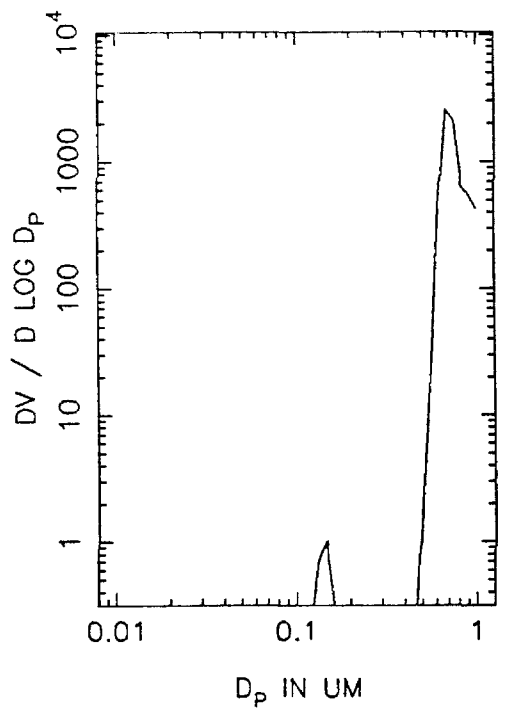

T=3.5 HOURS

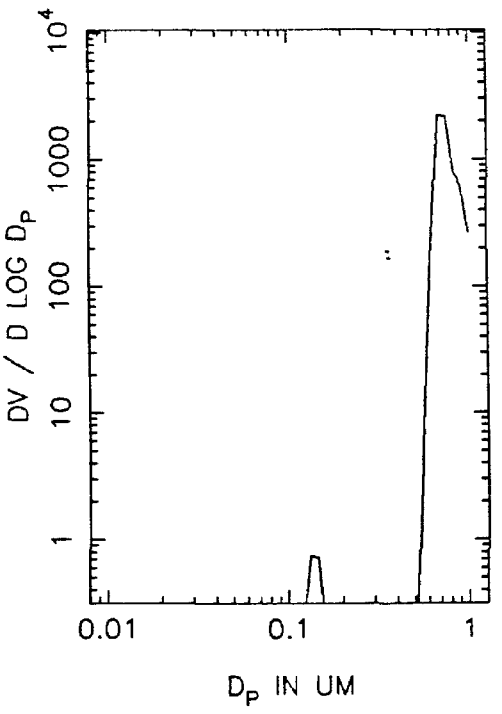

TI43 TOTAL NUMBER, SIDE A

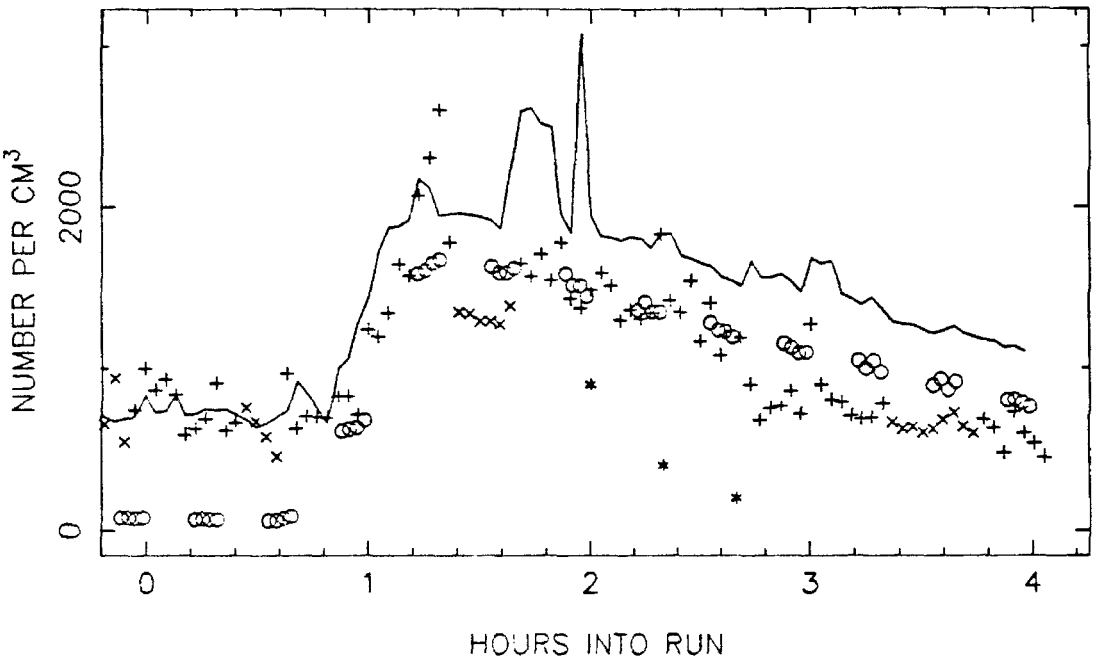

SIDE B

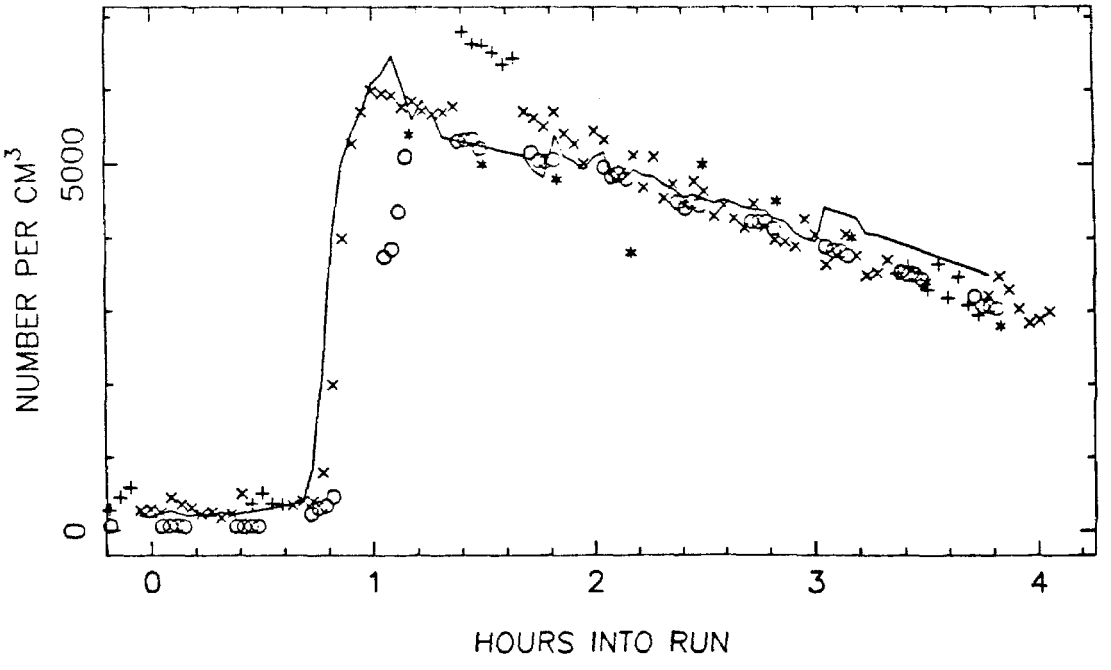

TI43 VOLUME IN THE AEROSOL PHASE, SIDE A

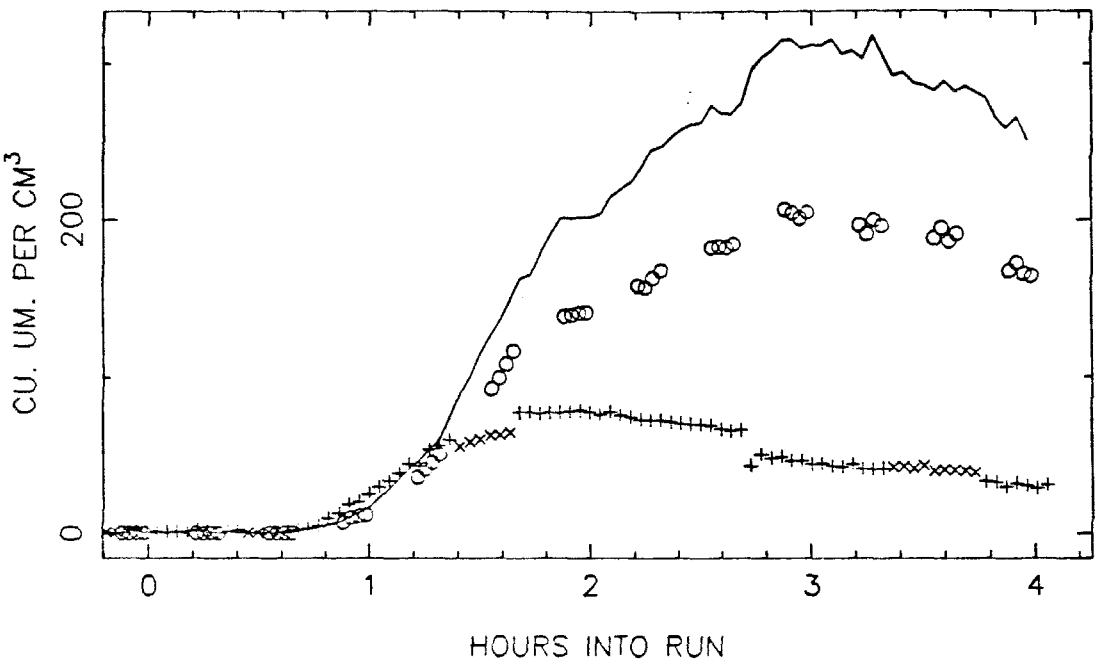

SIDE B

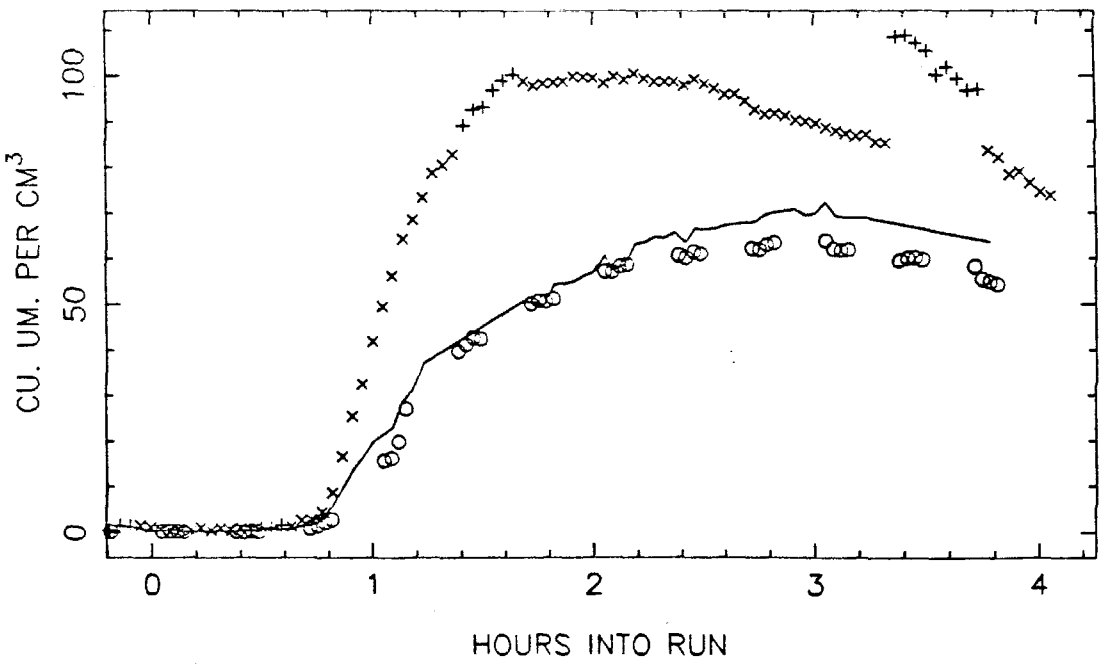

TI43 MEAN PARTICLE SIZE, SIDE A

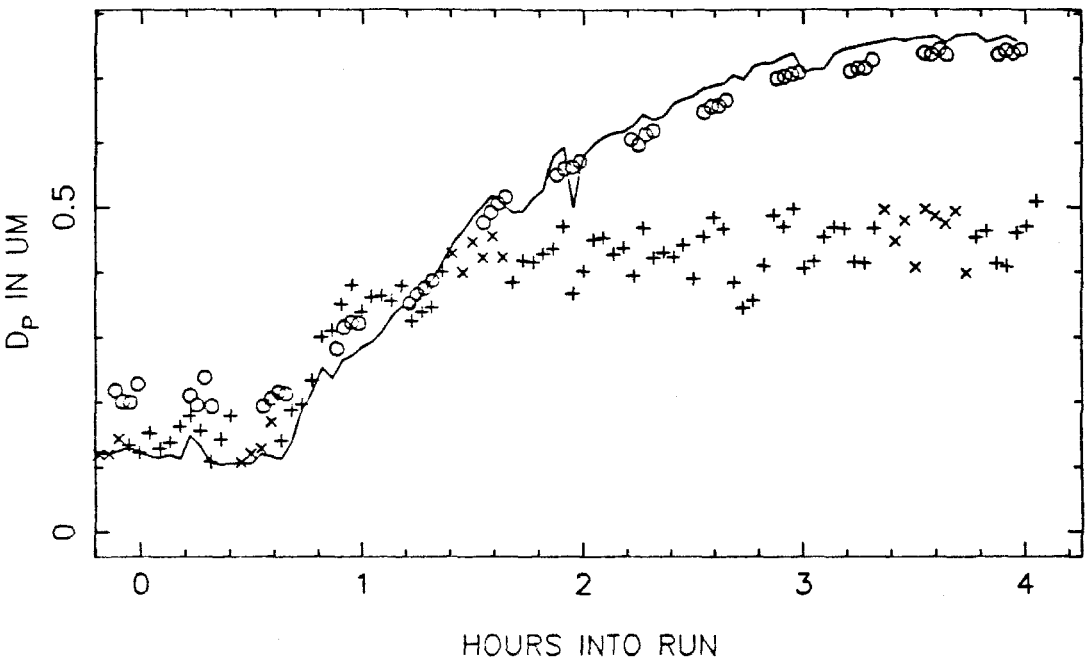

SIDE B

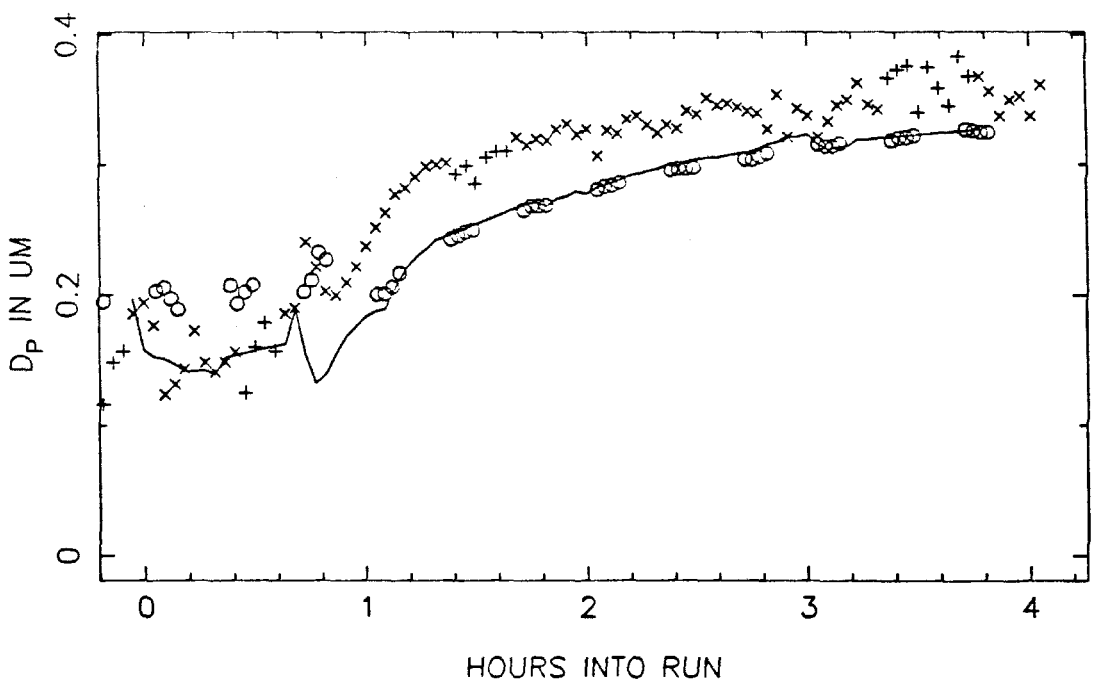

TI43A NUMBER DISTRIBUTION, T=0

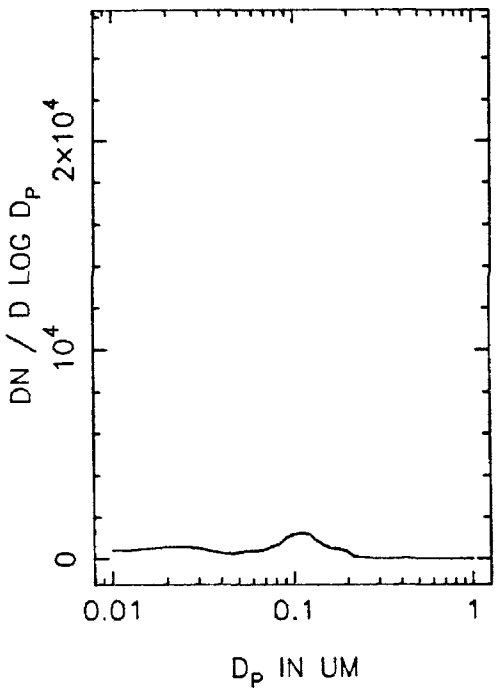

T=0.5 HOURS

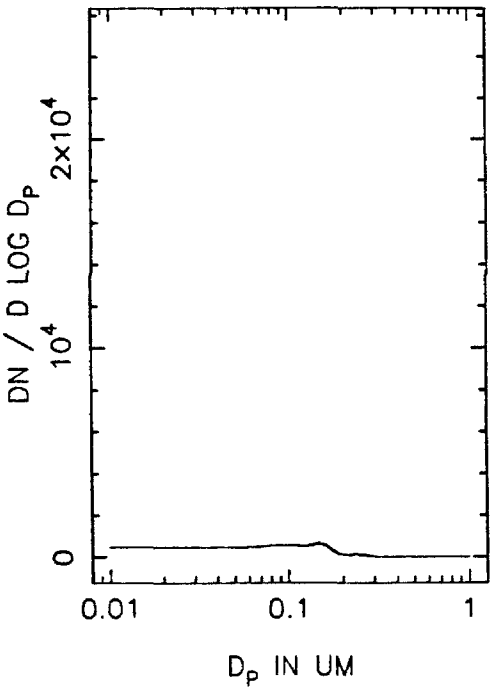

T=1.0 HOURS

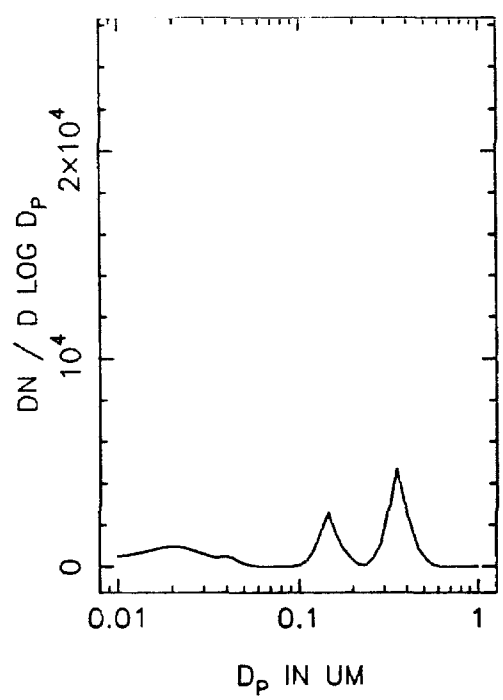

T=1.5 HOURS

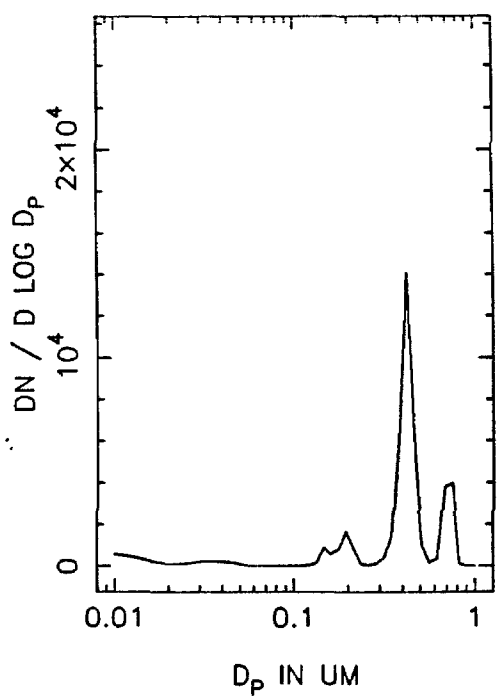

TI43A NUMBER DISTRIBUTION, T=2.0

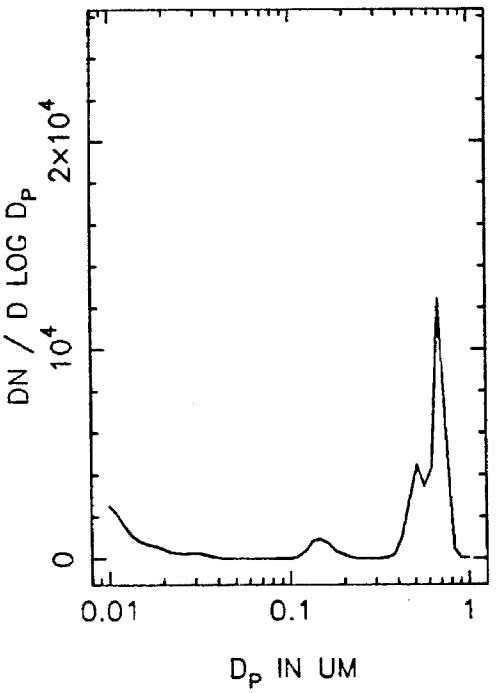

T=2.5 HOURS

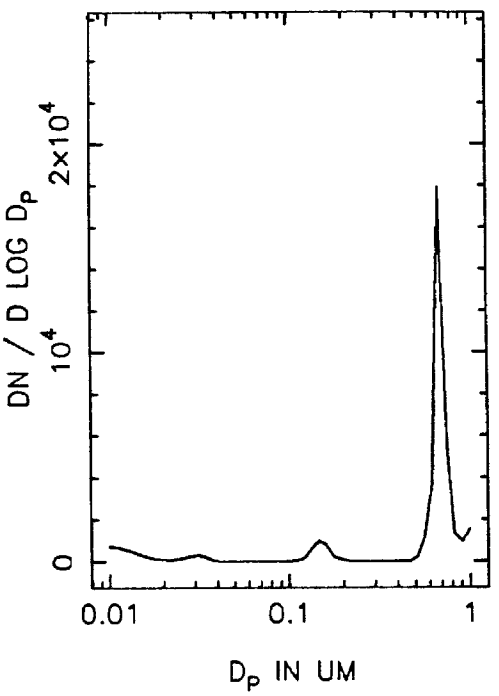

T=3.0 HOURS

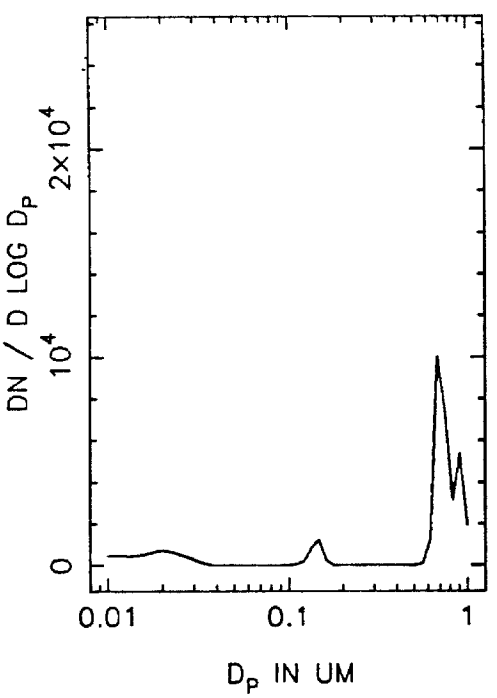

T=3.5 HOURS

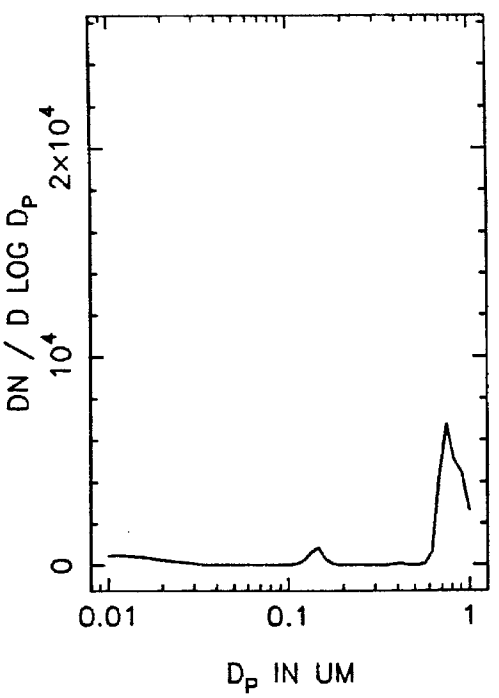

TI43A NUMBER DISTRIBUTION, T=4.0

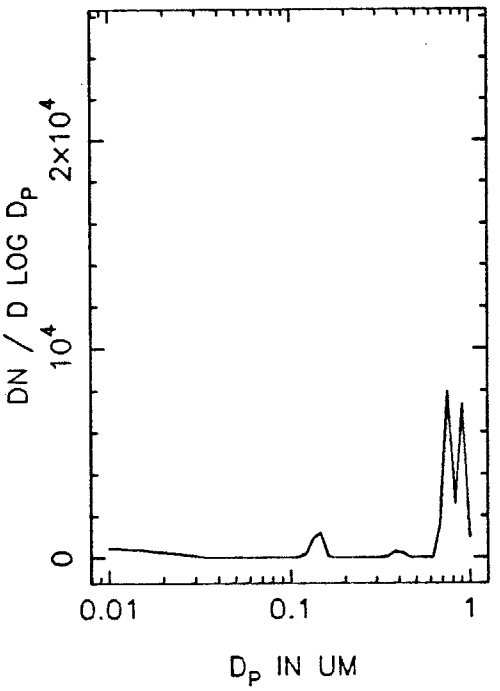

TI43A VOLUME DISTRIBUTION, T=0

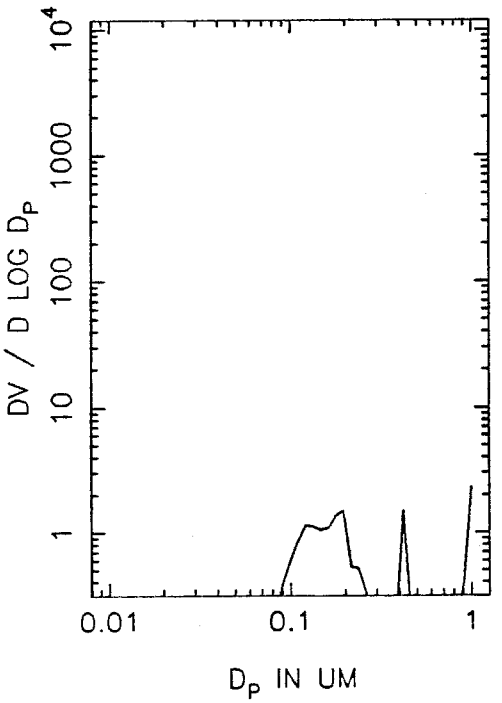

T=0.5 HOURS

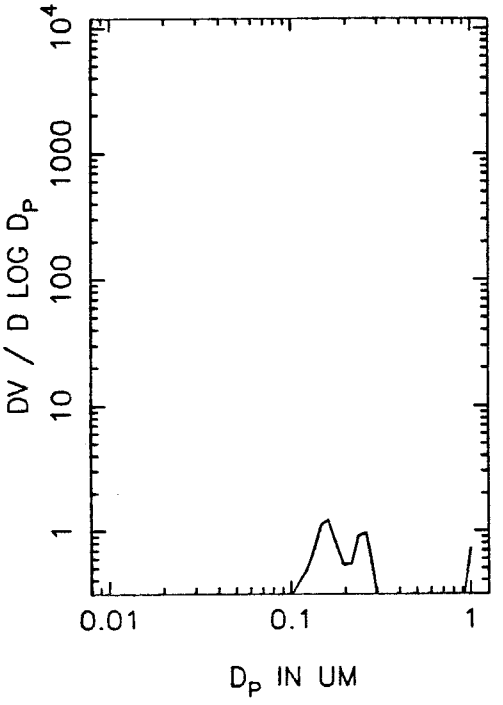

T=1.0 HOURS

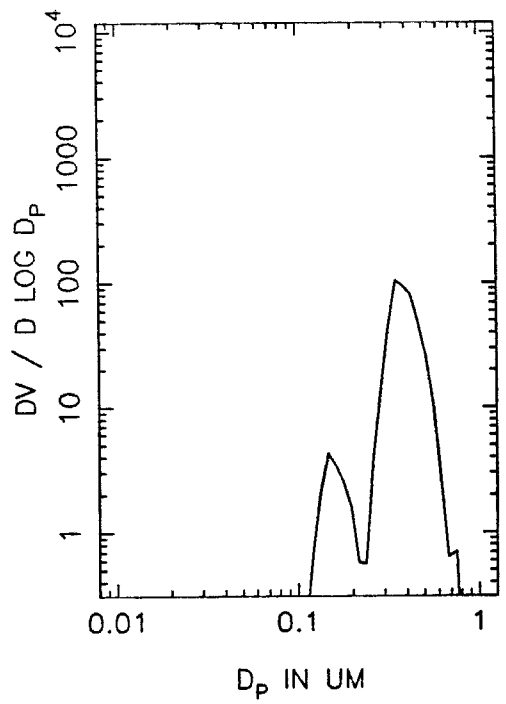

T=1.5 HOURS

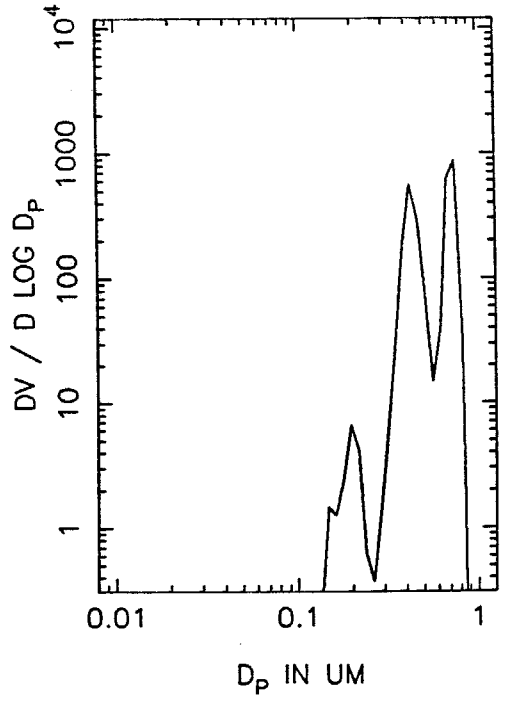

TI43A VOLUME DISTRIBUTION, T=2.0

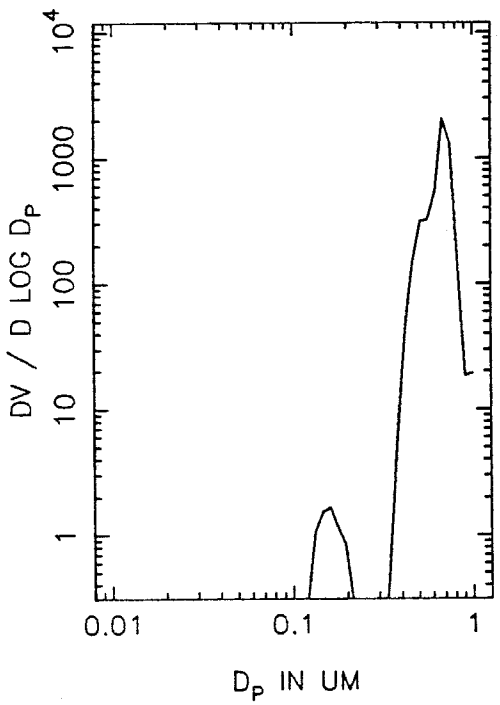

T=2.5 HOURS

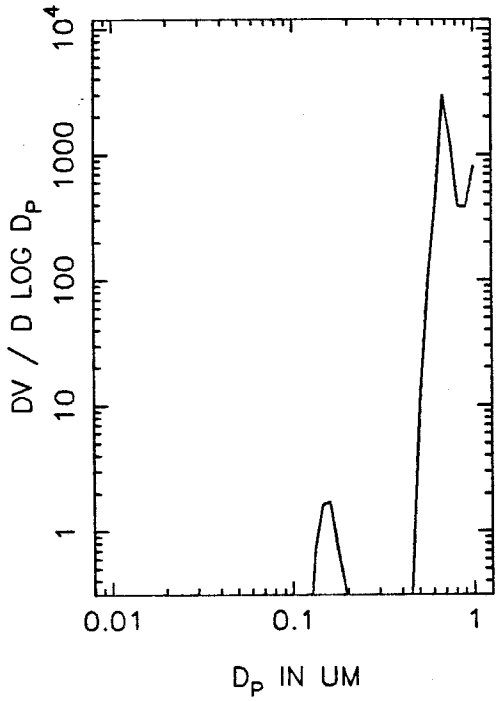

T=3.0 HOURS

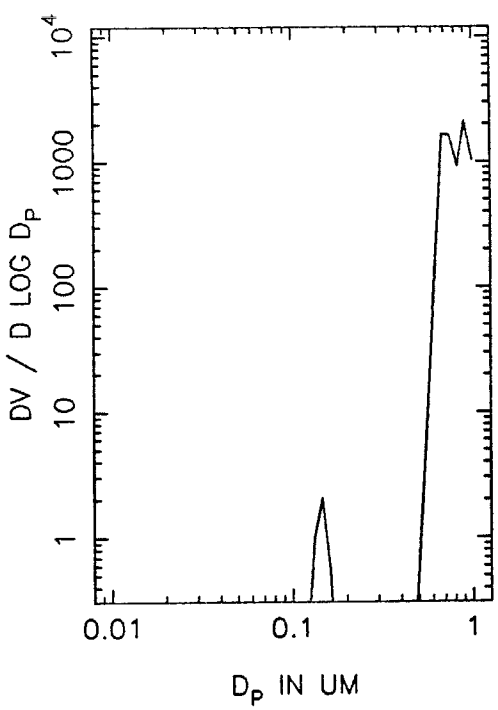

T=3.5 HOURS

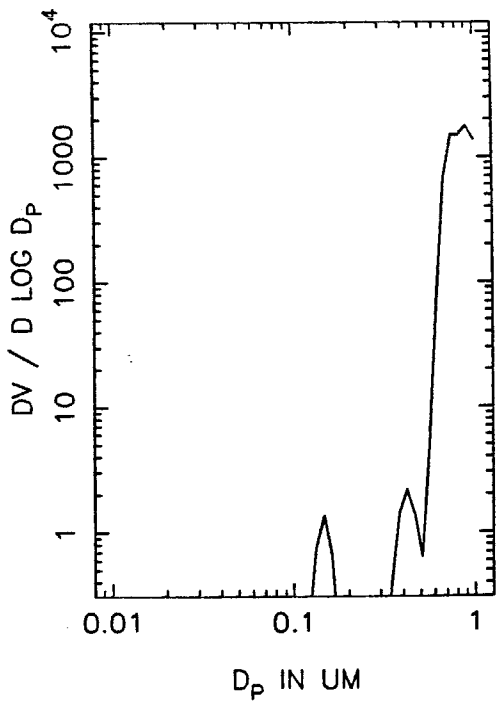

TI43A VOLUME DISTRIBUTION, T=4.0

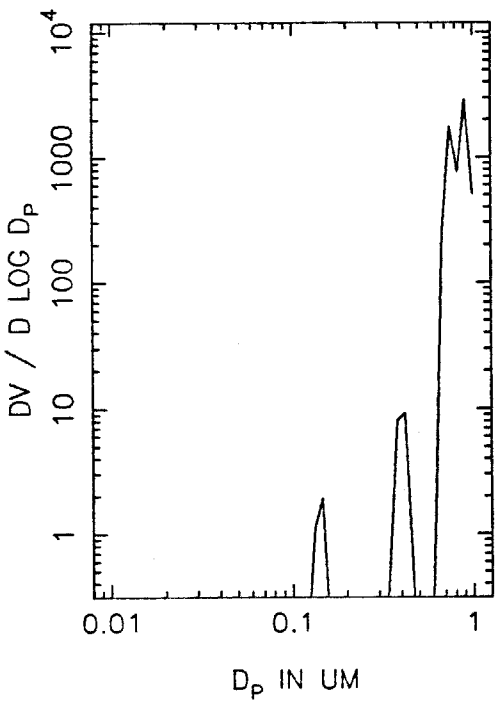

TI43B NUMBER DISTRIBUTION, T=0

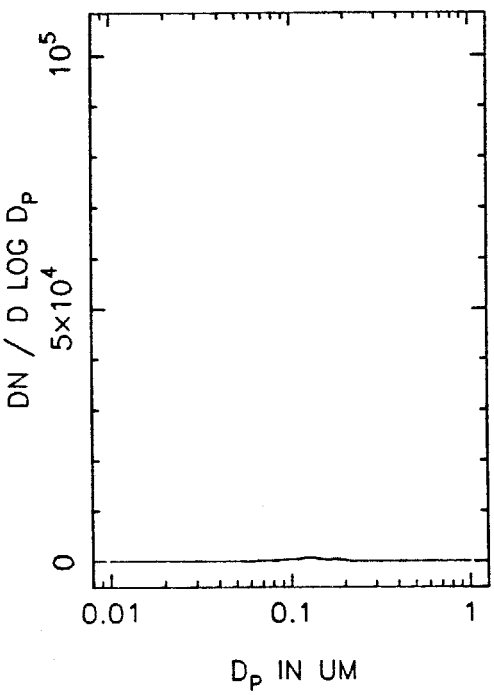

T=0.5 HOURS

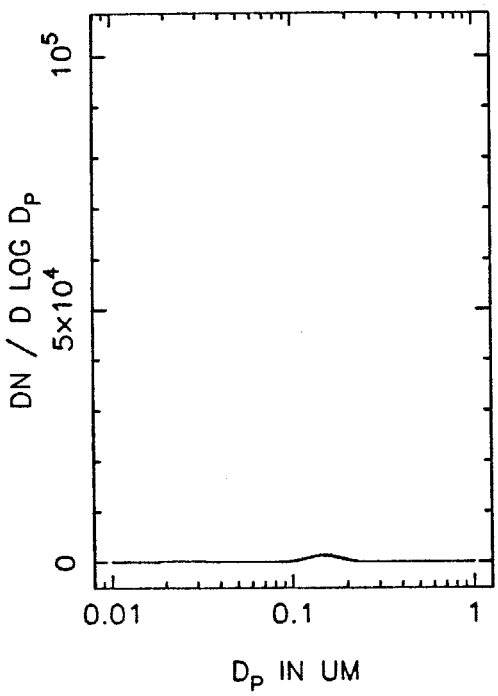

T=1.0 HOURS

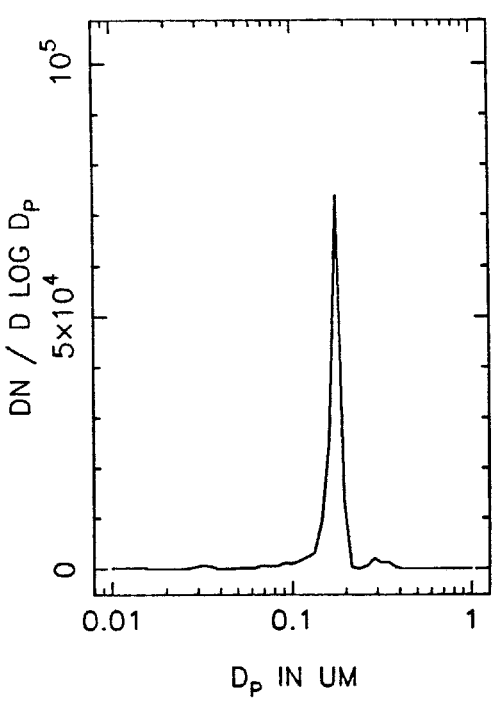

T=1.5 HOURS

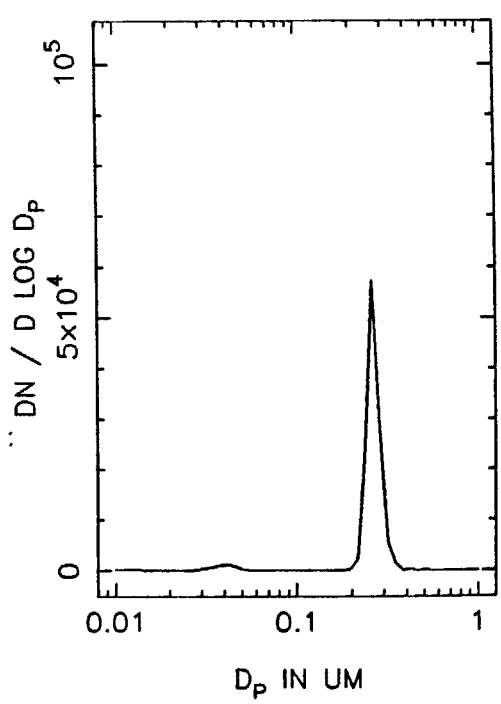

TI43B NUMBER DISTRIBUTION, T=2.0

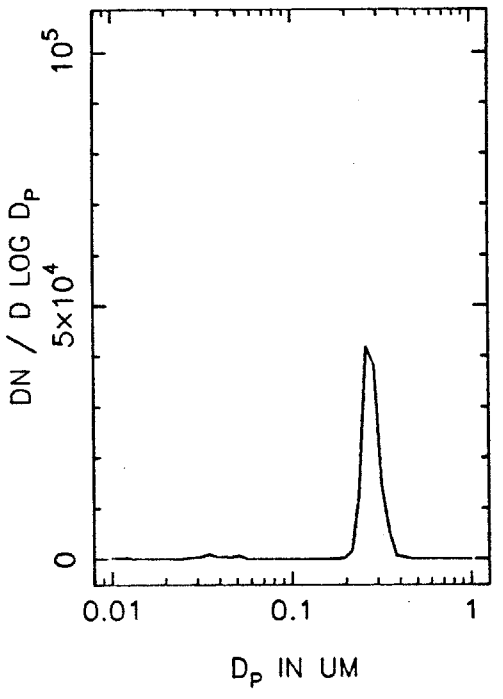

T=2.5 HOURS

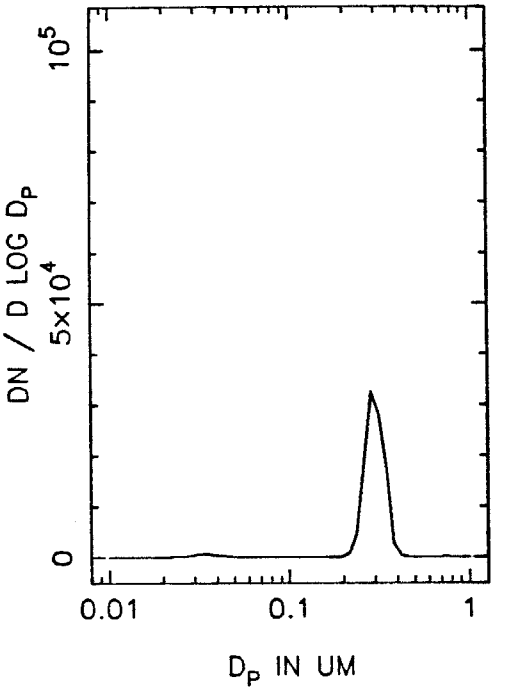

T=3.0 HOURS

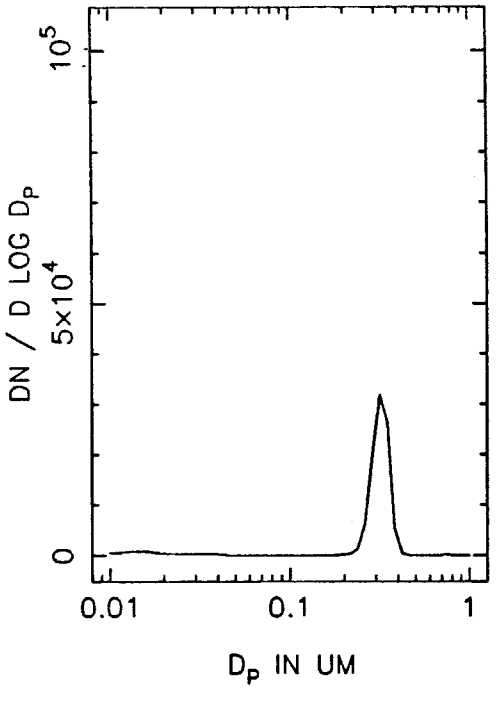

T=3.5 HOURS

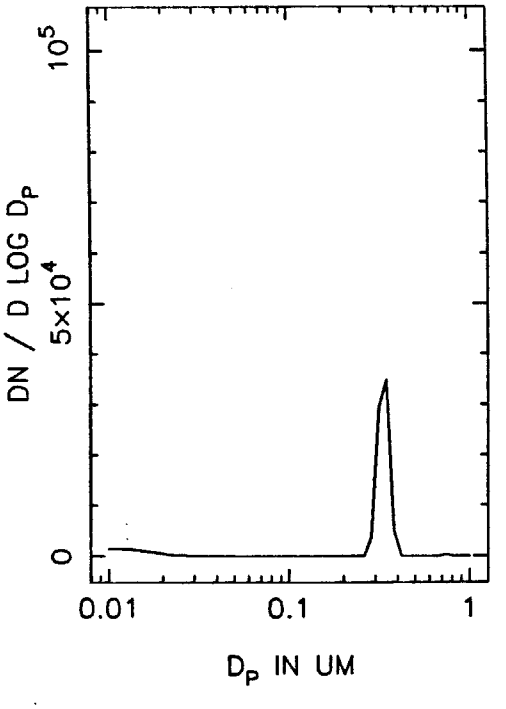

TI43B VOLUME DISTRIBUTION, T=0

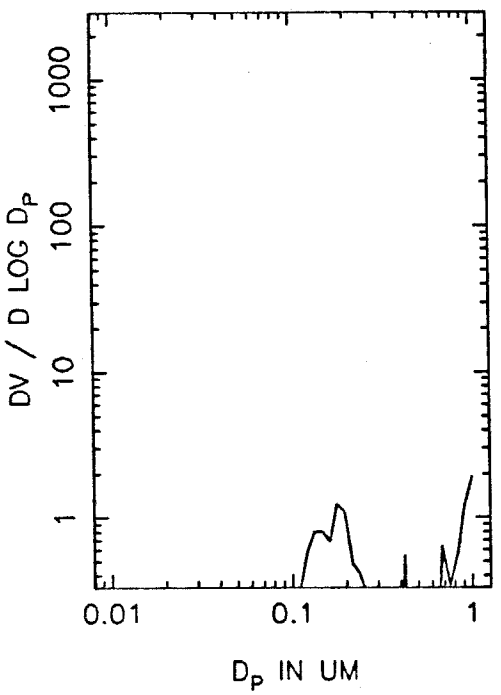

T=0.5 HOURS

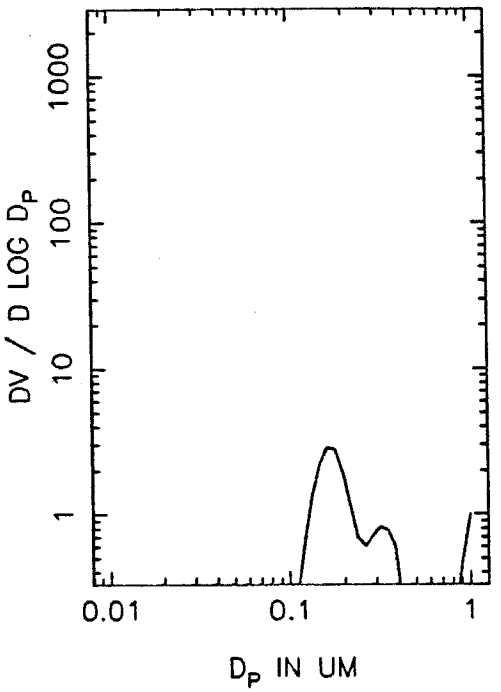

T=1.0 HOURS

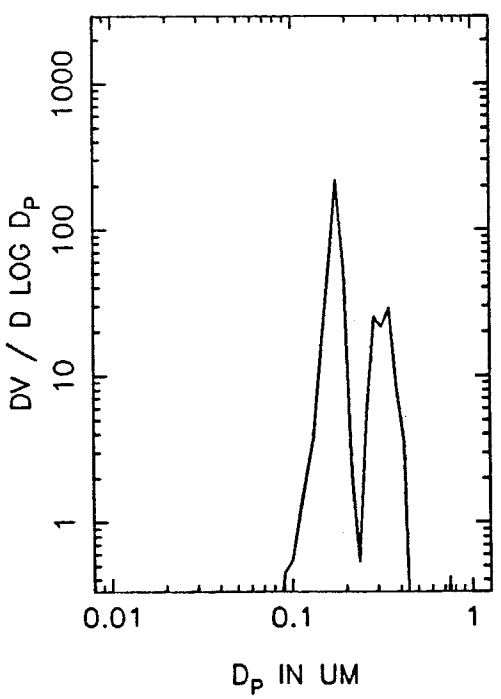

T=1.5 HOURS

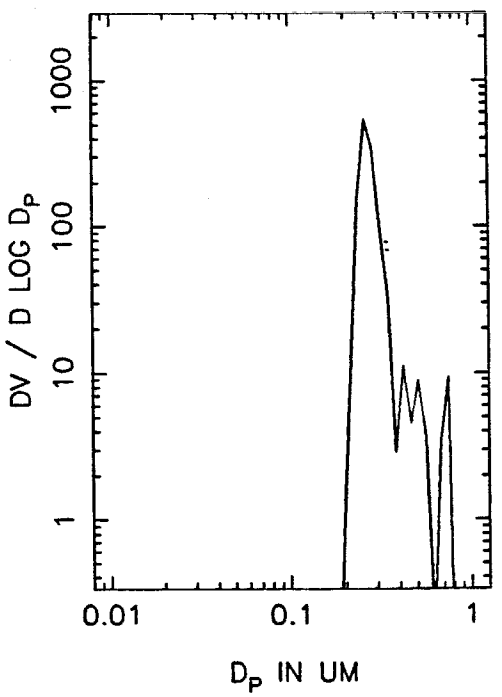

TI43B VOLUME DISTRIBUTION, T=2.0

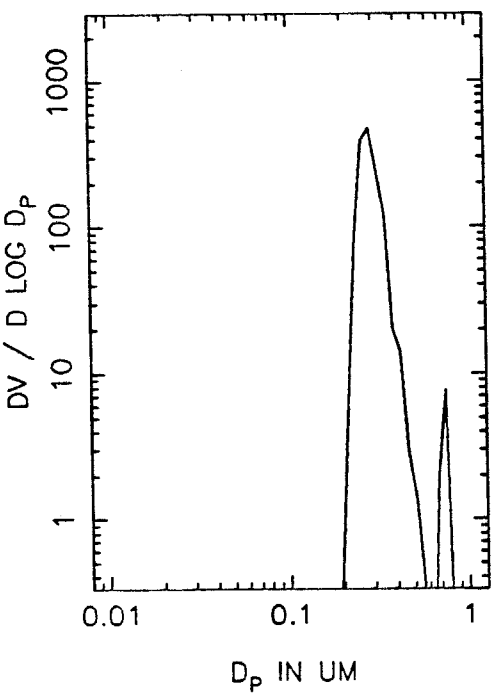

T=2.5 HOURS

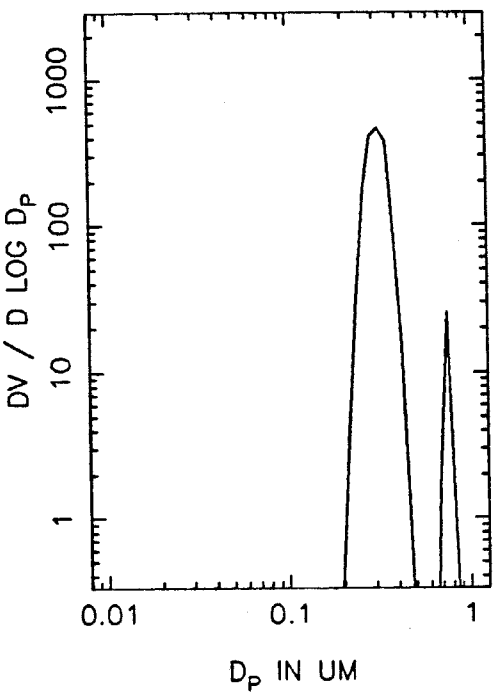

T=3.0 HOURS

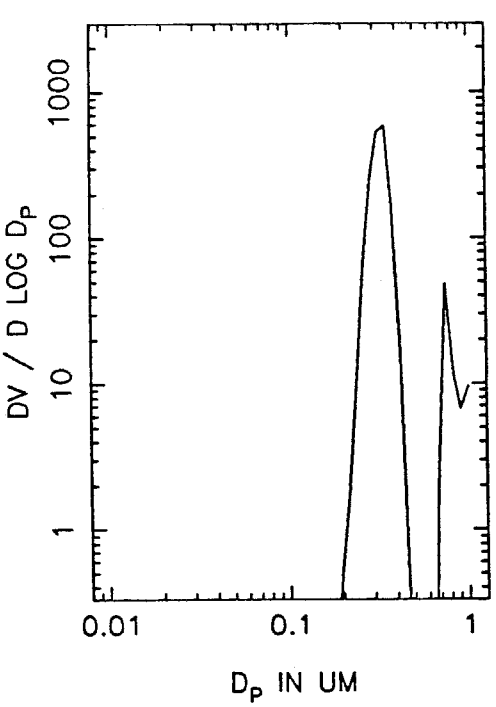

T=3.5 HOURS

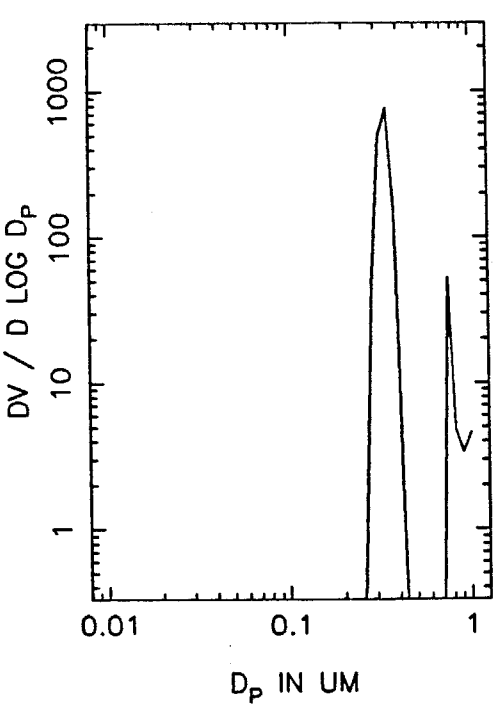

TO46 TOTAL NUMBER, SIDE A

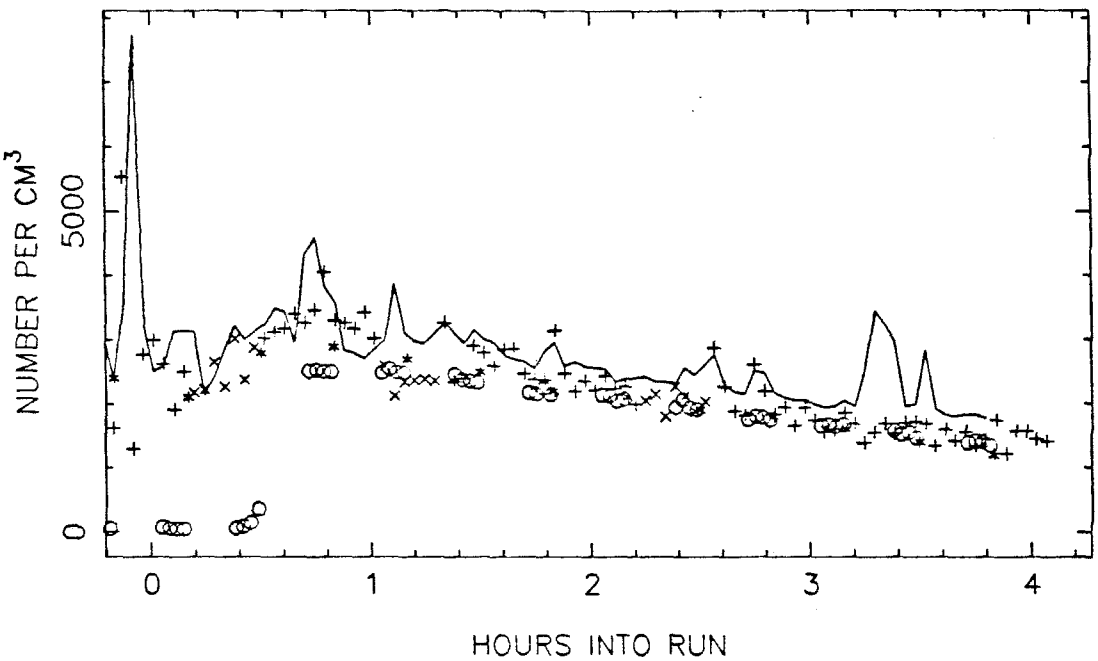

SIDE B

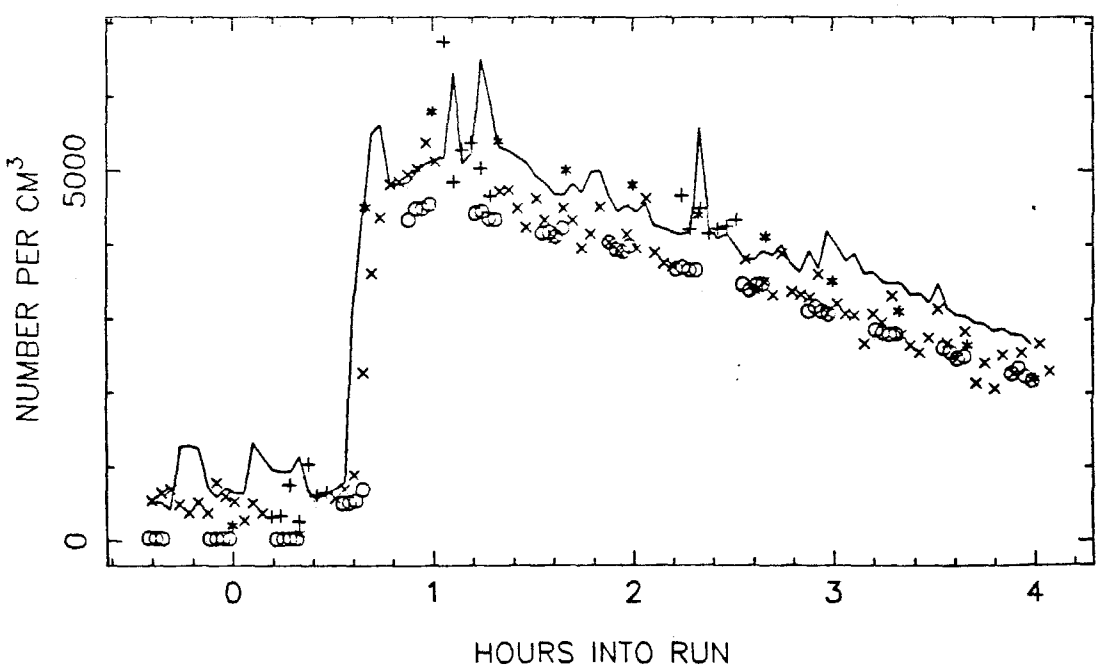

TO46 VOLUME IN THE AEROSOL PHASE, SIDE A

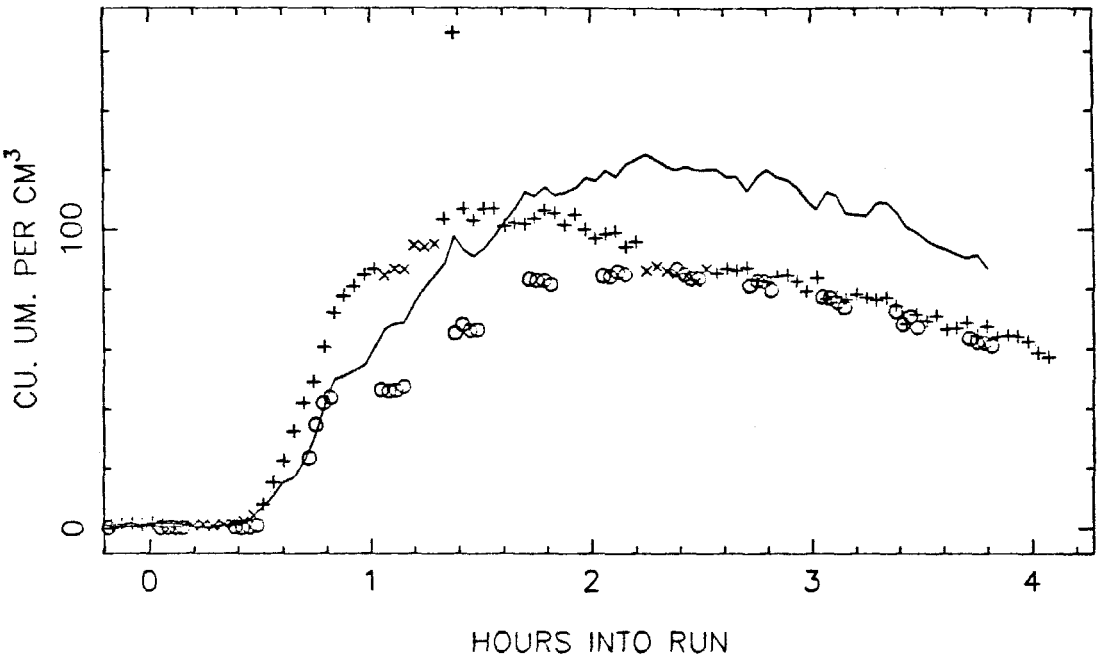

SIDE B

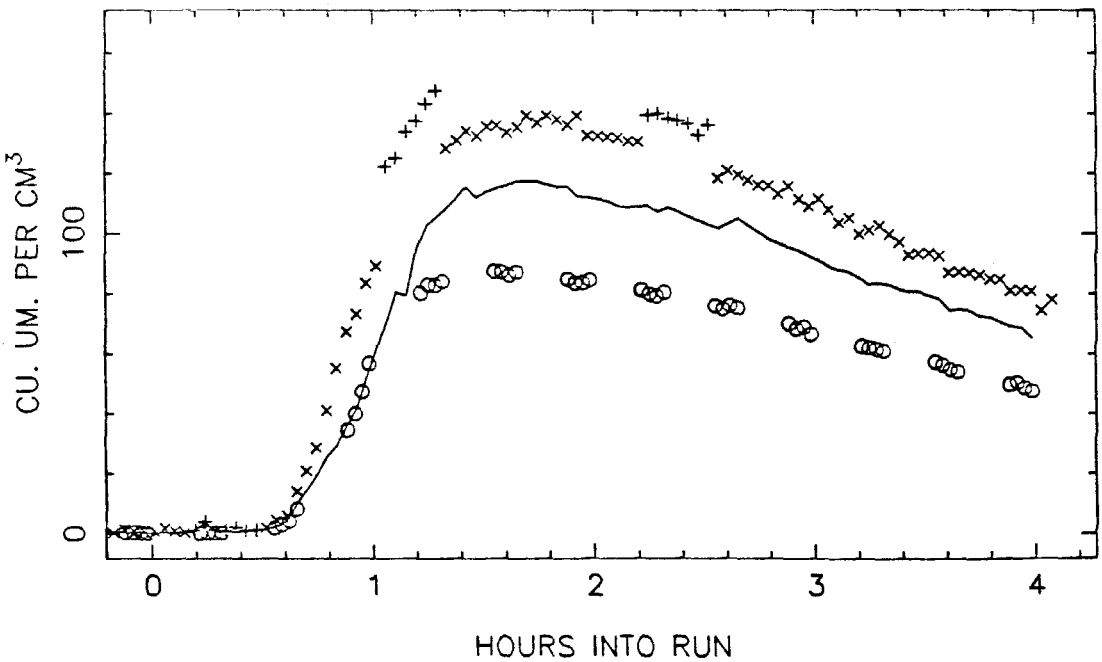

TO46 MEAN PARTICLE SIZE, SIDE A

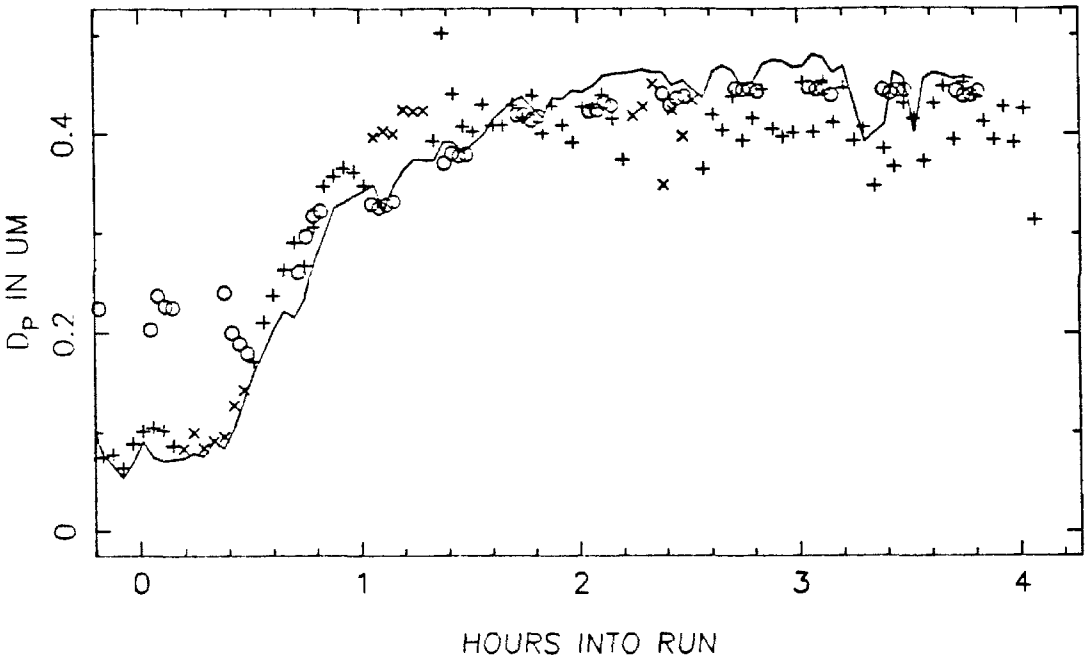

SIDE B

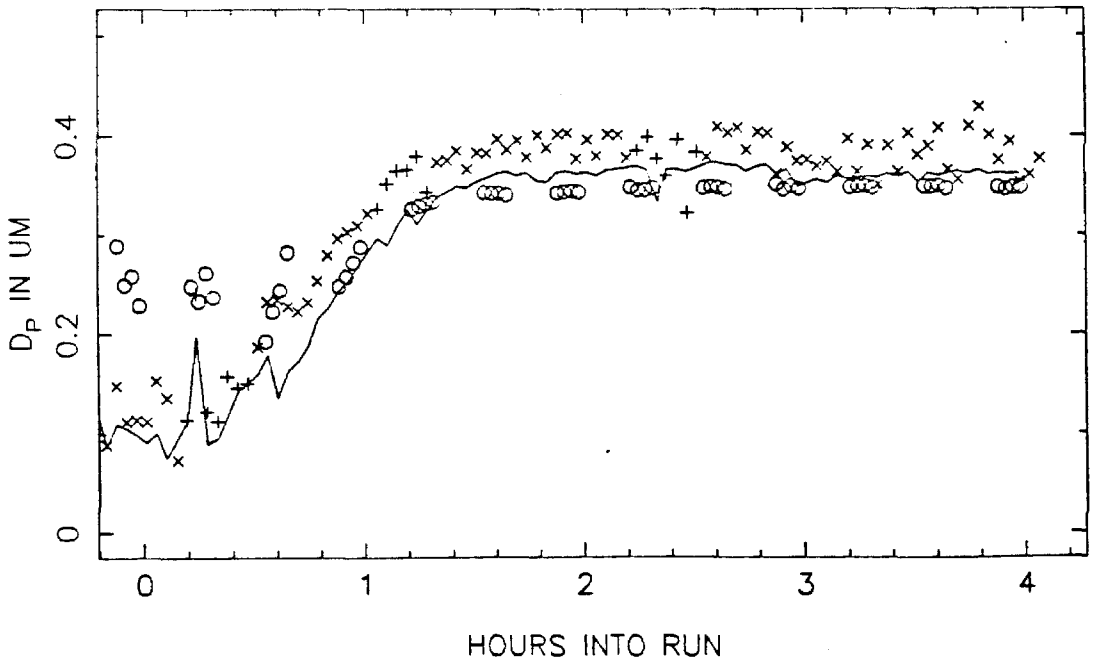

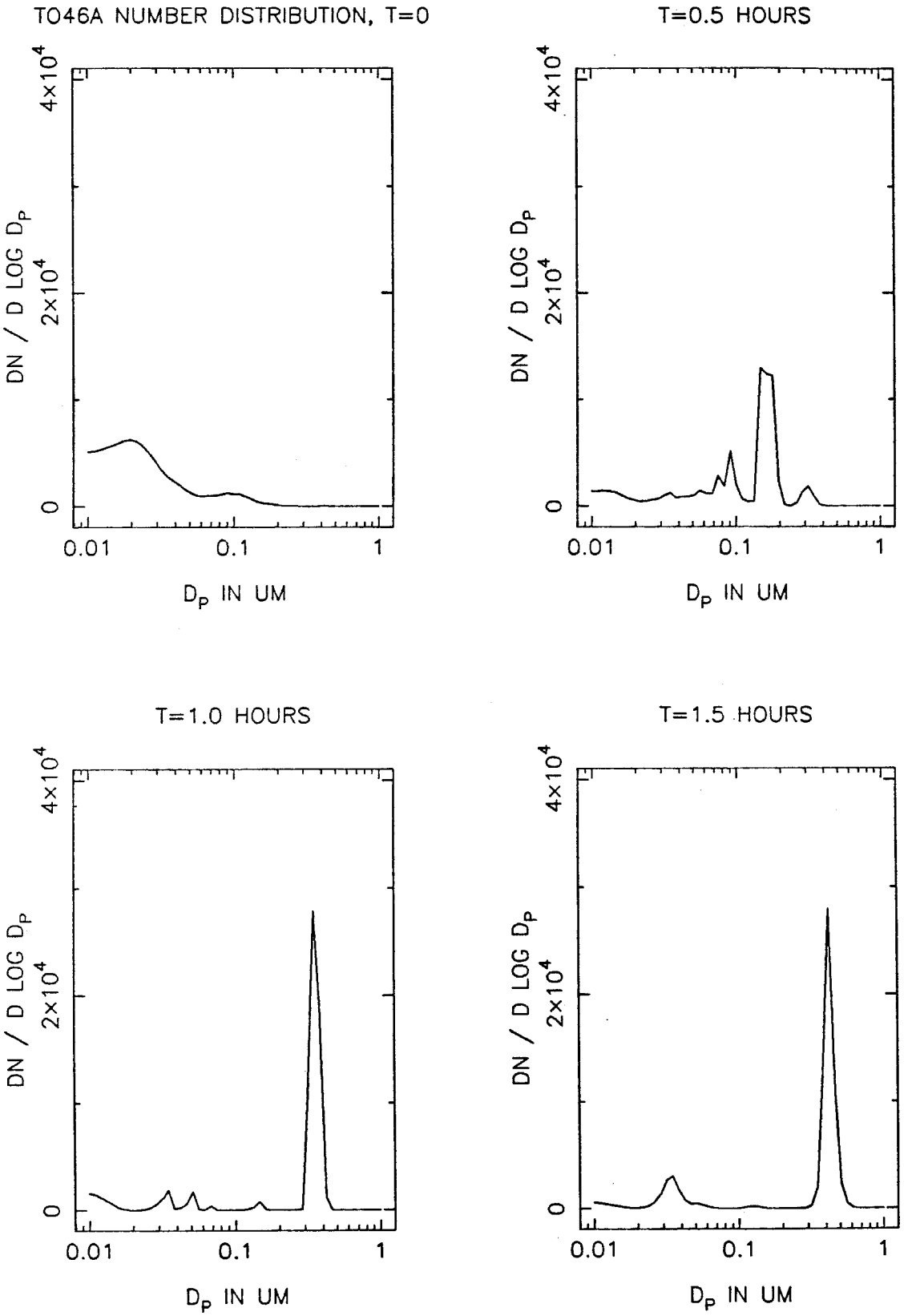
T046A NUMBER DISTRIBUTION, T=0
T=0.5 HOURS
T=1.0 HOURS
T=1.5 HOURS
DN / D LOG D_P
4×10^4
2×10^4
0
0.01
0.1
1
D_P IN UM

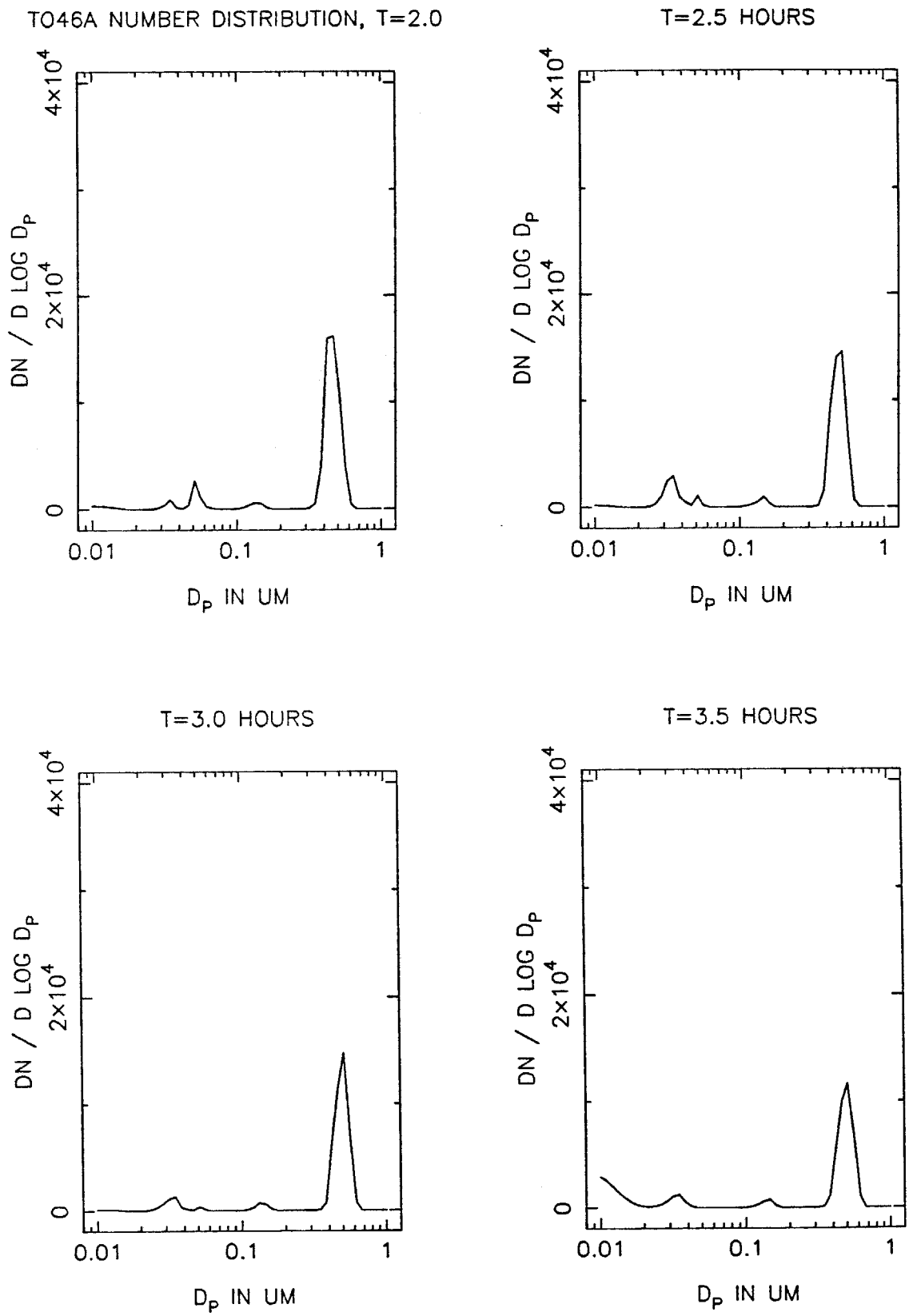
T046A NUMBER DISTRIBUTION, T=2.0
T=2.5 HOURS
T=3.0 HOURS
T=3.5 HOURS
DN / D LOG D_P
4×10^4
2×10^4
0
0.01
0.1
1
D_P IN UM

TO46A VOLUME DISTRIBUTION, T=0

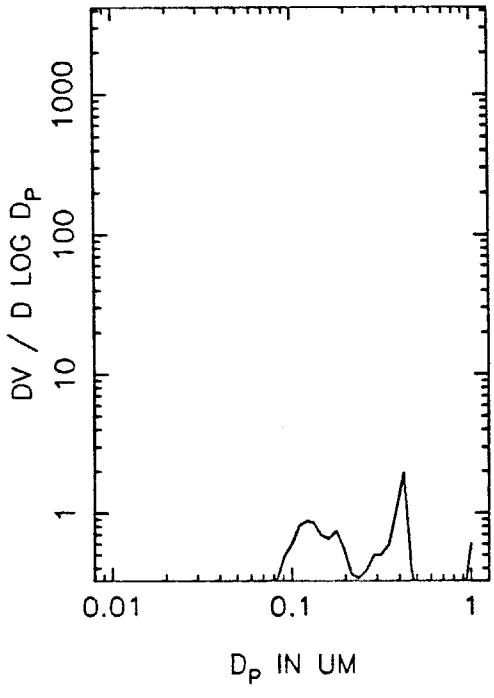

T=0.5 HOURS

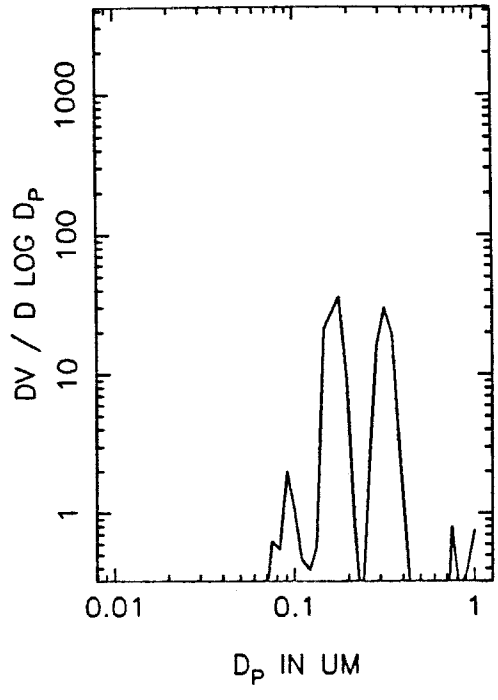

T=1.0 HOURS

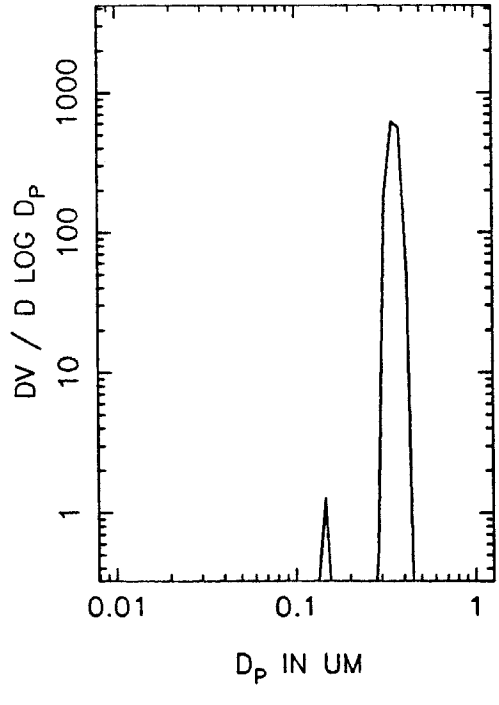

T=1.5 HOURS

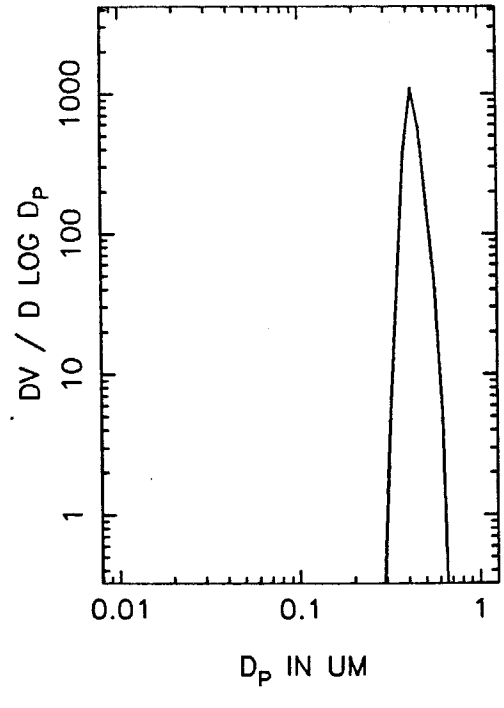

TO46A VOLUME DISTRIBUTION, T=2.0

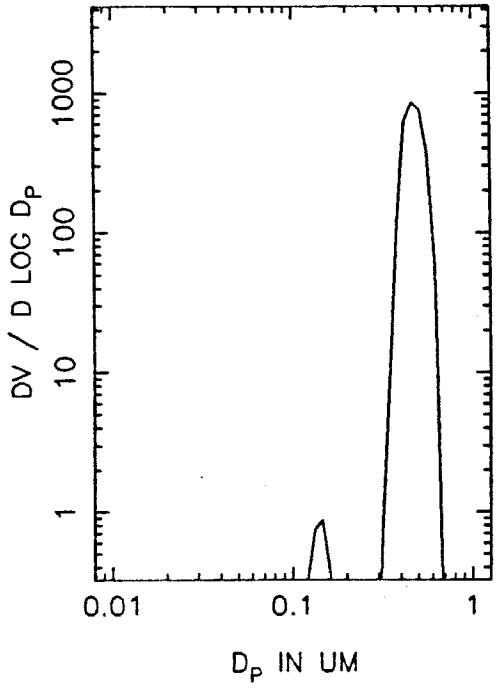

T=2.5 HOURS

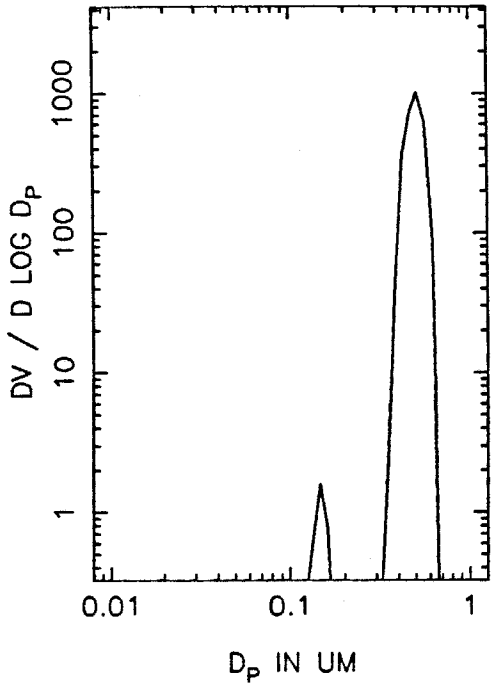

T=3.0 HOURS

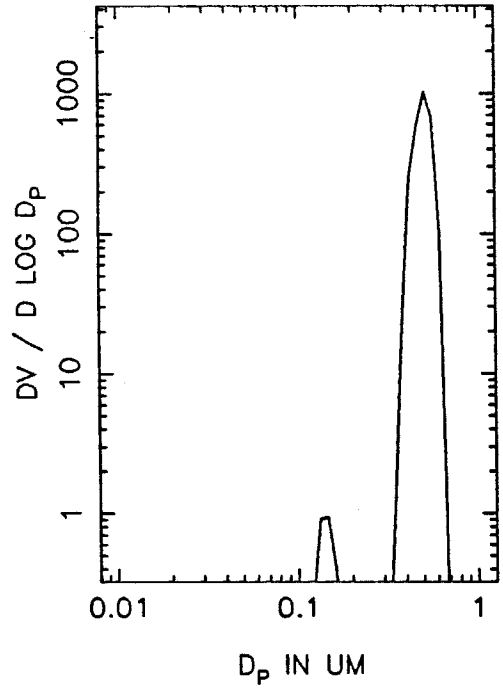

T=3.5 HOURS

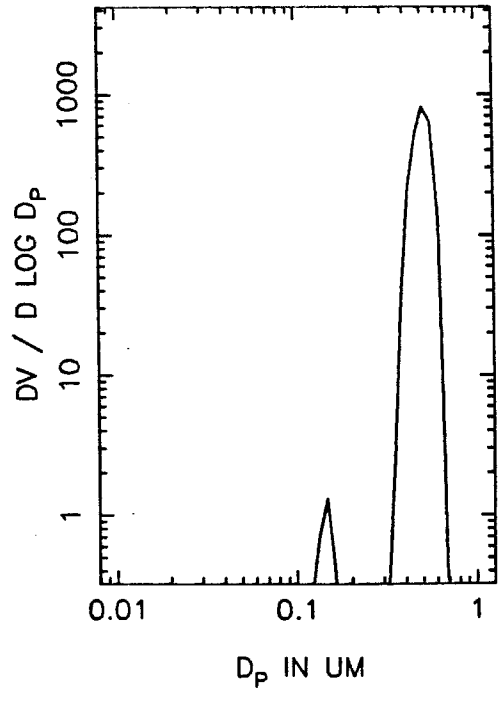

TO46B NUMBER DISTRIBUTION, T=0

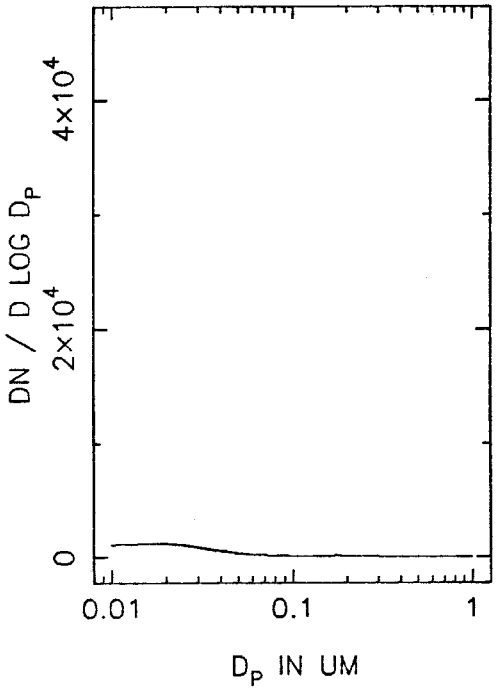

T=0.5 HOURS

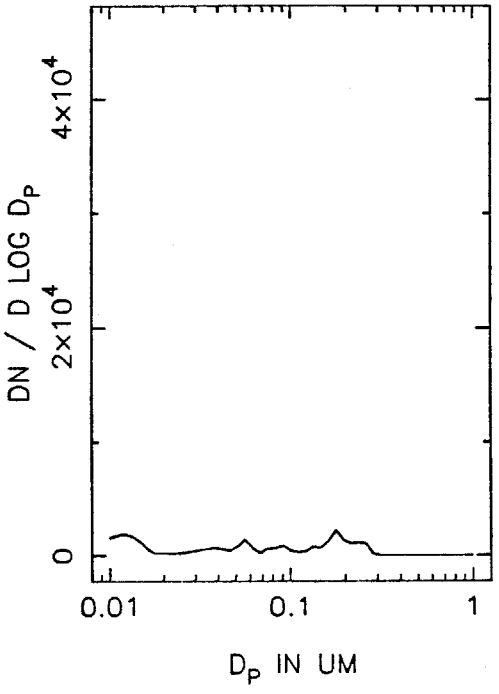

T=1.0 HOURS

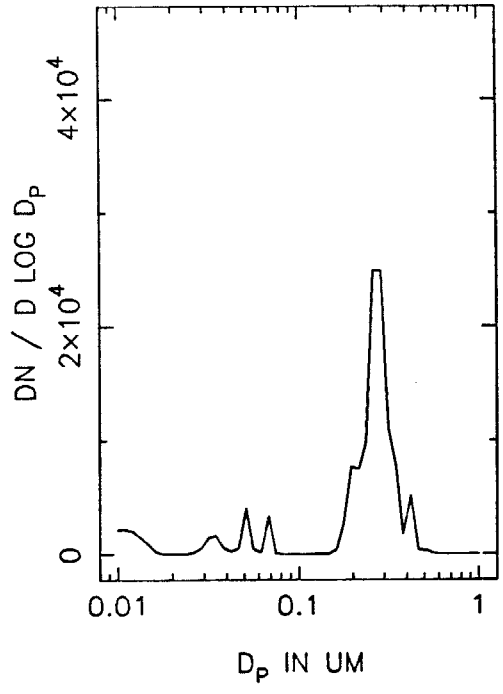

T=1.5 HOURS

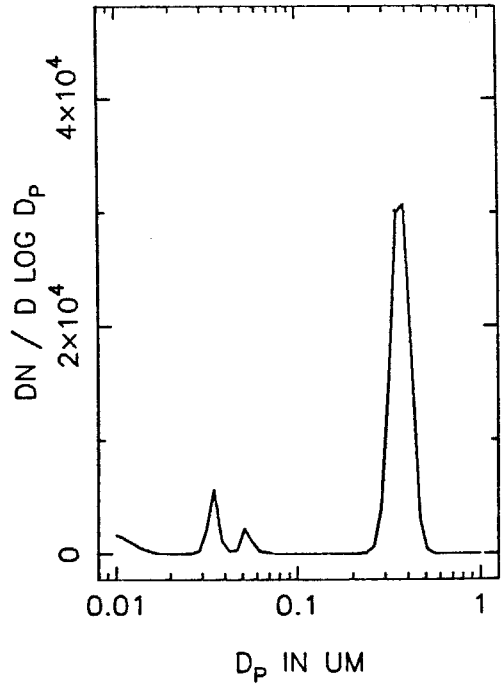

TO46B NUMBER DISTRIBUTION, T=2.0

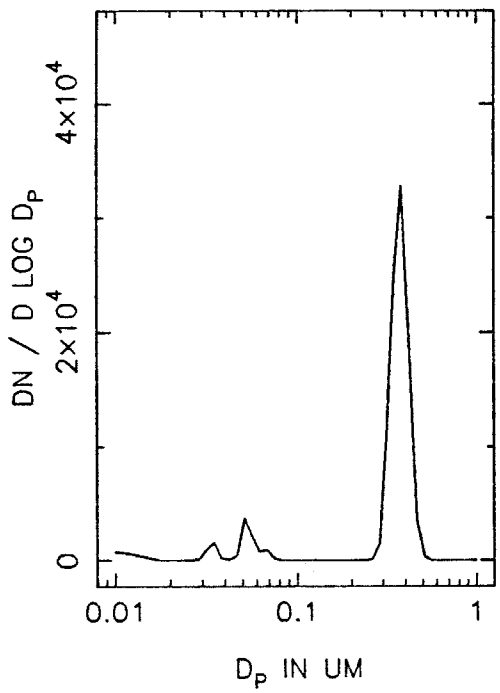

T=2.5 HOURS

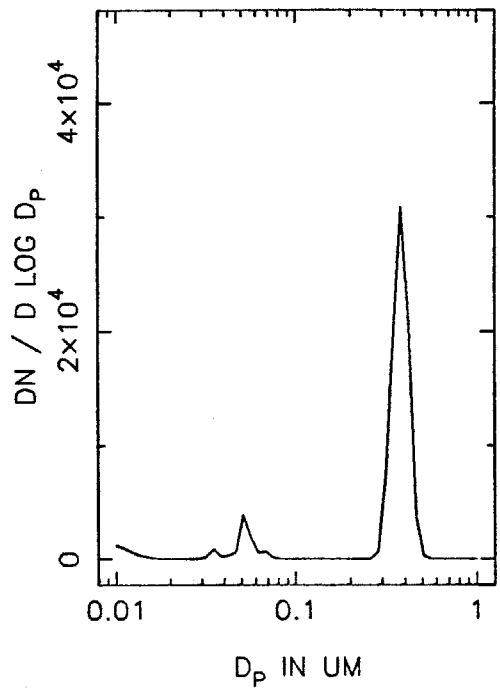

T=3.0 HOURS

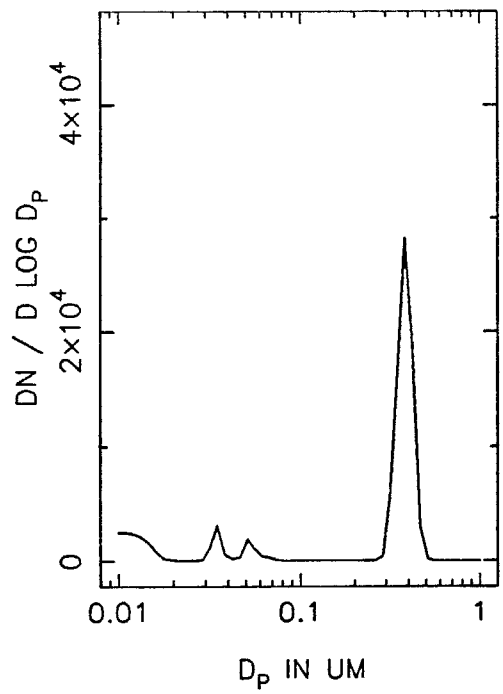

T=3.5 HOURS

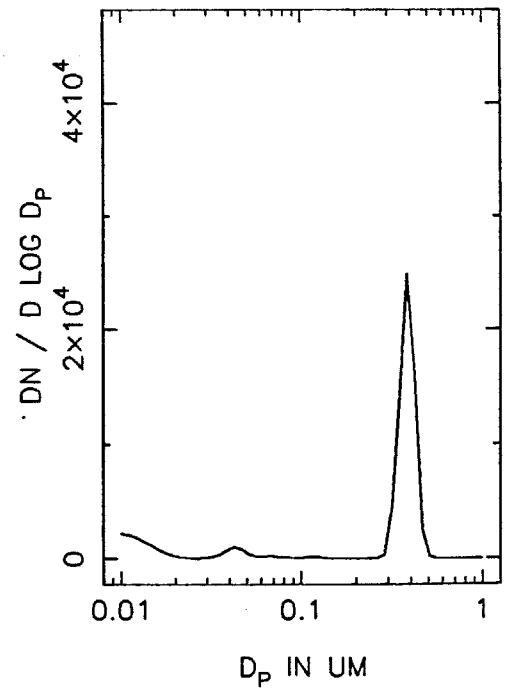

TO46B NUMBER DISTRIBUTION, T=4.0

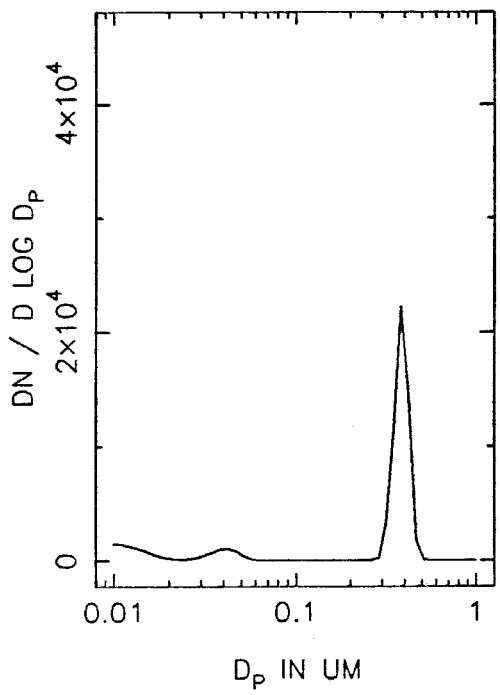

TO46B VOLUME DISTRIBUTION, T=0

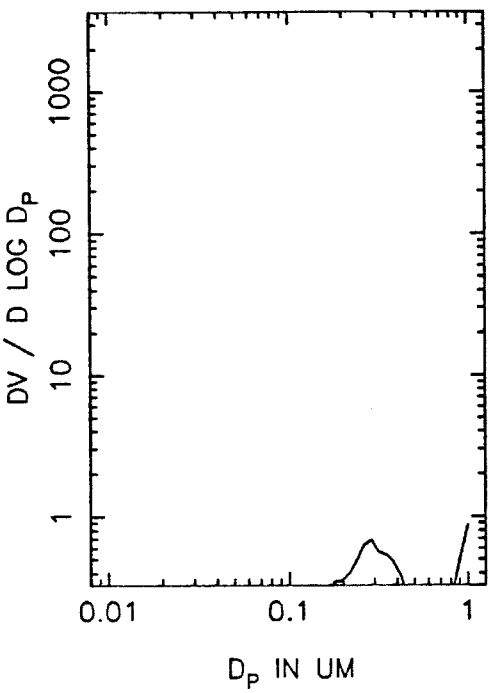

T=0.5 HOURS

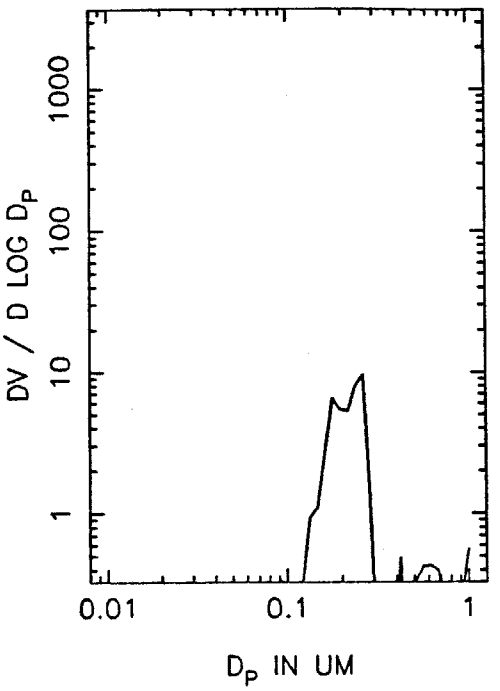

T=1.0 HOURS

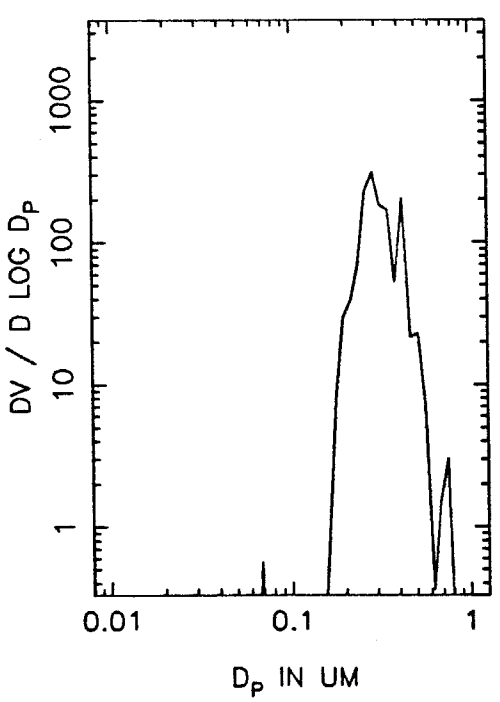

T=1.5 HOURS

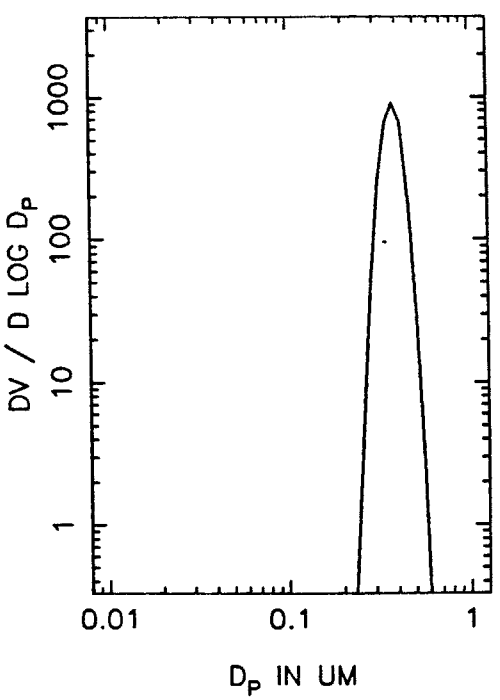

TO46B VOLUME DISTRIBUTION, T=2.0

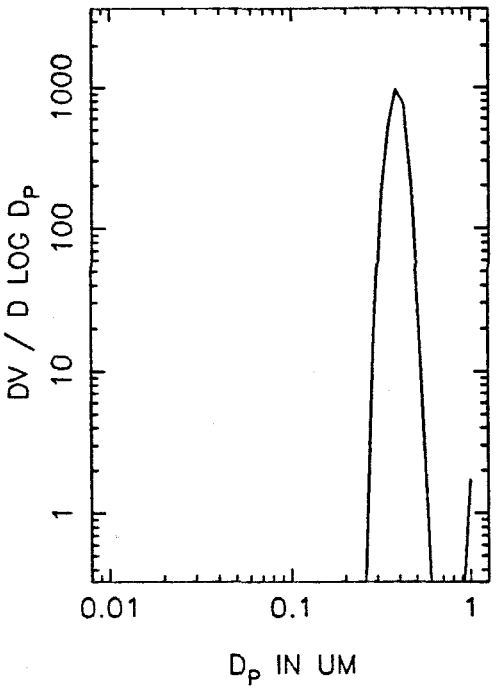

T=2.5 HOURS

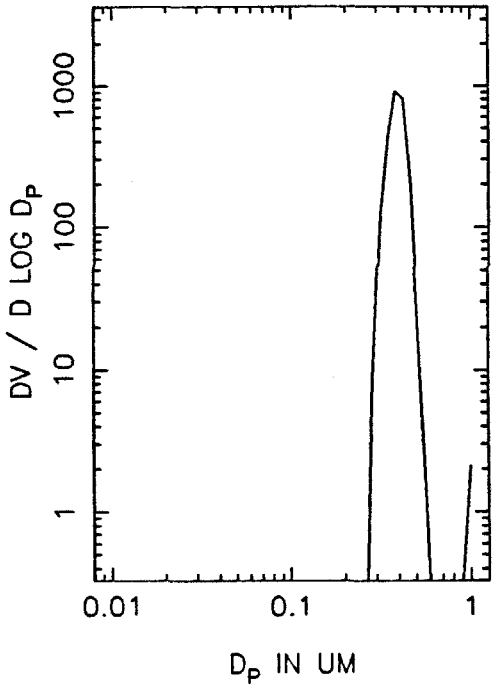

T=3.0 HOURS

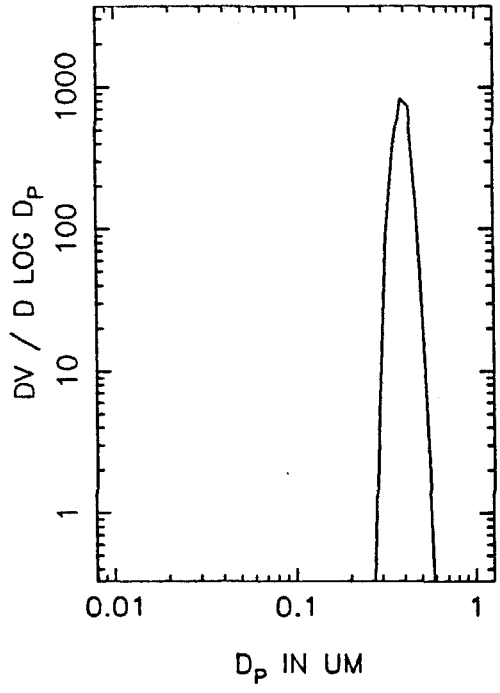

T=3.5 HOURS

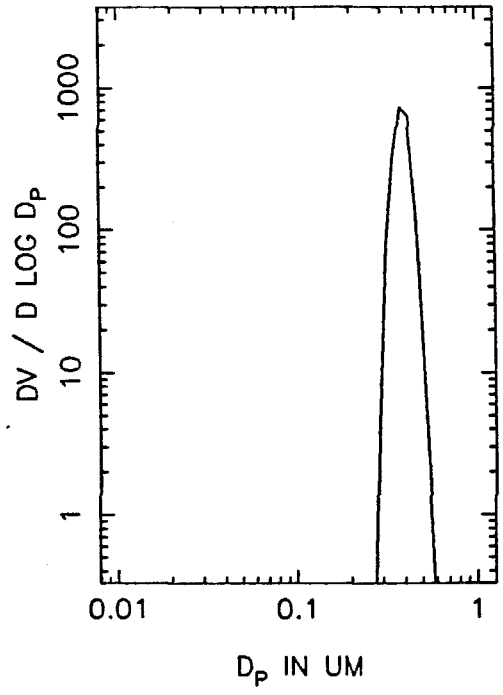

TO46B VOLUME DISTRIBUTION, T=4.0

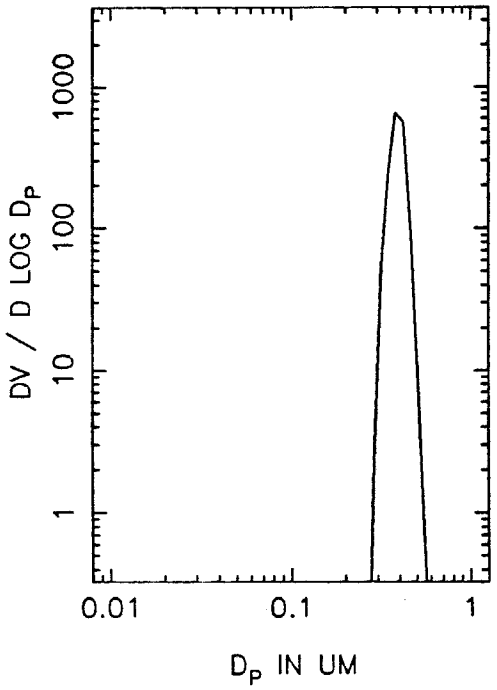

TN49 TOTAL NUMBER, SIDE A

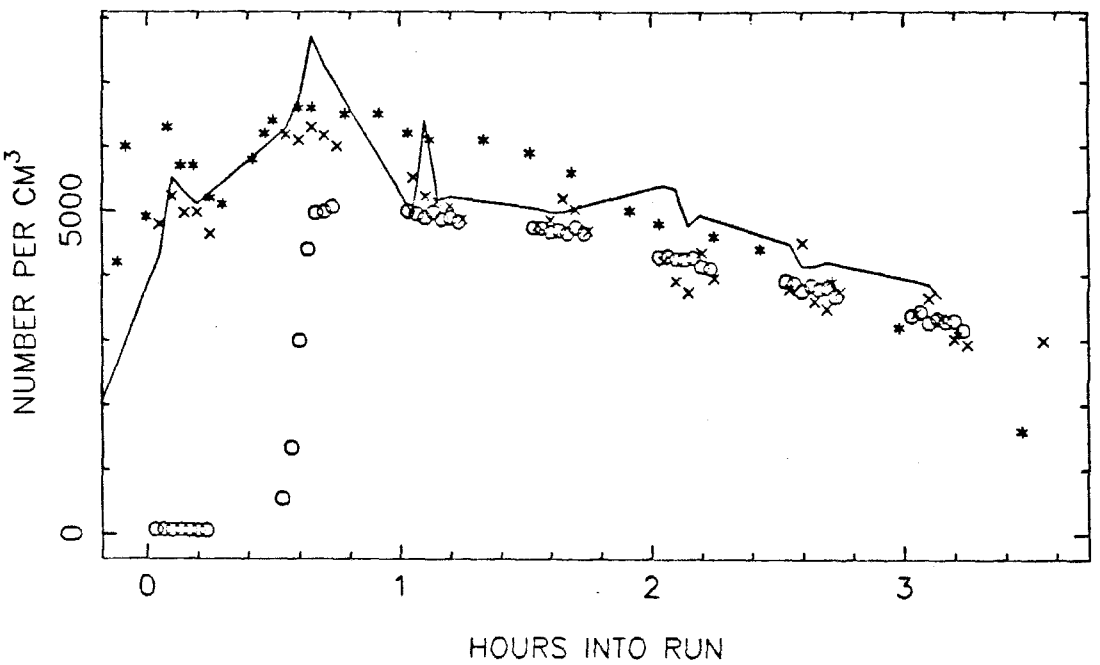

SIDE B

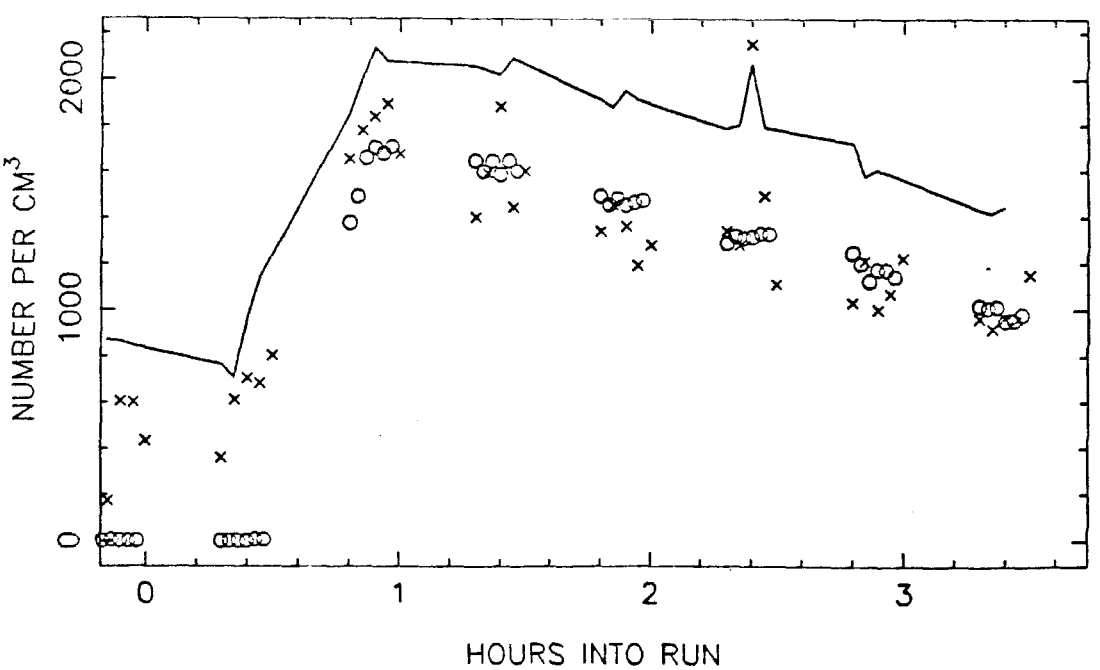

TN49 VOLUME IN THE AEROSOL PHASE, SIDE A

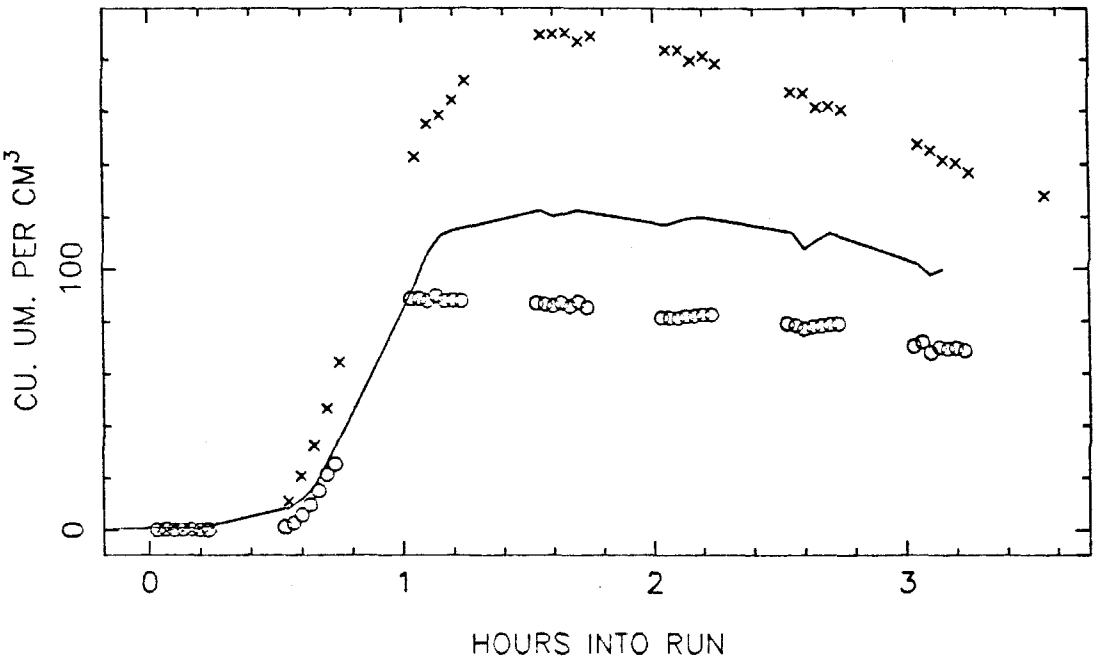

SIDE B

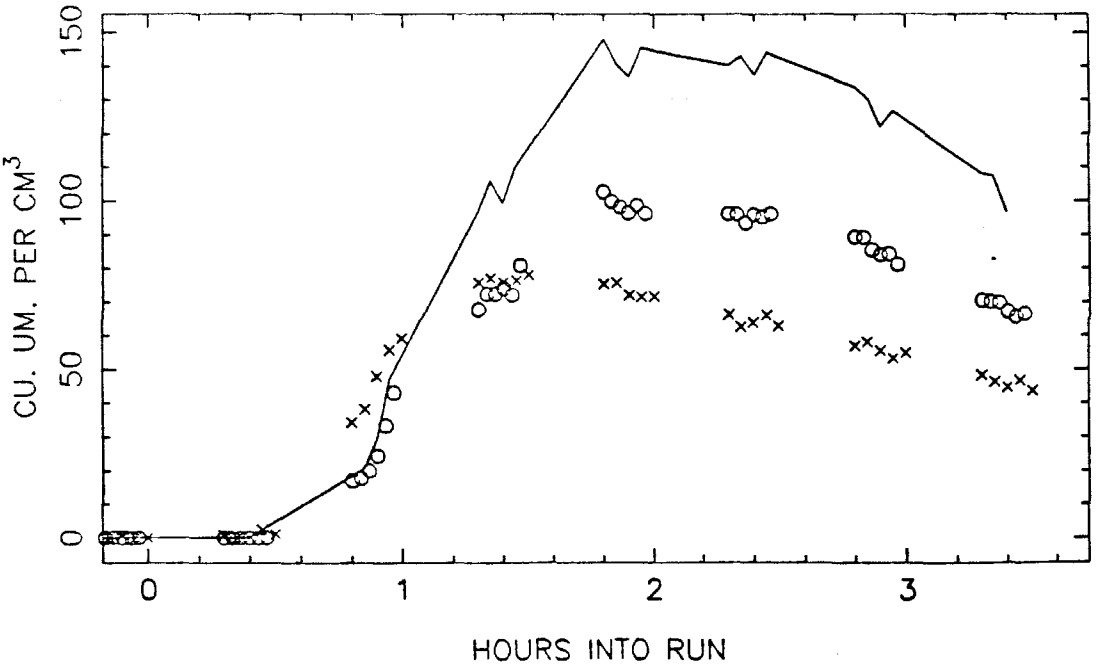

TN49 MEAN PARTICLE SIZE, SIDE A

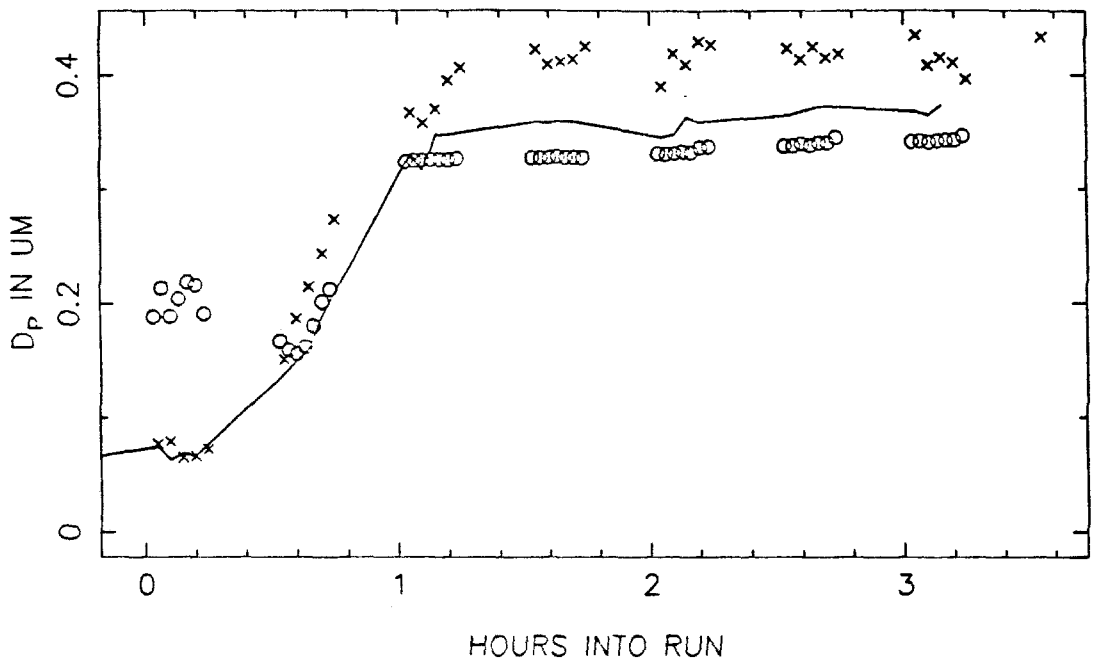

SIDE B

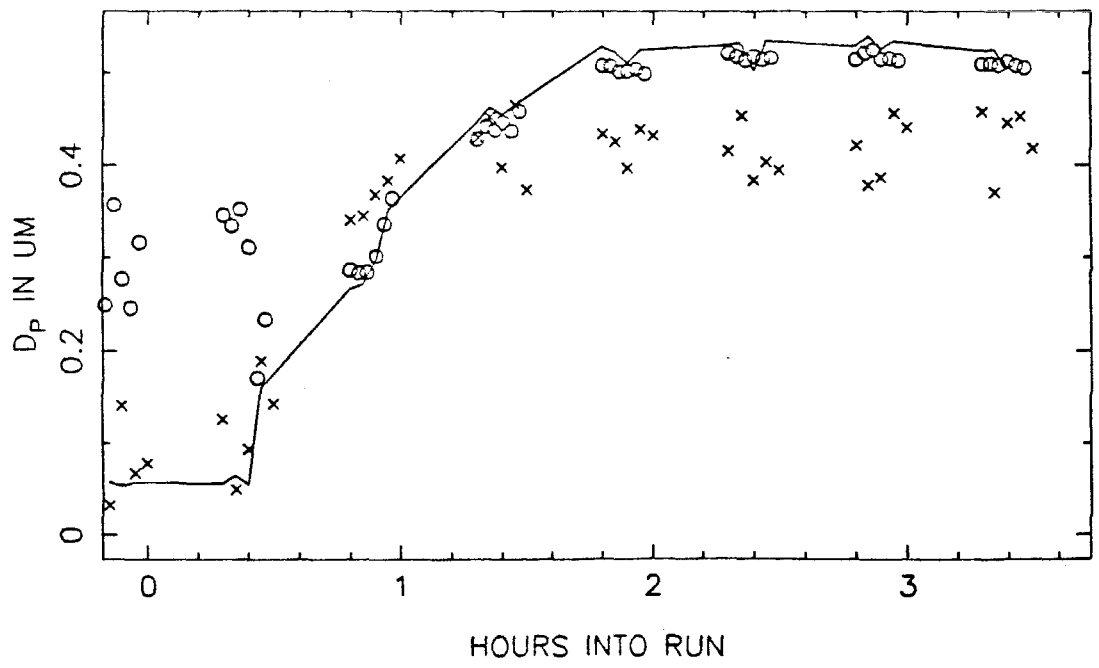

TN49A NUMBER DISTRIBUTION, T=0

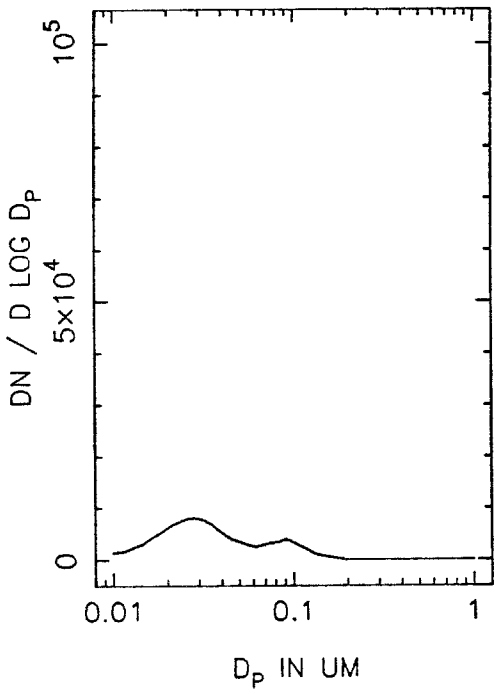

T=0.5 HOURS

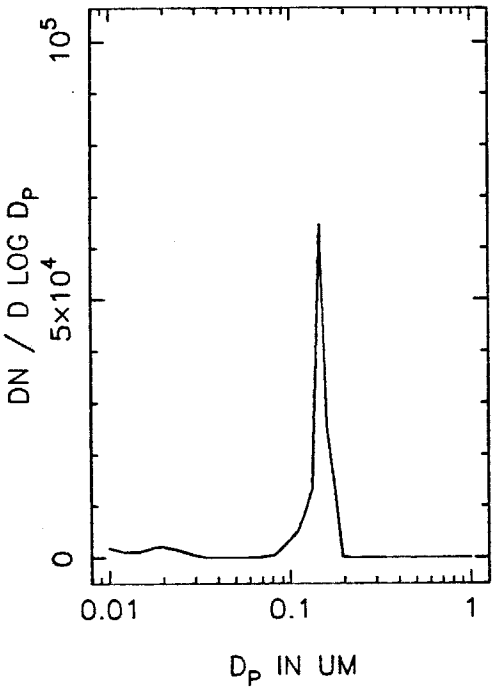

T=1.0 HOURS

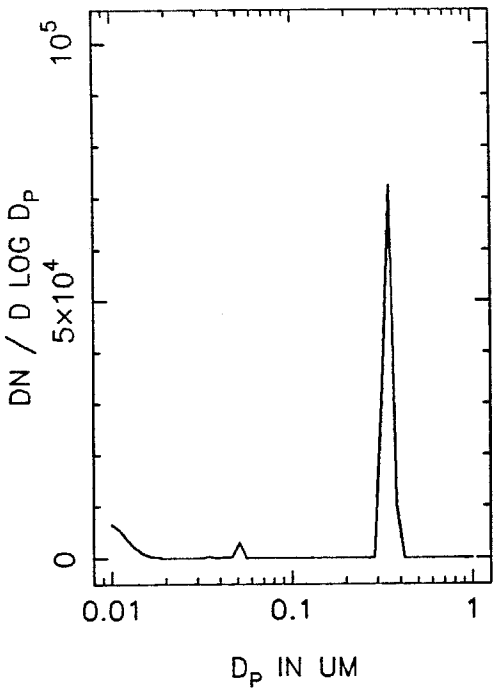

T=1.5 HOURS

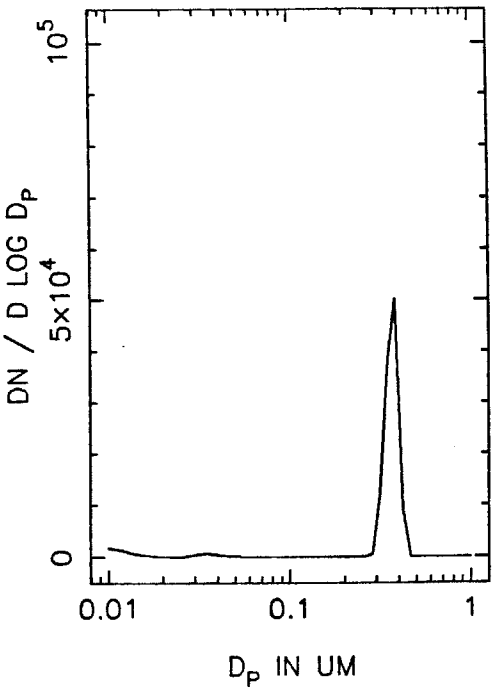

TN49A NUMBER DISTRIBUTION, T=2.0

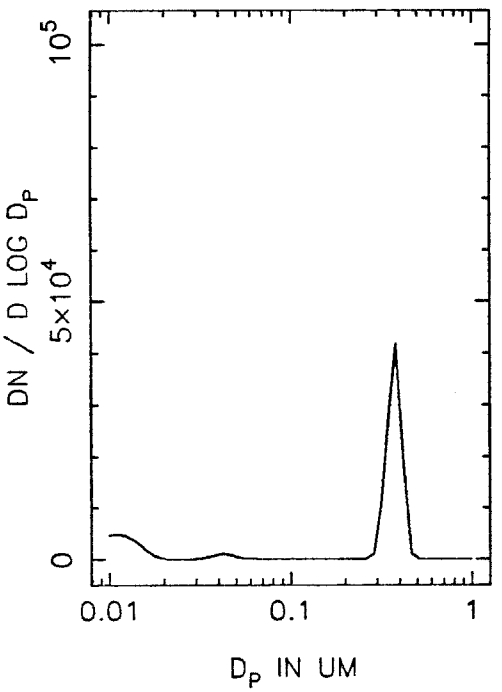

T=2.5 HOURS

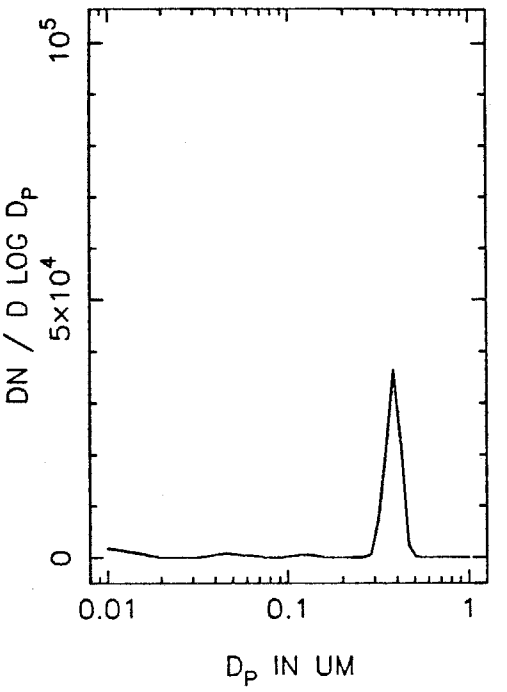

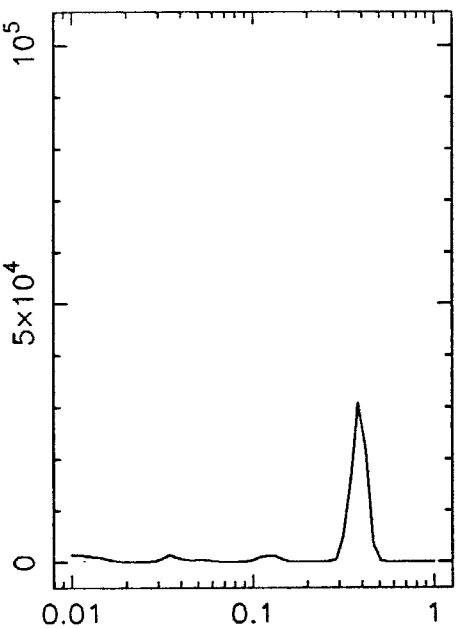

TN49A VOLUME DISTRIBUTION, T=0

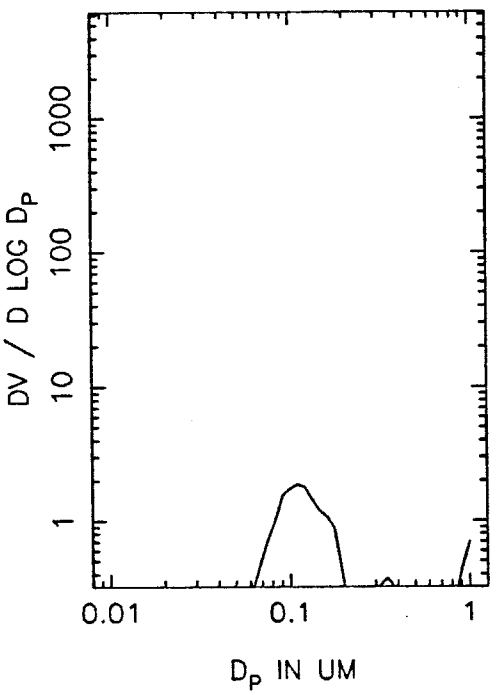

T=0.5 HOURS

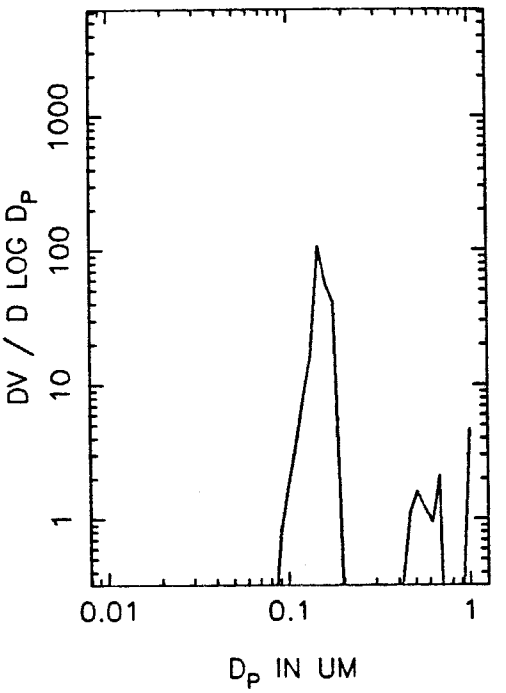

T=1.0 HOURS

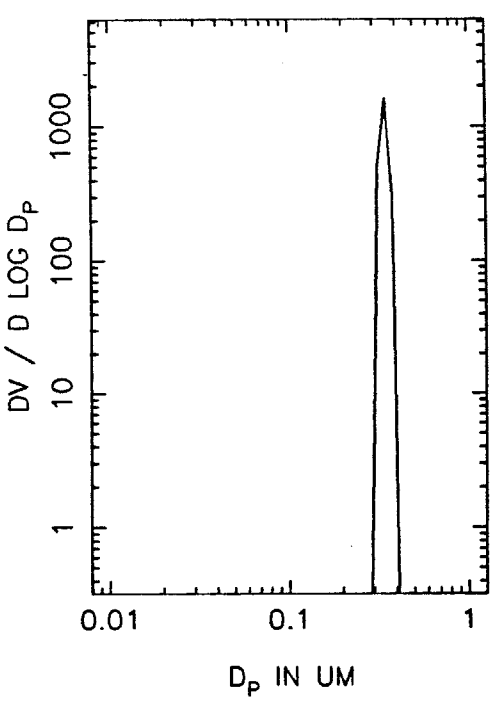

T=1.5 HOURS

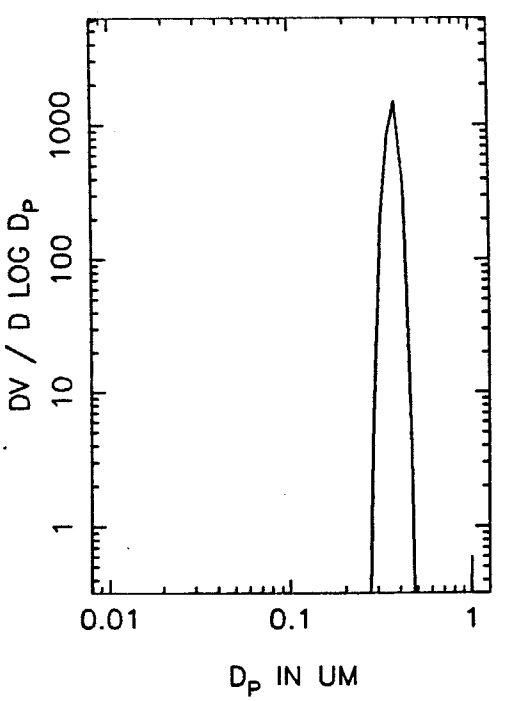

TN49A VOLUME DISTRIBUTION, T=2.0

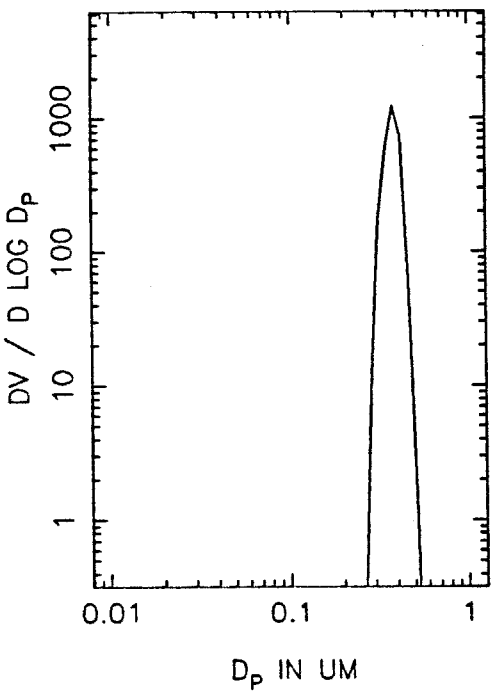

T=2.5 HOURS

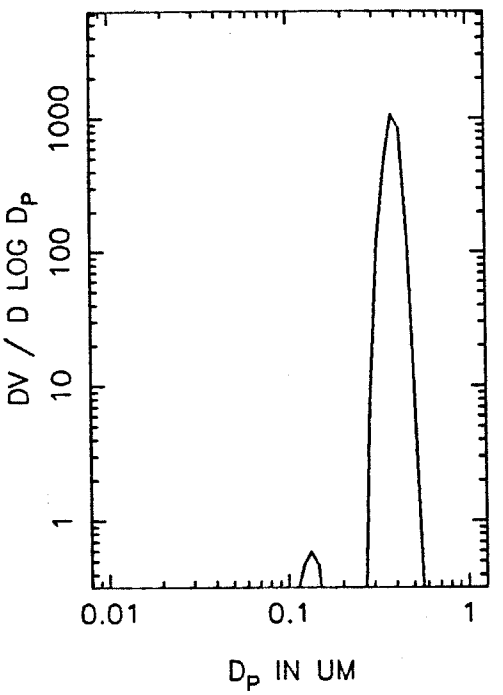

T=3.0 HOURS

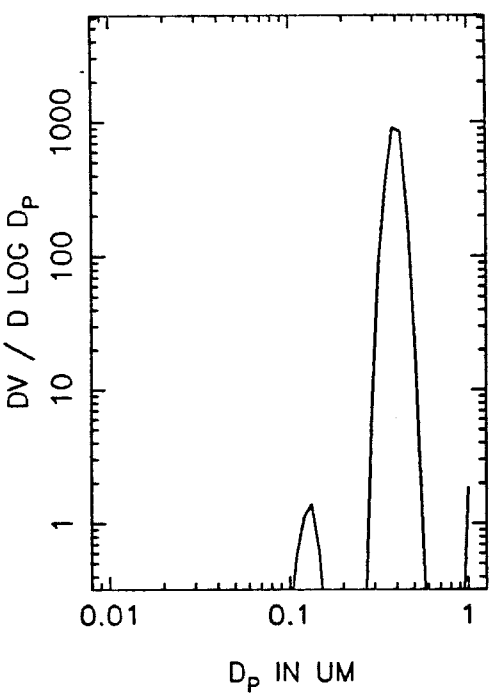

TN49B NUMBER DISTRIBUTION, T=0

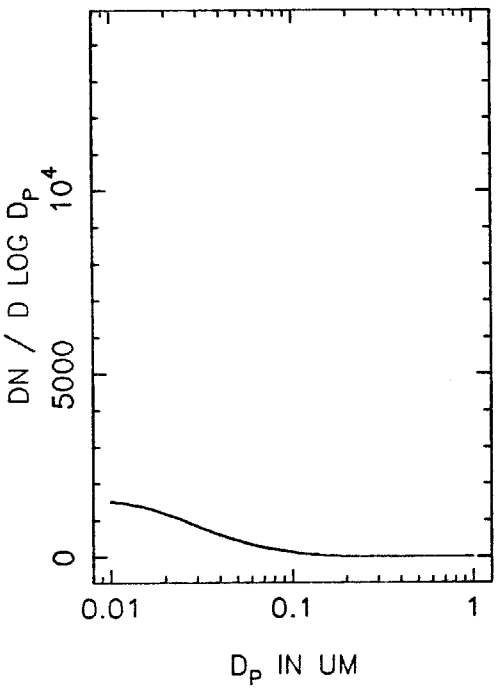

T=0.5 HOURS

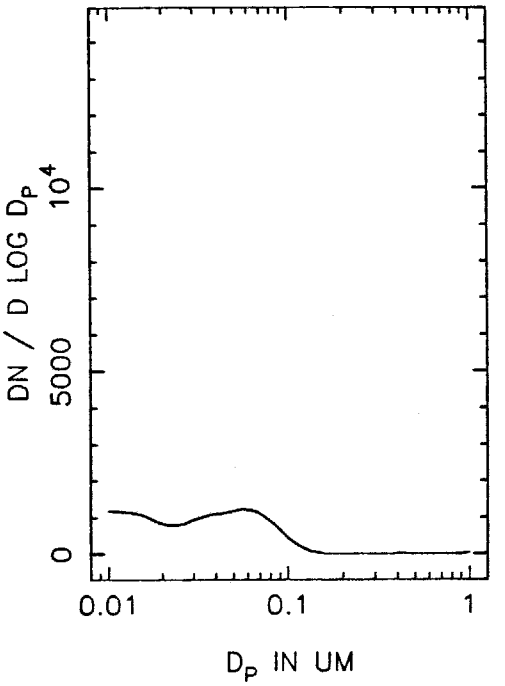

T=1.0 HOURS

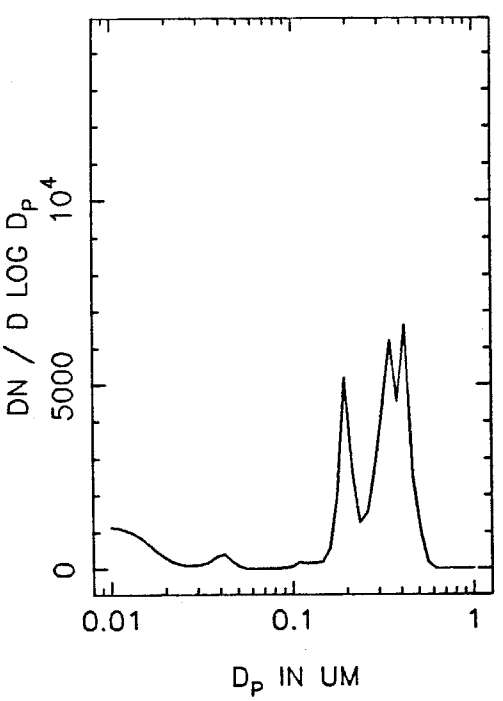

T=1.5 HOURS

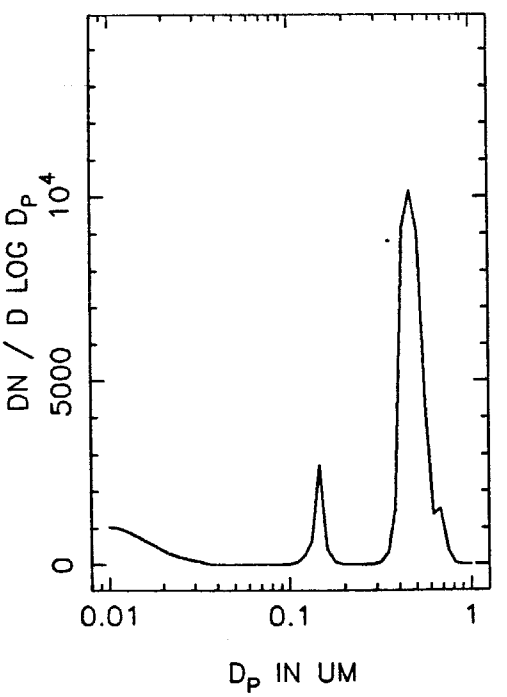

TN49B NUMBER DISTRIBUTION, T=2.0

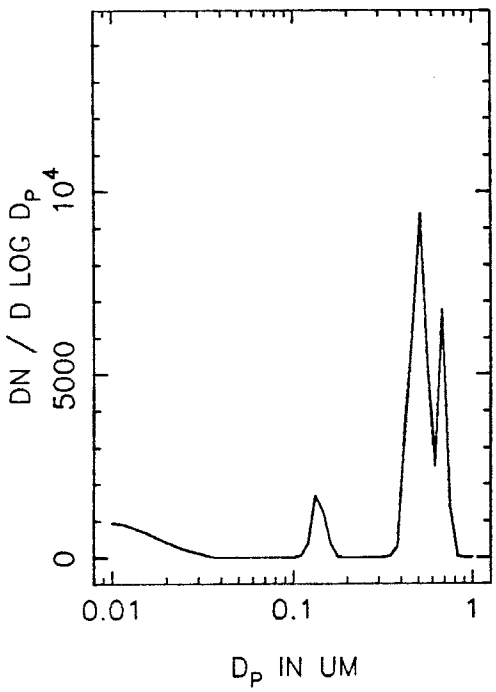

T=2.5 HOURS

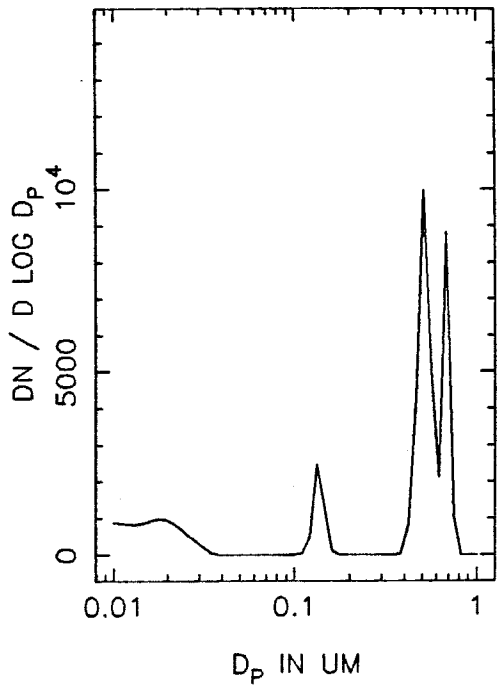

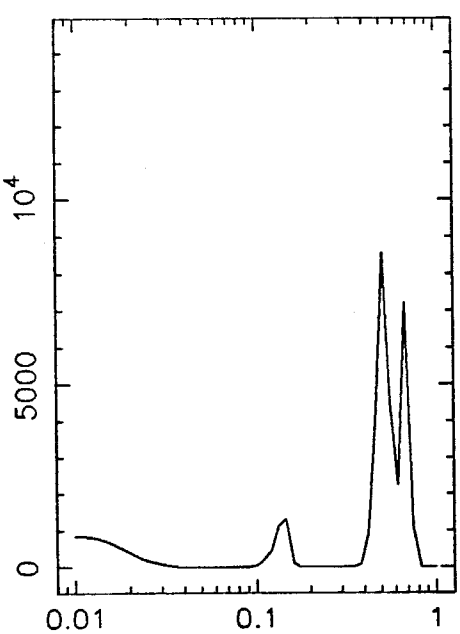

TN49B VOLUME DISTRIBUTION, T=0

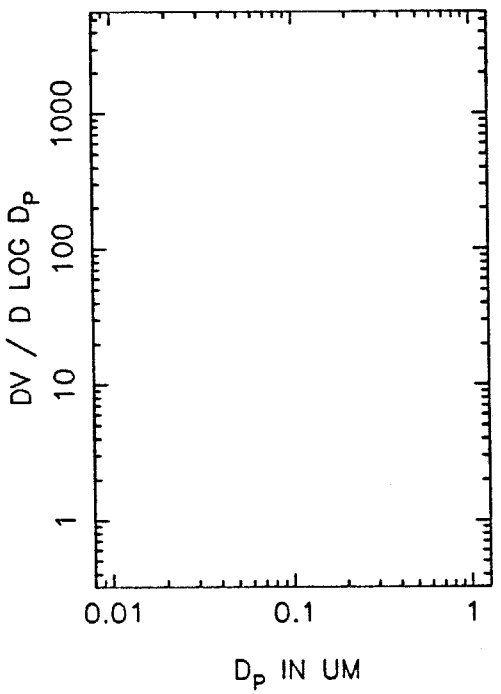

T=0.5 HOURS

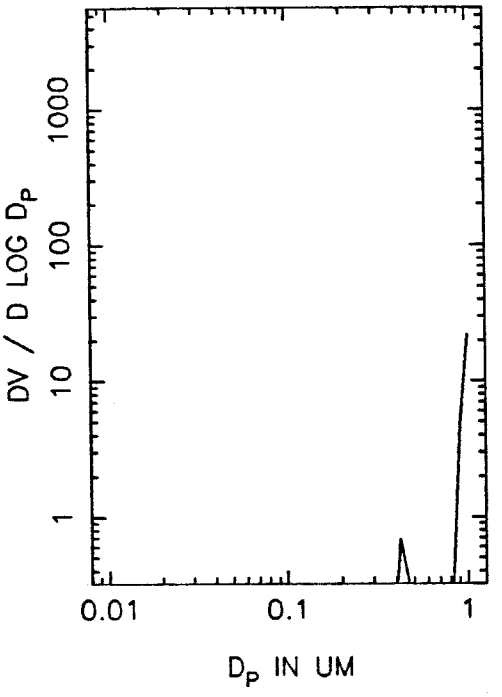

T=1.0 HOURS

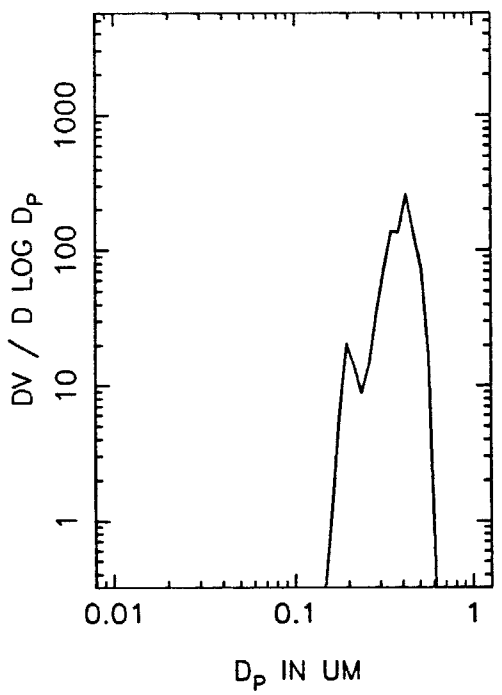

T=1.5 HOURS

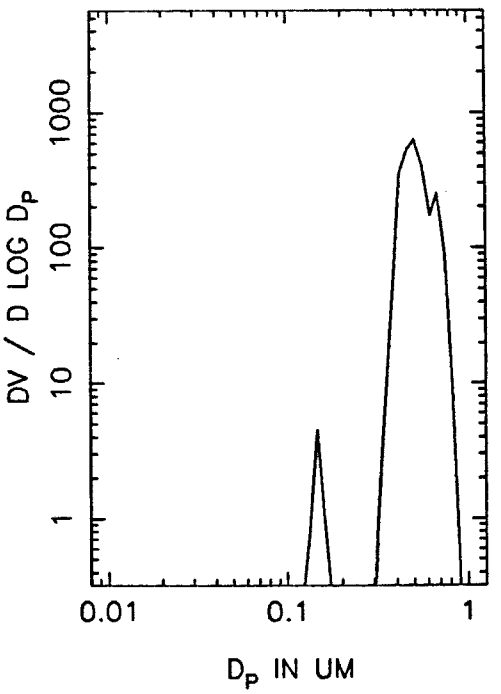

TN49B VOLUME DISTRIBUTION, T=2.0

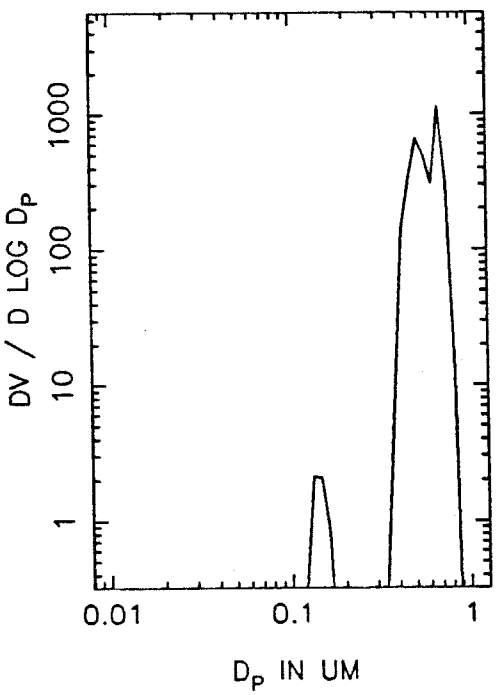

T=2.5 HOURS

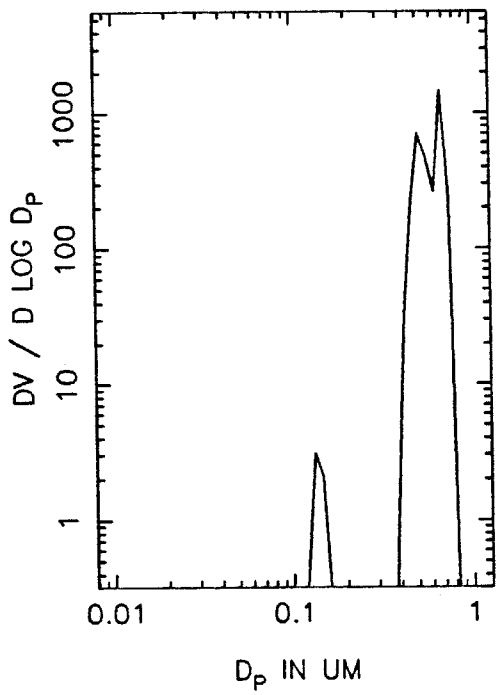

T=3.0 HOURS

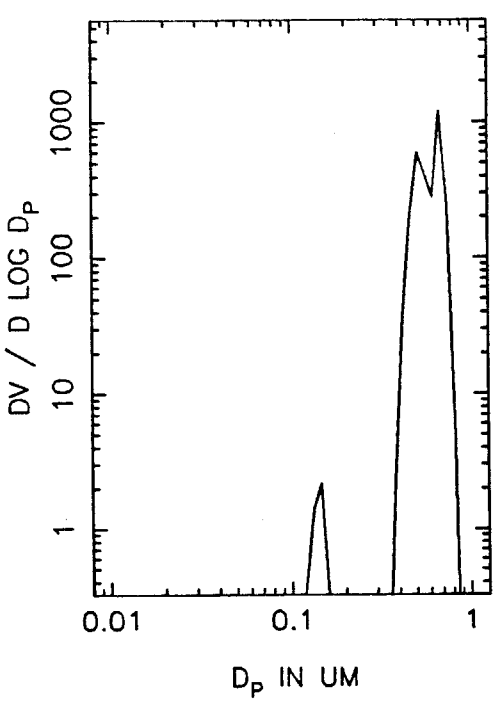

TN52 TOTAL NUMBER, SIDE A

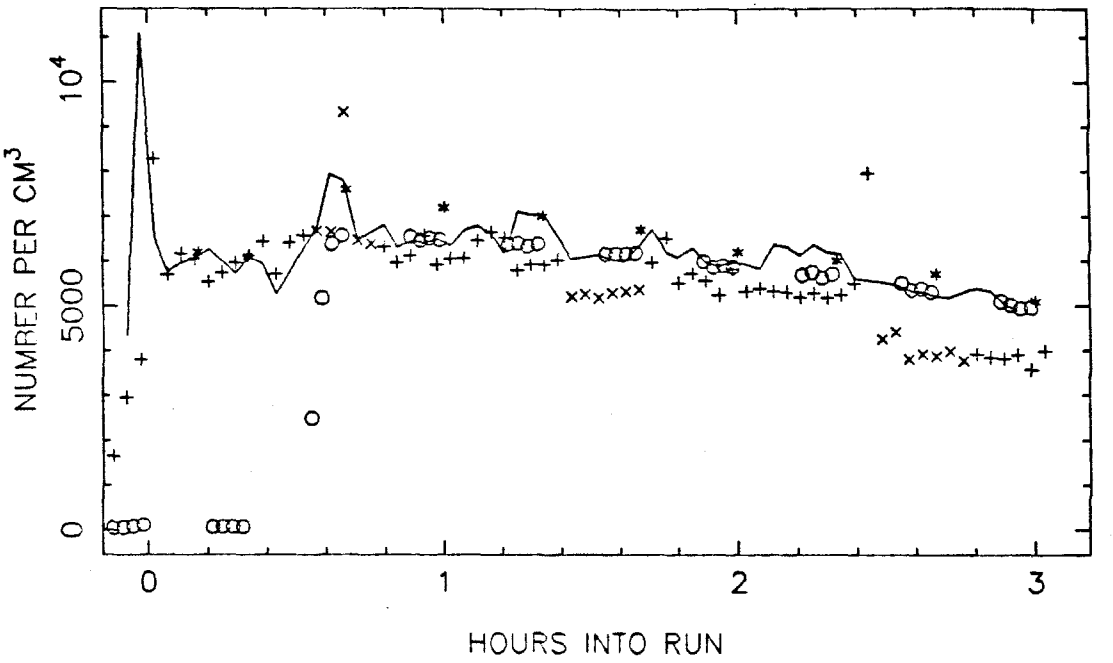

SIDE B

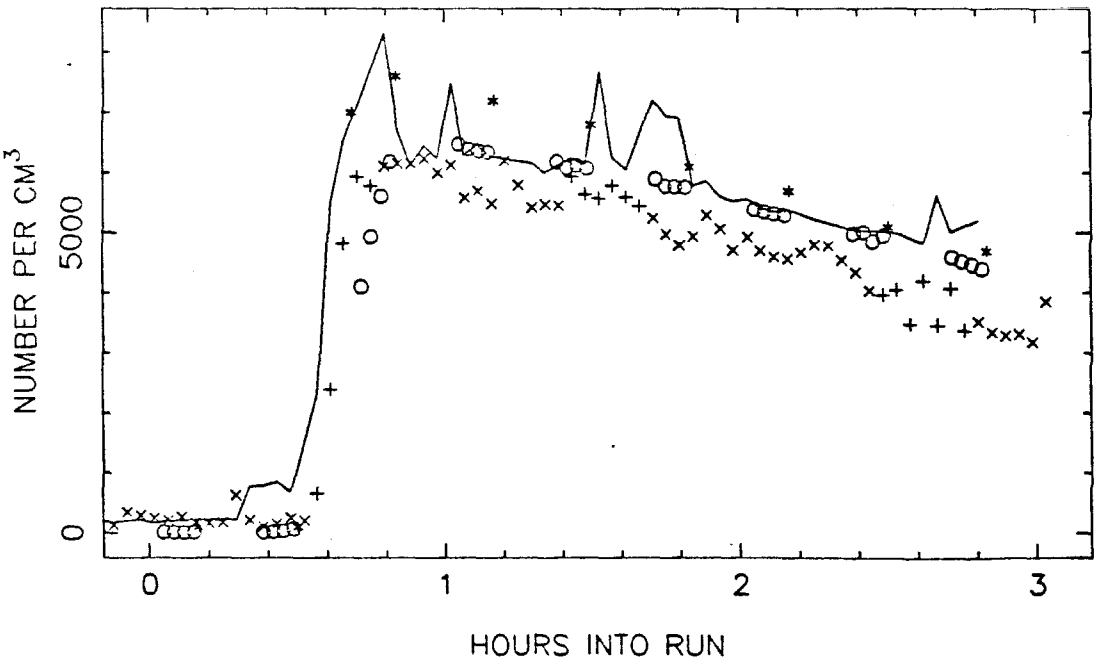

TN52 VOLUME IN THE AEROSOL PHASE, SIDE A

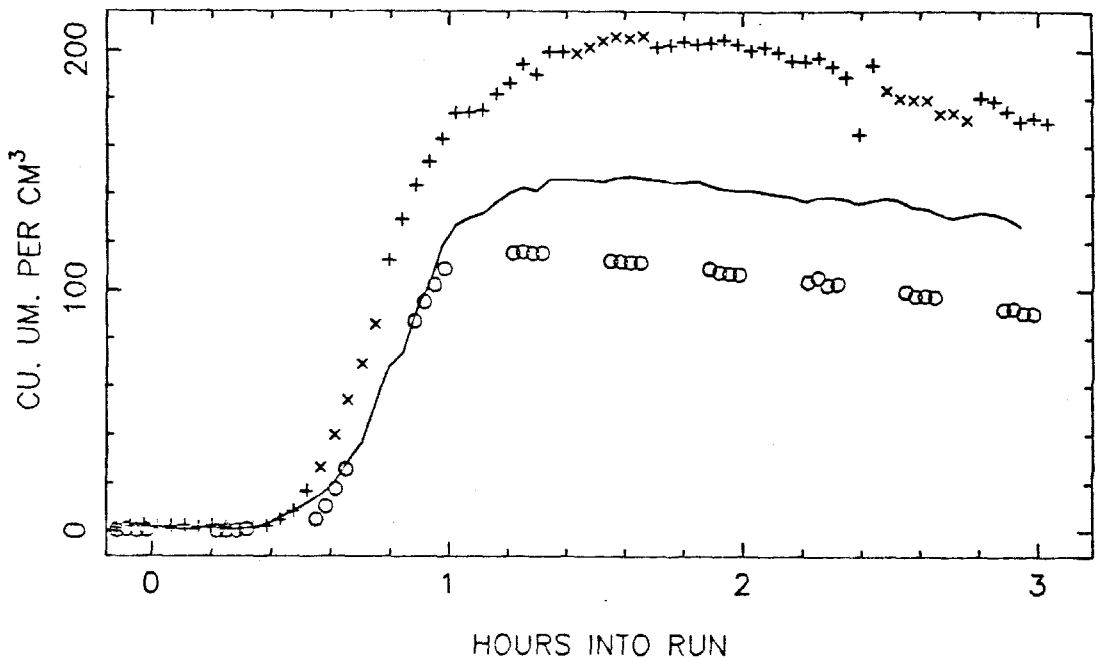

SIDE B

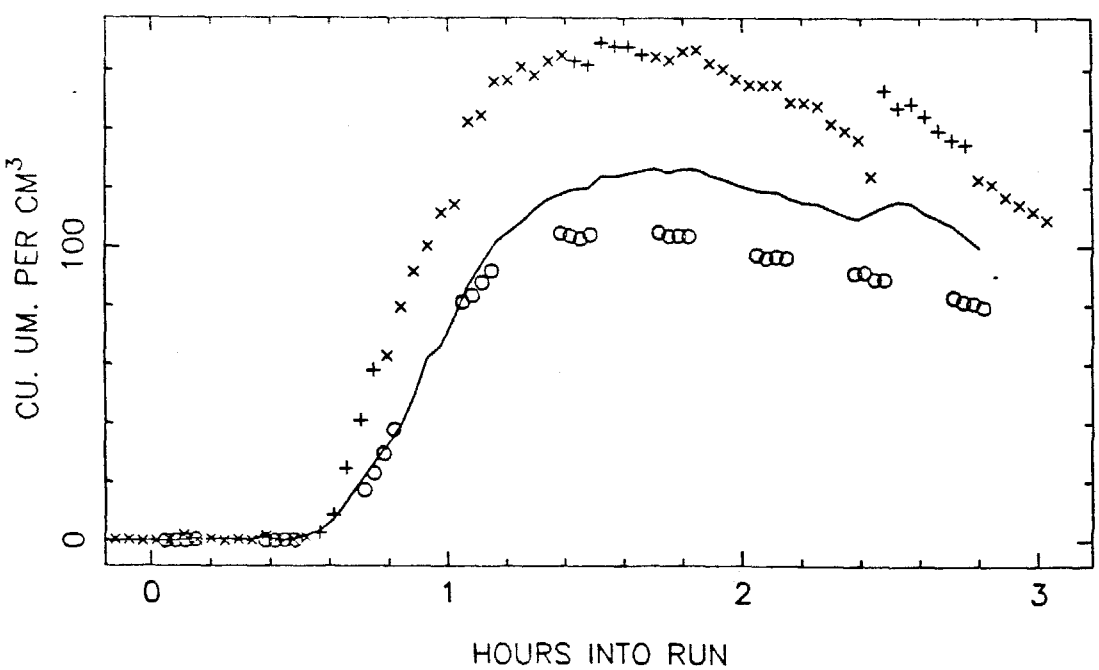

TN52 MEAN PARTICLE SIZE, SIDE A

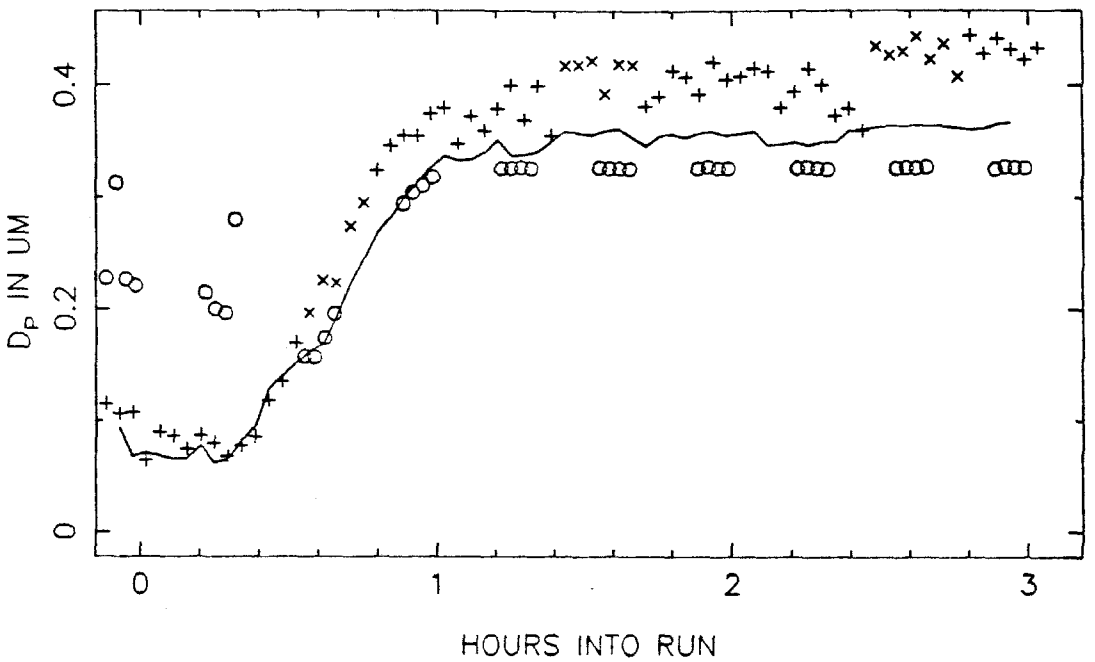

SIDE B

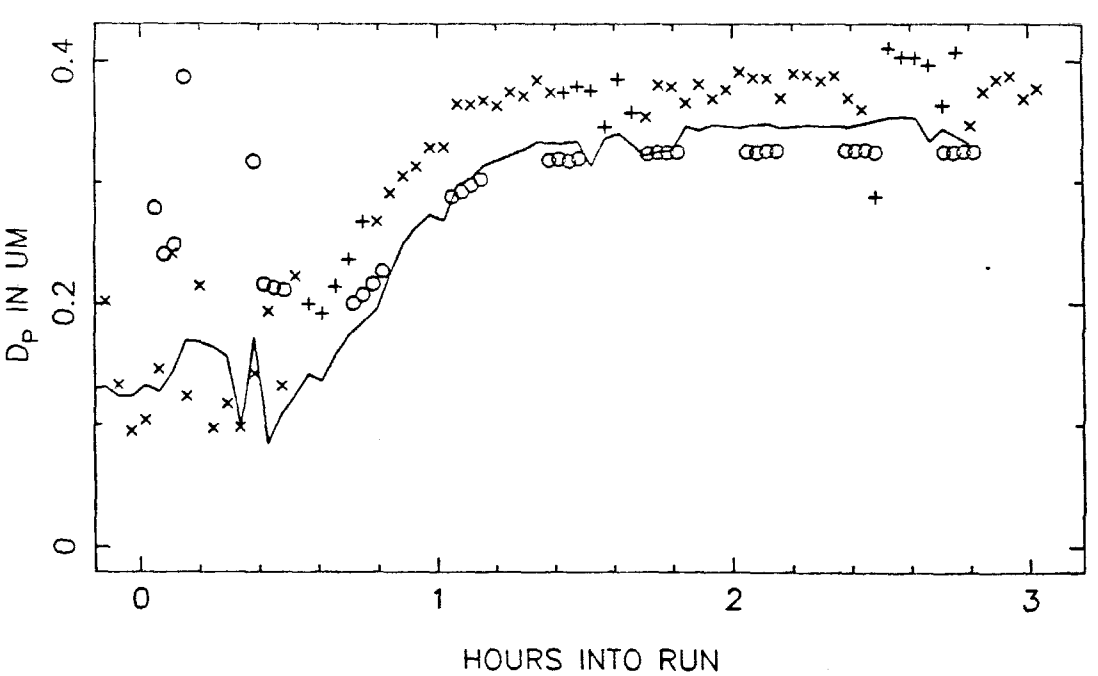

TN52A NUMBER DISTRIBUTION, T=0

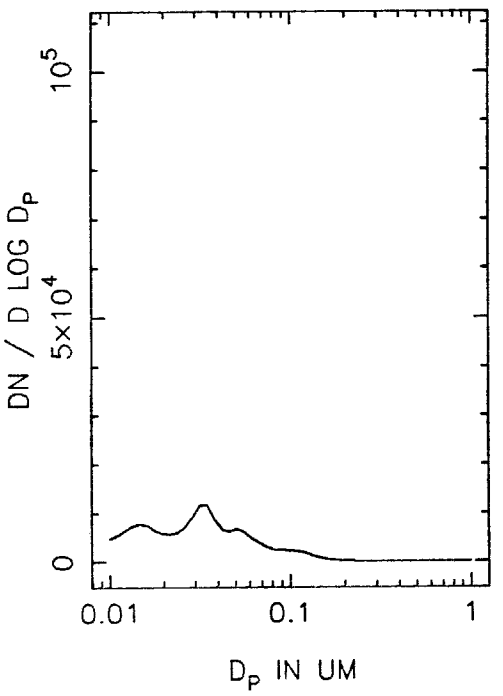

T=0.5 HOURS

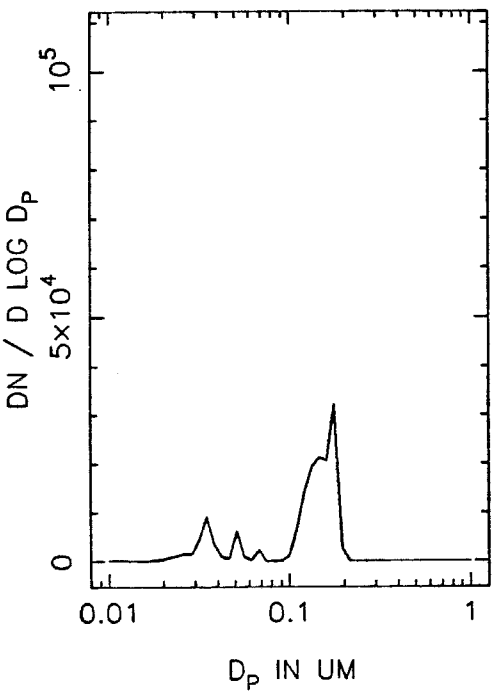

T=1.0 HOURS

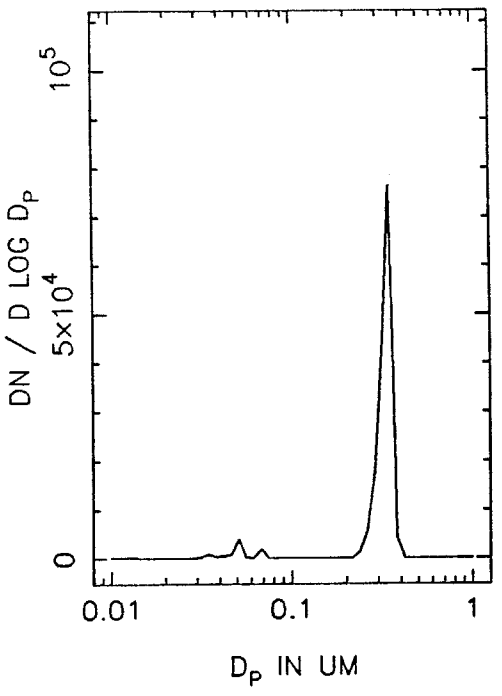

T=1.5 HOURS

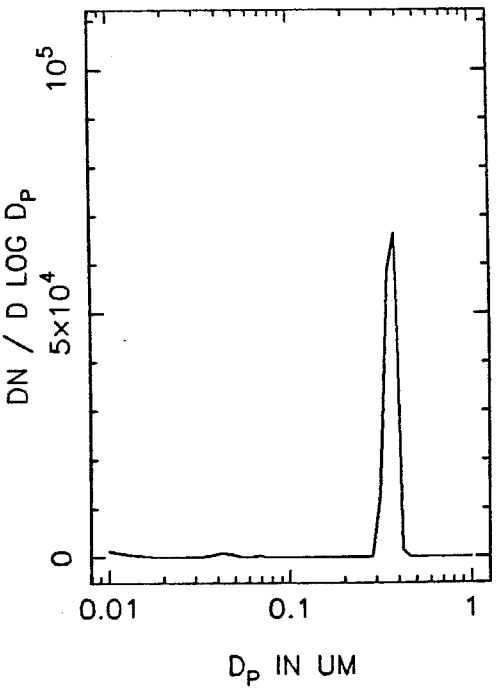

TN52A NUMBER DISTRIBUTION, T=2.0

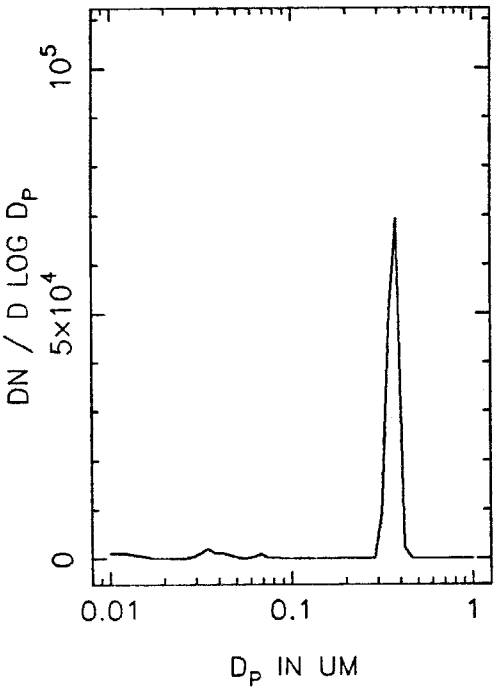

T=2.5 HOURS

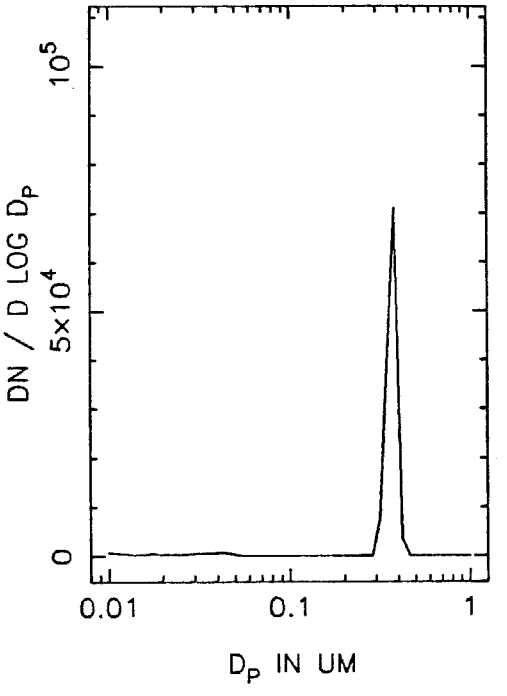

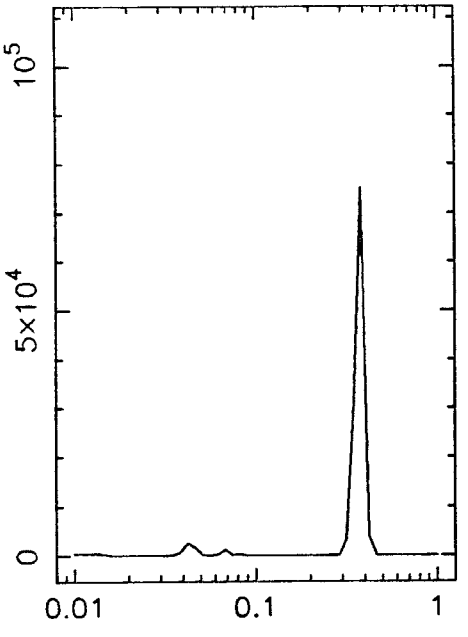

TN52A VOLUME DISTRIBUTION, T=0

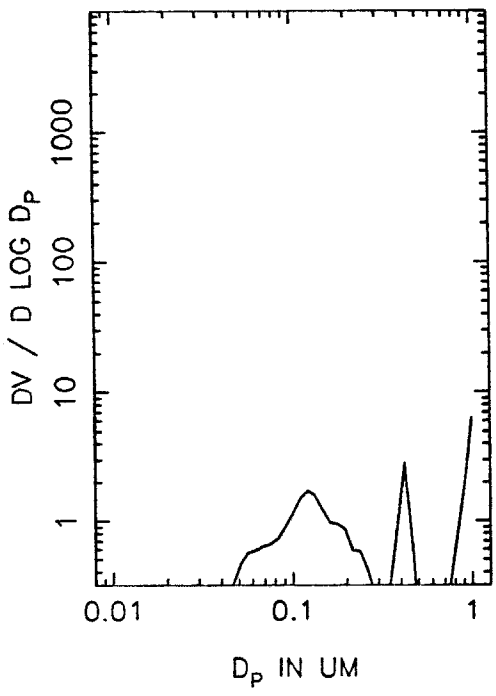

T=0.5 HOURS

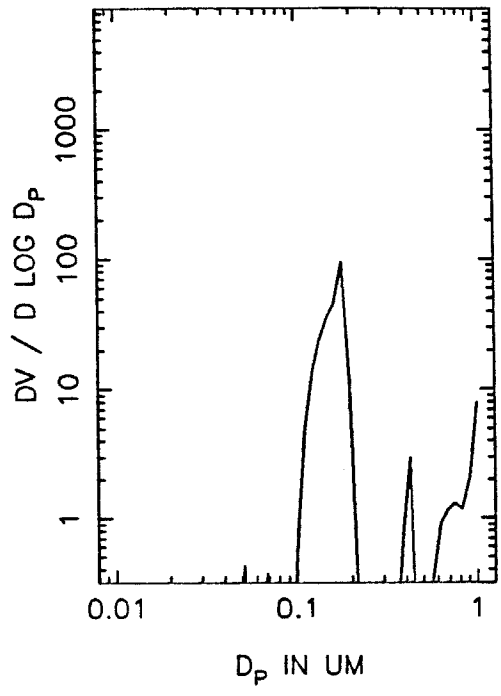

T=1.0 HOURS

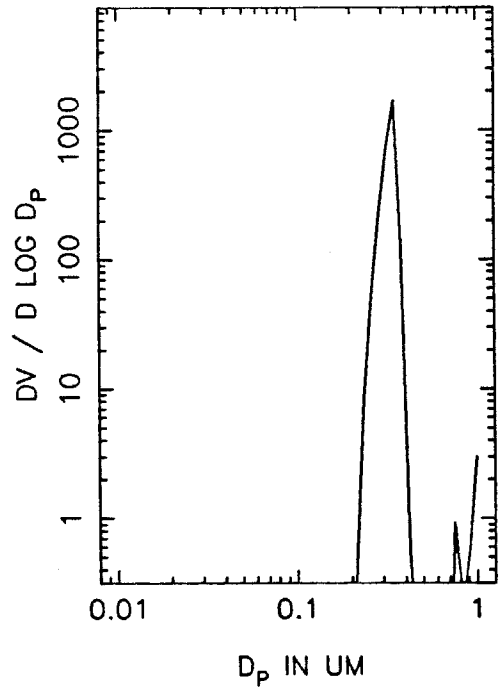

T=1.5 HOURS

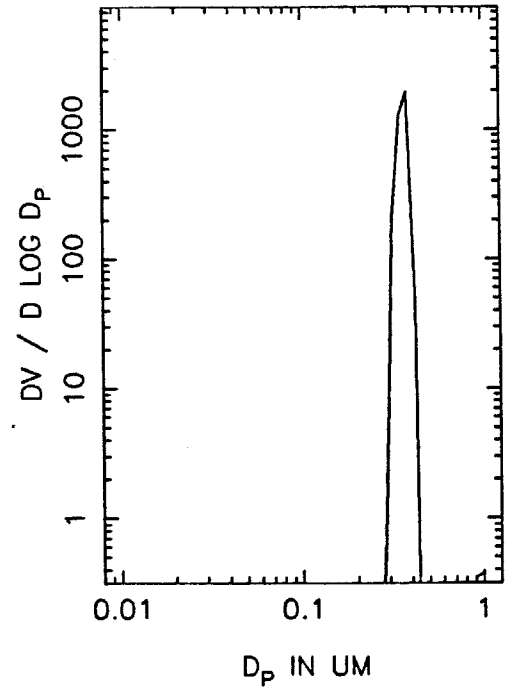

TN52A VOLUME DISTRIBUTION, T=2.0

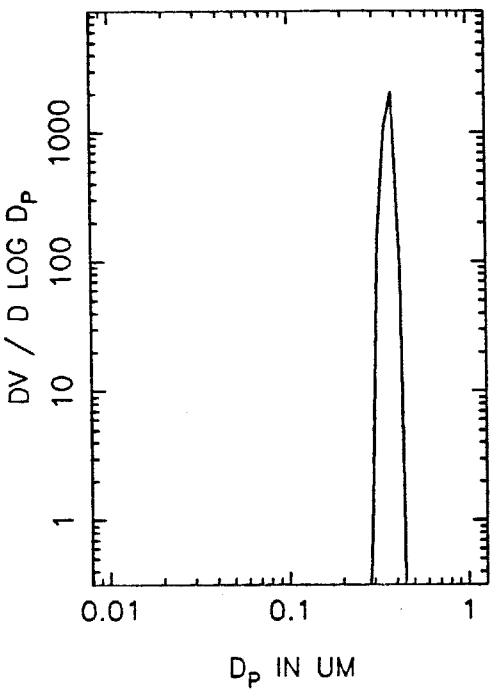

T=2.5 HOURS

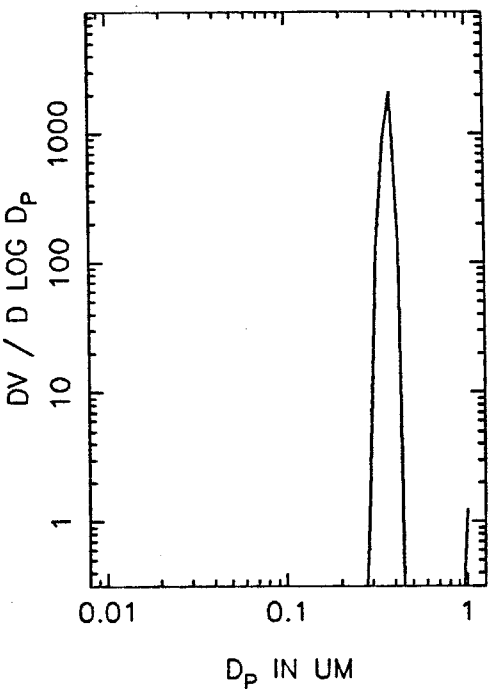

T=3.0 HOURS

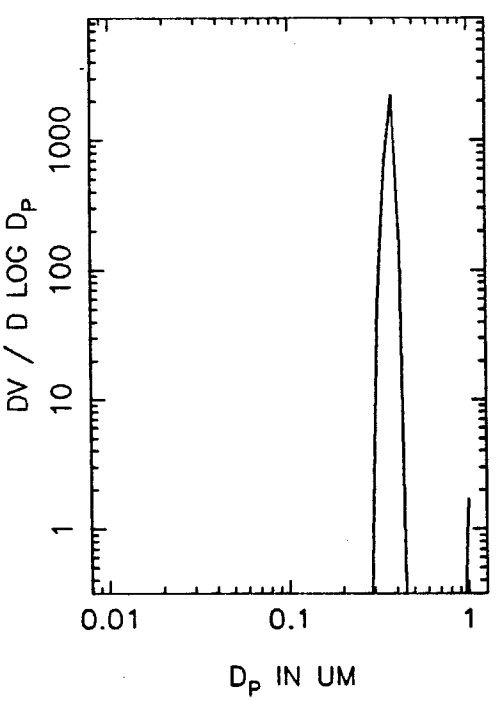

TN52B NUMBER DISTRIBUTION, T=0

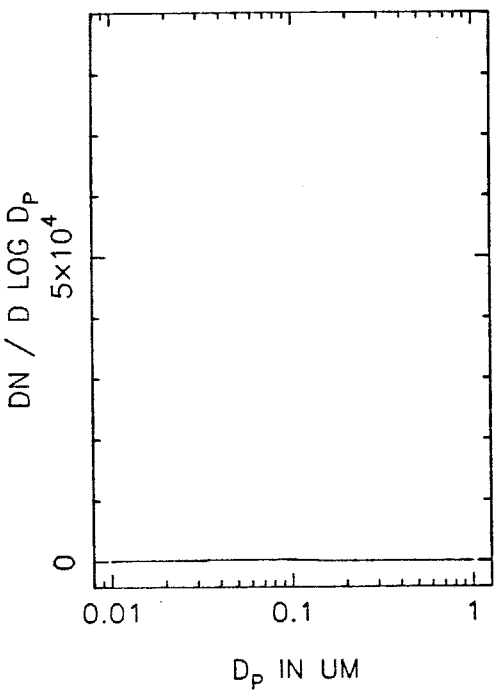

T=0.5 HOURS

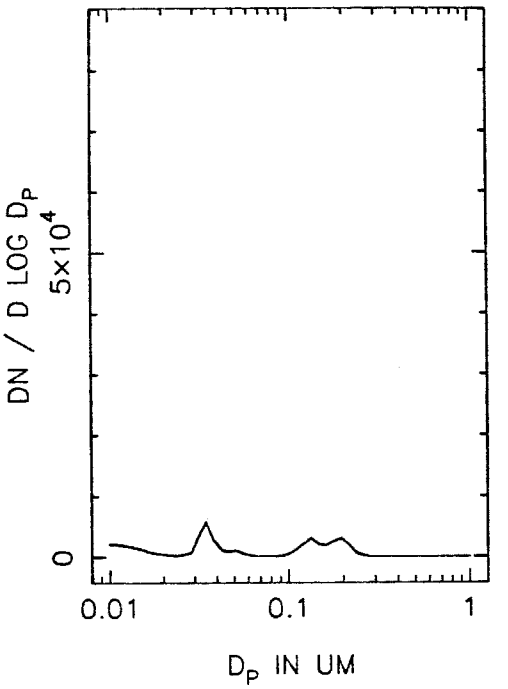

T=1.0 HOURS

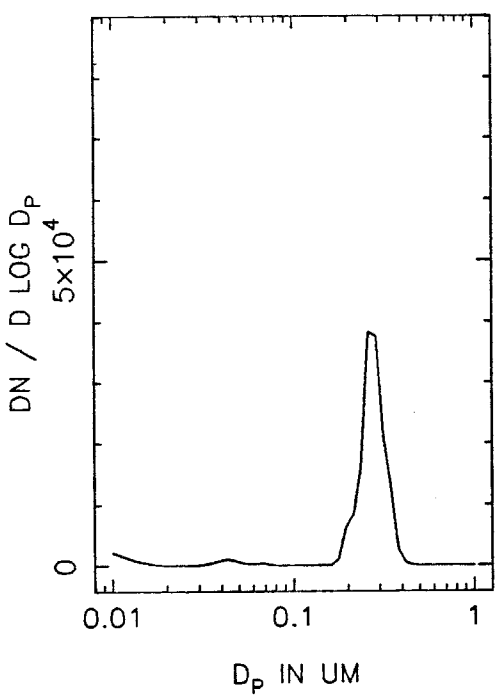

T=1.5 HOURS

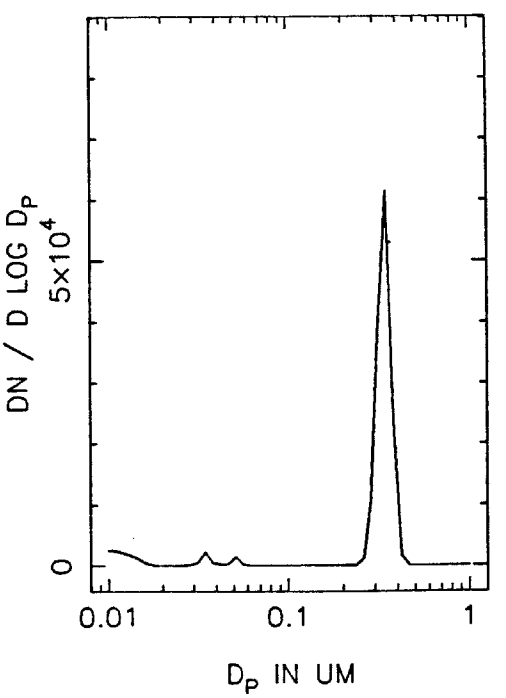

TN52B NUMBER DISTRIBUTION, T=2.0

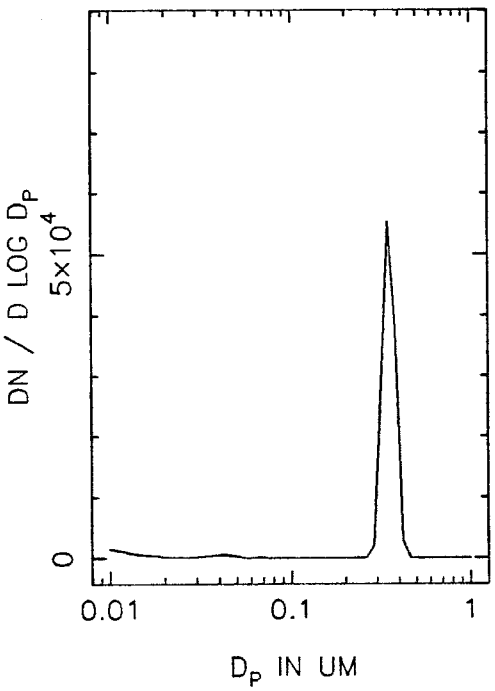

T=2.5 HOURS

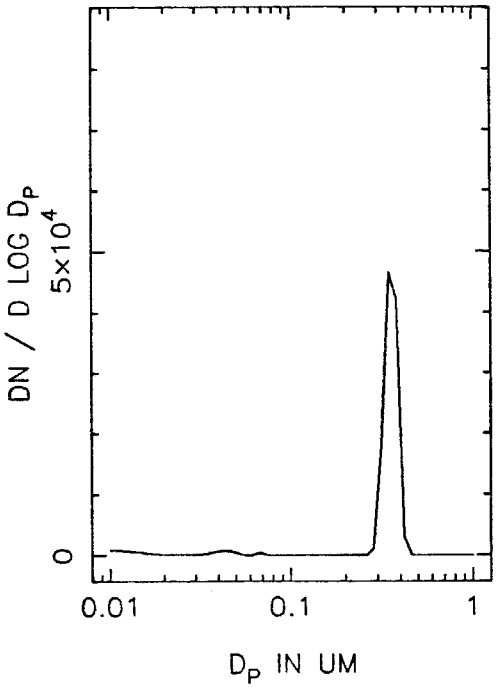

TN52B VOLUME DISTRIBUTION, T=0

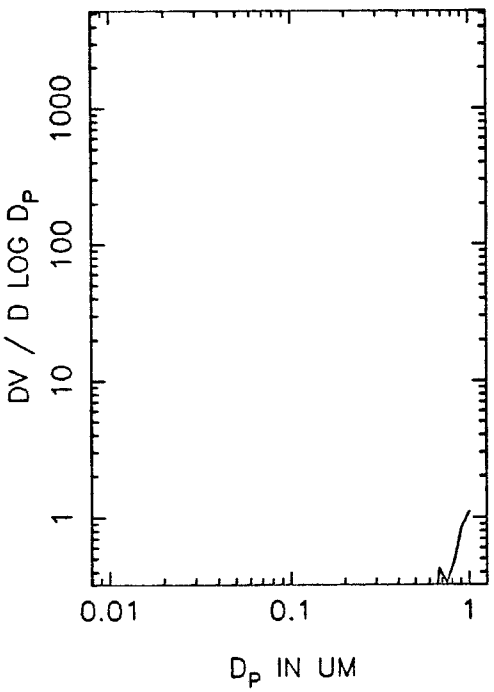

T=0.5 HOURS

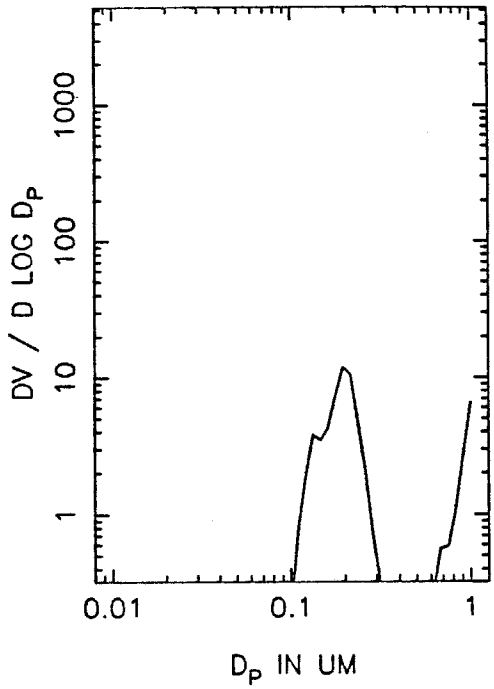

T=1.0 HOURS

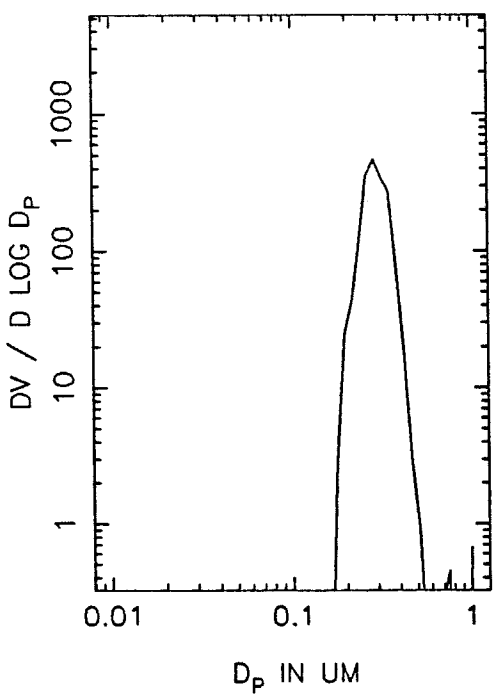

T=1.5 HOURS

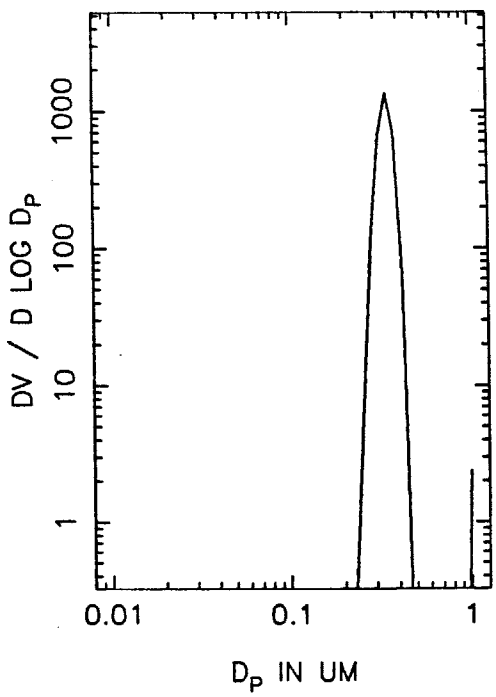

TN52B VOLUME DISTRIBUTION, T=2.0

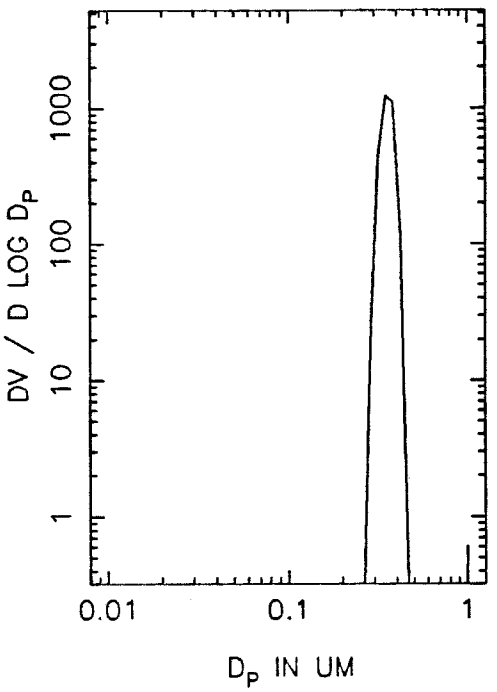

T=2.5 HOURS

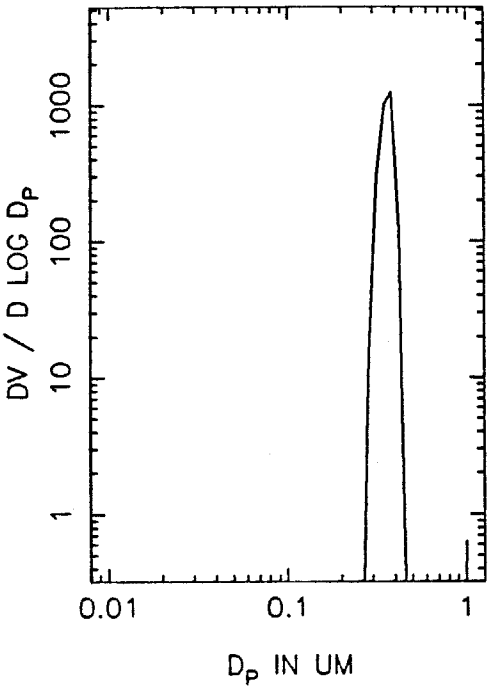

EC64 TOTAL NUMBER, SIDE A

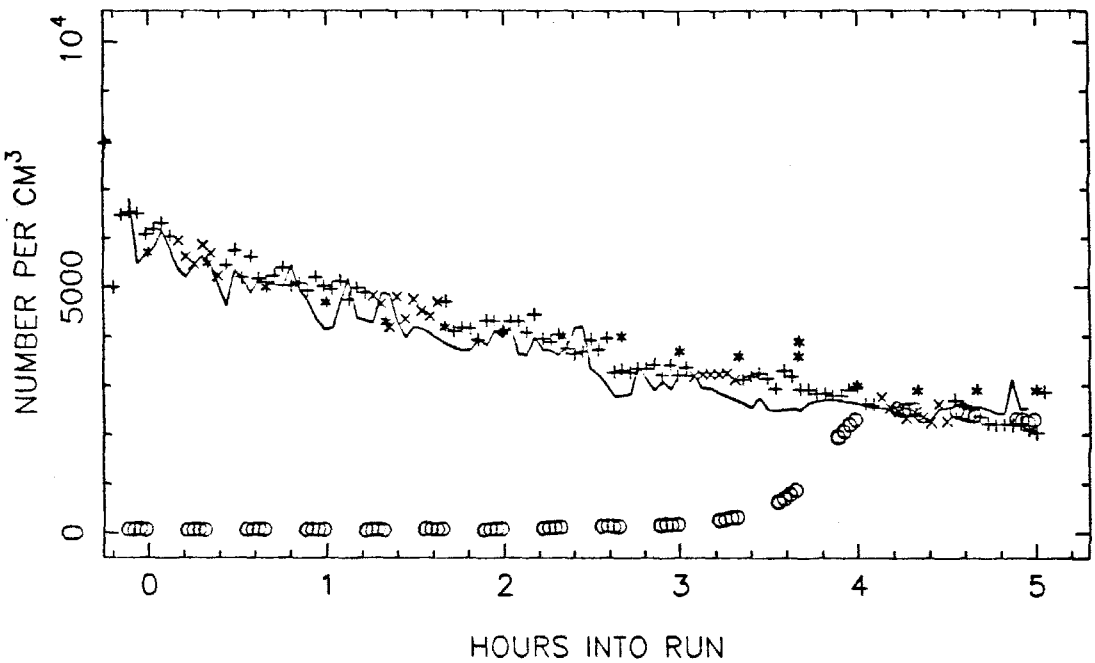

SIDE B

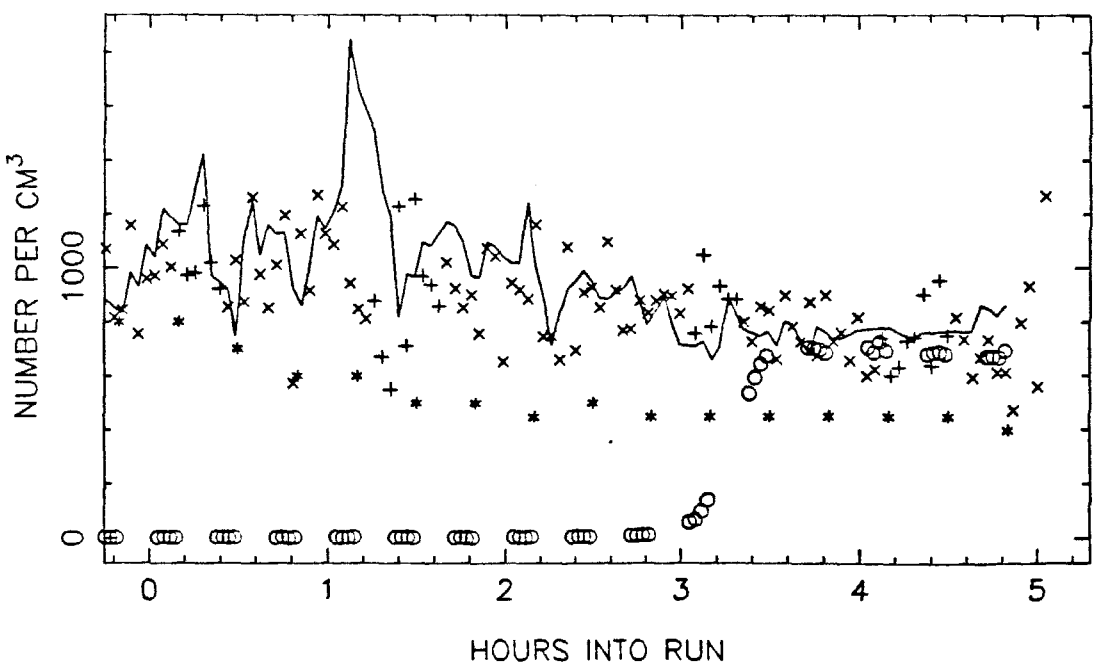

EC64 VOLUME IN THE AEROSOL PHASE, SIDE A

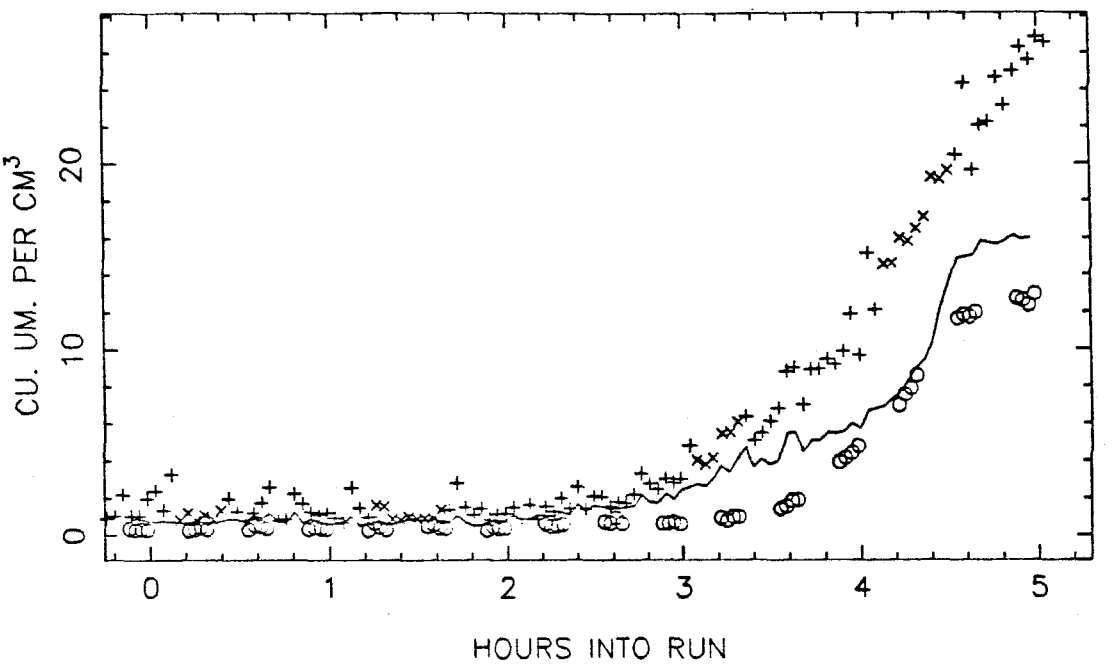

SIDE B

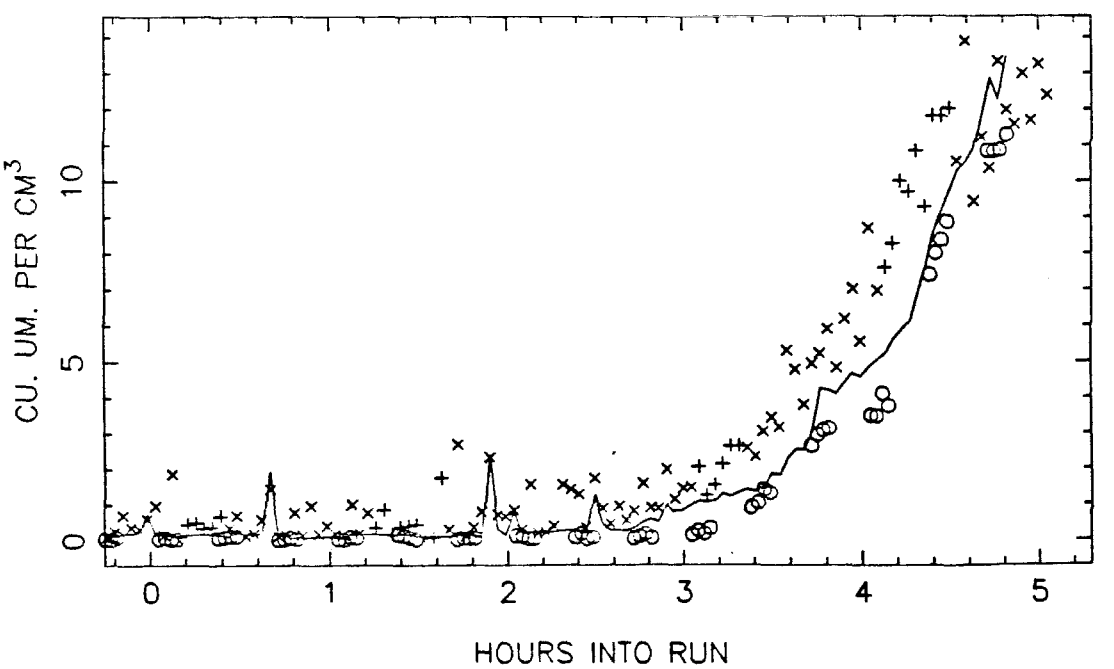

EC64 MEAN PARTICLE SIZE, SIDE A

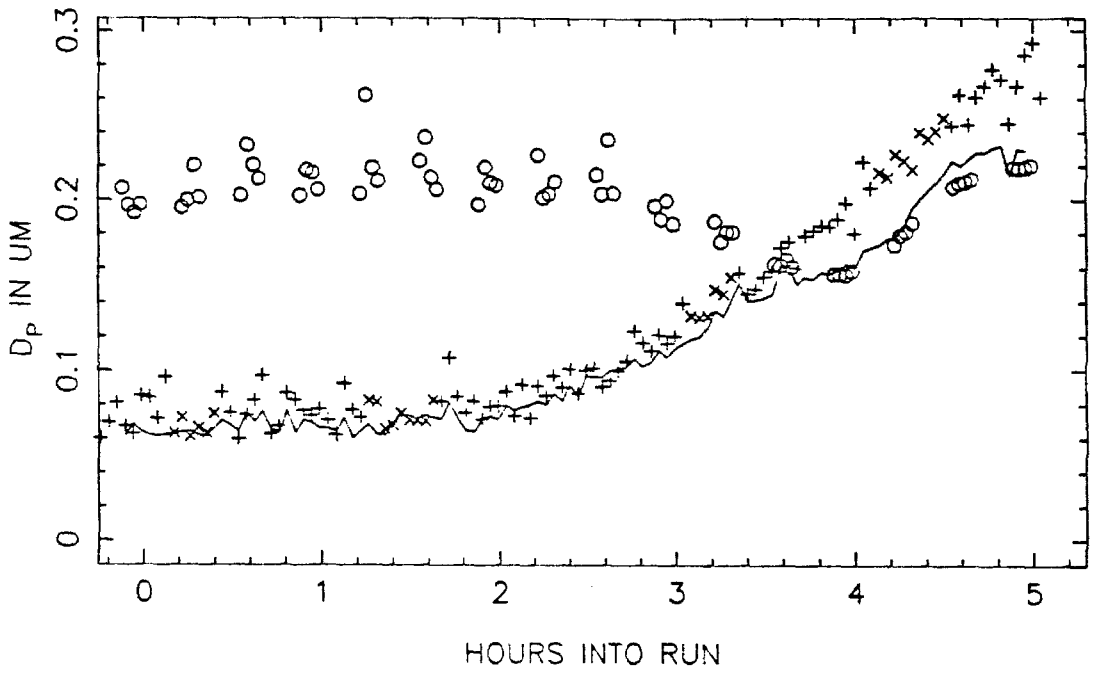

SIDE B

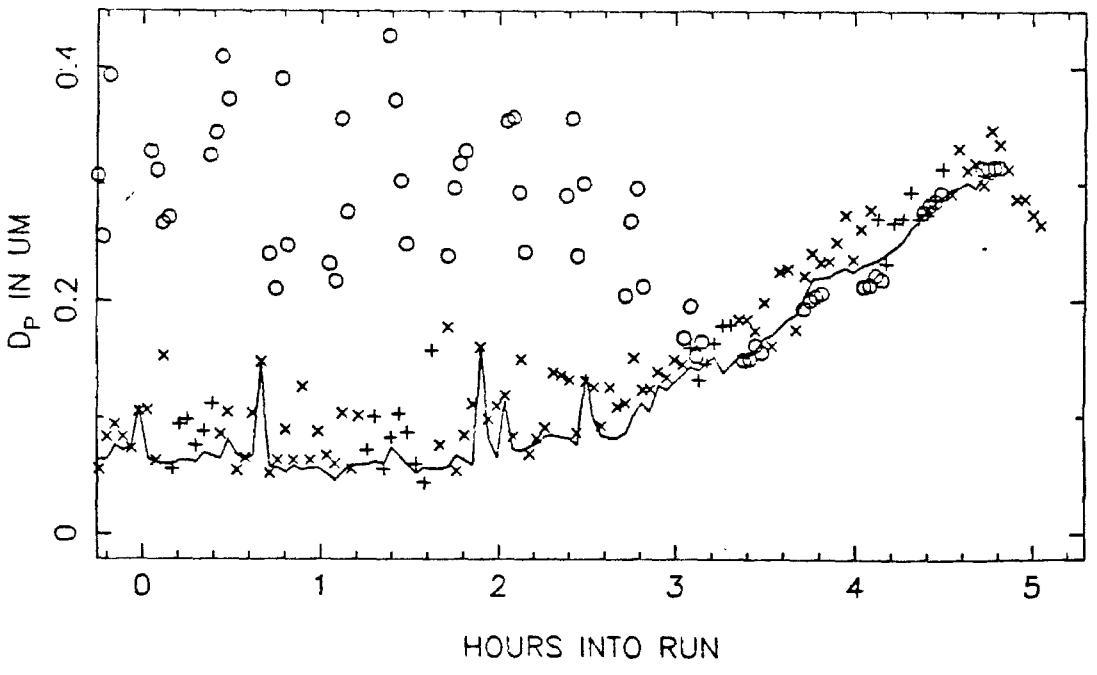

EC64A NUMBER DISTRIBUTION, T=0

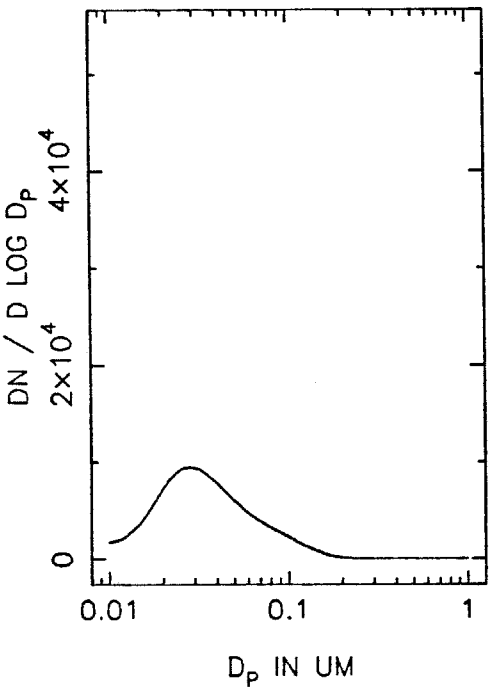

T=0.5 HOURS

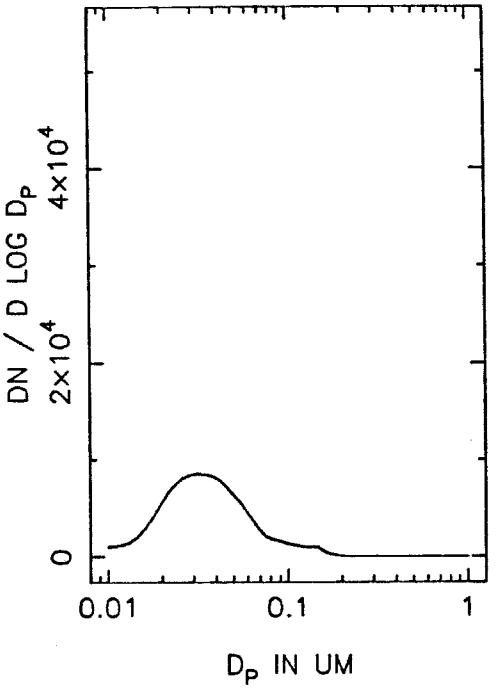

T=1.0 HOURS

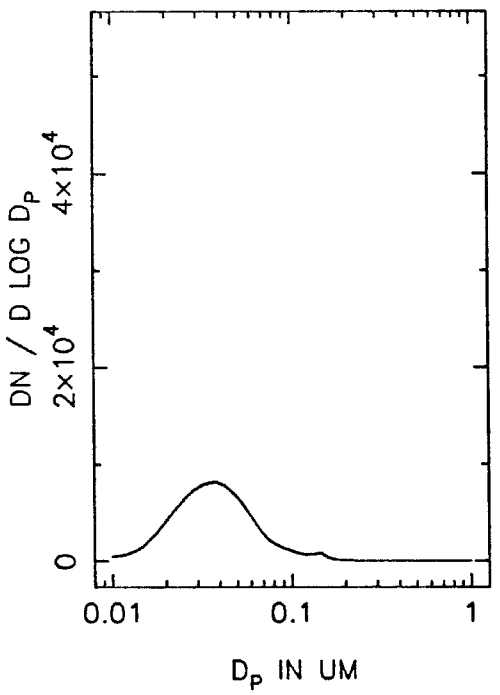

T=1.5 HOURS

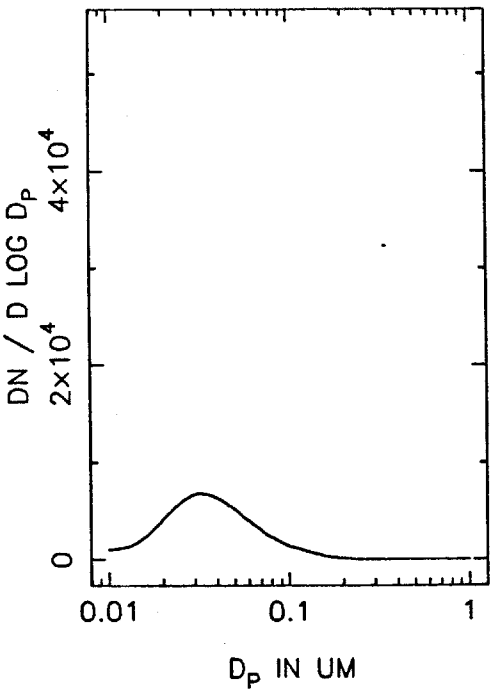

EC64A NUMBER DISTRIBUTION, T=2.0

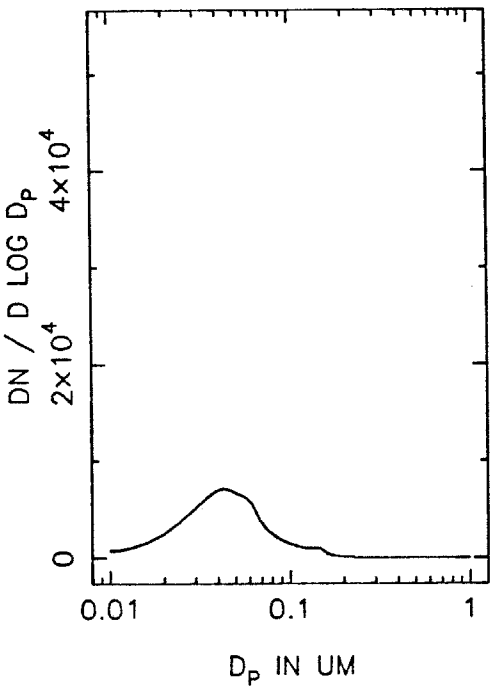

T=2.5 HOURS

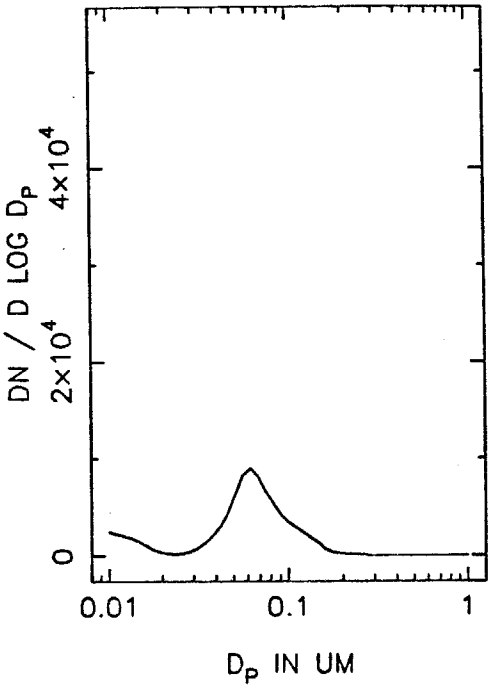

T=3.0 HOURS

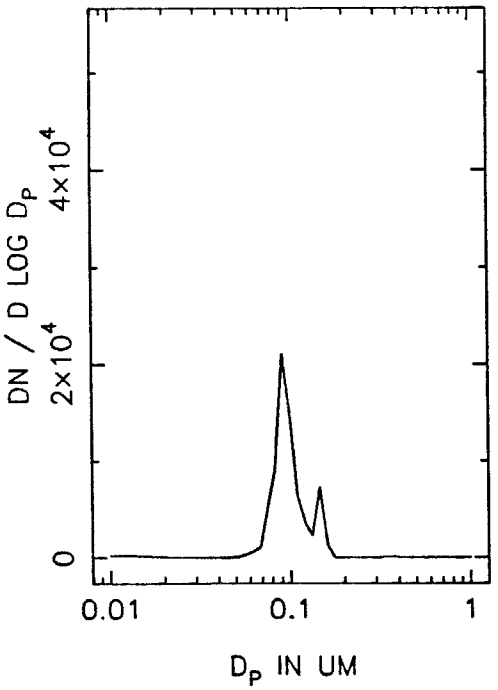

T=3.5 HOURS

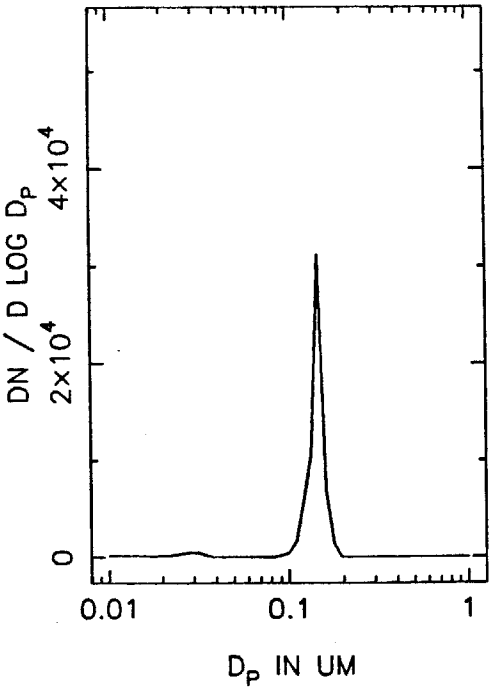

EC64A NUMBER DISTRIBUTION, T=4.0

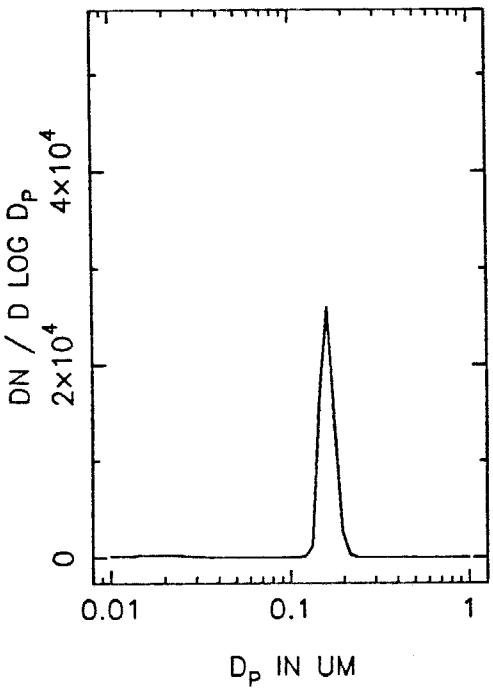

T=4.5 HOURS

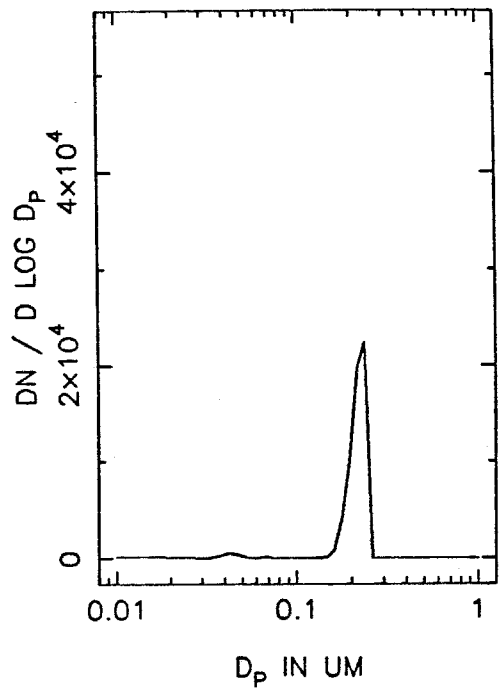

T=5.0 HOURS

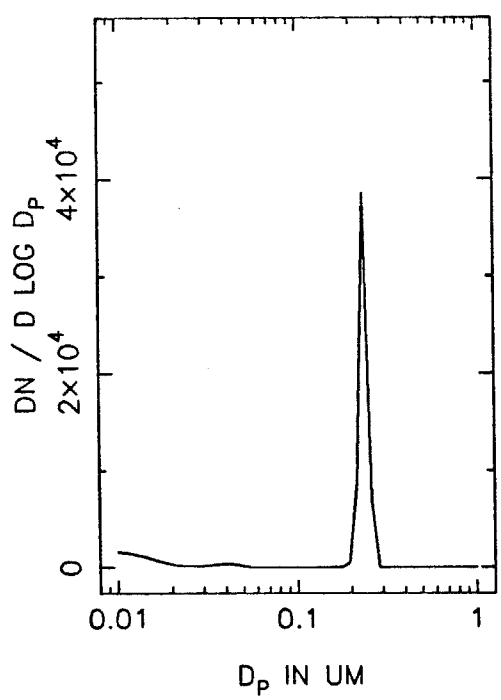

EC64A VOLUME DISTRIBUTION, T=0

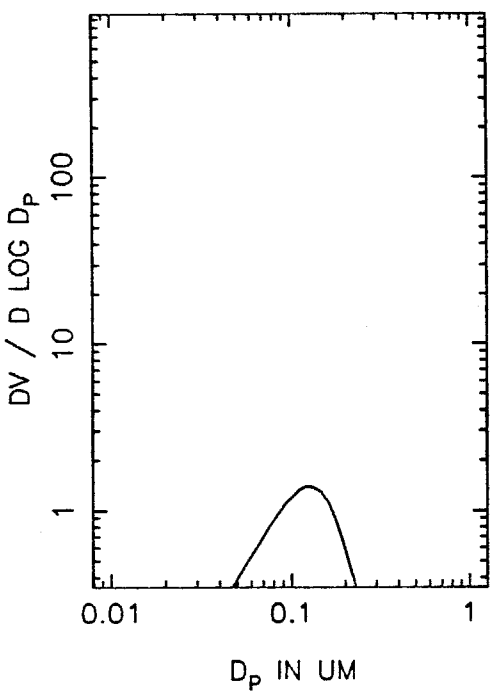

T=0.5 HOURS

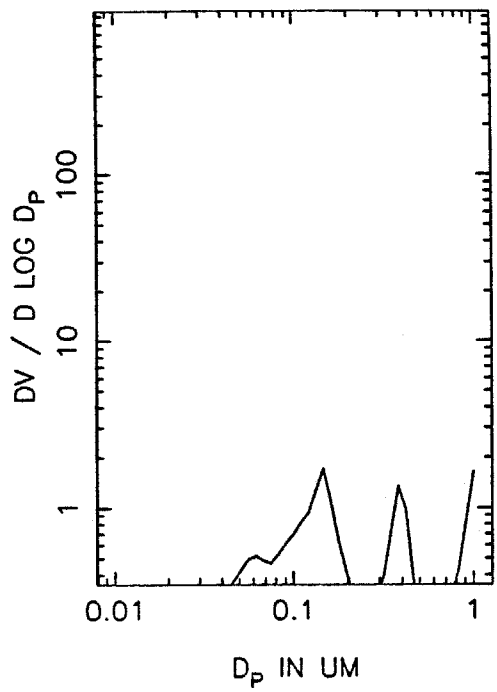

T=1.0 HOURS

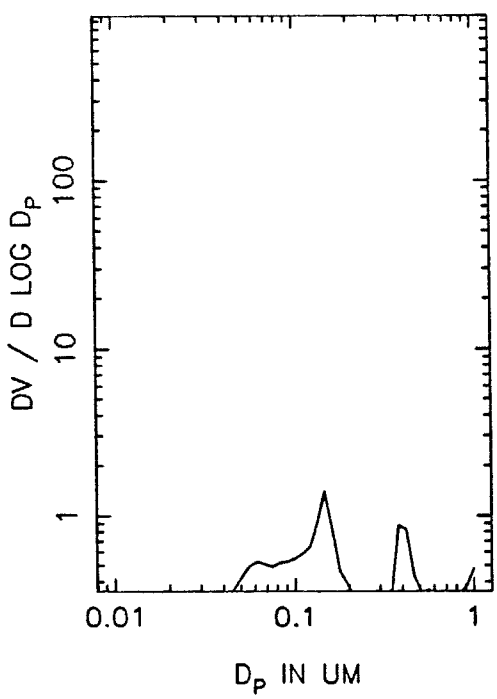

T=1.5 HOURS

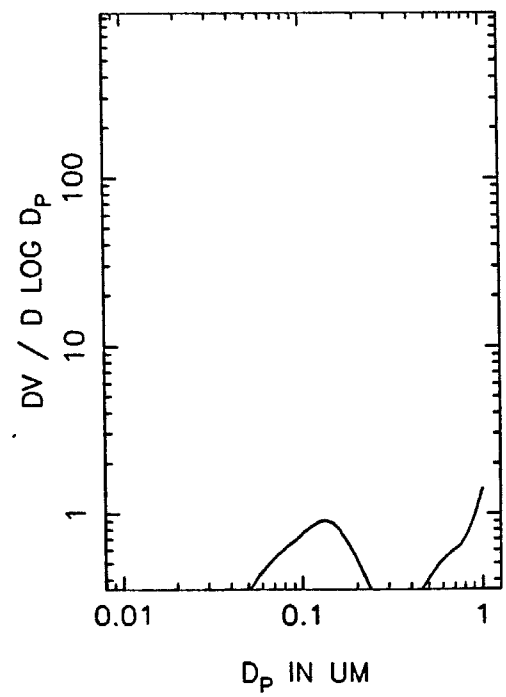

EC64A VOLUME DISTRIBUTION, T=2.0

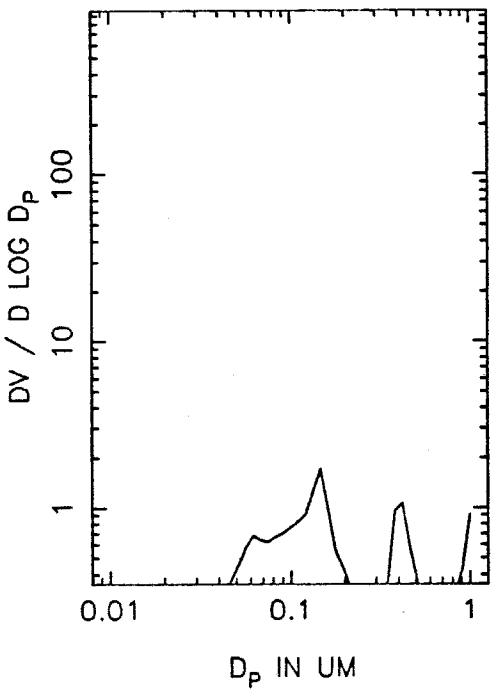

T=2.5 HOURS

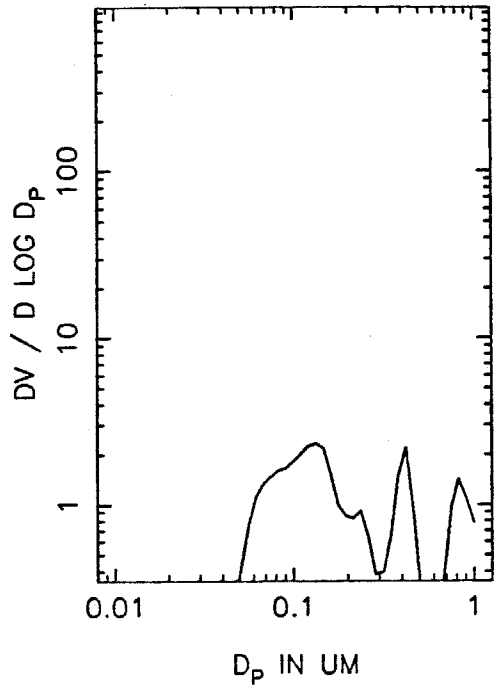

T=3.0 HOURS

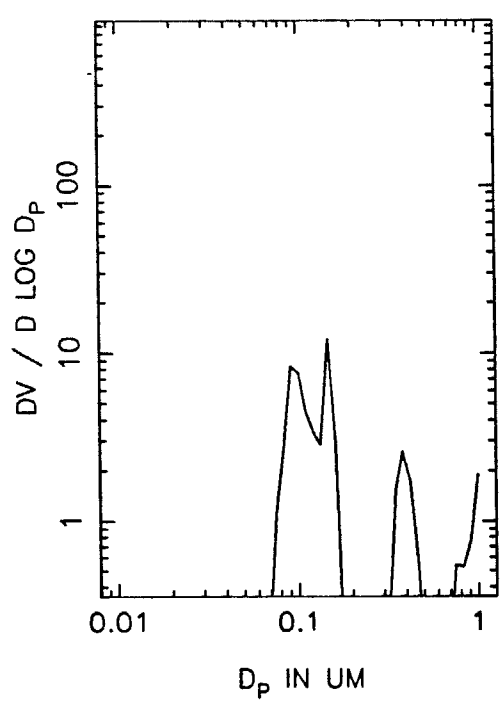

T=3.5 HOURS

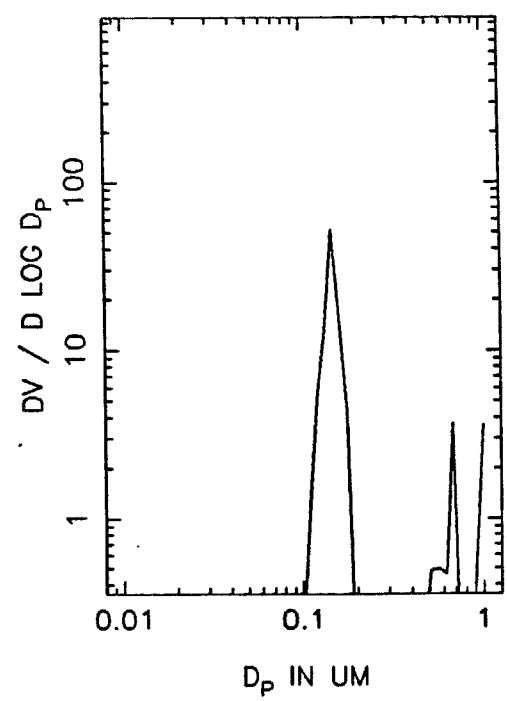

EC64A VOLUME DISTRIBUTION, T=4.0

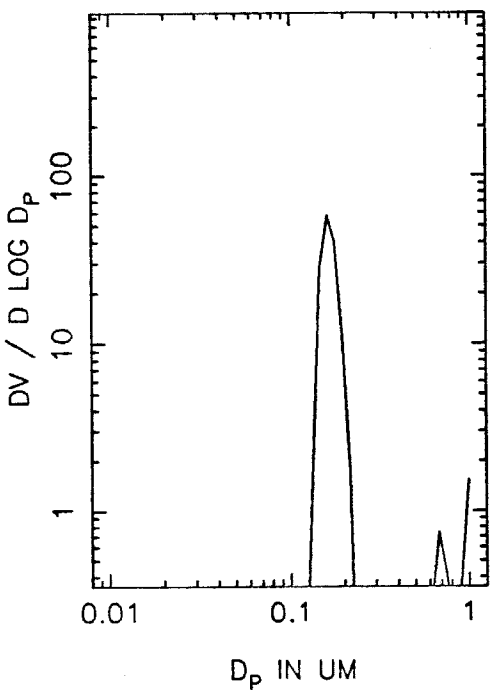

T=4.5 HOURS

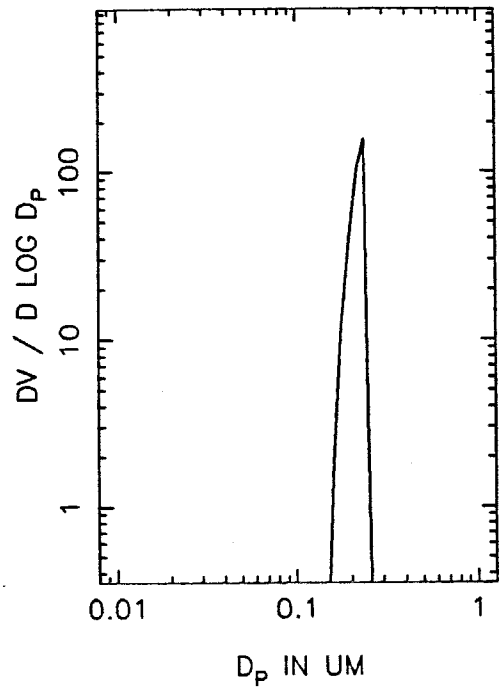

T=5.0 HOURS

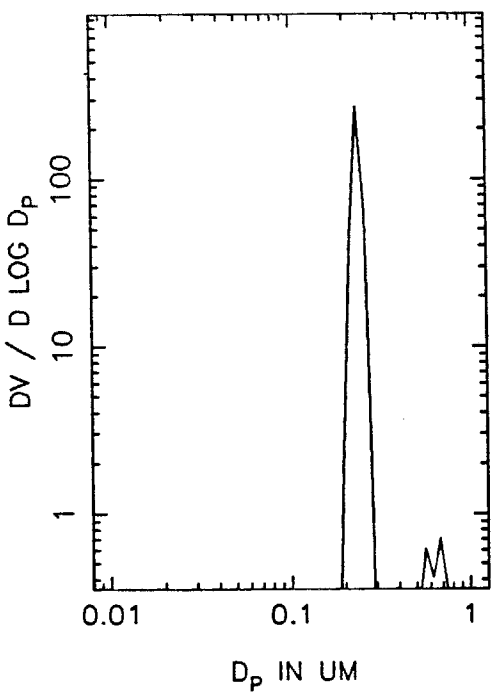

EC64B NUMBER DISTRIBUTION, T=0

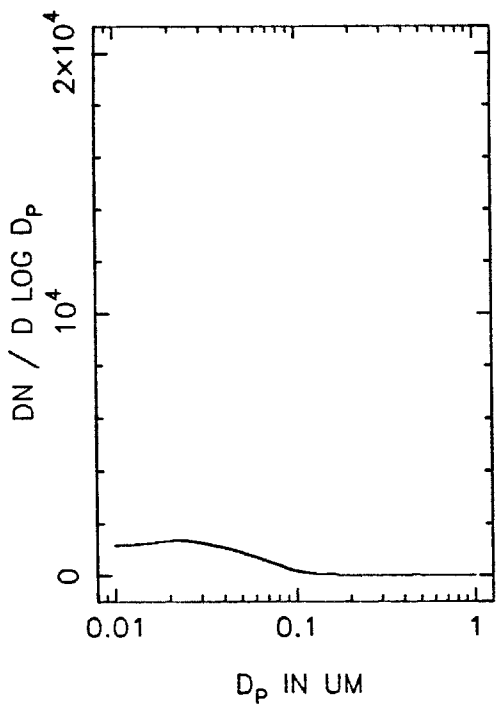

T=0.5 HOURS

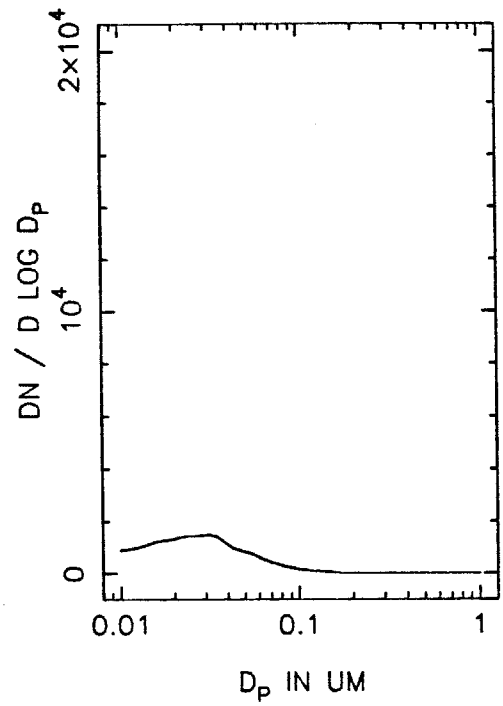

T=1.0 HOURS

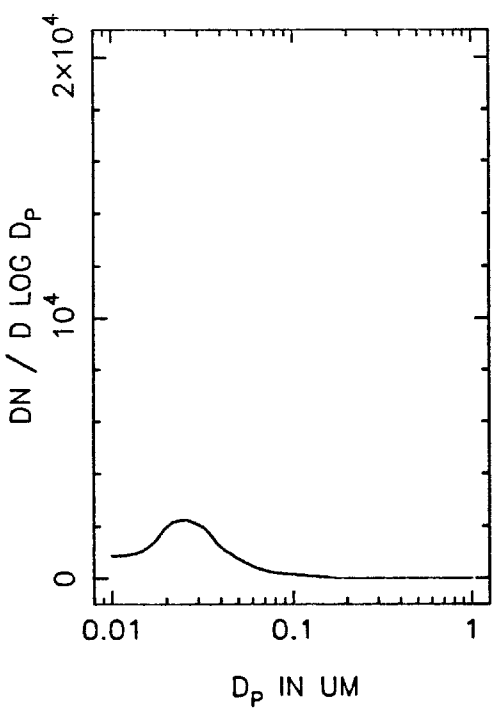

T=1.5 HOURS

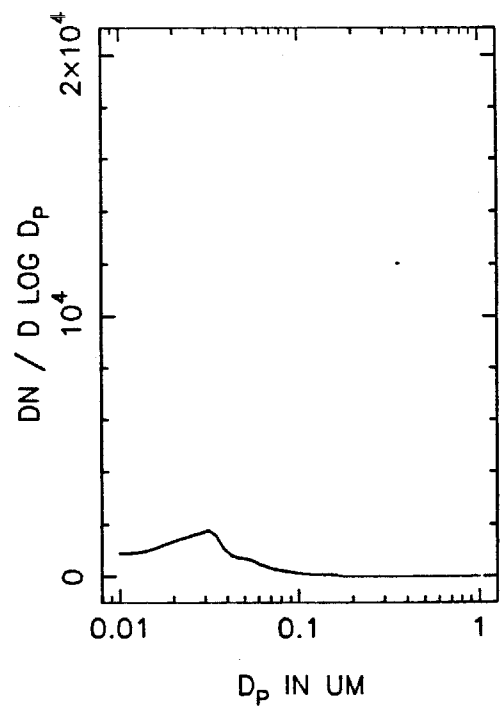

EC64B NUMBER DISTRIBUTION, T=2.0

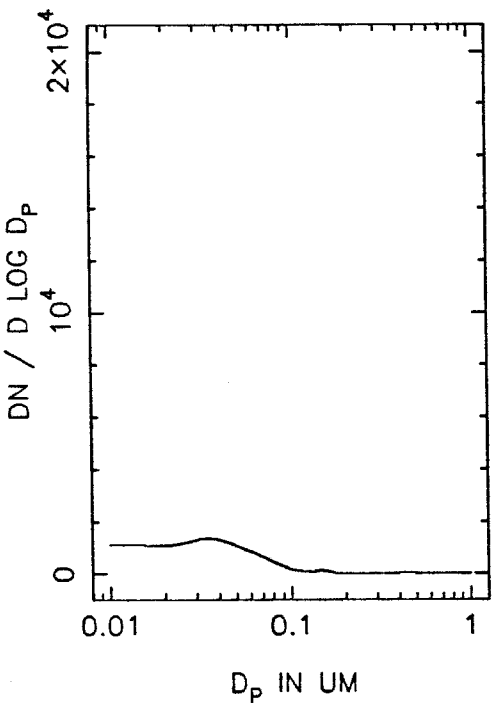

T=2.5 HOURS

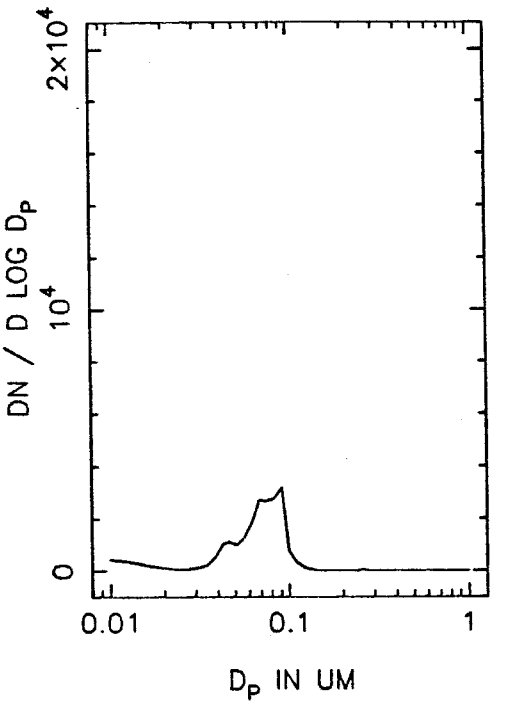

T=3.0 HOURS

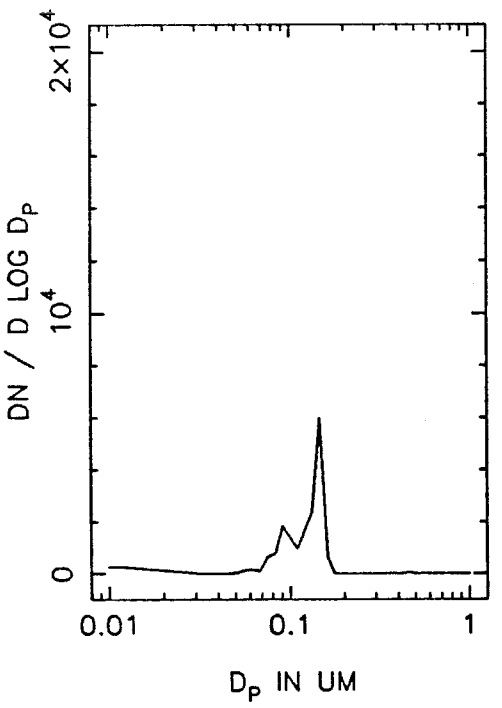

T=3.5 HOURS

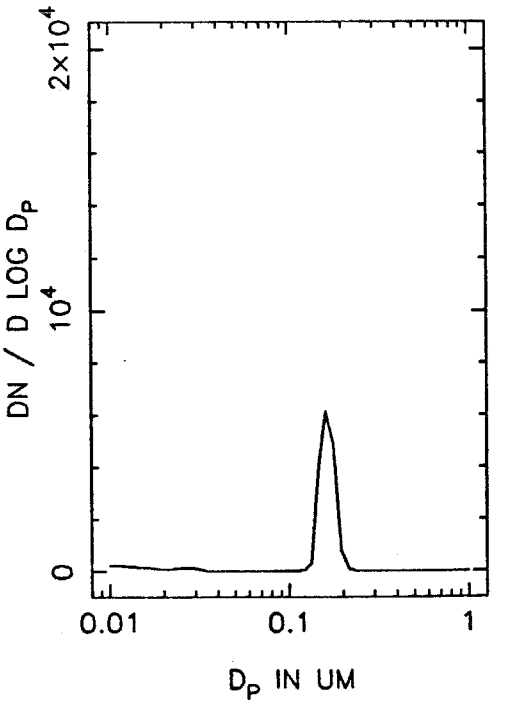

EC64B NUMBER DISTRIBUTION, T=4.0

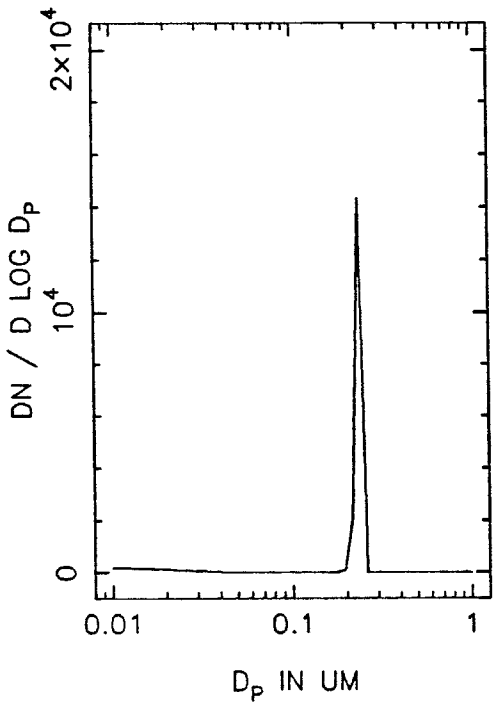

T=4.5 HOURS

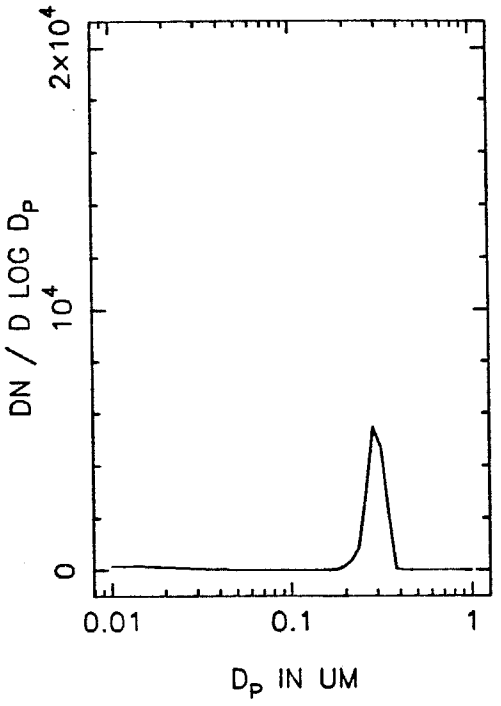

EC64B VOLUME DISTRIBUTION, T=0

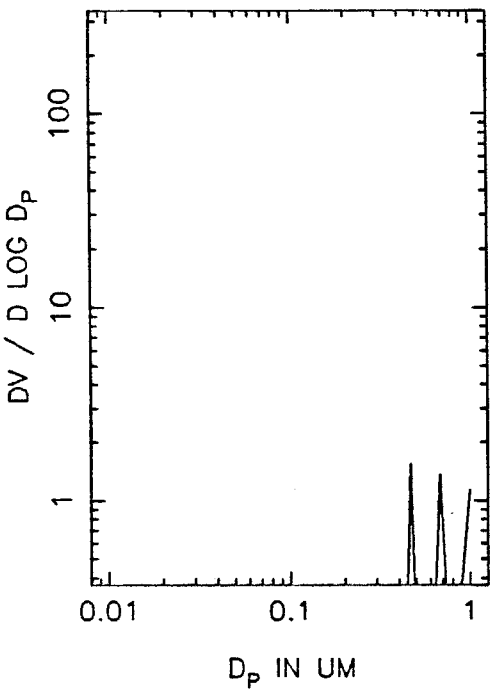

T=0.5 HOURS

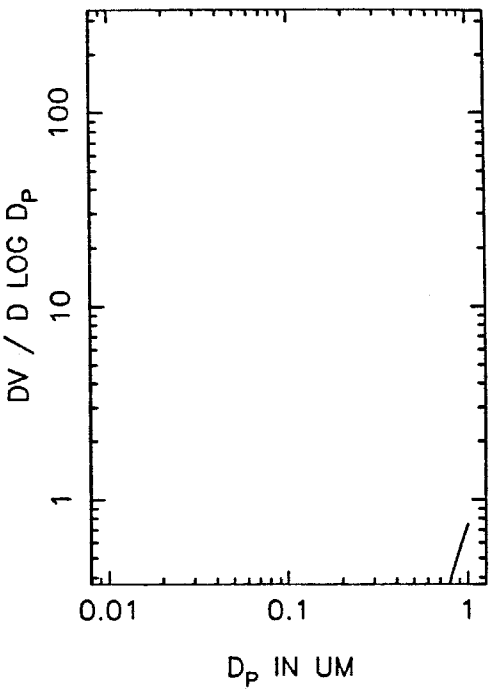

T=1.0 HOURS

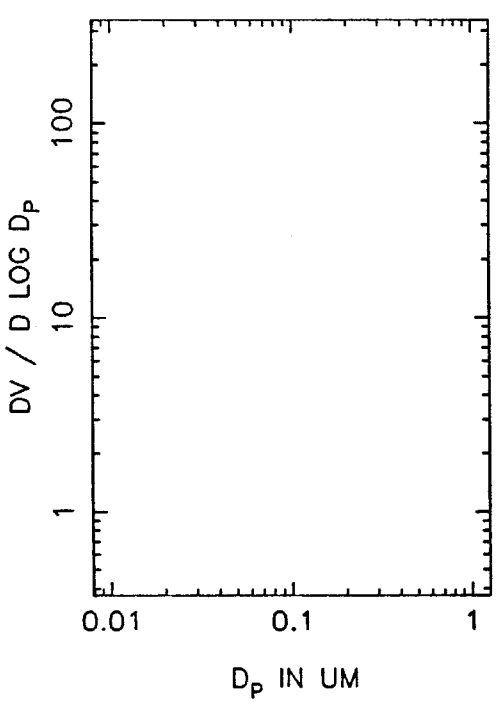

T=1.5 HOURS

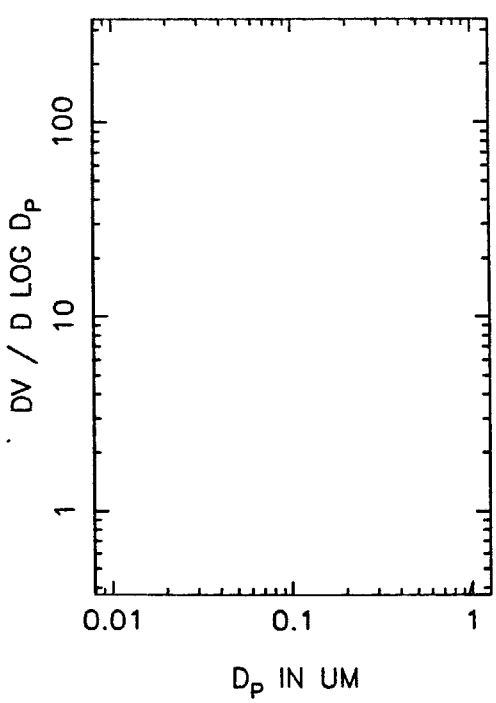

EC64B VOLUME DISTRIBUTION, T=2.0

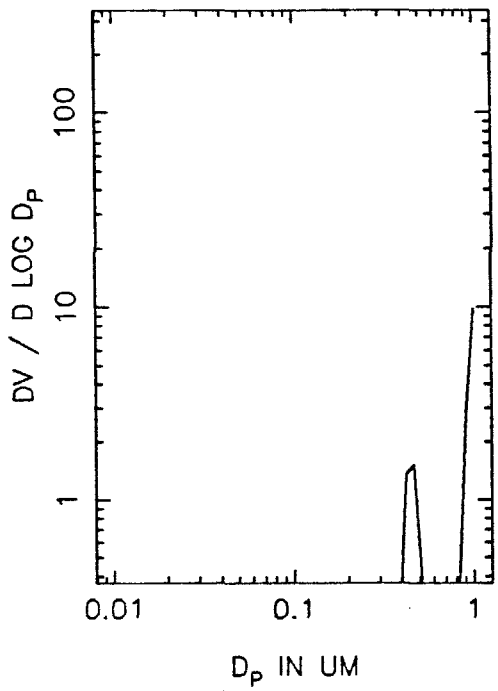

T=2.5 HOURS

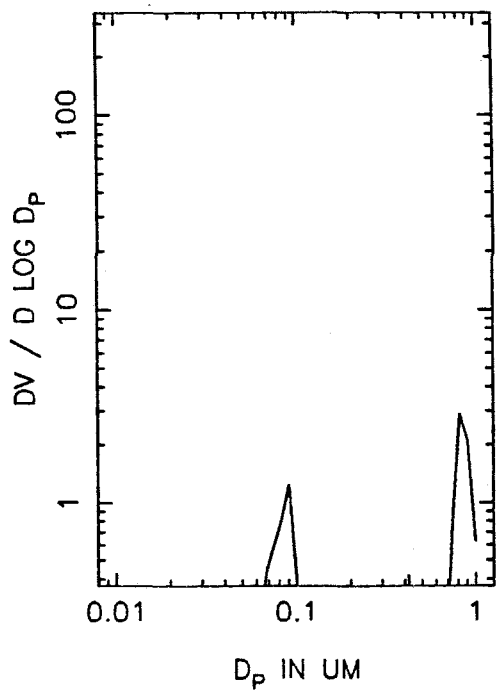

T=3.0 HOURS

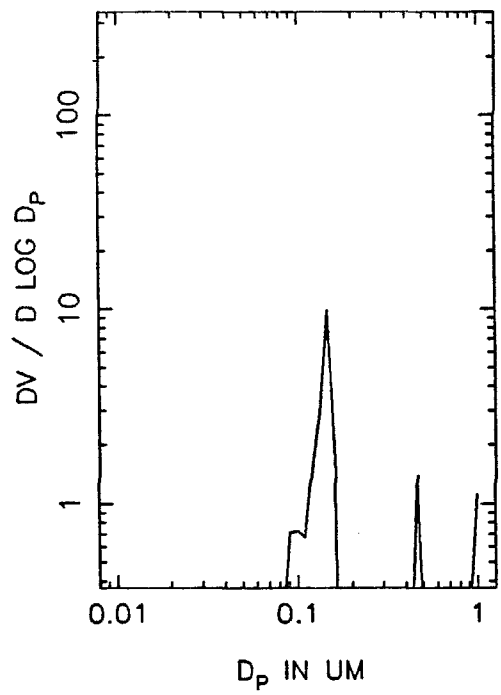

T=3.5 HOURS

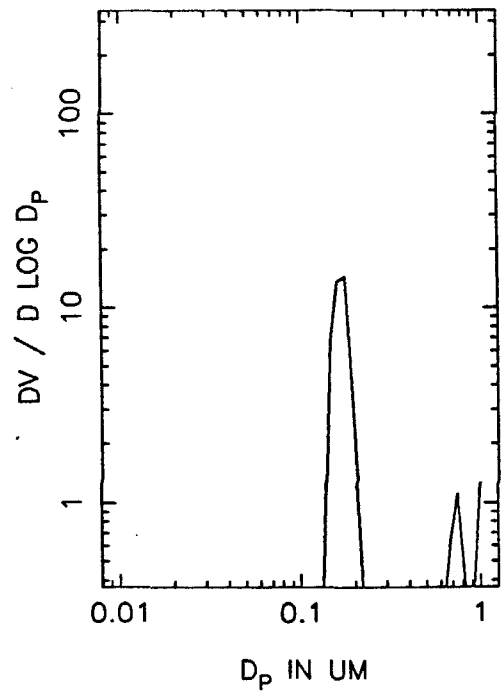

EC64B VOLUME DISTRIBUTION, T=4.0

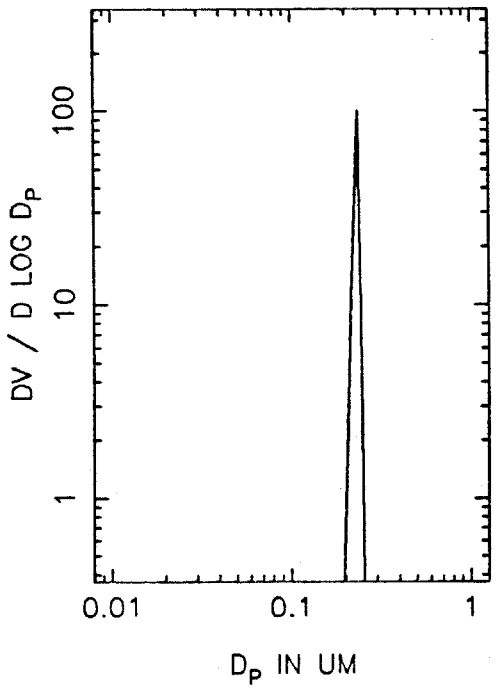

T=4.5 HOURS

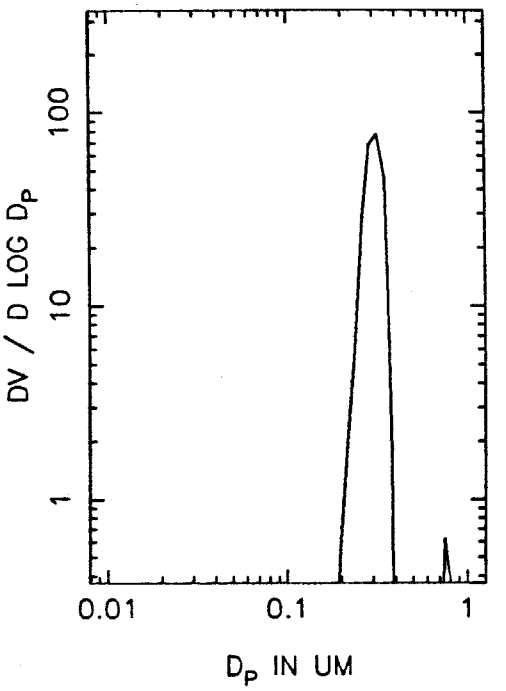

EH66 TOTAL NUMBER, SIDE A

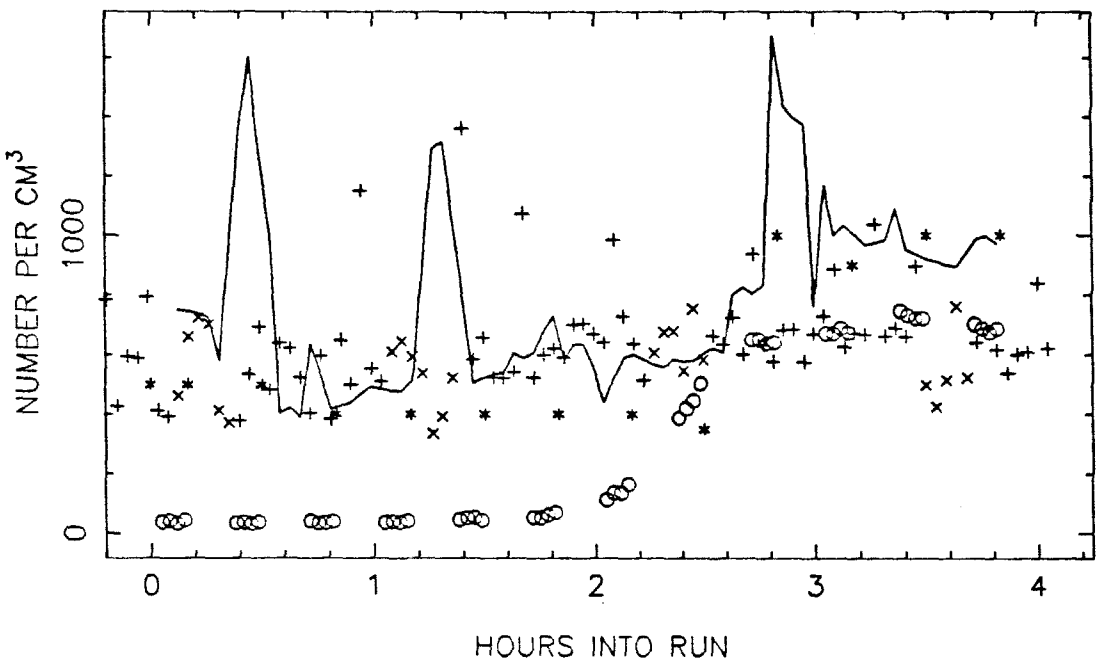

SIDE B

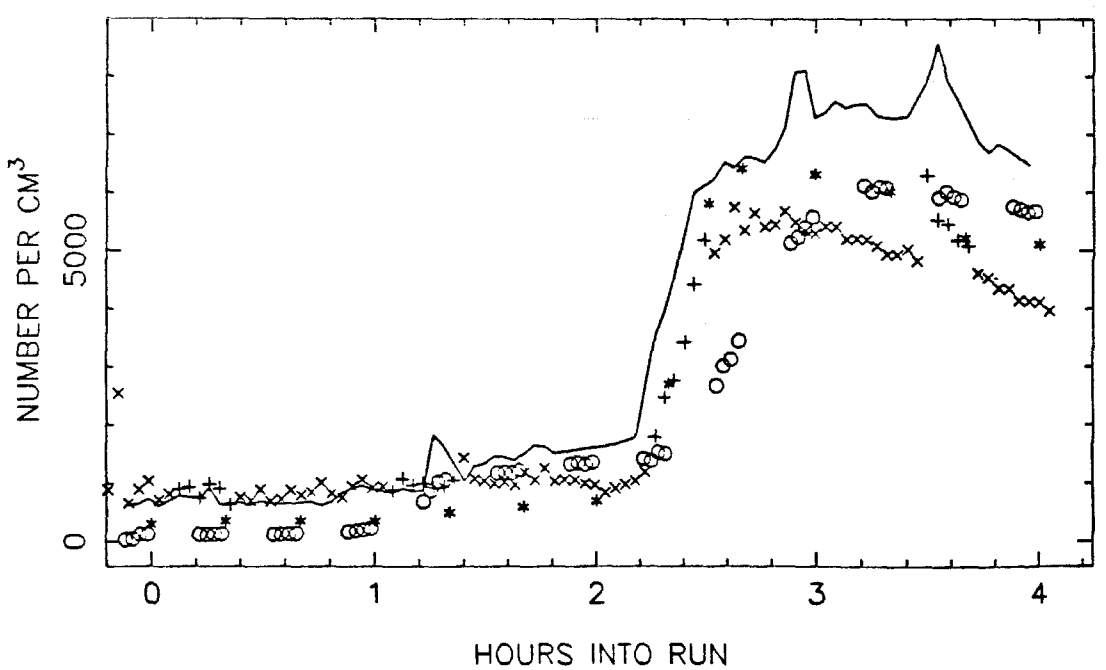

EH66 VOLUME IN THE AEROSOL PHASE, SIDE A

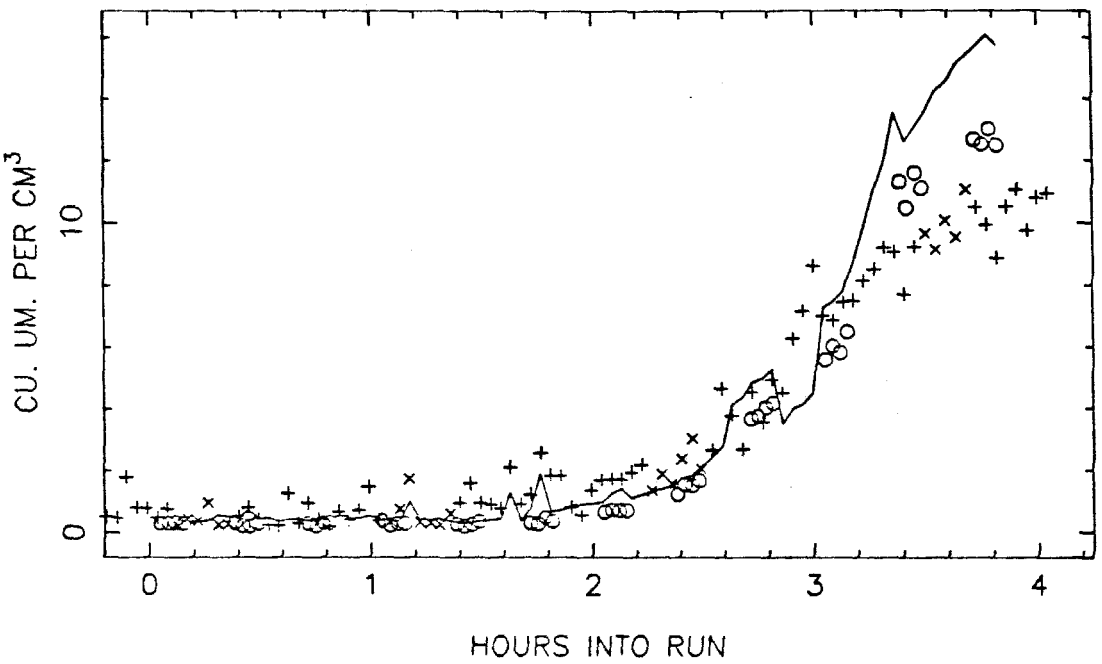

SIDE B

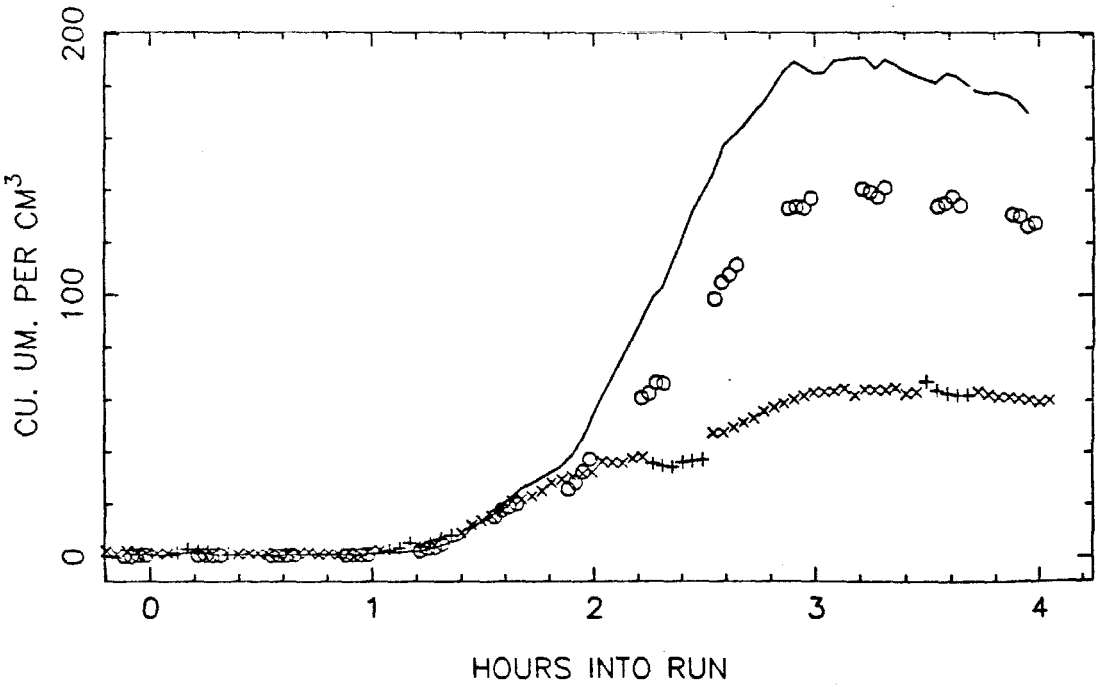

EH66 MEAN PARTICLE SIZE, SIDE A

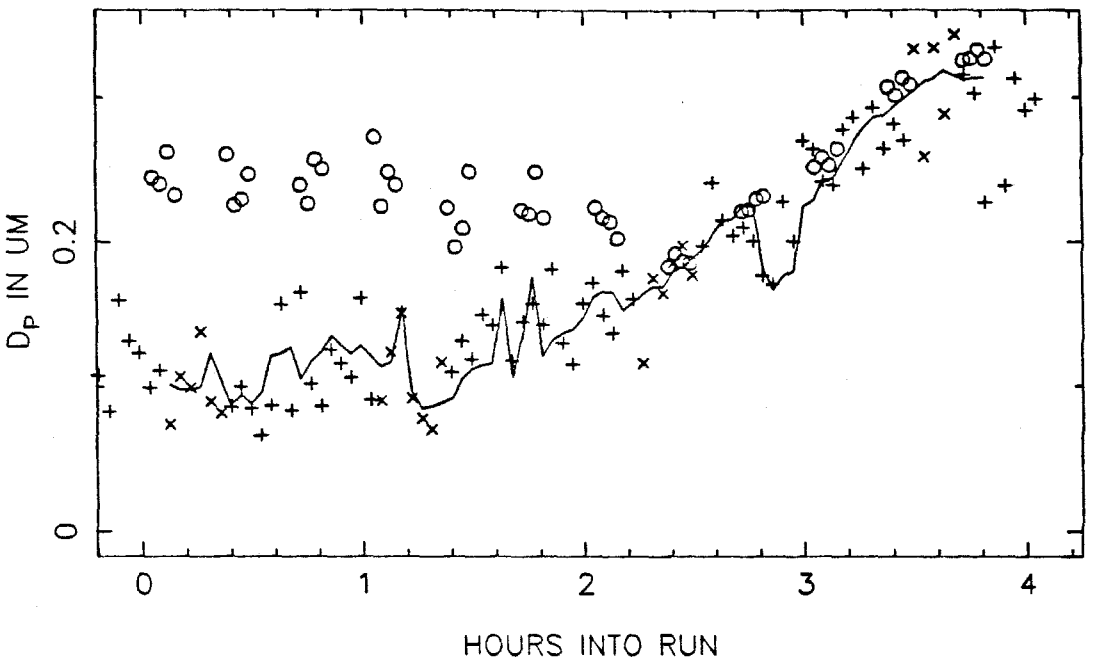

SIDE B

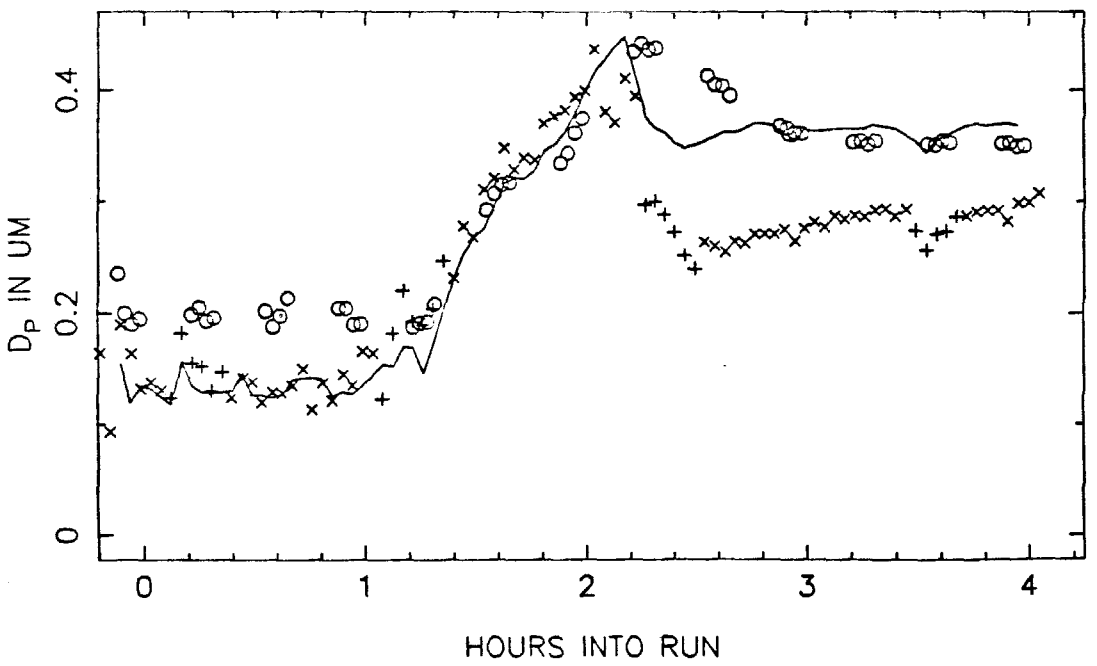

EH66A NUMBER DISTRIBUTION, T=0

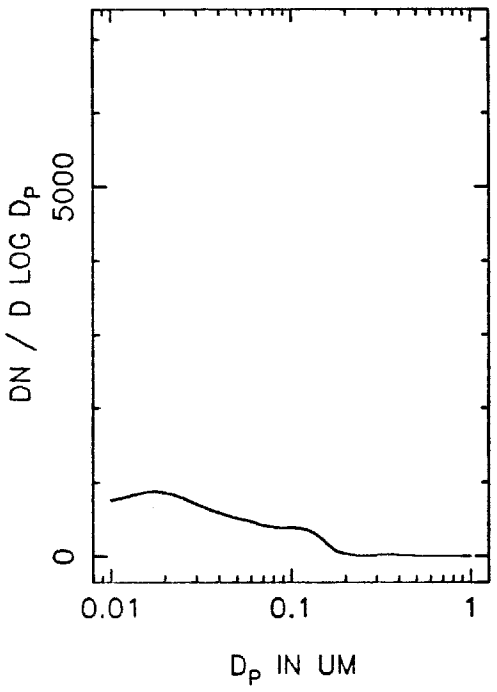

T=0.5 HOURS

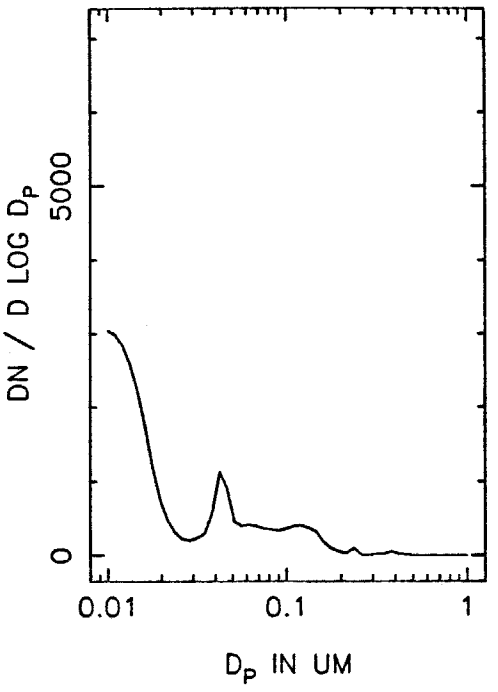

T=1.0 HOURS

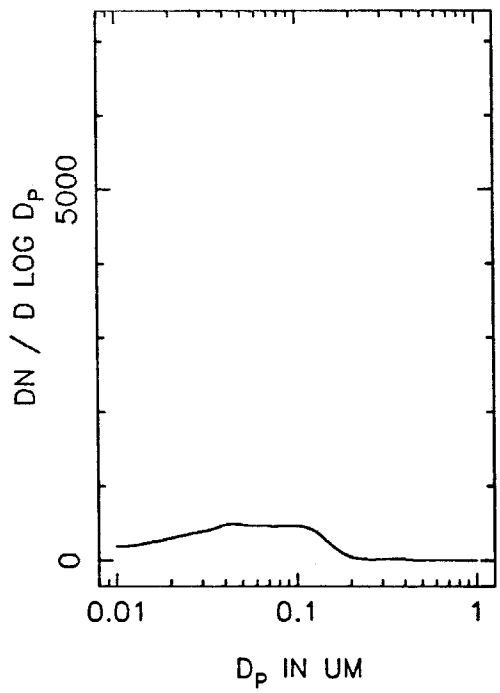

T=1.5 HOURS

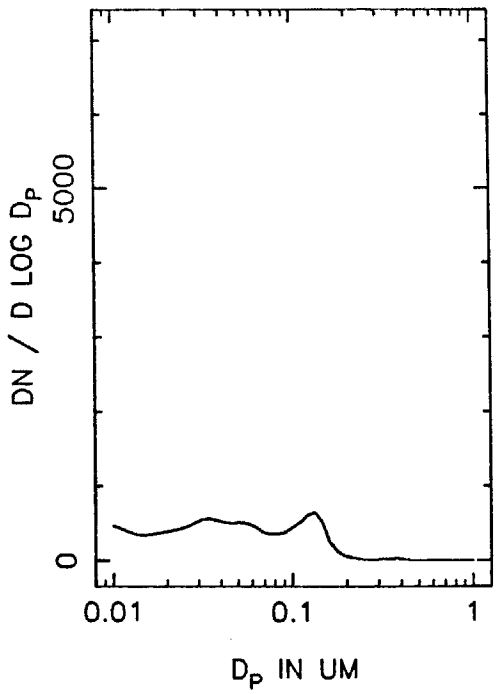

EH66A NUMBER DISTRIBUTION, T=2.0

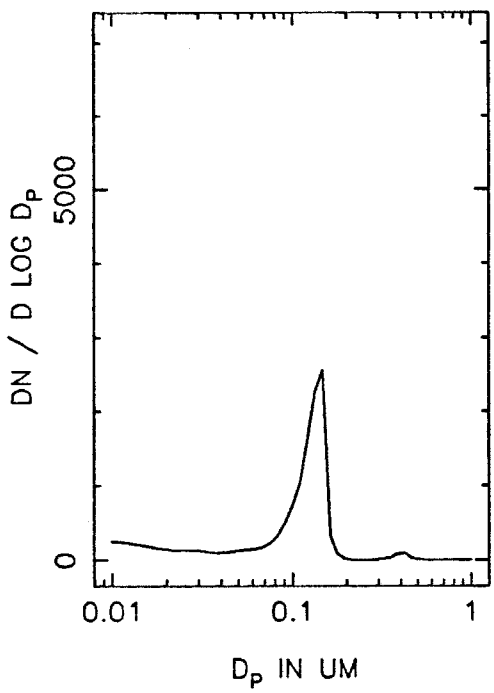

T=2.5 HOURS

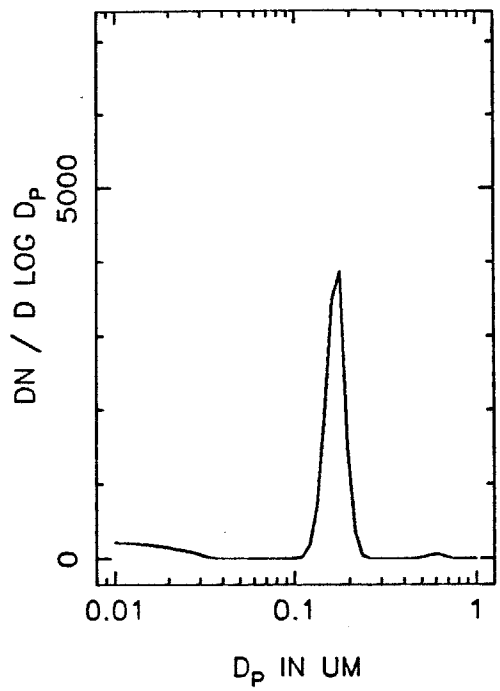

T=3.0 HOURS

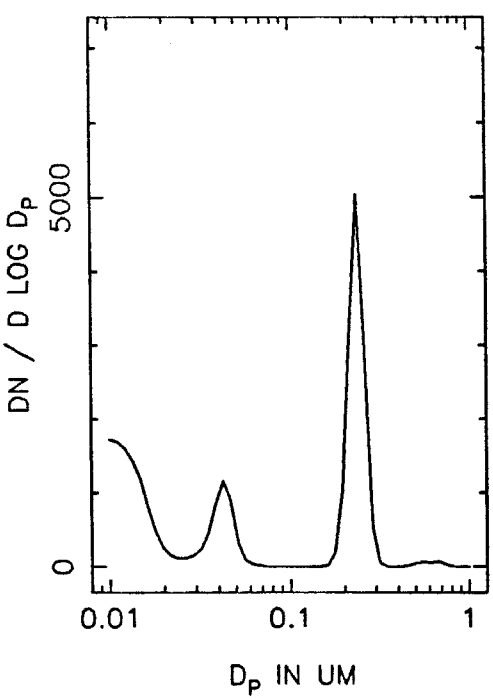

T=3.5 HOURS

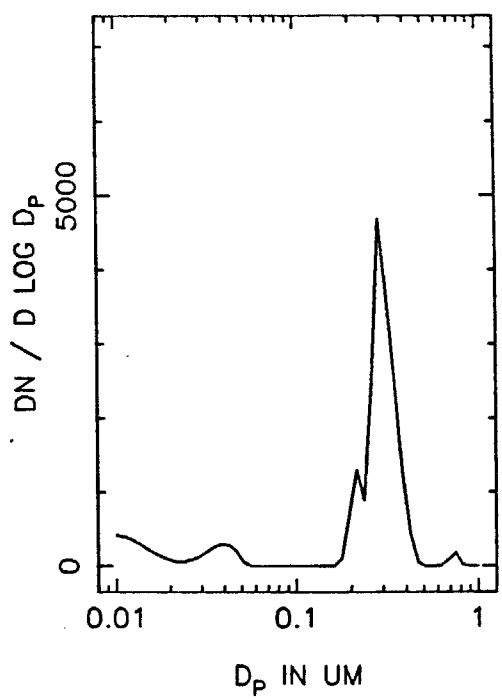

EH66A VOLUME DISTRIBUTION, T=0

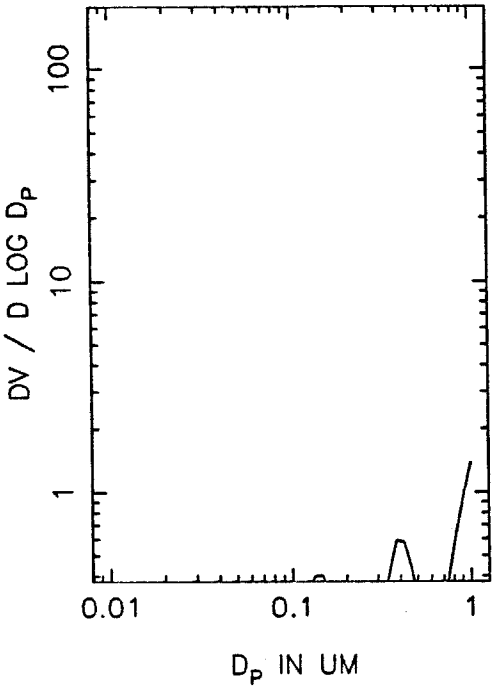

T=0.5 HOURS

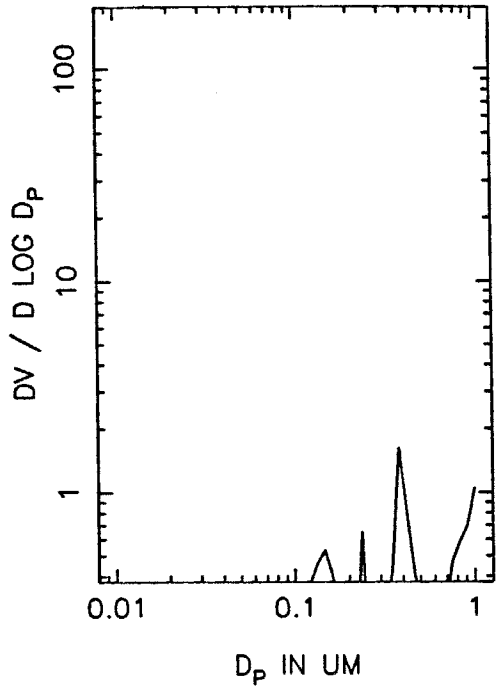

T=1.0 HOURS

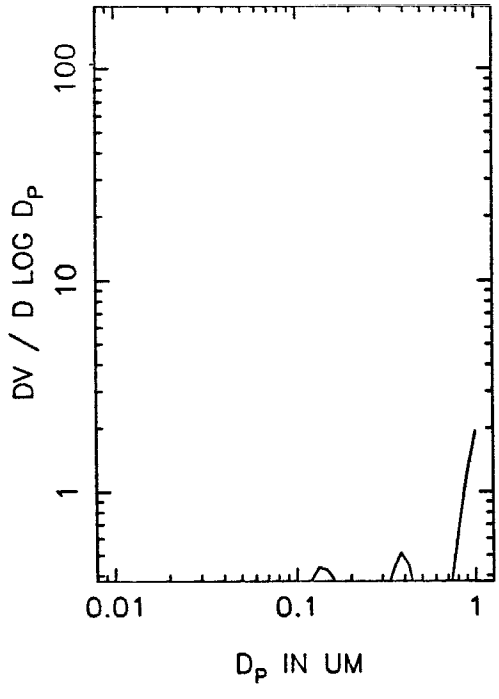

T=1.5 HOURS

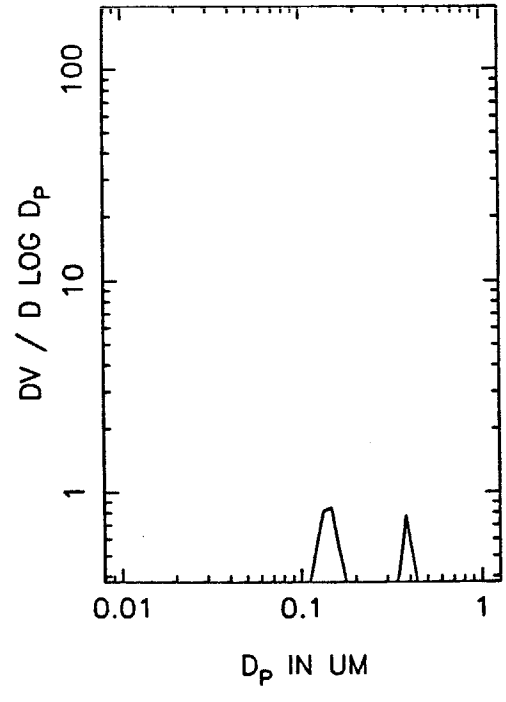

EH66A VOLUME DISTRIBUTION, T=2.0

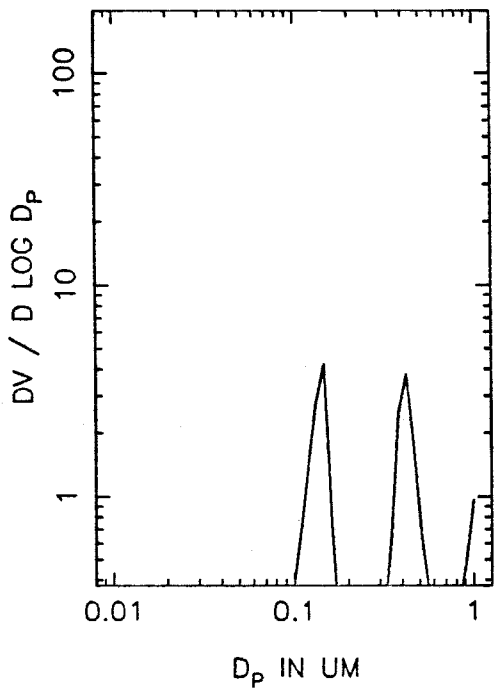

T=2.5 HOURS

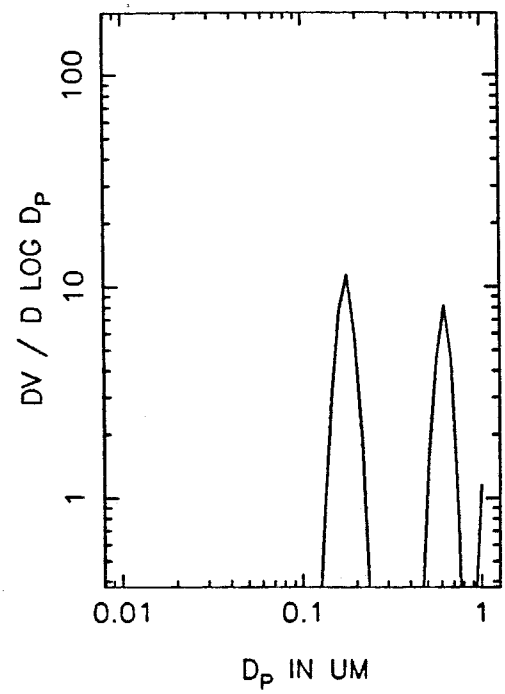

T=3.0 HOURS

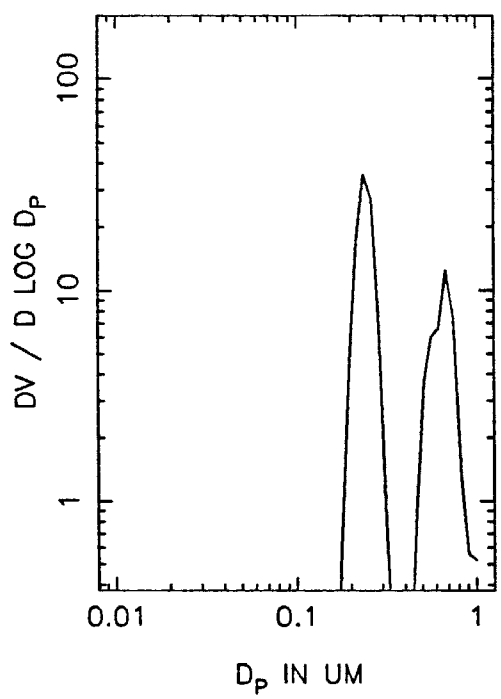

T=3.5 HOURS

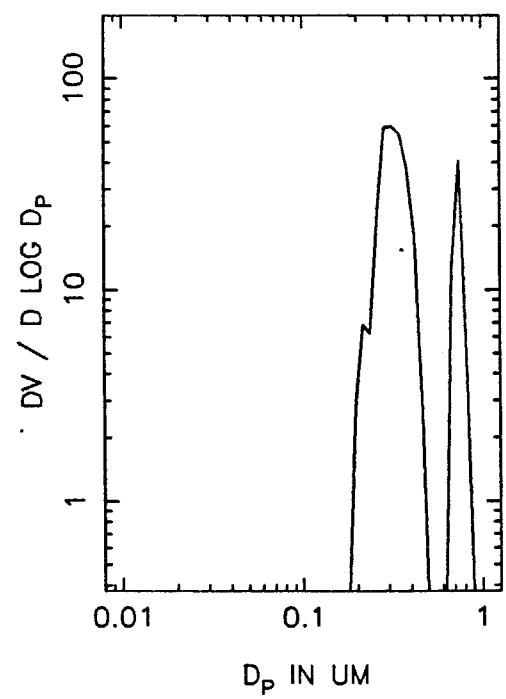

EH66B NUMBER DISTRIBUTION, T=0

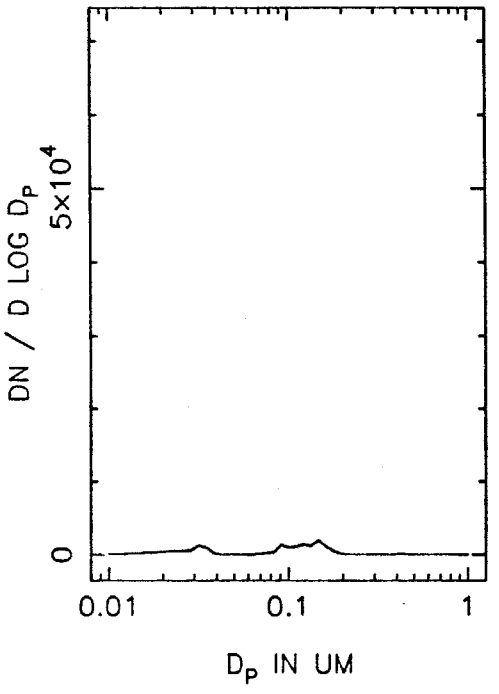

T=0.5 HOURS

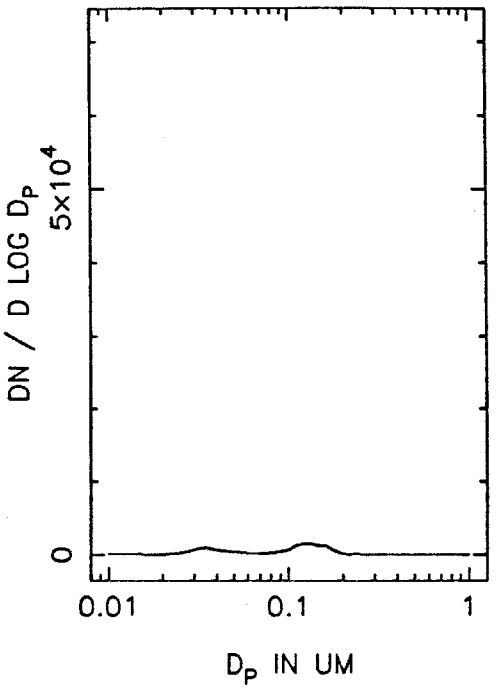

T=1.0 HOURS

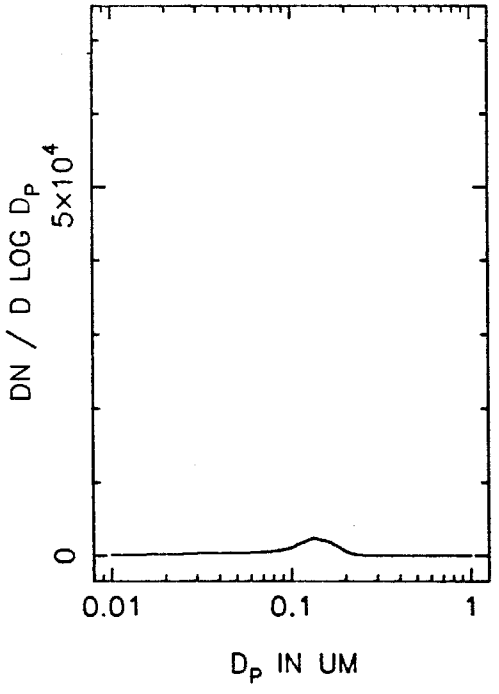

T=1.5 HOURS

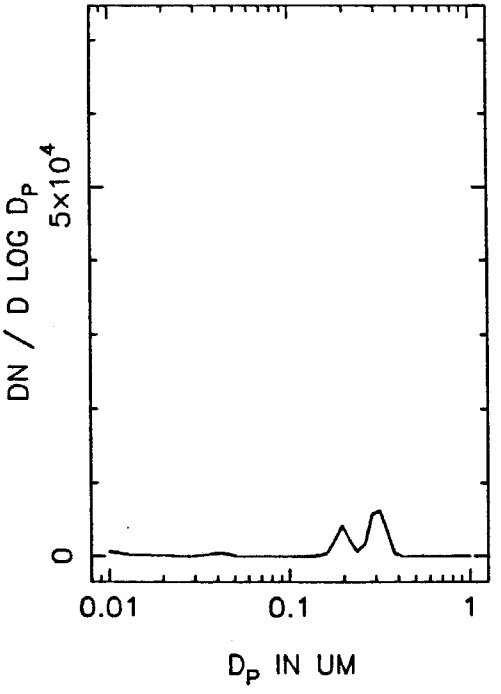

EH66B NUMBER DISTRIBUTION, T=2.0

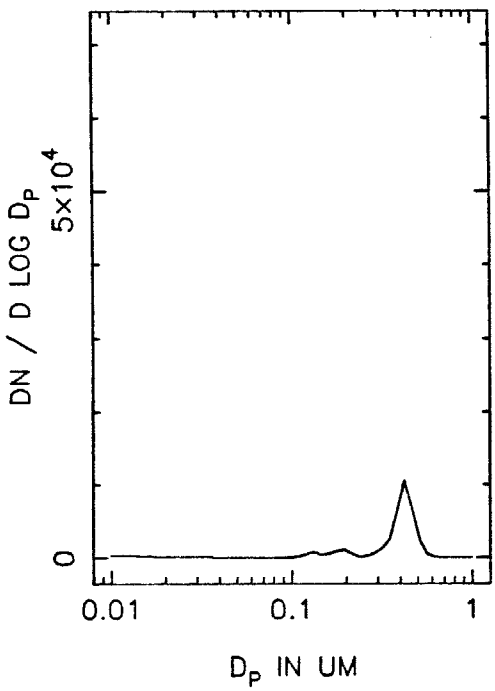

T=2.5 HOURS

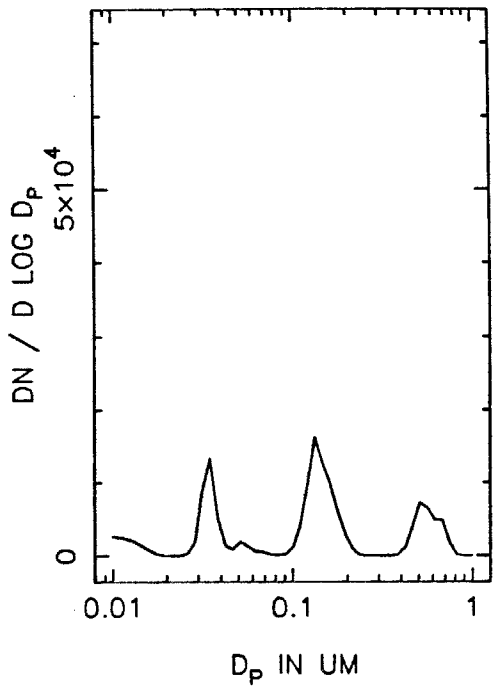

T=3.0 HOURS

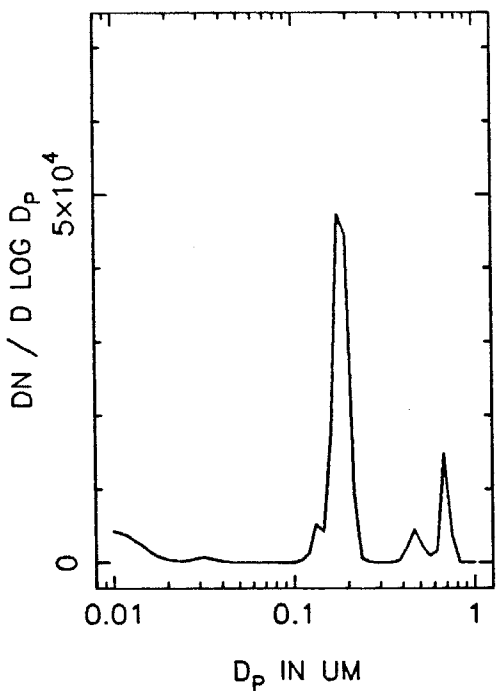

T=3.5 HOURS

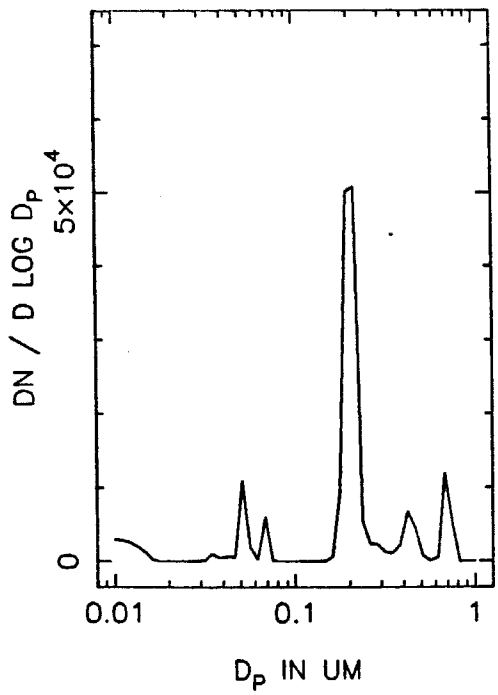

EH66B NUMBER DISTRIBUTION, T=4.0

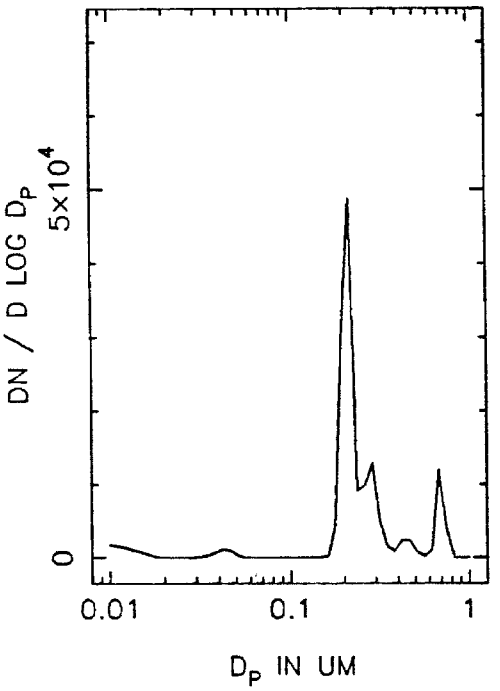

EH66B VOLUME DISTRIBUTION, T=0

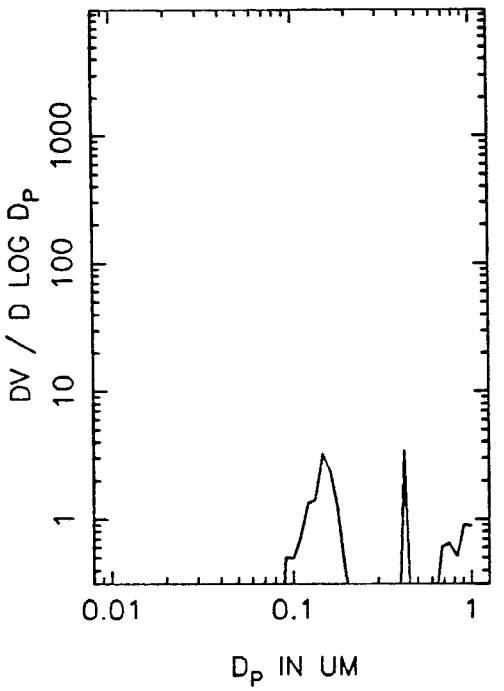

T=0.5 HOURS

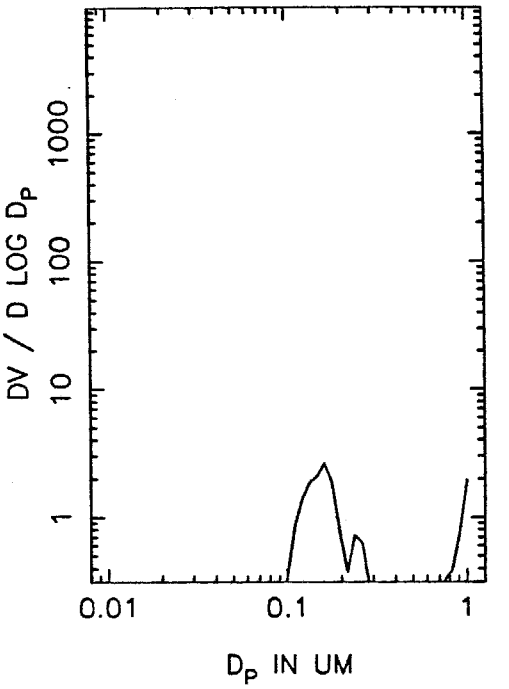

T=1.0 HOURS

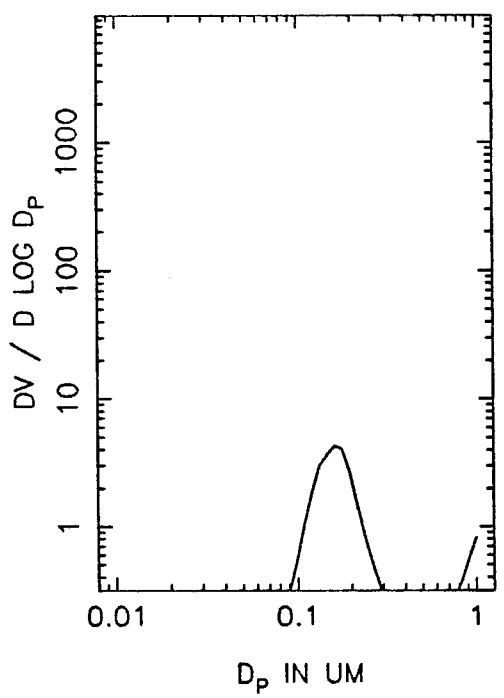

T=1.5 HOURS

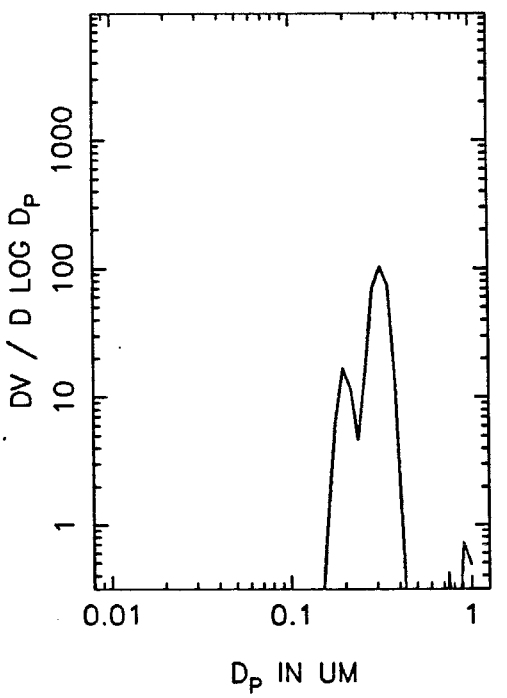

EH66B VOLUME DISTRIBUTION, T=2.0

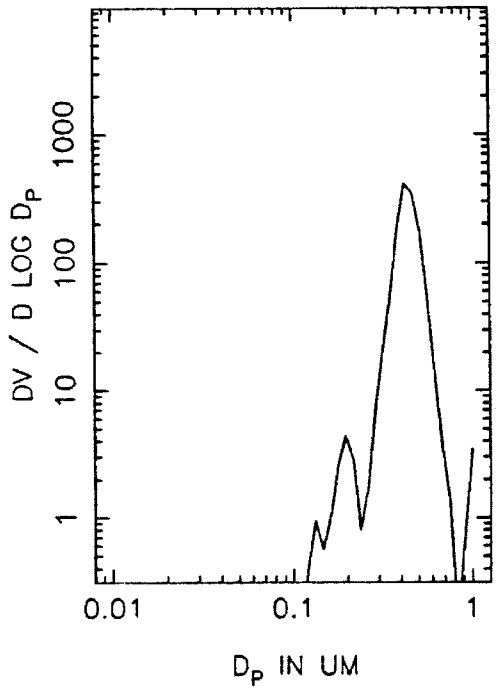

T=2.5 HOURS

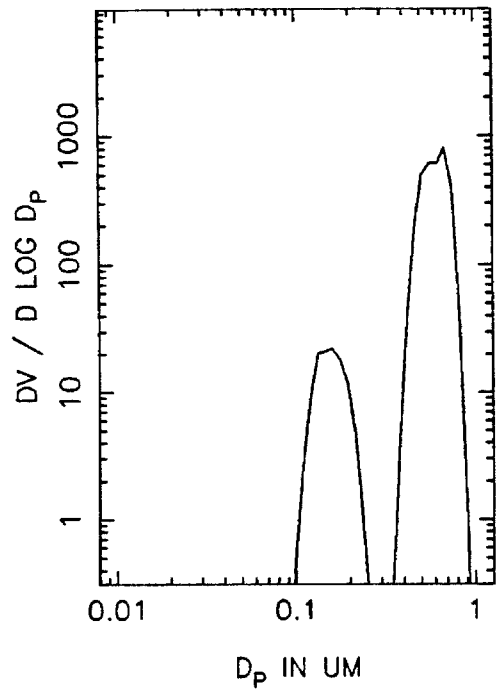

T=3.0 HOURS

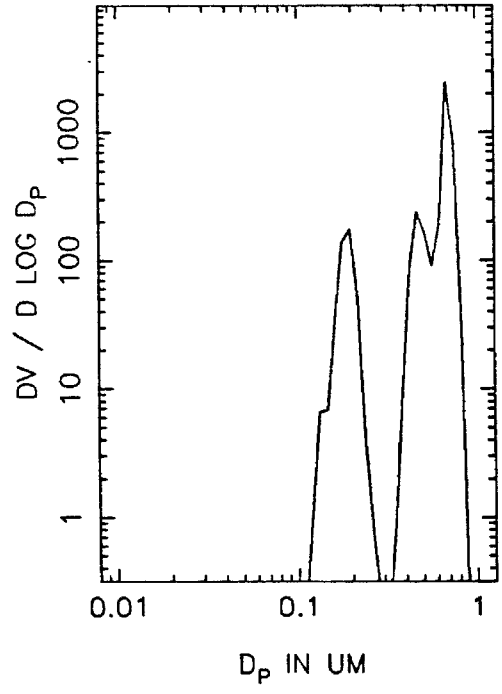

T=3.5 HOURS

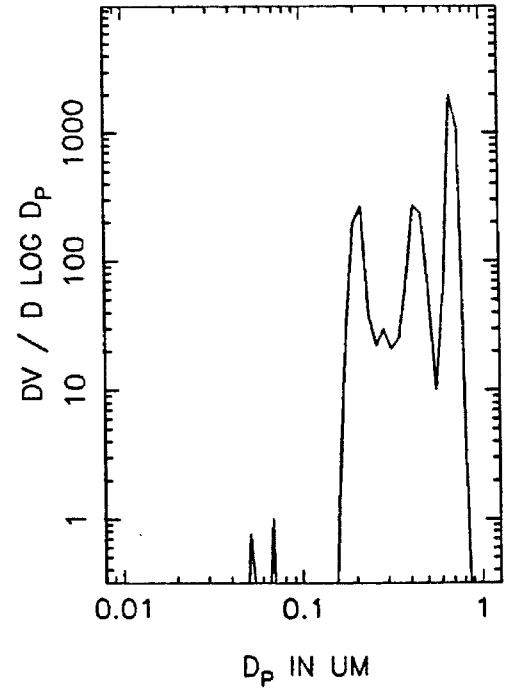

EH66B VOLUME DISTRIBUTION, T=4.0

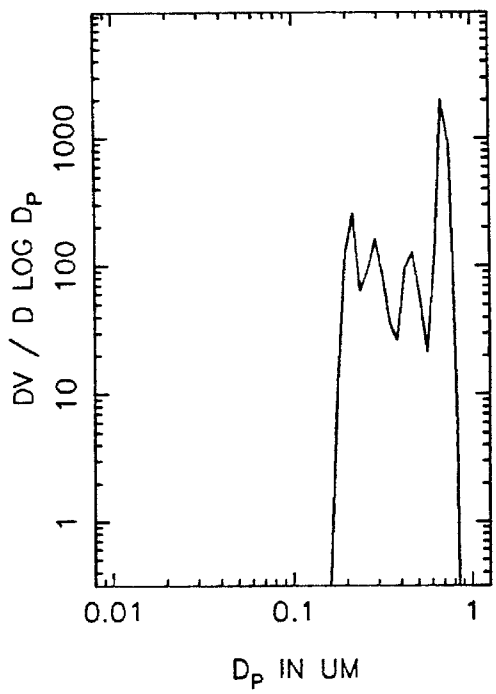

EM70 TOTAL NUMBER, SIDE A

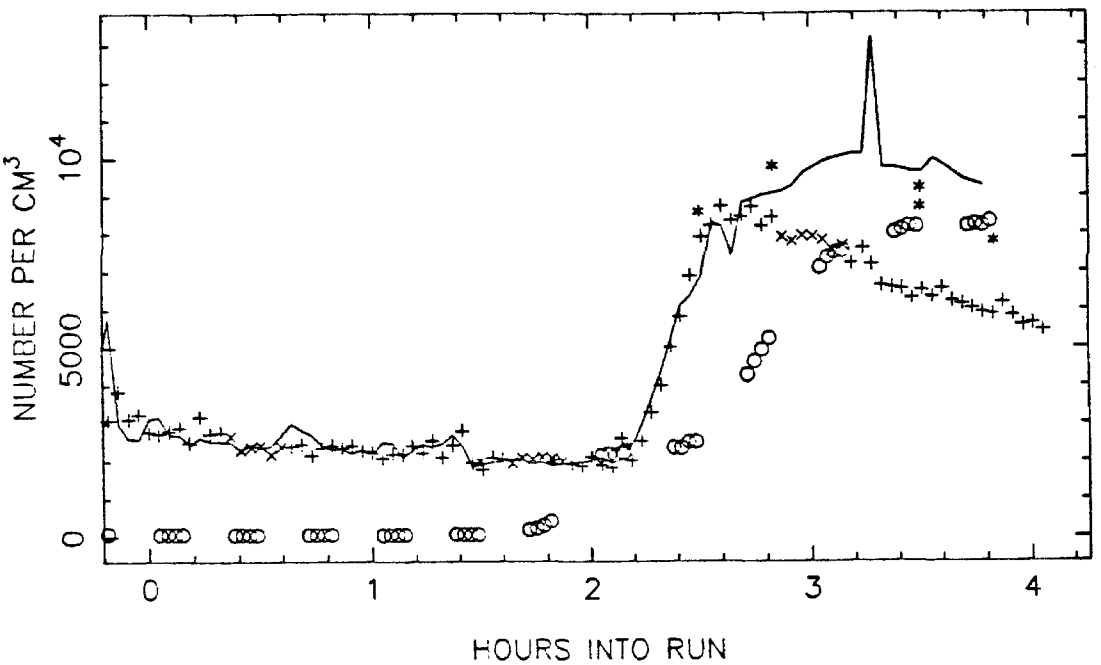

SIDE B

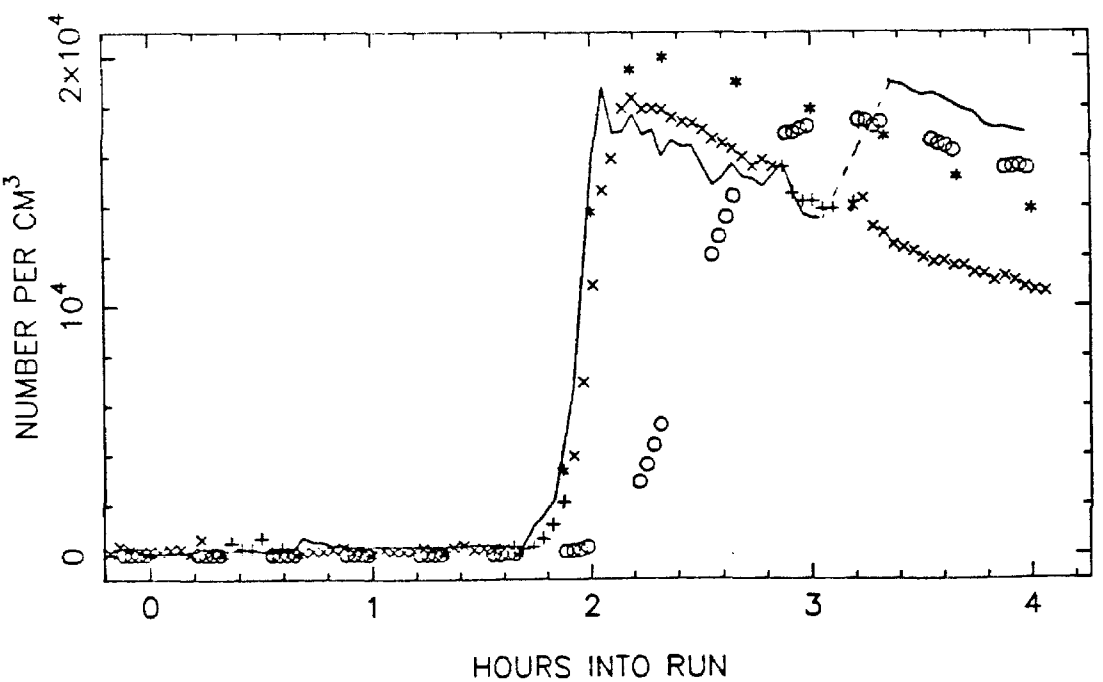

EM70 VOLUME IN THE AEROSOL PHASE, SIDE A

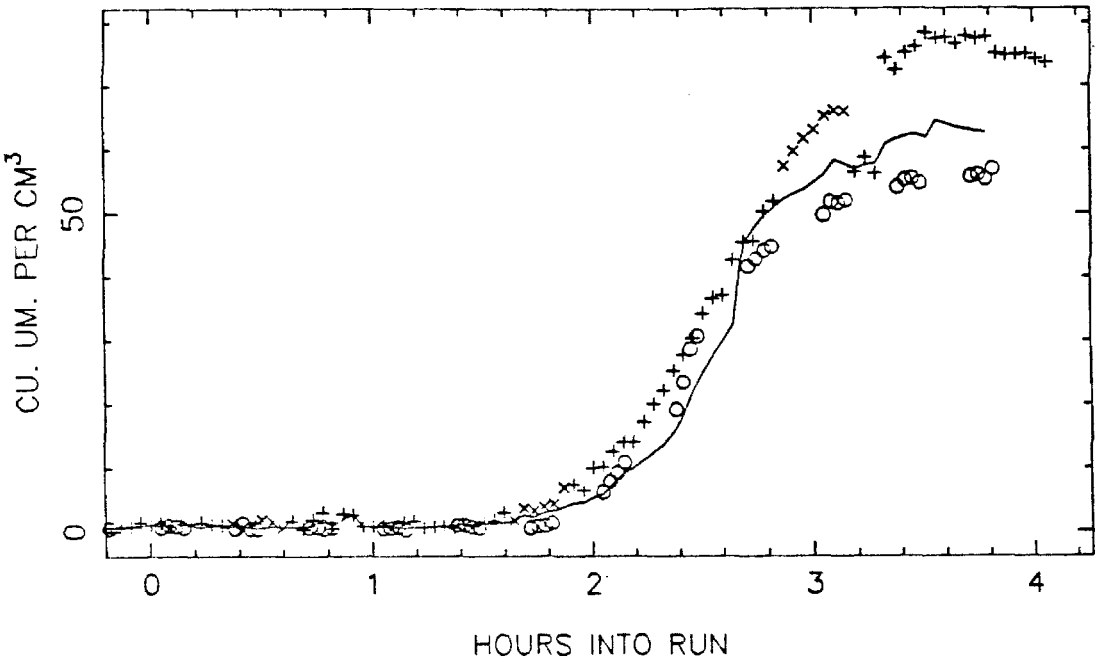

SIDE B

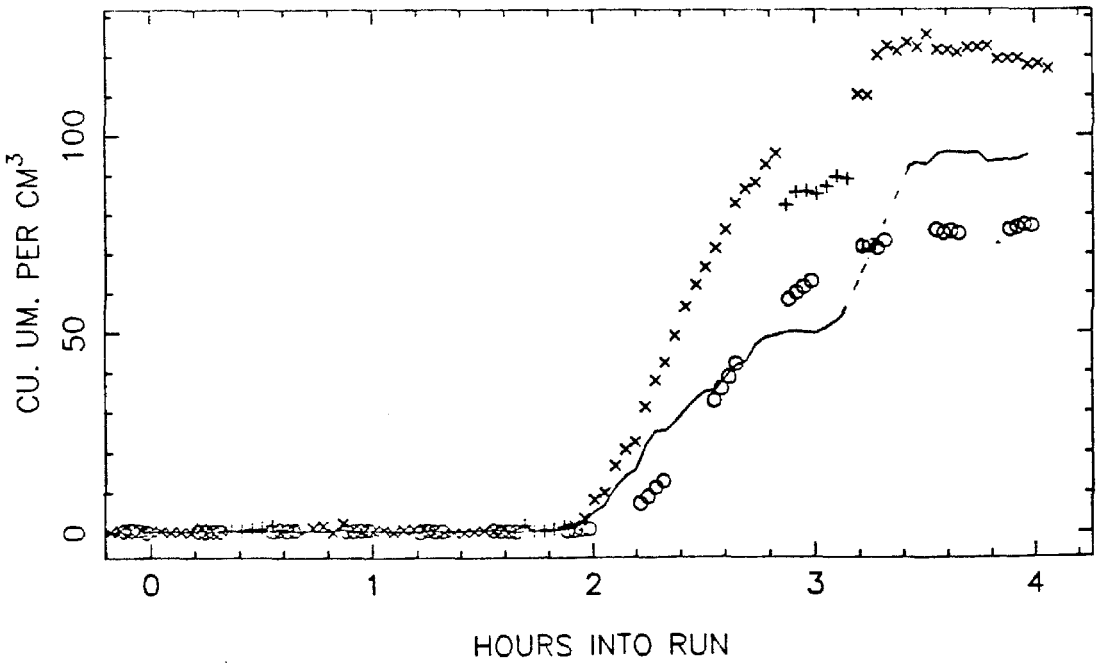

EM70 MEAN PARTICLE SIZE, SIDE A

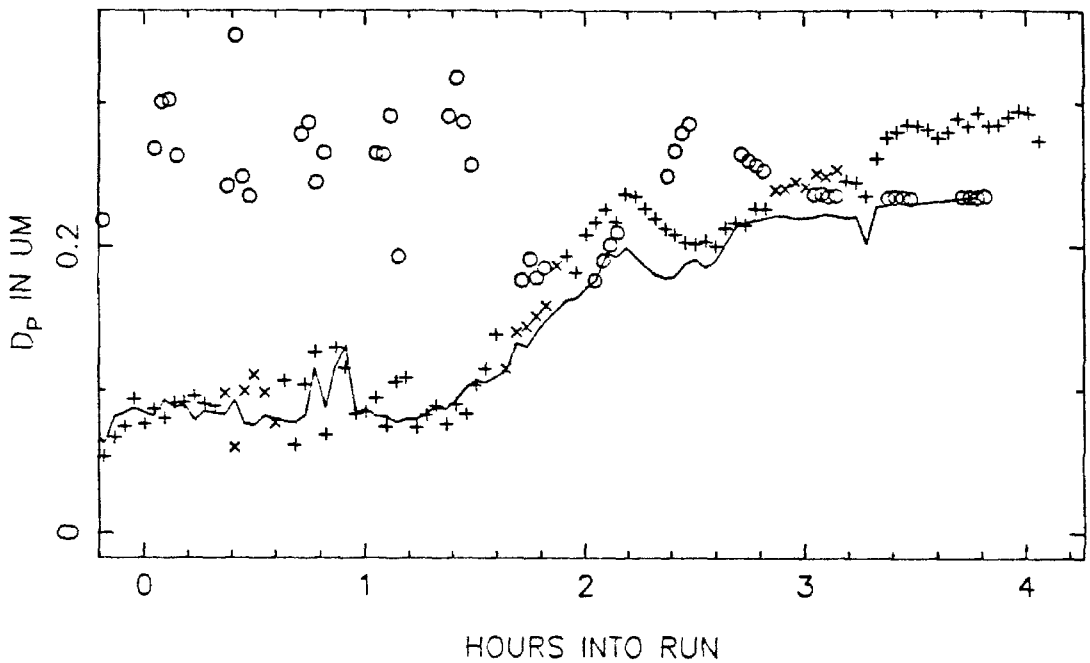

SIDE B

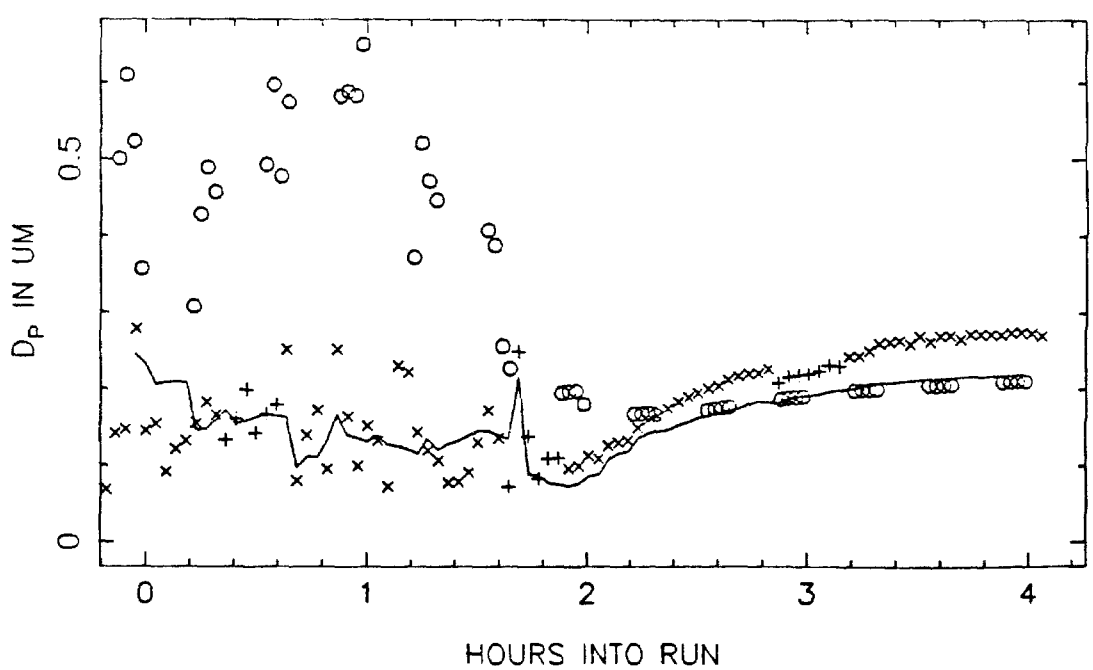

EM70A NUMBER DISTRIBUTION, T=0

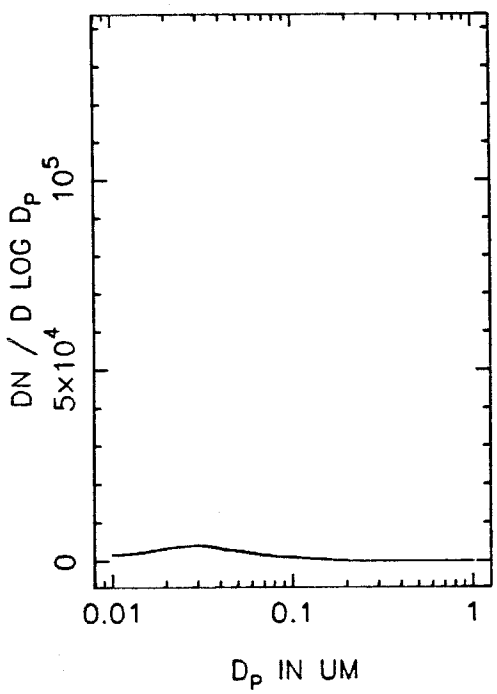

T=0.5 HOURS

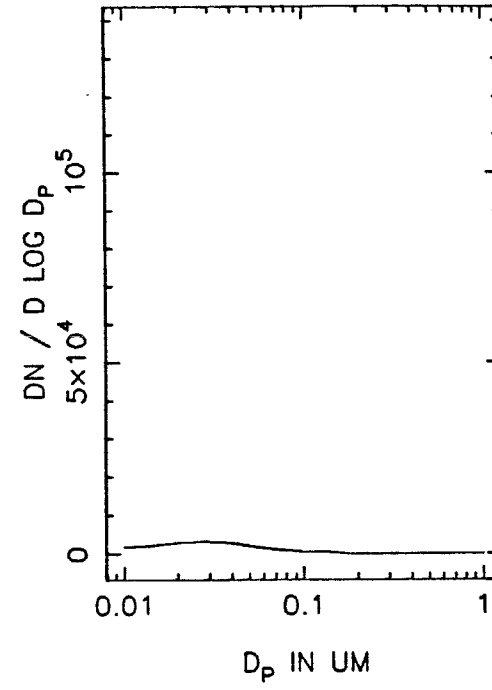

T=1.0 HOURS

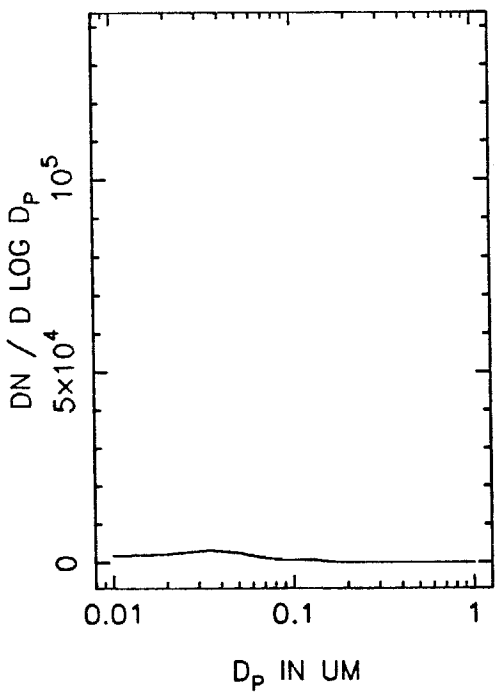

T=1.5 HOURS

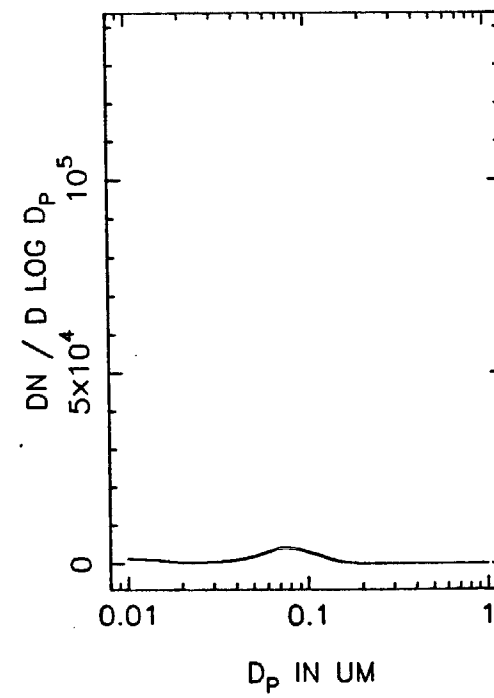

EM70A NUMBER DISTRIBUTION, T=2.0

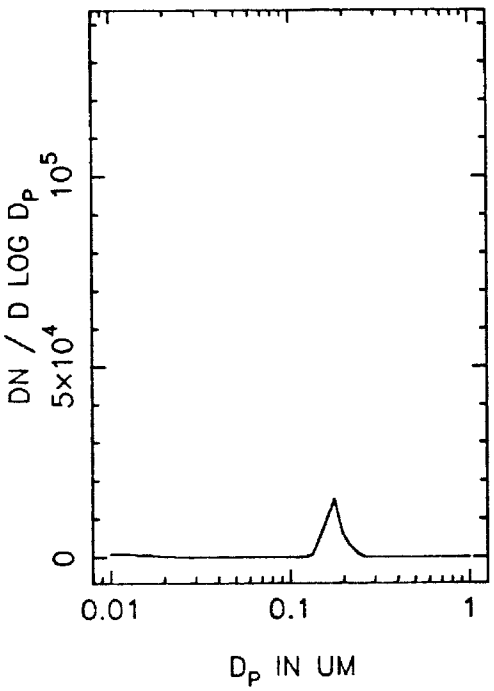

T=2.5 HOURS

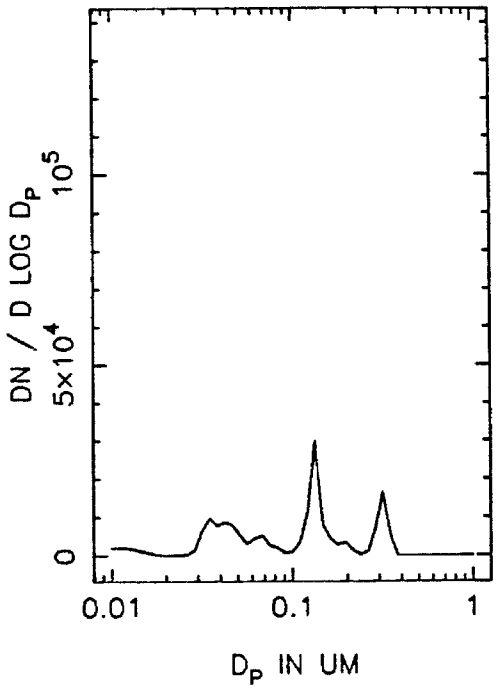

T=3.0 HOURS

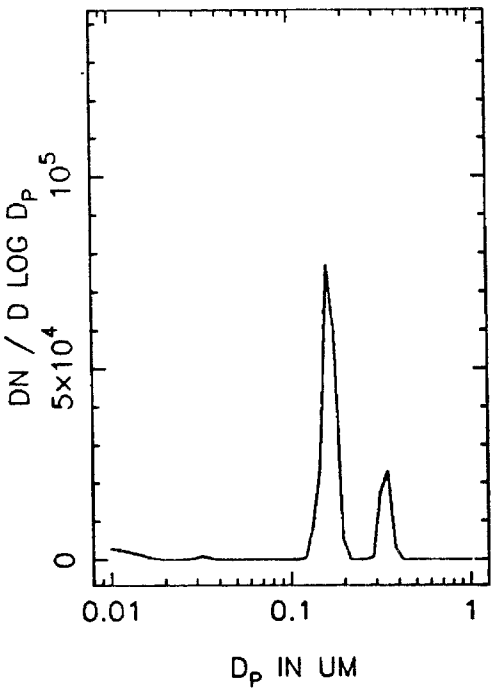

T=3.5 HOURS

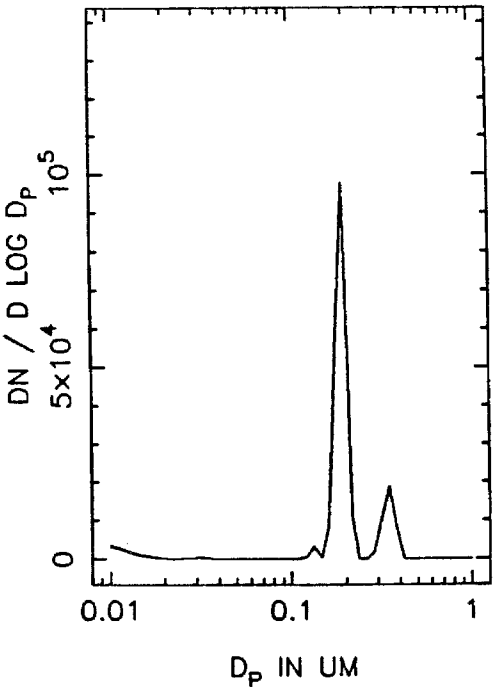

EM70A VOLUME DISTRIBUTION, T=0

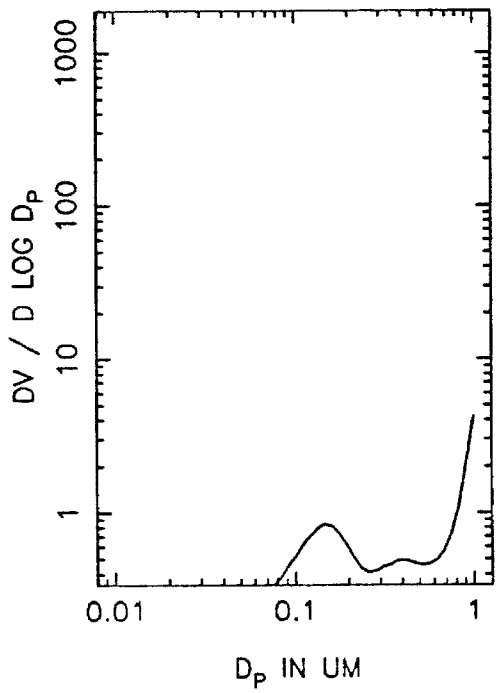

T=0.5 HOURS

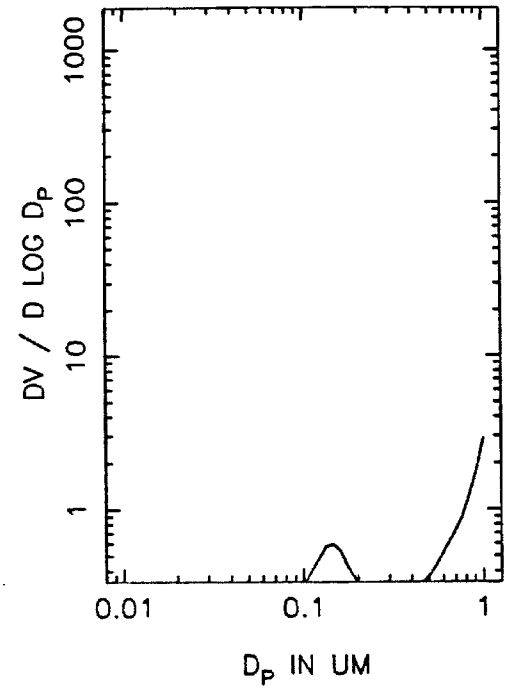

T=1.0 HOURS

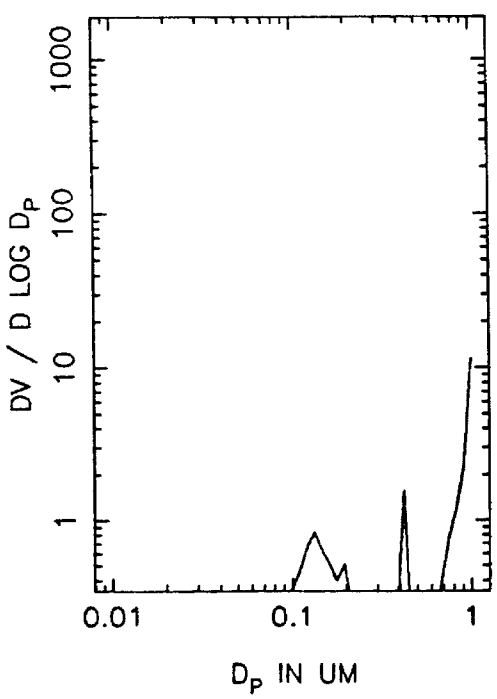

T=1.5 HOURS

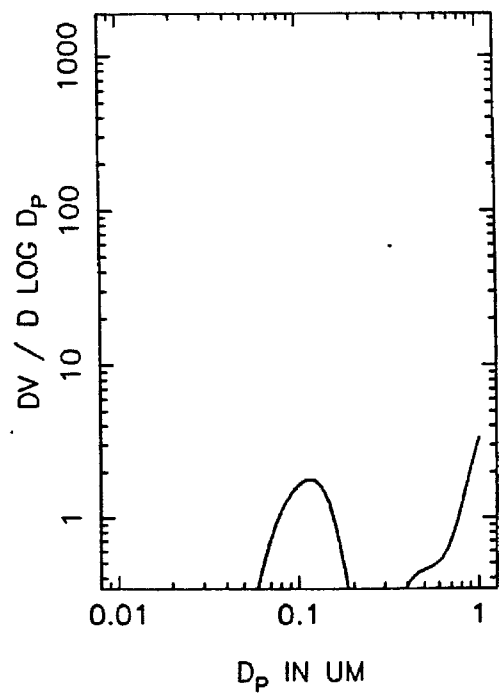

EM70A VOLUME DISTRIBUTION, T=2.0

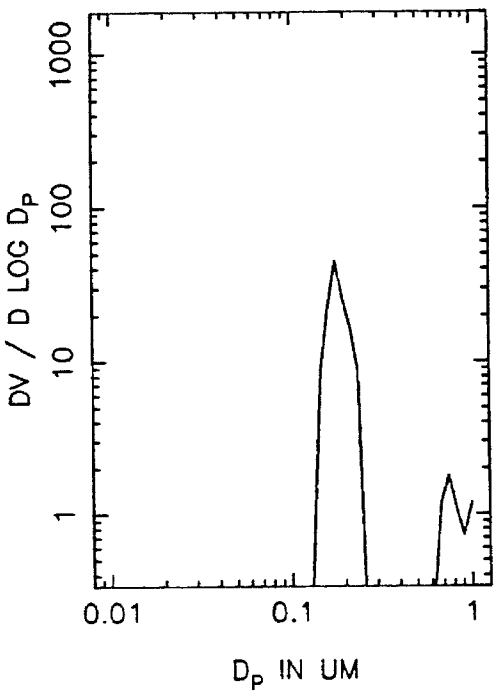

T=2.5 HOURS

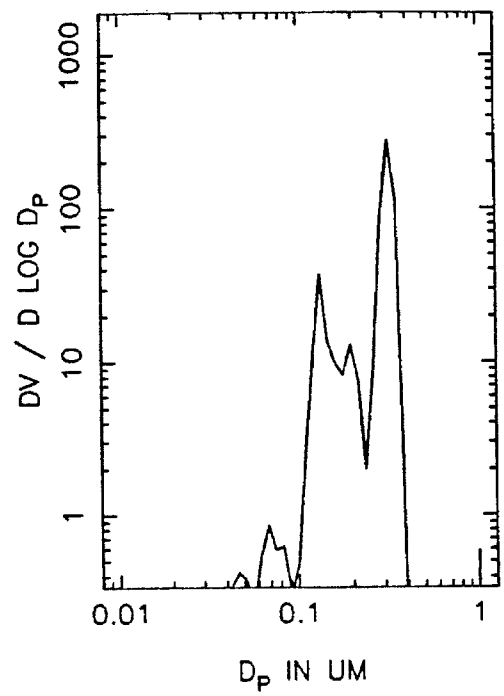

T=3.0 HOURS

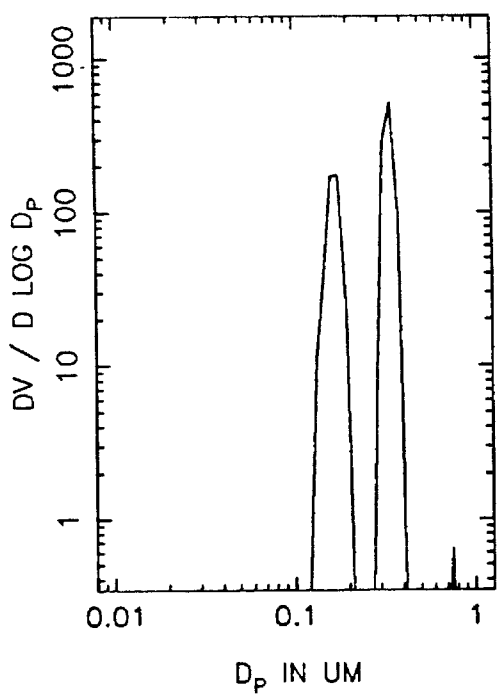

T=3.5 HOURS

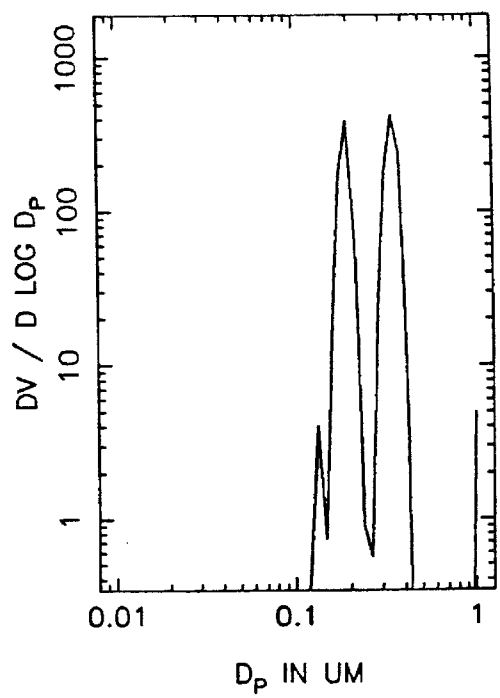

EM70B NUMBER DISTRIBUTION, T=0

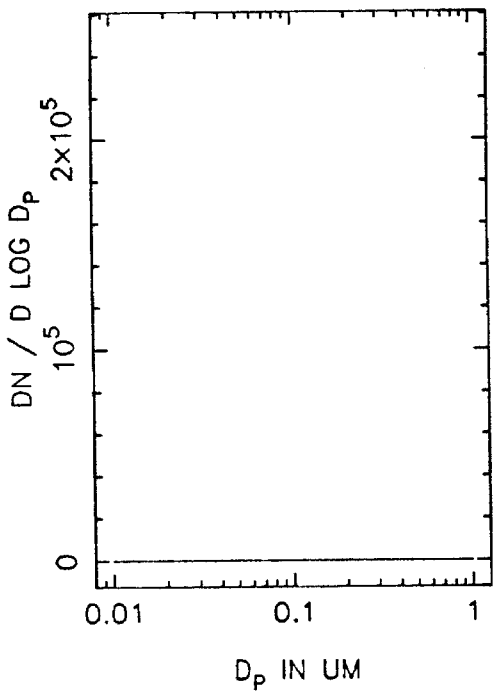

T=0.5 HOURS

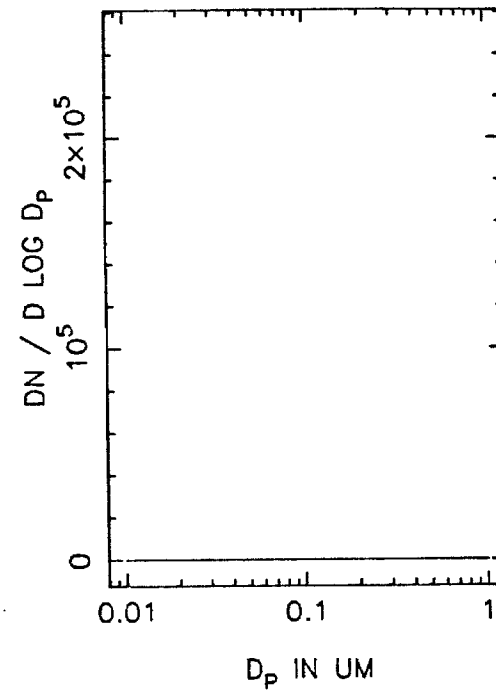

T=1.0 HOURS

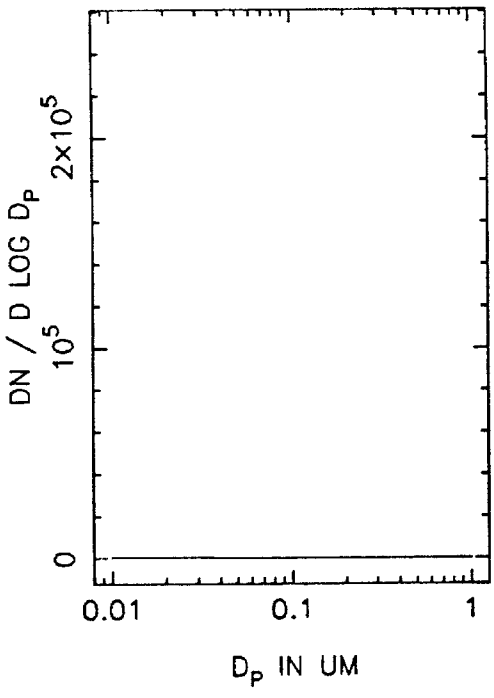

T=1.5 HOURS

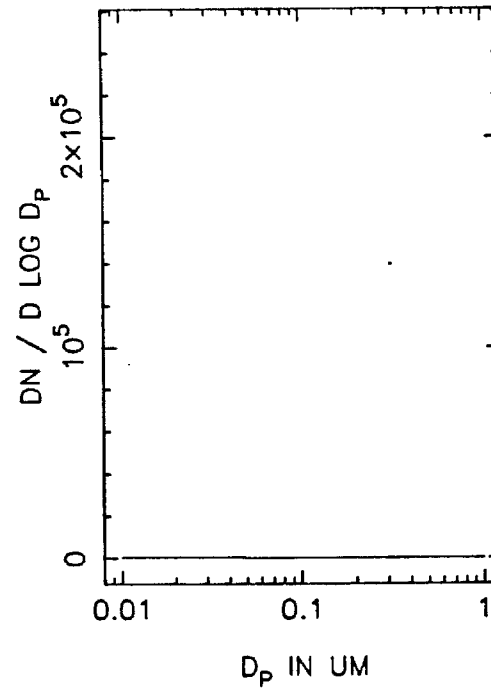

EM70B NUMBER DISTRIBUTION, T=2.0

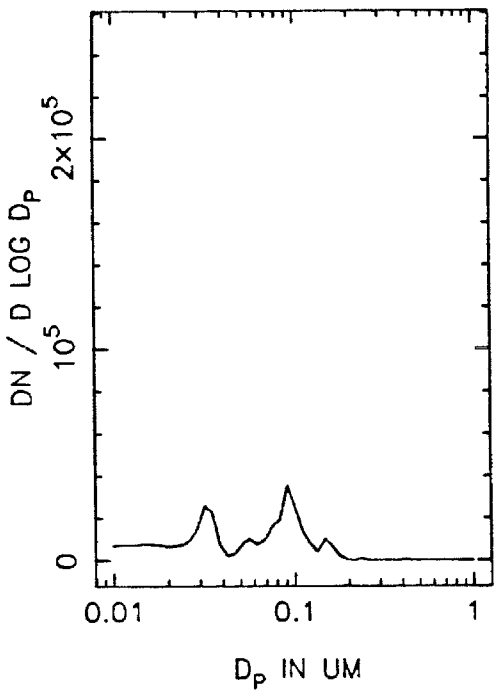

T=2.5 HOURS

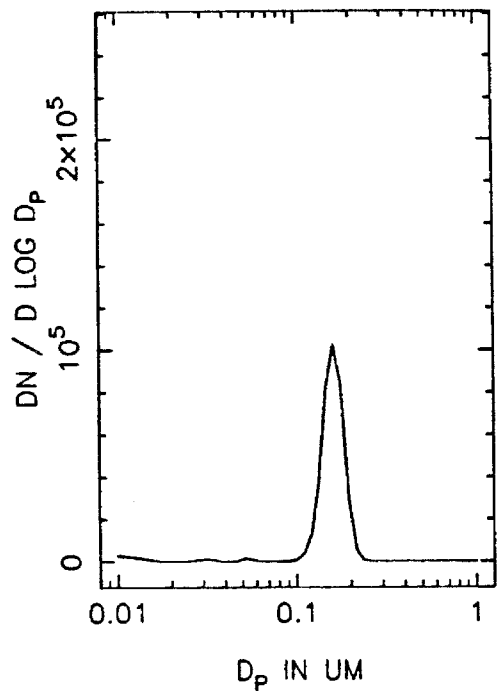

T=3.0 HOURS

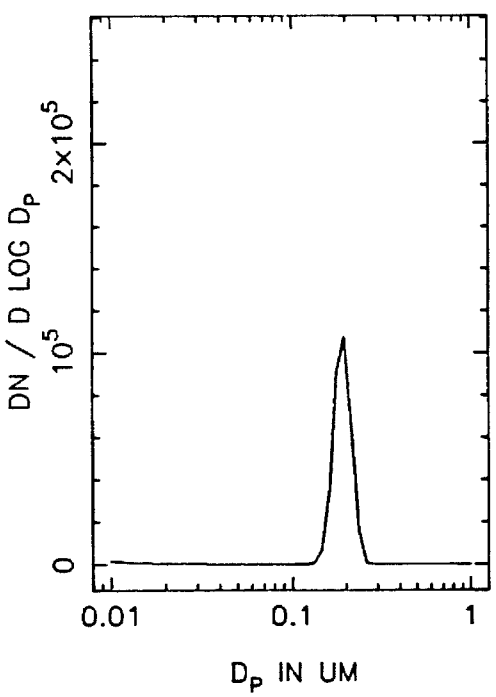

T=3.5 HOURS

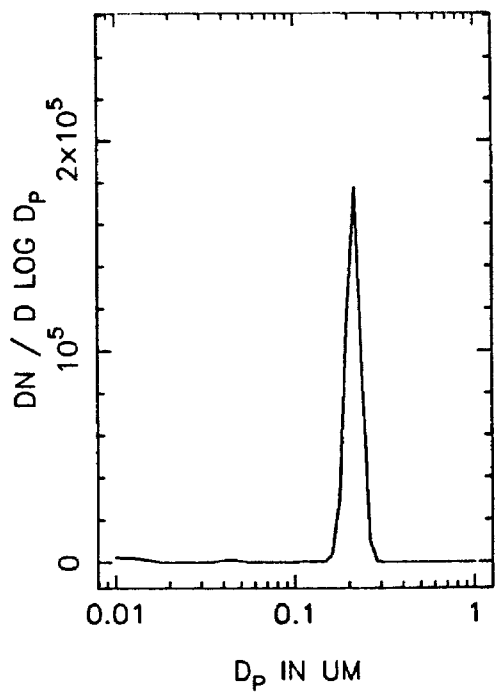

EM70B NUMBER DISTRIBUTION, T=4.0

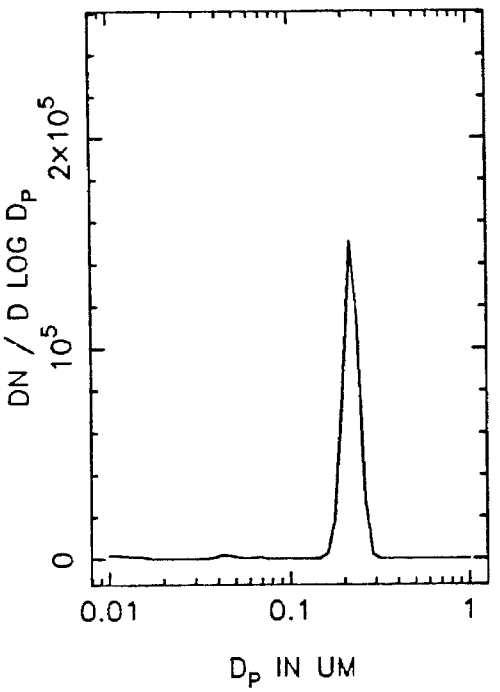

EM70B VOLUME DISTRIBUTION, T=0

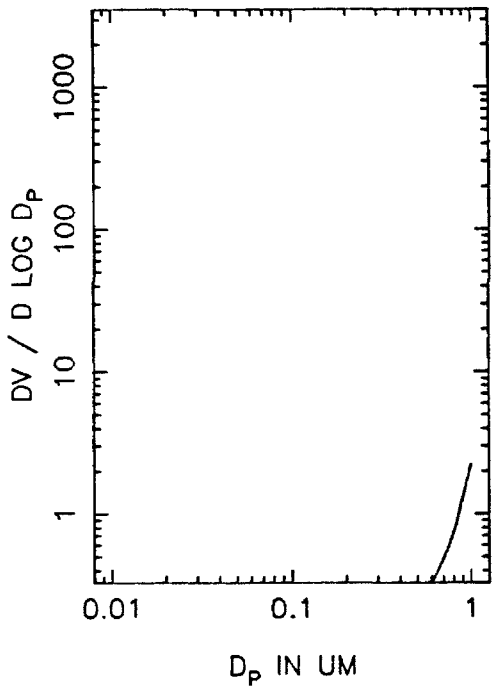

T=0.5 HOURS

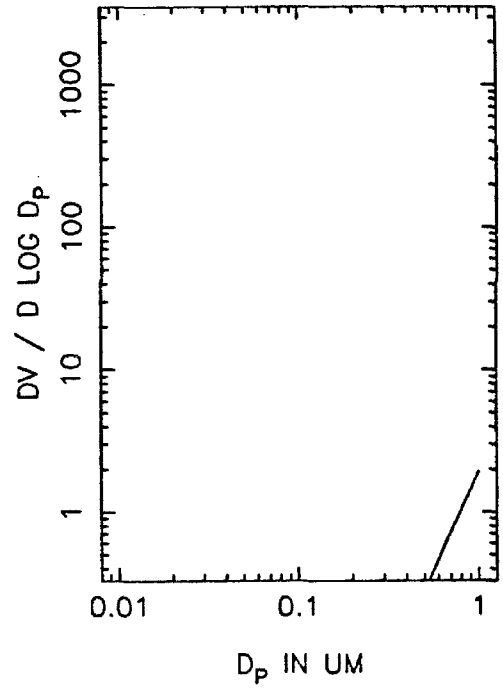

T=1.0 HOURS

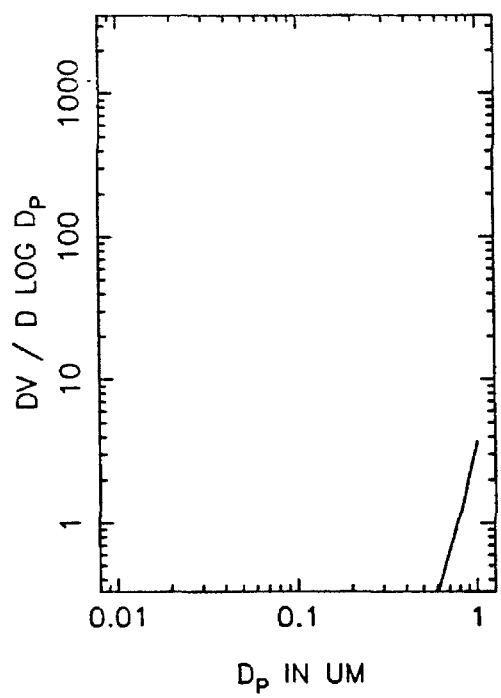

T=1.5 HOURS

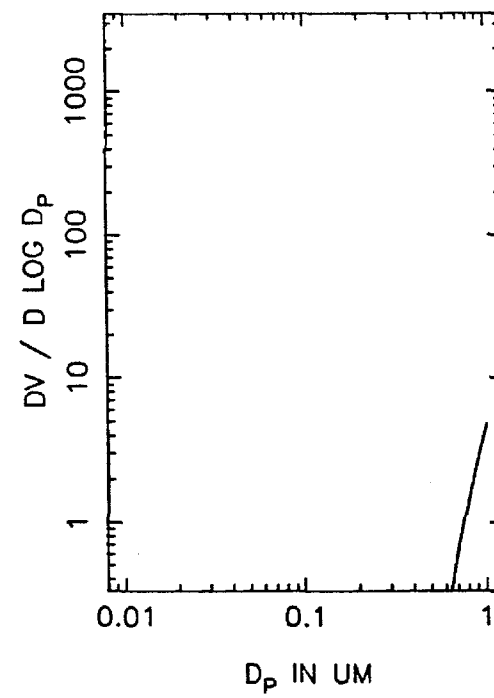

EM70B VOLUME DISTRIBUTION, T=2.0

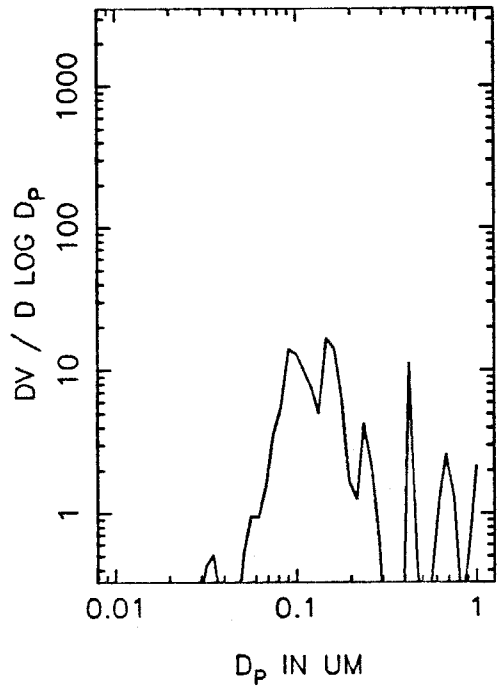

T=2.5 HOURS

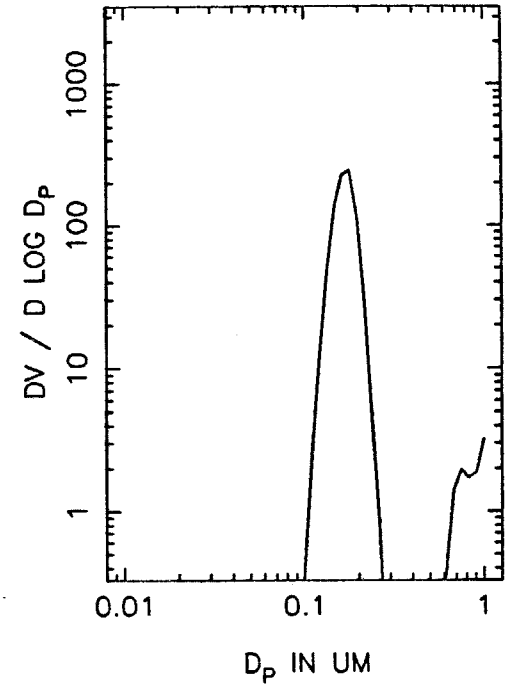

T=3.0 HOURS

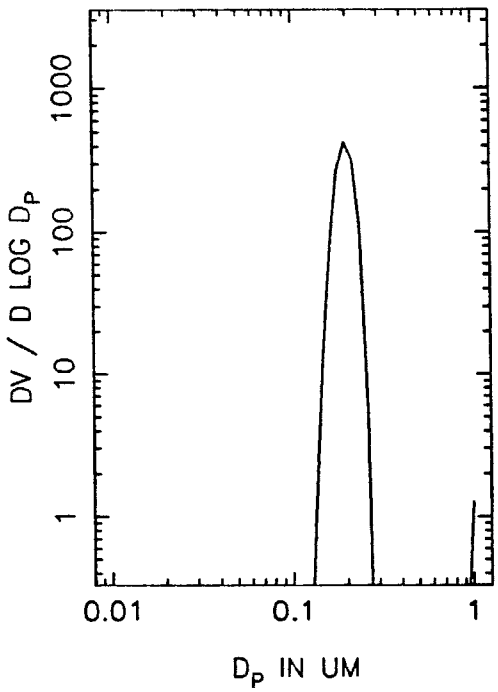

T=3.5 HOURS

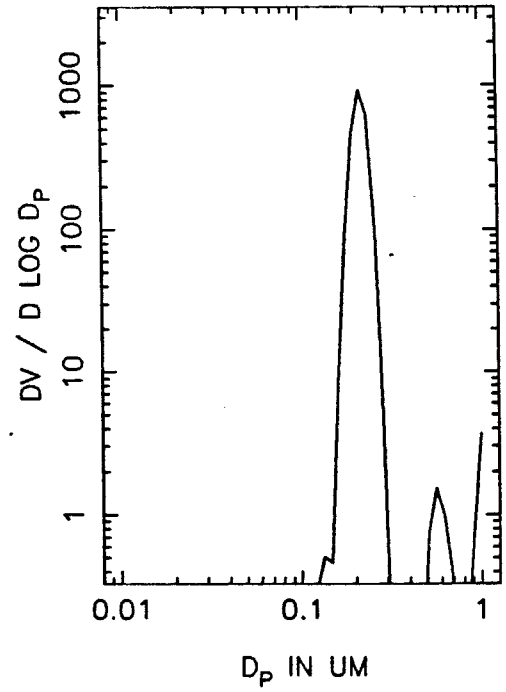

EM70B VOLUME DISTRIBUTION, T=4.0

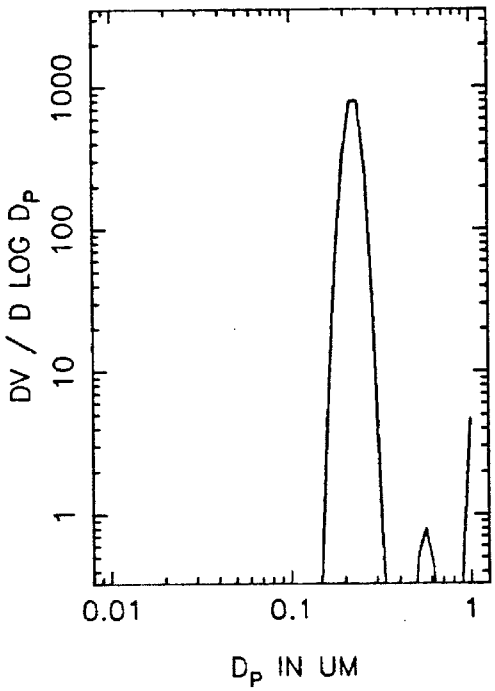

EL73 TOTAL NUMBER, SIDE A

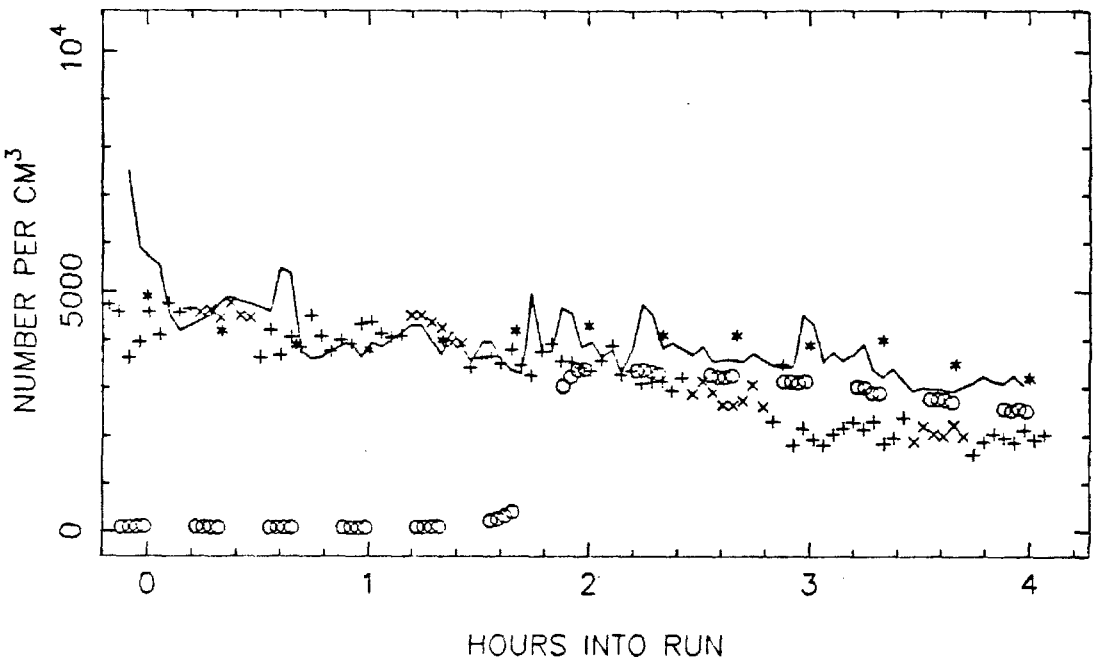

SIDE B

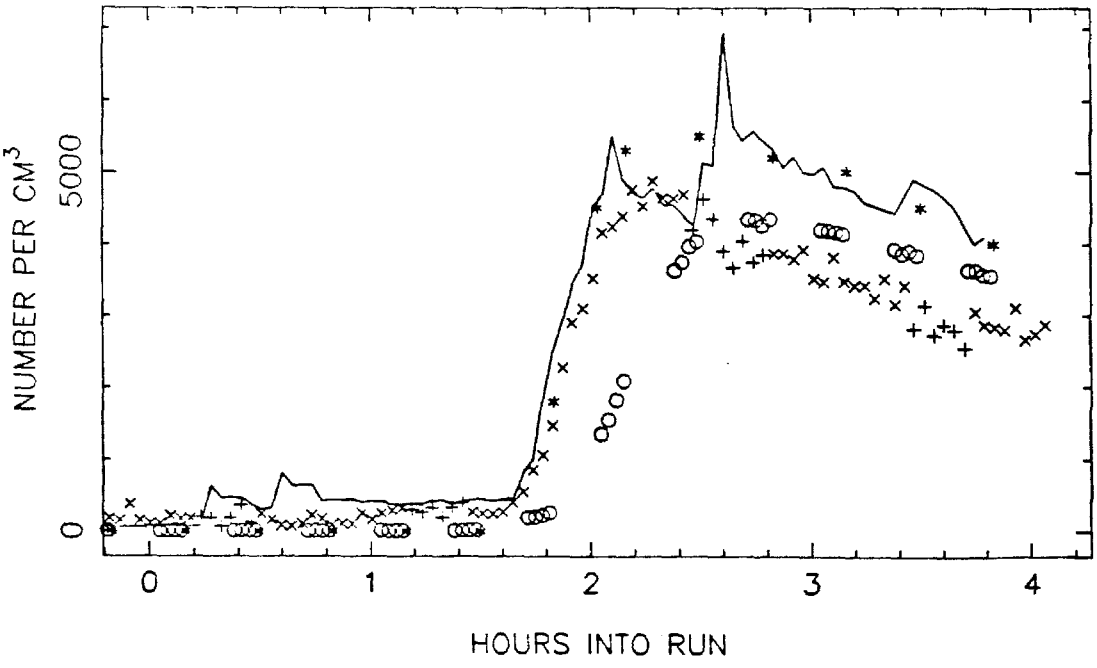

EL73 VOLUME IN THE AEROSOL PHASE, SIDE A

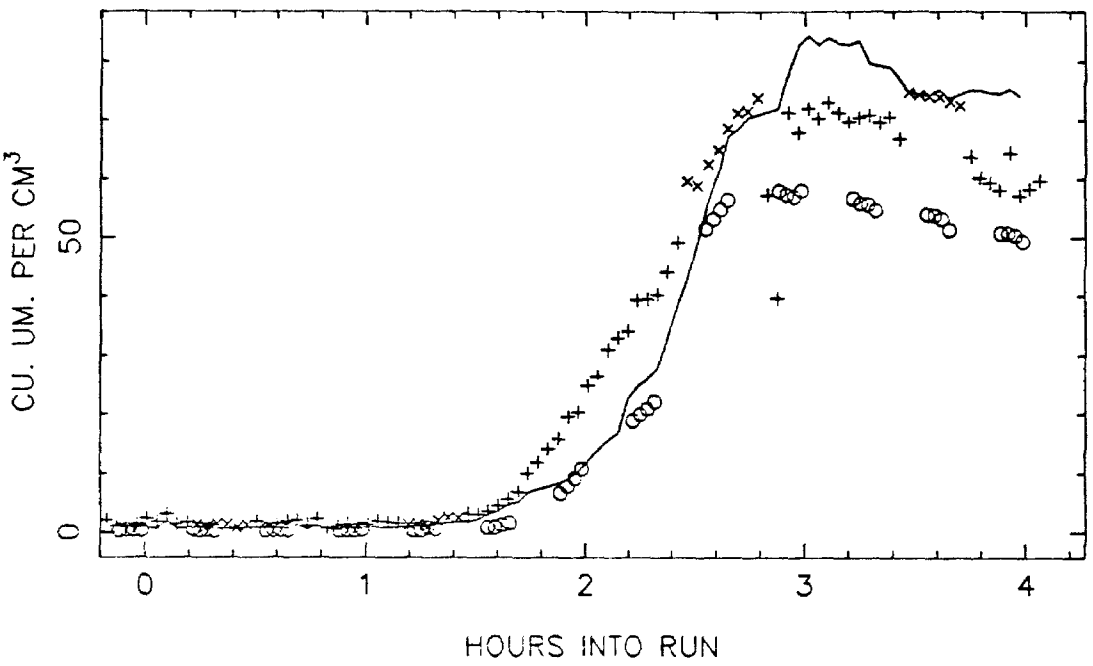

SIDE B

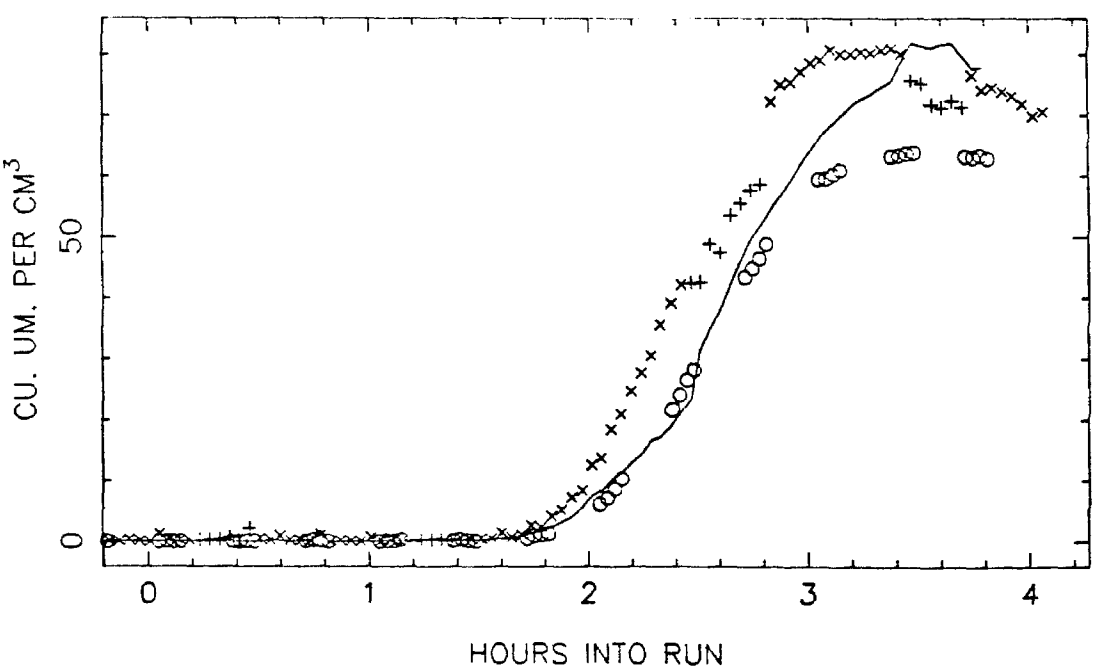

EL73 MEAN PARTICLE SIZE, SIDE A

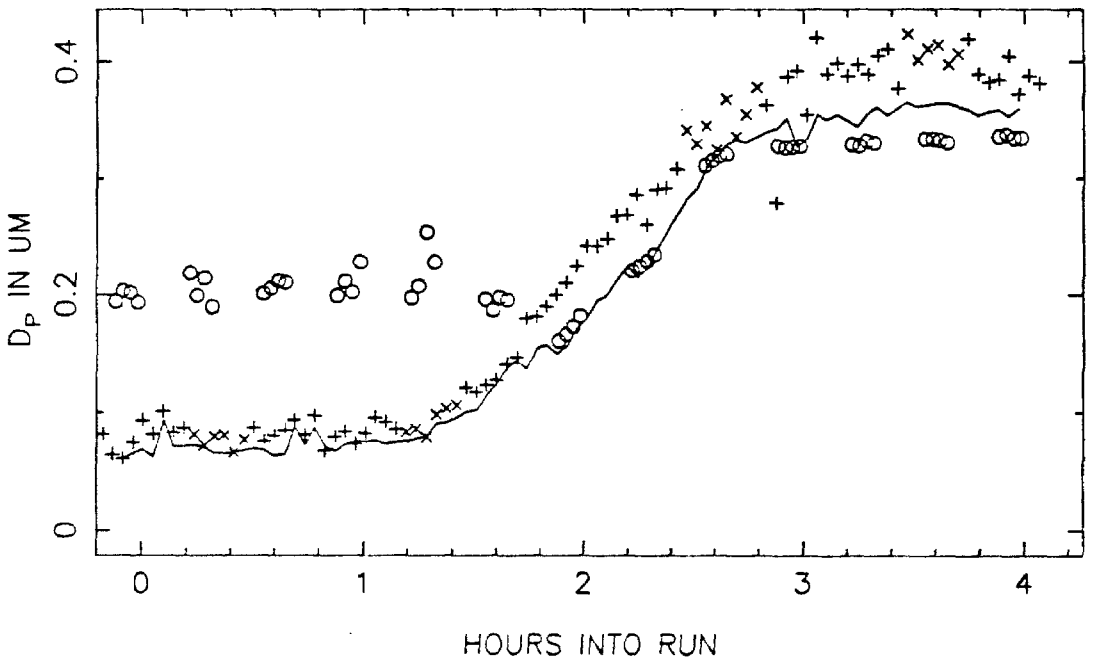

SIDE B

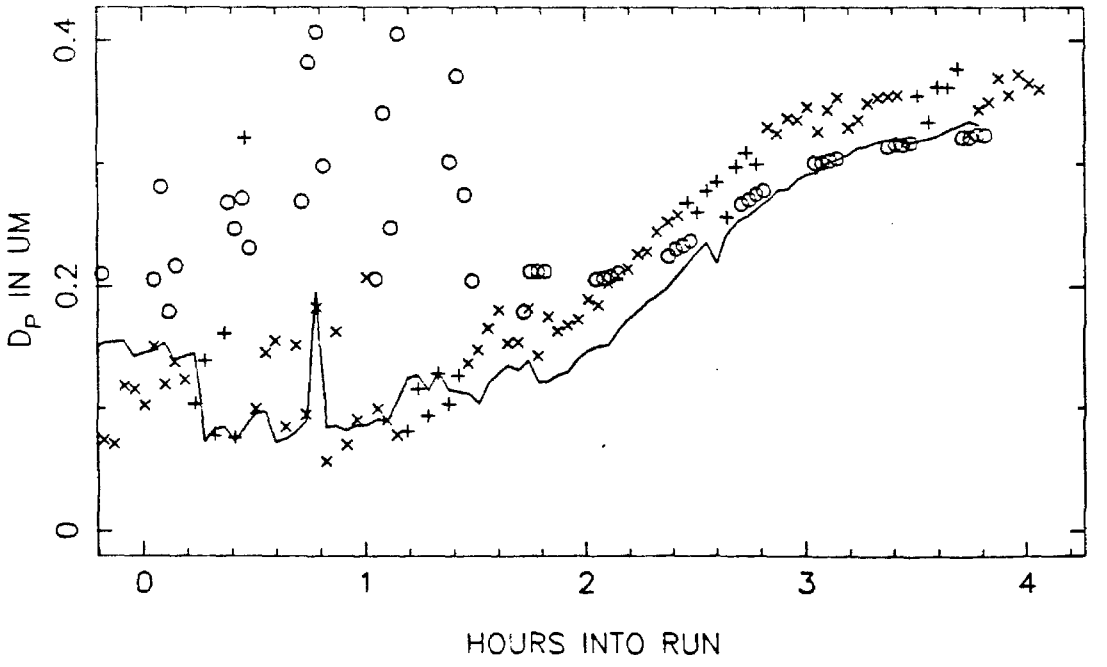

EL73A NUMBER DISTRIBUTION, T=0

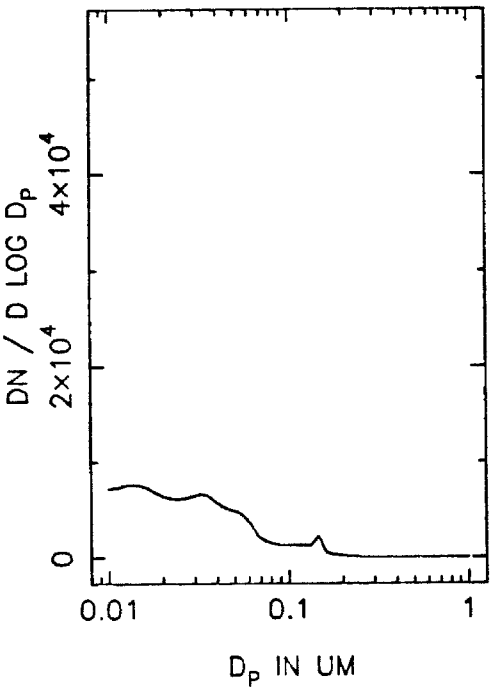

T=0.5 HOURS

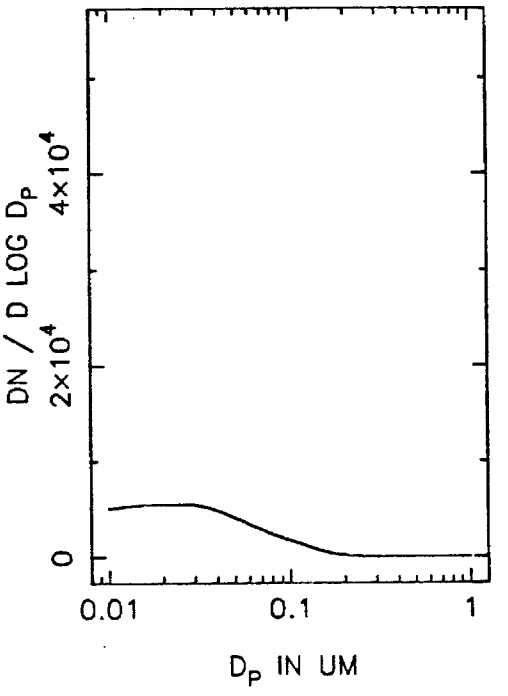

T=1.0 HOURS

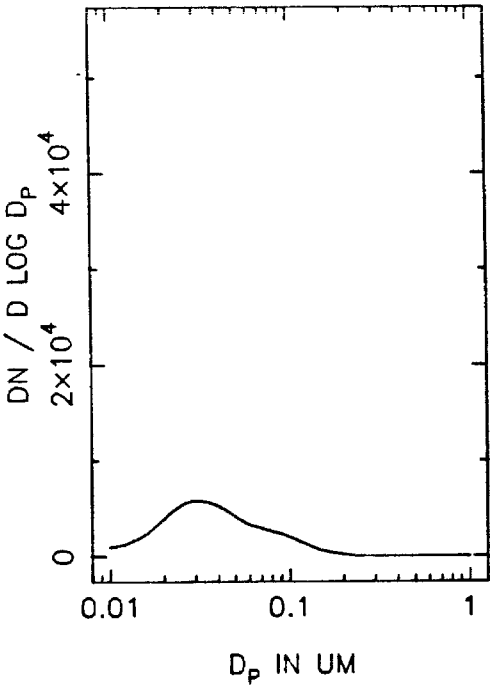

T=1.5 HOURS

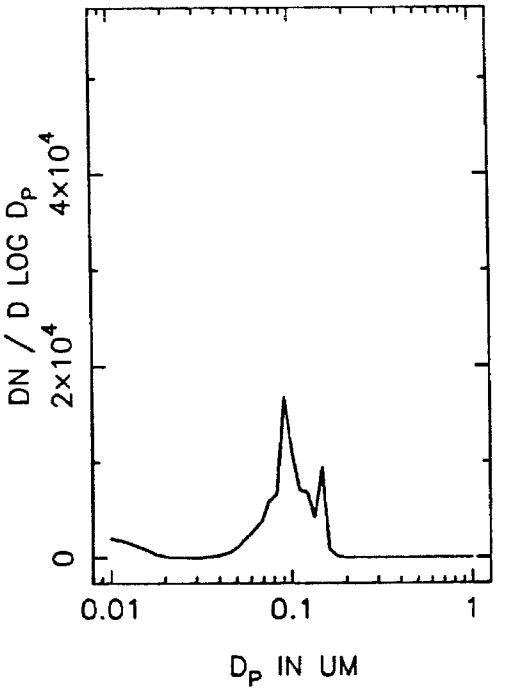

EL73A NUMBER DISTRIBUTION, T=2.0

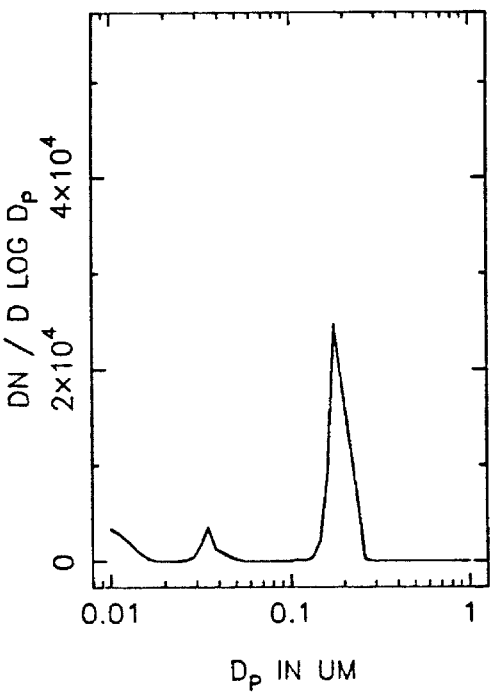

T=2.5 HOURS

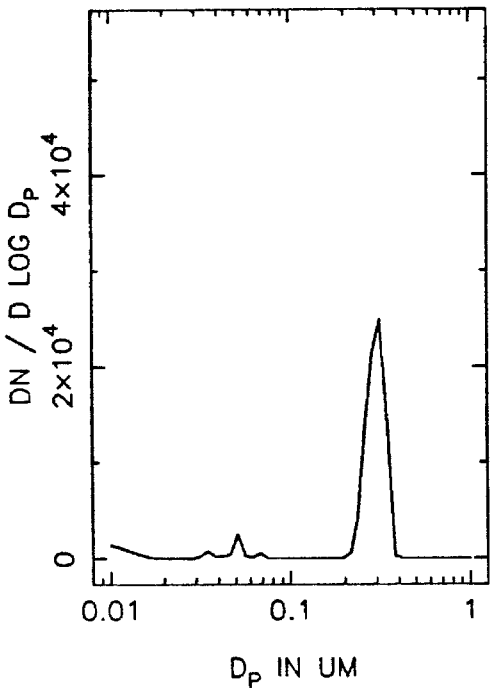

T=3.0 HOURS

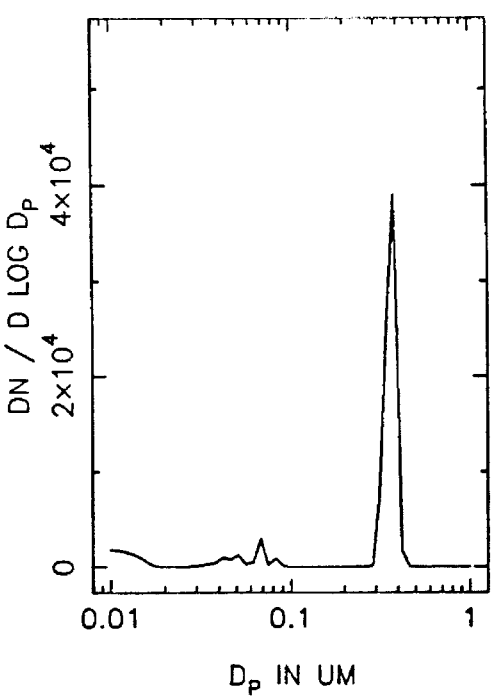

T=3.5 HOURS

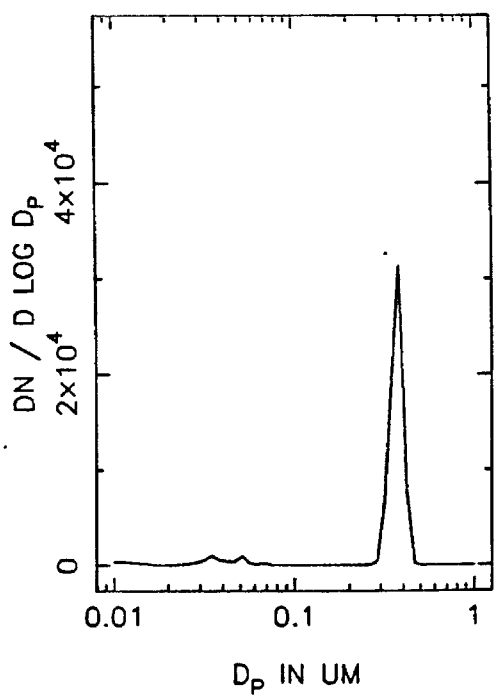

EL73A NUMBER DISTRIBUTION, T=4.0

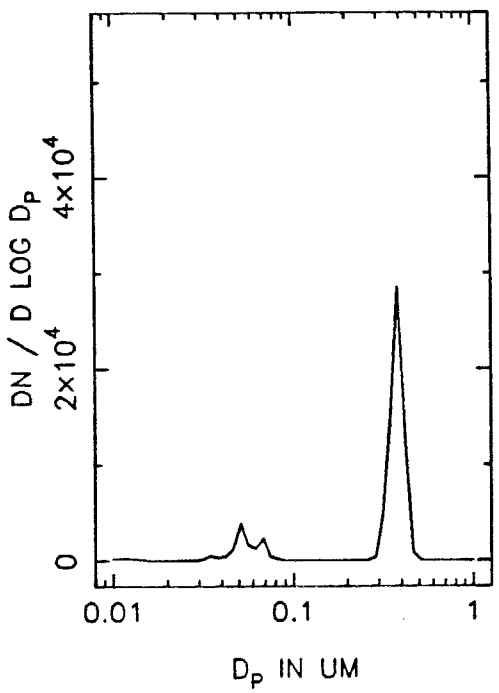

EL73A VOLUME DISTRIBUTION, T=0

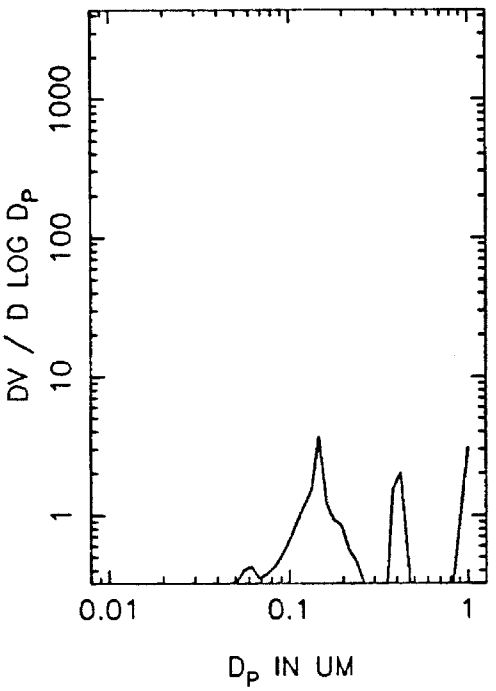

T=0.5 HOURS

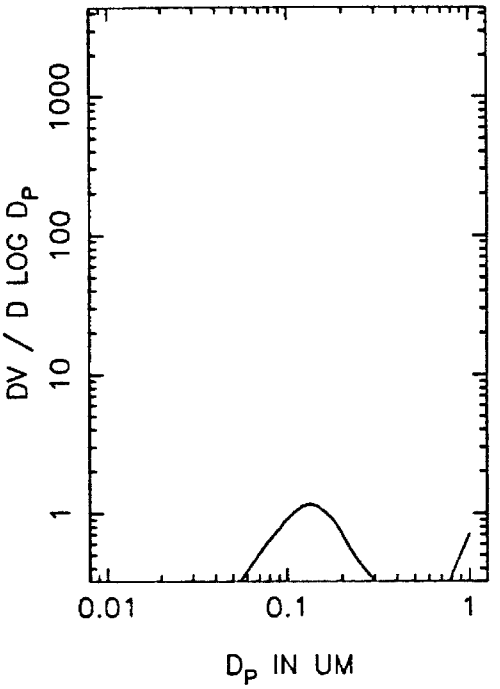

T=1.0 HOURS

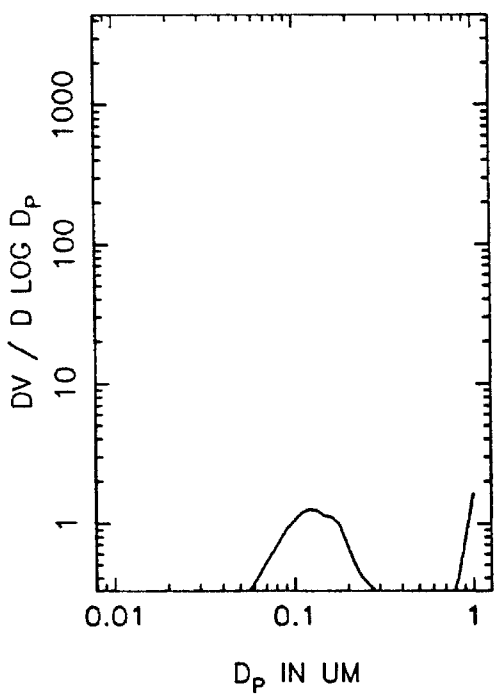

T=1.5 HOURS

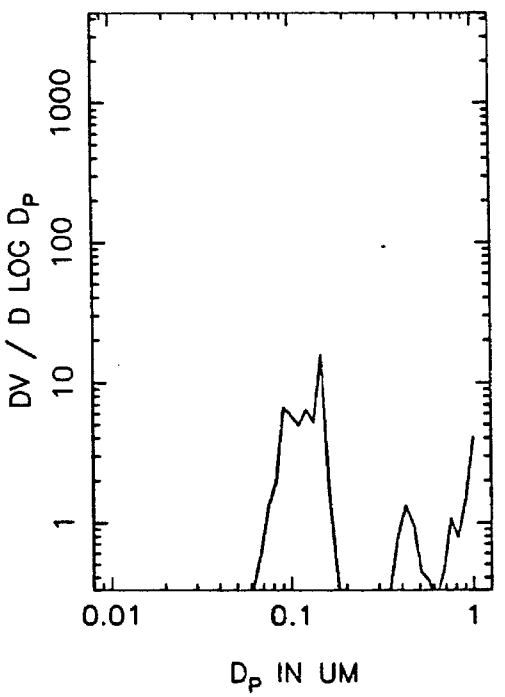

EL73A VOLUME DISTRIBUTION, T=2.0

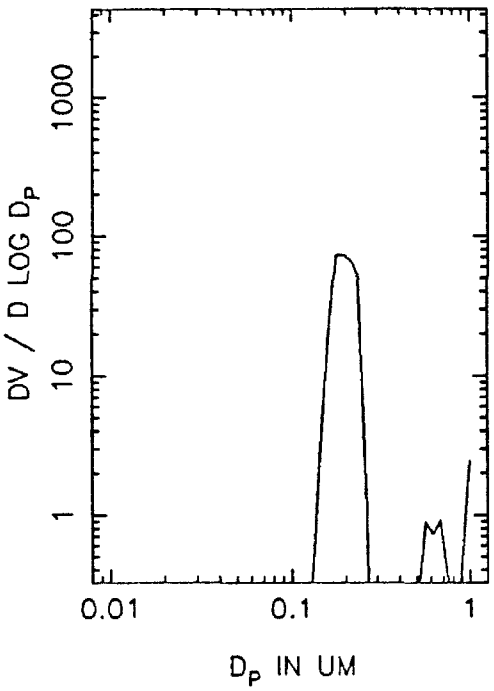

T=2.5 HOURS

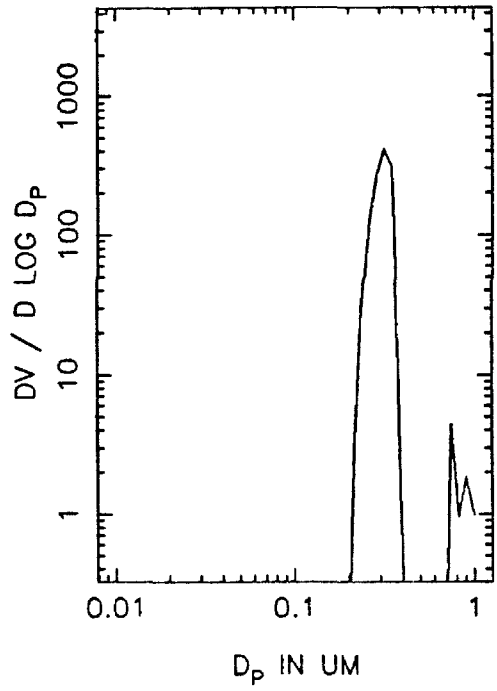

T=3.0 HOURS

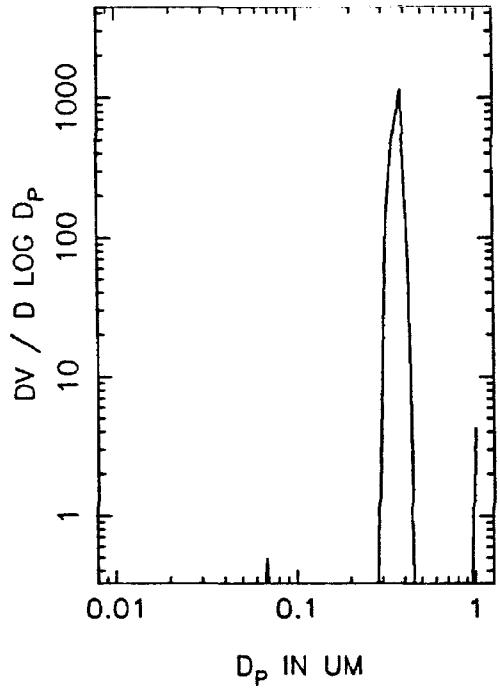

T=3.5 HOURS

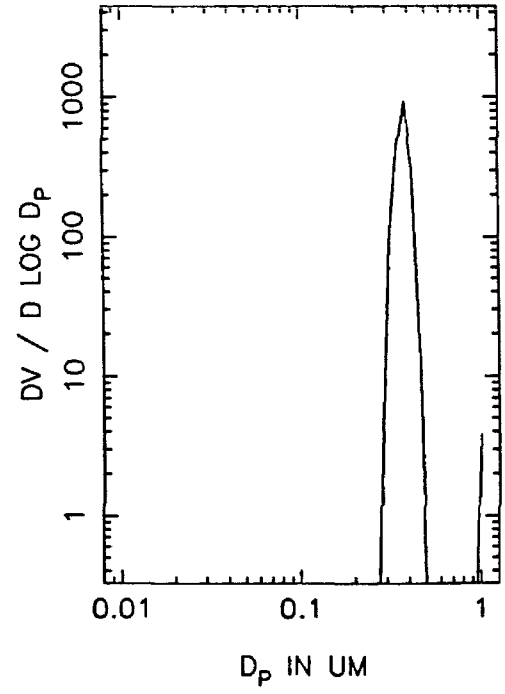

EL73A VOLUME DISTRIBUTION, T=4.0

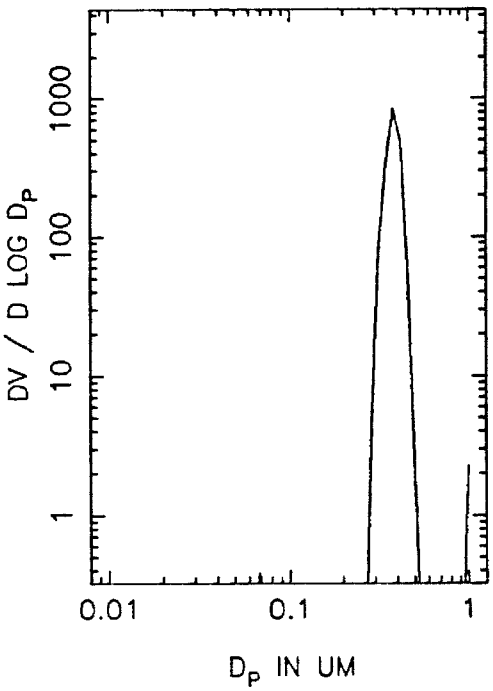

EL73B NUMBER DISTRIBUTION, T=0

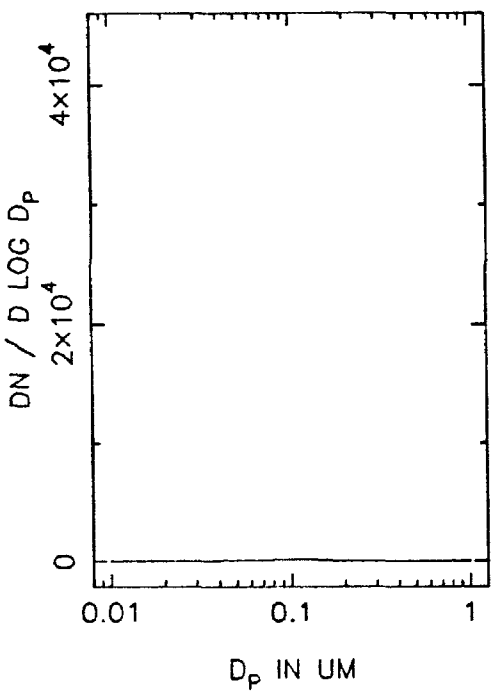

T=0.5 HOURS

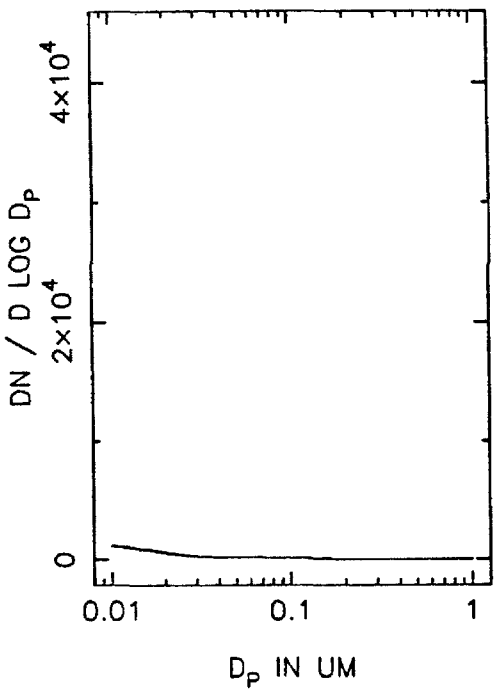

T=1.0 HOURS

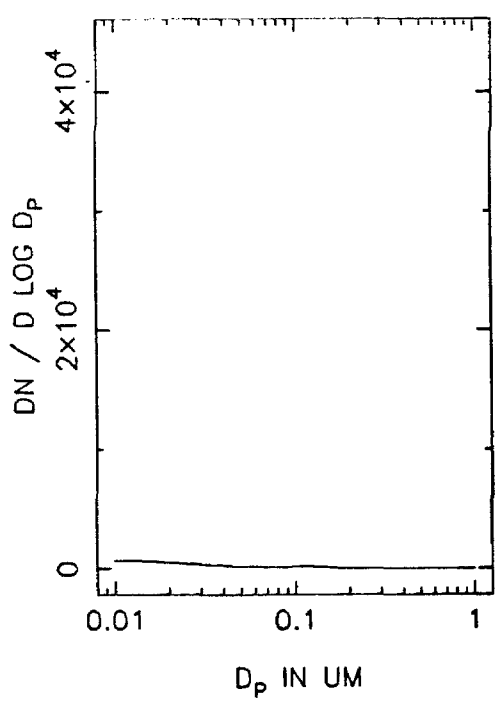

T=1.5 HOURS

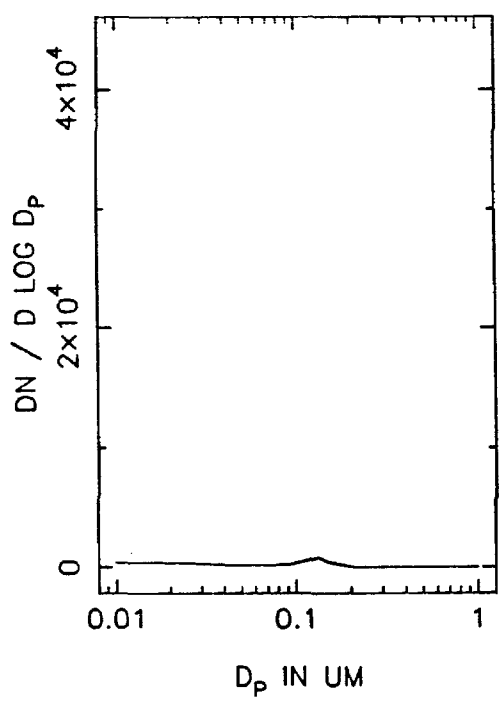

EL73B NUMBER DISTRIBUTION, T=2.0

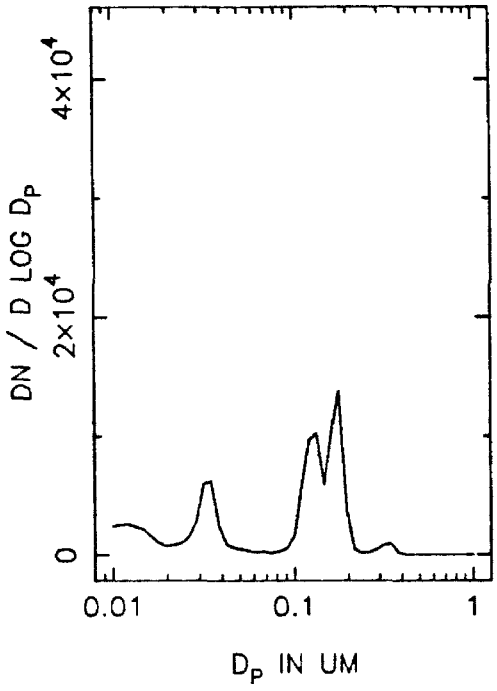

T=2.5 HOURS

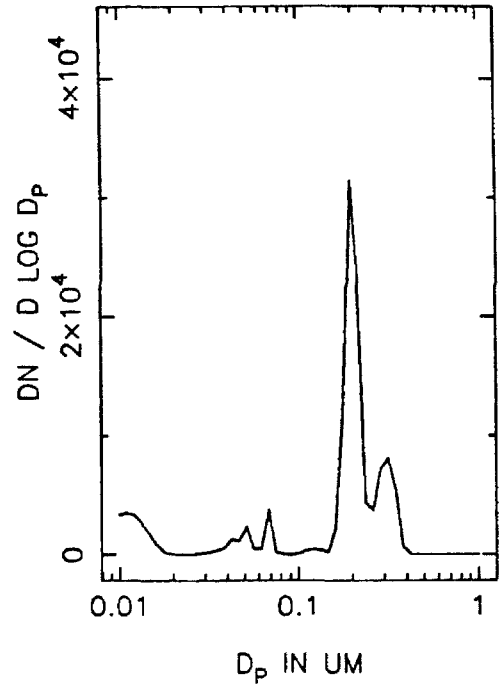

T=3.0 HOURS

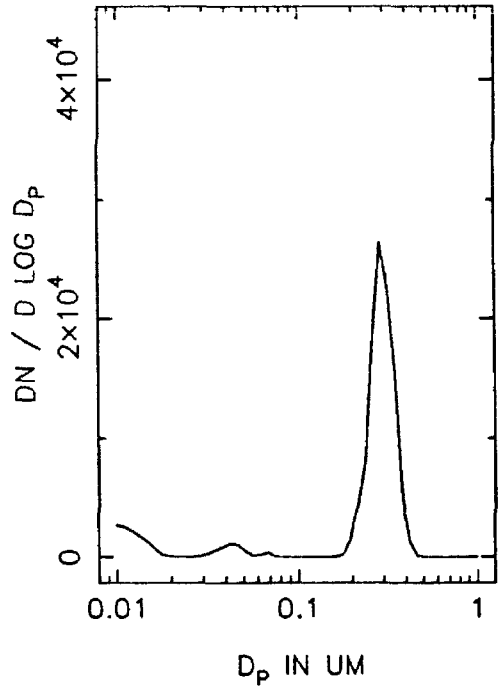

T=3.5 HOURS

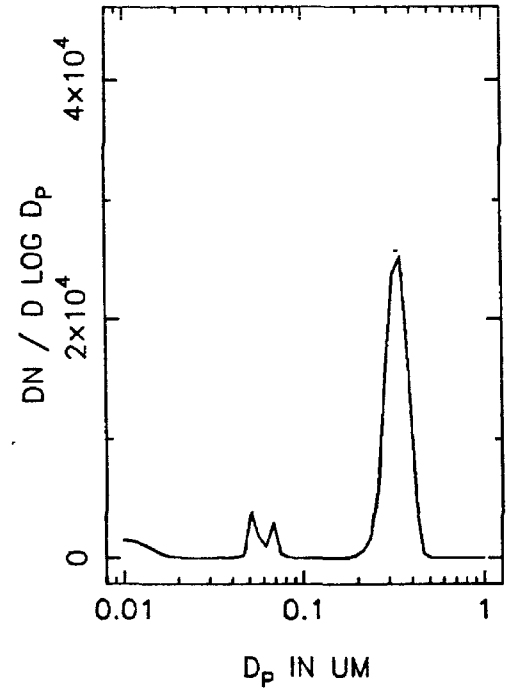

EL73B VOLUME DISTRIBUTION, T=0

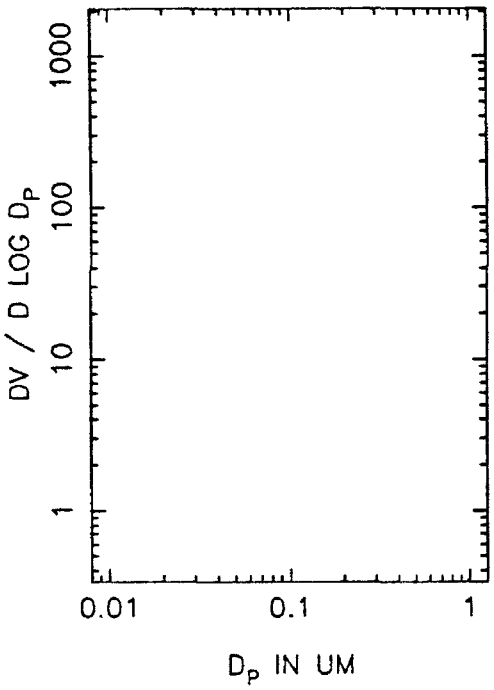

T=0.5 HOURS

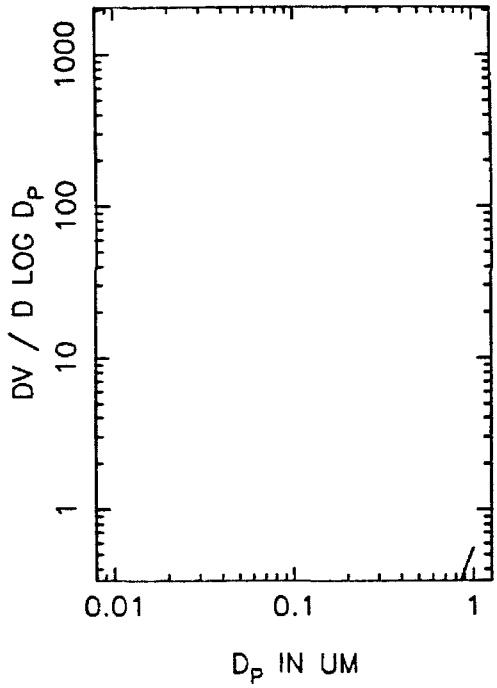

T=1.0 HOURS

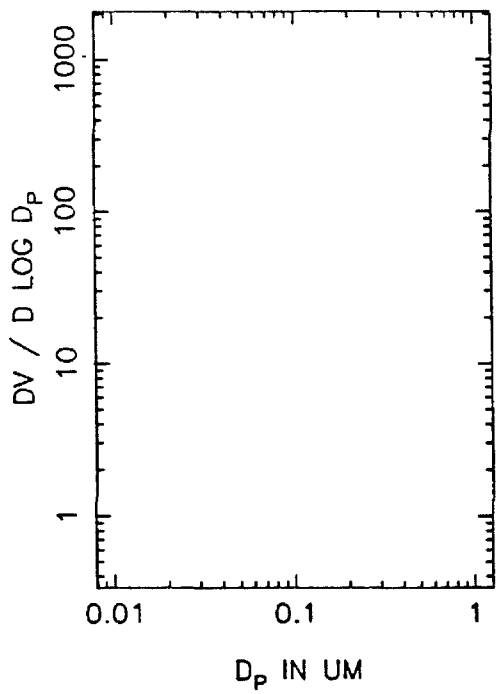

T=1.5 HOURS

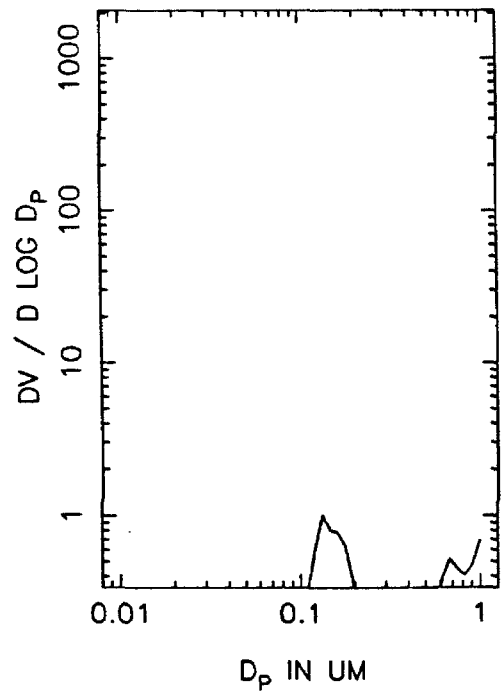

EL73B VOLUME DISTRIBUTION, T=2.0

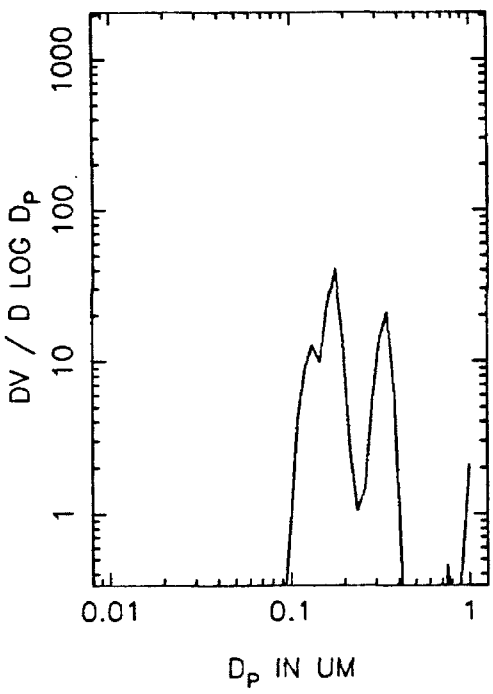

T=2.5 HOURS

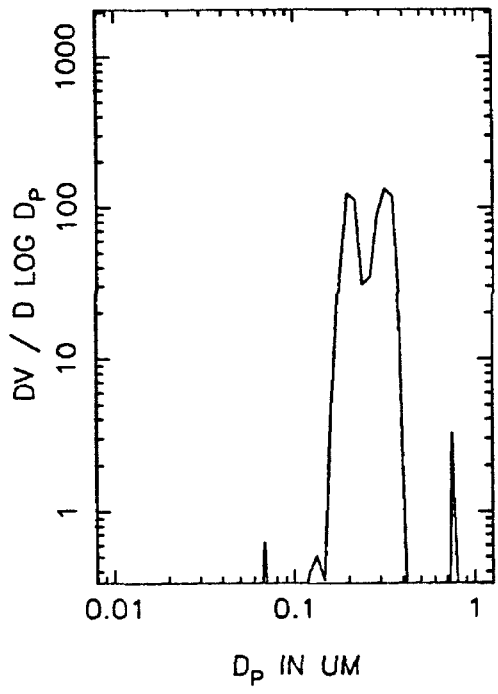

T=3.0 HOURS

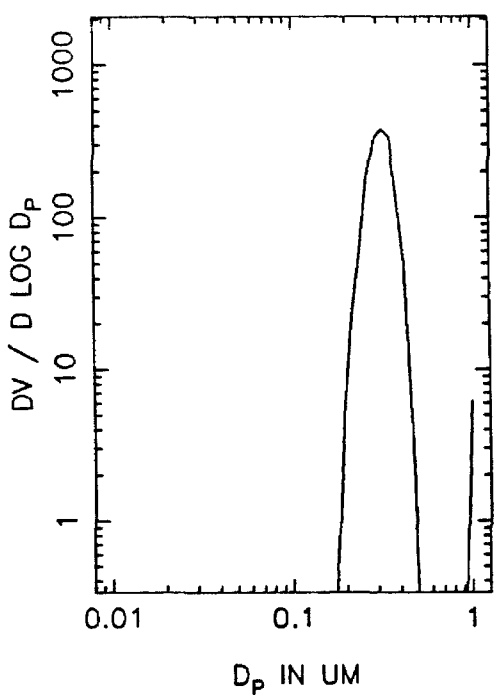

T=3.5 HOURS

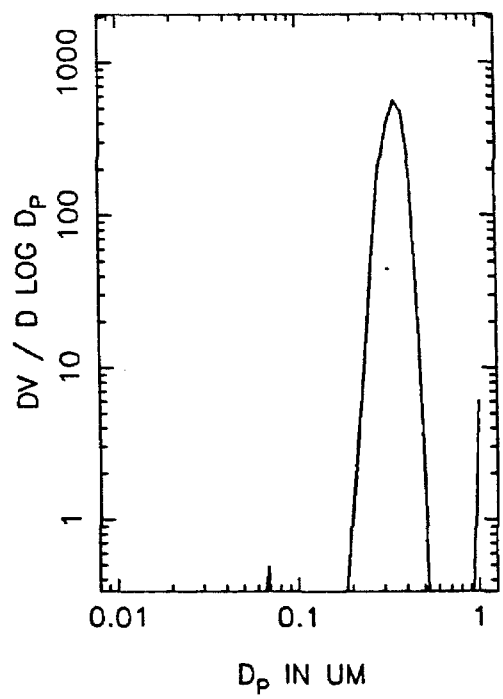

TXU75 TOTAL NUMBER, SIDE A

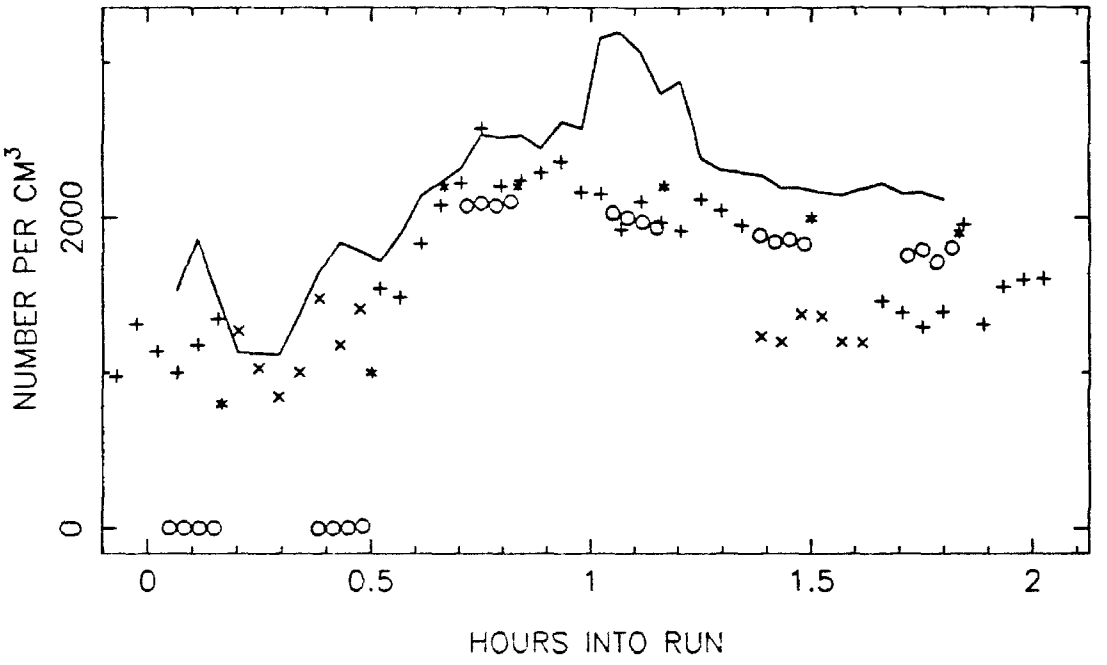

SIDE B

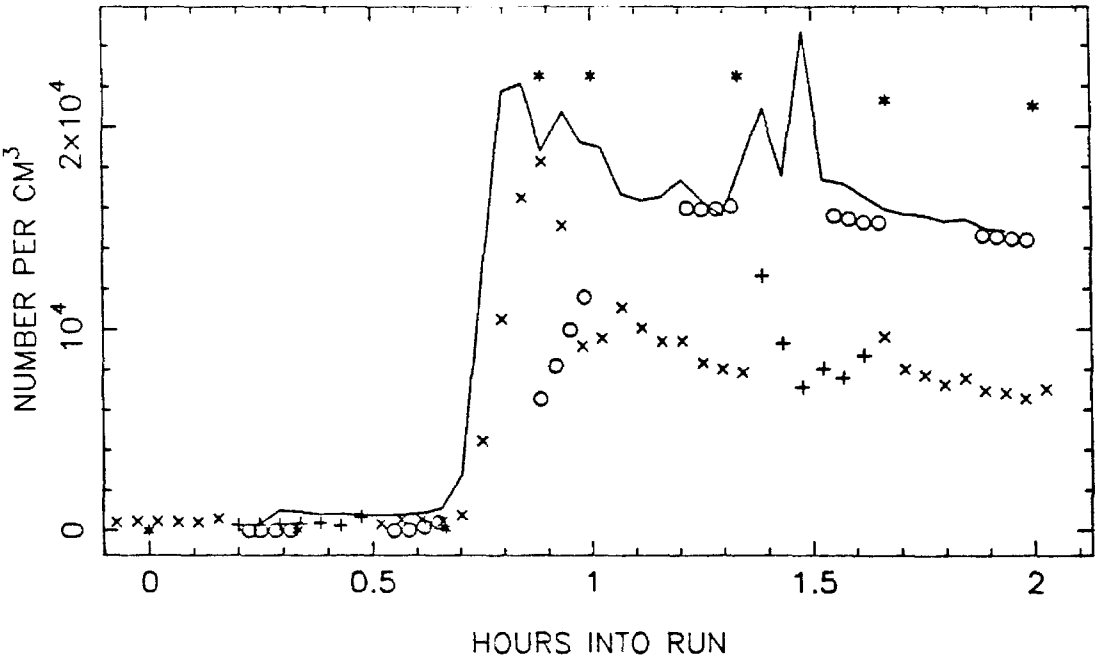

TXU75 VOLUME IN THE AEROSOL PHASE, SIDE A

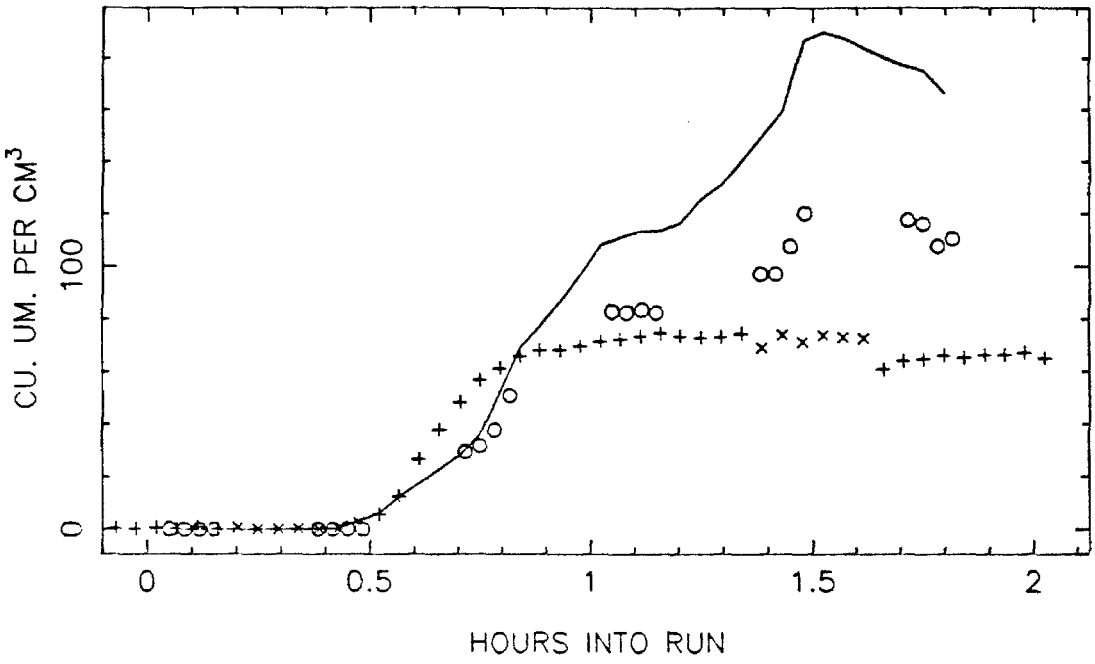

SIDE B

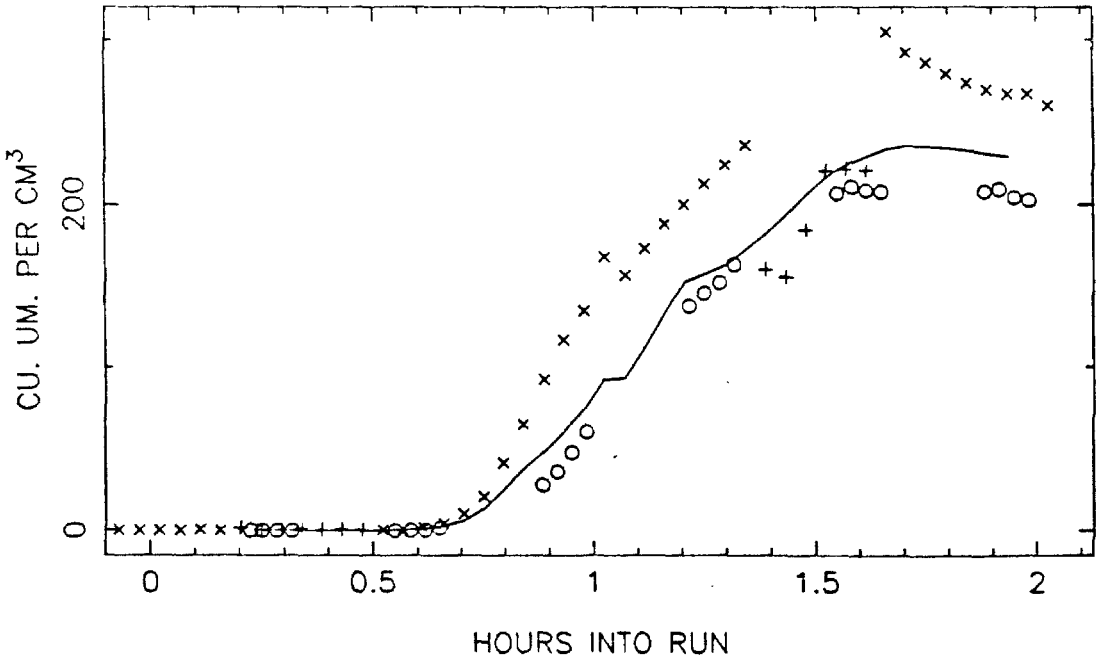

TXU75 MEAN PARTICLE SIZE, SIDE A

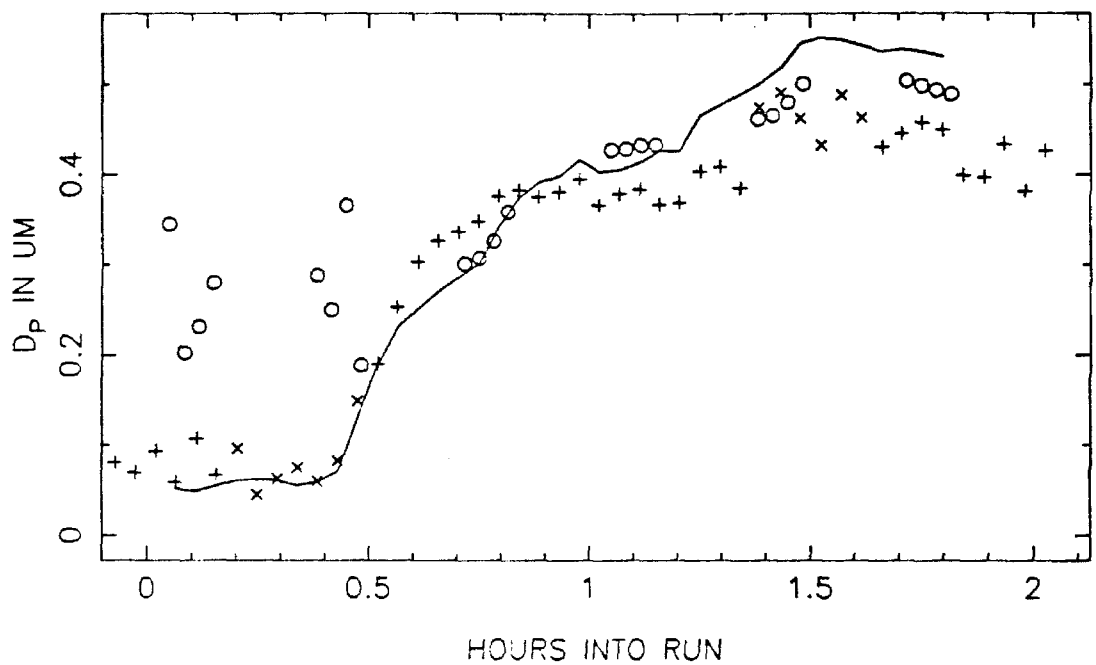

SIDE B

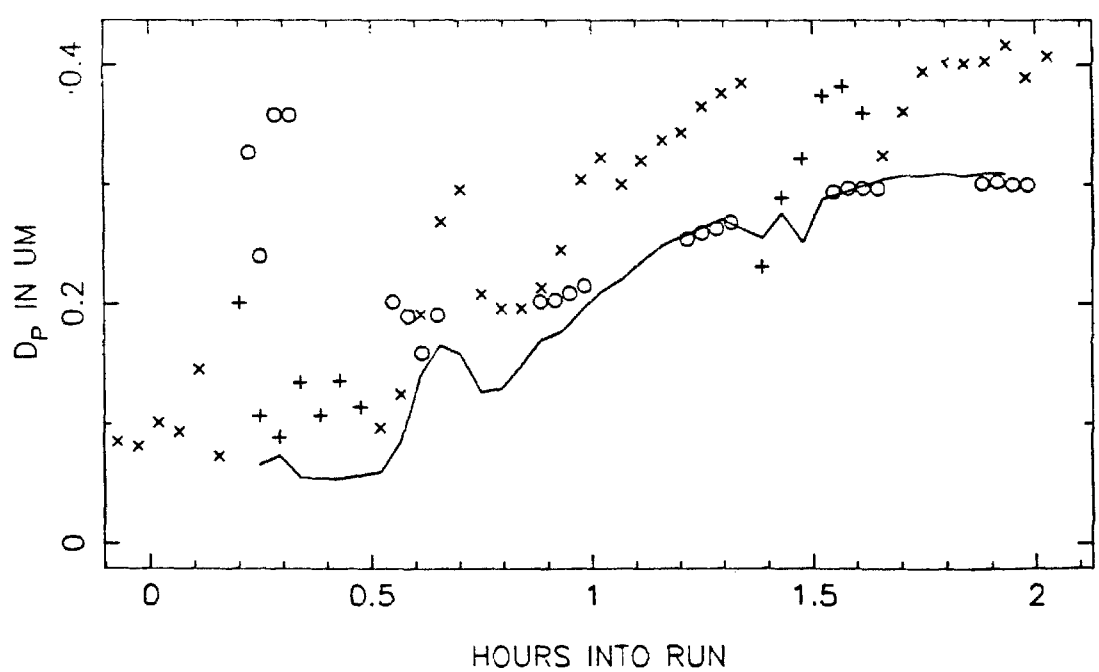

TXU75A NUMBER DISTRIBUTION, T=0

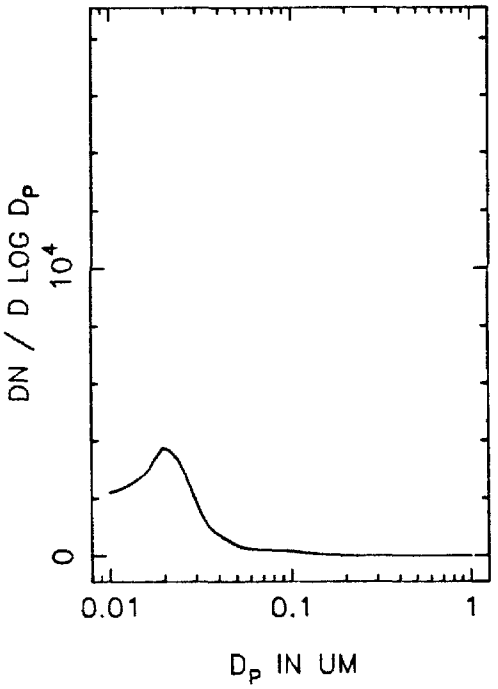

T=0.5 HOURS

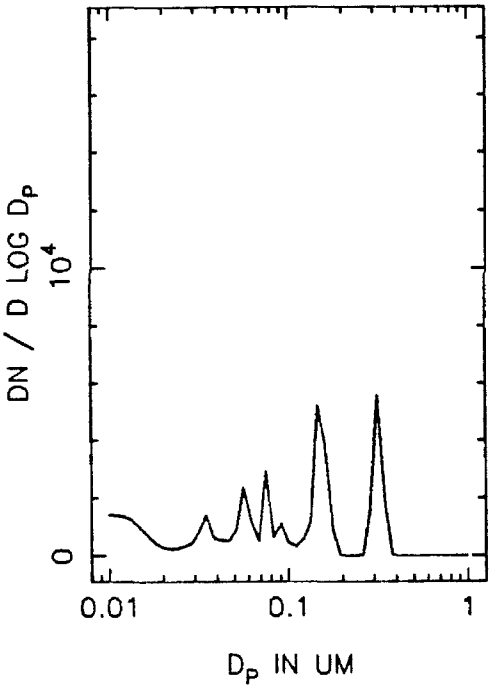

T=1.0 HOURS

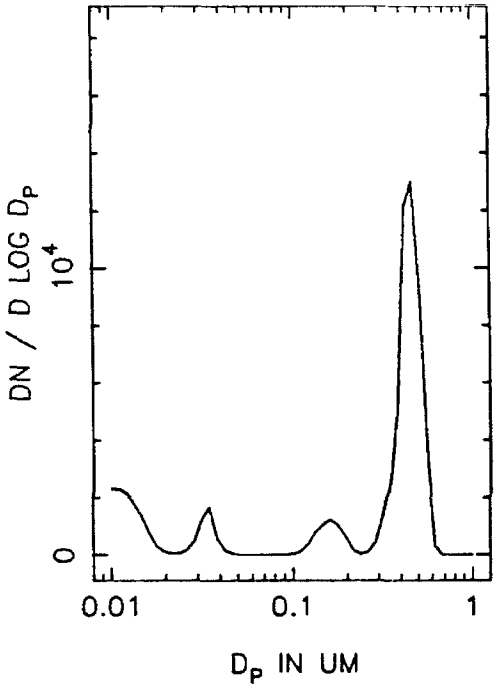

T=1.5 HOURS

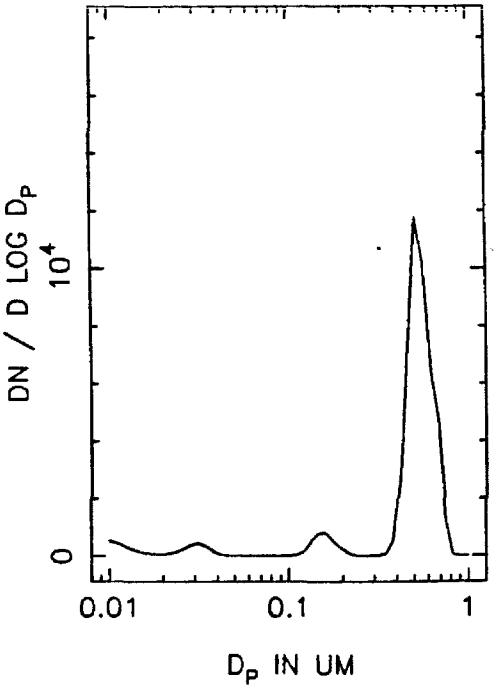

TXU75A VOLUME DISTRIBUTION, T=0

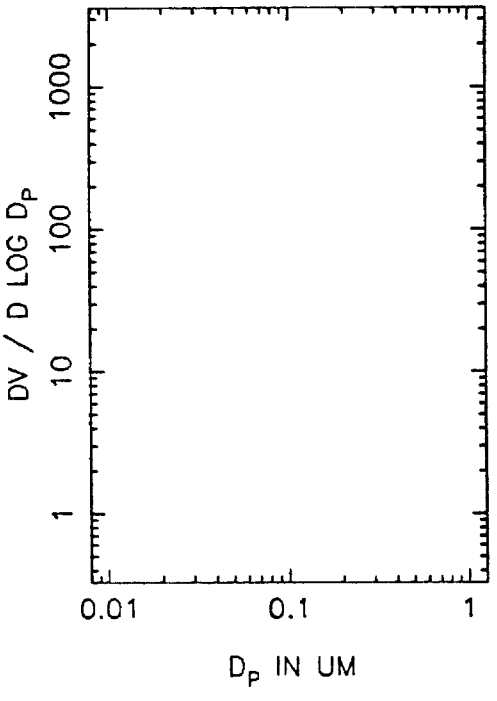

T=0.5 HOURS

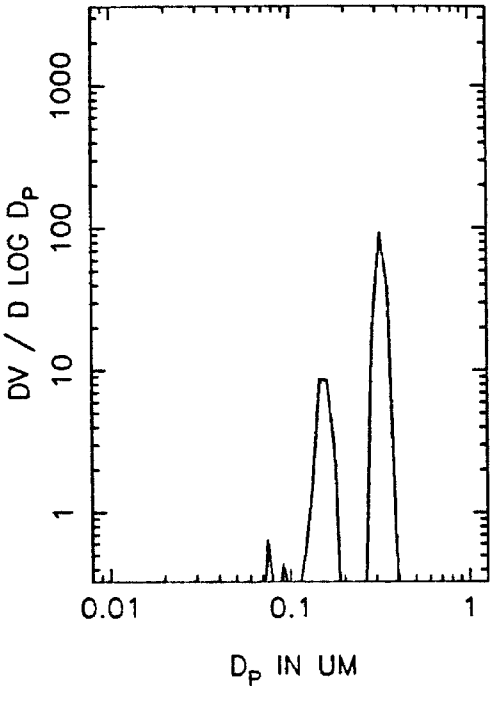

T=1.0 HOURS

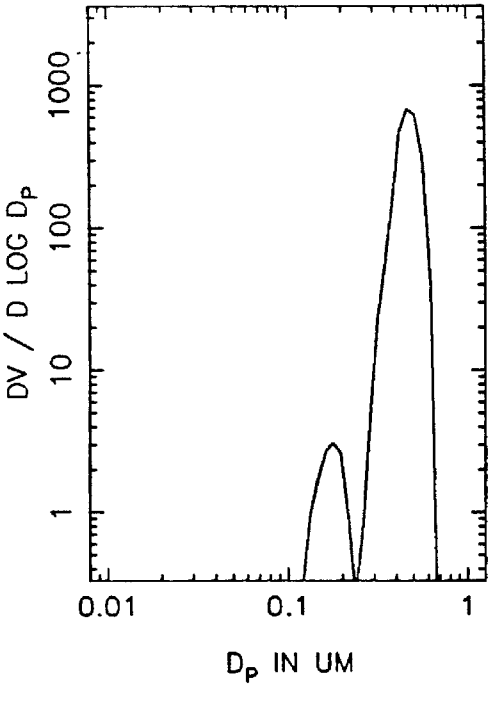

T=1.5 HOURS

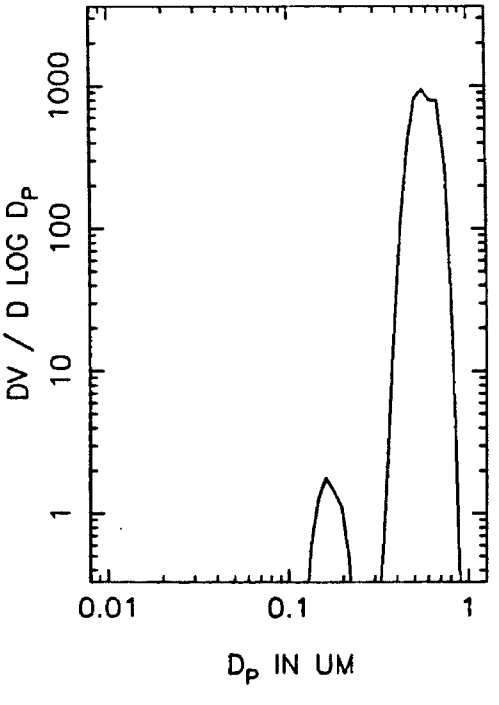

TXU75B NUMBER DISTRIBUTION, T=0

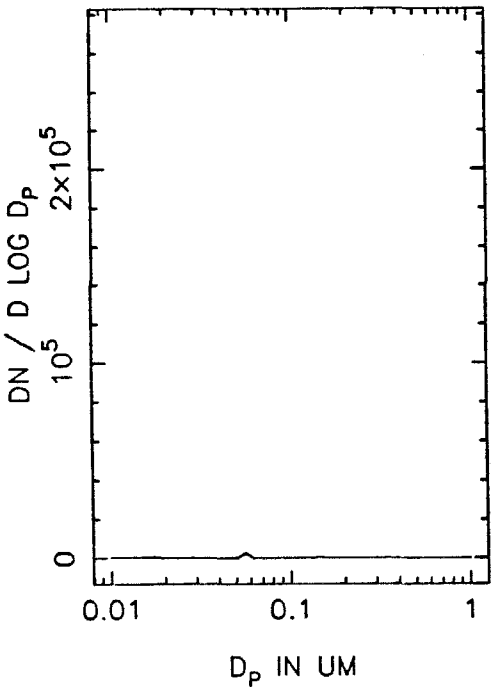

T=0.5 HOURS

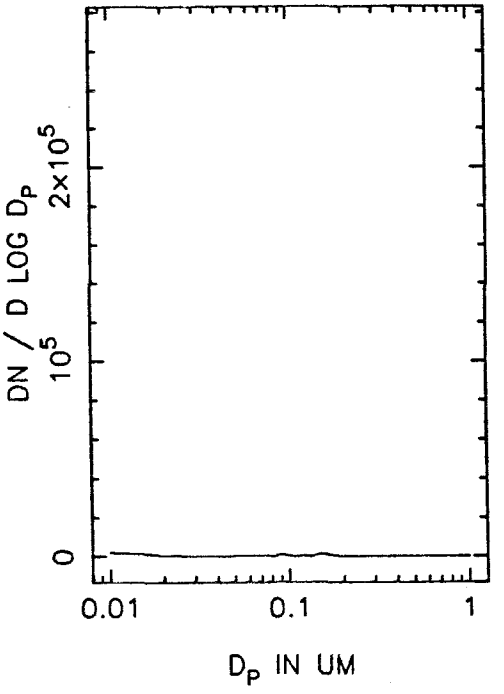

T=1.0 HOURS

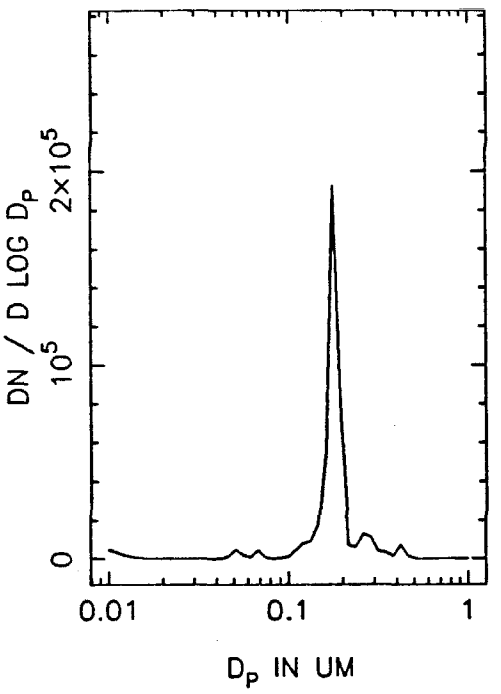

T=1.5 HOURS

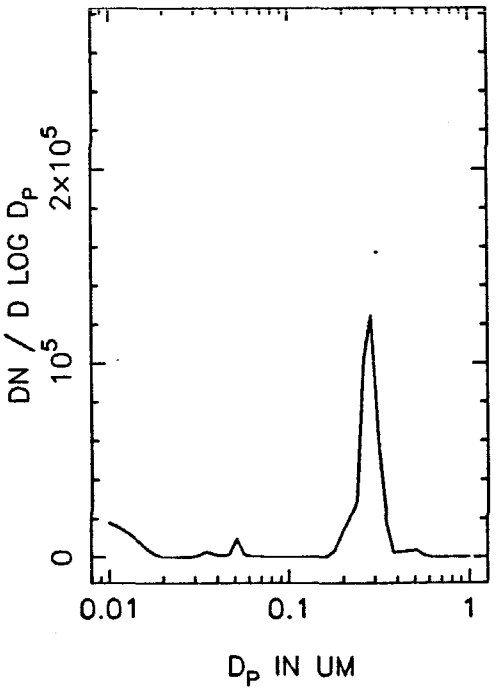

TXU75B NUMBER DISTRIBUTION, T=2.0

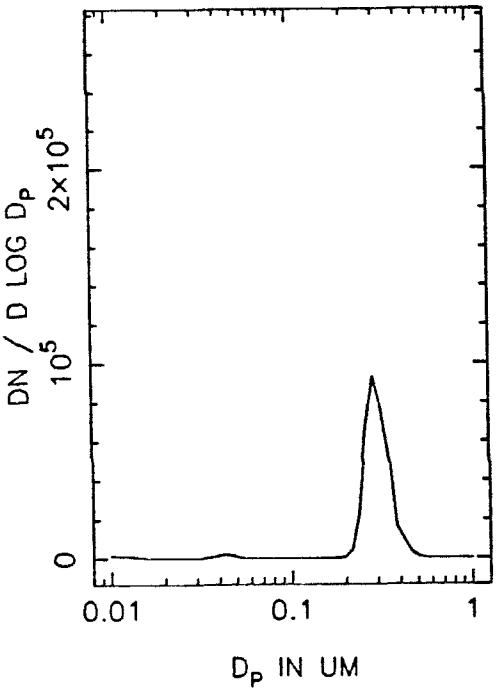

TXU75B VOLUME DISTRIBUTION, T=0

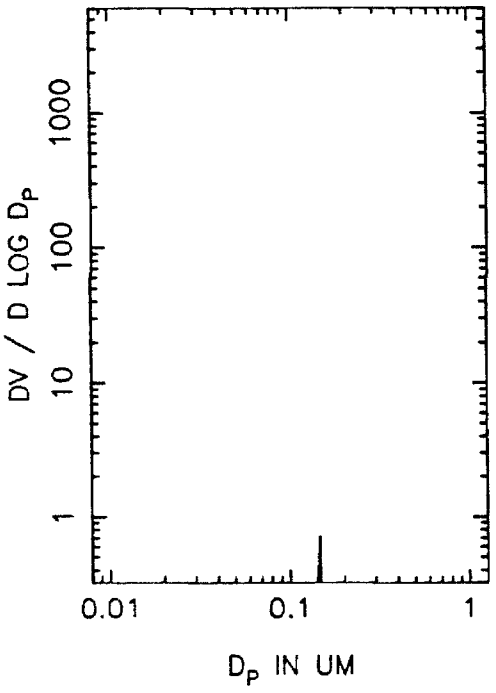

T=0.5 HOURS

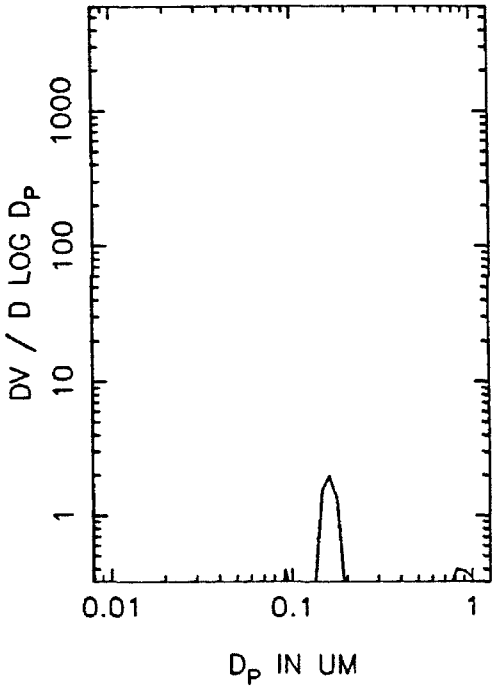

T=1.0 HOURS

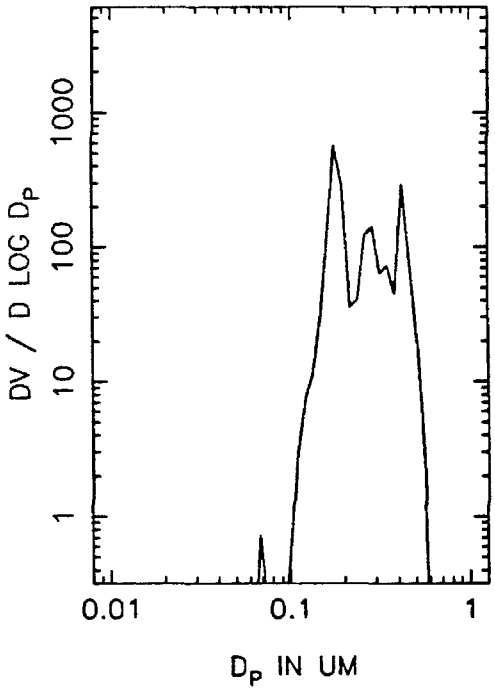

T=1.5 HOURS

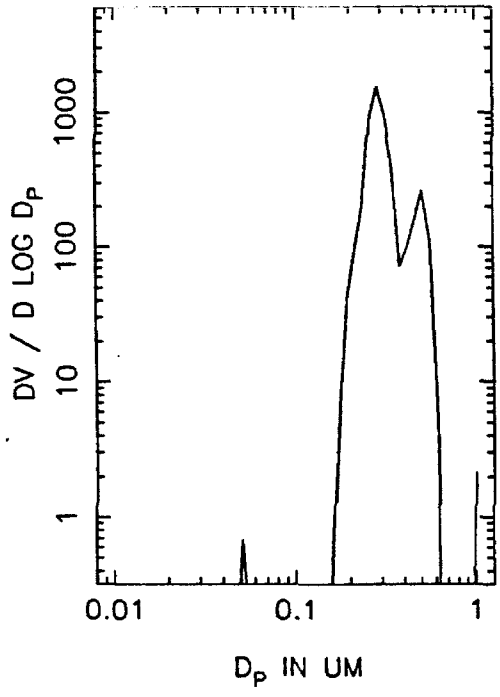

TXU75B VOLUME DISTRIBUTION, T=2.0

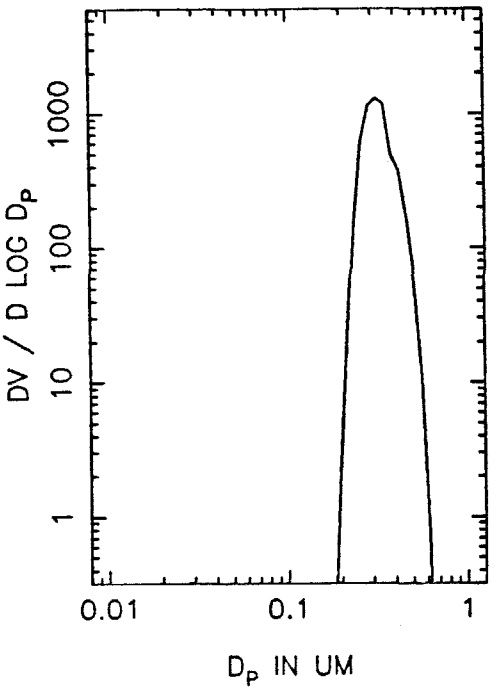

LEV77 TOTAL NUMBER, SIDE A

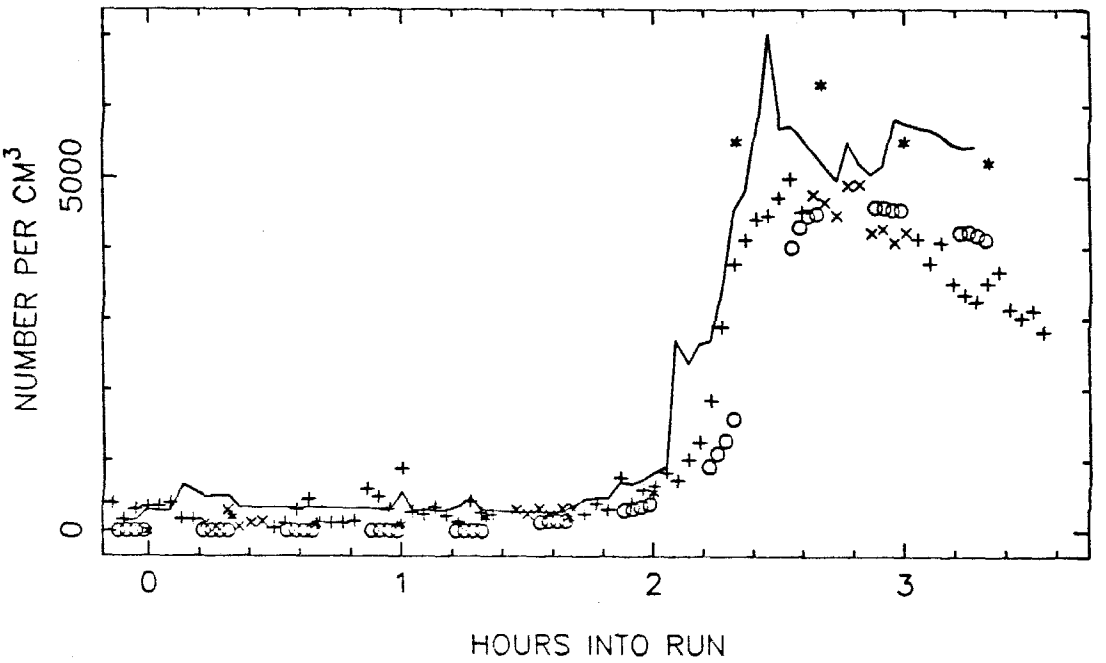

SIDE B

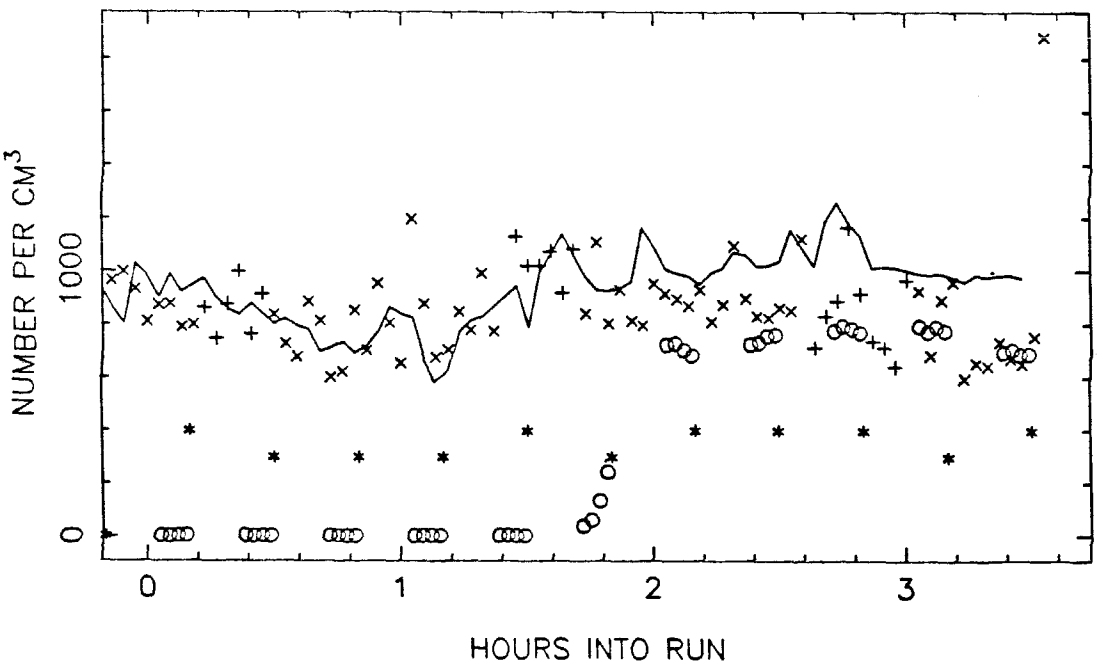

LEV77 VOLUME IN THE AEROSOL PHASE, SIDE A

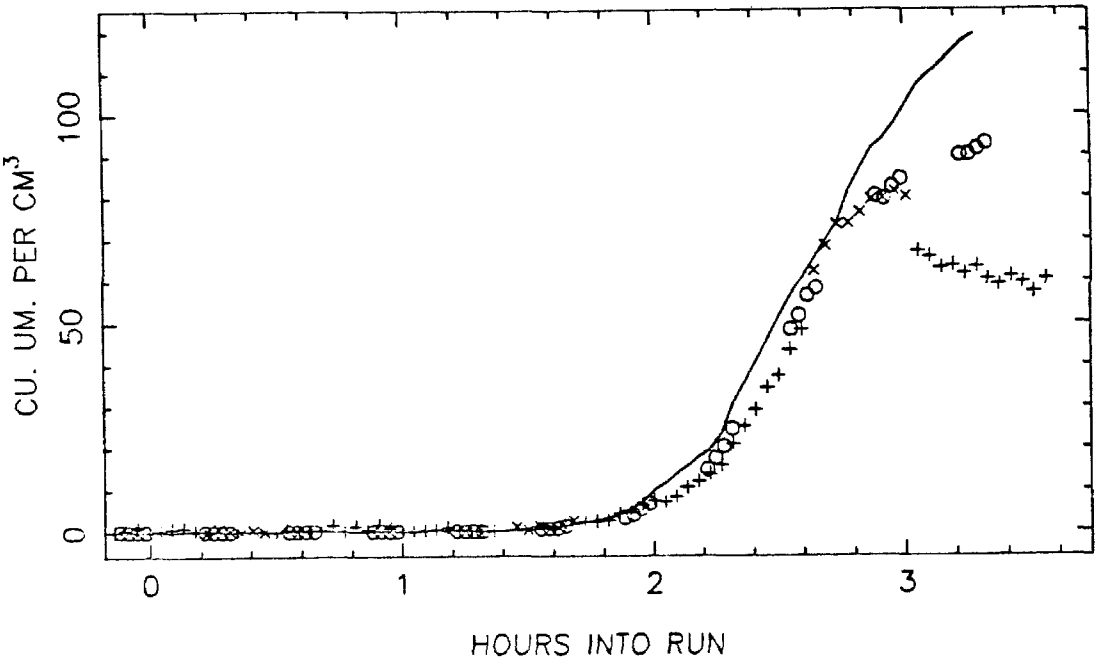

SIDE B

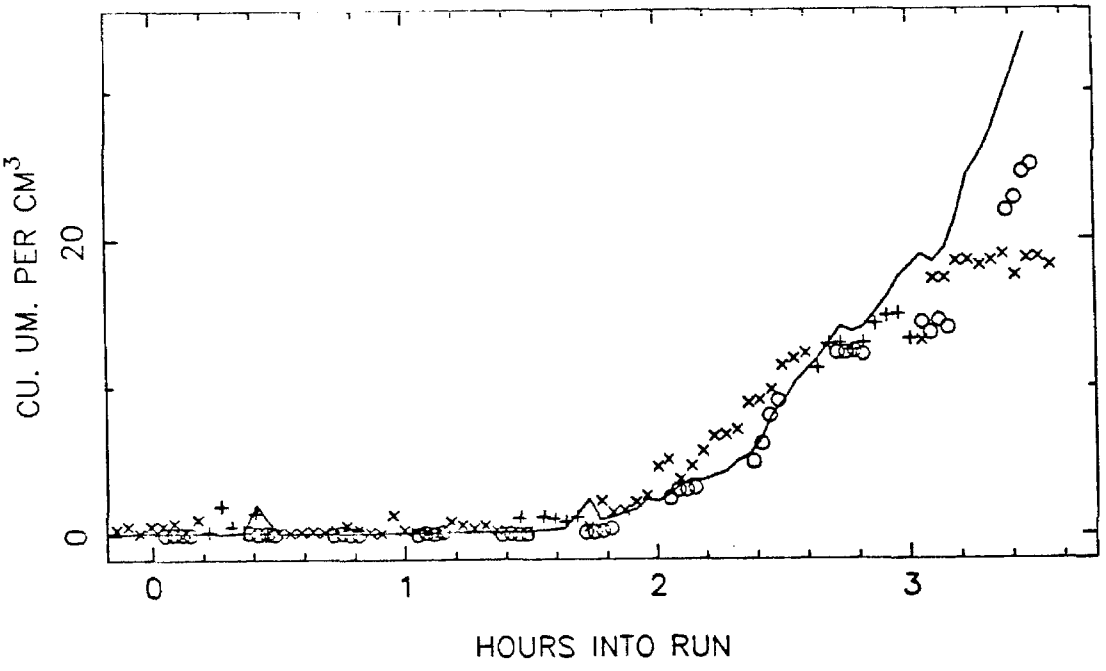

LEV77 MEAN PARTICLE SIZE, SIDE A

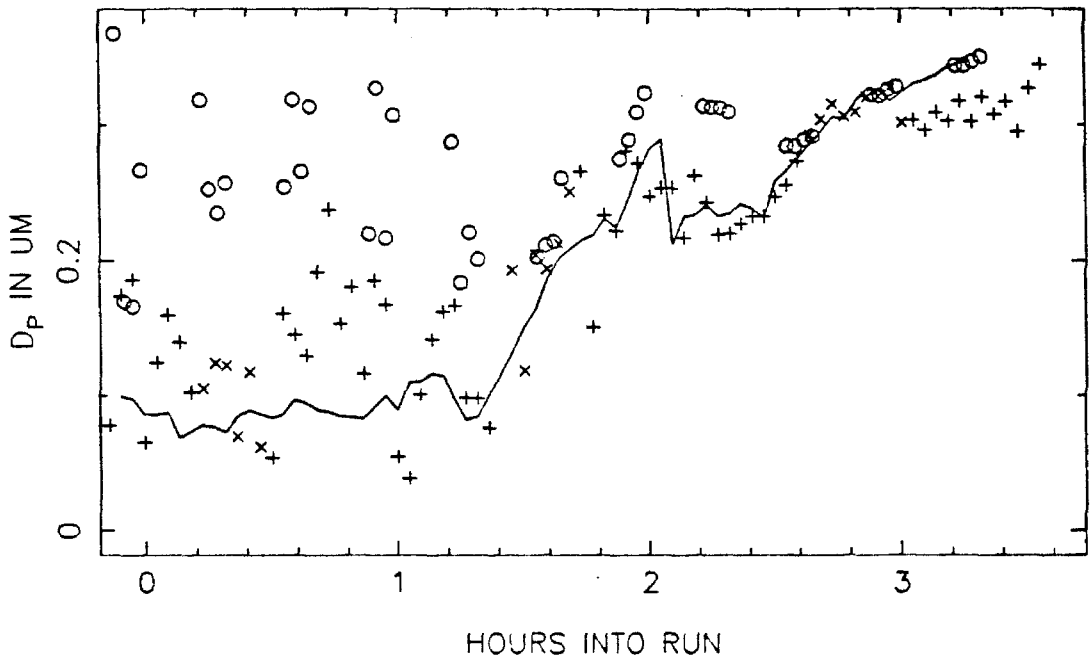

SIDE B

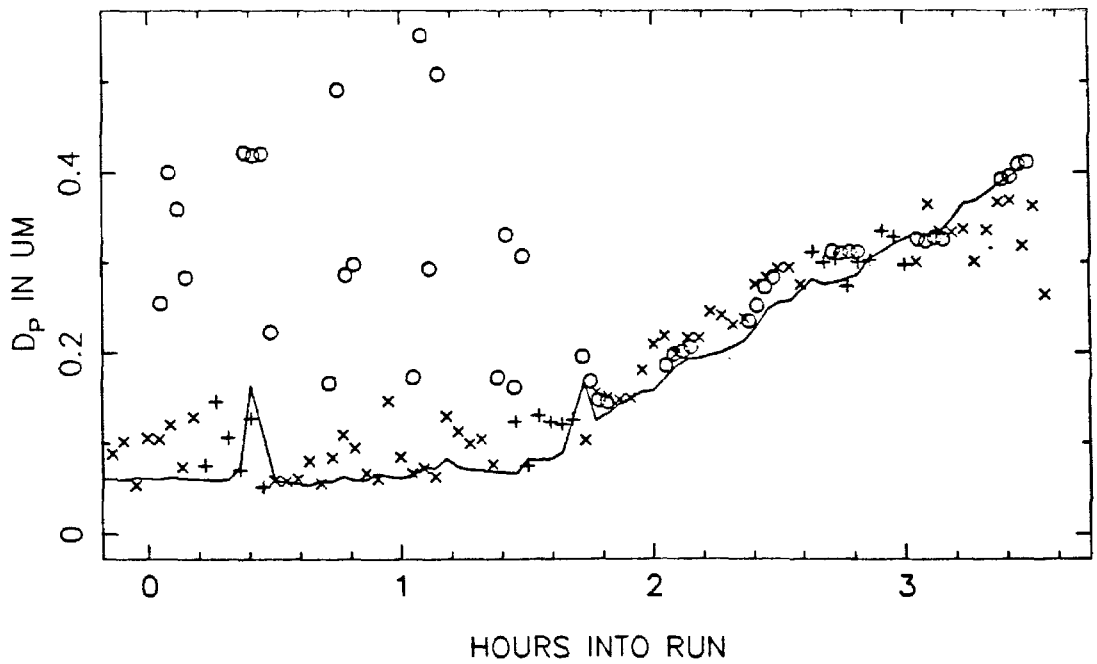

LEV77A NUMBER DISTRIBUTION, T=0

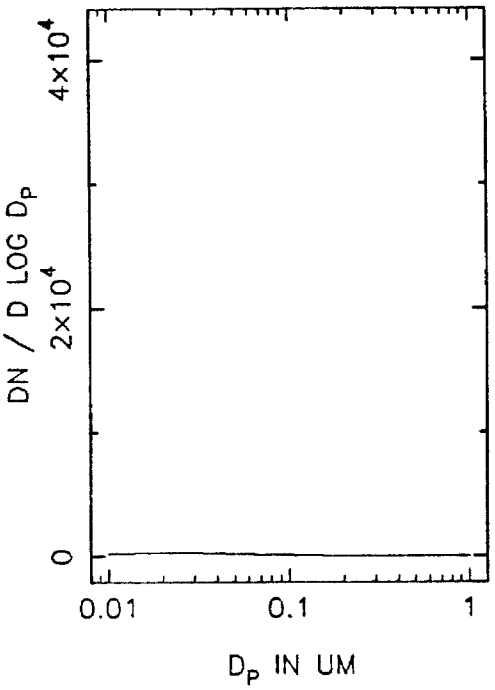

T=0.5 HOURS

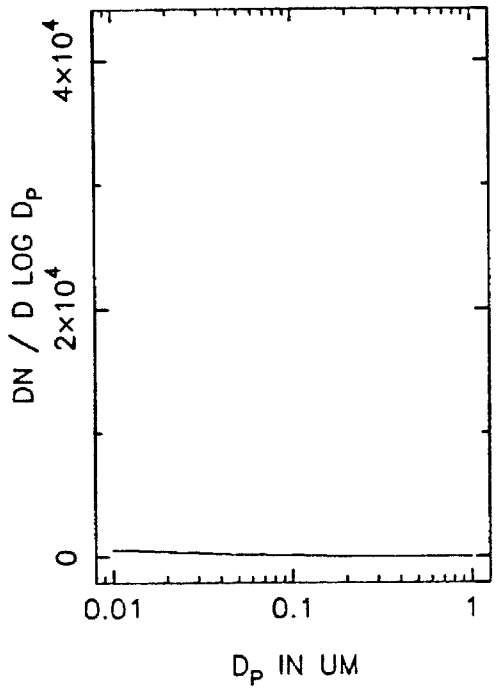

T=1.0 HOURS

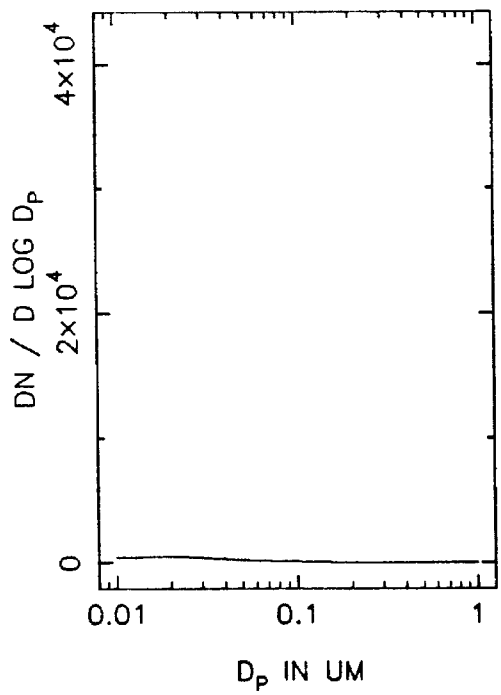

T=1.5 HOURS

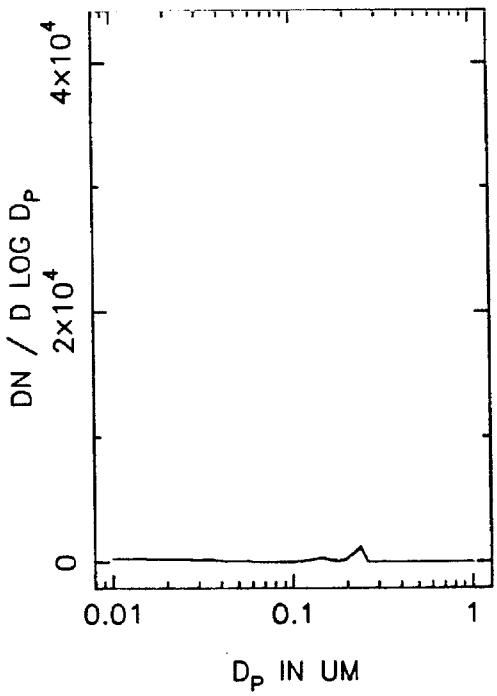

LEV77A NUMBER DISTRIBUTION, T=2.0

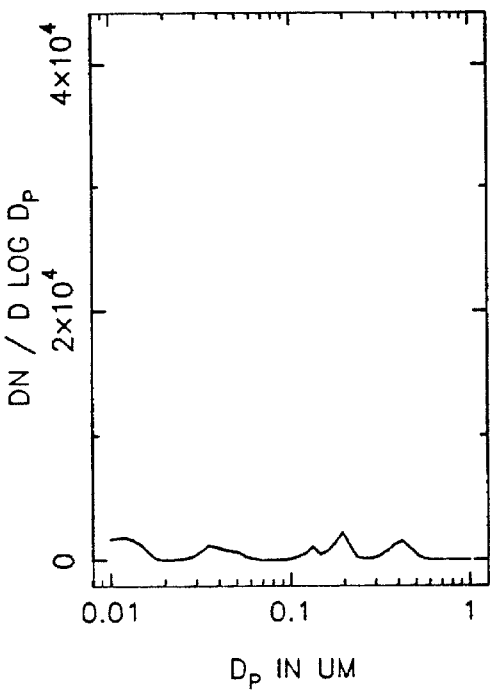

T=2.5 HOURS

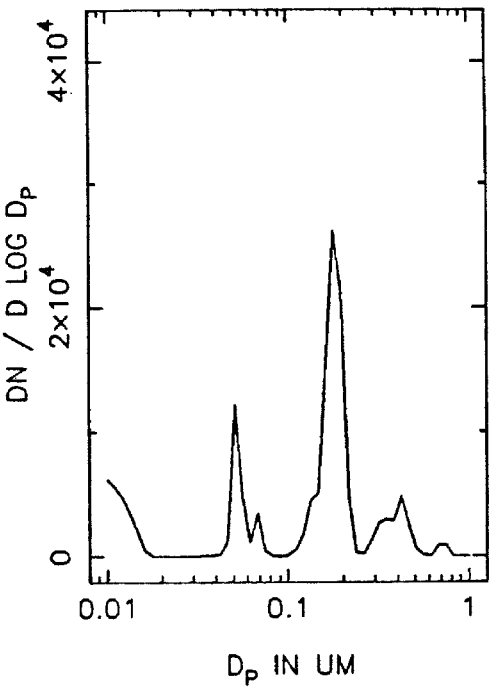

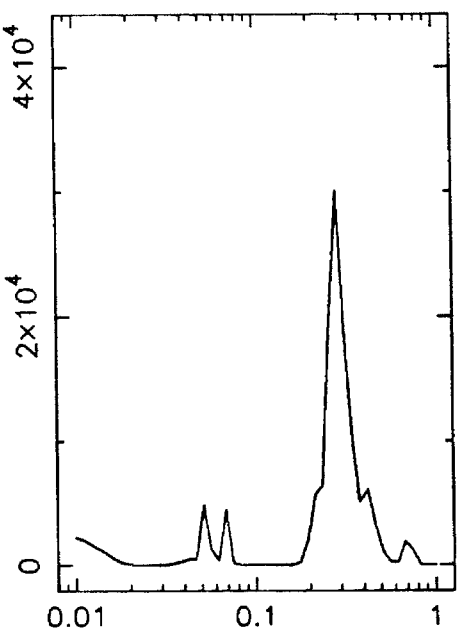

LEV77A VOLUME DISTRIBUTION, T=0

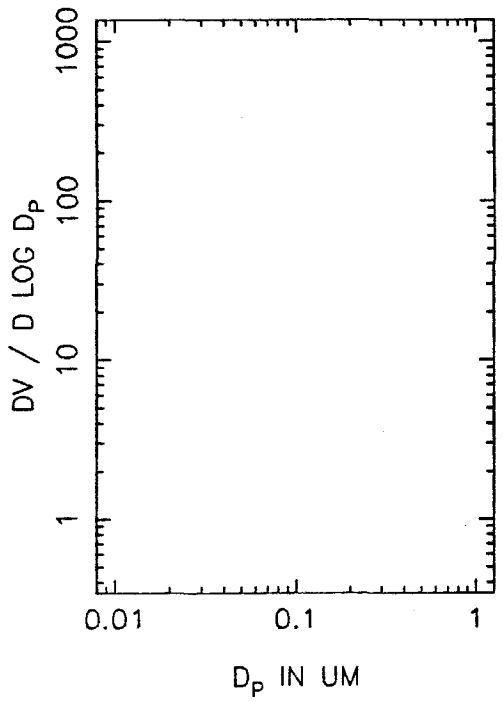

T=0.5 HOURS

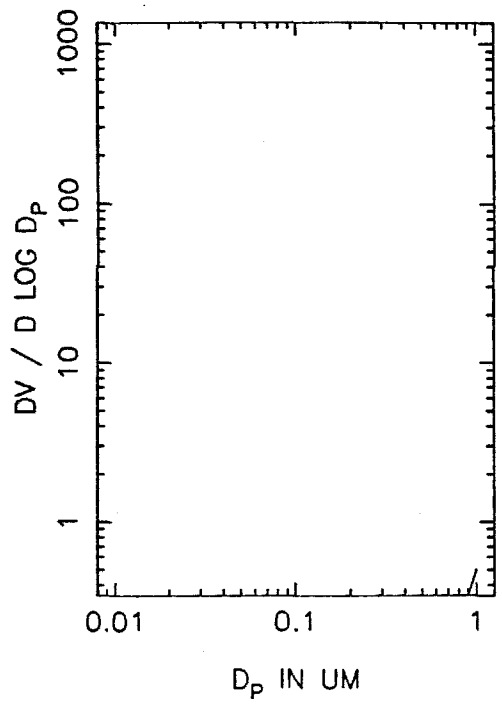

T=1.0 HOURS

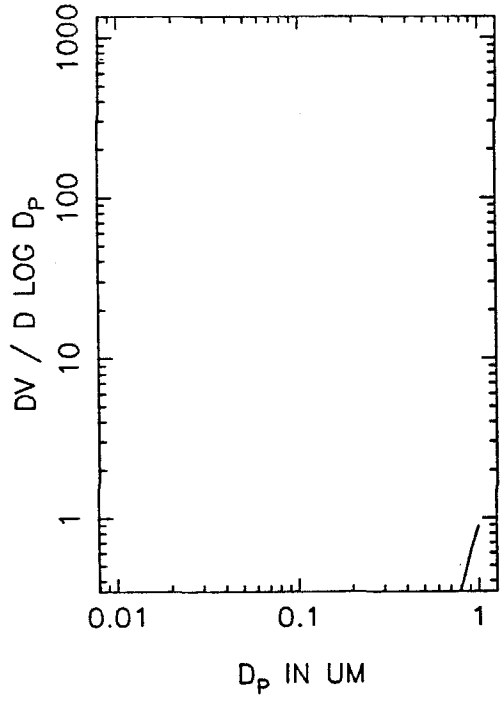

T=1.5 HOURS

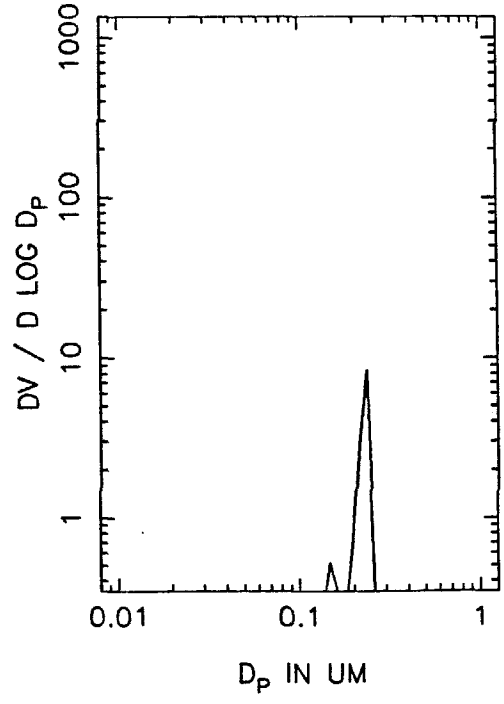

LEV77A VOLUME DISTRIBUTION, T=2.0

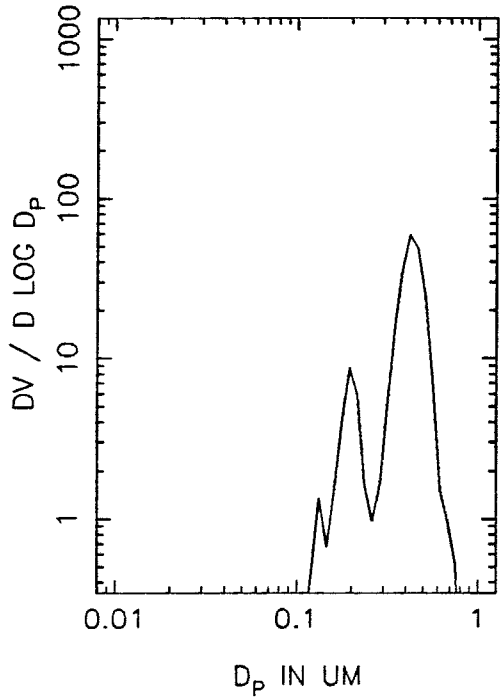

T=2.5 HOURS

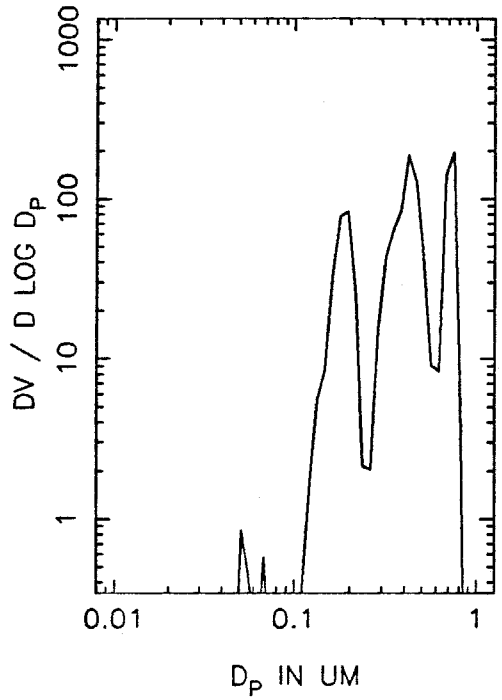

T=3.0 HOURS

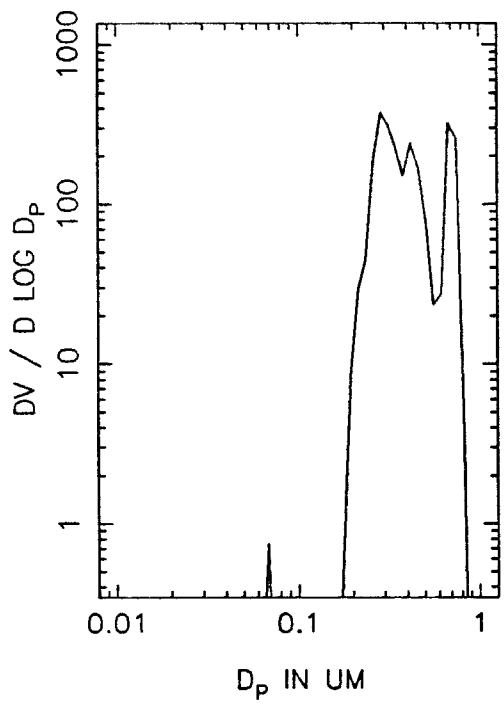

LEV77B NUMBER DISTRIBUTION, T=0

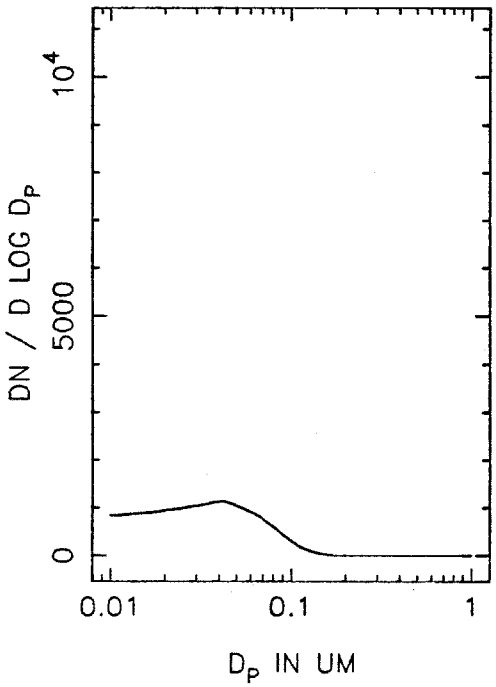

T=0.5 HOURS

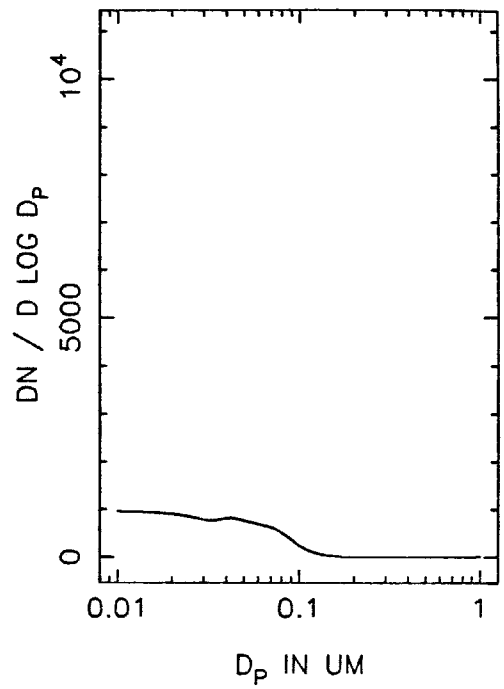

T=1.0 HOURS

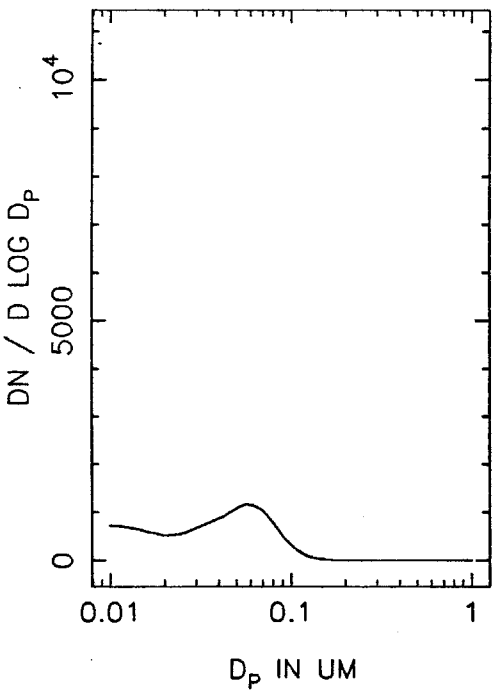

T=1.5 HOURS

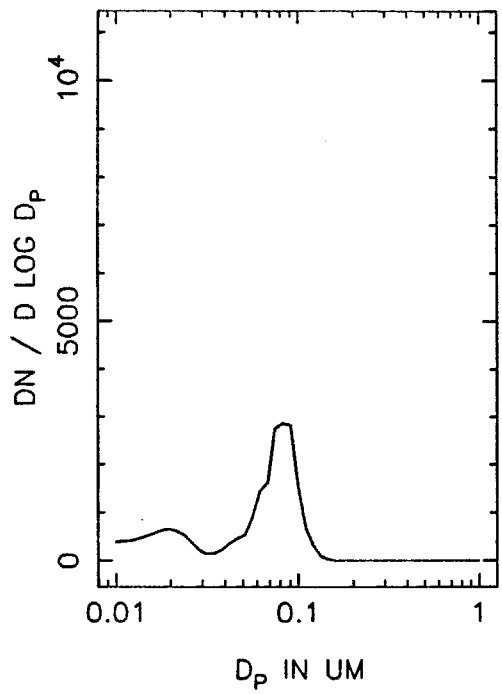

LEV77B NUMBER DISTRIBUTION, T=2.0

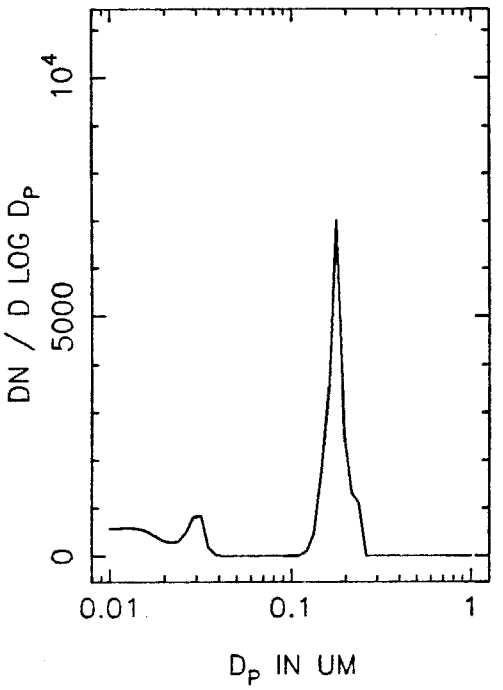

T=2.5 HOURS

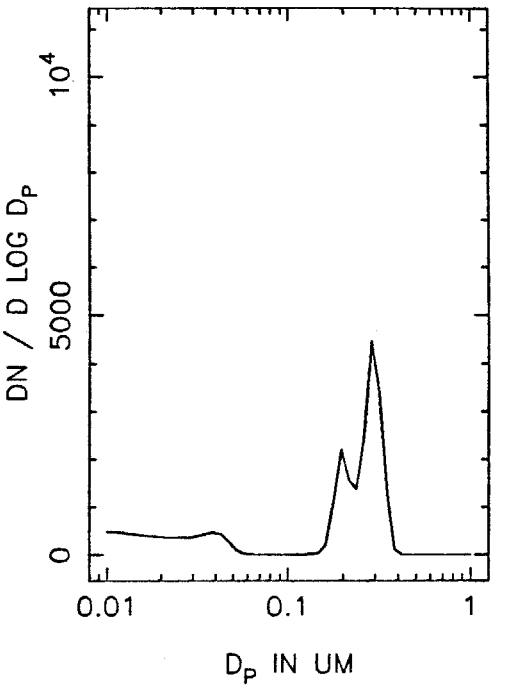

T=3.0 HOURS

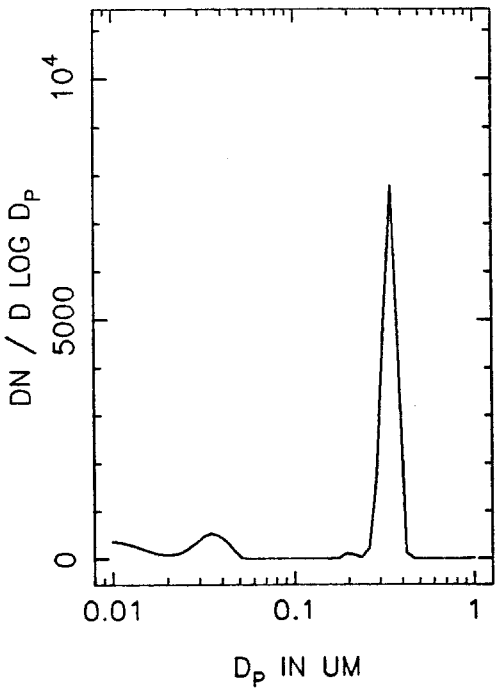

T=3.5 HOURS

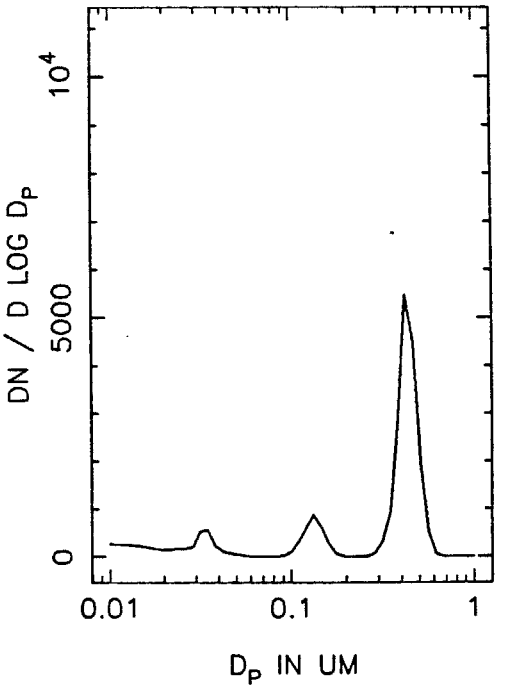

LEV77B VOLUME DISTRIBUTION, T=0

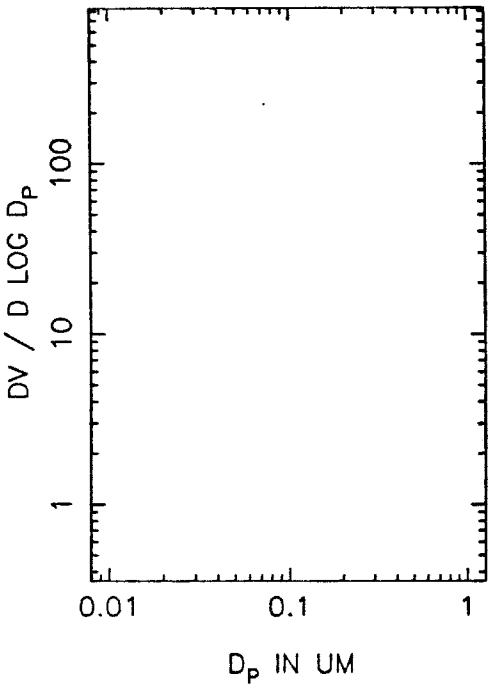

T=0.5 HOURS

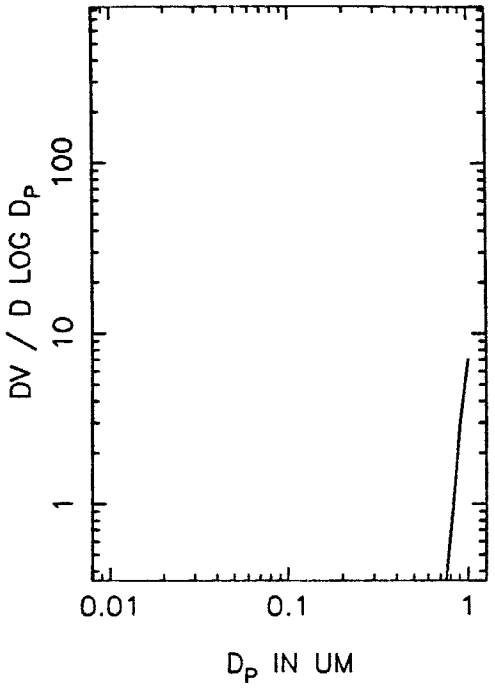

T=1.0 HOURS

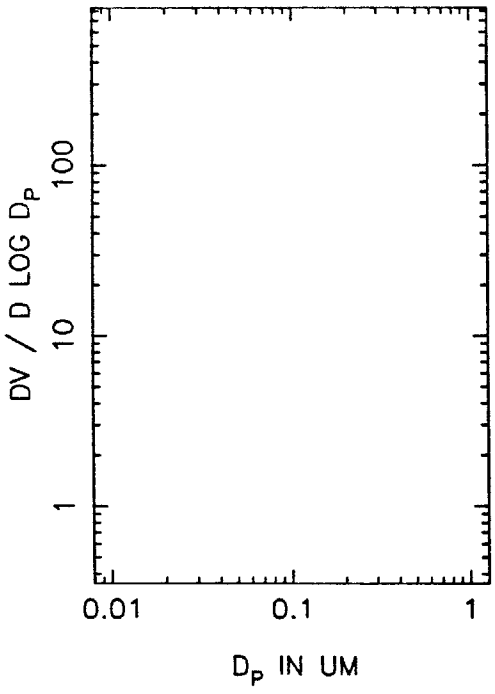

T=1.5 HOURS

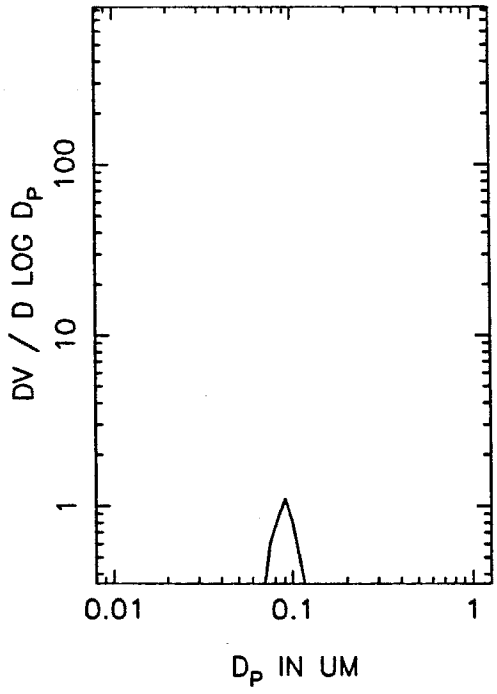

LEV77B VOLUME DISTRIBUTION, T=2.0

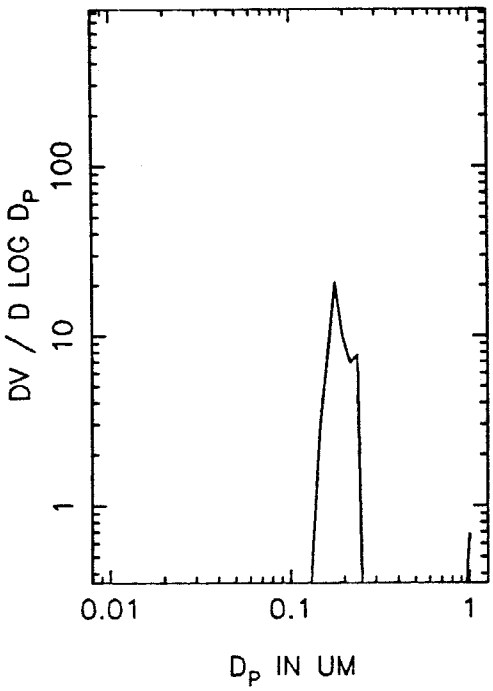

T=2.5 HOURS

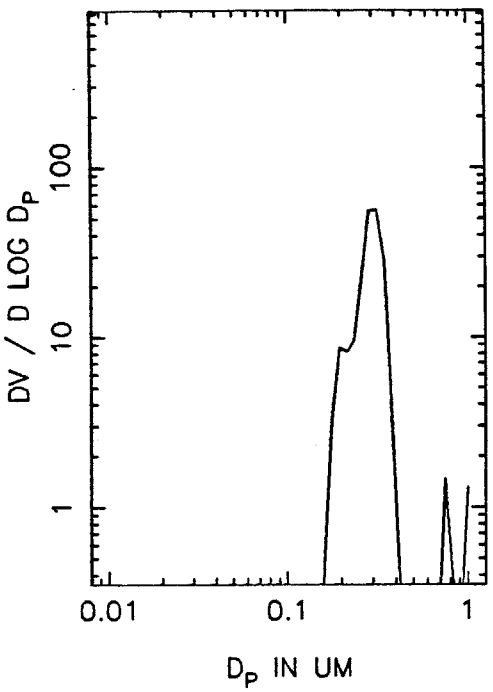

T=3.0 HOURS

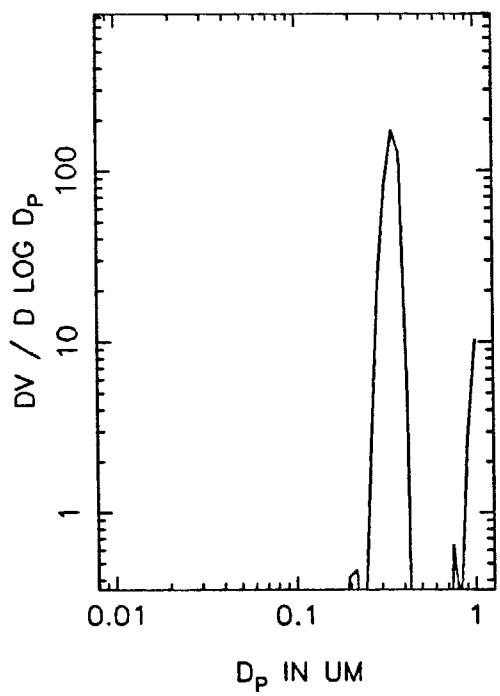

T=3.5 HOURS